Progress in Energy and Combustion Science 68 (2018) 29–64

Contents lists available at ScienceDirect

Progress in Energy and Combustion Science

journal homepage: www.elsevier.com/locate/pecs

Refinery co-processing of renewable feeds

Stella Bezergianni[a], Athanassios Dimitriadis[a], Oleg Kikhtyanin[b], David Kubička[b,*]

[a] *Centre for Research & Technology Hellas – CERTH, Chemical Process & Energy Resources Institute – CPERI, Thermi-Thessaloniki, 6th km Charilaou-Thermi Rd., Thermi-Thessaloniki 57001, Greece*
[b] *Technopark Kralupy, University of Chemistry and Technology Prague, Žižkova 7, 278 01 Kralupy nad Vltavou, Czechia*

ARTICLE INFO

Article History:
Received 11 September 2017
Accepted 21 April 2018
Available online xxx

Keywords:
Co-processing
Lipids
Bio-oil
HVO
Biofuels
Hydroprocessing
Fluid catalytic cracking (FCC)
Vegetable oils

ABSTRACT

Biofuels are called upon to play an important role, not only in reducing the associated greenhouse-gases emissions, but also in enabling the gradual independence from fossil sources, rendering low-carbon-highly-sustainable fuels. Today, the involvement of biomass-derived sources into existing petroleum refineries has a growing interest due to the increasing unpredictability of oil prices, environmental concerns and the necessity to secure an energy supply. Petroleum refineries already have a well-developed infrastructure to produce fuels and base chemicals and, consequently, would not require additional intensive investments for processing of alternative feedstocks. From this point of view, co-processing of biomass-derived feedstocks with petroleum fractions is an attractive option, which has already been industrially demonstrated in some cases. There are two main technologies that could be used for co-processing of biomass feedstocks with petroleum fractions, the first one being catalytic hydroprocessing and the second one being fluid catalytic cracking (FCC). Both technologies are found in virtually any conventional refinery. It is obvious that the co-processing of biomass-based feedstocks with petroleum fractions has the potential to play an important role in the near future. There are several research studies in literature that examine both technologies for co-processing. However, while there are many technological reviews that focus on stand-alone biofuel production (*e.g.*, FAME biodiesel, bioethanol, HVO *etc.*), a dedicated technological review on co-processing for production of hybrid fuels is still missing. Therefore, this paper is focused on presenting a state-of-the-art review on co-processing bio-based feedstocks with petroleum fractions via hydroprocessing and fluid catalytic cracking, looking at different potential feedstocks, catalysts, operating conditions, products and benefits in detail. As there is no specifically dedicated literature review in this field, the content of this review provides a guideline on co-processing of different bio-based feedstocks with petroleum fractions, aimed at delivering a technological assessment of the existing research efforts.

Contents

Abbreviations: ACE-R^{TM}, Advanced Cracking Evaluation; ACE^{TM}, Advanced Catalyst Evaluation; BEA, Zeolite Beta; BTY, Billion Metric Tons per Year; CAPEX, Capital Expenditures; CFPP, Cold Filter Plugging Point; CoMo, Cobalt-Molybdenum sulfided catalyst; CPO, Catalytic Pyrolysis Oil; CSO, Cottonseed Oil; CTO, Catalyst-to-Oil mass ratio; DMDBT, Dimethyldibenzothiophene; DOS, Days on Stream; DTA, Differential Thermal Analysis; EFAL, Extra-Framework Aluminum; EU, European Union; FAME, Free Fatty Acids Methyl Esters; FAO, Food and Agriculture Organization of the United Nations; FCC, Fluid Catalytic Cracking; FPO, Fast Pyrolysis Oil; FTIR, Fourier Transformed Infrared Spectroscopy; GC–MSD, Gas Chromatograph Mass Selective Detector; GHG, Green House Gas; GO, Gas Oil; HAGO, Heavy Atmospheric Gas Oil; HC, Hydrocarbons; HCO, Heavy Cycle Oil; HDA, Hydrodearomatization; HDC, Hydrocracking; HDC_a, Aromatic Hydrogenation; HDM, Hydrodemetallization; HDN, Hydrodenitrogenation; HDO, Hydrodeoxygenation; HDS, Hydrodesulfurization; HDT, Hydrotreating; HMM, High Molecular Mass; HPO, Hydrodeoxygenated Pyrolysis Oil; HVGO, Heavy Vacuum Gas Oil; HVOs, Hydrotreated Vegetable Oils; HYD, Hydrogenation; LAGO, Light Atmospheric Gas Oil; LCO, Light Cycle Oil; LHSV, Liquid Hourly Space Velocity; LMM, Low Molecular Mass; LPG, Liquefied Petroleum Gas; LR, Long Residue; MAT, Micro-activity Test Reactor; MON, Motor Octane Number; MS, Mass Spectrometry; NExBTL, Neste Biomass to Liquid; NiMo, Nickel-Molybdenum sulfided catalyst; NiW, Nickel-Tungsten sulfided catalyst; OPEX, Operating Expenses; PAH, Poly-aromatic Hydrocarbons; PFAD, Palm Fatty Acid Distillate; PIONA, Paraffins, Isoparaffins, Olefins, Naphthenes, Aromatics; REUSY, Rare Earth USY; RON, Research Octane Number; RSO, Rape Seed Oil; SFO, Sunflower Oil; SGO, Standard Gas Oil #4350; SRGO, Straight Run Gas Oil; SRVD, Straight Run Vacuum Distillate; TAN, Total Acid Number; TGA, Thermogravimetric Analysis; TPO, Temperature Programmed Oxidation; TFY, Total Fuel Yield; UK, United Kingdom; USY, Ultra stable Y zeolite (faujasite (FAU) structure according to the International Zeolite Association); VGO, Vacuum Gas Oil; WAF, Waste Animal Fats; WAG, Waste Animal Grease; WCO, Waste Cooking Oil; WHSV, Weight Hourly Space Velocity; ZSM-5, zeolite ZSM-5 (MFI structure according to the International Zeolite Association)

[*] Corresponding author.
E-mail address: david.kubicka@vscht.cz (D. Kubička).

https://doi.org/10.1016/j.pecs.2018.04.002
0360-1285/

1. Introduction

The world-wide depletion of crude oil and greenhouse-gases (GHG) emissions associated with the transportation sector has imposed the need for specific energy and climate targets towards energy security and solidarity via a growing decarbonized economy. Particularly for the transportation sector, biofuels are highlighted to play an important role, not only in reducing the associated GHG emissions, but also in enabling the gradual independence from fossil sources, rendering low-carbon-highly-sustainable fuels. Over the last several years, the EU and other countries have established specific action plans for the promotion of biofuels (Directive 2003/30/EC, Renewable Energy Directive 2009/28/EC, Amendment to the Fuel Quality Directive 2009/30/EC, *etc.*). On the 30th of November 2016, the Commission published its so-called ‘Winter Package’ of eight proposals to keep the European Union competitive as the clean energy transition changes the global energy markets. The Commission, backed by the Council, has embraced an ambitious plan for the European Union's electricity market. It will be a major instrument in realizing the transition to a low carbon economy by 2050. This means that EU citizens, as well as industrial users, should gradually switch to electricity not only as a source of light, heating and cooling, but also transportation. That electricity should, in turn, be generated or produced from low carbon sources, including, not only, non-fossil fuels such as hydro, solar and wind energy, but also biofuels, biomass and biogases [1]. It is obvious that biofuels are going to play a very important role in the near future.

The first-generation biofuels (biodiesel and bioethanol) are based on energy crops which limit their environmental benefits (GHG emissions) while leading to incompatibility problems with their fossil-based counterparts and combustion systems. For example, FAME (Free Fatty Acids Methyl Esters) biodiesel, produced via the transesterification of vegetable oils (sunflower, rape, soy, jatropha, *etc.*) has raised economic, environmental and social implications due to the associated “food *versus* fuel” debate, problematic by-products (glycerol) utilization, and fuel quality characteristics. More specifically, FAME's high viscosity, low energy content, high oxygen and water content, as well as high cloud and pour point, render technical limitations regarding its end-use (injector coking in diesel engines, microbial contamination of fuel tanks, quality degradation during long term storage [2–4], *etc.*). Similar limitations are also reported for the first-generation ethanol. Furthermore, air transport has acquired a significant role in the everyday life of the modern world. Consequently, there is increased interest in alternative fuels for aviation [5]. Aviation fuels are characterized by high energy density and, therefore, their production depends mainly on liquid hydrocarbon fuels. Moreover, good flow properties, thermal stability and low freezing are other important criteria that have to be met by alternative aviation fuels [6]. Consequently, FAME biodiesel is not acceptable as an aviation fuel due to its low energy density and high freezing point in comparison with jet fuels.

Due to all these disadvantages of the first-generation biofuels, alternative biofuels technologies are being explored. Today, the involvement of biomass-derived sources into existing petroleum refineries has a growing interest due to the increasing unpredictability of oil prices, environmental concerns (*e.g.*, increasing CO_2 level and climate change), and the necessity to secure an energy supply [7]. Petroleum refineries already have a well-developed infrastructure to produce fuels and base chemicals and, consequently, would not require additional intensive investments for the processing of alternative feedstocks. From this point of view, co-processing of biomass-derived feedstocks with petroleum fractions is an attractive option, which in some cases has found its practical realization already [8–12]. There are two main technologies that could be used for the co-processing of biomass feedstock with petroleum fractions, the first one is *catalytic hydroprocessing* and the second one is *fluid catalytic cracking (FCC)*. Both technologies are found in virtually any conventional refinery, as indicated in Fig. 1.

As far as catalytic hydroprocessing is concerned, it is a well-established and commonly-used refining technology generally employed to upgrade petroleum distillate fractions. There are two types of hydroprocessing technologies: catalytic hydrotreating (HDT) and catalytic hydrocracking (HDC), both of which are normally expected in a typical refinery, as depicted in Fig. 1. The catalytic hydrotreatment process is aimed at removing undesirable heteroatoms such as sulfur, nitrogen and oxygen as well as metals and the partial reduction (hydrogenation) of aromatics. It is applied to intermediate refinery streams which are fed to various conversion units (*e.g.*, FCC feed hydrotreating, naphtha pretreating prior to reforming, *etc.*). Catalytic hydrocracking is a conversion process that mainly aims to reduce the boiling point of petroleum fractions. Its feedstocks are generally heavier petroleum intermediate products

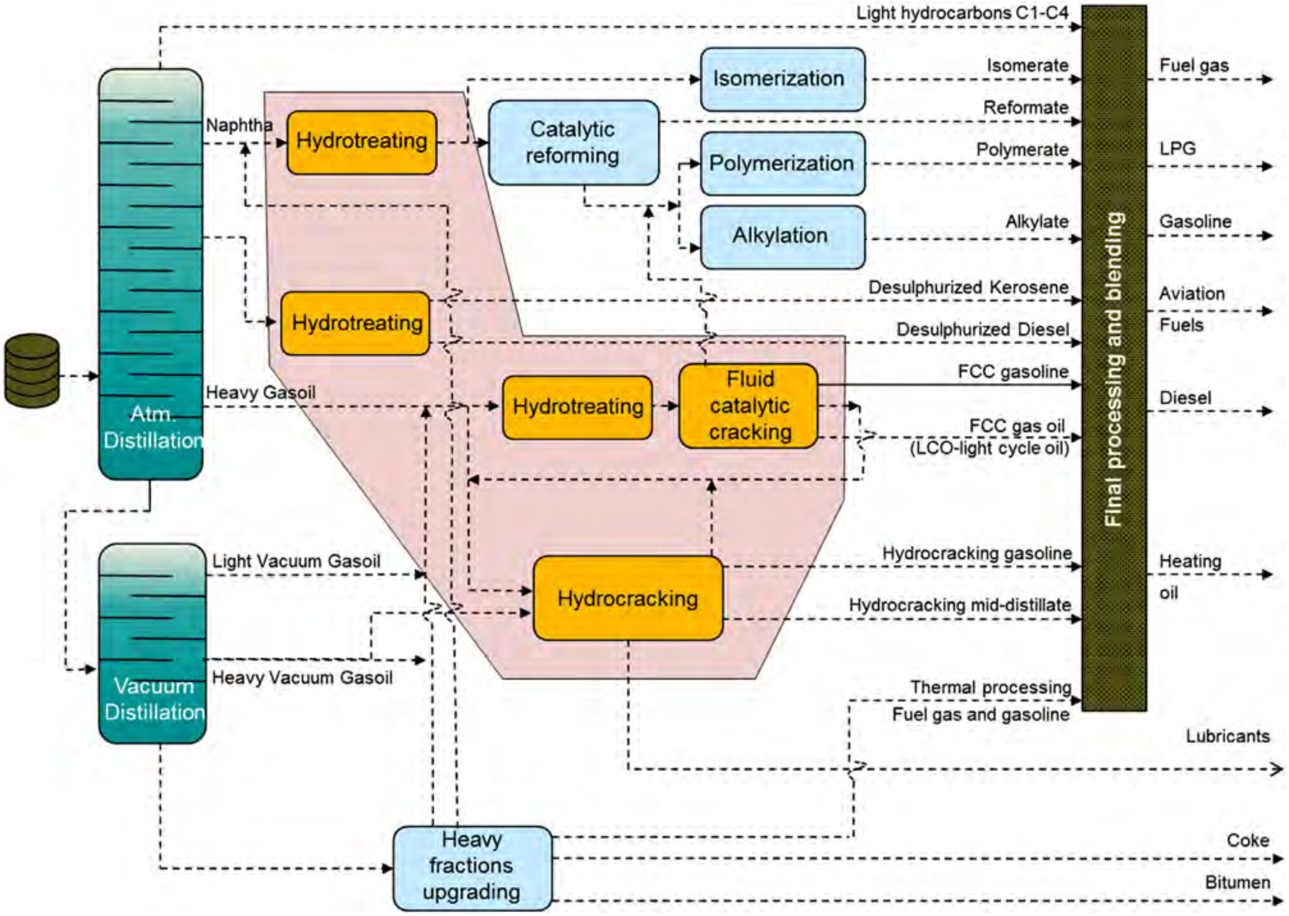

Fig. 1. Typical refinery scheme.

such as heavy gas oil, vacuum gas oil, *etc.* In fact, as the sulfur and aromatics specifications become stricter (*i.e.,* 10 ppm sulfur in diesel, the progressive reduction of aromatics) and the available crudes become heavier and sourer (higher sulfur amounts), catalytic hydroprocessing technologies are becoming dominant conversion units.

Over the last several years, catalytic hydroprocessing has been employed as an advanced biofuels technology over a wide range of bio-based feedstocks, primarily lipids, also. In general, the technology is currently available on an industrial scale, rendering hydrotreated vegetable oils (HVOs) or “green diesel” produced from edible lipids or “white diesel” produced from used cooking oils as “drop in” biofuels [13] for road transportation as well as the aviation sector [14]. The first commercial scale hydroprocessing plant for green diesel production, with a capacity of 170,000,000 metric tons per year was started up in the summer of 2007 at Neste Oil's Porvoo oil refinery in Finland. This technology is branded as “NExBTL” [8, 13, 15]. The produced biofuels are mainly paraffins in diesel, gasoline and jet fuel range, depending on the catalyst and operating conditions, with a high cetane number, a high heating value and a zero oxygen content [16]. The most important advantage of this technology includes high flexibility regarding the feedstock without compromising fuel quality [13]. During the catalytic hydroprocessing of bio-based feedstocks H_2O, CO, CO_2 and C_3H_8 are produced as side products. Nevertheless, such a technology is associated with high investment costs, which justifies high throughput plants only.

To minimize the high investment costs, the co-hydroprocessing of heavy petroleum fractions with bio-based feedstocks is currently being investigated, utilizing the underlying conversion capacity of existing refineries. This approach renders low-carbon hybrid (of partially bio- and partially fossil-origin) fuels of increased sustainability, while enabling the gradual decarbonization of the transportation and aviation sector via a biomass infusion in refineries. In addition, co-hydroprocessing has the potential of valorizing a variety of bio-based feedstocks including lipids, pyrolysis bio-oils, *etc.*, enabling operational flexibility and feedstock availability. The difference of stand-alone hydroprocessing of bio-based feedstocks for drop-in biofuels, which are blended with upgraded petroleum fractions leading to conventional fuels *vs* the co-processing approach rendering hybrid fuels, are compared in Fig. 2.

Regarding fluid catalytic cracking (FCC), it is the most widely used process in the petrochemical refinery for the conversion of the heavy fractions of crude oil (*e.g.,* vacuum gas oil (VGO) or long residue (LR)) to produce gasoline and propylene as the key products and other hydrocarbon fractions, such as C4 olefins or a middle distillate, *i.e.,* light cycle oil (LCO) [17, 18]. It is also among the refinery processes which can be successfully used for the co-processing of biomass-derived feedstocks and petroleum fractions. Oxygen which is abundantly present in bio-components is removed as CO/CO_2 and water during co-processing in FCC. Simultaneously, coke formed during the process can be successfully burned during the regeneration of a catalyst and the generated heat is used to provide heat for the FCC unit, *i.e.,* the catalyst acts as a heat carrier that supplies the energy needed for the endothermic cracking reaction to take place. In this way, all energy contained in the bio-feed is fully utilized in the process. The separation of water from hydrocarbons does not seem to be a problem. Moreover, some options to involve water into the water-gas shift reaction have been discussed by Corma et al. [18].

The chemistry, catalysts, and challenges involved in the production of biofuels by catalytic cracking of lignocellulosic- and

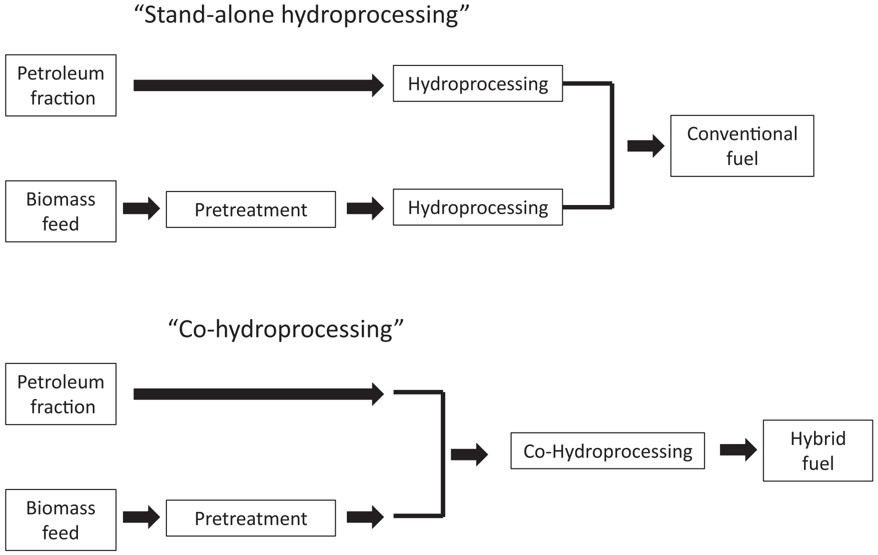

Fig. 2. Stand-alone biomass hydroprocessing for conventional fuel production by blending drop-in biofuel with petroleum-based fuel and biomass co-hydroprocessing for hybrid fuel production.

triglycerides-based feedstocks were considered by Huber and Corma [19] and Stöcker [20]. Nonetheless, the integration of catalytic cracking of petroleum-based feedstock with cracking of biomass-derived feedstocks to occur in a single FCC reactor remains a hot topic for investigation. The transformations of hydrocarbon fractions that occur in the FCC process include cracking reactions (cracking of alkanes, alkenes, naphthenes, and alkyl aromatics to lighter products), hydrogen transfer, isomerization, and coking reactions [21]. Additionally, Corma et al. [18] have proposed that the conversion of oxygenates from biomass-derived feedstocks in the FCC mainly occurs through a series involving five different classes of reactions: 1) dehydration reactions, 2) cracking of large oxygenated molecules to smaller molecules, 3) hydrogen-producing reactions, 4) hydrogen consuming reactions, and 5) production of larger molecules by C—C bond-forming reactions (aldol condensation or Diels–Alder reactions). All these reactions take place simultaneously, under FCC co-processing conditions, and their combination determines the chemical composition and characteristics of the final product.

Several reviews considering the FCC co-processing of biomass-derived and petroleum-derived feedstocks have been published to date [22–25]. While valuable information and conclusions related to co-processing of bio-based feedstocks have been provided, the information and relevant conclusions on the implementation of bio-based feedstocks co-processing in industrial FCC technology is scarce.

It is obvious that the co-processing of biomass-based feedstocks with petroleum fractions has the potential to play an important role in the near future. There are several research studies in the literature that examine both technologies (hydroprocessing and fluid catalytic cracking) for co-processing. However, while there are many technological reviews that focus on stand-alone biofuel production (*e.g.*, FAME biodiesel, bioethanol, HVO, *etc.*), a technological review on co-processing for hybrid fuels production is scarce. There are only a few reviews published in recent years that deal with co-processing. The review of Melero et al. [26] is focused mostly on chemistry, catalysis and challenges involved in the production of biofuels from biomass in conventional refineries, however it does not discuss the effect of the operating conditions, type of catalyst and biomass to fossil feedstock blending ratios in detail. Similarly, the two reviews of Al-Sabawi et al. [22, 27] consider the use of biomass-derived oils and their blends with petroleum feedstocks in hydroprocessing and FCC processing, respectively. However, a major part of these reviews deals with the processing of either individual bio-derived oils or model compounds. Consequently, a detailed discussion on the technological aspects is not provided. Moreover, there have been new developments since these three reviews were published in 2012. The very recent review of Stefanidis et al. [28] is focused very narrowly – it considers only FCC co-processing of petroleum feeds with differently prepared bio-oils.

Therefore, this paper is focused on presenting a state-of-the-art review on co-processing bio-based feedstocks with petroleum fractions via co-hydroprocessing and via fluid catalytic cracking, looking at different potential feedstocks, catalysts, operating conditions, products and benefits in detail. As a result, the content of this review provides a recent guideline on co-processing of different bio-based feedstocks with petroleum fractions, aimed at delivering a technological assessment of the existing research efforts in which goes beyond the previous reviews addressing co-processing of bio-based feedstocks.

2. Feedstocks

One of the main advantages of co-processing is the ability to combine a variety of bio- and fossil-based feedstocks/fractions without compromising product quality. Moreover, due to co-processing, fossil feedstocks can be saved and used in other processes. In this section, the range of fossil- and bio-based feedstocks that are being co-processed are determined and compared.

2.1. Petroleum fractions

Before examining the key bio-based feedstocks that can be introduced in a refinery via co-processing, the fossil-based fractions that are the best candidates for co-processing with bio-based feedstocks should be examined. The most commonly used fossil based feeds for co-hydroprocessing according to literature are straight run gas oil (SRGO) [29–32], straight run diesel, also called light atmospheric gas oil (LAGO) [33–36], heavy atmospheric gas oil (HAGO) [37] and heavy vacuum gas oil (HVGO) [38]. The fossil-based FCC feedstocks also suitable for co-processing applications include distillate fractions, such as vacuum- and heavy vacuum gas-oils or FCC cycle oils (light and heavy cycle oils), as well as atmospheric distillation residue, *i.e.*, short or long residue. The properties of petroleum-based feedstocks are presented in Table 1.

Table 1
Properties of various fossil-based feedstocks for co-hydroprocessing.

Properties	Kerosene	SRGO	LAGO	HAGO	VGO	HVGO	LCO
Density [g/ml]	0.79	0.83–0.84	0.85–0.86	0.85–0.86	0.84–0.92	0.91–0.97	0.95–0.96
Sulfur [wt%]	–	0.72–1.35	1.76	1.20–1.30	0.19–2.02	0.35–3.59	3.50
N [wppm]	–	127–570	140	195–473	29–1900	1600–1800	1000
O [wt%]	–	–	–	0–0.50	0–0.28	0.37	–
Cetane index	–	54.4	–	–	–	–	26.2
Aromatics [wt%]	–	27–33	27–43	30	23	59	76–87
Viscosity [mm^2/s]	–	2.7–3.0	2.4–5.0	–	8.9–10.8	–	2.5–2.7
10wt	176	234–277	215–266	254	253–400	337–400	227–257
30wt	183	296	280	308	329–437	390–430	276
50 wt	190	276	306	334	373–460	427–455	262–295
70 wt	198	326	331	359	422–495	468–490	327
90 wt	212	310–350	346–371	392	492–550	530–550	313–368
Ref.	[67]	[41, 42, 44, 68, 69]	[29, 31, 35, 48]	[45–47, 49]	[52, 54, 55, 62, 70]	[30, 38, 71]	[41, 42, 44]

Straight run gas oil (SRGO) is obtained by crude oil distillation and is the dominant feedstock for diesel fuel production. It is characterized by a low aromatic content, a high cetane index and a boiling point range from 234 °C to 350 °C [39, 40]. SRGO is a good candidate for co-processing due to its low sulfur content and a suitable boiling point range. Due to its favorable properties, SRGO has been examined as feedstock for co-hydroprocessing [41, 42].

Other possible streams for diesel production like light cycle oil (LCO) are only used sparingly. Light cycle oil (LCO) is a lighter petroleum product characterized by a high sulfur, nitrogen and aromatic content and a low cetane number/index. It contains a large amount of gas oil boiling point range multi-substituted aromatics (40–60%) and tetralins (20–30%), in which the side chains are very short paraffins, so their cetane numbers are low [42]. Nevertheless, the increasing presence of fluid catalytic cracking units (FCC) in conversion refineries produces large amounts of LCO. The quality of LCO could be improved by itself or by the conversion together with other refinery streams and/or in mixtures of alternative raw materials [43]. With the co-processing of triglycerides and middle distillates (*e.g.,* LCO containing gas oils) not only can the applicability of the low-quality gas oil fractions as fuel be solved, but diesel fuel with a biocomponent content can be produced. In general, a common practice is to feed LCO in a mixture with SRGO to the hydrotreater [44]. For the above reason, LCO is a feedstock that is not preferable for co-hydroprocessing by itself with lipid-based feeds. Instead, the co-hydroprocessing of blends of SRGO and LCO and bio-based feeds is preferred [4]. Several studies have examined co-hydroprocessing blends of SRGO and LCO with different types of lipids. For instance, the co-hydroprocessing of different prepared mixtures from straight run gas oil (70–100%), light cycle oil (0–10%) and waste animal fat (0–20%) was carried out to yield fuels that would satisfy the requirements of the EN 590:2013 standard [4, 41]. A similar study of co-hydroprocessing was also carried out for a straight run gas oil (70–85%), light cycle oil (15%) and waste cooking oil (0–15%) mixture [42].

Light Atmospheric Gas Oil (LAGO) is a cheap liquid petroleum distillate heavier than naphtha, with an approximate boiling range from 205 °C to 343 °C, low TAN (0.45 mg KOH g^{-1}) and 12 °C pour point. Heavy Atmospheric Gas Oil (HAGO) is a heavier petroleum distillate compared to LAGO, with a high sulfur content and is also used for diesel production. A common practice for these two feedstocks is to pass them through hydrotreaters to reduce the sulfur content and break the large molecules, rendering high quality blending components for diesel production [45–47]. Both LAGO and HAGO have been examined for co-hydroprocessing with lipid-based feedstocks for hybrid fuel production. LAGO has been tested in different blends with waste soya oil [48], sunflower oil [29, 32], rapeseed oil [35], tallow oil [35] and tall oil [35]. While HAGO was examined in blends with waste cooking oil during co-hydroprocessing [45–47, 49].

Heavy Vacuum Gas Oil or HVGO is part of the petroleum hydrocarbon heavy distillate family. HVGO is produced in a Vacuum Distillation Unit, through the separation of the heaviest fraction from the atmospheric distillation column. It is a heavy and viscous product and is only used as an intermediary. It is also known as cat feed, which is feedstock for fluid catalytic crackers used to make gasoline, gasoil and many other by-products. There are two main uses of HVGO. The first one is for gasoline production via the fluidized catalytic cracker which is a refining unit that cracks the HVGO in the presence of a catalyst, to produce a gasoline rich mix of products. And the second one is for diesel and kerosene production via a hydrocracker which is a refining unit that cracks the HVGO using hydrogen to produce a mixture of products rich in middle distillates. As HVGO is a heavy feed similar to vegetable oils, it has been investigated as a possible feedstock for co-hydroprocessing in blends with canola oil and sunflower oil both in hydrocracking [30, 38] and catalytic cracking (FCC) [50]. From the above research, it is obvious that there are numerous fossil-based feedstocks that could be used in blends with bio-based feeds for hybrid fuel production as shown in Table 1.

Vacuum gas oil (VGO) is the most widespread feedstock for FCC processes. It is the top product from the vacuum distillation of the atmospheric residue. It mainly consists of paraffins, naphthenes and aromatics and has a boiling range of 280–580 °C. VGO contains sulfur and nitrogen compounds which can act as catalyst poisons [51]. VGO is the most common petroleum distillate which is used in studies on the FCC co-processing in blends with different lignocellulosic [52–60] and triglycerides-based feedstocks [61, 62]. Sometimes VGO is subjected to hydrotreatment prior to its co-processing in FCC units to decrease the content of sulfur and nitrogen which could influence catalyst deactivation [51, 63–66]. It is worth noting that the properties of VGO (density, viscosity, boiling point range, *etc.*) may vary in different studies. For example, it is suggested that the usual feedstocks used in Brazil are heavier than those used in the USA or Europe [53].

2.2. Lipids

Triglycerides present in vegetable oils, waste oils or animal fats are characterized as a suitable raw material for high quality fuels production. The most common edible oils for co-hydroprocessing that have been examined in the literature are, palm oil [36], rapeseed oil [34, 35], soybean oil [36], sunflower oil [29–32], while Jatropha oil [33] is the most common non-edible oil studied as a co-hydroprocessing feedstock. As far as residual feedstocks are concerned, several types have been studied such as used cooking oils/ waste cooking oils (WCO) [42, 46], waste soya oil [72], waste

Table 2
Properties of various edible, non-edible and residual lipids.

Properties	Canola oil	Corn oil	Waste soya oil	Jatropha oil	Sunflower oil	Rapeseed oil	Palm oil	Soybean oil	Waste animal fat	Waste lard	Free fatty acids
Density [g/ml]	0.923	0.912	0.9148	0.919	0.923	0.920	0.912	0.923	0.884	0.893	0.921
Sulfur [wppm]	208	100	42	19	100	100	100	100	270	270	2
N [wppm]	192.7				7	16	1.6	3.9	232	480	
O [wt%]	8.31				11.5	10.62	11.33	10.5		11	
Pour Point [°C]		−40	−6	−6	−15	−19		−12			
Viscosity [mm^2/s]		35.1		35.391	31.1	37.3	43	33.1		42.4	24.05
Iodine value (g/100 g)	110–126	127–133		82–98	120–134	94–120	50–55	125–128	50–60	58–65	
10 wt%	541.2					580	552	576			362
30 wt%	609.8					590	572	587			
50 wt%						596	581	594			378
70 wt%	617.2					601	587	599			
90 wt%	619.8					642	618	639			460
Ref.	[38, 78]	[78–80]	[48]	[33, 78]	[29, 67, 78]	[34, 36, 69, 71, 78,79, 81]	[36, 62, 78]	[36, 62, 78, 79]	[4, 41]	[37, 78]	[76, 77]

vegetable oils [48] and animal grease [4, 41]. Here, we provide a brief overview of different lipid-based feedstocks that can be used for co-hydroprocessing in existing refineries. Their properties are summarized in Table 2.

2.2.1. *Edible oils*

Although edible oils are traditionally used for the 1st generation biodiesel production (FAME), they can also be used for co-hydroprocessing with petroleum fractions for hybrid fuel production.

The co-hydroprocessing of different edible oils with petroleum fractions has been widely explored by many researchers in recent years. Rapeseed oil was examined as a possible bio-based feedstock for co-hydroprocessing with light atmospheric gas oil (LAGO). More specifically, Walendziewski et al. [34] examined 10 wt% and 20 wt% blends of rape oil with LAGO and noticed the possibility to control rapeseed oil hydrogenolysis in the presence of gas oil by proper process parameters. Mikulec et al. [35] also investigated the co-hydroprocessing of rapeseed oil in 5–6 vol% with LAGO for hybrid fuel production. Hancsok et al. [69] examined the co-hydroprocessing of rapeseed oil with SRGO at variable blends (0%, 5%, 8%, 12%, 50% and 100% rapeseed oil). Sunflower oil was also examined as a possible biomass feedstock for co-hydroprocessing with petroleum fractions such as LAGO [29, 31], HVGO [30] and kerosene [67] in a variety of blending ratios (95/5, 85/15, 75/25, 30/70 petroleum fraction/sunflower oil) for diesel and jet fuel production. Chen et al. [38] have studied the co-hydroprocessing of low-grade raw canola oil with HVGO under typical hydroprocessing conditions; it was found that during co-hydroprocessing, more diesel but less gasoline was produced in comparison to pure HVGO. Finally, Watkins et al. [36] analyzed soybean, palm and rapeseed oil to better understand the possible chemistry that would occur if they were processed in a conventional hydrotreater with SRGO at blending ratios from 10% to 80%. Although there are also other types of edible oils that could be good candidates for co-hydroprocessing from a technological point of view, there is a lack of literature due to the "food *versus* fuel" debate for edible oils that limits the prospects of their wide-spread use.

2.2.2. *Non-edible oils*

The "food *versus* fuel" debate that stigmatized edible oils accelerated the emergence of non-edible oils as a preferable alternative. Non-edible oil plants such as Jatropha, sea mango or rubber tree are well adapted to arid/semi-arid conditions and require low fertility and moisture demand to grow [73]. In addition, fatty acids and oils can also be recovered during wood pulping rendering the so-called tall oils. With respect to their utilization for FAME biodiesel, non-edible oils can reduce the production cost by 20–40% [22]. Similarly, non-edible oils seem to be a better choice for hybrid fuels production as they do not raise the price of food production and have been investigated as suitable candidates. The most famous non-edible oil is Jatropha. Its co-hydroprocessing with SRGO was investigated in detail by Satyarthi et al. [33]. Based on studying a wide range of blending ratios (10–50% Jatropha oil blended in SRGO) they showed that the final products consist of hydrocarbons in the diesel fuel range. Furthermore, no significant effect on the sulfur content of the final products was observed and the catalyst performance was found to be stable after 150 h of operation.

2.2.3. *Residual oils*

As in the case for non-edible oils, the "food *versus* fuel" debate motivated scientists to focus on the 2nd generation of biomass feedstocks, which are based on residual biomass only such as used/waste cooking oil [45], waste animal fats [4, 41], *etc.* These feedstock sources have, however, higher amounts of so-called free fatty acids and water in comparison with edible and non-edible oils and may, thus, need pre-treatment before processing.

Waste cooking oil (WCO) is a feedstock which can be used in the production of hybrid biofuels through several methodologies and is available in satisfactory quantities. Today, used cooking oil is the main residual feedstock that is increasingly being exploited worldwide. Based on Wiltsee [74], 4–5 kg per capita per year of WCO can be collected, which when applied to the *ca.* 500 million inhabitants of the EU28, corresponds to 2–2.5 million metric tons per year of WCO. Other similar studies in Europe have shown even more optimistic results, such as that in the UK (United Kingdom) alone, there is the potential of 1 million metric tons of WCO that can be collected or 16 kg per capita [75], which when extrapolated to the EU28 population corresponds to 8 million metric tons per year of WCO. Furthermore, in the EU28, approximately 2.5 million metric tons of fats from the rendering industry are produced which can be exploited similarly. Specifically, waste animal fats are characterized by low sulfur, nitrogen and oxygen content (see Table 2) and low TAN approximately 0.85 mg KOH g^{-1} [4, 41].

Although waste oils are residual feedstocks with a very low cost, one of their main disadvantages however is the large-scale collection, which has not been solved yet. Other relatively high amounts of residual triglyceride feedstocks that can be used for co-hydroprocessing are formed in a variety rendering facilities. In these plants, various fatty materials, meal, fodders are made from the waste of slaughterhouses and carcasses of livestock. The most abundant product of these rendering plants is the technical grade brown lard, which is characterized by a high water content of approximately 4400 mg/kg [37] and high TAN (~16.5 mg KOH g^{-1}). Baladincz and Hancsok have examined a two stage co-hydroprocessing of waste

Table 3
Blending ratio during co-hydroprocessing of lipid feedstocks and fossil feedstocks.

Bio-based feedstock	Petroleum fractions	Bio-content, wt%	Reference
Edible oils			
Canola oil	Heavy vacuum gas oil	5, 10, 20	[38]
Rapeseed oil	Light gas oil, straight run vacuum distillate, straight run gas oil	5, 10, 20	[34, 35, 69, 71]
Sunflower oil	Gas oil, heavy vacuum gas oil, straight run gas oil	5, 10, 15, 20, 25, 30, 40	[29–32]
Sunflower oil	Kerosene	70	[67]
Olive oil	Liquid paraffins	20	[80]
Corn oil	Liquid paraffins	20	[80]
Palm oil	Straight run diesel	10	[36]
Soybean oil	Straight run diesel	10–80	[36]
Non-edible			
Jatropha oil	Straight run diesel	10, 20, 30, 40, 50	[33]
Wastes			
Waste cooking oil	Straight run gas oil, light cycle oil	0–15	[42]
Waste cooking oil	Heavy atmospheric gas oil	0–30	[45–47, 49]
Waste soya oil	Gas oil	10, 25, 40	[72]
Waste vegetable oil	Gas oil	10, 25, 40	[48]
Waste animal grease	Straight run gas oil, light cycle oil	5–20	[4, 41]
Waste lard	Heavy gas oil	5–30	[37]
Free fatty acids	Untreated gas oil + LCO	5–20	[76]

animal fats with heavy gas oil fraction for second-generation paraffinic biofuels [37, 41]. Another residual feedstock is free fatty acids. The hydrotreatment of fatty acids blended in gas oil fractions and the quality of the resulting hydrotreated products from the point of view of diesel fuel standard requirements were investigated in a couple of papers [76, 77].

2.2.4. *Lipid content*

During the co-hydroprocessing of bio-based feedstocks with petroleum fractions, the bio-content plays an important role with respect to final product yields and the quality as well as to the hydrogen consumption, as shown in Table 3 where different blending ratios of co-hydroprocessing are compared. Toth et al. [29] mentioned that a higher vegetable oil content in the feed causes a lower yield of the organic liquid products. This statement can be explained by the hypothesis that the liquid product yield of gas oil hydroprocessing is higher than the yield of hydroprocessing of neat lipids. While yields of liquid hydrocarbons > 95% are achieved when hydrotreating SRGO, the hydroprocessing of lipids produces only 80–90% of liquid hydrocarbons, the remainder being propane (5%), water and CO, CO_2 and CH_4. Furthermore, in another study of the same authors investigating waste cooking oil and FCC light cycle oil blends (10–15%), they concluded that increasing the triglyceride content of feedstocks above 15% is not recommended, as the sulfur removal reactions are suppressed due to the high oxygen content [42]. Similar results have also been reported for the co-processing of SRGO, LCO and animal fats, where the yields of the liquid hydrocarbon products decreased with the increase in the fat bio-content of the feedstock [4, 41]. Hancsok et al. [69] found that the yield of the middle distillate fraction (target fraction) decreased linearly with the increasing amount of vegetable oil in the feedstock because the theoretical yields of paraffin mixtures obtained by deoxygenation of triglycerides can only be 81–86 wt% depending on the extent of the key reactions (*i.e.*, hydrodeoxygenation and decarboxylation).

On the other hand, Rana et al. [48] mentioned that an increase of waste oils content in the feed leads to higher product yields. Rana et al. [48] after studying hybrid fuel production via the co-hydroprocessing of waste vegetable oil and LAGO reported that the final product consisted mostly of diesel-range hydrocarbons (60–90% yields) and a small amount of kerosene range-hydrocarbons (10–35% yields). According to Chen et al. [38], during the co-hydroprocessing of canola oil with heavy vacuum gas oil (blending ratio 95/5, 90/10 and 80/20) the gasoline yields range from 1.2 wt% to 8.6 wt% while for diesel it ranges from 27 wt% to 38 wt%. Bezergianni et al. [45, 46, 49] who examined waste cooking oil from restaurants and households as a potential residual bio-feedstock for hybrid fuels with heavy atmospheric gas oil in a variety of blends (10–30%) found that the optimum blending ratio according to the hydrogen consumption is up to 10% WCO as the H_2 consumption increased by 7% only as shown in Fig. 3. Besides WCO, waste soya oil with gas oil was also examined by Tiwari et al. [72] who found that blends can be easily deoxygenated into hydrocarbons under hydroprocessing conditions using laboratory prepared hydroprocessing catalysts supported on mesoporous silica and silica–alumina.

2.3. *Pyrolysis bio-oils*

In addition to lipids, bio-oils have been recently considered as a promising alternative bio-based feedstock due to the favorable origin from a non-food biomass. In general, bio-oils can be obtained by fast heating of a solid biomass, typically a lignocellulosic biomass including wood, forestry and agricultural residues, to temperatures around 400–500 °C in the absence of oxygen (fast or flash pyrolysis), a liquid oil with yields up to 70–80 wt% is produced [82, 83]. This fast pyrolysis oil (FPO) is a free-flowing liquid at room temperature which is green, brown or black in color, depending upon the chemical composition and the amount of microcarbon content [84]. It approximates to a biomass in an elemental composition and consists of a very complex mixture of oxygenated hydrocarbons formed

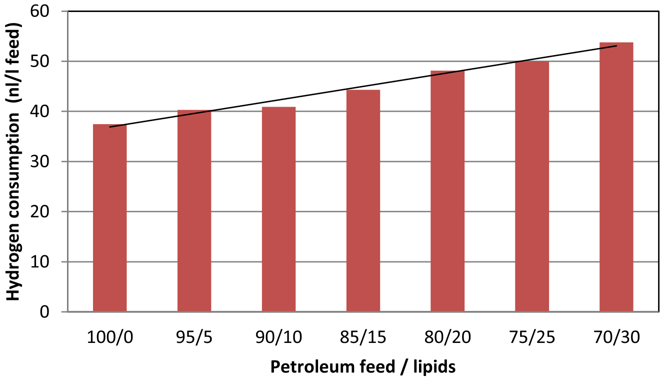

Fig. 3. Effect of lipid content in hydrogen consumption (lipid = waste cooking oil, petroleum feed = HAGO) [45].

during the decomposition of lignin and (hemi-)cellulose with an appreciable proportion of water from both the original moisture and reaction product [84]. Solid char (5–10 wt%) and gas (20–30 wt%) are also produced. Lower process temperatures and longer vapor residence times favor the production of charcoal. High temperatures and longer residence times increase the biomass conversion to gas, while moderate temperatures and a short vapor residence time are optimum for producing liquids. After cooling and condensation, a dark brown homogenous liquid is formed which has a heating value of about half that of a conventional fuel oil. A high yield of liquid is obtained with most biomass feeds low in ash. FPO has, however, a low energy density, and low thermal and chemical stability due to the high oxygen and unsaturation degree [82, 85]. The presence of oxygenates and unsaturated compounds as well as the admixtures of basic elements which can behave as catalysts result in the occurrence of secondary reactions, such as polymerization, condensation, *etc.* [82, 86]. Consequently, density increases while volatility decreases under FPO storage.

The complex composition of bio-oils and their physical-chemical properties together with their instability under storage prevent the direct blending of bio-oils with petroleum fractions. While blending is a prerequisite for the successful co-processing by hydrotreating, FCC can be theoretically accomplished without blending the bio-oil with a petroleum fraction. To allow blending, the high polarity of the bio-oil accompanied by its high content of water need to be reduced. Nonetheless, it is not necessary to remove oxygen completely for the successful blending as blends, *e.g.*, with triglycerides containing up to 12 wt% are feasible, *i.e.*, the reduction of the polarity is necessary to make blending possible. Two different upgrading routes are generally considered for improving bio-oil properties before its co-processing with hydrotreating or FCC feedstocks.

First, the low quality of FPO can be improved by introducing a post-pyrolysis mild hydro-treating step to produce an upgraded hydrodeoxygenated pyrolysis oil (HPO), which is more stable and possesses higher energy density than the starting bio-oil, FPO [82, 87, 88]. Among the large variety of catalysts employed for bio-oil HDO, good results have been achieved with noble and base metals supported on carbon and zeolitic materials [89]. Although these catalysts can be very effective for strongly reducing the oxygen content of the bio-oil, the high hydrogen consumption and pressure can increase the costs of HPO production. Elliot [90] pointed out important challenges in this field, such as the verification of the long-term operability of precious metal catalysts in continuous flow systems, the understanding of the effect of sulfur-containing compounds present in the bio-oils and the utilization of the upgraded bio-oil as a feedstock for the production of finished fuels.

Second, the quality of the bio-oil can be improved by performing an ordinary fast pyrolysis of the biomass in the presence of catalysts, mostly an FCC catalyst [91, 92]. The addition of catalysts to the pyrolysis system enhances the desired reactions that include cracking, decarbonylation, decarboxylation, hydrocracking, hydrodeoxygenation, and hydrogenation [93]. Additionally, metals present in the original biomass (Na, K, Mg, Ca) can be accumulated during pyrolysis on the catalyst surface, create additional basic active sites and, hence, cause the deterioration of the catalyst performance [94]. When a proper catalyst and conditions are used, the resulting bio-oil after catalytic pyrolysis (CPO) has a lower oxygen content and is more stable than the bio-oil from fast pyrolysis (FPO). This is achieved at the expense of the liquid yield [54]. Nevertheless, although the presence of a catalyst can change the quality and yield of the bio-oil produced from a catalytic pyrolysis process, the FCC catalyst is a very active one producing mainly water and coke. Thus, it does not seem to be an appropriate catalyst for this application and other zeolitic materials have been considered for this application. According to Fermoso et al. [89], the best results in CPO production were obtained over a ZSM-5 zeolite due to its high selectivity toward the formation of aromatic hydrocarbons. However, this catalyst suffers from a strong deactivation due to the formation of carbonaceous deposits as well as excessive decarbonylation reactions. This implies a significant loss of both carbon and chemical energy that would otherwise be in the organic liquid products. No doubt, more research is needed to identify a more suitable catalyst for the suggested catalytic pyrolysis process to maximize the liquid yield [95] and, at the same time, to improve its properties.

The characteristics of FPO, HPO and CPO which have been used in the co-processing with fossil feedstocks, typically in FCC, are summarized in Table 4 using different literature sources.

The data in Table 4 shows that the elemental composition and physical-chemical characteristics of the bio-oils are greatly affected by their origin and pre-treatment. In general, a reduction in the dry bio-oil yield, water amount and density of the FPO is achieved by its hydrotreatment. As a consequence, both hydrogen and carbon content increase in the HPO at the expense of the oxygen content. Simultaneously, a slight increase in its heating value is observed. The addition of a catalyst to the thermal pyrolysis process results in a lower yield (about 2×) of bio-oil organic compounds (CPO). The lower oil yields stem from oxygen removal in the form of water, CO_2 and CO, coke formation on the catalyst and an increase in hydrocarbon gas yield. Nevertheless, a comparison of the elemental composition of FPO and CPO shows that the hydrogen content in the differently prepared bio-oils is very similar.

More importantly, Table 4 also evidences a large variation in the characteristics of bio-oils prepared by the same method. In particular, water content in the FPO may vary from 15% to 62%. Accordingly, the elemental composition of the resulting bio-oil also varies in a wide range: the oxygen and carbon content changes from 25% to 61% and from 29% to 65%, respectively [59, 96]. The content of sulfur and nitrogen in the FPO also falls in a wide range of 0.01–0.4% [59,

Table 4
Physical properties of differently prepared bio-oils.

Physical property	Typical value FPO	HPO	CPO
Yield of bio-oil from biomass, wt	46.4–69.0	24.0	26.8–35.0
Water content, wt	15–61.7	2.1–15.9	7.4–30.8
Specific density, cm^3/g	1.05–1.25	0.93	1.0
pH value	2.5–3.8		3.7
Element content, wt			
C	29.4–65	63–84.4	66–73.1
H	5–8.5	8–10.6	7–7.4
O	25–61.7	4.9–28	19.5–27
N	0.2–4.3	0–4.9	<0.1
S	≤0.4	0–0.11	<0.2
Heating value, MJ/kg	16–27.9	25.2–46.0	30.5
Viscosity at 40–50 °C, cP	11.2–100		1–3.4
References	[22, 52–54, 59, 60, 82, 84, 95–97]	[52, 55, 57, 60, 82, 97–99]	[54, 57, 60, 95, 96, 98]

82] and 0.2–4.3% [52, 82], respectively. Moreover, even after the hydrotreating of FPO at $T = 300\,°C$ both the sulfur and nitrogen content in the resulting HPO may remain at a high level of 0.1% and 4.9%, respectively [52]. In most cases, a similar starting biological material was used for the preparation of the bio-oils, such as pine wood [53, 55, 57, 60] or poplar [59, 97]. Consequently, the characteristics of the bio-oils used for co-processing with petroleum feeds depend not only on the method of their preparation (*e.g.,* fast pyrolysis, catalytic pyrolysis or pyrolysis followed by deoxygenation) or on the origin of the starting biological materials used for bio-oil production, but also on other factors, including the conditions of the pyrolysis process, the pyrolysis technology used, the use of a catalyst (in the case of a CPO) or the conditions for the separation of aqueous and organic components after completing the pyrolysis procedure. Indeed, Gueudré et al. [57] pointed out that the composition of the co-processed pyrolytic oils strongly depends on the various upgrading steps implemented after the initial pyrolysis of the biomass feedstock. Comparing the characteristics of bio-oils from different studies, Agblevor et al. [96] made a conclusion that the CPO from their study might be similar to those from the partially hydrogenated bio-oils from [82] with respect to the O/C ratios.

3. Co-processing in hydroprocessing units

3.1. Hydroprocessing technology

Hydroprocessing is a catalytic process that enables targeted catalytic reactions with the addition of hydrogen. The aim of hydroprocessing is to increase the hydrogen-to-carbon ratio and to almost completely remove undesirable heteroatoms such as sulfur, nitrogen, oxygen and some metals. Furthermore, in some cases, hydroprocessing also targets to the reduction of olefin and the aromatic content of the feedstock. The key reactions involved in hydroprocessing include hydrodesulphurization (HDS), hydrodenitrogenation (HDN), hydrodemetallization (HDM), hydrogenation (HYD) and hydrodeoxygenation (HDO). HDS and HDN enable sulfur and nitrogen removal respectively [100], both of which are environmentally driven, aiming to mitigate SO_X and NO_X emissions of fuel combustion. HDM reactions focus on the removal of the present metals that severely poison the conversion catalysts during downstream refinery processes. HYD reactions favor the saturation of feedstocks and the reduction of aromatics, when required, and they are also a perquisite for further conversion reactions such as hydrocracking. HDO reactions are necessary for the removal of oxygen compounds, which are not desired in certain refinery products such as kerosene. HDO reactions are particularly important for bio-based feedstocks some of which might contain as much as 50 wt% oxygen. For this reason, HDO reactions are of high importance during the hydroprocessing or co-hydroprocessing of bio-based feedstocks.

In general, catalytic hydroprocessing is widely employed in all refineries worldwide to upgrade fossil-based intermediate streams. Each hydroprocessing plant within a refinery focuses on a single or a combination of the aforementioned reactions depending on the application, rendering multiple hydroprocessing plants within a single refinery. The availability and flexibility of the underlying refinery hydroprocessing plants render this process a suitable candidate for the parallel conversion of bio-based feedstocks/intermediates within a refinery. Furthermore, in many cases some refinery streams are of such low quality (*e.g.,* having high polyaromatic and sulfur contents) that their individual upgrading to fuels is not profitable, such as the light cycle oil (LCO) formed in an FCC plant which is being co-hydroprocessed with SRGO [42]. In such cases, co-hydroprocessing with liquid bio-based feedstocks and/or intermediates may better justify their upgrading, while in some cases even improve the exploitation potential of such low-quality refinery streams. All the targeted hybrid fuels produced via co-hydroprocessing of bio-based with petroleum streams can fulfill the high-bio-content-fuels requirements of the relevant directives of the European Union as described in the introduction section, by utilizing existing infrastructures.

In general, there are two pathways during biomass hydroprocessing, the first one is hydrodeoxygenation in which 1 triglyceride molecule consumes 12 hydrogen molecules to form 3 normal hydrocarbons with an even number of carbon atoms in their molecules, *e.g.,* n-octadecane (n-$C_{18}H_{38}$), and the second one is hydrodecarboxylation in which 1 triglyceride molecule consumes 3 hydrogen molecules to form 3 normal hydrocarbons with an odd number of carbon atoms in their molecules, *e.g.,* n-heptadecane (n-$C_{17}H_{36}$) as they are depicted in Fig. 4 [38]. Typically, the main products for hydrogenation of triglycerides are hydrocarbons (n-alkanes) and by-products are propane, water, CO and CO_2 [101]. A byproduct is a product with lower economic value than the main product.

During the co-hydroprocessing of bio-based feedstocks with fossil feeds, the products consist of a gas phase, a water phase and an organic liquid phase [29] as schematically represented in Fig. 5. The

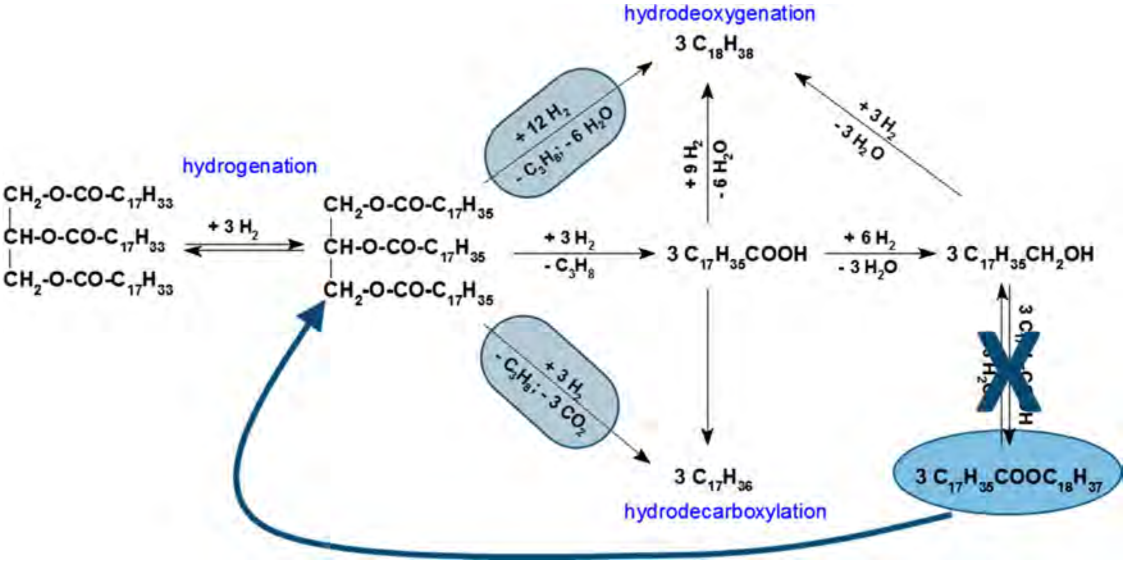

Fig. 4. Pathways of hydroprocessing triglycerides [38].

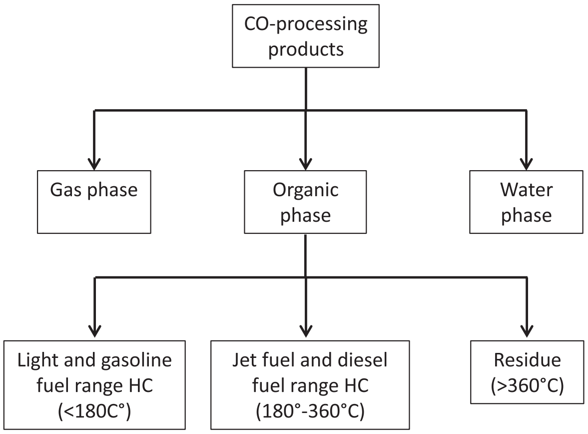

Fig. 5. Products from the co-processing of petroleum fraction with lipid feedstocks.

desired organic phase product is a liquid product containing hydrocarbons, some unreacted oxygen compounds [81] and a small amount of dissolved water. Depending on the bio- and fossil-based feedstocks co-hydroprocessed, the organic phase consists of three different fractions: a) a light product (hydrocarbons of a boiling point range of 0–180 °C), b) a mid-distillate product (a boiling point from 180 to 360 °C), and c) a heavy residue (with a boiling point over 360 °C). The aqueous phase is formed during the hydrodeoxygenation (HDO) and decarbonylation reactions of the bio-based part of the feedstock, and can be separated from the desired organic phase via sedimentation. Finally, the gas phase, besides the excess of hydrogen, also contains methane, carbon monoxide and carbon dioxide, which are by-products of the deoxygenation reactions (hydrodeoxygenation, decarbonylation, decarboxylation), propane formed from the triglyceride molecules cleavage, hydrogen sulfide and ammonia produced from the HDS and HDN reactions of the fossil part of the feedstock, and a small amount of light hydrocarbon by-products ($C_1–C_4$) formed during cracking reactions.

The yields and properties of the organic liquid phase depend on the operating conditions of the process, the type of catalyst as well as the feedstock (the type of bio-and fossil-based feedstock and bio-content). In principle, the more severe the process parameters and the higher the feedstock bio-content, the lower the density of the organic phase product [34]. In the next section, the effect of the co-hydroprocessing operating parameters is summarized based on the available literature.

3.2. Operating parameters

3.2.1. Co-hydroprocessing of lipids with fossil fractions

The most important factors of hydroprocessing are the operating conditions, *i.e.*, reaction pressure, reaction temperature, space velocity and hydrogen-to-oil ratio, and catalyst. Table 5 presents different studies that have been carried out in co-hydroprocessing at various operating conditions.

Reaction pressure: Hydrogen pressures during co-processing range from 20 bars to 110 bars (Table 5), affecting the HDS reactions as well as product yields. High hydrogen pressures are necessary for the hydrogen demanding reactions and its role is to increase the availability of hydrogen in the liquid phase. Special attention should be paid when co-processing feedstocks, such as lipids that have a high concentration of olefinic bonds, as saturation reactions consume large amounts of hydrogen. Changes in pressure affect the extent of the major (hydrodeoxygenation, decarboxylation and decarbonylation) and secondary reactions (strongly exothermic methanation and endothermic reverse water-gas-shift reaction), *i.e.*, the selectivity is influenced. The reaction pressure also affects the yields of the final products, as the liquid organic product yields decrease with increasing pressure and temperature in the case of gas oil and vegetable oil blends [29]. On the other hand, according to Sankaranarayanan et al. [31] an increase in pressure (30–60 bars) increased the conversion of vegetable oil in the blend (20% vegetable oil) by up to 15% depending on the catalyst (> 96% conversion was achieved) (see Fig. 6), as the conversion of the vegetable oil occurs through hydrocracking and hydrogenolysis reactions that consume hydrogen. Eller *et al.* [67] noticed that the extent of the aromatic saturation increased with the increasing pressure during jet fuel production. Furthermore, during the co-hydroprocessing of SRGO, LCO and waste animal fats, an increase in pressure (from 40 to 70 bars) promoted the conversion of triglycerides resulting in higher yields (from 92% to 94%) of the organic liquid product [4]. Similar results were also observed by Sagi et al. [76] who found that a higher pressure is advantageous for HDO and HDS reactions, while higher pressures also allowed products with ultra-low sulphur content, even at an increased LHSV, to be obtained. Moreover, in the case of the two-stage co-hydroprocessing of waste lard (10% blend) with HAGO, at temperatures above 320 °C an increase in pressure (from 20 to 80 bars) caused a small reduction in organic liquid product yields by 2% due to hydrocracking reactions [37].

Reaction temperature: Most hydrotreatment units operate at a temperature range from 290 to 400 °C. Toth et al. [29] mentioned that during the co-hydroprocessing of vegetable oil with a SRGO at 80 bars and 3 h^{-1} LHSV (Liquid Hourly Space Velocity), the increase in temperature (from 300 to 380 °C) increased the conversion and yields of the organic liquid product from 86% to 92% [29]. Similar results were also observed by Chen et al. [38] during the co-hydroprocessing of canola oil with HVGO, the yield of the organic liquid products and feed conversion increased with the increase in temperature from 360 to 395 °C. It was noticed that 80/20 HVGO/canola oil feed had the highest conversion while pure HVGO had the lowest one. They concluded that canola oil was easier to crack than HVGO. Consequently, to achieve the same organic product content or conversion, feeds with canola oil content required lower reaction temperatures than pure HVGO. As a result, the higher the canola oil concentration in the feed, the lower the reaction temperature that is required. Bezergianni and Dimitriadis [105] mentioned that a higher temperature favored heteroatom removal without affecting conversion; however, the addition of WCO favored the conversion of the organic liquid product without affecting sulfur and nitrogen removal. Eller et al. [67] reported that the optimum temperature range during the co-hydroproccesing of kerosene with sunflower oil for jet fuel production is 320–330 °C. In the case of co-hydroprocessing straight run gas oil, LCO and animal fats, the yields of the organic liquid product increased until a temperature of 340 °C and then decreased with a further increase in temperature, which was due to hydrocracking reactions that take place parallel to the hydrogenation and aromatic ring opening reactions [4, 41]. Similar trends were also observed during the two-stage co-hydroprocessing of waste lard with heavy gas oil, the yield of the main hydrogenated product fraction slightly decreased with an increase in temperature [37].

In conclusion, the discussed studies show that temperatures higher than 340 °C favor conversion as well as organic liquid yields during the co-processing of vegetable oils with petroleum fractions. However, the results are different when animal fats are co-processed with petroleum fractions. In this case, mid-range temperatures (320–340 °C) favor conversion, but with a further increase in temperature, the yields of the main liquid product decrease due to hydrocracking reactions that take place in addition to hydrogenation and saturation. A general conclusion that can be drawn is that when vegetable oils are co-processed with petroleum fractions, higher temperatures (360–390 °C) are preferable, on the other hand when the biomass consists of animal fats, mid-range temperatures (320–340 °C) are optimal.

Table 5
Operating conditions during the co-hydroprocessing of bio-based feeds (lipids and pyrolysis bio-oils) with petroleum fractions.

Feed type	Catalyst	*P*, bar	*T*, °C	H_2/Oil, v/v	LHSV, h^{-1}	Product yields, wt%	Remarks	Ref.
The co-processing of lipids with petroleum fractions								
HVGO/Canola oil	NiMo/Al_2O_3	80–110	360–395	800	1–2.5	36–40	Conversion increased with Temp.	[38]
LAGO/Waste soya oil	Ni-W/SiO_2–Al_2O_3	50	340–380	500	2 and 4	80–95	Yields depends from cat and conditions	[48]
HDT LAGO/Jatropha oil	CoMo and NiMo in alumina	50	350		1.2 (WHSV)	90	Yields of C15–C18 hydrocarbons over 90 wt%	[33]
HVGO/Sunflower oil	NiMo/Al_2O_3	50	300–450	1600	4.97	~87	Yields increase with vegetable oil content and reactor temperature	[30]
LAGO/Sunflower oil	commercial transition metal/Al_2O_3 catalysts	50–80	300–380	600	0.75–3	85–97	More than 15% vegetable oil reduce desulfurization efficiency	[29]
Refinery gas oil/Soya oil	NiMo/Al_2O_3	50	340–380	1500	2–4	85–95	85–95 wt% diesel yields <10 wt% kerosene yields	[72]
Refinery gas oil/Soya oil	NiW/SiO_2–Al_2O_3	50	340–380	1500	2–4	45–80	45–80 wt% diesel yields 15–50 wt% kerosene yields	[72]
Kerosene/Sunflower oil	Pt (0.4 wt%)/H-mordenite	30–70	260–340	400–600	1–2	12–24	Longer reaction time leads to lower liquid product yields	[67]
SRGO/Rapeseed oil	NiMoP/Al_2O_3	60	350–360	600	1.5	81–86	Increasing rapeseed oil content reduce liquid product yields	[69]
SRGO/Sunflower oil	NiMo-γ-alumina	30–60	320–350	500	1–4	95.5% conversion	Increase of WHSV decrease conversion to 64% for 4 h^{-1}	[31]
SRGO/Sunflower oil	NiMo-γ-alumina + 15% zeolite beta	30–60	320–350	500	1–4	>95% conversion	Increase of WHSV decrease conversion to 81% for 4 h^{-1}	[31]
SRGO/Sunflower oil	NiMo-γ-alumina + 30% zeolite beta	30–60	320–350	500	1–4	100% conversion	Increase of WHSV decrease conversion to 90% for 4 h^{-1}	[31]
LAGO/Rapeseed oil	NiMo/Al_2O_3	30–50	320–380	500	2	95	95 wt% yields at temperature range 350–380 °C and hydrogen pressure 5 MPa	[34]
LAGO + Palm fatty acid distillate (PFAD)	CoMo/Al_2O_3	25	280–350	630	0.75	30–40	The higher amount of PFAD slightly facilitated deoxygenation reaction, but impeded hydrodesulfurization reaction	[77]
Untreated gas oil + LCO + Fatty acids	NiMo/Al_2O_3	40–70	320–380	600	1–2	93.5–98.6	Gas-oil boiling range products with high yield can be produced from 10 to 20% fatty acid by-product and 10% light cycle oil containing feedstocks	[76]
SRGO + LCO + waste cooking oil	CoMo/Al_2O_3	30	320–380	420	1 –3	95–99	Optimum parameters: $T = 360$ °C, $P = 30$ bar, LHSV = 1 h^{-1}, H_2/Oil = 420 Nm^3/m^3 and 15% WCO content	[42]
HAGO/WCO	NiMo/Al_2O_3	56	350	500	1	92	increasing WCO in the feedstock does not limit the targeted HAGO hydrotreating reactions	[45]
HAGO/WCO	NiMo/Al_2O_3	56	330–370	500	1		presence of WCO in the feed has a positive effect on the HDS and HDN reactions rates for NiMo	[46]

(*continued*)

Table 5 (*Continued*)

Feed type	Catalyst	*P*, bar	*T*, °C	H_2/Oil, v/v	LHSV, h^{-1}	Product yields, wt%	Remarks	Ref.
HAGO/WCO	CoMo/Al_2O_3	56	330–370	500	1		Presence of WCO in the feed has a negative effect on the HDS and HDN reactions rates for CoMo	[46]
SRGO + LCO + waste animal fats (WAF)	NiMo/Al_2O_3	40–70	300–380	600	0.75–2	94.5	Optimum feed composition: 75% SRGO, 10% LCO, 15% WAF. Optimum conditions: $T = 340$ °C, $P = 70$ bar, LHSV: 1.0 h^{-1}, H_2/feed ratio: 600 Nm^3/m^3	[4]
SRGO + LCO + waste animal grease (WAG)	NiMo/Al_2O_3	40–70	300–380	600	0.7–3	78.1	Optimum parameters: $T = 340$ °C, $P = 70$ bar, LHSV = 1.0 h^{-1}, H_2/Oil = 600 Nm^3/m^3 Optimum blend: 75% SRGO + 10% LCO + 15% lipids	[41]
HAGO/waste lard	NiMo/Al_2O_3 and Pt/SAPO-11	20–80	300–380	600	0.75–1–1.5	91.7–93.6	2-stage co-hydroprocessing, 1st stage with NiMo/Al_2O_3 and 2nd stage with Pt/SAPO-11	[37]
SRVD/rapeseed oil	NiMo	180	400–420	1000	1	98–99	There was not observed any significant deactivation of the catalyst with lipids addition	[71]
LAGO/rapeseed oil	NiMo/Al_2O_3	55	380	1000	1	93.5–98.2	6.5 vol% the proportion of rapeseed oil n-C_{17}/n-C_{18} 1.64	[35]
LAGO/tallow oil	NiMo/Al_2O_3	55	380	1000	1	93.5–98.2	6.5 vol% the proportion of rapeseed oil n-C_{17}/n-C_{18} 0.7	[35]
LAGO/tall oil	NiMo/Al_2O_3	55	380	1000	1	93.5–98.2	6.5 vol% the proportion of rapeseed oil n-C_{17}/n-C_{18} 0.84	[35]
LAGO/rapeseed oil	NiMo/TiO_2	55	380 °C	1000	1	93.5–98.2	6.5 vol% the proportion of rapeseed oil n-C_{17}/n-C_{18} 2.32	[35]
LAGO/rapeseed oil	NiW/NaY	55	380	1000	1	93.5–98.2	6.5 vol% the proportion of rapeseed oil n-C_{17}/n-C_{18} 3.80	[35]
LAGO/rapeseed oil	NiW/TiO_2	55	380	1000 Nm^3/m^3	1	93.5–98.2	6.5 vol% the proportion of rapeseed oil n-C_{17}/n-C_{18} 2.40	[35]
LAGO/rapeseed oil	NiW/ZrO_2	55	380	1000 Nm^3/m^3	1	93.5–98.2	6.5 vol% the proportion of rapeseed oil n-C_{17}/n-C_{18} 0.94	[35]
The co-processing of pyrolysis bio-oil with petroleum fractions								
4,6-DMDBT /Guaiacol	ReS_2 catalysts supported on SiO_2 and γ-Al_2O_3	50	300	–	–	–	Batch reactor HDS rates decreased for both catalysts used in the co-processing reaction in comparison with the rates obtained for the separate experiments	[102]
SRGO/ethanol as oxygenate compound	CoMo/Al_2O_3	50	330	400	1	–	Mixed of SRGO with 2.4% w/w of retentate enriched in > 220–400 Da and 2.4% w/w of ethanol due to immiscibility problems of bio-oil with SRGO	[68]
SRGO/2-propanol, cyclopentanone, anisole, guaiacol, propanoic acid, ethyldecanoate	CoMo/Al_2O_3	30–50	330	–	1	–	Compounds tested one at a time. Results indicate that the co-treatment of some fractions of biomass derivates (containing alcohols, ketones, and ethers) with hydrocarbons is feasible	[103]

(*continued*)

Table 5 (*Continued*)

Feed type	Catalyst	*P*, bar	*T*, °C	H_2/Oil, v/v	LHSV, h^{-1}	Product yields, wt%	Remarks	Ref.
SRGO/Guaiacol	$CoMo/Al_2O_3$	40	280–360	15 ml H_2/min with 2 g/h	1–2	–	In the presence of SRGO and under deep desulfurization conditions, no inhibiting effect on HDS activity was observed due to guaiacol conversion	[104]

Space velocity: A key parameter of hydroprocessing is space velocity, which is defined either in terms of WHSV (weight hourly space velocity) or LHSV (liquid hourly space velocity). WHSV is defined as the mass feed flow-rate per dry catalyst mass loaded in the reactor. LHSV is defined as the feed volume flow-rate per catalyst volume inside the reactor. The inverse of the space velocity is the contact (residence) time, *i.e.,* it provides information for how long the feed is in contact with the catalyst under the operating conditions. The space velocity applied in the hydrotreating processes ranges from 1 to 4 h^{-1}. Rana et al. [48] examined the co-hydroprocessing of waste vegetable oil (from soya oil) with SRGO, and determined that by increasing the space velocity, it is possible to increase the yield of middle distillate hydrocarbons (C_{15}–C_{18}) with negligible cracking. Furthermore, Dimitriadis and Bezergianni [47] reported that lower LHSVs favor saturation reactions (thus increasing hydrogen consumption) while heteroatom removal, conversion and diesel yield are unaffected. Hence, higher LHSV is considered more suitable for co-hydroprocessing of HAGO/WCO [47]. According to Sagi et al. [4, 76], a reduction of LHSV was favorable for the improvement in the conversion at lower reaction temperatures; however, as the prolonged residence time favors the formation of lighter compounds by cracking. During the two-stage co-hydroprocessing experiments, Baladincz and Hancsok [37] observed that the triglyceride conversion is favored by a decrease in LHSV, however, the hydrocracking activity of the catalyst is increased as well, lowering the liquid organic product yield. Similar results were also found by Toth et al. [29] who noticed an increase in organic liquid yields with a decrease in WHSV. A general conclusion is that the optimum LHSV for co-hydroprocessing in the reaction temperature range of 320 to 360 °C varies from 1 to 2 h^{-1}.

Hydrogen-to-oil ratio: In principle, increasing the hydrogen flow-rate improves the HDS effectiveness since HDS is proportional to the partial pressure of hydrogen. In addition, when having a constant feed flow-rate, increasing the hydrogen flow-rate contributes to the vaporization of a large amount of the feed. Satyarthi et al. [33] claimed that by increasing hydrogen flow, the desulfurization activity is better in the co-hydroprocessing of Jatropha oil with straight run gas oil, and estimated that up to 30 wt% Jatropha oil can be processed without affecting the final sulfur content of the product. Similar results were also obtained by Dimitriadis and Bezergianni [47] in the co-hydroprocessing of waste cooking oil with heavy atmospheric gas oil. They showed that a higher H_2/liquid feed ratio favors saturation and heteroatom removal as there is an excess of hydrogen for the reactions to take place as shown in Fig. 7. In general, hydroprocessing is a technology that consumes hydrogen, the addition of a biomass feedstock in the co-hydroprocessing increases the hydrogen consumption of the overall process rather substantially. The amount of additional hydrogen consumed is obviously dependent on the type of feedstock, *i.e.,* bio-oil or lipids (saturated or unsaturated) and the reaction path that is related to the mechanism and kinetics of the process [101]. A very important parameter that affects the hydrogen consumption is the degree of saturation of the initial feedstock, more specifically palm oil and animal fats are highly saturated feeds and offer the advantage of lower hydrogen consumption when the target is renewable diesel. Other lipid feeds that contain high amounts of unsaturated fatty acids (27–40% C18:3) are camelina oil, linseed oil and algae oil which are preferable for aviation renewable fuels [106], plausibly because of the cyclization of the unsaturated chains producing substituted naphthenic hydrocarbons. According to literature, the most

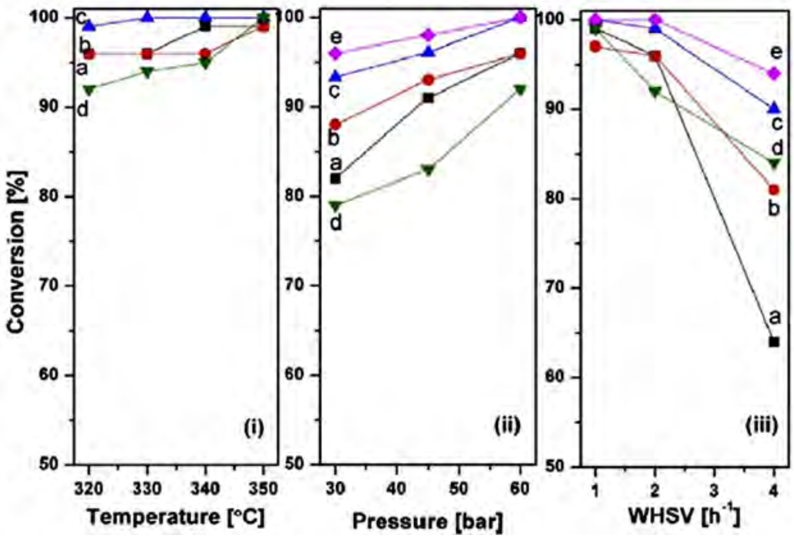

Fig. 6. The influence of process parameters on the conversion of oil/fatty acids in various oil/fatty acid-diesel blends [Conditions: (i) 60 bars, WHSV (h^{-1}), 2; (ii) 320 °C, WHSV (h^{-1}), 2; (iii) 60 bars, 320 °C; H_2/feed (v/v), 500 STP for all runs; data based on a single experiment] (a) 20% oil–diesel blend; Ni–Mo–Al; (b) 20% oil–diesel blend, Ni–Mo–15BEA; (c) 20% oil–diesel blend, Ni–Mo–30BEA; (d) 40% oil–diesel blend, Ni–Mo–30BEA; (e) 20% oil (+ 10% oleic acid)–diesel blend, Ni–Mo–30BEA [31].

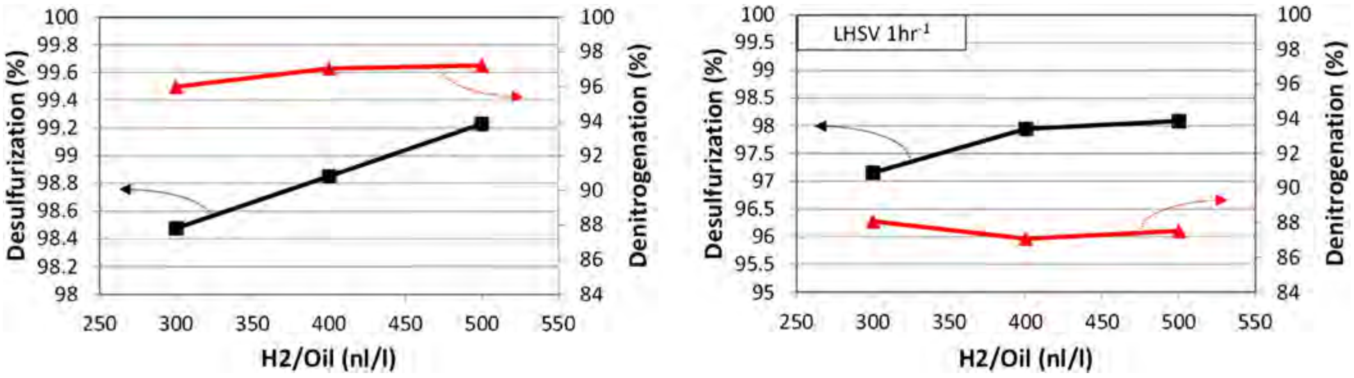

Fig. 7. Effect of LHSV 0.66 h^{-1} (dash line) and 1 h^{-1} (solid line) and H_2/Oil ratio (300, 400 and 500 L H_2/L feed on desulfurization (■) and denitrogenation (◆) reactions during co-hydroprocessing of HAGO/WCO blend (90/10 V/V%) at $T = 350$ °C, $P = 5.6$ MPa [47].

common practice for co-hydroprocessing is to use an H_2/Oil ratio from 420 to 590 nL H_2/L liquid feed.

3.2.2. *Co-hydroprocessing of bio-oils with fossil fractions*

The key aspect of any prospective refinery co-processing is the influence of the added feedstock, *i.e.*, bio-oil or pre-hydrotreated bio-oil, on the base petroleum feedstock, *i.e.*, straight-run gas oil or vacuum gas oil. Apart from the immiscibility issues that will have a plausibly more severe impact on upgrading in the liquid phase processes over catalysts in a fixed bed (hydrotreating / hydrocracking) than on the gas phase cracking over a fluidized catalyst bed (FCC), the chemical inhibition effects are of importance as well. In this context, the hydrotreating of atmospheric gas oil would be the most sensitive process as it affords a final refinery product, *i.e.*, diesel that is limited by strict standards. For instance, any inhibition by the oxygenates will limit the hydrodesulphurization activity and, thus, render reaching the 10 ppm S limit very challenging.

Up to now, there is only limited information on the co-processing of bio-oil or pre-hydrotreated bio-oil in the open literature. More specifically, there is just one study that examines the direct co-processing of a real bio-oil with petroleum fractions (straight run gas oil) [68]. Pinheiro et al. [68] studied the co-hydrotreatment of a bio-oil (produced from hardwood) with SRGO. In order to achieve this goal, the bio-oil was separated into four fractions by membrane fractionation and one of the fractions was mixed with the SRGO and co-hydrotreated over a $CoMo/Al_2O_3$ catalyst at 330 °C, 5 MPa, 1 h^{-1} (LHSV) and 400 SL/L H_2/HC_{outlet}. An inhibition effect on the HDS, HDN and HDC_a (aromatic hydrogenation) reactions was observed in the presence of the bio-oil fraction. This inhibition was due to the presence of CO and CO_2 formed during the reaction and not due to the oxygen compounds present in the bio-oil itself [68]. The very few studies that exist [103, 107, 108] mostly examine model compounds such as guaiacol with atmospheric gas oil to simulate the effect of a bio-oil in an existing petroleum refinery.

Several of these studies investigate the effect of bio-oil-representative compounds on the hydrotreating performance, *i.e.*, hydrodesulphurization (HDS), hydrodenitrification (HDN) and hydrodearomatization (HDA), over commercial hydrotreating catalysts [102, 103, 108–110]. Under standard hydrotreating conditions, *i.e.*, at > 330 °C, > 3 MPa and 1 h^{-1}, typical oxygenates covering the variety of functionalities present in bio-oils, such as anisole, guaiacol, 2-propanol, cyclopentanone, propionic acid and ethyl decanoate, have been completely deoxygenated when co-processed with straight-run gas oil (SRGO) over a commercial CoMo catalyst [103]. The concentration of these oxygenates in the SRGO was in the range 1.0–4.0 wt%. The results indicate that oxygenates rendering only water as a deoxygenation by-product do not inhibit the HDS, HDN and HDA performance of the catalyst, whereas a strong inhibition of the HDS, HDN and HDA activity was found in the case of propionic acid and ethyl decanoate [103]. It was shown that the inhibition is not due to the oxygenates themselves, but rather due to the inhibiting effect of CO and CO_2, *i.e.*, the by-products of deoxygenation [108]. The formation of carbon oxides is a consequence of the decarboxylation and / or decarbonylation reactions. Under hydrotreating conditions, it is virtually impossible to distinguish these pathways due to the rapid establishment of equilibrium between CO and CO_2 by the water-gas-shift and the reversed water-gas-shift reactions [108]. The inhibition effect of the addition of 1.16 wt% propionic acid or of 3.13 wt% ethyl decanoate in the SRGO could be expressed in technological terms as a need for an increase in the co-processing temperature by 11 °C to achieve the same level of desulfurization as in the case of SRGO. In the case of HDN, the necessary temperature increment would be 16 or 18 °C, respectively, while in the case of HDA, the co-processing temperature would need to be increased by 6 or 5 °C, respectively, in comparison with SRGO hydrotreating to have the same content of aromatics in all reaction effluents [103].

Among the other studied oxygenates, anisole and guaiacol, deserve particular attention. Though they are completely deoxygenated under the experimental conditions, the yield of the products, *i.e.*, cyclohexane and benzene, were much lower than expected. Only 10.7 and 17.0 mol% of cyclohexane and benzene (< 0.5 mol%) were formed in the co-processing of anisole and guaiacol, respectively, with SRGO [103]. This indicates that these aromatic oxygenates probably undergo, at standard hydrotreating conditions, condensation reactions yielding compounds undistinguishable from hydrocarbons present in the SRGO [103]. Under their experimental conditions, the authors [103] have ruled out the possibility of excessive coke formation that was proposed by others [100, 110] for guaiacol deoxygenation. It has to be noted that these studies were performed on oxygenates dissolved in hexadecane in a batch reactor at temperatures 260–300 °C. Consequently, the conversion of guaiacol was limited to 60% and phenolics (phenol and catechol) were the only reaction products, *i.e.*, only partial deoxygenation through demethoxylation took place [110]. In agreement with Pinheiro et al. [103], Bui et al. [108] has reported the absence of an HDS inhibition when co-processing guaiacol (5000 ppm) with SRGO over a commercial CoMo catalyst at temperatures above 320 °C and at an LHSV of 1 h^{-1}. However, they have observed the inhibition of the HDS activity outside the typical range of hydrotreating conditions, namely at 300 °C and 2 h^{-1}, *i.e.*, at shorter contact times. With a reference to older studies focusing on the upgrading/co-processing of coal liquids, they explain the inhibition of the HDS activity by competitive adsorption of between phenols originating from guaiacol and sulfur-containing compounds, such as benzo- and dibenzothiophenes [108]. In quantitative terms, the addition of 5000 ppm of guaiacol led to a decrease in the HDS conversion to *ca.* 30% from about 70% established for SRGO at 300 °C. At 340 °C, the HDS conversion decreased from *ca.* 92% (SRGO) to approximately 88% when 5000 ppm guaiacol was added to the SRGO [108].

An inhibition of the HDS activity of a commercial CoMo catalyst was observed not only for the co-processing of model compounds. It was also reported by Mercader et al. [107] for the co-processing of an SRGO with hydrotreated (*i.e.,* partially deoxygenated) bio-oils in weight ratio 70-to-30. It was observed that the competition between the HDS and HDO reactions did not result in permanent catalyst deactivation [107]. The bio-oils were obtained by water addition to the whole pyrolysis oil resulting in phase separation into organic and aqueous fractions. It has to be noted that depending on the type, the hydrotreated bio-oil used in the co-processing was diluted in isopropanol 2:1 or 1:1 on a weight basis to reduce its viscosity [107]. Hence, it has to be kept in mind that the dilution might have affected the co-processing in a positive way. Moreover, the experiments have not been performed under fully typical hydrotreating conditions, namely at 380 °C and at LHSV of 2 h^{-1}. Due to the different dilution of both bio-oils tested, it is difficult to compare the inhibition effect in a quantitative way – the sulfur content increased from 136 ppm found for SRGO hydrotreating to *ca.* 2000 ppm for the less diluted bio-oil and to 376 ppm for the more diluted bio-oil. Interestingly, deoxygenation of the bio-oil was not complete at these experimental conditions and phenolics were found in the product [107]. This is in line with the review of Furimsky [100] showing the carbon-oxygen bond in phenolics as one of the most refractory bonds in hydrotreating.

3.3. *Catalysts for co-hydroprocessing*

The selection of optimum catalysts for the co-hydroprocessing of bio-based feedstocks with those derived from petroleum is of utmost importance as it determines not only the product yield and quality, but also the duration of the co-processing operation, *i.e.,* the maximum catalyst life expectancy is targeted. The hydrotreating catalyst selection for co-hydroprocessing is a major challenge for two reasons: a) Catalyst activity varies significantly, as commercial catalysts are optimized for different feedstocks, *i.e.,* feedstocks with high sulfur concentration or heavy feedstocks (containing large molecules) or feedstocks with high oxygen concentration *etc.* b) Currently there are only a few commercial hydrotreatment catalysts available for bio-based feedstock/intermediate processing [111]. Consequently, the evaluation of different hydrotreating catalysts for the co-hydroprocessing of biomass feeds with petroleum fractions is a very important research area. Table 5 presents studies focusing on the co-hydroprocessing of bio-based feeds with fossil fuels using various catalysts.

The most common catalysts used in co-hydroprocessing are common hydrotreating catalysts based on cobalt–molybdenum (CoMo) [29, 45] and nickel–molybdenum (NiMo) [45, 48] sulfides. In general, CoMo catalysts are the most appropriate for desulfurization, while they exhibit low activity for the removal of nitrogen and the saturation of aromatic compounds while NiMo catalysts exhibit higher activity in nitrogen reduction and the saturation of aromatics, while they are less efficient for sulfur removal [112, 113].

The use of typical hydroprocessing catalysts for the deoxygenation of triglycerides during co-hydroprocessing raises two important issues. Firstly, the high oxygen content of triglycerides can result in increased continuous sulfur leaching from the catalyst surface and hence its gradual deactivation. Hence, an additional source of sulfur to replenish it on the surface is needed. However, the primary reason of the catalyst deactivation is coking which depends considerably upon the operating parameters as well as the blending ratio of the initial feed (fossil fraction and bio-based content) [33]. Secondly, compared to petroleum derived feedstocks, triglyceride molecules, as well as some oligomers present in the bio-oils, are bulkier and to overcome diffusion limitations, large pore-size catalysts, *i.e.,* catalysts with larger mean pore size than normally used in common hydrotreating catalysts, are required [72].

The co-hydroprocessing of different blends of canola oil with HVGO over NiMo/γAl_2O_3 was studied by Chen et al. [38], their results have shown that no effects were observed on the HDS and HDN reactions when canola oil was added in the initial fossil feed. Similar results were also reported by Bezergianni et al. [46] who compared the efficiency of a commercial NiMo with a commercial CoMo catalyst on the co-hydroprocessing of the fossil fraction (heavy atmospheric gas oil) blended with waste cooking oil (WCO). Their findings have shown that the HDS efficiency of a NiMo-type catalyst was not affected by the addition of WCO, while the efficiency of the CoMo-type catalyst was severely hindered from 95% of pure HAGO to 80% for the 70/30 HAGO/WCO blend. The efficiency of a NiMo-type catalyst during co-hydroprocessing was also studied by Rana et al. [48] who concluded that the hydrodeoxygenation pathway becomes more dominant with an increasing soya oil content in the feed.

During the hydroprocessing of triglyceride feeds, H_2O, CO_2, CO, and light alkanes are produced as by products [39, 40]. It is obvious that these by-products also produced during the co-processing of bio-based feeds with fossil fractions. As CO_2 constitutes one of the main by-products of co-hydrotreatment reactions, Bezergianni and Dagonikou [39] investigated the effect of CO_2 as a by-product during the co-hydroprocessing of gas-oil and triglycerides, over a commercial CoMo/Al_2O_3 catalyst. The aim of the study was to identify the influence of CO_2 on the effectiveness of heteroatom removal and saturation reactions. It was shown that the presence of CO_2 limits both the heteroatom removal (sulfur and nitrogen) and saturation reactions. Similar effects were reported by Pinheiro et al. [114] also. Bezergianni et al. [40] also examined the influence of H_2O and CO in the potential biomass catalytic co-hydroprocessing with fossil-based fractions to produce hybrid fuels. It was found that the H_2O role is neutral on the HDS and HDN removal. However, CO has a suspending role due to the inhibition of the catalyst active sites [40]. The weak inhibiting effect of H_2O on the hydrogenation reactions was also confirmed by Laurent and Delmon [110].

As it was already mentioned, the NiMo- and CoMo-type catalysts are the most common catalysts for co-hydroprocessing, however other types of catalyst have been explored in terms of their efficiency in co-hydroprocessing, such as NiW catalysts [35]. NiW catalysts mostly favor decarboxylation and decarbonylation reactions during co-hydroprocessing and are more appropriate when increasing triglyceride content in the feed [48], thus the hydrogen consumption is lower when NiW catalysts are used as decarbonylation/decarboxylation pathways consume less hydrogen compared to hydrodeoxygenation, which is more favored over NiMo catalysts. Nevertheless, hydrogen consumption also depends on the system pressure as well as the successive hydrogenation of CO and CO_2, which was limited in the case of NiW catalysts. To sum up, hydrodeoxygenation is favored by NiMo while decarboxylation and decarbonylation are favored over NiW. Furthermore, different support materials for NiMo as well as NiW catalyst were also investigated, such as Al_2O_3, TiO_2, NaY and ZrO_2. Nonetheless, in the cases of catalyst support with a low specific surface (ZrO_2), the level of desulphurization was much lower when compared to the commercial catalyst [35].

According to Tiwari et al. [72] the use of a NiW catalyst on an acidic-alumina also results in lower diesel range hydrocarbons (250–380 °C) compared with NiMo/Al_2O_3 due to more cracking of hydrocarbons over NiW catalyst due to its higher acidity. Thus, NiW catalysts are more suitable for the production of kerosene range products. Similar results were also found by Rana et al. [48] who reported that diesel yields over NiW catalyst are 2–20% lower compared with NiMo.

Also, the effect of a zeolite beta (BEA) content in NiMo catalyst was investigated. Sankaranarayanan et al. [31] has studied the efficiency of NiMo-BEA-gamma-alumina catalyst on co-hydroprocessing of straight run gas oil with sunflower oil. It was found that the large amount of zeolite (0–30%) in the catalyst helped in cracking the triglyceride molecules and enhanced the HDS activity of the NiMo catalyst.

Another approach to co-hydroprocessing is to combine various compositions of hydrogenation catalysts in the catalyst bed, more specifically to use different catalyst layers in the catalyst bed. This approach was investigated by Toth et al. [29] who used three commercial transition metal/Al_2O_3 catalysts with different compositions. The aim of this approach was to exploit the different activity of the three layers (protection/pre-hydrogenation, hydrodesulphurization/hydrodeoxygenation and isomerization) resulting in fuel components with slightly better cold flow properties. Similarly, Albemarle [111] has proposed a so-called Bio-STAX system that is a solution consisting of several different commercial catalysts loaded at a specific place in the reactor and considering the constraints of the unit, such as the H_2/oil ratio, outlet pressure, capacity of quenching, and intended VO addition (type and amount). The distribution (placement) of the catalysts in the reactor reflects the main factors affecting the kinetics of the individual feed components conversion [115].

Two-stage co-hydroprocessing is another approach for biofuel production. Baladincz and Hancsok [37] examined the possibility of a two stage co-hydroprocessing of waste lard with heavy gas oil. The first step, hydrogenation using NiMo/γ-Al_2O_3, was followed by an isomerization step on a custom-made Pt/SAPO-11 catalyst. After the first step, the product liquid yields were 95.1–95.5%, the triglyceride part was fully converted and the cetane number ranged from 56 to 58. After the second step (isomerization), the product yields were 91.4–92.4% and the cetane number ranged from 54 to 55. The isomerization step aimed at improving the CFPP properties was successful as the CFPP temperatures were between −15 to −20 °C.

Until now, different catalyst approaches for co-hydroprocessing of triglycerides with fossil fuels were analyzed, however besides the product quality, the expected catalyst decay rate is also a very important factor for determining the suitability of a hydrotreating catalyst in industry. The catalyst deactivation rate is associated with the overall refinery planning and has a significant economic impact. Bezergianni et al. [46] has examined the deactivation rate of a commercial CoMo/γ-Al_2O_3 and a NiMo/γ-Al_2O_3 catalyst during the co-hydroprocessing of waste cooking oil and heavy atmospheric gas oil blends. The deactivation rate was evaluated in terms of the loss of HDS efficiency of each catalyst with the increasing days of the experiment, *i.e.*, days on stream (DOS). Their results have shown that after 26 DOS, the deactivation rate of the NiMo/γ-Al_2O_3 catalyst (20%) was less significant when compared with the CoMo/γ-Al_2O_3 catalyst (30%) rendering NiMo as a better choice for lipids containing feedstocks. Also, Šimáček and Kubička [71] noticed no catalyst deactivation with a 5% addition of rapeseed oil in a straight run vacuum distillate with a NiMo catalyst.

As mentioned above, as far as co-hydroprocessing of pyrolysis bio-oil with petroleum fractions is concerned, there are very few studies in the literature and most of them use model compounds to simulate the bio-oil content. The most common model compound is guaiacol. First, it should be noted that hydrotreatment of a bio-oil in a stand-alone process, faces some disadvantages that are important for the life of a catalyst. More specifically, the HDO reaction of 2-methoxyphenol (guaiacol), which was studied over commercial hydrotreating catalysts such as CoMoS/Al_2O_3 and NiMoS/Al_2O_3 [104, 116], has shown that there is a need to add sulfur to the bio-oil in order to keep the active sites of the catalyst stable because the bio-oil is a sulfur free feedstock. However, with the addition of a sulfur source such as hydrogen sulfide, an adverse effect occurrs. The addition of this source has been reported to diminish the activity of NiMo catalyst through competitive adsorption between H_2S and the hydrogenolysis and hydrogenation sites present on the catalyst surface [109]. The co-hydroprocessing of bio-oil with fossil-based feeds on the other hand, is a technology that can eliminate this effect. The hydrodeoxygenation of guaiacol (HDO) in co-processing with gas oil (HDS) makes it unnecessary to add external sources of sulfur as the gas oil already has enough sulfur content [108]: the H_2S produced during the HDS of the gas oil acts as a sulfiding agent which extends the lifetime of the HDS catalyst.

Pinheiro et al. [68, 114] investigated the co-hydroprocessing of model compounds as well as of pretreated bio-oil in SRGO (Straight Run Gas Oil) blends by using CoMo/γ-Al_2O_3. The main conclusion was that oxygenated model compounds which produce water by deoxygenation had no impact on the hydrotreatment of the SRGO under deep HDS conditions whereas inhibition occurs at lower temperature [104]. Sepuvelda et al. [102] claimed that ReS_2 supported over alumina displayed higher activities compared to commercial reference catalysts, for this reason they investigated the co-hydroprocessing of guaiacol and 4,6-dimethyldibenzothiophene over ReS_2 catalysts supported on SiO_2 and γ-Al_2O_3. Their results have shown that guaiacol and 4,6-DMDBT compounds compete for the same active sites. Thus, guaiacol inhibited the HDS reaction for the two catalysts which is in agreement with the results observed by Bui et al. [104] over NiMoS/Al_2O_3 catalysts. Another observation was that the HDS efficiency reduced for both catalysts while the HDO efficiency increased for the ReS_2/Al_2O_3 catalyst only. The reduction of HDS efficiency was due to the competitive adsorption between guaiacol and 4,6-dimethyldibenzothiophene on the active sites while the increase of HDO efficiency was due to the inhibition of the demethylation pathway beneficial to the demethoxylation route.

Unfortunately, there is a lack of literature in the co-hydroprocessing of pyrolysis bio-oil with fossil-based feedstocks. The most commonly used catalysts up to now are CoMo/Al_2O_3 and NiMoS/Al_2O_3, however, further studies with different types of catalyst should take place in the future to better understand the effect of the catalyst type on the extent of the HDO and HDS reactions and to learn about the stability of these catalysts under co-hydroprocessing conditions.

Co-processing of bio-based feedstocks, particularly of lipids, has already reached commercial status. However, it is not easy to collect specific data about these technologies and their status. For example, renewable diesel fuel has been produced by ConocoPhillips at its refinery in Whitegate, Cork, Ireland [9], since 2006, but detailed information about the real capacity, the content of the lipids, in the hydrotreated feedstock, is not available [111]. Similarly, Petrobras [117] has developed a process in which triglycerides (vegetables oils and/or animal fats) can be co-hydroprocessed with a fossil-based feedstock at up to 20%. The bio- and fossil-based feedstock is hydroprocessed at 220–350 °C, improving the quality of the diesel oil produced [118]. The plan of Petrobras was to have the process implemented in at least three of its refineries by the end of 2007. However, the implementation was put on hold in 2008 due to high soybean oil prices that should have been the main feedstock [111, 117]. Furthermore, Haldor Topsoe supplies its deoxygenation catalyst to three undisclosed refineries in Australia, Europe, and the USA co-processing bio-feedstocks in the range of 0–5%, 2–5%, and 10–20%, respectively [111]. The feedstocks typically include animal fats, for example, chicken fat in the USA, and other unspecified bio-feedstocks. In Preem, Sweden, Haldor Topsoe has supplied its deoxygenation catalyst for the co-processing of raw tall oil (20–30% of the feed). Apart from co-processing, the Haldor Topsoe catalyst is used by Cetane Energy, USA, to process neat animal fat and algae oil [111].

4. Co-processing in catalytic cracking units

Catalytic cracking, *i.e.,* FCC, is a versatile workhorse of modern refineries and holds a potential to upgrade various bio-based feedstocks through their cracking and deoxygenation. This section will, thus, review the results on the co-processing of petroleum fractions with bio-based feedstocks in catalytic cracking units. In general, the co-processing of rapeseed oil (RSO) with petroleum oil in FCC conditions seems to be a more advantageous process in comparison with the transformation of RSO alone due to several reasons. Firstly, there is a substantial difference between the global consumption of petroleum (4.02 billion metric tons per year (BTY)) and the production of vegetable oils (0.12 BTY) [115]. Due to the lower availability of vegetable oils, the most preferable option is to integrate them into existing refining schemes than to create a new production. Secondly, it is suggested that potential synergy may be gained through co-processing the two different feedstocks, *i.e.,* aromatic (VGO) *versus* paraffinic (RSO) [50]. Indeed, in most cases, increased conversion was observed during FCC processing of blends of RSO with petroleum oil compared to conventional feedstock alone [50, 119]. From a technological point of view, the co-processing of vegetable oils with conventional FCC feeds seems to be a simpler process than the corresponding co-processing using bio-oil as a co-feed (Sections 4.2.1 and 4.2.2). Firstly, vegetable oils are homogeneous mixtures and mix well with petroleum oils, thus eliminating the occurrence of such technological problems as the separation of the constituents, pipe plugging, *etc.* Secondly, seed oils possess high crackability which is derived from their low thermal stability. Indeed, pure crude palm oil can be successively exposed to thermal cracking by means of free radicals in the preheating zone of the FCC reactor [120]. Černý et al. [121] have shown that canola oil underwent thermal cracking over glass beads with nearly 20% conversion to gaseous and gasoline range products at 500 °C. Besides, thermal cracking of canola oil was investigated in a continuously operating pilot plant at different cracking temperatures (450 580 °C) using silica sand as the bed material [122]. It was found that the total fuel yield ($TFY = (m_{gas} + m_{gasoline} + m_{LCO})/m_{feed}$) at 450 °C was about 77.2 wt% and increased with higher temperatures. Thirdly, the usual conditions of the FCC unit are severe enough to ensure the catalytically induced decomposition of the triglycerides of carbonic acids by means of decarboxylation, decarbonylation, or dehydration reactions to yield a mixture of different hydrocarbons. Despite the apparent advantages of such co-processing, only a limited number of publications dealt with this subject [50]. Nevertheless, the information available from open literature makes it possible to draw some conclusions about the peculiarities of carrying out the co-processing of vegetable and petroleum oils.

The co-processing of bio-oil with petroleum feeds under FCC conditions causes less technological challenges in comparison with cracking neat bio-oil. In the former case, such problems as plugging can be avoided due to the usually used ratios between these feeds when blended [22]. Nevertheless, possible problems during the catalytic experiments should be assumed and prevented if possible. Therefore, special attention should be paid to the choice of feedstocks and experimental units used in the co-processing experiments also. Using large scale FCC units (pilot or experimental) seems to be the most suitable choice, because they allow for carrying out the experiments under conditions as close as possible to those used in the real FCC process. Nevertheless, the operation of such units is obviously an expensive issue which substantially limits the possibility to perform a broad research. Therefore, small laboratory installations which, however, must be able to mimic FCC cycles are more often operated.

The thermal and oxidative stability of triglycerides (vegetable oil and animal fats) and bio-oils is another important issue that has to be considered. The stability of bio-based feedstocks may cause storage problems due to the changes in density, viscosity, acidity, and an increase in polymer formation [123]. In particular, triglycerides can form polymers under storage which result in gumming problems in heat exchangers and the hottest parts prior to the reactor. In turn, the instability of the pyrolysis oil is mainly attributed to lignin oligomers formed during pyrolysis [84]. Furthermore, the presence of acids in bio-based feedstocks can lead to corrosive problems: triglycerides may contain small admixtures of free fatty acids, while oxygenated compounds such as phenols and carboxylic acids contribute to the corrosiveness of bio-oils. Melero et al. [124] investigated the oxidative and thermal stability of mixtures of vegetable oils, animal fats and used cooking oils with petroleum feedstocks and suggested that these mixtures can be stable for a period of at least 180 days. To diminish the corrosivity of bio-based feedstocks, the same methods are used as those applied in the case of acidic crude oils (acidic crude oil means that the acid number is > 0.5 mg KOH/g, and high TAN crude means that the acid number is > 1.0 mg KOH/g [125]. These methods usually include (i) blending high TAN with low TAN crude; (ii) upgrading construction materials, and (iii) using corrosion inhibitors. In addition, the stability of the bio-oil can be improved also through flash pyrolysis, hydrotreating or zeolite upgrading (see Section 4.2.2).

4.1. Catalytic cracking technology

Laboratory-scale equipment is mostly used when investigating the co-processing of bio-based feedstocks in catalytic cracking. This allows controlling the process operationally and investigating the influence of various variables on the characteristics of products. Several types of laboratory equipment have been used to study the co-processing of bio-oils and petroleum feedstocks. These include:

- Microactivity test (MAT) reactor, which is a fully automatic, computerized and standardized (ASTM D3907) laboratory unit [82, 98, 99]. This equipment can adjust its time on stream time, catalyst/oil ratio, reaction temperature, the regeneration times and temperature, gas flow, and other parameters for each independent experiment. The catalyst loading is usually ≤ 10 g, and the reaction cycle consists of cracking, stripping, regeneration and purging steps performed in a single reactor. This equipment is mainly used as a tool for catalyst screening [126]. Nevertheless, the simulation of the processes which happen in an industrial FCC unit is rather complicated in the MAT equipment because of the inherent fluid dynamics differences between a fixed bed and a fluidized bed, but also other important aspects associated with large contact times [61]. It was also pointed out [62] that a higher yield of liquid can be obtained in the products with a fixed-bed reactor, but the olefinic content of the gas product is much lower.

- The group of Schuurman and Mirodatos used a laboratory unit with a fixed-bed quartz reactor containing 1.0 g of a catalyst [55, 56, 60, 70]. It was suggested that the equipment is validated with respect to a microactivity test reactor (MAT) by benchmarking experiments. Similar to MAT units, the reaction cycle consists of *in situ* cracking, stripping the under flow of inert gas, regeneration and purge.
- A specially designed and patented riser simulator reactor which permits operation on a laboratory scale under similar conditions to the FCC unit [58, 59]. This is an internal recycle reactor where the catalyst is fluidized continuously (during the reaction run) with an internal impeller for thrusting the gas (feed and products) throughout the catalyst bed. It was suggested that the riser simulator is ideal for simulating the conditions employed in industrial FCC units, particularly in terms of reaction time and fluidization [59]. In contrast to MAT units, the regeneration of a catalyst and the determination of coke amount using the mass loss of the spent catalyst were performed by ex situ combustion in a thermo balance.

- Advanced Catalyst Evaluation (ACE^{TM}) by BASF Inc. [96] or Advanced Cracking Evaluation (ACE-R^{TM}) by Kayser Technology [52]. In both cases, the catalyst charge is 9 g. As in the case of MAT units, the reaction cycle consists of cracking, stripping, regeneration and purging steps.
- Laboratory-scale once-through micro-riser [127] that operates in an isothermal plug-flow regime and simulates realistic FCC conditions.
- Laboratory-scale two-stage riser fluid catalytic cracking unit having the advantage of a catalyst relay, staged reaction, optimum residence time and great catalyst to oil ratio [62]. Fresh feedstock is injected into the first stage riser and recycling oil into the second stage. Both risers share a common disengage unit and regenerator. Thus, the fresh feedstock and the recycling oil are in contact with regenerated catalyst.
- FCC pilot plant. Most research works on the co-processing of RSO with petroleum oil on a pilot scale were performed using a pilot-scale FCC unit built at the Vienna University of Technology [51, 64]. It is suggested that in this continuous working reaction/regeneration system, steady state operation can be performed, which allows high comparability with large-scale FCC plants.

All these set-ups are intended for an effective and operational evaluation of the performance of the modified FCC catalysts and different FCC feedstocks. They can provide important information on suitable process parameters also (conversion, temperature) for upgrading new/alternative feeds with respect to a standard FCC feed (*i.e.,* a kind of relative measure). The following examples show that the mentioned experimental units are widely used to collect data on the influence of various parameters on the qualitative and quantitative characteristics of products obtained in the co-processing of bio-oils and petroleum feedstocks.

However, it can be questioned whether the results obtained by catalyst testing in laboratory units simulate the real catalyst performance during commercial operation in some way. Biswas and Maxwell [17] pointed out that the major drawback of the laboratory testing methods is the long cat/oil contact time (10–100 s) compared to the commercial operation (approximately 1 s). This increases the contribution of hydrogen transfer reactions in the overall conversion, thus decreasing the olefinicity and increasing the aromatic and alkane contents of the gasoline fraction. Then, the fixed bed MAT systems are non-steady state processes because the catalyst has a higher activity at the onset of the test than at its end, so the product slate and conversion change continually throughout an experiment. The long contact time also results in a different conversion-coke selectivity behavior from that of a commercial unit and causes excessive over-cracking at low conversion levels. Accordingly, Pinho et al. [53] pointed out that coke results obtained in circulating FCC pilot risers were frequently lower than those observed at lab scale experiments. Hence, knowledge about the experimental unit set-up and operating conditions is essential to draw correct conclusions, particularly when predicting future performance in an industrial scale unit.

Comparing experiments performed in the conventional MAT devices and the once-through micro-riser reactor Dupain et al. [127] have concluded that the MAT experiments were usually performed at lower temperatures (400–500 °C) than the conventional FCC temperatures (525–575 °C). Also, the different hydrodynamic behavior caused deviations in the observed phenomena. It may result in differences in the distribution of reaction products as well as the content of oxygenates (CO_2, CO and H_2O). Nevertheless, Dupain et al. [127] have suggested that the both testing devices (the MAT and the micro-riser) ensured the catalytic cracking of unsaturated vegetable oils and fatty acids and resulted in the formation of a highly aromatic organic liquid product. In general, it may be concluded that, regardless of the type of equipment used, the purpose of the studies is to understand the co-processing of the blends of vegetable and petroleum feedstocks in the context of FCC technology to meet legislative requirements for a biofuel component in gasoline and diesel.

4.2. *Operating parameters*

4.2.1. *Co-processing of lipids*

The following section summarizes the results and observations reported in the published studies on the influence of the operational conditions which influence the co-processing of RSO and conventional petroleum-derived feedstocks under FCC conditions, and the generalized information is presented in Table 6.

Table 6
Operating conditions during the FCC co-processing of lipids with petroleum fractions.

No	Feedstock		Percent biomass in the feedstock, %	Catalyst	Reactor	Catalyst loading	*T*, °C	Catalyst-to-Oil mass ratio	Ref.
	Biomass component	Petroleum component							
1	Palm oil, soybean oil, nonedible animal fats, waste cooking oil	VGO	30	E-CAT	MAT	1.5–9	565	1–6	[61]
2	Rapeseed oil	VGO	10	E-CAT (10% ZSM-5 additive)	MAT	4	525	2–12	[65]
3	Cottonseed oil, sunflower oil	VGO	10	E-CAT, Halloysite nanotubes	MAT	11	480–540	WHSV = 21 h^{-1}	[63]
4	Sunflower, rapeseed, mustard and palm oils	VGO	0–100	E-CAT	MAT		450–527	4	[66]
5	Palm oil	VGO	50; 100	USY + ZSM-5	Laboratory-scale two-stage riser fluid catalytic cracking unit		500–520	6–8	[62]
6	Canola oil	HAGO	15	E-CAT	Advanced Catalyst Evaluation (ACE^{TM}) unit	9	490–530	4–11	[50]
7	FAME	VGO	0–100	E-CAT	FCC pilot plant		550		[128]
8	Rapeseed oil	VGO	7.5; 15	E-CAT	FCC pilot plant				[119]
9	Rapeseed oil	VGO	0–100	E-CAT	FCC pilot plant	9–11 kg	500–600	3–4	[51]
10	Rapeseed, soybean and palm oil	VGO	0–100	E-CAT	FCC pilot plant	9–11 kg	500–600	3–4	[64]

Reaction temperature: Ng et al. [50] reported that the conversion of a blend of canola oil with HAGO increased as the temperature increased from 490 to 530 °C and it was higher than the conversion of neat HAGO (Fig. 8A). It was explained as a higher temperature is the driving force to (1) promote cracking, thus producing more gases and lighter liquid products, and (2) reduce the catalyst poisoning effect (by basic nitrogen in the feed), which is more pronounced at lower temperatures.

The increased cracking at elevated reaction temperature resulted in the growth of the yield of LPG (Fig. 8B) which was always higher for HAGO + Canola Oil than for HAGO due to the higher content of aliphatic chains in the former feed. The gasoline yield from HAGO + Canola Oil feed increased when increasing the temperature from 490 to 510 °C because of the enhanced cracking of the feed and reduced nitrogen poisoning of the catalyst (Fig. 8C). However, the gasoline yield slightly decreased from 510 to 530 °C due to the gradual exhaustion of gasoline precursors. These precursors are saturated hydrocarbons and monoaromatics plus other crackable components that predominantly contribute to the production of gasoline and its derived products, *i.e.,* dry gas, LPG, and catalytic coke. In contrast, the gasoline yield was virtually constant over the whole temperature range. The LCO yield decreased from *ca.* 22% to 18–19% consistent with the increasing temperature (from 490 to 530 °C) (Fig. 8D) which is a driving force to crack large molecules (*e.g.*, those in LCO) to smaller ones (*e.g.*, those in gasoline and gases). Obviously, at the same temperature, the blend always exhibits a slightly lower LCO yield than HAGO (by 0–2%) indicating that the blend is more crackable than its counterpart. The coke content in the catalysts increased from 3.5% to 4% with the growth of temperature from 490 to 530 °C as it was formed through the polymerization of aromatic hydrocarbons in the cracked liquid product together with the condensation reaction involving the vegetable oil [50]. Similar results were obtained by [66] when studying the co-processing of sunflower oil with VGO. The increase in the reaction temperature from 450 to 510 °C resulted in the increase of conversion from 79.2% to 88.7% and the yield of gaseous reaction products from 18.0% to 40.1%, while the yields of gasoline and LCO decreased from 43.5% to 31.2% and from 16.2% to 9.3%, correspondingly. Investigating the co-processing of cottonseed (CSO) and sunflower oils (SFO) with VGO at the temperature range of 480–540 °C, Abbasov et al. [63] found that the optimal conversion has been achieved at 500 °C in all the cases and varied at a 65–75% range. At higher temperatures ($T = 520–540$ °C), rapid coking of the catalyst blocked active sites while at lower temperatures ($T = 480$ °C) the reaction speed was very low.

The catalyst-to-oil mass ratio: The severity of the catalytic cracking process can be modified not only by reaction temperature but also by changing the catalyst-to-oil mass ratio (CTO). Melero et al. [61] investigated the FCC co-processing of 30% palm oil in VGO and found that, as the CTO increased from 3 to 6, a higher yield to gaseous products (from 2 to 3.8 wt% and from 11.5 to 23 wt% for dry gas and LPG, respectively) and coke (from 1 to 4.7 wt%) as well as a lower production of LCO (from 26 to 17 wt%) was achieved. The gasoline fraction showed a peculiar tendency with the CTO. It was suggested that gasoline is an unstable cracking product because it is obtained from heavier cuts and it is possible to crack further if the severity of the cracking process is adequate. This fact makes it probable that the gasoline which should rise with an increase of the severity will be cracked to lighter products and hence end up mainly as LPG. Because of the presence of this opposite phenomenon, gasoline shows a maximum in the yield (46–47 wt%) with an increase in the CTO. The location of this maximum appears in a different position, and it is more significant depending on the features of the feedstock.

Similar results were obtained in the study of Ng et al. [50]. They observed the increase of conversion with CTO and tended to level off at high CTOs. They claimed that this could be expected, as higher CTO ratios (as high as 9–11) provide proportionally more active acid sites of the catalyst to crack a given amount of feed molecules. However, the cracking rate is reduced at high CTOs once the crackable components in the feed are gradually exhausted. Both dry gas and LPG also increased with the CTO, while the gasoline yield increased

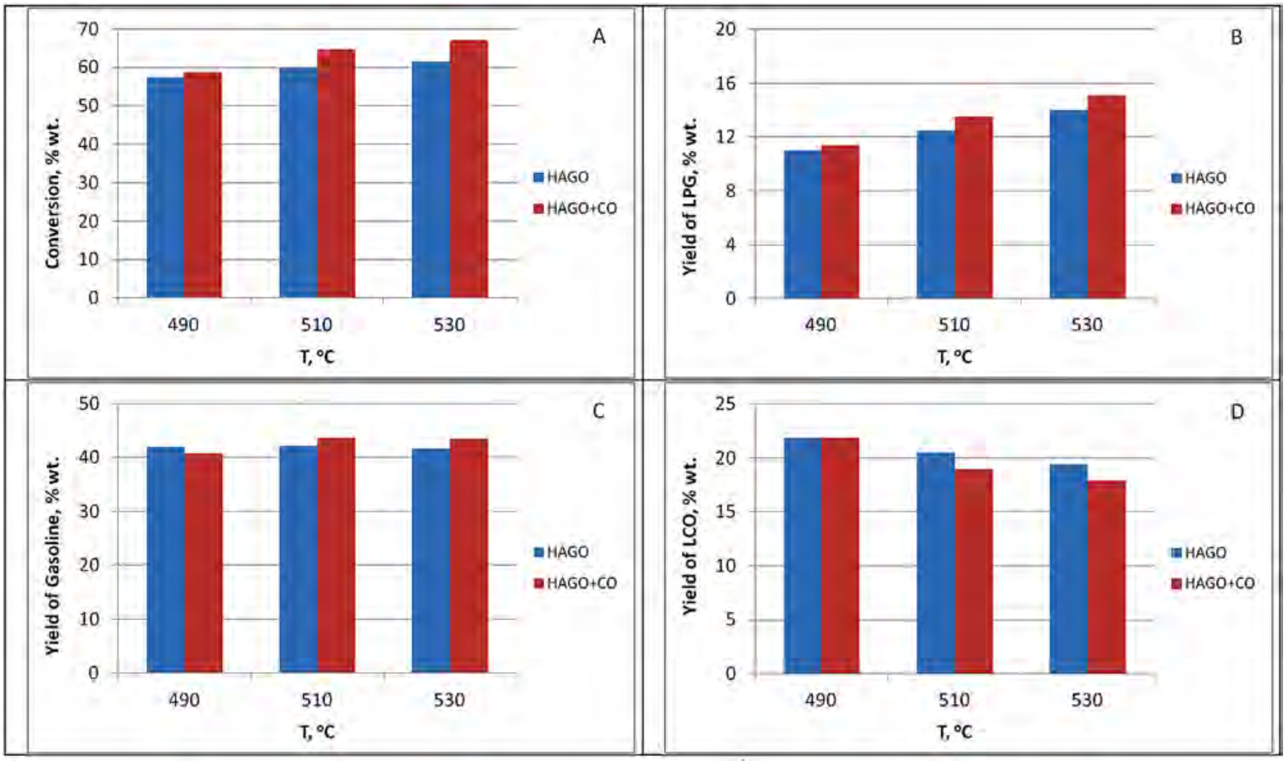

Fig. 8. Co-processing of HAGO and canola oil (CO) (85:15, v/v) dependent on the reaction temperature. Catalyst-to-Oil = 4 [50].

with the CTO, but only up to a certain point (CTO ≈ 7–9) at which the yield started to decline. The authors explained this trend by the gradual depletion of gasoline precursors and the accelerated conversion of gasoline into gases and coke at high CTOs. The LCO yield also decreased monotonously and parallel with the CTO, approaching the limit of the LCO precursors defined as the sum of different aromatic compounds, while the coke yield increased linearly with the CTO.

In contrast to the results from [50, 61], the decrease in gaseous reaction products (dry gas and LPG) and considerable increase in gasoline and stable content of LCO were observed with the growth of the CTO in [65]. The authors explained the obtained results by the additional joint transformations of rapeseed oil and HVGO feedstock compounds which comprised several effects: the enhancement of hydrogen transfer reactions (easier formation of carbenium ions) by olefin intermediates formed during rapeseed oil cracking and lowering the further cracking of gasoline-range hydrocarbons due to a competitive sorption effect of C_{15}–C_{17} olefins which have a higher tendency to form surface carbenium ions than the ones from the gasoline fraction.

The bio-content ratio: The influence of the RSO (Rape Seed Oil) content in the co-processing blend was investigated in several articles [61, 63, 64, 66]. Doronin et al. [66] using a lab-scale MAT unit showed that co-conversion of VGO and RSO under catalytic cracking conditions increased both the total conversion of the blend feed and the yields of gasoline fraction, and the maximum promoting effect was provided by the addition of 5–10 wt% vegetable oil. The authors suggested that the addition of a small amount of lipids (up to 25 wt%) promotes the activation of paraffinic and naphthenic hydrocarbons in the petroleum feedstock by hydrogen transfer reactions. In the process, hydrocarbons of petroleum feedstock serve as hydrogen donors, while the primary semi-products of vegetable oil thermal cracking, *i.e.*, C_{15}–C_{17} olefins are hydrogen acceptors. According to the proposed scheme, carbocations formed by the interaction of the olefins with the catalyst active acid site react with paraffinic and naphthenic hydrocarbons in the petroleum feedstock. Consequently, hydrogen transfer reactions result in the formation of aromatic hydrocarbons and isoparaffins and, thus, in an increased VGO conversion.

At a high concentration of olefins (a 25–75 wt% content of vegetable oil in the blend feed), the contribution of the secondary transformations was great due to pronounced reactivity of the olefins. This resulted in the formation of a large amount of mono- and polyaromatic hydrocarbons. Strong adsorption of these compounds on the acid sites of the catalyst led to their deactivation, thus lowering the catalyst activity.

Bielansky et al. [51] successfully converted the blends of VGO and different vegetable oils in a fully continuous FCC small scale pilot plant. They pointed out that no fundamental modifications were necessary and no difficulties in the system occurred during the test runs. The total fuel yield (gas + gasoline) decreased as the content of rapeseed oil in the blend increased from 0% to 100%. The decrease in total fuel yield at higher rapeseed oil ratios was attributed by the authors to the oxygen content of the feed that notably influenced the cracking gas amount. Indeed, the amount of gasoline was roughly constant for the different feeds studied, but the yield of the cracking gas gradually decreased from 37.5 to 24.0 wt% with the increase in the rapeseed oil content in the feed from 0% to 100%. The decrease in gas production from pure vegetable oils in comparison with petroleum feeds or their blends was also observed in other studies [65, 127]. In contrast, Melero et al. [61] found an increased formation of gaseous products (dry gas and LPG) as the palm oil content in the feed increased. According to Bielansky et al. [51], the yield of LCO depended on the origin of used vegetable oil, while the coke yields were approximately constant for all the investigated conditions. Based on the nearly linear trends for the lumps with different blends of vegetable oils and VGO, the authors assumed that the reaction rate of both feeds was similar and no synergetic effects seemed to occur.

A general observation was found in different studies [61, 64, 66]: the number of double bounds in the fatty acids (in the order soybean, rapeseed, palm oil) enhances the number of alkylation, cyclization and dehydrogenation reactions. It increases the total yield of liquid cracking product and the content of aromatic hydrocarbons, which are formed by aromatization of olefins, with a simultaneous decrease in the yields of paraffinic and olefinic hydrocarbons. It was also suggested [64] that, despite that aromatics in the gasoline increase the octane number, they are undesired from an environmental point of view.

Initial triglycerides are oxygen-containing compounds, while the final products should be oxygen-free hydrocarbons. Consequently, FCC processing should promote the effective deoxygenation of the triglyceride-base molecules. It is believed [61] that the usual conditions of the FCC unit are severe enough to decompose the heavy oxygenated hydrocarbons by means of decarboxylation, decarbonylation, or dehydration reactions to yield a mixture of different hydrocarbons, while oxygen molecules end up mainly as carboxylic gases (CO and CO_2) and, above all, water. Bielansky et al. [51] established that about 13 times more water than carbon dioxide was formed during the co-processing, indicating that most of the oxygen in the feed was converted into water. A similar suggestion was also made by Tian et al. [62]. Bielansky et al. [51] pointed out that the change in the quality of the produced gasoline by adding vegetable oils to the feedstock is of high importance. Two basic quality standards are the octane numbers as well as the oxidation stability. In their study increasing bio-oil content in the feedstock in the range of 0–100% increased the research octane number (RON) by two units while the motor octane number (MON) stayed approximately constant. Additionally, the increase of oil content in the feed (0–100%) also gradually enhanced oxidation stabilities. Abbasov et al. [63] also found that acid values of liquid reaction product have increased only marginally upon the addition of triglycerides, indicating an effective decarboxylation process. Tian et al. [62] performed the elemental analysis of the reaction products and found that oxygen content of the liquid products were relatively low (0.32–0.58%) *i.e.*, oxygen was present predominantly in the form of H_2O, CO and CO_2. Similarly, Lovas et al. [65] suggested that the use of the catalytic system consisting of FCC-ECAT + 10 wt% of FCC-ZSM-5 suppressed the content of the oxygenates under the detection limit of the GS-MS apparatus as their amount throughout the whole CTO ratio range was on the level of a ten thousandth of weight percent.

Analysis of the water phase was performed in [64]. It was found that the pH value of this phase was slightly basic for a low vegetable oil content in the blends but became acidic at ratios above 40%. Water samples from the co-processing had significant contents of acetic and propionic acids (600–1700 ppm) while the concentration of formic and butyric acids was smaller ($\leq$ 300 ppm).

4.2.2. Co-processing of bio-oils

In most cases, the co-processing of different bio-oils (flash pyrolysis bio-oil (FPO), catalytic pyrolysis oil (CPO), and hydrotreated pyrolysis oil (HPO)) and petroleum fractions is performed at reaction temperatures which are usual for ordinary FCC processing, *i.e.*, about 530 °C [17]. Nevertheless, examples on the study of reaction temperature outside this range on the co-processing parameters are also known.

Reaction temperature: As could be expected, the overall conversion increased as the temperature was increased both in the case of the co-processing of HPO with LCO [99] and the FPO with VGO [58]. Samolada et al. [99] found that the increase in reaction temperature from 500 °C to 550 °C during the co-processing of HPO and LCO resulted in a substantial increase in the conversion from 18% to 32%. On the contrary, the coke content decreased because the

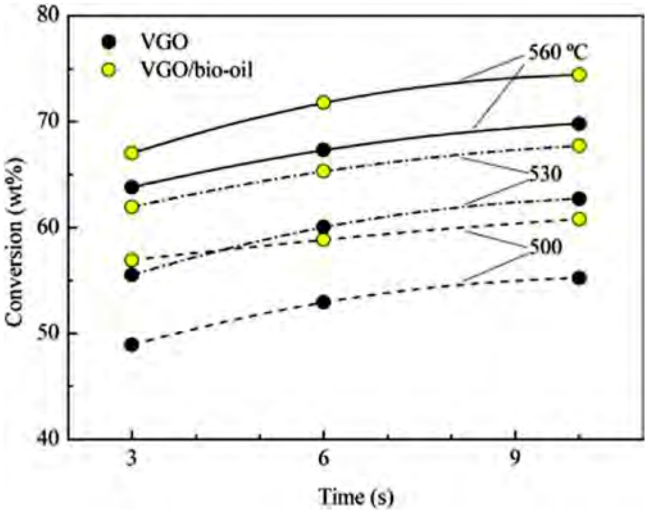

Fig. 9. The change of feed conversion with the reaction time in the catalytic cracking of VGO and VGO/bio-oil (20 wt% in bio-oil) at different reaction temperatures [58].

incremental conversion mainly produced gasoline and light gases. They also suggested that higher temperatures should be avoided to prevent secondary cracking reactions producing additional coke and/or gases. Nonetheless, the authors decided to perform all further experiments at 550 °C since a conversion lower than 20 wt% was declared undesirable. Unfortunately, no information on the processing of pure LCO under same reaction condition was provided.

Ibarra et al. [58] investigated the effect of temperature and reaction time on the conversion of pure VGO and the blend (80% VGO with 20% FPO) (Fig. 9). First of all, the blend conversion was higher than the conversion of VGO over the whole operating range what the authors attributed to the synergistic effect of the joint cracking since the conversion of neat bio-oil was in the range 55–65%, while the conversions of VGO and the blend were in the range 49–68% and 56–74%, respectively. Furthermore, the conversion substantially increased as the temperature was increased from 500 to 560 °C. The evolution of the product yields with the conversion for the cracking of the VGO/bio-oil blend and the individual feeds allowed the following conclusions to be made. The dry gas yield increased due to methane and ethane produced by the thermal cracking of oxygenates from the raw bio-oil. The LPG yield also increased due to the cracking of heavy molecular weight components leading to the compounds in this lump, as well as those in the dry gas. The coke yield increased with increasing conversion in the cracking. This was attributed to the fact that under the conditions studied, an increase in temperature and reaction time mainly promoted coke formation reactions by condensation of heavy volatile compounds rather than the cracking of these volatile compounds that are intermediates in the coke formation. The yield of oxygenates decreased to 2.1 wt% as the conversion increased to 70 wt% which shows that the oxygenate conversion is significant [58]. Considering the distribution of residual oxygenates among different products, it was noted that no oxygenates were found in the LCO fraction, but the presence of unconverted oxygenate compounds in the gasoline lump was due to their low reactivity.

The catalyst-to-oil mass ratio: The effect of the catalyst-to-oil mass ratios (CTO) on the performance of the bio-oil and petroleum oil co-processing was investigated in several studies [55, 60, 70, 96]. Table 7 evidences that this parameter varied over a wide range of 1–9 thus allowing for significantly modifying the conversion and yields. Agblevor et al. [96] demonstrated that the CPO was stable enough to be co-processed with a standard FCC feed to produce various fractions of hydrocarbon fuels. First, a blend of 15 wt% CPO and 85 wt% Standard #4350 Gas oil, *i.e.,* a SRGO, was evaluated and compared with the benchmark (Standard #4350 Gas oil) at a 70% constant conversion. The authors found that the blending of the Standard #4350 Gas oil with 15 wt% CPO did not have any obvious adverse effect on the yield of various cracked fractions, especially the gasoline fraction (Fig. 10A). Based on this result, they suggested that at a catalyst to oil ratio of 6, the CPO/gas oil blends can be used to produce gasoline with similar yields as petroleum gas oil thus constituting a true replacement for gasoline produced entirely from petroleum.

Agblevor et al. [96] also investigated the effects of catalyst to oil ratios (CTO) and suggested that the co-processing of CPO with gas oil was very sensitive to the CTO ratio because this ratio affected the conversion and subsequently the product yields and other parameters. They found that with a decreasing CTO ratio, the overall conversion also decreased. It resulted in the corresponding decrease in both dry gas and LPG yields. The coke yield also showed a decrease: as the CTO ratio was decreased, the catalyst could not promote coke forming reactions. These results are similar to what has been traditionally observed for the cracking FCC feed. In contrast, the HCO and LCO yields increased as the CTO decreased what was also attributed to the lower conversion. The authors pointed out that the almost constant yield of gasoline from this process was observed with a variation of the CTO ratio. The minimal change in the gasoline yields was attributed to the attainment of a pseudo steady state, where the change in the CTO ratio, generated more gasoline from the LCO/HCO, but the gasoline subsequently was converted into LPG. Similar results, *i.e.,* an increase in the overall conversion, gas and coke yield and LCO and bottom decrease with the growth of the CTO ratio were observed in other studies [55, 57, 60, 70, 99].

The examples of the co-processing of FPO, CPO and HPO with petroleum feedstocks at FCC conditions using laboratory scale units (MAT and ACE) are summarized in Table 7 which contains information on the type of both bio- and petroleum feeds, their ratio in the reaction mixture and catalysts used for the co-processing as well as variations in reaction conditions.

From experiments on the catalytic cracking of pure bio-oils in the FCC process, it was summarized that reactor plugging might be a crucial issue because char and coke formation was substantial, even at low reaction temperatures [99, 131–133]. Consequently, bio-oil cracking resulted in irreversible catalyst deactivation by dealumination of the zeolite component mainly because of the high oxygen content in the feed and substantial water steam presence in the reaction medium. Based on these conclusions, it was suggested that the quality of the raw bio-oil with a high content of oxygenates, *i.e.,* produced by fast pyrolysis, is too low to be co-processed directly with a petroleum feed in a standard FCC process [54, 82, 107]. Therefore, upgrading the FPO, mostly by hydrotreatment to remove the most reactive components in the bio-oil, is often performed prior to its co-processing with the petroleum feedstock [52, 55, 56, 82, 107]. Moreover, it was also suggested that the more upgraded HPO afforded lower coke and dry gas yields during FCC [82]. Correspondingly, most published studies have investigated the co-processing of bio-oil stabilized by hydrogenation step (*i.e.,* HPO feedstock with the lowest oxygen content and, therefore the lowest plugging problems) with conventional FCC feedstocks, vacuum gas oil (VGO) or light cycle oil (LCO) to assess the suitability of using HPO as a potential co-feed [52, 55, 56, 82].

The basic parameters of HPO co-processing with petroleum feedstocks were reviewed in [22, 24]. To mention briefly, the influence of HPO added to petroleum-based feedstocks on the conversion level observed in the FCC co-processing is not yet fully understood. It could depend either on the type of the fossil feed [70] or on the type of the catalysts being used, because the properties of the equilibrium catalysts were often not specified in the studies [22]. The data in Table 7 indicates that the co-processing results could be significantly affected by the properties of bio-oils as these vary in a great extent in different studies. As to product distribution, the cracking of the bio-

Table 7
Operating conditions during the FCC co-processing of pyrolysis bio-oils with petroleum fractions.

No	Feedstock		Percent biomass in the feedstock, %	Catalyst	Reactor	Catalyst loading, g	*T*, °C	Catalyst-to-oil mass ratio	Remarks	Ref.
	Biomass component	Petroleum component								
1	HPO	Long residue	20	E-CAT	MAT	10	520	3–8	Mild hydrogenation of FPO ("stabilization") is enough to enable co-processing	[82]
2	HPO	VGO	20	E-CAT, HY, ZSM-5	MAT	0.5 or 1	500	1–6	The competition for zeolite sites between the cracking route and the deoxygenation of oxygenates	[55]
3	HPO	VGO	10	E-CAT	MAT	1	500	3	The processing of bio-oil oxygenates favors then bio-coke and the bio-light gases production	[56]
4	HPO	LCO	15	E-CAT	MAT	–	500–550	2–6	Produced bio-gasoline has a high RON number (96) and meets the EU specifications.	[99]
5	HPO	VGO	20	E-CAT	MAT	1	500	2.9–5.9	Oxygen removal from HDO oxygenates consumes H_2 coming from hydrocarbon cracking	[70]
6	HPO	VGO	10	E-CAT	MAT	3–7	560	1.5–7	The effect of bio-oil upgrading severity on naphtha quality and coke content was evaluated	[129]
7	HPO	Atmospheric distillation residue	0–20	E-CAT	MAT	1	520	2.5–3	A higher CTO ratio should be used for the conversion of HPO in the standard FCC unit in a conventional refinery.	[97]
8	CPO	Gulf coast standard gas oil	15	E-CAT	Advanced Catalyst Evaluation (ACE^{TM}) unit	9	538	4–9	Hydrogen transfer from the cracking of gas oil to bio-oil eliminates the oxygen in the fuel without external H_2	[96]
9	FPO	VGO	20	E-CAT	A riser simulator reactor	–	500–560	6	Synergistic effect of the joint cracking of the VGO/bio-oil blends is observed	[58]
10	FPO	VGO	20	E-CAT	A riser simulator reactor	–	500	6	Existence of two significantly different pathways of catalyst deactivation during co-processing	[59]
11	CPO/ HPO	VGO	10	E-CAT	MAT	2	500	3–9	Higher concentration of alkylphenols in gasoline fraction by co-processing of CPO compared to HPO	[60]

(*continued on next page*)

Table 7 (*Continued*)

No	Feedstock		Percent biomass in the feedstock, %	Catalyst	Reactor	Catalyst loading, g	T, °C	Catalyst-to-oil mass ratio	Remarks	Ref.
	Biomass component	Petroleum component								
12	HPO/ CPO	VGO	10	E-CAT	MAT	2	500	3–6	Mechanistic scheme for coke formation under co-processing conditions is provided	[57]
13	FPO/CPO/	VGO	5–30	E-CAT	MAT	10	482	1 or 3	Bio-oil concentration during co-processing should remain low to avoid high coke formation	[98]
14	HPOFPO/HPO	VGO	5–20	E-CAT	Advanced Catalyst Evaluation (ACE- R^{TM}) unit	9	530	5	Removal of char particles from FPO by membrane filtration under vacuum	[52]
15	HPO produced from CPO	LGO/VGO	2	E-CAT	FCC small-scale pilot plant unit	–	520	–	Presence of the bio-oil favors gasoline and diesel production but increases coke yield	[95]
16	CPO	VGO	2–10	E-CAT	Pilot-plant FCC unit	–	525	5	At 15% CPO riser coke and feeder blockage were sometimes observed	[54]
17	FPO	VGO	10–20	E-CAT	A demonstration-scale FCC unit	450 kg	540–560	3	The FCC carbon efficiency was approximately 30%	[53]
18	FPO	VGO	5–10	E-CAT	A demonstration-scale FCC unit	450 kg	540		9-month-old bio-oil did not cause operating problems in the FCC unit	[130]

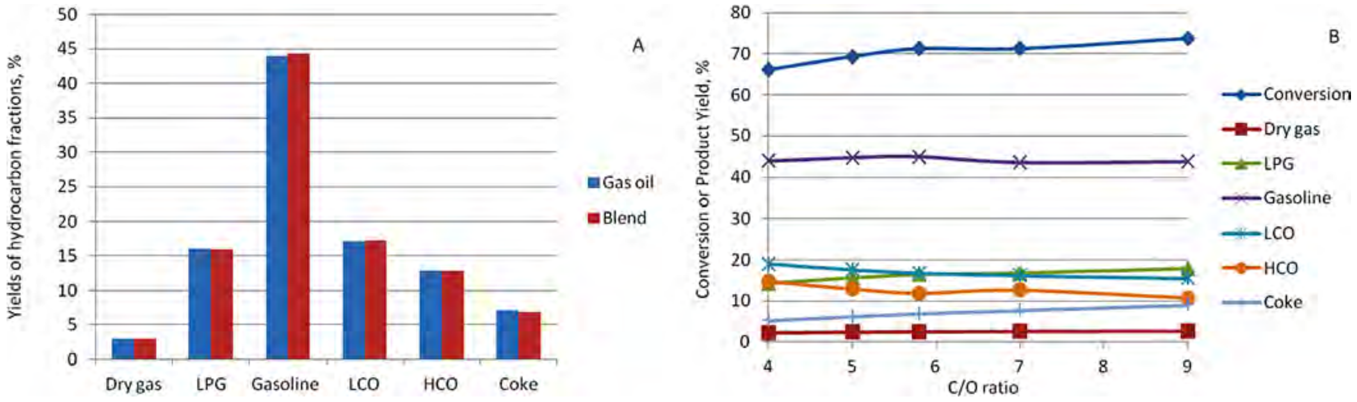

Fig. 10. A – Yields of hydrocarbon fractions obtained from the co-processing of CPO/gas oil (15/85) blends and gas oil at a 70% conversion. B – Influence of catalysts to oil ratio on the feed conversion as well as the yields of dry gas, LPG, gasoline, LCO, HCO, and coke during the FCC cracking of CPO/gas oil (15/85) blends [96].

oil/VGO mixture provided higher low-value dry gas (H_2, CO, CO_2, and C1–C2) yields and lower liquefied petroleum gas (LPG) yields than a pure VGO feed [70]. While there are discrepancies in the literature with respect to the yield of gasoline and LCO [70, 99], there is agreement concerning the increase in coke content during co-processing in comparison with the cracking of pure VGO [70, 82, 99]. As an exception, Huynh et al. [97] observed no significant difference in the observed coke yield between the co-feeding and neat conventional feed, independent of the CTO ratios. However, no explanation of the observed trend was provided by the authors.

The co-processing of hydrogenated pyrolysis oils (HPO) with fossil feeds in refineries constitutes a promising route toward the production of greener transportation fuels. Nevertheless, an obvious disadvantage of the bio-oil hydrotreatment to oxygen content close to 5 wt% is the necessity to use significant quantities of hydrogen which would make the technology economically unviable [98]. Gueudré et al. [129] found that the best naphtha quality (in terms of RON, MON, and paraffins, isoparaffins, olefins, naphthenes, aromatics (PIONA) composition) could be achieved with mildly hydrotreated pyrolysis liquids corresponding to an H_2 consumption of 202 NL/kg$_{\text{bio-oil}}$.

To decrease the cost of bio-oil hydrotreatment, Mercader et al. [82] used milder conditions for FPO upgrading. They concluded that bio-oils do not require complete hydrodeoxygenation to decrease coke formation and prevent unsuccessful FCC co-processing. Thus, the goal of the upgrading should be the elimination of the highly reactive components and functional groups with minimized hydrogen consumption only. Nonetheless, such upgrading technology is still under development and requires the use of an expensive noble metal catalyst [82, 107]. Therefore, eliminating the costly hydrogenation step by a catalytic pyrolysis step can be considered as a competitive approach to bio-oil upgrading by hydrotreating [54, 60]. Recent publications show that both FPO and CPO can be used directly in mixture with petroleum feed for FCC co-processing [58, 59, 96] also.

The co-processing of CPO with different types of gas oils was successfully demonstrated by Agblevor et al. [96]. They studied the co-processing of 15 wt% CPO blended with 85 wt% straight run standard fluid catalytic cracking feed (Gulf Coast standard #4350 Gas oil). For the same conversion of 70% for both the standard gas oil and the CPO/gas oil blends, the gasoline yield was 44 wt%, light cycle oil (LCO) 17 wt%, heavy cycle oil (HCO) 13 wt%, and LPG 16 wt%. The liquid fractions produced from the co-processing were rich in aromatic hydrocarbons, contained bio-carbons, and less than one percent oxygen. The coke yield for the blends was 6.64–6.81 wt% which was lower compared to the standard gas oil run (7.06 wt%). It was attributed to be hydrogen transferred from the cracking of the standard gas oil to the bio-crude oil which subsequently eliminated the oxygen in the fuel without external hydrogen addition.

Ibarra et al. [58] investigated the catalytic cracking of a blend of raw bio-oil produced by fast pyrolysis (20 wt%) and VGO (80 wt%) in a patented riser simulator reactor with an in-built impeller. The authors found the existence of a relationship between the mechanisms for the cracking of the hydrocarbons in the VGO and oxygenates in the bio-oil which had great impact on the yields and lump concentrations. A favorable synergistic effect was observed on the LPG ($C_3$and C_4) and gasoline (C_5–C_{12}) yields (higher values than expected in the absence of synergy), while the formation of CO_2 and CO was lowered. Moreover, co-feeding prevented coke formation, which lowered catalytic deactivation. In total, a deoxygenation degree of 95 wt% was obtained, with a total liquid fuel yield of 52.8 wt% and a gasoline yield of 31.6 wt%, with a low oxygenate fraction ($<$ 4 wt%) which contained carboxylic acids, aldehydes, ketones, and phenols.

The above examples show that not only HPO but also CPO and FPO may be considered as a promising bio-additive to petroleum-derived feedstock for FCC co-processing. Nevertheless, considering the results from different studies, it is difficult to evaluate the efficiency of the different bio-oils as a bio-additive in the co-processing and to make any conclusion about the influence of the type of bio-oil on the co-processing characteristics because of the differences in the properties of the bio-oils, reaction conditions, *etc.* Hence, publications dealing with comparative studies on the co-processing of differently prepared bio-oils with petroleum feeds at similar conditions are of an increased interest.

Naik et al. [52] compared the co-processing of petroleum derived VGO with either FPO or HPO in a laboratory scale Advanced Cracking Evaluation (ACE-R) unit. The authors suggested that low blending ratios of 5:95 and 10:90 of FPO with VGO was extremely suitable to produce light olefins, mainly LPG, at the expense of gasoline range hydrocarbons. In contrast, a decrease in dry gas yield and an increase in liquid hydrocarbons were observed with an increase in the FPO blending ratio with VGO up to 20:80. Nevertheless, the authors concluded that the FPO containing 32 wt% of oxygen seemed to be less suitable for the co-processing of VGO with FPO for higher gasoline yield, as the FPO containing the lignin-derived monomers could not be successfully cracked with the FCC catalysts. In contrast, the co-processing of HPO with VGO resulted in an increase in the yields of gasoline and LCO as compared to the co-processing of FPO with VGO, at the similar blending ratio of 5:95. The FCC distillate from the co-processing of FPO with VGO contained more iso-paraffinic CH3 substructure components, whereas the distillate fraction from the co-processing HPO with VGO contained more paraffinic CH3 substructures. The coke yield was found to be within the measurement uncertainty limit, and in fact, lower than in the cracking of the neat VGO over the same equilibrium FCC catalyst. Hence, HPO may be considered for co-processing with VGO in the FCC unit without many modifications in the process configuration and catalyst, whereas the co-processing of FPO would require some modifications.

Analyzing the properties of FPO, Thegarid et al. [60] suggested that this kind of bio-oil cannot be co-processed directly with fossil feed to liquid fuels due to their oxygen rich composition, low heating value, immiscibility with hydrocarbon fuels, chemical instability, high viscosity and corrosiveness, and concluded that the co-processing has to be preceded by an upgrading step such as hydrodeoxygenation. They compared a bio-oil that has been produced by catalytic pyrolysis (CPO) with an upgraded one (partially deoxygenated) thermal pyrolysis oil (HPO) in co-processing with VGO under FCC conditions. The main differences between the VGO processing and the HPO/VGO co-processing were found to be in the increased coke production, less hydrogen, more olefins and aromatics and the presence of alkyl-phenols in the case of HPO co-processing with VGO. If comparing CPO/VGO and HPO/VGO co-processing, small but significant differences in the product distribution and quality were observed. The excess of oxygen in the CPO as compared with HPO resulted in higher hydrogen consumption due to water formation, explaining the lower hydrogen production in comparison with HPO/VGO and the higher concentration of olefins and aromatics, especially at high feed conversion. Another specificity of the CPO was that it contained heavier components most likely consisting of lignin polymers. Consequently, a higher concentration of alkylphenols was found in the gasoline fraction when co-processing CPO as compared to HPO co-processing. Additionally, the higher gasoline yield during the CPO co-processing than in the HPO co-processing observed during the co-processing was ascribed to the reduced rate of cracking of the gasoline fraction due to its higher aromatic character. Nevertheless, these differences such as the higher concentration of unconverted phenolics in the gasoline or its higher content of aromatics could be reduced by further catalyst development both on the pyrolysis as well as on the FCC side. Taken together, it was concluded that the hydrogenation step could be eliminated by the addition of a suitable catalyst in the biomass pyrolysis step, thus reducing the biomass upgrading costs significantly.

Lindfors et al. [98] studied the co-processing of three differently prepared bio-oils, *i.e.,* dry thermal bio-oil (FPO), catalytic pyrolysis oil (CPO), and hydrotreated pyrolysis oil (HPO). CPO oil and HPO oil had lower carbonyl contents and lower oxygen contents but a higher content of low-molecular-mass (LMM) lignin in comparison with FPO. On the other hand, the amount of high-molecular-mass (HMM) lignin was higher in the CPO oil as compared to the HPO oil, as evidenced from the chemical composition of the bio-oil feeds determined using a solvent fractionation scheme (Fig. 11).

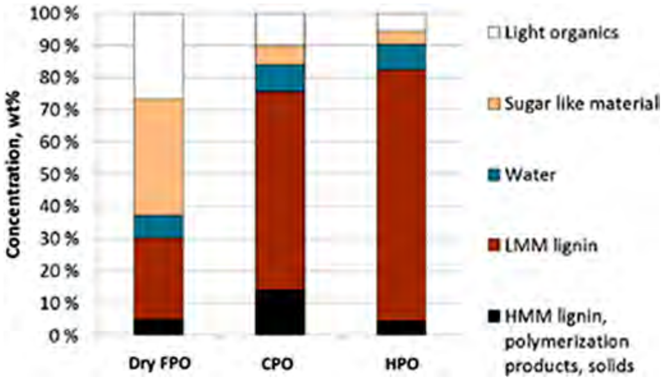

Fig. 11. Chemical composition of the dry bio-oil, catalytic pyrolysis oil, and hydrotreated oil determined by a solvent fractionation scheme [98].

Table 8
Feedstock conversion and yield of different products for MAT runs with blends (20 wt% bio-oils in VGO) (from [98]).

Product	VGO	VGO + 20% FPO	VGO + 20% CPO	VGO + 20% HPO
Conversion (gas + coke + gasoline), wt%	30	41	40	38
Liquid, wt%	85	69	74	76
Gas, wt%	10	14	12	12
Coke, wt%	5	10	10	8

In the co-processing of the dry FPO with VGO in different ratios, it was found that good mass balances in experiments with this bio-oil could be obtained only when using low bio-component concentrations, while at higher bio-oil concentrations coking was a problem when carrying out the experiments [98]. This led to the conclusion that the bio-oil concentration should be low during co-processing. That is why all comparative experiments on the co-processing of dry FPO, CPO, and HPO were performed with the oil content of 20 wt%. The obtained results showed that the bio-oil properties influenced the process. The co-processing of dry FPO resulted in a slightly lower liquid yield compared to the partly upgraded bio-oils, but the differences in the product distribution between different oils were very small in total (Table 8). Unfortunately, the experiments were not performed at the same conversion level and, consequently, the higher conversion in the case of co-processing than in case of neat VGO processing prevents a fair comparison of VGO processing with the bio-oils co-processing. Nonetheless, the comparison of different bio-oils co-processing is possible as a conversion of about 40% was reached in these experiments. Moreover, the chemical compounds present in the liquid products from the co-processing experiments were almost identical to those found in the product from VGO cracking. The main compounds identified by GC – MSD (Mass Selective Detector) were alkyl benzenes, naphthalenes, and straight-chain hydrocarbons, while no oxygen-containing compounds were detected. Nevertheless, coke formation was higher for FPO and the more aromatic CPO in comparison with HPO. The high coke yield with the dry FPO was partly caused by the sugar-like material in the oil (Fig. 11). Indeed, Carlson et al. [134] investigated the fast pyrolysis of glucose in presence of HZSM-5 and found that at high pyrolysis temperatures, glucose is dehydrated to form anhydro-sugars and furans. The latter compounds are easily polymerized and further ultimately decompose to unsaturated coke which represents large graphitic species like those observed on the external surface of the ZSM-5 during the conversion of methanol to hydrocarbons [135]. The difference in the coke yield between the HPO and CPO co-processing can be attributed to their different chemical compositions: the latter oil clearly contained more high-molecular-mass (HMM) lignin, which was a highly probable precursor for coke formation or direct fouling of the catalyst. In contrast to this, the HDO process decreased the oxygen content of the bio-oil while simultaneously boosting its hydrogen content. This change resulted in the saturation of many ring structures, thus making the bio-oil less prone toward coking [98].

Gueudré et al. [57] put an emphasis on the study of coke chemistry occurring in FCC on ultra-stable zeolite Y (USY) catalysts during the co-processing of VGO blended with various types of upgraded bio-oils produced by fast pyrolysis of lignocellulosic biomass, namely HPO and CPO. The yield of gasoline fraction was changed only slightly after blending HPO or CPO with VGO, while the yield of the LCO fraction decreased in the presence of the bio-oils. This could be explained by the lower average molecular weight of the bio-oils in comparison with VGO. Besides, the coke fraction was markedly increased in the presence of the bio-oils, though almost independently of the nature/composition of the added bio-oil (HPO or CPO). This could be attributed to the higher reactivity (due to the presence of oxygenates and unsaturated compounds) of the bio-oil in comparison with VGO. The investigation of the spent catalysts with TPO/TGA/DTA/MS and FTIR helped to conclude that the cracking of the bio-oils involved the consumption of most of the hydrogen present in the feedstock (lignin fragments) by hydrogen transfer reactions leading to highly dehydrogenated coke deposits. Nevertheless, slightly more carbon was accumulated on the spent catalyst samples (USY) after co-processing CPO with VGO than after neat VGO cracking. This was attributed to a higher oxygen content and larger lignin fragments in the non-hydrotreated catalytic pyrolysis bio-oil. Hence, it was concluded that the formation of additional coke (about 4%) under co-processing conditions may have a strong impact on the catalyst regeneration during the FCC cycle. Indeed, according to a rule of thumb generally accepted in FCC operation, an increase of 0.1 wt% in the delta coke (delta coke = coke yield/cat/oil ratio) might increase the regenerator temperature by about 20 °C. Accordingly, an increase of about 4% in the coke yield at a cat/oil of 6 would lead to an increase in the regenerator temperature of about 130 °C, which might create irreversible hydrothermal damage to the circulating catalyst [57]. No doubt, the increased coke formation during the co-processing of petroleum fractions with the bio-oil is considered as an apparent drawback which should be avoided.

It is worth noting that most of the above examples are related to the simulation of FCC co-processing on a laboratory level using a fixed-bed MAT reactor with a catalyst loading of several grams. In this case, regardless of the type of bio-oil used, an increase in coke formation was observed [55, 56, 60, 82, 98, 99]. However, an increased coke formation was not reported when the co-processing was performed using a fluidized-bed MAT reactor [88, 107] or a lab-scale riser simulator reactor [58, 59, 96]. Agblevor et al. [96] reported that when performing the FCC co-processing experiments using an ACE unit, the hydrogen and coke yields in the co-processing of bio-oil with Standard Gas Oil (SGO) and in cracking neat SGO showed considerable differences. In co-processing, 8.2% less hydrogen was produced than in the processing of SGO which was attributed to the bio-oil being hydrogen deficient. However, the hydrogen yield in co-processing was higher than it should have been expected provided that all the oxygen in the bio-oil was converted into water. Consequently, the authors suggested that part of the oxygen was rejected as CO or CO_2 rather than converted into water or over-cracking took place during co-processing. Agblevor et al. [96] also observed that the coke yield in the co-processing was lower than in the SGO processing. They attributed this to the inhibition effect of the bio-oil on the coke formation reactions. They explained this effect by the presence of steam and *in-situ* generated hydrogen from the cracking of the SGO, which moderated the coke formation reactions in spite of the low H/C ratio.

Comparing the above-discussed results obtained on different experimental units, it is obvious that the choice of reactor type is a crucial factor to be considered when evaluating the prospects of the bio-oil co-processing and evaluating the product selectivities.

Pilot- and demo-scale FCC units similar to real industrial FCC units are clearly a better choice to carry out experiments when studying bio-oil co-processing with petroleum fractions. Nevertheless, access to such kinds of equipment is limited, their operation is complicated and costly, and they also require access to an adequate feed supply [28]. Therefore, the examples of using larger pilot scale installations with process flow operation similar to industrial FCC units for co-processing are rare. Nevertheless, studies on the co-processing of bio-oils with petroleum fractions performed on an enlarged pilot scale provides sufficient information on the features of the experiments derived from the difference in the unit construction and size.

Lappas et al. [95] performed experiments on the co-processing of a hydrotreated heavy bio-oil fraction with a conventional VGO using a small-scale FCC pilot plant unit which was operated in full catalyst circulation mode with continuous regeneration and consisted of a riser reactor, a stripper, a lift-line and a fluid bed as the regenerator system. In total, the pilot plant was fully automated and its process control system was based on a special industrial control system. The authors suggested that the main problem with the blend of the above heavy hydrotreated fraction with conventional VGO could be the plugging of the injection nozzle of the small-scale FCC pilot plant. To overcome this issue, they diluted the HPO with LCO (15/85 by weight) and the mixture was finally blended with a conventional FCC feed (VGO). The total mixture of the LCO + HPO was 15 wt%. Experiments in the unit showed that the VGO/HPO co-feed produced about 1 wt% more gasoline and more LCO in comparison with the VGO feed, *i.e.*, the hydrotreated bio-oil components favored cracking into gasoline and diesel components. It was concluded, therefore, that the selectivity of some FCC products was favored by the presence of an HPO [95].

Expectedly, the coke yield was higher in the case of co-processing, however, the slight increase in coke yield was affordable for the FCC process from the technological point of view [95]. In contrast to the previously described products, all LPG gas yields were lower when the bio-oil was added in the feed. In general, it was concluded that the performed tests showed that co-feeding a petroleum VGO with a thermally hydrotreated bio-oil is technically viable for FCC units running with good quality feedstocks (and thus having excess coke burning capacity). Nevertheless, more experimental work is necessary to clarify any additional effects, for example, the influence of the bio-oil concentration (as co-feed) on the FCC product yields and selectivities, as well as on the quality of these products [95].

Wang et al. [54] collected data on the FCC bio-oil co-processing in an automated pilot-plant FCC unit. The pilot plant was operated in full catalyst circulation mode with continuous regeneration and consisted of a riser reactor, stripper, lift line, and fluidized bed as the regenerator. The catalyst circulation was achieved with two slide valves, and it was controlled in a manner similar to that in a commercial FCC unit. The authors studied the effect of a CPO addition (10%) to VGO and found that the co-processing of the blend gave nearly equivalent oxygenate content and also similar selectivities to gasoline, bottom oil, and coke as the catalytic cracking of neat VGO, suggesting that the CPO was a suitable feedstock for FCC co-processing. At the same time, the dry gas, including hydrogen and light hydrocarbons, obviously reduced in the co-processing experiment because of the hydrogen transfer between the bio-feedstock and the VGO. The co-processing experiments also resulted in the formation of CO, CO_2 and water; however, their amounts in the CPO co-processing case were much lower than in the FPO co-processing. Consequently, the authors concluded that the co-processing of CPO with petroleum fractions was highly promising for biomass conversion into biofuel.

Pinho et al. [53, 130] provided information on bio-oil co-processing with a petroleum fraction on the largest scale which was successful so far. They performed catalytic tests in a demonstration-scale fluid catalytic cracking unit equipped with a pseudo-adiabatic riser reactor and a continuous catalyst regenerator, operating under steady state conditions. The catalyst inventory was 450 kg and the total feed rate was controlled at 150 kg/h. In contrast to lab-scale reactors the use of the demonstration-scale unit allowed for the successful co-processing of the VGO mixed with 10 and 20 wt% FPO, even though the bio-oil and conventional petroleum fractions are poorly miscible or even totally immiscible due to the high polarity of the bio-oil [53]. The successful experiment with a high FPO content in the mixture was achieved by using two different axial injection positions in the FCC riser reactor. The authors concluded that the bio-oil could be directly co-processed without any type of hydrodeoxygenation and with a regular gas oil FCC feed containing up to 20 wt% bio-oil. The blend of the bio-oil and VGO was cracked into valuable products such as LPG and gasoline rendering similar product yields as those obtained from neat VGO when the feed contained up to 10 wt% bio-oil. However, there was a clear drop in the gasoline yield when 20% bio-oil was added to the feed due to the dilution effect caused by water. The same trend was observed for LCO yields, while the bottoms yields increased slightly when 20% bio-oil was added to the feed. The introduction of a 10% bio-oil in the riser reactor did not significantly increase coke, whereas the use of 20% clearly increasedthe coke yield. Most of the oxygen present in the bio-oil was removed as water. Nevertheless, special care must also be dedicated to the tanks used for the bio-oil storage and feed lines in the FCC unit to deal with the high acidity of the bio-oil. Moreover, alkaline metals present in the bio-oil may destroy the zeolite in the FCC catalyst and higher make-up rates would have to be employed to ensure FCC equilibrium catalyst activity [53].

In a recent article, Pinho et al. [130] demonstrated the effect of aging a bio-oil on the technical feasibility of co-processing a raw bio-oil with VGO. The tests conducted with the same bio-oil in two different experimental test series showed that while a 9-month-old bio-oil did not cause operating problems in the FCC unit, a 21-month aged bio-oil may affect the operating conditions. Nevertheless, the authors suggested the necessity of more data to further investigate the optimization of the co-processing. It was suggested, based on the MAT results [60, 98], that coke formation during the co-processing is excessively high when raw (untreated) bio-oil is used as a bio-component. Hence, raw bio-oil hydrotreatment to reduce the high concentration of heteroatoms has been recommended prior to contact with petroleum feeds. In contrast, Pinho et al. [53] proposed that a considerable increase in coke production even at low bio-oil amounts was a consequence of using small-scale units. Based on the results obtained in a demonstration-scale fluid catalytic cracking unit they tried to explain which characteristics inherent to small-scale units could stand up for the differences in yields observed in a much larger scale unit. First, a single feed line used in most of the FCC laboratory-scale units enormously complicates the feeding of bio-oils in the co-processing experiments because bio-oils are not miscible with petroleum streams and may result in an inhomogeneous feed entering the reactor. Moreover, excessive heating of the feed lines, above 50 °C, promotes bio-oil polymerization and causes plugging. However, such a low temperature is not suitable for VGO feeding because it causes an increase in the VGO viscosity and impairs the proper dispersion in the feed nozzle. Insufficient feed dispersion increases the amount of coke deposited on the catalyst and damages the catalyst selectivity. These problems may be, however, overcome in larger scale units, when different feed lines are used to segregate the bio-oil from the VGO (or other fossil stream), allowing adequate heating and dispersion of each feed. Indeed, in pilot scale installations which have a technological scheme similar to real FCC units, biomass feedstocks can be injected at a number of different positions of the FCC reactor relative to the VGO feed, *i.e.,* before the VGO, with the VGO, after the VGO feed, or even in the regenerator or in a separate riser reactor. These different zones involve different temperatures and catalytic activities [19].

Second, large scale units can overcome the issues related to the presence of high molecular weight molecules (cellulose, hemi-cellulose and lignin) which are not destroyed in the fast pyrolysis process [136]. In a real FCC unit, the bio-oil can be injected at the bottom of the riser, before the regenerated catalyst contacts the VGO. Consequently, it may be cracked at higher temperatures and the catalyst-to-oil (CTO) mass ratios (at the bottom of the riser, the local CTO ratio is approximately 10 times higher and the catalyst temperature is approximately 690 °C). The thermal shock between the hot regenerated catalyst and the large bio-oil molecules promotes their quick thermal cracking, transforming them into smaller molecules, which can then penetrate the catalyst pores and react there. If such thermal cracking is not possible, the bio-oil will not vaporize completely; a part of it will remain in a liquid form and will most likely be deposited as coke on the catalyst. Consequently, the deposited coke will decrease the catalyst selectivity and deteriorate the FCC yield profile. However, most of the equipment used on a laboratory scale, such as MAT reactors or ACE units, work isothermally and the entire reactor is kept uniformly at the same temperature, which is unrealistic for an industrial FCC operation. In this case, the thermal shock between the hot catalyst and the bio-oil is not possible. The non-vaporized fraction of the bio-oil will remain liquid and hence yield more coke. Thus, although MAT reactors and ACE units are economical options for the investigation of most of FCC applications using distillate petroleum feeds, they are inadequate to deal with heavy feeds, such as atmospheric residues and bio-oils [53]. Similarly, Wang et al. [54] also suggested that the oxygen in the bio-oil can be removed almost completely in their FCC co-processing study and a low oxygen content in the final product in comparison with results from other lab-scale cracking experiments, which was attributed to the difference in the operation scale and to the benefits of thermal shock effect in the pilot-scale unit.

4.3. *Catalysts*

The processes that take place in the FCC reactor are based on several types of reactions, including protolytic cracking (cleavage of carbon–carbon bonds), hydrogen transfer, and isomerization [137]. The same reactions should apparently occur in the case of the co-processing of petroleum and bio-based feedstocks. Moreover, the FCC process in this case has to ensure the removal of oxygen from the bio-based feedstock by dehydration, decarboxylation, and decarbonylation because the final product should be substantially oxygen-free to meet the requirements for motor fuels [18, 93]. FCC equilibrium (E-CAT) catalysts which are used in refineries demonstrate high effectiveness in this kind of reactions. Such typical catalysts usually contain 10–30 wt% faujasite zeolite (USY or REUSY) dispersed in a matrix consisting typically of silica–alumina, alumina, clay (kaolin) and special additives (*i.e.,* NO_X reduction additives, gasoline sulfur reduction additives, CO combustion, promoters, ZSM-5 as an additive to produce light olefins).

In most cases, the FCC co-processing of petroleum and vegetable oils or bio-oil proceeds in presence of refinery-generated equilibrium catalysts (E-CAT) (Tables 6 and 7) which are very effective in the production of valuable reaction products as well as in removing oxygen from the biomass by transformation into CO_2, CO, and water without using hydrogen [18]. Nevertheless, several studies tried to answer the question in which respect the addition of other catalysts changed the conversion of the blends and the distribution of the reaction products. Dupain et al. [127] found that the addition of ZSM-5 enhanced the cracking of vegetable oils thus resulting in higher gas yield but lower LCO and gasoline yields compared to the E-CAT alone. Similar results were obtained in [65]. However, no data was provided for the comparative co-processing experiments without/with ZSM-5 addition to the E-CAT.

Abbasov et al. [63] investigated the co-processing of VGA and vegetable oils using the mixture of E-CAT and halloysite nanotubes (natural clay nanotubes with large 5–20 inner lumen) as a catalyst. It increased the conversion of the feedstock by 3–5% which contributed to the additional increase in the gasoline and LPG at the expense of the LCO. The addition of the halloysite also promoted the efficiency of skeletal isomerization, resulting in the increase of branched paraffins and alkyl benzenes. Moreover, the coke yield was reduced by 7–10% due to the faster desorption of the reaction products from the nanotube mesopores. It was, therefore, concluded that the blends of E-CAT and halloysite nanotubes represented an improved catalyst for the mixtures of heavy petroleum distillates and vegetable oils which ensured the increase of aromatic content and the gasoline octane number rating by two units.

Moreover, studies on the possible relationships between the catalyst structure (nature and composition of the catalysts) and the co-processing performances are also known. Fogassy et al. [55] investigated the effect of the catalyst structure on the quality of the products formed by the co-processing of HPO with VGO. They performed a detailed mechanistic study on the possibility of biofuel production by co-processing in comparison with pure vacuum gas oil (VGO) processing using three different porous materials containing micropores and/or mesopores, FCC, HY and HZSM-5. The structure of the zeolites, in terms of pore size and Si/Al ratio (unit cell size), was found to influence the catalytic cracking reactions both for the VGO and for the VGO/HPO feed and thus to affect the conversion level and the product distribution. It was suggested that VGO/HPO co-processing leads to lower product formation rates than the processing of VGO alone, except for the coke formation and the formation of more unsaturated components (essentially aromatics). The data for both VGO cracking and co-processing followed the published trends with acid site density. These results were explained by the restricted access of the oxygenated compounds from HDO, like the heaviest VGO molecules, into the zeolite pores. Therefore, pre-cracking and deoxygenation (dehydroxylation and decarbonylation) occurred on the extra-framework structure (silica–alumina matrix or EFAL deposits for steamed samples). This process resulted in coke formation; indeed, due to their polar nature and fully accessible basic oxygen electronic doublet, the oxygenated compounds originating from the HPO adsorb much more strongly on the active sites (Brùnsted and Lewis acid sites) than the less polar hydrocarbons [138]. This excessive coke formation led to pore blocking and lower reaction rates. Another key mechanistic feature explaining the observed effects of co-processing on the product quality was the competition for hydrogen (protons or hydrides) through the zeolite interface, required by the oxygenates cracking process. This resulted in an increase in olefins and aromatics as well as the LPG fraction and more bottom and coke formation. Based on these findings, the authors suggested the existence of a high interest to tune the zeolite structural parameters in order (i) to increase the methoxy-phenol conversion and (ii) to decrease the coke deposition from oxygenates.

5. Product quality

As the hydroprocessing of lipids renders a paraffinic fuel, it is obvious that an increase in the bio-based content in the blend results in lower densities of the final hybrid fuel as a part of the produced hydrocarbons are paraffins with low density [37, 81]. During the co-hydroprocessing of straight run gas oil (SRGO), light cycle oil (LCO) and animal fats, the addition of LCO to SRGO increases the density because of its high aromatic content, but the addition of waste fat offsets that [4]. Obviously, the density of the hybrid products was reduced as an effect of the triglyceride conversion and the aromatics saturation. In general, lipids transformed mainly in the C_{15}–C_{18} n-alkanes and their densities are much lower (740–770 kg/m^3) compared to conventional diesel fuels [35].

As far as the effect of triglycerides on the sulfur content of the final product is concerned, the effect is not yet clear. Some studies claim that the sulfur content of the organic product decreased with the addition of a bio-based feedstock. As lipid-based feeds are virtually sulfur free, their addition results in lower sulfur content of the blend which may be responsible for lowering of the sulfur content in the liquid products, typically diesel. Baladincz and Hancsok [37] found that during co-hydroprocessing, the triglyceride content is converted to paraffins and the sulfur, nitrogen and oxygen content of the feedstock are decreased. Bezergianni et al. [45] noticed that HDS reactions are not affected by the addition of waste cooking oil in the feedstock which is in agreement with the results of Huber et al. [30] who claimed that the hydrotreating of vegetable oil and HDS probably occurs on different catalytic sites that were, however, not specified. On the other hand, according to Toth et al. [29], oxygen containing compounds (triglycerides, other oxygen containing products) bind strongly to the active sites of the desulfurization catalyst and hence limit the desulfurization reactions. Consequently, when higher vegetable oil contents were used, the sulfur content in the products increased. An amount of vegetable oil higher than 15% reduced the desulphurization efficiency, indicating that the removal of both heteroatoms (S and O) took place on the same active sites of the catalyst. Hence, the deoxygenation reactions restricted the desulphurization reactions because of the intake of large quantities of oxygen with the triglyceride molecule of the vegetable oil [139].

Another important property of the resulting middle distillate that is affected by the lipid content in the co-processing feed is the CFPP (cold filter plugging point). The higher the lipid content, the higher the CFPP, due to the paraffinic nature of the hybrid fuel [29]. As normal paraffins have a high melting point, their presence in the diesel fuel negatively affects the CFPP, which is a critical parameter for winter operability. During the co-hydroprocessing of waste animal grease and LCO, a positive correlation was observed between the CFPP value of the product and the content of the grease in the feed [41]. According to Toth et al. [81], only the products derived from less than 10% rapeseed oil containing feedstocks were able to meet the European standard for summer quality diesel fuel in temperate zones (EN 590). Balandincz and Hanscok proposed the addition of an isomerization step to improve the CFPP properties of the final product [37]. The problem of poor cold flow properties can also be tackled using proper “cold flow improvers” for decreasing the size of the wax crystallites, during the cooling of the fuel or inhibiting the wax formation starting [45]. However, it has been reported that the conventional commercial cold flow improvers are inefficient when the content of bio-derived paraffins exceeds 10% [140].

The total aromatics content of the final products decreased compared to that of the petroleum feedstocks because the lipid-based feeds are aromatics free [4, 81]. Furthermore, during the co-hydroprocessing of gas oil with triglyceride feedstocks, the aromatics and PAH content decreases in comparison with gas oil feed only due to the transformation of triglycerides to alkanes [35]. This gives the advantage to refineries to produce lower aromatic products, which will be more and more valuable if the future regulations will continue becoming stricter and yet a lower limit for total aromatics in diesel fuel will be imposed.

In addition, paraffins, originating from the deoxygenation of the lipids in the feed, increase the cetane number/index of the fuel [36, 37], as long chain paraffins have the best ignition quality characteristics between the hydrocarbons. According to experiments by Chen et al. [38], the cetane index of the corresponding diesel fraction from hydrocracking of heavy vacuum gas oil was 40 and it increased to 55 when a blend containing 20% of canola oil was upgraded, improving the quality of the diesel product in this way.

As far as kinematic viscosity is concerned, it decreased with an increasing temperature and pressure, due to the triglyceride conversion, the aromatics saturation and cracking reactions [37]. Furthermore, an increase in the products’ viscosity was also observed with the increase in the concentration of the triglycerides in the feedstock [81]. This happens because a higher triglyceride containing feedstock crates more viscous n-paraffins.

Being glyceryl esters of fatty acids (triglycerides), lipids contain a significant concentration of chemically-bound oxygen (10–14%). The oxygen moiety reacts under normal hydrotreating conditions with hydrogen to form water or is released as CO_2. If water is formed in large quantities it may adversely affect the catalyst by weakening it, or may cause a redistribution in the active metals and loss of surface area due to phase transformation of the support. However, at blending ratios up to 10%, the oxygen content is below 1.5 wt% and,

Table 9
Properties of hybrid fuels from the co-hydroprocessing of lipids.

Biomass feed	Petroleum fraction	Yields, wt%	Density, kg/m^3	*S*, wppm	*N*, wppm	Cetane index	Kinematic viscosity, mm^2/s	CFPP, °C	Remarks	Ref.
Canola oil	HVGO	36–40		20–600	5–160	40–55			S and N content depends on the blend and the product (diesel or gasoline)	[38]
Waste soya oil	GO	80–90	820–860			43–54			Depends on catalyst and conditions	[48]
Jatropha oil	Straight run diesel fraction	~90	840–823	219–309			3.332–3.692		Depends on catalyst CoMo or NiMo	[33]
Rapeseed oil	Straight run vacuum distillate	98–99	807–827	9–12	8–11	57–60	2–3.2	−27 to −19	Depends on *T* (°C)	[71]
Rapeseed oil	Light gas oil	~95	834–836				2.86–3.74		Depends from the conditions	[34]
Waste animal grease	Straight run gas oil + light cycle oil	78	825	4.9	8.7	≥51	2.56	−4	Optimum blend 75% SRGO, 10% LCO, 15% grease	[41]
Waste lard	Heavy gas oil	91–94	838–844	38	3	55	4.5–4.55	8	2-stage co-hydroprocessing	[37]

thus, it is unlikely to form enough water to cause significant problems.

Studies have shown that the addition of lipid-based feeds into an existing refinery improve the product quality [45]. Co-hydroprocessing is a key technology to produce high quality hybrid fuels that meet fuel specifications. A very important issue is the selection of the appropriate catalyst or a combination of catalysts to ensure petroleum grade HDS at the requested level below 10 ppm and, also, to be able to transform triglycerides to hydrocarbons. Hydroprocessing of lipid feedstocks converts triglycerides into normal paraffins. As a result, in the case of co-hydroprocessing, the increase of lipid content results in higher paraffinic content in the final product. This leads to a final product with a higher cetane number and heating value which improves the combustion efficiency of the engines. However, if the content of lipids is too high, then problems with cold flow properties will occur. Table 9 presents the properties of hybrid fuels from various studies.

Aromatic and naphthenic hydrocarbons, together with both linear and branched paraffins and olefins, are the main products of the FCC of petroleum fractions. Since in the co-processing of petroleum-derived and bio-derived feedstocks, the resulting feedstock mixture mostly consists of the former component, the quality of the produced gasoline and diesel fractions are mostly determined by the characteristics of the petroleum feed and reaction conditions. Nevertheless, the presence of oxygen atoms and unsaturated bonds in the bio-based feedstock affect the cracking process as well as the hydrogen consumption through hydrogen transfer reactions.

The fraction of aromatic hydrocarbons and polar aromatics (large molecular phenols and aromatic acids) in the FPO are considered as the primary sources for the formation of aromatic hydrocarbons during the bio-oil co-feeding with a petroleum distillate [99]. The composition of bio-gasoline produced during the FCC co-processing of LCO and FPO in a MAT unit was compared to that of an ordinary FCC gasoline. The main differences consisted in the lower amount of olefins and naphthenes, while the content of the total aromatics, especially toluene, was higher when co-processing FPO. It contributed to a rise in the RON from 92.2 for an ordinary FCC gasoline to 95.8 for a bio-gasoline. Consequently, it was suggested [99] that the composition of the bio-gasoline produced by the FCC co-processing of FPO was compatible with the EU specifications for an environmentally acceptable gasoline.

Pinho et al. [53] investigated the properties of a gasoline fraction produced by co-processing of VGO and FPO in a demonstration-scale FCC unit in detail. The benzene and total aromatics concentration increased from 0.8 to 1.4 and from 38 to 44 wt%, correspondingly, when increasing the content of VGO from 67% to 74%. Nevertheless, heavy cracked naphtha (HCN, 80–220 °C) produced from a blend containing 20% of bio-oil contained more aromatics than that produced from neat VGO (53.8 wt% and 50 wt%, respectively). Consequently, the octane numbers of the HCN cuts increased when the FPO was added to the VGO as a co-feed from 83.3 to 84.4 (MON) and from 95.8 to 96.5 (RON). Phenol and alkylphenols were identified and quantified in gasoline derived from the co-processing of VGO and FPO by ion chromatography. Nevertheless, it was suggested that the presence of these compounds might only be barely harmful to the gasoline quality because the phenolics are traditionally believed to stabilize the cracked gasoline and increase its octane number [53].

Bielansky et al. [51, 64] found that liquid products formed during the FCC co-processing of VGO with rapeseed oil in all ranges of feedstock compositions (0–100%) were practically oxygen free while water and carbon dioxide were the only oxygen-contained by-products of the RSO cracking. The analysis of the gasoline range of the pure VGO and pure rapeseed oil feedstocks showed that the content of the aromatics and olefinic naphthenes increased while the naphthenes, n-olefins and i-paraffins declined. The increase in the RSO content in the feedstock was accompanied by an increase in the RON and MON up to approximately 100 and 86, respectively, reported for the neat rapeseed-oil-derived gasoline. Moreover, the oxidation stability increased at higher rapeseed oil admixtures, and a necessary value of 360 according to EN228 could be reached without any further refinement steps with RSO rich blends.

6. Sustainability

6.1. *Co-hydroprocessing*

The current biofuels market has become much more transparent in comparison to its early stages. Until 2020 the key production and consumption region of biodiesel will be the European market. There are many benefits of biofuels including domestic production of fuels, decreased greenhouse gas emissions, decreased dependence on fossil fuels, improvement of rural economies and increased national security [4, 80].

The conventional HVO investment and operating costs involving the stand-alone hydrotreating of lipid feedstocks have been reported to be about 50% lower than the FAME costs by some [141, 142] while others have reported the costs to be comparable with those of FAME installations of the first generation biodiesel technologies [11, 143, 144] depending on the feedstock costs and by-product revenues. The corresponding hydroprocessing by-product, propane, is not so versatile and may not reduce the cost of HVO much. However, the cost of the catalytic hydroprocessing can be reduced by locating the plant at an existing petroleum refinery [142, 145]. Based on the same study, according to petroleum refineries, the modification cost of an existing hydrotreating unit to produce HVO is small, lowering the overall cost of the technology in this way. Another important aspect of HVO is that stand-alone hydroprocessing of lipids requires a two-stage process, consisting of mild-hydrotreating followed by an isomerization stage [146–148] leading to a high operating cost mainly due to the requirements for the hydroprocessing catalyst and hydrogen. Furthermore, by using a residual lipid-based feedstock such as waste cooking oil or animal fats, the production costs of the final diesel product (including 7% v/v HVO biofuel) reduce compared to the current market diesel scenario where diesel fuel contains 7% v/v FAME biodiesel. This is obvious as the production cost of the HVO biofuel from waste cooking oils is lower than that of FAME from fresh oils. In addition to that, the costs of the hydroprocessing lipid feedstocks are in some studies stipulated to be about 50% of the transesterification processing costs [141, 142]. Moreover, the use of residual biomass further reduces the production costs of the final diesel blend as according to the Directive 2009/28/EC, residual biomass feeds are eligible for double counting [149]. For instance, 3.5% v/v HVO (from residual lipids) counts as 7% v/v biofuel in the final diesel blend reducing the cost of the final market diesel in that way. In addition to that, methane which is a by-product of stand-alone hydroprocessing is a valuable gas that can also be sold on the market increasing the profits of the refinery, while propane, which is also a by-product of the process, can be processed by steam reforming to cover a part of the extra hydrogen needs for hydroprocessing of lipids. Finally the possibility of integrating H_2 from renewable energy sources could possibly further diminish the production cost of stand-alone hydroprocessing [150]. However, the high investment cost for new constructions makes this technology profitable only for large scale production. Finally, another important issue that raises the production cost of HVO is the transportation cost of feedstock which can be faced by constructing the unit close to feedstock provider companies [26].

The economic limitations of stand-alone hydroprocessing bio-based feedstock can be overcome via co-hydroprocessing of lipid-based feeds with petroleum fractions. This approach enables the use of existing refinery infrastructure, maintaining the same operating conditions, producing the same quality products and avoiding the establishment of parallel systems, which reduce capital and operating expenditures (CAPEX and OPEX, respectively) [30, 106]. The more beneficial option from an economic point of view is to add a small amount of lipid-based feedstock in an existing petroleum refinery for co-hydroprocessing with a fossil stream as shown in Fig. 2. This would allow the refineries to meet national mandates on biofuels. The final product is already in the diesel, gasoline, jet range, *etc.* with very good properties as was discussed in Section 5.

However, the addition of lipid-based feeds into a refinery results in an increase of hydrogen consumption. For example, Jatropha oil has an oxygen content 10–11 wt%, on the other hand, straight run diesel (LAGO) fraction has a sulfur content 0.5–2 wt%. According to a recent study [33], when adding Jatropha oil to LAGO fraction, the amount of oxygen introduced to the catalyst was higher than the decrease in sulfur content in the feed. As a result, to remove oxygen and sulfur as H_2O and H_2S, the hydrogen consumption was increased. Furthermore, the hydrogen consumption also depends on the type of lipids, highly saturated fatty feedstock sources (such as tallow and palm oil) that require less hydrogen than more unsaturated feedstock options (such as rapeseed) [144]. Consequently, the careful choice of lipid feedstock could result in lower hydrogen demands. The hydrogen consumption is an important issue from an industrial point of view; a process with lower hydrogen demands would be more economical. It may be possible for a typical diesel hydrotreater to easily co-process low amounts of lipid-based feeds (10%) with their existing conditions with a nominal increase in hydrogen consumption [48], for example, the addition of 5–10% of WCO increased hydrogen consumption by just 6.25% (Fig. 3), indicating that WCO integration up to 10% can be achieved without significant operating cost increase [45]. Another possible way to decrease hydrogen consumption is by selecting a more appropriate catalyst. From the reaction stoichiometry point of view (Fig. 4), hydrodeoxygenation is more hydrogen-demanding (*ca.* 4 times more) than decarboxylation/decarbonylation reactions, as hydrodeoxygenation is more favored over the NiMo catalyst than over NiW catalyst, the use of NiW catalyst seems to be a better choice for reducing the hydrogen consumption during co-hydroprocessing [72]. Nonetheless, this is true only when the consecutive reduction of CO_2 to methane can be avoided. If not, the decarboxylation pathway with complete the CO_2 reduction to methane and would consume more H_2 than the hydrodeoxygenation route [101, 111]. In addition to the catalyst choice, hydrodeoxygenation/decarboxylation selectivity can be affected by reaction conditions, most notably hydrogen pressure [151]. Furthermore, Kalnes et al. [11] mention that fossil energy use in HVO production can be reduced by producing H_2 from by-products like propane.

Another advantage of co-hydroprocessing is the reduction of production cost when waste lipids are used. The addition of 5–10% waste cooking oil or waste animal fats into the refinery leads to high economic benefits for the refinery. The cost of waste cooking oil or waste animal fats is much lower compared to the cost of fossil fuel and FAME biodiesel. Thus, by replacing 5–10% of fossil fuel or FAME biodiesel content with waste cooking oil the economic benefits of the refinery increased proportionally with the waste bio-content [152]. In addition to that, as it was already discussed in a previous section, straight run gas oil with light cycle oil, which is a low-quality fossil feed, in blends with lipid-based feedstocks can be co-processed. In this way, saving of crude oil could be reached with the increased use of LCO for diesel fuel production instead of straight run gas oil which is used for automotive fuels. As a result, more automotive fuels can be produced from straight run gas oil [4].

Due to the increased hydrogen consumption in co-processing, different hydrogen resources have to be carefully considered. Considering the overall sustainability, renewable resources should be preferred. A possibility that is easy to implement even in the current refineries is the steam reforming of propane and methane formed during co-hydroprocessing [153, 154]. A promising hydrogen production route might be the aqueous phase reforming relying typically on carbohydrate solutions originating, *e.g.*, from the processing of lignocellulosic biomass or by-products such as glycerol from other processes [155-158]. Sugar concentrations of up to 60% were used and an efficiency (defined as lower heating value of the produced hydrogen divided by the lower heating value of the feedstock) of > 55% was achieved [156]. Catalyst stability and moderate space-time yields still need to be further improved [156]. Moreover, according to a research project in Greece “Biofuels 2G” [150], another possibility to reduce the cost of the process is to use solar hydrogen to cover the extra hydrogen needed for co-hydroprocessing. This technique has an extra investment cost for a solar hydrogen production unit which, however, has a good pay-back time and could decrease the overall cost of the process [152]. Finally, increased hydrogen demands for co-processing are less important for some refineries that have excess hydrogen produced by natural gas steam reforming. To conclude, the role of lipids is not to totally replace the fossil fuels, but only part of them as sustainably available lipids are not abundant enough. Consequently, the extra H_2 demands for their co-hydroprocessing are not so high and can be covered with the methods described above.

The increased hydrogen consumption due to co-processing is closely related to the blending ratio. While the reports show that hydrotreating feeds containing up to 30% of lipids is technologically feasible, the availability of a suitable, *i.e.*, sustainably obtained, biomass has to be kept in mind. Unlike fossil fuels, a biomass is typically a seasonal product, and hence it is not a simple question of absolute amounts available, but also of the time when it is available. As average refinery hydrotreating capacity exceeds 30 thousand barrels per day [159], only low continuous blending ratios, *i.e.*, $<$ 5% of bio-components in fossil fuel fractions, seem to be realistic. Due to the seasonal aspects, higher temporary blending ratios could be, however, expected.

Finally, there are some technological and market challenges in biofuels production that remain, however, they are not insurmountable. The most important is the storage and handling of the feedstock due to lower thermal and oxidation stability of lipids and bio-oils. The corrosion of the process equipment and the poisoning of the catalyst due to corrosive properties and impurities (such as alkali metals) of bio-based feedstock and the higher cost of biomass in a period of low crude oil prices make biofuels less competitive [160].

In general, by comparing the two alternatives, *i.e.*, stand-alone HVO production with co-processing of lipid-based feedstocks with petroleum fractions, it is obvious that the second approach is economically more attractive. This is a consequence of investment cost being very small as there are no requirements for a new unit construction as in the case of "stand alone" processes. Hence, the profits for a refinery might be substantial.

From a biomass availability point of view, the main challenge is how to supply the necessary quantities to a refinery. Other challenges include the seasonal and geographical variation of the biomass feedstock composition and properties and the establishment of suitable transportation chains. These issues can be addressed by locating low-capacity biorefineries close to biomass-producing areas, thus reducing the transportation cost. Another possible option is to create temporary storage biomass facilities before the transportation to the refineries. In general, there are some studies that have developed mathematical models aimed at building an efficient logistic system [161–163].

As far as GHG emissions are concerned, the use of lipids for co-processing results in lower GHG emissions compared to pure fossil hydroprocessing [152] However, GHG emissions reduction depends on the source of lipids. More specifically, waste feedstock sources are better than native feedstock because of the smaller upstream impacts. Waste cooking oils have low energy demand which is related to the collection of the oils and pretreatment. Regarding tall oil, it was concluded by Tornvall et al. [164] that it is preferable from an environmental point of view instead of rapeseed in an energy and GHG perspective. According to Sunde et al. [144], tall oil is the most feasible feedstock, followed by used vegetable or cooking oil. Tall oil is a byproduct or waste from the main process of pulp production, for this reason it only carries the environmental loads related to the treatment of black liquor. Palm oil is cultivated with best practice on fallow or degraded land without soil losses, due to its high yields; it has favorable environmental profile compared to other vegetable oils [165]. Rapeseed oil may, however, perform better in cases where palm oil production is related to high soil carbon emissions or when the palm oil production processes are not environmentally optimized. The rapid increase in demand for palm oil has resulted in the clearing of rainforests to establish palm oil plantations with ecological impacts due to loss of rainforest biodiversity and pollution [166]. The clearing of rainforests or usage of peaty soil for palm oil production may create large soil carbon debts that may take decades to pay off [167, 168]. It is obvious that there are many aspects that influence the GHG emissions when the co-processing of lipid based with fossil-based feedstocks takes place. To conclude, a recent study from California Air Resources Board [160] proposes options for the quantification of low-carbon fuel mass/volume and for estimation of carbon intensities for fuels produced through co-processing. This study presents a preliminary framework and methods for estimating low-carbon fuel content of co-processed fuels for consideration and feedback from stakeholders.

6.2. *FCC co-processing*

When evaluating the concept of co-processing bio-oil with petroleum fractions in FCC units, it is important to not only consider the quantitative parameters (reaction conditions, the overall conversion, the yield of different fractions) and the qualitative evaluation of products composition and properties, but also to get an understanding on the amount of renewable carbon that is being effectively concentrated in the liquid fractions. For this purpose, the ^{14}C (renewable carbon) concentration is determined by accelerator mass spectrometry combined with isotope ratio mass spectrometry [53, 54, 56]. Fossil fuels are virtually ^{14}C-free, while bio-oil contains the present-day "natural" amount of ^{14}C. Fogassy et al. [56] showed that an initial 8.5 wt% bio-carbon content of the initial mixed feed composed of HPO (10 wt%) and VGO (90 wt%) was not statistically distributed among the products. Thus, the gas and especially the coke fractions contained significantly more bio-carbon than expected from the statistical distribution (10.6 wt% and 15.8 wt%, respectively). In contrast, the total liquid fraction (including the unreacted feed) a bio-carbon content lower than the initial feed content (7.5 wt%). After correction for the unconverted liquid fraction, which represents the LCO and bottom fraction, and assuming these fractions still contained the initial 8.5 wt% of bio-carbon, the content of the renewable carbon in the liquid product, gasoline, was even lower, about 7.2 wt%. Similar results were also obtained by Wang et al. [54] in the study of co-processing of CPO with VGO. The authors found that the renewable carbon in the gasoline product was about 7 wt%, while the bio-carbon in LCO fraction was slightly higher (7.3 wt%). The difference was explained by the increased polyaromatics content in the latter fraction.

Pinho et al. [53] pointed out that when 20% FPO was co-processed with a petroleum fraction, the renewable carbon content in the gasoline cuts varied between 3 and 5 wt%, whereas the biocarbon in the heavier cuts, *i.e.*, the LCO and bottoms, was 5 and 6 wt%, respectively. For 10 wt% FPO in the feed, 2 wt% renewable carbon were obtained in the total liquid product. Considering that the carbon content in the FPO was 42.35 wt%, the catalytic cracking produced a liquid effluent with approximately one-third of the renewable carbon present in the bio-oil. The same result was obtained using either 10% bio-oil or 20% bio-oil, *i.e.*, approximately one-third of the renewable carbon (on weight basis) present in the bio-oil was preserved in the liquid effluent. Recent results of the same authors [130] provided further evidence that for a similar reference feed (VGO), FCC conditions, and bio-oil origin approximately one-third of the renewable carbon from the bio-oil ends up in the liquid products for a bio-oil usage between 5 wt% up to 20 wt%. Like in co-hydroprocessing, large industrial FCC installations with an average capacity of nearly 40 thousand barrels per day [159], combined with the local biomass availability will not allow such large blending ratios on a continuous basis. Hence, less than 5% of bio-components in the feedstocks seem to be attainable on a continuous basis.

Research activities related to the co-processing of petroleum-derived and biomass-derived feedstocks under FCC conditions is a new area having a big potential to grow. The production of renewable fuels may be driven by several forces, including the unpredictable change of petroleum prices, governmental mandates and subsidies as well as commitments to Green House Gas reduction. Despite these incentives, current growth in the production of renewable fuels marginally meets expectations; moreover, little integration of renewable fuels with petroleum refineries is observed [169]. This increases the cost of production, since it does not take advantage of any existing infrastructure for the production and distribution of fuels. No doubt that additional economic prerequisites have to be created for the intensification of biofuel production in existing oil refineries.

The broad availability and low cost of biomass-derived feedstock are essential prerequisites for the economic efficiency and, consequently, the successful development of renewable fuel technologies. In this respect, the production of vegetable oil worldwide is very promising: it is constantly increasing and exceeded 185 million metric tons in 2016/2017 [170]. Mostly, vegetable oils are used in the food sector. Nevertheless, the global consumption of major vegetable oils (food *versus* industrial uses) can vary significantly and depends on the type of vegetable oil. Olive, sunflower, cottonseed oils are predominantly used in the food sector while palm kernel oil is mostly used in industrial applications, and coconut, rapeseed and soybean oils occupy an intermediate position [171]. Due to the significant consumption of vegetable oils in the food sector they could only replace a very small fraction of transportation fuels. Nevertheless, the ever-increasing demand for biofuels has a significant effect on the ratio between the food and industrial uses of vegetable oils. In turn, the necessity to increase the involvement of vegetable oils in the production of biofuels affects the cost of vegetable oils. In general, there is a good correlation between the price of vegetable oils and crude oil, which began to be noticeable about 10 years ago. The prices of energy and agriculture products are interrelated for two main reasons [172, 173]. Firstly, they are related via production costs as many agricultural products are energy intensive due to the high energy content of the fertilizers and other chemicals used and due to the high costs of harvesting and transport relative to the value of production. Secondly, they are related via substitution with biofuel varieties. According to Mitchell [173], biodiesel was responsible for approximately one-third of the increase in vegetable oil consumption in 2004–2007. In recent years, the cost of vegetable oils is in the range of 0.45–0.65 USD/l [169, 174] being higher than the current price for crude oil in the range of 0.3–0.4 USD/l. Based on these values, a conclusion is made that at current prices of vegetable oils and the limited availability of this kind of biomass, it is not attractive for producing biofuels without government subsidies [169].

Lignocellulosic biomass has a major advantage over vegetable oils in its larger availability and lower cost. Globally, more than 90% of plant biomass consists of lignocellulose and amounts to about 200×10^9 metric tons/year, among which 4–10% has an immense potential for biofuel generation [175]. Several studies reported the cost of producing bio-oil via fast pyrolysis to range between 0.11 and 0.65 USD per liter [176–179]. The broad availability of a lignocellulosic biomass and the low cost of its transformation to FPO makes this feedstock potentially attractive for its FCC co-processing with petroleum fractions. Nevertheless, it is assumed that FPO processing requires more commercial development and is also limited by the availability of pyrolysis oil, since commercially it is still in its infancy. In the long term, however, the focus must be on the effective utilization of cellulosic biomass [169]. It is worth noting that a lack of information is available on the cost of FPO upgrading to produce more stable and less oxygenated bio-oils, for example, by a hydrogenation step. Moreover, several other issues may affect the economic and operational viability of co-processing [180]:

- Differences in the stability of the biogenic feedstocks during storage and handling.
- The presence of water and oxygenated organic compounds in the biogenic feedstocks which can cause equipment corrosion and can affect yields and conversion rates.
- The potential for alkali metals in biogenic feedstocks to deactivate catalysts.
- Differences in yields between pilot and commercial scale projects.

Some of these problems can be mitigated based on findings from ongoing research and development activities. These can be carried out by using equipment varied in size, as shown in the previous sections. Accordingly, the obtained results being used for the feasibility studies may vary in dependence on the capacity of an experimental unit. Therefore, despite the successes in the co-processing of bio-derived and petroleum-derived feedstocks in a demonstration scale FCC riser reactor [130], more experimental data is needed for further optimization of the whole process.

7. Conclusions

The current biofuels market has become more transparent in comparison to their early stages. There are many benefits of biofuels including the domestic production of fuels, decreased greenhouse gas emissions, decreased dependence on fossil fuels, improvement of rural economies and increased national security. The co-processing approach enables the use of the existing refinery infrastructure while maintaining the nominal operating conditions, producing high quality products and avoiding the establishment of parallel systems, which consecutively reduces CAPEX and OPEX. The more beneficial option from an economic point of view is to add a small amount of bio-based feedstock in an existing petroleum refinery for co-processing with a fossil stream. This would allow the refineries to meet national mandates on biofuels. One of the main advantages of co-processing is the ability to combine a variety of bio- and fossil-based feedstocks/fractions without compromising product quality. Moreover, fossil resources are saved because of co-processing that can be used in other processes. There are two main technologies that could be used for co-processing of biomass feedstock with petroleum fractions, the first one is catalytic hydroprocessing and the second one is fluid catalytic cracking (FCC). Both technologies are found in virtually any conventional refinery.

The most commonly used fossil-based feeds for co-processing are straight-run gas oil (SRGO), light atmospheric gas oil (LAGO), heavy atmospheric gas oil (HAGO) and heavy vacuum gas oil (HVGO). The fossil-based FCC feedstocks suitable also for co-processing applications include distillate fractions, such as vacuum- and heavy vacuum gas-oils or FCC cycle oils, as well as atmospheric distillation residues. Triglycerides present in vegetable oils, waste oils or animal fats are characterized as a suitable raw material for high quality fuels production. The most common edible oils for co-hydroprocessing are palm oil, rapeseed oil, soybean oil, sunflower oil, while Jatropha oil is the most common non-edible oil. As far as residual feedstocks are concerned, several types have been studied such as used cooking oils/waste cooking oils, waste soya oil, waste vegetable oils and animal greases. In addition to lipids, bio-oil has been recently been considered as a promising alternative bio-based feedstock due to its favorable origin from non-food biomass. In general, bio-oil can be obtained by fast heating of a solid biomass, typically a lignocellulosic biomass including wood, forestry and agricultural residues.

The most important factors of co-hydroprocessing are operating conditions, *i.e.*, reaction pressure, reaction temperature, space velocity and hydrogen-to-oil ratio, and catalyst. It may be possible for a typical diesel hydrotreater to easily co-hydroprocess low percentages of lipid-based feeds ($<$ 10%) under nominal conditions with only a marginal increase in hydrogen consumption. Catalysts used in the co-hydroprocessing with lipids are common hydrotreating catalysts based on cobalt-molybdenum (CoMo) and nickel-molybdenum (NiMo). Other types are NiW catalysts while the effect of zeolite beta (BEA) content in NiMo catalyst has also been explored. Finally, another approach is to combine various compositions of hydrogenation catalysts in the catalyst bed. Unfortunately, there is a lack of literature in the co-hydroprocessing of pyrolysis bio-oil with fossil-based feedstocks. The most commonly used catalysts for the co-hydroprocessing of pyrolysis bio-oil with fossil-based feedstocks up to now are $CoMo/Al_2O_3$ and $NiMo/Al_2O_3$, however, further studies with different types of catalysts should be undertaken in the future to better understand the effect of catalyst type on the extent of HDO and HDS reactions.

Furthermore, studies have shown that the addition of lipid-based feeds into an existing refinery improves the product quality. Co-hydroprocessing is a key technology to produce high quality hybrid fuels that meet fuel specifications. Another advantage is the reduction of the production cost when waste lipids are used. The addition of 5–10% waste cooking oil or waste animal fats into the refinery leads to high economic benefits for the refinery. As far as GHG emissions are concerned, the use of lipids results in lower GHG emissions compared to pure fossil hydroprocessing. Nonetheless, it has to be kept in mind that co-processing results in an increased H_2 consumption in comparison with the hydrotreatment of fossil fractions.

Considering FCC co-processing, processes that take place in the FCC reactor are based on several types of reactions, including (protolytic) cracking, hydrogen transfer, and isomerization. The same reactions should apparently occur in the case of the co-processing of petroleum and bio-based feedstocks. When evaluating the concept of co-processing bio-oil with petroleum fractions in FCC units, it is important to consider not only the quantitative parameters (reaction conditions, the overall conversion, the yield of different fractions) and the qualitative evaluation of products composition and properties, but also to get an understanding on the amount of renewable carbon that is being effectively concentrated in the liquid fractions. Research activities related to the co-processing of petroleum-derived and biomass-derived feedstocks under FCC conditions is a new area having a big potential to grow.

Different bio-oils (HPO as well as CPO and FPO) may be considered as promising bio-additives to petroleum-derived feedstocks for FCC co-processing. Nevertheless, considering results from different studies, it is difficult to evaluate the efficiency of different bio-oils as a bio-additive in the co-processing and to make any conclusion about the influence of the type of bio-oil on the co-processing characteristics because of the differences in the properties of the bio-oils, reaction conditions, *etc.* Hence, publications dealing with comparative studies on the co-processing of differently prepared bio-oils with petroleum feeds at similar conditions are of an increased interest.

Today, petroleum refineries already have a well-developed infrastructure to produce fuels and base chemicals and, consequently, would not require additional intensive investments for the processing of alternative feedstocks. In general, co-processing either via hydroprocessing or FCC-processing is a very promising technique to integrate bio-based feedstocks in a petroleum refinery for hybrid fuels production, which in some cases already has found its practical realization. The benefits for a refinery are plenty, not only in reducing the associated GHG emissions, but also in enabling the gradual independence from fossil sources, rendering low-carbon-highly-sustainable fuels.

References

[1] Hancher L, Winters BM. The EU winter package, briefing paper, February 2017. Allen & Overy LLP 2017, 2017, p. 1–17.

[2] Diya'uddeen BH, Aziz ARA, Daud W, Chakrabarti MH. Performance evaluation of biodiesel from used domestic waste oils: a review. Process Saf Environ Prot 2012;90(3):164–79.

[3] Swain PK, Das LM, Naik SN. Biomass to liquid: a prospective challenge to research and development in 21st century. Renew Sustain Energy Rev 2011;15 (9):4917–33.

[4] Sagi D, Baladincz P, Varga Z, Hancsok J. Co-processing of FCC light cycle oil and waste animal fats with straight run gas oil fraction. J Clean Prod 2016;111:34–41.

[5] Viguie JC, Ullrich N, Porot P, Bournay L, Hecquet M, Rousseau J. BioTfueL project: targeting the development of second-generation biodiesel and biojet fuels. Oil Gas Sci Technol – Rev D Ifp Energies Nouvelles 2013;68(5):935–46.

[6] Hari TK, Yaakob Z, Binitha NN. Aviation biofuel from renewable resources: routes, opportunities and challenges. Renew Sustain Energy Rev 2015;42:1234–44.

[7] Primo A, Garcia H. Zeolites as catalysts in oil refining. Chem Soc Rev 2014;43 (22):7548–61.

[8] Aatola H, Larmi M, Sarjovaara T, Mikkonen S. Hydrotreated Vegetable Oil (HVO) as a renewable diesel fuel: trade-off between NOx, particulate emission, and fuel consumption of a heavy duty engine. SAE Int J Engines 2009;1(1):1251–62.

[9] ConocoPhillips begins production of renewable diesel. Biodiesel Magazine; 2007, http://www.biodieselmagazine.com/articles/1481/conocophillips-begins-production-of-renewable-diesel; [accessed 23.08.2017].

[10] Azevedo JSd. Presentation in biofuels Houston summit III. Houston; 2008.

[11] Kalnes T, Marker T, Shonnard DR. Green diesel: a second generation biofuel. Int J Chem Reactor Eng 2007;5. Article A48.

[12] Rekoske J. Sustainable aviation fuels. Farnborough Air Show; 2010.

[13] Bezergianni S, Dimitriadis A. Comparison between different types of renewable diesel. Renew Sustain Energy Rev 2013;21:110–6.

[14] Eller Z, Varga Z, Hancsok J. Advanced production process of jet fuel components from technical grade coconut oil with special hydrocracking. Fuel 2016;182:713–20.

[15] Lopez-Ruiz JA, Pham HN, Datye AK, Davis RJ. Reactivity and stability of supported Pd nanoparticles during the liquid-phase and gas-phase decarbonylation of heptanoic acid. Appl Catal A – General 2015;504:295–307.

[16] Eller Z, Varga Z, Varga G, Hancsok J. Biocomponent containing jet fuel production with using coconut oil. In: Varbanov PS, Klemes JJ, Liew PY, Yong JY, Stehlik P, editors. Proceedings of the 17th conference on process integration, modelling and optimisation for energy saving and pollution reduction; 2014. Pts 1–3. Chemical Engineering Transactions, 392014, p. 547.

[17] Biswas J, Maxwell IE. Recent process-related and catalyst-related developments in fluid catalytic cracking. Appl Catal 1990;63(2):197–258.

[18] Corma A, Huber GW, Sauvanaud L, O'Connor P. Processing biomass-derived oxygenates in the oil refinery: catalytic cracking (FCC) reaction pathways and role of catalyst. J Catal 2007;247(2):307–27.

[19] Huber GW, Corma A. Synergies between bio- and oil refineries for the production of fuels from biomass. Angew Chem Int Ed 2007;46(38):7184–201.

[20] Stocker M. Biofuels and biomass-to-liquid fuels in the biorefinery: catalytic conversion of lignocellulosic biomass using porous materials. Angew Chem Int Ed 2008;47(48):9200–11.

[21] Corma A, Miguel PJ, Orchilles AV. The role of reaction temperature and cracking catalyst characteristics in determining the relative rates of protolytic cracking, chain propagation, and hydrogen-transfer. J Catal 1994;145(1):171–80.

[22] Al-Sabawi M, Chen JW. Hydroprocessing of biomass-derived oils and their blends with petroleum feedstocks: a review. Energy Fuels 2012;26(9):5373–99.

[23] Vogt ETC, Weckhuysen BM. Fluid catalytic cracking: recent developments on the grand old lady of zeolite catalysis. Chem Soc Rev 2015;44(20):7342–70.

[24] Graca I, Lopes JM, Cerqueira HS, Ribeiro MF. Bio-oils upgrading for second generation biofuels. Ind Eng Chem Res 2013;52(1):275–87.

[25] Kubička D, Kikhtyanin O. Opportunities for zeolites in biomass upgrading lessons from the refining and petrochemical industry. Catal Today 2015;243:10–22.

[26] Melero JA, Iglesias J, Garcia A. Biomass as renewable feedstock in standard refinery units. Feasibility, opportunities and challenges. Energy Environ Sci 2012;5(6):7393–420.

[27] Al-Sabawi M, Chen JW, Ng S. Fluid catalytic cracking of biomass-derived oils and their blends with petroleum feedstocks: a review. Energy Fuels 2012;26 (9):5355–72.

[28] Stefanidis SD, Kalogiannis KG, Lappas AA. Co-processing bio-oil in the refinery for drop-in biofuels via fluid catalytic cracking. Wiley Interdiscip Rev: Energy Environ. 2017:e281.

[29] Toth C, Baladincz P, Hancsok J. Production of bio gas oil containing diesel fuel with upgraded cold flow properties by co-processing. In: Varbanov PS, Lam HL, Klemes JJ, Pierucci S, Klemes JJ, editors. Proceedings of the 15th international conference on process integration, modelling and optimisation for energy saving and pollution reduction; 2012. p. 613–8.

[30] Huber GW, O'Connor P, Corma A. Processing biomass in conventional oil refineries: production of high quality diesel by hydrotreating vegetable oils in heavy vacuum oil mixtures. Appl Catal A – General 2007;329:120–9.

[31] Sankaranarayanan TM, Banu M, Pandurangan A, Sivasanker S. Hydroprocessing of sunflower oil-gas oil blends over sulfided Ni–Mo–Al-zeolite beta composites. Bioresour Technol 2011;102(22):10717–23.

[32] Toth C, Baladincz P, Hancsok J. Production of biocomponent containing gas oil with the coprocessing of vegetable oil-gas oil mixture. Top Catal 2011;54 (16–18):1084–93.

[33] Satyarthi JK, Chiranjeevi T, Gokak DT, Viswanathan PS. Studies on co-processing of jatropha oil with diesel fraction in hydrodesulfurization. Fuel Process Technol 2014;118:180–6.

[34] Walendziewski J, Stolarski M, Luzny R, Klimek B. Hydroprocesssing of light gas oil–rape oil mixtures. Fuel Process Technol 2009;90(5):686–91.

[35] Mikulec J, Cvengros J, Jorikova L, Banic M, Kleinova A. Second generation diesel fuel from renewable sources. J Clean Prod 2010;18(9):917–26.

[36] Watkins B, Olsen C, Sutovich K, Petti N. New opportunities for co-processing renewable feeds in refinery processes. Catalagram 2008;103:1–13.

[37] Baladincz P, Hancsok J. Fuel from waste animal fats. Chem Eng J 2015;282:152–60.

[38] Chen JW, Farooqi H, Fairbridge C. Experimental study on co-hydroprocessing canola oil and heavy vacuum gas oil blends. Energy Fuels 2013;27(6):3306–15.

[39] Bezergianni S, Dagonikou V. Effect of CO_2 on catalytic hydrotreatment of gas-oil. Can J Chem Eng 2015;93(6):1017–23.

[40] Bezergianni S, Dagonikou V, Sklari S. The suspending role of H_2O and CO on catalytic hydrotreatment of gas-oil; myth or reality? Fuel Process Technol 2016;144:20–6.

[41] Baladincz P, Szepesi M, Hancsok J. Co-processing of FCC light cycle oil and waste animal fats with straight run gas oil fraction. Chem Eng Trans 2014;39:1159–64.

[42] Toth C, Sagi D, Hancsok J. Diesel fuel production by catalytic hydrogenation of light cycle oil and waste cooking oil containing gas oil. Top Catal 2015;58 (14–17):948–60.

[43] Dukanovic Z, Glisic SB, Cobanin VJ, Niciforovic M, Georgiou CA, Orlovic AM. Hydrotreating of straight-run gas oil blended with FCC naphtha and light cycle oil. Fuel Process Technol 2013;106:160–5.

[44] Ancheyta J, Aguilar-Rodriguez E, Salazar-Sotelo D, Betancourt-Rivera G, Leiva-Nuncio M. Hydrotreating of straight run gas oil-light cycle oil blends. Appl Catal A – General 1999;180(1-2):195–205.

[45] Bezergianni S, Dimitriadis A, Karonis D. Diesel decarbonization via effective catalytic co-hydroprocessing of residual lipids with gas-oil. Fuel 2014;136:366–73.

[46] Bezergianni S, Dimitriadis A, Meletidis G. Effectiveness of CoMo and NiMo catalysts on co-hydroprocessing of heavy atmospheric gas oil-waste cooking oil mixtures. Fuel 2014;125:129–36.

[47] Dimitriadis A, Bezergianni S. Co-hydroprocessing gas-oil with residual lipids: effect of residence time and H_2/oil ratio. J Clean Prod 2016;131:321–6.

[48] Rana BS, Kumar R, Tiwari R, Kumar R, Joshi RK, Garg MO, et al. Transportation fuels from co-processing of waste vegetable oil and gas oil mixtures. Biomass Bioenergy 2013;56:43–52.

[49] Bezergianni S, Kalogianni A, Dimitriadis A. Catalyst evaluation for waste cooking oil hydroprocessing. Fuel 2012;93(1):638–41.

[50] Ng SH, Al-Sabawi M, Wang JS, Ling H, Zheng Y, Wei Q, et al. FCC coprocessing oil sands heavy gas oil and canola oil. 1. Yield structure. Fuel 2015;156:163–76.

[51] Bielansky P, Reichhold A, Schonberger C. Catalytic cracking of rapeseed oil to high octane gasoline and olefins. Chem Eng Process 2010;49(8):873–80.

[52] Naik DV, Kumar V, Prasad B, Poddar MK, Behera B, Bal R, et al. Catalytic cracking of jatropha-derived fast pyrolysis oils with VGO and their NMR characterization. RSC Adv 2015;5(1):398–409.

[53] Pinho AD, de Almeida MBB, Mendes FL, Ximenes VL, Casavechia LC. Co-processing raw bio-oil and gasoil in an FCC Unit. Fuel Process Technol 2015;131:159–66.

[54] Wang YX, He T, Liu KT, Wu JH, Fang YM. From biomass to advanced bio-fuel by catalytic pyrolysis/hydro-processing: hydrodeoxygenation of bio-oil derived from biomass catalytic pyrolysis. Bioresour Technol 2012;108:280–4.

[55] Fogassy G, Thegarid N, Schuurman Y, Mirodatos C. From biomass to bio-gasoline by FCC co-processing: effect of feed composition and catalyst structure on product quality. Energy Environ Sci 2011;4(12):5068–76.

[56] Fogassy G, Thegarid N, Schuurman Y, Mirodatos C. The fate of bio-carbon in FCC co-processing products. Green Chem 2012;14(5):1367–71.

[57] Gueudre L, Thegarid N, Burel L, Jouguet B, Meunier F, Schuurman Y, et al. Coke chemistry under vacuum gasoil/bio-oil FCC co-processing conditions. Catal Today 2015;257:200–12.

[58] Ibarra A, Rodriguez E, Sedran U, Arandes JM, Bilbao J. Synergy in the cracking of a blend of bio-oil and vacuum gasoil under fluid catalytic cracking conditions. Ind Eng Chem Res 2016;55(7):1872–80.

[59] Ibarra A, Veloso A, Bilbao J, Arandes JM, Castano P. Dual coke deactivation pathways during the catalytic cracking of raw bio-oil and vacuum gasoil in FCC conditions. Appl Catal B – Environ 2016;182:336–46.

[60] Thegarid N, Fogassy G, Schuurman Y, Mirodatos C, Stefanidis S, Iliopoulou EF, et al. Second-generation biofuels by co-processing catalytic pyrolysis oil in FCC units. Appl Catal B – Environ 2014;145:161–6.

[61] Melero JA, Clavero MM, Calleja G, Garcia A, Miravalles R, Galindo T. Production of biofuels via the catalytic cracking of mixtures of crude vegetable oils and nonedible animal fats with vacuum gas oil. Energy Fuels 2010;24:707–17.

[62] Tian H, Li CY, Yang CH, Shan HH. Alternative processing technology for converting vegetable oils and animal fats to clean fuels and light olefins. Chin J Chem Eng 2008;16(3):394–400.

[63] Abbasov V, Mammadova T, Aliyeva N, Abbasov M, Movsumov N, Joshi A, et al. Catalytic cracking of vegetable oils and vacuum gasoil with commercial high alumina zeolite and halloysite nanotubes for biofuel production. Fuel 2016;181:55–63.

[64] Bielansky P, Weinert A, Schonberger C, Reichhold A. Catalytic conversion of vegetable oils in a continuous FCC pilot plant. Fuel Process Technol 2011;92 (12):2305–11.

[65] Lovas P, Hudec P, Hadvinova M, Haz A. Conversion of rapeseed oil via catalytic cracking: effect of the ZSM-5 catalyst on the deoxygenation process. Fuel Process Technol 2015;134:223–30.

[66] Doronin VP, Potapenko OV, Lipin PV, Sorokina TP. Catalytic cracking of vegetable oils and vacuum gas oil. Fuel 2013;106:757–65.

[67] Eller Z, Holló A, Hancsók J. Production of low reduced aromatic jet fuel from sunflower oil–kerosene mixture. In: Proceedings of the 20th European biomass conference and exhibition. Italy: Milan; 2012. p. 18–22.

[68] Pinheiro A, Hudebine D, Dupassieux N, Charon N, Geantet C. Membrane fractionation of biomass fast pyrolysis oil and impact of its presence on a petroleum gas oil hydrotreatment. Oil Gas Sci Technol – Revue D Ifp Energies Nouvelles 2013;68(5):815–28.

[69] Hancsók J, Krár M, Kasza T, Kovács S, Tóth C, Varga Z. Investigation of hydrotreating of vegetable oil-gas oil mixtures. J Environ Sci Eng 2011;5:500–7.

[70] Fogassy G, Thegarid N, Toussaint G, van Veen AC, Schuurman Y, Mirodatos C. Biomass derived feedstock co-processing with vacuum gas oil for second-generation fuel production in FCC units. Appl Catal B – Environ 2010;96 (3–4):476–85.

[71] Šimáček P, Kubička D. Hydrocracking of petroleum vacuum distillate containing rapeseed oil: evaluation of diesel fuel. Fuel 2010;89(7):1508–13.

[72] Tiwari R, Rana BS, Kumar R, Verma D, Kumar R, Joshi RK, et al. Hydrotreating and hydrocracking catalysts for processing of waste soya-oil and refinery-oil mixtures. Catal Commun 2011;12(6):559–62.

[73] Atabani AE, Silitonga AS, Ong HC, Mahlia TMI, Masjuki HH, Badruddin IA, et al. Non-edible vegetable oils: a critical evaluation of oil extraction, fatty acid compositions, biodiesel production, characteristics, engine performance and emissions production. Renew Sustain Energy Rev 2013;18:211–45.

[74] Wiltsee G. Urban waste grease resource assessment. National Renewable Energy Laboratory; 1998. Contract No.: NREL/SR-570-26141.

[75] Thornley P, Tomei J, Upham P, Panoutsou C, Yates N. Supergen biomass and bioenergy consortium theme 6 resource assessment feedstock properties. The University of Manchester; 2008.

[76] Sagi D, Hollo A, Varga G, Hancsok J. Co-hydrogenation of fatty acid by-products and different gas oil fractions. J Clean Prod 2017;161:1352–9.

[77] Boonyasuwat S, Tscheikuna J. Co-processing of palm fatty acid distillate and light gas oil in pilot-scale hydrodesulfurization unit over commercial CoMo/Al_2O_3. Fuel 2017;199:115–24.

[78] Blin J, Brunschwig C, Chapuis A, Changotade O, Sidibe S, Noumi ES, et al. Characteristics of vegetable oils for use as fuel in stationary diesel engines – towards specifications for a standard in West Africa. Renew Sustain Energy Rev 2013;22:580–97.

[79] Demirbas A. Chemical and fuel properties of seventeen vegetable oils. Energy Sources 2003;25(7):721–8.

[80] Jeczmionek L, Porzycka-Semczuk K. Hydrodeoxygenation, decarboxylation and decarbonylation reactions while co-processing vegetable oils over a NiMo hydrotreatment catalyst. Part I: thermal effects – theoretical considerations. Fuel. 2014;131:1–5.

[81] Toth C, Baladincz P, Hancsok J. Production of biocomponent containing diesel fuel in one step. In: Proceedings of the 45th international petroleum conference. Slovak Republic: Bratislava; 2011. p. 1–15.

[82] Mercader FD, Groeneveld MJ, Kersten SRA, Way NWJ, Schaverien CJ, Hogendoorn JA. Production of advanced biofuels: co-processing of upgraded pyrolysis oil in standard refinery units. Appl Catal B – Environ 2010;96(1-2):57–66.

[83] Pimentel D, Patzek TW. Ethanol production using corn, switchgrass, and wood; biodiesel production using soybean and sunflower. Nat Resour Res 2005;14 (1):65–76.

[84] Bridgwater AV. Review of fast pyrolysis of biomass and product upgrading. Biomass Bioenergy 2012;38:68–94.

[85] Oasmaa A, Czernik S. Fuel oil quality of biomass pyrolysis oils – state of the art for the end user. Energy Fuels 1999;13(4):914–21.

[86] Gagnon J, Kaliaguine S. Catalytic hydrotreatment of vacuum pyrolysis oils from wood. Ind Eng Chem Res 1988;27(10):1783–8.

[87] Lin YC, Huber GW. The critical role of heterogeneous catalysis in lignocellulosic biomass conversion. Energy Environ Sci 2009;2(1):68–80.

[88] Mercader FD, Groeneveld MJ, Kersten SRA, Venderbosch RH, Hogendoorn JA. Pyrolysis oil upgrading by high pressure thermal treatment. Fuel 2010;89 (10):2829–37.

[89] Fermoso J, Pizarro P, Coronado JM, Serrano DP. Advanced biofuels production by upgrading of pyrolysis bio-oil. Wiley Interdiscip Rev: Energy Environ 2017;6 (4):e245.

[90] Elliott DC. Biofuel from fast pyrolysis and catalytic hydrodeoxygenation. Curr Opin Chem Eng 2015;9:59–65.

[91] Elliott DC. Historical developments in hydroprocessing bio-oils. Energy Fuels 2007;21(3):1792–815.

[92] Sharma RK, Bakhshi NN. Catalytic upgrading of pyrolysis oil. Energy Fuels 1993;7(2):306–14.

[93] Mortensen PM, Grunwaldt JD, Jensen PA, Knudsen KG, Jensen AD. A review of catalytic upgrading of bio-oil to engine fuels. Appl Catal A – General 2011;407 (1–2):1–19.

[94] Stefanidis SD, Kalogiannis KG, Pilavachi PA, Fougret CM, Jordan E, Lappas AA. Catalyst hydrothermal deactivation and metal contamination during the in situ catalytic pyrolysis of biomass. Catal Sci Technol 2016;6(8):2807–19.

[95] Lappas AA, Bezergianni S, Vasalos IA. Production of biofuels via co-processing in conventional refining processes. Catal Today 2009;145(1–2):55–62.

[96] Agblevor FA, Mante O, McClung R, Oyama ST. Co-processing of standard gas oil and biocrude oil to hydrocarbon fuels. Biomass Bioenergy 2012;45:130–7.

[97] Huynh TM, Armbruster U, Atia H, Bentrup U, Phan BMQ, Eckelt R, et al. Upgrading of bio-oil and subsequent co-processing under FCC conditions for fuel production. React Chem Eng 2016;1(2):239–51.

[98] Lindfors C, Paasikallio V, Kuoppala E, Reinikainen M, Oasmaa A, Solantausta Y. Co-processing of dry bio-oil, catalytic pyrolysis oil, and hydrotreated bio-oil in a micro activity test unit. Energy Fuels 2015;29(6):3707–14.

[99] Samolada MC, Baldauf W, Vasalos IA. Production of a bio-gasoline by upgrading biomass flash pyrolysis liquids via hydrogen processing and catalytic cracking. Fuel 1998;77(14):1667–75.

[100] Furimsky E. Catalytic hydrodeoxygenation. Appl Catal A – General 2000;199 (2):147–90.

[101] Kubičková I, Kubička D. Utilization of triglycerides and related feedstocks for production of clean hydrocarbon fuels and petrochemicals: a review. Waste Biomass Valoriz 2010;1(3):293–308.

[102] Sepulveda C, Escalona N, Garcia R, Laurenti D, Vrinat M. Hydrodeoxygenation and hydrodesulfurization co-processing over ReS2 supported catalysts. Catal Today 2012;195(1):101–5.

[103] Pinheiro A, Hudebine D, Dupassieux N, Geantet C. Impact of oxygenated compounds from lignocellulosic biomass pyrolysis oils on gas oil hydrotreatment. Energy Fuels 2009;23(1):1007–14.

[104] Bui VN, Laurenti D, Delichere P, Geantet C. Hydrodeoxygenation of guaiacol. Part II: support effect for CoMoS catalysts on HDO activity and selectivity. Appl Catal B – Environ 2011;101(3–4):246–55.

[105] Bezergianni S, Dimitriadis A. Temperature effect on co-hydroprocessing of heavy gas oil-waste cooking oil mixtures for hybrid diesel production. Fuel 2013;103:579–84.

[106] Chen S. Green oil production by hydroprocessing. Int J Clean Coal Energy 2012;1(4):43–55.

[107] Mercader FD, Groeneveld MJ, Kersten SRA, Geantet C, Toussaint G, Way NWJ, et al. Hydrodeoxygenation of pyrolysis oil fractions: process understanding and quality assessment through co-processing in refinery units. Energy Environ Sci 2011;4(3):985–97.

[108] Bui VN, Toussaint G, Laurenti D, Mirodatos C, Geantet C. Co-processing of pyrolisis bio oils and gas oil for new generation of bio-fuels: hydrodeoxygenation of guaiacol and SRGO mixed feed. Catal Today 2009;143(1–2):172–8.

[109] Laurent E, Delmon B. Study of the hydrodeoxygenation of carbonyl, carboxylic and guaiacyl groups over sulfided CoMo/gamma-Al_2O_3 and NiMo/gamma-Al_2O_3 catalysts.1. Catalytic reaction schemes. Appl Catal A – General. 1994;109 (1):77–96.

[110] Laurent E, Delmon B. Study of the hydrodeoxygenation of carbonyl, carboxylic and guaiacyl groups over sulfided CoMo/gamma-Al_2O_3 and NiMo/gamma-Al_2O_3 catalysts. 2. Influence of water, ammonia and hydrogen-sulfide. Appl Catal A – General 1994;109(1):97–115.

[111] Kubička D, Tukač V. Hydrotreating of triglyceride-based feedstocks in refineries. In: Murzin DY, (ed.), Chemical engineering for renewables conversion. Advances in Chemical Engineering; Elsevier; 422013, p. 141–94.

[112] Topsoe H, Egeberg RG, Knudsen KG, Topsoe H. Future challenges of hydrotreating catalyst technology. Abstracts of Papers of the American Chemical Society. 2004;228:U659-U.

[113] Jechura J. Hydroprocessing: hydrotrerating & hydrocracking. 2017, http://inside.mines.edu/~jjechura/Refining/08_Hydroprocessing.pdf; [accessed 23.08.2017].

[114] Pinheiro A, Dupassieux N, Hudebine D, Geantet C. Impact of the presence of carbon monoxide and carbon dioxide on gas oil hydrotreatment: investigation on liquids from biomass cotreatment with petroleum cuts. Energy Fuels 2011;25:804–12.

[115] Demirbas A. Biorefinery technologies for biomass upgrading. Energy Sources Part A – Recovery Util Environ Effects 2010;32(16):1547–58.

[116] Grange P, Laurent E, Maggi R, Centeno A, Delmon B. Hydrotreatment of pyrolysis oils from biomass: reactivity of the various categories of oxygenated compounds and preliminary techno-economical study. Catal Today 1996;29 (1–4):297–301.

[117] Petrobras http://www.reuters.com/article/us-biofuel-summit-hbio-petrobras-idUSN1660193320080116; 2008 [accessed 23. 8. 2017] [press release].

[118] Gomes JR, Bezergianni S, Zotin JL, Sousa-Aguiar EF. Biofuels generation via hydroconversion of vegetable oils and animal fats. In: Rinaldi R, (ed.), Catalytic hydrogenation for biomass valorization. RSC (Royal Society of Chemistry) energy and environment series. 132015. p. 204–22.

[119] Watkins B, Olsen C, Sutovich K, Deady J, Petti N, Wellach S. New opportunities for coprocessing renewable feeds in the refinery process. Hydrocarbon Eng 2009;14(1):49–58.

[120] Twaiq FAA, Bhatia S, Zabidi NAM. Catalytic cracking of palm oil over zeolite catalysts: statistical approach. Int Islam Univ Malysia Eng J 2001;2(1):13–21.

[121] Černý R, Kubů M, Kubička D. The effect of oxygenates structure on their deoxygenation over USY zeolite. Catal Today 2013;204:46–53.

[122] Fimberger J, Swoboda M, Reichhold A. Thermal cracking of canola oil in a continuously operating pilot plant. Powder Technol 2017;316:535–41.

[123] Geller DP, Adams TT, Goodrum JW, Pendergrass J. Storage stability of poultry fat and diesel fuel mixtures: specific gravity and viscosity. Fuel 2008;87(1):92–102.

[124] Melero JA, Calleja G, Garcia A, Clavero M, Hernandez EA, Miravalles R, et al. Storage stability and corrosion studies of renewable raw materials and petrol mixtures: a key issue for their co-processing in refinery units. Fuel 2010;89 (3):554–62.

[125] Qing W. Processing high TAN crude: part I. Digital refining: processing, operations & maintenance [internet]. 2010. Available from: http://www.digitalrefining.com/article/1000524#.WmHY4YWcFXY.

[126] Corma A, Martinez C, Melo FV, Sauvanaud L, Carriat JY. A new continuous laboratory reactor for the study of catalytic cracking. Appl Catal A – General 2002;232(1–2):247–63.

[127] Dupain X, Costa DJ, Schaverien CJ, Makkee M, Moulijn JA. Cracking of a rapeseed vegetable oil under realistic FCC conditions. Appl Catal B – Environ 2007;72 (1–2):44–61.

[128] Weinert A, Bielansky P, Reichhold A. Upgrading biodiesel into oxygen-free gasoline: new applications for the FCC-process. In: Dan Y, (ed.), Proceedings of international conference on environmental science and development. APCBEE Procedia;12012, p. 147–52.

[129] Gueudre L, Chapon F, Mirodatos C, Schuurman Y, Venderbosch R, Jordan E, et al. Optimizing the bio-gasoline quantity and quality in fluid catalytic cracking co-refining. Fuel 2017;192:60–70.

[130] Pinho AD, de Almeida MBB, Mendes FL, Casavechia LC, Talmadge MS, Kinchin CM, et al. Fast pyrolysis oil from pinewood chips co-processing with vacuum gas oil in an FCC unit for second generation fuel production. Fuel 2017;188:462–73.

[131] Adjaye JD, Bakhshi NN. Catalytic conversion of a biomass-derived oil to fuels and chemicals.1. Model-compound studies and reaction pathways. Biomass Bioenergy 1995;8(3):131–49.

[132] Vitolo S, Bresci B, Seggiani M, Gallo MG. Catalytic upgrading of pyrolytic oils over HZSM-5 zeolite: behaviour of the catalyst when used in repeated upgrading-regenerating cycles. Fuel 2001;80(1):17–26.

[133] Horne PA, Williams PT. Upgrading of biomass-derived pyrolytic vapours over zeolite ZSM-5 catalyst: effect of catalyst dilution on product yields. Fuel 1996;75(9):1043–50.

[134] Carlson TR, Jae J, Lin YC, Tompsett GA, Huber GW. Catalytic fast pyrolysis of glucose with HZSM-5: the combined homogeneous and heterogeneous reactions. J Catal 2010;270(1):110–24.

[135] Bjorgen M, Svelle S, Joensen F, Nerlov J, Kolboe S, Bonino F, et al. Conversion of methanol to hydrocarbons over zeolite H-ZSM-5: on the origin of the olefinic species. J Catal 2007;249(2):195–207.

[136] da Cunha ME, Schneider JK, Brasil MC, Cardoso CA, Monteiro LR, Mendes FL, et al. Analysis of fractions and bio-oil of sugar cane straw by one-dimensional and two-dimensional gas chromatography with quadrupole mass spectrometry (GC×GC/qMS). Microchem J 2013;110:113–9.

[137] Sadeghbeigi R. Fluid catalytic cracking handbook. 2nd ed. Houston, TX: Gulf Professional Publishing; 2000. p. 369.

[138] Huuska M, Rintala J. Effect of catalyst acidity on the hydrogenolysis of anisole. J Catal 1985;94(1):230–8.

[139] Toth C, Baladincz P, Kovacs S, Hancsok J. Producing clean diesel fuel by co-hydrogenation of vegetable oil with gas oil. Clean Technol Environ Policy 2011;13(4):581–5.

[140] Šimáček P, Kubička D, Šebor G, Pospíšil M. Fuel properties of hydroprocessed rapeseed oil. Fuel 2010;89(3):611–5.

[141] Stumborg M, Wong A, Hogan E. Hydroprocessed vegetable oils for diesel fuel improvement. Bioresour Technol 1996;56(1):13–8.

[142] Marker TL. Opportunities for biorenewables in oil refineries USDOE Office of Energy Efficiency and Renewable Energy (EERE). 2005; Report No.: DOE-GO15085Final doi: 10.2172/861458.

[143] Kalnes TN, Koers KP, Marker T, Shonnard DR. A technoeconomic and environmental life cycle comparison of green diesel to biodiesel and syndiesel. Environ Prog Sustain Energy 2009;28(1):111–20.

[144] Sunde K, Brekke A, Solberg B. Environmental impacts and costs of hydrotreated vegetable oils, transesterified lipids and woody BTL – a review. Energies 2011;4(6):845–77.

[145] Holmgren J, Marinangeli R, Marker T, McCall M, Petri J, Czernik S, et al. Opportunities for biorenewables in petroleum refineries. UOP-Honeywell.

[146] Hancsok J, Krar M, Magyar S, Boda L, Hollo A, Kallo D. Investigation of the production of high cetane number bio gas oil from pre-hydrogenated vegetable oils over Pt/HZSM-22/Al_2O_3. Microporous Mesoporous Mater 2007;101 (1–2):148–52.

[147] Hancsok J, Kovacs S, Polczmann G, Kasza T. Investigation the effect of oxygenic compounds on the isomerization of bioparaffins Over Pt/SAPO-11. Top Catal 2011;54(16–18):1094–101.

[148] Kasza T, Kallo D, Hancsok J. Quality improvement of bio-paraffin mixtures. Fuel 2014;120:1–7.

[149] Directive 2009/28/EC, 2009.

[150] BIOFUELS-2G - 2nd generation biofuels for urban environment, 2017. http://biofuels2g.gr/index.php?lang=en; [accessed 23.8.2017].

[151] Kubička D. Future refining catalysis - introduction of biomass feedstocks. Collect Czech Chem Commun 2008;73(8–9):1015–44.

[152] SustainDiesel webpage, 2017. http://www.sustaindiesel.gr/; [accessed 23.8.2017].

[153] Schadel BT, Duisberg M, Deutschmann O. Steam reforming of methane, ethane, propane, butane, and natural gas over a rhodium-based catalyst. Catal Today 2009;142(1–2):42–51.

[154] Silberova B, Venvik HJ, Holmen A. Production of hydrogen by short contact time partial oxidation and oxidative steam reforming of propane. Catal Today 2005;99(1–2):69–76.

[155] Davda RR, Shabaker JW, Huber GW, Cortright RD, Dumesic JA. A review of catalytic issues and process conditions for renewable hydrogen and alkanes by aqueous-phase reforming of oxygenated hydrocarbons over supported metal catalysts. Appl Catal B – Environ 2005;56(1–2):171–86.

[156] Holladay JD, Hu J, King DL, Wang Y. An overview of hydrogen production technologies. Catal Today 2009;139(4):244–60.

[157] Huber GW, Dumesic JA. An overview of aqueous-phase catalytic processes for production of hydrogen and alkanes in a biorefinery. Catal Today 2006;111 (1–2):119–32.

[158] Murzin DY, Garcia S, Russo V, Kilpio T, Godina LI, Tokarev AV, et al. Kinetics, modeling, and process design of hydrogen production by aqueous phase reforming of xylitol. Ind Eng Chem Res 2017;56(45):13241–54.

[159] Robinson PR, Dolbear GE. Hydrotreating and hydrocracking: fundamentals. In: Hsu CS, Robinson PR, editors. Practical advances in petroleum processing. New York, NY: Springer; 2006.

[160] Co-processing of low carbon feedstocks in petroleum refineries, https://www.arb.ca.gov/fuels/lcfs/lcfs_meetings/053017draft_discussion_paper_coprocessing.pdf; 2017. Draft discussion paper, [accessed 23.8.2017] 30.5.2017.

[161] Sokhansanj S, Kumar A, Turhollow AF. Development and implementation of integrated biomass supply analysis and logistics model (IBSAL). Biomass Bioenergy 2006;30(10):838–47.

[162] Hess JR, Wright CT, Kenney KL. Cellulosic biomass feedstocks and logistics for ethanol production. Biofuels Bioproducts Biorefining 2007;1(3):181–90.

[163] Eksioglu SD, Acharya A, Leightley LE, Arora S. Analyzing the design and management of biomass-to-biorefinery supply chain. Comput Ind Eng 2009;57 (4):1342–52.

[164] Törnvall U, Börjesson P, Tufvesson LM, Hatti-Kaul R. Original research: biocatalytic production of fatty epoxides from rapeseed & tall oil derivatives: process & environmental evaluation. Ind Biotechnol 2009;5(3):184–92.

[165] Germer J, Sauerborn J. Estimation of the impact of oil palm plantation establishment on greenhouse gas balance. Environ Dev Sustain 2008;10(6):697–716.

[166] Fitzherbert EB, Struebig MJ, Morel A, Danielsen F, Bruhl CA, Donald PF, et al. How will oil palm expansion affect biodiversity? Trends Ecol Evol 2008;23 (10):538–45.

[167] Fargione J, Hill J, Tilman D, Polasky S, Hawthorne P. Land clearing and the biofuel carbon debt. Science 2008;319(5867):1235–8.

[168] Reijnders L, Huijbregts MAJ. Palm oil and the emission of carbon-based greenhouse gases. J Clean Prod 2008;16(4):477–82.

[169] Holmgren J, Gosling C, Couch K, Kalnes T, Marker T, McCall M, et al. Refining-biofeedstock-Innovation. https://www.uop.com/wp-content/uploads/2012/12/UOP-Refining-Biofeedstock-Innovation-Tech-Paper.pdf; 2007 [accessed 23.08.2017]. PTQ119-25.

[170] Global vegetable oil production. https://www.statista.com/statistics/263978/global-vegetable-oil-production-since-2000-2001/; 2017 [accessed 23.08.2017].

[171] Production, supply, and distribution online. United States Department of Agriculcure- Foreign Agricultural Service, https://apps.fas.usda.gov/psdonline/app/index.html#/app/home; 2017 [accessed 23.08.2017].

[172] Baffes J. The energy/non-energy price link: channels, issues and implications. In: Isabelle Piot-Lepetit, Robert Mapos'Barek, editors. Methods to analyse agricultural commodity price volatility. New York: Springer-Verlag; 2011. p. 31–44.

[173] Mitchell D. A note on rising food prices. The World Bank Development Prospects Group; 2008. Contract No.: Policy research working paper 4682, https://openknowledge.worldbank.org/bitstream/handle/10986/6820/WP4682.txt [accessed 23.08.2017] .

[174] Lane J. Rise in vegetable oil prices continues: report. Biofuels Digest 2016 http://www.biofuelsdigest.com/bdigest/2016/11/27/rise-in-vegetable-oil-prices-continues-report/ [accessed 23.08.2017].

[175] Kumar JSP, Gujjala SLK, Dash A, Talukdar B, Banerjee R. Biodiesel production from lignocellulosic biomass using oleaginous microbes. In: Kuila A, Sharma V, editors. Lignocellulosic biomass production and industrial applications. Wiley-Scrivener; 2017. p. 65–92.

[176] Cottam ML, Bridgwater AV. Technoeconomic modeling of biomass flash pyrolysis and upgrading systems. Biomass Bioenergy 1994;7(1–6):267–73.

[177] Gregoire CE, Bain RL. Technoeconomic analysis of the production of biocrude from wood. Biomass Bioenergy 1994;7(1–6):275–83.

[178] Wright MM, Daugaard DE, Satrio JA, Brown RC. Techno-economic analysis of biomass fast pyrolysis to transportation fuels. Fuel 2010;89 S2-S10 doi: https://doi.org/10.1016/j.fuel.2010.07.029.

[179] Brown TR, Thilakaratne R, Brown RC, Hu GP. Techno-economic analysis of biomass to transportation fuels and electricity via fast pyrolysis and hydroprocessing. Fuel 2013;106:463–9.

[180] California Air Resources Board. https://www.arb.ca.gov/fuels/lcfs/lcfs_meetings/020717_staffdiscussionpaper.pdf; 2017; [accessed 23.08.2017].

Stella Bezergianni obtained a Chemical Engineering diploma from the Aristotle University of Thessaloniki Greece and Ph.D. in Chemical Engineering from Lehigh University in USA. She started her career as an advanced engineer at ExxonMobil Research & Engineering in USA and later as a senior engineer in the ESSO Nederland BV refinery in the Netherlands. After her four-year industrial experience, she pursued a research career in the Centre for Research and Technology Hellas (CERTH) in Greece as a researcher, a position she presently holds. She is currently the head of the hydroprocessing group of CERTH, focusing on the technology development and optimization of hydroprocessing for biofuels production. Dr. Bezergianni is the scientific advisor of various European and National research projects as well as of research activities in collaboration with national and international industrial partners. She is an author of numerous scientific publications in technical journals, conference proceedings and monographs. She has acted as the president of the Energy and the Competitiveness and Innovation committees of the Central Macedonia Section of the National Technical Chamber of Greece and a member of the Agro-technology Committee of the American-Hellenic Chamber of Commerce. Finally, she has received scientific and innovation awards.

Athanasios Dimitriadis obtained a Mechanical Engineer diploma from the University of West Macedonian – Aristotle University of Thessaloniki in 2008. During his studies he had a two-month internship in the Hellenic Petroleum Refinery in Thessaloniki in 2005. In 2010 he started working in the Centre for Research and Technology Hellas as a head engineer in HydPro of CPERI/CERTH, a position he currently holds. His research activities involve the production and evaluation of environmentally friendly fuels and biofuels, development of new technologies for 2nd and 3rd generation biofuels production, as well as optimization of hydroprocessing for biofuels production. Since 2012 he is a Ph.D. candidate under the supervision of Prof. Z. Samaras of the Aristotle University of Thessaloniki, working on experimental and theoretical investigation of the effect of Hydrotreated Vegetable Oils (HVOs) on the operation of internal combustion engines and their anti-pollution systems. He is co-author of numerous scientific publications in technical journals and conference proceedings. He also has participated in various European and National research projects as well as in research activities in collaboration with national and international industrial partners.

Oleg Kikhtyanin graduated from Novosibirsk University in 1984 and has since then worked in Institute of Catalysis (Novosibirsk) under the supervision of Prof. K.G. Ione and Dr. G.V. Echevsky. He received his Ph.D. in physical chemistry in 2012 from Tomsk University. He has worked on cracking, hydroisomerization, aromatization and other processes. In 2013 he has joined the lab of Dr. David Kubička at UniCRE (Litvínov, Czech Republic) as a research fellow. He is since 2017 a researcher at University of Chemistry and Technology in Prague. His current scientific interests are heterogeneous catalysts for the production of valuable products from bio-derived sources.

David Kubička is a research scientist at the University of Chemistry and Technology Prague (UCTP). He graduated from UCTP in 1999 at the Department of Petroleum Technology and Petrochemistry. He obtained his Ph.D. in chemical engineering at Abo Akademi University in 2005 at the Laboratory of Industrial Chemistry. He worked at the Research Institute of Inorganic Chemistry (VUAnCH/UniCRE) belonging to petrochemical company Unipetrol from 2006 to 2015, first as a researcher and later as the head of a research program Renewable and Environmental Technologies (RENTECH). He was responsible for numerous scientific as well as industrial research projects. He obtained an award for the best doctoral thesis in the field of catalysis in Finland in 2004–2006 and an award of the CEO of Unipetrol in 2012. In 2016, he joined Technopark Kralupy belonging to the University of Chemistry and Technology Prague. He also holds an academic position at the Department of Petroleum Technology and Alternative Fuels at UCTP. His current scientific interests include heterogeneous catalysis and its application for biomass valorization. At present, he is the chairman of the Czech Catalysis Society.

Catalysis Reviews: Science and Engineering, 55:1–78, 2013
Copyright © Taylor & Francis Group, LLC
ISSN: 0161-4940 print / 1520-5703 online
DOI: 10.1080/01614940.2012.685811

Application of Molecular Sieves in Transformations of Biomass and Biomass-Derived Feedstocks

David Kubička[1], Iva Kubičková[1], and Jiří Čejka[2]

[1]Research Institute of Inorganic Chemistry – UniCRE-RENTECH, Litvínov, Czech Republic
[2]J. Heyrovský Institute of Physical Chemistry, Academy of Sciences of the Czech Republic, Prague, Czech Republic

Molecular sieves (zeolites, mesoporous materials, hierarchic systems, two-dimensional zeolites) are important acid catalysts for transformations of biomass into required products. This article covers the upgrading potential of different types of biomass based on their source and discusses the reaction pathways of their transformations emphasizing the role of molecular sieve catalysts. As typical examples, catalytic pyrolysis, deoxygenation, transesterification, dehydration, isomerization, and condensation reactions were chosen. Properties and chemical/textural characteristics of the most important molecular sieve catalysts are briefly discussed and related to their catalytic behavior in biomass transformations. Finally, potential of novel molecular sieve catalysts towards biomass upgrading is highlighted and some examples of novel zeolitic materials are addressed.

Keywords Biomass, Molecular sieves, Zeolites, Catalytic transformations, Sugars, Triglycerides, Glycerol, Terpenes, Lignocellulose

1. INTRODUCTION

Recent years can be described as the beginning of renaissance of utilization of renewable energy resources. Renewable resources, the exclusive energy carriers worldwide for many centuries, were pushed aside in the last 150 years by fossil energy resources (1) (at first coal, later on petroleum and natural

---

Received 26 November 2011; accepted 30 March 2012.

Address correspondence to David Kubička, Research Institute of Inorganic Chemistry – UniCRE-RENTECH, Chempark Litvínov, 436 70 Litvínov, Czech Republic. E-mail: david.kubicka@vuanch.cz

gas) that made possible a fast industrialization for most parts of the world. The wide-spread use of fossil resources can be attributed to their high energy content (both per m^3 as well as per t) and relatively easy accessibility. As a result, more than 85% of our energy demand is currently satisfied by fossil resources, mainly petroleum, followed by natural gas and coal (Fig. 1a) (1, 3).

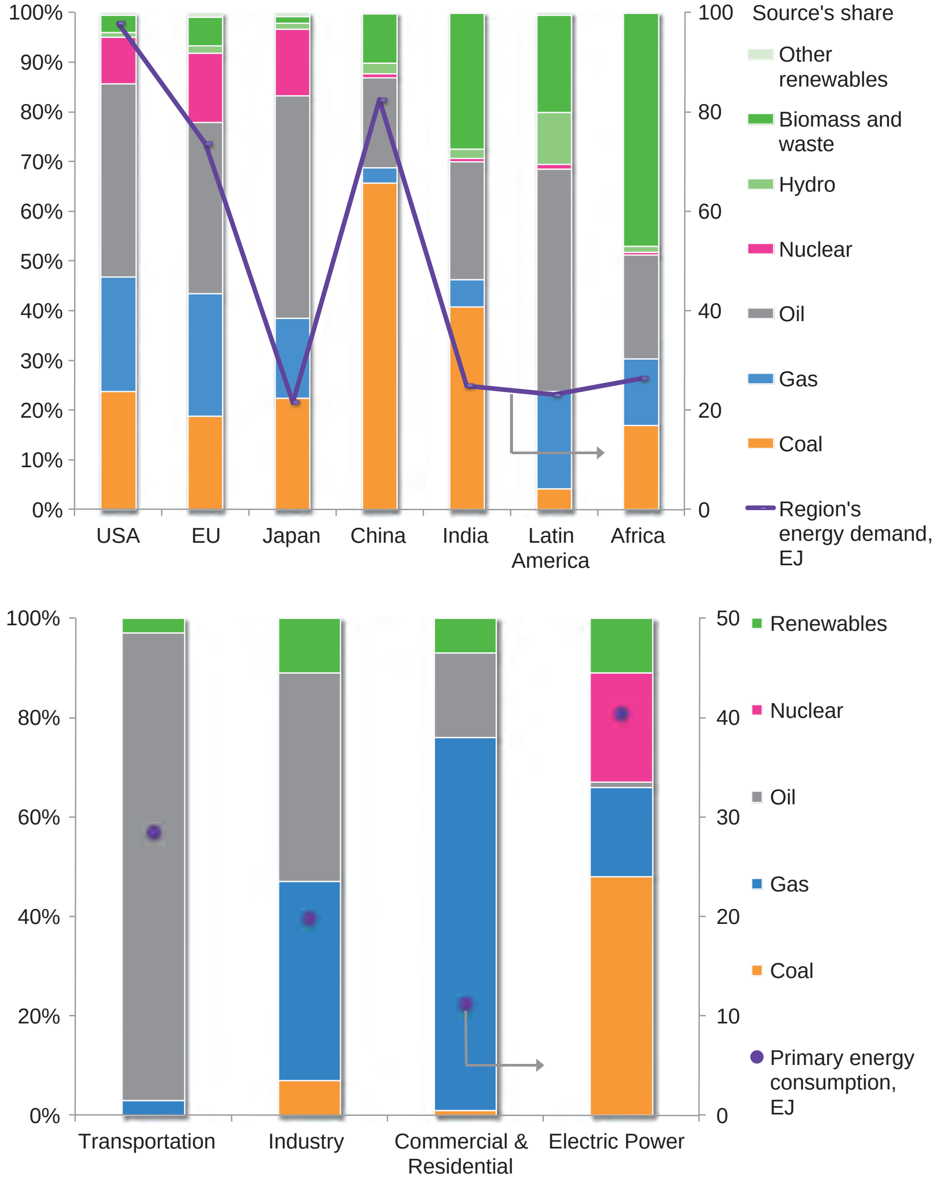

Figure 1: (a) Share of primary energy resources in different regions (1); b) share of primary energy resources in different sectors (U.S. data) (4) (color figure available online).

The dependence on fossil resources is particularly pronounced in the developed regions (U.S., Japan, and Europe) and in the transportation sector (Fig. 1b) (1,4). Apart from the undeniable benefits of fossil fuels, their use is connected with adverse environmental effects. In particular, the global use of fossil fuels was accompanied by a rapid growth in carbon dioxide emission (5–7). It was recently confirmed that consumption of fossil fuels accounts for the majority (*ca.* 56%) of global anthropogenic greenhouse-gas emissions (5).

The exhaustible nature of fossil resources together with their negative environmental impact dictates their gradual replacement by inexhaustible resources, i.e., renewable ones (8). There is a wide variety of renewable energy resources having different potential to contribute to our energy supply. With the exception of geothermal energy, all renewable resources available on the Earth can be considered as a form of solar energy (9). In its direct form, solar energy can be used for heat and electricity production (concentrating solar power, photovoltaics). In its indirect form, it can be harvested as the energy of wind and water (hydropower, e.g., of rivers), typically for electricity production or as biomass having a wider range of energy as well as non energy uses. In addition, tidal energy mostly due to the gravitational force of the Moon can be used for electricity production (e.g., in South Korea, one such unit is under constraction).

The current global primary energy supply (2008) is about 492 EJ/yr (5, 10) out of which *ca.* 63.5 EJ/yr, i.e., 12.9%, originated from renewable resources (Fig. 2) (5). Bioenergy, i.e., energy produced from biomass, provided *ca.* 50 EJ/yr (5,10) and can be divided into two main groups: (a) traditional biomass and (b) modern biomass. The term traditional biomass refers to the

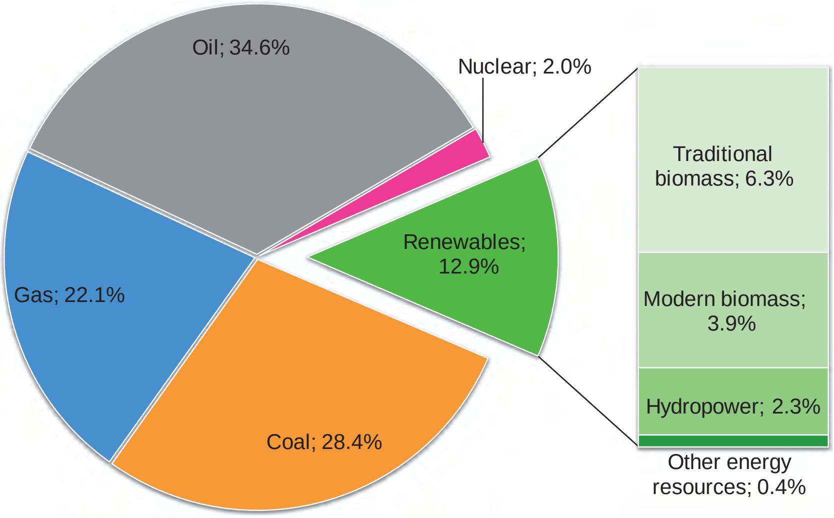

Figure 2: Energy resources portfolio in 2008 (5) (color figure available online).

use of biomass for cooking, heating, and lighting, being characterized by very low-energy efficiency (10–20%) and represents about 75% of the primary energy supplied by biomass. The rest is provided by the so-called modern biomass including electricity and combined heat and power generation, heating of residential, public and commercial buildings, and road transport fuels. The average energy efficiency of the currently used modern biomass technologies is >50% (5).

Renewable energy resources have not only large potential to mitigate climate change by lowering greenhouse gases (GHG) emissions, but also provide additional benefits, contributing to: (a) social and economic development; (b) reduction of negative impacts on the health and environment; and (c) securing energy supply and access (5, 8, 10–12). Based on lifecycle assessment (LCA), electricity production using renewable energy resources leads to significantly lower GHG emissions than those connected with fossil fuels use. Moreover, the GHG emissions from renewable energy technologies can often be lower than from fossil fuel technologies employing carbon capture and storage (CCS). When using non harvest wastes and residues, bioenergy generation can even make it possible to avoid GHG emissions (5). This cannot be achieved with any other source of energy. An additional benefit of bioenergy is that, unlike some other renewable resources, particularly direct solar (photovoltaics and concentrating solar power) and wind energy, it provides constant and controllable energy output (5).

Energy is stored in biomass owing to photosynthesis, i.e., a process converting carbon dioxide and water to organic compounds, typically carbohydrates, and oxygen. The required energy is supplied by photons having wavelength in the range of 400–740 nm, which represents about 49% of the incident solar energy (13). The maximum theoretical yield of photosynthesis is 4.6 and 6.0% for C3 (e.g., sugar beet, eucalyptus, etc.) and C4 plants (e.g., sugar cane, corn, miscanthus, etc.), respectively, where C3 and C4 denote the photosynthesis cycle (13).The maximum yields reported so far were 3.7% for C4 plants and 2.4% for C3 plants with an overall average being 0.5% (13, 14). Even highly efficient sugar cane crop stores only around 1% of the annual incident solar energy as biomass (15,16). The projections for fast-growing algae estimate solar energy conversion up to 4.2%, but the actual annual conversion efficiencies above 2% are rare (15). On the other hand, the solar energy reaching Earth's surface every hour is 430 EJ (13), the amount of energy comparable with the current annual global primary energy consumption (492 EJ) (5). The estimated natural annual biomass replacement corresponds to an energy supply of approximately 3000 EJ (17), i.e., it is about three times higher than the predicted global primary energy consumption in 2050 (600 to 1000–1200 EJ/yr) (5, 10). The energy content of lignocellulosic biomass is about 450–490 MJ/kmol of carbon. In order to convert lignocellulosic biomass into a high-energy density fuel, such as gasoline having 604 MJ/kmol of carbon, almost one quarter of carbon has to be released as CO_2 if biomass is the only feedstock used (18).

However, our possibilities to exploit this energy sustainably are currently very limited. The estimates of available energy from biomass vary in a wide range depending on the assumptions made (5, 12, 19–22). For example, "IPCC Special Report on Renewable Energy Sources and Climate Chase Mitigation" reviewing literature up to 2007 estimated the upper limit of the technical potential in 2050 being about 500 EJ. Residues originating from forestry, agriculture, and organic wastes could contribute by 40–170 EJ/yr. Surplus products (surplus forestry products, energy crops from surplus land, and marginal land products) could yield up to 250–290 EJ/yr. Another 140 EJ/yr could be recovered owing to improvements in agricultural and livestock management (5). Due to the existence of various restrictions, the review concluded that the potential deployment levels of biomass for energy by 2050 could be in the range of 100–300 EJ/yr (5).

Unlike the other renewable energy resources, biomass can be used not only for power production (i.e., heat and electricity) but also to produce many chemicals and liquid fuels. Transportation is currently dependent on liquid fuels providing several important advantages over electrically driven vehicles. These include significantly greater amount of usable energy per unit weight (20–40 times!), easy storage, handling, and refueling (3, 16).

Biomass as the only renewable source of carbon (11) becomes an important feedstock of chemical industry well before oil, gas, and coal reserves are consumed. As biomass growth depends on availability of CO_2, one can argue that CO_2 is the primary renewable source of carbon. The key to successful deployment of biomass in the current value chains is to achieve economic, environmental, and social sustainability of the entire biomass lifecycle. In biomass upgrading to chemicals and liquid fuels, assuming that biomass was produced in accordance with all sustainability criteria, the core challenge is the maximum efficiency (both material as well as energy efficiency) of any biomass conversion process to final products. Deployment of innovative green catalytic methodologies (homogeneous, heterogeneous, and enzymatic) will be thus inevitable (11, 23, 24). There are several useful methods of measuring the environmental impact of conversion processes, namely E factor (kg waste per kg of product), atom economy, and environmental quotient (takes into account not only the amount of waste, but also its nature/toxicity (11, 23, 24).

There is a wide variety of biomass-derived raw materials and hence a multitude of transformation pathways, but only the most efficient ones will reach a commercial stage. As suggested above, catalytic systems facilitating these transformations with maximum selectivity and minimum energy requirements will play a key role. Among many plausible catalytic systems, molecular sieves have a special place. They are a versatile class of micro- and mesoporous (or both) materials, the properties of which can be tailored for specific applications owing to their easy modifiability. The most important tunable properties of molecular sieves include: (a) their structure (size, shape, and connectivity of pores) controlling the molecular traffic to and from active sites; and (b) both inherent Lewis and Brønsted acid sites as well as supported, e.g., metallic sites, while acido-basic properties determining their reactivity with different guest-molecule functionalities can be adjusted (25).

Recently, several excellent reviews discussing different aspects of biomass and biomass-derived feedstocks focused on biomass to transportation fuels (1, 26–28), biomass to chemicals (29), biomass to fine and specialty chemicals (30, 31), catalytic transformations of lignocellulosic materials (32, 33), biomass-derived oxygenates to fuels and chemicals (34, 35), utilization of triglycerides (36, 37), glycerol to value-added products (38, 39), sugars to furan derivatives (40), and catalytic valorization of lignin (41) have been published. In general, these studies are mostly centered on the reaction pathways. In the present work and in contrast to previous reviews, we attempt to review the topic from a different perspective, namely our goal is to understand the catalytic role of micro- and mesoporous molecular sieves in different biomass-related applications. Some aspects of zeolite application in biomass upgrading were very recently reviewed by Taarning et al. (42–44). Moreover, application of zeolites in organic syntheses was meticulously reviewed by van Bekkum and Kouwenhoven (45, 46).

The main goal of this review is to assess the currently investigated potential uses of micro- and mesoporous catalysts in transformation of biomass-derived raw materials and to discuss their further opportunities. After a concise description of different biomass-derived raw materials based on their complexity, the selected transformations of biomass-based feedstocks over micro- and mesoporous materials are discussed with the particular focus on the role of micro- and mesoporous catalysts and their characteristic properties, such as acidity, shape selectivity, etc., in these transformations. Further on, the most relevant types and properties of molecular sieves, such as three-dimensional (3D) zeolites (i.e., conventional microporous molecular sieves), two-dimensional (2D) zeolites with limited connectivity in the third dimension, mesoporous molecular sieves, and hierarchic molecular sieves, will be shortly introduced and their specific properties will be analyzed in light of the desired transformations, i.e., the needs for conversion of biomass-derived raw materials. Finally, some future trends and opportunities will be highlighted.

2. BIOMASS COMPOSITION AND POSSIBLE ROUTES IN ITS UPGRADING

Any terrestrial organic matter can be in principle denoted as biomass (19), i.e., wood, agricultural, and forestry residues, energy crops, human and animal excrements, and industrial and municipal biodegradable wastes (12). Biomass is the most important primary source of energy for mankind; it serves as food, fodder, and fuel resource. Thus, it is essential to maintain a balance between biomass production for fuel and chemical applications, on the one hand, and food and fodder applications on the other hand, in other words to avoid fuel vs. food competition (15).

Biomass can be classified using many different criteria. Regarding energy and chemicals production two are particularly important, namely biomass origin and biomass chemical composition. Based on its origin, biomass can be classified into three groups: (a) residues from agriculture and forestry (sustainably available waste); (b) dedicated energy crops and surplus forestry production (dedicated fuel crops); and (c) organic waste (15, 21). The energy crops potential is estimated to be between 200–600 EJ/yr while the potential of residues is assumed to reach 62–325 EJ/yr in 2050 (19). According to its chemical composition, biomass can be classified as: (a) lignocellulosic biomass (wood, forestry, and agricultural residues); (b) carbohydrate biomass (starch- or sucrose-rich plants); (c) triglyceride biomass (oil seed plants); and (d) extractives biomass (e.g., essential oils, terpenes, etc.); see Fig. 3 for examples. Some plants can be classified into two categories. For example, sugar cane belongs to both (a) and (b), and rapeseed can be classified into (a) and (c) when waste from the primary production (sucrose or triglycerides, respectively) are utilized. The current production of different biomass raw materials (Fig. 4) clearly demonstrates the dominance of lignocellulosic biomass; more than 80% of biomass feedstocks for energy are derived from wood and shrubs (5). Traditional biomass applications (i.e., fuel wood) being dominantly used have a very low efficiency (10–20%), thus, the energy supply from this amount of biomass is inferred to increase up to 3–6 times by using it in modern biomass applications.

The global potential of lignocellulosic biomass is significantly larger than that of the remaining types (5), particularly being less dependent on favorable climatic and soil conditions and hence requiring fewer inputs of agrochemicals and competing less with food production (21). On the contrary, carbohydrate and triglyceride biomass are important food crops and their use for fuel production is in direct competition with food production except when only surplus production is used. For example, it has been estimated that in Europe alone 5–9 EJ/yr of energy crops (with an average yield of 100 GJ/ha/yr) could be produced in 2030 using land freed up owing to improvement of food crop yields (22). Algae are the most promising non lignocellulosic biomass feedstock not competing directly with food and fodder production. It consists mainly of carbohydrates, lipids, and proteins produced in yields per hectare (49) estimated to be 790–4550 GJ/ha/yr. This considerably exceeds the yields of palm oil and sugar cane (192 and 124 GJ/ha/yr, respectively) (50).

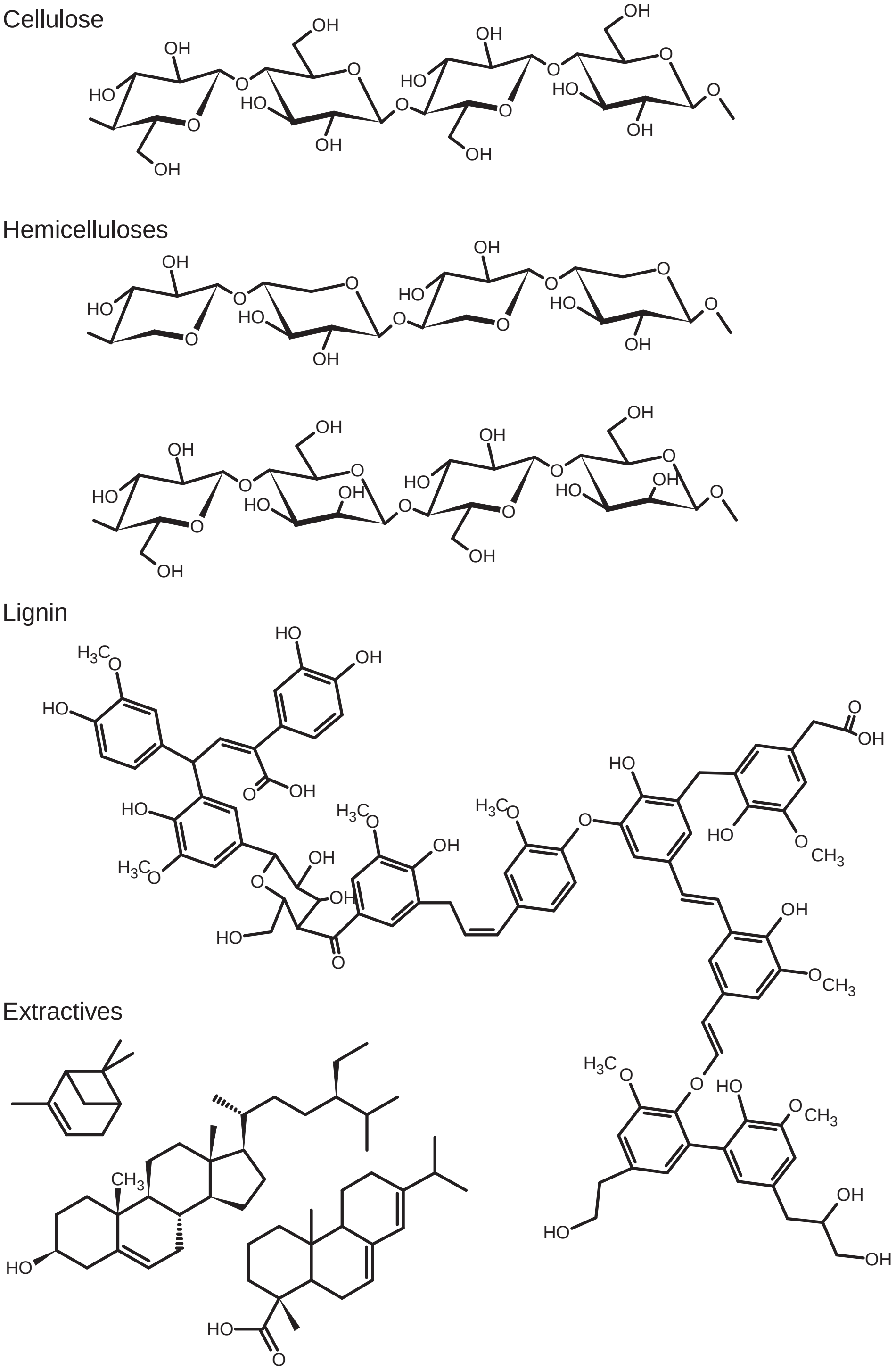

Figure 3: Chemical structures of the principal biomass components – lignin, cellulose, hemicelluloses (xylan, glucomannan), and typical extractives (α-terpene, β-sitosterol, abietic acid) (47, 48).

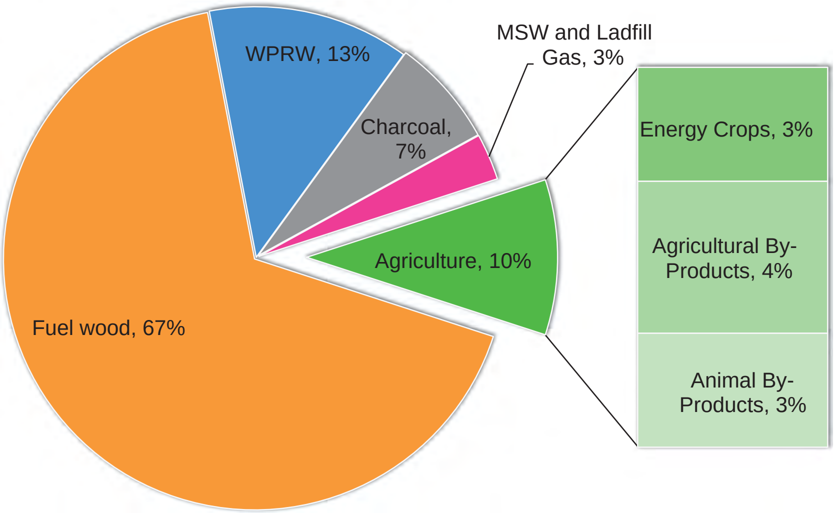

Figure 4: Global primary biomass sources for energy production, based on (5). MSW - municipal solid waste; WPRW - wood processing residues and wastes (color figure available online).

Different strategies for biomass raw materials valorization can be used depending primarily on the chemical composition of the feedstock. The lignocellulosic biomass, i.e., the most abundant biomass resource, consists of three polymers, namely cellulose, hemicellulose, and lignin being accompanied by extractives, e.g., terpenes (Fig. 3). The concentrations of these main components vary substantially depending not only on the plant type (51) but also on the local environment (Fig. 5). This diversity in composition presents yet another challenge for lignocellulosic biomass upgrading. Different thermo-chemical concepts have been reported for the primary upgrading of lignocellulosic biomass and reviewed by several authors (1, 17, 18, 32, 33, 52–58). These include selective deconstruction, yielding the individual polymers, or unselective treatments such as pyrolysis or gasification, affording the so-called pyrolysis oil (bio-oil) and synthesis gas (mixture of CO and H_2), respectively.

The former approach is similar to the current pulp production and offers an advantage of tailoring the secondary upgrading reaction conditions specifically for each polymer type. Moreover, specific transformation (valorization) chains for cellulose (and hexoses), hemicellulose (and pentoses), lignin (and phenols), and extractives can be envisaged as each of the chains will need specific upgrading conditions (including catalyst) and will afford different products and/or chemical intermediates. In principal, this approach relies upon targeted depolymerization and its main advantage would be the possibility to derive selectively several “platform chemicals,” e.g., levulinic acid, glycerol, 5-hydroxymethylfurfural, or hydroxypropionic acid (29, 30, 59–63). Those could

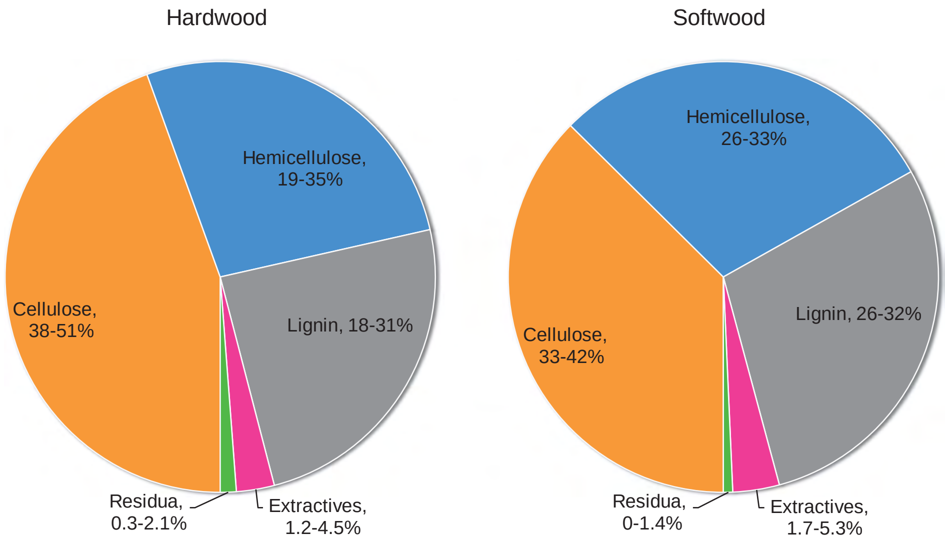

Figure 5: Average composition of woody biomass, based on (51) (color figure available online).

be further transformed into final products or intermediates of various chemical syntheses (e.g., monomers). The most promising platform chemicals to be derived from carbohydrates are depicted in Fig. 6 (59).

Molecular sieves are the most important group of heterogeneous catalysts nowadays in refining and petrochemistry and they are promising catalytic systems to enhance significantly transformations of biomass, as will be shown here. The step-wise biomass deconstruction (i.e., primary upgrading) could be in principle based on the current pulping technologies affording cellulose, hemicellulose, and lignin. For upgrading of other raw materials than those currently used in pulping it has to compete with the relatively "simple" and well-proven pyrolysis and gasification technologies. As a result, new less-demanding pulping procedures allowing easy separation of the three polymers and their dissolution are sought. Ionic liquids might provide such a solution in the future (52, 64–66).

The latter, non selective, approach relies primarily on pyrolysis and gasification. The details of the technologies are outside of the scope of this review and can be found elsewhere, see, e.g., (53–57, 67). Pyrolysis affords a liquid product, bio-oil, that can be further upgraded to fuel components or chemical intermediates (53, 67–69). The obvious advantage of this approach is a relatively broad portfolio of feedstocks, ranging from wood and forestry residues to various agricultural residues, being processed to obtain a liquid product. At the same time, the volumetric energy density increases. The disadvantage of bio-oil is its complex composition, high concentration of water, low pH, and instability, which is a challenge for efficient catalytic upgrading

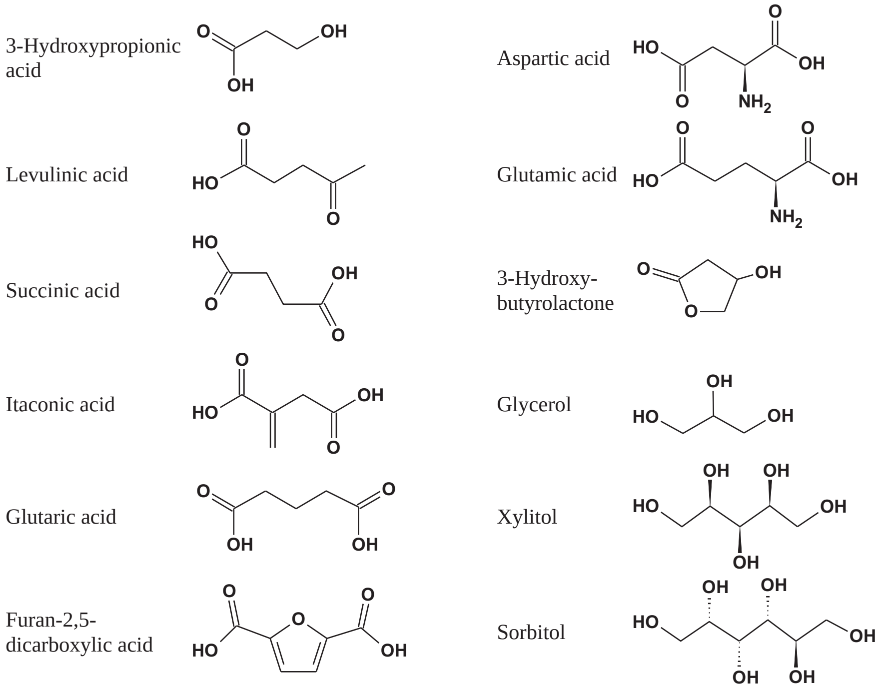

Figure 6: Suggested platform chemicals derived from biomass feedstocks (59, 61).

(deoxygenation) of bio-oil (69, 70). On the other hand, gasification yields a simple and versatile product: synthesis gas that can be processed using well-mature technologies, such as Fischer-Tropsch synthesis (71). The main challenge of this approach lies in scaling down the gasification technology to make it economical also for the scattered biomass resources. The advantage, on the other hand, is rather obvious: principally, any product can be synthesized using synthesis gas (see Fig. 7 (72)). The applicability of molecular sieves in synthesis gas-related transformations was also demonstrated (73–76), but the details are out of the scope of this article as these can be considered as general petrochemical transformations rather than biomass-related.

The non lignocellulosic biomass raw materials are significantly less complex. Following their isolation from the original plants (sugar cane, sugar beet, rapeseeds soybeans, etc.) they can be directly converted into final products. Sugars are usually fermented affording ethanol or butanol while lipids react with methanol or hydrogen to yield the corresponding methyl esters or hydrocarbons, respectively (36, 37). Various extractives such as terpenes, fatty acids, and sterols (Fig. 3) are raw materials for production of fine chemicals, isoeugenol, matairesinol, β-sitostanol, verbenol, and verbenone, to name a few (29, 30). After isolation, their transformation to useful petrochemicals (e.g., cymenes) is comparatively easy since they typically contain less oxygen and

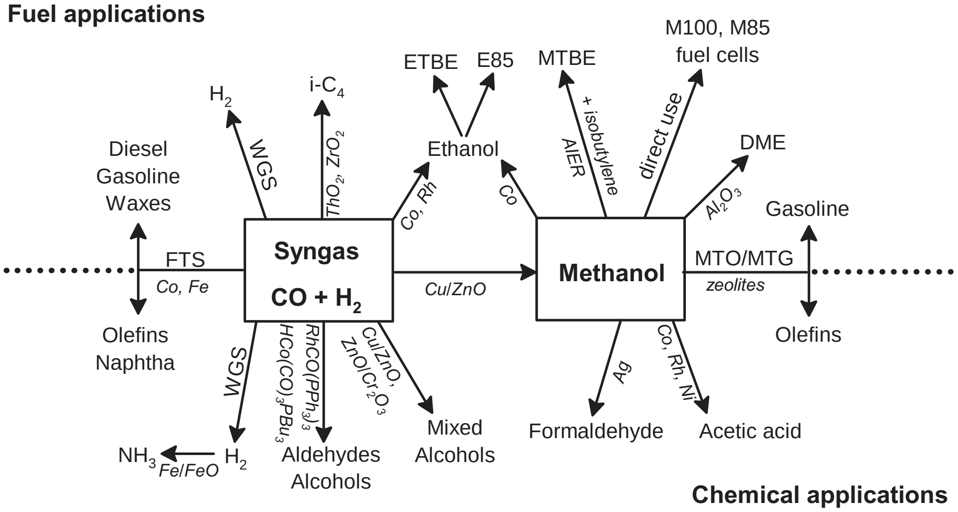

Figure 7: Synthesis options from synthesis gas (72). FTS – Fischer-Tropsch synthesis; WGS – water-gas shift; AIER – acid ion-exchange resins; MTO/G – methanol-to-olefins/gasoline; DME – dimethyl ether; E/MTBE – ethyl/ methyl *tert*-butyl ether; E85/M100 – fuel containing 85 % ethanol/ 100 % methanol.

have a relatively low molecular weight. Nonetheless, they are significantly less abundant than the main components of lignocellulosic biomass.

The wide variety of biomass-derived feedstocks (related to their origin as well as composition) implies that there is no general route to their upgrading but there exists a broad range of alternative processing routes. In principle, biomass upgrading into value-added products can be tackled by a "bottom-up approach" or a "top-down approach." The "bottom-up approach" one relies on conversion of the simplest building blocks in organic chemistry obtainable from any biomass feedstock, i.e., carbon monoxide and hydrogen (being called synthesis gas or syngas), into virtually any chemical compound containing carbon, hydrogen, and sometimes also oxygen. Some of the applications of syngas are depicted in Fig. 7. The "top-down approach" approach is based on a step-wise deconstruction of the complex biomass-derived feedstocks into simpler building blocks, sometimes denoted as platform chemicals, and on the design of specific transformation routes affording desired products from these platform chemicals. The complexity of biomass-derived feedstocks, including the "deconstruction products/intermediates" is schematically shown in Fig. 8. In the present article, we have decided to focus on the "top-down approach," i.e., we discuss at first the transformations of the most complex biomass feedstock, i.e., lignocellulosic biomass, followed by transformations of sugars and sugar alcohols, triglycerides, glycerol, short-chain aldehydes and ketones, and terpenes. In this way, the complete transformation chain, e.g.,

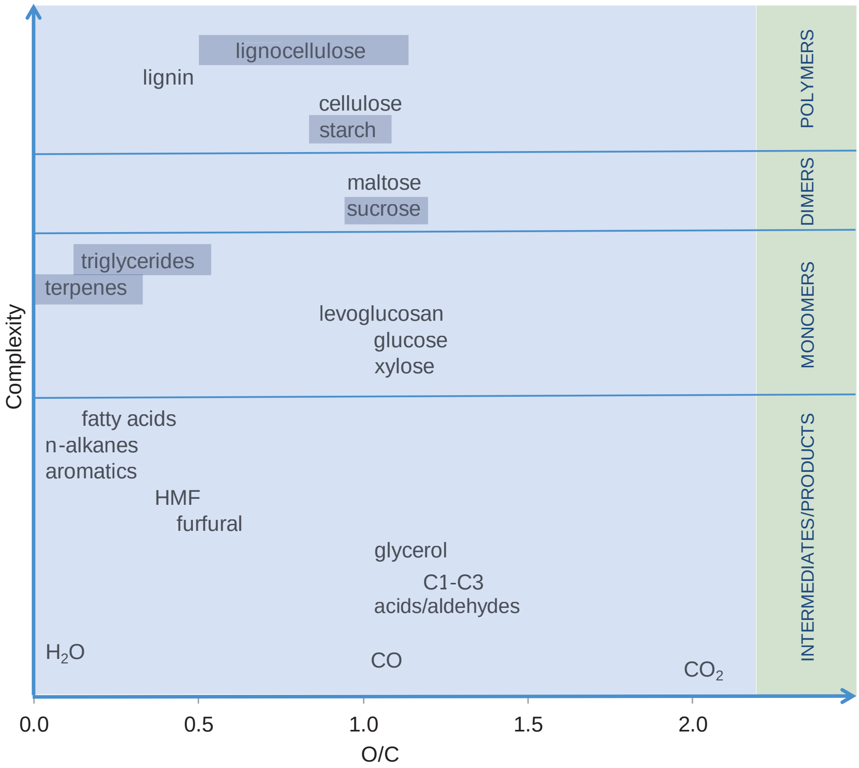

Figure 8: Schematic representation of biomass-derived feedstocks based on their complexity and oxygen content. The primary feedstocks obtainable directly from nature are depicted in square boxes (color figure available online).

lignocellulose – cellulose – glucose – 5-hydroxymethylfurfural, can be easily followed.

Here, we strictly look at the role of heterogeneous catalysts, molecular sieves in particular, in valorization of some of the most promising biomass-derived raw materials in detail. The next part is thus devoted to the current developments in conversion of lignocellulosic biomass, triglycerides, glycerol, sugars and sugar alcohols, aldehydes, and ketones from biomass pyrolysis, terpenes, and phenols.

3. BIOMASS-RELATED APPLICATIONS OF MICRO- AND MESOPOROUS CATALYSTS

3.1. Transformations of Lignocellulosic Biomass

The main objective is to break down bulky molecules originating from biomass to rather low molecular-weight intermediates and to facilitate their (partial) deoxygenation to achieve intermediates useful in the production of high value-added products. Owing to the complexity of biomass feedstocks, their conversion involves a wide variety of chemical reactions connected with oxygen elimination (dehydration, decarboxylation, decarbonylation) and rearrangement of C–C bonds (cracking, oligomerization, alkylation, isomerization, cyclization, and aromatization). The simplest method of lignocellulosic biomass "deconstruction" to lower molecular weight chemical intermediates is its pyrolysis. The main challenge of biomass pyrolysis is the low selectivity to specific intermediates, i.e., a rather wide variety of products is formed, imposing thus challenging upgrading of the intermediates into final products.

3.1.1. Pyrolysis

The main purpose of biomass pyrolysis is to convert the heterogeneous solid material into a liquid product, so-called bio-oil or pyrolysis oil. The by-products of this transformation include gaseous products, typically light hydrocarbons and carbon oxides, and coke, i.e., solid product of condensation and dehydrogenation reactions deposited on the catalyst (53–55, 69, 77). Apart from obtaining a liquid product that can be rather easily handled, volumetric energy density is also increased reducing thus the transportation cost per unit of energy transported. This is particularly important for processing of waste materials, such as straw. The liquid product can be further upgraded using heterogenous catalysts to yield hydrocarbons in gasoline and diesel fuel range as the most important desired products with heavier hydrocarbons being the main by-products. Due to the chemical and thermal instability issues, high polarity, and corrosiveness of pyrolysis oils (68, 70), different concepts of biomass pyrolysis have been proposed to maximize the yields of the most valued products to be used as automotive fuel components.

Two basic approaches to biomass pyrolysis can be distinguished: (a) thermal pyrolysis followed by subsequent catalytic treatment of either pyrolytic vapors or of the bio-oil and (b) addition of catalyst directly into the pyrolysis process (i.e., changing the purely thermal process to a combined thermo-catalytic process). While in the latter case a large external surface area of the catalyst may be important (advantageous), in the former one the molecular sieving properties play an important role (due to limiting coking) — similar to the FCC process. Comparison of different studies concerning catalytic pyrolysis of biomass and interpretation of their results requires extreme caution particularly in connection with the various experimental setups (e.g., fluidized vs. fixed bed, experimental vs. analytical pyrolysis, etc.), experimental conditions used and inconsistency of data reported by different authors.

The catalytic upgrading of biomass-pyrolysis vapors using zeolite catalysts (ZSM-5) was pioneered already in the 1980's and 1990's by Diebold and Scahill (78–80), and Horne and Williams (81–84). Oxygen content of the pyrolysis oil originating from fluidized bed pyrolysis at 550°C could be reduced from 33 wt.% (in absence of ZSM-5) to about 13 wt.% when the vapors were treated over ZSM-5 fixed bed at 550°C. At the same time, the overall concentration of CO and CO_2 in the gaseous products increased from 13.4% to about 31% (81, 84). The coke deposited on the catalyst was shown to contain significant quantities of oxygen that decreased with the reaction time from 34.4 wt.% after 30 min to *ca.* 16.4 wt.% after 120–180 min and to lead to catalyst activity decline as evidenced by the gradual decrease of monocyclic and polycyclic aromatics (82). Nonetheless, the formation of aromatic hydrocarbons (both mono- and polycyclic) was significantly promoted by ZSM-5 while the concentration of oxygenates decreased (82, 83). The ZSM-5 catalyst could be regenerated (air, 550°C, 8 h) to recover partially its activity, as evidenced by the decreased yields of gases and aqueous phase after 3 regeneration cycles (30.0 and 15.8 wt.% vs. 36.9 and 18.0 wt.% for fresh catalyst). Further regenerations did not affect the catalyst performance (85).

A comparison of H-ZSM-5 with partially exchanged Na-ZSM-5, zeolite Y, and activated aluminaindicated the superiority of a medium pore zeolite (ZSM-5) over a large pore one (Y) in conversion of biomass-pyrolysis vapors as evidenced by a higher yield of pyrolysis oil and gases over medium pore zeolites (Table 1) (86). Increasing concentration of sodium decreases the amount of acid sites and may partly decrease the available reaction volume in the channel system. As the location of aluminum controlling the positions of sodium in ZSM-5 (87) depends on the synthesis conditions of an individual sample (88), no general conclusion can be made for this issue. Owing to the sterical limitations inside the pores of ZSM-5, formation of larger coke molecules is prevented. Consequently, the coke deposited on ZSM-5 catalysts amounted to *ca.* 12 wt.% as compared with *ca.* 19 wt.% deposited on Y zeolite (86). Similar amounts of coke (18.5 wt.%) were found also on activated alumina (86), as there are no pore size restrictions preventing coke formation and growth.

In recent studies, the amount of coke in fluidized bed pyrolysis decreased in the order Y > Beta >Mordenite > ZSM-5 and Y > Beta > Ferrierite reflecting the pore size/connectivity and structure of zeolites (89, 90). The surface area of all spent catalysts dropped dramatically (below 100 m^2/g), but could be restored after regeneration by burning off the carbonaceous deposits (89). The increasing concentration of strong Brønsted acid sites, i.e., those retaining pyridine at 450°C, per unit surface area was shown to enhance the extent of deoxygenation over zeolite Beta (the concentration of strong Lewis acid sites was roughly the same for 3 of the 4 studied catalysts), as evidenced by the decreasing yield of organic oil and increasing yield of aqueous phase. Unfortunately, information about coke levels on the spent catalysts was not provided (91). A comparison of different molecular sieves and experimental setups is given in Table 1.

Table 1: Comparison of catalytic pyrolysis results using zeolite catalysts in different experimental setups.

Primary bed / T, °C	Secondary bed / T, °C	Catalyst / Si/Al	Feed	Product yields, wt.%[a]				Ref
				Gas	Oil	Char	Coke	
Fluid / 550	Fixed / 500	ZSM-5	Mixed wood[d]	37.8	6.0	17.1	11.9	(85, 86)
		Na-ZSM-5		36.9	5.5	16.8	12.5	
		Y		29.6	1.1	17.5	19.1	
		Al_2O_3		28.2	3.1	17.1	18.4	
Fluid / 400	Fluid / 450	H-Beta/12.5[b]	Pine wood dust, 355–500 μm	10.6	37.8	18.6	2.8	(90)
		Fe-Beta/12.5[b]		12.7	37.0	19.3	3.7	
Fluid / 450	-	H-Beta/12.5	Pine wood dust, 355–500 μm	49.5	15.1	10.4	11.2	(89)
		H-ZSM-5/11.5		52.1	20.7	9.0	5.2	
		H-Y/6		51.1	9.0	6.5	16.7	
		H-MOR/10		48.1	17.6	12.7	7.2	
Fluid / 450	-	H-Beta/12.5	Pine wood dust, 355–500 μm	49.4	15.8	21.7[c]		(91)
		H-Beta/75		52.8	12.3	21.5[c]		
Fluid / 400	Fluid / 450	H-Beta/12.5	Pine wood dust, 355–500 μm	36.3	21.7	23.1	2.1	(92)
		H-Beta/12.5 +Bentonite		37.2	16.6	23.0	4.2	
		Bentonite		37.5	21.2	21.1	2.4	
Fixed / 550	Fixed / 550	Al-MCM-41	Milled spruce wood	7.7	11.0	-	51.3[e]	(96)
		Al-SBA-15		11.4	19.3	-	48.4[e]	
		Fe-MCM-41	Lignocell/miscanthus[d]	8.6/17.1	8.8/16.0	-	52.0/34.8[e]	(97)
		Cu-MCM-41		9.7/14.4	11.4/17.5	-	36.5/29.0[e]	
		Zn-MCM-41		8.3/5.8	13.0/14.2	-	35.0/39.7[e]	
Fixed / 550	Fixed / 550	MCM-41	Lignocell[d]	9.9	19.8	-	32.7[e]	(98)
		Al-MCM-41-50		7.5	22.6	-	37.4[e]	
		Al-MCM-41-50S[f]		11.2	12.9	-	41.1[e]	

[a] The balance to 100% is water.
[b] Yield of unidentified products H – 20.3 wt.%, Fe – 16.9 wt.%.
[c] Including coke yield.
[d] Total mass balance higher than 90%.
[e] Includes also yield of charcoal.
[f] Steamed at 750°C.

Application of a dual bed system (1st bed – thermal pyrolysis at 400°C; 2nd bed – catalytic upgrading of vapors at 450°C) instead of a single fluidized catalytic bed (450°C) resulted in considerably lower formation of coke on spent catalysts (2.1 and 0.6 wt.% vs. 11.2 and 5.2 wt.% for zeolites Beta and ZSM-5, respectively). At the same time, the yields of char and gaseous products decreased for both zeolites from *ca.* 22 to about 10 wt.% and *ca.* 50 wt.% to *ca.* 37 wt.% (89, 92). It can be speculated that owing to the close contact of biomass with catalyst in the single bed part of the char is deposited on the external catalyst surface and reported as coke. Moreover, the deoxygenation performance of the dual system seems to be better as increased yields of water were obtained (13.5 vs. 16.5 wt.%) and further improvement (to *ca.* 19 wt.%) was reported by using hybrid zeolite/bentonite catalysts (35/65 wt.%) (89, 92). When ion-exchanged with iron (3.4 wt.% Fe), the catalytic performance of zeolite Beta was modified only slightly, the yield of water increased to 14.0 wt.% (90) indicating a minor improvement in deoxygenation catalyst activity. Similar improvement was also observed as a result of modification of zeolite Y and Ferrierite (90). On the other hand, modification of ZSM-5 with gallium (1 wt.%) resulted in enhanced aromatization activity as evidenced by the increased concentration of monoaromatics (e.g., toluene – 10.4 vs. 5.7 wt.%, xylenes – 10.9 vs. 6.4 wt.%) and suppressed gas formation (93). The gaseous products consisted typically of carbon oxides (>80%) accompanied by C_1-C_4 hydrocarbons.

To investigate the effect of different oxygenates on the cracking process, a series of model compounds was cracked under biomass-pyrolysis conditions over ZSM-5 (Si/Al = 50) (94). Cracking of anisole, a representative of phenolic compounds, at 500°C differed substantially from other oxygenates (methanol, furfural, and cyclopentanone). The non phenolic oxygenates afforded mainly C_7-C_{10} aromatics, phenol, and its alkyl derivatives were the main products of anisole cracking. Hence, phenolics (originating from lignin fraction of biomass) were suggested to be detrimental for the catalytic upgrading of pyrolysis liquids (94).

Recently, a screening of different catalysts (ZSM-5, MgO, NiO, Al_2O_3, ZrO_2, TiO_2, FCC catalyst, etc.) in in-situ catalytic upgrading of pyrolysis vapors originating from fast pyrolysis of beech-wood-derived feed has been performed by Stefanidis et al. (95). Considering their very different properties, including specific surface areas and acidity, the performance of the catalysts was rather similar. It can be hence concluded that the fixed bed setup allows describing mainly the thermal pyrolysis process and the role of catalysts is rather difficult to interpret.

Catalytic performance of modified Al-MCM-41, Si-SBA-15, and Al-SBA-15 catalysts in fixed-bed biomass (milled spruce wood) pyrolysis was compared with a commercial equilibrium FCC catalyst (96) (typically consisting of amorphous alumina-silica matrix, USY as the main cracking catalyst, 15–25 wt.%, and ZSM-5 as an additive, <5 wt.%). Very high yields of coke, even if the coke reported here consists in fact of coke and char, were obtained in these experiments (42–52 wt.%; Table 1) as compared with the fluidized bed experiments discussed above. The lowest coke yield was obtained with the FCC catalyst. As the yield of coke and char decreases, the yields of desired liquid products increase hand in hand with the yield of gaseous products. Unfortunately, not a clear conclusion can be drawn on the effect of MCM-41 dimensions, only Cu-modified MCM-41 afforded less coke than the unmodified MCM-41 catalysts due to an oxidation ability of Cu species (96). Detailed investigation of metal-modified MCM-41 catalysts (Fe, Cu, Zn) confirmed the effect of Cu (97). The organic liquid products (OLP) from beech wood pyrolysis over MCM-41 catalysts were rich in hydrocarbons (14–30 wt.% of OLP) and polycyclic aromatic hydrocarbons (25–44 wt.% of OLP) while the metal-containing MCM-41 catalysts afforded more oxygenates, mainly alcohols, carbonyls, and acids (97). Moreover, different types of biomass (spruce and miscantus) behaved differently, in terms of product yields over various catalysts used (MCM-41, SBA-15, Cu-MCM-41, FCC catalyst) (96, 97).

Unfortunately, results reported for MCM-41 catalysts with similar Si/Al (34 and 30, and 51 and 50) (97, 98) using the same experimental setup and procedure as well as the same feedstock differ greatly, e.g., the reported coke yields were 45–50 wt.% (97) vs. 37–38 wt.% (98). This makes the understanding of such effects as varying acidity and pore size by synthesis (96, 97) or steaming (98) very difficult if not impossible. One of the reasons could be the different synthesis protocol for individual Al-containing MCM-41 catalysts. It was shown earlier that the concentration of accessible Al is much lower than the overall Al concentration and depends on the synthesis strategy (99). Conventional Al-MCM-41 (Si/Al = 50) was also compared with its mesoporous analogues (MSU-S) synthesized from H-Beta (Si/Al = 50) seeds (100). The application of MSU-S catalysts resulted in a decreased yield of total liquid product (32–38 vs. 48 wt.%) consisting of organic and aqueous phase, i.e., total pyrolysis bio-oil, and increased yield of coke (43–49 vs. 37 wt.%). However, the main difference was in the organic liquid product composition. The MSU-S catalysts afforded *ca.* 39 and 50 wt.% of polyaromatics and heavy compounds, respectively, in the organic phase, while the corresponding concentrations obtained over MCM-41 were 7 and 9 wt.%, respectively (100). Concurrently, the formation of oxygenates was severely minimized with MSU-S catalysts (100). The differences in the behavior of Al-MCM-41 and MSU-S are attributed to a higher acidity (particularly Brønsted one) in the case of MSU-S, which arises from the presence of Beta seeds (101).

The influence of mesoporosity on the performance of ZSM-5, the most promising catalyst for biomass pyrolysis so far, was investigated using two types of mesoporous ZSM-5 catalysts, prepared either by direct synthesis using mesopore-directing agent or by desilication of primarily synthesized ZSM-5 crystals (102). The directly synthesized mesoporous ZSM-5 catalyst outperformed both the conventional ZSM-5 as well as mesoporous ZSM-5 synthesized from zeolite seed crystals (all Si/Al = 17.5–20.1) by yielding the most aromatics (C_6–C_9) in the organic phase (*ca.* 29 wt.% vs. *ca.* 20 and 2 wt.%, respectively). The selectivity of this catalyst to C_6–C_9 aromatics was further improved by its incipient wetness impregnation with 1 wt.% Ga, their concentration in the organic product increased to about 38 wt.% (102). It has been shown that excess of Ga (5 wt.%) resulted in suppressed formation of aromatics, plausibly due to the reduced catalyst acidity. Moreover, gallium was reported to suppress both gas and coke yields while the total yield of bio-oil increased (102), which could be explained by dimerization and cyclization of gaseous products affording liquid phase aromatics. One can expect that too high concentrations of Ga in the form of oxide nanoparticles block the entrances to the zeolite channel system and the promoting effect is minimized at the expense of a low catalytic activity.

Carlson et al. (103, 104) applied a more fundamental approach to biomass pyrolysis. The authors demonstrated the effect of the hydrogen-to-carbon efficient ratio ($H/C_{eff,}$ defined as (H – 2O) / C) (104) predetermining the maximum theoretical yield of hydrocarbons as the lignocellulosic feedstocks having H/C_{eff} in the range 0–0.5 are hydrogen deficient (105). In line with these limitations, xylitol ($H/C_{eff} = 2/5$) afforded more aromatics than glucose ($H/C_{eff} = 0$) – *ca.* 45 vs. 30 wt.% in their pyrolysis over ZSM-5 (Si/Al = 60). The yields from cellulose and cellobiose pyrolysis (both having $H/C_{eff} = 0$) were similar to those of glucose indicating that glucose is a suitable model compound for cellulose pyrolysis (103). The yields of aromatics from glucose pyrolysis (600°C, catalyst-to-feed = 19, 240 s) declined in the order ZSM-5 >> silicalite > Beta > SiO_2-Al_2O_3 ≈ Y (being >10 for silicalite and Beta, and 0 for SiO_2-Al_2O_3 and Y). Large quantities of coke (>50 wt.%) were formed over Beta, SiO_2-Al_2O_3, and Y (103). These results evidence the utmost importance of the catalyst structure as only medium pore zeolites prevent excessive coking; it would be interesting to see the results performed with much lower amounts of catalysts. Moreover, the catalyst acidity is essential too, as demonstrated by the superior performance of ZSM-5 over silicalite. Apart from the catalyst structure, a fast heating rate and high catalyst-to-feed ratio are crucial for minimizing coke yields (103). It has been suggested that two main steps are involved in glucose pyrolysis: (a) fast thermal decomposition via retro–aldol condensation or dehydration and (b) aromatics formation inside the zeolite pores (104) confirming the need for a close contact between catalyst and feedstock molecules and optimum catalyst properties, particularly in terms of its pore dimensions and acidity.

In this context, the role of zeolite pore size and shape selectivity on the conversion of glucose to aromatics was studied as well (106). The yield of aromatics could be correlated with the zeolite pore size. The highest yields of aromatics (up to 35% in the case of ZSM-5) were reported for the medium-pore zeolites with pore size in the range 0.52–0.56 nm, while small- and large-pore zeolites afforded no or low yields of aromatics, respectively (106). In addition, large-pore zeolites facilitated carbonaceous deposits formation, whereas oxygenated products and carbon oxides were the main products over small-pore zeolites besides coke (106). Conversion of a wide spectrum of chemical intermediates originating from biomass (thermal) pyrolysis was thoroughly investigated by Gayubo et al. (107–109) using a ZSM-5 catalyst (Si/Al = 24). As the attention is specifically focused on alcohols, phenols, aldehydes, ketones, and acids, the results will be addressed in the appropriate section below.

3.1.2. Depolymerization

Besides pyrolysis, liquid-phase conversion of cellulose under rather mild reaction temperature (185°C) and hydrogen pressure (20 bar) was investigated over mesoporous molecular sieve (Al)MCM-48 with or without Pt. The primary products included sugars, such as glucose and xylose, that were further hydrogenated to sugar alcohols (sorbitol and xylitol) and/or dehydrated to furfural derivatives (furfural, furfuryl alcohol, 5-hydroxymethyl furfural) (110). The same research group has also focused on detailed investigation of catalytic transformation of levoglucosan (1-6-anhydro-β-D-glucopyranose), i.e., an important product of cellulose pyrolysis, over different molecular sieves, such as Beta, MCM-22, MCM-36, and MCM-48 (111,112,113). Over acidic zeolite Beta (Si/Al = 25) ca. 90% conversion of levoglucosan was achieved in liquid phase at 150°C and 20 bar; the main product being glucose accompanied by 5-hydroxymethyl furfural (111). On the contrary, under gas phase conditions (300°C, atmospheric pressure) glycolaldehyde, formaldehyde, acetic acid, and acetaldehyde were the main condensable products over H-Beta. The significantly lower concentration and strength of acid sites in MCM-48 in comparison with H-Beta (2 vs. 143 μmol/g) are plausibly the main reason for much lower conversion (30%) over MCM-48 under liquid phase conditions (111). In fact, this conversion is only slightly higher than in the case of non-catalytic experiment (conversion 20%) (111).

More liquid oxygenates (glycolaldehyde, formaldehyde, acetic acid acetaldehyde, furfural, and 5-methyl furfural) were obtained from levoglucosan over mesoporous molecular sieves (pillared MCM-36 and MCM-41) at 300°C and atmospheric pressure than over microporous MCM-22 (112, 113). For instance, at a short contact time, 0.005 min, the molar yield of furfural and glycolaldehyde were 0.06 and 0.33, respectively, over MCM-41 while only 0.01 and 0.17, respectively, over MCM-22 (112). By swelling of MCM-22 and subsequent pillaring of swollen MCM-22, MCM-36 was obtained and its performance in levoglucosan conversion was compared to that of the parent MCM-22. To investigate the influence of acidity, MCM-36 catalysts with Si/Al equal to 47, 65, and 92 were synthesized. Their Bronsted acidity decreased with the decreasing Al content from 87 to 36 μmol/g (113). The lowest (molar) yields of glycolaldehyde, the main reaction product, were obtained over MCM-22 (0.1 over 0.25 g of catalyst). However, the glycolaldehyde molar yield varied in the range 0.28–0.38 for the 3 MCM-36 catalysts without a clear correlation with their Bronsted acidity (113).

Zeolites were also applied in hydrolysis of polysaccharides. For instance, inulin, was hydrolyzed to fructose over a zeolite with conversion 95% within 2 h at reaction temperature 100°C (114). More importantly, cellulose was successfully converted to a mixture of sugar alcohols by using Pt and Ru modified zeolite USY (2.5 wt. % Pt or Ru) at 190°C and initial hydrogen pressure of 5 MPa (115). The yield of sorbitol and mannitol was 25 and 6%, respectively. As the supports yielded only very low yields of glucose (ca. 2 % in case of USY), it was inferred that the supported metals promoted cellulose hydrolysis in addition to hydrogenating glucose to sorbitol and mannitol (115).

In summary, ZSM-5-derived catalysts outperform other zeolites or aluminosilicates (Beta, USY, Mordenite and amorphous aluminosilicates (86, 89, 102, 104, 116, 117) owing to their optimum pore dimensions and architecture preventing formation of large coke precursors accelerating rapid catalyst deactivation and favoring, in particular, deoxygenation and aromatization reactions. This has been confirmed for lignocellulosic biomass (saw dust) (116, 117) as well as for various model compounds (cellulose, glucose, xylitol) (104, 116, 117) and pyrolysis oils and vapors (102, 120). Apart from the decisive role of channel dimensions and connectivity, the density and strength of Brønsted acid sites and modification by other active phases, particularly metals, are the key parameters affecting primarily the selectivity. Similar experiments shall be carried out with catalysts exhibiting zeolite acidity but not limiting the reaction space, like various MCM-22-related materials and other two-dimensional zeolites (118, 119).

3.2. Transformations of Triglycerides

Triglycerides are the main components of vegetable oils and animal fats (>95%). In contrast to lignocellulosic biomass, the composition of vegetable oils is rather well defined/uniform and the content of oxygen is significantly lower (*ca.* 11 wt.%). In addition, they can be directly upgraded into fuel components partially replacing fossil fuels. Consequently, the utilization of triglycerides for production of biodiesel (fatty acids methyl esters, FAME) by transesterification with methanol affording FAME and glycerol (121, 122) is one of the most mature technologies producing fuels or chemicals from renewables. Despite its maturity, the technology does not fully comply with the green chemistry principles as significant amounts of waste streams are formed. It is based on using a homogeneous catalyst (typically NaOH, KOH, or CH_3ONa) requiring separation from the products (FAME)

(122). This separation includes neutralization and washing resulting in large quantities of waste water streams generated (up to three liters of waste water for each liter of biodiesel) (123). Moreover, utilization of glycerol, the main by-product, is essential as it represents *ca.* 10 wt.% of the raw material. However, it typically contains catalyst residues, salts, and water, thus, its upgrading to a quality suitable for chemical syntheses is very demanding (124). Consequently, alternatives to homogeneous transesterification are sought. The most investigated ones include transesterification using heterogeneous catalysts (124–126), deoxygenation yielding diesel-range hydrocarbons (36, 37), and catalytic cracking affording for olefins and aromatics (127–129). These are schematically depicted in Fig. 9 (36). The application of molecular sieves is important especially in transesterification and catalytic cracking of triglycerides, even though mesoporous molecular sieves were occasionally studied also for deoxygenation (130, 131). While basic catalysts were primarily studied in heterogeneously-catalyzed transesterification, e.g., alkali-metals doped or exchanged molecular sieves, acidic catalysts, mostly zeolites and mesoporous molecular sieves have been investigated for catalytic cracking of triglycerides (127–129). Hence, the topics will be discussed separately.

3.2.1. Transesterification

The key parameters of heterogeneous transesterification catalysts are their basicity and stability with the main challenge being preventing the leaching of the active basic components. Due to their ion-exchange properties, zeolites modified by alkali metals have been proposed as suitable

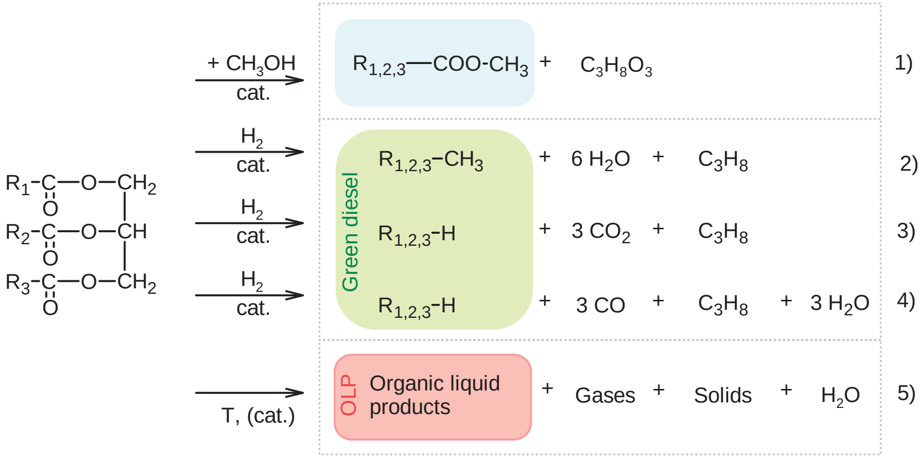

Figure 9: A simplified scheme of the main reaction paths in transformation of triglycerides into biofuels via catalytic processes: (1) transesterification; (2) hydrodeoxygenation; (3) hydrodecarboxylation; (4) decarbonylation; and (5) cracking/catalytic cracking based on (36) (color figure available online).

heterogeneous transesterification catalysts (125, 126). Other catalytic systems include basic oxides (such as MgO, CaO) (132–136), mixed oxides (e.g., hydrotalcites) (124, 137–140) and impregnated alumina catalysts (141–143) including mesoporous alumina (144).

Owing to its high ion-exchange capacity and hence possibility to achieve high density of basic cations, NaX has been studied extensively (141, 145). It was reported that modification of the parent NaX zeolite with KOH (145, 146) or NaO_x (141) was crucial to achieve basic sites of the high strength (i.e., >15 on the Hammett indicators scale) resulting in a high catalyst activity. Alternatively, thermally treated titanosilicate ETS-10 exhibited higher conversion than 90% similarly to NaO_x/NaX zeolite (141). Only a minor reduction of conversion was observed when the catalyst (NaO_x/NaX) was reused. It could be tied to the partial leaching of sodium. A severe drop in conversion (from 85% to 49%) after one reuse cycle was observed for the KOH/NaX catalyst and it was attributed to the leaching of KOH (145). Among KI modified catalysts, zeolite KL and NaX exhibited lower activity in comparison KI/Al_2O_3, which was explained by their lower base strength. The modified zeolites showed also lower activity than KI/ZnO having a similar base strength, which was attributed to possible differences in the amount of basic sites (143). It seems, however, more plausible that the pore dimensions of the zeolites prevent the bulky molecules of triglycerides from entering the zeolite pores and hence limiting the access of reactants to the active basic sites located inside the microporous structure.

Potassium-modified mesoporous molecular sieves, as well as delaminated zeolites (MCM-41, SBA-15, and ITQ-6, respectively). were also active in triglycerides transesterification with methanol, but exhibiting a severe decrease in conversion (e.g., K-ITQ-6 from 97% over fresh catalyst to only 56% in the second cycle) (147, 148). It could be attributed to potassium leaching, as its concentration on the catalyst dropped from 1.59 wt.% to 0.51 wt.% (147). Despite similar conversion of triglycerides over K-ITQ-6 and K-MCM-41 (64 and 58%, respectively, both having $Si/Al = \infty$), the yield of biodiesel differed tremendously (56 and 3%, correspondingly). It has been suggested that it may be a consequence of the higher hydrophobicity of potassium-modified ITQ-6, nonetheless, the potassium loading of MCM-41 was also significantly lower (0.22 vs. 1.59 wt.% K on ITQ-6) (147). As both supports were purely siliceous, a high level of leaching of K is not surprising as the cations are only loosely bounded to the surface.

Acidic forms of zeolites Y, ZSM-5, and Beta have been studied together with other solid acidic catalysts (ion-exchange resins, sulfated zirconia) by Kiss et al. (149). Only a small increase in the conversion of dodecanoic acid reacting with 2-ethylhexanol has been observed for the zeolites (conversion ca. 40% in a non catalytic experiment and 42–44% in a zeolite-catalyzed experiment (H-ZSM-5, Y, Beta) after 120 min at 130°C and alcohol to acid molar ratio 1:1) as compared with the non catalyzed reaction. This has been explained by limited diffusion of the bulky triglycerides into the zeolite pores (147, 149). Conversion in the same range (*ca.* 40%) was also reported for zeolite beta (150, 151). An increase in conversion (from 40 to *ca.* 50%) was observed when the zeolite was ion-exchanged with La cations. The increase was attributed to enhanced concentration of external Brønsted acid sites owing to La introduction resulting in presence of Si-OH-La and La-OH groups (150). The hydrophilicity of the surface of acidic zeolites has been also suggested to explain their low transesterification activity (147). One can argue that La^{3+} cations (Lewis sites) can also contribute to a higher acidity, resulting then in higher conversion.

The co-existence of acidic and basic active sites in zeolites provides a potential advantage for processing of feedstocks containing free fatty acids (FFAs) requiring conventionally a two-step treatment, .i.e., first esterification of FFAs using an acid catalyst and subsequently transesterification of triglycerides using a basic catalyst. This advantage has been demonstrated for transesterification of a feedstock containing FFAs (total free acidity 5.58%) using K-ITQ-6 and KOH. While with both catalysts virtually complete conversion of triglycerides was achieved, although under different reaction conditions, conversion of FFAs was different — more than 90% of FFAs were converted over K-ITQ-6, but only *ca.* 45% with KOH (147). The conversion of fatty acids in esterification over Al-MCM-41 after 90 minutes was shown to increase with decreasing Si/Al ratio, i.e., increasing concentration of acid sites. The conversion of palmitic acid increased from 55% to 80% when bulk Si/Al ratio decreased from 32 to 8 (152).

In conclusion, despite some promising results achieved with alkali-metal-modified zeolites (Table 2), the possibility of increasing their basic sites strength while simultaneously creating a stable catalyst, i.e., with limited leaching of alkali cations, is still challenging. Consequently, the first commercial heterogeneous transesterification catalyst (process EsterfipH by Axens) consists of mixed oxides (Zn, Al) (124).

3.2.2. Catalytic Cracking

The modern cracking processes rely typically on the tunable acido-basic properties and molecular-sieving ability of zeolites. As these properties are of importance for any catalytic cracking process, most of the studies dealing with catalytic cracking of triglycerides focused on zeolites and related microporous-mesoporous molecular sieves (127–129, 155–157). Since the molecular dimensions of triglycerides exceed those of zeolite channels, significant effort has been oriented towards developing composite catalysts, so-called microporous/mesoporous molecular sieves (158). These materials provide two levels of molecular sieving: mesopores can accommodate even triglycerides, but only the intermediates originating from their cracking can enter the micropores and undergo not only further cracking, but also aromatization reactions.

Table 2: Comparison of zeolite performance in transesterification of vegetable oils.

Catalyst	Conditions	Basicity	Conversion/Yield of methyl ester	Reference
NaX	150°C, 24 h, SBO, MeOH/SBO = 6, 10 wt.% cat.	S = 3.26	38.8/23.9	(141)
KX		S = 3.07	40.9/31.5	
NaOx/NaX			100/94	
ETS-10	60°C, 24 h, SBO, MeOH/SBO = 6, 10 wt.% cat.	S = 3.68	100/95.8	
NaX		S = 3.26	19.4/6.8	
NaOx/NaX			95.4/84.2	
ETS-10		S = 3.68	96.5/80.7	
KOH/NaX	65°C, 8 h, SBO, MeOH/SBO = 10, 3 wt.% cat., 10 wt.% KOH	15 < H_ < 18.4	85.6/-	(145)
KI/NaX	65°C, 8 h, SBO, MeOH/SBO = 15, 2 wt.% cat., 35 wt.% KI	9.3 < H_ < 15	12.9/-	(143)
KI/KL		9.3 < H_ < 15	28.3/-	
KI/Al2O3		15 < H_ < 18.4	87.4/-	
H-X	100°C, 24 h, WFO, MeOH/WFO = 15, 5 wt.% cat.		8/0.5	(147)
K-MCM-41			58/3	
K-ITQ-6			62/53	

SBO – soyabean oil; WFO – waste fruit oilseeds; NaOx/NaX – NaX occluded with 3 sodium azide/supercage; S – Sandersons intermediate electronegativity; H_ — Hammett indicator strength.

In a near future, even "two-dimensional" zeolites possessing limited size of the third-dimension could provide a better catalytic performance (159–161).

The products of catalytic cracking of triglycerides over zeolites such as ZSM-5 or Beta, comprise hydrocarbon gases (C_3–C_5 paraffins and olefins), so-called organic liquid product (OLP, i.e., mixture of aliphatic and aromatic hydrocarbons with traces of oxygenates) and coke (127, 128). Deoxygenation is achieved during cracking of triglycerides and carbon oxides and water are formed as well (127, 128, 155). Obviously, OLP is the most desired product for potential fuel and petrochemical applications. It consists of hydrocarbons in the boiling point range of gasoline due to cracking reactions, diesel and also vacuum distillates originating from condensation reactions (127, 128, 155). The yield and composition of OLP is particularly affected by the following factors: (a) reaction conditions; (b) strength of Brønsted acid sites of the catalyst; (c) concentration of Brønsted acid sites; and (d) structure of the catalyst (in particular, pore dimensions and connectivity). The cracking is typically investigated at atmospheric pressure and temperatures ranging from 350–550°C.

Among zeolites, ZSM-5, Beta, and USY were studied most extensively in catalytic cracking of triglycerides (127, 128, 157, 162–164). While gaseous and gasoline-range hydrocarbons are the main products over ZSM-5, USY and Beta exhibit higher selectivity towards diesel-range hydrocarbons (128). ZSM-5 is a medium-pore zeolite (cf. Table 4) and its pore dimensions virtually prohibit the formation of diesel-range hydrocarbons (linear hydrocarbons in diesel-range could be in principle formed, however due to slow diffusion they would crack before leaving ZSM-5 pores), while they can be easily formed in the large pore zeolites. The pore dimensions affect also the rate of coke formation. It increases in the order H-ZSM-5 < H-Beta < H-USY (128). The higher coking rate of USY, in comparison with zeolite Beta, can be ascribed to the presence of cavities in USY zeolite allowing the formation of bulky coke precursors. Owing to its strong acidity and unique pore dimensions and architecture, ZSM-5 afforded rather selectively aromatics (aromatic yield was 80–95 wt. % of OLP), particularly benzene and toluene. When comparing the performance of different structural types of zeolites, the overall yield of hydrocarbons decreases in the order H-ZSM-5 > silicalite > H-Mordenite > H-Y. The yield of aromatics correlated with the overall yield of hydrocarbons over zeolites, while amorphous silica-alumina provided significant yields of aliphatic hydrocarbons (>20 wt.% vs. <5 wt.% over ZSM-5) (127).

The composite microporous/mesoporous materials were investigated with the intention to enhance diesel-range hydrocarbons, being nowadays more valuable from the fuel applications point of view than gasoline-range hydrocarbons (165). The composite micro/mesoporous catalysts (H-ZSM-5/MCM-41, H-Beta/MCM-41, H-ZSM-5/SBA-15) outperformed both the microporous as well as mesoporous parent materials in terms of yields of gasoline fraction and aromatics (Table 3). This indicates the importance of optimum balance between acidity of active sites and diffusion of reactants and products. Also, the overall yield of OLP increased (156, 157, 166). The improved yields of aromatics could be attributed to pre-cracking of triglycerides in the mesopores and the enhanced access of the intermediates into the micropores (156) or by the possibility of coke deposition in the mesopores preventing the fast blockage of micropores.

Vegetable oils were also cracked to hydrocarbon components (mainly aromatics, iso-paraffins, and iso-olefins) belonging both in gasoline and diesel fuel range under typical FCC conditions (commercial FCC catalyst, reaction temperature 485–585°C, contact time <5 s) (167). Oxygen was removed predominantly in the form of water plausibly by dehydration and aromatics were the main products, confirming thus results of the previously discussed studies. Moreover, co-processing of vegetable oils with vacuum distillates was investigated (168, 169). The addition of rapeseed oil (up to 30 %) to vacuum gas oil (VGO), a typical FCC feedstock, resulted in a decreased yield of liquid hydrocarbon products. At the same time, the yield of C_3/C_4 olefins was enhanced from 8.7–9.5 wt.% when increasing rapeseed oil concentration from 0 to 10 wt.% (168). Only traces of oxygenates, such as carboxylic acids, were detected in the liquid products. Likewise, the catalytic cracking of animal fats afforded aliphatic hydrocarbons at lower cracking temperature (400°C) and

Table 3: Comparison of molecular sieves performance in catalytic cracking of vegetable oils and fatty acids.

Catalyst	Conditions	Conversion, %	Product yields, wt.%[a] Gas	OLP[a]	Water	Coke	Gasoline in OLP, wt.%	Aromatics[b] in OLP, wt.%	Ref
HZSM-5	450°C, $2.5\ h^{-1}$, fatty acids mixture, atm. pressure	89.9	25.7	54.1	8.8	1.4	37.0	48.3	(156)
MCM-41		69.5	17.9	34.6	7.4	9.6	25.7	6.6	
CMZ20[c]		86.8	19.5	57.5	8.3	1.5	43.7	54.0	
SBA-15		61.4	9.5	41.0	33.7	7.2	20.7	–	
CSZ20[c]		97.6	33.2	56.6	7.2	0.6	39.6	54.8	
H-Beta	450°C, $2.5\ h^{-1}$, waste palm oil, atm. pressure	70.9	10.9	41.4	7.0	11.6	16.1	–	(166)
MCM-41		72.7	14.4	41.4	7.4	9.4	30.3	–	
CMB20[d]		67.8	9.1	43.7	6.4	8.6	30.6	–	
H-Beta/MCM-41[e]		87.6	13.4	57.1	6.4	10.7	28.9	–	
HZSM-5-50[f]		96.8	17.4	–	6.8	1.7	44.6	53.1	(157)
MCM-41-64[f]		92.8	9.6	–	6.7	11.8	31.3	–	
CMZ20[c]-76[f]		94.0	17.8	–	–	3.0	45.4	51.4	
CMZ20[c]-12[f]		91.1	11.4	–	–	2.5	38.0	46.1	

[a] Organic liquid product.

[b] Total benzene, toluene, and xylene.

[c] Composite of MCM-41 (M) or SBA-15 (S) and HZSM-5 with 20% of mesophase in the synthesis gel.

[d] Composite of MCM-41 (M) and H-Beta (B) with 20% of mesophase in the synthesis gel.

[e] Physical mixture.

[f] Si/Al ratio.

alkyl aromatic hydrocarbons at higher cracking temperatures (550°C) (170). This shift was attributed to the significantly enhanced rate of the cyclization reactions at the elevated temperatures. Moreover, the indigenous vegetable oil impurities, such as phosphorus or calcium, were shown to deteriorate the catalyst cracking activity considerably (168).

In summary, it can be inferred that the yield of hydrocarbons from triglyceride cracking increases with the decreasing pore diameter of the investigated zeolites. Consequently, the primary decomposition of triglycerides has to occur on the external surface of zeolite crystals, as triglycerides cannot fit into the medium- or large-pore zeolite channels. In contrast, the increasing pore dimensions result in increasing yield of carbonaceous deposits and hence a lower yield of gaseous and liquid hydrocarbons. More importantly, the results suggest that the effect of pore structure is more important than that of the catalyst acidity and that the primary conversion is rather a thermal process than a catalyzed one (by the acid sites of zeolites). This means that the product distribution is determined primarily by the shape selective characteristics of the catalyst (155), catalyst acidity being also of some importance. Furthermore, it may be proposed that a careful optimization of the pore architecture at both micropores, as well as mesopores, provides a tool for selectivity fine tuning in the case of cracking of bulky biomass-derived reactants.

It should be noted that triglycerides and related feedstocks can be converted selectively into hydrocarbons using hydrotreating catalysts. This process has been commercialized by Neste Oil (process NexBTL). Currently, four production units with a total capacity of nearly 2 Mt/y are operated worldwide (171). While the deoxygenation step relies on other than molecular sieve catalysts, the subsequent mild isomerization step (165) is catalyzed most probably by Pt modified zeolites. As this is a conventional refining technology, it is not discussed here. Nonentheless, mesoporous molecular sieves modified by CoMo were shown to be viable deoxygenation catalysts though less active than the alumina supported ones (130, 131).

Bio-oil, the desired product of biomass flash pyrolysis, needs to be further upgraded before it can be used as a component for automotive fuels blending. Two principal refinery alternatives include deep hydrotreating (172, 173) and fluid catalytic cracking (FCC) (174). Hydrotreating of bio-oils necessitates a two-step process where in the first step the most reactive components (e.g., aldehydes) are saturated under mild reaction conditions (<250°C, 10 MPa). Only then complete deoxygenation of bio-oil under the required severe reaction conditions (>350°C, 20 MPa) can be achieved without excessive coking (172). Similarly, direct introduction of bio-oil in the FCC process was shown to be not feasible as the rate of coke formaton is too high (174). Hence, a pretreatment to remove the components responsible for rapid coking prior to catalytic cracking (FCC) was suggested (175). Following bio-oil upgrading at 230°C and

29 MPa, the product could be blended in an FCC feed (long residue) up to a concentration of 20 wt.% and co-processed. The products were oxygen free despite the high oxygen concentration in the feed (17–28%). The propensity to coke formation (expressed by the MCRT results) decreased with the increasing HDO pretreatment temperature and hence with the decreasing oxygen content in bio-oil (the MCRT value dropped from 14 to 2 when the oxygen content decreased from 28 to 15%, which corresponds to upgrading temperature increase from 230 to 330°C) (175). The discussed difficulties of further upgrading of (thermal) flash pyrolysis bio-oils explain the research interest in catalytic pyrolysis as it includes partial deoxygenation leading to more stable bio-oil product.

3.3. Transformations of Sugars and Sugar Alcohols

Sugars (carbohydrates) are the main building blocks of cellulose and hemicellulose, which makes them the most abundant biomass-derived renewable raw materials. Consequently, their efficient utilization in production of renewable fuels and chemicals is essential. Carbohydrates are mostly transformed by fermentation to yield important industrial chemicals, such as ethanol, butanol, and lactic acid as well as prospective platform chemicals (e.g., 3-hydroxypropionic acid, succinic acid, etc.) (29, 31, 59, 61). The largest heterogeneously catalyzed process for sugar transformations is hydrogenation of glucose affording sorbitol (capacity 650 kt/y in 2008), an intermediate in vitamin C production (176, 177).

As a result of extensive research efforts focused on development of new processes utilizing renewable raw materials, zeolites were suggested for separations (e.g., carbohydrate separations (178, 179), 1,3 propanediol from glucose and glycerol separation (Na-ZSM-5 membrane) (180), production of oxygenated platform chemicals, such as levulinic acid, 5-hydroxymethylfurfural, and sorbitol (181–195) oxygenated fuel components (197, 198), and production of hydrocarbons, mainly olefins and aromatics (106, 199–202). Other applications include glucose isomerization to fructose (187, 203–206), glucose oxidation to hydroxyacids (207, 208), and synthesis of alkyl glucosides (191, 208–210).

The main challenge in catalytic transformation of sugars into hydrocarbons is the necessity to perform the conversion in aqueous phase as sugars are thermally unstable under gas phase conditions. Generally, three main classes of reactions are involved: C–C bond cleavage (e.g., retro aldol condensation, decarbonylation), C–O bond cleavage (e.g. dehydration), and hydrogenation reactions (see Fig. 10) (200). Brønsted acidity is crucial for dehydration reactions, while supported noble metal clusters catalyze hydrogenation and C–C bond cleavage reactions (200).

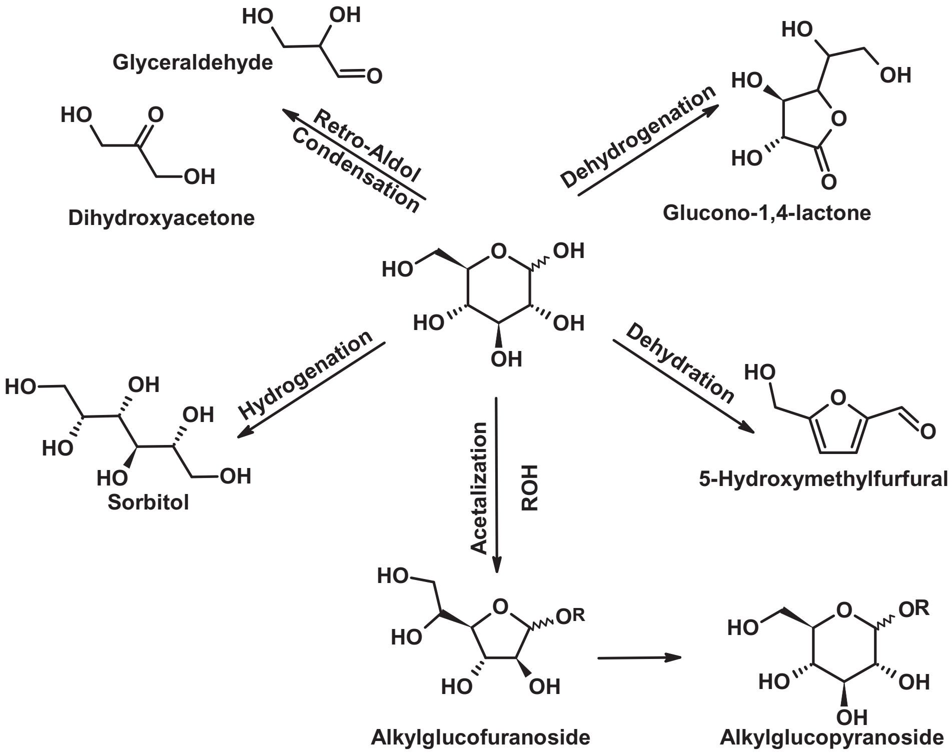

Figure 10: Possibilities of glucose conversion to useful oxygenated intermediates (59, 199).

3.3.1. *Aromatization*

H-ZSM-5 facilitates selective formation of aromatics suitable for gasoline pool from carbohydrates (104, 211). Similarly to lignocellulosic biomass and triglycerides, the appropriate acidity and pore dimensions are vital for securing high selectivity to aromatics at a minimum coking rate. Apart from the catalyst properties, the yields of aromatics and olefins depend severely on the feedstock composition, namely on its hydrogen to carbon effective ratio (H/C_{eff}), defined as $(H - 2O) / C$ (104, 202) or in more general way as $(H - 2O - 2S - 3N) / C$ (211). It was demonstrated that biomass-derived feedstocks with H/C_{eff} less than 1 (e.g., glucose, sorbitol, glycerol) deactivate the ZSM-5 catalyst more quickly than feedstocks with H/C_{eff} larger than 1. Furthermore, the aromatic and olefin carbon yields increase with increasing H/C_{eff} ratio. It has been suggested to hydrogenate feedstocks deficient in hydrogen to reach an H/C_{eff} ratio of *ca.* 1.2 to improve aromatic and olefin production (202). Mixtures with an overall H/C_{eff} ratio in the range 1.3–1.6 have been recommended to avoid catalyst deactivation and to increase the yield of desired hydrocarbons (211). This was demonstrated by upgrading carbohydrate- (e.g., glucose, xylose, sucrose) methanol mixtures (50% solution) over ZSM-5 at 510°C, atmospheric pressure and *ca.* 2 g_{mix}/g_{cat}.h (211) where methanol enhanced the H/C_{eff} ratio and subsequently the yield of hydrocarbons. The yield of hydrocarbons dropped with increasing kinetic diameters of the reactants (glucose vs. sucrose) suggesting the importance of accessibility to the channel system of ZSM-5 (211). When the 4:1 methanol-to-glucose solution was used instead of glucose alone, the yield of hydrocarbons was enhanced from less than 20 to about 45 wt.% (211). It should be noted that besides carbohydrates also methanol can be converted under these reaction conditions to hydrocarbons.

It can be concluded that due to inherent feedstock limitations (low H/C_{eff}), carbohydrates can be efficiently converted to hydrocarbons, typically aromatics and short-chain olefins, only when processed in the presence of a hydrogen donor, e.g., methanol, or after hydrogen pretreatment yielding intermediates having sufficiently high H/C_{eff}. Otherwise, the yields of valuable products are prohibitively low due to excessive coking.

Application of more selective catalytic strategies, such as dehydration or hydrogenation, provides a very promising route to important future chemical intermediates, so-called platform chemicals, such as 5-hydroxymethylfurfural (HMF), levulinic acid (LA), or sorbitol. The production of sorbitol by heterogeneously catalyzed hydrogenation is a commercial process (176, 177). With Ru/H-USY (3 wt.% Ru), starch hydrolysates underwent combined hydrolysis/hydrogenation to yield sorbitol and mannitol solutions in one-pot synthesis (45, 189). Brønsted acid sites at the external surface hydrolyze amylose, which is too bulky to enter zeolite Y pores, to glucose that is hydrogenated to sorbitol over Ru sites located both inside zeolite channels as well as on the external surface (45). Essentially complete conversion was achieved after 1 h at 180°C and 5.5 MPa and the selectivity to sorbitol was >95% (45).

3.3.2. Dehydration

The synthesis of HMF from glucose and fructose was demonstrated to be feasible over microporous (H-Y, H-Mordenite) (181,182) as well as other molecular sieves MCM-20 or MCM-41 (182) (Fig. 11). Mesoporous MCM-41 promoted the cleavage of the glucose - pyranose ring owing to their suitable dimensions of intraparticle voids (pores) (182). The reaction is probably catalyzed by Brønsted acid sites. The decomposition of glucose was even faster over microporous materials, but resulted in a significant formation of coke and hence decreased selectivity to HMF and its subsequent decomposition products, i.e., organic acids (formic acids, 4-oxopentanoic (levulinic) acid). Formic acid was the main product with selectivity up to 60 % followed by HMF (selectivity up to 30 %) (182). In contrast, fructose could be converted to HMF with selectivity > 80 %, yield > 70 % over H-Mordenite. The selectivity decreased with its dealumination and hence with the increasing volume of mesopores. It has been speculated that the pore structure hinders HMF

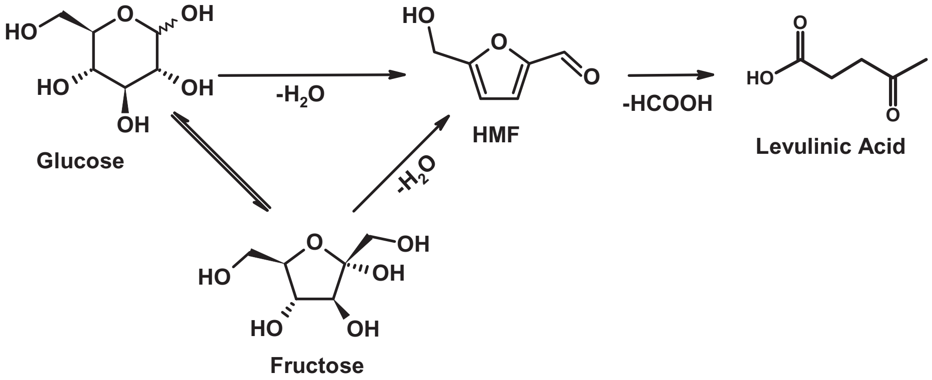

Figure 11: Transformation of glucose to yield 5-hydroxymethyl furfural and levulinic acid, based on (182).

rearrangement into heavy products (i.e., coke precursors) (181). HMF could be also obtained rather selectively over functionalized SBA-15 (selectivity 71%, conversion 84%). The increasing hydrophobicity of the silanes used in functionalization was suggested to affect positively the selectivity towards HMF (212). Significantly lower yields were obtained, for instance, over Al-TUD-1 (*ca.* 20 wt.%), the by-products of which were speculated to be soluble polymers rather than coke, which was attributed to prevailing Lewis acidity and weak Brønsted acidity of the catalyst (190).

Analogously, zeolites (H-Y, H-Mordenite, Si/Al *ca.* 10) convert xylose into furfural with selectivity >90% at conversion 30% in water/toluene (but only *ca.* 50% at similar conversion in water/methyl isobutyl ketone). Obviously, the solvent choice affecting furfural extraction from the aqueous phase influenced the overall process (183). Comparable catalytic performance exhibited also the significantly less acidic Al-TUD-1, particularly in terms of concentration and strength of Brønsted acid sites, providing 60% yield of furfural at 90% conversion (190). In comparison with monosacharides, disaccharides (sucrose, cellobiose) and xylan were easily hydrolyzed (100% conversion) over Al-TUD-1 to corresponding sugars being subsequently partially dehydrated affording furfural and HMF (190). Direct route to HMF from cellulose using ionic liquids has been recently reported (186). Zeolite Y added in an ionic liquid facilitated cellulose hydrolysis to glucose and disaccharides. The superiority of zeolite Y over sulfonated resins and sulfuric acid was explained by the fact that HY did not catalyze the subsequent hydrolysis of HMF that was the main consecutive reaction in strong acids (186).

Consecutive rehydration of HMF affords levulinic acid (LA), another important intermediate. Usually, this reaction is catalyzed by mineral acids, as the yields over solid acids reported so far were unsatisfactory (184, 213). For example, the maximum yield of LA obtained over HY was about 20 wt.% as it was consumed in secondary reactions due to its diffusion-limited transport in the zeolite pores (213). The yield of LA obtained from glucose was almost doubled (36 wt.%) over a composite micro/mesoporous catalyst (having ZSM-5 structure) synthesized through hetero-crystal seeding method (184). While glucose conversion increased with the decreasing Si/Al ratio (130 to 12), the yield of LA exhibited an optimum at Si/Al = 15, which has been explained by the higher extent of fragmentation reactions over the more acidic catalyst affording lactic acid as a by-product. Its yield was 19.1 and 6.8% for catalyst with Si/Al equal to 12 and 15, respectively (184).

3.3.3. Isomerization

Apart from enzymes, namely D-glucose ketoisomerase which is a very efficient catalyst, zeolites can be also used to catalyze isomerization of glucose to fructose (204, 205), which is of importance for instance in glucose conversion to HMF. Two heterogeneously catalyzed routes have been reported. The first one relies on the use of alkaline-cation-exchanged zeolites and selectivity to fructose in the range 60–80% was achieved at conversions 20–30 %. However, cation leaching (> 10 %) remains a challenge (NaX, KX) (204). The other approach uses Sn-Beta or Ti-Beta as a solid catalyst and glucose (aqueous solution) is converted in a mixture of glucose, fructose and mannose (46:31:9 wt. %) (205). Glucose isomerization to fructose over Sn-Beta was also used in designing a biphasic system (H_2O/THF/NaCl) allowing the isomerization to proceed at pH *ca.* 1 favorable for direct fructose dehydration to HMF by a mineral acid (HCl). This one-pot synthesis approach was successfully applied for glucose (HMF selectivity 70% at 76% conversion) as well as for starch (HMF selectivity 69% at 75% conversion). On the other hand, the conversion of cellobiose was only 36% (selectivity to HMF 36%) (187). Moreover, glucose and fructose can be separated using CaX or CaY while mannose and glucose separation can be achieved using BaX or BaY (46)

It was shown that the isomerization of glucose to fructose does not proceed over medium-pore zeolite (TS-1) and is considerably slower over modified MCM-41 (Sn-MCM-41, Ti-MCM-41) (205). In contrast, basic titanosilicates (ETS-10, ETS-4, AM-4) and mixed alkali silicates (AV-1, AV-2, TOB) (203) were active and except ETS-10 catalysts gave better results than Na-X zeolite—fructose yields were above 30% while only 20–25% over NaX and ETS-10 catalysts. The best performance at 100°C was achieved over ETS-4 (glucose conversion 48%, fructose selectivity 84%) (203). Sorbitol, a product of glucose hydrogenation, is commercially dehydrated to isosorbide and reacted with, e.g., lauric acid to afford “green” plasticizers. The traditional synthesis using, e.g., sulfonic acid resin could be replaced by MCM-41 functionalized with sulfonic groups. In one-pot synthesis using sorbitol and lauric acid in molar ratio 1:6 as raw materials dilaurylisosorbide was obtained with 95% selectivity at 33%

conversion of lauric acid at 110°C (46). On the other hand, no conversion was observed over H-Beta (Si/Al = 12.5) (46).

Lactic acid and alkyl lactate can be obtained by dehydration and isomerization of triose sugars (dihydroxyacetone, glyceraldehyde that can be obtained, e.g., by oxidation of glycerol as discussed below) over zeolite catalysts (192, 193, 195), amorphous aluminosilicates and silicoaluminophosphates (194) in water or alcohol solutions. Apart from being a very valuable monomer for biodegradable plastics, lactic acid offers also a promising utilization of glycerol. Unlike most of the up-to-now discussed applications of zeolites in renewable raw materials upgrading, production of lactic acid from triose sugars relies on Lewis acidity of the catalyst (192–195). It was demonstrated that the lactic acid and its methyl ester can be efficiently produced over Sn/Beta (192) as well as H-USY (Si/Al = 6) having significant concentration of Lewis acid sites (*ca.* 200 μmol/g) (193). Similarly, increasing Lewis acidity in zeolite Beta by isomorphous substitution of silicon for Ti or Zr or due to steaming (leading to formation of extra-framework Al species) increased the yield of methyl lactate (from *ca.* 5% for Al-Beta to about 30–40 for Ti-Beta, Zr-Beta and steamed Al-Beta) (192). The highest reported selectivity was, however, obtained over an amorphous aluminosilicate with Si/Al = 10 (conversion 25%, selectivity 96%) (194). A concerted action of Brønsted and Lewis acid sites was suggested to be essential as trioses (dihydroxyacetone, glyceraldehyde) were first dehydrated over Brønsted acid sites with medium acid strength present in USY to pyruvic aldehyde before reacting with an alcohol over Lewis acid sites to afford the corresponding alkyl lactate (195). Strong Brønsted acid sites were shown to be detrimental for catalyst activity as they catalyze the formation of diethyl acetal of pyruvic aldehyde, thus decreasing the selectivity towards the desired lactate (194, 195). It follows that Lewis acidic zeolites may find future applications in isomerization of oxygenates, particularly of the carbohydrate type, the challenge being to prevent strong adsorption leading to severe catalyst coking and deactivation. Moreover, finding the optimum balance between Brønsted and Lewis acid sites of the appropriate strength remains a challenge to be solved (194, 196).

3.3.4. Esterification and Oxidation

In addition, several more specialized zeolite applications for carbohydrate transformations were suggested as well (197, 198, 207, 209, 210). Proton-form zeolites (H-Y, H-Beta, MCM-22, H-ZSM-5, H-Mordenite) were shown to be active and selective in synthesis of alkyl glucosides that could be used as environmentally friendly detergents (209). The highest yields of alkyl glucofuranosides and pyranosides were obtained from D-glucose and *n*-butanol when zeolite Beta was used (>90%) (209). Hydrophilic zeolites were less efficient due to a strong competitive adsorption of polar compounds, i.e., zeolites with high Si/Al ratio are preferable (209, 210). In fact, optimum Si/Al ratios were reported depending on the zeolite preparation method, being around 100 for dealuminated and 30 for as synthesized zeolite Beta (210). Moreover, zeolite crystal sizes in excess of 0.35 μm were shown to influence strongly the zeolite activity by diffusion (210). Ketalization of monosaccharides with acetone over H-Beta and H-Y was successfully demonstrated by Maksimov et al. (197, 198). The ketals, obtained in yields above 50%, were suggested as prospective high octane number components (197).

Ti-containing zeolites (TS-1, Ti-MCM-41, and titanated zeolites Y, L, and Mordenite) were investigated as glucose oxidation catalysts (207). Glucose oxidation by hydrogen peroxide afforded various hydroxyacids, the main being gluconic acid resulting from the aldehyde group oxidation (maximum selectivity nearly 30% at conversions 20–30%). Neither conversion nor selectivity of glucose oxidation depended on the pore size or titanium species (207). Titanosilicates (TS-1) were also used to oxidize furans, e.g., 2,5-dimethyl furan that can be obtained by selective hydrogenation of 5-hydroxymethyl furfural, i.e., a product of dehydration of fructose or glucose (40, 46). Nearly complete conversion of 2,5-dimethyl furan was achieved in 3 h in acetonitrile at 25°C when using H_2O_2 as an oxidant. Diones, *cis-* and *trans*-hex-3-ene-2,5-dione, were obtained with 85% selectivity at 94% conversion (46,214). Oxidation of furan was complete in about 5 hours at 20°C in acetonitrile and the main products were maleic and fumaric dialdehydes with overall selectivity 80% (214).

Although molecular sieves can be used for direct conversion of sugars into hydrocarbons, their physico-chemical properties play only a secondary role, as the yields are limited severely a priori by feedstock composition (its H/C_{eff}). Consequently, it appears that more attention shoud be paid to selective conversions of sugars, e.g., by partial dehydration, to platform chemicals, such as 5-hydroxymethyl furfural (HMF), levulinic acid, or furfural, that can be further transformed to a wide range of valuable products including fuel components. Molecular sieve pore dimensions, surface polarity, and acidity are key parameters decisive for minimizing undesired side reactions resulting in coking and catalyst rapid deactivation.

3.4. Glycerol Transformations

Glycerol has a special place among biomass-derived feedstocks, as it is obtained with high selectivity as a by-product of biodiesel production by transesterification of triglycerides with methanol. Its amount corresponds to *ca.* 10 wt. % of the starting triglycerides and hence it is crucial, from the economic point of view, to utilize it for production of high-added-value products. Each carbon atom of glycerol bears a functional group, thus, it has many

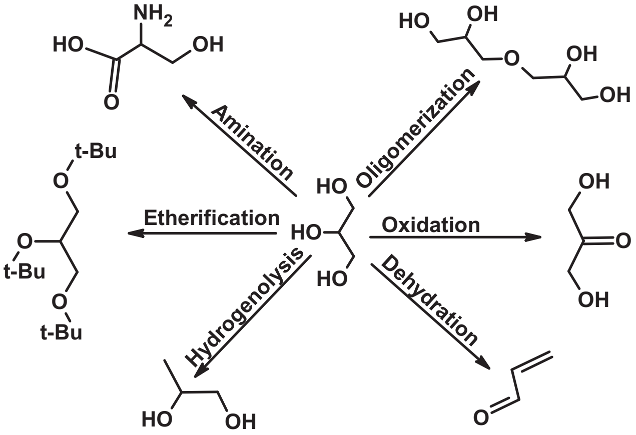

Figure 12: Main catalytic routes of glycerol transformation, based on (215, 216).

application opportunities and belongs to platform chemicals. Some basic chemical transformations of glycerol utilizing various heterogeneous catalysts are depicted in Fig. 12. Only the transformations over micro- and mesoporous catalysts are discussed here. Nonetheless, it should be mentioned that there are successful applications using other types of catalyst, e.g. for conversion of glycerol to epichlorhydrine that was commercialized recently (217).

3.4.1. Dehydration

Among many reaction pathways available for glycerol (see Fig. 12), dehydration to acrolein offers the highest application potential for zeolites. Acrolein is currently produced by selective oxidation of propylene and it is used primarily for the production of acrylic acid and its esters. Various zeolites and zeotypes (H-Beta, H-Y, H-Mordenite, H-ZSM-5, H-Ferrierite, ZSM-22, SAPO-34) were found as active catalysts in glycerol dehydration to acrolein (218–224). It was demonstrated that the reaction is sensitive to many reaction parameters, namely specific surface area, pore architecture, and total acidity, the external surface area, and presence of extra-framework alumina (EFAL) species (223, 218). As the channel systems of zeolites are typically quickly filled with carbonaceous deposits due to the reactivity of glycerol-dehydration products, only the external surface sites can contribute to glycerol conversion. Consequently, the highest conversion (*ca.* 94 vs. 30–76% over zeolites after 2 h on stream) has been obtained over silica-alumina (315°C, 0.1 MPa, 8.3 mol% $C_3H_8O_3$ and 76.3 mol% H_2O in He), i.e., the material with the largest external surface area (218). It also follows that the particle size of the zeolite crystals plays a significant role with nano-crystals (ZSM-5, Si/Al *ca.* 65, 20–60 nm) outperforming bulkier crystals (*ca.* 20 μm) (219). Analogously, a commercial

ZSM-5 additive for fluid catalytic cracking containing 15 wt.% ZSM-5 (Si/Al = 50) was found to afford high acrolein yields (molar carbon yield 55–62%, conversion >85%) at 350°C in a moving bed reactor (Microdowner, residence time 0.5—1.0 s) (220). With respect to that it can be inferred that two-dimensional zeolites can be more resistant to deactivation due to much higher external surface compared with conventional zeolites.

Nonetheless, selectivity rather than activity is crucial in this case. It was suggested that Brønsted rather than Lewis acid sites are responsible for high acrolein selectivity (221, 222), which can also explain the drop in acrolein selectivity with increasing concentration of EFAL species in Ferrierite (218). Moreover, high density of Brønsted sites has been beneficial for acrolein formation when comparing different nanocrystalline HZSM-5 catalysts (Si/Al 14, 18, 65, 145, ∞) with similar crystal size (0.02–3 μm) (219). Unfortunately, it was not possible to synthesize different ZSM-5 zeolites with identical crystal size and Si/Al ratio varying over a wide range to enable a rigorous analysis of the influence of Brønsted acid sites density. The strength of acid sites, determined by Hammet indicators, was correlated with the selectivity of glycerol dehydration to acrolein (222). Catalysts having acid strength in the range $-8.2 \leq H_0 \leq -3.0$ (e.g., H-ZSM-5 or SAPO-34) exhibited the highest acrolein selectivity (60–70%), while stronger acids ($H_0 \leq -8.2$, e.g., H-Beta) and weaker acids ($-3.0 \leq H_0 \leq +6.8$, e.g., siliceous SBA-15) afforded lower acrolein selectivities (40–50% and <30%, respectively) (222). The decreased acrolein selectivity over catalysts having stronger acidity was attributed to more severe coking (222). It should be noted that the acidity measurement by Hammet indicators may underestimate the acidity of zeolites due to the rather bulky nature of the indicators (222). From the mechanistic point of view, an FTIR study of glycerol dehydration over ZSM-5 concluded that the hydroxyl group on the second carbon atom was dehydrated first rather selectively (221).

In addition to frequently investigated gas-phase dehydration of glycerol, the liquid phase reaction (250°C, 70 bar, 20 wt.% glycerol in water) was recently reported over a series of microporous and mesoporous catalysts by de Oliveira et al. (225). Both catalyst acidity (the density and strength of the acid sites) and structure determine the catalyst activity — hence, proton forms of Beta zeolite, Mordenite, and Y zeolite exhibited the highest conversion ≥90% after 10 h (20 mg catalyst, 20 ml aqueous glycerol solution) followed by H-ZSM-23 (conversion *ca.* 80%) having, in addition to less accessible pore system for glycerol, also a lower density of acid sites (about one third to one half of the other zeolites) determined by TPD of ammonia. The lowest conversion, *ca.* 40%, was observed for the mesoporous siliceous SBA-15 (225). Acrolein was exclusively formed over H-Y, H-Mordenite, and H-ZSM-23. In contrast, H-Beta yielded primarily unidentified products and hydroxyacetone (225) but the reported differences in the strength of the acid sites (that were suggested by the authors to explain the differences in acrolein selectivity) do not provide a clear explanation for the observed deviation of the acrolein selectivity over H-Beta in comparison with the other zeolites. When reused for the second time, the conversion over all catalysts dropped to *ca.* 5–10% (225). A plausible explanation for this decline is coke deposition. The authors concluded that pore blockage can be expected only in the case of zeolites, particularly ZSM-23 and Mordenite, hence the deactivation should be rather attributed to specific adsorption of coke or its precursors on the active (Brønsted acid) sites (225).

3.4.2. Acetalization

Apart from acrolein production, dehydration of glycerol over acidic zeolites (H-Beta, H-Y), saponite, and mesoporous molecular sieves (MCM-41) was also proposed to replace the traditional epichlorhydrine route to glycerol oligomers (226). While zeolite Beta has been studied most extensively, the selectivity to diglycerol has been improved by using MCM-41. The increase in the hydrophobic character of the catalysts (e.g., due to their dealumination) may affect the interaction of glycerol with the surface and result in modified selectivity (226). The wider range of hydrophilic-hydrophobic character of the biomass-derived feedstocks presents thus yet another challenge to their transformation using micro- and mesoporous solids. Optimization of the polarity/acidity of hydrophobic zeolites has a great potential for improving the performance of these catalysts in upgrading glycerol-water mixtures by reacting glycerol with aldehydes to yield cyclic acetals (227).

In the presence of water (up to 31 wt.%), hydrophobic zeolite Beta was found to be more active in acetalization of glycerol with formaldehyde than *p*-toluenesulfonic acid and Amberlyst resin that were more active in absence of water (227). For example, under comparable reaction conditions (25 mg catalyst, 1.115 g CH_2O, 1.220 g $C_3H_8O_3$, and 100°C) the yield of glycerol formals was *ca.* 65% over zeolite Beta and only *ca.* 50% over Amberlyst-36. Strong adsorption of polar products caused zeolite Beta deactivation. This can be partially suppressed by appropriate solvent and modification of catalyst surface hydrophobicity (227). For example, zeolite Beta can be synthesized in fluoride media to obtain a catalyst having less polar surface, i.e., being more hydrophobic due to fewer silanol defects. This way of preparation afforded indeed a more stable catalyst towards deactivation. As the hydrophobicity increases with the increasing Si/Al ratio, i.e., with decreasing concentration of active sites, an optimum between number of active sites and activity decline due to deactivation (hydrophobicity of the catalyst surface) in acetalization of glycerol with formaldehyde was found for zeolite Beta to be at Si/Al of about 50 prepared in fluoride media (227).

3.4.3. *Esterification*

Another well-established application for glycerol is triacetin production traditionally employing mineral acids as homogeneous catalysts. In an attempt to use heterogeneous catalysts in esterification of glycerol by acetic acid, a heteropoly acid ($H_3PMo_{12}O_{40}$) has been encapsulated in the cages of NaUSY zeolite and an active and stable heterogeneous catalyst was obtained (228). The activity of NaUSY was increased up to 6 times when heteropoly acid (HPA) was encapsulated in its cages (from *ca.* 3.10^{-3} mol/h.m_{cat} to about 17.10^{-3} mol/h.m_{cat}) and an optimum concentration of HPA was found to be in the range 0.013–0.019 $g_{HPA}/g_{zeolite}$ (228). The introduction of HPA also improved the selectivity towards acetins (sum of mono-, di-, and triacetin) to $>98\%$ from original 90% observed for NaUSY. Moreover, the main product over HPA/NaUSY was diacetin in contrast to monoacetin over NaUSY (228).

3.4.4. *Etherification*

Etherification of isobutene with glycerol is a new approach aimed at glycerol utilization as a fuel component. Typically homogeneous catalysts, such as *p*-toluenesulfonic acid, and ion-exchange resins, e.g., Amberlyst, have been investigated. They suffer, however, from thermal stability issues (229–231). Moreover, they can also be poisoned by typical impurities of glycerol originating from biodiesel production, i.e., methanol, salts and water (217). As an alternative, zeolites H-Beta and H-Y were studied (230, 231). High conversions of glycerol ($>80\%$) were obtained over both zeolite Beta (Si/Al = 12.5) and Y (Si/Al = 15) at 60°C using dioxane as solvent and molar ratio of isobutylene to glycerol equal to 4:1. The reaction proceeded significantly faster over H-Beta (80% conversion in 60 min) than over H-Y (80% conversion in 400 min) (230). As the formation of tri-*tert*-butylether is sterically hindered over Beta, di-*tert*-butylether was the main product and etherification equilibrium was reached (230). The remaining isobutylene was then consumed by the competing oligomerization reaction yielding C_8 olefins allowing thus the reverse reaction (de-etherification) to take place. As a consequence, the conversion of glycerol decreased after the initial 60 min (230). Both glycerol etherification and isobutylene oligomerization were significantly slower over H-Y resulting thus in higher glycerol conversion after 480 min (88.7%) and also higher yields of di- and tri-*tert*-butylethers than over H-Beta (230).

A treatment of HY zeolite with citric or nitric acids (231) resulted in introduction of mesoporosity and also in modification of the catalyst acidity. The concentration of weak acid sites was lowered more extensively than the concentration of strong acid sites and, in some cases, the strength of the acid sites was increased as well (231). Consequently, increased conversion and selectivity to di-*tert*-butylglycerols were observed (231). A further shift enhancing yields of di- and tri-*tert*-butylglycerols (> 90 %) wasachieved with SBA-15 modified by terminal sulfonic groups, in particular arenesulfonic groups, i.e., moderately strong acid centers (232).

3.4.5. Aromatization

Glycidol, another industrially relevant derivative of glycerol, can be obtained from glycerol carbonate by its conversion at 175°C and 35 mbar over zeolite A. Glycidol is obtained in a yield of 86% and purity of 99% (217). In addition to applications using the high degree of glycerol functionalization discussed so far, the use of zeolites to convert glycerol into alkylaromatics was also proposed (224). Whereas one-dimensional zeolites (ZSM-22, Mordenite) afforded only oxygenates, mainly acrolein and acetol, 3D zeolites (USY, ZSM-5) yielded alkyl aromatics C_8–C_{10} at 300–400°C and 0.1–2 MPa (224). Nonetheless, acrolein was the main product over all zeolites. All zeolites, but Mordenite, had Si/Al of 40–45. Mordenite (Si/Al = 8) was partially ion-exchanged by Na to achieve similar acid sites density to the other zeolites. This is not easily achieved as our earlier report evidenced that Na is mainly exchanged into 8-rings, which are not available for aromatic hydrocarbons (233). Further increase in the yield of alkylaromatics was achieved by applying a dual bed concept, dehydration catalyst (Pd/ZnO) in the first bed and aromatization catalyst (H-ZSM-5) in the second bed. The molar carbon yield of aromatics increased from 21 to 35% when dual bed was used instead of ZSM-5 (400°C, 2 MPa, W/F = 0.5h). No aromatics were formed over the first bed catalyst (Pd/ZnO) (224). In general, the formation of aromatics was favored by longer contact time, higher temperature and pressure (224).

It can be seen that glycerol is a versatile feedstock that can be converted over micro- and mesoporous materials to a broad spectrum of products depending on the reaction conditions as well as catalyst functionality (in particular, acidity – type, strength; pore architecture and dimensions; polarity). Most of the products have a high added value and can be thus considered promising valorization alternatives for glycerol. In some cases, the transformation of glycerol over zeolites could replace the current production based on fossil resources (e.g., acrolein production from propylene) while in other cases it aims at new products (e.g., lactic acid/alkyl lactate production from dihydroxyacetone and glyceraldehyde obtainable by glycerol oxidation).

3.5. Transformations of Low Molecular Weight Aldehydes and Ketones

Biomass decomposition reactions (e.g., fast pyrolysis) yield typically low-molecular-weight products that find direct application only with difficulties. Among low-molecular-weight aldehydes and ketones, typically C_1-C_6 aldehydes and C_3-C_6 ketones are found in bio-oils, i.e., products of biomass fast pyrolysis. Due to their low molecular weight, simple deoxygenation is not suitable for their valorization, e.g., as fuel components. Consequently, condensation reactions, such as aldol condensation or Michael reaction, are necessary to increase the molecular weight of the products and their applicability either as fuel components or as specialty chemicals. Aldehyde and ketones find a broad range of applications in fine chemicals synthesis, which is beyond the scope of this review despite some of them are catalyzed by micro- and mesoporous molecular sieves; for details see (30, 234–245). For more details about heterogeneously catalyzed transformations of biomass-derived aldehydes and ketones see the thorough review by Mäki-Arvela et al. (30).

Transformations of low molecular-weight aldehydes and ketones include a very broad scope of reactions involving a wide variety of reactants and products. These are typically oriented towards production of fine chemicals and rely on dedicated resources, such as acetone or acetaldehyde production. In contrast, biomass pyrolysis products are typically very complex mixtures. To provide some insights in the upgrading of bio-oils or other biomass sources of low-molecular-weight oxygenates studies using relevant model compounds are reviewed in this chapter. The aim is to demonstrate the possibility of bio-oil utilization by selective molecular weight increase accompanied by an improved stability of the product. Consequently, we focus here solely on the conversion of: (a) short-chain aliphatic aldehydes and ketones (i.e., formaldehyde, acetaldehyde, propionaldehyde, and acetone); (b) cyclic aldehydes (i.e., furfural, 5-hydroxymethyl furfural); and (c) aromatic aldehydes (benzaldehyde) being typically found in bio-oils using micro- and mesoporous molecular sieves. Transformation of these intermediates is of the utmost importance for efficient processing and utilization of bio-oils. Besides being suitable candidates for valorization by condensation reactions, particularly by aldol condensation, aldehydes and ketones were also identified as coke precursors in bio-oil upgrading (246) and as fermentation inhibitors (247). Particular attention is hence paid to aldol condensation (248–250) and to improving the quality of bio-oils and fermentation broths (107–109, 246, 247). Another relevant class of reactions, synthesis of acetals, and ketals (197, 198, 251) as possible automotive fuel components over zeolites and mesoporous molecular sieves was discussed above.

3.5.1. Olefins from Short Aldehydes and Ketones

Reactions of various aldehydes and ketones (e.g., acetaldehyde, acetone, butanone) over a catalyst comprising 25 wt.% of ZSM-5 zeolite (Si/Al = 24), bentonite (30 wt.%), and fused alumina (45 wt.%). were investigated by Gayubo et al. at reaction temperatures 200–450°C (107–109). Moreover, the behavior of these principal intermediates in biomass pyrolysis was compared with other important pyrolysis intermediates, namely alcohols, phenols, and acids.

Acetaldehyde underwent polycondensation reactions in the preheating zone (400°C), 50% of acetaldehyde fed in the reactor formed coke even before reaching the catalyst bed (108). Consequently, deep hydrotreating of bio-oil fractions necessitates a priori removal of aldehydes either by hydrotreating under significantly milder conditions or by physical separation to avoid extensive catalyst coking. Acetone, on the other hand, yielded butenes by oligomerization followed by dehydration and cracking. Butenes can be successively oligomerized into heavier olefins (108). Alkali metal-exchanged zeolite Beta was very recently shown to afford selectively isobutylene, the highest isobutylene yield of 55% being obtained over K-Beta (249). The high selectivity was attributed to low diffusion resistance to isobutylene owing to 12-ring openings and 3D architecture of zeolite Beta channels as well as to elimination of the strongest acid sites due to ion-exchange by alkali metals. Both factors lead to suppression of isobutylene consecutive reactions being responsible for coking (249). Ethylene, propylene, and isobutylene have been obtained over ZSM-5 zeolites (250). Despite having similar acidity and specific surface area, the nano-sized ZSM-5 (30–40 nm) afforded significantly more stable acetone conversion (>90% after 500 min time-on-stream, TOS) as compared with macro-sized ZSM-5 (2000 nm) where the conversion dropped after 500 min TOS to <20%. The initial acetone conversion was 100% for both catalysts (250). Nonetheless, larger external surface and hence higher concentration of acid sites accessible on the nano-sized ZSM-5 made more feasible the secondary reactions affording aromatics due to reduced spatial limitations. Consequently, substantially higher C_2-C_4 olefin selectivity (up to 90%) was obtained over the partially deactivated macro-sized ZSM-5 in comparison with the nano-sized one (*ca.* 30%) (250). However, the increased selectivity was a result of significantly decreased conversion (from 100% to ca. 20%) being accompanied by a substantial drop in selectivity to aromatics (from ca. 55% at 100% conversion vs. 0% at 20% conversion). The yield of C_2-C_4 olefins over the nano-sized ZSM-5 at high conversion conditions (>97%) was increased from 28 to 45% as a result of deactivation of acid sites located on the external surface by catalytic cracking of diphenylsilane. Simultaneously, the yield of aromatics decreased from 54 to 36% (250).

Similar results to those of Tago et al. (250) were observed also for transformation of alcohols (1-propanol, 2-propanol). Propene, the primary dehydration product, was oligomerized and partly cracked to yield C_4^+ olefins (107). The product distributions of pyrolysis oil upgraded over ZSM-5 were similar to those obtained when pure oxygenates were transformed and coking was the principal reason for the catalyst deactivation (109). It can be thus inferred that high temperature (>200°C) treatment of oxygenates present in biomass pyrolysis oils over acidic zeolites (e.g., ZSM-5) results in severe catalyst coking, i.e., in loss of the yield of gaseous and liquid biomass-derived carbon-containing products. In such case, even ZSM-5 zeolite, usually the most stable against deactivation, is not resistant against coking. To achieve maximum utilization of the biomass-derived carbon, low-temperature conversion processes affording products with higher molecular weight and improved thermal stability, such as aldol condensation, should be preferred.

3.5.2. Aldol Condensation

Aldol condensation reactions (Fig. 13), relying traditionally on the use of a homogeneous base catalyst, such as NaOH, belong among the most promising reactions for valorization of renewable raw materials. The increased awareness of green chemistry principles as well as the focus on complex conversions of biomass-derived feedstocks, such as pyrolysis oils (bio-oils), intensified the efforts to find suitable heterogeneous catalysts for condensation reactions. In addition to typical base catalysts like various zirconia-based catalysts (MgO-ZrO_2, $Ce_xZr_{1-x}O2$) (252–254) or hydrotalcites (255, 256), also alkali-metal forms of zeolites, usually with low Si/Al ratios (257–263), were used.

The increasing basicity of zeolite Y (HY < NaY < KY) enhances the reaction rate in the aldol condensation of n-butanal to 2-ethyl-2-hexanal reaction (257). Moreover, the presence of both acid (weak Lewis acid) and basic sites was important for enhancing the catalyst activity, which was evidenced by a higher activity of alkali-cation-exchanged zeolite Y (CsNa, Na, LiNa) in comparison with the strongly basic MgO (257). This assumption was confirmed by poisoning acid and basic sites by ammonia and CO_2, respectively, resulting in reduced steady-state rate of the aldol condensation (from 1.99×10^{-4} to ca. 0.66×10^{-4} moles of formed 2-ethyl-2-hexanal per g of catalyst and hour) (257). Cooperation between basic and acid sites was used as a plausible explanation for the enhanced performance of ZSM-5, when modified with MgO, in formaldehyde and acetaldehyde condensation to acrolein (259). The

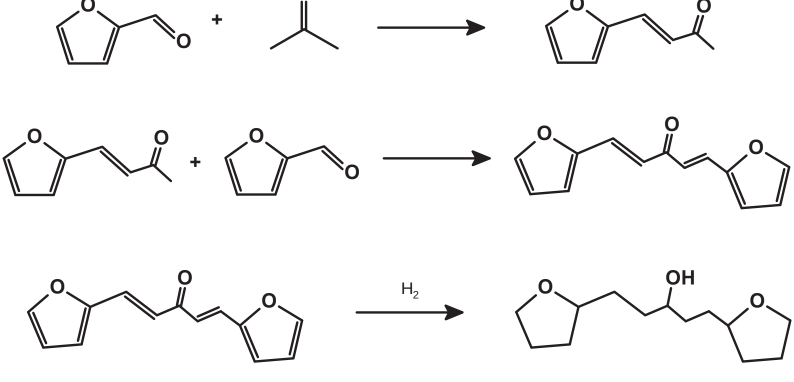

Figure 13: Schematic depiction of aldol condensation of furfural and acetone followed by hydrogenation of reaction product over heterogeneous catalysts.

conversion at 400°C increased from ca. 35 to 60% with the increasing MgO loading from 2 to 8 wt.%, but it decreased to ca. 55% when MgO loading was increased to 10 wt.% as some of the active sites inside the porous structure of ZSM-5 became inaccessible (259). Similar conversion as in the case of 4 wt.% MgO/ZSM-5 was observed over MgO-loaded (4 wt.%) SiO_2 and zeolite Y, but their selectivity to acrolein was lower owing to their larger pores allowing formation of polycondensation products (259).

Acrolein synthesis was also investigated using a series of metallosilicalites having ZSM-5 structure containing Fe, Ga, B, and Al, introduced by isomorphous substitution for Si. It was concluded that the catalyst activity in aldol condensation increased with increasing concentration of accessible Brønsted acid sites of medium strength. The selectivity, on the other hand, increased with decreasing strength of Brønsted acid sites since strong acid sites enhance particularly the rate of secondary reactions (260). Consequently, conversion of acetaldehyde increased with increasing concentration of acid sites, while coking resistance and selectivity to acrolein and crotonaldehyde (products of aldol condensation) decreased (261). The feasibility of aldol condensation over acidic zeolites can be also deduced from the adsorption studies of acetaldehyde and acetone on a ZSM-5 zeolite using FTIR spectroscopy (248, 264). Even at low partial pressures of acetaldehyde the authors observed conversion of adsorbed acetaldehyde into crotonaldehyde (264).

In some cases the catalysts for aldol condensation were modified by noble metals, e.g., Pd, to achieve simultaneous hydrogenation of the condensation products (254). More frequently, however, the hydrogenation step was performed over metal-supported silica-alumina catalysts or molecular sieves (e.g., MCM-41, H-Y) (265). Pd-modified molecular sieves yielded exclusively alkanes while the use of other Pd-modified catalysts led solely to ketones (Pd/C) or mixtures of ketones and alkanes (Pd/Al_2O_3, Pd/SiO_2-Al_2O_3) in hydrogenation of condensation products of 5-hydroxymethylfurfural and acetone (265). The remarkable selectivity of Pd-modified molecular sieves can be associated with highly dispersed Pd particles and combination of metal and acid active sites facilitating furan ring-opening reaction.

Condensation reactions are the key to successful valorization of low-molecular-weight products obtained typically by biomass pyrolysis. Owing to the possibility to employ zeolites as basic catalysts and tune their basicity, they can catalyze aldol condensation reactions. By optimizing the acido-basic properties their catalytic performance can be improved. Apart from oxygenates that can be deoxygenated over supported noble metal catalysts (possible on a molecular sieve) affording fuel-range hydrocarbons, low olefins (ethylene, propylene, isobutylene) can be obtained as well. In this instance, the pore dimensions and architecture play an important role, on the one hand, they impose diffusional limitations promoting the extent of secondary reactions while on the other hand they restrict the formation of large coke precursors. Hence, small zeolite crystals (i.e., short diffusional path lengths) with deactivated-blocked external surface area (to suppress formation of coke) afford the highest selectivities.

3.6. Terpenes Transformations

Terpenes belong to a relatively small class of renewable raw materials (in comparison with lignocellulose) that is denoted as “extractives,” as they can be separated by extraction from biomass, typically plants. They are the primary constituents of essential oils and find various applications as fragrances. By chemical transformations (isomerization, hydrogenation, oxidation) their application potential can be substantially expanded. The main terpenes include α-pinene and β-pinene extracted from turpentine oil (a by-product from wood pulping) and limonene originating from citrus oil (31) (for structures of the most important terpenes, see Fig. 14). Catalytic transformations of terpenes were reviewed in detail by Swift, Ravasio et al., and Monteiro and Veloso (266–268). Therefore, here we revisit only the principle transformation routes of terpenes over (modified) micro- and mesoporous materials comprising isomerization of α-pinene (269–271), dehydrogenation of pinenes to

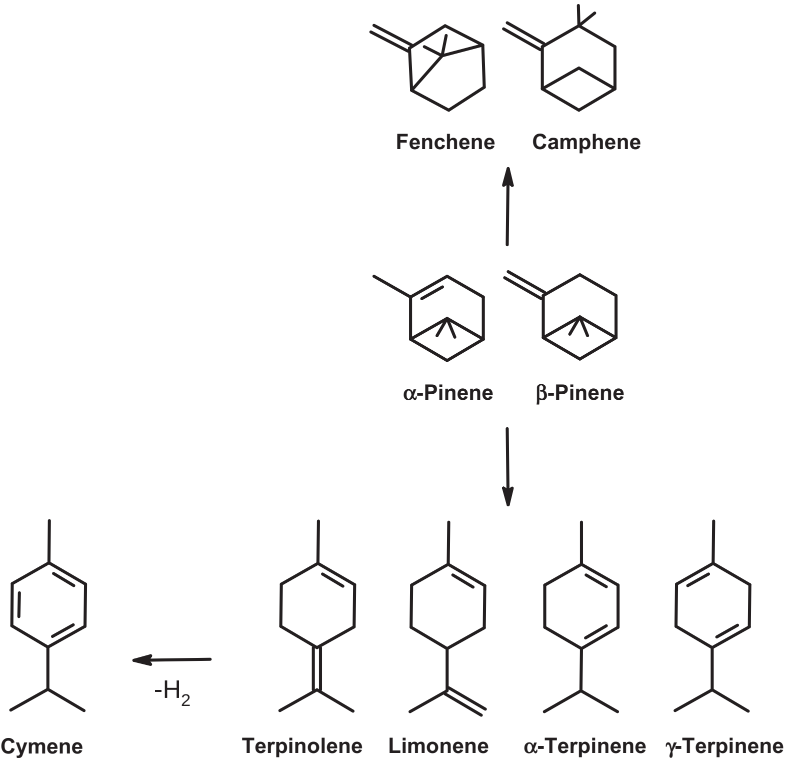

Figure 14: Isomerization of α-pinene over acidic catalysts (270).

p-cymene (272), alkoxylation of limonene (273), epoxidations of α-pinene and limonene (274–276), and rearrangement of α-pinene oxide (277).

3.6.1. Isomerization

The isomerization of α-pinene (Fig. 14) is the most widely investigated reaction of terpenes, as it affords interesting chemical intermediates, such as camphene, limonene, terpinene, or cymenes being subsequently essential for a number of fine chemical syntheses (29). The activity and selectivity of catalysts in α-pinene isomerization are significantly influenced by the strengths of Brønsted acid sites and their distribution originating, for instance from the zeolite framework irregularities (269). Catalysts having the largest external surface areas afforded the highest conversions. For example, conversion of α-pinene in its isomerization to camphene and limonene was 7 and 99 for zeolite Beta having Si/Al = 10 and $S_{ext} = 43\ m^2/g$ and for zeolite Beta with Si/Al = 27, $S_{ext} = 227\ m^2/g$, respectively (269). On the other hand, despite their significantly larger external surface areas ($S_{ext} > 700\ m^2/g$), MCM-41 catalysts (Si/Al = 12 and ∞) exhibited substantially lower conversion. Whereas the purely siliceous MCM-41 showed a negligible conversion of α-pinene (2.9%), the conversion of α-pinene over aluminum-containing MCM-41 (Si/Al = 12) was nearly 45% evidencing the importance of catalyst acidity (269). In addition to acidity, the presence of mesopores facilitating the transport of α-pinene to active sites is important as well (269) as evidenced by low conversions over medium-pore ZSM-5 or one-dimensional Mordenite, i.e., zeolites in which diffusional limitations play important role. The low conversion over these zeolites can be related to their smaller external surface area originating probably from their larger crystal size. In this context, the performance of faujasite and mordenite zeolites dealuminated to a different degree (dealumination 20–90%) was studied (278). A combined yield of camphene and limonene, the most desired isomerization products, was as high as 68% over dealuminated mordenite. However, the increasing pore diameter due to extensive dealumination favored formation of heavier by-products. At the same time, an optimum dealumination was reported maximizing pinene conversion (original mordenite Si/Al = 7, dealuminated mordenite Si/Al = 50) (278). This demonstrates the importance of a balance between accessibility and amount of Brønsted acid sites. Isomerization of α-pinene was also accomplished over natural zeolites, such as clinoptilolite and montmorillonite (266).

To improve the performance of the parent zeolites (ZSM-5, ZSM-12), desilication treatment (leading to the pore surface cleaning and to formation of mesopores) was suggested (279). A treatment of ZSM-5 zeolite with 1.0 M NaOH increased α-pinene conversion at 75°C from *ca.* 11% to about 27%, while the selectivity to the main products, i.e., camphene and limonene, remained virtually unaltered (about 34% to camphene as well as limonene) (279). This approach based on dissolving of a part of silica domains in zeolites by basic treatment, provides zeolites with much larger surface areas and a higher concentration of acid sites on the external surface (280). This will be discussed in more detail later on in this article.

The importance of the presence of mesopores allowing for more accessible acid sites and faster diffusion was also demonstrated by the successful application of mesoporous molecular sieves prepared by direct assembly of nanoclustered zeolitic precursors (named MSU $S_{(BEA)}$). On a series of MSU $S_{(BEA)}$ catalysts with various Si/Al ratios (30–150), an influence of the concentration of acid sites on the catalyst activity was shown and an optimum Si/Al ratio (Si/Al = 67) was found (271). The volcano-shaped dependence of yield of camphene and limonene (max. 91%) as a function of the accessible acid sites (determined by adsorption of 2,6-di-*tert*-butylpyridine) was attributed to changes in both hydrophobicity and in concentration of acid sites (271). While the number of acid sites increased with the increasing Al concentration, i.e., decreasing Si/Al, the hydrophobicity decreases and consequently adsorption of the non polar reactant is less favorable. Similarly, introduction of mesopores to H-Ferrierite by its mild dealumination resulted in an increased α-pinene conversion (from 72 to 97% after the treatment with 0.25 M HCl). The treatment was accompanied by an increase in the selectivity to limonene and simultaneous decrease in the selectivity to camphene. The overall selectivity to these products remained virtually unaltered (*ca.* 85 %) (270). However, more severe dealumination resulted in less active catalysts due to reduction of their Brønsted acidity (270). The initial activity of 4.28 $\text{mmol}_{\alpha\text{-pinene}}/(\text{g}_{\text{cat}}.\text{min})$ (acidity 1.29 mmol $H^+/\text{g}_{\text{cat}}$) increased after the first treatment to 5.01 $\text{mmol}_{\alpha\text{-pinene}}/(\text{g}_{\text{cat}}.\text{min})$ (acidity 0.92 mmol $H^+/\text{g}_{\text{cat}}$), but declined severely after consecutive treatments to 2.31 $\text{mmol}_{\alpha\text{-pinene}}/(\text{g}_{\text{cat}}.\text{min})$ after the third treatment when acidity dropped to only 0.32 mmol $H^+/\text{g}_{\text{cat.}}$ As expected, isomorphous substitution of Al by B, Ti, and V yielded catalysts with insignificant activity evidencing the importance of Brønsted acid sites (281).

3.6.2. Dehydrogenation and Epoxidation

The dehydrogenation of pinenes to *p*-cymene, an important chemical intermediate (e.g., for *p*-cresol production), requires the use of a bifunctional catalyst. Most importantly, the strength of the acid sites needs to be carefully optimized as too weak acid sites cannot open selectively the cyclobutane ring while too strong acids sites favor side reactions (cracking, oligomerization) (272). The metal function (e.g., Pd) controls the hydrogenation/dehydrogenation catalyst activity, i.e., the yield of aromatics. The yield of aromatics increased at complete conversion of α-pinene from 3 to 67% as a result of Pd introduction (0.5 wt.%) on a silica support (272). Apart from various metals (Ni, Cu, Pt, Pd) supported on alumina, silica, or active carbon (266), H-ZSM-5 was shown to be active in dehydrogenation of limonene to *p*-cymene. When promoted with cerium (1 wt.% Pd, 2 wt.% Ce) the initial selectivity to *p*-cymene increased from 17 to 50 % at complete conversion of limonene. Simultaneously, deactivation was suppressed (282). A further increase in selectivity (to 80% at complete conversion) was obtained as a result of replacing H-ZSM-5 by its sodium form (282).

The porous structure of highly dealuminated zeolites NaX and NaY has been utilized to entrap homogeneous catalytic complexes (such as (R,R)-(N,N0)-bis(3,5-di-tert-butylsalicylidene)-1,2-diphenylethylene-1,2-diaminocobalt complex) using a "ship-in-a-bottle" synthesis approach. The complex was synthesized in mesopores generated by the dealumination procedure and being surrounded by micropores. These catalysts were efficient for epoxidation of α-pinene and limonene (275). The entrapment of the organometallic complex was achieved without a significant loss of its activity and selectivity while allowing easy separation from the reaction mixture (275). The epoxidation of α-pinene was also successfully catalyzed by Ti-Beta (274) and Ti-MCM-41 (276). Titanium-modified mesoporous silicas (Ti-MCM-41, Ti-HMS; Si/Ti = ca. 50) were shown to afford exclusively α-pinane oxide in oxidation of α-pinene by *t*-butyl hydroxyperoxide at conversion of α-pinane $<10\%$ (283). Upon introduction of trivalent cations like Al, B, or Fe, mild acidity was introduced resulting in the formation of 1,2-pinanediol i.e., a product of opening of the epoxy ring. Due to a mild acidity, the ring is opened selectively, i.e., without promoting secondary reactions of oxidation products (283). The method of Ti incorporation was shown to be of key importance for catalyst activity; Ti-MCM-41 catalyst with Ti introduced during the sol-gel synthesis had 2–10 times lower TOF (depending on the reactant) than Ti-MCM-41 where Ti was was grafted from a titanocene solution (267). In contrast to Ti-Beta, where epoxidation of double bond in the side chain was preferential due to steric reasons (284), the porosity features did not have a significant influence in the case of Ti-modified silicas (MCM-41, Aerosil, etc.) (267).

The subsequent conversion of α-pinene oxide to campholenic aldehyde, an important fragrance precursor, is typically performed in the presence of homogeneous Lewis acid catalysts ($ZnCl_2$, $ZnBr_2$ salts) (31). Homogeneous catalyst can be replaced by solid Lewis acid catalyst, such as Ti-Beta achieving high yields ($>$ 95 %). The excellent performance was attributed to the presence of isolated, well-dispersed Ti sites in the silica-based zeolite support (i.e., without any Brønsted acid sites), optimum hydrophobicity/hydropholicity, and the transition-state shape selectivity imposed by the channel structure of zeolite Beta (274). In fact, one pot synthesis of campholenic aldehyde from α-pinene was addressed by Suh et al. (285, 286). The catalyst is required to have both epoxidation as well as mild Lewis acidic functions and hence Ti-HMS was used as a catalyst. To suppress side reactions, it is crucial to remove water and molecular oxygen from the reaction media and oxidant (*t*-butyl hydroxyperoxide, TBHP) (286). For instance, in the presence of water α-pinene is transformed primarily to verbenone (selectivity 51%) and campholenic aldehyde (selectivity 23%) while in absence of water campholenic aldehyde is obtained with selectivity of 82% at 350 K and 1:1 molar ratio of α-pinene to TBHP (285).

3.6.3. Alkoxylation and Hydration

In addition to oxidation and isomerization, alkoxylation and hydration of terpenes over large-pore zeolite catalysts (H-Beta, H-Y, H-Mordenite) providing some flavor and fragrance intermediates was reported (273, 287). In the alkoxylation of limonene and α-pinene, H-Beta was found more active and selective catalyst than H-Mordenite and H-Y, which was attributed to its suitable acid sites and pore size and shape (273). Zeolite H-Beta prepared by fluoride-mediated synthesis (Si/Al = 15–>10 000) exhibited less internal defects (silanol groups) than base-mediated synthesis (Si/Al = 7.5–40). A more hydrophobic character of H-Beta zeolite provided higher yields of dihydromyrcenol from dihydromyrcene over several zeolites Beta with different Si/Al ratios. An optimum Si/Al ratio equal to 27 for Beta synthesized in fluoride media exhibiting the highest yield (59%) of the desired product (at nearly 100% selectivity) was reported as well (287). Hence, this is an example where the zeolite hydrophobicity determines the catalytic performance. Last but not least, immobilized Grubbs catalysts on mesoporous SBA-15 and MCM-41 exhibit a high activity and selectivity in metathesis of citronellene (288).

The potential of terpenes consists particularly of their valorization as raw materials for fine chemicals syntheses. Several aspects pertaining to molecular sieves, namely structure, acid sites (type, strength, concentrations) and surface polarity, are essential for successful application of molecular sieves in these transformations as high selectivity is of utmost importance in contrast to, e.g., triglyceride transformations.

4. MICROPOROUS AND MESOPOROUS MATERIALS IN BIOMASS UPGRADING

In previous sections of this article it was evidenced that different types of zeolites and mesoporous materials exhibit interesting catalytic activities and selectivities in various reaction of biomass upgrading. This part addresses briefly the main properties of different micro- and mesoporous molecular sieves, the catalytic behavior of which was already discussed. In addition, their future potential is provided based on the analysis of their chemical and structural features.

Table 4: Structure characteristics of some zeolites relevant to the transformations of biomass.

Zeolite	IZA Code	Channel dimensionality	Channel type	Pore dimensions (nm)
Beta	BEA	3D	12	0.76 x 0.64
			12	0.55 x 0.55
L	LTL	1D	12	0.71
Mordenite	MOR	1D	12	0.70 x 0.67
MCM-22[a]	MWW	3D	10	0.55 x 0.40
SSZ-33		3D	12-12-10	0.64 x 0.70 0.70 x 0.59 0.51 x 0.45
Y[b]	FAU	3D	12	0.74
ZSM-5	MFI	3D	10	0.53 x 0.56
			10	0.51 x 0.55
ZSM-11	MEL	3D	10	0.53 x 0.54
ZSM-12	MTW	1D	12	0.55 x 0.59
ZSM-22	TON	1D	10	0.44 x 0.55

[a] Two independent channel systems, one possessing large cavities with 12- ring pockets on the "external" surface with dimensions 0.71 x 0.71 nm.

[b] Cavities in the channel intersection.

Zeolites as crystalline microporous aluminosilicates are the most important group of industrial heterogeneous catalysts with applications ranging from refining and petrochemistry up to environmental catalysis and synthesis of fine chemicals (289). About 200 different structural types of zeolites have been recognized differing in the size, shape and connectivity of their channels exhibiting from 8 to 30-rings (290–292). Some structural characteristics of zeolites relevant to biomass upgrading are given in Table 4. The size of zeolite channel entrances is critical for application of zeolites in catalysis, particularly in shape-selective one, but still it did not overcome substantially 1 nm. The tailored control of textural and chemical properties of zeolites remains a big challenge. To enhance the application potential of zeolites for transformations of bulky substrates, including biomass, different approaches have been investigated in recent years (decades). In principle, three procedures were developed and each of them will be briefly commented now: (a) synthesis of two-dimensional (2D) zeolites either directly or post-synthesis by transformation of 3D to 2D structures (118, 293–295); (b) micro-mesoporous materials (hierarchical systems) prepared by different direct or post-synthesis methods (101, 296–298); and (c) purely mesoporous materials (144, 299–303). Each of these synthetic approaches provides porous materials with enhanced diffusion properties differing in acidic character, however, no shape-selective behavior can be expected.

Zeolites as crystalline microporous materials exhibit various pore architectures starting from 8-rings up to recently identified 30-ring channels. Schemes of the most frequently used zeolites for transformations of biomass

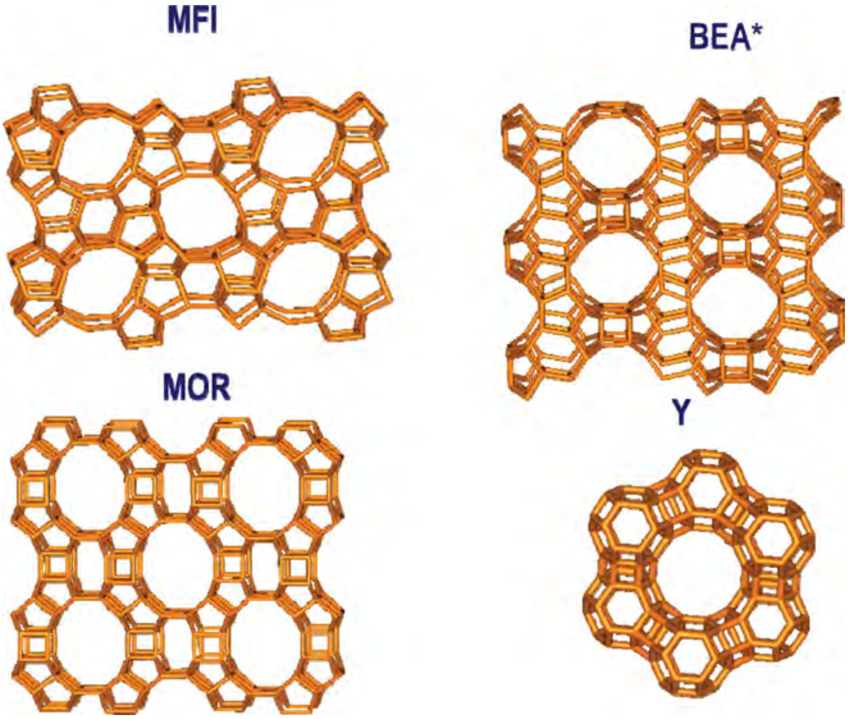

Figure 15: Schemes of the structures of zeolites ZSM-5, Beta, Mordenite, and Y (color figure available online).

are given in Fig. 15. Particularly, with increasing pore size, these are less and less spherical and can be elliptical or with even more complicated shapes (290). This makes the evaluation of the accessibility of acid sites much more complex, especially for large organic substrates. Generally, the activity of zeolites increases with increasing size of the pores and their dimensionality, although some exceptions have also been described (298).

Most of reactions described in this contribution are acid catalyzed reactions. The acidic features of zeolites stem from the presence of three-valent aluminum atoms (generally, three-valent heteroatoms, e.g., Fe, Ga, B) in the aluminosilicate frameworks. When the negative charge of the framework is compensated by protons, Brønsted acid sites are formed. Depending on the structure and chemical composition (variation of Si/Al or replacement of Al by B, Fe, Ga), the strength of acid sites can be adjusted for a particular catalytic reaction. Si/Al ratio can be changed from low values (Si/Al equal to 1 is the limiting value due to the Lowenstein rule) up to infinity (Si/Al $= \infty$). Decreasing concentration of aluminum in the framework results in a lower amount of acid sites, as well as in a higher hydrophobicity of the zeolite. By optimizing concentration of acid sites and hydrophobicity of the zeolite, tuning of catalytic properties can be performed. In addition to Brønsted sites (protons located in bridging Si-OH-Al groups), Lewis acid sites can be also present being associated with another coordination of aluminum or extra-framework aluminum species (304, 305). The concentrations of individual Brønsted and Lewis acid sites depend on the structural type of zeolite, synthesis conditions and post-synthesis treatment. Particularly, at temperatures above 500°C, dehydroxylation proceeds easily leading to the formation of Lewis acid sites.

While zeolites impose sterical restrictions on bulky organic molecules due to the size of their channel openings, catalysts exhibiting zeolite properties can be applied as well if the reaction can proceed on the external surfaces of zeolite crystals. This can be achieved by decreasing crystal size of zeolites leading to nanocrystals or with zeolites having high aspect ratio obtained by direct synthesis (e.g., MCM-22) (306). As the most striking feature of zeolite synthesis, it was observed that although zeolites are generally crystalline materials with three-dimensional (3D) ordering of their structures, some zeolites are synthesized via layered precursors (159, 307–309). The precursor is either further transformed into 3D zeolites via post-synthesis treatment or to delaminated, pillared or stabilized forms (160). The synthesis of zeolite lamellar precursors opens new possibilities to tailor the textural features of zeolites in a broad range. As a further step in designing new zeolite materials in contrast to accidental findings of 2D zeolitic precursors is the synthesis of 2D (lamellar, single-nanosheet) ZSM-5 zeolites using designed structure-directing agents by Ryoo and coworkers (294, 295, 310, 311). This approach represents a real breakthrough in the synthesis of lamellar (single nano-layers) providing a high application potential for catalysis and transformation or formation of bulky organic molecules. When forming layered zeolites with fully (delaminated materials) or partly separated (pillared) layers, these materials can exhibit micro-meso porosity (hierarchic systems, e.g., MCM-36 (307)) or just mesoporosity (compact zeolitic layers without any micropores, e.g., ITQ-6 with ferrierite layers (312)). For application in catalysis, both microporous and particularly mesoporous systems can be applied depending on the size/shape of reactant molecules. For transformation of bulky compounds, active sites located on the external surface or, in other words, on the zeolitic layers are responsible for their catalytic activities. There are few examples showing higher resistance to coke formation when compared with conventional zeolites (311). The acid sites are again of Brønsted and Lewis type as in conventional zeolites. In addition, external surface of zeolite layers is rich in silanol groups. They are usually almost neutral but can contribute to adsorption of reactants of products if not to the reaction. Recently, it was shown for the first time that zeolite UTL can be transformed from 3D structure to 2D layer system by treatment in water/acid conditions with preservation of the structure of UTL layers (Fig. 16; (161)). synthesis opens new opportunities for the future synthesis of wide variety of 2D zeolites having different acidic

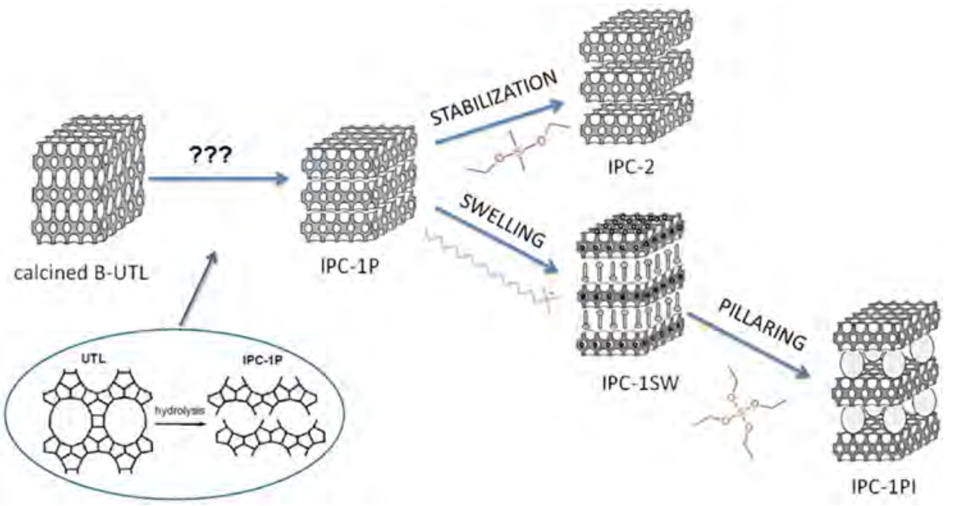

Figure 16: Scheme of post-synthesis transformation of 3D structure of zeolite UTL to 2D systems including stabilized (IPC-2) and pillared (IPC-1PI) materials (color figure available online).

properties. It is evident that zeolitic layers will not work as traditional shape selective catalysts but their primary application will be in bulky chemicals synthesis/transformation.

Another approach to overcome the limitations imposed by small channel entrances of zeolites with preservation of their chemical properties is based on direct or post-synthesis treatments resulting in the formation of mesopores. Zeolites combining micropores with mesopores are usually called hierarchic materials. Two particular methods were developed: (a) direct synthesis with a secondary template (inducing mesoporosity) (313, 314) and (b) post-synthesis treatment leading to a partial destruction of the crystals by selective removal of some building units (280, 315). The first procedure uses, e.g., carbon black particles as “secondary templates” in the synthesis mixture together with a template for the synthesis of zeolite. As a result, the individual particles are partly or completely covered by the zeolitic structure as evidenced by 3D TEM images. Calcination removes the template and carbon particles opening both micropores and mesopores inside the crystals and enlarging the external surface. Mesopores are accidentally distributed throughout individual crystals depending on the homogeneity of the reaction mixture. The second approach stems from the fact that silicate materials dissolve under basic conditions. Under optimized conditions (pH, temperature, concentration, time), a part of silicate framework is dissolved forming mesopores. This is general procedure as documented by a number of zeolite structural types investigated up-to-date, including zeolites ZSM-5, ZSM-12, mordenite, Beta, SSZ-35, ZSM-22, etc.; for complete list of zeolites, see (316). There is a clear distinction between the role of micro- and mesopores in catalytic reactions. Each porosity level in the hierarchical structure exhibits complementary task: while the micropores hold catalytically active sites, the access to the pores is facilitated mesopores. Addition of mesopores to the zeolite crystals also has other important effects: (a) due to a decrease in the diffusion pathways in the micropores, shape selectivity is usually diminished (298); or (b) much larger external surface is formed, which can lead to a high activity for reactions of bulky substrates or leading to bulky products not penetrating into/being formed in the micropore system of zeolites (317). In a similar way to 2D zeolites, acid sites in hierarchic zeolites are located both in the micropores as well as on the external surface, substantially enlarged by the presence of mesopores (surface roughness). In such a case, acid sites in micropores are catalytically active for transformations of small reactants with enhanced transport through mesopores, or acid sites on the external surface catalyze reaction of bulky substrates. It should be noted that both Brønsted and Lewis acid sites are involved in these reactions.

Finally, catalytic behavior of mesoporous molecular sieves is discussed as well. In contrast to conventional, 2D or hierarchic zeolites, mesoporous molecular sieves are of amorphous character exhibiting predominantly only Lewis acid sites. This makes them usually less active, particularly for those reactions requiring Brønsted acid sites (303). The first mesoporous molecular sieves were synthesized after 1990 like MCM-41 and MCM-48 (299, 318) as silicates or aluminosilicates, shortly followed by mesoporous aluminas (144) and other chemical compositions and structures (319–321). Recently, significant advances have been achieved in the synthesis of mesoporous molecular sieves, particularly related to the enlargement of the pore diameters. Group of Ryoo described the facile synthesis route to the MCM-48-like ordered mesoporous silicas with pores ranging from 4–12 nm by controlling the amounts of butanol and silica source in the synthesis mixture (322). In addition, Cao with coworkers (323) succeeded in enlargement of the pores of SBA-15 from 10 to 26 nm by optimizing of solubilization of swelling agents in micellar solution. Such large pore sizes enable the diffusion of bulky substrates, even some bio-related compounds to the inner surface of mesoporous molecular sieves. For the catalytic purposes, mesoporous catalysts with a narrow pore size distribution and highly acidic accessible surface (preferentially of Brønsted type) are highly demanding. Synthetic approaches including recrystallization of amorphous pore walls (324) or using nanozeolitic particles as building blocks being organized into mesoporous structure with an interesting potential for catalytic applications (101, 325, 326) were proposed but optimization of their properties is still needed.

There is no doubt about a high practical potential and economic viability of most of molecular sieves briefly discussed here. Their main advantages for catalytic applications in biomass transformations are:

- high thermal and hydrothermal stability of zeolites and their related analogs, being higher than those of mesoporous molecular sieves;
- increased accessibility of active sites in mesoporous, two-dimensional, and hierarchic zeolites than over conventional 3D zeolites;
- tailored acidity of Brønsted and Lewis acid sites in zeolites, 2D, and hierarchical systems, while mainly Lewis acid sites are available in mesoporous catalysts.

Although not discussed in detail, all these catalysts are easily regenerated usually without a significant loss in their activity.

Some more general conclusions about the applicability of molecular sieves (all types discussed in this section) can be drawn when considering the most important characteristics of these materials with regard to the transformations of different biomass-derived raw materials. Location, type, and accessibility of active sites are of critical importance for molecular sieves to operate as active catalysts. There is a clear limitation as for the channel entrances to the zeolite systems. Thus, only molecules with kinetic diameters smaller than entrance windows (reactant shape-selectivity) can be transformed. Thus, the reactant shape selectivity can be used advantageously when transforming primary (cracking) products of biomass upgrading by selective deoxygenation/dehydration of sugars or phenolics, aromatization of sugars or triglycerides, and condensation/aromatization of short aldehydes, ketones, and acids present typically in bio-oils. In addition, glycerol and terpenes have an easy access to internal channel structure of zeolites. Glycerol can be converted by dehydration or aromatization relying on the product shape selectivity in the latter case. Terpenes can undergo isomerization, epoxidation, and dehydrogenation inside zeolite channels and transition-shape and product selectivity might improve overall transformation selectivity.

As soon as more bulky molecules need to be upgraded, mesoporous molecular sieves or two-dimensional zeolites are primary candidates. While pore dimensions of mesoporous catalysts can again be theoretically a limiting factor, particularly in the case of lignocellulosic biomass and its main constituents, the accessibility of active sites on “flat” surfaces of two-dimensional zeolites should be advantageous. Of course, when treating bulky molecules, reacting part of the molecule needs to access intimately the active site. Thus, confinement effect in the structure of mesoporous molecular sieves might play a significant role. Thus, for reactions like triglycerides deoxygenation or cracking or oligosaccharides dehydration or cracking, mesoporous molecular sieves or two-dimensional zeolites should be preferred. Having said this, one has to consider also the local arrangement of these catalysts. While active sites in two-dimensional zeolites will be mostly located on the external surface (or close to it, e.g., in cups of MCM-22 zeolite), mesoporous catalysts like

SBA-15 exhibit substantial “surface roughness.” In such case, the accessibility for bulky molecules can be hindered as well and not due to slow diffusion in the mesopores. In contrast, the walls of MCM-41 do not exhibit “surface roughness” and could be favorable for reactions of substrates smaller than 4–5 nm. On the other hand, the “surface roughness” could be beneficial for stabilizing supported metal (or other active) clusters that provide, e.g., hydrogenation/dehydrogenation functionality.

The type of acidity can also be important for the course of the reaction. While Brønsted sites are highly advantageous for most of acid catalyzed reactions, Lewis sites are very efficient for particular reactions requiring electron donor-acceptor interaction. The type of acidity together with the concentration and strength of the acid sites influences significantly or even determines the characted of guest-host interaction (i.e., reactant-zeolite/molecular sieve interaction). Brønsted sites and their concentration and strength are essential not only for cracking reactions. With repect to biomass-derived feedstocks they play a vital role especially in dehydration reactions (e.g., glycerol to acrolein conversion or glucose to aromatics). Depending on the type of the desired product, a short contact time, i.e., short diffusion path length (e.g., in case of acrolein formation), or bifunctional catalysts, i.e., metal clusters accompanying the Brønsted sites (e.g., to improve catalyst stability by suppressing carbonaceous deposits formation) may be necessary to improve the catalytic performance. Lewis acid sites introduced typically by incorporation of Ti or Sn are key to successful oxidation as demonstrated by the example of terpenes epoxidation and glucose oxidation or to isomerization of sugar solutions in aqueous phase. The power of tunability of acidic properties can be evidenced by the example of transformation of trioses into alkyl lactates where concerted action of Brønsted sites (dehydration) and Lewis sites (alkylation) is crucial.

5. CONCLUSIONS AND OUTLOOK

Biomass-derived feedstocks will inevitably find a prominent place among resources for the chemical industry as they are the only renewable source of carbon on the Earth. The current prognoses suggest that a significant part of our predicted consumption of energy resources can be derived from biomass sustainably. Owing to the scattered nature and diversity of biomass raw materials, energy, and raw material efficient processes will be necessary to maximize the potential of the new raw material basis for sustainable development of the chemical industry. Learning from the previous experience, one has to recognize the indispensable role of heterogeneous catalysis in maximizing the material and energy utilization of petroleum. As a consequence, we still have time ahead of us when we can use this very convenient, but finite, energy resource and develop processes for utilization of novel energy resources, such as biomass. In a similar way, we can expect that heterogeneous catalysts, and particularly those based on molecular sieves, will play a dominant role in efficient biomass transformation.

Molecular sieves are a very broad class of catalytically active materials. Owing to their unique nature they can be "shaped" in many different ways to catalyze a multitude of desired/desirable biomass transformations with the maximum thermodynamically feasible efficiency. Among the many exclusive features of micro- and mesoporous materials, two stand out, namely pore architecture (including pore dimensions, pore connectivity, and internal and external specific surface area) and acidity/basicity (more preciously strength, density, and location of the sites, and type of the sites: acidic/basic, Lewis/Brønsted). In addition to the wide variability of materials obtainable by direct synthesis, the as-synthesized materials can be modified by different post-synthetic treatments modifying their primary properties as well as adding new functionalities.

The main challenge, typical for any catalytic process development, is matching the catalyst properties with those of feedstocks and products so that the maximum energy and material efficiency are achieved. Biomass transformations include conversion of a broad range of chemical species of varying sizes; the common feature of most of these being a high content of chemically bound oxygen. Obviously, the accessibility of the active sites by the reactants is essential and modern methodologies enhancing the molecular transport to and from active sites are employed. Apart from the widely used post-synthetic modifications leading to mesoporosity in microporous molecular sieves, mesoporous materials have been developed as well. Nonetheless, the concentration and strength of the active (acidic) sites in these materials is generally low limiting their applicability. Consequently, the attention can be expected to turn more-and-more to the recently discovered 2D zeolites that could bring a breakthrough as they combine easy accessibility of active sites while allowing for adjusting their concentration and strength over a rather wide span.

Microporosity will, nonetheless, remain a key parameter for many applications relying on shape selectivity. In biomass transformations, particularly product and transition-state shape selectivity preventing formation of coke precursors inside the pore system leading to rapid deactivation/blockage of active sites are of a high importance due to the instability of many reaction intermediates in biomass reactions. In a nutshell, the tunable pore size and architecture of micro- and mesoporous materials offers wide range of possibilities for conversion of various biomass-derived feedstocks. It can be concluded, based on the examples discussed above, that the rational design of these catalysts, controlling molecular traffic as well as limiting undesired transformations and catalyst deactivations, form a corner stone of robust catalysts development.

Physico-chemical properties of molecular sieves predetermine the guest-host (i.e., reactant-zeolite) interactions and are hence crucial for application of molecular sieves as catalysts. Acidity (Brønsted or Lewis) plays a vital role in many transformations of biomass-derived feedstocks and it can be designed for specific applications. Not only the type of acid sites, but also their strength and concentration can be varied by selection of: (a) the zeolite type (structure); (b) zeolite chemical composition (typically Si/Al ratio); (c) synthesis and activation (calcination) procedure; and (d) post-synthesis treatments and modifications. This versatility and adjustability of molecular sieves properties makes them strong candidates for successful transformation of various biomass-derived feedstocks despite the many challenges lying ahead. In brief, the physico-chemical character of molecular sieves can be designed to provide properties that are essential for particular chemical reaction to take place: catalysts containing solely Brønsted or Lewis acid sites with different density of these sites can be prepared. Their strength can be varied as well, but it is more challenging as it depends on the structure of the material as well. Moreover, synthesis or post-synthetic modifications allow modifying molecular sieves to contain basic cations and metallic (hydrogenation/dehydrogenation) sites and to have different hydrophobic/hydrophilic character.

ACKNOWLEDGMENT

The authors thank the Grant Agency of the Czech Republic for financial support (Centre of Excellence – P106/12/G015).

REFERENCES

[1] Huber, G.; Iborra, S.; Corma, A. Synthesis of Transportation Fuels from Biomass: Chemistry, Catalysts, and Engineering. *Chem. Rev.* **2006**, *106*(9), 4044–4098.

[2] World Energy Outlook. OECD/IEA 2009, http://www.iea.org, 2009.

[3] Manganaro, J.; Chen, B.; Adeosun, J.; Lakhapatri, S.; Favetta, D.; Lawal, A.; Farrauto, R.; Dorazio, L.; Rosse, D. Conversion of Residual Biomass into Liquid Transportation Fuel: An Energy Analysis. *Energ. Fuels* **2011**, *25*(6), 2711–2720.

[4] Annual Energy Review. U.S. Energy Information Administration, DOE/EIA-0384(2009), http://www.eia.gov/aer, 2009.

[5] Edenhofer, O.; Pichs-Madruga, R.; Sokona, Y.; Seyboth, K.; Matschoss, P.; Kadner, S.; Zwickel, T.; Eickemeier, P.; Hansen, G.; Schlömer, S.; von Stechow, C., Eds. *IPCC Special Report on Renewable Energy Sources and Climate Change Mitigation*; Cambridge University Press: Cambridge, UK, New York, 2011.

[6] Choi, S.; Drese, J.; Jones, C. Adsorbent Materials for Carbon Dioxide Capture from Large Anthropogenic Point Sources. *ChemSusChem* **2009**, *2*(9), 796–854.

[7] Sayari, A.; Belmabkhout, Y.; Serna-Guerrero, R. Flue Gas Treatment via CO_2 Adsorption. Chem. Eng. J. **2011**, *171*(3), 760–774.

[8] Ragauskas, A.J.; Williams, C.K.; Davison, B.H.; Britovsek, G.; Cairney, J.; Eckert, C.A.; Frederick, W.J.; Hallett, J.P.; Leak, D.J.; Liotta, C.L.; Mielenz, J.R.; Murphy, R.; Templer, R.; Tschaplinski, T. The Path Forward for Biofuels and Biomaterials. *Science* **2006**, *311*(5760), 484–489.

[9] Centi, G.; van Santen, R.A., Eds., *Catalysis for Renewables: From Feedstock to Energy Production*; Wiley-VCH Verlag: Weinheim, Germany, 2007.

[10] Bauen, A.; Berndes, G.; Junginger, M.; Londo, M.; Vuille, F. *Main Report - Bioenergy – a Sustainable and Reliable Energy Source. A Review of Status and Prospects.* IEA BIOENERGY: ExCo: 2009:06. http://www.ieabioenergy.com, 2009.

[11] Sheldon, R. Utilisation of Biomass for Sustainable Fuels and Chemicals: Molecules, Methods and Metrics. *Catal. Today* **2011**, *167*(1), 3–13.

[12] Gold S. Bio-Energy Supply Chains and Stakeholders. *Mitig. Adapt. Strat. Global Change* **2011**, *16*(4), 439–462.

[13] Zhu, X.-G.; Long, S.; Ort, D. What is the Maximum Efficiency with which Photosynthesis Can Convert Solar Energy into Biomass? *Curr. Opin. Biotechnol*. **2008**, *19*(2), 153–159.

[14] Okkerse, C.; Van Bekkum, H. From Fossil to Green. *Green Chem.* **1999**, *1*(2), 107–114.

[15] Agrawal, R.; Singh, N. Solar Energy to Biofuels. *Ann. Rev. Chem. Biomol. Eng*. **2010**, *1*, 343–364.

[16] Singh, N.; Delgass, W.; Ribeiro, F.; Agrawal, R. Estimation of Liquid Fuel Yields from Biomass. *Environ. Sci. Technol.* **2010**, *44*(13), 5298–5305.

[17] Demirbas, A. Biomass Resource Facilities and Biomass Conversion Processing for Fuels and Chemicals. *Energy Convers. Manage*. **2001**, *42*(11), 1357–1378.

[18] Agrawal, R.; Singh, N. Synergistic Routes to Liquid Fuel for a Petroleum-Deprived Future. *AIChE J.* **2009**, *55*(7), 1898–1905.

[19] Offermann, R.; Seidenberger, T.; Thrän, D.; Kaltschmitt, M.; Zinoviev, S.; Miertus, S. Assessment of Global Bioenergy Potentials. *Mitig. Adapt. Strat. Global Change* **2011**, *16*(1), 103–115.

[20] de Vries, B.; van Vuuren, D.; Hoogwijk, M. Renewable energy Sources: Their Global Potential for the First-Half of the 21st Century at a Global Level: An Integrated Approach. *Energ. Policy* **2007**, *35*(4), 2590–2610.

[21] Beringer, T.; Lucht, W.; Schaphoff, S. Bioenergy Production Potential of Global Biomass Plantations under Environmental and Agricultural Constraints. *GCB Bioenerg.* **2011**, *3*, 299–312.

[22] de Wit, M.; Londo, M.; Faaij, A. Productivity Developments in European Agriculture: Relations to and Opportunities for Biomass Production. *Renew. Sust. Energ. Rev.* **2011**, *15*(5), 2397–2412.

[23] Sheldon, R.A. Atom Efficiency and Catalysis in Organic Synthesis. *Pure Appl. Chem.* **1998**, *72*(7), 1233–1246.

[24] Sheldon, R.A. The E factor: fifteen years on. *Green Chem*. **2007**, *9*(12), 1273–1283.

[25] Čejka, J.; Centi, G.; Perez-Pariente, J.; Roth, W.J. Zeolite-based Materials for Novel Catalytic Applications: Opportunities, Perspectives and Open Problems. *Catal. Today*, **2012**, *179*, 2–15.

[26] Petrus, L.; Noordermeer, M. Biomass to Biofuels, a Chemical Perspective. *Green Chem.* **2006**, *8*(10), 861–867.

[27] van Bekkum, H. Application of Zeolites in the Upgrading of Renewables. in: Čejka, J.; Perez-Pariente, J.; Roth, W.J., Eds. *Zeolites: From Model Materials to Industrial Catalysts*; Transworld Research Network: Kerala, India, 2008, pp. 299–332.

[28] Barrault, J.; Clacens, J.-M.; Pouilloux, Y. Selective Oligomerization of Glycerol over Mesoporous Catalysts. *Top. Catal.* **2004**, *27*(1–4), 137–142.

[29] Corma, A.; Iborra, S.; Velty, A. Chemical Routes for the Transformation of Biomass into Chemicals. *Chem. Rev.* **2007**, *107*(6), 2411–2502.

[30] Mäki-Arvela, P.; Holmbom, B.; Salmi, T.; Murzin, D. Recent Progress in Synthesis of Fine and Specialty Chemicals from Wood and Other Biomass by Heterogeneous Catalytic Processes. *Catal. Rev. Sci. Eng.* **2007**, *49*(3), 197–340.

[31] Gallezot, P. Catalytic Routes from Renewables to Fine Chemicals. *Catal. Today* **2007**, *121*, 76–91.

[32] Centi, G.; Lanzafame, P.; Perathoner, S. Analysis of the Alternative Routes in the Catalytic Transformation of Lignocellulosic Materials. *Catal. Today* **2011**, *167*, 14–30.

[33] Lange, J.-P. Lignocellulose Conversion: An Introduction to Chemistry, Process and Economics. *Biofuels Bioprod. Biorefining* **2007**, *1*(1), 39–48.

[34] Chheda, J.; Huber, G.; Dumesic, J. Liquid-Phase Catalytic Processing of Biomass-Derived Oxygenated Hydrocarbons to Fuels and Chemicals. *Angew. Chem. Int. Ed. Engl.* **2007**, 46(38), 7164–7183.

[35] Simonetti, D.; Dumesic, J. Catalytic Production of Liquid Fuels from Biomass-Derived Oxygenated Hydrocarbons: Catalytic Coupling at Multiple Length Scales. *Catal. Rev. Sci. Eng.* **2009**, *51*(3), 441–484.

[36] Kubičková, I.; Kubička, D. Utilization of Triglycerides and Related Feedstocks for Production of Clean Hydrocarbon Fuels and Petrochemicals: A Review. *Waste. Biomass. Valor.* **2010**, *1*, 293–308.

[37] Lestari, S.; Mäki-Arvela, P.; Beltramini, J.; Lu, G.; Murzin, D. Transforming Triglycerides and Fatty Acids into Biofuels. *ChemSusChem* **2009**, *2*(12), 1109–1119.

[38] Pagliaro, M.; Ciriminna, R.; Kimura, H.; Rossi, M.; Pina, C.D. From Glycerol to Value-Added Products. *Angew. Chem. Int. Ed.* **2007**, *46*, 4434–4440.

[39] Pagliaro, M.; Ciriminna, R.; Kimura, H.; Rossi, M.; Pina, C. Recent Advances in the Conversion of Bioglycerol into Value-Added Products. *Eur. J. Lipid Sci. Technol*. **2009**, *111*(8), 788–799.

[40] Tong, X.; Ma, Y.; Li, Y. Biomass into Chemicals: Conversion of Sugars to Furan Derivatives by Catalytic Processes. *Appl. Catal. A Gen.* **2010**, *385*(1–2), 1–13.

[41] Zakzeski, J.; Bruijnincx, P.; Jongerius, A.; Weckhuysen, B. The Catalytic Valorization of Lignin for the Production of Renewable Chemicals. *Chem. Rev.* **2010**, *110*(6), 3552–3599.

[42] Taarning, E.; Osmundsen, C.; Yang, X.; Voss, B.; Andersen, S.; Christensen, C. Zeolite-Catalyzed Biomass Conversion to Fuels and Chemicals. *Energ. Environ. Sci.* **2011**, *4*(3), 793–804.

[43] Climent, M.J.; Corma, A.; Iborra, S. Converting Carbohydrates to Bulk Chemicals and Fine Chemicals over Heterogeneous Catalysts. *Green Chem.* **2011**, *13*(3), 520–540.

[44] Perego, C.; Bianchi, D. Biomass Upgrading through Acid–Base Catalysis. *Chem. Eng. J.* **2010**, *161*(3), 314–322.

[45] van Bekkum, H.; Kouwenhoven, H.W. Zeolites in Organic Cascade Reactions. *Stud. Surf. Sci. Catal.* **2005**, *157*, 311–336.

[46] van Bekkum, H.; Kouwenhoven, H.W. Progress in the Use of Zeolites in Organic Synthesis. *Stud. Surf. Sci. Catal.* **2007**, *168*, 947–998.

[47] Ek, M., Gellerstedt, G., Henriksson, G., Eds. *Pulp and Paper Chemistry and Technology, Volume 1: Wood Chemistry and Wood Biotechnology*; de Gruyter: Berlin, 2009.

[48] Ritter, S. News of the Week: A Fast Track to Green Gasoline. *Chem. Eng. News* **2008**, *86*(16), 10.

[49] Foley, P.; Beach, E.; Zimmerman, J. Algae as a Source of Renewable Chemicals: Opportunities and Challenges. *Green Chem.* **2011**, *13*(6), 1399–1405.

[50] Singh, A.; Nigam, P.; Murphy, J. Renewable Fuels from Algae: An Answer to Debatable Land Based Fuels. *Bioresour. Technol.* **2011**, *102*(1), 10–16.

[51] Liu, S. Woody Biomass: Niche Position as a Source of Sustainable Renewable Chemicals and Energy and Kinetics of Hot-Water Extraction/Hydrolysis. *Biotechnol. Adv.* **2010**, *28*(5), 563–582.

[52] Mäki-Arvela, P.; Anugwom, I.; Virtanen, P.; Sjöholm, R.; Mikkola, J. Dissolution of Lignocellulosic Materials and its Constituents using Ionic Liquids-A Review. *Ind. Crop. Prod.* **2010**, *32*(3), 175–201.

[53] Bridgwater, A. Review of Fast Pyrolysis of Biomass and Product Upgrading. *Biomass Bioenerg.* **2011**, *38*, 68–94.

[54] Bridgwater, A.; Peacocke, G. Fast Pyrolysis Processes for Biomass. *Renew. Sust. Energ. Rev.* **2000**, *4*(1), 1–73.

[55] Bulushev, D.; Ross, J. Catalysis for Conversion of Biomass to Fuels via Pyrolysis and Gasification: A Review. *Catal. Today* **2011**, *17* (1), 1–13.

[56] Maniatis, K. Progress in Biomass Gasification: An Overview. in: *Progress in Thermochemical Biomass Conversion*, Bridgwater, A.V., Ed.; Blackwell Science: Oxford, 2008.

[57] Goyal, H.; Seal, D.; Saxena, R. Bio-fuels from Thermochemical Conversion of Renewable Resources: A Review. *Renew. Sust. Energ. Rev.* **2008**, *12*(2), 504–517.

[58] Digman, B.; Joo, H.; Kim, D.-S. Recent Progress in Gasification/ Pyrolysis Technologies for Biomass Conversion to Energy. *Environ. Prog. Sustain. Energ.* **2009**, *28*(1), 47–51.

[59] Todd, A.; Holladay, J.E.; White, J.F. *Top Value Added Chemicals from Biomass - Volume I, Results of Screening for Potential Candidates from Sugars and Synthesis Gas*; Pacific Northwest National Laboratory: Richland, Washington, 2004.

[60] Bozell, J.J.; Holladay, J.E.; Johnson, D.; White, J.F. *Top Value Added Chemicals from Biomass. Volume II – Results of Screening for Potential Candidates from Biorefinery Lignin*; Pacific Northwest National Laboratory, Richland, Washington, 2007.

[61] Bozell, J.; Petersen, G. Technology Development for the Production of Biobased Products from Biorefinery Carbohydrates - The US Department of Energy's "Top 10" Revisited. *Green Chem.* **2010**, *12*(4), 539–554.

[62] Rosatella, A.; Simeonov, S.; Frade, R.; Afonso, C. 5-Hydroxymethylfurfural (HMF) as a Building Block Platform: Biological Properties, Synthesis and Synthetic Applications. *Green Chem.* **2011**, *13*(4), 754–793.

[63] Della Pina, C.; Falletta, E.; Rossi, M. A Green Approach to Chemical Building Blocks. The Case of 3-hydroxypropanoic Acid. *Green Chem.* **2011**, *13*(7), 1624–1632.

[64] Kilpeläinen, I.; Xie, H.; King, A.; Granstrom, M.; Heikkinen, S.; Argyropoulos, D. Dissolution of Wood in Ionic Liquids. *J. Agric. Food Chem.* **2007**, *55*(22), 9142–9148.

[65] Zhu, S.; Wu, Y.; Chen, Q.; Yu, Z.; Wang, C.; Jin, S.; Ding, Y.; Wu, G. Dissolution of Cellulose with Ionic Liquids and its Application: A Mini-Review. *Green Chem.* **2006**, *8*(4), 325–327.

[66] Li, B.; Asikkala, J.; Filpponen, I.; Argyropoulos, D. Factors Affecting Wood Dissolution and Regeneration of Ionic Liquids. *Ind. Eng. Chem. Res.* **2010**, *49*(5), 2477–2484.

[67] Yaman, S. Pyrolysis of Biomass to Produce Fuels and Chemical Feedstocks. *Energ. Conv. Manage.* **2004**, *45*(5), 651–671.

[68] Zhang, Q.; Chang, J.; Wang, T.; Xu, Y. Review of Biomass Pyrolysis Oil Properties and Upgrading Research. *Energ. Conv. Manage.* **2007**, *48*(1), 87–92.

[69] Czernik, S.; Bridgwater, A. Overview of Applications of Biomass Fast Pyrolysis Oil. *Energ. Fuels* **2004**, *18*(2), 590–598.

[70] Oasmaa, A.; Elliott, D.; Muller, S. Quality Control in Fast Pyrolysis Bio-Oil Production and Use. *Environ. Prog. Sustain. Energ*. **2009**, *28*(3), 404–409.

[71] Steynberg, A. P. Fischer–Tropsch Technology. In: Steynberg, A.P., Dry, M.E., Eds. *Studies in Surface Science and Catalysis (Volume 152)*; Elsevier: Amsterdam, **2004**, 1–63.

[72] Spath, P. L., Dayton, D. C. *Preliminary Screening — Technical and Economic Assessment of Synthesis Gas to Fuels and Chemicals with Emphasis on the Potential for Biomass-Derived Syngas*; Pacific Northwest National Laboratory: Richland, Washington, 2003.

[73] Khodakov, A.Y.; Chu, W.; Fongarland, P. Advances in the Development of Novel Cobalt Fischer-Tropsch Catalysts forSynthesis of Long-Chain Hydrocarbons and Clean Fuels. *Chem. Rev.* **2007**, *107*, 1692–1744.

[74] Martinez, A.; López, C.; Márquezand, F.; Díaz, I. Fischer–Tropsch Synthesis of Hydrocarbons over Mesoporous Co/SBA-15 Catalysts: The Influence of Metal Loading, Cobalt Precursor, and Promoters. *J. Catal.* **2003**, *220*, 486–499.

[75] Martinez, A.; Lopez, C. The Influence of ZSM-5 Zeolite Composition and Crystal Size on the in situ Conversion of Fischer–Tropsch Products over Hybrid Catalysts. *Appl. Catal. A Gen.* **2005**, *294*, 251–259.

[76] Garcia-Trenco, A.; Vidal-Moya, A.; Martínez, A. Study of the Interaction between Components in Hybrid CuZnAl/HZSM-5 Catalysts and its Impact in the Syngas-To-DME Reaction. *Catal. Today* **2012**, *179*, 43–51.

[77] Elliott, D.C. Historical Developments in Hydroprocessing Bio-oils. *Energ. Fuels* **2007**, *21*, 1792–1815.

[78] Diebold, J.; Chum, H.; Evans, R.; Milne, T.; Reed, T.; Scahill, J. Low-Pressure Upgrading of Primary Pyrolysis Oils from Biomass and Organic Wastes. *Symposium Papers - Energy from Biomass and Wastes*, Washington, D.C., April

7, 1986; Klass, D.L. Ed., Inst. of Gas Technology: Chicago, Illinois, 1987, pp. 801–830.

[79] Diebold, J.; Scahill, J. *Biomass to Gasoline (BTG): Upgrading Pyrolysis Vapors to Aromatic Gasoline with Zeolite Catalysis at Atmospheric Pressure.* ACS Division of Fuel Chemistry, Preprints *32*(2), Washington, D.C., **1987**, 297–307.

[80] Diebold, J.P.; Scahill, J.W. Conversion of Wood to Aromatic Gasoline with Zeolite Catalysts. *Energ. Prog.* **1988**, *8*(1), 59–66.

[81] Horne, P.; Williams, P. Premium Quality Fuels and Chemicals from the Fluidised Bed Pyrolysis of Biomass with Zeolite Catalyst Upgrading. *Renew. Eng.* **1994**, *5*(5–8), 810–812.

[82] Horne, P.; Nugranad, N.; Williams, P. Catalytic Coprocessing of Biomass-Derived Pyrolysis Vapours and Methanol. *J. Anal. Appl. Pyrolysis* **1995**, *34*(1), 87–108.

[83] Horne, P.; Williams, P. Upgrading of Biomass-Derived Pyrolytic Vapours over Zeolite ZSM-5 Catalyst: Effect of Catalyst Dilution on Product Yields. *Fuel* **1996**, *75*(9), 1043–1050.

[84] Williams, P.; Horne, P. Characterisation of Oils from the Fluidised Bed Pyrolysis of Biomass with Zeolite Catalyst Upgrading. *Biomass Bioenerg*. **1994**, *7*(1–6), 223–236.

[85] Williams, P.; Horne, P. The Influence of Catalyst Type on the Composition of Upgraded Biomass Pyrolysis Oils. *J. Anal. Appl. Pyrolysis* **1995**, *31*(C), 39–61.

[86] Williams, P.; Horne, P. The Influence of Catalyst Regeneration on the Composition of Zeolite-Upgraded Biomass Pyrolysis Oils. *Fuel* **1995**, 74(12), 1839–1851.

[87] Kučera, J.; Nachtigall, P. Coordination of Alkali Metal Ions in ZSM-5: A Combined Quantum Mechanics/Interatomic Potential Function Study. *Phys. Chem. Chem. Phys.* **2003**, *5*(15), 3311–3317.

[88] Gábová, V.; Dědeček, J.; Čejka, J. Control of Al Distribution in ZSM-5 by Conditions of Zeolite Synthesis. *Chem. Commun.* **2003**, *9*(10), 1196–1197.

[89] Aho, A.; Kumar, N.; Eränen, K.; Salmi, T.; Hupa, M.; Murzin, D. Catalytic Pyrolysis of Woody Biomass in a Fluidized Bed Reactor: Influence of the Zeolite Structure. *Fuel* **2008**, *87*(12), 2493–2501.

[90] Aho, A.; Kumar, N.; Lashkul, A.; Eränen, K.; Ziolek, M.; Decyk, P.; Salmi, T.; Holmbom, B.; Hupa, M.; Murzin, D. Catalytic Upgrading of Woody Biomass Derived Pyrolysis Vapours over Iron Modified Zeolites in a Dual-Fluidized Bed Reactor. *Fuel* **2010**, *89*(8), 1992–2000.

[91] Aho, A.; Kumar, N.; Eränen, K.; Salmi, T.; Hupa, M.; Murzin, D. Catalytic Pyrolysis of Biomass in a Fluidized Bed Reactor: Influence of the Acidity of H-Beta Zeolite. *Process Saf. Environ. Protect.* **2007**, *85*(5 B), 473–480.

[92] Aho, A.; Kumar, N.; Eränen, K.; Hupa, M.; Salmi, T.; Murzin, D. Zeolite-Bentonite Hybrid Catalysts for the Pyrolysis of Woody Biomass. *Stud. Surf. Sci. Catal.* **2008**, *174*(B), 1069–1074.

[93] Park, H.; Dong, J.-I.; Jeon, J.-K.; Yoo, K.-S.; Yim, J.-H.; Sohn, J.; Park, Y.-K. Conversion of the Pyrolytic Vapor of Radiata Pine over Zeolites. *J. Ind. Eng. Chem.* **2007**, *13*(2), 182–189.

[94] Horne P.; Williams, P. Reaction of Oxygenated Biomass Pyrolysis Model Compounds over a ZSM-5 Catalyst. *Renew. Eng.* **1996**, *7*(2), 131–144.

[95] Stefanidis, S.; Nitsos, C.; Kalogiannis, K.; Iliopoulou, E.; Lappas, A.; Triantafyllidis, K. Catalytic Upgrading of Lignocellulosic Biomass Pyrolysis Vapours: Effect of Hydrothermal Pre-Treatment of Biomass. *Catal. Today* **2011**, *167*(1), 37–45

[96] Adam, J.; Antonakou, E.; Lappas, A.; Stöcker, M.; Nilsen, M.; Bouzga, A.; Hustad, J.; Oye, G. In situ Catalytic Upgrading of Biomass Derived Fast Pyrolysis Vapours in a Fixed Bed Reactor using Mesoporous Materials. *Micropor. Mesopor. Mat.* **2006**, 96(1–3), 93–101.

[97] Antonakou, E.; Lappas, A.; Nilsen, M.; Bouzga, A.; Stöcker, M. Evaluation of Various Types of Al-MCM-41 Materials as Catalysts in Biomass Pyrolysis for the Production of Bio-Fuels and Chemicals. *Fuel* **2006**, *85*(14–15), 2202–2212.

[98] Iliopoulou, E.; Antonakou, E.V.; Karakoulia, S.; Vasalos, I.; Lappas, A.; Triantafyllidis, K. Catalytic Conversion of Biomass Pyrolysis Products by Mesoporous Materials: Effect of Steam Stability and Acidity of Al-MCM-41 Catalysts. *Chem. Eng. J.* **2007**, *134*, 51–57.

[99] Dědeček, J.; Žilková, N.; Čejka, J. Experimental Study of the Effect of Si/Al Compsition on the Aluminum Distribution in (Al)MCM-41. *Micropor. Mesopor. Mat.* **2001**, 44–45, 259–266.

[100] Triantafyllidis, K.; Iliopoulou, E.; Antonakou, E.; Lappas, A.; Wang, H.; Pinnavaia, T. Hydrothermally Stable Mesoporous Aluminosilicates (MSU-S) Assembled from Zeolite Seeds as Catalysts for Biomass Pyrolysis. *Micropor. Mesopor. Mat.* **2007**, *99*(1–2), 132–139.

[101] Prokešová, P.; Žilková, N.; Mintova, S.; Bein, T.; Čejka, J. Catalytic Activity of Micro/Mesoporous Composites in Toluene Alkylation with Propylene. *Appl. Catal. A Gen*. **2005**, *281*(1–2), 85–91.

[102] Park, H.; Heo, H.; Jeon, J.-K.; Kim, J.; Ryoo, R.; Jeong, K.-E.; Park, Y.-K. Highly Valuable Chemicals Production from Catalytic Upgrading of Radiata Pine Sawdust-Derived Pyrolytic Vapors over Mesoporous MFI Zeolites. *Appl. Catal. B Environ.* **2010**, *95*(3–4), 365–373.

[103] Carlson, T.R.; Tompsett, G.A.; Conner, W.C.; Huber, G.W. Aromatic Production from Catalytic Fast Pyrolysis of Biomass-Derived Feedstocks. *Top. Catal.* **2009**, *52*, 241–252.

[104] Carlson, T.; Jae, J.; Lin, Y.-C.; Tompsett, G.; Huber, G. Catalytic Fast Pyrolysis of Glucose with HZSM-5: The Combined Homogeneous and Heterogeneous Reactions. *J. Catal.* **2010**, *270*(1), 110–124.

[105] Vispute, T.; Zhang, H.; Sanna, A.; Xiao, R.; Huber, G. Renewable Chemical Commodity Feedstocks from Integrated Catalytic Processing of Pyrolysis Oils. *Science* **2010**, *330*(6008), 1222–1227.

[106] Jae, J.; Tompsett, G.; Foster, A.; Hammond, K.; Auerbach, S.; Lobo, R.; Huber, G. Investigation into the Shape Selectivity of Zeolite Catalysts for Biomass Conversion. *J. Catal.* **2011**, *279*(2), 257–268.

[107] Gayubo, A.; Aguayo, A.; Atutxa, A.; Aguado, R.; Bilbao, J. Transformation of Oxygenate Components of Biomass Pyrolysis Oil on a HZSM-5 Zeolite. I. Alcohols and pPhenols. *Ind. Eng. Chem. Res.* **2004**, *43*(11), 2610–2618.

[108] Gayubo, A.; Aguayo, A.; Atutxa, A.; Aguado, R.; Olazar, M.; Bilbao, J. Transformation of Oxygenate Components of Biomass Pyrolysis Oil on a HZSM-5 Zeolite. II. Aldehydes, Ketones, and Acids. *Ind. Eng. Chem. Res.* **2004**, *43*(11), 2619–2626.

[109] Gayubo, A.; Aguayo, A.; Atutxa, A.; Prieto, R.; Bilbao, J. Deactivation of a HZSM-5 Zeolite Catalyst in the Transformation of the Aqueous Fraction of Biomass Pyrolysis Oil into Hydrocarbons. *Energ. Fuels* **2004**, *18*(6), 1640–1647.

[110] Käldström, M.; Kumar, N.; Murzin, D. Yu. Valorization of Cellulose over Metal Supported Mesoporous Materials. *Catal. Today* **2011**, *167*, 91–95.

[111] Käldström, M.; Kumar N.; Salmi T.; Murzin, D. Yu. Levoglucosan Transformation over Aluminosilicates. *Cell. Chem. Technol.* **2010**, *44*(4–6), 203–209.

[112] Käldström, M.; Kumar N.; Heikkilä, T.; Tiitta, M.; Salmi T.; Murzin, D. Yu. Transformation of Levoglucosan over H-MCM-22 Zeolite and H-MCM-41 Mesoporous Molecular Sieve Catalysts. *Biomass Bioenerg.* **2011**, *35*(5), 1967–1976.

[113] Käldström, M.; Kumar N.; Heikkilä, T.; Murzin, D. Yu. Pillared H-MCM-36 Mesoporous and H-MCM-22 Microporous Materials for Conversion of Levoglucosan: Influence of Varying Acidity. *Appl. Catal. A Gen.* **2011**, *397*(1–2), 13–21.

[114] Mäki-Arvela, P.; Salmi, T.; Holmbom, B.; Willför, S.; Murzin, D.Yu. Synthesis of Sugars by Hydrolysis of Hemicelluloses – A Review. *Chem. Rev.* **2011**, *111*, 5638–5666.

[115] Fukuoka, A.; Dhepe, P.L. Catalytic Conversion of Cellulose into Sugar Alcohols. *Angew. Chem. Int. Ed.* **2006**, *45*, 5161–5163.

[116] French, R.; Czernik, S. Catalytic Pyrolysis of Biomass for Biofuels Production. *Fuel Process. Technol.* **2010**, *91*(1), 25–32.

[117] Torri, C.; Reinikainen, M.; Lindfors, C.; Fabbri, D.; Oasmaa, A.; Kuoppala, E. Investigation on Catalytic Pyrolysis of Pine Sawdust: Catalyst Screening by Py-GC-MIP-AED. *J. Anal. Appl. Pyrolysis* **2010**, *88*(1), 7–13.

[118] Roth, W.J.; Dorset, D. Expanded View of Zeolite Structures and Their Variability based on Layered Nature of 3-D Frameworks. *Micropor. Mesopor. Mater.* **2011**, *142*(1), 32–36.

[119] Roth, W.; Dorset, D.; Kennedy, G. Discovery of New MWW Family Zeolite EMM-10: Identification of EMM-10P as the Missing MWW Precursor with Disordered Layers. *Micropor. Mesopor. Mater.* **2011**, *142*(1), 168–177.

[120] Vitolo, S.; Bresci, B.; Seggiani, M.; Gallo, M. Catalytic Upgrading of Pyrolytic Oils over HZSM-5 Zeolite: Behaviour of the Catalyst when Used in Repeated Upgrading-Regenerating Cycles. *Fuel* **2001**, *80*(1), 17–26.

[121] Ma, F.; Hanna, M. Biodiesel Production: A Review. *Bioresour. Technol*. **1999**, *70*(1), 1–15.

[122] Meher, L.; Vidya Sagar, D.; Naik, S. Technical Aspects of Biodiesel Production by Transesterification-A Review. *Renew. Sust. Energ. Rev.* **2006**, *10*(3), 248–268.

[123] *Biodiesel Safety and Best Management Practices for Small-Scale Noncommercial Use and Production*, State College, PA: The Pennsylvania State University, 2008, www.cas.psu.edu

[124] Bournay, L.; Casanave, D.; Delfort, B.; Hillion, G.; Chodorge, J. New Heterogeneous Process for Biodiesel Production: A Way to Improve the Quality and the Value of the Crude Glycerinproduced by Biodiesel Plants. *Catal. Today* **2005**, *106*, 190–192.

[125] Yan, S.; Dimaggio, C.; Mohan, S.; Kim, M.; Salley, S.; Ng, K. Advancements in Heterogeneous Catalysis for Biodiesel Synthesis. *Top. Catal.* **2010**, *53*(11–12), 721–736.

[126] Semwal, S.; Arora, A.; Badoni, R.; Tuli, D. Biodiesel Production using Heterogeneous Catalysts. *Bioresour. Technol.* **2011**, *102*(3), 2151–2161.

[127] Katikaneni, Sai P.R.; Adjaye, J.D.; Bakhshi, N.N. Catalytic Conversion of Canola Oil to Fuels and Chemicals over Various Cracking Catalysts. *Can. J. Chem. Eng.* **1995**, *73*(4), 484–497.

[128] Twaiq, F.A.; Zabidi, N.A.M.; Bhatia, S. Catalytic Conversion of Palm Oil to Hydrocarbons: Performance of Various Zeolite Catalysts. *Ind. Eng. Chem. Res.* **1999**, *38*, 3230–3237.

[129] Danuthai, T.; Jongpatiwut, S.; Rirksomboon, T.; Osuwan, S.; Resasco, D. Conversion of Methylesters to Hydrocarbons over Zn-modified H-ZSM-5 Zeolite Catalyst. *Catal. Lett.* **2009**, *132*(1–2), 197–204.

[130] Kubička, D.; Šimáček, P.; Žilková, N. Transformation of Vegetable Oils into Hydrocarbons over Mesoporous-Alumina-Supported CoMo Catalysts. *Top. Catal.* **2009**, *52*, 161–168.

[131] Kubička, D.; Bejblová, M.; Vlk, J. Conversion of Vegetable Oils into Hydrocarbons over CoMo/MCM-41 Catalysts. *Top. Catal.* **2010**, *53*(3–4), 168–178.

[132] Dossin, T.F.; Reyniers, M.; Berger, R.J.; Marin, G.B. Simulation of Heterogeneously MgO-Catalyzed Transesterification for Fine-Chemical and Biodiesel Industrial Production. *Appl. Catal. B Environ.* **2006**, *67*, 136–148.

[133] Granados, M.; Poves, M.; Alonso, D.; Mariscal, R.; Galisteo, F.; Moreno-Tost, R.; Santamaría, J.; Fierro, J. Biodiesel from Sunflower Oil by Using Activated Calcium Oxide. *Appl. Catal. B Environ.* **2007**, *73*(3), 317–326.

[134] Di Serio, M.; Tesser, R.; Casale, L.; D'Angelo, A.; Trifuoggi, M.; Santacesaria, E. Heterogeneous Catalysis in Biodiesel Production: The Influence of Leaching. *Top. Catal*. **2010**, *53*(11–12), 811–819.

[135] Yang, Z.; Xie, W. Soybean Oil Transesterification over Zinc Oxide Modified with Alkali Earth Metals. *Fuel Process. Technol.* **2007**, *88*(6), 631–638.

[136] Encinar, J.; González, J.; Pardal, A.; Martínez, G. Rape Oil Transesterification over Heterogeneous Catalysts. *Fuel Process. Technol.* **2010**, *91*(11), 1530–1536.

[137] Cantrell, D.G.; Gillie, L.J.; Lee, A.F.; Wilson, K. Structure-Reactivity Correlations in MgAl Hydrotalcite Catalysts for Biodiesel Synthesis. *Appl. Catal. A Gen.* **2005**, *287*, 183–190.

[138] Di Serio, M.; Cozzolino, M.; Giordano, M.; Tesser, R.; Patrono, P.; Santacesaria, E. From Homogeneous to Heterogeneous Catalysts in Biodiesel Production. *Ind. Eng. Chem. Res.* **2007**, *46*(20), 6379–6384.

[139] Navajas, A.; Campo, I.; Arzamendi, G.; Herníndez, W.; Bobadilla, L.; Centeno, M.; Odriozola, J.; Gandía, L. Synthesis of Biodiesel from the Methanolysis of Sunflower Oil Using PURAL(R) Mg-Al Hydrotalcites as Catalyst Precursors. *Appl. Catal. B Environ.* **2010**, *100*(1–2), 299–309.

[140] Hsin, T.-M.; Chen, S.; Guo, E.; Tsai, C.-H.; Pruski, M.; Lin, V.S.Y. Calcium Containing Silicate Mixed Oxide-Based Heterogeneous Catalysts for Biodiesel Production. *Top. Catal.* **2010**, *53*(11–12), 746–754.

[141] Suppes, G.; Dasari, M.; Doskocil, E.; Mankidy, P.; Goff, M. Transesterification of Soybean Oil with Zeolite and Metal Catalysts. *Appl. Catal. A Gen*. **2004**, *257*, 213–223.

[142] Arzamendi, G.; Campo, I.; Arguiňarena, E.; Sánchez, M.; Montes, M.; Gandía, L. Synthesis of Biodiesel with Heterogeneous NaOH/Alumina Catalysts: Comparison with Homogeneous NaOH. *Chem. Eng. J.* **2007**, *134*(1–3), 123–130.

[143] Xie, W.; Li, H. Alumina-Supported Potassium Iodide as a Heterogeneous Catalyst for Biodiesel Production from Soybean Oil. *J. Mol. Catal. A Chem.* **2006**, *255*, 1–9.

[144] Marquez-Alvarez C.; Žilková N.; Perez-Pariente J.; Čejka, J. Synthesis, Characterization and Catalytic Applications of Organized Mesoporous Aluminas. *Catal. Rev. Sci. Eng.* **2008**, *50*(2), 222–286.

[145] Xie, W.; Huang, X.; Li, H. Soybean Oil Methyl Esters Preparation Using NaX Zeolites Loaded with KOH as a Heterogeneous Catalyst. *Bioresour. Technol.* **2007**, *98*, 936–939.

[146] Xie, W.; Peng, H.; Chen, L. Transesterification of Soybean Oil Catalyzed by Potassium Loaded on Alumina as a Solid-Base Catalyst. *Appl. Catal. A Gen.* **2006**, *300*(1), 67–74.

[147] Macario, A.; Giordano, G.; Onida, B.; Cocina, D.; Tagarelli, A.; Giuffré, A. Biodiesel Production Process by Homogeneous/Heterogeneous Catalytic System using an Acid-Base Catalyst. *Appl. Catal. A Gen.* **2010**, *378*(2), 160–168.

[148] Abdullah, A.; Razali, N.; Lee, K. Optimization of Mesoporous K/SBA-15 Catalyzed Transesterification of Palm Oil Using Response Surface Methodology. *Fuel Process. Technol*. **2009**, *90*(7–8), 958–964.

[149] Kiss, A.; Dimian, A.; Rothenberg, G. Solid Acid Catalysts for Biodiesel Production - Towards Sustainable Energy. *Adv. Synth. Catal.* **2006**, *348*, 75–81.

[150] Shu, Q.; Yang, B.; Yuan, H.; Qing, S.; Zhu, G. Synthesis of Biodiesel from Soybean Oil and Methanol Catalyzed by Zeolite Beta Modified with La^{3+}. *Catal. Commun.* **2007**, *8*(12), 2159–2165.

[151] Karmee, S.; Chadha, A. Preparation of Biodiesel from Crude Oil of Pongamia Pinnata. *Bioresour. Technol.* **2005**, *96*(13), 1425–1429.

[152] Carmo, J.A.; de Souza, L.; da Costa, C.; Longo, E.; Zamian, J.; da Rocha Filho, G. Production of Biodiesel by Esterification of Palmitic Acid over Mesoporous Aluminosilicate Al-MCM-41. *Fuel* **2009**, *88*(3), 461–468.

[153] Goncalves, A.; Lopes, J.; Lemos, F.; Ramoa Ribeiro, F.; Prazeres, D.; Cabrai, J.; Aires-Barros, M. Zeolites as Supports for Enzymatic Hydrolysis Reactions. Comparative Study of Several Zeolites. *J. Mol. Catal. B: Enzym.* **1996**, 1(2), 53–60.

[154] Brito, A.; Borges, M.; Otero, N. Zeolite Y as a Heterogeneous Catalyst in Biodiesel Fuel Production from Used Vegetable Oil. *Energ. Fuels* **2007**, *21*(6), 3280–3283.

[155] Idem, R.; Katikaneni, S.; Bakhshi, N. Catalytic Conversion of Canola Oil to Fuels and Chemicals: Roles of Catalyst Acidity, Basicity and Shape Selectivity. *Fuel Process. Technol.* **1997**, *51*(1), 101–125.

[156] Ooi, Y.-S.; Zakaria, R.; Mohamed, A.R.; Bhatia, S. Catalytic Conversion of Fatty Acids Mixture to Liquid Fuel and Chemicals over Composite Microporous/Mesoporous Catalysts. *Energ. Fuels* **2005**, *19*, 736–743.

[157] Twaiq, F.; Mohamad, A.; Bhatia, S. Performance of Composite Catalysts in Palm Oil Cracking for the Production of Liquid Fuels and Chemicals. *Fuel Process. Technol.* **2004**, *85*(11), 1283–1300.

[158] Čejka, J.; Mintova, S. Perspectives of Micro/Mesoporous Composites in Catalysis. *Catal. Rev. Sci. Eng.* **2007**, *49*(4), 457–509.

[159] Roth, W. Synthesis of Delaminated and Pillared Zeolitic Materials. in: Čejka, J., van Bekkum, H., Corma, A., Schüth, F., Eds., *Introduction to Zeolite Science and Practice*; Elsevier: Amsterdam, 2007, pp. 221–239.

[160] Roth, W.J.; Čejka, J. Two-Dimensional Zeolites: Dream or Reality? *Catal. Sci. Technol.* **2011**, *1*(1), 43–53.

[161] Roth, W.J.; Shvets, O.V.; Shamzhy, M.; Chlubná, P.; Kubů, M.; Nachtigall, P.; Čejka, J. Postsynthesis Transformation of Three-Dimensional Framework into a Lamellar Zeolite with Modifiable Architecture. *J. Amer. Chem. Soc.* **2011**, *133*(16), 6130–6133.

[162] Dandik, L.; Aksoy, H.; Erdem-Senatalar, A. Catalytic Conversion of Used Oil to Hydrocarbon Fuels in a Fractionating Pyrolysis Reactor. *Energ. Fuels* **1998**, *12*(6), 1148–1152.

[163] Yarlagadda, P.; Yaollang, H.; Bakhshl, N. Effect of Hydrothermal Treatment of HZSM-5 Catalyst on Its Performance for the Conversion of Canola and Mustard Oils to Hydrocarbons. *Ind. Eng. Chem. Prod. Res. Dev.* **1986**, *25*, 251–257.

[164] Katikaneni, S.; Adjaye, J.; Bakhshi, N. Studies on the Catalytic Conversion of Canola Oil toHydrocarbons: Influence of Hybrid Catalysts and Steam. *Energ. Fuels* **1995**, *9*, 599–609.

[165] Kubička, D. Future Refining Catalysis – Introduction of Biomass Feedstocks. *Collect. Czech. Chem. Commun.* **2008**, *73*(8–9), 1015–1044.

[166] Ooi, Y.-S.; Zakaria, R.; Mohamed, A.R.; Bhatia, S. Synthesis of Composite Material MCM-41/Beta and its Catalytic Performance in Waste Used Palm Oil Cracking. *Appl. Catal. A Gen.* **2004**, *274*, 15–23.

[167] Dupain, X.; Costa, D.; Schaverien, C.; Makkee, M.; Moulijn, J. Cracking of a Rapeseed Vegetable Oil under Realistic FCC Conditions. *Appl. Catal. B Environ.* **2007**, *72*(1–2), 44–61.

[168] Bormann, K.; Tilgner, H.; Moll, H.-J. Rape Seed Oil as a Feed Component for the Catalytic Cracking Process. *Erdoel Erdgas Kohle* **1993**, *109*(4), 172–176.

[169] Bormann, K.; Tilgner, H. On the Influence of Rape Seed Oil Triglycerides on the Catalytic Cracking of Petroleum Distillate. *Erdoel Erdgas Kohle* **1994**, *110*(2), 75.

[170] Stadlbauer, E.; Altensen, R.; Bojanowski, S.; Donnevert, G.; Fiedler, A.; Hossain, S.; Rossmanith, J.; Schilling, G. Production of Hydrocarbons from Animal Fat by Thermocatalytic Cracking. *Erdoel Erdgas Kohle* **2006**, *122*(2), 64–69.

[171] Neste Oil, http://www.nesteoil.com/default.asp?path=1,41,11991,12243,13565; accessed on February 22, 2012.

[172] Elliott, D. Historical Developments in Hydroprocessing Bio-oils. *Energ. Fuels* **2007**, *21*, 1792–1815.

[173] French, R.; Hrdlicka, J.; Baldwin, R. Mild Hydrotreating of Biomass Pyrolysis Oils to Produce a Suitable Refinery Feedstock. *Environ. Prog. Sustain. Energ.* **2010**, *29*, 142–150.

[174] Samolada, M.C.; Baldauf, W.; Vasalos, I.A. Production of a Bio-Gasoline by Upgrading Biomass Flash Pyrolysis Liquids via Hydrogen Processing and Catalytic Cracking. *Fuel* **1998**, *77*(14), 1667–1675.

[175] de Miguel Mercader, F.; Groeneveld, M.; Kersten, S.; Way, N.; Schaverien, C.; Hogendoorn, J. Production of Advanced Biofuels: Co-processing of Upgraded Pyrolysis Oil in Standard Refinery Units. *Appl. Catal. B Environ.* **2010**, *96*, 57–66.

[176] Lichtenthaler, F. W. *Carbohydrates: Occurrence, Structures and Chemistry*; Ullmann's Encyclopedia of Industrial Chemistry, 2010.

[177] van Gorp, K.; Boerman, E.; Cavenaghi, C.; Berben, P. Catalytic Hydrogenation of Fine Chemicals: Sorbitol Production. *Catal. Today* **1999**, *52*(2–3), 349–361

[178] Sherman, J.; Chao, C. Carbohydrate Separations using Zeolite Molecular Sieves. *Stud. Surf. Sci. Catal.* **1986**, *28*(C), 1025–1032.

[179] Cheng, Y.; Lee, T. Separation of Fructose and Glucose Mixture by Zeolite Y. *Biotechnol. Bioeng.* **1992**, *40*(4), 498–504.

[180] Li, S.; Tuan, V.; Falconer, J.; Noble, R. Effects of Zeolite Membrane Structure on the Separation of 1,3-propanediol from Glycerol and Glucose by Pervaporation. *Chem. Mater.* **2001**, *13*(5), 1865–1873.

[181] Moreau, C.; Durand, R.; Razigade, S.; Duhamet, J.; Faugeras, P.; Rivalier, P.; Pierre, R.; Avignon, G. Dehydration of Fructose to 5-hydroxymethylfurfural over H-Mordenites. *Appl. Catal. A Gen.* **1996**, *145*(1–2), 211–224.

[182] Lourvanij, K.; Rorrer, G. Reaction Rates for the Partial Dehydration of Glucose to Organic Acids in Solid-Acid, Molecular-Sieving Catalyst Powders. *J. Chem. Technol. Biotechnol*. **1997**, *69*(1), 35–44.

[183] Moreau, C.; Durand, R.; Peyron, D.; Duhamet, J.; Rivalier, P. Selective Preparation of Furfural from Xylose over Microporous Solid Acid Catalysts. *Ind. Crop. Prod.* **1998**, *7*(2–3), 95–99.

[184] Zeng, W.; Cheng, D.-G.; Zhang, H.; Chen, F.; Zhan, X. Dehydration of Glucose to Levulinic Acid over MFI-type Zeolite in Subcritical Water at Moderate Conditions. *React. Kinet. Mechan. Catal.* **2010**, *100*(2), 377–384.

[185] Sui, X.; Lin, L. Clean conversion of glucose to levulinic acid catalyzed by ZSM-5. *Huaxue Fanying Gongcheng Yu Gongyi/Chem. React. Eng. Technol.* **2010**, *26*(1), 74–78, 87.

[186] Tan, M.; Zhao, L.; Zhang, Y. Production of 5-hydroxymethyl Furfural from Cellulose in CrCl2/Zeolite/BMIMCl System. *Biomass Bioenerg.* **2011**, *35*(3), 1367–1370.

[187] Nikolla, E.; Román-Leshkov, Y.; Moliner, M.; Davis, M. “One-pot” Synthesis of 5-(hydroxymethyl)Furfural from Carbohydrates Using Tin-Beta Zeolite. *ACS Catal*. **2011**, *1*(4), 408–410.

[188] Holm, M.; Saravanamurugan, S.; Taarning, E. Conversion of Sugars to Lactic Acid Derivatives Using Heterogeneous Zeotype Catalysts. *Science* **2010**, *328*(5978), 602–605.

[189] Gallezot, P. Direct Routes from Biomass to End-Products. *Catal. Today* **2011**, *167*(1), 31–36.

[190] Lima, S.; Antunes, M.; Fernandes, A.; Pillinger, M.; Ribeiro, M.; Valente, A. Acid-Catalysed Conversion of Saccharides into Furanic Aldehydes in the Presence of Three-Dimensional Mesoporous Al-TUD-1. *Molecules* **2010**, *15*(6), 3863–3877.

[191] Richel, A.; Laurent, P.; Wathelet, B.; Wathelet, J.-P.; Paquot, M. Current Perspectives on Microwave-Enhanced Reactions of Monosaccharides Promoted by Heterogeneous Catalysts. *Catal. Today* **2011**, *167*(1), 141–147.

[192] Taarning, E.; Saravanamurugan, S.; Holm, M.; Xiong, J.; West, R.; Christensen, C. Zeolite-Catalyzed Isomerization of Triose Sugars. *ChemSusChem* **2009**, *2*(7), 625–627.

[193] West, R.; Holm, M.; Saravanamurugan, S.; Xiong, J.; Beversdorf, Z.; Taarning, E.; Christensen, C. Zeolite H-USY for the Production of Lactic Acid and Methyl Lactate from C3-sugars. *J. Catal.* **2010**, *269*(1), 122–130.

[194] Pescarmona, P.; Janssen, K.; Stroobants, C.; Molle, B.; Paul, J.; Jacobs, P.; Sels, B. A High-Throughput Experimentation Study of the Synthesis of Lactates with Solid Acid Catalysts. *Top. Catal.* **2010**, *53*(1–2), 77–85.

[195] Pescarmona, P.; Janssen, K.; Delaet, C.; Stroobants, C.; Houthoofd, K.; Philippaerts, A.; De Jonghe, C.; Paul, J.; Jacobs, P.; Sels, B. Zeolite-Catalysed Conversion of C3 Sugars to Alkyl Lactates. *Green Chem.* **2010**, *12*(6), 1083–1089.

[196] Corma, A.; Garcia, H. Lewis Acids: From Conventional Homogeneous to Green Homogeneous and Heterogeneous Catalysis. *Chem. Rev.* **2003**, *102*(10), 3837–3892

[197] Maksimov, A.; Nekhaev, A.; Shlyakhtitsev, D.; Varfolomeev, S.; Vol'Eva, V.; Nikiforov, G. Synthesis of the Components of Engine Fuels on the Basis of Renewable Raw Materials: Trends and Prospects. *Pet. Chem.* **2010**, *50*(5), 325–331.

[198] Maksimov, A.; Nekhaev, A.; Ramazanov, D.; Arinicheva, Y.; Dzyubenko, A.; Khadzhiev, S. Preparation of High-Octane Oxygenate Fuel Components from Plant-Derived Polyols. *Pet. Chem*. **2011**, *51*(1), 61–69.

[199] Huber, G.; Dumesic, J. An Overview of Aqueous-Phase Catalytic Processes for Production of Hydrogen and Alkanes in a Biorefinery. *Catal. Today* **2006**, *111*(1–2), 119–132.

[200] Li, N.; Huber, G. Aqueous-Phase Hydrodeoxygenation of Sorbitol with Pt/SiO_2-Al_2O_3: Identification of Reaction Intermediates. *J. Catal.* **2010**, *270*(1), 48–59.

[201] Li, N.; Tompsett, G.; Huber, G. Renewable High-Octane Gasoline by Aqueous-Phase Hydrodeoxygenation of C_5 and C_6 Carbohydrates over Pt/Zirconium Phosphate Catalysts. *ChemSusChem* **2010**, *3*(10), 1154–1157.

[202] Zhang, H.; Cheng, Y.-T.; Vispute, T.; Xiao, R.; Huber, G. Catalytic Conversion of Biomass-Derived Feedstocks into Olefins and Aromatics with ZSM-5: The Hydrogen to Carbon Effective Ratio. *Energ. Environ. Sci.* **2011**, *4*(6), 2297–2307.

[203] Lima, S.; Dias, A.; Lin, Z.; Brandão, P.; Ferreira, P.; Pillinger, M.; Rocha, J.; Calvino-Casilda, V.; Valente, A. Isomerization of d-glucose to d-fructose over Metallosilicate Solid Bases. *Appl. Catal. A Gen.* **2008**, *339*(1), 21–27.

[204] Moreau, C.; Durand, R.; Roux, A.; Tichit, D. Isomerization of Glucose into Fructose in the Presence of Cation-Exchanged Zeolites and Hydrotalcites. *Appl. Catal. A Gen.* **2000**, 193(1–2), 257–264.

[205] Moliner, M.; Román-Leshkov, Y.; Davis, M. Tin-Containing Zeolites are Highly Active Catalysts for the Isomerization of Glucose in Water. *Proc. Natl. Acad. Sci. U. S. A.* **2010**, *107*(14), 6164–6168.

[206] Roman-Leshkov, Y.; Moliner, M.; Labinger, J.; Davis, M. Mechanism of Glucose Isomerization using a Solid Lewis Acid Catalyst in Water. *Angew. Chem. Int. Ed.* **2010**, *49*(47), 8954–8957.

[207] Velarde, A.; Bartl, P.; Nießen, T.; Hoelderich, W. Hydrogen Peroxide Oxidation of D-Glucose with Titanium-Containing Zeolites as Catalysts. *J. Mol. Catal. A Chem.* **2000**, *157*(1–2), 225–236.

[208] Xavier, N.; Lucas, S.; Rauter, A. Zeolites as Efficient Catalysts for Key Transformations in Carbohydrate Chemistry. *J. Mol. Catal. A Chem.* **2009**, *305*(1–2), 84–89.

[209] Corma, A.; Iborra, S.; Miquel, S.; Primo, J. Preparation of Environmentally Friendly Alkylglucoside Surfactants Using Zeolites as Catalysts. *J. Catal.* **1996**, *161*(2), 713–719.

[210] Camblor, M.; Corma, A.; Iborra, S.; Miquel, S.; Primo, J.; Valencia, S. Beta Zeolite as a Catalyst for the Preparation of Alkyl Glucoside Surfactants: The Role of Crystal Size and Hydrophobicity. *J. Catal.* **1997**, *172*(1), 76–84.

[211] Chen, N.; Degnan Jr., T.F.; Koenig, L. Liquid Fuel from Carbohydrates. *CHEMTECH* **1986**, *16*(8), 506–511.

[212] Crisci, A.; Tucker, M.; Lee, M.-Y.; Jang, S.; Dumesic, J.; Scott, S. Acid-Functionalized SBA-15-type Silica Catalysts for Carbohydrate Dehydration. *ACS Catal.* **2011**, 1(7), 719–728.

[213] Lourvanij, K.; Rorrer, G. Reactions of Aqueous Glucose Solutions Over Solid-Acid Y-Zeolite Catalyst at 110-160°C. *Ind. Eng. Chem. Res.* **1993**, *32*(1), 11–19.

[214] Wahlen, J.; Moens, B.; De Vos, D.E.; Alsters, P.L.; Jacobs, P.A. Titanium Silicalite 1 (TS-1) Catalyzed Oxidative Transformations of Furan Derivatives with Hydrogen Peroxide. *Adv. Synth. Catal.* **2004**, *346*, 333–338.

[215] Brandner, A.; Lehnert, K.; Bienholz, A.; Lucas, M.; Claus, P. Production of Biomass-Derived Chemicals and Energy: Chemocatalytic Conversions of Glycerol. *Top. Catal.* **2009**, *52*, 278–287.

[216] Sels, B.; D'Hondt, E.; Jacobs, P. *Catalytic Transformation of Glycerol*. in: Centi, G., van Santen, R.A., Eds., *Catalysis for Renewables*; Wiley-VCH: Weinheim, 2007. pp. 223–255.

[217] Paglario, M.; Rossi, M. *The Future of Glycerol: New Uses of a Versatile Raw Material*; RSC Publishing: Cambrige, 2008.

[218] Kim, Y.; Jung, K.-D.; Park, E. A Comparative Study for Gas-Phase Dehydration of Glycerol over H-Zeolites. *Appl. Catal. A Gen.* **2011**, *393*(1–2), 275–287.

[219] Jia, C.-J.; Liu, Y.; Schmidt, W.; Lu, A.-H.; Schüth, F. Small-sized HZSM-5 Zeolite as Highly Active Catalyst for Gas Phase Dehydration of Glycerol to Acrolein. *J. Catal.* **2010**, *269*(1), 71–79.

[220] Corma, A.; Huber, G.W.; Sauvanaud, L.; O'Connor, P. Biomass to Chemicals: Catalytic Conversion of Glycerol Water Mixtures into Acrolein, Reaction Network. *J. Catal.* **2008**, *257*, 163–171.

[221] Yoda, E.; Ootawa, A. Dehydration of Glycerol on H-MFI Zeolite Investigated by FT-IR. *Appl. Catal. A Gen.* **2009**, *360*(1), 66–70.

[222] Chai, S.-H.; Wang, H.-P.; Liang, Y.; Xu, B.-Q. Sustainable Production of Acrolein: Investigation of Solid Acid-Base Catalysts for Gas-Phase Dehydration of Glycerol. *Green Chem.* **2007**, *9*(10), 1130–1136.

[223] Pathak, K.; Reddy, K.; Bakhshi, N.; Dalai, A. Catalytic Conversion of Glycerol to Value Added Liquid Products. *Appl. Catal. A Gen.* **2010**, *372*(2), 224–238.

[224] Hoang, T.; Zhu, X.; Danuthai, T.; Lobban, L.; Resasco, D.; Mallinson, R. Conversion of Glycerol to Alkyl-Aromatics over Zeolites. *Energ. Fuels* **2010**, *24*(7), 3804–3809.

[225] de Oliveira, A.S.; Vasconcelos, S.J.; de Sousa, J.R.; de Sousa, F.F.; Filho, J.M.; Oliveira, A.C. Catalytic Conversion of Glycerol to Acrolein over Modified Molecular Sieves: Activity and Deactivation Studies. *Chem. Eng. J.* **2011**, *168*(2), 765–774.

[226] Martin, A.; Richter, M. Oligomerization of Glycerol - A Critical Review. *Eur. J. Lipid Sci. Technol.* **2011**, *113*(1), 100–117.

[227] Ruiz, V.; Velty, A.; Santos, L.; Leyva-Pérez, A.; Sabater, M.; Iborra, S.; Corma, A. Gold Catalysts and Solid Catalysts for Biomass Transformations: Valorization

of Glycerol and Glycerol-Water Mixtures Through Formation of Cyclic Acetals. *J. Catal.* **2010**, *271*(2), 351–357.

[228] Ferreira, P.; Fonseca, I.; Ramos, A.; Vital, J.; Castanheiro, J. Esterification of Glycerol with Acetic Acid over Dodecamolybdophosphoric Acid Encaged in USY Zeolite. *Catal. Commun.* **2009**, *10*(5), 481–484.

[229] Klepáčová, K.; Mravec, D.; Bajus, M. Tert-Butylation of Glycerol Catalysed by Ion-Exchange Resins. *Appl. Catal. A Gen.* **2005**, *294*(2), 141–147.

[230] Klepáčová, K.; Mravec, D.; Kaszonyi, A.; Bajus, M. Etherification of Glycerol and Ethylene Glycol by Isobutylene. *Appl. Catal. A Gen.* **2007**, *328*(1), 1–13.

[231] Xiao, L.; Mao, J.; Zhou, J.; Guo, X.; Zhang, S. Enhanced Performance of HY Zeolites by Acid Wash for Glycerol Etherification with Isobutene. *Appl. Catal. A Gen.* **2011**, *393*(1–2), 88–95.

[232] Melero, J.; Vicente, G.; Morales, G.; Paniagua, M.; Moreno, J.; Roldán, R.; Ezquerro, A.; Pérez, C. Acid-Catalyzed Etherification of Bio-Glycerol and Isobutylene over Sulfonic Mesostructured Silicas. *Appl. Catal. A Gen.* **2008**, *346*(1–2), 44–51.

[233] Čejka, J.; Kotrla, J.; Krejčí, A. Disproportionation of Trimethyl Benzenes over Large Pore Zeolites: Catalytic and Adsorption Study. *Appl. Catal. A Gen.* **2004**, *277*(1–2), 191–199.

[234] Corma, A.; Fornés, V.; Martín-Aranda, R.; García, H.; Primo, J. Zeolites as Base Catalysts: Condensation of Aldehydes with Derivatives of Malonic Esters. *Appl. Catal.* **1990**, *59*(1), 237–248.

[235] Corma, A.; J. Climent, M.; Carcía, H.; Primo, J. Formation and Hydrolysis of Acetals Catalysed by Acid Faujasites. *Appl. Catal.* **1990**, *59*(1), 333–340.

[236] Climent, M.; Corma, A.; Garcia, H.; Primo, J. Zeolites as Catalysts in Organic Reactions: Condensation of Aldehydes with Benzene Derivatives. *J. Catal.* **1991**, *130*(1), 138–146.

[237] Joshi, M.; Narasimhan, C.; Mukesh, D. HZSM-5-catalyzed Shape-Selective Formation of Diacetates. *Zeolites* **1995**, *15*(7), 597–600.

[238] Kumar, P.; Hegde, V.; Kumar, T. An Efficient Synthesis of Diacetates from Aldehydes Using Beta Zeolite. *Tetrahedron Lett.* **1995**, *36*(4), 601–602.

[239] Climent, M.; Corma, A.; Iborra, S.; Navarro, M.; Primo, J. Use of Mesoporous MCM-41 Aluminosilicates as Catalysts in the Production of Fine Chemicals: Preparation of Dimethylacetals. *J. Catal.* **1996**, *161*(2), 783–789.

[240] Kulkarni, S.; Ramachandra Rao, R.; Subba Rao, Y.; Subrahmanyam, M.; Rama Rao, A. Synthesis of 3,5-lutidine from Propionaldehyde over Modified ZSM-5 Catalysts. *Appl. Catal. A Gen.* **1996**, *136*(1), L1–L6.

[241] Hölderich, W.; Röseler, J.; Heitmann, G.; Liebens, A. The Use of Zeolites in the Synthesis of Fine and Intermediate Chemicals. *Catal. Today* **1997**, *37*(4), 353–366.

[242] Hölderich, W. Environmentally Benign Manufacturing of Fine and Intermediate Chemicals. *Catal. Today* **2000**, *62*(1), 115–130.

[243] Rodriguez, I.; Climent, M.; Iborra, S.; Fornés, V.; Corma, A. Use of Delaminated Zeolites (ITQ-2) and Mesoporous Molecular Sieves in the Production of Fine Chemicals: Preparation of Dimethylacetals and Tetrahydropyranylation of Alcohols and Phenols. *J. Catal.* **2000**, *192*(2), 441–447.

[244] Ballini, R.; Bigi, F.; Gogni, E.; Maggi, R.; Sartori, G. Zeolite as Base Catalyst: Nitroaldolic Condensation. *J. Catal.* **2000**, *191*(2), 348–353.

[245] Ono, Y. Solid Base Catalysts for the Synthesis of Fine Chemicals. *J. Catal.* **2003**, *216*(1–2), 406–415.

[246] Gayubo, A.; Aguayo, A.; Atutxa, A.; Valle, B.; Bilbao, J. Undesired Components in the Transformation of Biomass Pyrolysis Oil into Hydrocarbons on an HZSM-5 Zeolite Catalyst. *J. Chem. Technol. Biotechnol.* **2005**, *80*(11), 1244–1251.

[247] Ranjan, R.; Thust, S.; Gounaris, C.; Woo, M.; Floudas, C.; Keitz, M.; Valentas, K.; Wei, J.; Tsapatsis, M. Adsorption of Fermentation Inhibitors from Lignocellulosic Biomass Hydrolyzates for Improved Ethanol Yield and Value-Added Product Recovery. *Micropor. Mesopor. Mat.* **2009**, *122*(1–3), 143–148.

[248] Kubelková, L.; Čejka, J.; Nováková, J. Surface Reactivity of ZSM-5 Zeolites in Interaction with Ketones at Ambient Temperature (a FT-IR Study). *Zeolites* **1991**, *11*(1), 48–53.

[249] Tago, T.; Konno, H.; Ikeda, S.; Yamazaki, S.; Ninomiya, W.; Nakasaka, Y.; Masuda, T. Selective Production of Isobutylene from Acetone over Alkali Metal Ion-Exchanged BEA Zeolites. *Catal. Today* **2011**, *164*(1), 158–162.

[250] Tago, T.; Konno, H.; Sakamoto, M.; Nakasaka, Y.; Masuda, T. Selective Synthesis for Light Olefins from Acetone over ZSM-5 Zeolites with Nano- and Macro-Crystal Sizes. *Appl. Catal. A Gen.* **2011**, *403*(1–2), 183–191.

[251] Perez-Mayoral, E.; Martin-Aranda, R.M.; Lopez-Peinado, A.J.; Ballesteros, P.; Zukal, A.; Čejka, J. Green Synthesis of Acetals/Ketals: Efficient Solvent-Free Process for the Carbonyl/Hydroxyl Group Protection Catalyzed by SBA-15 Materials. *Top. Catal.* **2009**, *52*(1–2), 148–152.

[252] Chheda, J.; Dumesic, J. An Overview of Dehydration, Aldol-Condensation and Hydrogenation Processes for Production of Liquid Alkanes from Biomass-Derived Carbohydrates. *Catal. Today* **2007**, *123*(1–4), 59–70.

[253] Gangadharan, A.; Shen, M.; Sooknoi, T.; Resasco, D.; Mallinson, R. Condensation Reactions of Propanal over $Ce_xZr_{1-x}O_2$ Mixed Oxide Catalysts. *Appl. Catal. A Gen.* **2010**, *385*(1–2), 80–91.

[254] Faba, L.; Díaz, E.; Ordóñez, S. Performance of Bifunctional Pd/Mx Ny O (M = Mg, Ca; N = Zr, Al) Catalysts For Aldolization-Hydrogenation of Furfural-Acetone Mixtures. *Catal. Today* **2011**, *164*(1), 451–456.

[255] Liu, H.; Xu, W.; Liu, X.; Guo, Y.; Guo, Y.; Lu, G.; Wang, Y. Aldol Condensation of Furfural and Acetone on Layered Double Hydroxides. *Kinet. Catal.* **2010**, *51*(1), 75–80.

[256] Ordóñez, S.; Díaz, E.; León, M.; Faba, L. Hydrotalcite-Derived Mixed Oxides as Catalysts for Different C-C Bond Formation Reactions from Bioorganic Materials. *Catal. Today* **2011**, *167*(1), 71–76.

[257] Rode, E.; Gee, P.; Marquez, L.; Uemura, T.; Bazargani, M. Aldol Condensation of Butanal over Alkali Metal Zeolites. *Catal. Lett* **1991**, *9*, 103–114.

[258] Wierzchowski, P.; Zatorski, L. Aldol Condensation in Gaseous Phase by Zeolite Catalysts. *Catal. Lett.* **1991**, *9*(5–6), 411–414.

[259] Dumitriu, E.; Hulea, V.; Bilba, N.; Carja, G.; Azzouz, A. Synthesis of Acrolein by Vapor Phase Condensation of Formaldehyde and Acetaldehyde over Oxides Loaded Zeolites. *J. Mol. Catal.* **1993**, 79(1–3), 175–185.

[260] Dumitriu, E.; Hulea, V.; Fechete, I.; Auroux, A.; Lacaze, J.-F.; Guimon, C. The Aldol Condensation of Lower Aldehydes over MFI Zeolites with Different Acidic Properties. *Micropor. Mesopor. Mat.* **2001**, *43*(3), 341–359.

[261] Ungureanu, A.; Royer, S.; Hoang, T.; Trong On, D.; Dumitriu, E.; Kaliaguine, S. Aldol Condensation of Aldehydes over Semicrystalline Zeolitic-Mesoporous UL-ZSM-5. *Micropor. Mesopor. Mat.* **2005**, *84*(1–3), 283–296.

[262] Cobzaru, C.; Oprea, S.; Dumitriu, E.; Hulea, V. Gas Phase Aldol Condensation of Lower Aldehydes over Clinoptilolite Rich Natural Zeolites. *Appl. Catal. A Gen.* **2008**, *351*(2), 253–258.

[263] Shen, W.; Tompsett, G.; Hammond, K.; Xing, R.; Dogan, F.; Grey, C.; Jr., W.C.; Auerbach, S.; Huber, G. Liquid Phase Aldol Condensation Reactions with MgO-ZrO2 and Shape-Selective Nitrogen-Substituted NaY. *Appl. Catal. A Gen.* **2011**, *392*(1–2), 57–68.

[264] Diaz C.D.C.; Locatelli, S.; Gonzo, E.E. Acetaldehyde Adsorption on HZSM-5 Studied by Infrared Spectroscopy. *Zeolites* **1992**, *12*(7), 851–857.

[265] Chatterjee, M.; Matsushima, K.; Ikushima, Y.; Sato, M.; Yokoyama, T.; Kawanami, H.; Suzuki, T. Production of Linear Alkane via Hydrogenative Ring Opening of a Furfural-Derived Compound in Supercritical Carbon Dioxide. *Green Chem.* **2010**, *12*(5), 779–782.

[266] Swift, K.A.D. Catalytic Transformations of the Major Terpene Feedstocks. *Top. Catal.* **2004**, *27*(1–4), 143–155.

[267] Ravasio, N.; Zaccheria, F.; Guidotti, M.; Psaro, R. Mono- and Bifunctional Heterogeneous Catalytic Transformation of Terpenes and Terpenoids. *Top. Catal.* **2004**, *27*(1–4), 157–168.

[268] Monteiro, J.L.F.; Veloso, C.O. Catalytic Conversion of Terpenes into Fine Chemicals. *Top. Catal.* **2004**, *27*(1–4), 169–180.

[269] Dimitrova, R.; Gündüz, G.; Spassova, M. A Comparative Study on the Structural and Catalytic Properties of Zeolites Type ZSM-5, Mordenite, Beta and MCM-41. *J. Mol. Catal. A Chem.* **2006**, *243*(1), 17–23.

[270] Rachwalik, R.; Olejniczak, Z.; Jiao, J.; Huang, J.; Hunger, M.; Sulikowski, B. Isomerization of Alfa-Pinene over Dealuminated Ferrierite-Type Zeolites. *J. Catal.* **2007**, *252*(2), 161–170.

[271] Wang, J.; Hua, W.; Yue, Y.; Gao, Z. MSU-S Mesoporous Materials: An Efficient Catalyst for Isomerization of Alfa-Pinene. *Bioresour. Technol.* **2010**, *101*(19), 7224–7230.

[272] Roberge, D.; Buhl, D.; Niederer, J.; Hölderich, W. Catalytic Aspects in the Transformation of Pinenes to p-cymene. *Appl. Catal. A Gen.* **2001**, *215*(1–2), 111–124.

[273] Hensen, K.; Mahaim, C.; Hölderich, W. Alkoxylation of Limonene and Alpha-Pinene over Beta Zeolite as Heterogeneous Catalyst. *Appl. Catal. A Gen.* **1997**, *149*(2), 311–329.

[274] Kunkeler, P.; Van der Waal, J.; Bremmer, J.; Zuurdeeg, B.; Downing, R.; Van Bekkum, H. Application of Zeolite Titanium Beta in the Rearrangement of Alfa-Pinene Oxide to Campholenic Aldehyde. *Catal. Lett.* **1998**, *53*(3–4), 135–138.

[275] Schuster, C.; Hölderich, W. Modification of Faujasites to Generate Novel Hosts for 'Ship-in-a-Bottle' Complexes. *Catal. Today* **2000**, *60*(3), 193–207.

[276] Casuscelli, S.; Eimer, G.; Canepa, A.; Heredia, A.; Poncio, C.; Crivello, M.; Perez, C.; Aguilar, A.; Herrero, E. Ti-MCM-41 as Catalyst for Alfa-Pinene Oxidation. Study of the Effect of Ti Content and H_2O_2 Addition on Activity and Selectivity. *Catal. Today* **2008**, *133–135*(1–4), 678–683.

[277] Alaerts, L.; Séguin, E.; Poelman, H.; Thibault-Starzyk, F.; Jacobs, P.A.; De Vos, D. Probing the Lewis Acidity and Catalytic Activity of the Metal-Organic Framework ($Cu_3(BTC)_2$) (BTC = Benzene-1,3,5-tricarboxylate). *Chem. Eur. J.* **2006**, *12*(28), 7353–7363.

[278] López, C.M.; Machado, F.J.; Rodríguez, K.; Méndez, B.; Hasegawa, M.; Pekerar, S. Selective Liquid-Phase Transformation of α-pinene over Dealuminated Mordenites and Y-Zeolites. *Appl. Catal. A Gen.* **1998**, *173*, 75–85.

[279] Mokrzycki, L.; Sulikowski, B.; Olejniczak, Z. Properties of Desilicated ZSM-5, ZSM-12, MCM-22 and ZSM-12/MCM-41 Derivatives in Isomerization of Alfa-Pinene. *Catal. Lett.* **2009**, *127*(3–4), 296–303.

[280] Groen, J.; Zhu, W.; Brouwer, S.; Huynink, S.; Kapteijn, F.; Moulijn, J.; Pérez-Ramírez, J. Direct Demonstration of Enhanced Diffusion in Mesoporous ZSM-5 Zeolite Obtained via Controlled Desilication. *J. Amer. Chem. Soc.* **2007**, *129*(2), 355–360.

[281] Gündüz, G.; Dimitrova, R.; Yilmaz, S.; Dimitrov, L. Liquid Phase Transformation of Alfa-Pinene over Beta Zeolites Containing Aluminium or Boron, Titanium and Vanadium as Lattice Ions. *Appl. Catal. A Gen.* **2005**, *282*(1–2), 61–65.

[282] Weyrich, R.A.; Hölderich, W.F. Dehydrogenation of α-limonene over Ce Promoted, Zeolite Supported Pd Catalysts. *Appl. Catal. A Gen.* **1997**, *158*, 145–162.

[283] Trong On, D.; Kapoor, M.P.; Joshi, P.N.; Bonneviot, L.; Kaliaguine, S. Catalytic Epoxidation of α-pinene over Bifunctional Mesoporous Molecular Sieves. *Catal. Lett.* **1997**, *44*, 171–176.

[284] van der Waal, J.C.; Rigutto, M.S.; van Bekkum, H. Zeolite Titanium Beta as a Selective Catalyst in the Epoxidation of Bulky Alkenes. *Appl. Catal. A Gen.* **1998**, *167*, 331–342.

[285] Suh, Y.-W.; Kim, N.-K.; Ahn, W.-S. Rhee, H.-K. Redox-Mesoporous Molecular Sieve as a Bifunctional Catalyst for the One-Pot Synthesis of Campholenic Aldehyde from α-pinene. *J. Mol. Catal. A Chem.* **2001**,*174*, 249–254.

[286] Suh, Y.-W.; Kim, N.-K.; Ahn, W.-S. Rhee, H.-K. One-Pot Synthesis of Campholenic Aldehyde from α-pinene over Ti-HMS Catalyst II: Effects of Reaction Conditions. *J. Mol. Catal. A Chem.* **2003**, *198*, 309–316.

[287] Botella, P.; Corma, A.; Nieto, J.; Valencia, S.; Lucas, M.; Sergio, M. Selective Hydration of Dihydromyrcene to Dihydromyrcenol over H-Beta Zeolite. Influence of the Microstructural Properties and Process Variables. *Appl. Catal. A Gen.* **2000**, *203*(2), 251–258.

[288] Bek, D.; Balcar, H.; Žilková, N.; Zukal, A.; Horáček, M.; Čejka, J. Grubbs Catalysts Immobilized on Mesoporous Molecular Sieves via Phosphine and Pyridine Linkers. *ACS Catal* **2011**, *1*(7), 709–718.

[289] Čejka, J.; Corma, A; Zones, S. Eds., *Zeolites and Catalysis: Synthesis, Reactions and Applications*; Wiley-VCH: Weinheim, 2010.

[290] Sun, J.; Bonneau, C.; Cantín, Á.; Corma, A.; Díaz-Cabanas, M.; Moliner, M.; Zhang, D.; Li, M.; Zou, X. The ITQ-37 Mesoporous Chiral Zeolite. *Nature* **2009**, *458*(7242), 1154–1157.

[291] Shvets, O.; Kasian, N.; Zukal, A.; Pinkas, J.; Čejka, J. The Role of Template Structure and Synergism between Inorganic and Organic Structure Directing Agents in the Synthesis of Utl Zeolite. *Chem. Mater.* **2010**, *22*(11), 3482–3495.

[292] Shvets, O.; Shamzhy, M.; Yaremov, P.; Musilová, Z.; Procházková, D.; Čejka, J. Isomorphous Introduction of Boron in Germanosilicate Zeolites with UTL Topology. *Chem. Mater*. **2011**, *23*(10), 2573–2585.

[293] Corma, A.; Fornes, V.; Pergher, S.; Maesen, T.; Buglass, J. Delaminated Zeolite Precursors as Selective Acidic Catalysts. *Nature* **1998**, *396*(6709), 353–356.

[294] Choi, M.; Na, K.; Kim, J.; Sakamoto, Y.; Terasaki, O.; Ryoo, R. Stable Single-Unit-Cell Nanosheets of Zeolite MFI as Active and Long-Lived Catalysts. *Nature* **2009**, *461*(7261), 246–249.

[295] Na, K.; Chol, M.; Park, W.; Sakamoto, Y.; Terasakl, O.; Ryoo, R. Pillared MFI Zeolite Nanosheets of a Single-Unit-Cell Thickness. *J. Amer. Chem. Soc.* **2010**, *132*(12), 4169–4177.

[296] Perez-Ramirez, J.; Christensen, C.H.; Egeblad, K.; Christensen, C.H.; Groen, J. Hierarchical Zeolites: Enhanced Utilisation of Microporous Crystals in Catalysis by Advances in Materials Design. *Chem. Soc. Rev.* **2008**, *37*(11), 2530–2542.

[297] Peréz-Ramirez, J.; Verboekend, D.; Bonilla, A.; Abelló, S. Zeolite Catalysts with Tunable Hierarchy Factor by Pore-Growth Moderators. *Adv. Funct. Mater.* **2009**, *19*(24), 3972–3979.

[298] Musilová-Pavlačková, Z.; Zones, S.; Čejka, J. Post-Synthesis Modification of SSZ-35 Zeolite to Enhance the Selectivity in p-xylene Alkylation with Isopropyl Alcohol. *Top. Catal.* **2010**, *53*(3–4), 273–282.

[299] Kresge, C.T.; Leonowicz, M.E.; Roth, W.J.; Vartuli, J.C.; Beck, J. Ordered Mesoporous Molecular Sieves Synthesized by a Liquid-Crystal Template Mechanism. *Nature* **1992**, *359*(6397), 710–712.

[300] Corma, A. From Microporous to Mesoporous Molecular Sieve Materials and Their Use in Catalysis. *Chem. Rev.* **1997**, *97*(6), 2373–2419.

[301] Žilková, N.; Zukal, A.; Čejka, J. Synthesis of Organized Mesoporous Alumina Templated with Ionic Liquids. *Micropor. Mesopor. Mat.* **2006**, *95*(1–3), 176–179.

[302] Schüth, F. Engineered Porous Catalytic Materials. *Ann. Rev. Mater. Res*. **2005**, *35*, 209–238.

[303] Martín-Aranda, R.M.; Čejka, J. Recent Advances in Catalysis over Mesoporous Molecular Sieves. *Top. Catal.* **2010**, *53*(3–4), 141–153.

[304] Cruz, J.M.; Corma A.; Fornes, A. Framework and Extra-Framework Aluminum Distribution in (NH4)2F6Si-dealuminated Y-zeolites – Relevance to Cracking Catalysts. *Appl. Catal.* **1989**, *50*(3), 287–293.

[305] Corma, A.; Martinez, A.; Martinez, C. The Role of Extra Framework Aluminum Species in USY Catalysts during Isobutane/2-Butene Alkylation. *Appl. Catal. A Gen.* **1996**, *134*(1), 169–182.

[306] Leonowicz, M.; Lawton, J.; Lawton, S.; Rubin, M. MCM-22: A Molecular Sieve with Two Independent Multidimensional Channel Systems. *Science* **1994**, *264*(5167), 1910–1913.

[307] Roth, W.; Kresge, C.; Vartuli, J.; Leonowicz, M.; Fung, A.; McCullen, S. MCM-36: The First Pillared Molecular Sieve with Zeolite Properties. *Stud. Surf. Sci. Catal.* **1995**, *94*(C), 301–308.

[308] Zukal, A.; Dominguez, I.; Mayerová, J.; Čejka, J. Functionalization of Delaminated Zeolite ITQ-6 for the Adsorption of Carbon Dioxide. *Langmuir* **2009**, *25*(17), 10314–10321.

[309] Schreyeck, L.; Caullet, P.; Mougenel, J.-C.; Guth, J.-L.; Marler, B. A Layered Microporous Aluminosilicate Precursor of FER-type Zeolite. *J. Chem. Soc. Chem. Commun.* **1995**, (21), 2187–2188.

[310] Na, K.; Jo, C.; Kim, J.; Cho, K.; Jung, J.; Seo, Y.; Messinger, R.; Chmelka, B.; Ryoo, R. Directing Zeolite Structures into Hierarchically Nanoporous Architectures. *Science* **2011**, *333*(6040), 328–332.

[311] Kim J.; Park, W.; Ryoo, R. Surfactant-Directed Zeolite Nanosheets: A High-Performance Catalyst for Gas-Phase Beckmann Rearrangement. *ACS Catal* **2011**, *1*(4), 337–341.

[312] Schreyeck, L.; Caullet, P.; Mougenel, J.C.; Guth, J.L.; Marler, B. PREFER: A New Layered (Alumino) Silicate Precursor of FER-type Zeolite. *Microporous Mesoporous Mater*. **1996**, *6*, 259–271.

[313] Jacobsen, C.; Madsen, C.; Houzvicka, J.; Schmidt, I.; Carlsson, A. Mesoporous Zeolite Single Crystals. *J. Amer. Chem. Soc.* **2000**, *122*(29), 7116–7117.

[314] Janssen A.; Schmidt, I.; Jacobsen, C.; Koster, A.; de Jong, K. Exploratory Study of Mesopore Templating with Carbon during Zeolite Synthesis. *Micropor. Mesopor. Mater.* **2003**, *65*(1), 59–75.

[315] van Miltenburg, A.; Pawlesa, J.; Bouzga, A.M.; Žilková, N.; Čejka, J.; Stoecker, M. Alkaline Modification of MCM-22 to a 3D Interconnected Pore System and its Application in Toluene Disproportionation and Alkylation. *Top. Catal.* **2009**, *52*(9), 1190–1202.

[316] Verboekend, D.; Groen, J.C.; Pérez-Ramírez, J. Interplay of Properties and Functions upon Introduction of Mesoporosity in ITQ-4 Zeolite. *Adv. Funct. Mater.* **2010**, *20*(9), 1441–1450.

[317] Koo, J.-B.; Jiang, N.; Saravanamurugan, S.; Bejblová, M.; Musilová, Z.; Čejka, J.; Park, S.-E. Direct Synthesis of Carbon-Templating Mesoporous ZSM-5 Using Microwave Heating. *J. Catal.* **2010**, *276*(2), 327–334.

[318] Beck, J.S.; Vartuli, J.C.; Roth, W.J.; Leonowicz, M.E.; Kresge, C.T.; Schmitt, K.D.; Chu, C.T.-W.; Olson, D.H.; Sheppard, E.W.; McCullen, S.B.; Higgins, J.B.; Schlenker, J. A New Family of Mesoporous Molecular Sieves Prepared with Liquid Crystal Templates. *J. Amer. Chem. Soc*. **1992**, *114*(27), 10834–10843.

[319] Zhao, D.; Huo, Q.; Feng, J.; Chmelka, B.; Stucky, G. Nonionic Triblock and Star Diblock Copolymer and Oligomeric Sufactant Syntheses of Highly Ordered, Hydrothermally Stable, Mesoporous Silica Structures. *J. Amer. Chem. Soc.* **1998**, *120*(24), 6024–6036.

[320] Miyahara, M.; Vinu, A.; Ariga, K. Adsorption Myoglobin over Mesoporous Silica Molecular Sieves: Pore Size Effect and Pore-Filling Model. *Mater. Sci. Eng. C* **2007**, *27*(2), 232–236. .

[321] Sawant, D.; Balasubramanian, V.; Justus, J.; Halligudi, S.; Bose, A.; Ariga, K.; Mori, T.; Vinu, A. Novel Highly Acidic Nanoporous Cage Type Materials and Their Catalysis. *Top. Catal.* **2009**, *52*(1–2), 111–118.

[322] Kim, T.-W.; Kleitz, F.; Paul, B.; Ryoo, R. MCM-48-like Large Mesoporous Silicas with Tailored Pore Structure: Facile Synthesis Domain in a Ternary Triblock Copolymer-Butanol-Water System. *J. Amer. Chem. Soc.* **2005**, *127*(20), 7601–7610.

[323] Cao L.; Man, T.; Kruk, M. Synthesis of Ultra-Large-Pore SBA-15 Silica with Two-Dimensional Hexagonal Structure Using Triisopropylbenzene as Micelle Expander. *Chem. Mater.* **2009**, *21*(6), 1144–1153.

[324] Kloestra K.; Van Bekkum, H.; Jansen, J. Mesoporous Material Containing Framework Tectosilicate by Pore-Wall Recrystallization. *Chem. Commun.* **1997**, (23), 2281–2282.

[325] Liu Y.; Zhang, W.; Pinnavaia, T. Steam-Stable MSU-S Aluminosilicate Mesostructures Assembled from Zeolite ZSM-5 and Zeolite Beta Seeds. *Angew. Chem. Int. Ed.* **2001**, *40*(7), 1255–1258.

[326] Prokešová P.; Mintova, S.; Čejka, J.; Bein, T. Preparation of Nanosized Micro/Mesoporous Composites. *Mater. Sci. Eng. C* **2003**, *23*(6–8), 1001–1005.

Catalysis Today 243 (2015) 10–22

Contents lists available at ScienceDirect

Catalysis Today

journal homepage: www.elsevier.com/locate/cattod

Review

Opportunities for zeolites in biomass upgrading—Lessons from the refining and petrochemical industry

David Kubička*, Oleg Kikhtyanin

Research Institute of Inorganic Chemistry, UniCRE-RENTECH, Areál Chempark Záluží, 436 70 Litvínov, Czech Republic

ARTICLE INFO

Article history:
Received 22 June 2014
Received in revised form 22 July 2014
Accepted 24 July 2014
Available online 23 September 2014

Keywords:
Zeolites
Molecular sieves
Biomass
Triglycerides
Sugars
Cracking
Isomerization
Aldol condensation.

ABSTRACT

New technologies ensuring the production of valuable products from renewable raw materials would greatly benefit our society by satisfying the ever-growing needs while reducing environmentally harmful waste and emissions. The present paper reviews the possibilities of microporous and mesoporous materials as catalysts in conversion of biomass-derived raw materials. Proven industrial applications from the refining and petrochemical sector are used as the basis for discussing the potential of new renewable-raw-materials-based processes. The examples of different studies on the applicability of zeolites as catalysts in processes requiring splitting or formation of carbon–carbon bond, isomerization, deoxygenation (including dehydration), etc. are given. The perspectives of the application of zeolites for the valorization of biomass are evaluated and several challenges are generalized, aiming at a better understanding of the relationship between physical and chemical properties of microporous materials and their behavior in the transformation of biomass-derived feedstocks.

Contents

1. Introduction

Zeolites possess an array of unique properties that turned them into a crucial class of industrial adsorbents and heterogeneous catalysts [1,2]. Apart from their widespread use in various adsorption and separation applications, such as desiccants [3], air separation [4] or separation of iso-paraffins from *n*-paraffins [5], they revolutionized the refining and petrochemical industry by enhancing significantly the raw material efficiency and increasing dramatically the environmental acceptability of these large-scale industrial processes.

The industrial success of zeolites has inspired intensive investigations leading to discovery of new structures and to better understanding of their functionalities and the relations between synthesis and zeolite properties [6–8], on the one hand, and between zeolite properties and their catalytic performance, on the other hand. As a result, more than 200 structures have been described up to date and new synthesis strategies have been demonstrated, including 2D zeolites, hierarchical zeolites to name a few [9–12], expanding the zeolite base to an unprecedented

---

[*] Corresponding author. Tel.: +420 476163735; fax: +420 475 212 079.
E-mail address: david.kubicka@vuanch.cz (D. Kubička).

http://dx.doi.org/10.1016/j.cattod.2014.07.043

magnitude [13,14]. Despite the enormous effort, the number of industrially applied zeolites remains limited to a handful of structures [15,16].

The first milestone, i.e. development of the fluid catalytic cracking (FCC) process relying on the use of zeolites to convert extensively the atmospheric crude oil distillation residue to automotive fuel components, contributed to and at that time unimaginable growth in transport that continues to current days. It was followed by severe negative impact of the expanding industrial activities on the environment and thus life quality on the Earth. The increased public awareness resulted in strong demand for environmentally friendly processes, the second milestone, and zeolites made it possible by replacing homogeneous catalysts used for alkylation reactions and increasing the raw material efficiency, improving the product quality and facilitating separation processes.

In the recent years, the issue of the vast dependence on fossil resources including their sustainability and the related carbon dioxide emissions has become the focal concern of our time. As biomass is the only renewable source of carbon (apart from CO_2), its sustainable utilization is crucial for addressing the current challenge of replacing to the maximum possible extent the fossil resources used by the chemical industry by renewable ones. While in the energy sector and to a limited extent also in the transportation sector renewable electricity sources, e.g. solar or wind energy, can be employed, most of the chemical industry and transportation fuels production have to rely on biomass utilization. Taking into account the historical developments in petroleum processing, it can be anticipated that zeolites, or more generally molecular sieves, have the potential to play "the game-changing role" once again [17].

The goal of this paper is to identify the opportunities and challenges for application of zeolites in transformation of biomass and biomass-derived feedstocks. Due to the vast possibilities and many review papers as well as a high number of particular studies devoted to biomass transformations, we have decided to approach the topic from a yet different perspective. The paper will discuss at first briefly the key properties of zeolites that made their widespread use possible and connect them to particular examples of industrial processes. Once the link between properties of zeolites and industrial processes is established, relevant case studies will be described/analyzed focusing on the analogy between the petrochemical processes and possible biomass transformation routes. The case studies will reflect the applicability of zeolites to processes requiring carbon–carbon bond splitting, formation or rearrangement, i.e. cracking, alkylation or skeletal isomerization, respectively, as well as to processes relying on functionalization or defunctionalization that include, for instance, oxidation, esterification or deoxygenation (including dehydration), respectively. Finally, the particular opportunities and challenges will be generalized to provide a broader perspective of the application of zeolites for valorization of biomass and its possible impact on the chemical industry.

2. Key properties of zeolites and molecular sieves

The vast variety of synthesis routes and post-synthesis modifications applicable to zeolites and molecular sieves, in general, is the key to creation of catalytic materials with an enormous variety in their properties encompassing structural, textural, chemical and acido-basic properties. The possibility to tune up zeolite properties so that they match the needs of the chemical transformations is at the heart of their industrial success.

Zeolites can be described as microporous crystalline aluminosilicates. The zeolite structure consists of interconnected SiO_4 and $[AlO_4]^-$ tetrahedra (the central atom of a tetrahedron is called a T-atom). The immense number of the tetrahedra connections leading to formation of (i) pores having different dimensions (e.g. 8-, 10- or 12-ring channels, i.e. having 8, 10 or 12 T-atoms in the ring defining the pore), (ii) intersecting pores and thus 1D, 2D or 3D pore architecture and (iii) cavities is the origin of the wide variety of structures (>200) known today. The synthesis of a particular structure is determined by the specific synthesis conditions (synthesis gel composition, pH, temperature, etc.) and, in some cases, the use of structure directing agents. The stability of the zeolite crystalline structures limits the size (diameter) of the zeolite channels (pores) to less than 1 nm (14-ring channels). As a consequence of their ordered microporous structure, zeolites have relatively large specific surface areas, typically in the range 300–800 m^2/g. It follows that they can accommodate large number of molecules on their surface provided these molecules can penetrate the zeolite porous structure. Moreover, the basic structural characteristics of zeolites provide them with two salient features—shape selectivity and acidity—that widely determine their practical application.

The commeasurable size of the zeolite channels and raw materials, reaction intermediates and/or products is the origin of shape selectivity of zeolites. There are commonly distinguished three basic scenarios—(i) smaller reactants can reach the active sites inside zeolites pores and be transformed while the larger ones cannot (reactant shape selectivity), (ii) smaller products can be formed and diffuse out of the pores while the larger ones are either not formed or diffuse very slowly and are converted before they can leave the pores (product shape selectivity) and (iii) due to the sterical restrictions inside zeolite pores some transition states can be formed while others cannot and thus only the former products can be produced (transition-state shape selectivity). The size of biomass related feedstocks will often be of the same order of magnitude as the size of zeolite channels and thus it has to be anticipated that shape selectivity and diffusion will play an important role.

The difference in valence of the T atoms—silicon is tetravalent while aluminum only trivalent—introduces a negative charge to the zeolite framework that needs to be compensated by a cation. The cation is exchangeable, i.e. this is the origin of the ion-exchange properties of zeolites that makes it possible to introduce various functionalities to the framework. Alkali metals provide the zeolite with basic properties, while their replacement with protons introduces Brønsted acidity to zeolites. Moreover, the ion exchange can be used to introduce metal cations (e.g. Cu or Pt) that after reduction will afford a bifunctional catalyst possessing an acidic function (the proton) and a hydrogenation component (the metal). Obviously, the acido-basic character of zeolites is closely related to their chemical composition, i.e. the more framework Al atoms the higher concentration of Brønsted acid sites. Traditionally, zeolites can be depending on their structure synthesized in a wide range of Si/Al ratios, i.e. in a wide range of concentration of acid sites. It has also to be noted that not all aluminum atoms are typically incorporated in the zeolite structures and the so-called extra-framework aluminum (EFAL) species are present that introduce Lewis acidity in zeolites.

Unlike mineral acids that have well-defined uniform acidity, the strength of the acid sites in zeolites is determined by the local environment in zeolites, i.e. on the type of T atom, its concentration, local geometry (e.g. Si—O—T angle) and the distribution of the T atom in the framework [18,19]. For instance, the strength of Brønsted acid sites is the highest when the next nearest T atoms to the Al T-atom are Si atoms [20]. The presence of EFAL in the vicinity of Brønsted acid sites also affects the strength of these sites [21]. Besides the adjustment of Si/Al ratio during the synthesis, various post-synthesis treatments, particularly dealumination by steaming or acid leaching, are often used to either adjust the Si/Al ratio outside the range attainable by direct synthesis or to remove EFAL to improve the accessibility of active sites in the pores [22–26]. Moreover, dealumination or desilication treatments are also applied to create mesoporosity in zeolite crystal and thus enhance mass transfer [27–29]. The acidity can be also varied by using another T-atom instead of Al. Consequently, catalysts (i) having reduced acid sites strengths (e.g. boro- or gallosilicates, silicoaluminophosphates), (ii) containing exclusively Lewis acid sites (e.g. stannosilicates) or (iii) being neutral/non-acidic (silicates or germano- and titanosilicates) can be synthesized [30–33].

The accessibility of active (acid) sites is due to the rather bulky nature of many biomass-derived feedstocks, such as triglycerides, disaccharides, etc., together with their relatively high reactivity in comparison with petroleum-derived feedstocks, a key challenge for biomass transformations. Thus, new strategies are being intensively sought. Among them two are of particular interest—hierarchical (micro/mesoporous) materials and delaminated (2D) zeolites [34–39]. In both cases, the strategy relies on maintaining the acid sites of the original zeolite, however in the former case the zeolite structure is incorporated in a mesoporous one decreasing thus the diffusion lengths in the zeolite while in the latter case the external surface containing the acid sites is maximized maximizing thus the accessibility of the active sites.

A specific characteristic of zeolites important for biomass-related conversions is the hydrophobicity/hydrophilicity of zeolite surface that may affect some of the biomass transformation routes due to inhibition/competing adsorption effects [40–42].

The zeolite properties, as listed here, can be affected strongly by the reaction media. Apart from coking, the effect of steam or hot liquid water on zeolites and their properties is a key factor which has to be taken into account when considering biomass transformations as these can take place in aqueous media. The interaction of zeolite catalysts with hot aqueous medium occurs also in different refining and petrochemical processes, such as oxidative regeneration of zeolites where catalysts are exposed to water vapors formed as a result of the burning of carbonaceous deposits. In the presence of steam, a ratio between intra-framework (InAl) and extra-framework (ExAl) Al atoms, i.e. between Brønsted and Lewis acid sites can change [43]. In its turn, the presence of ExAl species leads to improved hydrothermal stability of zeolite, increased Lewis acidity and thus changes in catalytic activity, etc. Examples of petrochemical processes with water as one of the reaction products include methanol-to-olefins, methanol-to-gasoline as well as the upgrading of products obtained during Fischer–Tropsch synthesis. The hydrothermal stability of zeolites is of particular importance when changing from fossil feedstocks (with zero-to-low water content) to non-petroleum, biomass-derived feedstocks (with low-to-medium-to-high water content). However, in contrast to the considerable number of publications on hydrothermal stability in the presence of steam, the number of studies dealing with the behavior of zeolites in hot liquid water is limited [43–46].

Ravenelle et al. [43] studied the stability of zeolites in hot liquid water and found that ZSM-5 was stable up to 200 °C independent of its Si/Al ratio, whereas various zeolite Y samples were degraded to a level that depended on their Si/Al ratio. It was stated that the degradation of Y zeolites by condensed water mostly occurs through hydrolysis of Si—O—Si bonds rather than dealumination, which is the dominant degradation pathway under steaming conditions. Hydrolysis leads to the formation of an amorphous material, and this process tends to increase with increasing Si/Al ratio, thus being the opposite of the stability of zeolites against steaming. Lutz et al. [45] investigated the treatment of various zeolites with liquid water up to $T = 240\,^{\circ}$C and showed that MFI and MOR materials were relatively stable under such treatment, while FAU and BEA underwent strong decomposition. These examples prove the existence of a problem in maintaining the properties of zeolites in hot aqueous medium which should be considered when developing new processes using water-rich feedstocks.

A way to solve this problem was proposed by Resasco et al. [46] who were using hydrophobic zeolites as catalysts for reactions in hot aqueous media. The hydrophobic barrier necessary to prevent the contact of the zeolite with the liquid water was formed by silylation of the zeolite with organosilanes. The hydrophobicity increased without significantly reducing the density of acid sites. As a result, while at 200 °C the crystalline structure of an untreated HY zeolite collapses after a few hours of contact with aqueous medium, the functionalized hydrophobic zeolites kept their structure practically unaltered. Another approach to improving the hydrothermal stability of zeolites has been proposed in [44]. In this work, the layer which protects zeolite against water under hydrothermal conditions was generated by 'alkaline' or 'acid' alumination with sodium aluminosilicate or hydroxo-oxo-aluminum cations, correspondingly. The formed surface layer blocked the terminal OH groups and the energy-rich Si—O—Si bonds on the crystal surface, where the water molecules attack the zeolite framework. It may be assumed that the development of new processes based on the use of water-rich feedstocks, including those derived from biomass, would give additional impulse to studies aiming to improve hydrothermal stability of zeolite catalysts.

The in-situ change of the zeolite properties, e.g. due to aqueous media, has to be taken into account when determining and interpreting the physicochemical properties of zeolites. For instance, Lewis acid sites can be formed due to dehydration of Brønsted acid sites. Consequently, the ratio between those two types of acid sites may be different under working catalyst conditions from that determined by FTIR of adsorbed pyridine which is preceded by high-temperature pretreatment (favoring surface dehydration).

3. Case studies

It is obvious that zeolites and molecular sieves, in general, offer an array of useful properties that can be adjusted to particular needs of a wide range of chemical reactions. The tunable acidic properties together with controllable porosity (including shape selectivity) made zeolites the catalyst of choice for carbon–carbon bond rearrangements. The key applications are catalytic cracking and hydrocracking that allow reducing the molecular weight of heavy petroleum fractions and thus increasing their application range and value. As the key biomass constituents are high-molecular-weight materials, such as vegetable oils or disaccharides, or polymers, i.e. cellulose, hemicelluloses and lignin, the primary objective for their valorization is the reduction of their molecular mass. By analogy, catalytic cracking or hydrocracking are the industrially mature technologies to be applied and their possibilities in biomass upgrading will be explored below for catalytic cracking and hydrocracking of triglycerides and catalytic pyrolysis of biomass.

Another class of important carbon–carbon bonds rearrangements are isomerization reactions, such as *n*-alkanes to iso-alkanes isomerization to improve, depending on the feedstock, octane number or cold-flow properties of automotive fuels, or isomerization of xylenes to deviate from thermodynamic equilibrium and maximize the yield of the most valuable *p*-xylene. In both cases, shape selectivity of zeolites plays an important role as it permits targeted formation of the desired products while avoiding formation of the undesired ones, e.g. due to cracking. Apart from the pore-size constraint leading to shape selectivity, fine tuning of acid sites distribution and strength is paramount to minimize the undesirable isomerization on the external surface and excessive cracking. From biomass perspective, isomerization is the key to valorizing *n*-alkane-rich fractions from triglycerides deoxygenation as well as to facilitating sugar transformations yielding either fructose from glucose or rare sugars as it will be shown here.

Finally, zeolites can be used also for formation of carbon–carbon bonds, typically by alkylation of aromatics. This approach could be used for the transformations of aromatics and phenols obtainable from lignin conversion. As the application of these principles to biomass-derived aromatics is rather straightforward, we shall focus on other type of carbon–carbon forming reactions, namely condensations that are together with acylation reactions being increasingly investigated and even industrially used in the synthesis of fine chemicals [47]. These reactions involve often the use of oxygenated (polar) compounds and are thus very valuable for demonstrating the effect of other characteristics of zeolites, such as hydrophilic/hydrophobic properties, that are highly pertinent to biomass related transformations. Nonetheless, the acido-basic and textural properties will continue to be of prime importance which will be demonstrated on the example of aldol condensation that represents both a petrochemical synthesis (of fine chemicals) as well as transformation of bio-based raw materials to, e.g. fuel components.

In addition to carbon–carbon bond rearrangements, zeolites are important catalysts for functionalization/defunctionalization of raw materials that include oxidation and deoxygenation reactions, in particular. Titanosilicates are very important industrial oxidation catalysts affording epoxides. Evidently, structural properties and the incorporation of titanium are the key aspects. With respect to biomass, olefinic raw materials, such as triglycerides or the corresponding acids and terpenes, are the relevant feedstocks. Apart from these, a specific class of zeolite-based catalysts containing exclusively Lewis acid sites will be included here as they have shown an interesting potential in conversion of sugars and lactic acid (methyl lactate).

In the following text, the selected case studies are described in detail demonstrating the potential of zeolites/molecular sieves in each particular area.

3.1. Catalytic cracking

Fluid catalytic cracking (FCC) is the largest catalytic process and it is the reason for zeolite Y being the most produced and consumed zeolite in catalytic applications worldwide accounting for 95% of the tonnage of zeolite catalysts [48]. The catalyst used in FCC has evolved in a very complex catalyst in which ultra-stabilized zeolite Y (USY) plays an essential role though it makes up only between 20 and 40% of the final catalyst. The remainder consists of the catalytically active matrix (composed of amorphous aluminosilicate and binder) and an array of additives aimed, e.g. at boosting gasoline octane number (using ZSM-5 zeolite) or trapping NO_x and SO_x emissions during continuous catalyst regeneration [5]. The main role of the matrix is to pre-crack bulky feedstock molecules into intermediates that can reach the highly active acid sites located in the pores of zeolite USY, the key active component of the FCC catalyst.

Acid sites density and strength are the key properties of USY zeolite used in FCC catalysts as they determine the products yields and quality, e.g. gasoline octane number, as well as coke formation. Both parameters depend on the Si/Al ratio. The maximum cracking activity was reported for Si/Al ratio in the range 5–8 at which all framework Al atoms are isolated [49]. In addition to acidic properties, the textural properties play an important role. Apart from the molecular sieving effect of the matrix as well as USY and ZSM-5 that governs the product distribution and makes possible its adjustment, e.g. between gasoline and propylene, the USY mesoporosity and the presence of extra-framework aluminum (EFAL) species originating from the dealumination process were shown to affect the cracking performance significantly [50]. Moreover, dealumination by steaming provides the catalyst with sufficient hydrothermal stability that is crucial for its regenerability.

The bulky nature of many biomass feedstocks makes the use of cracking catalysts attractive for molecular weight reduction. In addition to carbon–carbon bond cracking which is almost exclusive reaction in petroleum feedstock cracking, the splitting of carbon–oxygen bonds plays an important role in upgrading of biomass feedstocks. Since carbon–oxygen bonds are weaker than carbon–carbon bonds, a lower strength and density of acid sites should be sufficient to achieve desired conversion of biomass feedstocks, i.e. to avoid over-cracking and the related excess formation of gaseous products. It also follows that the hierarchical porous structure of FCC catalysts can be advantageous as it will allow controlling the molecular traffic. This is particularly valid for cracking of triglycerides, while in the case of lignocellulosic biomass cracking, catalytic cracking has to be preceded by thermal degradation of the polymers, i.e. lignin, cellulose and hemicelluloses, as the polymers cannot reach the catalyst active sites. It has been proposed to combine the thermal and catalytic steps and the process is called catalytic pyrolysis.

Catalytic cracking of triglycerides as an alternative process to their direct deoxygenation has the advantage of being accomplished in the absence of hydrogen. On the other hand, it results in a broad spectrum of products ranging from gases to carbonaceous deposits and the yield of the desired products is thus significantly limited in comparison to hydrogen-consuming deoxygenation [51]. The different alternatives of triglycerides upgrading are summarized in Fig. 1 [17]. An extensive review on the possibilities of the

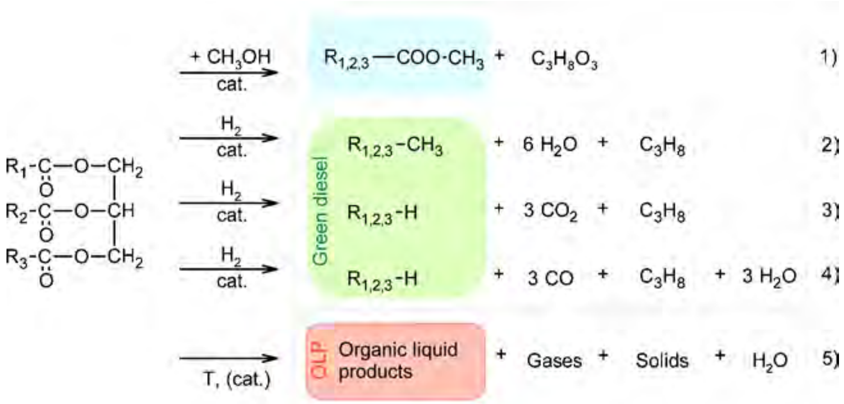

Fig. 1. A simplified scheme of the main reaction paths in transformation of triglycerides into biofuels via catalytic processes: (1) transesterification, (2) hydrodeoxygenation, (3) hydrodecarboxylation, (4) decarbonylation, (5) cracking/catalytic cracking [17]. Reprinted by permission of Taylor & Francis LLC (http://www.tandfonline.com).

transformation of biomass-derived feedstocks using conventional refinery processes, including the FCC process, has been reported by Huber and Corma [52].

It was shown that structural and textural properties of acidic zeolites affected their activity and selectivity in alkane cracking [53,54]. Recent studies show that the same characteristics also introduce a significant impact on the behavior of zeolites in the deoxygenation of triglycerides and carboxylic acids. Zeolites of different structural types, mesoporous materials and their composites were used as objects of these studies [55–58]. Main products of catalytic cracking of vegetable oils are hydrocarbon gases gasoline fraction (mostly aromatics) and diesel, and the ratio between them depends on the physicochemical characteristics of applied materials.

However, the studies using the industrial equilibrium FCC catalysts are the most interesting ones from the application point of view. It has been demonstrated that addition of triglycerides (vegetable oils or animal fats) into vacuum gas oil (VGO) shifts the product distribution towards lighter products, i.e. gaseous products (typically C_3 and C_4 fraction) and gasoline [59–62]. Oxygen was released in the form of water and to a minor extent also CO and CO_2. Only traces of oxygenates were detected in the liquid products [60,61]. It was established that the naturally occurring contaminant of triglycerides, such as calcium and phosphorus, have a pronounced negative impact on the catalyst activity [60].

Apart from the commercial FCC catalysts, neat zeolites have been investigated extensively for catalytic cracking of triglycerides to provide fundamental insights into the role of acidity and structural properties as well as the impact of feedstock structure. For instance, Černý et al. have reported that over USY catalyst under MAT conditions (MAT = micro-activity test standardized for FCC catalysts evaluation), both the degree of unsaturation and the nature of the carbon–oxygen bond are essential for the final product distribution [63]. Most interestingly, fatty alcohols afforded better yields of the valuable iso-alkanes in the gasoline product than fatty acids and triglycerides. Moreover, triglycerides yielded more condensation products which was attributed to their thermal pre-cracking and the increased degree of unsaturation of the feedstock resulted in enhanced formation of aromatics [63].

In an attempt to understand the effect of zeolite structure, a comparison of catalytic properties of MFI, BEA and FAU was performed in the conversion of canola oil [58]. Hence, zeolite samples with similar SiO_2/Al_2O_3 ratios were consciously chosen to give a clearer indication of the effect of the zeolite structure and the density of acid sites on the cracking products. For gaseous hydrocarbons, the structural type of zeolite determined not only the yield of gaseous products, which decreased in the following order: BEA > FAU > MFI, but also the composition of obtained hydrocarbons. MFI, the zeolite with 10-ring pores, produced the most C_3 molecules, while BEA with 12-ring pores produced the most C_4, and FAU, also with 12-ring pore mouths but including large cages, produced the most C_5 [58]. The yield of organic liquid product decreased in the following order: MFI > BEA > FAU. Cracking of canola oil over 10-membered ring MFI produced predominantly gasoline which mostly consisted of aromatics [58]. Between the two 12-membered ring zeolites BEA produced slightly more aromatics than FAU at the studied reaction temperatures. The influence of SiO_2/Al_2O_3 ratio on the behavior of catalysts was also studied for BEA zeolite. The increase of SiO_2/Al_2O_3 from 25 to 300 increased the yield of gasoline range products but did not result in the growth of aromatics yield giving maximal value at $SiO_2/Al_2O_3 = 50$ [58]. Differences in the yield and composition of the liquid products the authors explained by shape selective processes which proceeded inside zeolitic pore structure. The structural type of zeolites also affects the formation of coke in the catalysts. Upon completion of the reaction, MFI showed a significantly lower coke amount in catalyst than the 12-ring materials BEA and FAU due to the difference in the pore size. The difference in the coke amount in 12-ring zeolites, BEA and FAU, the authors explained by the presence of the FAU supercages with a free diameter about 25% larger than the free diameter of the pores. This cage allowed more room for condensation and polymerization which results in even more coke. The same condensation and polymerization mechanism to coke formation was also consistent with lower coke yields on materials with higher SiO_2/Al_2O_3 ratios which were observed on both BEA and FAU materials.

Similar results were obtained by other authors when studying the conversion of ginger oil over MFI, BEA and FAU [64]. MFI zeolites consistently produced the highest gasoline fraction yields, while FAU catalysts generally performed poorly in gasoline yield. On the other hand, FAU and BEA catalysts produced more coke than MFI, what was attributed to the possibility for multiple molecules to condensate inside porous space of zeolites. Moreover, coke formation was facilitated by supercages present in FAU structure; in these supercages, molecules larger than the pore mouth can form and thus remain trapped in the cage. Hence zeolites that favor coke formation are less suitable as liquid yields are targeted. Zeolites with low SiO_2/Al_2O_3 ratios and having pore structures which reduce interactions of multiple molecules were favored. FAU, widely used in fluid catalytic cracking processes, gave poor yields of liquids from ginger oil and was basically unsuitable for this process. MFI gave the highest liquid yield but also produced the highest yield of benzene which is undesirable for gasoline. However, if aromatics for renewable petrochemicals would be the goal, MFI appears the clear choice. Finally, high SiO_2/Al_2O_3 BEA was a good choice for high liquid yields for fuels where benzene is undesired.

Further improvement in the properties of catalysts for cracking of plant oils is possible if using composite materials. Twaiq et al. [65] reported cracking reactions of palm oil over a composite material containing zeolite ZSM-5 and mesoporous molecular sieve which was prepared by coating ZSM-5 crystals with a layer of mesoporous molecular sieve. The catalytic performance of the prepared samples in the palm oil conversion was compared with those obtained from pure HZSM-5 and MCM-41 materials. Palm oil conversion of 80–100 wt% and yield of gasoline fraction of 38–47 wt% (mostly aromatics) were obtained from the composite catalysts which was superior in comparison with HZSM-5 and MCM-41. Similarly, other composite catalysts, such as BEA-MCM-41 were reported to outperform both the zeolite and the mesoporous material [57,65,66].

Biomass pyrolysis has been proposed as the key conversion technology for solid biomass upgrading as it allows increasing the energy density of biomass, for instance from ca. 2 GJ/m^3 to ca. 25 GJ/m^3 in the case of straw pyrolysis [67] and making transport and further processing of biomass more economical than the alternative technologies of gasification and hydrolysis [68]. Nonetheless, the main targeted product of biomass pyrolysis, i.e. bio-oil, is very difficult to process/upgrade due to its very complex composition with high content of oxygenates, low stability and high acidity and water content [69]. As a result, suitable upgrading technologies are sought. Catalytic pyrolysis has been suggested as a viable technology as it allows improving the properties of the bio-oil by increasing its energy value, decreasing its acidity and improving its stability [69]. Generally two approaches are considered, catalytic treatment of the vapors originating from thermal pyrolysis and the use of a catalyst directly in the pyrolysis process instead of an inert heat carrier [69–71]. The catalysts of choice for the upgrading are typically zeolites or molecular sieves [17,69–71] since they possess modifiable acidity and large surface areas allowing rather efficient dehydration/deoxygenation of the vapors. Moreover, catalytic pyrolysis with catalysts mixed directly with finely grinded lignocellulosic biomass has been demonstrated already at an industrial scale by Kior [69,72]. When looking at the process, it is obvious that it is a modification of the fluidized catalytic cracking discussed above. The most widely studied zeolites include FAU, i.e. the key component of commercial FCC catalysts, and MFI that is used as an additive boosting the production of aromatics and light olefins [69,71].

The investigations of the catalytic pyrolysis have been usually performed in fluidized or fixed bed setup in the first stage (pyrolysis/thermal cracking stage) followed by catalytic upgrading of the pyrolysis vapors in the second stage in a fixed-bed reactor with reaction temperatures in the range 400–550 °C [73–78]. The products consisted mainly of gaseous products (yielded typically in the range 30–50%), whereas the yields of the desired liquid bio-oil were limited to 5–20% [73–78]. Significant amounts of carbon (20–50%) from the feed are converted into carbonaceous deposits or char causing fast deactivation of the catalysts [73–78]. The structure of zeolites, in particular, the pore size and connectivity have been shown to affect the coking; the use of FAU zeolite resulted in more pronounced catalyst coking in comparison with MFI zeolite (19 vs 12%) [79]. Similar dependency, i.e. amount of coke decreasing in the order 3D-12 ring zeolites (FAU, BEA) > 1D 12 ring zeolites (MOR) > 3D-10 ring zeolites (MFI, FER) has been reported by other authors [73,74]. Strong Brønsted acidity has been linked with the superior deoxygenation activity of zeolite with BEA structure [79]. It has to be noted that a rigorous comparison of the results of the catalytic pyrolysis experiments is virtually impossible as (i) different experimental setups are used (often based on the so-called micropyrolysis unit designed a GC utility) that are characterized by different heat and mass transport parameters that are of utmost importance for the pyrolysis course, (ii) different catalysts with a limited amount of characterization data are used (only some of the following important characteristics, i.e. concentration of acid sites, their accessibility, strength and type are reported) not allowing drawing unambiguous conclusions about the relationship between catalyst properties and performance and (iii) the experimental conditions (e.g. temperature, contact time, biomass particle size, biomass feedstock, etc.) differ over a rather wide range making it thus difficult to interpret the experimental data.

The group of Huber has focused on the investigation of glucose and cellobiose (i.e. sugar representing cellulose, the most abundant component of lignocellulosic biomass) as well as other biomass-derived oxygenates (xylitol and furan) under fast pyrolysis conditions using various zeolites [80–83] in addition to their studies using lignocellulosic biomass [84,85]. In accordance with other findings, the catalyst selected for most of their investigations was MFI in proton form and modified [82,83]. When reviewing the performance of 13 zeolite structures, MFI was found to afford significantly more aromatics (35%) than the other zeolites; the second highest yield of aromatics was 25% over ZSM-11. Both of these zeolites have pore openings of 5.5 Å. On the other hand, large pore zeolites (pore openings >6 Å, e.g. BEA, FAU) or zeolites with pore openings <5 Å (e.g. FER) were found to yield <5% aromatics [82]. This clearly evidences the importance of the shape selectivity on formation aromatics, as the yield of coke was 30 and 45% for MFI and ZSM-11, while it was >60% for the large pore zeolites [82]. It was suggested that the coke is formed via furan intermediates (i.e. dehydration products) of oligomeric nature that decompose ultimately to coke [81]. Fast heating rates and high catalyst to feed ratios were thus proposed, in addition to the proper catalyst structure selection, as the key parameters allowing minimizing the coke formation [80]. These results were, however, achieved using a special pyroprobe that allows high heating rates (1000 °C/s) and with high catalyst-to-feed ratios (>10) that would be difficult to achieve in a real industrial process.

Recently, Rezai et al. [86] reviewed the production of aromatics and olefins by catalytic cracking of biomass-derived oxygenates using acidic and metal-modified zeolites as catalysts. They concluded that the major challenge is to restrict the main competing reaction, i.e. coking, and that the key characteristics of the cracking catalysts determining the product distribution include their acidity and structural features (pore size and shape, and crystal size) [86]. For further development they recommend to (i) increase content of/retain hydrogen in the hydrocarbon products (by supplying hydrogen donors/promote decarboxylation over dehydration), (ii) control the accessibility of zeolite pores (by controlling the size and shape of the pores), (iii) optimize catalyst acidity, i.e. the type, concentration and strength of acid sites and (iv) fundamental investigation of the relationship between acidity and pore structure [86].

3.2. Hydrocracking/hydroisomerization

Conventional hydrocracking and hydroisomerization catalysts represent bifunctional systems in which metal component is responsible for hydrogenation/dehydrogenation stages and acidic component carries out the isomerization of intermediate carbenium cations and their cracking producing fragments with lower molecular weight. Hydrotreatment catalysts with the only metal component, such as sulfided CoMo, NiMo, NiW on alumina or Pd/C, successfully participate in the deoxygenation of triglycerides by the reactions which include hydrogenation, decarboxylation and decarbonylation [51]. The main reaction pathways are depicted in Fig. 1. As the result of these reactions, the formation of diesel hydrocarbon fraction which consists primarily of *n*-C15 to *n*-C18 alkanes takes place. However, these mono-functional catalysts are inactive in the following isomerization of *n*-alkanes due to the absence of (strong) acid sites. Obviously, the addition of acidic component into catalytic material with hydrogenating properties should result in the further transformation of *n*-alkanes obtained, thereby changing the composition of the reaction products. This would be a direct parallel with the commercial dewaxing via hydroisomerization of *n*-alkanes to isoalkanes that relies on the use of bifunctional catalysts, such as Pt/ZSM-22, Pt/ZSM-23 or Pt/SAPO-11, allowing isomerization restricted to mono- and di-branched products [87–90]. However, to date the amount of work aimed for one-step hydroconversion of plant oils in the presence of bifunctional zeolite catalyst is rather limited.

In an attempt to develop a bifunctional catalyst, the influence of adding BEA zeolite (0–30%) to conventional NiMo/γ-Al_2O_3 was studied for hydroprocessing of mixtures of sunflower oil and a straight run gas oil [91]. The increasing content of zeolite in the catalyst resulted in enhanced conversion of the feed. The authors suggested that this result confirmed the role of the zeolite in the conversion of the oil molecules. However, C17–C18 *n*-alkanes were the main reaction products of oil hydroconversion, which indicates that the catalyst cannot be denoted as a bifunctional one. The absence of hydrocarbons with lower molecular weight and C17–C18 isoalkanes in reaction products was attributed to a fast hydrogenation of the intermediate olefins [91]. Consequently, the olefins could not reach the acid sites, either due to the disbalance between the two functions or rather due to too large distance between the metallic and acidic sites, as balance between both functions and their proximity are the key parameters of bifunctional catalysts [92–95].

The effect of different active sites and supports on the properties of NiMo/γ-Al_2O_3, Pt/H-Y and Pt/HZSM-5 in the hydroconversion of rapeseed oil was investigated in [96]. Both zeolite catalysts showed high activity in the conversion of the feedstock under the selected reaction conditions. The hydrotreating of rapeseed oil on Pt/H-ZSM-5 produced a higher yield of gasoline (C_5–C_{12} fraction) than diesel (C_{13}–C_{22} fraction). The higher production of cracked products with the 10-ring zeolite suggested that the acid sites of Pt/H-ZSM-5 are stronger than those of Pt/H-Y. The milder acidity of the Pt-HY catalyst led to a larger production of green diesel than green gasoline. Nevertheless, compared with the yield of diesel obtained over $NiMo/Al_2O_3$ the yield of green diesel over Pt/zeolite catalysts was low. The acid sites of zeolites favored the production of iso-paraffins, which are desirable for the diesel to have a low pour point, indicating the bifunctional character of the catalysts.

Hierarchical mesoporous zeolites were studied in the hydroconversion of triglycerides and free fatty acids obtained from algae and Jatropha seeds to produce jet fuel (kerosene) range hydrocarbons [97]. Based on the screening of various mesoporous and microporous supports, it was concluded that a mesoporous molecular sieve support is necessary to obtain high and stable activity along with high yield of isomerized product. Besides, with the right balance of acid sites and hydrogenation–dehydrogenation sites, it might be possible to improve the yield as well as the isomerization selectivity. When converting triglycerides, a specially prepared catalyst with Ni–W phase loaded on acidic ZSM-5 support with hierarchical structure and intra-crystalline mesoporosity yielded 40–45% C9–C15 hydrocarbons and high isomerization selectivity (iso/*n*-alkanes = 2–6). Further, when using a hierarchical mesoporous ZSM-5 with higher acidity, larger surface area but lower zeolitic crystallinity, the jet range hydrocarbons yield reached 54% with moderately high isomerization selectivity (iso/*n*-alkanes = 2.6). The authors attributed the high yield and selectivity to the desired balance between the hydrogenation and cracking functionalities of the catalyst [97].

It is generally accepted that hydroconversion of long-chain *n*-alkanes over bifunctional catalysts proceeds with high selectivity towards isomerization route if a microporous material possessing specific structural characteristics, namely a one-dimensional pore system with pore size of 0.5–0.6 nm is used as acidic component [98–100]. Examples of such microporous systems include ZSM-22 and ZSM-23 zeolites as well as substituted microporous aluminophosphates, especially SAPO-11. The latter material exhibits a high efficiency for the isomerization of *n*-paraffins (waxes) at high conversion with little cracking [98,101]. By using Pt/SAPO-11 the Blechner Center has developed a novel process which produces high-quality green diesel fuel from vegetable and animal oil in one stage [102–105]. The authors of this process claimed that, after 150 h of TOS, i.e. under pseudo-steady-state operation, the catalyst ensured not only feed hydrodeoxygenation and isomerization of *n*-alkanes but also produced naphthenes and aromatics in parallel with the other reactions. As a result, a superior renewable diesel called Isodiesel was produced from animal and vegetable oils in a one-stage process. The total duration of the catalytic experiment was 650 h, during which a reaction product characterized by cetane index of >65, oxidation stability of 0.3 mg/100 mL, cloud point of −6 °C and high-frequency reciprocating rig (HFRR) lubricity of <300 lm was produced [105].

A one-step hydrotreatment of vegetable oil combining deoxygenation and isomerization to directly produce low cloud point, high-quality diesel was also reported by Wang et al. [106]. In this study SAPO-11 and ZSM-22 were used as acidic carriers for the preparation of bifunctional Pt-containing catalysts. Over these catalysts, 100% conversion of soybean oil was obtained with total selectivity to alkanes of 100% while selectivity to isomeric compounds was 63%.

The properties of Pt/SAPO-11 catalysts in the hydroconversion of plant oils to isomeric alkanes depend not only on the nature of applied metal and the structural characteristics of microporous component. Chen et al. showed [107] the influence of Si/Al ratio in SAPO-11 and Pt loading on the behavior of Pt/SAPO-11 in the hydroconversion of Jatropha oil. The growth of Si content in SAPO-11 resulted in the increase of the number of medium acidic sites, what, in turn, enhanced the isomerization activity of the catalysts. Over catalyst with the optimal Si content (Si/Al = 0.4), the complete conversion of triglycerides was achieved with different Pt loadings, and the highest ratio of $\text{iso-}C_{15-18}/n\text{-}C_{15-18}$ was nearly 22 when using 3 wt% Pt/SAPO-11. It was also shown that deoxygenation, isomerization and cracking reactions were strongly dependent on Pt loading; when the Pt loading was increased, the isomerization and cracking activities of Pt/SAPO-11 catalyst were enhanced significantly.

Bifunctional catalysts with the composition other than Pt/SAPO-11 can be used for the selective production of iso-alkanes from triglycerides. Hydroconversion of sunflower oil over Pd/SAPO-31 revealed prospects of this catalytic system for the one-stage hydroconversion of vegetable oil to produce hydrocarbon-based biodiesel with improved low-temperature properties [108]. At optimal reaction conditions and the initial time of the process (TOS = 2 h), triglycerides conversion was 100% and the $\text{i-}(C_{17}+C_{18})/n\text{-}(C_{17}+C_{18})$ ratio exceeded 10. As the duration of the experiment increased, the activity of the catalyst gradually decreased what was manifested in a decline in the content of isomeric reaction products. The comparison of the physicochemical properties of fresh and used catalysts showed that the degradation of the catalytic properties of Pd/SAPO-31 could be generally attributed to a decrease in Pd dispersion. The authors suggested that low Pd dispersion not only decreased the activity of the bifunctional catalyst in hydrocarbons isomerization, but might also result in incomplete conversion of intermediate oxygenated products which blocked acidic sites of SAPO-31. Indeed, it was shown that the increase of Pt content in Pt/SAPO-31 substantially increased the duration of the stable activity of the catalyst in hydroconversion of sunflower oil simultaneously keeping high selectivity to *n*-alkanes isomerization [109].

Unlike isomerization of hydrocarbons that necessitates the use of bifunctional catalyst, such as metal-modified zeolites discussed above, isomerization of sugars can be accomplished by the use of acidic catalysts alone. As glucose is the most abundant monosaccharide, its efficient utilization/valorization is of paramount importance. A key route to value-added products is the dehydration of glucose to 5-hydroxymethyl furfural (HMF) that serves as a platform chemical for many applications, e.g. levulinic acid, dihydroxymethylfuran, dimethylfuran, etc. [110]. A basic scheme of these transformations is shown in Fig. 2. Similarly, xylose obtainable from hemicelluloses can be dehydrated to furfural, another platform molecule. It has been demonstrated that conversion of fructose to HMF is significantly more facile than that of glucose [111,112]. Hence, glucose to fructose isomerization is essential for efficient glucose transformation to HMF. Various zeolites have been shown to be active as isomerization catalysts [111,113]. It was shown that water has an inhibiting effect on the isomerization reaction over zeolites, and methanol was recommended as the most suitable solvent due to the easiest formation of alkylfructoside (in comparison with other alcohols) that allowed for the highest yields of fructose after fructoside hydrolysis [113]. Both zeolite structure and acidity were seen to have an impact on glucose conversion. Due to limited pore dimensions, MFI zeolites yielded only small amounts of fructose (<10%) regardless their Si/Al ratio. Similarly, MOR afforded also limited yields of fructose and no fructoside. On the other hand, FAU and BEA structures yielded significant amounts of fructose and methylfructoside that approached the equilibrium value of 55% [113]. It was clearly seen that high concentration of acid sites was beneficial as with the increasing Si/Al ratio the yields of fructose and methylfructoside decreased [113]. The isomerization results also indicated that the optimum ratio between Brønsted and Lewis acid sites (ca. 2) was crucial for obtaining near-equilibrium fructose yields due to efficient hydrolysis of the methylfructoside intermediate [113,114].

In addition to zeolites, Sn-BEA was demonstrated to be an effective isomerization catalyst during conversion of hexoses and pentoses to lactic acid [115,116]. At 100 °C, equilibrium

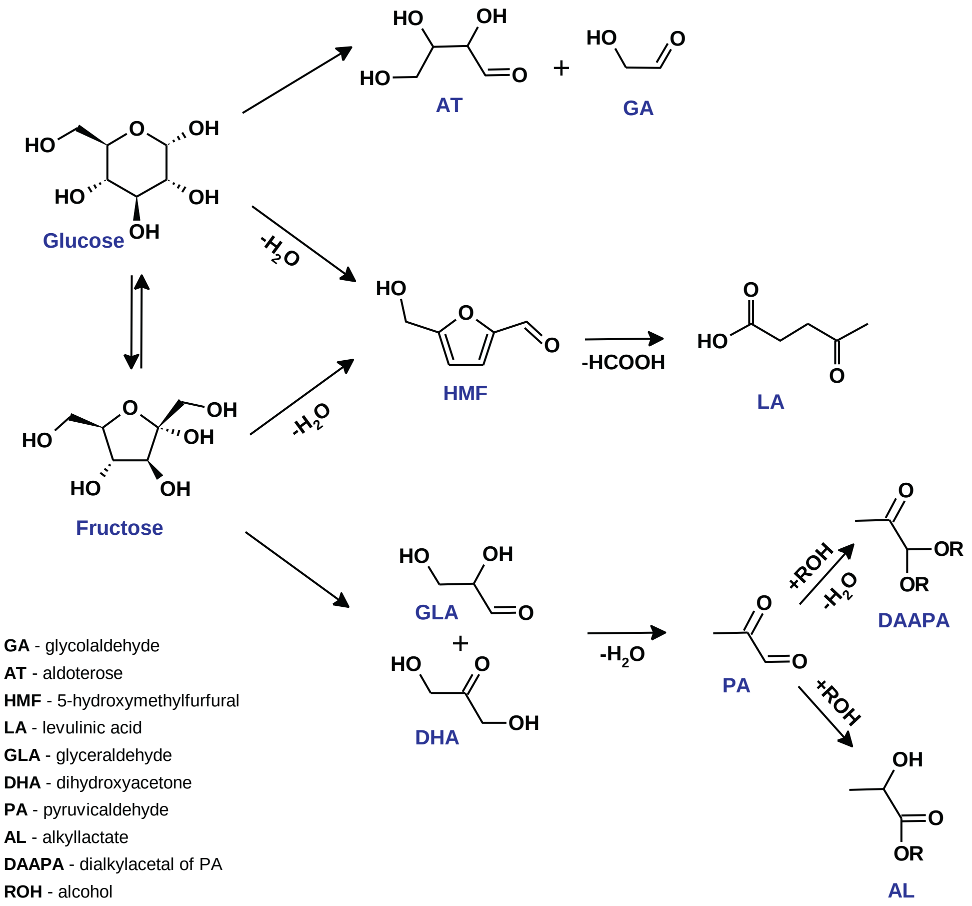

Fig. 2. An overview of the transformation pathways for upgrading of sugar-based feedstocks, including isomerization, dehydration and retro-aldol condensation reactions.

distribution among aldoses and ketoses was achieved for various sugars including glucose and xylose. It can thus be inferred that Sn-BEA could be the catalyst of choice to produce rare sugars, e.g. lyxose or xylulose from xylose, for special applications [115,116].

3.3. Fine chemicals synthesis—condensation reactions

The condensation reactions are important reactions in synthetic organic chemistry for the lengthening the backbone of resulting molecules. Generally such kind of the reactions may occur in acidic or basic medium, and catalytic functions of acid and base have been well established [117]. Catalysts such as sodium hydroxide or sulfuric acid in the liquid phase are used commonly in industry [118], but these processes introduce a lot of disadvantages, i.e. corrosion of equipment, safety and environmental problems, complex separation scheme, etc. Therefore, the solid acid and basic heterogeneous catalysts as potential catalysts for condensation of different organic molecules have attracted attention during past decades [119,120]. Zeolites have been demonstrated to be suitable catalysts for many pharmaceutical, such as synthesis of Ibuprofen or Naproxen [47,121–123] and fine chemical applications, such as various fragrances and flavors [47,124]. Among these, the syntheses of acetanisole and acetoveratrole have been commercialized using BEA and FAU zeolites, respectively [125,126]. In addition to conventional zeolites, including BEA, FAU, MOR and MFI used in carbon–carbon-bond forming reactions, Ti-BEA and Sn-BEA have been demonstrated to be efficient isomerization (e.g. alpha-pinene isomerization) and oxidation (Baeyer-Villiger oxidation using Lewis acid catalysts), respectively [127–129]. The potential of these catalysts in biomass transformations will be discussed in the next case study.

Biomass-derived feedstocks, particularly those originating from cellulose and hemicelluloses, consist typically of C_5 and C_6 molecules with carbonyl and hydroxyl groups. Their reactivity can be used for their further valorization in condensation reactions. In fact, should the goal be the production of automotive fuel components, an increase of the molecular mass through carbon–carbon bond formation is necessary. Considering the chemical structure of the biomass-related feedstocks, aldol condensation could be an efficient reaction pathway to increase the molecular mass efficiently. Aldol condensation, among other types of similar reactions, proceeds as a cross-condensation between two molecules of different aldehydes or ketones, or as self-condensation between two of the same aldehyde or ketone molecules having α-hydrogen atoms [117,130,131]. The acid-catalyzed C—C bond formation occurs via an initial keto–enol tautomerization of alkanal (or alkanone) to form the conjugate enol. The sequential nucleophilic attack of the alpha carbon in enol to the protonated carbonyl group of alkanal (or alkanone) creates an inter-molecular C—C bond, thus lengthening the carbon backbone and forming a beta-hydroxy alkanal (or alkanone), also known as an aldol. The base-catalyzed C—C bond formation involves the formation of a resonance-stabilized enolate and its sequential nucleophilic attack to the carbonyl group of an alkanal or alkanone to evolve the aldol. Both acid- and base-catalyzed reactions share a common sequential dehydration step that transforms the beta-hydroxyl alkanal (or alkanone) to an alkenal or alkenone, respectively, to complete a catalytic turnover. Since the acid–base properties of zeolites can be tailored in a relatively broad range, they can be considered as promising catalytic systems for this reaction because they have fixed and stable structural characteristics, high surface area and can possess either acidic or basic active sites.

Most studies on aldol condensation over zeolites deal with catalysts possessing basic properties. Aldol condensation over zeolites in cationic forms and treated with alkali metals for generation of basic properties have been known for several decades. In 1970s and 1980s, Isakov et al. [132,133] studied properties of various solid catalysts for the vapor-phase aldolization of different compounds. In these studies, the catalytic activity of alkali metal zeolite followed the order of CsNaY > NaY > LiNa > MgO > Al_2O_3. Other examples of the use of zeolites in aldol condensation include: vapor-phase reaction of formaldehyde with methyl propionate using X, Y and ZSM-5 treated with NaOH, KOH, CsCl and NaN_3 [134], the aldol condensation of *n*-butanal to 2-ethyl-2-hexenal over Y zeolites with Li, Na and Cs cations [135], acetaldehyde self-condensation over type X zeolites [136], the aldol condensation of propanal to 2-methylpentenal in the presence of alkali ion-exchanged zeolites and comparing them with other basic materials [137], the condensation reaction of propionic acid and formaldehyde over ion-exchanged X zeolites, with and without occluded cesium [138]. All these studies revealed a similar trend: the activity of cationic forms of zeolites in aldolization increased in accordance with the trend of catalyst basic strength, so that cesium-containing zeolites exhibited the best catalytic properties. Thus, the results obtained using alkali ion-exchanged zeolites as catalysts for the aldol condensation of propanal to 2-methylpentenal [137] indicated the dependence of catalytic properties of the samples on the type of alkali metal ion exchanged into zeolite cage. The conversions obtained followed the order Cs–X > Rb–X > K–X > Na–X which was in agreement with the order of basicity for these solids. Nevertheless, in comparison with conventional basic catalysts, such as hydrotalcites, alkali-containing zeolites possessed poor activity. The conversion of propanal varied from 22 to 42% with 92–94% selectivity of 2-methylpentenal using various alkali ion exchanged zeolites, while under the same reaction conditions activated hydrotalcite showed the maximum conversion (97%) of propanal with 99% selectivity of 2-methylpentenal. This difference in the properties was explained that alkali ion-exchanged zeolites are weaker basic materials in comparison with hydrotalcites.

The catalytic behavior of X zeolite exchanged with cesium and impregnated with cesium species was studied using the aldol condensation reaction between glyceraldehyde acetonide and acetone producing the corresponding α,β-unsaturated carbonyl compound [130]. These catalysts were active for the studied reaction. The activity of X zeolite exchanged and impregnated with cesium species was close to that for Mg–Al hydrotalcite. However, these catalysts differed in selectivity (a lower selectivity to diacetone alcohol was observed over the zeolite), which was explained by differences in the strength of basic sites.

Acidic zeolites were also studied as catalysts for aldol condensation. Conversion of acetophenone, cyclohexanone and acetone over various acidic zeolites H-Y, H-USY, H-beta and H-MCM-22 was studied in [139]. The catalytic properties of zeolites depended on the structural properties as well as on the strength and concentration of acid sites. Thus, in acetophenone condensation the activity of MWW and BEA zeolites showed the following trend: aluminosilicate > gallosilicate > ferrisilicate. On the other hand, the yield of reaction products depended on the concentration of acid sites accessible to reactant molecules. Dumitriu et al. [140] studied the properties of ZSM-5 samples with different Si/Al ratio, as well as Ga-, Fe- and B-substituted MFI samples in the aldol condensation of acetaldehyde and formaldehyde. Both the conversion and the product selectivity were substantially influenced by the Si/M^{3+} ratio and the nature of substituting element. In the aldol condensation of acetaldehyde and formaldehyde, the activity of the samples decreased in the order: B > Fe > Ga > Al-ZSM-5, which was attributed to the concentration of accessible Brønsted sites of medium strength. However, in terms of the selectivity for cross-aldol condensation the activity of the zeolite was related to the presence of strong acid sites, i.e. following the reverse order: Al > Ga > Fe > B-ZSM-5.

Many studies have been devoted to the investigation of the effect of properties of zeolites as catalysts for acetone self-condensation [130,141–145]. This reaction attracts an attention for study since acetone is readily available product on chemical market. First of all, it is a secondary product in propylene oxide production and in phenol synthesis from cumene [146]. Also, the development of technologies for the production of commodity chemicals, energy, and materials from renewable bio-based feedstocks provides additional sources of acetone supply. It can be produced from abundantly available biomass, such as agricultural wastes, by ABE (acetone–butanol–ethanol) fermentation [147]. Besides, acetone can be produced by the catalytic steam reforming of bio-ethanol [148], biomass pyrolysis [149,150] and the transformation of different biomass wastes, such as sewage sludge, fermentation residues and livestock manure [151–153].

Similar to other aldol condensation reactions, acetone self-condensation proceeds over both acidic and basic zeolites [141,142,154,155]. It is postulated [141] that the aldol condensation of acetone over bases leads to diacetone alcohol that dehydrates to mesityl oxide. Further, aldol condensation of mesityl oxide with another acetone molecule gives trimeric compounds which result in the formation of isophorone and mesitylene. When acidic catalysts are used for acetone aldolization, diacetone alcohol is also produced but it decomposes into isobutene and acetic acid. Aromatic and aliphatic compounds are formed from isobutene oligomerization. According to these considerations, it was found that lower silica-to-alumina ratios in FAU zeolites favored the basic route of the reaction, i.e. increased mesityl oxide formation and decreased isobutene formation. The increase in cesium content led to the mesityl oxide hydrogenation to methylisobutylketone, suggesting that hydrogenation activity was related to the nature of the cation.

Tago et al. [143] studied the effect of crystal size on catalytic activity and stability of acidic ZSM-5 samples in acetone self-condensation. As compared with the macro-sized zeolite, the nano-sized zeolite exhibited a high activity over a long lifetime. However, because the nano-sized zeolite possesses a large external surface area, undesirable reactions forming aromatics from the produced light olefins occurred on the acid sites located at the external surface or in its vicinity. After passivation of the external surface of nano-sized ZSM-5 with different silanes, the catalyst exhibited high olefins and low aromatics yields even at high acetone conversion.

The acidity of the zeolites, which affected the catalytic activity as well as the isobutylene selectivity, could be also controlled using the ion-exchanged treatment [142]. Ion exchange of H-BEA zeolite with different alkali metals decreased the acidity of the catalysts in the order: H-BEA > Na-BEA > K-BEA > Rb-BEA > Cs-BEA, and the order of their catalytic activity in acetone conversion was the same. Though H-BEA zeolite showed a high acetone conversion at the initial reaction time, the activity of the catalyst drastically decreased due to coke formation. In contrast, the alkali metal ion-exchanged BEA zeolites exhibited high isobutylene selectivity and decreased coke formation at high acetone conversion conditions. Similar results were obtained also in other studies [144,156] when studying the properties of BEA zeolites exchanged with mono- and divalent cations in acetone conversion. It was shown that ion-exchange decreased Brønsted acidity and increased Lewis acidity. As a consequence, metal-exchanged zeolites showed decreased

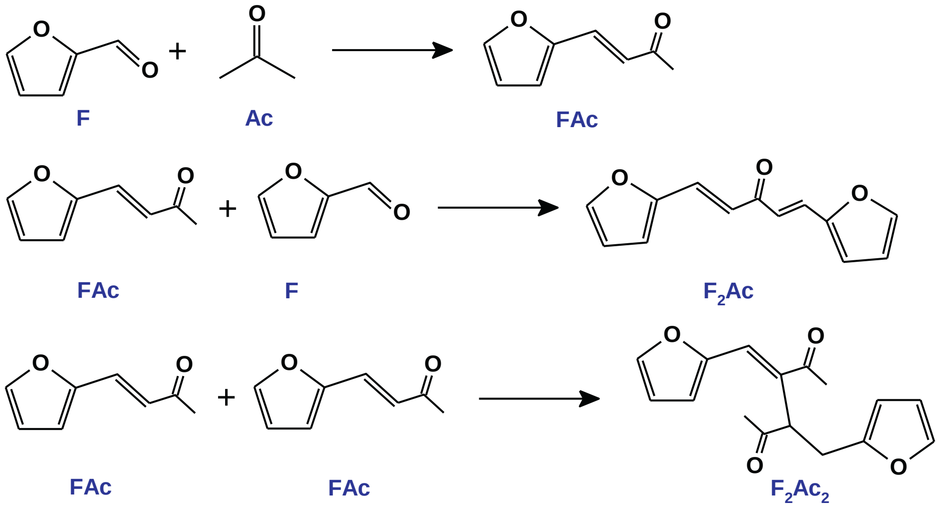

F - furfural
Ac - aceton
FAc - 4-(furan-2-yl)but-3-en-2-one
F_2Ac - 1,5-di(furan-2-yl)penta-1,4-dien-3-one
F_2Ac_2 - 4-(furan-2-yl)-5-(furan-2-ylmethyl)hept-3-ene-2,6-dione

Fig. 3. A simplified scheme of aldol condensation and dimerization pathways in conversion of acetone and furfural.

activity in aldol condensation but increased selectivity to isobutylene.

Moreover, structural properties of zeolites can change their selectivity to the reaction products. Regardless of the crystalline framework acetone self-condensation over zeolites resulted in the formation of diacetone alcohol, mesityl oxide and phorone as reaction products, since their molecular dimensions are comparable with the dimensions of the zeolitic channels [145]. However, unlike the medium pore MFI zeolite, the large pore BEA, FAU and micro-mesoporous silica–aluminas afforded isophorone as the final product that was absent over MFI due to sterical reasons.

The successful use of zeolites in the aldol condensation of various aldehydes and ketones indicates that these materials can be also used as catalysts for the production of valuable products from other biomass-derived sources. Furanic compounds (furfural or hydroxymethylfurfural) can be obtained by acid hydrolysis of monomeric products, generally sugars, produced from hemicellulose- and cellulose-rich feedstocks, and serve as platform chemicals in many applications [17,157–161]. Among them, aldol condensation of furanic compounds with acetone is intensively studied, because it permits obtaining various valuable products, for example, those which can be used for producing of hydrocarbon fractions to be used in fuel blending. A basic reaction scheme of the aldol condensation of furfural with acetone is given in Fig. 3. This reaction is usually carried out in the presence of basic catalysts, for example hydrotalcites [162–164]. So far, only few studies compared the properties of acidic and basic zeolites in this reaction. The comparison of the properties of solid base catalysts $MgO–ZrO_2$, NaY and nitrided zeolite Y (Nit-NaY) prepared by treating zeolites with ammonia in aldol condensations of furaldehydes with acetone and propanal was performed in [165]. Nit-NaY exhibited catalytic activity for aldol condensation comparable to MgO–ZrO2 and much higher than that of NaY, pointing thus to the increased base strength of Nit-NaY due to replacing the bridging oxygen with the lower electronegativity nitrogen. However, the used procedure for obtaining this material resulted in a partial loss of crystallinity of the FAU-type crystal structure, and the Nit-NaY sample was found to be unstable under the reaction conditions due to leaching of the framework nitrogen resulting in the loss of catalytic activity.

Recently [166,167] acidic zeolites of different structural types were shown to possess appreciable activity in aldol condensation of furfural with acetone and resulted in a formation of products of aldehyde–ketone interaction, which are usually obtained when performing this reaction over basic catalysts. However, it was shown that zeolites catalysts additionally promote the dimerization of the classical condensation products (Fig. 3). This can be considered as a distinguishing feature of the aldol condensation over solid acid catalysts. A comparison of results obtained for zeolites of different structural types showed that their catalytic behavior was mainly influenced by their both structural and textural properties. Wide-pore three-dimensional BEA and FAU zeolites afforded higher furfural conversion in comparison with medium-pore MFI and with wide-pore mono-dimensional MOR [166]. Furthermore, the formation of the above-mentioned dimer was the highest over FAU, in which the presence of large cages inside zeolite structure promoted the formation of this bulky compound. In the course of the reaction, the activity of all acidic zeolites decreased quickly due to coke formation inside the zeolite pores, but the activity was fully restored after calcination in air leading to coke removal. Nevertheless, the crystalline framework also affected the coke formation in zeolites. The comparison of the properties of several MWW samples in aldol condensation of furfural and acetone [167] showed that the deactivation MCM-36 catalysts, i.e. a pillared (2D) material, was more severe than that of MCM-22 and MCM-49 having conventional 3D structure. It was attributed to the reaction taking place in supercages, which are present in MCM-22 and MCM-49 but absent in MCM-36, as the acidic sites located in these supercages are protected by 10-ring channels from severe coking [167].

3.4. Partial de-functionalization of sugars—platform chemicals by dehydration

Petroleum-derived fractions exhibit only very limited extent of functionalization, typically by sulfur that is removed in the process of fuel production, whereas biomass-derived feedstocks are almost exclusively functionalized by hydroxyl, carbonyl or carboxyl groups. Consequently, there are no direct examples from the petrochemical industry for de-functionalization of biomass-derived feedstocks. A parallel can be found perhaps in the deoxygenation process that is focused on removing any oxygen from the raw materials and turning them into hydrocarbons. As suggested above, any effective and efficient biomass valorization necessitates the transformation of the basic building blocks, i.e. sugars and phenols, into so-called platform chemicals that can become the cornerstones of future chemical industry. Their potential arises from their versatile transformation pathways leading to products having high added value. Sugars obtained by hydrolysis of cellulose and hemicelluloses can be turned either to furanic compounds, furfural and 5-hydroxymethylfurfural (HMF), through dehydration [160,161] or to lactic acid and its esters via dehydration and retro-aldol condensation [160,168]. Fig. 2 summarizes the main transformation routes.

As discussed above, isomerization of glucose to fructose precedes its dehydration to HMF. The experimental data indicate that conversion of glucose to HMF is not simply proportional to the concentration of acid sites in BEA zeolites. It has been suggested that the nature of acid sites is crucial. BEA catalysts with predominating Brønsted acidity afford lower conversion of glucose and higher formation of by-products than BEA with predominating Lewis acidity (prepared by steaming) [111]. It can be inferred that Lewis acidity is responsible for the isomerization step while Brønsted acidity determines the dehydration activity of the catalyst [111]. Isomerization of glucose was found to be the rate-limiting step. The key to maximizing the HMF yield is the proper balance between isomerization and dehydration activity, i.e. between Lewis and Brønsted acidity, allowing fast fructose dehydration before the undesired side reactions of fructose over Lewis acid sites can take place [111]. The optimization between the number and the strength of acid sites was suggested already by Moreau et al.in 1996 [112]. Using a series of MOR, the optimum Si/Al was reported to be around 10–11. The initial reaction rate of fructose dehydration decreased by more 25% both in case there were more acid sites, but weaker ones (Si/Al ca. 7) and in case there were less acid sites but stronger ones (Si/Al ca. 15–18) [112]. The authors also found that high HMF selectivity is the consequence of limited pore size of MOR that prevents side reactions. An increased extent of the side reactions was observed as the mesopores volume of the MOR catalysts increased [112]. Similar dependencies were reported also for dehydration of xylose to furfural [169].

The authors focusing on dehydration of sugars to esters of levulinic acid [170] have reported shape selective behavior of zeolites catalysts as well. Due to size constraints, ethyl levulinate was not formed over MFI and MOR catalysts, whereas it could be obtained although in low concentration over 3D large pore zeolites, FAU and BEA. However, a sulfonated mesoporous catalyst (SO_3H-SBA-15) yielded ethyl levulinate as the main reaction product [170]. The disadvantage of this catalytic system was its low isomerization activity due to the low strength of the acid sites. As a result, ethyl levulinate was obtained only from fructose and, to a smaller extent, sucrose (a disaccharide consisting of fructose and glucose). On the other hand, glucose and cellobiose (a disaccharide consisting of two glucose molecules) yielded exclusively an etherification product, ethyl glucopyranoside [170].

Lactic acid is an important intermediate with a vast application potential [168,171]. Among other routes, it can be obtained by transformation of trioses and hexoses sugars over heterogeneous acidic catalysts, such as zeolites and related materials. A screening of zeolite catalysts (FAU, BEA, MOR, MFI) having different structural and acidic characteristics revealed that selectivity to lactic acid in conversion of triose sugars decreased with the increasing Si/Al ratio and increasing Brønsted acidity character [114,172]. It could be concluded that Lewis acidity is essential for highly selective transformation of trioses to lactic acid or lactates as is the choice of solvent; while water promoted degradation and side reactions in methanol the yields of methyl lactate exceeded 90% [114,172]. This was further confirmed by investigated different catalysts with BEA structure prepared by isomorphous substitution (Al, Si, Ti, Zr, Sn-BEA) [173]. Sn-BEA was superior to all the other catalysts indicating not only that solely Lewis acidity is needed for converting trioses to lactates, but also that strong Lewis acid sites are important [173]. On the other hand, Brønsted acid sites were shown to be responsible for the formation of acetals. Further substantiation of the role of different type of acid sites was obtained from different steaming of Al-BEA and Al-FAU zeolites that led to different distribution of Al (framework vs. extra-framework Al). It was suggested that only strong Brønsted acid sites afforded while weak Brønsted acid sites yielded together with Lewis acid sites alkyl lactates [172,173].

Obviously, the transformation pathways grow even more complex when hexoses are used instead of trioses. The essential challenge is the extent of side reactions leading to very low carbon balances of the experiments (in the range of 50–70%) [115]. In general, the absence of acid sites (Si-BEA) affords only partial dehydration, whereas Brønsted acidity promotes dehydration and formation of HMF and levulinic acid [116]. On the other hand, Lewis acidity (Sn-,Ti-, Zr-BEA) facilitates the retro-aldol condensation resulting in the formation of lactate, vinylglycolate and glycolaldehyde dimethyl acetal as the main identified products [115].

4. Conclusions and outlook

The present review highlights the existence of numerous analogies between the behavior of zeolites and other microporous materials in the processes of oil refining, petrochemistry and fine organic synthesis, on the one hand, and in the transformation of biomass and biomass-derived feedstocks, on the other hand. The influence of structural, textural and acid–base characteristics of zeolites on their activity and selectivity in the processing of renewable chemicals provides a broad possibility for studies and opportunities for new catalytic applications. Nonetheless, significant focused research effort is still needed to understand the role of the key parameters of microporous and mesoporous materials for the obtaining valuable products from renewable raw materials and address the main challenges that so far prevent industrial applications of these catalysts in biomass upgrading processes. Among the main challenges, the following ones need to be mentioned:

1. *Reactions in aqueous phase*. Many processes dealing with biomass upgrading and its transformation to platform chemicals proceed in water-containing medium, be it water used as solvent or water as one of the products. Therefore, it is of utmost importance to study catalytic properties of zeolites in the conversion of biomass-derived organic molecules not only in “ideal”, i.e. water-free conditions, but also in the presence of water, i.e. using relevant biomass-derived feedstocks.
2. *Deactivation of catalysts*. Many reactions of organic molecules result in zeolites gradually losing their activity due to the accumulation of non-desorbed compounds (coke) in their porous space. The examples of the present review show that the severe deactivation is observed in the case of the transformation of renewables. Therefore, the long-term stability of microporous catalysts in the reactions needs to be addressed, including studies on limiting the extent of coking reactions as well as on re-using the catalysts and restoring of their catalytic properties.
3. *Access of reactants to active sites and diffusion of reaction products*. Bulky molecules with complex structure and high molecular weight are of increased value. Therefore, the issues related to both the improved access of reagent molecules to active sites and easy removal of reaction products from catalyst surfaces are very

relevant. In this regard, the study of the properties of nano-sized or hierarchical materials, 2D zeolite-like materials, the influence of increased mesoporosity, etc., is one of the keys to unlocking the potential of micro- and mesoporous catalysts.

Intensification of studies in these (and other) fields can be expected in the next years leading to applications of microporous materials as catalysts for the obtaining valuable products from biomass-derived feedstocks. Obviously, that the unique properties of zeolites and related materials that have already found application in oil refining and petrochemistry, will be also in demand in new renewable-based technologies.

Acknowledgments

This publication is a result of project no. P106/12/G015 supported by the Czech Science Foundation which is being carried out in the UniCRE centre (CZ.1.05/2.1.00/03.0071) whose infrastructure was supported by the European Regional Development Fund and the state budget of the Czech Republic.

References

[1] J. Čejka, A. Corma, S.I. Zones, Zeolites and Catalysis: Synthesis, Reactions and Applications, Wiley-VCH, Weinheim, Germany, 2010.
[2] J. Čejka, H. van Bekkum, A. Corma, F. Schüth, Introduction to the Zeolites Science and Practice, Vol. 168, 3rd rev. ed, Elsevier, Amsterdam, The Netherlands, 2007.
[3] R. Staudt, M. Thommes, Zeolites: From Model Materials to Industrial Catalysts, Transworld Research Network, Kerala, 2009, pp. 207.
[4] G. Bellussi, A. Carati, R. Millini, Zeolites and Catalysis: Synthesis, Reactions and Applications, Wiley-VCH, Weinheim, Germany, 2010.
[5] M.S. Rigutto, R. van Veen, L. Huve, Stud. Surf. Sci. Catal. 168 (2007) 855–913.
[6] W.J. Roth, P. Nachtigall, R.E. Morris, P.S. Wheatley, V.R. Seymour, S.E. Ashbrook, P. Chlubná, L. Grajciar, M. Položij, A. Zukal, O. Shvets, J. Čejka, Nat. Chem. 5 (2013) 628–633.
[7] D.P. Serrano, J.M. Escola, P. Pizarro, Chem. Soc. Rev. 42 (2013) 4004–4035.
[8] M. Milina, S. Mitchell, P. Crivelli, D. Cooke, J. Pérez-Ramírez, Nat. Commun. 5 (2014) 3922.
[9] W.J. Roth, Stud. Surf. Sci. Catal. 168 (2007) 221–239.
[10] W.J. Roth, O.V. Shvets, M. Shamzhy, P. Chlubná, M. Kubů, P. Nachtigall, J. Čejka, J. Am. Chem. Soc. 133 (2011) 6130–6133.
[11] M. Opasenko, W. O'Neil Parker Jr., M. Shamzhy, E. Montanari, M. Bellettato, M. Mazur, R. Millini, J. Čejka, J. Am. Chem. Soc. 136 (2014) 2511–2519.
[12] F. Solânea, O. Ramos, K. Mendelssolm, H.O. de Pietre, Pastore, RSC Adv. 3 (2013) 2084–2111.
[13] W.J. Roth, P. Nachtigall, R.E. Morris, J. Čejka, Chem. Rev. 114 (2014) 4807–4837.
[14] Y. Li, J. Yu, Chem. Rev. (2014), http://dx.doi.org/10.1021/cr500010r.
[15] T.F. Degnan, Top. Catal. 13 (2000) 349–356.
[16] S.I. Zones, Micropor. Mesopor. Mater. 144 (2001) 1–8.
[17] D. Kubička, I. Kubičková, J. Čejka, Catal. Rev. Sci. Eng. 55 (2013) 1–78.
[18] C.T.-W. Chu, C.D. Chang, J. Phys. Chem. 89 (1985) 1569–1571.
[19] J.A. Rabo, G.C. Gajda, Catal. Rev. Sci. Eng. 31 (1989) 385–430.
[20] J. Weitkamp, M. Hunger, Stud. Surf. Sci. Catal. 168 (2007) 525–553.
[21] W.O. Haag, R.M. Lago, P.B. Weisz, Nature 309 (1984) 589–591.
[22] H. Stach, U. Lohse, H. Thamm, W. Schirmer, Zeolites 6 (1986) 74–90.
[23] A. Gola, B. Rebours, E. Milazzo, J. Lynch, E. Benazzi, S. Lacombe, L. Delevoye, C. Fernandez, Micropor. Mesopor. Mater. 40 (2000) 73–83.
[24] Y. Fan, X. Bao, X. Lin, G. Shi, H. Liu, J. Phys. Chem. B 110 (2006) 15411–15416.
[25] J.P. Marques, I. Gener, P. Ayrault, J.C. Bordado, J.M. Lopes, F.R. Ribeiro, M. Guisnet, Comptes Rendus Chim. 8 (2005) 399–410.
[26] M. Boveri, C. Márquez-Álvarez, M. Ángel Laborde, E. Sastre, Catal. Today 114 (2006) 217–225.
[27] R.A. Beyerlein, C. Choi-Feng, J.B. Hall, B.J. Huggins, G.J. Ray, Top. Catal. 4 (1997) 27–42.
[28] L.R. Aramburo, L. Karwacki, P. Cubillas, S. Asahina, D.A. de Winter, M.R. Drury, I.L. Buurmans, E. Stavitski, D. Mores, M. Daturi, P. Bazin, P. Dumas, F. Thibault-Starzyk, J.A. Post, M.W. Anderson, O. Terasaki, B.M. Weckhuysen, Chemistry 17 (2011) 13773–13781.
[29] J.C. Groen, J.A. Moulijn, J. Pérez-Ramírez, Micropor. Mesopor. Mater. 87 (2005) 153–161.
[30] C.T.W. Chu, C.D. Chang, J. Phys. Chem. 89 (1985) 1569–1571, R.C. Deka, N. Tajima, K. Hirao, J. Molec. Structure: Theochem 535 (2001) 31–38.
[31] J. Weitkamp, M. Hunger, Stud. Surf. Sci. Catal. 168 (2007) 787–835.
[32] Z. Kang, X. Zhang, H. Liu, J. Qiu, K.L. Yeung, Chem. Eng. J. 218 (2013) 425–432.
[33] N. Kasian, E. Verheyen, G. Vanbutsele, K. Houthoofd, T.I. Koranyi, J.A. Martens, C.E.A. Kirschhock, Micropor. Mesopor. Mater. 166 (2013) 153–160.
[34] W.J. Roth, C.T. Kresge, J.C. Vartuli, M.E. Leonowicz, A.S. Fung, S.B. McCullen, Stud. Surf. Sci. Catal. 94 (1995) 301–308.
[35] A. Corma, V. Fornés, J.M. Guil, S. Pergher, Th.L.M. Maesen, J.G. Buglass, Micropor. Mesopor. Mater. 38 (2000) 301–309.
[36] M.S. Holm, E. Taarning, K. Egeblad, C.H. Christensen, Catal. Today 168 (2011) 3–16.
[37] J. Čejka, S. Mintova, Catal. Rev. Sci. Eng. 49 (2007) 457–509.
[38] D. Verboekend, J. Perez-Ramirez, ChemSusChem 7 (2014) 753–764.
[39] W. Roth, J. Čejka, Catal. Sci. Technol. 1 (2011) 43–53.
[40] I. Batonneau-Gener, A. Yonli, S. Hazael-Pascal, J. Pedro Marques, J. Madeira Lopes, M. Guisnet, F. Ramôa Ribeiro, S. Mignard, Micropor. Mesopor. Mater. 110 (2008) 480–487.
[41] T. Mochida, R. Ohnishi, N. Horita, Y. Kamiya, T. Okuhara, Micropor. Mesopor. Mater. 101 (2007) 176–183.
[42] P.A. Zapata, Y. Huang, M.A. Gonzalez-Borja, D.E. Resasco, J. Catal. 308 (2013) 82–97.
[43] R.M. Ravenelle, F. Schüßler, A. D'Amico, N. Danilina, J.A. van Bokhoven, J.A. Lercher, C.W. Jones, C. Sievers, J. Phys. Chem. C 114 (2010) 19582–19595.
[44] W. Lutz, W. Gessner, R. Bertram, I. Pitsch, R. Fricke, Microporous Mater. 12 (1997) 131–139.
[45] W. Lutz, H. Toufar, R. Kurzhals, M. Suckow, J. Int. Adsorp. Soc. 11 (2005) 405–413.
[46] P.A. Zapata, J. Faria, M. Pilar Ruiz, R.E. Jentoft, D.E. Resasco, J. Am. Chem. Soc. 134 (2012) 8570–8578.
[47] M. Bejblová, D. Procházková, J. Čejka, ChemSusChem 2 (2009) 486–499.
[48] W. Vermeiren, J.-P. Gilson, Top. Catal. 52 (2009) 1131–1161.
[49] A. Corma, A. Martinez, Stud. Surf. Sci. Catal. 157 (2005) 337–366.
[50] A. Corma, V. Fornes, A. Martinez, F.V. Melo, O. Pallota, Stud. Surf. Sci. Catal. 37 (1988) 495–503.
[51] I. Kubičková, D. Kubička, Waste Biomass Valor. 1 (2010) 293–308.
[52] W. Huber, A. Corma, Angew. Chem. Int. Ed. 46 (2007) 7184–7201.
[53] A. Corma, V. Gonzalez-Alfaro, A.V. Orchillks, Appl. Catal. A: Gen. 129 (1995) 203–215.
[54] H. Konno, T. Okamura, T. Kawahara, Y. Nakasaka, T. Tago, T. Masud, Chem. Eng. J. 207–208 (2012) 490–496.
[55] F.A. Twaiq, A.R. Mohamed, S. Bhatia, Micropor. Mesopor. Mater. 64 (2003) 95–107.
[56] F.A. Twaiq, N. Asmawati, M. Zabidi, A.R. Mohamed, S. Bhatia, Fuel Process. Technol. 84 (2003) 105–120.
[57] Y.-S. Ooi, R. Zakaria, A.R. Mohamed, S. Bhatia, Energy Fuels 19 (2005) 736–743.
[58] D. Chen, N.I. Tracy, D.W. Crunkleton, G.L. Price, Appl. Catal. A: Gen. 384 (2010) 206–212.
[59] A. Corma, G.W. Huber, L. Sauvanaud, P. O'Connor, J. Catal. 247 (2007) 307–327.
[60] K. Bormann, H. Tilgner, H.J. Moll, Erdol Erdgas Kohle 109 (1993) 172–176.
[61] K. Bormann, H. Tilgner, Erdol Erdgas Kohle 110 (1994) 75–77.
[62] E.A. Stadlbauer, R. Altensen, S. Bojanowski, S. Donnevert, A. Fiedler, S. Hossain, J. Rossmanith, G. Schilling, Erdol Erdgas Kohle 122 (2006) 64–69.
[63] R. Černý, M. Kubů, D. Kubička, Catal. Today 204 (2013) 46–53.
[64] Y. He, S.E. Barnes, D.W. Crunkleton, G.L. Price, Fuel 96 (2012) 469–475.
[65] F.A.A. Twaiq, A.R. Mohamad, S. Bhatia, Fuel Process. Technol. 85 (2004) 1283–1300.
[66] Y.-S. Ooi, R. Zakaria, A.R. Mohamed, S.S. Bhatia, Appl. Catal. A Gen. 274 (2004) 15–23.
[67] N. Dahmen, 2nd Generation Synthetic Biofuels, in: Lurgi Biodiesel Conference, Potsdam 19-21.9.2007, 2007.
[68] R.P. Anex, A. Aden, F.K. Kazi, J. Fortman, R.M. Swanson, M.M. Wright, J.A. Satrio, R.C. Brown, D.E. Daugaard, A. Platon, G. Kothandaraman, D.D. Hsu, A. Dutta, Fuel 89 (2010) S29–S35.
[69] A.V. Bridgwater, Biomass Bioenergy 38 (2012) 68–94.
[70] T. Dickerson, J. Soria, Energies 6 (2013) 514–538.
[71] D.A. Bulushev, J.H.R. Ross, Catal. Today 171 (2011) 1–13.
[72] http://www.kior.com/
[73] A. Aho, N. Kumar, K. Eränen, T. Salmi, M. Hupa, D. Murzin, Fuel 87 (2008) 2493–2501.
[74] A. Aho, N. Kumar, A. Lashkul, K. Eränen, M. Ziolek, P. Decyk, T. Salmi, B. Holmbom, M. Hupa, D. Murzin, Fuel 89 (2010) 1992–2000.
[75] J. Adam, E. Antonakou, A. Lappas, M. Stöcker, M. Nilsen, A. Bouzga, J. Hustad, G. Oye, Micropor. Mesopor. Mater. 96 (2006) 93–101.
[76] E. Antonakou, A. Lappas, M. Nilsen, A. Bouzga, M. Stöcker, Fuel 85 (2006) 2202–2212.
[77] E. Iliopoulou, E.V. Antonakou, S. Karakoulia, I. Vasalos, A. Lappas, K. Triantafyllidis, Chem. Eng. J. 134 (2007) 51–57.
[78] K. Triantafyllidis, E. Iliopoulou, E.V. Antonakou, A. Lappas, H. Wang, T. Pinnavaia, Micropor. Mesopor. Mater. 99 (2007) 132–139.
[79] P. Williams, P. Horne, Fuel 74 (1995) 1839–1851.
[80] T.R. Carlson, G.A. Tompsett, W.C. Conner, G.W. Huber, Top. Catal. 52 (2009) 241–252.
[81] T.R. Carlson, J. Jae, Y.-C. Lin, G.A. Tompsett, G.W. Huber, J. Catal. 270 (2010) 110–124.
[82] J. Jae, G.A. Tompsett, A.J. Foster, K.D. Hammond, S.M. Auerbach, R.F. Lobo, G.W. Huber, J. Catal. 279 (2011) 257–268.
[83] Y.-T. Cheng, Z. Wang, C.J. Gilbert, W. Fan, G.W. Huber, Angew. Chem. Int. Ed. 51 (2012) 11097–11100.
[84] Y.-T. Cheng, J. Jae, J. Shi, W. Fan, G.W. Huber, Angew. Chem. Int. Ed. 51 (2012) 1387–1390.

[85] T.R. Carlson, Y.-T. Cheng, J. Jae, G.W. Huber, Energy Environ. Sci. 4 (2011) 145–161.
[86] P.S. Rezaei, H. Shafaghat, W.M. Ashri, W. Daud, Appl. Catal. A: Gen. 469 (2014) 490–511.
[87] S.J. Miller, Stud. Surf. Sci. Catal. 84 (1994) 2319–2326.
[88] V.T. Nghiem, G. Sapaly, P. Mériaudeau, C. Naccache, Topics Catal. 14 (2001) 131–138.
[89] J.A. Martens, R. Parton, L. Uytterhoeven, P.A. Jacobs, G.F. Froment, Appl. Catal. 76 (1991) 95–116.
[90] W. Huybrechts, J.W. Thybault, B.R. De Waele, G. Vanbutsele, K.J. Houthoofd, F. Bertinchamps, J.F.M. Denayer, E.M. Gaigneaux, G.B. Marin, G.V. Baron, P.A. Jacobs, J.A. Martens, J. Catal. 239 (2006) 451–459.
[91] T.M. Sankaranarayanan, M. Banu, A. Pandurangan, S. Sivasanker, Bioresource Technol. 102 (2011) 10717–10723.
[92] L.B. Galperin, S.A. Bradley, T.M. Mezza, Appl. Catal. A: Gen. 219 (2001) 79–88.
[93] T.F. Degnam, C.R. Kennedy, AlChE J. 39 (1993) 607–614.
[94] T.J. McCarthy, G.-D. Lei, W.M.H. Sachtler, J. Catal. 159 (1996) 90–98.
[95] M. Höchtl, A. Jentys, H. Vinek, J. Catal. 190 (2000) 419–432.
[96] R. Sotelo-Boyas, Y. Liu, T. Minowa, Ind. Eng. Chem. Res. 50 (2011) 2791–2799.
[97] D. Verma, R. Kumar, B.S. Rana, A.K. Sinha, Energy Environ. Sci. 4 (2011) 1667–1671.
[98] S.J. Miller, Micropor. Mater. 2 (1994) 439–449.
[99] V.T. Nghiem, G. Sapaly, P. Mériaudeau, C. Naccache, Top. Catal. 14 (2001) 131–138.
[100] K.-C. Park, S.-K. Ihm, Appl. Catal. A: Gen. 203 (2000) 201–209.
[101] T. Blasco, A. Chica, A. Corma, W.J. Murphy, J. Agundez-Rodriguez, J. Perez Pariente, J. Catal. 242 (2006) 153–161.
[102] M. Herskowitz, M.V. Landau, I. Reizner, M. Kaliya, Production of diesel fuel from vegetable and animal oil, US Patent 2006/0207116 (2006).
[103] M. Herskowitz Reaction system for production of diesel fuel from vegetable and animals oils, US Patent 2008/066374 (2008).
[104] M. Herskowitz, M.V. Landau, I. Reizner, Diesel fuel from vegetable and animal oils blended with alkyl levulinates, WO 2010/106536 A1 (2010).
[105] M. Herskowitz, M.V. Landau, Y. Reizner, D. Berger, Fuel 111 (2013) 157–164.
[106] C. Wang, Z. Tian, L. Wang, R. Xu, Q. Liu, W. Qu, H. Ma, B. Wang, ChemSusChem 5 (2012) 1974–1983.
[107] N. Chen, S. Gong, H. Shirai, T. Watanabe, E.W. Qian, Appl. Catal. A: Gen. 466 (2013) 105–115.
[108] O.V. Kikhtyanin, A.E. Rubanov, A.B. Ayupov, G.V. Echevsky, Fuel 89 (2010) 3085–3092.
[109] M.Yu. Smirnova, O.V. Kikhtyanin, A.E. Rubanov, L.I. Trusov, G.V. Echevskii, Catal. Ind. 5 (2013) 253–259.
[110] A.A. Rosatella, S.P. Simeonov, R.F.M. Frade, C.A.M. Afonso, Green Chem. 13 (2011) 754–793.
[111] R. Otomo, T. Yokoi, J.N. Kondo, T. Tatsumi, Appl. Cat. A: Gen. 470 (2014) 318–326.
[112] C. Moreau, R. Durand, S. Razigade, J. Duhamet, P. Faugeras, P. Rivalier, P. Ros, G. Avignon, Appl. Cat. A: Gen. 145 (1996) 211–224.
[113] S. Saravanamurugan, M. Paniagua, J.A. Melero, A. Riisager, J. Am. Chem. Soc. 135 (2013) 5246–5249.
[114] R.M. West, M.S. Holm, S. Saravanamurugan, J. Xiong, Z. Beversdorf, E. Taarning, C.H. Christensen, J. Catal. 269 (2010) 122–130.
[115] M.S. Holm, Y.J. Pagán-Torres, S. Saravanamurugan, A. Riisager, J.A. Dumesic, E. Taarning, Green Chem. 14 (2012) 702–706.
[116] M.S. Holm, S. Saravanamurugan, E. Taarning, Science 328 (2010) 602–605.
[117] D.S. Kemp, V. Frank, Organic Chemistry, Worth Publishers, 1980, pp. 839–845.
[118] R.T. Morrison, R.N. Boyd, Organic Chemistry, Prentice-Hall, Englewood Cliffs, NJ, 1992, Chapter 21.
[119] H. van Bekkum, H.W. Kouwenhoven, Stud. Surf. Sci. Catal. 157 (2005) 311–336.
[120] H. van Bekkum, H.W. Kouwenhoven, Stud. Surf. Sci. Catal. 168 (2007) 947–998.
[121] J. Klisáková, L. Červený, J. Čejka, Appl. Catal. A: Gen. 272 (2004) 79–86.
[122] P. Andy, J. Garcia-Martinez, G. Lee, H. Gonzalez, C.W. Jones, M.E. Davis, J. Catal. 192 (2000) 215–223.
[123] P. Moreau, A. Finiels, P. Meric, F. Fajula, Catal. Lett. 85 (2003) 199–203.
[124] K. Bauer, D. Garbe, H. Surburg, Common Fragrance and Flavor Materials, Wiley-VCH, Weinheim, 2001.
[125] P. Metivier, in: R.A. Sheldon, H. Van Bekkum (Eds.), Fine Chemicals through Heterogeneous Catalysis, Wiley-VCH, Weinheim, 2001, p. 161.
[126] M. Guisnet, M. Guidotti, in: E.G. Derouane (Ed.), Catalysts for Fine Chemicals Synthesis—Microporous and Mesoporous Solid Catalysts, Vol. 4, Wiley, West Sussex, 2006.
[127] P.J. Kunkeler, J.C. van der Waal, J. Bremmer, B.J. Zuurdeeg, R.S. Downing, H. van Bekkum, Catal. Lett. 53 (1998) 135–138.
[128] A. Corma, S. Iborra, M. Mifsud, M. Renz, M. Susarte, Adv. Synth. Catal. 346 (2004) 257–262.
[129] M. Boronat, A. Corma, M. Renz, G. Sastre, P.M. Viruela, Chem. Eur. J. 11 (2005) 6905–6915.
[130] C.O. Veloso, C.A. Henriques, A.G. Dias, J.L.F. Monteiro, Catal. Today 107–108 (2005) 294–301.
[131] F. Lin, Y. Chin, J. Catal. 311 (2014) 244–256.
[132] Y.I. Isakov, Kh.M. Minachev, N.Y. Usachev, Izv. Akad. Nauk SSSR, Ser. Khim 5 (1972) 1175.
[133] Y.I. Isakov, N.Ya. Usachev, T.A. Isakova, Kh. Minachev, Izv. Akad. Nauk SSSR, Ser. Khim. (1985) 1965.
[134] P.T. Wierzchowski, L.W. Zatorski, Catal. Lett. 9 (1991) 411–414.
[135] E.J. Rode, P.E. Gee, L.N. Marquez, T. Uemura, M. Bazargani, Catal. Lett. 9 (1991) 103–113.
[136] Y.-C. Chang, A.-N. Ko, Appl. Catal. A: Gen. 190 (2000) 149–155.
[137] S.K. Sharma, P.A. Parikh, R.V. Jasra, J. Mol. Catal. A: Chem. 278 (2007) 135–144.
[138] J. Li, J. Tai, R.J. Davis, Catal. Today 116 (2006) 226–233.
[139] T. Komatsu, M. Mitsuhashi, T. Yashima, Stud. Surf. Sci. Catal. 142 (2002) 667–674.
[140] E. Dumitriu, V. Hulea, I. Fechete, A. Auroux, J.-F. Lacaze, C. Guimon, Micropor. Mesopor. Mater. 43 (2001) 341–359.
[141] C.O. Veloso, J.L.F. Monteiroa, E.F. Sousa-Aguiar, Stud. Surf. Sci. Catal. 84 (1994) 1913–1920.
[142] T. Tago, H. Konno, S. Ikeda, S. Yamazaki, W. Ninomiya, Y. Nakasaka, T. Masuda, Catal. Today 164 (2011) 158–162.
[143] T. Tago, H. Konno, M. Sakamoto, Y. Nakasaka, T. Masuda, Appl. Catal. A: Gen. 403 (2011) 183–191.
[144] A.J. Cruz-Cabeza, D. Esquivel, C. Jiménez-Sanchidrián, F.J. Romero-Salguero, Materials 5 (2012) 121–134.
[145] C. Flego, C. Perego, Appl. Catal. A: Gen. 192 (2000) 317–329.
[146] J.F. Knifton, P.S.E. Dai, Catal. Lett. 57 (1999) 193–197.
[147] T.W. Jesse, T.C. Ezeji, N. Qureshi, H.P. Blaschek, J. Ind. Microbiol. Biotechnol. 29 (2002) 117–123.
[148] T. Nishiguchi, T. Matsumoto, H. Kanai, K. Utani, Y. Matsumura, W.-J. Shen, S. Imamura, Appl. Catal. A: Gen. 279 (2005) 273–277.
[149] A.G. Gayubo, A.T. Aguayo, A. Atutxa, R. Aguado, M. Olazar, J. Bilbao, Ind. Eng. Chem. Res. 43 (2004) 2619–3262.
[150] S.D. Stefanidis, K.G. Kalogiannis, E.F. Iliopoulou, A.A. Lappas, P.A. Pilavachi, Bioresour. Technol. 102 (2011) 8261–8267.
[151] E. Fumoto, Y. Mizutani, T. Tago, T. Masuda, Appl. Catal. B: Environ. 68 (2006) 154–159.
[152] S. Funai, Y. Satoh, K. Tajima, T. Tago, T. Masuda, Top. Catal. 53 (2010) 654–658.
[153] S. Funai, T. Tago, T. Masuda, Catal. Today 164 (2011) 443–446.
[154] A.G. Panov, J.J. Fripiat, J. Catal. 178 (1998) 188–197.
[155] G.J. Hutchings, P. Johnston, D.F. Lee, C.D. Williams, Catal. Lett. 21 (1993) 49–53.
[156] D. Esquivel, A.J. Cruz-Cabeza, C. Jiménez-Sanchidrián, F.J. Romero-Salguero, Micropor. Mesopor. Mater. 142 (2011) 672–679.
[157] J. Bozell, G. Petersen, Green Chem. 12 (2010) 539–554.
[158] A. Corma, S. Iborra, A. Velty, Chem. Rev. 107 (2007) 2411–2502.
[159] P. Mäki-Arvela, B. Holmbom, T. Salmi, D. Murzin, Catal. Rev. Sci. Eng. 49 (2007) 197–340.
[160] E. Taarning, C. Osmundsen, X. Yang, B. Voss, S. Andersen, C. Christensen, Energ. Environ. Sci. 4 (2011) 793–804.
[161] M.J. Climent, A. Corma, S. Iborra, Green Chem. 13 (2011) 520–540.
[162] L. Faba, E. Díaz, S. Ordóñez, Appl. Catal. B: Environ. 142–143 (2013) 387–395.
[163] L. Hora, V. Kelbichová, O. Kikhtyanin, O. Bortnovskiy, D. Kubička, Catal. Today 223 (2014) 138–147.
[164] L. Hora, O. Kikhtyanin, L. Čapek, O. Bortnovskiy, D. Kubička, Catal. Today (2014), http://dx.doi.org/10.1016/j.cattod.2014.03.010.
[165] W. Shen, G.A. Tompsett, K.D. Hammond, R. Xing, F. Dogan, C.P. Grey, W.C. Conner Jr., S.M. Auerbacha, G.W. Huber, Appl. Catal. A: Gen. 392 (2011) 57–68.
[166] O. Kikhtyanin, V. Kelbichová, D. Vitvarová, M. Kubů, D. Kubička, Catal. Today 227 (2014) 154–162.
[167] O. Kikhtyanin, P. Chlubná, T. Jindrová, D. Kubička, Dalton Trans. 43 (2014) 10628–10641.
[168] P. Mäki-Arvela, I.L. Simakova, T. Salmi, D. Yu, Murzin, Chem. Rev. 114 (2014) 1909–1971.
[169] C. Moreau, R. Durand, D. Peyron, J. Duhamet, P. Rivalier, Ind. Crops Products 7 (1998) 95–99.
[170] S. Saravanamurugan, A. Riisager, Catal. Commun. 17 (2012) 71–75.
[171] M. Dusselier, T. Van Wouve, A. Dewaele, E. Makshina, B.F. Sels, Energy Environ. Sci. 6 (2013) 1415–1442.
[172] P. Pescarmona, K.P.F. Janssen, C. Delaet, C. Stroobants, K. Houtboofd, A. Philippaerts, C. De Jonghe, J.P. Paul, P.A. Jacobs, B.F. Sels, Green Chem. 12 (2010) 1083–1089.
[173] E. Taarning, S. Saravanamurugan, M.S. Holm, J. Xiong, R.M. West, C.H. Christensen, ChemSusChem 2 (2009) 625–627.

WILEY-VCH

Edited by Mark Crocker and
Eduardo Santillan-Jimenez

Chemical Catalysts for Biomass Upgrading

11

Upgrading of Lipids to Hydrocarbon Fuels via (Hydro)deoxygenation

David Kubička

University of Chemistry and Technology Prague, Technopark Kralupy, Žižkova 7, 278 01 Kralupy nad Vltavou, Czech Republic

In memoriam of Professor Victor Teixeira da Silva, an outstanding scientist and friend.

11.1 Introduction

Production of hydrocarbon fuels relies on the upgrading of various feedstocks with the aim to remove heteroatoms – such as sulfur, nitrogen, and oxygen – and to modify their molecular structure to improve their fuel properties. In traditional (petroleum-based) refineries, hydrodesulfurization (HDS) is the key upgrading operation that ensures environmental acceptability of the fuels due to (i) elimination of SO_x emissions and (ii) protection of catalysts in the exhaust gas converters allowing efficient abatement of pollutants including unburned hydrocarbons, carbon monoxide, and NO_x. While deoxygenation is not a concern when upgrading petroleum distillate fractions, it is of the utmost importance in the upgrading of biomass-derived feedstocks, which typically contain at least 10 wt% of organically bound oxygen. However, deoxygenation is not driven by environmental concerns; rather, it aims at improving the thermochemical stability of fuels and increasing their energy content.

Recent efforts aimed at minimizing the impacts of fossil fuels in the environment – mainly due to the increase in atmospheric CO_2 concentration resulting from fossil fuel combustion – have encouraged worldwide research of biofuels, i.e. renewable (biomass-derived) transportation fuels. Biofuels are generally classified into three generations: the first generation relies on food crops and includes bioethanol from sugar and starch plants as well as biodiesel derived from edible vegetable oils; the second generation is produced from lignocellulosic feedstocks as well as from nonedible oils and waste oils and fats; and the third generation is based on aquatic biomass (e.g. algae). The current shift toward the second- and the third-generation biofuels, as mandated by the proposed RED II directive [1], for instance, enhances the importance of deoxygenation as a robust, versatile technology capable of dealing with a wide variety of feedstocks.

Chemical Catalysts for Biomass Upgrading, First Edition. Edited by Mark Crocker and Eduardo Santillan-Jimenez.

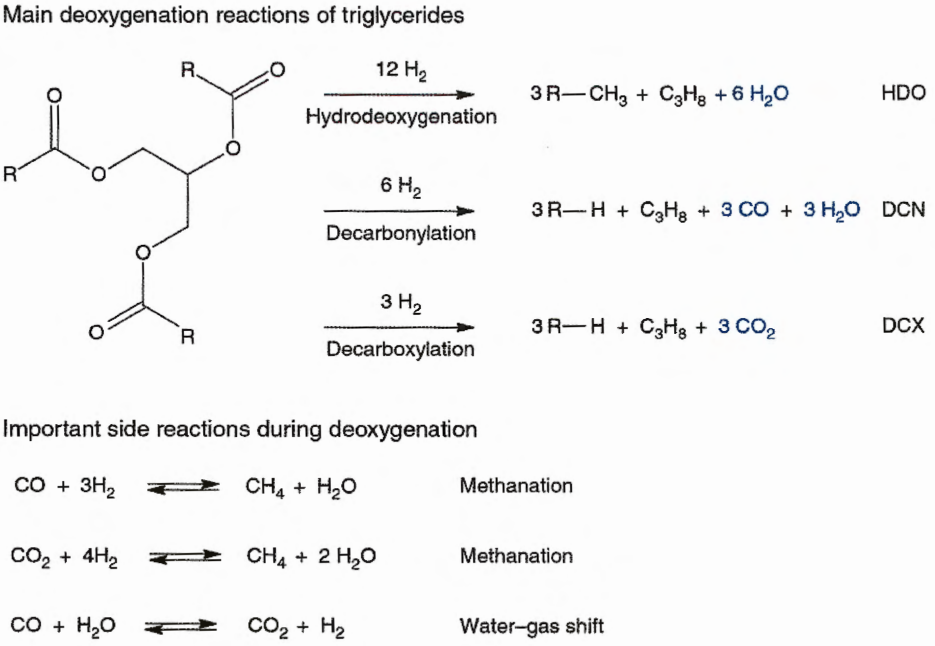

Figure 11.1 Main deoxygenation reactions and important parallel reactions.

Deoxygenation encompasses four main different types of chemical reactions that take place under reducing conditions – namely, hydrodeoxygenation (HDO), dehydration, decarbonylation (DCN), and decarboxylation (DCX) – ultimately resulting in three main oxygen-containing products, i.e. water, carbon monoxide, and carbon dioxide (Figure 11.1). In addition, other products (such as alcohols) originating from demethoxylation or hydrogenolysis reactions involving ethers and esters, respectively, could be considered as deoxygenation products as well. This makes the deoxygenation chemistry more complex than that of HDS and hydrodenitrification (HDN), which under reducing conditions yield hydrogen sulfide and ammonia, respectively, as the only heteroatom-containing by-products. Obviously, the rich chemistry of deoxygenation has its origins in the complex composition of biomass; however, even relatively simple oxygenates, such as triglycerides (TGs), can undergo a wide range of deoxygenation reactions depending on the catalyst and reaction conditions employed.

Although deoxygenation can be applied to any feedstock containing oxygenates and much attention is currently focused on the deoxygenation of bio-oils – i.e. organic liquids produced by fast pyrolysis of particularly lignocellulosic biomass – the deoxygenation of lipids and lipid-derived feedstocks (mainly comprising TGs and free fatty acids [FFAs]) has already been implemented at industrial scale and is currently the prevailing application of deoxygenation processes. This is a consequence of (i) their well-defined and constant structure and composition and (ii) the possibility to convert the lipids rather easily into hydrocarbon mixtures with superior fuel properties. Therefore, the focus of this chapter will be on the chemistry of deoxygenation and on deoxygenation catalysts using TGs and other lipid-based feedstocks as a model system. Additional details can be found in several reviews published in the last decade [2–10].

11.2 Feedstocks

TGs, which are esters of three fatty acid molecules and a glycerol molecule, are the main constituents of vegetable oils and animal fats together with minor amounts of other components such as phospholipids and tocopherols. The fatty acid moieties present in the most abundantly produced vegetable oils, i.e. palm, soybean, rapeseed (canola), and sunflower oil, are typically between 14 and 22 carbon atoms (C_{16} and C_{18} being the most prevalent ones) in length. Similarly, C_{16} and C_{18} fatty acid chains are the most abundant in the TGs making up animal fats, such as beef tallow, pork lard, and chicken fat [11]. The global annual production of vegetable oils and animal fats has more than doubled in the last 20 years and is currently nearly 200 MMt [12]. The production of animal fats is estimated to be about 14% of the total oil and fat production [11], i.e. ca. 30 Mt. Recently, algal oils have attracted enormous attention due to their remarkable potential, which stems from their superior annual productivity per unit area in comparison with vegetable oils (>50 t/ha for algal oil [13] vs. 3.5–5 t/ha for palm oil [14] and <1 t/ha for other vegetable oils [14]) and the prospect of using nonagricultural land. Other TG feedstocks include used or waste cooking oils and nonedible vegetable oils, such as Jatropha oil. Side-streams from vegetable oil or wood processing (e.g. crude tall oils), which contain significant concentrations of FFAs, can be used as feedstocks to produce fuels as well.

TGs mainly consist of either unsaturated fatty acid moieties (in the case of oils) or saturated fatty acid moieties (in the case of fats), which affects their stability during deoxygenation in the presence of hydrogen as cyclization reactions may occur [15] as well as the overall hydrogen consumption. The overall chain length of the fatty acid moieties (C_{14}–C_{22}) is particularly suitable to produce diesel and/or kerosene fuels that consist of hydrocarbons comprising between 10 and 20 carbon atoms.

The suitable carbon–carbon chain lengths together with their relatively uniform reactivity, absence of water, easy storage and handling, and straightforward production by physical and/or chemical extraction are the salient advantages of TGs over other biomass-derived raw materials, such as bio-oils. Direct conversion of TGs via transesterification has been used to produce fatty acids methyl esters (FAMEs) or biodiesel, mainly because of the ability of the latter to be mixed with (or replace) hydrocarbon fuels [16]. This simple technology allows the processing of highly purified nonacidic feedstocks [16] to afford first-generation biofuels, waste streams being much more difficult to upgrade through biodiesel production. In contrast, deoxygenation technologies can deal not only with waste TG-based feedstocks but also with feeds with high concentrations (or made exclusively) of FFAs, i.e. virtually any lipid-based feedstock can be upgraded by deoxygenation to hydrocarbon fuels. Moreover, sustainability data (in terms of the overall greenhouse gas emissions savings) demonstrate that deoxygenation is a more favorable conversion pathway from an environmental standpoint than transesterification [17].

Finally, the quality of the final biofuel has to be considered as well. Biodiesel can certainly serve as a biofuel, but it has to either be blended with diesel (current EU limit is maximum 7 vol%) to be used as mixed biodiesel–diesel fuel in unmodified vehicles or be used in engines purposely designed or modified to employ neat (100%) biodiesel. Indeed, these fuels usually require adaptations to be made to engine systems. Moreover, due to the oxygen content and unsaturation of most alkyl chains within FAMEs, the chemical, thermal, and oxidative stability as well as the energy content are lower for biodiesel than for diesel fuel [6]. In contrast, hydrocarbons obtained via deoxygenation of TGs are fully compatible with diesel fuel and diesel fuel-based infrastructure and even superior to petroleum-derived diesel as their combustion produces less harmful emissions (due to the absence of aromatics and sulfur).

11.3 Chemistry

Although the structure of TGs is fairly simple, depending on the deoxygenation reaction conditions and the catalyst employed, they are susceptible to a surprisingly wide variety of conversion pathways. The rudimentary differentiation of deoxygenation routes is based on their primary oxygen-containing product lacking an alkyl chain, i.e. inorganic oxygenates. There are three such products: water, carbon monoxide, and carbon dioxide. When carbon oxides are formed, the resulting hydrocarbons have one carbon atom less than the original fatty acid moieties. Since natural oils and fats exclusively contain fatty acid moieties with even carbon number, the resulting hydrocarbons are characterized by an odd carbon number. Depending on the nature of the carbon oxide, the process is called DCN, yielding CO, or DCX, producing CO_2 (Figure 11.1). On the other hand, the formation of water is not accompanied by a carbon atom loss from the original fatty acid moiety, and thus, the hydrocarbons formed have an even number of carbons. HDO and dehydration are the possible reactions affording water, dehydration applying only to the alcohols produced via the stepwise HDO of esters and acids. It should be noted that under hydrotreating conditions, the hydrogenation of carbon oxides may also take place, yielding additional water and methane (Figure 11.1). This intertwined nature of conversion pathways makes the exact evaluation of the underlying chemistry challenging. Also, the formation of water and carbon oxides may inhibit the catalyst performance, e.g. CO is well known as a potent catalyst poison. Finally, the reaction pathway followed has an important effect on the overall hydrogen consumption.

A closer look at the conversion of TGs under hydrotreating conditions reveals that their transformation to hydrocarbons consists of several consecutive and parallel reactions. The most facile reaction in the presence of hydrogen is the saturation of the double bonds. Most studies show that the key intermediate in the deoxygenation of TGs are fatty acids that can be formed either via hydrogenolysis or hydrolysis. This justifies the use of fatty acids as model compounds, albeit the reactivity of the acids has been shown to be lower than that of esters [18]. Considering the absence of water in the feedstocks as well as the mild acidity (if any) of the catalysts employed, hydrogenolysis rather than hydrolysis represents the main reaction through which TGs are converted to fatty acids along the pathway toward hydrocarbons. In principle, the carbon–oxygen bond in esters can be cleaved either in the alpha or beta position with respect to the carboxylic group. Nevertheless, cleavage in the alpha position is not very common, albeit it does take place under rather harsh conditions (>15 MPa) over bimetallic formulations such as CuCr, ZnCr, or CuZn. In fact, the industrial production of a wide range of alcohols, such as fatty acid alcohols or hexanediol, relies on the use of the Adkins catalyst (CuCr) [19]. However, these catalysts are not very active (if at all) in deoxygenation. Thus, hydrogenolysis in the beta position ultimately yielding three fatty acid molecules and propane precedes the actual deoxygenation, as oxygen is not released from the organic molecules during hydrogenolysis. Plausible intermediates of this pathway, including propylstearate and propanediol distearate, have been identified among the reaction products at low conversions [20–22]. Since diglycerides have also been observed [10, 23, 24], hydrolysis may also take place to some extent.

Subsequently, actual deoxygenation proceeds either via DCX, DCN, or HDO, the reaction(s) followed depending both on the catalyst and the reaction conditions applied. DCX/DCN was shown to be favored over group 10 metals (Ni, Pt, Pd), while molybdenum or tungsten-based catalysts (Mo_2C, MoS_2, sulfided NiMo, CoMo, NiW) predominantly promote HDO [25]. Although sulfided catalysts can be generally regarded as selective toward the HDO pathway [25], the selectivity patterns over sulfides are rather complex, NiS being selective to DCX/DCN [20] and sulfided NiW allowing the tuning of the HDO/(DCX + DCN) products ratio by adjusting reaction conditions (particularly hydrogen pressure and, to a lesser extent, reaction temperature) [26]. Indeed, when decreasing the hydrogen pressure from 7 MPa to just 0.7 MPa, the HDO/(DCX + DCN) ratio dropped from ca. 3 to about 0.3 over a sulfided NiW catalyst at 280 °C [26]. As mentioned earlier, FFAs are typical intermediates of both reaction pathways that are often accompanied by alcohols and fatty acid esters [6, 25]. Aldehydes, which constitute other likely intermediates, were observed scarcely [25], plausibly because aldehydes and ketones are the most reactive oxygenates under deoxygenation conditions in general and hydrotreating conditions in particular [27].

Frequently, two or more of the aforementioned pathways may occur simultaneously, which makes the elucidation of the complete transformation scheme complex and challenging (see Figure 11.2). In general, DCX is favored by lower pressure and higher reaction temperature, while HDO is operative at lower reaction temperatures and higher hydrogen pressures. The DCN pathway was shown to be effective when a suitable enol-keto tautomerization equilibrium is established under the reaction conditions. While DCX produces simply carbon dioxide and a hydrocarbon, there are several oxygenated intermediates along the HDO pathway. These include an aldehyde, i.e. the first partial hydrogenation/deoxygenation product that is successively reduced to an alcohol, which in turn represents the second partial hydrogenation/deoxygenation product.

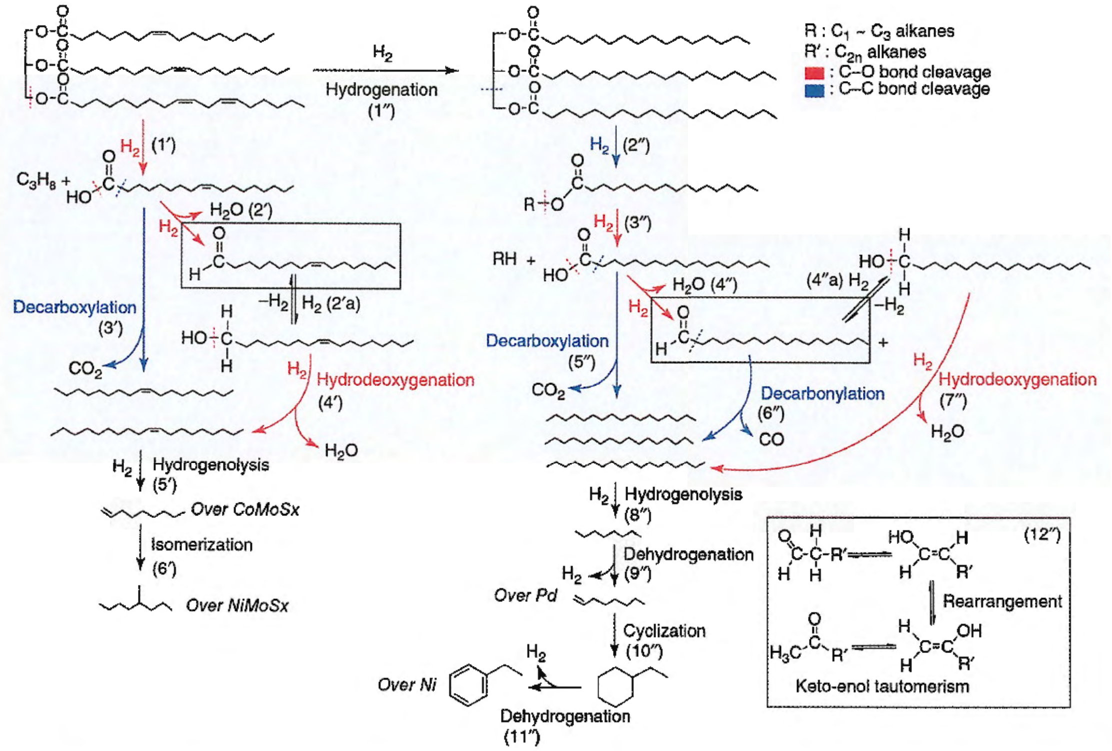

Figure 11.2 Detailed reaction scheme for the deoxygenation pathways of triglycerides. Source: Reprinted with permission from Kim et al. 2014 [28]. Copyri
2014, Elsevier.

The formation of these organic products is accompanied by formation of water. Finally, the alcohol is dehydrated/hydrodeoxygenated to produce a hydrocarbon and an additional water molecule. In addition, the fatty alcohol can also react with a fatty acid to yield a fatty ester and water. Strictly speaking, this esterification can also be considered a deoxygenation reaction. Under specific reaction condition, fatty esters can be produced in yields exceeding 30 wt% [29].

Ultimately, liquid phase hydrocarbons can be obtained from TGs in 81–85 wt% yield, depending on whether the selective DCX (affording the lower yield value) or the HDO pathway is operative. The other final products include propane (5 wt%) and either CO_2 (15 wt%) or water (12 wt%). It should be noted that all yield calculations are based on the complete conversion of tristearin to hydrocarbons, propane, and the primary deoxygenation product while also assuming that CO_2 is not hydrogenated. Consequently, hydrogen consumption ranges from 1 to 3 wt%, which is in the same order of magnitude as hydrogen consumption in hydrocracking and approximately an order of magnitude higher than hydrogen consumption in conventional hydrotreating. This shows that HDO is a hydrogen-intensive process; however, it also implies that by a proper choice of catalyst and/or reaction conditions, significant savings can be achieved. In particular, close attention has to be paid to controlling the successive hydrogenation of the primary CO_2 or CO to methane. Hence, two main selective deoxygenation alternatives have been widely studied: deoxygenation in the presence of H_2 and deoxygenation in the absence of H_2 [25].

In addition, deoxygenation can also be achieved via cracking, often using zeolites as catalysts. The topic has attracted great attention as hydrogen is not needed. However, this route is highly unselective and produces a wide range of hydrocarbons and shorter oxygenates [6, 25], while the catalysts, typically zeolites, have to be frequently reactivated by burning off the coke deposits. Moreover, the wide molecular weight range of the hydrocarbon products, many of which fall outside of the targeted kerosene/diesel fuel range, is undesired. Therefore, this transformation path is outside of the scope of this chapter. Due to the very close relationship between the catalyst nature and the observed product distribution, specific details of deoxygenation reaction pathways will be presented in the succeeding text as part of a discussion of different catalytic systems.

FFAs, fatty acid esters, and specific TGs are generally used as model compounds to represent vegetable oils in deoxygenation studies. Based on an extensive literature review, Gosselink et al. [25] have concluded that while all of them are suitable model compounds for deoxygenation in the presence of hydrogen, FFAs and fatty acid esters are inappropriate model systems for deoxygenation in absence of hydrogen. Furthermore, in order to suppress undesired side reactions (e.g. cracking and coking), the use of hydrogen during deoxygenation has been deemed necessary [25].

11.4 Technologies

The industrial application of a process dedicated to the transformation of TGs into superior quality kerosene and diesel fuel components has been pioneered by the Finnish refining company Neste Oyj. The process is known as NEXBTL, and there are currently four installations, two at the refinery in Porvoo, Finland (210 kt/yr each); one in Rotterdam, The Netherlands (1000 kt/yr); and one in Singapore (1000 kt/yr). The first unit was built in Porvoo in 2007 and the last one (to date) in Rotterdam in 2011. Nowadays, a diesel fuel produced solely by the NEXBTL technology is marketed in Finland as "Neste MY Renewable Diesel." An alternative process, called Ecofining™, was developed by ENI in collaboration with Honeywell-UOP. Since 2013, three commercial units have been installed, one in Norco, USA (500 kt/yr currently being expanded to 900 kt/yr); one in Venice, Italy (375 kt/yr with a second unit in progress); and one in Paramount, USA (125 kt/yr with focus on green jet fuel) [30]. The Finnish company UPM started producing a renewable diesel, called BioVerno, from crude tall oil in its biorefinery in Lapeenranta, Finland (ca. 100 kt/yr) in 2015 [31]. Finally, the refining company Total announced in 2015 the construction of the first industrial version of the Vegan™ process developed by Axens with a renewable diesel production capacity of 500 kt/yr, start-up being expected in 2018 [32]. There are also other potential producers of renewable diesel, such as the Canadian SBI Bioenergy Inc., which has signed an agreement with Shell [33], or the Finnish St1 Nordic Oy, which announced it intends to start renewable diesel production by 2020 [34]. These industrial developments over the past decade demonstrate not only the potential of renewable diesel technologies but also their technical and economic viability.

Apart from the UPM hydrotreatment process that uses exclusively crude tall oil, other technologies rely on the use of a variety of TG-containing feedstocks that allows for more flexibility. Notably, there is a clear strategy on the part of all producers to reduce the carbon footprint of their renewable diesel technologies by relying mostly on waste-based feedstocks, such as waste cooking oils, residual oils, waste fats, etc. For instance, the feeds for the NEXBTL technology consisted of >60% wastes and residues as far back as 2014. Obviously, feed pretreatment and quality control play a crucial role. As the general scheme of industrial deoxygenation technologies is rather similar, the concept will be demonstrated here using the NEXBTL process as an example. After removing the undesired impurities, such as phosphorus as well as alkali and alkaline earth metals, the feedstock enters the hydrotreating reactor where deoxygenation takes place at 300–350 °C and 5 MPa of hydrogen pressure over a sulfided catalyst [35]. The liquid hydrocarbon product stream from the hydrotreating reactor then enters the second-stage reactor where hydroisomerization takes place at 300–350 °C and 4 MPa of hydrogen pressure to convert the *n*-alkanes formed in the deoxygenation stage into *iso*-alkanes with better fuel properties. Specifically, the cold flow properties are considerably improved. Also, by adjusting the reaction conditions in the second stage, mild hydrocracking instead of selective hydroisomerization may take place, thus producing renewable kerosene. Recently, Neste announced that it has started to commercially produce bio-propane, i.e. the by-product of TG deoxygenation, at its facility in Rotterdam, The Netherlands (40 kt/yr) [36].

In addition, aiming at reducing investment costs, coprocessing TG-based feedstocks with petroleum feeds in existing hydrotreating units has gained significant attention. A commercial technology, called H-BIO, was developed by Petrobras over a decade ago. However, despite having been industrially tested at six refineries, it appears not to be currently employed and FAMEs biodiesel is used as the biocomponent in diesel blends [37]. Another coprocessing technology using tall oil as the renewable feed has been installed in the Preem Gothenburg refinery using a catalytic system developed by Haldor-Topsoe [38]. Further plans to produce renewable diesel from crude tall oil have also been announced recently by SunPine in Pitea, Sweden [39].

11.5 Catalysts

The most promising deoxygenation catalysts can be classified into three groups, namely, (i) transition metals, such as Co, Ni, and Pt-group metals; (ii) sulfides of transition metals, mostly nickel and cobalt-promoted molybdenum sulfides; and (iii) transition metal carbides and phosphides, mainly of Ni, Mo, and W. The following sections will discuss the most salient features as well as the respective advantages and disadvantages of these catalysts. First, the sulfided catalysts currently at the heart of commercial technologies will be discussed, after which the two main challengers to these formulations – i.e. metallic catalysts and carbide/phosphide-based catalysts – will be addressed.

The crucial aspects of all catalysts include, besides their activity, their selectivity and the stability of their performance as a function of time on stream (TOS). In deoxygenation, the selectivity to undesired (typically cracking) products, is very low when using the three groups of catalysts mentioned earlier as they typically use nonacidic supports, such as alumina. Hence, the key selectivity issue is the relative extent of HDO and DCX /DCN reactions, which determines both the yield of organic liquids and, at the same time, the extent of hydrogen consumption. Theoretically, the lower the extent of HDO, the lower the hydrogen consumption. As mentioned earlier, this assumes that the subsequent hydrogenation of any CO or CO_2 evolved does not take place. The stability of the catalysts (which dictates the stability of their performance) is a critical parameter for their industrial viability. So far, sulfided (HDS) catalysts are used industrially even though the feedstocks are mostly sulfur-free. Consequently, in order to prevent their fast deactivation, an external source of sulfur has to be added, which is one of the key driving forces for the development of sulfur-free catalysts. Catalyst stability is also closely related to the quality of the feedstock, as some of the natural components of oils and fats have a detrimental impact on the activity of deoxygenation formulations. Thus, all of these issues will be addressed in the following text as part of the discussion of different deoxygenation catalysts.

11.5.1 Sulfided Catalysts

Sulfided (HDS) catalysts are the most widespread hydrogenation (hydrotreating) catalysts in the petroleum upgrading arena. They consist mostly of alumina-supported MoS_2 promoted either with NiS or CoS, albeit catalysts with both promoters are also used in some applications. Alternatively, NiS-promoted

WS_2 is also used, though mostly for hydrocracking applications. Considering the similarity of desulfurization and deoxygenation, it is not surprising that sulfided hydrotreating catalysts have attracted considerable attention as catalysts for the deoxygenation of TGs and have already been used in commercial processes [38].

From a reaction pathway point of view, the HDS catalysts appear to be nonspecific, i.e. they catalyze DCX, DCN, and HDO reactions, although HDO is often the prevailing reaction [18, 40]. However, it has been reported that HDO was practically the only pathway observed when using MoS_2 without any promoters, whereas DCX/DCN was the exclusive reaction pathway when NiS or CoS were employed [20]. This may indicate that the different phases in HDS catalysts favor different reaction pathways. It should also be noted that the activity of both MoS_2 and NiS catalysts was 3.5 and 22 times lower, respectively, than that of a NiMoS catalyst at 260–280 °C and 3.5 MPa [20], which is indicative of a synergy effect analogous to that reported in HDS. The absence of fatty alcohols and aldehydes in the products obtained over NiS indicated that DCX rather than DCN (via keto-enol tautomerization) was the preferred reaction path. Fatty esters were reported to be important intermediates over both NiMoS and MoS_2 catalysts with selectivities of 20–30% being observed at TG conversions of 30–90% [20]. A comparison between promoted (with Ni or Co as promoters) and unpromoted (Mo only) sulfided catalysts was performed by Brillouet et al. [41] using decanoic acid as a model compound. In line with previous reports, both Ni and Co were found to promote DCN and inhibit HDO [41]. It was suggested that an increase in the basicity of sulfur anions neighboring Co or Ni present in the sulfided promoted phase may be responsible for the enhancement of DCN [41]. The work of Brillouet et al. also showed that acids adsorb strongly on the surface, thus inhibiting the deoxygenation of other compounds [41]. The strong adsorption of acids may also explain their lower reactivity relative to esters during deoxygenation [18].

Experimental studies using unsupported sulfides (MoS_2, Ni_3S_2, and Ni-promoted MoS_2) as catalysts for the deoxygenation of ethyl decanoate in the gas phase (250 °C, 1.5 MPa) accompanied by density functional theory (DFT) calculations have confirmed the concurrence of HDO and DCX/DCN over promoted MoS_2, with MoS_2 and Ni_3S_2 favoring HDO and DCX/DCN, respectively [42]. In fact, the presence of the Ni_3S_2 phase in the promoted MoS_2 was deemed to be responsible for the DCX/DCN [42]. DFT calculations revealed the dehydrogenation pathway of aldehyde to alkenoyl and/or ketene intermediate to be favored on the Ni_3S_2 surface relative to MoS_2 surfaces [42]. The latter has been further supported by a recent study of Wagenhofer et al., who suggested that HDO takes place via an aldehyde intermediate on MoS_2 (whose strongly bound electron-poor sulfur did not allow α-hydrogen abstraction) and DCN occurs via the ketene intermediate on Ni-MoS_2 (whose labile electron-rich sulfur favors α-hydrogen abstraction and ketene formation) [43].

In contrast to many studies on supported and unsupported promoted MoS_2 catalysts [20, 42] (and references therein), Zhang et al. reported the conversion of waste cooking oil over an unsupported CoMoS catalyst (300/375 °C, 9 MPa) where DCX/DCN – not HDO – was the main reaction ($C_{18}/C_{17} = 0.6$ vs. 1.5–2.5) [44]. The authors suggested that for supported catalysts, the Lewis acidity of the supports may affect selectivity [44]. This contradicts another study focused on unsupported NiMoS [42], although differences in the reaction setup (batch liquid phase vs. flow gas phase) and conditions (375 °C, 9 MPa vs. 250 °C, 1.5 MPa) employed may account for the discrepancy.

As reported by Kubička [26], the preferred deoxygenation pathway could be completely altered just by varying reaction conditions; indeed, while HDO was the main path over a NiWS catalyst at 310 °C and 7 MPa (C_{18}/C_{17} = ca. 3), DCX prevailed at 280 °C and 0.7 MPa (C_{18}/C_{17} = ca. 0.3) [26]. Furthermore, the presence or absence of H_2S was shown to affect the distribution of deoxygenation products dramatically, DCX reactions being enhanced significantly when dimethyl disulfide (DMDS) was added to the TG feed (to generate H_2S and protect the catalyst from desulfurization and the associated loss of activity) [45]. Tellingly, during the deoxygenation of rapeseed oil over a CoMoS catalyst at 310 °C and 3.5 MPa, the C_{18}/C_{17} ratio decreased from ca. 3.5–4.0 when no DMDS was co-fed to about 1.0–1.5 when DMDS was co-fed, which was attributed to the increased catalyst acidity in presence of H_2S [45]. Finally, the support was also found to influence both the activity and selectivity of supported sulfided catalysts [29]. The use of an inert support (e.g. SiO_2) for the NiMoS active phase resulted in DCX dominating over HDO, whereas HDO was the main reaction pathway when other supports (such as Al_2O_3 or TiO_2) were employed [29]. This was particularly pronounced in the case of NiMoS/TiO_2, with C_{18}/C_{17} exceeding the value of 10 [29]. Apart from the active NiMoS cluster size decreasing based on the support nature in the order $TiO_2 > Al_2O_3 > SiO_2$, differences in the structure of this phase were also ascertained. Specifically, the population of octahedral Ni species in the oxide form of the catalyst (i.e. the precursor before the final activation via sulfidation) was significantly higher in the silica-supported catalyst than in the other two formulations [29]. Chen et al. also found a relationship between the acidity of the support and the preferred deoxygenation pathway on a supported NiMoS active phase. Due to a higher acidity, $NiMoO_4^-$ and MoO_3 sulfided phases dominated on SAPO-11 and DCX/DCN was the preferred deoxygenation route, while Mo^{4+} polymeric octahedral sulfided phases prevailed on Al_2O_3 and HDO was the favored deoxygenation pathway [46].

Kubička and Horáček have clearly demonstrated the loss of activity of a sulfided NiMo catalyst during rapeseed oil deoxygenation when H_2S was absent in the reactor [45], the yield of hydrocarbons dropping 30% over 144 hours TOS without added DMDS (as a source of H_2S) and only 5% over 250 hours when DMDS was constantly added. Moreover, the authors showed catalyst deactivation to be partly reversible, as the deoxygenation performance of the catalyst could be revived after introducing a feed containing DMDS for a short period. However, further cycles with and without DMDS clearly indicated that some of the changes to the catalyst caused in the absence of H_2S (DMDS) are permanent, so a minimum level of H_2S has to be maintained to ensure stable long-term catalyst performance [45].

The inhibition effects of water, hydrogen sulfide, and ammonia, i.e. plausible catalyst poisons present during deoxygenation, were studied for various oxygenates by Laurent and Delmon [47]. Even high concentrations of water were reported to have only a very minor inhibiting effect on the conversion of an ester and a ketone [47]. Hydrogen sulfide was found to promote conversion of carboxylic esters, while it suppressed the activity of NiMoS in the conversion of ketonic groups [47]. On the other hand, ammonia inhibited strongly the conversion of carboxylic esters, but did not affect the hydrogenation of ketonic groups [47]. Although only minor inhibition of deoxygenation reactions by water was observed [47], water was shown to deteriorate significantly the overall catalyst activity, which dropped to one-third of the initial level [48]. This was attributed mainly to partial oxidation of NiS to NiO by water and to a lesser extent to recrystallization of y-alumina to hydrated boehmite resulting in a decrease in surface area [48]. The adverse effect of water was also observed by Wang et al. [49], who reported the formation of a MoO_3 phase during deoxygenation in the absence of a sulfiding agent due to the desulfidation of the catalyst resulting from the exchange of oxygen (from oxygenates) with the sulfur in the catalyst active phase.

Apart from coke deposition – which is a natural cause of deactivation in all transformations of carbon-containing feedstocks – and the aforementioned catalyst desulfidation and partial oxidation, trace elements inherently present in TG feedstocks (such as P, Na, K, Mg, Ca) can cause severe catalyst deactivation [45]. These elements are associated with phospholipids and deposit on the catalyst surface in the form of phosphates, causing pore blockage and deactivation [45]. The most severe deactivation effect is observed for waste-TG streams with an excess of P (relative to metals), which result in the formation of phosphoric acid (instead of phosphates) and in rapid oligomerization followed by coking [45]. Hence, these trace elements must be removed before the TG feedstocks can be deoxygenated.

Due to their robustness and proven reliability in HDS, sulfided catalysts are currently used commercially to deoxygenate lipid-based feedstocks into hydrocarbon fuels. However, it is necessary to introduce a source of sulfur into the process to keep the catalyst in its active form. Moreover, better selectivity control in terms of HDO vs. DCX/DCN – which necessitates more fundamental knowledge on catalyst structure–activity relationships – and minimized CO_x hydrogenation to improve the overall hydrogen economy are key challenges to be tackled.

11.5.2 Metallic Catalysts

Supported metal catalysts, including transition metals (such as Ni or Co) and noble metals (such as Pt, Pd, or Ru) are effective in the hydrogenation of a wide variety of functionalities including double and triple bonds as well as carbonyl groups. Moreover, the aforementioned metals have also been shown to be active in DCX, which makes them of interest for the upgrading of TGs or fatty acids. Two key lines of research have been followed – deoxygenation under H_2-rich atmospheres [28, 50, 51] and deoxygenation in H_2-poor conditions (or even in absence of H_2) [10, 50, 52, 53]. From the reaction stoichiometry point of view, DCX of saturated fatty acids does not consume any hydrogen to yield saturated hydrocarbons, whereas conversion of a saturated TG would require 3 mol of H_2 to produce saturated hydrocarbons (see Figure 11.1). Thus, many efforts have focused on leveraging this fact. Kubičková et al. [50] upgraded stearic acid and ethyl stearate using 5 wt% Pd/C at 300–360 °C under He, H_2, and 5 vol% H_2 in Ar to obtain *n*-heptadecane along with some heptadecenes. This suggest that both DCX and DCN are operative under the reaction conditions. The highest turnover frequency (TOF) was obtained when using 5 vol% H_2 in Ar [50]. In addition to C_{17} olefins, C_{17} aromatics were also observed in the absence of hydrogen [50], indicating that H_2 was important to prevent dehydrogenation reactions and, hence, protect the catalyst from deactivation. The formation of unsaturated products was higher when ethyl stearate was used [50] as could be expected from stoichiometric considerations, ethylene and ethane also being detected in the gaseous products.

Snåre et al. [53], screened various supported-metal catalysts for activity in the deoxygenation of stearic acid under He, carbon-supported formulations significantly outperforming their alumina-supported analogues [53]. High conversion was also achieved on Ru/MgO, which yielded selectively a C_{35} symmetrical ketone, i.e. a ketonization product of stearic acid, likely due to the basic character of the MgO support although other carriers have also shown high selectivity toward this product at low conversions. On the other hand, the HDO activity of all catalysts was negligible. Due to the inert atmosphere, formation of oligomerization products was pronounced over most catalysts but particularly over Ni-containing formulations (>20% selectivity), which also exhibited substantial cracking activity (ca. 20% selectivity) [53]. The various reaction pathways proposed are summarized in Figure 11.3.

Crocker and coworkers tested carbon-supported Ni, Pt, and Pd catalysts for activity in the conversion of TGs at 350 °C under a N_2 atmosphere [52]. These authors confirmed that oxygen was eliminated as CO and CO_2 [52]. It was

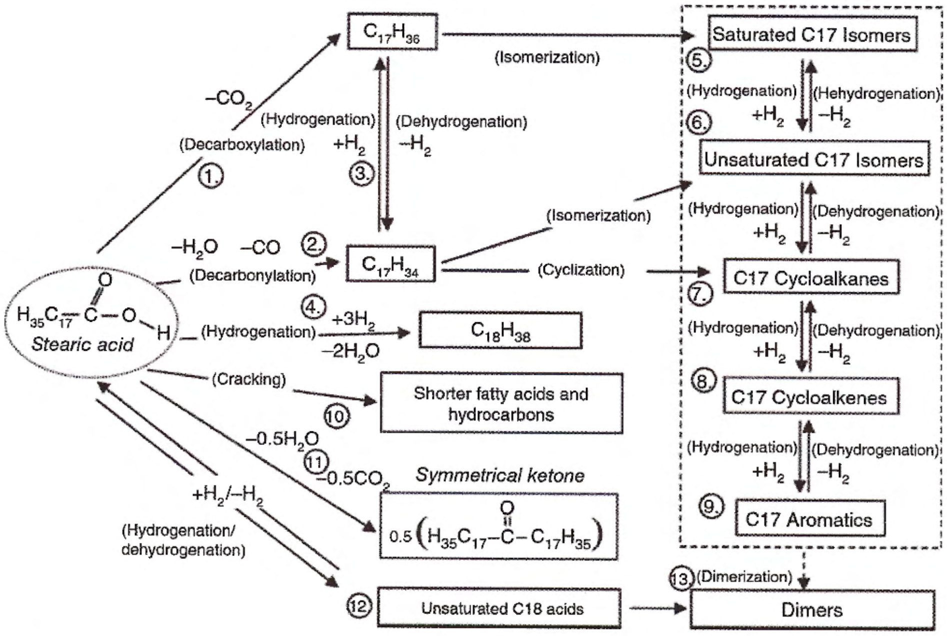

Figure 11.3 Scheme of stearic acid deoxygenation over supported metallic catalysts under inert atmosphere. Source: Reprinted with permission from Snåre et al. 2006 [53]. Copyright 2006, American Chemical Society.

explained that an initial β-elimination step was followed by the DCX of the released fatty acid, C—C bonds scission affording either a C_{17} hydrocarbon (if scission occurred between the ester carbonyl carbon and the α carbon of the hydrocarbon chain) or a C_{15} hydrocarbon and ethylene (if scission took place between the β and γ carbon atoms) [52]. Increasing the degree of unsaturation of the lipids led to increased cracking, especially over the Ni catalyst [52]. Carbon-supported Pt and Pd were less active both in deoxygenation and in cracking than Ni/C [52]. Further investigation of Ni-based catalysts showed that a Ni–Al layered double hydroxide (LDH) catalyst was particularly suited for regeneration as the regenerated catalyst outperformed the fresh formulation, which was attributed to the formation of strong basic sites during regenerative calcination. Also, hydrogen was convincingly shown to curb the deposition of carbonaceous species on the catalyst surface [54]. Moreover, promotion of 20 wt% Ni/Al_2O_3 with 5 wt% Cu resulted in suppressed cracking activity, the formation of diesel-like hydrocarbons being significant especially when upgrading yellow grease [55]. Besides Cu, the use of Sn as promoter was also shown to improve the selectivity of Ni/alumina catalysts to diesel-like hydrocarbons during the conversion of tristearin at 350 °C [56].

Zhao and coworkers studied the transformation of palmitic acid over various Ni-containing catalysts in a batch reactor operated at 260 °C and 12 bar both in the presence and absence of H_2 [57]. They found that reducible supports with oxygen vacancies – such as ZrO_2 – adsorbed palmitic acid via the carboxylic group. This resulted in oxygen elimination and the formation of a ketene, which is hydrogenated to hexadecanal on Ni sites (in the presence of H_2) or reacts with another adsorbed palmitate to yield a symmetrical ketone (in the absence of H_2) [57]. In parallel, palmitic acid is also reduced directly to hexadecanal that is then decarbonylated, both of these reactions occurring on Ni sites [57]. Ni/ZrO_2 exhibited a higher rate of deoxygenation of palmitic acid than Ni/SiO_2 and Ni/Al_2O_3 due to the active contribution of the support to the deoxygenation reaction [57]. Similarly, the rate is further enhanced over zeolite-supported Ni as the dehydration of hexadecanol (which is in equilibrium with hexadecanal) is faster than the other reaction pathways [57]. Consequently, hexadecane is the main reaction product, which is not the case for Ni on supports that do not possess significant Brønsted acidity [57]. This pathway was corroborated by modifying ZrO_2 with SiO_2, which led to the introduction of Brønsted acid sites – accompanied also by a significant surface area increase (from 72 to 193 m^2/g) – and accelerated the deoxygenation of stearic acid by HDO rather than DCN [58]. Likewise, high deoxygenation activity was achieved over Ni supported on hierarchical nanosized MFI exhibiting both excellent Ni dispersion and large number of accessible acid sites [59].

Ni and Co supported on Al- and Si-SBA-15 having large specific surface area (and mild acidity in the case of Al-SBA-15) have also been tested for activity in the deoxygenation of methyl esters in a flow reactor at 300–340 °C and 3 MPa H_2 [51]. In line with the results from Lercher and coworkers [58], Ni/Si-SBA-15 showed lower activity than Ni/Al-SBA-15 and a negligible selectivity to HDO, whereas HDO was the main reaction pathway over Ni/Al-SBA-15 (about 60% of $C_{17} + C_{18}$ hydrocarbons at 300 °C) [51]. Interestingly, Si-SBA-15-supported Co was more active than Ni and showed significant selectivity to HDO (about

20% of $C_{17} + C_{18}$ hydrocarbons at 300 °C), which increased to 70–80% over Co/Al-SBA-15 [51]. Both Al-SBA-15-supported catalysts exhibited low cracking activity, high yields of diesel-range hydrocarbons (>90 wt%) being obtained during the whole six hour TOS period investigated [51]. At 340 °C, the initial yield of desired isomers exceeded 25 wt%, albeit it dropped to about 10 wt% after six hours TOS [51]. Surprisingly, Co/Al-SBA-15 yielded more isomers than Ni/Al-SBA-15 at 300 °C. Nonetheless, the yield decreased rapidly from 15 to 6 wt%, still twice the yield obtained over Ni/Al-SBA-15 that remained constant at about 3 wt% [51].

The isomerization activity of deoxygenation catalysts is of high interest as it would allow converting TGs directly into the most desired diesel-range fuel components, i.e. *iso*-alkanes. Commercially, this is achieved in a two-stage setup, with the *n*-alkanes stemming from the deoxygenation of lipids being upgraded in a second reactor over a commercial isomerization/mild hydrocracking catalyst. In addition to mesoporous supports such as Al-SBA-15, attention has been mainly directed at SAPO materials, such as SAPO-11 and SAPO-31, which exhibit mild acidity thus limiting excessive cracking [60–63]. Kikhtyanin et al. [60] have shown that sunflower oil could be converted exclusively to hydrocarbons in the diesel fuel range over Pd/SAPO-31 at 320–350 °C and 2 MPa H_2 with a high initial selectivity to C_{17} and C_{18} *iso*-alkanes (*iso*–/*n*-alkanes >10). This ratio, however, dropped dramatically within 24 hours TOS to virtually zero indicating severe deactivation, which was attributed to a drop in Pd dispersion (from 50% to 11%) [60]. Full soybean oil conversion and a high isomerization selectivity (*iso*-alkanes representing 60–85% of all produced alkanes) was also observed over Pt/SAPO-11 and Pt/ZSM-22 at 357 °C, 4 MPa H_2 and three hours TOS [63]. While SAPO-11 favored isomerization (<4% selectivity to liquid cracking products), ZSM-22 promoted cracking reactions (50–60% selectivity to liquid cracking products) [63]. Unfortunately, the stability of the catalysts was not reported in this contribution. In the deoxygenation of palm oil, a good liquid product yield – ca. 60% (the theoretical maximum being 80–85%) – and good isomerization selectivity (ca. 50%) were obtained in a 35 hour TOS experiment using 7 wt% Ni/SAPO-11 at 360 °C and 4 MPa H_2 [61].

When metallic catalysts are employed, it is obvious that the product selectivity can be fine-tuned by the choice of (i) the active metal, (ii) the support, and (iii) the reaction conditions in general and the gas atmosphere in particular, all of which determine the preferred reaction pathway. However, the choice of support has uniquely important consequences. Indeed, partially reducible supports may enhance DCN/DCX pathways, while non-reducible supports with Brønsted acid sites (e.g. molecular sieves) may on the one hand shift the preferred pathway toward HDO and on the other hand promote both desirable isomerization and undesirable cracking reactions. The long-term TOS stability of these catalysts remains a challenge to be addressed.

11.5.3 Metal Carbide, Nitride, and Phosphide Catalysts

Metal carbides, nitrides, and phosphides are an emerging class of robust hydrogenation catalysts that offer several advantages over the other types of deoxygenation catalysts. Most importantly, they are much more affordable than noble metal catalysts and do not require the sulfur-containing additives that are essential when sulfided catalysts are employed. As with supported-metal catalysts, deoxygenation over carbide-, nitride-, and phosphide-based formulations has been investigated under both hydrogen-rich and hydrogen-poor conditions.

Molybdenum carbide supported on alumina was investigated as a catalyst in the deoxygenation of sunflower oil (633 K, 5 MPa) by Sousa et al. [64]. Conversion of TGs into alkanes was described as a two-step process consisting of thermal cracking of TGs yielding FFAs followed by hydrogenation of the double bonds and of the carboxylic group of the FFAs [64]. Both CO and CO_2 were absent among the reaction products indicating that DCX and/or DCN reactions did not take place and that HDO was the exclusive deoxygenation reaction pathway [64]. Nonetheless, the occurrence of DCX and/or DCN reactions cannot be completely excluded as methane – which could be formed by CO_x hydrogenation (including that of the CO_x formed through the thermal cracking of the FFAs) – was found in the reaction products [64]. The Mo_2C/Al_2O_3 catalyst was found to provide a more stable performance in terms of both activity and product distribution than sulfided formulations [64]. Moreover, the activity of molybdenum carbide was claimed to be higher than that of molybdenum sulfide [64], which also operates via HDO [20].

Therefore, supported Mo_2C catalyst offer several advantages, including (i) low to negligible formation of CO and CO_2, (ii) stable operation without the necessity to supply a source of sulfur (as is the case for sulfided catalysts), and (iii) direct HDO of FFAs, which obviates the need to convert acids into esters prior to their deoxygenation [64].

Unsupported and active charcoal-supported Mo_2C were some of the first catalysts tested for activity in the deoxygenation of vegetable oils and related model compounds (e.g. stearic acid, methyl stearate) over carbides at 280–300 °C and 1–2 MPa hydrogen pressure [65]. HDO products such as *n*-octadecane were the predominant products obtained over supported Mo_2C with yields around 90% and 75% when esters and stearic acid were used, respectively. At the same time, DCX/DCN products were formed in ca. 4% yield from esters and ca. 13% yield from stearic acid [65]. The performance of the unsupported Mo_2C was inferior to that of the supported Mo_2C [65]. The activated charcoal-supported Mo_2C favored the HDO of esters, aldehydes, and alcohols, whereas Pd nanoparticles supported on $BaSO_4$ favored the DCN pathway producing hydrocarbons with one carbon atom less than in the original lipid [65]. This was also observed for the deoxygenation of hexadecanol [65], which could be explained by invoking the equilibrium between the alcohol and the aldehyde [25]. In the case of stearic acid, the HDO pathway was favored by both catalytic systems. Thus, it was suggested that aldehydes and olefins (rather than carboxylic acids) were the intermediates in the conversion of esters [65]. In contrast to methyl stearate and methyl palmitate, full conversion was not reached when deoxygenating vegetable oils under the same reaction conditions (conversions being 85–95%) [65].

The performance of tungsten and molybdenum carbide supported on carbon nanofibers (CNFs) in the deoxygenation of oleic acid was studied at 350 °C and 5 MPa H_2 pressure by Hollak et al. [66]. These authors found Mo_2C/CNF to be more active and stable than W_2C/CNF. Mo_2C/CNF was highly selective to *n*-octadecane, steric acid being the main reaction intermediate. On the other hand, W_2C/CNF produced olefins in significant yields (up to 50% before being hydrogenated) [66]. This was explained by higher hydrogenation rates being achieved over Mo_2C/CNF, which was also suggested to be the reason behind the superior stability of Mo_2C/CNF in terms of catalytic activity [66]. HDO was found to be the main reaction pathway over both catalysts, DCX products being produced in 7% and 15% molar yield at complete deoxygenation over Mo_2C and W_2C, respectively [66]. This difference was attributed to the higher sensitivity of W_2C/CNF toward oxidation [66].

It was also established that the particle size of the supported carbides (Mo_2C, W_2C) is a decisive factor determining their deoxygenation activity and stability [67]. It was shown that larger carbide particles were more resistant against full oxidation to crystalline metal oxides, thus providing a more stable catalytic phase [67]. At the same time, the TOF over Mo_2C/CNF increased by an order of magnitude when the carbide particle size was increased from 2 to 10 nm [67]. The increase in particle size also resulted in a change in the preferred reaction pathway. Indeed, while the *n*-octadecane produced by HDO was practically the sole hydrocarbon product over 2 nm Mo_2C/CNF, almost equal amounts of C_{17} and C_{18} hydrocarbons were formed over 10 nm Mo_2C/CNF at 300 °C and 3 MPa H_2 [67]. At the same time, the formation of the C_{36} esterification product was greatly diminished. The main oxygenated intermediates included octadecanol and octadecanal and the formation of C_{17} hydrocarbons was assigned to the DCN of the aldehyde [67].

The experiments with octadecanol and octadecanal clearly demonstrated that under a N_2 atmosphere octadecanal was selectively converted to unsaturated C_{17} hydrocarbons over Mo_2C/CNF, whereas stearic acid did not react at all [67]. Octadecanol yielded both C_{17} and C_{18} hydrocarbons (with preference to C_{18} over 2 nm Mo_2C and to C_{17} over 10 nm Mo_2C) indicating that the dehydrogenation of the alcohol to the aldehyde was followed by DCN [67]. In contrast, W_2C/CNF invariably yielded C_{18} hydrocarbons in very large excess likely due to the oxophilic nature of tungsten carbide, the WO_x domains formed on the surface of W_2C/CNF catalyzing alcohol dehydration [67].

Mo_2C supported on different carbon supports – such as reduced graphene oxide (RGO), glassy spherical carbon, activated carbon, and mesoporous carbon was studied by Kim et al. [68]. When using Mo_2C/RGO nanocomposites prepared by the supercritical alcohol route, 30–60% higher hydrocarbon yields were obtained in the HDO of oleic acid at 350 °C, 4.5 MPa H_2 and 2 h^{-1} liquid hourly space velocity (LHSV) [68]. The higher efficiency of the RGO-supported Mo_2C was attributed to a uniform distribution of Mo_2C particles and the large pore size of the support allowing the efficient transport of reactants to the active sites [68]. A decrease in soybean oil conversion of 13% was observed over Mo_2C/RGO during six hours on stream, which was significantly less than the 42% drop in conversion observed over a commercial $CoMoS/Al_2O_3$ catalyst [68]. Nevertheless, it seems that the authors did not add any sulfur to the feed, which would have a detrimental effect on the performance of the $CoMoS/Al_2O_3$ catalyst.

Theoretical DFT studies of the preferred reaction pathways have been performed using short chain (e.g. propionic, butyric) acids as model compounds [69, 70]. The orthorhombic Mo_2C (100) has a surface terminated in either Mo or C. The Mo-terminated surface was shown to favor the HDO path as a result of the low barrier for oxygenates, while the C-terminated surface was preferable for the DCX of propanoic acid due to low barrier for O–H scission [69]. Butyric acid deoxygenation over an hexagonal Mo_2C (101) surface was reported to proceed through the dissociative adsorption of the acid followed by the hydrogenation of the adsorbed acyl to adsorbed butanal [70]. The direct decomposition of acyl to produce propane, CO, and water was found to be less energetically favorable and hence not competitive [70]. Butanal was then hydrogenated to butanol via butoxyl – which was the preferred adsorbed species – followed by butanol dissociation to butyl and hydroxyl species and final hydrogenation of these species to form butane and water [70]. However, it should be noted that neither the structure nor the chain length of the model compounds employed provide a realistic representation of TGs, and steric effects might affect the predicted outcomes.

A NiMo carbide and nitride supported over ZSM-5, i.e. an acidic support, were also used in the deoxygenation of soybean oil at 360–450 °C and 4.5 MPa by Wang et al. [71]. At 450 °C and a LHSV of $1.5\,h^{-1}$, full conversion of the soybean oil was achieved, but differences in the gas phase products were noticed. The nitride exhibited higher selectivity to CO, CO_2, and CH_4 than the carbide catalyst, indicating not only a higher DCX/DCN activity but also a higher methanation activity [71]. Nonetheless, significant amounts of carboxylic acids were observed in the product mixtures recovered after three and eight days on stream at 360 and 450 °C, respectively, indicating severe deactivation of the NiMo nitride catalyst [71]. The latter was explained invoking strong adsorption of water. In general, the NiMo carbide was found to be more selective to higher hydrocarbons. Based on a comparison between a Mo-carbide/ZSM-5 catalyst (10 wt% loading) and a 3 NiMo-carbide/ZSM-5 formulation (the same metal loading and Ni/Mo ratio = 0.5, 1, and 1.5), the lack of Ni was claimed to be responsible for insufficient hydrogen activation and for the high extent of polymerization reactions eventually leading to reactor plugging [71]. In addition, the yield of organic liquid products decreased as the Ni/Mo ratio increased [71], plausibly due to the hydrogenolytic activity of Ni.

Nguyen et al. [72] reported that – in contrast to 5 wt% Ni/H-Y and 5 wt% Ni/SiO_2 – an unsupported Mo_2N/MoO_2 catalyst (nitride/oxide ratio = 1.2) showed noteworthy resistance to deactivation during the deoxygenation of crude Chlorella algal oil at 300 °C and 3 MPa H_2. However, the conversion over the nitride catalyst was only 14% after six hours of reaction, compared with the 35 and 12% values reached over Ni/H-Y and Ni/SiO_2, respectively [72]. In line with the findings of Wang et al. [71], only low yields (<10%) of hydrocarbons were obtained and fatty acids represented the main reaction products [72].

In addition to carbides and nitrides [25, 64–68, 71–73], transition metal phosphides have recently gained significant attention as deoxygenation catalysts [74–81]. Peroni et al. convincingly showed that HDO was the key reaction pathway during the upgrading of palmitic acid over WP, while DCN of the intermediate aldehyde was a significant reaction route over Ni_2P and MoP catalysts at 4 MPa

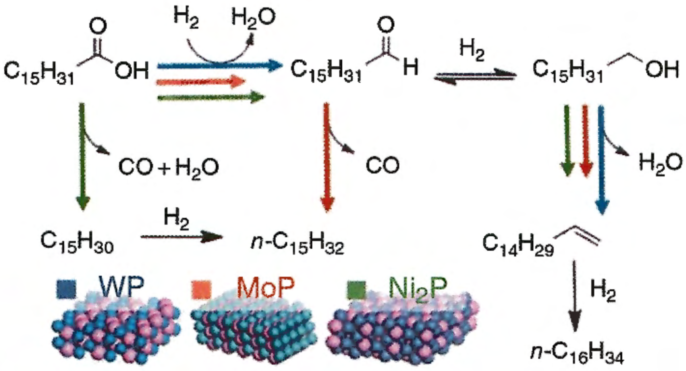

Figure 11.4 Deoxygenation of palmitic acid over different phosphides. Source: Reprinted with permission from Peroni et al. 2017 [77]. Copyright 2017, American Chemical Society.

and 180–300 °C [77] as depicted in Figure 11.4. Furthermore, the dehydration of the intermediate alcohol was correlated with the Lewis acidity of the phosphide catalysts and only Ni_2P catalyzed the dehydration to the ketene followed by the DCN of the latter [77]. However, weak Brønsted acid sites were not strong enough to dehydrate the intermediate alcohol [77]. The activation energies of palmitic acid deoxygenation spanned from 57 kJ/mol for MoP to 129 kJ/mol for WP [77]. The activity could be increased by addition of citric acid, which limited the growth of oxide precursors during the synthesis step and of phosphide crystals during calcination. However, citric acid addition also resulted in partial coverage of the metal surface by residual carbon [77].

Despite the obvious advantage offered by WP in terms of the highest retention of renewable carbon in the liquid deoxygenation products, Ni_2P catalysts have attracted most attention. Indeed, conversion of both fatty acids and their methyl esters has been extensively studied over zeolite- and mesoporous molecular sieve-supported Ni_2P [74, 75, 79, 80], as well as over carbon- and silica-supported Ni_2P [76, 78, 81].

Ni_2P supported on acidic H-ZSM-22 [75] was compared with unsupported $Ni_{12}P_5$ and unmodified H-ZSM-22 (Si/Al = 70) in the solvent-free deoxygenation of palmitic acid at ambient pressure at 310–360 °C under a flow of 5% H_2 in Ar. Full conversion was reached over all catalysts besides the unsupported Ni_xP, while the yield of liquid hydrocarbons increased with the increasing supported Ni_xP phase content from 14% to 46% for 5 wt% Ni_xP/H-ZSM-22 and 60 wt% Ni_xP/H-ZSM-22, respectively [75]. These yields are, however, significantly lower than the theoretical maximum of 83% (assuming only DCX/DCN take place). This is a consequence of gaseous products formation due to cracking reactions [75]. Nonetheless, as the Ni_xP loading increased, less cracking was observed due to the corresponding decrease in catalyst Lewis acidity [75]. The $Ni_{12}P_5$ phosphide phase was suggested to be the most active in DCN and DCX reactions (the optimum crystal size being 20–24 nm), while the acid sites of the support were active in isomerization and cracking reactions [75]. Albeit pentadecane was reported to be the main deoxygenation product over Ni_xP/H-ZSM-22 [75], over Ni_xP/MCM-41 both *n*-hexadecane (a HDO product) and *n*-pentadecane (a DCX/DCN product) were observed during the deoxygenation of methyl palmitate at 3 MPa of H_2 pressure and 290–350 °C [74]. However, this could be attributed to the difference in reaction pressure (0.1 MPa, 5% H_2 in Ar vs. 3 MPa H_2). Indeed, an increase in H_2 pressure has been reported to enhance HDO selectivity at the expense of DCX/DCN selectivity, the $C_{18}/(C_{18} + C_{17})$ ratio increasing from 0.2 to 0.6 upon increasing the pressure from 0.3 to 4 MPa over 15% Ni_xP/SBA-15 at 250 °C [79]. In contrast, the aforementioned ratio did not depend on H_2 pressure, and DCX/DCN was the preferred route over 15% Ni/SBA-15, which afforded deoxygenation product mixtures comprising >95% DCX/DCN products [79].

Interestingly, during the deoxygenation of methyl palmitate, the selectivity to HDO and DCX/DCN was found to be a function of Ni_xP loading on MCM-41, the nC_{16}/nC_{15} ratio decreasing from 60/35 to 35/60 when the Ni_xP loading was increased from 5 to 20 wt% [74]. At the same time, irrespective of the phosphide loading, all catalysts exhibited virtually the same TOF (0.43–0.44 s^{-1}) [74], which suggests that the same sites are active in both HDO and DCX/DCN reactions and/or that the intrinsic activity of different sites is very similar. In addition, at short contact times (3.3 minutes) and low conversions, DCX/DCN prevailed significantly (n-C_{15}/n-C_{16} ca. 6), while at longer contact times (20 minutes), the excess of the DCX/DCN products was only 1.4 [74]. In addition to the hydrogenolysis of the methyl ester yielding an acid and methane, direct formation of aldehyde and methanol was proposed as well [74].

By varying the Ni/P ratio in the range 1.25–3.33, it was established that increasing the concentration of P resulted in a decrease in the conversion of methyl palmitate (from 95% to 60% at 290 °C) and lower selectivity to HDO [74]. Similarly, a significantly lower activity was reported for SBA-15-supported Ni_3P than for Ni_xP/SBA-15 with Ni/P = 0.5–2 during the deoxygenation of methyl oleate at 3 MPa and 250–340 °C [80]. The phosphorus-deficient phase (Ni_3P) also showed higher selectivity to DCX/DCN than to HDO being thus more similar to Ni/SBA-15 than to other Ni_xP/SBA-15 catalysts [80]. The best performance, in terms of conversion and selectivity to HDO products, was provided by catalysts rich in Ni_2P and $Ni_{12}P_5$ phases, whereas an excess of P (Ni/P = 0.5) had a detrimental effect on the catalyst activity due to the formation of large Ni_xP crystallites [80].

No cracking activity was reported over Ni_2P/SBA-15 (all Si-SBA-15) [79] and over Ni_xP/MCM-41 (Al content not reported) [74], which might be due to the absence of acid sites in the supports. A comparison with Ni/SBA-15 demonstrates that the cracking/hydrocracking activity of supported Ni_xP is negligible, which allows for high renewable carbon retention in the liquid products, whereas supported Ni (even on a neutral support) promotes cracking significantly, particularly at higher reaction temperatures [79]. This is corroborated by the long-term testing of Ni_2P (25 wt%) supported on SiO_2 and HY under hydrocracking conditions (370 °C, 3 MPa) [81]. Indeed, the liquid hydrocarbon yields reached 78–82% over both catalysts, but virtually no cracking took place over Ni_2P/SiO_2 (gasoline fraction <1%), while as much as 20 wt% of light hydrocarbon (HC) liquids (boiling below 150 °C) were produced over Ni_2P/HY [81]. However, the extent of the cracking reactions decreased with increasing

TOS from the initial 20 wt% (20 hours TOS) to about 5 wt% (150 hours TOS), while the soybean oil was completely deoxygenated [81]. The decline in the hydrocracking activity was attributed to the adverse effect of the water generated during deoxygenation on catalyst acidity, specifically through the conversion of Lewis acid sites (hydroxylaluminum ions) into neutral $Al(OH)_3$, which blocks the access of reagents to Brønsted acid sites [81].

Silica-supported Ni_2P catalysts having a crystallite size in the range 3–12 nm were prepared using different SiO_2 supports including SBA-15 and MCM-41 and tested for activity in the deoxygenation of methyl laureate at 2 MPa H_2 and 200–340 °C [82]. The TOF was found to be directly proportional to the Ni_2P crystallite size, increasing from 0.064 to 0.151 s^{-1} for a crystallite size of 3 and 12 nm, respectively [82]. The lower TOF values over the smaller Ni_2P crystallites were attributed to a stronger interaction between Ni and P in these crystallites [82]. In contrast to the results reported for Ni_xP/SBA-15 catalysts, DCX/DCN was always preferred over HDO reactions with (DCX + DCN)/HDO in the range 2–4 [82], likely due to the lower H_2 pressure affecting the HDO/(DCX + DCN) ratio [79] and the higher temperature promoting DCX/DCN at the expense of HDO reactions [82]. Based on previous reports [79], an HDO/(DCX + DCN) ratio equal to unity would be expected in the deoxygenation of methyl oleate at 250 °C, so a ratio of about 2 at 300 °C [82] seems to be in line with these results. In contrast with previous work demonstrating that Lewis rather than Brønsted acidity affects the deoxygenation selectivity [77], Brønsted acidity originating from a P surplus has been linked to changes in selectivity [82]. Indeed, the acid Brønsted acid sites were associated with both the DCN and the HDO pathways (involving alcohol dehydration) [82], these acid sites also being deemed responsible for the esterification reaction taking place and resulting in the formation of lauryl laureate [82]. Similar observations were also made for sulfided catalysts, for which the increased acidity due to presence of H_2S (HS^-) promoted DCX/DCN at the expense of HDO reactions and the formation of esters through the reaction between fatty acids and fatty alcohols [45].

As with metallic catalysts, carbides, nitrides, and phosphides of transition metals provide some flexibility to adjust the selectivity to HDO and DCX/DCN pathways, thus allowing some degree of control over hydrogen consumption. They can be operated at a similar range of reaction conditions, which makes them an attractive alternative to noble metal-based catalysts due to their lower cost. Moreover, in contrast to metallic catalysts that preferentially yield DCX/DCN products, HDO can be the main reaction pathway over carbides, nitrides, and phosphides, which results in a higher retention of renewable carbon in the liquid organic products. As with the other catalytic systems discussed, the long-term stability of their performance remains a major challenge to be overcome.

11.6 Conclusions and Outlook

Several advances in the deoxygenation of lipid-based feedstocks has enabled the commercialization of the resulting technology by several companies, and new investments in additional industrial units have been announced. The recent focus on more sustainable feedstocks – such as waste lipids or algal oils – increases the need not only for improving the robustness of the catalysts but also for a meticulous pretreatment of the feedstocks to eliminate catalyst poisons, including alkali and alkaline earth metals and phosphorus. The availability of (sustainable) lipid-based feedstock is one of the factors limiting the widespread use of deoxygenation technology, other factors including the selectivity and long-term stability of deoxygenation catalysts.

Significant progress in understanding the underlying chemistry has been achieved recently. HDO, DCN, and DCX have been identified as the main deoxygenation reactions taking place. The intrinsic selectivity (toward specific reaction paths) of different active phases has been revealed along with the parameters that affect it, the nature and properties of the support, promoters, reaction gas, or reaction conditions having been described. In general, catalysts based on molybdenum sulfides and carbides favor HDO, while DCX and DCN are the preferred reaction pathways over nickel- and noble metal-based catalysts.

Although sulfided catalysts necessitate addition of H_2S (or a source thereof) to maintain their activity, they represent the only deoxygenation catalysts used in commercial deoxygenation technologies. This is due to their robustness and the vast experience of industry with these catalysts. Nonetheless, from both a technical and an environmental point of view, sulfur-free catalysts are highly desirable. Consequently, transition metal catalysts as well as their carbides, nitrides, and phosphides have attracted significant attention as promising alternatives.

The understanding of the intrinsic activity and selectivity of deoxygenation catalysts provides an opportunity to fine-tune their selectivity and to control hydrogen consumption. However, more effort is needed to develop catalysts with a controlled distribution of the desired active sites. Additionally, the stability of these active sites has to be further improved so they can be rendered tolerant to the oxygen-containing inorganic compounds produced, namely, water, CO, and CO_2. The use of promoters and of suitable supports with optimized properties (particularly textural and acid–base properties) is a research area with significant potential for improvement.

Finally, in line with the principles of green chemistry, consolidation of the two stages currently employed to upgrade lipids – i.e. deoxygenation followed by either isomerization or mild hydrocracking to afford high quality diesel fuel and kerosene, respectively – into a single-stage process should be attempted. Despite some promising results, catalysts in general (and isomerization formulations in particular) still suffer from fast deactivation that results in a rapid deterioration of their performance. Thus, the bifunctional catalysts needed to address this issue must be improved further.

References

1 Eur-Lex. Renewable energy directive. http://eur-lex.europa.eu/legal-content/EN/TXT/?uri=CELEX:52016PC0767R%2801%29 (accessed 10 April 2018).

2 Dawes, G.J.S., Scott, E.L., Le Notre, J. et al. (2015). Deoxygenation of biobased molecules by decarboxylation and decarbonylation – a review on the role of heterogeneous, homogeneous and bio-catalysis. *Green Chem.* 17 (6): 3231–3250.

3 Hermida, L., Abdullah, A.Z., and Mohamed, A.R. (2015). Deoxygenation of fatty acid to produce diesel-like hydrocarbons: a review of process conditions, reaction kinetics and mechanism. *Renewable Sustainable Energy Rev.* 42: 1223–1233.

4 James, O.O., Maity, S., Mesubi, M.A. et al. (2012). A review on conversion of triglycerides to on-specification diesel fuels without additional inputs. *Int. J. Energy Res.* 36 (6): 691–702.

5 Kordulis, C., Bourikas, K., Gousi, M. et al. (2016). Development of nickel based catalysts for the transformation of natural triglycerides and related compounds into green diesel: a critical review. *Appl. Catal., B* 181: 156–196.

6 Kubičková, I. and Kubička, D. (2010). Utilization of triglycerides and related feedstocks for production of clean hydrocarbon fuels and petrochemicals: a review. *Waste Biomass Valorization* 1 (3): 293–308.

7 Pattanaik, B.P. and Misra, R.D. (2017). Effect of reaction pathway and operating parameters on the deoxygenation of vegetable oils to produce diesel range hydrocarbon fuels: a review. *Renewable Sustainable Energy Rev.* 73: 545–557.

8 Rogers, K.A. and Zheng, Y. (2016). Selective deoxygenation of biomass-derived bio-oils within hydrogen-modest environments: a review and new insights. *ChemSusChem* 9 (14): 1750–1772.

9 Zhao, C., Bruck, T., and Lercher, J.A. (2013). Catalytic deoxygenation of microalgae oil to green hydrocarbons. *Green Chem.* 15 (7): 1720–1739.

10 Santillan-Jimenez, E. and Crocker, M. (2012). Catalytic deoxygenation of fatty acids and their derivatives to hydrocarbon fuels via decarboxylation/decarbonylation. *J. Chem. Technol. Biotechnol.* 87 (8): 1041–1050.

11 Woodgate, S.L. and van der Veen, J.T. (2014). Fats and oils – animal based. In: *Food Processing. Principles and Applications* (eds. S. Clark, S. Jung and B. Lamsal), 481–500. Wiley.

12 Global production of vegetable oils from 2000/01 to 2017/18. https://www.statista.com/statistics/263978/global-vegetable-oil-production-since-2000-2001/ (accessed 10 April 2018).

13 Sheehan, J., Dunahay, T., Benemann, J., and Roessler, P. (1998). A Look Back at the U.S. Department of Energy's Aquatic Species Program: Biodiesel from Algae. *Contract No.: NREL/TP-580-24190.* National Renewable Energy Laboratory.

14 Johnston, M., Foley, J., Holloway, T. et al. (2009). Resetting global expectations from agricultural biofuels. *Environ. Res. Lett.* 4: 1–9.

15 da Rocha Filho, G.N., Brodzki, D., and Djéga-Mariadassou, G. (1993). Formation of alkanes, alkylcycloalkanes and alkylbenzenes during the catalytic hydrocracking of vegetable oils. *Fuel* 72 (4): 543–549.

16 Ma, F. and Hanna, M.A. (1999). Biodiesel production: a review. *Bioresour. Technol.* 70 (1): 1–15.

17 EU (2009). Directive 2009/28/EC of the European Parliament and of the Council on the promotion of the use of energy from renewable sources.

18 Laurent, E. and Delmon, B. (1994). Study of the hydrodeoxygenation of carbonyl, carboxylic and guaiacyl groups over sulfided CoMo/γ-Al_2O_3 and NiMo/γ-Al_2O_3 catalysts: I. Catalytic reaction schemes. *Appl. Catal., A* 109 (1): 77–96.

19 Turek, T., Trimm, D.L., and Cant, N.W. (1994). The catalytic hydrogenolysis of esters to alcohols. *Catal. Rev. Sci. Eng.* 36 (4): 645–683.

20 Kubička, D. and Kaluža, L. (2010). Deoxygenation of vegetable oils over sulfided Ni, Mo and NiMo catalysts. *Appl. Catal., A* 372 (2): 199–208.

21 Gousi, M., Andriopoulou, C., Bourikas, K. et al. (2017). Green diesel production over nickel-alumina co-precipitated catalysts. *Appl. Catal., A* 536: 45–56.

22 Robota, H.J., Alger, J.C., and Shafer, L. (2013). Converting algal triglycerides to diesel and HEFA jet fuel fractions. *Energy Fuels* 27 (2): 985–996.

23 Liu, Y.Y., Sotelo-Boyas, R., Murata, K. et al. (2011). Hydrotreatment of vegetable oils to produce bio-hydrogenated diesel and liquefied petroleum gas fuel over catalysts containing sulfided Ni–Mo and solid acids. *Energy Fuels* 25 (10): 4675–4685.

24 Choudhary, T.V. and Phillips, C.B. (2011). Renewable fuels via catalytic hydrodeoxygenation. *Appl. Catal., A* 397 (1–2): 1–12.

25 Gosselink, R.W., Hollak, S.A.W., Chang, S.W. et al. (2013). Reaction pathways for the deoxygenation of vegetable oils and related model compounds. *ChemSusChem* 6 (9): 1576–1594.

26 Kubička, D. (2008). Future refining catalysis – introduction of biomass feedstocks. *Collect. Czech. Chem. Commun.* 73 (8–9): 1015–1044.

27 Elliott, D.C. (2007). Historical developments in hydroprocessing bio-oils. *Energy Fuels* 21 (3): 1792–1815.

28 Kim, S.K., Han, J.Y., Lee, H.S. et al. (2014). Production of renewable diesel via catalytic deoxygenation of natural triglycerides: comprehensive understanding of reaction intermediates and hydrocarbons. *Appl. Energy* 116: 199–205.

29 Kubička, D., Horáček, J., Setnička, M. et al. (2014). Effect of support-active phase interactions on the catalyst activity and selectivity in deoxygenation of triglycerides. *Appl. Catal., B* 145: 101–107.

30 Anderson, J. (2017). *Green Transportation Fuels from UOP*. Biomass Research and Development (BR&D) Board.

31 Kotrba, R. (2018). UPM's \$206M renewable diesel plant begins commercial production. *Biodiesel Magazine* http://www.biodieselmagazine.com/articles/277480/upms-206m-renewable-diesel-plant-begins-commercial-production (accessed 10 April 2018).

32 Perotta, L. (2016). Hydroconversion of renewable lipids into biojet and biodiesel: a flexible solution becoming a reality. *ERTC 21st Annual Meeting*, Lisbon, Portugal (15 November 2016).

33 Lane, J. (2018). Shell goes carbon negative, signs commercial-scale deal with SBI. *Biofuels Digest*. http://www.biofuelsdigest.com/bdigest/2017/07/02/shell-enters-carbon-negative-signs-commercial-scale-deal-with-sbi/ (accessed 10 April 2018).

34 BioenergyInternational (2018). St1 plans to extend its advanced biofuels production into renewable diesel. *Bioenergy International*. https://

bioenergyinternational.com/biofuels-oils/st1-plans-extend-advanced-biofuels-production-renewable-diesel (accessed 10 April 2018).

35 Hodge, C. (2006). NExBTL renewable diesel. *California Air Resources Board Workshop on Regulatory and Non-Regulatory Fuels-Related Activities*, Sacramento, CA, USA.

36 Guzman, D.D. (2018). Neste starts bio-propane production. *Green Chemicals Blog*. https://greenchemicalsblog.com/2018/03/19/neste-starts-bio-propane-production/ (accessed 10 April 2018).

37 Palombo, F. (2013). Developing technologies for biofuels. *Eco-Mobility 2013, 8th A3PS Conference*, Vienna, Austria (3–4 October 2013).

38 Kubička, D. and Tukač, V. (2013). Hydrotreating of triglyceride-based feedstocks in refineries. In: *Chemical Engineering for Renewables Conversion*, Advances in Chemical Engineering, vol. 42 (ed. D.Y. Murzin), 141–194. San Diego, CA: Elsevier – Academic Press. ISBN: 978-0-12-386505-2.

39 Moran, D. (2018). SunPine to build a new crude tall diesel plant in Sweden. *Biorefineries Blog*. https://biorrefineria.blogspot.cz/2018/04/sunpine-to-build-new-crude-tall-diesel-plant-in-sweden.html (accessed 10 April 2018).

40 Donnis, B., Egeberg, R.G., Blom, P., and Knudsen, K.G. (2009). Hydroprocessing of bio-oils and oxygenates to hydrocarbons. Understanding the reaction routes. *Top. Catal.* 52 (3): 229–240.

41 Brillouet, S., Baltag, E., Brunet, S., and Richard, F. (2014). Deoxygenation of decanoic acid and its main intermediates over unpromoted and promoted sulfided catalysts. *Appl. Catal., B* 148: 201–211.

42 de Brimont, M.R., Dupont, C., Daudin, A. et al. (2012). Deoxygenation mechanisms on Ni-promoted MoS_2 bulk catalysts: a combined experimental and theoretical study. *J. Catal.* 286: 153–164.

43 Wagenhofer, M.F., Barath, E., Gutierrez, O.Y., and Lercher, J.A. (2017). Carbon–carbon bond scission pathways in the deoxygenation of fatty acids on transition-metal sulfides. *ACS Catal.* 7 (2): 1068–1076.

44 Zhang, H.P., Lin, H.F., Wang, W.Z. et al. (2014). Hydroprocessing of waste cooking oil over a dispersed nano catalyst: kinetics study and temperature effect. *Appl. Catal., B* 150: 238–248.

45 Kubička, D. and Horáček, J. (2011). Deactivation of HDS catalysts in deoxygenation of vegetable oils. *Appl. Catal., A* 394 (1–2): 9–17.

46 Chen, H., Wang, Q.F., Zhang, X.W., and Wang, L. (2015). Effect of support on the NiMo phase and its catalytic hydrodeoxygenation of triglycerides. *Fuel* 159: 430–435.

47 Laurent, E. and Delmon, B. (1994). Study of the hydrodeoxygenation of carbonyl, carboxylic and guaiacyl groups over sulfided $CoMo/\gamma\text{-}Al_2O_3$ and $NiMo/\gamma\text{-}Al_2O_3$ catalyst: II. Influence of water, ammonia and hydrogen sulfide. *Appl. Catal., A* 109 (1): 97–115.

48 Laurent, E. and Delmon, B. (1994). Influence of water in the deactivation of a sulfided $NiMo\gamma\text{-}Al_2O_3$ catalyst during hydrodeoxygenation. *J. Catal.* 146 (1): 281–291.

49 Wang, H., Li, G.L., Rogers, K. et al. (2017). Hydrotreating of waste cooking oil over supported CoMoS catalyst catalyst – deactivation mechanism study. *Mol. Catal.* 443: 228–240.

50 Kubičková, I., Snåre, M., Eränen, K. et al. (2005). Hydrocarbons for diesel fuel via decarboxylation of vegetable oils. *Catal. Today* 106 (1): 197–200.

51 Ochoa-Hernandez, C., Yang, Y.X., Pizarro, P. et al. (2013). Hydrocarbons production through hydrotreating of methyl esters over Ni and Co supported on SBA-15 and Al-SBA-15. *Catal. Today* 210: 81–88.

52 Morgan, T., Grubb, D., Santillan-Jimenez, E., and Crocker, M. (2010). Conversion of triglycerides to hydrocarbons over supported metal catalysts. *Top. Catal.* 53 (11–12): 820–829.

53 Snåre, M., Kubičková, I., Mäki-Arvela, P. et al. (2006). Heterogeneous catalytic deoxygenation of stearic acid for production of biodiesel. *Ind. Eng. Chem. Res.* 45 (16): 5708–5715.

54 Santillan-Jimenez, E., Morgan, T., Shoup, J. et al. (2014). Catalytic deoxygenation of triglycerides and fatty acids to hydrocarbons over Ni–Al layered double hydroxide. *Catal. Today* 237: 136–144.

55 Santillan-Jimenez, E., Loe, R., Garrett, M. et al. (2018). Effect of Cu promotion on cracking and methanation during the Ni-catalyzed deoxygenation of waste lipids and hemp seed oil to fuel like hydrocarbons. *Catal. Today* 302: 261–271.

56 Loe, R., Santillan-Jimenez, E., Morgan, T. et al. (2016). Effect of Cu and Sn promotion on the catalytic deoxygenation of model and algal lipids to fuel-like hydrocarbons over supported Ni catalysts. *Appl. Catal., B* 191: 147–156.

57 Peng, B.X., Zhao, C., Kasakov, S. et al. (2013). Manipulating catalytic pathways: deoxygenation of palmitic acid on multifunctional catalysts. *Chem. Eur. J.* 19 (15): 4732–4741.

58 Foraita, S., Liu, Y., Haller, G.L. et al. (2017). Controlling hydrodeoxygenation of stearic acid to *n*-heptadecane and *n*-octadecane by adjusting the chemical properties of Ni/SiO_2-ZrO_2 catalyst. *ChemCatChem* 9 (1): 195–203.

59 Schreiber, M.W., Rodriguez-Nino, D., Gutierrez, O.Y., and Lercher, J.A. (2016). Hydrodeoxygenation of fatty acid esters catalyzed by Ni on nano-sized MFI type zeolites. *Catal. Sci. Technol.* 6 (22): 7976–7984.

60 Kikhtyanin, O.V., Rubanov, A.E., Ayupov, A.B., and Echevsky, G.V. (2010). Hydroconversion of sunflower oil on Pd/SAPO-31 catalyst. *Fuel* 89 (10): 3085–3092.

61 Liu, Q.Y., Zuo, H.L., Zhang, Q. et al. (2014). Hydrodeoxygenation of palm oil to hydrocarbon fuels over Ni/SAPO-11 catalysts. *Chin. J. Catal.* 35 (5): 748–756.

62 Ahmadi, M., Nambo, A., Jasinski, J.B. et al. (2015). Decarboxylation of oleic acid over Pt catalysts supported on small-pore zeolites and hydrotalcite. *Catal. Sci. Technol.* 5 (1): 380–388.

63 Wang, C.X., Tian, Z.J., Wang, L. et al. (2012). One-step hydrotreatment of vegetable oil to produce high quality diesel-range alkanes. *ChemSusChem* 5 (10): 1974–1983.

64 Sousa, L.A., Zotin, J.L., and da Silva, V.T. (2012). Hydrotreatment of sunflower oil using supported molybdenum carbide. *Appl. Catal., A* 449: 105–111.

65 Han, J.X., Duan, J.Z., Chen, P. et al. (2011). Molybdenum carbide-catalyzed conversion of renewable oils into diesel-like hydrocarbons. *Adv. Synth. Catal.* 353 (14–15): 2577–2583.

66 Hollak, S.A.W., Gosselink, R.W., van Es, D.S., and Bitter, J.H. (2013). Comparison of tungsten and molybdenum carbide catalysts for the hydrodeoxygenation of oleic acid. *ACS Catal.* 3 (12): 2837–2844.

67 Stellwagen, D.R. and Bitter, J.H. (2015). Structure-performance relations of molybdenum- and tungsten carbide catalysts for deoxygenation. *Green Chem.* 17 (1): 582–593.

68 Kim, S.K., Yoon, D., Lee, S.C., and Kim, J. (2015). Mo_2C/graphene nanocomposite as a hydrodeoxygenation catalyst for the production of diesel range hydrocarbons. *ACS Catal.* 5 (6): 3292–3303. https://doi.org/10.1021/acscatal.5b00335.

69 Kim, S.K., Kim, J., and Lee, S.C. (2017). Surface-termination dependence of propanoic acid deoxygenation on Mo_2C. *Catal. Commun.* 99: 61–65.

70 Shi, Y., Yang, Y., Li, Y.W., and Jiao, H.J. (2016). Theoretical study about Mo_2C(101)-catalyzed hydrodeoxygenation of butyric acid to butane for biomass conversion. *Catal. Sci. Technol.* 6 (13): 4923–4936.

71 Wang, H.L., Yan, S.L., Salley, S.O., and Ng, K.Y.S. (2012). Hydrocarbon fuels production from hydrocracking of soybean oil using transition metal carbides and nitrides supported on ZSM-5. *Ind. Eng. Chem. Res.* 51 (30): 10066–10073.

72 Nguyen, H.S.H., Maki-Arvela, P., Akhmetzyanova, U. et al. (2017). Direct hydrodeoxygenation of algal lipids extracted from *Chlorella alga*. *J. Chem. Technol. Biotechnol.* 92 (4): 741–748.

73 Al Alwan, B., Salley, S.O., and Ng, K.Y.S. (2015). Biofuels production from hydrothermal decarboxylation of oleic acid and soybean oil over Ni-based transition metal carbides supported on Al-SBA-15. *Appl. Catal., A* 498: 32–40.

74 Guan, Q., Wan, F., Han, F. et al. (2016). Hydrodeoxygenation of methyl palmitate over MCM-41 supported nickel phosphide catalysts. *Catal. Today* 259: 467–473.

75 Liu, Y.H., Yao, L., Xin, H. et al. (2015). The production of diesel-like hydrocarbons from palmitic acid over HZSM-22 supported nickel phosphide catalysts. *Appl. Catal., B* 174: 504–514.

76 Pan, Z.Y., Wang, R.J., Nie, Z.Y., and Chen, J.X. (2016). Effect of a second metal (Co, Fe, Mo and W) on performance of Ni_2P/SiO_2 for hydrodeoxygenation of methyl laurate. *J. Energy Chem.* 25 (3): 418–426.

77 Peroni, M., Lee, I., Huang, X. et al. (2017). Deoxygenation of palmitic acid on unsupported transition-metal phosphides. *ACS Catal.* 7 (9): 6331–6341.

78 Xin, H., Guo, K., Li, D. et al. (2016). Production of high-grade diesel from palmitic acid over activated carbon-supported nickel phosphide catalysts. *Appl. Catal., B* 187: 375–385.

79 Yang, Y.X., Ochoa-Hernandez, C., O'Shea, V.A.D. et al. (2012). Ni_2P/SBA-15 as a hydrodeoxygenation catalyst with enhanced selectivity for the conversion of methyl oleate into *n*-octadecane. *ACS Catal.* 2 (4): 592–598.

80 Yang, Y.X., Ochoa-Hernandez, C., Pizarro, P. et al. (2015). Influence of the Ni/P ratio and metal loading on the performance of NixPy/SBA-15 catalysts for the hydrodeoxygenation of methyl oleate. *Fuel* 144: 60–70.

81 Zarchin, R., Rabaev, M., Vidruk-Nehemya, R. et al. (2015). Hydroprocessing of soybean oil on nickel-phosphide supported catalysts. *Fuel* 139: 684–691.

82 Yang, Y., Chen, J., and Shi, H. (2013). Deoxygenation of methyl laurate as a model compound to hydrocarbons on Ni_2P/SiO_2, Ni_2P/MCM-41, and Ni_2P/SBA-15 catalysts with different dispersions. *Energy Fuels* 27 (6): 3400–3409.

Catalysis Today 227 (2014) 154–162

Contents lists available at ScienceDirect

Catalysis Today

journal homepage: www.elsevier.com/locate/cattod

Aldol condensation of furfural and acetone on zeolites

Oleg Kikhtyanin[a], Vendula Kelbichová[a], Dana Vitvarová[b], Martin Kubů[b],
David Kubička[a,*]

[a] Research Institute of Inorganic Chemistry, RENTECH-UniCRE, Chempark Litvínov, Záluží–Litvínov, 436 70, Czech Republic
[b] J. Heyrovský Institute of Physical Chemistry, Academy of Sciences of the Czech Republic, v.v.i., Dolejškova 3, 182 23 Prague, Czech Republic

ARTICLE INFO

Article history:
Received 26 July 2013
Received in revised form 13 October 2013
Accepted 18 October 2013
Available online 27 November 2013

Keywords:
Aldol condensation
Oligomerization
Zeolites
Acidity
Coke formation
Regeneration

ABSTRACT

Zeolites of different structural types were used as catalysts for aldol condensation of furfural and acetone in batch reaction conditions at $T = 20$–$100\,^{\circ}$C and time 0–24 h. To establish a relation between physico-chemical and catalytic properties of microporous materials, the samples were characterized by SEM, N_2 adsorption, FTIR and TGA. It was found that the acidic solids possessed appreciable activity in the reaction and resulted in a formation of products of aldehyde–ketone interaction. Nevertheless, furfural conversion decreased rapidly due to coke formation inside zeolite pores. Simultaneously with a general route of the reaction observed for basic catalysts, dimerization of the condensation product on acidic sites occurred. It was supposed that catalytic behavior of zeolites considerably affected by their both structural and textural properties. Experiments with re-used samples showed that zeolites totally restored their activity and selectivity after calcination at 530 °C.

1. Introduction

In conditions of unpredictable prices for conventional hydrocarbon sources, it is of a great importance to develop new technologies based on non-traditional, renewable energy supplies. At present, significant research attention is focused on the transformation of waste biomass into fuels and valuable chemicals [1,2]. The primary transformation of biomass can proceed by different routes resulting in a formation of bio-oil (by liquefaction and/or pyrolysis), sugar solutions, etc. [1–6]. Acetone, which is obtained as a product of acetic acid decomposition (ketonization), and furanic compounds that are afforded by sugars hydrolysis are among the final products of the successive transformation steps involved in conversion of the starting complex biomass mixtures. Furanic compounds and acetone, being aldehydes and a ketone by chemical origin, may further react with each other via aldol condensation in the presence of the corresponding catalyst [7–9]. In this respect, aldol condensation seems to be a useful tool to increase a length of carbon chain and to produce heavier reaction products from comparatively light initial reagents. The aldol condensation step is of particular importance in upgrading of bio-oils since these light molecules would be otherwise converted into low-value gaseous products during bio-oil deoxygenation that is necessary to improve its stability and enhance its fuel properties [10].

Aldol condensation of aldehydes and ketones is a well-known reaction of organic synthesis and it proceeds in the presence of catalysts with either basic or acidic properties. Most often basic catalysts are used for this reaction because they possess high activity in conversion of reagents and high selectivity toward the desired reaction products (Scheme 1). Sodium hydroxide is a recognized catalyst for aldol condensation, which permits to carry out the reaction even at room temperature [8]. Nevertheless, high corrosivity of this compound and the increasing demands for environmental friendliness of new technologies result in a necessity of using heterogeneous catalytic systems with similar basic properties. Catalysts derived from hydrotalcite-like (HTC) materials as well as other mixed oxide systems were found to be good heterogeneous catalysts with basic properties, which were successively employed as catalysts for aldol condensation [11–14]. It is known that re-hydrated HTC materials allow carrying out aldol condensation between furfural and acetone with high furfural conversion already at 50–60 °C [13]. Nevertheless, a number of published works dealing with the properties of HTC materials indicate significant disadvantages of these materials; in particular high sensitivity to the ambient CO_2 and problems with re-using the HTC-based catalysts in successive catalytic runs [11,15,16].

Solid catalysts with acidic properties are used seldom as catalysts for aldol condensation in comparison with basic heterogeneous catalysts. Zeolites, being materials with pronounced and controllable acidic properties, seem to be suitable materials for this purpose. Indeed, it is known that acidic zeolites

---

* Corresponding author. Tel.: +420 476163735.
E-mail address: david.kubicka@vuanch.cz (D. Kubička).

0920-5861/$ – see front matter © 2013 Elsevier B.V. All rights reserved.
http://dx.doi.org/10.1016/j.cattod.2013.10.059

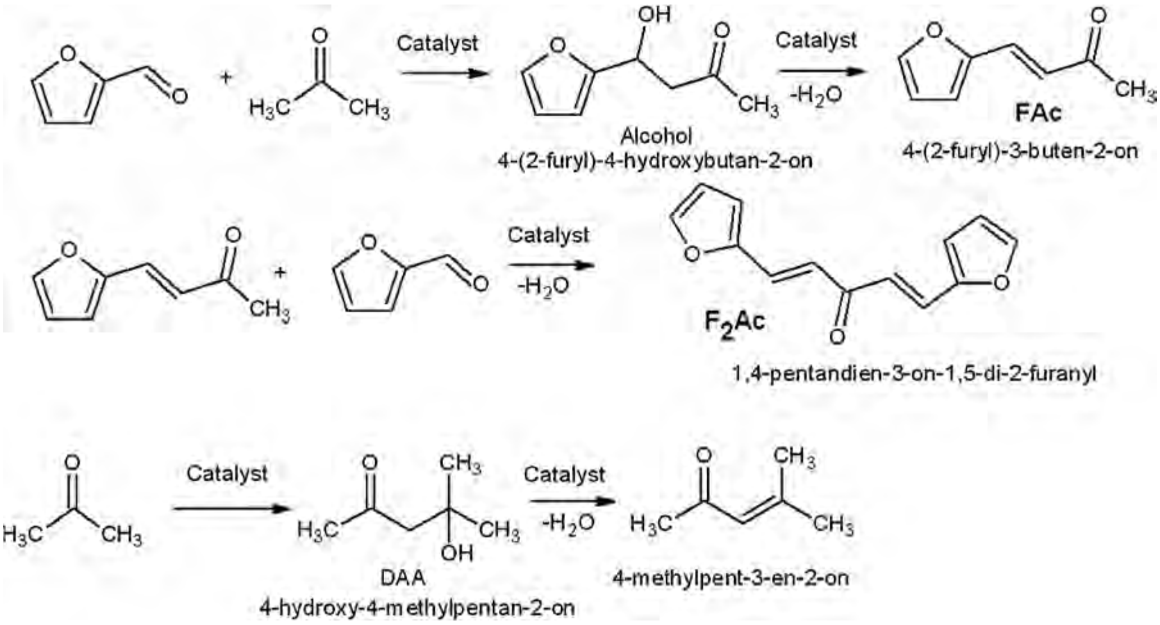

Scheme 1. Aldol condensation between furfural and acetone over acidic or basic catalysts.

of different structural types can catalyze condensation of various aldehydes and ketones [17–19]. However, the examples of using zeolites as catalysts for aldol condensation are still few. Therefore, further investigation to gain deeper understanding of the suitability of these microporous materials as catalysts for reactions of different biomass-derived aldehydes and ketones are required to promote the development of efficient biomass transformation routes into fuel components and valuable chemicals.

The present work aims at understanding of the relationship between the properties of zeolites of different structural type and their catalytic performance in aldol condensation of furfural and acetone. Both activity and selectivity of these materials are correlated with their physico-chemical properties.

2. Experimental

2.1. Supply and preparation of catalysts

Zeolite samples for the study (NH_4-ZSM-5(23), NH_4-ZSM-5(50), NH_4-BEA(25), NH_4-BEA(38), NH_4-MOR(20), HSDUSY(80), HSUSY(5)) were provided by Zeolyst International. The numbers in parentheses designate SiO_2/Al_2O_3 molar ratio of the samples as given by the manufacturer. The transformation of NH_4-form of zeolites to the corresponding H-form was carried out by calcination in air at 500 °C for 4–6 h. The effect of chemical composition of the samples on their physico-chemical and catalytic properties was investigated by using materials of the same structural type with different SiO_2/Al_2O_3 molar ratio.

2.2. Physico-chemical characterization

The shape and size of the zeolite crystals were determined by scanning electron microscopy (SEM, Jeol, JSM-5500LV). The textural properties of the samples were determined by nitrogen physisorption at 77 K using an ASAP 2020 (Micromeritics) static volumetric apparatus. In order to attain sufficient accuracy in the accumulation of the adsorption data, the ASAP 2020 was equipped with pressure transducers covering the 133 Pa, 1.33 kPa and 133 kPa ranges. The zeolite samples were outgassed under turbomolecular pump vacuum before starting the adsorption experiments. The zeolite samples were outgassed at 110 °C (heating rate 1 °C/min starting from the ambient temperature) until the residual pressure of 0.5 Pa was obtained. After further heating at 110 °C for 1 h the temperature was increased until the temperature 300 °C (heating rate 1 °C/min) was achieved. This temperature was maintained for 6 h.

Acidic properties of zeolites were examined by IR spectroscopy of adsorbed pyridine on Nicolet 6700 spectrometer equipped with MCT detector. Pyridine adsorption proceeded at 150 °C for 20 min at partial pressure 3 Torr, followed by 20 min evacuation at 150 °C. The concentrations of Brønsted and Lewis acid sites were calculated from integral intensities of the individual bands characteristic of pyridine adsorbed on Brønsted acid sites (BAS, at 1545 cm^{-1}) and on Lewis acid sites (LAS, at 1455 cm^{-1}) and molar absorption coefficients of $\varepsilon(B) = 1.67 \pm 0.1$ cm μmol^{-1} and $\varepsilon(L) = 2.22 \pm 0.1$ cm μmol^{-1}, respectively [20]. The spectra were recorded with a resolution of 4 cm^{-1} by collection of 128 scans for a single spectrum. Prior to the adsorption of pyridine, self-supporting wafers of samples were activated in situ by overnight evacuation at temperature 450 °C.

2.3. Catalysis

Properties of zeolite samples were investigated in aldol condensation of furfural and acetone. The catalytic experiments were carried out in a 100 ml stirred batch reactor (a glass flask reactor with magnetic stirring for the experiments at 20 and 60 °C, Parr stirred autoclave for the experiments at 100 °C). Before the start of the catalytic runs at 20 and 60 °C, 2 g of catalyst was mixed together with a stirred mixture of 39.5 g acetone and 6.5 g of furfural (acetone/furfural molar ratio 10/1, pre-heated to the desired reaction temperature, 20 or 60 °C) and kept at the reaction temperature for 2–24 h under intensive stirring. For autoclave experiments, 2 g of catalyst was mixed together with the reaction mixture of the above composition and loaded into the autoclave. After initiation of the heating the desired temperature was achieved in

~60 min, and the autoclave was kept at $T = 100\,^{\circ}\mathrm{C}$ for additional 0, 2 or 8 h.

Analysis of the reaction products was performed on an Agilent 7890A GC unit equipped with a flame ionization detector using a HP-5 capillary column (30 m/0.32 ID/0.25 μm). The obtained products were identified based on the standard reference compounds as well as additional GC-MS analyses.

3. Results and discussion

3.1. Physico-chemical characterization

The performed XRD analysis confirmed that all the samples were phase-pure zeolites of the declared structure with a high degree of crystallinity. Fig. 1 shows SEM images of the zeolite samples. It

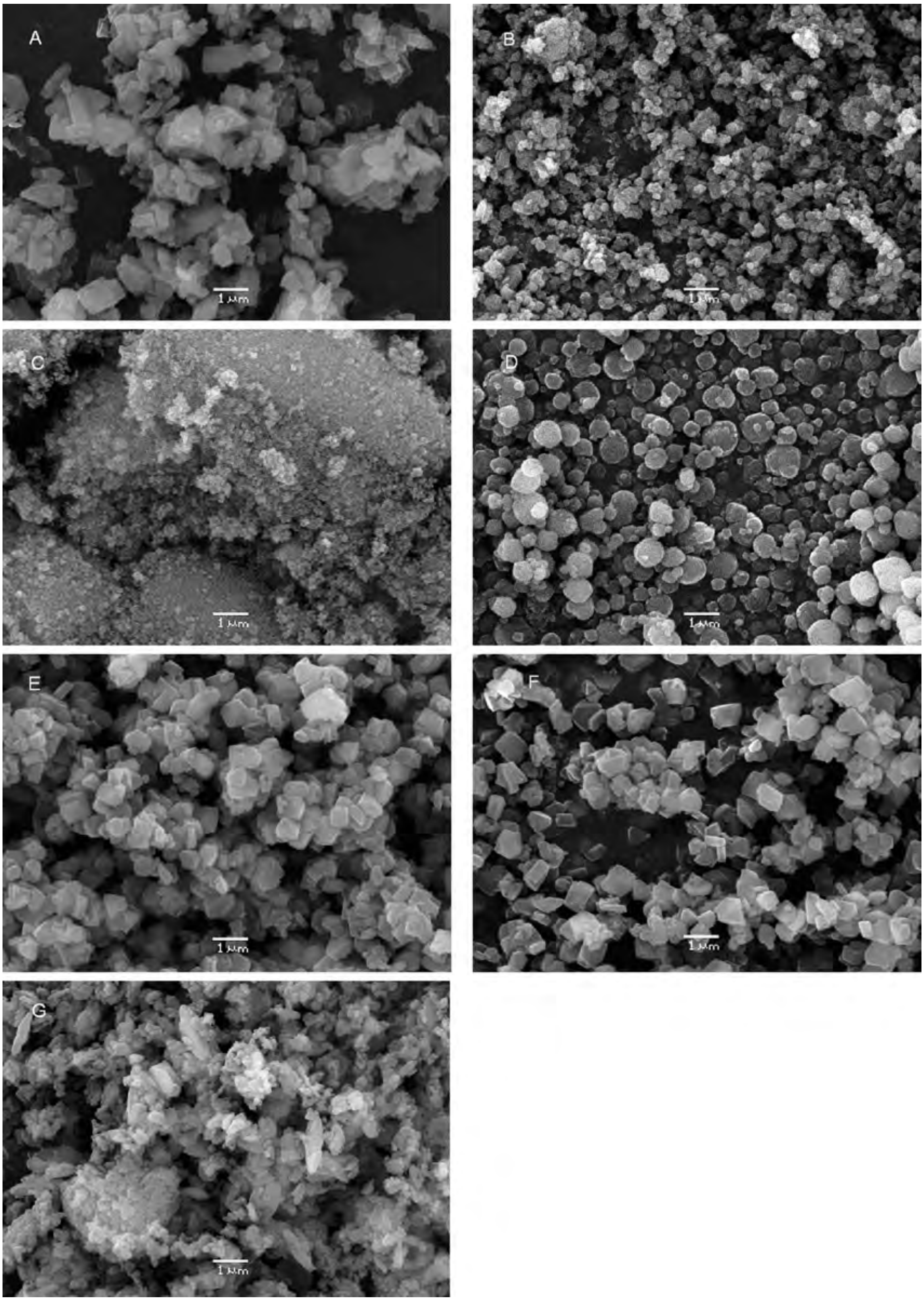

Fig. 1. SEM images of zeolites samples. (A) NH_4-ZSM-5(23), (B) NH_4-ZSM-5(50), (C) NH_4-BEA(25), (D) NH_4-BEA(38), (E) HSDUSY(80), (F) HSUSY(5), (G) NH_4-MOR(20).

Table 1
Textural properties of zeolite samples.

Sample	BET (m^2/g)	S_{ext} (m^2/g)	V_{mic} (cm^3/g)	V_{meso} (cm^3/g)	V_{tot} (cm^3/g)	D_{BJH} (Å)
HZSM-5(23)	378	99	0.126	0.055	0.210	10.9
HZSM-5(50)	398	133	0.118	0.102	0.255	10.0
HBEA(25)	608	222	0.174	0.851	1.017	9.2
HBEA(38)	617	134	0.218	0.036	0.334	–
HSDUSY(80)	840	294	0.246	0.210	0.536	13.6
HSUSY(5)	588	94	0.226	0.166	0.388	7.4
HMOR(20)	471	55	0.190	0.015	0.269	–

BET, surface area (from BET method); V_{mic}, micropore volume (from *t*-plot method); V_{meso}, mesopore volume (from BJH method); V_{int}, interparticle space volume; V_{tot}, total pore volume at $p/p_0 = 0.97$; *D*, average pore diameter (from BJH method, for mesoporous samples).

can be seen that the size and shape of the crystals of MFI zeolites differ between the samples with different Al content (Fig. 1A and B). NH_4-ZSM-5(23) sample is represented by well-defined individual crystals of 0.5–1 μm. In contrast, the crystals of NH_4-ZSM-5(23) do not possess a certain shape and their size varies from 100 to 300 nm. The crystals of two samples with BEA structure are also different (Fig. 1C and D). NH_4-BEA(25) consists of very large agglomeration of small crystals with the size smaller than 100 nm. SEM image of NH_4-BEA(38) indicates the presence of spherical particles in a wide range of 0.2–1 μm. Crystal morphology of two FAU samples is similar: they consist of crystals with dimensions of 0.2–1 μm (Fig. 1E and F). The size of crystals of MOR zeolite lies in the same wide range of 0.2–1 μm (Fig. 1G).

The adsorption characteristics of zeolites of different structural types are presented in Table 1. Obviously, BET surface is determined by a structural type of the zeolite material. This value is the highest for the three-dimensional wide-pore BEA (608–617 m^2/g) and FAU (588–840 m^2/g) materials, while the lowest value is observed for medium-pore MFI (378–398 m^2/g). MOR zeolite, which belongs to one-dimensional wide-pore microporous systems, takes an intermediate position. Both BEA samples have similar BET surface values, despite the fact that, according to SEM, their crystal morphology varies significantly. This can be explained by assuming that the particles of H-BEA(38) zeolite with a visual size of 0.2–1 μm consist in fact of very small crystals similar to those of H-BEA(25) zeolite. The differences in the micropore volume of the samples are similar to those observed for the BET surface: the highest value V_{mic} is observed for BEA and FAU zeolites, and the lowest - for MFI. Besides, the results presented in Table 1 indicate that mesoporosity of the samples varies to a great extent. For example, the mesopore volume is in the range 0.055–0.1 cm^3/g for MFI samples and in the range 0.166–0.21 cm^3/g for FAU samples. In the case of BEA zeolites the difference in mesoporosity is more pronounced: it reaches 0.85 cm^3/g for H-BEA(25), but it is almost absent for H-BEA(38) (Figs. 2 and 3).

The concentration of strong BAS and LAS present in the samples was determined by FTIR of adsorbed pyridine (Table 2). Both the amount of these sites and BAS/LAS ratio depend to a large extent on the Al content in the samples. For zeolites of the same structural type an increase in Al content results in an increased concentration of LAS and, as a result, in a decreased BAS/LAS ratio. For MFI materials an increase of the SiO_2/Al_2O_3 ratio leads to a decreased

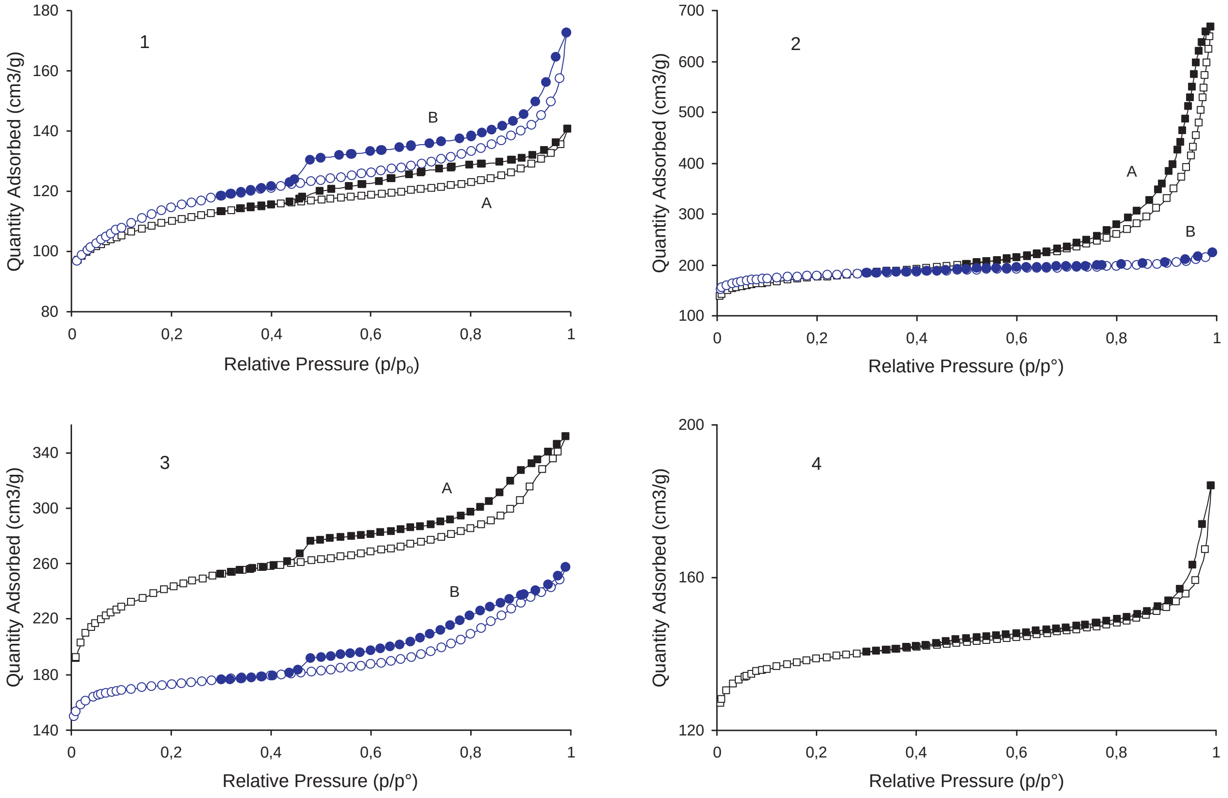

Fig. 2. Isotherms of zeolite samples. 1 – HZSM-5 (A – HZSM-5(23), B – HZSM-5(50)), 2 – HBEA (A – HBEA(25), B–HBEA(38)), 3 – FAU (A – HSDUSY(80), B – HSUSY (5)), 4 – HMOR(20).

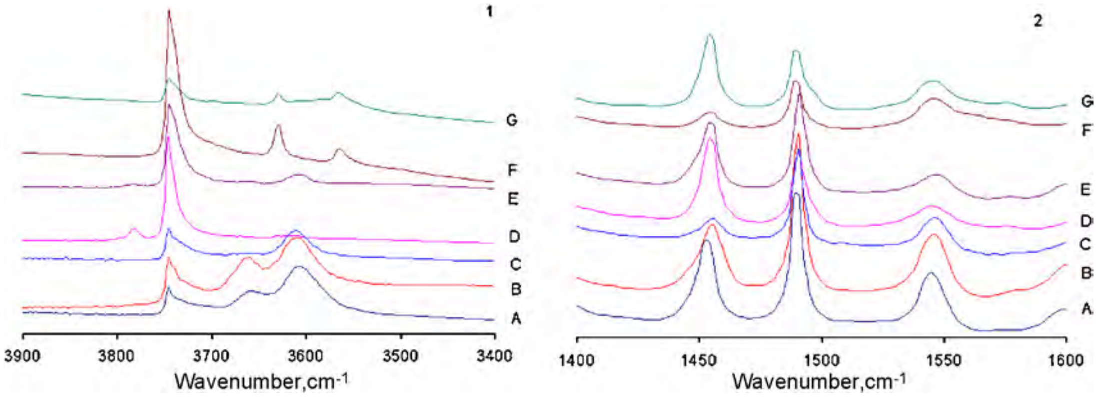

Fig. 3. IR spectra in the OH vibration region (1) and spectra after pyridine adsorption (2). (A) HMOR(20), (B) HZSM-5(23), (C) HZSM-5(50), (D) HBEA(25), (E) HBEA(38), (F) HSDUSY(80), (G) HSUSY (5).

Table 2
Acidic properties of zeolite samples obtained by FTIR method.

Sample	C_{LAS} (mmol/g)	C_{BAS} (mmol/g)	C_{LAS}/C_{BAS}
HZSM-5(23)	0.220	0.353	1.6
HZSM-5(50)	0.049	0.183	3.73
HBEA(25)	0.255	0.138	0.54
HBEA(38)	0.179	0.142	0.79
HSDUSY(80)	0.068	0.104	1.53
HSUSY(5)	0.223	0.127	0.57
HMOR(20)	0.241	0.282	1.17

concentration of BAS, but for BEA and FAU zeolites the same trend is not obvious.

3.2. *Catalysis*

3.2.1. *The catalytic performance of the zeolites*

Table 3 contains the results on furfural conversion over zeolites with different structural types and nature of the compensating cations (NH_4^+ and H^+). It can be clearly seen that the properties of the investigated zeolites substantially influence their activity in aldol condensation. Regardless of the type of crystal framework, all the samples in the NH_4-form possess very low activity in the reaction. In contrast, the application of zeolites in the H-form results in a noticeable increase of furfural conversion, especially at high reaction temperature. The difference in the catalytic performance between the samples in NH_4- and H-forms unambiguously proves that aldol condensation of furfural and acetone takes place with the participation of acidic sites of zeolites. A correlation of the catalytic performance of the zeolite samples with their physico-chemical characteristics permits to evaluate the key factors determining the activity of zeolites in aldol condensation of furfural and acetone.

Table 3
Furfural conversion (%) at different reaction temperatures (after 2 h of the reaction).

Sample	Reaction temperature (°C)		
	20	60	100
NH_4-ZSM-5(23)	0	0	0
HZSM-5(23)	0	1.5	6.4
NH_4-ZSM-5(50)	0	0	0.7
HZSM-5(50)	0	3.1	9.5
NH_4-MOR	0	0	0.7
HMOR(20)	0	1.1	6.8
NH_4-BEA(25)	0	0	7.1
HBEA(25)	2.8	19.7	38.5
NH_4-BEA(38)	0	0	6.2
HBEA(38)	6.5	22.6	29.0
HSDUSY(80)	1.6	10.4	21.8
HSUSY(5)	0	1.3	12.0

It is evident that crystal structure of zeolites introduces considerable influence on their behavior in the reaction. Medium pore MFI zeolites and wide-pore mono-dimensional MOR zeolite possess low activity, and furfural conversion over these catalysts does not exceed 10% even at $T = 100$ °C (Table 3). On the other hand, the activity of wide-pore zeolites with three-dimensional crystal framework increases when they are transformed into H-form, and furfural conversion over BEA zeolites achieves 30% at $T = 100$ °C after 2 h of the reaction. It can be assumed that in addition to the crystal structure additional characteristics, for example, textural and acidity properties, influence the catalytic properties of the molecular sieves. However, taking together FTIR data with catalytic results it becomes obvious that not only the acidic properties of zeolites introduce a decisive influence on their catalytic activity in the reaction. A comparison of acidic properties of the two iso-structural HBEA samples indicates that BAS concentration in these materials is similar, and LAS concentration is higher for the sample with higher Al content, namely HBEA(25). At the same time, their activity in aldol condensation is approximately the same. It leads to the conclusion that the reaction between furfural and acetone over zeolites proceeds with participation of BAS rather than LAS. Nonetheless, comparison of two FAU samples shows that HSDUSY(80) with lower BAS and, in particular, LAS, concentrations is more active in the reaction than HSUSY(5). The same tendency also occurs in the case of two MFI zeolites: activity of HZSM-5(50) with lower acidity is higher compared with that of HZSM-5(23). These dependences lead to the conclusion that the acidity of the zeolite is not the single factor that determines the catalytic performance of the investigated zeolites in aldol condensation.

Study of textural characteristics of zeolites and their SEM data show that materials with smaller crystal sizes possess larger values of BET surface area and external surface area. Obviously, the larger the external surface, the greater is the amount of pore openings available for the access of the reactant molecules into the internal pore system. Indeed, when correlating the activity of the catalysts with their textural characteristics, it is seen that the materials with larger BET surface values exhibit higher activity in the reaction. Summarizing the results, it can be concluded that the activity of zeolites in aldol condensation of furfural and acetone increases when wide-pore three-dimensional microporous materials with small crystal size are used.

Furfural conversion over different zeolites in dependence on reaction time at $T = 60$ and 100 °C is shown on Fig. 4. It is seen that furfural conversion increases very fast during the initial period of the reaction, and after approximately 2 h the catalysts achieve a quasi-stationary state, i.e. the conversion of furfural increases only very slightly. Among the wide-pore materials, BEA zeolites are the most active microporous materials at any

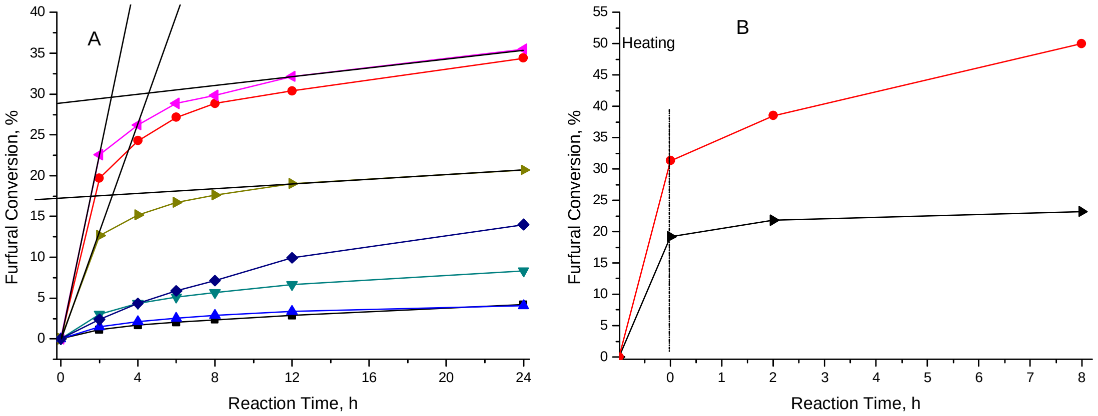

Fig. 4. Conversion of furfural over different zeolites in H-form at 60 °C (A) and 100 °C (B). (■) HMOR(20), (▲) HZSM-5(28), (▼) HZSM-5(50), (◆) HSUSY(5), (►) HSDUSY(80), (•) HBEA(25), (◄) HBEA(38).

reaction time as compared to FAU zeolites. An evaluation of the initial and quasi-stationary reaction rates can be performed using the angles of the slopes of the lines derived from the kinetic curves in the range 0–2 h and 4–24 h, respectively. The calculations show that for BEA and FAU zeolites the initial and quasi-stationary reaction rates differ by more than an order of magnitude ($W_{\text{ini}}/W_{\text{quasi}} = \text{tg}\alpha_{0-2}/\text{tg}\alpha_{4-24} = 30 - 40$), which indicates severe deactivation.

The composition of the reaction products obtained on zeolites with different structure types substantially depends on the activity of the catalysts or more specifically on the level of furfural conversion. For the samples with low activity, i.e. MFI and MOR zeolites, FAc is as the major reaction product with selectivity ≥95% in the range of reaction temperatures 20–100 °C. The single by-product in this case is the corresponding alcohol, which is in line with the consecutive reaction mechanism and proves its fast dehydration to FAc on acidic sites of zeolites (Scheme 1). The use of the wide-pore three-dimensional zeolites results in an increased furfural conversion, and, as a result, the composition of the products formed in aldol condensation also changes. The yield of the reaction products as a function of furfural conversion observed over HBEA(25) and HSDUSY(80) catalysts at $T = 60\,°\text{C}$ is plotted in Fig. 5A. FAc is the major compound formed in the reaction, and its yield increases linearly as the furfural conversion increases. The corresponding alcohol is absent among the reaction products due to its total and fast dehydration at this reaction temperature. Independently on the furfural conversion, the content of F_2Ac, i.e. the subsequent condensation product (Scheme 1), is very low. This proves that at given reaction conditions the subsequent condensation of the second furfural molecule with FAc hardly occurs. An explanation might be the low concentration of furfural, or more plausibly, the limited dimensions of the pores that hinder the formation and diffusion of the bulky F_2Ac product.

Simultaneously, the formation of a heavier reaction product than F_2Ac is observed (Fig. 4). GC–MS analysis of this compound proves its molecular weight to be 272. The molecular mass corresponds to a dimer of FAc and it can thus be assumed that this compound is a result of dimerization of olefinic FAc molecule on acid sites of zeolites (Scheme 2). However, at present it remains still unclear at which double bond the dimerization occurs and additional experiments will be carried out to clarify this issue. The content of this dimer $(FAc)_2$ also increases with the growth of the furfural conversion. Fig. 5 also shows that yield of this dimer compound is larger when using HSDUSY zeolite as a catalyst compared with HBEA(25). Taking into account the data on textural and acidic properties of these zeolites (Tables 1 and 2) it may be assumed that the formation of this dimer readily occurs inside microporous volume of zeolites, and large cages of FAU structure are the most suitable for this reaction route. Similar composition of reaction products and their dependence on furfural conversion are observed when the reaction temperature is increased to 100 °C (Fig. 5B).

The formation of this dimer compound was not yet reported in literature dealing with aldol condensation on HTC materials and other basic catalysts. By comparing the composition of the reaction products which is observed on basic materials (double oxides) and on acidic materials (zeolites) it could be concluded that for

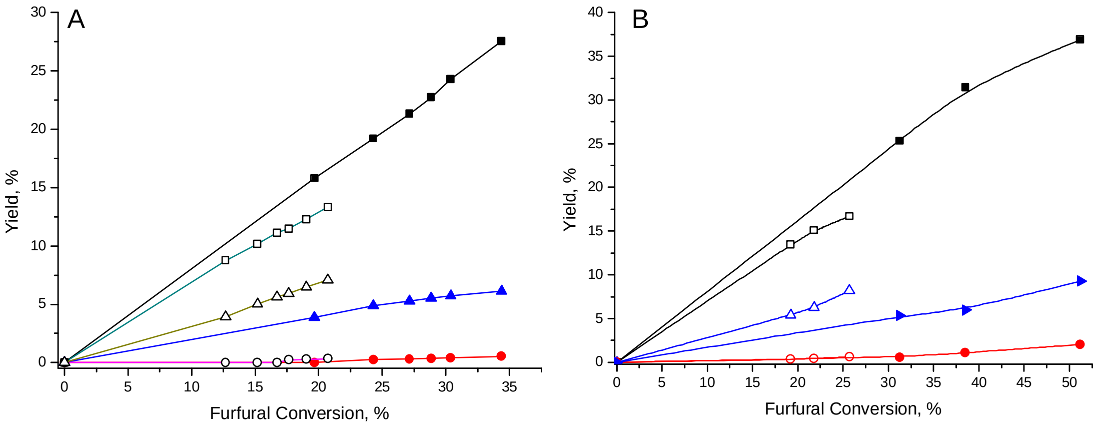

Fig. 5. Yield of reaction products formed in aldol condensation of furfural and acetone over HBEA(25) (■,•,▲) and HSDUSY(80) (□, ○, Δ) at 60 °C (A) and 100 °C (B). (■) FAc, (•) F_2Ac, (▲) $(FAc)_2$.

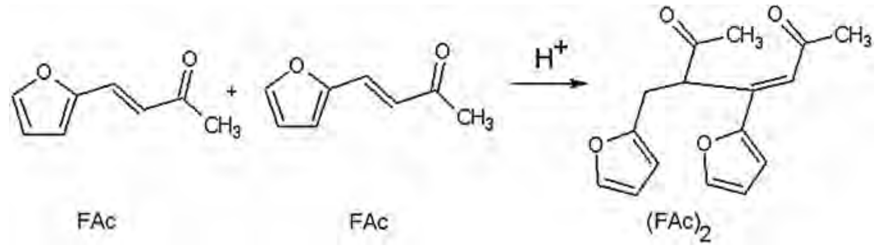

Scheme 2. Formation of dimer product from FAc compound.

both types of catalysts FAc is the primary general product of aldol condensation which is formed by dehydration of the corresponding alcohol. A further transformation of the formed FAc compound proceeds by different routes on either basic or acid catalysts. The consecutive aldol condensation of FAc to F_2Ac takes readily place over HTC, i.e. basic catalysts, while zeolites favor mostly dimerization of FAc to $(FAc)_2$ due to the presence of unsaturated bonds in FAc which can readily interact with Brønsted acid sites.

3.2.2. TGA of the spent catalysts

As shown by the catalytic tests, the activity of zeolites in aldol condensation of furfural and acetone is high at the beginning of the reaction but rapidly decreases with the increasing time of the experiment. The samples recovered from the reactor are black in color suggesting a big amount of coke deposits in them. The catalysts after reaction were thus abundantly washed with ethanol to remove any organics from external surface of the zeolite crystals, and the content of the carbonaceous deposits inside micropore volume was investigated by TGA (Fig. 6).

Two regions of weight loss, low-temperature (LT) and high-temperature (HT), are clearly found on the curves. Regardless of the atmosphere in which the experiments have been carried out the maximum of the LT peak is observed in the range of 57–78 °C, which corresponds to the removal of residual light compounds from the samples. The weight loss in this region is in the range 3.2–6.5% (Table 4).

The position and intensity of the DTG peaks located in HT region depend both on the structural type of the zeolite samples and on the conditions of the thermal analysis. Heating of the spent HBEA(25) sample in nitrogen atmosphere results in appearance of a broad peak with maximum at 400 °C and weight loss of 5.3%. If the experiment is performed in oxidative atmosphere, two HT peaks are observed: at 380 °C with a weight loss of 4.1% and at 459 °C with weight loss of 6.5% (Fig. 6). It may be concluded that peaks at 380–400 °C correspond to desorption of heavy reaction products from the zeolite pores while the latter peak is attributed to the oxidative destruction of the non-desorbed compounds, which cannot escape from the internal zeolite volume. Fig. 6 also shows that DTG profiles are nearly identical for all investigated zeolites and the findings can be summarized as follows: carbonaceous deposits formed during aldol condensation of furfural and acetone are removed from the internal volume of microporous materials in two stages. At 300–360 °C occurs either removal of light reaction products or thermal degradation of heavier substances. At 450–510 °C takes place burning of the residual coke compounds in the oxidative atmosphere.

3.2.3. Catalytic properties of re-used samples

It is known that oxidative treatment does not result in a total restoration of the catalytic activity of HTC materials in aldol condensation [13]. This disadvantage substantially reduces the prospects of these materials as catalysts for practical use. Unlike

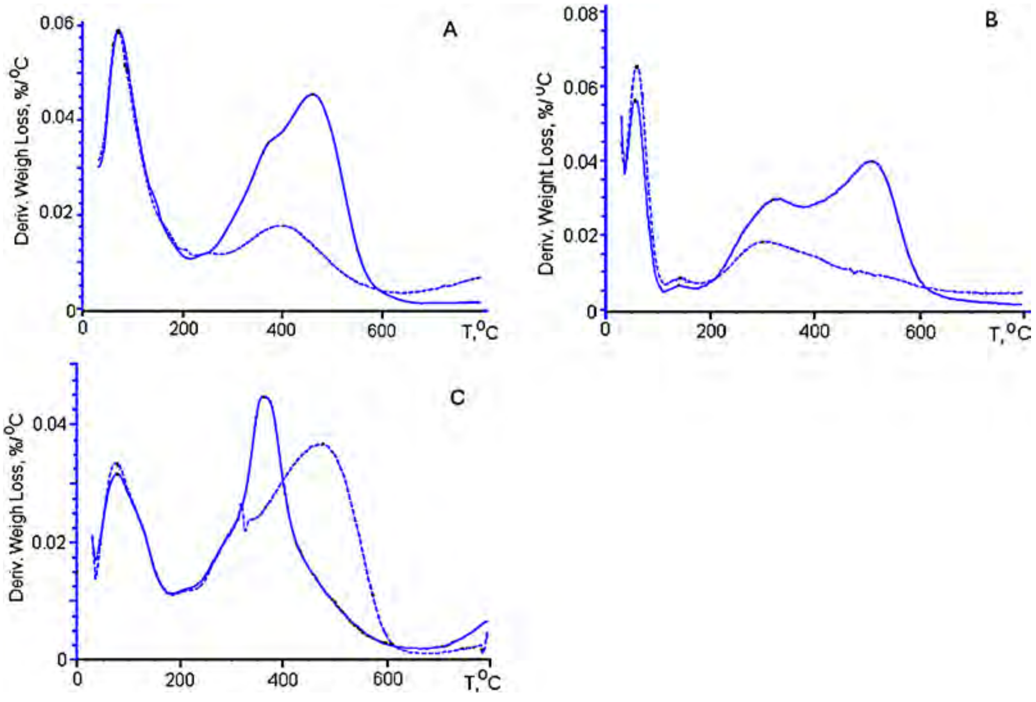

Fig. 6. DTG profiles obtained in inert (dotted line) and oxidative (solid line) ambience for HBEA(25) (A), HSDUSY(80) (B) and HZSM-5(23) (C).

Table 4
Results of TGA for zeolite samples carried out in inert (nitrogen) and oxidative (oxygen) atmospheres.

Sample	Conditions of TGA experiments	Temperature region (°C)	Maximum value on DTG curve (°C)	Weight loss (%)
HBEA(25)	N_2	20–200	70	6.5
		200–600	400	5.3
	O_2	20–200	72	6.2
		200–600	380; 459	4.1; 6.2
HSDUSY(80)	N_2	20–200	60;	3.3;
			142	0.7
		200–600	301	6.4
	O_2	20–200	57; 140	3.2; 0.5
		200–600	318; 510	4.5; 6.7
HZSM-5(23)	N_2	20–200	78	3.5
		200–600	362	8.1
	O_2	20–200	78	3.6
		200–600	338; 477	3.2; 6.7

Table 5
Catalytic properties of the re-used catalysts after washing with ethanol and calcination at 530 °C in comparison with the fresh HBEA(25) sample. $T_{reac.}$ = 100 °C (except for *, $T_{reac.}$ = 60 °C), time of the reaction – 2 h.

Sample	Furfural conversion (%)	Selectivity (%)		
		FAc	F_2Ac	$(FAc)_2$
HBEA(25), 1st run	38.5	79.5	3.7	16.8
HBEA(25), 2nd run (washed with ethanol)	20.2	88.5	4.6	6.9
HBEA(25), 2nd run (calcined at 530 °C)	40.2	71.8	3.6	24.6
*HBEA(25), T = 60 °C (conversion ca. 20%)	19.8	80.2	0	19.8

HTC, most zeolites are known to be very resistant to oxidative regeneration up to T = 500–550 °C and totally restore their properties during their re-using as catalysts in different organic reactions.

It is seen from Table 5 that washing of HBEA(25) with an excess of ethanol does not restore the initial activity of HBEA(25) completely, and furfural conversion over the washed sample attains only 20% comparing with 39% for the fresh catalyst. Additionally, a change in the composition of the reaction products formed on the washed sample is also observed: the selectivity toward the first product of aldol condensation, FAc, increases and the selectivity toward dimer product, $(FAc)_2$, correspondingly, decreases. Provided that the microporous volume of this zeolite after reaction and washing is still filled with carbonaceous deposits, the moderate decrease in conversion of furfural for the washed sample proves that aldol condensation of furfural and acetone can proceed with participation of both internal and external acid sites of HBEA(25). At the same time, a significant decrease of the selectivity toward $(FAc)_2$ indicates that this product predominantly is formed inside micropore volume of HBEA(25) where a close interaction of two FAc molecules can be ensured. Moreover, a comparison of the reaction products observed at equal furfural conversion (ca. 20%) for two different samples HBEA(25), i.e. for the coked one at 100 °C and washed and for the fresh one at 60 °C also reveal that $(FAc)_2$ is formed independently on the conversion level if the micropores are free from any deposits. After calcination of the coked zeolite at 530 °C both furfural conversion and the composition of the reaction products attain values observed for the fresh sample (Table 1).

On the other hand, the selectivity toward F_2Ac is higher over the coked HBEA(25) i.e. over the catalyst that has some of the acid sites blocked, as compared with the fresh one tested at 60 °C at equal furfural conversion of 20%. The observed difference in selectivity of the catalysts allows concluding that the formation of F_2Ac takes place easily either with the participation of the active sites located on the external surface of the zeolite crystals or with those having lower acidic strength. Thus, the optimization of the physico-chemical characteristics of the zeolite materials, including their textural and acidic properties, could be a key factor for directing the interaction between furfural and acetone to the desired reaction route.

4. Conclusion

The presented results show that the acidic zeolites possess rather good activity in aldol condensation of furfural and acetone and their catalytic properties are determined by the structural type, as well as by their textural and acidic characteristics. The highest conversion of furfural is observed when using wide pore zeolites with a three-dimensional crystalline framework. The obtained results suggest that Brønsted acid sites are essential in the transformation. In the presence of a solid acidic catalyst the reaction between furfural and acetone results in the formation of FAc, which is also the primary product of the aldol condensation in the presence of basic catalysts. However, the following transformation of FAc proceeds by different reaction routes. Unlike basic materials, the properties of the zeolites contribute to the formation of $(FAc)_2$ compound which is formed via dimerization of the olefinic FAc on the acid sites. During the reaction, the activity of the investigated zeolites decreases due to the formation of carbonaceous deposits inside their micropores. Nevertheless, their catalytic properties in aldol condensation of furfural and acetone can be completely restored by calcination at temperatures above 500 °C. The objectives for the future investigations should be focused on an increase of the activity of zeolites in the reaction and on improvement of their stability by optimization of both physico-chemical properties of the microporous materials and the reaction conditions.

Acknowledgements

The authors thank the Czech Science Foundation for the financial support (Center of Excellence – P106/12/G015). The project (P106/12/G015) is being carried out in the UniCRE center (CZ.1.05/2.1.00/03.0071) in the Research Institute of Inorganic Chemistry.

References

[1] G. Huber, S. Iborra, A. Corma, Chem. Rev. 106 (9) (2006) 4044–4098.
[2] D. Kubička, I. Kubičková, J. Čejka, Catal. Rev. Sci. Eng. 55 (2013) 1–78.
[3] A.V. Bridgwater, Biomass Bioenerg 38 (2012) 68–94.
[4] D.L. Klass, Biomass for Renewable Energy, Fuels and Chemicals, Academic Press, San Diego, 1998.

[5] G.W. Huber, A. Corma, Angew. Chem. Int. Ed. 46 (2007) 7184–7201.
[6] Y. Sun, J. Cheng, Bioresour. Technol. 83 (2002) 1–11.
[7] G.W. Huber, J.N. Chheda, C.J. Barret, J.A. Dumesic, Science 308 (2005) 1446–1450.
[8] R.M. West, Z.Y. Liu, M. Peter, C.A. Gärtner, J.A. Dumesic, J. Mol. Catal. A: Chem. 296 (2008) 18–27.
[9] A.V. Rong Xing, H. Subrahmanyam, Olcay, G.P. Wei Qi, H. van Walsum, G.W. Pendse, Huber, Green Chem. 12 (2010) 1933–1946.
[10] T.N. Pham, D. Shi, D.E. Resasco, Appl. Catal. B: Environ. (2013), http://dx.doi.org/10.1016/j.apcatb.2013.01.002.
[11] D.P. Debecker, E.M. Gaigneaux, G. Busta, Chem. Eur. J. 15 (2009) 3920–3935.
[12] I. Sádaba, M. Ojeda, R. Mariscal, R. Richards, M. López Granados, Catal. Today 167 (2011) 77–83.
[13] L. Faba, E. Diaz, S. Ordõnez, Appl. Catal. B: Environ. 113–114 (2012) 201–211.
[14] M.J. Climent, A. Corma, S. Iborra, A. Velty, Green Chem. 4 (2002) 474–480.
[15] Chunli Xu, Yuan Gao, Xihong Liu, Ruirui Xin, Zhen Wang, RSC Adv. 3 (2013) 793–801.
[16] S. Abelló, D. Vijaya-Shankar, J. Pérez-Ramírez, Appl. Catal. A: Gen. 342 (2008) 119–125.
[17] E. Dumitriu, V. Hulea, I. Fechete, A. Auroux, J.-F. Lacaze, C. Guimon, Microporous Mesopororous Mater. 43 (2001) 341–359.
[18] A. Ungureanu, S. Royer, T.V. Hoang, D. Trong On, E. Dumitriu, S. Kaliaguine, Microporous Mesopororous Mater. 84 (2005) 283–296.
[19] T. Komatsu, M. Mitsuhashi, T. Yashima, Stud. Surf. Sci. Catal. 142 (2002) 667–674.
[20] C.A. Emeis, J. Catal. 141 (1993) 347–354.

Dalton Transactions

PAPER

Cite this: *Dalton Trans.*, 2014, **43**, 10628

Peculiar behavior of MWW materials in aldol condensation of furfural and acetone

Oleg Kikhtyanin,[a] Pavla Chlubná,[b] Tereza Jindrová[a] and David Kubička*[a]

MWW family of different structural types (MCM-22, MCM-49, MCM-56 and MCM-36) was used as catalysts for aldol condensation of furfural and acetone studied in a batch reactor at 100 °C, autogenous pressure and a reaction time of 0–4 h. To establish a relation between physico-chemical and catalytic properties of microporous materials, the samples were characterized by XRD, SEM, N_2 adsorption, FTIR and TGA. It was found that the acidic solids possessed appreciable activity in the reaction and resulted in the formation of products of aldehyde–ketone interaction. Surprisingly, MCM-22 and MCM-49, *i.e.* three-dimensional materials containing internal supercages, exhibited higher activity than two MCM-36 catalysts with two-dimensional character having larger accessible external surface area due to expansion of the interlayer space by swelling and pillaring treatments. Moreover, all MWW family catalysts gave higher conversion than the large-pore zeolite BEA. Nevertheless, furfural conversion decreased rapidly for all the studied materials due to coke formation. Unexpectedly, the deactivation was found to be more severe for MCM-36 catalysts than for MCM-22 and MCM-49, which was attributed to the reaction taking place also in supercages that are protected by 10-ring channels from severe coking. In contrast the cups located on the external surface were coked rapidly.

Received 19th January 2014,
Accepted 23rd April 2014

DOI: 10.1039/c4dt00184b

www.rsc.org/dalton

1. Introduction

Production of valuable chemicals as well as fuels from renewable raw materials is a key technological challenge facing modern society at the beginning of the 21st century. The development of efficient technologies, relying on the use of natural renewable resources, is an essential step for ensuring social security and stability and mitigating the increasing environmental threats connected with the extensive use of fossil fuels.[1]

Transformation of lignocellulosic and, in particular, waste biomass into fuels and valuable chemicals is considered to be one of the most promising directions as it allows avoiding competition with food and fodder production.[1,2] Cellulose-rich feedstocks can be successively treated to form different monomeric products, generally sugars.[3–5] These can be further converted by acid hydrolysis to furanic compounds (furfural or hydroxymethylfurfural) that can serve as platform chemicals in many applications.[6–8] Among them, aldol condensation has great potential as it allows increasing the carbon atom chain length beyond six carbon atoms, which is the limit for sugars. Furanic compounds thus can be valorized by aldol condensation with acetone in the presence of suitable heterogeneous catalysts like MgO–ZrO_2,[7] alkali and alkaline earth oxides,[9–15] alkali-exchanged zeolites (Cs-BEA),[16] MCM41,[17,18] aluminophosphate oxynitrides,[19] ion-exchange resins,[20,21] and activated Mg–Al hydrotalcites.[22–26] Alternatively, a biphasic system with NaOH as a catalyst was also proposed.[27] The needed acetone may be obtained by ketonization of acetic acid[28] that is an important product of biomass pyrolysis. This route has attracted significant interest, because hydrogenation/hydrodeoxygenation of these aldol condensation products leads to various hydrocarbons suitable for blending in conventional diesel fuel and kerosene.[29]

Aldol condensation of aldehydes and ketones is a classical reaction of organic synthesis, which takes place in the presence of both acidic and basic catalysts. Homogeneous basic catalysts such as sodium hydroxide are most often used for this purpose.[29–31] They possess high activity in conversion of reactants and high selectivity towards the desired reaction products. Unfortunately, their environmental friendliness is not satisfactory, particularly for large scale applications, due to the need for neutralization and separation of the homogeneous catalysts from the liquid products. Consequently, solid basic catalysts have attracted widespread interest as they could be helpful in overcoming the deficiencies of the currently used catalysts. The most studied basic solid catalysts include metal oxides or double mixed oxides, such as MgO,[32]

---

[a] Research Institute of Inorganic Chemistry, RENTECH-UniCRE, Chempark Litvínov, Záluží – Litvínov, 436 70, Czech Republic. E-mail: david.kubicka@vuanch.cz; Tel: +420-476163735

[b] J. Heyrovský Institute of Physical Chemistry, Academy of Sciences of the Czech Republic, v.v.i., Dolejškova 3, 182 23 Prague, Czech Republic

$MgO–Al_2O_3$,[33–35] $MgO–ZrO_2$ [29,36] and TiO_2.[37] Recently, also MOFs have been recognized as highly active catalysts in different condensation reactions.[38,39] Despite the intensive research efforts, the heterogeneous basic catalysts suffer from several major drawbacks such as high sensitivity to the ambient CO_2 and difficulties connected with re-using the hydrotalcite-based catalysts in successive catalytic runs,[40–42] which limits their widespread industrial use. Therefore, along with the optimization of the properties of the solid basic catalysts, attention is focused on alternative solid catalysts for aldol condensation. In this respect, solid acid catalysts have been recognized as promising candidates.

Among solid acid catalysts, zeolites are considered versatile and tunable acidic catalysts exhibiting good activity and selectivity in various reactions of organic synthesis ranging from petrochemical to fine chemical applications.[1,43–48] Zeolites were also investigated as catalysts for aldol condensation in the past.[49–51] In our recent work[52] it was shown that the acidic zeolites possess rather good activity in aldol condensation of furfural and acetone and their catalytic properties are determined by the structural type, as well as by their textural and acidic characteristics. The highest conversion of furfural was observed when using wide pore zeolites with a three-dimensional crystalline framework, the best result being obtained over zeolite BEA. It was also shown that during the reaction, the activity of all investigated zeolites decreased due to the formation of carbonaceous deposits inside their micropores. Therefore, to compete with the solid basic materials as catalysts for aldol condensation it is necessary to optimize the properties of zeolites with the aim to increase their activity in the reaction and to improve their stability, *i.e.* resistance to coking. Layered two-dimensional materials exhibit a better accessibility of their active sites than the classical three-dimensional zeolites and could thus make the activity enhancement possible. About fifteen zeolite frameworks have been found to form two-dimensional zeolite forms and among them MWW is the first and most famous example.[53–56]

In this respect, materials with MWW framework topology occupy a special place among a large variety of different micro- and mesoporous materials as this family consists of more than ten members, *e.g.* MCM-22, MCM-36, MCM-49, MCM-56 and others, which have the same MWW topology but a different arrangement of the layers (different interlayer bonding and distances).[57] The unifying feature of all MWW materials is the presence a layered crystalline unit in their structure, so-called “MWW monolayer”, with a thickness of 25 Å, which contains a two-dimensional 10-MR sinusoidal channel pore system and large cups (7.1 Å Ø, 7.0 Å depth) on the [0 0 1] crystal surface.[58,59] As a result of agglomeration of such layered species during hydrothermal treatment of aluminosilicate gel in the presence of hexamethyleneimine (HMI) an intermediate product is formed. It is designated as MCM-22 (P), the layered precursor. Upon calcination of this reaction product, the condensation of the monolayers occurs leading to creation of a new independent pore system, constituted by large supercages (7.1 Å Ø, 18.2 Å height) accessible through 10-ring openings (4.0 Å × 5.5 Å),[58] thus forming a three-dimensional crystal framework of MCM-22 zeolite with two independent pore systems.

Formation of MCM-36 occurs through the subsequent swelling of the MCM-22(P) precursor by the addition of cetyltrimethylammonium hydroxide followed by pillaring treatment using tetraethoxysilane (TEOS).[53,60] As a consequence, the space between the “MWW monolayers” is expanded and internal mesoporous space is generated. Thus, MCM-36 provides free access to all large cups, located on the external surface of “MWW monolayers”. Nevertheless, it should be underlined that the pillars consist of amorphous and inactive silica and thus they dilute the concentration of active sites. Their nature remains unknown.

Zeolite MCM-49 possesses nearly the same framework topology as the calcined MCM-22 (only the average unit cell *c*-parameter is 0.2 Å longer in MCM-49).[61] However, unlike the latter, MCM-49 is formed by a direct synthesis route, avoiding the formation of intermediate lamellar MCM-22(P). This is achieved by optimizing the composition of the initial reaction mixture and the conditions of its hydrothermal treatment. When hexamethyleneimine is used as a structure directing agent, MCM-49 generally has a lower Si/Al molar ratio (<13) than MCM-22P does (>13). A factor that influences the formation of either MCM-22P or MCM-49 is the molar ratio of the organic cation R_o (SDA) to the inorganic cations R_i (*e.g.* Na, K, or Rb). When the ratio R_o/R_i is typically less than 2.0, the formation of MCM-49 is favoured. By analogy with MCM-22, the crystalline framework of MCM-49 consists of two independent pore systems, which are both accessible through 10-ring apertures with diameters of 4.0 × 5.9 Å for the sinusoidal channels and 4.0 × 5.4 Å for the entrances to the supercages.[62]

Apart from MCM-22, zeolite MCM-49 crystallizes through its delaminated intermediate designated as MCM-56. MCM-56 is synthesized from the same synthetic gel as MCM-49 but with a more careful control for crystallization time and temperature.[63] The structure of this zeolite consists of disordered agglomeration of “MWW monolayers” without in-registry alignment in the *c* direction and no interlayer links. Due to this, MCM-56 has a higher concentration of large cups exposed to the crystal surface than the MCM-49.

Owing to their properties, MWW materials have been used in a number of different applications, and it has been found that they can be considered promising catalysts for several organic reactions, for example for isobutene–2-butene alkylation,[64] as well as alkylation of benzene with propylene.[65] The uniqueness of these catalysts is that they combine the properties of both conventional zeolite systems and layered materials. The expansion of the areas of application of MWW materials necessitates a deeper understanding of the impact of structural features on their activity in conversion of organic molecules.

This paper presents a comparative study focusing on (i) characterization of MCM-22, MCM-36, MCM-49 and MCM-56 materials with a number of physico-chemical methods, and (ii) investigation of their catalytic properties in aldol condensation of furfural and acetone. In addition, wide-pore zeolite Beta that has shown the best performance among the zeolite catalysts investigated previously in aldol condensation of furfural and acetone was included in the study for comparison.

2. Experimental

2.1. Synthesis of MWW materials

2.1.1. MCM-22. 7.31 g of 50% water solution of NaOH was added to 400 g of water. 7.44 g of sodium aluminate (40–45% Na_2O, 50–56% Al_2O_3, Aldrich) was added and stirred until it dissolved. Then, 232.29 g of Ludox AS-30 was added. The mixture became thick and was stirred until a homogeneous gel was formed. Then, 38.34 g of HMI was added and the final mixture was stirred for 2 hours. The reaction mixture was charged into a Teflon-lined steel autoclave. Crystallization proceeded at 143 °C with inside stirring and autogenous pressure for 96 hours. The solid product was collected by filtration, washed with distilled water and dried in an oven at 60 °C overnight.

MCM-22P was heated in nitrogen at 500 °C for 3 hours and a temperature ramp of 2 °C min^{-1}, cooled to about 130 °C, and then calcined in air at 540 °C for 6 hours with the ramp of 2 °C min^{-1}. The calcined MCM-22 product was ion-exchanged into NH_4^+ form by treating four times with 1.0 M NH_4NO_3 solution for 4 hours at room temperature.

2.1.2. MCM-36(1). 1.16 g of NaOH was dissolved in 251.2 g of water and mixed with 1.68 g of sodium aluminate (40–45% Na_2O, 50–56% Al_2O_3, Aldrich). Then, 80 g of Ludox AS-30 was added. The mixture became thick and was stirred until a homogeneous gel was formed. Then, 38.34 g of HMI was added and the final mixture was stirred for 2 hours. The reaction mixture was charged into a Teflon-lined steel autoclave. Crystallization proceeded at 150 °C under agitation and autogenous pressure for 7 days. The solid product was collected by filtration, washed with distilled water and dried in the oven at 60 °C overnight.

10 g of uncalcined MCM-22(P) was added to 200 ml of 25% solution of C_{16}TMA-OH prepared by ion-exchange from chloride form. The slurry was stirred overnight at ambient temperature. The product MCM-22SW was separated by centrifugation, properly washed with water and dried at 60 °C.

Pillaring was carried out with 12.44 g of MCM-22SW in 373 ml of TEOS (Aldrich). The mixture was stirred and heated at 85 °C under reflux overnight. The solid was isolated by centrifugation and dried at ambient temperature. Then, about 1500 ml of water was added to 14.37 g of dried powder and stirred overnight (hydrolysis). The product was centrifuged again and dried at 60 °C. Final calcinations were carried out under nitrogen at 482 °C for 3 hours and a temperature ramp of 3 °C min^{-1}, cooled to about 130 °C and then calcined in air at 540 °C for 6 hours with a ramp of 2 °C min^{-1}. The calcined product MCM-36(1) was ion-exchanged into NH_4^+ form by treating four times with 1.0 M NH_4NO_3 solution for 4 hours at room temperature.

Table 1 Molar chemical compositions of reaction mixtures for the synthesis of MWW zeolites

Sample	Al_2O_3	SiO_2	Na_2O	HMI	H_2O
MCM-22	1	30	2.52	10	815
MCM-36(1)	1	46	3	20	1960
MCM-36(2)	1	36	3	20	1875
MCM-49	1	25	2.45	8.15	440
MCM-56	1	25	2.45	8.15	440

2.1.3. MCM-36(2). The preparation method of this sample was substantially the same as that for MCM-36(1), with the only exception that only 62 g of Ludox AS-30 was taken.

2.1.4. MCM-49. 9 g of 50% NaOH water solution was added to 396 g of water. 9.75 g of sodium aluminate (40–45% Na_2O, 50–56% Al_2O_3, Aldrich) was added and stirred until dissolving. Then, 77.1 g of silicon dioxide (Aldrich, nanopowder, particle size 10–20 nm) was added. The mixture was stirred for 10 minutes and then 40.8 g of HMI was added and the gel was stirred for 15 minutes. Crystallization proceeded at 143 °C under agitation and autogenous pressure for 93 hours. The solid product was collected by filtration, washed with distilled water and dried in the oven at 60 °C overnight.

MCM-49 was heated in nitrogen at 482 °C for 3 hours and a temperature ramp of 3 °C min^{-1}, cooled to about 130 °C, and then calcined in air at 540 °C for 6 hours with a ramp of 2 °C min^{-1}. The calcined product MCM-49 was ion-exchanged into NH_4^+ form by treating it four times with 1.0 M NH_4NO_3 solution for 4 hours at room temperature.

2.1.5. MCM-56. The preparation method of this sample was substantially the same as that for MCM-49, with the only exception that the time of hydrothermal synthesis was 33 hours.

Molar compositions of reaction mixtures used for the synthesis of different MWW samples are presented in Table 1. The relationship between different structures of the MWW family is depicted in Scheme 1.

2.2. Characterization methods

The crystallographic structures of MWW zeolites were determined by X-ray powder diffraction using a Bruker AXS D8 Advance diffractometer, working with the Cu K_α line (λ = 0.154 nm) in the 2θ range of 4–40°.

Nitrogen adsorption/desorption isotherms were measured on a Micromeritics GEMINI II 2370 volumetric Surface Area Analyzer at −196 °C to determine the surface area, pore volume and pore size distribution. Before the sorption measurements, all samples were degassed on a Micromeritics FlowPrep 060 instrument under helium at 300 °C (heating rate 10 °C min^{-1}) for 4 h. The specific surface area was evaluated by the BET method[66] using adsorption data in the range of relative pressure from p/p_0 = 0.05 to p/p_0 = 0.25. The *t*-plot method[67] was applied to determine the volume of micropores (V_{mic}). The adsorbed amount at relative pressure p/p_0 = 0.98 reflects the total adsorption capacity (V_{tot}).

The concentration of Lewis (L) and Brønsted (B) acid sites was determined after adsorption of d_3-acetonitrile (Ac) by FTIR

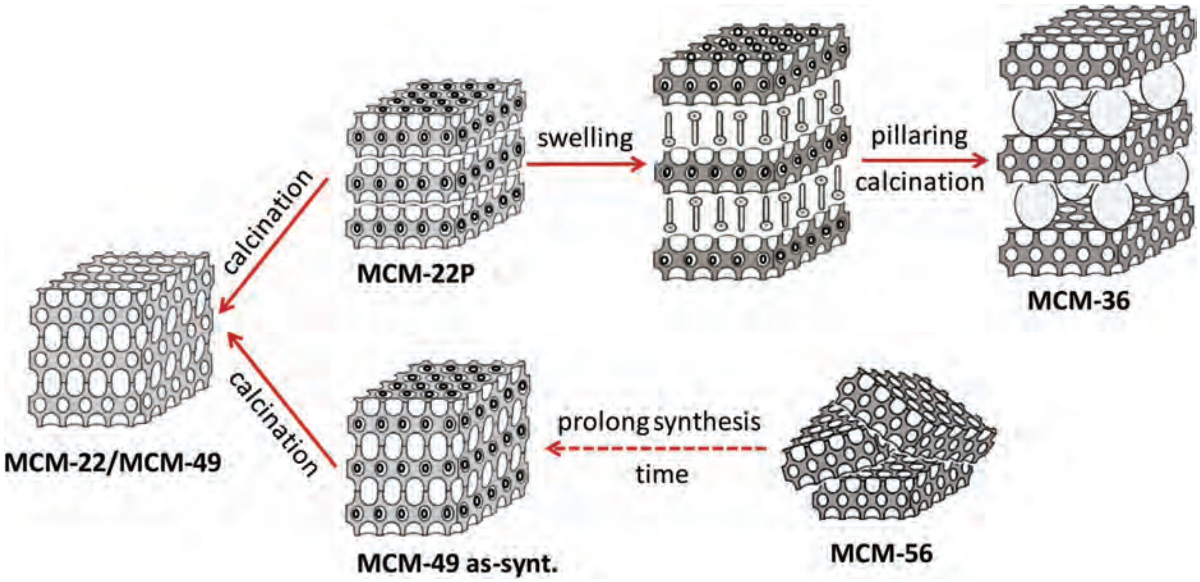

Scheme 1 MWW family presented by MCM-22P, MCM-49 and MCM-56 prepared by direct synthesis and MCM-36 prepared by post-synthetic modification of MCM-22P. The red dot-line presents the assumed transformation of delaminated form MCM-56 into regular 3D MCM-49 if the synthesis time is prolonged.

spectroscopy on a Nicolet Protégé 460 Magna with a transmission DTGS and MTC/A detector. Zeolites were pressed into self-supporting wafers with a density of 8.0–12.0 mg cm^{-2} and activated *in situ* at 450 °C overnight. Before adsorption d$_3$-acetonitrile was degassed by freezing and thawing cycles. d$_3$-Acetonitrile was adsorbed at ambient temperature for 30 min at a partial pressure of 900 Pa, followed by desorption for 20 min. All spectra were recorded with a resolution of 4 cm^{-1} by collecting 128 scans for a single spectrum at room temperature. The experimental data were recalculated to a normalized wafer (density of 10 mg cm^{-2}). The concentrations of Lewis and Brønsted acid sites were evaluated from the integral intensities of bands at 2323 cm^{-1} (Lewis acid sites) and at 2294 cm^{-1} (Brønsted acid sites) using extinction coefficients ε (L) = 3.6 cm μmol^{-1} and ε (B) = 2.05 cm μmol^{-1}.[68]

The presented IR spectra both for d$_3$-acetonitrile and for 2,6-di-*tert*-butyl-pyridine (DTBP) are not correlated to the standard mass. A large probe molecule DTBP was used to determine the concentration of acid sites located on the external surface of zeolites.[69] The adsorption of DTBP was performed at 150 °C at equilibrium probe vapor pressure with the zeolite wafer for 15 min. Desorption proceeded at the same temperature for 1 h followed by collection of spectra at room temperature.

The size and shape of zeolite crystals were examined by scanning electron microscopy (SEM, JEOL, JSM-5500LV). For the measurement, crystals were coated with a thin platinum layer by sputtering in the vacuum chamber of a BAL-TEC SCD-050.

Thermogravimetric analysis of the zeolite catalysts was performed using a TA Instruments TGA Discovery series equipment and operating at a heating ramp of 10 °C min^{-1} from room temperature to 900 °C under the flow of nitrogen (20 mL min^{-1}, Linde 3.0). Approximately15 mg of sample was heated in an open alumina crucible.

2.3. Reaction studies

The properties of zeolite samples were investigated in aldol condensation of furfural and acetone. The catalytic experiments were carried out in a 200 ml stirred batch reactor (Parr autoclave) at 100 °C. Before the start of the catalytic runs, 0.5 g of catalyst was mixed together with a mixture of 19.75 g of acetone and 3.25 g of furfural (acetone/furfural molar ratio 10/1) and loaded into the autoclave. After initiation of the heating the desired temperature was achieved in ~60 min, and the autoclave was kept at T = 100 °C for an additional 0, 2 or 4 h.

Analysis of the reaction products was performed on an Agilent 7890A GC unit equipped with a flame ionization detector using a HP-5 capillary column (30 m/0.32 ID/0.25 μm). The obtained products were identified based on the standard reference compounds. Catalytic activity is expressed in terms of conversion, which is defined as the fraction of furfural which has reacted. Selectivity was calculated by dividing the percentage of furfural moles presented in the products by total moles of converted furfural.

3. Results and discussion

3.1. Catalyst characterization

3.1.1. XRD. XRD patterns of the MWW materials are depicted in Fig. 1. Although all the prepared materials possess the same MWW topology of the layers, the differences in the layer arrangement can be recognized on the basis of XRD pat-

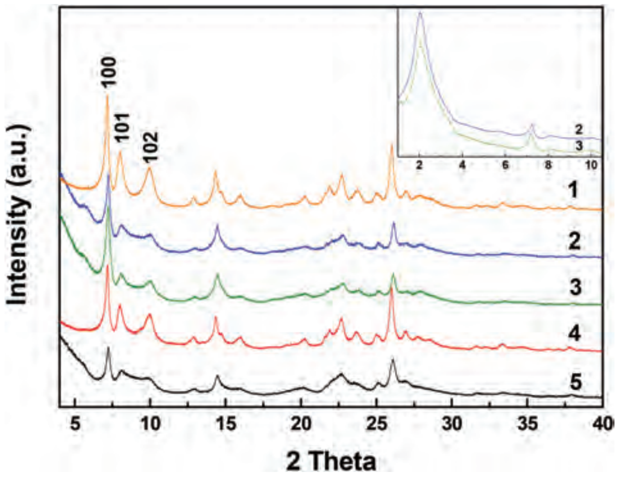

Fig. 1 XRD patterns of MWW samples. (1) MCM-22, (2) MCM-36(1), (3) MCM-36(2), (4) MCM-49, (5) MCM-56.

terns. The XRD patterns of MCM-22 and MCM-49, as the three-dimensional zeolites, differ from the others and show three well-defined peaks corresponding to (100) (2θ = 7.1–7.2°), (101) ($2\theta \approx 8°$) and (102) ($2\theta \approx 10°$) reflections, which is in good agreement with previous reports[70] and proves good crystallinity and phase purity of these materials. In contrast, the two-dimensional MWM forms (MCM-56 and MCM-36) have a broad band between 8° and 10° indicating the disappearance of atomic order in the third dimension, along the *c*-axis. In addition, both MCM-36 samples are distinctly characterized by a high intensity low angle peak around ≈2 °C, corresponding to a *d*-spacing of about 5 nm. It corresponds well to an idea of MWW layers of *ca.* 2.5 nm thick separated by around 2.5 nm interlayer space filled partially with amorphous silica pillars.[53] Similarly, in MCM-56 the broad band between 8° and 10° indicates that the material is composed of thin layers that extend in the *a* and *b* directions with a lack of order in the *c*-axis direction.[63] As the intermediate to MCM-49, delaminated MCM-56 is not fully crystalline and an amorphous part is most probably present evaluated from lower intensities of diffraction lines in comparison to fully crystalline MCM-49. Based on the analysis of XRD patterns it can be concluded that a series of materials with MWW topology differing in layer arrangement was prepared in the pure phase (with the exception of MCM-56, which has an amorphous part present).

3.1.2. SEM. Fig. 2 shows SEM images of the MWW materials. The morphology of the individual crystals of all materials shows a thin plate-like shape that is a characteristic of MWW. The samples differ somewhat with regard to the size of individual crystals and their aggregation. The crystal size can be influenced by the synthesis time as is demonstrated on the row MCM-22 (96 hours) ≥ MCM-49 (93 hours) > MCM-56 (33 hours, the intermediate to MCM-49). The individual crystals of MCM-22, MCM-49 and MCM-56 have a length of 0.2–0.5 μm and a thickness of about 0.1 μm. In the case of MCM-36 materials the aggregation of individual crystals is visible as they underwent swelling and pillaring treatments under relatively severe conditions. In the case of MCM-36 the length of crystals is about 1 μm. It was pointed out that the large crystals of MCM-36 might have been previously hidden in the aggregates and became visible only upon swelling and pillaring treatments.[70]

3.1.3. N_2 adsorption. The textural parameters of the prepared MWW materials were evaluated based on nitrogen isotherms (Fig. 3(A)). MCM-22 and MCM-49 zeolites have very similar isotherms typical of microporous materials according to the IUPAC classification.[71] It was mentioned above that MCM-22 and MCM-49 crystallize as aggregates of thin sheets. As a result we observe a narrow hysteresis loop at higher relative pressure in both zeolites corresponding to nitrogen condensation in interlayer voids of the aggregates. The BET surface areas for MCM-22 and MCM-49 are similar, 505 and 455 $m^2\ g^{-1}$, as well as the micropore volumes, 0.151 and 0.165 $cm^3\ g^{-1}$, respectively (for more details see Table 2). Delaminated MCM-56 has the nitrogen isotherm with a distinctive hysteresis loop corresponding to the adsorption in the interlayer space of delaminated MWW layers. As MCM-56 is the intermediate to MCM-49 and cannot be fully crystalline (discussion *vide supra*), also the BET surface area is lower in comparison to MCM-49, 401 *vs.* 455 $m^2\ g^{-1}$. Nevertheless, both materials differ noticeably in the micropore and total volume when the micropore volume for MCM-56 and MCM-49 is 0.113 and 0.165 $cm^3\ g^{-1}$ and the total pore volume 0.701 and 0.459 $cm^3\ g^{-1}$, respectively (see Table 2). The higher micropore volume in MCM-49 is caused by the presence of the regular three-dimensional framework with a 10-ring two-dimensional channel system and the presence of supercages. On the other hand, in MCM-56 the supercages were not formed as the layers are not condensed and irregularly aggregated. The layers are expected to be connected only by hydrogen bonds. The pillared materials MCM-36 possess isotherms with a gradual increase in the adsorbed amount in the relative pressure range p/p_0 0.01–0.3. It is typical of mesopore materials with the mesopore size below 4 nm.[72] Also the high surface areas for both MCM-36 materials, 606–762 $m^2\ g^{-1}$, indicate the formation of a new mesopore structure. The micropore volumes decreased in comparison to MCM-22, 0.062–0.097 $cm^3\ g^{-1}$. This is related to the presence of amorphous silica pillars, which form a considerable part of the material. Alike MCM-56, in MCM-36 materials supercages were not formed and MWW layers have only large cups on the surface and 10-sinusoidal channel system inside the layers. The mesopore size distribution of pillared MCM-36 (1) and (2) materials (displayed in Fig. 3(B)) is centered at 2.3 and 2.5 nm, nicely corresponding to the data determined from XRD patterns (see section 3.1.1).

The type of obtained isotherms reflects the structural differences between the samples. Thus, isotherms of MCM-22 and MCM-49 with the same structural characteristics are very close to those typical of microporous solids,[73] showing a fast increase in the adsorbed amount occurring at very low p/p_0, followed by long almost horizontal plateau extending up to the high p/p_0 values. A very narrow hysteresis loop observed for these samples at high p/p_0 values indicates the presence of

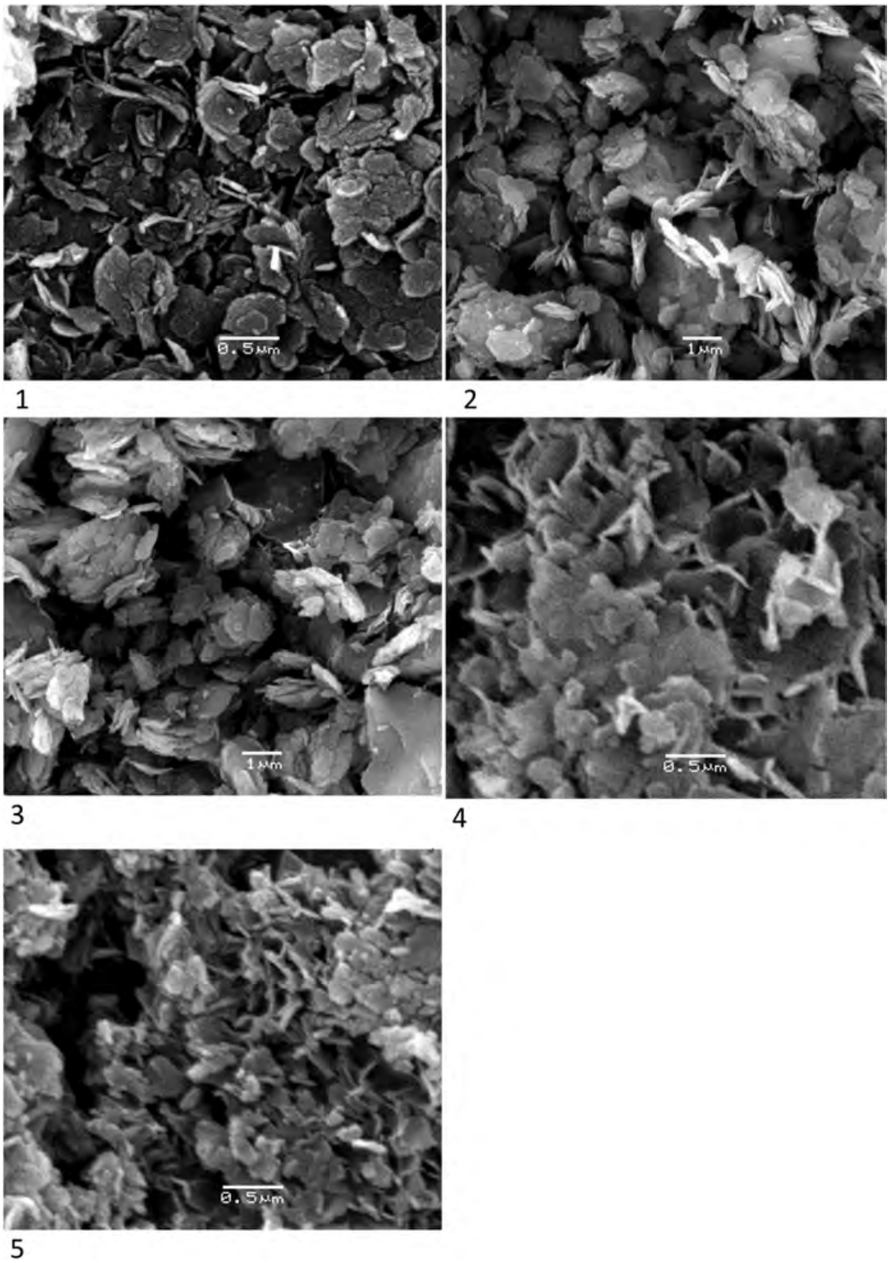

Fig. 2 SEM images of zeolites samples. (1) MCM-22, (2) MCM-36(1), (3) MCM-36(2), (4) MCM-49, (5) MCM-56.

some slit-shaped, wide mesopores (or narrow macropores) or platelet particles,[73] most probably originating from the aggregation of the lamellar particles.

A change in the shape of the isotherms for two MCM-36 samples reflects the structural changes in these materials caused by the swelling followed by pillaring. The marked increase in the adsorption capacity of MCM-36 up to p/p_0 = 0.3–0.4 evidences capillary condensation and indicates the presence of mesopores created by pillaring. At higher p/p_0 there is a clear hysteresis loop of type H4 characteristic of layered materials.[74,75]

In comparison with MCM-22, the isotherm of MCM-56 shows a slightly lower N_2 adsorption amount at p/p_0 = 0–0.6. It proves a slight decrease in the amount of micropores in this sample due to the absence of bonding between "MCM-22 monolayers". In higher p/p_0 region of the N_2 isotherm the adsorption amount increases very fast due to a well-developed interlamellar space formed by MCM-22 sheets arrayed in a disordered manner forming the so-called partially delaminated structure.[63,76]

The values of the calculated specific surface areas and total pore volumes are summarized in Table 2.

All the prepared samples possess high BET area. The observed differences in BET area between the samples are in full agreement with their structural features. The smallest BET

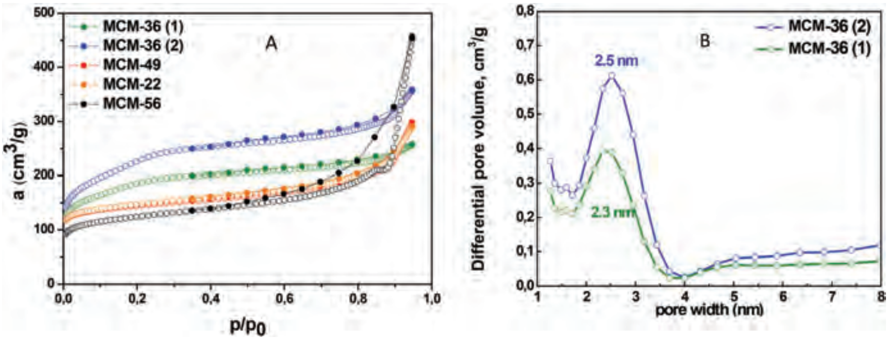

Fig. 3 (A) Nitrogen isotherms of the investigated MWW materials. Open circles – adsorption branch, closed circles – desorption branch. (B) The mesopore size distribution for pillared MCM-36 materials.

Table 2 Textural properties of MWW materials determined from nitrogen adsorption measured at 77 K

Sample	BET ($m^2\ g^{-1}$)	$S_{ext.}$ ($m^2\ g^{-1}$)	V_{mic} ($cm^3\ g^{-1}$)	V_{tot} ($cm^3\ g^{-1}$)
H-MCM-22	505	176	0.151	0.449
H-MCM-36(1)	762	656	0.062	0.553
H-MCM-36(2)	606	430	0.097	0.398
H-MCM-49	455	134	0.165	0.459
H-MCM-56	401	181	0.113	0.701
H-BEA(25)	608	222	0.174	1.017

BET – specific surface area (from the BET method). V_{mic} – micropore volume (from the *t*-plot method). V_{tot} – total pore volume at $p/p_0 = 0.97$.

area (401 $m^2\ g^{-1}$) is observed for delaminated MCM-56 sample representing a disordered agglomeration of MCM-22 monolayers without in-registry alignment in the *c* direction with no interlayer links. For MCM-22 and MCM-49 samples the BET area increases to 505 and 455 $m^2\ g^{-1}$, respectively, due to the ordering of "MCM-22 monolayers" in the vertical direction resulting in the formation of a three-dimensional crystalline framework and creation of 12-ring supercages between the layers. The further growth of the *c* parameter of the crystalline framework due to the introduction of the silica pillars not only influences the BET area, but also results in a substantial increase of the external surface area for both MCM-36 samples (Table 2).

The largest volume of micropores is observed for MCM-22 and MCM-49 samples as their pore system consists of "MWW monolayers" and large cylindrical supercages between them. It is obvious that delaminated materials not having supercages and channels connecting them have lower micropore volume regardless of whether the layers remain disordered (MCM-56) or connected by siliceous pillars (MCM-36). At the same time, the disordered arrangement of "MWW monolayers" in MCM-56 generates significant inner mesoporosity in this sample. It was shown[76,77] that pillaring may also result in the formation of mesopores. However, according to ref. 77, the volume of the formed mesopores depends on the pillaring procedure. Hence, it is not surprising that the two MCM-36 samples studied here have different mesopore volumes; MCM-36(1) exhibits considerably larger mesopore volume in comparison with MCM-36(2) (Table 2). Taking into account the difference in Si/Al ratio in the reaction mixture for the preparation of these samples (Table 1), it may be assumed that the mesopore volume of the final MCM-36 materials is determined not only by the pillaring procedure, but also by the properties of the intermediate MCM-22P material.

Table 2 also shows that the BET area of BEA used as a reference sample differs only slightly from the values determined for MWW samples. However, the BEA sample has a significantly higher V_{tot} due to the well-developed mesoporosity of this material.

3.1.4. Acidity. IR spectra of MCM-22, MCM-36, MCM-49 and MCM-56 in the region of OH stretching vibration are shown in Fig. 4. The well expressed absorption band at 3745 cm^{-1} is assigned to the terminal silanol groups exposed at the external surface. This band is the most intensive for two MCM-36 samples compared with MCM-22 and MCM-49 which can be explained by the presence of silicate pillars in the structure and the increased access to the MWW sheets, *i.e.* increased external specific surface area as indicated also by the nitrogen physisorption results (Table 2). Similarly, the rela-

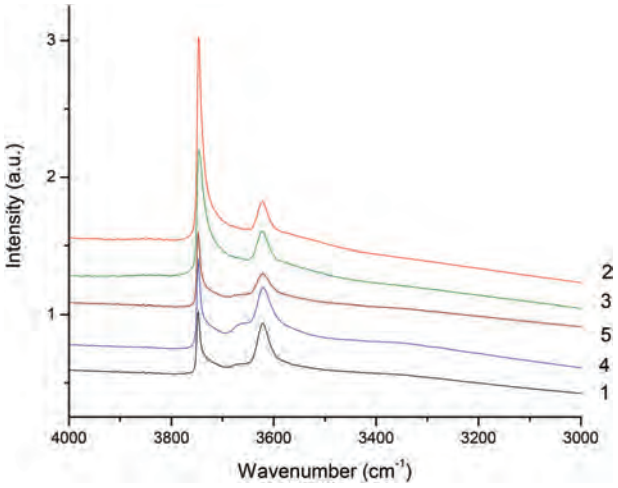

Fig. 4 Region of OH stretching vibration of the studied zeolites. (1) MCM-22, (2) MCM-36(1), (3) MCM-36(2), (4) MCM-49, (5) MCM-56.

tively low intensive band for Si–OH groups in MCM-56 material correlates well with the low external surface area and also the fact that MCM-56 is not a fully crystalline material (discussion *vide supra*) (Table 2).

The band at 3620 cm^{-1} is attributed to the acidic bridging Si(OH)Al hydroxyls associated with the framework Al. The intensity of this band is the highest for MCM-22 and MCM-49 due to a high structural ordering of these zeolites. It is also seen that both delamination (MCM-56) and pillaring (MCM-36) result in a partial degradation of the Brønsted acid centers. This is in accordance with previous results.[64,78] The difference between the two MCM-36 samples should be also noted. The intensity of the band at 3620 cm^{-1} is slightly lower for MCM-36(1) in comparison with MCM-36(2). Fig. 4 also shows that spectra of OH-groups of MCM-22, MCM-49 and MCM-56 contain a very weak band between 3660 and 3670 cm^{-1}, which is characteristic of OH groups located on extra-framework aluminum (EFAL) centers.[79] It was suggested that some of these aluminum-containing species may have rather strong Brønsted-type acidity.[80]

It is generally accepted that acid sites in the MWW family materials can have in principle three different locations depending on packing arrangement of "MWW monolayers".[62] For delaminated MCM-56 these centers can be present in the sinusoidal 10-ring channels and in cups located on the external surface of the crystals. In addition to these two possible locations, MCM-22 and MCM-49 also contain acid sites in large supercages formed by condensation of "MWW monolayers" that are accessible by another network of 10-ring pores. Similarly to MCM-56, MCM-36 material does not contain large supercages. However, it can be expected that the pillaring procedure can also result in a decrease of accessibility to acid sites located in the cups due to their blocking by the silicate pillars.

Small basic molecules, such as pyridine or d_3-acetonitrile, can easily enter the 10-ring channels of zeolites and can be used as probes for acid sites located inside supercages and the 2D sinusoidal pore system of MWW family materials. Conversely, large basic molecules, such as 2,6-di-*tert*-butyl-pyridine (DTBP) cannot enter the 10-ring, so they are adsorbed only on the Brønsted acid sites located on the external surface of such zeolitic materials.[69] Thus, DTBP was used to determine the concentration of the external acid sites of the prepared MWW materials, while the total concentration of Brønsted and Lewis acid sites, respectively, was evaluated by FTIR of the adsorbed d_3-acetonitrile (Ac).

Table 3 Acidic properties of the samples determined by FTIR using d-acetonitrile and DTBP as probe molecules

Sample	C_B (DTBP) (mmol g^{-1})	C_B (Ac) (mmol g^{-1})	C_L (Ac) (mmol g^{-1})	Si/Al (Ac)^b
H-MCM-22	0.044	0.335	0.247	19.1
H-MCM-36(1)	0.067	0.196	0.177	29
H-MCM-36(2)	0.053	0.249	0.245	21.6
H-MCM-49	0.036	0.317	0.537	11
H-MCM-56	0.050	0.210	0.380	16
H-BEA^a	0.125	0.353	0.220	—

^{a} Concentration of acid sites in BEA zeolite was determined by pyridine-FTIR. ^{b} Calculated from the Ac adsorption data.

The concentrations of acid sites in the studied zeolites determined with both probing molecules, Ac and DTBP, is presented in Table 3. It can be seen that the highest concentration of Brønsted acid sites (BAS), 0.335 mmol g^{-1} and 0.317 mmol g^{-1}, is observed for three-dimensional MWW zeolites with the largest micropores volume, MCM-22 and MCM-49, respectively. It is in good agreement with the high intensity of the band of bridged OH-groups at 3620 cm^{-1} for these samples (Fig. 4). The concentration of BAS in MCM-36 and MCM-56 is lower, which is in line with the lower intensity of the band at 3620 cm^{-1}. The lower concentrations of BAS in MCM-36 can be explained by the presence of silica pillars, which generally dilute the concentrations of active sites. It was already mentioned above that MCM-56 is not fully crystalline and it is also reflected in its acidity. Since the MCM-36 materials were prepared from MCM-22P precursors differing in Si/Al ratio, it is reasonable that the final pillared MCM-36 also differ in the acid site concentrations. It should be additionally noted that MCM-49 and MCM-56 possess an increased concentration of Lewis acid sites (LAS), which is most probably a consequence of their higher Al content in comparison with MCM-22 and MCM-36 materials.

The concentration of external Brønsted acid sites determined by DTBP-FTIR reflects differences in structural features of the investigated MWW materials. The largest concentration of the external BAS is observed for MCM-36 and MCM-56, which correlates with their larger external surface and the increased concentration of large cups exposed to the outside and hence the improved accessibility of acid sites. Similarly, the lower concentration of external BAS in MCM-22 and MCM-49 is due to their lower external surface area and thus less cups per gram of catalyst.

Table 3 also shows that the reference BEA sample possesses a relatively high concentration of BAS, both total and those located on the external surface, 0.353 and 0.125 mmol g^{-1}, respectively, which is a consequence of high aluminum content and its good textural characteristics (Table 2). Besides, the high concentration of acid sites in BEA determined by DTBP-FTIR can be partially attributed to the penetration of DTBP into the pores of BEA and its interaction with both external and internal Brønsted acid sites.[69]

3.2. Catalyst performance

3.2.1. Conversion and selectivity. It was shown in ref. 52 that consecutive interaction of furfural and acetone over acidic and basic catalysts results in the formation of the following main products: FAc (produced by dehydration of an intermediate alcohol) and F_2Ac (Scheme 2). A distinctive feature of this reaction over zeolites is the formation of an additional reaction product, $(FAc)_2$, which is formed by dimerization of FAc, *i.e.* it is not a direct aldol condensation product. Additionally, self-condensation of acetone also takes place to a small extent

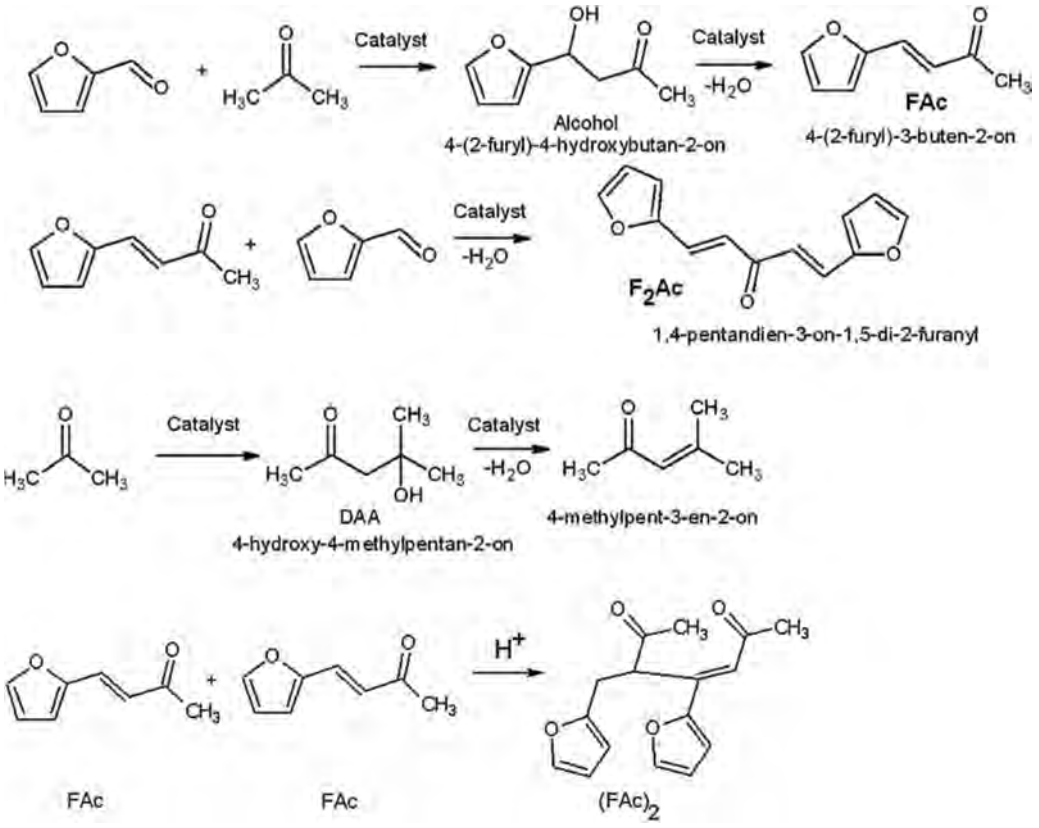

Scheme 2 Aldol condensation between furfural and acetone over acidic catalysts.[52]

leading to diacetone alcohol (DAA) that is subsequently dehydrated and affords mesityl oxide (Scheme 2).

Furfural conversion over MWW materials in aldol condensation of furfural and acetone is depicted in Fig. 5 and 6. Fig. 5(A) shows furfural conversion obtained over different catalysts after 2 hours of the reaction. It is seen that the activity of all MWW samples is higher than the activity of BEA zeolite which was used as the reference sample. It can be concluded that MWW materials exhibit better activity than the other zeolites investigated so far for the aldol condensation of furfural and acetone as the following activity sequence was reported previously: BEA > FAU > MOR > MFI.[52] Considering the high BET area and acidity of the reference BEA sample, this might be surprising and indicates that other factors, such as the specific structural features of MWW materials, play an important role. Among the MWW samples, MCM-22 was the most active in aldol condensation with furfural conversion of 60% after 2 hours of the reaction. The conversion of furfural over MCM-49 and MCM-56 was only slightly lower being 55 and 52%, respectively, after 2 hours. Finally, the lowest conversion of 30 and 35% was obtained over MCM-36(2) and MCM-36(1), respectively, *i.e.* the pillared materials. It can be concluded that introduction of silicate pillars between the "MWW monolayers" resulted in deterioration of the catalytic properties of

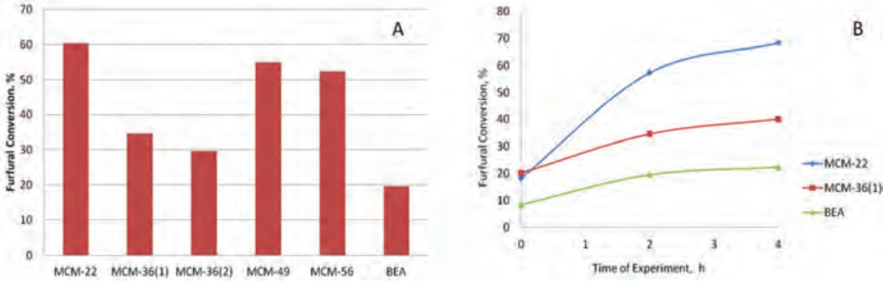

Fig. 5 (A) Furfural conversion obtained on different catalysts after 2 hours of the reaction at 100 °C and autogenous pressure. (B) Dependence of furfural conversion on the duration of reaction at 100 °C and autogenous pressure.

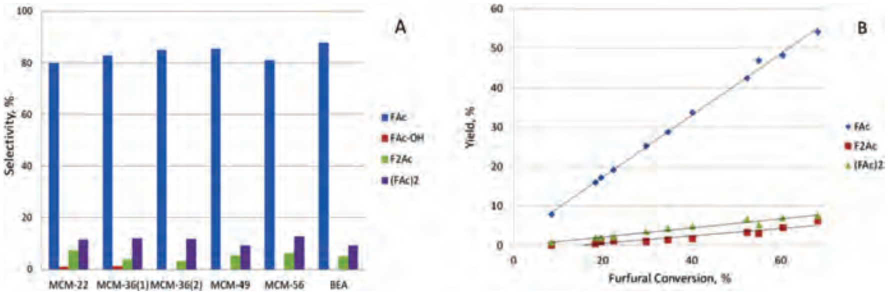

Fig. 6 (A) Selectivity towards the main reaction products in aldol condensation of furfural and acetone over different catalysts after 2 hours at 100 °C and autogenous pressure. (B) Dependence of the yield of reaction products on furfural conversion for all studied MWW samples at 100 °C and autogenous pressure and reaction time from 0 to 4 hours.

these materials in aldol condensation. This is quite surprising, taking into account the larger external surface and better accessibility of acid sites which can be deduced from the DTBP-FTIR results according to which the concentration of the external BAS is 20–50% larger in MCM-36 than in MCM-22. Moreover, increased activity of MCM-36 as compared with MCM-22 was reported for a number of organic reactions.[64,78,81] Additional insight can be obtained when looking at the time dependence of furfural conversion. Fig. 5(B) shows that at $t_{\text{reac.}} = 0$ (*i.e.* when reaching $T = 100$ °C inside the batch stirred reactor, which takes about 1 hour) the furfural conversion over MCM-36(1) is slightly higher than over MCM-22 catalyst, 20 *vs.* 18%. When analyzing the shape of the conversion as a function of time curve it can be evidenced that the reaction rate over MCM-22 exceeds that observed for MCM-36(1) and BEA. This is a clear indication of catalyst deactivation that was reported also previously for this reaction system.[52] The aspect of coke formation in these zeolites and its impact on catalyst performance will be discussed in the present article.

Apart from furfural conversion, selectivity towards the main products is an important parameter of the overall catalyst evaluation. The selectivity data are summarized for all investigated catalysts after 2 hours of the reaction (Fig. 6(A)). Generally, the composition of the reaction products obtained over MWW samples corresponds to that observed for zeolites with different structural types.[52] For all the catalysts in the present study FAc is the main reaction product formed with selectivity ≥80%. In accordance with the generally accepted reaction network, this compound is formed on acidic sites by dehydration of the corresponding alcohol, FAc–OH.[52] Other reaction products include F_2Ac formed by condensation of a furfural molecule with FAc as well as $(FAc)_2$. It was shown in ref. 52 that the latter compound is a result of dimerization of two (olefinic) FAc molecules. Apparently, the formation of this dimer is a distinctive feature of aldol condensation of furfural and acetone carried out in the presence of acidic catalysts as this product was not observed when hydrotalcites, *i.e.* basic catalysts, were used.[33] The yields of FAc, F_2Ac and $(FAc)_2$, respectively, increased linearly with the growth of furfural conversion (Fig. 6(B)) with no obvious dependence on the structural features of the studied catalysts. The obtained results confirm that aldol condensation of furfural and acetone over acidic catalysts takes place as one and the same sequence of successive transformations, and furfural conversion is kinetically governed and no molecular sieving effect is observed. This could mean that at least the secondary reactions proceed on the external surface. However, when comparing the concentration of the external BAS with the observed conversion (Table 3, Fig. 5), they do not correlate. In fact, the conversion after 2 hours appears to decrease with increasing concentration of external Brønsted acid sites, *i.e.* those determined by DTBP-FTIR (Table 3). This suggests that some of the reactions might proceed at the internal surface that is significantly larger in the case of MCM-22 and MCM-49 (Table 2) that also exhibit higher conversion than both MCM-36 catalysts.

It was shown in ref. 52 that the conversion over large-pore three-dimensional zeolites in aldol condensation of furfural and acetone is considerably higher compared with medium-pore three-dimensional or wide-pore mono-dimensional materials. This has been attributed to the constrained space within MFI and MOR pores for the formation of aldol condensation products. Consequently, the observed, though very low conversion, over MFI and MOR was attributed to the activity of the external acid sites.[52] From this point of view, it is hard to believe that the sinusoidal 10-ring channels of MWW materials could be responsible for the high activity of these materials in aldol condensation, which is even higher than that of BEA zeolite, while MFI was virtually inactive although its 10-ring pores are slightly larger than those of MWW materials (MFI, 5.3 × 5.6 and 5.1 × 5.5 Å *vs.* MWW, 5.1 × 4.1 and 5.5 × 4.0 Å). This points to the conclusion that apart from the external surface acid sites, the acid sites located in the supercages of MWW are of great importance for catalytic transformations. Considering the dimensions of acetone and furfural, 4.1 × 2.4 × 2.7 Å and 5.2 × 3.5 × 1.7 Å, these molecules can reach the supercages of MWW through the 10-ring pores, where they could form the first aldol condensation product, FAc (8.9 × 3.6 × 2.2 Å), while the formation of the second aldol condensation product, F_2Ac (13.3 × 5.3 × 1.9 Å), in the supercages is highly unlikely. Since FAc is a rather flat molecule it might be able to diffuse out from the supercages through the 10-ring channels. In contrast, the intersections of the 10-ring pores in MFI may not accommodate even FAc, which would explain the very low activity of MFI reported earlier.[52] More importantly, it can help explain the significantly higher conversion over MCM-22 and MCM-49 in comparison with MCM-36 catalysts that possess only cups at the external surface, but no supercages. This conclusion is supported by the catalytic performance of the two MCM-36 catalysts, where MCM-36(1) shows higher activity than MCM-36(2) despite having lower total concentration of acid sites (Table 3) but higher concentration of surface acid sites. It proves that the interaction of furfural and acetone over these samples generally takes place in the large cups of the external surface of crystallites.

In lamellar MCM-56, the concentration of acidic centers determined by DTBP-FTIR is also slightly lower than that in MCM-36(2) (0.50 *vs.* 0.53 mmol g^{-1}), but its activity in aldol condensation is close to that of MCM-22 and MCM-49 (Fig. 5). MCM-56 is an intermediate crystalline product in the MCM-49 synthesis: the increase of crystallization time results in the condensation of the lamellar monolayers of MCM-56 into the three-dimensional MCM-49 framework. It could be assumed that the MCM-56 sample may contain a small admixture of condensed MCM-49, which is confirmed by the splitting of the XRD reflection at $2\theta = 8$–$10°$. In that case there should be available supercages and the observed MCM-56 activity would be higher than what would be expected solely on the basis of the concentration of acid sites determined by DTBP-FTIR.

Taking into account the structural features of MWW materials, an assumption could be made that their catalytic activity may be considerably influenced by the location and concentration of Brønsted acid sites. Nevertheless, with respect to Lewis acid sites the situation is not as clear. Comparing the acidic properties of the samples (Table 3) with their activity in furfural conversion (Fig. 5) it can be concluded that the catalytic properties of MWW materials show poor correlation with the concentration of Lewis acid sites. This observation is in total agreement with our results obtained for different zeolites used as catalysts in aldol condensation.[52] However, there is not yet enough information available to make a definitive conclusion about the role of Lewis acid sites both in the transformation of the feed molecules and in coke formation. Apparently, a comprehensive understanding of the impact of various acid sites is possible only after an additional study of a series of molecular sieve samples having the same structure but different Brønsted/Lewis acid sites ratios.

3.2.2. Deactivation of catalysts.

Based on the conversion time dependence, it has been concluded that the activity of MWW materials in aldol condensation continuously decreases with increasing length of the experiment (Fig. 5B). All the catalysts after reaction are black in color suggesting that they have accumulated a significant amount of carbonaceous deposits (coke). Hence, after thorough washing with acetone, the samples were studied by TGA/DTG to evaluate the content and possibly also the distribution of carbonaceous deposits on the spent catalysts.

Two regions of weight loss, low-temperature (LT) and high-temperature (HT), are observed on DTG curves (Fig. 7). The LT region consists of two peaks, at 70–80 °C and 140–150 °C corresponding to the residual organic substances (acetone, ethanol, furfural, mesityl oxide) and water removal. The weight loss at this stage is equal to 4.4–6.4% for all the samples. The position and intensity of the DTG peaks located in the HT region show rather poor dependence on structural features of MWW. Nevertheless, several conclusions can be made. Clearly distinguishable peaks with maxima at 320–340 °C and 507–563 °C are observed on the DTG curves of all samples. Since MWW materials have a dual pore system, it could be assumed that the two peaks on the DTG curve correspond to the removal of coke from large cups on the external surface of the zeolite crystals ($T = 320$–340 °C) and from the 10-ring sinusoidal channels ($T = 507$–563 °C). The determined weight loss associated with each of these peaks is in line with this assumption. The largest weight loss in the range of $T = 320$–340 °C is observed for MCM-36 and MCM-56 samples (Table 4) with

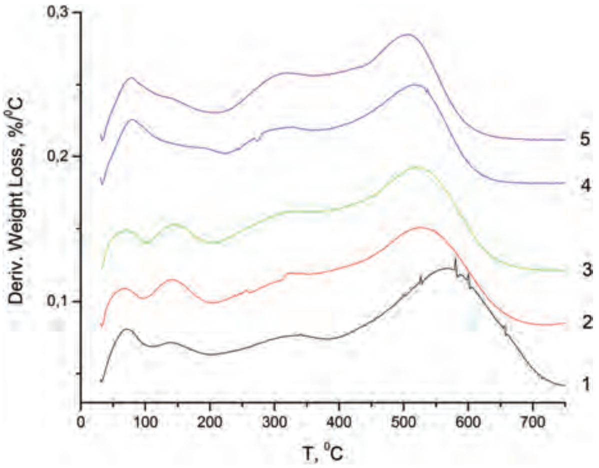

Fig. 7 DTG profiles of spent MWW materials obtained in oxidative atmosphere (air). (1) MCM-22, (2) MCM-36(1), (3) MCM-36(2), (4) MCM-49, (5) MCM-56.

Table 4 Results of TGA for MWW zeolite samples carried out under oxidative (oxygen) atmospheres

Sample	Temperature region (°C)	Maximum value on DTG curve (°C)	Weight loss (%)
MCM-22	20–200	72; 145	5.0
	200–750	331	6.0
		563	17.4
MCM-36(1)	20–200	72; 144	4.6
	200–750	341	7.3
		526	12.5
MCM-36(2)	20–200	72; 146	4.4
	200–750	334	7.6
		521	12.1
MCM-49	20–200	72; 170	6.4
	200–750	332	5.3
		521	11.8
MCM-56	20–200	72; 151	6.2
	200–750	320	7.8
		507	10.8

easily accessible external large cups due to the delamination and pillaring. On the other hand, MCM-22 with a well-developed microporosity (Table 2) has the highest weight loss at $T \approx 560$ °C (17.4%). However, the MCM-49 sample with crystal structure and value of micropore volume similar to those of MCM-22 appears to be an exception from these considerations. Taking into account the high concentration of LAS in MCM-49 (Table 3), it may be assumed that these active sites could be inactive or less active in coke formation on the MCM-49 crystals.

3.2.3. Conversion and selectivity over coked samples. To evaluate the influence of carbonaceous deposits on the catalytic properties of MWW materials, the catalyst samples after reaction were separated from the organic phase, washed with excess of ethanol, dried at 120 °C for 12 hours and re-used in the aldol condensation under the same reaction conditions. The results are presented in Table 5.

It is seen that furfural conversion over both re-used MCM-36 samples decreased drastically to about 5–7% from about 30–35% obtained over the fresh catalysts (Table 5). At the same time, the conversion of furfural over re-used MCM-22 and MCM-49 samples decreased only to 33–38% from the original 55–60% conversion of furfural. The results suggest that rapid formation of carbonaceous deposits which are poorly soluble in ethanol occurs in the cups located both on the external surface of MWW monolayers and in the mesoporous pillared space between these layers. On the other hand, in MCM-22 and MCM-49 possessing large supercages, the coking rate and growth of the carbonaceous deposits are limited, which makes it possible to remove such carbonaceous deposits from supercages by a simple washing with ethanol. Taking into account the structural differences between condensed and laminated/pillared MWW materials it can be assumed that the main reason for the different catalytic properties of the studied samples MWW is concerned with the presence of supercages located between "MWW monolayers" which are accessible through 10-ring pores.

It follows that the presence of cups on the surface of "MWW monolayers" or supercages (double cups) in the structure of MWW materials introduces a positive impact on the aldol condensation activity of these materials in comparison with conventional microporous crystalline materials, zeolites, as it is apparent from the comparison with the reference sample, a wide-pore three-dimensional BEA sample.

Table 5 Comparison of catalytic properties of fresh and used MWW materials. $T = 100$ °C, $t = 2$ hours, autogenous pressure

		Selectivity[a] (%)		
Sample	Furfural conversion (%)	FAc	F_2Ac	$(FAc)_2$
MCM-22	60.4	82.1	6.7	11.5
MCM-22-coked	33.0	91.7	3.5	4.8
MCM-36(1)	34.6	83.7	3.2	13.1
MCM-36(1)-coked	5.6	100	0	0
MCM-36(2)	29.7	84.8	2.8	12.4
MCM-36(1)-coked	7	94.9	0	5.1
MCM-49	55.0	85.4	5.4	9.2
MCM-49-coked	37.6	92.5	2.9	4.5

[a] FAc–OH was not observed among the reaction products.

4. Conclusions

A number of MWW materials (MCM-22, MCM-49, MCM-56 and MCM-36) were used as catalysts for the aldol condensation of furfural and acetone. Their performance was compared to that of large-pore zeolite BEA in a batch reactor at 100 °C, autogenous pressure and a reaction time of 0–4 h. To establish the relationship between the physico-chemical and catalytic properties of these micro/mesoporous materials, the samples were characterized by XRD, SEM, N_2 adsorption, FTIR and TGA. It was found that the acidic solids possessed appreciable activity in the reaction and their use resulted in the formation of products of aldehyde–ketone interaction. Surprisingly, MCM-22 and MCM-49, *i.e.* condensed materials containing supercages, exhibited higher activity than two MCM-36 catalysts having larger accessible external surface area than the condensed materials due to delamination and pillaring. This was explained by the participation of the active sites located in the supercages in the reaction in addition to the active sites present in the cups located on the external surface of MWW materials. Moreover, all MWW family catalysts gave higher conversion than the large-pore zeolite BEA. Nevertheless, furfural conversion decreased rapidly for all catalysts due to coke formation. Unexpectedly, the deactivation was found to be more severe for MCM-36 catalysts than for MCM-22 and MCM-49, which was attributed to the reaction taking place also in supercages that are protected by 10-ring channels from severe coking. In contrast, the cups located on the external surface were coked rapidly which resulted in low conversion over MCM-36 catalysts as well as in a shift in product selectivities. The selectivity to F_2Ac and $(FAc)_2$, *i.e.* products that can be formed due to their dimensions only on the external surface, was lower over coked catalyst than over fresh ones as a result of decreased concentration of the active sites on the external surface.

Acknowledgements

This publication is a result of project no. P106/12/G015 supported by the Czech Science Foundation which is being carried out in the UniCRE centre (CZ.1.05/2.1.00/03.0071) whose infrastructure was supported by the European Regional Development Fund and the state budget of the Czech Republic. The authors are very grateful to Jiří Čejka and Dana Vitvarová, both from the J. Heyrovský Institute of Physical Chemistry, Academy of Sciences of the Czech Republic, for stimulating discussions and FTIR characterization of the catalysts, respectively.

References

1 D. Kubička, I. Kubičková and J. Čejka, *Catal. Rev. Sci. Eng.*, 2013, **55**, 1–78.

2 C. Somerville, H. Youngs, C. Taylor, S. C. Davis and S. P. Long, *Science*, 2010, **329**, 790–792.

3 G. W. Huber and A. Corma, *Angew. Chem., Int. Ed.*, 2007, **46**, 7184–7201.

4 D. L. Klass, *Biomass for Renewable Energy, Fuels and Chemicals*, Academic Press, San Diego, 1998.

5 Y. Sun and J. Cheng, *Bioresour. Technol.*, 2002, **83**, 1–11.

6 X. Hu, L. Wu, Y. Wang, Y. Song, D. Mourant, R. Gunawan, M. Gholizadeh and C.-Z. Li, *Bioresour. Technol.*, 2013, **133**, 469–474.

7 J. N. Chheda, G. W. Huber and J. A. Dumesic, *Angew. Chem., Int. Ed.*, 2007, **46**, 7164–7183.

8 D. R. Dodds and R. A. Gross, *Science*, 2007, **318**, 1250–1251.

9 C. Gutsche, D. Redmore, R. Buriks, K. Nowotny, H. Grassner and C. Armbruster, *J. Am. Chem. Soc.*, 1967, **89**, 1235.

10 Y. Shigemasa, K. Yokoyama, H. Sashiwa and H. Saimoto, *Tetrahedron Lett.*, 1994, **35**, 1263.

11 G.-W. Wang, Z. Zhang and Y.-W. Dong, *Org. Process Res. Dev.*, 2004, **8**, 18.

12 Z. Zhang, Y.-W. Dong and G.-W. Wang, *Chem. Lett.*, 2003, **32**, 966.

13 V. K. Díez, C. R. Apesteguía and J. I. Di Cosimo, *J. Catal.*, 2006, **240**, 235.

14 C. Noda, G. P. Alt, R. M. Werneck, C. A. Henriques and J. L. F. Monteiro, *Braz. J. Chem. Eng.*, 1998, **15**, 120.

15 I. Di Cosimo, V. K. Diez and C. R. Apesteguia, *Appl. Catal., A*, 1996, **137**, 149.

16 M. J. Climent, A. Corma, S. Iborra and J. Primo, *J. Catal.*, 1995, **151**, 60.

17 B. M. Choudary, M. L. Kantam, P. Sreekanth, T. Bandopadhyay, F. Figueras and A. Tuel, *J. Mol. Catal. A: Chem.*, 1999, **142**, 361.

18 J. Yu, S. Y. Shiau and A. Ko, *Catal. Lett.*, 2001, **77**, 165.

19 M. J. Climent, A. Corma, H. García, R. Guil-López, S. Iborra and V. Fornés, *J. Catal.*, 2001, **193**, 385.

20 H. Naka, Y. Kaneda and T. Kurata, *J. Oleo Sci.*, 2001, **50**, 813.

21 V. Subramoni, V. K. Rajeevan and B. R. Prasad, *Ion Exch. Technol.*, 1984, 367.

22 J. C. A. A. Roelofs, A. J. van Dillen and K. P. de Jong, *Catal. Today*, 2000, **60**, 297.

23 M. J. Climent, A. Corma, S. Iborra and A. Velty, *Catal. Lett.*, 2002, **79**, 157.

24 C. Noda Pérez, C. A. Pérez, C. A. Henriques and J. L. F. Monteiro, *Appl. Catal., A*, 2004, **272**, 229.

25 S. Abelló, F. Medina, D. Tichit, J. Pérez-Ramírez, J. C. Groen, J. E. Sueiras, P. Salagre and Y. Cesteros, *Chem. – Eur. J.*, 2005, **11**, 728.

26 F. Winter, X. Xia, B. P. C. Hereijgers, J. H. Bitter, A. J. van Dillen, M. Muhler and K. P. de Jong, *J. Phys. Chem. B*, 2006, **110**, 9211.

27 R. M. West, Z. Y. Liu, M. Peter, C. A. Gärtner and J. A. Dumesic, *J. Mol. Catal. A: Chem.*, 2008, **296**, 18–27.

28 T. N. Pham, D. Shi and D. E. Resasco, *Appl. Catal., B*, 2014, **145**, 10–23.

29 C. J. Barrett, J. N. Chheda, G. W. Huber and J. A. Dumesic, *Appl. Catal., B*, 2006, **66**, 111–118.

30 R. M. West, Z. Y. Liu, M. Peter, C. A. Gärtner and J. A. Dumesic, *J. Mol. Catal. A: Chem.*, 2008, **296**, 18–27.

31 R. Xing, A. V. Subrahmayam, H. Olcay, W. Qi, P. van Walsum, G. Pendse and G. W. Huber, *Green Chem.*, 2010, **12**, 1933–1946.

32 A. S. Ndou, N. Plint and N. J. Coville, *Appl. Catal., A*, 2003, **251**, 337–345.

33 L. Hora, V. Kelbichová, O. Kikhtyanin, O. Bortnovskiy and D. Kubička, *Catal. Today*, 2014, **223**, 154–162.

34 D. Tichit, M. N. Bennani, F. Figueras, R. Tessier and J. Kervennal, *Appl. Clay Sci.*, 1998, **13**, 401–415.

35 B. F. Sels, D. E. de Vos and P. A. Jacobs, *Catal. Rev. Sci. Eng.*, 2001, **43**, 443–488.

36 W. Shen, G. A. Tompsett, K. D. Hammond, R. Xing, F. Dogan, C. P. Grey, W. C. Conner Jr., S. M. Auerbach and G. W. Huber, *Appl. Catal., A*, 2011, **392**, 57–68.

37 P. A. Zapata, J. Faria, M. P. Ruiz and D. E. Resasco, *Top. Catal.*, 2012, **55**, 38–52.

38 A. Dhakshinamoorthy, M. Opanasenko, J. Čejka and H. Garcia, *Adv. Synth. Catal.*, 2013, **355**, 247–268.

39 A. Dhakshinamoorthy, M. Opanasenko, J. Čejka and H. Garcia, *Catal. Sci. Technol.*, 2013, **3**, 5209–5240.

40 D. P. Debecker, E. M. Gaigneaux and G. Busta, *Chem. – Eur. J.*, 2009, **15**, 3920–3393.

41 C. Xu, Y. Gao, X. Liu, R. Xin and Z. Wang, *RSC Adv.*, 2013, **3**, 793–801.

42 S. Abelló, D. Vijaya-Shankar and J. Pérez-Ramírez, *Appl. Catal., A*, 2008, **342**, 119–125.

43 E. Taarning, C. Osmundsen, X. Yang, B. Voss, S. Andersen and C. Christensen, *Energy Environ. Sci.*, 2011, **4**(3), 793–804.

44 C. Perego and D. Bianchi, *Chem. Eng. J.*, 2010, **161**(3), 314–322.

45 H. van Bekkum and H. W. Kouwenhoven, *Stud. Surf. Sci. Catal.*, 2007, **168**, 947–998.

46 A. Corma, S. Iborra and A. Velty, *Chem. Rev.*, 2007, **107**(6), 2411–2502.

47 P. Mäki-Arvela, B. Holmbom, T. Salmi and D. Murzin, *Catal. Rev. Sci. Eng.*, 2007, **49**(3), 197–340.

48 M. Bejblová, D. Procházková and J. Čejka, *ChemSusChem*, 2009, **2**, 486.

49 E. Dumitriu, V. Hulea, I. Fechete, A. Auroux, J.-F. Lacaze and C. Guimon, *Microporous Mesoporous Mater.*, 2001, **43**, 341–359.

50 A. Ungureanu, S. Royer, T. V. Hoang, D. Trong On, E. Dumitriu and S. Kaliaguine, *Microporous Mesoporous Mater.*, 2005, **84**, 283–296.

51 T. Komatsu, M. Mitsuhashi and T. Yashima, *Stud. Surf. Sci. Catal.*, 2002, **142**, 667–674.

52 O. Kikhtyanin, V. Kelbichová, D. Vitvarová, M. Kubů and D. Kubička, *Catal. Today*, 2014, **227**, 154–162.

53 W. J. Roth, C. T. Kresge, J. C. Vartuli, M. E. Leonowicz, A. S. Fung and S. B. McCullen, *Stud. Surf. Sci. Catal.*, 1995, **94**, 301.

54 F. S. O. Ramos, M. K. De Pietre and H. O. Pastore, *RSC Adv.*, 2013, **3**, 2084.

55 W. J. Roth, P. Nachtigall, R. E. Morris, P. S. Wheatley, V. R. Seymour, S. E. Ashbrook, P. Chlubná, L. Grajciar, M. Položij, A. Zukal, O. Shvets and J. Čejka, *Nat. Chem.*, 2013, **5**, 628.

56 W. J. Roth, P. Nachtigall, R. E. Morris and J. Čejka, *Chem. Rev.*, 2014, DOI: 10.1021/cr400600f, article ASAP.

57 W. J. Roth, in *Introduction to Zeolite Science and Practice*, ed. J. Čejka, H. V. Bekkum, A. Corma, F. Schuth, Elsevier Science, 2007, vol. 168.

58 M. E. Leonowicz, S. L. Lawton, R. D. Partridge, P. Chu and M. K. Rubin, *Science*, 1994, **264**, 1910.

59 S. L. Lawton, M. E. Leonowicz, R. D. Partridge, P. Chu and M. K. Rubin, *Microporous Mesoporous Mater.*, 1998, **23**, 109–117.

60 S. Maheshwari, C. Martínez, M. T. Portilla, F. J. Llopis, A. Corma and M. Tsapatsis, *J. Catal.*, 2010, **272**, 298–308.

61 S. Lawton, A. Fung, G. Kennedy, L. Alemany, C. Chang, G. Hatzikos, D. Lissy, M. Rubin, H. Timken and S. Steuernagel, *J. Phys. Chem.*, 1996, **100**, 3788.

62 K. Liu, S. Xie, S. Liu, G. Xu, N. Gao and L. Xu, *J. Catal.*, 2011, **283**, 68–74.

63 G. G. Juttu and R. F. Lobo, *Microporous Mesoporous Mater.*, 2000, **40**, 9–23.

64 Y. J. He, G. S. Nivarthy, F. Eder, K. Seshan and J. A. Lercher, *Microporous Mesoporous Mater.*, 1998, **25**, 207–224.

65 Y. Zhang, H. Xing, P. Yang, P. Wu, M. Jia, J. Sun and T. Wu, *React. Kinet. Catal. Lett.*, 2007, **90**, 45–52.

66 S. Brunauer, P. H. Emmet and E. Teller, *J. Am. Chem. Soc.*, 1938, **62**, 309.

67 B. C. Lippens and J. H. de Boer, *J. Catal.*, 1965, **4**, 319.

68 B. Gil, S. I. Zones, S.-J. Hwang, M. Bejblová and J. Čejka, *J. Phys. Chem. C*, 2008, **112**, 2997.

69 A. Corma, V. Fornés, L. Forni, F. Márquez, J. M. Triguero and D. Moscotti, *J. Catal.*, 1998, **179**, 451–458.

70 P. Chlubná, W. J. Roth, A. Zukal, M. Kubů and J. Pavlatová, *Catal. Today*, 2012, **179**, 35–42.

71 K. S. W. Sing, D. H. Everett, F. A. W. Haul, L. Mouscou, R. A. Pierotti, J. Rouquerol and T. Siemieniewska, *Pure Appl. Chem.*, 1985, **57**, 603.

72 M. Kruk, M. Jaroniec and A. Sayari, *J. Phys. Chem. B*, 1997, **101**, 583.

73 F. Rouquerol, J. Rouquerol and K. Sing, *Adsorption by Powders and Porous Solids, Principles Methodology and Applications*, Academic Press, London, 1999.

74 J. S. Beck, J. C. Vartuli, W. J. Roth, M. E. Leonowicz, C. T. Kresge, K. D. Schmitt, C. T.-W. Chu, D. H. Olson, E. W. Sheppard, S. B. McCullen, J. B. Higgins and J. L. Schlenker, *J. Am. Chem. Soc.*, 1992, **114**, 10834.

75 O. Franke, J. Rathousky, G. Schulz-Ekloff, J. Stárek and A. Zukal, in *Zeolites and Related Microporous Materials: State of the Art 1994, Studies in Surface Science and Catalysis*, ed. J. Weitkamp, H. G. Karge, H. Pfeifer and W. Hölderich, vol. 84, Part B, Elsevier, Amsterdam, 1994, p. 77.

76 A. Corma, U. Diaz, V. Fornés, J. M. Guil, J. Martínez-Triguero and E. J. Creyghton, *J. Catal.*, 2000, **191**, 218–224.

77 S. Laforge, P. Ayrault, D. Martin and M. Guisnet, *Appl. Catal., A*, 2005, **279**, 79–88.

78 A. Corma, V. Fornes, J. Martinez-Triguero and S. B. Pergher, *J. Catal.*, 1999, **186**, 57–63.

79 A. Lercher, C. Grundling and G. Eder-Mirth, *Catal. Today*, 1996, **27**, 353.

80 B. Gil, B. Marszałek, A. Micek-Ilnicka and Z. Olejniczak, *Top. Catal.*, 2010, **53**, 1340.

81 E. J. A. Schweitzer and P. F. Van den Oosterkamp, *Microporous Mesoporous Mater.*, 1998, **20**, 397.

Catalysis Today 243 (2015) 158–162

Contents lists available at ScienceDirect

Catalysis Today

journal homepage: www.elsevier.com/locate/cattod

Toward understanding of the role of Lewis acidity in aldol condensation of acetone and furfural using MOF and zeolite catalysts

Oleg Kikhtyanin[a,*], David Kubička[a], Jiří Čejka[b,c]

[a] Research Institute of Inorganic Chemistry – UniCRE-RENTECH, Chempark Litvínov, 436 70 Litvínov, Czech Republic
[b] J. Heyrovský Institute of Physical Chemistry, Academy of Sciences of the Czech Republic, v.v.i., Dolejškova 3, CZ-182 23 Prague 8, Czech Republic
[c] Center of Research Excellence in Petroleum Refining and Petrochemicals, King Fahd University of Petroleum & Minerals, Dhahran 31261, Saudi Arabia

ARTICLE INFO

Article history:
Received 16 June 2014
Received in revised form 28 July 2014
Accepted 18 August 2014
Available online 9 September 2014

Keywords:
Metal organic framework
Aldol condensation
Acidic catalysis
Lewis acidity
Brønsted acidity

ABSTRACT

The aldol condensation of furfural and acetone allow producing higher value products from simple organic compounds resulting from biomass processing. In this paper, a number of metal organic framework (MOF) materials possessing Lewis acidity were investigated as catalysts in this reaction. Experiments were carried out under batch reaction conditions in Parr stirred autoclave at 100 °C during 0–4 h. The catalytic results indicated that the aldol condensation over MOFs took place with the participation of acidic rather than basic centers. The catalytic performance of these materials exhibited could not be explained by their reported Lewis acidity. Experiments with heat-activated and re-hydrated samples showed that Brønsted acid sites could also be present in MOFs as a consequence of interaction of metal cation with surrounding water molecules. As a consequence, the catalysts having such generated Brønsted acidity exhibited enhanced activity in the reaction.

1. Introduction

Geopolitical and environmental concerns faced by our society are reflected in the extensive research activities focused on production of automotive fuels and different valuable products using other resources than fossil ones. Among them, lignocellulosic biomass is considered as one of the most promising bio-based feedstocks for the production of fuels and other chemical products not competing with food crops, fodder, and natural habitat [1]. Furanic compounds (furfural, 5-hydroxymethlyfurfural) and acetone are readily available chemicals, which can be produced by biomass hydrolysis [2]. Additionally, acetone is available as a by-product in phenol production. Aldehydes and ketones can react by aldol condensation and afford higher added value products from simple and cheap ones. Aldol condensation proceeds in the presence of either basic or acidic catalysts [3,4]. The most effective industrially available methods rely on using liquid bases (NaOH or KOH) or mineral acid (H_2SO_4) as catalysts [3]. However, these catalysts pose a major environmental threat due to waste water production and equipment corrosion. To address this issue, new industrially viable catalysts must be developed.

Solid catalysts with acid–base character are considered as a promising alternative to homogeneous catalysts for aldol condensation of furfural and acetone [5–13]. In accordance with generally accepted reaction scheme, 4-(2-furyl)-4-hydroxybutan-2-on (alcohol FAc-OH; Scheme 1) is the primary intermediate product of the interaction between furfural and acetone. In the presence of catalysts having strong acidic or basic centers, this intermediate is easily dehydrated to 4-(2-furyl)-3-buten-2-on (FAc; Scheme 1), the primary product of aldol condensation. Further, F_2Ac (1,4 pentadiene-3-on-1,5-di-2-furanyl) formation takes place as a result of a consecutive reaction of FAc with another furfural molecule. When acidic zeolites are used as catalysts for the reaction, the formation of an additional product, $(FAc)_2$, occurs as a result of FAc dimerization over Brønsted acid sites (Scheme 1) [11].

Among solid catalysts, Al–Mg hydrotalcites and different metal oxides or double mixed oxides with basic character are considered as the most promising catalysts for this reaction [5–13]. The essential disadvantages of such basic catalysts are their high sensitivity to ambient CO_2, which transforms them into a catalytically inactive form and the lack of reliable methods for recovering their catalytic properties after regeneration [14–16]. Recently, zeolites were reported as catalysts for aldol condensation of acetone and furfural [11]. It was shown that by using zeolites the disadvantages of basic catalysts i.e. susceptibility to CO_2 and poor regenerability could be avoided. On the other hand, their activity in the aldol condensation of acetone and furfural is lower than that of

---

* Corresponding author.
E-mail address: oleg.kichtanin@vuanch.cz (O. Kikhtyanin).

http://dx.doi.org/10.1016/j.cattod.2014.08.016
0920-5861/

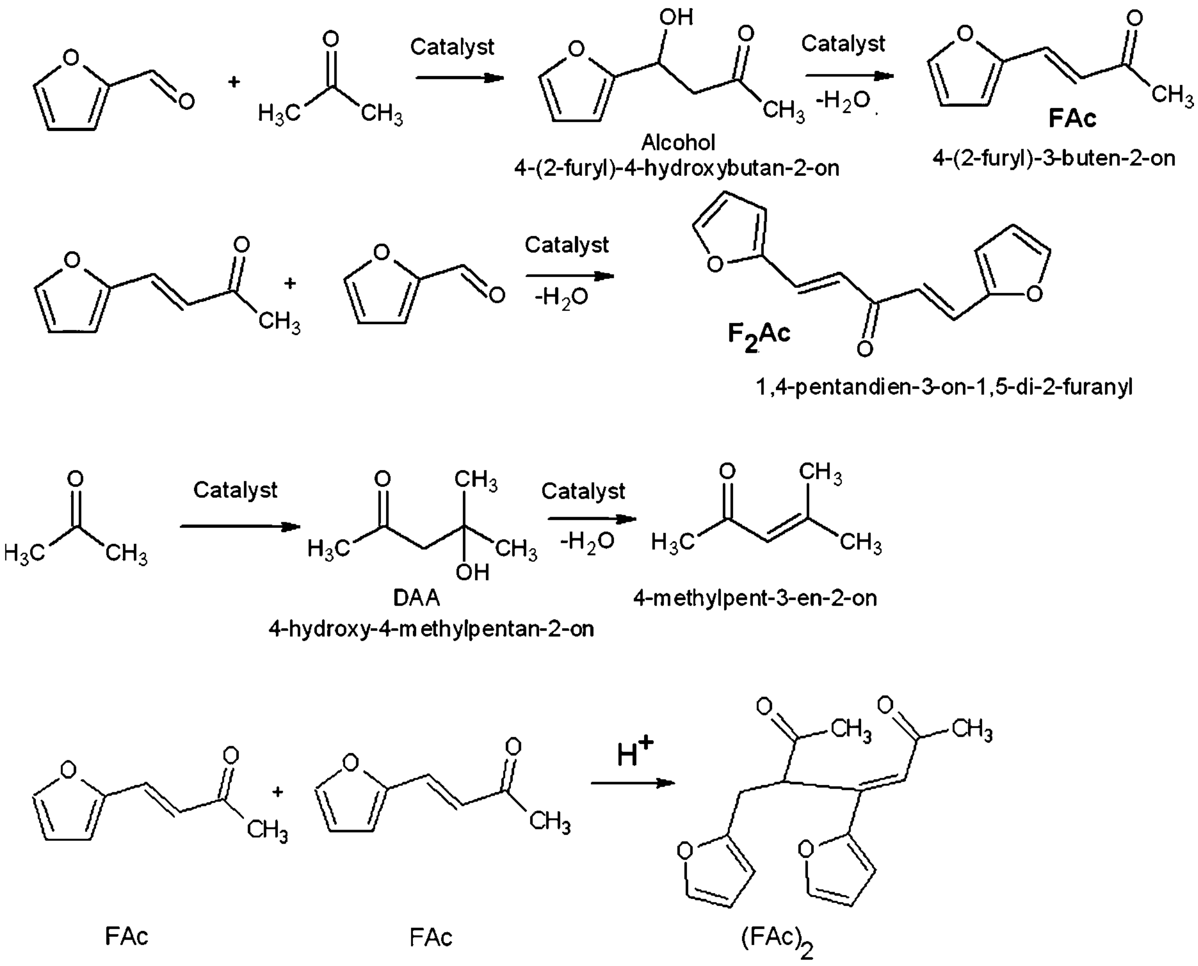

Scheme 1. Aldol condensation between furfural and acetone over acidic or basic catalysts and the formation of dimer product $(FAc)_2$ from FAc compound over acidic catalysts.

hydrotalcites. Moreover, they are rapidly deactivated due to coke formation during the reaction [11]. Obviously, the optimization of the properties of solid acidic catalysts in the aldol condensation of acetone and furfural is not possible without understanding the importance of different physico-chemical characteristics, especially the role of Brønsted (BAS) and Lewis acid sites (LAS), for the reaction. Unfortunately, zeolites contain generally both types of acidic centers, so an unambiguous conclusion about the degree of participation of BAS and LAS in the aldol condensation of furfural and acetone is virtually impossible. This problem can be overcome by using other solid acidic catalysts which possess only one type of acid sites.

MOFs are heterogeneous porous crystalline solids, which are characterized by reasonable thermal stability [17] and outstanding textural properties [18]. Unlike zeolites containing both Lewis and Brønsted acid sites [19–21], MOFs are assumed to possess mild Lewis acidity [22,23]. It makes them active in a number of organic reactions [24–27]. The presence of Lewis acidity in two commercially available MOF materials, Cu-BTC (copper benzene-1,3,5-tricarboxylate) and Fe-BTC (iron benzene-1,3,5-tricarboxylate), is well-documented [28,29]. Due to the presence of Lewis sites, Cu-BTC exhibits good catalytic properties in various reactions, such as the rearrangement of α-pinene oxide to campholenic aldehyde and the cyclization of citronellal to isopulegol [30], the Friedländer reaction between 2-aminobenzophenones and acetylacetone [23], coumarin synthesis by the Pechmann reaction [31], and Beckmann rearrangement [28].

Fe-BTC has also been reported to be a highly active catalyst for some reactions requiring Lewis acidity, such as methylation of amines [32], Claisen–Schmidt condensation between acetophenone and benzaldehyde [33], aldehyde acetalization and epoxide ring-opening reactions by methanol [34–36], the isomerization of α-pinene oxide [29]. To the best of our knowledge, no information yet is available about the use of MOFs as catalysts for aldol condensation of furfural and acetone. The performance of both Cu-BTC and Fe-BTC in this reaction is of a special interest since these materials with well-expressed Lewis acidity could provide information about the importance of such sites for the reaction between acetone and furfural.

To elucidate the role of Lewis and Brønsted acid sites in aldol condensation of acetone and furfural, the performance of several metal organic framework (MOF) catalysts with well-expressed Lewis acidity is compared with the performance of several zeolites possessing both Brønsted and Lewis acid sites.

2. Experimental

The following MOFs were purchased from Sigma-Aldrich Cu-BTC (Basolite C300), Fe-BTC (Basolite F300), Mg-formate (Basosiv M050), and ZIF-8 (Basolite Z1200). The zeolites used as reference catalysts included MFI (Si/Al = 11.5) and BEA (Si/Al = 19) obtained from Zeolyst. Their catalytic properties were investigated in aldol condensation of furfural and acetone. The catalytic experiments were carried out in a 200 ml stirred batch reactor (Parr autoclave) at

Table 1
Physico-chemical characteristics of MOFs (taken from [28]) and reference zeolite catalysts (taken from [11]).

Sample	BET, m^2/g	$D_{micropore}$, nm	V_{tot}, cm^3/g	V_{mic}, cm^3/g	C_{LAS} (mmol/g)	C_{BAS} (mmol/g)
Cu-BTC	1500	0.90, 0.50, 0.35		0.64	2.30	–
Fe-BTC	1060	0.86		0.33	2.56	–
MFI	378	0.51 × 0.55, 0.53 × 0.56	0.210	0.126	0.22	0.353
BEA	617	0.66 × 0.67, 0.56 × 0.56	0.334	0.218	0.179	0.138

100 °C. Before the start of the catalytic runs, 1.0 g (unless indicated otherwise) of the as-obtained catalyst was mixed together with a mixture of 19.75 g of acetone and 3.25 g of furfural (i.e. acetone-to-furfural molar ratio of 10-to-1) and loaded into the autoclave. After initiation of the heating the desired temperature, 100 °C, was achieved in ~60 min, and the autoclave was kept at $T = 100$ °C for an additional 2 or 4 h.

The Fe-BTC catalyst was also reactivated after the catalytic experiment by extraction of the soluble deposits using ethanol as a solvent as the conventional regeneration technique based on oxidation of the deposits is not suitable in the case of MOFs due to their low thermal stability.

Analysis of the reaction products was performed using an Agilent 7890A GC unit equipped with a flame ionization detector using a HP-5 capillary column (30 m/0.32 ID/0.25 μm). The obtained products were identified based on the standard reference compounds and GC–MS analysis of representative product samples. The catalytic activity is expressed in terms of conversion, which is defined as the fraction of furfural which was converted. The selectivity was calculated by dividing the percentage of furfural moles presented in the products by the total moles of converted furfural.

3. Results and discussion

Several MOF catalysts, i.e. Basosiv M050 and Basolite Z1200, exhibited only negligible activity in the aldol condensation of furfural and acetone (furfural conversion < 1%) and are thus not discussed here further. On the other hand, Cu-basolite (Cu-BTC) and Fe-basolite (Fe-BTC) were active in the reaction. These MOFs are commercially available materials and the textural and acidic properties of the samples under study were determined by Opanasenko et al. [28]. Hence, we used for our investigation the published data. The Cu-BTC possesses higher BET surface area (1500 m^2/g) than Fe-BTC (1060 m^2/g) and similar Lewis acid sites (LAS) concentration, 2.3 and 2.56 mmol/g, respectively (Table 1). While the concentration of LAS in Fe-BTC is only ca. 10% higher than in Cu-BTC, its BET area is ca. 30% lower and thus, judging from these physico-chemical characteristics, similar catalytic activity could be expected. Surprisingly, the furfural conversion during its aldol condensation with acetone over Cu-BTC is significantly lower in comparison with Fe-BTC (Fig. 1). Furfural conversion over Cu-BTC is 2.7% after 2 h of experiment whereas it is nearly 10 times higher over Fe-BTC, 26.2% (Table 2). It should also be noted that increasing the reaction time up to 4 h does not further increase the furfural conversion. Moreover, the Fe-BTC was re-used in aldol condensation after regeneration with ethanol and it showed better activity than Cu-BTC (conversion 13.7%), but lower than the fresh Fe-BTC catalyst (Fig. 1A). Elemental analysis of the organic reaction products proved that no leaching of Cu or Fe cations into the liquid phase took place. So, catalytic action of dissolved Fe^{3+} and Cu^{2+}cations could be neglected and only physico-chemical characteristics of Fe-BTC and Cu-BTC should be taken into account for the discussion of catalytic results.

Table 2
Catalytic properties of MOFs and reference zeolite samples in the aldol condensation of furfural and acetone.

Sample	Furfural conversion, %	Selectivity, %			
		FAc-OH	FAc	F_2Ac	$(FAc)_2$
Cu-BTC	2.7	30	70	0	0
Fe-BTC	26.2	8	71	20	1
MFI	6.4[a]	0[a]	100[a]	0[a]	0[a]
BEA	29[a]	0[a]	83[a]	5.5[a]	11.5[a]

[a] Taken from [11].

The previously reported results of aldol condensation of furfural with acetone over zeolites indicate that both Lewis and Brønsted acid sites might be involved in the reaction [11,37]. References on the study of Cu-BTC and Fe-BTC as catalysts for different organic reactions show [29–31] that the studied MOFs have a hard Lewis acid character. Unfortunately, our experiments with MOFs possessing similar Lewis acidity (Table 1) do not unambiguously explain the effect of LAS in aldol condensation of furfural with acetone as Fe-BTC affords 10 times higher conversion than Cu-BTC (Fig. 1; Table 2) under the same experimental condition despite having only 10% higher concentration of LAS (Table 1). Hence, the role of Lewis acidity remains unclear and further factors have to be taken into account.

It can be seen (Fig. 1B) that Cu-BTC exhibits only weak dehydrating properties; selectivity to alcohol, the primary product of the interaction between furfural and acetone, is as high as 46% after 2 h and reduces to 30% after 4 h of the reaction (Fig. 1B). The absence of the second condensation product, F_2Ac (Fig. 1B), serves as an additional evidence of the poor catalytic behavior of Cu-BTC. In contrast, the selectivity to alcohol over Fe-BTC is just 10% after 2 h of the reaction. Additionally, F_2Ac is found among the reaction products over this catalyst with a selectivity above 15% and when increasing the time of the experiment to 4 h. Moreover, $(FAc)_2$, i.e. a product ascribed to FAc dimerization [11], is observed in the products ($S = 1.4\%$) as well. The composition over the regenerated catalyst has changed: selectivity to alcohol increases to 22.1% while that to F_2Ac decreases to 8%.

From the comparison of the catalytic properties of MOFs with those of zeolites (Table 2) it can be elucidated that the acid sites in MOFs are weaker than those in zeolites as evidenced by their significantly lower dehydration activity of the primary alcohol product. In fact, FAc-OH is not observed among the products over zeolites at comparable conversion levels, though this may be influenced by the presence of Brønsted acid sites responsible for dehydration [38,39].

It was also demonstrated previously [11] that the formation of $(FAc)_2$ can be related to the Brønsted acidity present in zeolites; the selectivity was as high as 11.5% over zeolite BEA at conversion around 29%, i.e. similar to that observed for Fe-BTC. Thus, the presence of $(FAc)_2$ in the reaction products suggests that, first, the aldol condensation of furfural and acetone over Fe-BTC is definitely acid rather basic catalyzed reaction; second, the presence of not only LAS but also BAS in Fe-BTC. Indeed, it was proposed in [34] that weak Brønsted acid sites could be present in Fe-BTC due to the existence of structural defects. If so, the catalytic activity of MOF materials in the aldol condensation might be attributed to the presence of BAS rather than LAS since the Lewis acidic Cu-BTC affords only negligible furfural conversion. Moreover, the very recent theoretical calculations by P. Nachtigall et al. [40] have shown that LAS alone are not able to decrease the activation barrier for aldolization, while BAS decrease it.

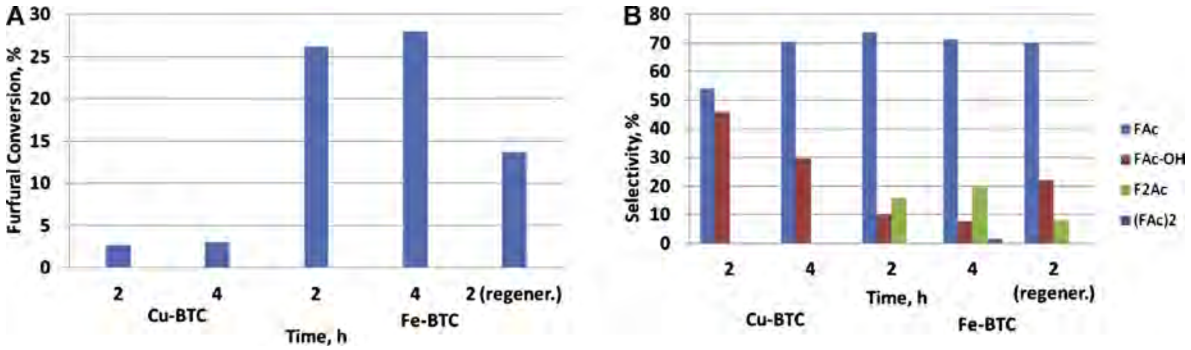

Fig. 1. Conversion of furfural over Cu-BTC and Fe-BTC (A) and the selectivity to the main aldol condensation products (B).

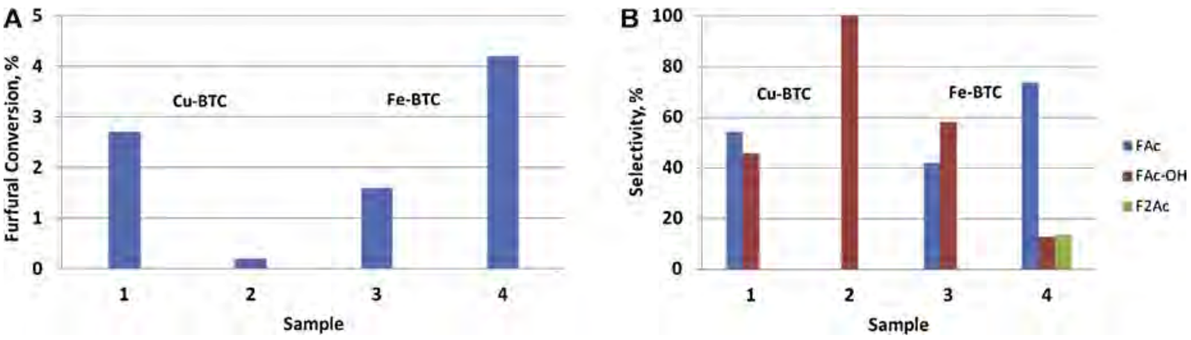

Fig. 2. Catalytic properties of activated Cu-BTC and Fe-BTC and rehydrated Fe-BTC samples. (A) Furfural conversion. (B) Products selectivity. 1 – As-received Cu-BTC. 2 – Cu-BTC activated at 150 °C. 3 – Fe-BTC activated at 150 °C. 4 – Activated and rehydrated Fe-BTC. Note: only 0.25 g of regenerated catalyst was used in the experiments with Fe-BTC.

The question remains, however, whether it is possible to attribute the existence of BAS in MOF materials exclusively to the presence of structural defects? To answer this question, we have performed a thermal activation of Cu-BTC and Fe-BTC at 150 °C to remove water which could be present in these materials. Fig. 2 shows that furfural conversion of thermally activated Cu-BTC decreases by an order of magnitude, the only reaction product being alcohol. The additional experiments with Fe-BTC were conducted using 0.25 g of the regenerated catalyst. Catalytic results obtained over the heat-treated samples have shown that furfural conversion over activated Fe-BTC is 1.6% and the reaction products consist of two compounds: FAc-OH with the selectivity of 58% and FAc with the selectivity of 42%. Another part of Fe-BTC sample activated at 150 °C was impregnated with a few drops of water, followed by drying in air for 24 h. The catalytic test of such re-hydrated sample evidenced an increase in the furfural conversion up to 4.2% (Fig. 2A). Also, the selectivity to alcohol was significantly reduced (from ca. 60% to about 14%), and the second condensation product F2Ac was obtained with the selectivity of 14% (Fig. 2B).

The results demonstrate that water present in the fresh, as-obtained Fe-BTC, introduces a promoting effect on the catalytic properties of the MOF material in comparison with the dried catalysts, plausibly due to the generation of BAS. It is also obvious (Fig. 2B) that the active sites present in Cu-BTC are not capable of the second aldol condensation step affording F_2Ac while this product is obtained over Fe-BTC. This suggests that the concentration of Brønsted acid sites in Cu-BTC is lower than in Fe-BTC or they are weaker than those in Fe-BTC. As in both catalysts a clear effect of water (moisture) is visible, it was investigated further.

To prove the importance of water for the presence of BAS in hydrated iron and copper MOF catalysts, additional experiments were carried out using copper and iron hydrated nitrates as catalysts for aldol condensation (Fig. 3). Furfural conversion over $Cu(NO_3)_2{\cdot}6H_2O$ was 1.1%, and the reaction products consisted of alcohol with a selectivity of 52.2% and FAc with a selectivity of

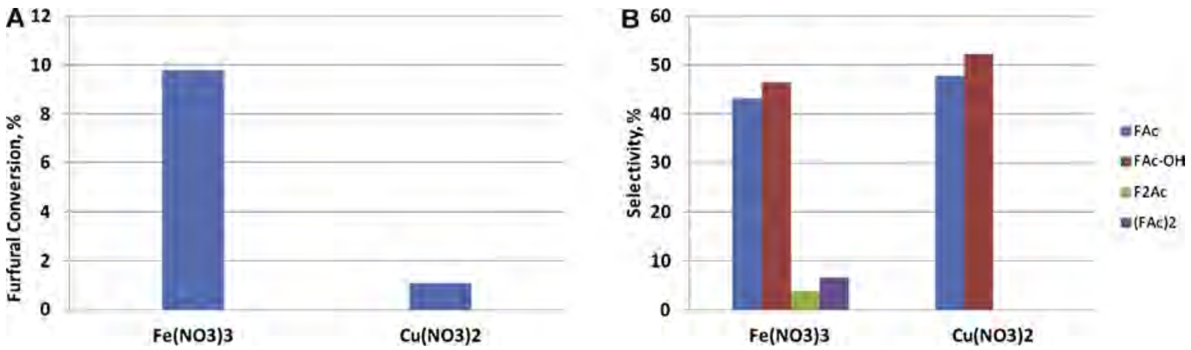

Fig. 3. Comparison of catalytic properties of iron and copper nitrates in the aldol condensation of furfural and acetone.

47.8%. Furfural conversion in the presence of $Fe(NO_3)_3{\cdot}9H_2O$ was 9.8% and the reaction products were not limited to FAc-OH and FAc, but F_2Ac with a selectivity of 3.8% and $(FAc)_2$ with a selectivity of 6.6% were also present. The last result shows that the hydrated iron nitrate definitely exhibits Brønsted acidity. Indeed, it is known that transition metal ions like Fe^{3+}or Cu^{2+} cannot be Brønsted acids by themselves (as they do not possess any proton to donate), but in water solutions they are causing the hydrolysis of water molecules being in their first coordination sphere. Thus, the existing metal aqua complex can be considered as donor of the proton, forming hydroxoaqua complex in the process and giving up H^+ ions to the medium. Water molecules co-ordinatively bound to one of these metal ions are more acidic than normal water molecules.

Taking into account the results of the catalytic tests, it can be suggested that even in organic medium Fe^{3+} cations in hydrated iron nitrate may act as donors for the neighboring water molecules, thus resulting in the appearance of H^+ ions. Unfortunately, the exact structure of Fe-BTC remains unknown due to its poor crystallinity [34] making it difficult to describe its interaction with water. However, similar catalytic properties of iron hydrated nitrate and iron 1,3,5-benzenetricarboxylate (Fe-BTC) make us suggest that Fe-BTC also contains bound water molecules acting, by analogy, as proton donors. As a result, Fe-BTC also possesses Brønsted acidity as evidenced by the formation of the dimerization product, $(FAc)_2$. Moreover, trivalent ions pull the electrons more strongly than divalent ions. That means that the hydrogen atoms in the ligand water molecules will have a greater positive charge in a trivalent ion, i.e. being more acidic. This could explain the string difference in the catalytic behavior of Cu-BTC and Fe-BTC.

4. Conclusions

Catalytic behavior of Fe-BTC and Cu-BTC in the aldol condensation of furfural and acetone suggests that the reaction proceeds with the participation of acidic rather than basic sites. Solid catalysts having exclusively Lewis acid sites possess substantially lower activity in the aldol condensation of acetone and furfural, as proved by the results over Cu-BTC in this reaction, particularly when sufficiently dried. Fe-BTC, which is also assumed as a material with Lewis acidity, shows a fairly good activity in the aldol condensation of acetone and furfural. Such catalytic behavior of Fe-BTC can be explained by the presence of (weak) Brønsted acid sites in addition to Lewis acid sites. These centers are present in Fe-BTC either due to the existence of structural defects, or due to the activating effect of Fe^{3+} cation on the surrounding (coordinated) water molecules, resulting in the appearance of H^+ ions in the reaction medium, i.e. of Brønsted acidity. The consequences of the generated Brønsted acidity in the catalyst are the increase in the activity of MOF materials and the change in the composition of reaction products. In particular, the formation of $(FAc)_2$ takes place which, in turn, may be considered as a proof for the presence of Brønsted acid sites in solid catalysts.

Acknowledgements

This publication is a result of project no. P106/12/G015 supported by the Czech Science Foundation which is being carried out in the UniCRE center (CZ.1.05/2.1.00/03.0071) whose infrastructure was supported by the European Regional Development Fund and the state budget of the Czech Republic.

References

[1] D. Kubička, I. Kubičková, J. Čejka, Catal. Rev. Sci. Eng. 55 (2013) 1–78.
[2] P. Maki-Arvela, T. Salmi, B. Holmbom, S. Willfor, D.Y. Murzin, Chem. Rev. 111 (2011) 5638–5666.
[3] R.T. Morrison, R.N. Boyd, Organic Chemistry, Prentice-Hall, Englewood Cliffs, 1992 (Chapter 21).
[4] D.S. Kemp, V. Frank, Organic Chemistry, Worth Publishers, 1980, pp. 839–845.
[5] A.S. Ndou, N. Plint, N.J. Coville, Appl. Catal. A: Gen. 251 (2003) 337–345.
[6] D. Tichit, M.N. Bennani, F. Figueras, R. Tessier, J. Kervennal, Appl. Clay Sci. 13 (1998) 401–415.
[7] B.F. Sels, D.E. de Vos, P.A. Jacobs, Catal. Rev. Sci. Eng. 43 (2001) 443–488.
[8] C.J. Barrett, J.N. Chheda, G.W. Huber, J.A. Dumesic, Appl. Catal. B: Environ. 66 (2006) 111–118.
[9] W. Shen, G.A. Tompsett, K.D. Hammond, R. Xing, F. Dogan, C.P. Grey, W.C. Conner Jr., S.M. Auerbach, G.W. Huber, Appl. Catal. A: Gen. 392 (2011) 57–68.
[10] P.A. Zapata, J. Faria, M.P. Ruiz, D.E. Resasco, Top. Catal. 55 (2012) 38–52.
[11] O. Kikhtyanin, V. Kelbichová, D. Vitvarová, M. Kubů, D. Kubička, Catal. Today 227 (2014) 154–162.
[12] L. Hora, V. Kelbichová, O. Kikhtyanin, O. Bortnovskiy, D. Kubička, Catal. Today 223 (2014) 138–147.
[13] L. Hora, O. Kikhtyanin, L. Čapek, O. Bortnovskiy, D. Kubička, Catal. Today (2014), http://dx.doi.org/10.1016/j.cattod.2014.03.010.
[14] D.P. Debecker, E.M. Gaigneaux, G. Busta, Chem. Eur. J. 15 (2009) 3920–3935.
[15] C. Xu, Y. Gao, X. Liu, R. Xin, Z. Wang, RSC Adv. 3 (2013) 793–801.
[16] S. Abelló, D. Vijaya-Shankar, J. Pérez-Ramírez, Appl. Catal. A: Gen. 342 (2008) 119–125.
[17] (a) H. Li, M. Eddaoudi, M. O'Keeffe, O.M. Yaghi, Nature 402 (1999) 276–279; (b) R.E. Morris, Nat. Chem. 3 (2011) 347–348.
[18] H.K. Chae, D.Y. Siberio-Perez, J. Kim, Y.B. Go, M. Eddaoudi, A.J. Matzger, M. O'Keeffe, O.M. Yaghi, Nature 427 (2004) 523–527.
[19] A. Corma, Chem. Rev. 95 (1995) 559–624.
[20] C.T. Kresge, M.E. Leonowicz, W.J. Roth, J.C. Vartuli, J.S. Beck, Nature 359 (1992) 710–712.
[21] R.M. Martín-Aranda, J. Čejka, Top. Catal. 53 (2010) 141–153.
[22] A. Corma, H. García, F.X. Llabrés i Xamena, Chem. Rev. 110 (2010) 4606–4655.
[23] E. Pérez-Mayoral, Z. Musilová, B. Gil, B. Marszalek, M. Položij, P. Nachtigall, J. Čejka, Dalton Trans. 44 (2012) 4036–4044.
[24] A. Dhakshinamoorthy, M. Opanasenko, J. Čejka, H. Garcia, Adv. Synth. Catal. 355 (2013) 247–268.
[25] F.X. Llabrés i Xamena, F.G. Cirujano, A. Corma, Microporous Mesoporous Mater. 157 (2012) 112–117.
[26] P. Horcajada, S. Surble, C. Serre, D.Y. Hong, Y.K. Seo, J.S. Chang, J.M. Greneche, I. Margiolaki, G. Ferey, Chem. Commun. (2007) 2820–2822.
[27] F.X. Llabrés i Xamena, O. Casanova, R. GaliassoTailleur, H. Garcia, A. Corma, J. Catal. 255 (2008) 220–227.
[28] M. Opanasenko, M. Shamzhy, M. Lamač, J. Čejka, Catal. Today 204 (2013) 94–100.
[29] A. Dhakshinamoorthy, M. Alvaro, H. Chevreau, P. Horcajada, T. Devic, C. Serre, H. Garcia, Catal. Sci. Technol. 2 (2012) 324–330.
[30] L. Alaerts, E. Séguin, H. Poelman, F. Thibault-Starzyk, P.A. Jacobs, D.E. De Vos, Chem. Eur. J. 12 (2006) 7353–7363.
[31] M. Opanasenko, M. Shamzhy, J. Čejka, ChemCatChem 5 (2013) 1024–1031.
[32] A. Dhakshinamoorthy, M. Alvaro, H. Garcia, Appl. Catal. A: Gen. 378 (2010) 19–25.
[33] A. Dhakshinamoorthy, M. Alvaro, H. Garcia, Adv. Synth. Catal. 352 (2010) 711–717.
[34] A. Dhakshinamoorthy, M. Alvaro, P. Horcajada, E. Gibson, M. Vishnuvarthan, A. Vimont, J.-M. Grenèche, C. Serre, M. Daturi, H. Garcia, ACS Catal. 2 (2012) 2060–2065.
[35] A. Dhakshinamoorthy, M. Alvaro, H. Garcia, Chem. Eur. J. 16 (2010) 8530–8536.
[36] A. Dhakshinamoorthy, M. Alvaro, H. Garcia, Adv. Synth. Catal. 352 (2010) 3022–3030.
[37] O. Kikhtyanin, P. Chlubná, T. Jindrová, D. Kubička, Dalton Trans. 43 (2014) 10628–10641.
[38] V.V. Ordomsky, J. van der Schaaf, J.C. Schouten, T.A. Nijhuis, ChemSusChem 5 (2012) 1812–1819.
[39] R. Weingarten, G.A. Tompsett, W. Curtis Conner Jr., G.W. Huber, J. Catal. 279 (2011) 174–182.
[40] M. Položij, M. Rubeš, J. Čejka, P. Nachtigall, ChemCatChem (2014), http://dx.doi.org/10.1002/cctc.201402411.

Journal of Molecular Catalysis A: Chemical 424 (2016) 358–368

Contents lists available at ScienceDirect

Journal of Molecular Catalysis A: Chemical

journal homepage: www.elsevier.com/locate/molcata

Aldol condensation of furfural with acetone over ion-exchanged and impregnated potassium **BEA** zeolites

O. Kikhtyanin[a,*], R. Bulánek[b], K. Frolich[b], J. Čejka[c,d], D. Kubička[a,e]

[a] Unipetrol Centre of Research and Education (UNICRE), Chempark Litvínov, 436 70 Záluží-Litvínov, Czech Republic
[b] Department of Physical Chemistry, Faculty of Chemical Technology, University of Pardubice, Studentská 573, CZ-532 10 Pardubice, Czech Republic
[c] J. Heyrovský Institute of Physical Chemistry, Academy of Sciences of the Czech Republic, v.v.i., Dolejškova 3, CZ-182 23 Prague 8, Czech Republic
[d] Center of Research Excellence in Petroleum Refining and Petrochemicals, King Fahd University of Petroleum & Minerals, Dhahran 31261, Saudi Arabia
[e] Technopark Kralupy VŠCHT Praha (University of Chemistry and Technology Prague), Žižkova 7, 278 01 Kralupy nad Vltavou, Czech Republic

ARTICLE INFO

Article history:
Received 24 June 2016
Received in revised form 9 September 2016
Accepted 12 September 2016
Available online 13 September 2016

Keywords:
Acetone
Furfural
Condensation
Potassium-**BEA**
Zeolite

ABSTRACT

Potassium-containing **BEA** zeolites were prepared by ion-exchange from NH_4-**BEA** with potassium nitrate aqueous solution or ion-exchange combined with impregnation. The samples were used as basic catalysts for aldol condensation of furfural and acetone studied in a batch reactor at 100 °C, autogenous pressure and a reaction time of 2 h. To establish a relationship between physico-chemical properties and catalytic behavior of **BEA** zeolites, the samples were characterized by XRD, N_2 adsorption, FTIR, calorimetry, and TGA. The ion-exchanged K-**BEA** catalysts exhibited low activity in the aldol condensation because of a weak strength of intrinsic basic sites. In contrast, the samples prepared by ion exchange combined with impregnation possessed strong basic sites, plausibly K_2O clusters, and demonstrated appreciable activity in the aldol condensation. TGA results proved that, in contrast to acidic zeolites, basic sites of impregnated **BEA** samples hardly contribute to the formation of heavy carbonaceous deposits during the reaction what could be advantageous for the stable behavior of catalysts.

1. Introduction

Efficient biomass valorization is one of the most prominent scientific challenges that chemists and chemical engineers have been facing in the recent years. The ability to tackle this challenge would be a significant step towards sustainable utilization of available resources on Earth since biomass constitutes an abundant renewable resource. Considering the energy needs of our society, transportation fuels are the sector with the highest growth of demand. However, there is a gap between the basic biomass building blocks having generally 5–9 carbon atoms in their molecules and the desired fuel components that have, in the case of kerosene and diesel fuel, typically between 10 and 20 carbon atoms in their molecules. Bridging this gap is a big challenge requiring to be addressed to valorize solid (lignocellulosic) biomass as a feedstock for transportation fuel production.

The increase in carbon chain length can be advantageously achieved by aldol condensation of short-chain aldehydes and ketones [1–4], such as furfural and acetone, as these can be produced in substantial amounts from biomass [5,6]. As a result, rather complex products with suitable molecular mass and structure can be obtained starting from comparatively simple reagents. Both the preparation of the initial reagents and their processing to complex heavier molecules could be regarded as a basis of the production of valuable products from biomass-based renewable feedstocks.

Aldol condensation of aldehydes and ketones is a well-known reaction of organic synthesis, which takes place in the presence of both acidic and basic catalysts [7]. Most often, aqueous basic hydroxide solutions are used as catalysts for this reaction because of their excellent activity and high selectivity toward the desired reaction products [8]. This is connected with high demands on the corrosive stability of equipment and produces a significant amount of waste water streams that must be treated [9]. These disadvantages together with the increasing demands for environmental friendliness of new technologies constitute a significant driving force for introducing solid basic materials as catalysts for aldol condensation. Hydrotalcite-like (HTC) materials as well as other mixed oxide systems have been recently successfully used as basic catalysts for aldol condensation [10–14]. Nevertheless, these materials have some significant disadvantages, such as high sensitivity to the

---

* Corresponding author.
E-mail address: oleg.kikhtyanin@unicre.cz (O. Kikhtyanin).

http://dx.doi.org/10.1016/j.molcata.2016.09.014
1381-1169/

ambient CO_2 and difficulties with re-using of the HTC-based catalysts in successive catalytic cycles [10,15,16]. Consequently, new solid catalysts for aldol condensation between acetone and furfural have been investigated [17–19].

Among heterogeneous catalysts, solid catalysts with acidic properties, in particular acidic zeolites of different structural types, have been shown to catalyze condensation of various aldehydes and ketones [20–22] including aldol condensation between acetone and furfural [18,23]. Activity of zeolites in this reaction was determined by the acidic as well as structural properties. Nevertheless, during the reaction the activity of the investigated zeolites decreased due to the formation of carbonaceous deposits inside their micropores [18].

In contrast to most inorganic solids the functionality of zeolites can vary from acidic to basic range and the change in their acido-basic character is achieved by performing relevant procedures and monitored by physico-chemical methods. Zeolites possessing basic sites were also repeatedly used as catalysts for different organic reactions [24,25]. In general, two types of basic centers can be discriminated in these materials. Firstly, zeolites possess “intrinsic basicity”, which is provided by the negative charges of the framework oxygen atoms in the proximity of tetrahedral Al atoms [26–28]. It is believed that these basic sites are relatively weak [26], but the basicity of zeolites can be enhanced by introducing excess of alkali species. These “hosted basic sites” are normally introduced by incipient wetness impregnation of corresponding basic compounds, mostly as their salts that are subsequently decomposed by heating [29,30]. Obviously, a ratio between “intrinsic” and “hosted” basic sites can be adjusted by the content of a basic metal introduced into a zeolite by either ion exchange or impregnation. The excess of alkali compounds as compared to the ion-exchange capacity of a zeolite can be achieved also by a different method. Davis and Hathaway [31] prepared **FAU** zeolites overloaded with alkaline oxides by ion-exchange using aqueous solution of Cs acetate followed by filtration of the catalysts without subsequent washing of the samples with excess of water. Romero et al. [32] enhanced the basic properties of the **X** zeolite during synthesis by controlling the washing stage of the synthesized zeolite, which allowed retaining the optimum amount of alkaline hydroxide. Independently on the preparation method, such zeolites with “hosted basic species” possessed rather strong basicity, which was proved by different methods [25,29,33]. These basic zeolites were investigated in different organic reactions including dehydrogenation of alcohols, olefins isomerization, side-chain alkylation of aromatics, condensations, etc. [24,25,34]. A special attention was paid to the stability of the prepared catalysts because supported alkali metals have been shown to be prone to leaching when upgrading biomass-derived feedstocks [6]. In some cases the leaching could be suppressed when using supports with a stronger support-alkali metal (oxide) interaction, such as zeolites [6 and References herein]. Despite the significant number of articles dealing with basic zeolites, there is a lack of information on the performance of catalysts prepared from the same parent zeolite sample but having a different ratio of “intrinsic” to “hosted” basicity. Moreover, the performance of zeolites with basic properties as catalysts for aldol condensation of furfural and acetone has not been reported yet.

The present study deals with the preparation of a series of **BEA** zeolite samples by ion-exchange (partial and complete) with aqueous KNO_3 solution followed by thorough washing or without any rinsing of the samples with excess of water after filtration. The properties of the prepared basic zeolites were examined by a number of physico-chemical methods and their catalytic behavior was investigated in aldol condensation of acetone and furfural. The primary aim of the study is to understand the fundamental role of acidic and basic sites in zeolite BEA in the aldol condensation of furfural and acetone. In particular, the catalytic activity and selectivity as well as the susceptibility to rapid deactivation in dependence on the acido-basic properties of the catalysts are addressed.

2. Experimental

2.1. Materials

The series of K-**BEA** samples was prepared using the same parent NH_4-**BEA** zeolite (Si/Al = 11.5) provided by Zeolyst (CP814E). The as-received NH_4-**BEA** zeolite was submitted to ion exchange using aqueous KNO_3 solutions with different concentration of the salt (0.1–1.1 M). The ion exchange was performed at 80 °C under stirring (200 RPM) for 2 h. Then the ion-exchanged samples were filtrated using a Buchner funnel. The first set of samples was thoroughly washed with a plenty of hot water to remove all extra potassium cations from the solids (IE series). These samples were designated as xK-**BEA** where x stands for molar concentration of KNO_3 in the aqueous solution used. The highest ion-exchanged level in **BEA** sample was obtained by three-times repeated ion-exchange procedure using 0.5 M aqueous KNO_3 solution. This sample was further designated as 3 × 0.5K-**BEA**. The second set of samples was not washed after filtration (IE + IMP series). The samples are designated as xK-N-**BEA**, where x stands for the molar concentration of KNO_3 in the aqueous solution used while N indicates that the samples were not washed after their filtration. All samples were then dried in ambient air overnight and calcined at T = 530 °C for 3 h.

2.2. Catalysts characterization

X-ray powder diffraction (XRD) patterns of the prepared calcined samples were recorded on a Philips MPD 1880 diffractometer working with the Cu Kα line ($\lambda = 0.154$ nm) in the 2θ range of 4°–40° at a scanning rate of 2θ of 2.4°/min. The relative crystallinity (%) of all materials was estimated from the line area of the experimental sample in the diffraction angle range of $2\theta = 22.5°$. In this case, H-**BEA** sample with the highest crystallinity was used as the reference.

The elemental composition was determined by X-ray fluorescence (XRF) using Philips PW 1401 equipped with an Rh RTG lamp. The UniQuant program was used to evaluate the results. BET areas and pore volumes were determined from nitrogen adsorption/desorption experiments performed at −196 °C using a Micromeritics ASAP 2020 after sample activation in vacuum at 300 °C for 12 h.

IR spectra of the prepared samples were recorded on Nicolet 6700 FTIR spectrometer equipped with a MCT detector. The concentrations of Brønsted and Lewis acid sites were calculated from the integral intensities of the individual bands characteristic for pyridine adsorbed on Brønsted acid sites (BAS, at 1545 cm^{-1}) and on Lewis acid sites (LAS, at 1455 cm^{-1}) using the molar extinction coefficients taken from [35]. Before the CO adsorption IR experiments, the self-supporting sample wafers were placed into a home-made IR cell and pre-treated in a dynamic vacuum (residual pressure $<10^{-4}$ mbar) overnight at 450 °C.

The calorimetric CO_2 adsorption experiments were carried out using an isothermal Tian-Calvet type microcalorimeter (BT 2.15, SETARAM) combined with a home-made volumetric/manometric device equipped with capacitance pressure gauges (Pfeiffer Vacuum). The dependence of the differential adsorption heat vs. adsorbed amount was obtained by numerical differentiation of the integral adsorption heat dependence on adsorbed amount data.

The amount of carbonaceous deposits in the catalysts after reaction and their type based on the degradation temperature was examined using a TA Instrument, TGA Discovery series equipment, operating at a heating ramp of 10 °C/min from room temperature to 800 °C in flowing air (20 mL/min).

Additional details on all characterization techniques used are provided in the Supplementary information.

2.3. Catalysis

Catalytic performance of the zeolite samples was investigated in aldol condensation of furfural (Sigma-Aldrich) and acetone (Lach-Ner, s.r.o., Czech Republic) pre-dried before the experiments with a molecular sieve. The catalytic experiments were carried out in a 300 mL Parr stirred autoclave at 100 °C. In a catalytic run, 2 g of freshly calcined (T = 530 °C) catalyst was mixed together with a stirred mixture of 39.5 g acetone and 6.5 g of furfural (acetone/furfural molar ratio 10/1). The desired temperature was achieved in ∼50–60 min after initiation of the heating, and the autoclave was then kept at T = 100 °C for additional 2 h. Analysis of the reaction products obtained after 2 h at the reaction temperature was performed using an Agilent 7890A GC equipped with a flame ionization detector and an HP-5 capillary column (30 m/0.32 ID/0.25 μm). The products were identified based on the standard reference compounds as well as additional GC–MS analyses.

Catalytic results of aldol condensation of furfural and acetone were described by conversion and selectivity parameters that were calculated as follows:

reactant conversion (t) (mol%) = 100 × (reactant$_{t=0}$ − reactantt) /reactant$_{t=0}$;

selectivity to product i = 100 × (mole of reactant converted to product i)/(total number of mole of reactant converted).

Carbon balance was monitored in all experiments as the total number of carbon atoms detected in each organic compound with C$_n$ atoms (where n = 3, 5, 8 ., etc.) divided by the initial number of carbon atoms in F + Ac feed:

$$\text{Cbalance\%} = (3\text{molC}_3 + 5\text{molC}_5 + \ldots \text{nmolC}_n)/(3\text{molC}_{3(t=0)} + 5\text{molC}_{5(t=0)}).$$

3. Results and discussion

3.1. XRD

The XRD powder diffraction patterns of all prepared catalyst samples calcined at T = 530 °C (see the Suppl. Info. (SI),) correspond to that of BEA zeolite [36]. The XRD patterns also evidence that no other crystalline phases present in the catalysts including no XRD-visible potassium clusters (K_2O or KNO_3). Among all catalyst samples, H-BEA possesses the highest intensity of the characteristic reflections corresponding to the BEA structure. The relative crystallinity of the calcined 0.5K-BEA and 3 × 0.5K-BEA samples is slightly lower (95–96%) due to the incorporated potassium. It means that the presence of K^+ ions in the cationic sites does not result in destruction of BEA framework during the ion-exchange process. In contrast, the calcination of samples prepared by the IE + IMP method affects their crystallinity more significantly: the relative crystallinity continuously decreases from 84% for 0.3K-N-BEA to 40% for 1.1K-N-BEA (Table 1). A decrease in the diffraction intensities of the impregnated zeolites is usually attributed either to the presence of the high content of non-framework species inside zeolite pores due to the high mass transfer coefficient of X-ray absorption by metal atoms or to a partial destruction of zeolite framework (amorphization) during calcination [29,32,37].

3.2. Chemical analysis

Chemical composition of the samples prepared by IE (Table 1) shows that the growth in KNO_3 concentration from 0.1 to 0.5 M results in an increase of K/Al ratio from 0.57 to 0.8. Nevertheless, even several successive exchange steps with intermediate filtration and washing of the zeolite powder with an excess of hot water do not afford a further increase in the potassium content in the resulting samples. It seems that the number of cationic positions in BEA zeolite that can be exchanged with alkali cations is limited.

As expected, ion-exchange combined with impregnation allows obtaining higher potassium content in the samples. For 0.1 M KNO_3 solution the difference between the two preparation methods, IE and IE + IMP, is low: K/Al ratio in 0.1K-BEA and 0.1K-N-BEA is 0.57 and 0.66, correspondingly (Table 1). However, the difference is more obvious for 0.3 M KNO_3 solution, giving K/Al = 1.07 in 0.3K-N-BEA (as compared to K/Al of 0.72 obtained by the IE method). A further increase in the concentration of KNO_3 solution results in a subsequent growth of the potassium content in the samples prepared by the IE + IMP method, K/Al ratio reaching values as high as 2.5 for 1.1K-N-BEA sample. K/Al ratio above 1 is an indication that the impregnation of BEA zeolite with KNO_3 results in a high content of extra-framework potassium species present inside the internal pore system of the zeolite as well as on its outer surface.

3.3. Nitrogen adsorption

Textural properties of the prepared samples were determined by N_2 physisorption and the results are presented in Table 1.

Irrespective of the concentration of KNO_3 solution and the number of consecutive ion-exchange steps, the ion-exchange of the parent BEA zeolite does not affect the porosity of the prepared samples: micropore volumes in the range of 0.166–0.170 cm^3/g are observed for all potassium-ion-exchanged catalysts. Nevertheless, the BET areas of these samples decrease from 608 m^2/g to 558–564 m^2/g. On the contrary, the IE + IMP method has a more substantial effect on the textural properties of the catalysts: for 1.1K-N-BEA the micropore volume and BET area decrease to 0.049 cm^3/g and 219 m^2/g, respectively, i.e. by more than 60%. The content of the crystalline phase based on the micropore volume of the samples is in good agreement with the XRD study (Table 1). In summary, XRD and N_2 physisorption data show that the IE + IMP preparation method leads to partial blocking of the zeolite pore system with extra-framework species and/or to partial destruction of the crystalline framework of BEA zeolite.

3.4. FTIR study of the changes upon calcination

The changes in FTIR spectra for the as-prepared 0.3K-N-**BEA** and 1.1K-N-**BEA** catalysts during their heating from room temperature to T = 400 °C are shown in Fig. 1. As the temperature increases from 25 to 400 °C, the bands with maximum at ≈3430 cm^{-1} and 1632 cm^{-1} corresponding to the stretching and bending water vibrations, respectively, lose their intensities. The intensity of the bands with maxima at 1398 and 1368 cm^{-1} (doublet; the bands are detected in all impregnated samples, with 1.1K-N-**BEA** having the highest intensity) decreases as well. According to [38,39], these bands can be attributed to bulk KNO_3 present inside the pore system of BEA zeolite. The observed change in the spectra proves that KNO_3 is gradually decomposed as the activation temperature increases but a certain amount of KNO_3 remains in 1.1K-N-**BEA** even after ca. 10 h of heating at 400 °C. As a result of this decomposition, K_2O species are apparently formed. Taking into account the data on textural properties of the prepared catalysts (Table 1) it can be concluded that both undecomposed KNO_3 precursor and the formed K_2O clusters block zeolite pores resulting in a lower adsorption capacity of the samples prepared by IE + IMP in comparison with the samples prepared by IE.

Table 1
Crystallinity, chemical composition and sorption properties of prepared samples.

Sample	Crystallinity (XRD), %	K:Al:Si atomic ratio	Micropore volume, cm^3/g	BET area, m^2/g	Crystallinity (N_2 sorption), %
H-**BEA**	100	0:1:13.0	0.17	608	100
0.1K-**BEA**	–	0.57:1:12.8	–	–	–
0.3K-**BEA**	–	0.72:1:13.0	–	–	–
0.5K-**BEA**	95	0.8:1:12.9	0.166	558	98
3x 0.5K-**BEA**	96	0.85:1:13.0	0.169	564	100
0.1K-N-**BEA**	–	0.66:1:12.8	–	–	–
0.3K-N-**BEA**	84	1.07:1:12.9	0.154	514	91
0.5K-N-**BEA**	67	1.2:1:12.9	0.133	438	78
0.7K-N-**BEA**	56	1.87:1:12.9	–	–	–
0.9K-N-**BEA**	48	2.23:1:14.7	–	–	–
1.1K-N-**BEA**	40	2.5:1:14.5	0.049	219	29

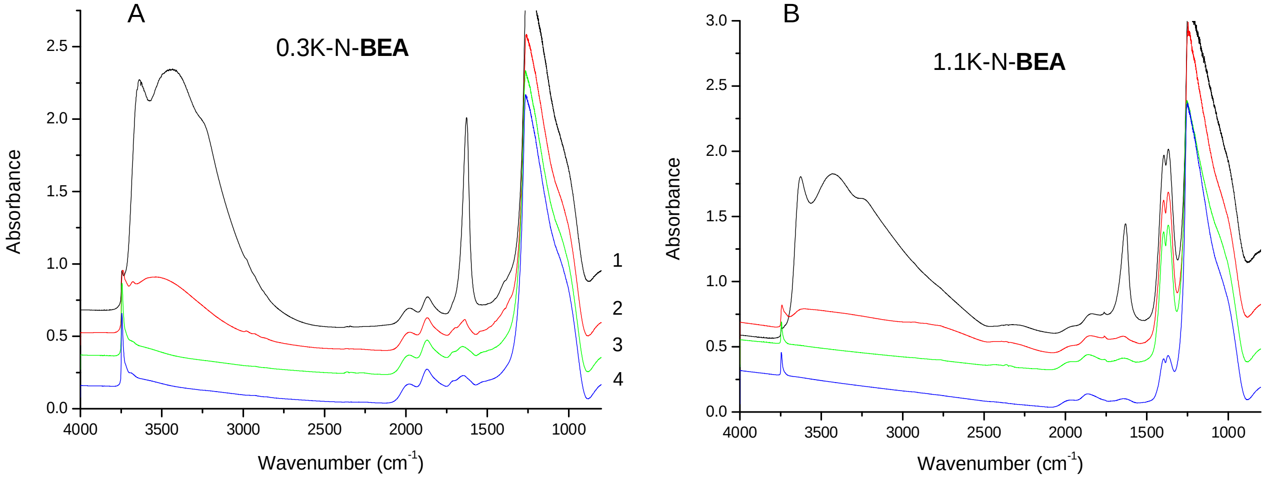

Fig. 1. FTIR spectra of samples calcined in dynamic vacuum in temperature range of 25–400 °C. 1–samples at T = 25 °C; 2–dehydration at T = 100 °C for 5 min; 3–dehydration at 400 °C for 25 min; 4–dehydration at T = 400 °C for 10 h.

3.5. The study of prepared samples by FTIR of adsorbed pyridine

IR spectrum of the parent H-BEA (see the *SI*) shows four clearly distinguishable OH bands at 3780, 3743, 3670 and 3610 cm^{-1}. In accordance with previous studies, the band at 3780 cm^{-1} is unequivocally attributed to hydroxyl groups related to tri-coordinated extra-framework Al species and the band at 3742 cm^{-1} is attributed to isolated silanols [33,40,41]. As pointed out in [33], all these species result from the presence of defects in the zeolite framework due to the small size of the zeolite crystallites of the parent H-BEA resulting in a large number of the external surface terminations. The band at 3610 cm^{-1} belongs to (Si—OH—Al) bridged species bearing a Brønsted acid proton. Finally, the band at 3670 cm^{-1} is due to hydroxyl groups bonded to extra-framework (or partially extra-framework) aluminum species [40,42,43]. It is accepted that the latter hydroxyls are much more acidic in comparison with silanols or OH– species observed on γ-Al_2O_3, but weaker than Brønsted bridged hydroxyl acid sites [40,44,45]. Besides, broad absorption band in the region of 3600–3000 cm^{-1} characteristic for hydrogen-bonded silanols [46] is observed in the spectrum.

After pyridine adsorption on H-BEA followed by its desorption at 150°C (removal of physisorbed pyridine) the bands at 3610 cm^{-1} and 3670 cm^{-1} totally disappear (see the *SI*) proving their acidic character. On the contrary, the band at 3745 cm^{-1} is, as expected, visually unchanged due to the lack of interaction between pyridine molecules and silanol groups. Interestingly, the band at 3780 cm^{-1} almost disappears after pyridine adsorption, but its remnants are still visible after pyridine desorption at 250 °C and higher. This indicates that most, but not all extra-framework Al species, interact with pyridine molecules and that the residual species either do not possess sufficient acidity to retain pyridine or they are inaccessible for pyridine molecules. Indeed, whether such hydroxyl groups in zeolites have any significant Lewis acidity is still a matter of discussion [40,41,46].

The decrease in the intensity of bands at 3610, 3670 and 3780 cm^{-1} after pyridine adsorption is accompanied by the appearance of bands at 1545 cm^{-1} and 1455 cm^{-1}, which are ascribed to the interaction of pyridine with strong Brønsted and Lewis acid centers, respectively (see the *SI*). The concentrations of Brønsted and Lewis acid sites (BAS and LAS, respectively) in the prepared samples are presented in Table 2. The concentrations of BAS and LAS in the parent acidic BEA zeolite are 0.138 and 0.255 mmol/g, respectively. The increase in the temperature of pyridine desorption from 150 to 450 °C results in a consistent and substantial decrease in the intensity of band at 1545 cm^{-1}. Simultaneously, the bands at 3610 cm^{-1} and 3670 cm^{-1} reappear in the spectra. The apparent dependence of the intensity of the band at 1545 cm^{-1} (BAS) on the desorption temperature (see the *SI*) suggests a significant difference in the strength of BAS in H-BEA zeolite (Table 2). In contrast, the intensity of band at 1455 cm^{-1} (LAS) varies to a lesser degree with the increasing desorption temperature indicating more homogeneous nature of LAS from their strength point of view. Almost half of all LAS in H-BEA are strong enough to bound pyridine even at 450 °C.

After ion-exchange of the parent BEA zeolite with 0.1 M KNO_3 solution, the FTIR spectrum of 0.1K-BEA sample shows the absence of the band at 3610 cm^{-1} (see the *SI*) proving that all bridged protons are easily exchanged with potassium cations. The inten-

Table 2
Concentration of Brønsted and Lewis acid sites in potassium-containing **BEA** zeolites determined by FTIR of adsorbed pyridine after its desorption at different temperatures.

Sample	$T_{des.}$, °C	$C_{BAS,}$ mmol/g	$C_{LAS,}$ mmol/g
H-BEA	150	0.138	0.255
	250	0.112	0.170
	350	0.060	0.144
	450	0.020	0.118
0.1K-BEA	150	0.020	0.180
	250	0.019	0.127
	350	–	0.068
	450	–	0.032
0.5K-BEA	150	–	0.117
	250	–	0.050
	350	–	0.034
	450	–	0.018
0.5K-N-BEA	150	–	–

sity of the band at 3670 cm^{-1} slightly increases, possibly due to partial hydrolysis of Si—O—Al bonds giving rise to the number of hydroxyls bonded with partially framework Al atoms (defective sites). Simultaneously, the band at 3780 cm^{-1} which characterizes hydroxyl groups related to tri-coordinated extra-framework Al species totally disappears. Bisio et al. [33] suggested that this could be explained by leaching of the related tri-coordinated extra-framework Al species in the exchange solution. Nevertheless, another explanation for the absence of the band at 3780 cm^{-1} in 0.1K-BEA sample may exist: ion-exchange of acidic protons in the bridged (Si-O-Al) species by potassium cations could prevent the transition of the tetrahedral framework Al atoms to extra-framework positions during the calcination process thus decreasing the intensity of band at 3780 cm^{-1}. The band at 1455 cm^{-1} is still present in the spectrum after pyridine adsorption, but having lower intensity (see the *SI*) suggesting that at least part of the extra-framework (or partially extra-framework) Al atoms characterized by the band at 3670 cm^{-1} could interact with pyridine as LAS. As a consequence, the LAS concentration decreases from 0.255 to 0.180 mmol/g due to the ion-exchange (Table 2). Simultaneously, a new band at 1445 cm^{-1} appears in the spectra after IE. The band at 1445 cm^{-1} was previously observed in the FTIR spectrum of ammonia adsorbed on ion-exchanged Cs-BEA sample and was attributed to NH_3 interaction with new LAS, namely Cs^+ cations whose acidity was significantly lower compared with tri-coordinated aluminum species [33]. This band could be attributed to the interaction of pyridine with potassium cations in 0.1K-BEA.

Despite the absence of the band at 3610 cm^{-1} in FTIR spectrum of 0.1K-BEA, the band at 1545 cm^{-1} which is characteristic of pyridinium cation is still present for this sample (see the *SI*). It indicates the existence of BAS in 0.1K-BEA sample although in a very low concentration of 0.020 mmol/g (Table 2). To explain this, it is necessary to consider the behavior of the band at 3670 cm^{-1} before and after pyridine adsorption. After pyridine adsorption the band at 3670 cm^{-1} completely disappears (see the *SI*), while the band at 1545 cm^{-1} appears. Further, the increase in the desorption temperature results in the decrease in the intensity of band at 1545 cm^{-1} and the re-appearance of band at 3670 cm^{-1}. Such a comparison allows concluding unambiguously that hydroxyl groups related to the partially extra-framework Al atoms behave as BAS being able to interact with pyridine and form pyridinium ions.

The increase in the concentrations of the ion-exchange KNO_3 solution and the increase in the number of consecutive steps of the ion exchange results in a further change in the FTIR spectra of 0.5K-BEA both before and after pyridine adsorption. The very weak band at 1545 cm^{-1} (BAS) is still present in the FTIR spectrum after pyridine adsorption (see the *SI*) indicating the possible presence of residual BAS in 0.5K-BEA sample, but it is close to the detection limit. However, a significant difference is observed for the ratio between the intensities of bands at 1455 (LAS) and 1445 cm^{-1}. It is seen that the depth of ion-exchange influences the amount of extra-framework Al species in the sample (which are LAS) after calcination procedure, hence the decreased intensity of band at 1455 cm^{-1}, and the high amount of pyridine molecules adsorbed on potassium cations (1445 cm^{-1}). The increase in the intensity of the 1445 cm^{-1} band is in line with the increased concentration of K^+ in ion-exchanged samples, while the decrease in the intensity of the 1455 cm^{-1} band supports the suggested limited formation of LAS during calcination due to the presence of potassium.

The band at 3670 cm^{-1} is absent in the FTIR spectrum of 0.5K-N-BEA sample prepared by IE + IMP (see the *SI*). As a consequence, no BAS are determined in this sample after pyridine adsorption as evidenced by the absence of the band at 1545 cm^{-1}. Moreover, the band at 1455 cm^{-1} is not present in the FTIR spectrum either, which indicates total absence of LAS in 0.5K-N-BEA. At the same time, the intensity of the band at 3745 cm^{-1} has decreased (see the *SI*). A similar result was observed in Ref. [33] when studying properties of Cs-overloaded BEA sample. In that work the reduced intensity of the band at 3745 cm^{-1} was explained by an acid-base reaction between silanols and the occluded metal oxidic particles formed during calcination. In our case the change in intensity of this band is observed simultaneously with a decrease in crystallinity of the sample and its BET area. The decreased intensity of the band at 3745 cm^{-1} may be also explained by a partial destruction of BEA crystal structure during the calcination of impregnated samples, resulting in the condensation of silanol groups and the formation of dense amorphous silica [33].

The absence of the band at 3670 cm^{-1} in the FTIR spectrum of the impregnated sample could have two possible explanations. First, as pointed out in [33], under dehydrated conditions at increased temperatures partially extra-framework Al species can act as “normal” framework tetrahedral Al with charge-compensating proton, which in turn is able to be ion-exchanged with salts of basic metals. However, it can be assumed that in the course of the destruction of BEA structure partially extra-framework Al atoms can be converted into totally extra-framework Al atoms followed by their transformation to amorphous silica (aluminosilica) phase. Hence, OH-groups in 0.5K-N-BEA sample are exclusively represented by silanol groups, which are characterized by the band at 3745 cm^{-1} (see the *SI*). The band at 1445 cm^{-1} which is characteristic for pyridine adsorbed on potassium cationic sites has high intensity, which is in accordance with the high exchange level of potassium in this sample. Additionally, all other samples prepared by the IE + IMP method produce similar FTIR spectra (not shown) and, like 0.5K-N-BEA, do not possess any acidity except for that connected with K^+ cations and characterized by the band at 1445 cm^{-1}.

3.6. *FTIR study of adsorbed CO*

Interaction of CO with K-BEA zeolites can bring information about potassium cations in ion-exchangeable sites of BEA zeolite. FTIR spectra of carbon monoxide adsorbed on 0.5K-BEA zeolite at liquid nitrogen temperature are shown in Fig. 2(A). Three main absorption bands are discernible in the spectra at 2168, 2149 and about 2120 cm^{-1}. According to [47], the band at 2168 cm^{-1} is ascribed to C—O stretching frequency of CO adsorbed on isolated single K^+ cation, the band at 2120 cm^{-1} corresponds to isocarbonyl species on isolated sites and the band at 2149 cm^{-1} is assigned to CO molecule interacting with two nearby K^+ cations in so-called dual cationic sites forming bridged complexes. The band at 2168 cm^{-1} is slightly red-shifted to frequency 2161 cm^{-1} when coverage increases as a consequence of dicarbonyl species formation, as it was explained in ref. [47]. Other ion-exchanged samples have a similar character of FTIR bands, indicating similar population

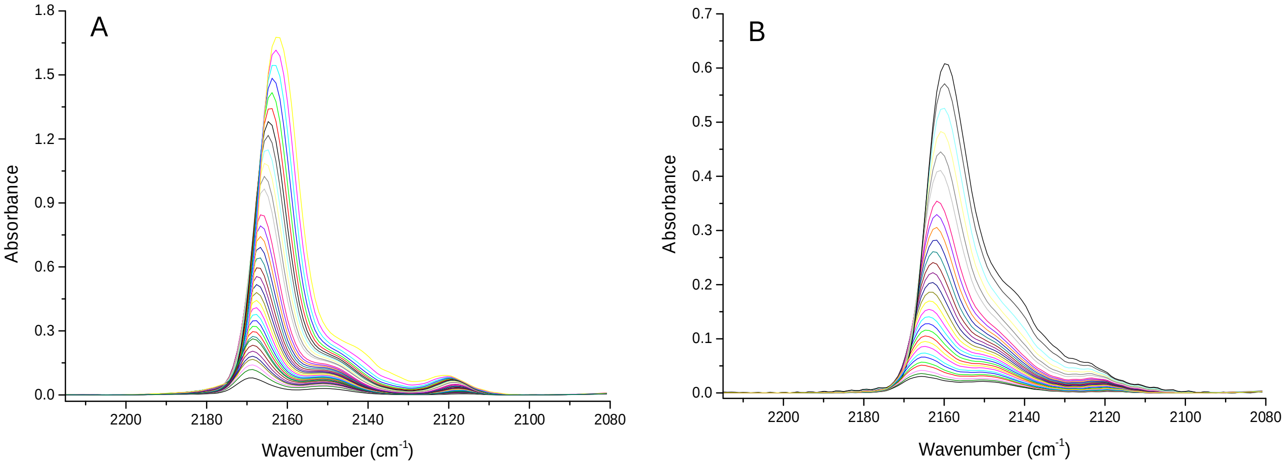

Fig. 2. FTIR spectra of adsorbed CO recorded at liquid nitrogen temperature on 0.5K-**BEA** (A) and 0.5K-N-**BEA** (B).

of exchanged K^+ cation in all ion exchanged catalysts, and intensities of IR spectra corresponding to the potassium concentration obtained by chemical analysis of these samples.

On the contrary, 0.5K-N-BEA exhibits a significantly lower intensity of the IR bands (Fig. 2(B)) compared to 0.5K-BEA zeolite. As complete ion-exchange degree in this sample is confirmed by FTIR of OH-groups (see the *SI*), the IR spectra intensities correspond to neither the total potassium content nor number of exchangeable sites. It can be due to two reasons. Firstly, reducing availability of K^+ cations for interaction with CO is due to zeolite channels to be blocked by a bulk phase, presumably K_2O. This explanation is supported by N_2 physisorption data, as both BET and micropore volume are lower for 0.5K-N-BEA sample in comparison with the parent material. Secondly, taking into account the XRD results, the decreased amount of adsorbed CO can be explained by a decrease in the content of the zeolite phase in the sample, i.e. a partial collapse of the crystalline BEA framework. This explanation can also be supported by data on nitrogen adsorption. Both the blocking and the partial destruction of the zeolite lattice influence the internal channel system and, as a consequence, reduce both micropore volume and the number of accessible Al-O-Si bonds, i.e. decrease the potentially available cationic exchange sites.

Besides the bands at 2168, 2149 and 2120 cm^{-1}, the spectra of adsorbed CO for 0.5K-BEA and 0.5K-N-BEA samples do not contain any additional bands. As 0.5 K-N-BEA sample is likely to contain K_2O oxidic species, it is possible to suggest that CO is not interacting with them. This is in complete agreement with the results of the study of Cs-overloaded BEA samples [33], which showed that no signal specific for CO adsorbed on Cs_2O exists.

3.7. Microcalorimetry and FTIR experiments with adsorbed CO_2

The basic character of potassium-modified **BEA** zeolites was probed by CO_2 adsorption microcalorimetry. The adsorption isotherms of CO_2 on **BEA** samples at T = 34 °C and corresponding calorimetric curves are depicted in Fig. 3. The adsorption isotherm of CO_2 on H-**BEA** is the lowest among all samples investigated and almost linear evidencing very weak interaction of adsorbed molecules with the zeolite. The initial adsorption heat (at very small coverage of adsorbed CO_2 of 0.01 mmol/g) is ≈ 35 kJ/mol and it gradually decreases to plateau at 28 kJ/mol extending from 0.02 to 0.075 mmol/g of adsorbed CO_2. This part of calorimetric curve can be associated with CO_2 adsorption on Al sites (structural defects) followed by adsorption on BAS. The range of adsorption heats corresponds well with heat of CO_2 adsorption on Brønsted sites in **BEA** zeolite determined by VTIR spectroscopy [48]. Further increase in the adsorbed amount results in a drop to about 25 kJ/mol followed by a very pronounced plateau up to 0.4 mmol/g – it indicates CO_2 interaction with zeolite framework by dispersive interaction [49]. The value of dispersion interaction of CO_2 with **BEA** seems to be reasonable; the adsorption heat of CO_2 on silicalite reported in literature is about 27 kJ/mol [50] which is slightly higher (by about 2 kJ/mol) in line with the fact that **MFI** framework is characterized by higher framework density (smaller channel size).

Nearly completely ion-exchanged 3 × 0.5K-**BEA** and 0.3K-N-**BEA** prepared by IE and IE + IMP, respectively, have very similar calorimetric curves and adsorption isotherms (Fig. 3). Practically coincident adsorption isotherms of both samples are in a very good agreement with their similarity in potassium content, crystallinity and pore volume. It also indicates very similar strength of CO_2 interaction. The initial heat of adsorption is around 55 kJ/mol and it gradually decreases to about 40 kJ/mol (at CO_2 adsorbed amount approx. 0.07 mmol/g) followed by a plateau up to the adsorbed amount of 0.27 mmol/g. Then, the adsorption heat decreases only very slowly to approximately 32 kJ/mol at the highest adsorbed amount (0.8 mmol/g). The initial value of 55 kJ/mol correlates well with data on K-**FER** and K-**MFI** [49,51–53] and can be assigned to the formation of bridged K-CO_2-K complexes (similar to CO vibration band at 2149 cm^{-1} which characterizes such dual cationic sites [47]). The adsorption heat in the range between 55 and 40 kJ/mol corresponds to the adsorption of CO_2 on K^+ ions in different local environments and the subsequent formation of geminal complexes results in further lowering the adsorption heat [54]. Calorimetric heats bring evidence on negligible amounts of strong basic centers in both samples.

Completely different is the situation in the 0.5K-N-**BEA** sample. The behavior of the curve for 0.5K-N-**BEA** is also very similar to the ion-exchanged samples but only at adsorbed amount higher than 0.08 mmol/g. Below this value, a very strong interaction between CO_2 and the sample is observed: the initial value is as high as 116 kJ/mol due to chemisorption reaction of CO_2 with strongly basic centers, possibly K_2O species, creating surface carbonates. The presence of very strong basic sites is also accompanied by a slightly lower adsorption CO_2 capacity for sample 0.5K-N-**BEA**: at 210 mbar CO_2 the adsorption capacity is 0.9 mmol/g in comparison with 1.05 mmol/g for ion-exchanged samples. This is in line with the decrease in pore volume and crystallinity of the sample (see Table 1).

The behavior of the curve for 1.1K-N-**BEA** is quite different from the other samples. It also exhibits initial strong CO_2 chemisorption similar to 0.5K-N-**BEA**, but the heat decreases faster than that for 0.5K-N-**BEA** and reaches values around 45 kJ/mol at CO_2

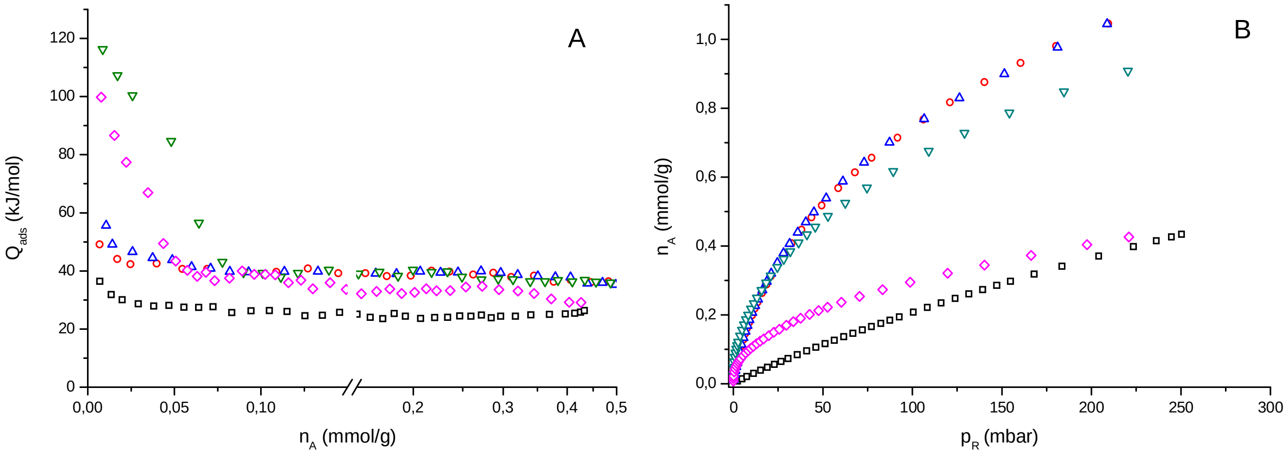

Fig. 3. Adsorption heat (A) and adsorption isotherms (B) for K-**BEA** samples in dependence on the amount of adsorbed CO_2. H-**BEA** (square), 3 × 0.5K-**BEA** (circle), 0.3K-N-**BEA** (up triangle), 0.5K-N-**BEA** (down triangle), 1.1K-N-**BEA** (diamond).

adsorbed amount 0.05 mmol/g. It means that the amount of accessible strongly basic sites is lower compared with 0.5K-N-**BEA** sample. After saturation of strong basic sites, the interaction of CO_2 with the sample is characterized by adsorption heats between 40 and 30 kJ/mol. It is similar as in the case of other, previously discussed, samples except the fact that the calorimetric curve is compressed into a narrower interval as a result of the limited adsorption capacity of this sample for CO_2: only 0.42 mmol/g of CO_2 is adsorbed at 210 mbar of CO_2, *i.e.* only 40% of the capacity of the ion-exchanged samples. The reasons for such a low capacity are obviously either the blocking of pores by K_2O or nitrate clusters, the partial collapse of **BEA** crystalline structure or inaccessibility of K^+ ions.

3.8. Catalysis

According to the general scheme of aldol condensation of furfural with acetone (see the *SI*), the intermediate compound, C8 aldol (FAc—OH) is formed as a primary condensation product. It is subsequently dehydrated into the first condensation C8 product (FAc). It successively reacts with another furfural molecule and the second condensation C13 product (F_2Ac) is formed, which is also a dehydrated product. Additionally, the formation of a heavier reaction product ($(FAc)_2$) may be observed as a result of dimerization of the olefinic FAc molecule on acid sites of zeolites [18,23]. Acetone conversion by self-condensation with the formation of diacetone alcohol, mesityl oxide, etc., was very low (below 1%) what allowed us excluding these results from a consideration.

Fig. 4 depicts furfural conversion and selectivity to the products of aldol condensation observed over H-**BEA** and potassium-containing samples prepared by ion-exchange followed by subsequent thorough washing of the prepared catalysts. The final furfural conversion (after 2 h) is 33% for H-**BEA** at T = 100 °C and it steadily decreases with the increasing potassium content in the catalysts. As a result, the furfural conversion drops down to ca. 5% at K/Al ≥ 0.7-0.8 (Fig. 4(A)). The declining furfural conversion is accompanied by a change in the product distribution (Fig. 4(B)). The composition of the observed reaction products on H-**BEA** similar to that reported for similar catalyst in our previous studies [18,23]: selectivities to FAc, F_2Ac and $(FAc)_2$ are 70, 3 and 25%, respectively. The growth in K/Al ratio results in a decrease in the selectivity to F_2Ac and $(FAc)_2$, whereas the selectivity towards FAc-OH and FAc increases. For 0.1K-BEA with low exchange level selectivity to FAc increases to 90%, and selectivity to $(FAc)_2$ dimer decreases to 3%. Reaction products over 0.5K-BEA consist exclusively of FAc and FAc-OH with a selectivity of 80% and 20%, respectively. As the micropore volumes and BET areas of these catalysts are almost the same as those of the parent H-**BEA** zeolite (Table 1), the decrease in the selectivity to F_2Ac and $(FAc)_2$ cannot be related with the change in textural properties of the 0.1K-**BEA** and 0.5K-**BEA**. However, it can be associated with the change in their acido-basic properties.

According to FTIR spectra for 0.1K-**BEA** and 0.5K-**BEA**, the samples with K/Al ratio above 0.5-0.6 do not contain strong bridged BAS characterized by the band at 3610 cm^{-1} (Table 2). Therefore, the observed Brønsted acidity in these samples (band at 1545 cm^{-1} after pyridine adsorption) is attributed to the presence of OH-groups attached to extra-framework or partially hydrolyzed framework Al atoms [42], which are characterized by the band at 3670 cm^{-1} in the FTIR spectrum (Fig. 2). The latter sites are able to interact with pyridine forming a protonated adduct; however, their amount is too low and their strength is decreased as proved by the low temperature of pyridine desorption (Table 2). The observed decrease in the furfural conversion and the change in the product composition over the ion-exchanged samples can be attributed to the reduced acidity of the catalysts. The absence of C8 aldol and the decreased selectivity to dimer $(FAc)_2$ observed for 0.1K-**BEA** (Fig. 4(B)) suggest that residual strong Brønsted acid sites are still present in the ion-exchanged samples with a low exchange degree. Nevertheless, the appearance of C8 aldol and the absence of $(FAc)_2$ in the reaction products for 0.3K-**BEA** and 0.5K-**BEA** is in line with the lack of Brønsted acidity in these catalysts proved by FTIR of adsorbed pyridine (Table 2). Fig. 4B also shows decreasing selectivity to FAc and increasing selectivity to FAc-OH for 3 × 0.5K-**BEA**, which reflects the further decrease in the amount and strength of residual acid sites after the consecutive ion exchange steps. The growth of exchange degree in K-**BEA** zeolites reduces their acidity, while their basicity (that is the basicity of the oxygens of cation-exchanged zeolites [26–28]), accordingly, increases. Nevertheless, the catalytic results obtained over ion-exchanged K-**BEA** samples prove that zeolites only with the intrinsic basicity possess poor activity in aldol condensation of furfural and acetone.

Similar to the ion-exchanged samples, furfural conversion over parent catalyst and those prepared by IE + IMP decreases in the order: H-**BEA** > 0.1K-N-**BEA** > 0.3K-N-**BEA** (Fig. 4(C)). Chemical analysis (Table 1) shows that this trend is observed as the K/Al ratio approaches unity. This result also confirms that zeolites with intrinsic basicity (*i.e.* with no extra-framework species acting as bases) possess poor catalytic activity in aldol condensation. With increasing potassium content (K/Al > 1), the activity of the samples in aldol condensation begins to rise and becomes even higher than that of the parent H-**BEA** zeolite (Fig. 4(C)). However, these samples contain no Brønsted acidic centers, but only silanol OH

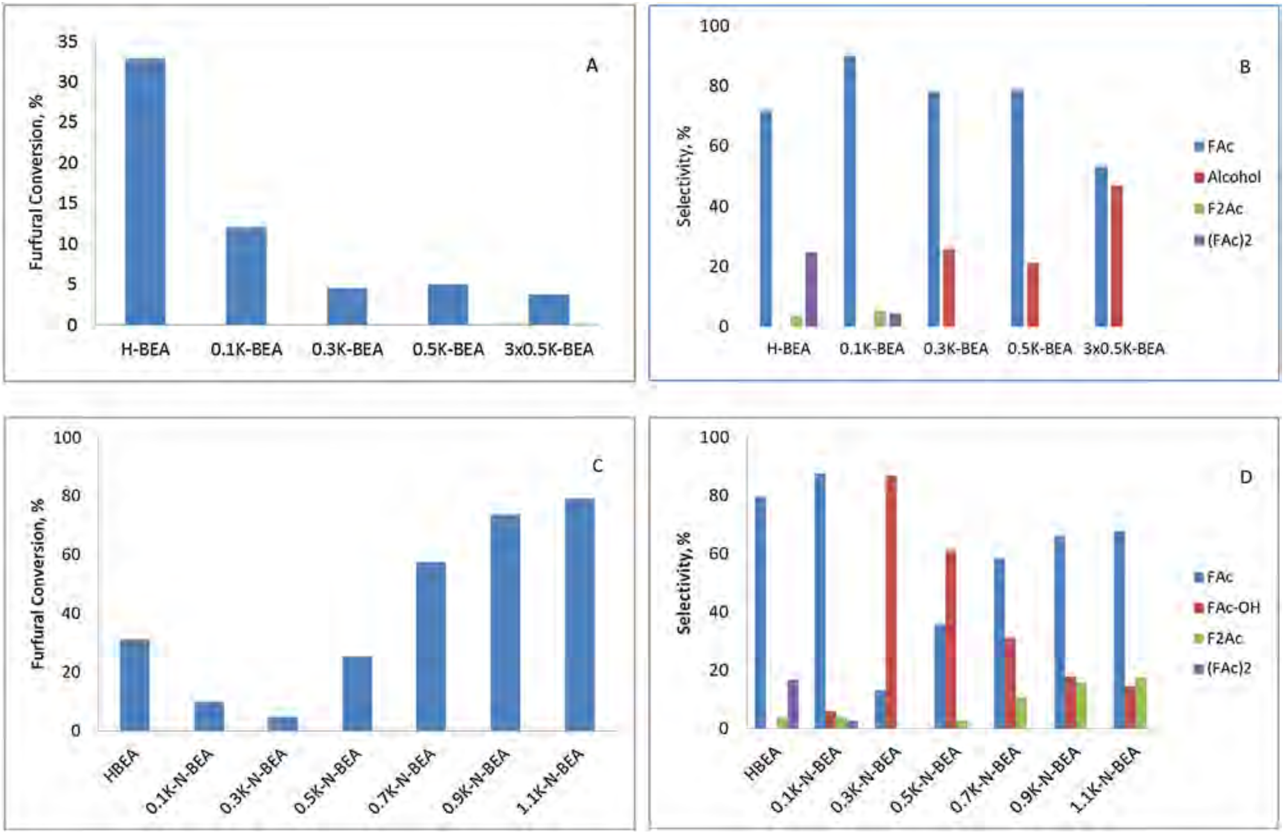

Fig. 4. Catalytic properties of K-BEA samples prepared by IE (A, B) or IE + IMP (C, D) methods. A, C – Furfural conversion; B, D – Products selectivity. T = 100 °C, time – 2 h.

groups as evidenced by FTIR data. By combining the results of the chemical analysis, FTIR and microcalorimetry, the presence of strong basic sites, plausibly K_2O clusters, can be expected. Hence, the observed activity of the samples prepared by IE + IMP can be explained by the presence of basic rather than acidic sites. Indeed, the results of calorimetry suggest that 0.5K-N-**BEA** and 1.1K-N-**BEA** samples contain very strong basic sites (Fig. 3), which could be responsible for the increased activity of the IE + IMP catalysts in the reaction. Nevertheless, the amount of the strongest basic sites determined by CO_2 microcalorimetry in 1.1K-N-**BEA** is lower than in 0.5K-N-**BEA** (the ratio of strong basic sites with adsorption heat higher than 45 kJ/mol is 0.05:0.077 mmol/g, respectively), but the furfural conversion on the former catalyst is much higher. This discrepancy can be attributed to a difference in the textural properties of these two samples. Most of the potassium species in 0.5K-N-**BEA** with a well-developed micropore volume and BET may be located in the internal pore space. These species can be successively probed by CO_2 with small molecular size, but they are inaccessible for organic reagents. In contrast, 1.1K-N-**BEA** possesses significantly worse textural properties due to either pore blockage with extra-framework species or the partial collapse of crystalline framework. In both cases the growth of potassium content in this sample increases the amount of K_2O clusters located principally on the external surface without any sterical limitations thus increasing the activity of high-potassium catalysts in aldol condensation.

From the selectivity point of view observed for the IE + IMP samples, the main change is in the absence of the dimer $(FAc)_2$ for catalysts with K/Al > 1 (Fig. 4(D)). This clearly indicates that when the K/Al ratio exceeds unity, there are no acid sites left able to catalyze the dimerization of the FAc product. The dimerization is the first step "*en route*" to the formation of condensation products that cause catalyst deactivation by blocking access to the active sites [18,23]. The absence of acid sites is thus further reflected by the decreased formation of heavier condensation products causing the catalyst deactivation as discussed below. At the same time, the selectivity towards FAc-OH shows a peculiar trend with a maximum around K/Al = 1. This behavior can be explained by dehydration of the alcohol either by acid sites (hence its low production or even absence in case of K/Al < 0.8) or by strong basic sites (hence its low production in case of K/Al ≥ 1.9). The "intrinsic" basic sites are apparently not strong enough to catalyze dehydration at the applied reaction temperature and hence the alcohol is the main reaction product observed for 0.3K-N-**BEA** and 0.5K-N-**BEA**. With the growth of potassium content in catalysts, the selectivity to alcohol decreases and selectivity to dehydrated compounds, FAc and F_2Ac, accordingly increases demonstrating a good correlation with furfural conversion. This allows suggesting the kinetically dependent character of the reaction which mainly proceeds on the external surface of catalysts with K/Al ≥ 1.

3.9. TGA study of the samples after reaction

Fig. 5 presents the results of thermal analysis of several potassium treated zeolites after catalytic experiments. The total weight loss varies in the range of 23–35% and does not exhibit a distinct dependence on the method of the samples preparation (Fig. 5A). Nevertheless, the type of the adsorbed species is apparently different in acidic H-**BEA** and basic K-**BEA** zeolites. The large and wide peak in the range of T = 500–750 °C observed on DTG curve for H-**BEA** (Fig. 5(B)) indicates the presence of highly condensed coke deposits formed by secondary transformation of the reaction products on acidic sites of the catalyst. For 0.3K-**BEA** and 3 × 0.5K-**BEA** samples, both prepared by IE, the position of peaks in the high-temperature region of DTG curve is shifted to 300–550 °C evidencing a change in the nature of the compounds being adsorbed in the samples with weaker acidity. The total amount of the adsorbed

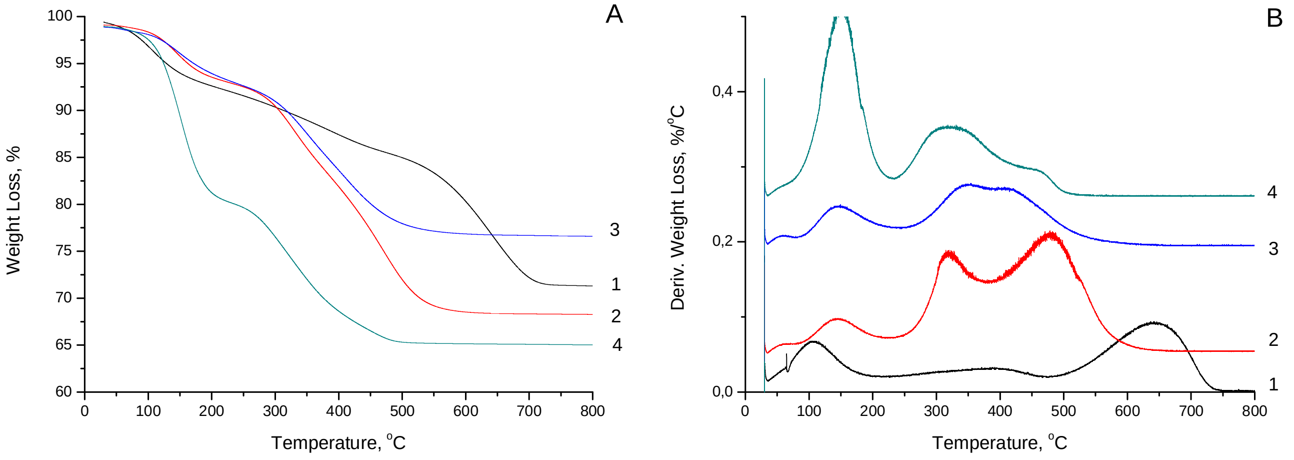

Fig. 5. TGA (A) and DTG (B) curves obtained for the samples under study. 1–H-**BEA**, 2–0.3K-**BEA**, 3–3 × 0.5K-**BEA**, 4–0.5K-N-**BEA**.

species in 0.5K-N-**BEA** prepared by IE + IMP is higher in comparison with the ion-exchanged samples as proved by TGA data (Fig. 5(A)). It correlates well with the increasing activity of 0.5K-N-**BEA** in aldol condensation, *i.e.* with the increase in the total amount of reaction products which are characterized by the presence of an intensive peak on DTG curve below T = 250 °C (Fig. 5(B)). Taken together, TGA results allow suggesting that basic sites of potassium treated **BEA** catalysts hardly contribute to the formation of heavy carbonaceous deposits (in contrast to acidic sites that promote a rapid deactivation by carbonaceous deposits [18,23]).

3.10. *Catalytic properties of K-**BEA** zeolites after regeneration and under storage*

In [18] it was shown that washing of H-BEA(25) with an excess of ethanol cannot restore its initial activity in aldol condensation, but the catalytic performance of H-BEA sample calcined in air at 530 °C is similar to that for fresh sample. The effect of the ethanol washing and the oxidative regeneration at 530 °C was also investigated for 0.5K-N-BEA. Table 3 presents catalytic data of this sample obtained after three consecutive cycles.

It is seen from Table 3 that, similar to experiments with H-BEA, washing of 0.5K-N-BEA with an excess of ethanol followed by drying at 80 °C for 1 h does not result in complete restoration of the initial activity of the catalyst in aldol condensation. The continuous decrease of furfural conversion observed in consecutive cycles of aldol condensation on basic zeolites allows assuming the formation of compounds during the reaction which cannot be removed by a simple treatment with a solvent. Nevertheless, the type of these adsorbed compounds differs from those observed on acidic H-BEA, as evidenced by TGA data (Fig. 5). Recently we have shown that furoic acid produced from furfural by Cannizzaro reaction may result in the progressive deactivation of the catalyst in aldol condensation thus decreasing its activity and making it difficult to recycle/reuse the catalyst without a regeneration step [55]. Indeed, furfuryl alcohol was identified among the reaction products formed during the reaction of furfural and acetone on basic BEA samples in the present study thus proving the occurrence of furfural conversion by Cannizzaro reaction on these catalysts. The results from Table 3 allow suggesting that furoate species formed due to the interaction of furoic acid produced by Cannizzaro reaction with strong basic sites of potassium-containing BEA zeolite are not removed by a simple washing with a solvent and are thus responsible for the successive loss of catalyst activity in consecutive catalytic runs.

Nevertheless, another effect responsible for the decreased activity of basic zeolites after reaction could be considered. The results in Table 3 show that in comparison with fresh sample the activity of the spent 0.5K-N-BEA sample regenerated in air at T = 530 °C decreases as well. It is also seen that increasing the number of regeneration cycles has virtually no influence on furfural conversion. Such behaviour of the catalyst could be explained by two reasons. First of all, the decrease in catalytic activity observed after the first regeneration cycle may be caused by leaching of potassium into reaction medium during the first reaction cycle. However, according to XRF measurements the K content in the catalyst after the reaction is the same as in the fresh one, so no leaching occurs during the reaction. Secondly, it may be also assumed that a high sensitivity to environment often observed for materials with expressed basic character could cause the decrease in the activity of potassium-containing zeolites. In this case, a decline in furfural conversion observed in the experiments with 0.5K-N-BEA washing between the consecutive catalytic runs could be concerned with the exposure of the catalyst to air during the drying stage. As a result, the decreasing activity of potassium-impregnated zeolites may be explained by both the blocking of basic sites with furoate species as the consequence of furfural conversion by Cannizzaro reaction and the high sensitivity of basic materials to environment during their treatment between consecutive runs.

The next example demonstrates that a contact between calcined potassium-impregnated BEA and air has a definite effect on the performance of the zeolite catalyst in aldol condensation. It is known that solid materials with basic properties such as hydrotalcites readily react with CO_2 and therefore it is difficult to avoid contamination from atmospheric CO_2 leading to carbonate anions [56]. As a consequence, rehydrated hydrotalcites can totally lose their activity in organic reactions after exposing to air [57]. The data in Table 4 show that the sample 0.7K-N-BEA also exhibits sensitivity to the environment. Aging of the calcined sample in air obviously reduces its activity in aldol condensation: the furfural conversion drops from 78 to 64% after 18 h and to 48% after 30 days of aging. The observed drop in activity causes a corresponding change in the composition of reaction products: the selectivity to the initial product of interaction between furfural and acetone, FAc-OH, increases, but the selectivity to the dehydrated product, FAc, and to the second condensation compound, F_2Ac, correspondingly, decreases. Assuming that the active sites in the potassium-containing zeolites prepared by IE + IMP are K_2O species, the decreased activity of the aged samples could be explained by the presence of catalytically inactive potassium carbonate formed by interaction of K_2O with CO_2 under storage. Since decomposition of potassium carbonate

Table 3
Catalytic performance of 0.5K-N-**BEA** in aldol condensation after three consecutive washing in ethanol (a) and regenerations at 530 °C (b). Reaction conditions: T = 100 °C, t = 2 h.

No. Exp.	Sample	Furfural Conversion, %	Selectivity, %		
			FAc	FAc-OH	F_2Ac
1	0.5K-N-**BEA** – freshly calcined at 530 °C	25.6	36.0	61.1	2.9
2a	1st washing in ethanol	19.6	31.4	65.9	2.7
3a	2nd washing in ethanol	16.1	28.5	69	2.5
4a	3rd washing in ethanol	11.8	24.1	74	1.9
2b	1st regeneration at 530 °C	17.1	28.2	69.4	2.4
3b	2nd regeneration at 530 °C	17.0	27.8	70.1	2.1
4b	3rd regeneration at 530 °C	18.6	33.1	64.6	2.3

Table 4
Catalytic properties of 0.7K-N-**BEA** sample calcined and aged for certain time in air. Reaction conditions: T = 100 °C, t = 2 h.

No. Exp.	Sample	Conversion, %	Selectivity, %		
			FAc	FAc-OH	F_2Ac
1	0.7K-N-**BEA**, freshly calcined	77.8	67.2	15.2	17.6
2	0.7K-N-**BEA**, calcined, aged for 18 h in air	64	60.1	25.9	14.1
3	0.7K-N-**BEA**, calcined, aged for one month in air	48.3	53.2	37.9	8.9

occurs at substantially higher temperature than zeolite regeneration takes place, the initial activity of the basic zeolite in aldol condensation cannot be totally restored in the following reaction cycles even after its calcination at T = 500–550 °C. Nevertheless, the moderate furfural conversion observed for potassium BEA zeolite even after its aging during one month proves that not all basic sites in the catalyst are sensitive to CO_2 and still able to catalyze aldol condensation. The determination of these "environmentally stable" basic sites in zeolites impregnated with potassium salts may be considered as a challenge for a forthcoming study.

4. Conclusions

The presented results show that the properties of potassium-containing BEA zeolites and their behavior as basic catalysts for aldol condensation of furfural and acetone depend to a great extent on the method of their preparation. Regular ion-exchange of parent NH_4-BEA zeolite with aqueous KNO_3 solution allows achieving potassium content in BEA samples up to K/Al = 0.8–0.85 even after several successive exchange steps. According to FTIR experiments of adsorbed pyridine, these samples do not possess strong Brønsted acid sites and the amount of strong Lewis acid sites is decreased. Additionally, a new band appears in Py-FTIR spectra of the prepared samples after ion exchange. This band characterizes the interaction of pyridine with potassium cations in the samples which are weak Lewis acid sites. The probing of basic properties of ion-exchanged K-BEA zeolites with CO_2 adsorption microcalorimetry reveals the absence of strong basic sites in these samples. As a consequence, furfural conversion decreases as the potassium content in the ion-exchanged catalysts increases to K/Al ca.0.7–0.8 proving that intrinsic basic sites in potassium-containing zeolites has scarce activity in aldol condensation of furfural with acetone. Unlike the ion-exchanged samples, K-BEA zeolites prepared by the combined IE + IMP preparation method exhibit a partial blocking of the zeolite pore system with extra-framework potassium species and/or a partial destruction of crystalline framework of BEA zeolite. FTIR experiments of adsorbed pyridine prove that these samples do not possess any acidity except for that connected with K^+ cations introduced by ion exchange.

Basic properties of the impregnated zeolites are more expressed: CO_2 adsorption microcalorimetry proves the presence of strong basic sites in these samples, which are plausibly extra-framework K_2O species. Such catalysts demonstrate high activity in aldol condensation at T = 100 °C, especially provided that the K_2O oxidic species are located on the external surface of zeolite crystals. The composition of reaction products proves that aldol condensation between furfural and acetone over the impregnated K-BEA samples proceeds by a reaction pathway similar to that observed for other basic materials. The good performance of the impregnated K-BEA zeolites is accompanied by the decreased amount of heavy carbonaceous deposits in the catalysts after reaction what could be advantageous for their stability.

Nevertheless, the activity of the impregnated K-BEA samples visibly decreases after their washing with a solvent in consecutive catalytic runs. Presence of furfuryl alcohol in the reaction products allows suggesting the occurrence of furfural conversion by Cannizzaro reaction on these catalysts. Furoic acid produced by this reaction interacts with strong basic sites of the impregnated K-BEA forming surface furoates and resulting in decreased catalyst activity in aldol condensation. On the other hand, the catalytic activity of basic zeolites after their oxidative regeneration in consecutive catalytic runs or after their storage in a calcined form on open air is also lower in comparison with freshly calcined sample. Presumably, it is caused by the interaction of strong basic sites in the catalysts with CO_2 from environment resembling another class of basic solids, rehydrated hydrotalcites. That is why further studies concerned with the preparation of zeolites with strong basic sites and the evaluation of their behavior in organic reactions are necessary.

Acknowledgement

The authors thank the Czech Science Foundation for the support (P106/12/G015).

Appendix A. Supplementary data

Supplementary data associated with this article can be found, in the online version, at http://dx.doi.org/10.1016/j.molcata.2016.09.014.

References

[1] G.W. Huber, J.N. Chheda, C.J. Barret, J.A. Dumesic, Science 308 (2005) 1446–1450.
[2] R. Xing, A.V. Subrahmanyam, H. Olcay, W. Qi, G.P. van Walsum, H. Pendse, G.W. Huber, Green Chem. 12 (2010) 1933–1946.
[3] Q. Deng, J. Xu, P. Han, L. Pan, L. Wang, X. Zhang, J.-J. Zou, Fuel Process. Technol. 148 (2016) 361–366.

[4] Q. Deng, G. Nie, L. Pan, J.-J. Zou, X. Zhang, L. Wang, Green Chem. 17 (2015) 4473–4481.
[5] D.L. Klass, Biomass for Renewable Energy, Fuels and Chemicals, Academic Press, San Diego, 1998.
[6] D. Kubička, I. Kubičková, J. Čejka, Catal. Rev. Sci. Eng. 55 (2013) 1–78.
[7] F.A. Carey, R.J. Sundberg, Advanced Organic Chemistry, Part B: Reactions and Synthesis, Fourth ed., Kluwer Academic Publishers, New York, 2002.
[8] R.M. West, Z.Y. Liu, M. Peter, C.A. Gärtner, J.A. Dumesic, J. Mol. Catal. A: Chem. 296 (2008) 18–27.
[9] C.J. Barrett, J.N. Chheda, G.W. Huber, J.A. Dumesic, Appl. Catal. B: Environ. 66 (2006) 111–118.
[10] D.P. Debecker, E.M. Gaigneaux, G. Busta, Chem. Eur. J. 15 (2009) 3920–3935.
[11] I. Sádaba, M. Ojeda, R. Mariscal, R. Richards, M. López Granados, Catal. Today 167 (2011) 77–83.
[12] L. Faba, E. Diaz, S. Ordõnez, Appl. Catal. B: Environ. 113–114 (2012) 201–211.
[13] M.J. Climent, A. Corma, S. Iborra, A. Velty, Green Chem. 4 (2002) 474–480.
[14] L. Hora, V. Kelbichová, O. Kikhtyanin, O. Bortnovskiy, D. Kubička, Catal. Today 223 (2014) 138–147.
[15] C. Xu, Y. Gao, X. Liu, R. Xin, Z. Wang, RSC Adv. 3 (2013) 793–801.
[16] S. Abelló, D. Vijaya-Shankar, J. Pérez-Ramírez, Appl. Catal. A: General 342 (2008) 119–125.
[17] W. Xu, X. Liu, J. Ren, H. Liu, Y. Ma, Y. Wang, G. Lu, Microporous Mesoporous Mat. 142 (2011) 251–257.
[18] O. Kikhtyanin, V. Kelbichová, D. Vitvarová, M. Kubů, D. Kubička, Catal. Today 227 (2014) 154–162.
[19] D.N. Thanh, O. Kikhtyanin, R. Ramos, M. Kothari, P. Ulbrich, T. Munshi, D. Kubička, Catal. Today (2016), http://dx.doi.org/10.1016/j.cattod.2015.11.027.
[20] E. Dumitriu, V. Hulea, I. Fechete, A. Auroux, J.-F. Lacaze, C. Guimon, Microporous Mesoporous Mat. 43 (2001) 341–359.
[21] A. Ungureanu, S. Royer, T.V. Hoang, D. Trong On, E. Dumitriu, S. Kaliaguine, Microporous Mesoporous Mat. 84 (2005) 283–296.
[22] T. Komatsu, M. Mitsuhashi, T. Yashima, Stud. Surf. Sci. Catal. 142 (2002) 667–674.
[23] O. Kikhtyanin, P. Chlubná, T. Jindrová, D. Kubička, Dalton Trans. 43 (2014) 10628–10641.
[24] J. Weitkamp, M. Hunger, U. Rymsa, Microporous Mesoporous Mat. 48 (2001) 255–270.
[25] R.J. Davis, J. Catal. 216 (2003) 396–405.
[26] D. Barthomeuf, Catal. Rev. Sci. Eng. 38 (1996) 521–612.
[27] D. Barthomeuf, Microporous Mesoporous Mat. 66 (2003) 1–14.
[28] D. Barthomeuf, J. Phys. Chem. B 109 (2005) 2047–2054.
[29] M. Laspéras, H. Cambon, D. Brunel, I. Rodriguez, P. Geneste, Microporous Mater. 7 (1996) 61–72.
[30] E.R. Silva, J.M. Silva, P. Massiani, F.R. Ribeiro, M.F. Ribeiro, Catal. Today 107 (2005) 792–799.
[31] M.E. Davis, P.E. Hathaway, J. Cat. 116 (1989) 263–278.
[32] M.D. Romero, G. Ovejero, A. Rodríguez, J.M. Gómez, J. Porous Mater. 11 (2004) 31–39.
[33] C. Bisio, P. Massiani, K. Fajerwerg, L. Sordelli, L. Stievano, E.R. Silva, S. Coluccia, G. Martra, Microporous Mesoporous Mat. 90 (2006) 175–187.
[34] M.D. Romero, G. Ovejero, A. Rodriguez, J.M. Gomez, Microporous Mesoporous Mat. 81 (2005) 313–320.
[35] C.A. Emeis, J. Catal. 141 (1993) 347–354.
[36] J.M. Newsam, M.M.J. Treacy, W.T. Koetsier, C.B. de Gruyter, Proc. R. Soc. Lond. A 420 (1988) 375–405.
[37] K.P. Volcho, S. Yu. Kurbakova, D.V. Korchagina, E.V. Suslov, N.F. Salakhutdinov, A.V. Toktarev, G.V. Echevskii, V.A. Barkhash, J. Mol. Catal. A: Chem. 195 (2003) 263–274.
[38] Z.-Q. Zou, M. Meng, J.-J. He, Mater. Chem. Phys. 124 (2010) 987–993.
[39] M.A. Peralta, B.S. Sánchez, M.A. Ulla, C.A. Querini, Appl. Catal. A: General 393 (2011) 184–188.
[40] I. Kiricsi, C. Flego, G. Pazzuconi, W.O. Parker, R. Millini, C. Perego, G. Bellussi, J. Phys. Chem. 98 (1994) 4627–4634.
[41] A. Vimont, F. Thibault-Starzyk, J.C. Lavalley, J. Phys. Chem. B 104 (2000) 286–291.
[42] S. Kotrel, J.H. Lunsford, H. Knözinger, J. Phys. Chem. B 105 (2001) 3917–3921.
[43] A. Zecchina, G. Spoto, S. Bordiga, Phys. Chem. Chem. Phys. 7 (2005) 1627–1642.
[44] A. Zecchina, S. Bordiga, G. Spoto, D. Scarano, G. Petrini, G. Leonfanti, M. Padovan, C. Otero Areán, J. Chem. Soc. Faraday Trans. 88 (1992) 2959–2969.
[45] M. Bjørgen, F. Bonino, S. Kolboe, K.-P. Lillerud, A. Zecchina, S. Bordiga, J. Am. Chem. Soc. 125 (2003) 15863–15868.
[46] E. Bourgeat-Lami, P. Massiani, F. Di Renzo, P. Espiau, F. Fajula, Appl. Catal. 72 (1991) 139–152.
[47] R. Bulánek, E. Koudelková, Microporous Mesoporous Mat. 151 (2012) 149–156.
[48] M.R. Delgado, C.O. Arean, Energy 36 (2011) 5286–5291.
[49] L. Grajciar, J. Čejka, A. Zukal, C. Otero Areán, G. Turnes Palomino, P. Nachtigall, ChemSusChem 5 (2012) 2011–2022.
[50] J.A. Dunne, R. Mariwala, M. Rao, S. Sircar, R.J. Gorte, A.L. Myers, Langmuir 12 (1996) 5888–5895.
[51] R. Bulánek, K. Frolich, E. Frýdová, P. Čičmanec, Topics Catal. 53 (2010) 1349–1360.
[52] R. Bulánek, K. Frolich, E. Frýdová, P. Čičmanec, J. Therm. Anal. Calor. 105 (2011) 443–449.
[53] A. Zukal, A. Pulido, B. Gil, P. Nachtigall, O. Bludský, M. Rubeš, J. Čejka, Phys. Chem. Chem. Phys. 12 (2010) 6413–6422.
[54] C.O. Areán, M.R. Delgado, G.F. Bibiloni, O. Bludský, P. Nachtigall, Chem. Phys. Chem 12 (2011) 1435–1443.
[55] O. Kikhtyanin, E. Lesnik, D. Kubička, Appl. Catal. A: General 525 (2016) 215–225.
[56] A. Vaccari, Catal. Today 41 (1998) 53–71.
[57] C. Moreau, J. Lecomte, A. Roux, Catal. Commun. 7 (2006) 941–944.

Applied Catalysis A, General 549 (2018) 8–18

Contents lists available at ScienceDirect

Applied Catalysis A, General

journal homepage: www.elsevier.com/locate/apcata

Characterization of potassium-modified FAU zeolites and their performance in aldol condensation of furfural and acetone

Oleg Kikhtyanin[a,b,*], Yadolah Ganjkhanlou[c], David Kubička[b], Roman Bulánek[c], Jiří Čejka[d]

[a] Unipetrol Centre of Research and Education (UNICRE), Chempark Litvínov, 436 70 Záluží-Litvínov, Czech Republic
[b] Technopark Kralupy, University of Chemistry and Technology Prague, Žižkova 7, 278 01 Kralupy nad Vltavou, Czech Republic
[c] Department of Physical Chemistry, Faculty of Chemical Technology, University of Pardubice, Studentská 573, 532 10 Pardubice, Czech Republic
[d] J. Heyrovský Institute of Physical Chemistry, Academy of Sciences of the Czech Republic, Dolejškova 2155/3, 182 23 Prague, Czech Republic

ARTICLE INFO

Keywords:
Aldol condensation
Biomass
Y zeolite
Dealumination
Furfural
Potassium

ABSTRACT

The effects of both Si/Al ratio and preparation method (ion exchange vs. impregnation) on the physico-chemical properties of potassium modified Y zeolites were studied in detail. The samples were used as basic catalysts for aldol condensation of furfural and acetone. A relationship between physico-chemical properties and catalytic performance of potassium-containing Y zeolites was established using XRD, N_2 physisorption, IR spectroscopy of adsorbed CO_2 and CO_2-TPD. Neither ion-exchange nor impregnation with KNO_3 removed completely all acid sites in Y (Si/Al = 2.5). Moreover, K_2O clusters were not formed under thermal activation of the samples prepared from the parent H-Y(2.5). As a consequence, both ion-exchanged and impregnated K-Y(2.5) possessed low activity in aldol condensation, but they had high ability to dehydrate reaction products. In contrast, thermal activation of USY zeolites (Si/Al = 15 and 40) impregnated with potassium resulted in the formation of K_2O species which, according to CO_2-IR spectroscopy and CO_2-TPD, were strong basic sites. It was concluded that the lower amount of proton sites available for an ion-exchange together with the larger mesopore volume and more defective crystalline framework promoted the accumulation of KNO_3 in the USY zeolites during the impregnation step. Subsequently, K_2O species were formed by thermal treatment. Impregnated and calcined USY zeolites possessed a superior catalytic activity in comparison with HY (Si/Al = 2.5). The presence of K_2O species as strong basic sites in K-impregnated USY zeolites was favorable for both the high activity of the catalysts in aldol condensation and the occurrence of the second condensation step.

1. Introduction

Biomass as a renewable organic source has become a promising and sustainable energy resource in recent years [1,2]. However, the carbon-chain length of biomass-derived molecules as starting building blocks is usually limited to 3–9 carbon atoms, which needs to be increased to the desired length of 8+ carbon atoms for their efficient application in producing transportation fuels. Aldol condensation of short-chain biomass-derived products, such as furfural and acetone, is an efficient route for practical utilization of biomass to obtain valuable compounds [3–6]. Sodium hydroxide solution is a well-known homogeneous catalyst for this reaction [7,8], however its corrosive properties and environmental issues connected with its use limit its industrial application. Consequently, enormous effort has recently been exerted to find an alternative heterogeneous catalyst for this reaction [9–12].

Aldol condensation can be catalyzed by both acidic and basic sites [7,8], therefore porous materials with either basic or acidic properties are relevant heterogeneous catalysts. Both pore-size confinement and the nature of active sites could influence their activity and alter the composition of reaction products. Moreover, the stability of the catalytic activity of these heterogeneous catalysts should be considered for their practical utilization as well. For example, hydrotalcite-like materials as solids possessing basic properties are studied as heterogeneous catalysts for aldol condensation [13–15], but their sensitivity to CO_2 from ambient atmosphere and low chemical stability restrict their widespread industrial application [16,17]. Zeolites are recyclable environmentally-friendly heterogeneous catalysts [18–20], which can facilitate this reaction due to their high stability, large surface area and high activity. Flego and Perego [21] investigated both effect of the acid site density and the pore dimension on a variety of acidic molecular sieves (small-, medium-, large-pore zeolites and amorphous micro-, mesoporous silica-aluminas) in acetone self-condensation. Ungureanu et al. [22] found that the catalytic activity of semicrystalline zeolitic-mesoporous UL-ZSM-5 materials in aldol condensation of acetaldehyde

---

* Corresponding author at: Technopark Kralupy, University of Chemistry and Technology Prague, Žižkova 7, 278 01 Kralupy nad Vltavou, Czech Republic
E-mail address: oleg.kikhtyanin@vscht.cz (O. Kikhtyanin).

http://dx.doi.org/10.1016/j.apcata.2017.09.017
Received 28 June 2017; Received in revised form 10 September 2017; Accepted 15 September 2017

with formaldehyde well correlated with the number of acid sites. Tago et al. [23] studied the possibility of light olefins production by cracking of isobutylene formed from aldol condensation products of acetone. Acidic FAU, BEA and MWW zeolites were used as catalysts in aldol condensation of furfural and acetone [10,24]. Nevertheless, the fast deactivation of acidic zeolites in condensation reactions limits their application for this purpose [4,22]. Acidic sites of conventional zeolites can catalyze side reactions (e.g. oligomerization) producing coke (heavy carbonaceous deposits) and deactivate the catalyst. Ion-exchanged metal zeolites were also reported to catalyze condensation reactions. The examples of these reactions include aldol condensation of n-butanal to 2-ethyl-2-hexenal over ion-exchanged NaY zeolites [25], aldol condensation of acetone over alkali cation exchanged X and Y zeolites [26], the condensation reaction of propionic acid and formaldehyde to form methacrylic acid using NaX, KX and CsX zeolites [27], solvent free aldol condensation of propanal to 2-methylpentenal using alkali ion-exchanged zeolites [28]. Potassium-modified BEA zeolite has been recently reported as catalysts active in aldol condensation of furfural and acetone [4]. The performance of potassium-containing BEA zeolites as basic catalysts for aldol condensation of furfural and acetone depends significantly on the method of their preparation. According to FTIR experiments of adsorbed pyridine, the ion-exchanged samples did not possess strong Brønsted acid sites and the amount of strong Lewis acid sites was decreased [4]. CO_2 adsorption microcalorimetry confirmed the absence of strong basic sites in these samples. Consequently, furfural conversion decreased as the potassium content in the ion-exchanged catalysts increased to K/Al ca.0.7–0.8 proving that intrinsic basic sites in potassium-containing zeolites have low activity in aldol condensation. In contrast, CO_2 adsorption microcalorimetry proved the presence of strong basic sites in impregnated samples, which were plausibly extra-framework K_2O species. Such catalysts demonstrated high activity in aldol condensation due to the participation of the K_2O species located on the external surface of zeolite crystals. The reliable performance of the impregnated K-BEA zeolites was accompanied by a decreased amount of heavy carbonaceous deposits in the catalysts after reaction, which could be advantageous for the stability of their catalytic activity. Nevertheless, the influence of Si/Al molar ratio in zeolites on the catalytic performance of potassium-containing zeolites in aldol condensation of furfural and acetone was not investigated so far.

The goal of the present study is to evaluate the effect of chemical composition and zeolite texture on the performance of the catalysts in aldol condensation of furfural and acetone. For that purpose, a series of potassium-modified Y zeolites with different Si/Al ratio was prepared by either ion exchange or impregnation methods. In order to fully understand the effect of different parameters on the activity and selectivity of the prepared catalysts, CO_2 as probe molecule for studying the basic sites [29] has been utilized (applying IR spectroscopy and TPD techniques). Accordingly, the structure and distribution of different basic sites in the samples were thoroughly investigated by this approach.

2. Experimental

2.1. Samples

Commercial HY and H-USY zeolites with the Si/Al ratio of 2.5, 15 and 40 provided by Zeolyst International (CBV 400, CBV 720 and CBV 780, respectively) were used as parent materials. To prepare potassium-containing samples, the starting zeolites were ion exchanged or impregnated with potassium according to a procedure described previously [4]. The as-received zeolites in proton form were ion-exchanged using an aqueous 0.7 M KNO_3 solution at 80 °C under 200 RPM stirring for 2 h followed by filtration of the prepared samples using a Buchner funnel. The first set of samples was thoroughly washed with a plenty of hot water to remove all extra potassium cations from the solids (IE series). The second set of samples was filtered but not washed (IMP series). All prepared materials were then dried in ambient air overnight and calcined at T = 530 °C for 3 h. These samples were labeled as: K-modification procedure (IE or IMP)-zeolite type(xx), where xx stands for Si/Al ratio of the parent zeolite, e.g. K-IMP-Y(40) denotes a potassium-containing faujasite having Si/Al ratio equal to 40 using the impregnation method to introduce potassium.

2.2. Characterization

X-ray powder diffraction (XRD) patterns of both as-prepared and freshly calcined samples were recorded on a Philips MPD 1880 diffractometer working with the Cu Kα line (λ = 0.154 nm) in the 2θ range of 4°–40° at a scanning rate of 2θ of 2.4°/min. Quantitative phase analysis of the samples was performed using the Rietveld structure refinement method employing Materials Analysis Using Diffraction (MAUD) software (Version 2.26) [30,31]. It allowed calculating lattice parameters (a), crystallite size (D) and microstrain (parameter characterizing the distortion of the structure) (ε) which have been provided in the Supplementary Information (see Table S1 in the *SI*). For each set of zeolites with the same Si/Al ratio, a sample with the highest crystallinity was used as a reference. The elemental composition was determined by X-ray fluorescence (XRF) using Philips PW 1401 equipped with a Rh RTG lamp. The UniQuant program was used to evaluate the results. Textural properties ("external" surface area and micro- and total pore volumes) were determined from nitrogen adsorption/desorption experiments performed at −196 °C after sample activation in vacuum at 300 °C for 12 h using a Micromeritics ASAP 2020 unit (It should be considered that BET model does not applied for interpreting the N_2 sorption results as it is not valid for microporous materials).

IR spectra of the prepared samples were recorded on a Nicolet 6700 FTIR spectrometer equipped with a MCT detector. The concentrations of Brønsted and Lewis acid sites were calculated from the integral intensities of the individual bands characteristic for pyridine adsorbed on Brønsted acid sites (BAS, $1545\,cm^{-1}$) and on Lewis acid sites (LAS, $1455\,cm^{-1}$) using the molar extinction coefficients of 1.13 and $1.28\,cm\mu mol^{-1}$ taken from [32]. Before the CO_2 adsorption experiments monitored by FTIR, the self-supporting wafers were placed into a home-made IR cell for transmission spectra measurement and pretreated in a dynamic vacuum (residual pressure $< 10^{-4}$ mbar) at 450 °C for 16 h. After that CO_2 with pressure of about 2 mbar was dosed into the cell at ambient temperature and the system was equilibrated for 20 min before evacuation. IR spectra recording proceeded (accumulating 8 scans with the resolution of $2\,cm^{-1}$) during the gradual cell evacuation using a turbomolecular pump at room temperature.

Temperature programmed desorption of CO_2 (CO_2-TPD) study was performed using a Micromeritics AutoChem II 2920 instrument. The desorbed products were followed by mass spectrometer Pfeiffer OmniStar GSD 300 (the molecular ion $m/z = 44$ was analyzed). Before TPD experiments, the samples were heated to 530 °C in He flow and treated in O_2 flow at the same temperature for 2 h. After cooling to RT, the samples were saturated with CO_2 (10% CO_2/He; 25 ml/min) for 25 min. The physisorbed CO_2 was flushed with He (25 ml/min) for 60 min. The end of both saturation and flushing were checked by mass signal stabilization. The CO_2-TPD proceeded with a temperature ramp of 10 °C/min from 25 to 500 °C in He flow of 25 ml/min.

2.3. Catalytic study

The catalytic performance of the prepared zeolite samples was investigated in aldol condensation of furfural (Sigma-Aldrich) and acetone (Lach-Ner, s.r.o., Czech Republic) pre-dried before the experiments with a molecular sieve. The catalytic experiments were carried out in a 300 ml Parr stirred autoclave at 100 °C. In a catalytic run, 2 g of a freshly calcined (T = 530 °C) catalyst was mixed together with a stirred mixture of 39.5 g acetone and 6.5 g of furfural (the acetone/

furfural molar ratio of 10/1). The desired temperature was achieved in ~50–60 min after initiation of the heating, and the autoclave was then kept at T = 100 °C for additional 2 h. Analysis of the reaction products obtained after 2 h at the reaction temperature was performed using an Agilent 7890A GC equipped with a flame ionization detector and an HP-5 capillary column (30 m/0.32 ID/0.25 μm). The products were identified based on the standard reference compounds as well as GC–MS analyses. Catalytic results of aldol condensation of furfural and acetone were described in terms of conversion and selectivity calculated as follows:

$Conversion\ (t)\ (mol\%) = 100 \times (reactant_{t=0} - reactant_t)/reactant_{t=0};$

Selectivity to product i = 100 × (mole of reactant converted to product i)/(total number of mole of reactant converted).

Carbon balance was monitored in all experiments as the total number of carbon atoms detected in each organic compound with Cn atoms (where n = 3, 5, 8,…, etc.) divided by the initial number of carbon atoms in F + Ac feed:

C balance% = (3molC3 + 5molC5 +…nmolCn)/(3molC3(t = 0) + 5molC5(t = 0)).

3. Results

3.1. XRD and chemical analysis

The XRD powder patterns of the parent zeolites used for the preparation of K-containing catalysts proved the phase purity of zeolites with FAU structure (see the *SI*, Fig. S1). After either IE or IMP treatment no other crystalline phases, including potassium clusters (K_2O or KNO_3), were detected in XRD patterns of the resulting samples (cf. Fig. S2 in the *SI*).

Chemical analysis of the prepared potassium-containing Y zeolites demonstrates (Table 1) that K content in the samples prepared by ion-exchange (IE) is lower for samples with higher Si/Al molar ratio. Ion-exchanged material K-IE-Y(2.5) possesses the largest K content of 5.94 wt.% due to its higher exchange ability, while K-IE-Y(40) has the lowest K content of 0.24 wt.% in agreement with the lowest number of sites available to cationic exchange. K/Al molar ratios of ion exchanged samples are 0.55, 0.41 and 0. 17 for K-IE-Y(2.5), K-IE-Y(15) and K-IE-Y(40) samples, respectively (i.e. below unity for all ion exchanged samples). It means that some acidic OH groups were not exchanged (due to short time for reaching of ion-exchange equilibrium or increasing hydrophobicity of the zeolite) [33]. Also presence of some extraframework Al atoms can contribute to the K/Al molar ratios below unity. [34]. The potassium content in the impregnated samples is from 4.0 to 6.9 wt.% (Table 1). For catalysts prepared from HY(2.5) the potassium content for ion-exchanged and impregnated samples is 5.9 and 6.9 wt.%, respectively, which corresponds to K/Al molar ratio of 0.55 and 0.63, respectively. In contrast, a difference in potassium content between ion-exchanged and impregnated high-silica zeolites increases in a great extent, from 1.34 to 4.56 wt.% and from 0.24 to 4.03 wt.% for ion-exchanged and impregnated samples prepared from HY(15) and HY(40), respectively. Accordingly, the achieved potassium content in K-IMP-Y(15) and K-IMP-Y(40) corresponds to K/Al molar ratio of 1.6–3.3, respectively, suggesting the presence of potassium species outside of ion-exchangeable sites (probably K_2O species) in these samples after their thermal activation.

Table 1
Chemical analysis and textural properties of potassium zeolite samples.

Sample	K[a], wt.%	K/Al molar ratio	S_{ext}, m[b]/g	V_{mic},[c], cm^3/g	V_{tot},[d], cm^3/g
HY(2.5)	–	–	8	0.332	0.388
K-IE-Y(2.5)	5.94	0.55	10	0.301	0.336
K-IMP-Y(2.5)	6.91	0.63	10	0.297	0.317
HY(15)	–	–	74	0.320	0.490
K-IE-Y(15)	1.34	0.41	84	0.302	0.490
K-IMP-Y(15)	4.56	1.61	82	0.144	0.346
HY(40)	–	–	81	0.286	0.536
K-IE-Y(40)	0.24	0.17	97	0.274	0.509
K-IMP-Y(40)	4.03	3.27	64	0.137	0.327

[a] K − potassium content.
[b] S_{ext} − surface area of mesopores and external surface of crystallites (from t-plot method).
[c] V_{mic} − micropore volume (from t-plot method).
[d] V_{tot} − total pore volume at p/p_0 = 0.97.

3.2. Nitrogen adsorption

Irrespective of Si/Al ratio in studied zeolites, all parent samples exhibit large micropore and total pore volumes (Table 1). Additionally, USY zeolites demonstrate improved porosity and increased surface area in comparison with HY(2.5) except surface of micropores represented in intercept of line in t-plots (cf. S_{ext} values in Table 1). The ion-exchange affects the pore volume of the prepared samples only insignificantly. Porosity of K-IMP-Y(2.5) sample are very similar to those of the ion-exchanged sample (Table 1) due to the assumed absence of excessive extra-framework potassium species in this sample. On the contrary, the impregnation method has a substantial effect on the textural properties of the low aluminum samples. The K-IMP-Y(15) sample has its micropore volume decreased to 0.144 cm^3/g. These values amount to about 50% reduction from those obtained for K-IE-Y(15) sample. For K-IMP-Y(40) the micropore volume decreases to 0.137 cm^3/g, which is again ~50% of those obtained for K-IE-Y(40) and HY(40) samples. This decrease in pore volumes can be associated with the potassium species that are not present in the ion-exchangeable sites (see IR and CO_2-TPD results).

3.3. SEM images

The SEM images, as well as textural properties (see Table 1), clearly show that dealumination procedure during USY zeolites preparation results in the formation of pores and defects on the external surface of zeolite crystals creating additional mesoporosity (Fig. 1). Due to the formation of K_2O clusters in the impregnated samples, we may speculate that some micropores of K-IMP-Y(15) and K-IMP-Y(40) samples are partially filled or blocked with K_2O as evidenced by the decrease in micropore volumes (Table 1). Moreover, some K_2O species may be also formed on the external surface of the zeolite particles. The relative reduction in mesopore density visible on the particle surface and surface roughness of the impregnated sample in SEM images supports this assumption (Fig. 1d and f in comparison with Fig. 1c and e). More interestingly, no obvious changes in the shape of the zeolite crystals upon impregnation are observed (compare K-IMP-Y(40) and K-IE-Y(40) or K-IMP-Y(15) and K-IE-Y(15) samples, Fig. 1), while the crystal structure parameters of these samples differ considerably (see the *SI*, Fig. S4 and Table S1). This observation suggests that partial distortion and destruction of the zeolite structure (which can be deduced from XRD data related to the structural changes) due to the impregnation step occurs, if any, inside the zeolite crystallites rather than on their external surface. If so, most K_2O species are also formed in the intra-crystalline volume, presumably in the supercages of Y structure.

3.4. FTIR study

3.4.1. The behavior of samples during thermal activation

Fig. 2 shows the changes in the IR spectra of the as-prepared and dried samples before and after thermal activation under vacuum at

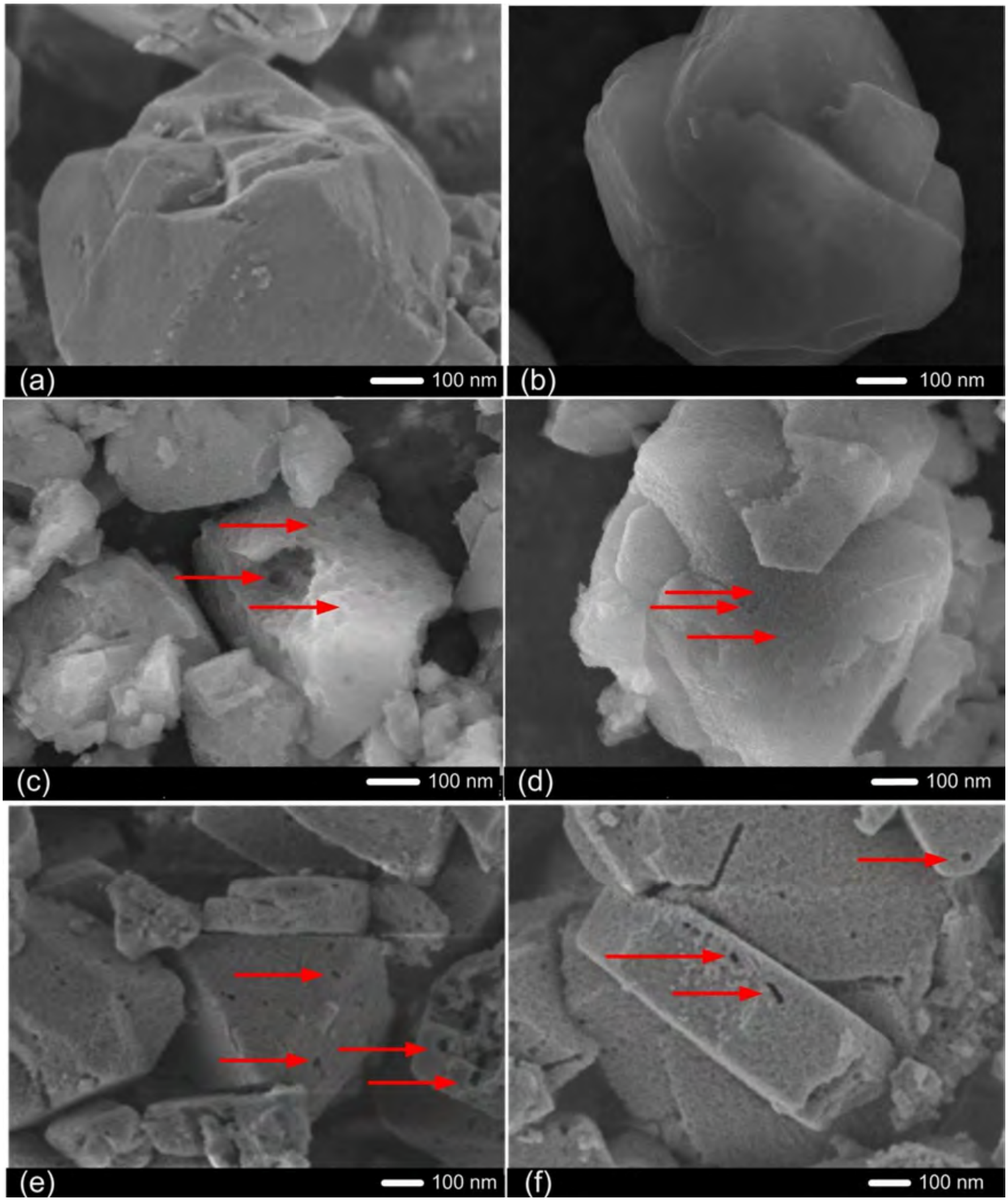

Fig. 1. SEM micrographs of (a) K-IE-Y(2.5) (b) K-IMP-Y(2.5) (c) K-IE-Y(15) (d) K-IMP-Y(15) (e) K-IE-Y(40) (f) K-IMP-Y(40).

450 °C for 16 h as well as IR spectra of parent zeolite. The observed bands between 3600 and 3000 cm^{-1} and ~1632 cm^{-1} in *as-prepared* samples corresponding to the stretching and bending water vibrations, respectively, lose their intensities upon heating and activation of the samples. In the IR spectra of the ion-exchanged samples before thermal activation, a broad peak at 3600–3000 cm^{-1} related to the interaction of active silanol groups with water is observed at a higher wavenumber (especially in the dealuminated Y zeolites, Fig. 2c and e). This band shifts to a lower wavenumber in the impregnated samples as the most active silanols are grafted with potassium (Fig. 2d and f). Additionally, the intensity of the doublet with maximum at 1396 and 1375/1367 cm^{-1} decreases as well. These bands can be attributed to the bulk KNO_3 present inside the pore system of the samples [35,36] and the disappearance of these bands after activation is an indication of nitrates decomposition. The signal of Brønsted sites (at 3630 and 3566 cm^{-1} [29]) is present in the IR spectra of neither ion-exchanged nor impregnated dealuminated zeolites after heat activation suggesting that almost all protons in these samples are exchanged with potassium. In contrast, the band at 3600 cm^{-1} is observed in the IR spectra of K-IE-Y (2.5) and K-IMP-Y(2.5) samples which could be related to remaining Brønsted sites [37] (IR spectrum of the parent HY(2.5) is also provided in Fig. 2).

3.4.2. *Study of acidic properties of potassium zeolites using infrared spectra of adsorbed pyridine (Py-FTIR)*

Upon pyridine adsorption new absorption bands appear at 1545 cm^{-1} and 1455 cm^{-1}, which are ascribed to the interaction of pyridine with strong Brønsted and Lewis acid sites, respectively (Fig. 3). The concentrations of BAS and LAS in K-IE-Y(2.5) are 0.21 and 0.34 mmol/g (Table 2), respectively, indicating that ion exchange does

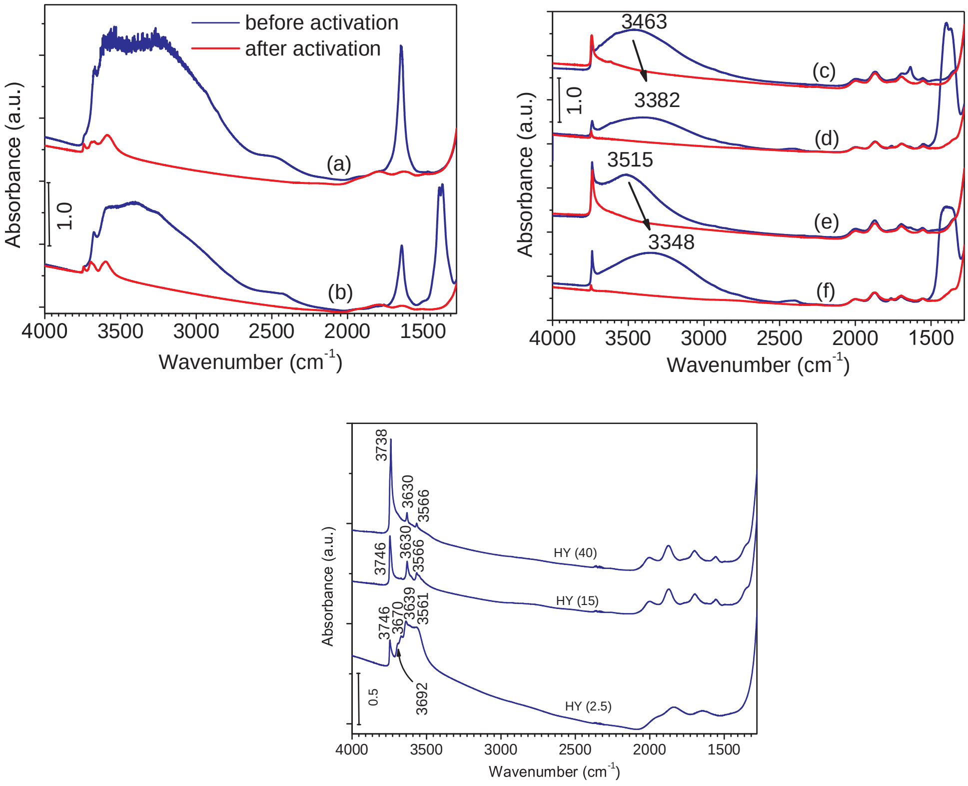

Fig. 2. FTIR spectra of samples before and after vacuum activation at 450 °C overnight (a) K-IE-Y(2.5) (b) K-IMP-Y(2.5) (c) K-IE-Y(15) (d) K-IMP-Y(15) (e) K-IE-Y(40) (f) K-IMP-Y(40). The FTIR spectra of parent zeolite with the label of HY(2.5), HY(15) and HY(30) is also provided (the bottom panel).

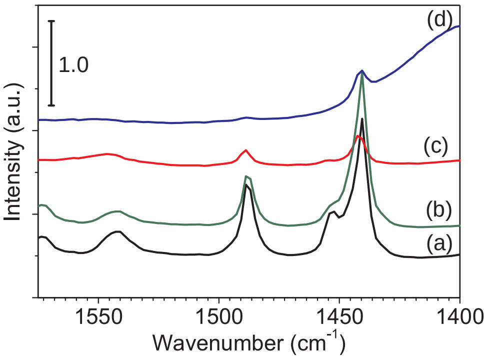

Fig. 3. Py-FTIR spectra of potassium Y samples. (a) K-IE-Y(2.5), (b) K-IMP-Y(2.5), (c) K-IE-Y(15), (d) K-IMP-Y(15).

Table 2
Concentration of Brønsted and Lewis acid sites as well as those due to the interaction of pyridine with potassium cations.

Sample	Brønsted acid sites, mmol/g	Lewis acid sites, mmol/g
HY(2.5)	0.127	0.223
K-IE-Y(2.5)	0.21	0.34
K-IMP-Y(2.5)	0.11	0.3
HY(15)	[a]	[a]
K-IE-Y(15)	0.03	0.03
K-IMP-Y(15)	0.01	0.02
HY(40)	0.104	0.068
K-IE-Y(40)	< 0.01	< 0.01
K-IMP-Y(40)	< 0.01	0.02

[a] Not measured.

not remove all acid sites in this sample that are available for interaction with pyridine. It is worth to note that IR study of pyridine adsorption is more sensitive than IR studying of the OH region and small number of acidic sites could be detected by pyridine adsorption method [29] while bands of acidic sites in the OH region disappeared. Simultaneously, a new band at 1445 cm^{-1} appears in the spectrum of K-IE-Y(2.5) after IE. It can be attributed to pyridine interacting with potassium cations located in the ion-exchangeable sites of the prepared samples, as proposed in [4]. Due to the impregnation step the BAS concentration in K-IMP-Y(2.5) decreases to 0.11 mmol/g, whereas the concentration of both LAS (0.3 mmol/g) and the sites which characterize potassium cations (band at 1445 cm^{-1}) is virtually unaffected. K-IE-Y(15) possesses only residual acidity with the concentration of both BAS and LAS equal to 0.03 mmol/g, while the concentration of these sites in K-IMP-Y (15) is even lower, 0.01 and 0.02 mmol/g, respectively. The intensity of the IR band ascribed to the interaction of pyridine with potassium cations in K-IE-Y(15) and K-IMP-Y(15) is similar in both samples and significantly lower as compared with K-IE-Y(2.5). This agrees with the decreased potassium content introduced into these samples by ion exchange. Finally, Py-FTIR data evidences that K-IE-Y(40) and K-IMP-Y (40) do not possess any acidity and the intensity of the IR band due to the interaction of pyridine with potassium cations is about ten-times lower, which is expected due to the high Si/Al ratio of the samples.

3.4.3. CO_2 adsorption

CO_2 adsorption on all catalysts has been also studied by means of IR spectroscopy at room temperature. IR bands after CO_2 adsorption can be divided in two groups (Fig. 4); the first category related to physisorption of linear CO_2 at 2350 cm^{-1} and the second one associated with chemisorption of carbonate-like species represented by low-frequency bands in the 1700–1300 cm^{-1} region [38]. The ν_3 absorption band of linear CO_2 is observed in spectra of all samples recorded under 2 mbars of CO_2 equilibrium pressure, whereas the low frequency bands related to the chemisorbed species are observed only in the impregnated samples (except for K-IMP-Y(2.5) sample). The chemisorbed species are more resistant to evacuation at room temperature as evidenced by presence of these IR bands in the spectra after 20 min evacuation, whilst the band at 2350 cm^{-1} completely disappeared. CO_2 chemisorbed on basic site could be characterized by splitting frequency of the corresponding bands (see the *SI*). The bands related to the chemisorbed

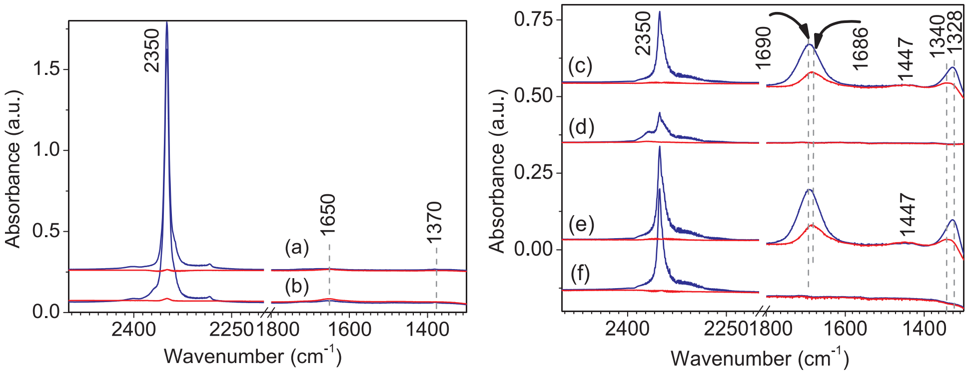

Fig. 4. FTIR spectra of adsorbed CO_2 (equilibrium pressure 2 mbars, 20 min of equilibration time, blue curves) recorded at RT on different samples (a) K-IMP-Y(2.5) (b) K-IE-Y(2.5) (c) K-IMP-Y(40) (d) K-IE-Y(40) (e) K-IMP-Y(15) (f) K-IE-Y(15) after 20 min of CO_2 evacuation at RT (red curves). (For interpretation of the references to colour in this figure legend, the reader is referred to the web version of this article.)

species are not observed in both K-IMP-Y(2.5) and K-IE-Y(2.5) indicating that the amount of K_2O in these catalysts is very low (Fig. 4a). Figs. 2 and 3 indicate that Brønsted acid sites are still remaining in K-IE-Y(2.5) and K-IMP-Y(2.5) after thermal activation and therefore ion exchange of potassium originating from the decomposition of excessive KNO_3 with Brønsted acid sites is preferred rather than the formation of K_2O species. In impregnated dealuminated zeolites (Fig. 4c and e), the bands of the chemisorbed species are observed at 1690 cm^{-1} and 1328 cm^{-1} which shift to 1686 and 1340 cm^{-1}, respectively, upon lowering the coverage by gradual desorption, demonstrating two different types of species with splitting frequencies ($\Delta\nu$) around 360 cm^{-1} and 346 cm^{-1} in the dealuminated impregnated samples. After evacuation, only the more stable type with the lower splitting frequency ($\Delta\nu$ = 346 cm^{-1}) remains (Fig. 4).

To summarize this section, the main band of asymmetric vibration, which is slightly shifted with increasing coverage indicates the presence of two kinds of carbonate species. According to literature [38] these are bidentate carbonates (see the *SI*, Scheme S1b). The splitting $\Delta\nu$ in the range of 300–370 cm^{-1} supports this suggestion. There is a very weak band at 1447 cm^{-1} suggesting that negligible amount of other type of carbonates with lower splitting frequency could also be present in the impregnated samples.

3.5. TPD of CO_2

Two well-resolved peaks are observed in CO_2-TPD curves of impregnated dealuminated Y zeolites (Fig. 5). Low-temperature peak (LT) having a maximum at ca. 50 °C is present in the TPD profiles of almost all the samples, while the high-temperature peak (HT) at temperature 135 °C is detected only in the TPD profiles of the impregnated Y zeolites with Si/Al molar ratios of 15 and 40. The CO_2 desorption is very weak in the case of the ion-exchanged samples in comparison with the impregnated ones (Fig. 5) which agrees with the IR results of CO_2 adsorption. Both the occurrence and intensity of the band in the IR spectra ascribed to the chemisorbed CO_2 species agree well with the intensity of the desorption peaks in the TPD patterns (Table 3). The intensity of the high-temperature desorption peak in the TPD curves of the dealuminated impregnated zeolites is larger than that for the low-temperature desorption peaks. On the other hand, K-IMP-Y(2.5) sample shows very weak CO_2 desorption in agreement with the absence of the chemisorbed species in the IR spectra (cf. Fig. 4).

Table 3
The amount of CO_2 desorbed from the samples during TPD experiments calculated from the intensity of low-temperature (LT) and high-temperature (HT) peaks and the comparison of these data with the integrated area of the IR bands related to chemisorbed CO_2.

Sample	LT peak on TPD curve		HT peak on TPD curve		Total n_{CO2}, µmol/g	Area (IR)
	T, °C	n_{CO2}, µmol/g	T, °C	n_{CO2}, µmol/g		
K-IE-Y(2.5)[a]						1.1
K-IMP-Y(2.5)	54	3.9	–	–	3.9	0.9
K-IE-Y(15)	31	0.9	–	–	0.9	0.9
K-IMP-Y(15)	50	18	136	66	84	25
K-IE-Y(40)	43	0.3	–	–	0.3	0.6
K-IMP-Y(40)	55	16	133	64	80	19

[a] TPD was not measured for this sample.

Based on the IR results reported above, the low-temperature peak can be ascribed to the carbonate species characterized with higher splitting frequency ($\Delta\nu$ around 360 cm^{-1}) whereas high-temperature peak related to the carbonate species with lower splitting frequency.

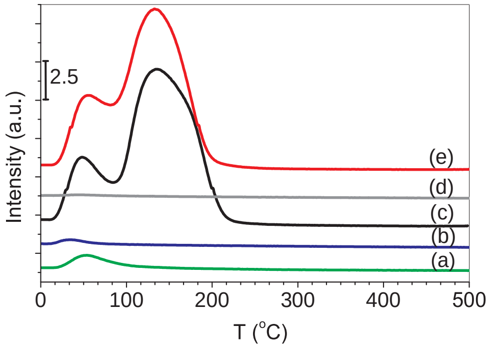

Fig. 5. CO_2-TPD measured on the samples **(a)** K-IMP-Y(2.5), **(b)** K-IE-Y(15), **(c)** K-IMP-Y(15), **(d)** K-IE-Y(40) and **(e)** K-IMP-Y(40).

3.6. Catalytic results

According to a general reaction scheme (see the *SI*, Scheme S2), aldol condensation of furfural with acetone leads to the formation of an aldol (FAcOH) as a primary product, which is often considered as an intermediate. It is successively dehydrated into the first condensation product C8 (FAc), which can react with another furfural molecule forming the second condensation product C13 (F_2Ac). Additionally, the formation of a heavier reaction product $(FAc)_2$ may be observed as a result of the dimerization of the olefinic FAc molecule in the presence of acid sites, for example, over acidic zeolites [10]. Acetone self-condensation with the formation of diacetone alcohol, mesityl oxide, etc., can be considered as a competing parallel reaction route, which should be taken into account. In the present study, however, the acetone conversion by this reaction route was below 3%, which allowed us neglecting it.

Special experiments with K-IE-Y(15) and K-IE-Y(40) were performed to evaluate the possibility of leaching, i.e., the partial dissolution of potassium oxidic species in a reaction medium and, as a consequence, the occurrence of a homogeneous reaction. The comparison of K/Al ratio in the samples before and after catalytic run by XRF method proved a similarity in their chemical compositions. Additionally, the analysis of reaction mixture by ICP method at the end

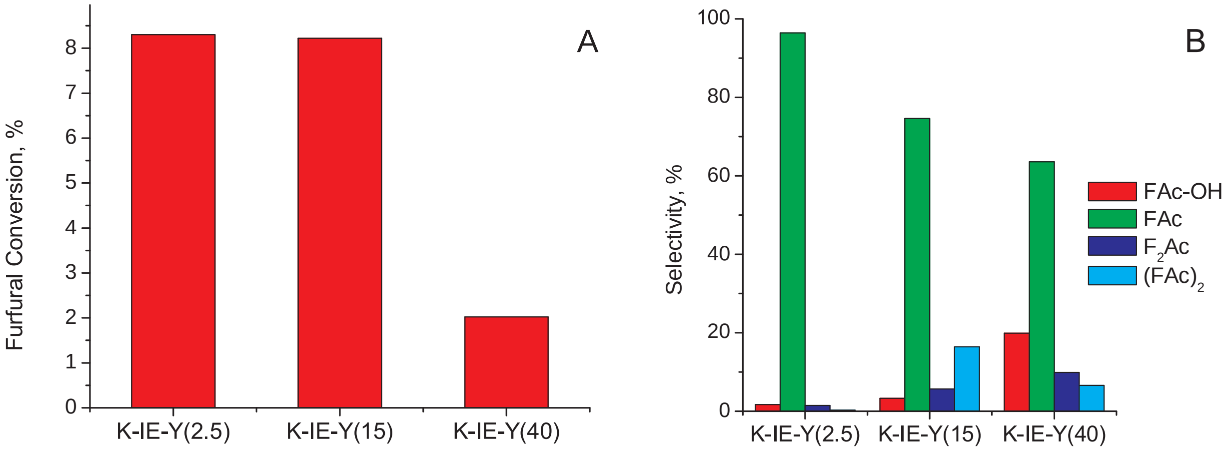

Fig. 6. Furfural conversion (A) and product selectivity (B) observed for ion-exchanged potassium Y zeolites.

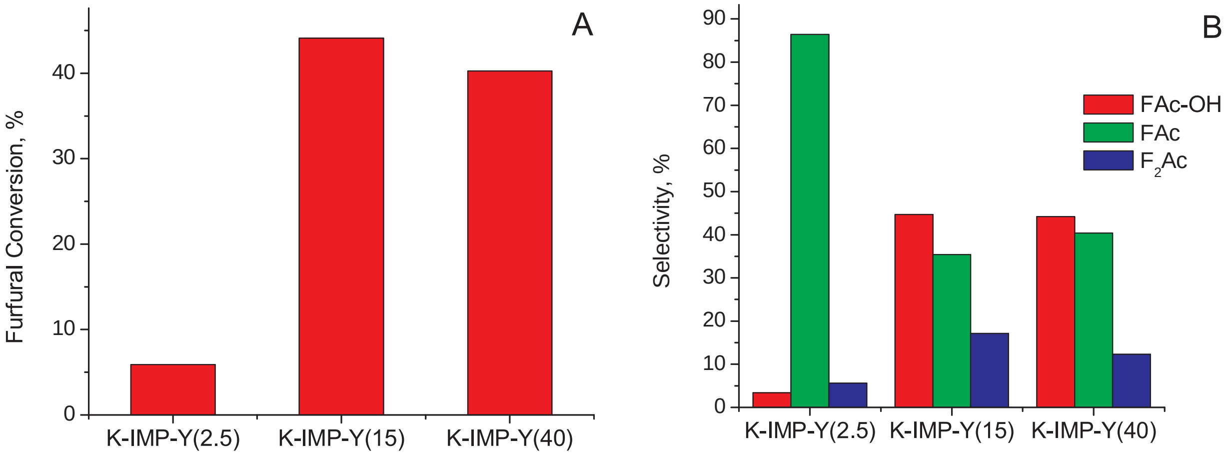

Fig. 7. Furfural conversion (A) and product selectivity (B) observed for impregnated potassium Y zeolites.

of a catalytic run and catalyst separation showed the absence of potassium in the organic phase. Based on these results it was concluded that furfural conversion and the composition of reaction products determined in performed catalytic experiments were concerned exclusively with the physico-chemical characteristics of the prepared zeolites.

Furfural conversion is 8.3% and 8.2% for K-IE-Y(2.5) and K-IE-Y (15), respectively (Fig. 6A). These values are lower than those obtained for acidic HY(2.5) zeolite (Fig. S7), but slightly higher than those observed for ion-exchanged K-BEA zeolites (being in the range of 4–5%) [4]. Furfural conversion on K-IE-Y(40) is substantially lower and does not exceed 2%.

Similarly to acidic zeolites (see the *SI*), FAc is the main reaction product obtained in aldol condensation of furfural and acetone on the ion-exchanged Y samples (Fig. 6B). Its selectivity is 96.4% on K-IE-Y (2.5) at 8.3% of furfural conversion, which could be the consequence of the successful FAcOH dehydration on the remaining acid sites present in the catalyst. The selectivity to F$_2$Ac, i.e. the second condensation product, as well as (FAc)$_2$, i.e. the dimerization product, is 1.5% and 0.3%, respectively. At similar conversion level (8.2%), selectivity to FAc on K-IE-Y(15) decreases to 74.6%, while that of FAcOH shows only slight increase to 3.3%. In contrast, the selectivity to bulkier compounds, F$_2$Ac and (FAc)$_2$, increases more significantly up to 5.7 and 16.4%, respectively, which could be related to a higher mesoporosity of this sample.

The conversion and selectivity over K-IE-Y(40) are slightly different from those over the K-IE-Y(15) sample (Fig. 6), which could be related to the lower density of both basic sites and residual acid sites in this catalyst (IR spectra have been presented in Fig. S5 of the *SI*). The latter are hardly detected by Py-FTIR in K-IE-Y(40), but their residual presence can be expected based on the catalytic data. It is evidenced from the ability to dehydrate the intermediate FAcOH to FAc (although the selectivity to FAcOH increases to 20% in this case) and the persistent presence of (FAc)$_2$ among reaction products. Notably, selectivity to F$_2$Ac observed on K-IE-Y(40) has the highest value of 10% among all ion-exchanged catalysts.

Most of the active sites participating in aldol condensation and further transformation of the primary products are in the supercages of FAU structure (both acidic and basic sites). Consequently, a difference in the composition of the reaction products formed on K-IE-Y(2.5) and K-IE-Y(15) or K-IE-Y(40) is concerned with the feasibility of the formation of the bulkier compounds under the steric constraints of the FAU structure or their ability to diffuse out from the supercages through the 12-rings (this will be discussed in more details in the discussion section). Furfural conversion on K-IMP-Y(2.5) is slightly higher in comparison with K-IE-Y(2.5), 5.9 and 8.3%, respectively (cf. Figs. 6 A and 7 A). The above-described characterization methods prove that the impregnation used for the preparation of K-IMP-Y(15) and K-IMP-Y (40), results in the formation of extra-framework potassium species (K/Al > 1), in contrast to K-IMP-Y(2.5), operating as strong basic sites. Consequently, furfural conversion on these impregnated catalysts increases to 44.1 and 40.3% (Fig. 7A), respectively, which is substantially higher in comparison with the ion-exchanged samples. Simultaneously, some changes in the composition of the reaction products were observed for K-IMP-Y(15) and K-IMP-Y(40) samples; the selectivity to FAc decreases to 35% and 40%, respectively, while selectivity to FAcOH and

F_2Ac increases accordingly (Fig. 7B). The increased FAcOH selectivity among the reaction products in the range of 44–45% implies that potassium species possess lower ability to dehydrate aldol (FAc-OH) in comparison with the residual acid sites. On the other hand, the basic sites derived from the potassium species favor the formation of F_2Ac. In addition, the impregnation step removes all residual Brønsted acid sites accessible to reactants, which is evidenced from the total absence of $(FAc)_2$ among the reaction products.

4. Discussion

Both acidic and basic sites in zeolite catalysts can catalyze aldol condensation. Data in Tables 2 and 3 evidence that catalysts prepared in present study contain both acidic and basic sites. It is therefore important to determine the contribution of each type of such sites to the catalytic performance of both ion-exchanged and impregnated zeolites. First of all, the low activity of K-IE-Y(40) in aldol condensation proves that the presence of either acidic or basic sites is necessary for the reaction to occur. Indeed, this catalyst possesses the lowest concentration of both acidic and basic sites and demonstrates the lowest activity with furfural conversion of 2.0%. In addition, Lewis acid sites can be excluded from further consideration since their concentration is the largest for K-IE-Y(2.5) and K-IMP-Y(2.5) in the range of 0.3-0.34 mmol/g (Table 2) while furfural conversion observed on these catalysts does not exceed 5.9-8.3% (Figs. 6 and 7). This result agrees with the conclusions from [12] that aldol condensation on acidic catalysts proceeds with the participation of Brønsted rather than Lewis acid sites. Therefore, differences in the catalytic performance of potassium-containing zeolites can be explained by considering the role of Brønsted acid sites and Brønsted and Lewis basic sites.

In our previous paper [4] we have shown that the increase in potassium content in ion-exchanged K-BEA zeolites decreased the concentration of Brønsted acid sites and, accordingly, resulted in a decline in furfural conversion. We concluded [12] that zeolites with decreased acidity and possessing intrinsic basicity (i.e. zeolites ion-exchanged with basic cations) possess poor activity in aldol condensation of furfural and acetone. A decrease in activity observed for ion-exchanged Y samples prepared in the present study in comparison with parent acidic Y zeolites confirms this conclusion (see Fig. 5 and Fig. S7 in the *SI*). Ion exchange results in the decreased Brønsted acidity of starting zeolites and creates an intrinsic basicity. As a consequence, a decrease in furfural conversion on the ion-exchanged zeolites is observed. The concentration of residual Bronsted acid sites which are not removed by the ion-exchange procedure in K-IE-Y(2.5) and K-IE-Y(15) is 0.2 and 0.03 mmol/g, correspondingly, while the concentration of these sites in K-IE-Y(40) is below the detection limit (Fig. 3 and Table 2). It allows concluding that the observed activity of the ion-exchanged zeolites in aldol condensation can be attributed to the residual acidity in these catalysts. Nevertheless, the possible contribution of the basic sites generated due to the ion-exchange procedure to the catalytic performance of these zeolites cannot be discarded.

CO_2-TPD data evidence the presence of a peak in the LT region of TPD curves for ion-exchanged zeolites (Fig. 5 and Table 3). Currently, it is impossible to answer unambiguously if this peak is characteristic exclusively for intrinsic basic sites. Nevertheless, independent on their origin, these sites in ion-exchanged catalysts have to be considered to participate in the reaction. Indeed, the comparison of two ion-exchanged USY catalysts shows that an increase in the concentration of LT sites from 0.3 to 0.9 μmol/g in K-IE-Y(40) and K-IE-Y(15), correspondingly (Table 3), results in the growth of furfural conversion from 2.0 to 8.2%, correspondingly. Therefore, the participation of these LT basic sites (instead of or together with acid sites) in aldol condensation can be expected.

Nevertheless, this conclusion should be made with care as K-IMP-Y (2.5) also contains even more similar LT basic sites (3.9 μmol/g), but the conversion of furfural on this catalyst is only 5.9%, i.e. lower than on K-IE-Y(15). Consequently, the comparison of the catalytic performance of K-IE-Y(2.5) and K-IE-Y(15) casts doubts on the participation of LT basic sites in aldol condensation. If so, only the residual concentration of acid sites determines the activity of ion-exchange Y zeolites in aldol condensation. Apparently, additional experiments are needed to determine the true role of intrinsic basic sites in zeolites in aldol condensation.

The presence of potassium in ion-exchanged zeolites has a significant effect on their catalytic performance, in terms of both activity and the composition of reaction products. Comparing the performance of the acidic and ion-exchanged catalysts derived from Y(2.5) zeolites (Fig. 6 and Fig.S7), it is seen that the presence of potassium in K-IE-Y (2.5) results in a slight decrease in the catalyst activity and prevents the formation of $(FAc)_2$ while the possibility to dehydrate of FAc-OH to FAc remains almost the same. Over HY(2.5), the dimer is formed with the participation of the accessible acid sites located in the supercages of Y zeolite. The Py-FTIR data (Fig. 3) evidence that ion exchange of protons with K^+ does not remove all acid sites, but the presence of larger potassium cations creates steric hindrances for the formation of bulky molecules formed in aldol condensation. Consequently, the conversion of furfural over K-IE-Y(2.5) sample in the reaction decreases, while the residual acid sites in the supercages are able to dehydrate FAc-OH to FAc, but the steric constraints prevent dimerization of FAc to bulky $(FAc)_2$. It is worth noting that selectivity to F_2Ac also decreases over K-IE-Y(2.5), supporting the proposed existence of steric constraints for the bulky reaction products to be formed on this catalyst.

Nevertheless, the consideration of the catalytic performance of Y zeolites based only on their acido-basic characteristics might be incomplete without taking into account other properties of the compared catalysts, e.g. the population of active centers in supercages or their textural properties. Comparing catalytic performance of HY(2.5) and HY(40) (see the SI, Fig. S7) shows that high furfural conversion on FAU zeolites can be achieved on a catalyst with significantly lower acidity. The increased values of both external surface area and total pore volume (Table 1) can explain the difference in the catalytic performance of the catalysts. On the other hand, the difference in furfural conversion and the composition of the reaction products observed for catalysts derived from Y(2.5) and USY zeolites depends on the possibility to form the reaction products, especially bulkier compounds, under the steric constraints of FAU structure or to diffuse from the supercages through 12-rings. The content of extra framework Al cations in HY(2.5) is substantially larger than in USY zeolites as evidenced by Py-FTIR data (Table 2). Presumably, these extra-framework Al cations may contribute to the creation of steric constraints at supercage windows and hinder diffusion of (bulkier) reaction products from the internal porous space. Additionally, the increased mesoporosity (Table 1) also favors diffusion of reaction products. Therefore, not only the total concentration of active sites (basic or acidic), but also their accessibility in the supercages, together with the possibility to form reaction products and to remove them from the supercages should determine the catalytic performance of Y zeolites.

The conversion of furfural on K-IE-Y(2.5) and K-IE-Y(15) is the same in the range of 8.2-8.3% (Fig. 6), nevertheless the concentration of residual acid sites in them differs by the factor of 7 (Table 2), and the concentration of potassium differs by the factor of 4.4 (Table 1). Hence, these significant differences in the concentration of both acid sites and intrinsic basic sites cannot explain the relatively high activity of K-IE-Y (15) in the reaction. The content of ion-exchanged cations in K-IE-Y(15) is too small to create steric constraints in supercages and to prevent either FAc interaction with another furfural molecule forming F_2Ac or FAc dimerization to $(FAc)_2$ on residual acid sites. Accordingly, the difference in the composition of the reaction products observed on K-IE-Y(2.5) and K-IE-Y(15) is related to either transition-state or product shape selectivity. However, it should be also considered that not all protons in supercages of the parent HY(15) can be exchanged with K^+. Thus, the contribution of the textural properties of zeolites with different Si/Al ratio to their catalytic performance cannot also be excluded to affect the reaction products distribution. Table 1 shows that micropore volumes of the K-IE-Y(2.5) and K-IE-Y(15) samples are quite similar, 0.301 and 0.302 cm^3/g, respectively, while their total pore volume differs significantly, 0.336 and 0.490 cm^3/g, respectively. Therefore, the lower number of acid and basic active sites in the K-IE-Y (15) could be compensated by its increased presence of mesopores, which makes the active sites in supercages more accessible for reactants and ensures a fast diffusion of the reaction products. In addition, mesopore surface contain high amount of OH groups connected with Si or Al in defective sites which can act as a weaker acid sites. These sites possess lower ability to dehydrate FAc-OH to FAc what is evidenced from the composition of reaction products at a similar furfural conversion level (Fig. 7B), so the strength of such defective acid centers should be lower than that of the conventional Brønsted sites residually present in K-IE-Y(2.5). Nevertheless, they are able to dimerize FAc and consequently the selectivity to $(FAc)_2$ attains 18% on K-IE-Y(15). The increase in the selectivity to the second condensation product F_2Ac from 1.5% to 5.8% is also in agreement with this assumption.

The amount of ion-exchanged potassium atoms in K-IE-Y(40) related with the amount of intrinsic basic sites is substantially lower in comparison with the above-discussed samples, and the concentration of the residual acid sites is lower than the detection limit. As a result of the very low number of both acid and basic active sites the conversion of furfural is very low (2%) despite the increased total pore volume of K-IE-Y(40) (total pore volume = 0.509 cm^3/g). Nevertheless, both F_2Ac and $(FAc)_2$ are also formed on K-IE-Y(40) with selectivity almost the same as for K-IE-Y(15). The obtained catalytic data suggest that a difference in the activity between the two ion-exchanged high-silica catalysts is caused by the difference in the population of active sites whose properties in the catalytic steps of aldol condensation are substantially similar.

The impregnation step substantially influences the properties of Y zeolites with different Si/Al ratio. Chemical analysis, CO_2 adsorption studies and IR spectroscopy prove the formation of K_2O species during decomposition of nitrates under the heat treatment of the impregnated K-IMP-Y(15) and K-IMP-Y(40). The CO_2-IR and CO_2-TPD results indicate that at least two types of basic sites are formed in the prepared zeolites after calcination. Upon CO_2 adsorption, chemisorbed carbonates with different symmetry were identified (see the *SI*) and two desorption peaks, low (T = 50 °C) and high (T = 135 °C) temperature peaks, were observed on the CO_2-TPD curves of impregnated K-IMP-Y (15) and K-IMP-Y(40) samples (Fig. 5). Unlike these samples, no excessive strong basic sites are present in K-IMP-Y(2.5) (Figs. 4 and 5) while the concentration of the residual acid sites decreases from 0.2 to 0.1 mmol/g (Table 3) as compared with the K-IE-Y(2.5) sample. As discussed above, a limited number of hydrated potassium cations can be located inside the supercages of HY zeolite during either IE or IMP stages, so not all protons located in the supercages are exchanged with potassium cations during ion-exchange in aqueous solution. Consequently, a part of Brønsted acid sites are still remaining in the micropore volume and no K_2O species are formed after the thermal activation of K-IMP-Y(2.5) due to solid-state ion-exchange. The acid-base properties of this catalyst result in further decrease of the furfural conversion in comparison with the K-IE-Y(2.5), while the composition of the reaction products remains unchanged: these consist of FAc as the main reaction product with a low content of FAcOH and F_2Ac. The decreased ion-exchange capacity of the dealuminated Y zeolites leads to a possibility to accumulate more KNO_3 molecules inside the supercages without an ion-exchange step. After the heat treatment of K-IMP-Y(15) and K-IMP-Y(40), these excessive nitrates are transformed to K_2O species located inside the porous structure of the catalysts. The amount of the internal K_2O species inside the zeolite Y supercages is the most important parameter affecting both the CO_2 adsorption capacity and the catalytic performance of the impregnated dealuminated Y samples. The basic sites derived from potassium species (i.e., K_2O) favor aldol condensation of furfural and acetone and the occurrence of the second condensation step resulting in the formation of F_2Ac (Fig. 7). In addition, due to the impregnation, all residual Brønsted acid sites in the dealuminated zeolites are removed (the proton is possibly replaced by a potassium cation) as evidenced by the total absence of $(FAc)_2$ among reaction products and by the Py-FTIR data (Table 2). Nevertheless, these basic sites possess lower dehydration ability in comparison with the acid sites, as evidenced when comparing the performance of K-IMP-Y(2.5) and the impregnated catalysts based on the dealuminated Y zeolites. The combination of both types of active sites could be essential for the effective occurrence of aldol condensation of furfural and acetone in the presence of potassium-containing zeolites: the basic sites ensure effective aldol condensation between aldehyde and ketone while the acid sites are responsible for the dehydration of the intermediate aldol.

As discussed above, the participation of intrinsic basic sites in aldol condensation cannot be totally excluded. Nevertheless, the activity of impregnated K-IMP-Y(15) and K-IMP-Y(40) catalysts in the reaction is substantially larger. Extra-framework K_2O species formed after the calcination of BEA zeolites impregnated with potassium nitrate were shown to be responsible for the enhanced catalytic activity of the catalysts [4]. Similarly, strong basic sites which are characterized by the HT peak in the CO_2-TPD curve contribute substantially to the catalytic performance of K-IMP-Y(15) and K-IMP-Y(40). The concentration of the HT basic sites in these catalysts is 66 and 64 μmol/g what is substantially larger than the concentration of LT basic sites (Table 3). Comparing acido-basic properties of different samples (Tables 2 and 3) with their catalytic performance (Figs. 5 and 6), both types of basic sites can be responsible for the catalytic performance of the prepared catalysts. In this case, different furfural conversion observed for ion-exchanged and impregnated catalysts could be concerned with the different concentration of LT and HT basic sites rather than with their strength. However, as discussed above, the role of the LT basic sites cannot be unequivocally determined because of the influence of the residual acid sites in the ion-exchanged samples.

Several types of basic sites which differ in their strength are also present in hydrotalcite-based materials which are well-known and widely used as catalysts for base-catalyzed reactions, such as aldol condensation. Nevertheless, there is not agreement in open literature, which kind of basic sites in the hydrotalcite-based materials are responsible more for the occurrence of the reaction. Díez et al. [39] suggested that the rate-limiting step of aldol condensation is the abstraction of proton from the acetone molecule that is essentially promoted by strong basic sites. Ordóñez et al. [40] also suggested that aldol condensation of furfural and acetone requires high density of strong basic sites. In contrast, Faba et al. [41] proposed that the rate-determining step of the reaction is promoted by medium-strength basic sites. Smoláková et al. [6] also found that higher furfural conversion was observed for catalysts with higher population of sites with medium strength. Based on these considerations, it is hardly possible to attribute the catalytic performance of impregnated K-USY zeolites to either LT or HT basic sites. Moreover, the unambiguous assignment of these two peaks is not yet clear. It can be proposed that they reflect either different nature of basic sites (intrinsic vs. oxidic), or different location of the K_2O clusters (i.e. on the external or internal surface of the zeolite crystals) or the adsorption mode of CO_2 on them (e.g. various symmetry of bidentate species). The former proposal is supported by the TPD patterns in which only a negligible LT peak is observable for K-IMP-Y (2.5) while the other potassium-impregnated samples exhibit strong LT and HT peaks.

A comparison of the results on potassium-containing Y zeolites obtained in the present work with those obtained in a previous study on potassium-modified BEA zeolites [4] indicates a similarity in the performance of both groups of basic materials. Regardless their structural type, potassium-containing zeolites prepared by ion exchange exhibit poor activity in aldol condensation of furfural and acetone, which may be attributed either to weak strength of the “intrinsic” basic sites or their low concentration. In contrast, the activity of catalysts prepared by impregnation is significantly higher due to the abundant presence of bulky potassium species (mainly K_2O clusters) in the porous space of zeolites. As the amount, size and distribution of these species in the catalysts are concerned, the performance of the impregnated zeolites in aldol condensation should depend on the parameters of a crystalline framework. Indeed, when comparing the performance of impregnated BEA [4] and Y zeolites (this study) with similar potassium content, differences in both furfural conversion and selectivity can be observed. Nevertheless, the activity of the basic zeolites in aldol condensation is lower compared to that of reconstructed hydrotalcites (HTCs), because furfural conversion on the latter catalysts attains 100% already after 10–20 min of the reaction at T = 25 °C [42] proving higher efficiency of Brønsted basic sites in HTCs compared to bulky potassium species in zeolites. Additionally, the selectivity to the reaction products observed on these two types of basic materials also differs: consecutive condensation steps occur readily on HTCs with opened layer structure [43] and in a significantly larger extent than on basic zeolites, even if they possess wide-pore 3D channel system with the pore opening of 0.7–0.8 nm. Nevertheless, the steric constrains imposed by zeolite pores could be advantageous in aldol condensation if high selectivity to the first condensation product is desired. The chemical stability of basic catalysts under the influence of reaction mixture is another issue to be addressed. It was shown that metal leaching could be discarded for both hydrotalcites and derived mixed oxides [15,42] and basic zeolites [4]. The absence of leaching effect was confirmed for the catalysts used in the present study, as described above. Therefore, for zeolite catalysts, the observation could be indeed attributed to the improved stability of potassium species trapped in the zeolitic porous space. Nevertheless, the stability of the entrapped oxidic potassium species in aqueous organic medium needs to be yet determined. The main cause of deactivation during aldol condensation is the formation of carbonaceous deposits. This deactivation is most severe with proton-form zeolites due to the oligomerization reactions taking place on the acid sites [10]. It leads to complete blocking of the porous system. On the other hand, coking is substantially diminished when using potassium-modified zeolites [4]. Hydrotalcites can keep their activity during the build-up of heavier products, but eventually they lose their activity rather rapidly [43]. Their regeneration is not straightforward and well-understood as it requires combining oxidation and rehydration cycles under controlled atmosphere to remove coke and restore the active hydrotalcite structure, respectively. From another hand the advantage of zeolite-based catalysts dwells in their rather facile regeneration during which stable but slightly lower activity than that of the fresh potassium zeolite can be maintained [4].

5. Conclusions

The results of the current work can be summarized as follows:

1. The chemical composition of parent HY zeolites influences significantly the content of potassium in samples prepared by ion exchange and impregnation. While K-HY samples with molar ratio Si/Al = 2.5 prepared by either ion exchange or impregnation had very similar K content, the impregnated HUSY zeolites (Si/Al = 15 and 40) contained significantly more potassium in comparison with their ion-exchanged counterparts. The difference is related with the amount of proton sites located in the supercages and potentially available for the ion exchange: i.e. the larger the population of the proton sites in the supercages, the larger the amount of the ion-exchanged potassium ions and the lower the probability for bulky potassium species to be formed after the impregnation step.
2. Y zeolites prepared by ion-exchange are active in aldol condensation of furfural and acetone, so the participation of intrinsic basic sites in zeolites may be assumed in the reaction. Nevertheless, these catalysts also contain residual acid sites which are also active in the reaction. Hence, the true the intrinsic activity of the intrinsic basic sites cannot be easily assessed.
3. The USY zeolites impregnated with potassium exhibited higher catalytic activity in aldol condensation of furfural and acetone in comparison with the ion-exchanged catalysts. The catalytic data together with catalysts characterization results allow concluding that potassium species formed by the thermal decomposition of nitrates are strong basic sites and mostly contribute to the catalytic activity of the impregnated USY zeolites due to their strength and high concentration. An additional advantage of these catalysts stems from their increased mesoporosity which can facilitate mass transfer of both reactants and reaction products.
4. The impregnated low-aluminum K-Y zeolites possessed the highest selectivity to FAcOH and F_2Ac, while the impregnated K-Y(2.5) produced FAc as the main reaction product formed by the dehydration of FAcOH. These features are related to the fast dehydration of FAcOH on the residual acidic sites of K-IMP-Y(2.5) or the fast occurrence of the second condensation step on the strong basic sites of the impregnated K-Y(15) and K-Y(40) zeolites, correspondingly.

Acknowledgement

The authors thank the Czech Science Foundation for the support (P106/12/G015).

Appendix A. Supplementary data

Supplementary data associated with this article can be found, in the online version, at http://dx.doi.org/10.1016/j.apcata.2017.09.017.

References

[1] A. Demirbas, Progress Energy Combust. Sci. 31 (2005) 171–192.
[2] P. McKendry, Bioresour. Technol. 83 (2002) 47–54.
[3] G.W. Huber, J.N. Chheda, C.J. Barrett, J.A. Dumesic, Science 308 (2005) 1446–1450.
[4] O. Kikhtyanin, R. Bulánek, K. Frolich, J. Čejka, D. Kubička, J. Mol. Catal. A: Chem. 424 (2016) 358–368.
[5] M.J. Climent, A. Corma, S. Iborra, Green Chem. 16 (2014) 516–547.
[6] L. Smoláková, K. Frolich, J. Kocík, O. Kikhtyanin, L. Čapek, Ind. Eng. Chem. Res. 56 (2017) 4638–4648.
[7] A.T. Nielsen, W.J. Houlihan, The Aldol Condensation, John Wiley & Sons, New Jersey, 1968.
[8] B.A. Hathaway, J. Chem. Educ. 64 (1987) 367.
[9] I. Sádaba, M. Ojeda, R. Mariscal, R. Richards, M.L. Granados, Catal. Today 167 (2011) 77–83.
[10] O. Kikhtyanin, V. Kelbichová, D. Vitvarová, M. Kubů, D. Kubička, Catal. Today 227 (2014) 154–162.
[11] D.N. Thanh, O. Kikhtyanin, R. Ramos, M. Kothari, P. Ulbrich, T. Munshi, D. Kubička, Catal. Today 277 (2016) 97–107.
[12] O. Kikhtyanin, D. Kubička, J. Čejka, Catal. Today 243 (2015) 158–162.
[13] K.K. Rao, M. Gravelle, J.S. Valente, F. Figueras, J. Catal. 173 (1998) 115–121.
[14] E. Suzuki, Y. Ono, Bull. Chem. Soc. Japan 61 (1988) 1008–1010.
[15] L. Hora, O. Kikhtyanin, L. Čapek, O. Bortnovskiy, D. Kubička, Catal. Today 241 (2015) 221–230.
[16] C. Xu, Y. Gao, X. Liu, R. Xin, Z. Wang, RSC Adv. 3 (2013) 793–801.
[17] S. Abelló, D. Vijaya-Shankar, J. Pérez-Ramírez, Appl. Catal. A: Gen. 342 (2008) 119–125.
[18] M. Moliner, C. Martínez, A. Corma, Angew. Chem. Intern. Ed. 54 (2015) 3560–3579.
[19] M.V. Opanasenko, W.J. Roth, J. Čejka, Catal. Sci. Technol. 6 (2016) 2467–2484.
[20] D. Kubička, I. Kubičková, J. Čejka, Catal. Rev. 55 (2013) 1–78.
[21] C. Flego, C. Perego, Appl. Catal. A: Gen. 192 (2000) 317–329.
[22] A. Ungureanu, S. Royer, T.V. Hoang, D. Trong On, E. Dumitriu, S. Kaliaguine, Micropor. Mesopor. Mater. 84 (2005) 283–296.
[23] T. Tago, H. Konno, M. Sakamoto, Y. Nakasaka, T. Masuda, Appl. Catal. A: Gen. 403 (2011) 183–191.
[24] O. Kikhtyanin, P. Chlubná, T. Jindrová, D. Kubička, Dalton Trans. 43 (2014) 10628–10641.
[25] E.J. Rode, P.E. Gee, L.N. Marquez, T. Uemura, M. Bazargani, Catal. Lett. 9 (1991) 103–114.
[26] C.O. Veloso, J.L.F. Monteiro, E.F. Sousa-Aguiar, Stud. Surf. Sci. Catal. 84 (1994) 1913–1920.
[27] J. Li, J. Tai, R.J. Davis, Catal. Today 116 (2006) 226–233.

[28] S.K. Sharma, P.A. Parikh, R.V. Jasra, J. Mol. Catal. A: Chem. 278 (2007) 135–144.

[29] S. Bordiga, C. Lamberti, F. Bonino, A. Travert, F. Thibault-Starzyk, Chem. Soc. Rev. 44 (2015) 7262–7341.

[30] L. Lutterotti, R. Ceccato, R.D. Maschio, E. Pagani, Mater. Sci. Forum 93 (1998) 278–281.

[31] L. Lutterotti, S. Gialanella, Acta Mater. 46 (1998) 101–110.

[32] M. Guisnet, P. Ayrault, J. Datka, Pol. J. Chem. 71 (1997) 1455–1461.

[33] A. Dyer, Stud. Surf. Sci. Catal. 157 (2005) 181–204.

[34] T.C. Keller, M. Položij, B. Puértolas, H.V. Thang, P. Nachtigall, J. Pérez-Ramírez, J. Phys. Chem. C 120 (2016) 4954–4960.

[35] Z.-Q. Zou, M. Meng, J.-J. He, Mater. Chem. Phys. 124 (2010) 987–993.

[36] M.A. Peralta, B.S. Sánchez, M.A. Ulla, C.A. Querini, Appl. Catal. A: Gen. 393 (2011) 184–188.

[37] S. Morin, A. Berreghis, P. Ayrault, N. Gnep, M. Guisnet, J. Chem. Soc. Faraday Trans. 93 (1997) 3269–3275.

[38] Q. Liu, A. Mace, Z. Bacsik, J. Sun, A. Laaksonen, N. Hedin, Chem. Commun. 46 (2010) 4502–4504.

[39] V.K. Díez, C.R. Apesteguía, J.I. Di Cosimo, J. Catal. 240 (2006) 235–244.

[40] S. Ordóñez, E. Díaz, M. León, L. Faba, Catal. Today 167 (2011) 71–76.

[41] L. Faba, E. Díaz, S. Ordóñez, Appl. Catal. B: Environ. 113–114 (2012) 201–211.

[42] O. Kikhtyanin, Z. Tišler, R. Velvarská, D. Kubička, Appl. Catal. A: Gen. 536 (2017) 85–96.

[43] O. Kikhtyanin, L. Hora, D. Kubička, Catal. Commun. 58 (2015) 89–92.

Catalysis Today 223 (2014) 138–147

Contents lists available at ScienceDirect

Catalysis Today

journal homepage: www.elsevier.com/locate/cattod

Aldol condensation of furfural and acetone over Mg—Al layered double hydroxides and mixed oxides

Lukáš Hora[a,*], Vendula Kelbichová[a], Oleg Kikhtyanin[a], Oleg Bortnovskiy[b], David Kubička[a]

[a] Research Institute of Inorganic Chemistry, UniCRE-RENTECH, Areál Chempark Záluží, 436 70 Litvínov, Czech Republic
[b] Eurosupport Manufacturing Czechia, Areál Chempark Záluží, 436 70 Litvínov, Czech Republic

ARTICLE INFO

Article history:
Received 7 February 2013
Received in revised form 26 August 2013
Accepted 5 September 2013
Available online 14 October 2013

Keywords:
Aldol condensation
Hydrotalcites
Mixed oxides
Furfural
Renewables

ABSTRACT

Liquid phase aldol condensation of furfural and acetone catalyzed by solid base catalysts (Mg—Al hydrotalcites and Mg—Al mixed oxides) has been investigated as a method to valorize short chain ketones obtainable from biomass pyrolysis for the production of higher-molecular-weight products usable as fuel components. The Mg/Al molar ratios of the investigated catalysts was varied in the range from 2 to 4 and their catalytic activity was tested at different reaction temperatures (20–100 °C) using several activation methods. Mg—Al hydrotalcites were used either after calcination as mixed oxides or after subsequent contact with liquid water or steam as rehydrated materials.

Both furfural-acetone condensation products, i.e. C_8 and C_{13}, were the desired products of aldol condensation reaction. Higher reaction temperature facilitated the dehydration step and enhanced the catalyst selectivity to both dehydrated products (C_8 and C_{13}). The best results were achieved with calcined catalyst sample having Mg/Al molar ratio equal to 3 at 100 °C (>95% furfural conversion and >90% selectivity to the desired products). The selectivity to the main by-product, diacetone alcohol, did not exceed 5% in any experiment. The ex situ rehydration of the calcined samples resulted in catalysts with a significantly lower activity, except the catalyst with Mg/Al molar ratio equal to 2. On the other hand, in situ rehydration caused catalyst activity improvement only in the case of the sample with Mg/Al molar ratio 3.

1. Introduction

The extensive use of fossil fuels has been a cornerstone of the rapid development during twentieth century, but it has also resulted in many adverse environmental impacts. Consequently, enormous research focus has recently been directed toward the sustainable utilization of renewable resources in an attempt to replace at least partially the finite fossil fuels resources [1,2]. The primary objective of these efforts is to maximize the sustainable utilization of biomass-derived feedstocks while minimizing environmental impacts (CO_2 emissions, loss of diversity, etc.) and avoiding competition with food and fodder production. It is particularly desirable to produce liquids fungible with conventional fuels and chemicals production from non-food crops [3–5].

A promising route to using the chemical potential of cellulose-rich feedstocks is their hydrolysis yielding furfural or hydroxymethylfurfural that are often denoted as platform chemicals [6–8]. For example, furfural can be obtained by acid hydrolysis of sugar cane bagasse, a residue from sugar cane processing, followed by extraction [9]. To exploit the full potential of furfural as a platform chemical its transformation by aldol condensation with acetone followed by hydrogenation/deoxygenation has been proposed to afford hydrocarbons, namely C_8 and C_{13} alkanes [10].

Typically, aldol condensation is catalyzed by homogenous base catalysts, such as sodium and calcium hydroxide. However, these processes generate significant waste water streams that must be treated (neutralized and cleaned) [10]. Apart from the negative environmental impact, the production cost is affected adversely. Consequently, many researchers focus on developing a new active and stable solid base catalyst (such as MgO [11], MgO—ZrO [10,12], ZnO, TiO_2 [13]) to replace the generally used homogenous catalysts [14,15]. Among the solid base catalysts, layered double hydroxides (LDH) also known as anionic clays or hydrotalcite like materials (HTC) have been also reported to be promising aldolization catalysts [16–19]. The main advantages of heterogeneous catalysts over homogeneous ones include easier catalyst recovery and recycling resulting in mitigation of the adverse environmental impacts, such as waste water treatment, and elimination of corrosion problems to name the most significant ones.

---

* Corresponding author.
E-mail address: lukas.hora@vuanch.cz (L. Hora).

0920-5861/$ – see front matter © 2013 Elsevier B.V. All rights reserved.
http://dx.doi.org/10.1016/j.cattod.2013.09.022

The name “hydrotalcites” is reserved for solids having structure closely related to that of the mineral hydrotalcite, that is, rhombohedral $Mg_6Al_2(OH)_{16}CO_3{\cdot}4H_2O$. Hydrotalcites consist of a brucite-like $[Mg(OH)_2]$ network wherein isomorphous substitution of Mg^{2+} ion by a trivalent cation M^{3+} occurs and the excess positive charge is compensated by gallery anions which are located in the interlayer along with water molecules [20–22]. The Mg—Al LDH can be used as catalysts either in the form of mixed oxides Mg(Al)O obtained by the calcination of an Mg—Al hydrotalcite precursor or in the rehydrated form of these calcined materials [23].

The aim of this work is to describe the effect of pretreatment of the hydrotalcite-based catalysts on their activity and selectivity in aldol condensation of furfural with acetone. Besides calcination of the hydrotalcite precursor, different rehydration procedures (ex situ vs. in situ and liquid vs. gas phase) have been performed and their impact on the yield of the desired aldol condensation products has been determined. Moreover, the effect of the Mg/Al ratio has been studied as well.

2. Experimental and materials

2.1. Materials

Mg—Al layered double hydrotalcites (LDH) with Mg/Al molar ratio ranging from 2:1 to 4:1 were provided by Eurosupport Manufacturing Czechia (ESMC). One sample, denoted HTC-feed, was used as a reference material. Their properties and activation procedures are described below. Furfural (Acros Organics, 99%) and acetone (Lach:Ner, p.a.) were used in the experiments.

2.2. Catalysts activation

Three different activation procedures were applied to transform the as-supplied LDH materials into catalysts–calcination, ex situ rehydration of the calcined material and in situ rehydration of the calcined material. The calcination of LDH was performed at 450 °C in air and mixed Mg—Al oxide catalysts were obtained. The temperature during calcination was raised at the rate of 10 °C/min to reach 450 °C and maintained at the final temperature for 16 h. The calcined mixed oxides were used as catalysts in aldol condensation reaction directly or after rehydration.

The ex situ rehydration was carried out either in liquid or gas phase. The liquid phase ex situ rehydration was performed in a stirred flask using demineralized water at 20 °C for 2 h under inert atmosphere (N_2). After the activation, the catalyst was separated by filtration and dried under vacuum at 60 °C for 2 h. The gas phase ex situ rehydration was carried out in a glass tube at 50 °C under flow of nitrogen gas saturated with water vapor for 16 h. The flow of wet nitrogen of 6 L/h was maintained for the specified period (16 h for 5 g of catalyst). Both types of ex situ treatments lead to full rehydration of the calcined materials (mixed oxides). The amount of water needed for the full rehydration of the mixed oxides was approximately 1 g of water per 1 g of mixed oxides.

The in situ rehydration was carried out only in liquid phase. It was achieved by addition of a small amount of demineralized water (0.2 mL) into the reaction mixture before immersing the calcined catalyst into the reactor. In this case, approximately 10% wt. of the mixed oxides was rehydrated.

The list of all tested catalysts including their names and activation procedure is shown in Table 1.

Table 1
List of the catalysts used for catalytic tests.

Catalyst name	Activation procedure
Cal. HTC-feed	Calcination
Cal. HTC 2:1	Calcination
Cal. HTC 3:1	Calcination
Cal. HTC 4:1	Calcination
ExWR HTC-feed	Full ex situ rehydration in liquid water
ExWR HTC 2:1	Full ex situ rehydration in liquid water
ExWR HTC 3:1	Full ex situ rehydration in liquid water
ExWR HTC 4:1	Full ex situ rehydration in liquid water
ExVR HTC-feed	Full ex situ rehydration in water vapor
ExVR HTC 2:1	Full ex situ rehydration in water vapor
ExVR HTC 3:1	Full ex situ rehydration in water vapor
ExVR HTC 4:1	Full ex situ rehydration in water vapor
InWR HTC-feed	Partial in situ rehydration in liquid water
InWR HTC 2:1	Partial in situ rehydration in liquid water
InWR HTC 3:1	Partial in situ rehydration in liquid water
InWR HTC 4:1	Partial in situ rehydration in liquid water

2.3. Catalysts characterization

The catalysts were characterized by several techniques to assess their structure, composition, surface area and pore volume. The crystallographic structures of dried LDH catalysts were determined by X-ray powder diffraction using a Philips MPD 1880, working with the Cu—K_α line ($\lambda = 0.154$ nm) in the 2Θ range of 5°–70° at a scanning rate of 2Θ of 2.4°/min. The elemental composition was determined by X-ray fluorescence using Philips PW 1401 equipped with an Rh RTG lamp. The UniQuant program was used to evaluate the results. The textural properties of the catalysts (specific surface area and pore volume) were measured by nitrogen physisorption at −196 °C using a Micromeritics ASAP 2020 surface area and porosity analyzer. The plausible leaching of the main metals (Mg, Al) from the catalysts into the reaction mixture during the reaction was evaluated by ICP–OES equipment.

Thermogravimetric analysis of the dried LDH catalysts was performed using a TA Instruments TGA Discovery series equipment and operating at heating ramp of 10 °C/min from room temperature to 900 °C in flowing nitrogen (20 mL/min, Linde 3.0). Approximately 15 mg of sample was heated in an open alumina crucible.

2.4. Reaction studies

The experiments were carried out in a 100 mL stirred batch reactor (a glass flask reactor for experiments at up to 50 °C, an autoclave for experiments at temperatures above 50 °C) in liquid phase. Before the start of an experiment, 2 g of catalyst was mixed together with a stirred mixture of 39.5 g acetone and 6.5 g furfural (acetone/furfural molar ratio 10:1, pre-heated to the desired reaction temperature in range from 20 to 100 °C) and kept at this temperature for 2 or 24 h under intensive stirring.

The experiments were carried out at the strictly controlled conditions. Every time the same heating rate of 5 °C per minute was used. The experiments carried out at up to 50 °C were performed with the catalyst added into the reaction mixture after reaching of the reaction temperature. The experiments carried out at 100 °C were performed with the presence of catalyst in reaction mixture from the beginning of the heating. No overshooting of the target temperature was observed.

The used acetone/furfural molar ratio and the absolute amounts of the reactants could result, in the case of complete conversion of furfural, in the formation of approximately 0.8 g of water. This amount of water equals approximately to 40% of the amount needed for a full rehydration of the mixed oxides (calcined hydrotalcites).

The samples of reaction mixtures were withdrawn from the reactor during the experiment at certain reaction times, filtered, and analyzed by an Agilent 7890A gas chromatograph equipped with a flame ionization detector (FID), using a HP 5 capillary column (30 m/0.32 mm ID/0.25 μm).

Table 2
Chemical composition of the catalysts.

Parameter/sample	Unit	HTC-feed	HTC 2:1	HTC 3:1	HTC 4:1
MgO	wt.%	50.5	59.07	70.86	75.25
Al_2O_3	wt.%	27.2	37.42	27.78	23.45
SiO_2	wt.%	0.19	0.23	0.37	0.25
CaO	wt.%	<0.01	1.09	0.43	0.52
TiO_2	wt.%	<0.01	0.31	0.05	0.29
Fe_2O_3	wt.%	0.10	1.18	0.14	0.14
Mg: Al	mol/mol	2.35	2.0	3.25	4.1

Table 3
Main textural characteristics of the catalysts.

Catalyst form	Dried		Calcined		Spent
Parameter Sample/unit	Specific area (BET) m^2/g	Pore volume cm^3/g	Specific area (BET) m^2/g	Pore volume cm^3/g	Specific area (BET) m^2/g^{-1}
HTC-feed	149.0	0.42	185.3	0.40	–
HTC 2:1	137.2	0.31	170.9	0.30	63.9
HTC 3:1	128.8	0.32	164.3	0.33	28.2
HTC 4:1	121.2	0.31	159.1	0.31	71.3

3. Results and discussion

3.1. Characterization of the catalyst

The catalytic materials were characterized in the as-obtained form to determine their composition (Table 2) and textural properties (Table 3). The main impurities in most of the samples were Fe, Ca, Ti, Si, particularly in the HTC 2:1 sample. On the other hand, the reference sample denoted HTC-feed was virtually free of all impurities, besides traces of Si and Fe. The pore volume of the HTC 2:1 to 4:1 samples was almost identical, around 0.31 cm^3/g, regardless the variation in Mg/Al ratio while the sample HTC-feed exhibited about 30% higher pore volume, 0.42 cm^3/g (Table 3). The specific surface areas of all dried samples were within the range 120–150 m^2/g, while the calcined samples exhibited specific surface areas in the range 159–186 m^2/g. Surprisingly, the sample HTC 2:1 exhibited about 30% higher BET surface area than HTC 3:1 and HTC 4:1 despite the fact that they all showed the same pore volume. This indicates that HTC 2:1 has a smaller particle size than the other two catalysts.

The structural data were obtained both for as-obtained (dried) and calcined catalysts – Figs. 1 and 2. A clear difference among the studied samples can be observed in case of the dried samples. In particular, the sample HTC-feed differs from the other samples as it has fewer distinguishable diffraction lines which indicate a lower degree of crystallinity. On the other hand, the HTC 2:1 shows a well-developed and characteristic hydrotalcite diffractogram (Fig. 1). With the increasing Mg/Al ratio, the clarity of diffractograms decreases which can be attributed to a lower crystallinity of these samples. Moreover, the XRD data indicate also the presence of other crystalline phases, namely MgO and $Mg(OH)_2$. The shape of the diffraction line belonging to MgO (at 43°) is virtually identical for HTC 2:1–4:1 indicating that the MgO crystallites are approximately of the same size. On the other hand, the line is significantly broadened in HTC-feed, which suggests that the MgO crystallites are smaller in this sample than in the other hydrotalcites.

The XRD patterns of the calcined samples (Fig. 2) indicate the presence of MgO crystalline phase only. While the shapes of the diffraction lines of HTC 2:1–4:1 are practically the same, reference sample HTC-feed shows dramatically wider and lower peaks. This indicates, in accordance with XRD patterns of dried sample, that HTC-feed is less crystalline than the other samples.

The TGA–DTA peaks obtained from the thermal analysis studies of the dried LDH catalysts are presented in Fig. 3 and Table 4. The course of the TGA curves exhibited a gradual weight loss process with two main events that are reflected as peaks in the DTA. In general, for all the hydrotalcite samples, the first step involves loss of interlayer water that occurs in between ambient temperature and about 125 °C. Dehydration takes place in two minor steps followed by a step at around 200 °C. The third step corresponds to the loss of OH^- groups and decomposition of $CO_3{}^{2-}$ in the LDH structure and can be observed at around 380–400 °C [26].

Table 4
TGA analysis of dried LDH catalysts.

Sample	1st peak (°C)	2nd peak (°C)	Weight loss		Residue
			30–450 °C	450–900 °C	
HTC feed	205	388	21.80%	0.41%	77.79%
HTC 2:1	105	330	17.15%	2.35%	80.50%
HTC 3:1	105	396	29.47%	3.48%	67.05%
HTC 4:1	113	388	23.43%	3.14%	73.43%

In our case the shapes of the TGA curves and the positions of the DTA peaks demonstrate differences among the used materials. The similar shape of the curves of the samples HTC 3:1 a HTC 4:1 suggest their similar structure (XRD patterns of these LDH materials are also similar, Fig. 1), differences are only in the total weight loss. The indistinctive course of the thermal analysis of the sample HTC 2:1 (as clearly visualized by the DTA peaks) was not expected, because its XRD patterns suggested the best hydrotalcite structure. This sample had the lowest weight loss from all the tested samples. Although the sample HTC feed did also not show a very indistinctive TGA curve, the DTA curves exhibit the presence of the two peaks characteristic for LDH.The catalysts were also analyzed by the XRD and TGA after their use in aldol condensation. The XRD results of calcined catalysts used at low reaction temperatures did not show any significant differences in the catalyst structures. The only crystalline phase observed was the MgO crystalline phase. The amount of water that can be produced in the reaction may be estimated as 0.4 g (furfural conversion about 50%), which is 20% of the catalyst weight and full re-hydration necessitates the water amount to be 100% of the catalyst weight. In line with this, the TGA results confirmed partial re-hydration of catalysts by the reaction water. The TGA results also indicated that there were not any carbonaceous deposits on the spent catalysts. Nonetheless, the specific surface of the spent catalysts significantly decreased (below 100 m^2/g). The leaching of the main elements, Mg and Al, was checked by ICP analysis of the reaction products mixtures. In all cases the content of Mg and Al in the obtained liquid products was below the detection limit of 20 mg/kg which corresponds to 0.15% of the mass of the

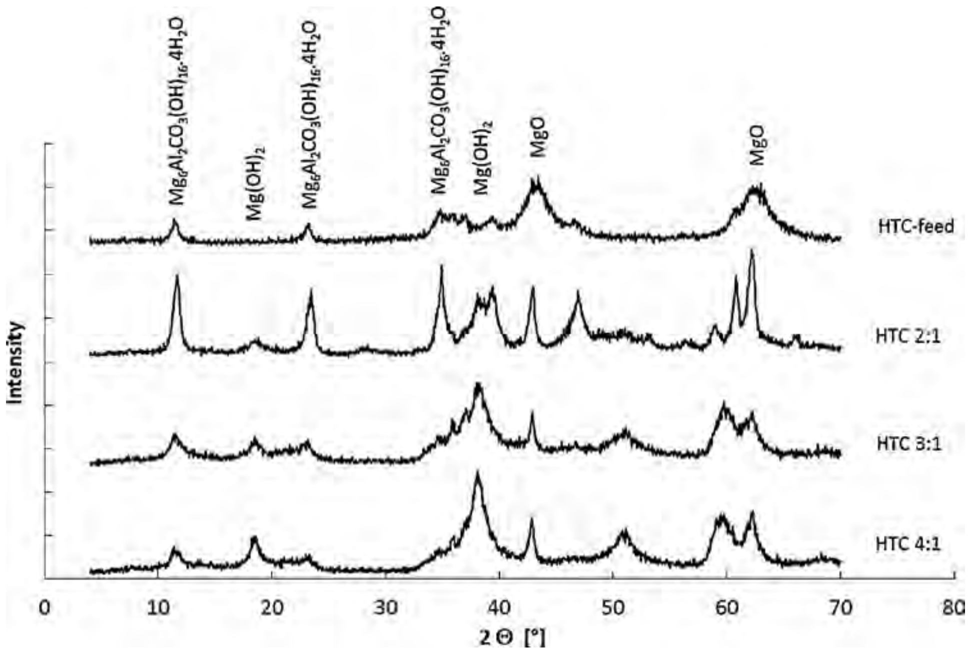

Fig. 1. X-ray diffraction patterns of the dried hydrotalcites.

used catalyst being present or dissolved in the total liquid reaction product.

3.2. Aldol condensation of furfural and acetone

3.2.1. Basic reaction behavior

The influence of the reaction temperature and time on furfural conversion and catalyst selectivity in the range 25–56 °C (reflux temperature) is shown in Fig. 4. Both reaction temperature and time have significant effect on the course of furfural conversion. As expected higher furfural conversions were obtained at higher temperatures. It can be inferred that the conversion of furfural is not limited by thermodynamic equilibrium.

The data also confirm the consecutive nature of several reaction steps (Fig. 4, Scheme 1). In particular, the intermediate product, C_8 alcohol (see Scheme 1), is preferentially formed in the initial period of the reaction as a primary condensation product. It is subsequently dehydrated into the first condensation C_8 product (FAc). A higher reaction temperature facilitates this dehydration process. FAc successively reacts with another furfural molecule and the second condensation C_{13} product (FA_2c) is formed, which is also a dehydrated product. It can be clearly seen that higher reaction temperature favors the formation of FAc and F_2Ac, respectively, resulting thus in an increased selectivity to these desired products. It can be concluded that the selectivity to alcohols decreases at the expense of the selectivity to formation of ketones with the increasing reaction temperature. The selectivity to diacetone

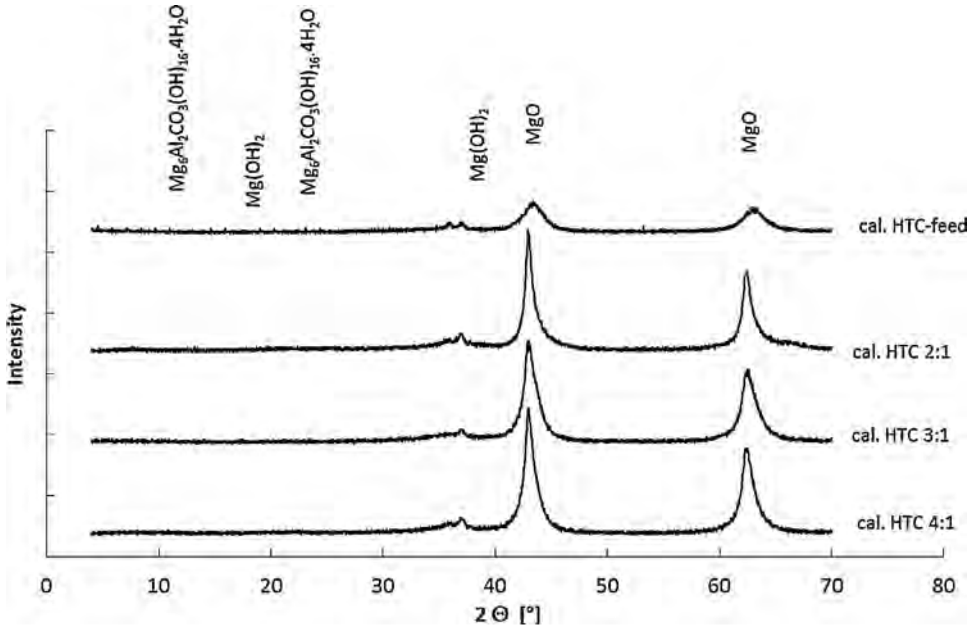

Fig. 2. X-ray diffraction patterns of the calcined hydrotalcites (mixed oxides).

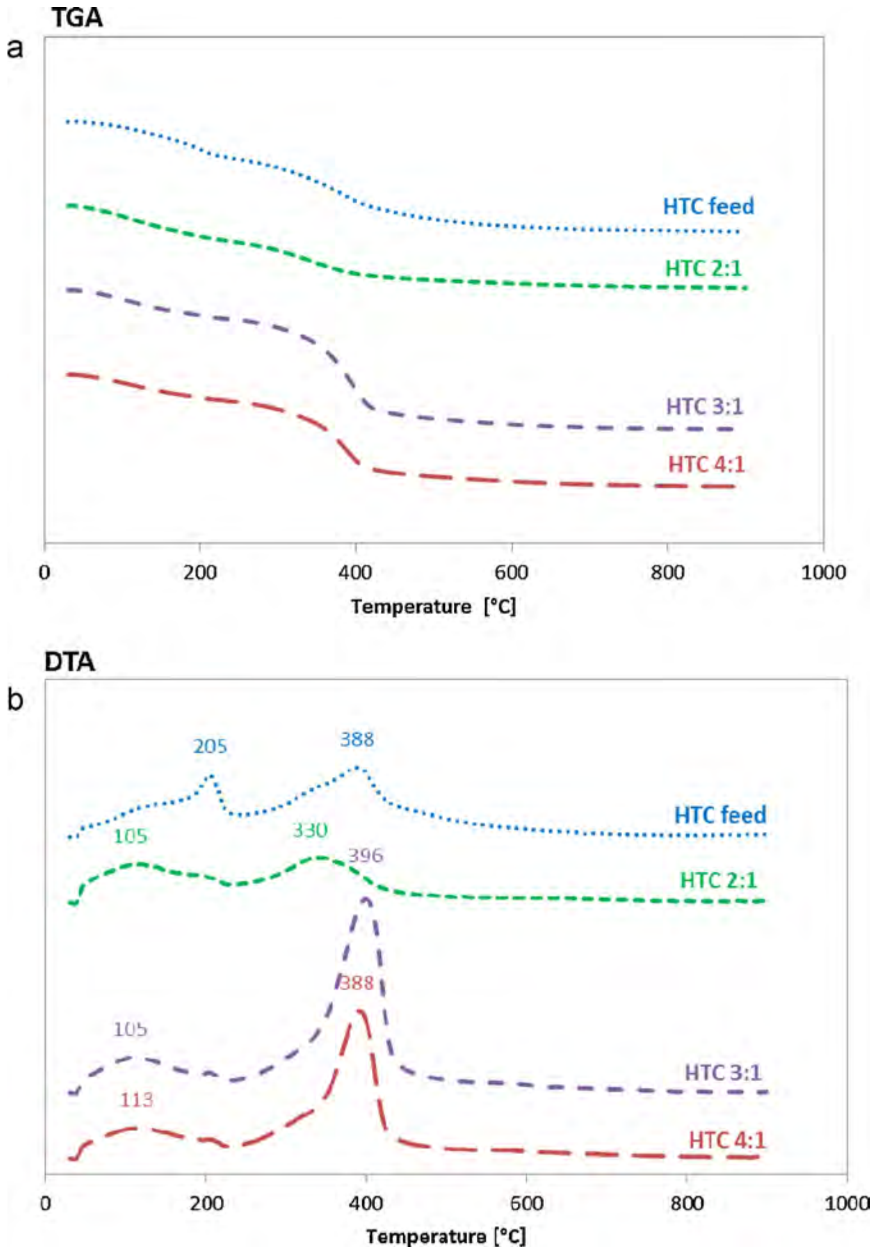

Fig. 3. TGA–DTA curves of dried of dried LDH catalysts.

alcohol (DAA), the main by-product, remains practically constant during the course of the reaction, i.e. it is not favored by the increased reaction temperature.

3.2.2. *Influence of the Mg/Al molar ratio of the calcined catalysts and reaction temperature*

The performance of the calcined LDH catalysts without any rehydration, i.e. mixed oxides catalysts, was investigated using catalysts with Mg/Al molar ratio between 2 and 4 at two reaction temperatures, 20 and 100 °C. The results are summarized in Fig. 5 where a comparison of furfural conversion and product distributions is given.

The results in the whole range of the investigated Mg/Al ratios are in accordance with the above described reaction behavior. Furfural conversions more than 95% were achieved at 100 °C with all catalysts except the catalyst denoted HTC 4:1 (Fig. 5). In this case the conversion was only around 62%. While the performance of HTC-feed, HTC 2:1 and HTC 3:1 is very similar at 100 °C, differences can be revealed at 20 °C. The highest conversion, about 30%, was achieved with catalyst HTC 3:1, while the conversion over HTC 2:1 and HTC 4:1 are significantly lower, ca. 20% and ca. 15%, respectively. It can be thus concluded that the Mg/Al ratio has an impact on the catalyst activity and that there is an optimum at a molar ratio Mg/Al around 3 (HTC 3:1).

There is a significant difference in product distribution depending on the reaction temperature regardless the mixed-oxide catalyst used (Fig. 5). While C_8 alcohol is formed almost exclusively (selectivity >90% at conversion <20%) at reaction temperature 20 °C, only minor concentrations of C_8 alcohol were observed over catalysts that afforded conversion >90% at 100 °C. On the other hand, over HTC 4:1 conversion of only about 60% was reached after 2 h and consequently significant selectivity to C_8 alcohol was still observed at the expense of selectivity to the desired FAc and F_2Ac products (Fig. 2). It can be concluded that at 20 °C the dehydration of C_8 alcohol to the desired C_8 product FAc is very slow as is the subsequent second condensation step to C_{13} product F_2Ac (Fig. 5). A

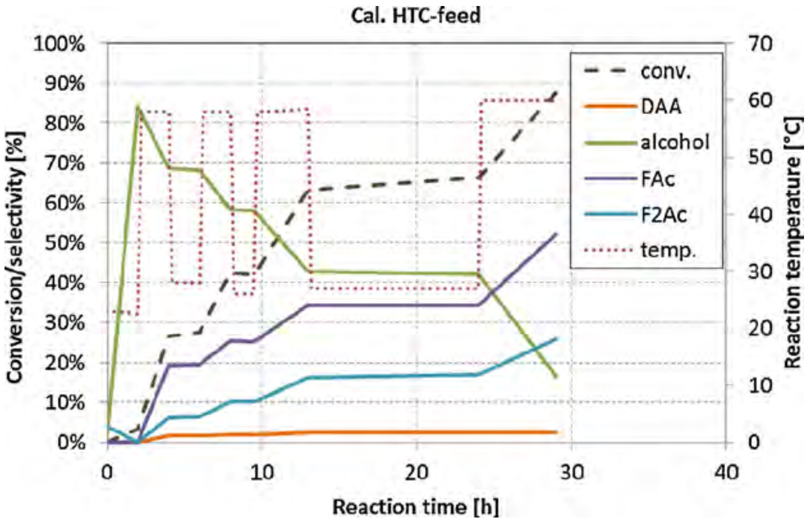

Fig. 4. Profile of furfural conversion and catalyst selectivity (products distribution) during reaction temperature switching between 25 and 56 °C in a 28-h experiment.

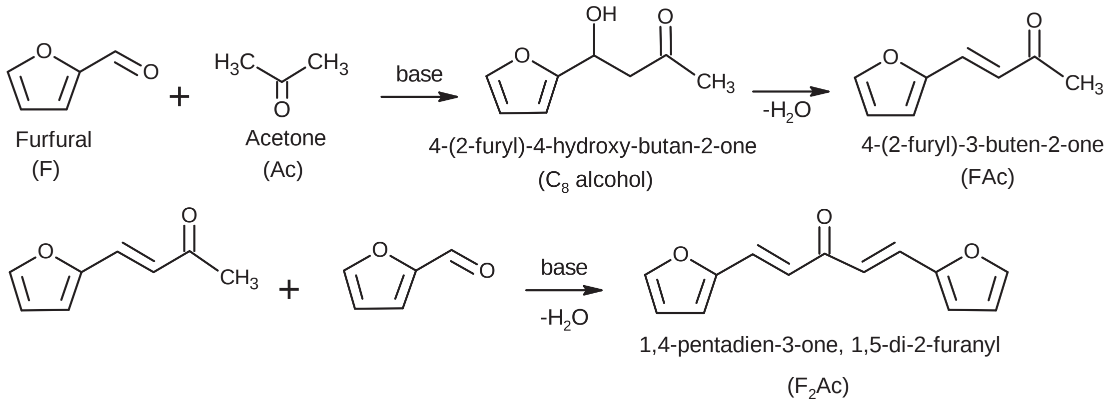

Scheme 1. Reaction scheme of the aldol condensation of furfural and acetone.

comparison of the product distributions with the phase composition of the catalysts indicates that at low temperature the formation of FAc and F_2Ac can be related to the presence of MgO and $Mg(OH)_2$ phases (although the dependence could not be expressed explicitly). A more detailed structural investigation is, however, needed to reach an unequivocal conclusion. The best results were achieved with HTC 3:1 catalyst that yielded almost exclusively FAc and F_2Ac products at nearly complete conversion

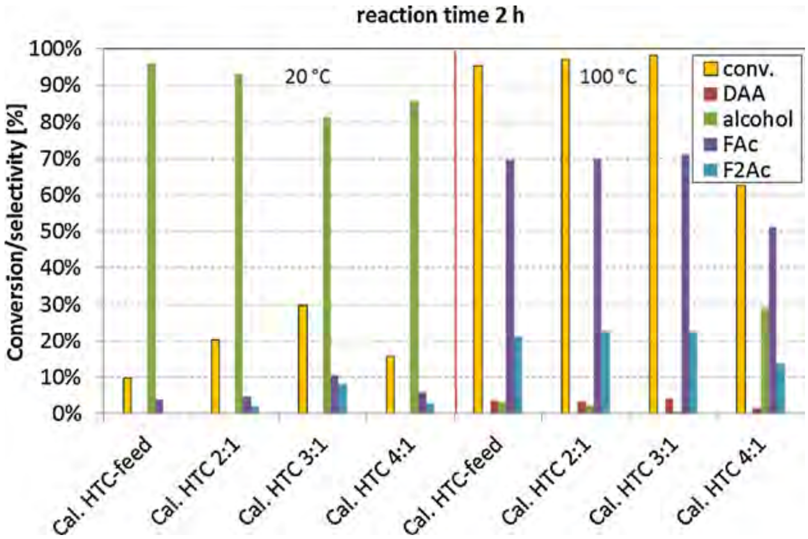

Fig. 5. Comparison of furfural conversions obtained over calcined catalysts with different Mg/Al molar ratio using reaction temperature 20 and 100 °C.

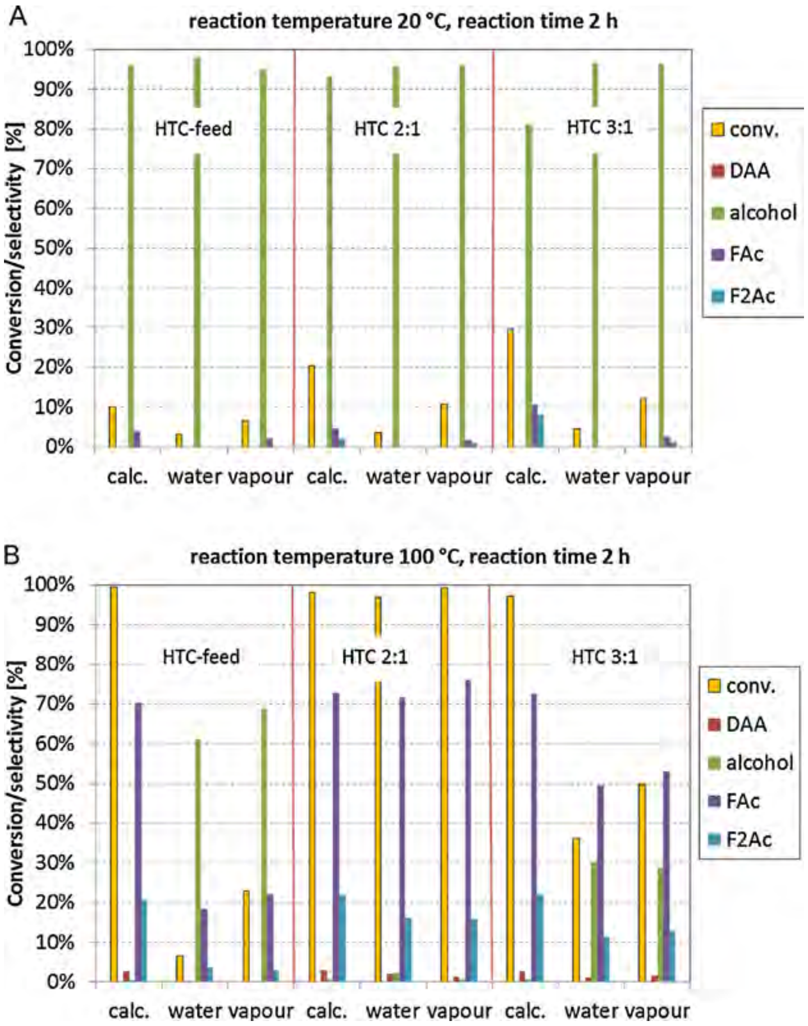

Fig. 6. Comparison of furfural conversion and product selectivity achieved over calcined and rehydrated catalysts with different Mg/Al molar ratio using reaction temperatures 20 (A) and 100 °C (B).

of furfural. The selectivity to diacetone alcohol (DAA) did not exceed 5% in any of the experiments. Moreover, the formation DAA was not detected at 20 °C (Fig. 5).

3.2.3. *Influence of ex situ rehydration on the catalyst activity and selectivity*

The activation of the calcined hydrotalcites (mixed oxides) with water or steam is often reported in the literature [24,25]. Hence, the three best calcined catalysts (HTC-feed, HTC 2:1 and HTC 3:1) were investigated after rehydration under the same reaction conditions as the calcined catalysts (20 and 100 °C, 2 h). Fig. 6 compares conversion of furfural and the product distribution over the calcined catalysts with the conversion of furfural and the product distribution over ex situ rehydrated catalysts, both liquid phase rehydrated (Ex-RW) and steam rehydrated (Ex-VR).

It can be clearly observed that at 20 °C the rehydration led to significant decrease in conversion for both ex situ rehydration methods. Moreover, the decrease in conversion for all investigated catalysts was more pronounced in the case of ex situ liquid phase rehydration than in the case of steam rehydration (Fig. 6). Due to the decrease in the conversion, the selectivity to the desired products (FAc and F_2Ac) dropped as well (Fig. 6). In contrast, the ex situ rehydration affected the catalyst performance at 100 °C differently. While over HTC-feed and HTC 3:1 the conversion of furfural dropped dramatically due to the rehydration, HTC 2:1 maintained its activity even after rehydration (Fig. 6). The conversion of furfural over HTC 2:1 stayed practically constant after all three activation procedures (Fig. 6). It is also interesting to note that the conversion over HTC 3:1 dropped less than over HTC feed and again the steam rehydrated catalysts afforded higher furfural conversions than the liquid phase rehydrated ones. A comparison with the structural data suggests that the catalytic materials exhibiting a lower relative crystallinity (HTC 3:1 and particularly HTC feed) are significantly affected by the rehydration procedure while HTC 2:1 catalyst with rather well-developed hydrotalcite structure is more resistant to any of the applied ex situ rehydration procedures. However, the plausible influence of the crystallinity of the LDH phase in the prepared catalyst samples on their catalytic behavior in aldol condensation requires additional investigation. Another explanation can be provided based on the analysis of the phase composition of the dried samples according to their XRD patterns (Fig. 1). All samples are a mixture of two main phases, hydrotalcite and MgO/$Mg(OH)_2$. Both hydrotalcite and MgO possess high initial activity for aldol condensation. Nevertheless, water which is formed in the course of the reaction may affect the properties of these two main phases differently. While the presence of water in the reaction mixture can even increase the activity of HTC materials in the condensation of aldehydes and ketones [26], MgO gradually loses its activity due to its continuous hydration and transformation to inactive $Mg(OH)_2$. As a consequence, the activity of the different materials in the study is determined in a great extent by the ratio between HTC and MgO phases, which is the highest in case of HTC

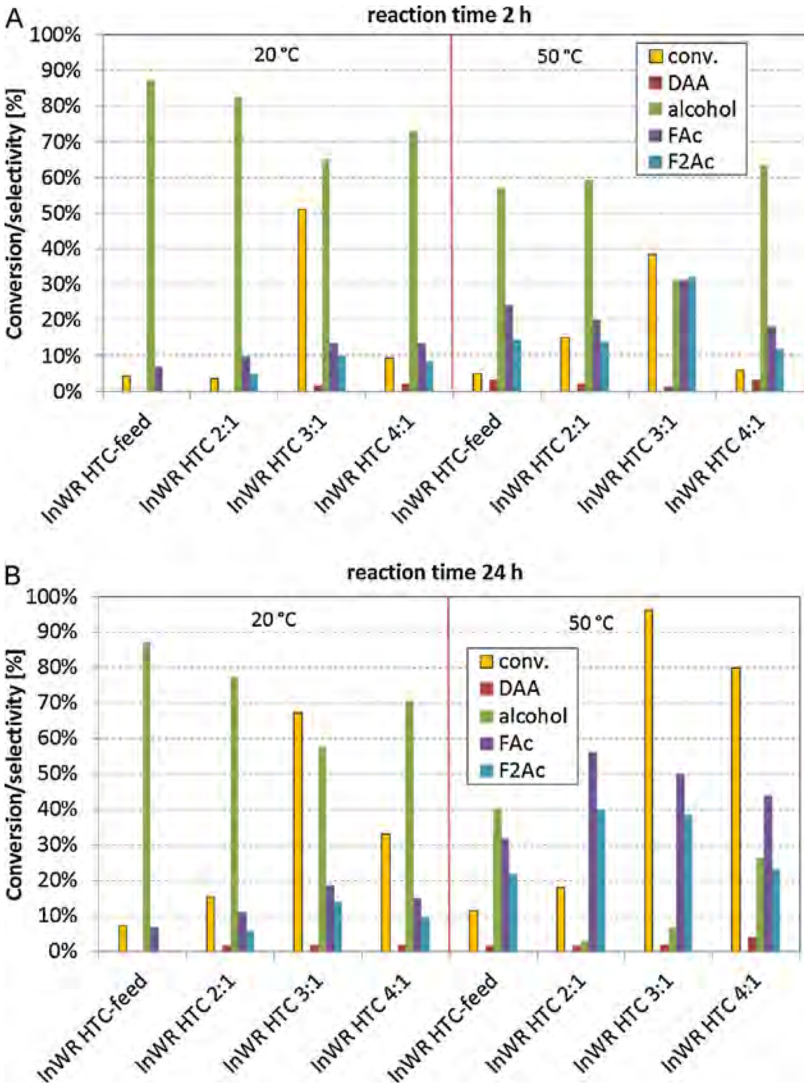

Fig. 7. Comparison of furfural conversion and catalyst selectivity achieved over calcined and in situ rehydrated catalysts with different Mg/Al molar ratio using reaction temperatures 20 and 50 °C for (A) 2 h and (B) 24 h.

2:1. In terms of the product distribution (Fig. 6), the rehydrated catalysts (except the HTC 2:1) show a higher selectivity to the intermediate C_8 alcohol not only at 20 °C, but also at 100 °C in comparison with the calcined catalysts. Due to the consecutive nature of the reactions, this could be explained by the lower conversion over the rehydrated catalysts. This conclusion is supported comparing the results obtained over the calcined HTC 4:1 (furfural conversion ca. 60%, selectivity to C_8 alcohol ca. 32%, Fig. 5) and over rehydrated HTC 3:1 (furfural conversion ca. 50%, selectivity to C_8 alcohol ca. 28%, Fig. 6). It is known that calcined HTC materials possess strong Lewis basicity, and their rehydration results in a Lewis-to-Brønsted sites transformation [27]. The obtained results show that rehydration, regardless the ex situ rehydration procedure, does not affect the reaction pathway and results in a comparable product composition at equal furfural conversion. In this case, the activity of both the calcined and the rehydrated catalyst samples as well as the composition of the obtained reaction products are determined by the amount of the accessible active sites (both Brønsted and Lewis) with the strength sufficient to activate the particular reactant molecule.

3.2.4. Influence of catalysts activation by in situ rehydration

The effect of ex situ rehydration indicates that the catalyst activity could be negatively influenced by air moisture, e.g. during catalyst handling, or by water dissolved in the raw materials. To verify this assumption a series of experiments were carried out at temperature 20 and 50 °C. Due to the relatively low reaction temperatures the reaction time was extended up to 24 h. A comparison of furfural conversions is given in Fig. 7. A rather peculiar behavior can be observed, the conversion over HTC 3:1 has increased in comparison with the calcined sample (Fig. 5 and Fig. 7), while it did drop in the case of liquid phase rehydration Fig. 6. The effect on the other catalysts was very similar to the one observed for the ex situ water rehydration. Another interesting observation is related to the conversion of furfural at 20 and 50 °C where a lower conversion was observed at the higher temperature in the case of HTC 3:1 and HTC 4:1 catalysts after 2 h (Fig. 7). This can be attributed to the influence of water that is inhibiting the catalyst activity, particularly at low reaction temperatures (Fig. 6) at which the intrinsic reaction rate is significantly lower.

To explain this behavior, it is helpful to look at the conversion of furfural as a function of reaction time (Fig. 8). When the calcined catalyst is not pre-hydrated, it behaves at 20 °C as a calcined catalyst and the effect of water addition can be observed only by the gradual decrease in the reaction rate. On the other hand, at 50 °C the catalyst activity is apparently affected at the very beginning of the experiment (due to the higher rate of inhibition by water) and

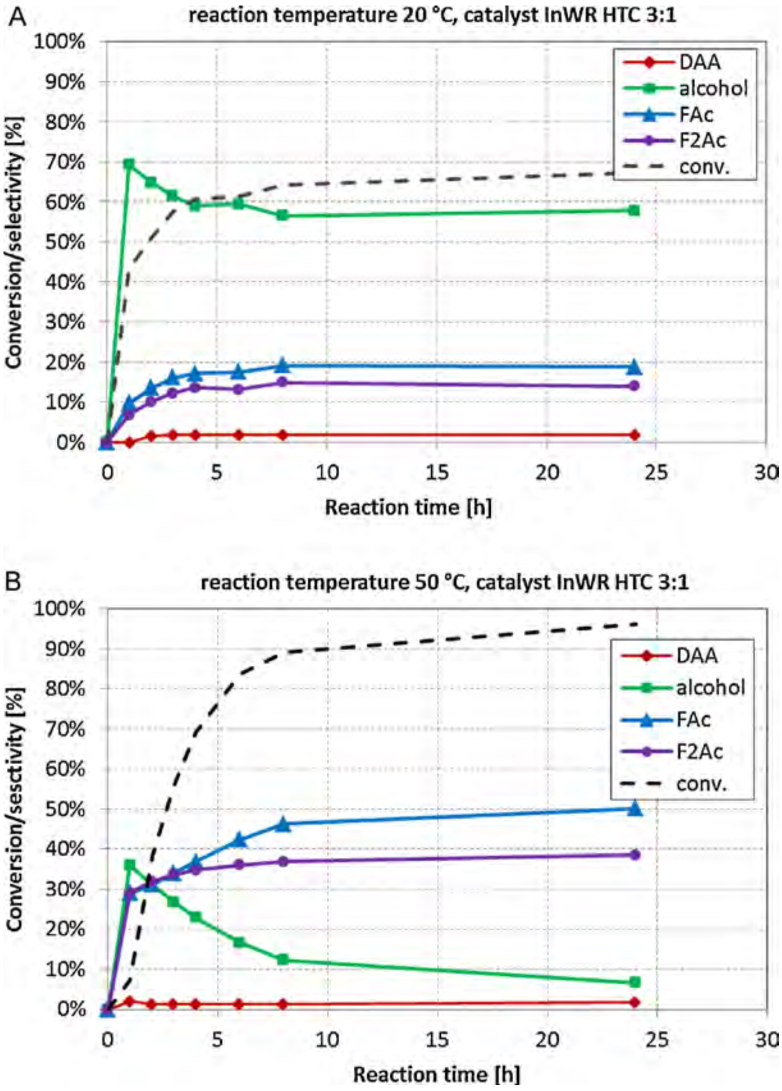

Fig. 8. Time evolution of furfural conversion and catalysts selectivity at reaction temperature (A) 20 °C and (B) 50 °C over catalyst HTC 3:1 rehydrated in situ.

consequently an induction period is observed (Fig. 8). When the reaction continues for a longer time, the final furfural conversion is higher at 50 °C than at 20 °C due to the higher reaction rate at the higher reaction temperature. It can be also seen that the reaction rate drops significantly with time (Fig. 8). After about 6 h the increase in conversion of furfural is a small one despite full conversion was not yet reached. The product distributions (Figs. 7 and 8) at 20 °C and after 2 and 24 h are very similar, dominant product being C_8 alcohol. In agreement with the previous results, the extent of dehydration is very limited at 20 °C.

Analogously with other experiments, higher reaction temperature favors the dehydration step and higher yields of the desired C_8 and C_{13} products (FAc and F_2Ac) were formed during reaction at 50 °C, particularly over HTC 3:1 catalyst. This tendency can be observed clearly when the product distributions are plotted as a function of reaction time (Fig. 8). While the apparent rate of formation of the C_8 alcohol is significantly higher than the apparent rate of formation of FAc and F_2Ac, the apparent rates of formation of these three products are virtually equal at 50 °C (Fig. 8). It can be also seen that at 50 °C the C_8 alcohol intermediate is virtually completely consumed in the successive reactions, while at 20 °C an equilibrium-like state is established, i.e. the selectivities to the products do not change (Fig. 8). It can be concluded that higher reaction temperatures, at least 50 °C, are needed to convert furfural fully into condensation products. The selectivity to the main by-product (DAA) again did not exceed 5%.

The differences of catalysts behavior after in situ rehydration can be also explained with the help of TGA analysis results. As it was presented above in the Fig. 3 and Table 4, HTC 3:1 and 4:1 show a more typical thermal decomposition profile of LDH than HTC-feed and HTC 2:1. This means, that after in situ rehydration (by a small amount of water) large amount additional active basic sites can be formed. As a result, the in situ rehydration might lead to improvement of the catalysts activity.

It can be concluded that in addition to the inherent structure of the HTC catalysts their pretreatment determines their final activity and selectivity. The observed peculiarities indicate that in fact the activity is very closely related to the rehydration process. Hence the process should be carefully monitored and investigated in more detail than it was done so far. We have already started working along this research line.

4. Conclusions

Mg—Al layered double hydrotalcites (LDH) with different Mg/Al molar ratio have been investigated as potential catalysts in aldol condensation of furfural with acetone at different reaction temperatures. Catalytic activity of the parent LDH materials has been studied in the form of mixed oxides (after calcination) and ex situ or in situ rehydrated samples. Their catalytic activity was affected both by reaction temperature and catalyst Mg/Al molar ratio. A significant effect of reaction temperature on the product distribution was observed. While C_8 alcohol formation was prevailing at the lower temperatures, higher temperatures supported C_8 alcohol dehydration and the formation of the desired FAc and F_2Ac products. The optimum Mg/Al molar ratio was found to be around 3. The best results were achieved with this catalyst at 100 °C (>95% furfural conversion and only a minor selectivity to C_8 alcohol). Selectivity to the main by-product DAA did not exceed 5%.

Ex situ rehydration (liquid and steam phase) led to a significant decrease in furfural conversion, which caused also a decrease of selectivity to the desired product (FAc and F_2Ac) in comparison with the calcined hydrotalcites, i.e. mixed oxides. This phenomenon was observed not only at 20 °C, but also at 100 °C. Only one catalyst, the one with Mg/Al molar ratio 2, preserved its high activity (furfural conversion more than 90%) and the desired product selectivity after rehydration treatment. The reason lies probably in the highest relative crystallinity of the as prepared (dried) hydrotalcite catalyst in comparison with the other catalysts that is transformed to more stable and active catalysts, i.e. catalyst with a lower relative content MgO active phase that is more sensitive to water.

Acknowledgments

Financial support from the Ministry of Industry and Trade of the Czech Republic (project FR-TI3/327) and Czech Science Foundation (P106/11/0773) is gratefully acknowledged. This publication was created in connection with the project Unipetrol research and education center Reg. CZ.1.05/2.1.00/03.0071, which is funded through the Operational Programme for Research and Innovation Development of the Structural Funds (specifically the European Regional Development Fund) and the state budget of the Czech Republic.

References

[1] G. Huber, S. Iborra, A. Corma, Chem. Rev. 106 (2006) 4044–4098.
[2] D. Kubička, I. Kubičková, J. Čejka, Catal. Rev. Sci. Eng. 55 (2013) 1–78.
[3] L.D. Schmidt, P.J. Dauenhauer, Nature 447 (2007) 914.
[4] J.R. Rostrup-Nielsen, Science 308 (2005) 1421–1422.
[5] C. Somerville, H. Youngs, C. Taylor, S.C. Davis, S.P. Long, Science 329 (2010) 790–792.
[6] X. Hu, L. Wu, Y. Wang, Y. Song, D. Mourant, R. Gunawan, M. Gholizadeh, C.-Z. Li, Bioresour. Technol. 133 (2013) 469–474.
[7] J.N. Chheda, G.W. Huber, J.A. Dumesic, Angew. Chem. Int. Ed. 46 (2007) 7164–7183.
[8] D.R. Dodds, R.A. Gross, Science 318 (2007) 1250–1251.
[9] S. Gámez, J.J. González-Cabriales, J.A. Ramírez, G. Garrote, M. Vázquez, J. Food Eng. 74 (2006) 78–88.
[10] C.J. Barrett, J.N. Chheda, G.W. Huber, J.A. Dumesic, Appl. Catal. B: Environ. 66 (2006) 111–118.
[11] A.S. Ndou, N. Plint, N.J. Coville, Appl. Catal. A: Gen. 251 (2003) 337–345.
[12] W. Shen, G.A. Tompsett, K.D. Hammond, R. Xing, F. Dogan, C.P. Grey, W.C. Conner Jr., S.M. Auerbach, G.W. Huber, Appl. Catal. A: Gen. 392 (2011) 57–68.
[13] P.A. Zapata, J. Faria, M.P. Ruiz, D.E. Resasco, Top. Catal. 55 (2012) 38–52.
[14] R. Xing, A.V. Subrahmayam, H. Olcay, W. Qi, P. van Walsum, G. Pendse, G.W. Huber, Green Chem. 12 (2010) 1933–1946.
[15] R.M. West, Z.Y. Liu, M. Peter, C.A. Gartner, J.A. Dumesic, J. Mol. Catal. A: Chem. 296 (2008) 18–27.
[16] D. Tichit, M.N. Bennani, F. Figueras, R. Tessier, J. Kervennal, Appl. Clay Sci. 13 (1998) 401–415.
[17] F. Prinetto, D. Tichit, R. Teissier, B. Coq, Catal. Today 55 (2000) 103–116.
[18] B.F. Sels, D.E. de Vos, P.A. Jacobs, Catal. Rev. Sci. Eng. 43 (2001) 443–488.
[19] F. Figueras, Top. Catal. 29 (2004) 189–196.
[20] V. Rives (Ed.), Layered Double Hydroxides: Present and Future, Nova Science, New York, 2001, pp. 251–411.
[21] S.M. Auerbach, K.A. Carrado, P.K. Dutta, Handbook of Layered Materials, Marcel Dekker, New York, 2004.
[22] X. Duan, D.G. Evans (Eds.), Layered Double Hydroxides, Structure and Bonding Series, vol. 119, Springer, Berlin, 2006.
[23] D. Tichit, D. Lutic, B. Coq, R. Durand, R. Teissier, J. Catal. 219 (2003) 167–175.
[24] H. Liu, W. Xu, X. Liu, Y. Guo, Y. Guo, G. Lu, Y. Wang, Kinet. Catal. 51 (2010) 75–80.
[25] M. Campanati, S. Franceschini, O. Piccolo, A. Vaccari, A. Zicmanis, Catal. Commun. 5 (2004) 145–150.
[26] C. Xu, Y. Gao, X. Liu, R. Xin, Z. Wang, RSC Adv. 3 (2013) 793–801.
[27] D.P. Debecker, E.M. Gaigneaux, G. Busca, Chem. Eur. J. 15 (2009) 3920–3935.

ChemPubSoc Europe
DOI: 10.1002/cctc.201701880
CHEMCATCHEM Full Papers

Using Mg-Al Mixed Oxide and Reconstructed Hydrotalcite as Basic Catalysts for Aldol Condensation of Furfural and Cyclohexanone

Oleg Kikhtyanin,*[a, b] David Kadlec,[a] Romana Velvarská,[a] and David Kubička[b]

This study presents results on aldol condensation of furfural and cyclohexanone in presence of Mg-Al hydrotalcite-derived materials as solid basic catalysts at reaction temperatures from 25 to 90 °C and a cyclohexanone to furfural molar ratio of 1–10. Mg-Al mixed oxide exhibited reasonable activity with furfural conversion of ca. 50% after 180 min of the reaction at $T = 90$ °C. The activity of reconstructed hydrotalcite was much higher with furfural conversion close to 100% at short reaction times. In comparison with Mg-Al mixed oxide, the initial reaction rate has increased 30–50 times. Under similar reaction conditions, cyclohexanone self-condensation on HTC-derived catalysts could not compete with aldol condensation because the former reaction was inhibited by produced water. The change in CH/F molar ratio influenced both furfural conversion and product selectivity; higher furfural content in the reaction mixture favored the second condensation step.

Introduction

The dependence of price and availability of fossil fuels on political and economic events worldwide as well as environmental concerns require the development of economical and energy-efficient processes for the sustainable production of fuels and chemicals.[1] Consequently, the production of advanced biofuels is becoming an increasingly actual and urgent task. Among available biomass resources, lignocellulose is the most appropriate long-term alternative to fossil carbon owing to its availability and socio-economic acceptability.[2–5] Nevertheless, the successful introduction of biofuels on the fuel market is still limited by their cost and the lack of effective methods for their production.[1,6,7]

While a plethora of alternatives to conventional road transport fuels has been put forward, including electrical or hydrogen-fueled vehicles, such alternatives are not yet available for air transport. In fact, it was suggested that "…no practical alternatives to kerosene-based fuels for commercial jet aircraft for the next several decades".[8] Therefore, biomass-derived aviation drop-in fuels meeting the demanding aviation fuel standards are of immense interest.[9–11] In this context, a high content of naphthenic hydrocarbons (>25%) and a proper hydrocarbon chain length (C9–C16) are essential providing a guideline for selecting appropriate biomass-derived feedstocks as well as for fuel synthesis strategies. From the lignocellulosic biomass point of view, it becomes obvious that 1) condensation reactions need to be applied as the monomeric units of the three lignocellulosic polymers have typically between 5 and 9 carbon atoms in the molecule and that 2) lignin monomeric units should be used to introduce the naphthenic structure into the final fuel molecules.

Aldol condensation, a well-known reaction of organic synthesis that proceeds in the presence of catalysts with either basic or acidic properties, is a versatile tool to produce complex molecules starting from simple aldehydes and ketones. With respect to biomass valorization, aldol condensation of furfural and acetone has been studied in detail, as after hydrogenation the reaction products have characteristics of high quality diesel fuel components.[12–14] Nonetheless, the resulting linear hydrocarbons would not be suitable for aviation fuels owing to their low volumetric energy density and high pour point.[9–11,15–17] In contrast, the selective depolymerization of lignin results in a variety of phenolic and aromatic molecules whose cyclic structure can provide the necessary characteristics of potential aviation fuels produced from biomass. To arrive at aviation fuel components, lignin-derived compounds should be processed by one of the following strategies: 1) aldol condensation of short-chain aldehydes with (substituted) cyclic ketones[18–21] obtained by partial hydrogenation of phenolics from lignin[22,23] or furanics[24–26], or 2) self-condensation of cyclic ketones,[27–30] or 3) alkylation of lignin-derived aromatics by short chain alcohols.[31,32] Furthermore, some biomass-derived compounds, such as terpenes, have cyclic aliphatic rings and can be directly used as high-density biofuel additives.[15,16]

The conversion of cyclic ketones into bi-cyclic biofuels by self-condensation reaction was reported in presence of homogeneous and heterogeneous catalysts, both acidic and basic,[27–30] followed by hydrodeoxygenation.[27] Aldol condensa-

---

[a] Dr. O. Kikhtyanin, D. Kadlec, R. Velvarská
Unipetrol Centre of Research and Education (UNICRE),
Chempark Litvínov, 436 70 Záluží-Litvínov (Czech Republic)
E-mail: oleg.kikhtyanin@vscht.cz

[b] Dr. O. Kikhtyanin, Dr. D. Kubička
Technopark Kralupy VŠCHT Praha
University of Chemistry and Technology Prague
Žižkova 7, 278 01 Kralupy nad Vltavou (Czech Republic)

Supporting information and the ORCID identification number(s) for the author(s) of this article can be found under: https://doi.org/10.1002/cctc.201701880.

tion of cyclic ketones with furanics in presence of NaOH as a basic catalyst in solvent-free[18] or aqueous solutions[19] followed by hydrogenation of produced compounds[18] have been recently shown to be a promising way to obtain alkylated naphthenic compounds. NaOH was demonstrated[18] to be a very good catalyst in solvent-free condensation of cyclopentanone/cyclohexanone and furfural/5-hydroxymethyl-furfural, whereas $Mg(OH)_2$, $Ca(OH)_2$, and Na_2CO_3 were nearly inactive (with conversion $<2.0\%$). This performance was explained by the inability of weak bases to activate cyclopentanone to form carbanion which is necessary for the condensation. Similar results were obtained by Hronec et al. when performing aldol condensation of cyclopentanone and furfural in aqueous solution.[19] They found that Na_2CO_3, $Ca(OH)_2$, and $MgO-ZrO_2$ were less active as catalysts compared to NaOH and concluded that it was beneficial to conduct the reaction either at higher reaction temperatures (80–100 °C) and low concentration of a base or at lower temperatures (ca. 40 °C) and higher concentration of a base. The above studies suggest that NaOH is a highly effective and the most promising catalyst for aldol condensation of cyclic ketones and furfural. Additionally it was suggested that, in contrast to NaOH solution, the use of solid base catalysts for this aldol condensation may cause technical problem of separation of the solid catalyst from solid reaction product.[19] On the other hand, several technical, economic, and environmental disadvantages which arise when using homogeneous catalysts have to be also taken into account.[20,33] From this point of view, using solid catalysts in aldol condensation with participating cyclopentanone/ cyclohexanone should have substantial benefits over homogeneous ones including minimization of waste streams resulting to reduced costs and environmental burden[34,35] and reducing corrosion issues.

Accordingly, catalysts which could compete with NaOH in catalyzing aldol condensation of furfural and cyclic ketones and thus favor the sustainability of the process have been sought intensively. Recent studies evidence that aldol condensation of furfural and cyclic ketones can be successfully performed in presence of heterogeneous catalysts as well. Wang et al.[21] performed aldol condensation of cyclopentanone and furfural over solid acid catalysts (ion-exchange resins and zeolites) under solvent-free conditions. Among investigated catalysts, Nafion exhibited the best performance. It showed good stability and did not deactivate during 4 catalytic runs. Meanwhile, a certain amount of humins was formed during the reaction. Ordóñez et al.[20] found that, in contrast to results of Hronec et al.,[19] Mg-Zr mixed oxide was a promising catalyst for the aqueous phase furfural and cyclopentanone aldol condensation working at mild conditions. They observed almost complete conversion of furfural in 4 hours at $T=293–323$ K and furfural to cyclopentanone molar ratio of 1. No doubt, studies on finding promising catalytic systems for aldol condensation of furfural and cyclic ketones should be continued and developed to allow sustainable production of naphthenic in the jet fuel range and thereby improving the sustainability of jet fuels.

Mg-Al mixed oxides and hydrotalcite-like materials have been successfully used as catalysts for aldol condensation reactions, mostly with the participation of furfural and/or acetone, under batch[33,36–39] as well as flow reaction conditions.[40] As-prepared hydrotalcite-like materials (HTC) are solids having structure closely related to that of the mineral hydrotalcite (HTC), that is, rhombohedral $Mg_6Al_2(OH)_{16}CO_3{\cdot}4H_2O$. The most known Mg-Al HTC consist of a brucite-like $[Mg(OH)_2]$ network wherein isomorphous substitution of Mg^{2+} ion by Al^{3+} occurs and the excess positive charge is compensated by gallery anions which are located in the interlayer along with water molecules.[41–43] The Mg-Al HTCs can be used as catalysts either in the form of mixed oxides Mg(Al)O with Lewis basicity obtained by calcination of the as-prepared Mg-Al precursor or in the form of reconstructed HTCs with Brønsted basicity as the rehydrated form of these calcined materials.[44] It is worth noting a special and constantly growing interest in activated hydrotalcites obtained by rehydration of the mixed oxides for different catalytic applications.[36,43–45] Nevertheless, to the present no information can be found in the literature on the catalytic performance of either Mg-Al mixed oxides or reconstructed HTCs in aldol condensation of cyclic ketones and furfural.

The aim of this work is to provide deeper understanding of the role of different functionalities in solid base catalysts derived from hydrotalcites in condensation reactions of cyclic ketones with aldehydes derived from biomass. Specifically, this work is focused on cyclohexanone self-condensation and furfural-cyclohexanone aldol condensation over an Mg-Al mixed oxide and a reconstructed HTC. The effects of reaction conditions as well as different basicity of the catalysts on their activity and selectivity in both reactions are described. Additionally, re-using of the catalysts in consecutive aldol condensation runs, which is vital from the sustainability point of view, is presented as well. Although relying on established raw materials and known catalytic systems, the presented original results shed light on some of the transformation peculiarities and demonstrate their unique potential to succeed in the quest for efficient upgrading of renewable aldehydes and ketones into a feedstock for aviation fuels production.

Results and Discussion

The Mg-Al hydrotalcite-derived catalysts used for aldol condensation of furfural and cyclohexanone have been investigated previously[36,46] and thus, for the sake of conciseness, their detailed physicochemical characterization is included in the Supporting Information, Table S1 and Figures S1–S5.

Both F and CH aldol condensation and CH self-condensation proceed simultaneously under the contact of F and CH mixture with Mg-Al mixed oxide or reconstructed hydrotalcite. A large consumption of CH by self-condensation reaction route could influence the results obtained in F and CH aldol condensation. Besides, CH self-condensation can afford products that could also be further upgraded to aviation fuel components. Consequently, this reaction was studied separately by varying the type of catalyst and reaction conditions.

Cyclohexanone self-condensation

Cyclohexanone self-condensation is a reversible reaction[28,29] that can be catalyzed by acidic[28,47,48] or basic catalysts.[27,29] According to the accepted reaction route (Scheme 1,[28,29] the adduct 1′hydroxy-[1,1′-bicyclohexyl]-2-one (D1) is formed first and then dehydrated in situ, yielding an isomeric mixture of reaction products, namely 2-(1-cyclohexen-1-yl)cyclohexanone (D2) and 2-cyclohexylidencyclohexanone (D3).

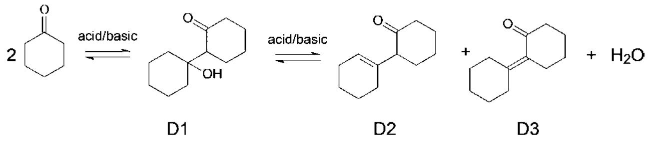

Scheme 1. The reaction pathway of cyclohexanone self-condensation.[28]

The conversion of cyclohexanone over the as-prepared HTC with no pronounced basicity increased with the growth of reaction temperature but did not exceed 3% at 90 °C after 3 hours of the experiment (Figure 1). The activity of both Mg-Al mixed oxide and reconstructed HTC was considerably larger proving the base-catalyzed character of this reaction. The observed catalytic performance of these catalysts would suggest that both Lewis basic sites in the Mg-Al mixed oxide and Brønsted basic sites in the reconstructed HTC are responsible for the reaction. Nevertheless, Tichit et al.[37] suggested that the pre-adsorption of water in a suitable amount on the surface of MgO or Mg-Al mixed oxide transforms the Lewis basic sites into active hydroxy groups (Brønsted basic sites) and increases the activity of the catalysts in acetone self-condensation, while a very high water amount inhibited the reaction.[37] The high complexity of the reaction system due to the thermodynamic equilibrium and water inhibition effects prevents unequivocal determination of the active basic sites. Nonetheless, it is clear that Brønsted basic sites are active in the reaction.

For both catalysts, Mg-Al mixed oxide and reconstructed HTC the interpretation of the obtained results is not straightforward as CH conversion over both the catalysts did not increase with the increase of reaction temperature. In contrast, Liang et al.[30] investigated cyclopentanone self-condensation over Mg-Zr mixed oxide and observed a sharp increase in conversion with the growth of reaction temperature. A careful comparison of CH conversion over the tested catalysts shows that there is a limiting value of ca. 3–4% conversion at 90 °C in the case of all three catalysts and ca. 10% conversion at 50 °C in the case of Mg-Al mixed oxide and reconstructed HTC (Figure 1). This would suggest that the reaction is either thermodynamically limited or severely inhibited by water and higher conversions can be achieved only in absence of water.

Such behavior can be supported, by analogy, by results on self-condensation of acetone to diacetone alcohol (DAA), which is a reversible reaction and the equilibrium concentration of DAA decreases with increasing temperature.[49] Assuming a similar mechanism for both acetone and cyclohexanone self-condensation in presence of basic catalysts, the decrease of cyclohexanone conversion with increasing temperature is thus not surprising. Furthermore, the hypothesis on the inhibiting effect of water is corroborated by the product distributions. As D1 is always the major condensation product, owing to the limited dehydration strength of the studied catalysts, the ratio of dehydrated to non-dehydrated products, that is, (D2+D3)/D1, is used as a measure expressing presence of water in the products (Figure 2). It is clearly seen that regardless the reaction temperature, the highest conversion is achieved when the (D2+D3)/D1 remained 0. As the ratio (D2+D3)/D1 increased to ca. 0.03–0.05, that is, water was formed by dehydration (this corresponds to about 3 to 5% selectivity to dehydration products), the conversion remained constant. This allows concluding that indeed water formation has a strong inhibiting effect on the CH self-condensation. First, it prevents the formation of enolate ion owing to interaction of cyclohexanone with basic hydroxy group on the surface of a catalyst. Second, water can reduce the production rate of dehydrated products D2 and D3. A similar conclusion was made when considering the kinetics of mesityl oxide formation in acetone self-condensation.[49] Consequently, it may be expected that an increase in cyclohexanone conversion can be achieved by removing water from the reaction mixture.

The above conclusions are further supported by the results of a study using NaOH as a basic catalyst where it was suggested[29] that CH self-condensation did not take place at temperatures lower than 100 °C. According to a proposed kinetic model,[29] water caused a remarkable decrease in the maximum conversion reachable, which was due to the growing extent of

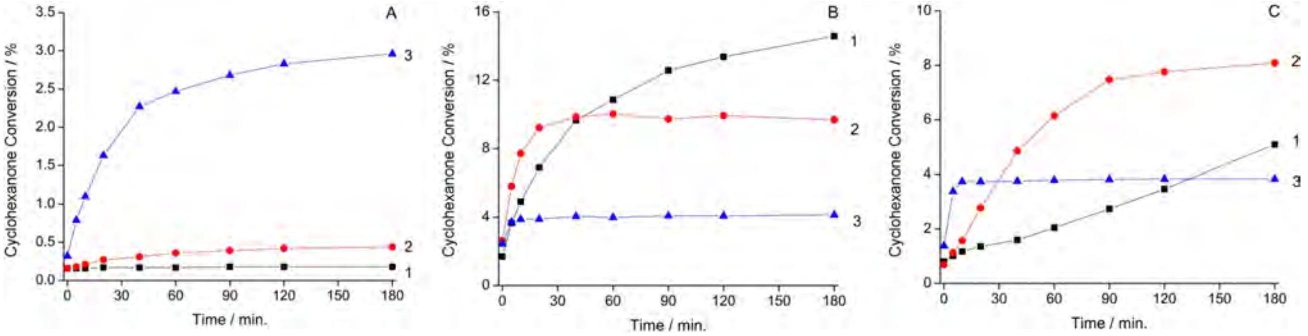

Figure 1. The influence of reaction temperature on cyclohexanone conversion over A) as-prepared HTC, B) Mg-Al mixed oxide, and C) reconstructed HTC. 1 = 25 °C, 2 = 50 °C, 3 = 90 °C.

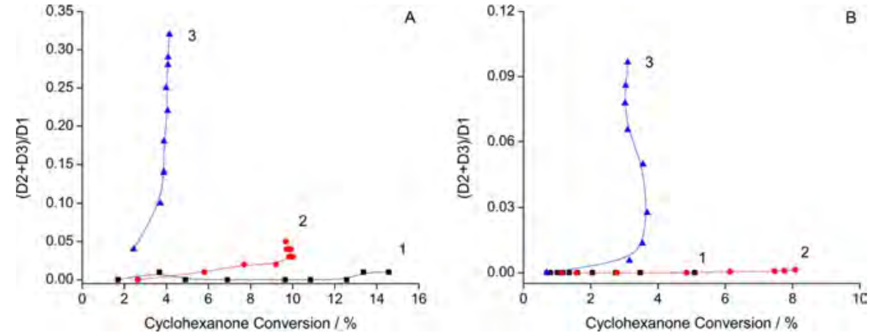

Figure 2. (D2 + D3)/D1 ratio observed in experiments on cyclohexanone self-condensation on A) Mg-Al mixed oxide and B) reconstructed HTC at different reaction temperatures: 1 = 25 °C, 2 = 50 °C, 3 = 90 °C.

the reverse reaction with increasing water concentration in the reaction mixture. Thus, it was concluded that the content of water in the media was a key parameter to control the desired cyclohexanone conversion.[29] The high conversions reported previously for Amberlyst-15 as an acidic catalyst in the range of 30–60 % at $T = 70–110\,°C$[28,48] contradict the current findings only seemingly. These experiments were conducted either at low reaction pressure or in a flow system and accumulation of water in the reaction mixture was thus avoided. The inhibiting effect of water was also found in the study for cyclohexanone self-condensation in presence of ion-exchange resin.[47]

The results also indicate that Mg-Al mixed oxide is more active in CH self-condensation compared to reconstructed HTC. The presence of water in the reaction mixture seems to be the crucial factor determining the activity of both Mg-Al mixed oxide and reconstructed HTC in the reaction. The slightly better performance of the mixed oxide catalyst could be attributed to the possibility of its reconstruction to HTC, which consumes part of the water formed during the dehydration of D1.

The negative effect of water on the catalyst behavior of the reconstructed Mg-Al HTC was confirmed by experiments in which water was either added to or removed from the reaction mixture. In Figure 3 A it is demonstrated that water added to CH obviously reduced the conversion of CH on the reconstructed HTC at $T = 25$ and 50 °C from 5.1 to 3.6 % and from 8.1 to 3.9 %, correspondingly, while at $T = 90\,°C$ CH conversion (ca. 3.1 %) did not change since at these reaction conditions water was formed abundantly by dehydration of the primary D1 product.

On the other hand, the removal of water from the reaction mixture (by performing the reaction at $T = 90–150\,°C$ without a cooler–condenser above the glass reactor and thus favoring water evaporation during the reaction) had a positive effect on the activity of the reconstructed HTC. This is obvious already at $T = 90\,°C$; when water could evaporate (that is, it was not condensed), CH conversion increased from 3.1 to 7.3 % (Figure 3 B). The growth in reaction temperature subsequently resulted in an increased activity of the reconstructed HTC, so that CH conversion attained 44 % at $T = 150\,°C$.

The results obtained during the study of CH self-condensation in presence of Mg-Al mixed oxide and reconstructed HTC allow making the following conclusions. First, the different nature of basic sites had only a small impact on the performance of the two catalysts in cyclohexanone self-condensation. Second, an increase in the reaction temperature promoted the increase in CH conversion only to a certain extent, which is possibly due to thermodynamic limitations. At the same time, the growth of reaction temperature increased the extent of dehydration of the intermediate aldol. Consequently, the formed water inhibited the catalyst activity and/or promoted the reverse reaction (retro-aldolization) leading ultimately to a lower CH conversion at 90 °C than at 25 °C. In other words, cyclohexanone conversion by self-condensation on the

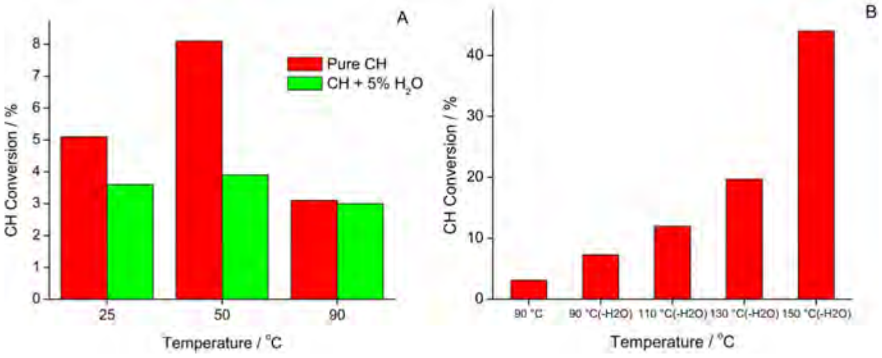

Figure 3. A) The catalytic performance of reconstructed HTC in converting pure cyclohexanone and its aqueous (5 % of water) solution. B) Cyclohexanone conversion in experiments with water separation from reaction mixture. Reaction time −180 min.

Mg-Al mixed oxide and the reconstructed HTC is very low at increased reaction temperatures when water is present in the reaction mixture. These results should be kept in mind when discussing results on aldol condensation of furfural and cyclohexanone.

Aldol condensation of furfural and cyclohexanone

A special experiment on F and CH aldol condensation in absence of a catalyst confirmed no any reaction occurred (furfural conversion was below 0.1% at $T=90\,^{\circ}$C after 3 hours). Introducing a catalyst into the reaction mixture initiated the reaction and resulted in the formation of several products. To identify them, a reaction mixture was analyzed by GC-MS. Based on the identification, the following reaction network is proposed (Scheme 2). It is worth noting that more than one compound with the same molecular weight was determined by GC-MS. A similar observation has been reported[20] and peaks belonging to compounds with the same number of carbon atoms were attributed to *cis* and *trans* isomers of the same molecule. By analogy with the results from the previous report,[20] all products with the same molecular weight were considered together in all GC analyses as a single compound.

It is worth noting that the conversion of cyclohexanone by self-condensation did not exceed 2% in all experiments on F + CH aldol condensation. The absence of the cyclopentanone self-condensation adducts during aldol condensation of furfural and cyclopentanone was also suggested.[20] As shown above, this can be explained by the formation of water by the dehydration of an aldol (FCH-OH), which is the primary product of aldol condensation of furfural and cyclohexanone. Being formed, water favors retro-aldolization in cyclohexanone self-condensation route. Accordingly, this reaction was excluded from the consideration of catalytic results on aldol condensation because of its negligible impact.

The effect of catalyst type and reaction temperature on furfural conversion and the composition of products obtained in aldol condensation of furfural and cyclohexanone were studied at CH/F molar ratio of 5. This choice was dictated by the formation of a yellow solid product in experiments with high furfural content. Similar observations were reported in other studies.[18–20] After separation from the reaction mixture, this solid product was dissolved in excessive benzene and analyzed by GC-MS which proved that it consisted mainly of F_2CH. Its formation disrupted the homogeneity of the reaction mixture and made it difficult (if possible) to periodically withdraw liquid samples to analyze the composition of the reaction products in dependence on reaction time. All experiments on the effect of reaction temperature and catalyst type with periodic sampling were therefore carried out at a high CH/F molar ratio of 5, which prevented the excessive occurrence of the second step of aldol condensation to form F_2CH. The used CH/F molar ratio additionally promoted the homogeneity of the reaction mixture by dissolving aldol condensation products in excessive cyclohexanone. It also allowed obtaining carbon balance values of ≥ 90% in all experiments, suggesting a small contribution of side reactions or of the excessive formation of oligomers by consecutive condensation steps.

Three Mg-Al-derived catalysts were investigated in F and CH aldol condensation: 1) as prepared Mg-Al hydrotalcite, 2) Mg-Al mixed oxide obtained by calcination of as prepared hydrotalcite at $T=450\,^{\circ}$C, and 3) reconstructed hydrotalcite obtained by liquid-phase rehydration of the Mg-Al mixed oxide. Among them, the as-prepared hydrotalcite showed very low activity; furfural conversion reached less than 3% after 3 hours at 90 °C. Thus, in the following discussion only the performance of the Mg-Al mixed oxide and the reconstructed HTC is considered. It also proves that thermal activation of the Mg-Al hydrotalcites before their use as catalysts is essential.

The conversion of furfural over Mg-Al mixed oxide and Mg-Al reconstructed HTC as a function of reaction time at three reaction temperatures (25, 50, and 90 °C) and constant feed composition (cyclohexanone/furfural molar ratio = 5) is shown in Figure 4. The conversion of furfural over Mg-Al mixed oxide increased from 7.1% to 51.9% after 180 min. of the reaction with the growth of reaction temperature from 25 °C to 90 °C. The catalytic activity increased dramatically when Mg-Al mixed oxide was rehydrated to form reconstructed Mg-Al HTC with furfural conversion close to 100% already after 60 min. of the reaction. It could not be explained by the differences in the textural properties of Mg-Al mixed oxide and reconstructed HTC, because BET surface areas of these catalysts were 180 and 43 $m^2\,g^{-1}$, respectively (see the Supporting Information). Although Mg-Al had larger surface area than the reconstructed HTC, it exhibited lower activity in the reaction. Accordingly, the increase in the catalytic activity demonstrates that by reconstruction of HTC structure suitable active sites are formed, namely the Lewis basic sites are converted into the more active Brønsted basic sites. The increase in the activity was quantified by estimating the initial reaction rate over Mg-Al mixed oxide and reconstructed HTC catalysts, respectively (Table 1). Depending on the reaction temperature, the initial reaction rate over the reconstructed Mg-Al HTC is 30 to 50 higher than that over the Mg-Al mixed oxide. It is noteworthy that complete conversion of furfural was not attained even after 3 hours, which contrasts with aldol condensation of furfural and acetone at similar reaction conditions.[36]

Figure 5 depicts a change in the composition of reaction products observed on Mg-Al mixed oxide and reconstructed HTC in dependence on F conversion at different reaction tem-

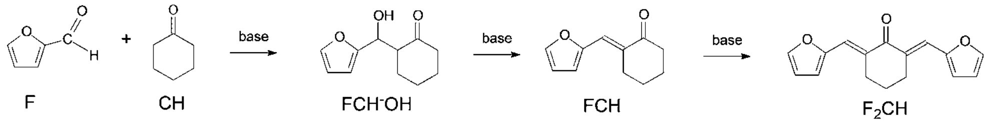

Scheme 2. The reaction pathway of aldol condensation of furfural and cyclohexanone.

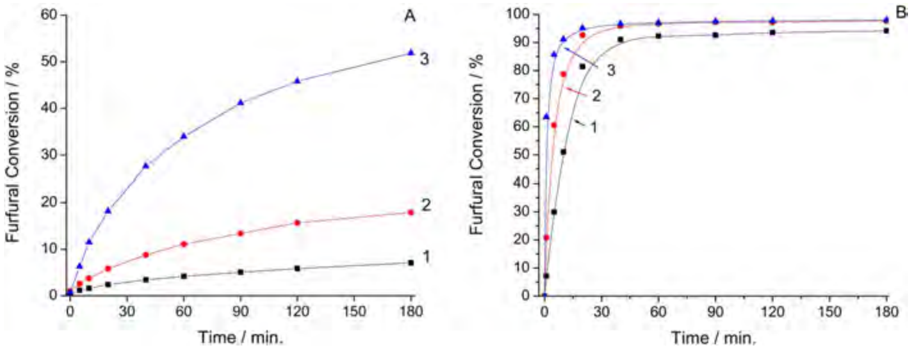

Figure 4. Furfural conversion in aldol condensation of furfural and cyclohexanone (CH/F molar ratio = 5) as a function of reaction time at 25, 50 and 90 °C over A) Mg-Al mixed oxide and B) reconstructed Mg-Al HTC.

peratures. According to the suggested reaction Scheme (Scheme 2), aldol (FCH–OH) is the initial product formed by the condensation of furfural and cyclohexanone. Indeed, its selectivity on Mg-Al mixed oxide is close to 100% at low F conversion (Figure 5 A1). The increase in reaction temperature favors FCH–OH dehydration as evidenced from the increase in selectivity to FCH (Figure 5 B1) and F_2CH (Figure 5 C1) at similar conversion levels. Selectivity to FCH-OH decreases (and, accordingly, selectivity to FCH and F_2CH increase) very fast at the

Table 1. Initial catalytic activity of Mg-Al mixed oxide and reconstructed Mg-Al HTC in aldol condensation of furfural and cyclohexanone (CH/F molar ratio = 5).

Temperature [°C]	$r_{in.}$ (MO) [mmol/(g min)]	$r_{in.}$ (HTC) [mmol/(g min)]	$r_{in.}$ (HTC)/$r_{in.}$ (MO)
25	0.3	9.7	32.3
50	0.7	28.2	40.3
90	1.7	86	50.6

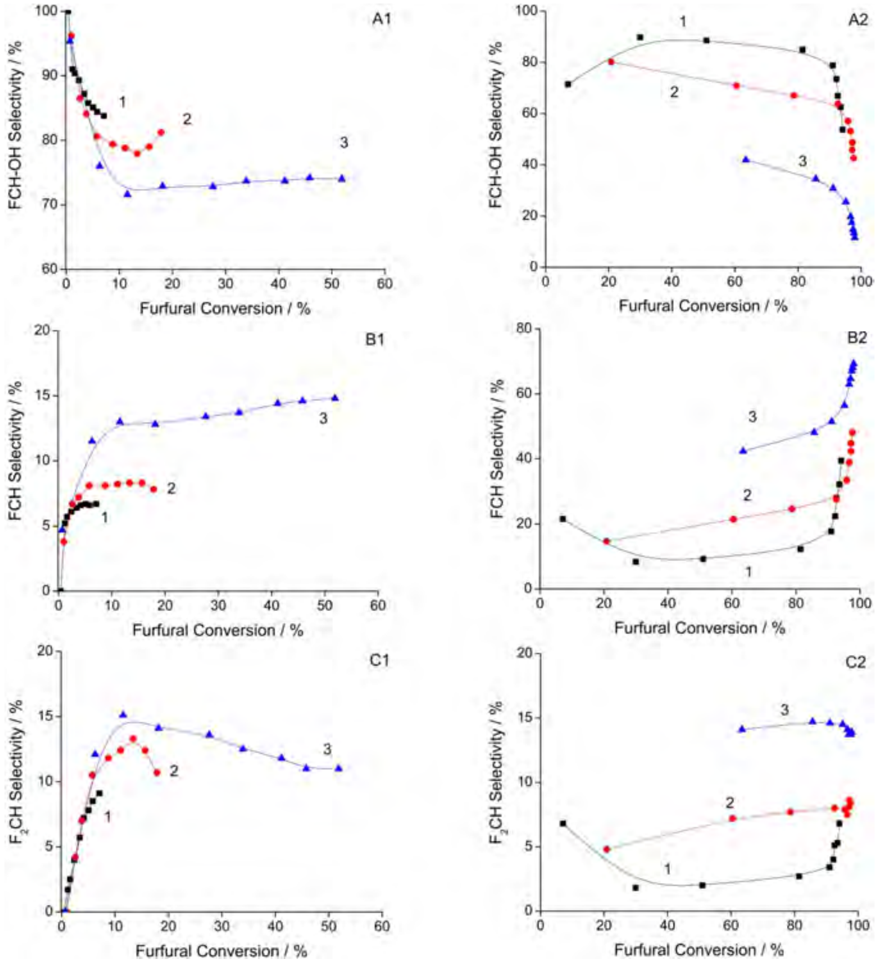

Figure 5. Selectivity to A) FCH-OH, B) FCH, and C) F_2CH observed in aldol condensation of furfural and cyclohexanone over Mg-Al mixed oxide (left) and reconstructed HTC (right). 1 = T = 25 °C, 2 = 50 °C, and 3 = 90 °C. CH/F molar ratio = 5.

beginning of the reaction at F conversion below 10% followed by a steady-state region. The observed change in the composition of the reaction products allows suggesting that the properties of Mg-Al mixed oxide are modified in the course of the reaction as discussed further.

Similar to experiments with Mg-Al mixed oxide, the increase of reaction temperature in experiments with reconstructed HTC facilitates FCH-OH dehydration to FCH and the formation of the second condensation product (F_2CH). The intermediate aldol (FCH–OH) is the most abundant reaction product at $T=$ 25 and 50 °C and F conversion below 80% (Figure 5 A2), but the changes in selectivity with increasing F conversion are rather peculiar. At $T=25$ °C, the initial FCH-OH selectivity is 71.5%; it increases to 89.7% at furfural conversion of about 30% followed by a small decrease to 84.9% with increasing F conversion. At higher reaction temperatures ($T=50$ °C and 90 °C), FCH-OH selectivity shows more common trend for an intermediate reaction product: it monotonously decreases with the increasing F conversion. Finally, as F conversion is approaching 100%, a sharp drop in FCH–OH selectivity is observed in all experiments (Figure 5 A2).

The change in selectivity to FCH observed on the reconstructed HTC exhibits an opposite trend to that observed for FCH-OH which is in accordance with the reaction route (Scheme 2). In general, the lower the selectivity to FCH-OH, the higher the selectivity to dehydrated FCH, and vice versa. At $T=25$ °C, the initial selectivity to FCH shows a notable decrease from 21.5 to 8.3% at the beginning of the reaction, a steady-state behavior in the range of F conversion between 30 and 80% and a sharp increase at higher F conversion (Figure 5 B2). In contrast, at 50 °C and 90 °C the constant increase in selectivity to FCH during all the experiments is observed. The change in the selectivity to F_2CH follows the same trend as observed for FCH, that is, a complex behavior at $T=25$ °C and a slight increase at higher reaction temperatures (Figure 5 C2). The absence of a sharp increase in F_2CH selectivity at $T=50$ and 90 °C at the end of experiments is probably concerned with the lack of furfural molecules available for the second condensation step at high conversion levels.

The selectivity to FCH at approximately the same conversion shown for both catalysts at each reaction temperature studied (Figure 6) indicates that indeed the dehydration performance of the reconstructed Mg-Al HTC is considerably better than that of Mg-Al mixed oxide. It can thus be inferred that the active sites in reconstructed HTC are intrinsically more active in dehydration than the sites in Mg-Al mixed oxide. However, there are some peculiarities observed in the product distribution when approaching complete furfural conversion (Figure 5), namely there is a sharp decrease in the selectivity to the FCH-OH accompanied by a sharp increase in the selectivity to its dehydration product, that is, FCH. Such behavior suggests that, when nearly all furfural is consumed, more active sites become available for the dehydration step. This could be a consequence either of competitive adsorption of furfural and FCH-OH on the basic sites (with furfural being preferentially adsorbed) or of recovery/regeneration of some active sites.

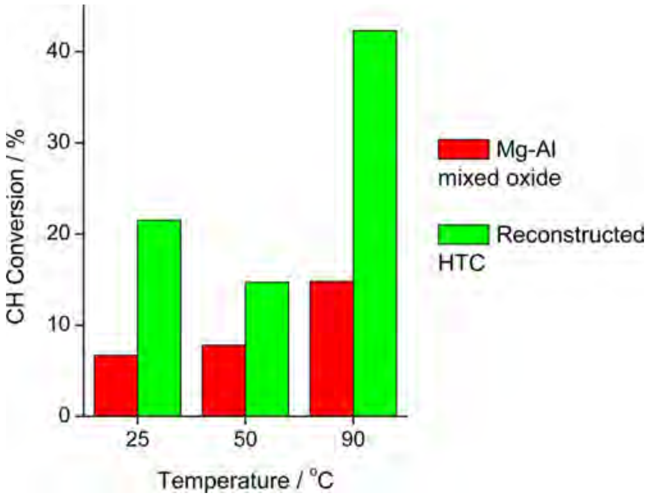

Figure 6. Selectivity to FCH at 25, 50, and 90 °C over Mg-Al mixed oxide (F conversions 7, 18, and 52%, respectively) and reconstructed Mg-Al HTC (F conversions 8, 20, and 63%, respectively) in aldol condensation of furfural and cyclohexanone (CH/F molar ratio = 5).

Detailed analysis of the product distribution provided evidence supporting the second hypothesis. It was shown that aldol condensation of furfural and acetone is affected by Cannizzaro reaction that yields furoic acid and furfuryl alcohol.[50] While furoic acid interacts with the basic sites of reconstructed HTC, presumably with interlayer hydroxy groups, forming interlayer furoates and is thus not seen among the reaction products, furfuryl alcohol can be detected. The amount of furfuryl alcohol depends, among other factors, on the reaction rate of aldol condensation of furfural and cyclohexanone, as this is a faster reaction consuming furfural in the reaction mixture. Hence, often the concentration of furfuryl alcohol in the reaction products is close to its detection limit. Nonetheless, in an experiment over reconstructed HTC at $T=25$ °C, furfuryl alcohol was reliably detected, and its yield is plotted as a function of the reaction time in Figure 7.

It is surprising to see that the yield of furfuryl alcohol passes through a maximum and decreases as furfural conversion approaches to 100%. Simultaneously, at furfural conversion ≥ 50% the formation of furfuryl ester of the furoic acid is observed (Figure 7). The occurrence of this compound among reaction products indicates the interaction of furfuryl alcohol with furoate species which are present in the interlayer of the spent catalyst. It follows that when furoic acid is consumed in the esterification reaction, some basic active sites become again available for other reactions. Judging by the peculiar selectivity profiles at near complete furfural conversion (Figure 5), dehydration of FCH–OH to FCH is one of them.

The results strongly suggest that aldol condensation of furfural and cyclohexanone is affected by deactivation owing to the formation of furoic acid by the Cannizzaro reaction from furfural, so two further aspects have been studied: reusing of the spent catalyst in several reaction cycles and the influence of CH/F molar ratio.

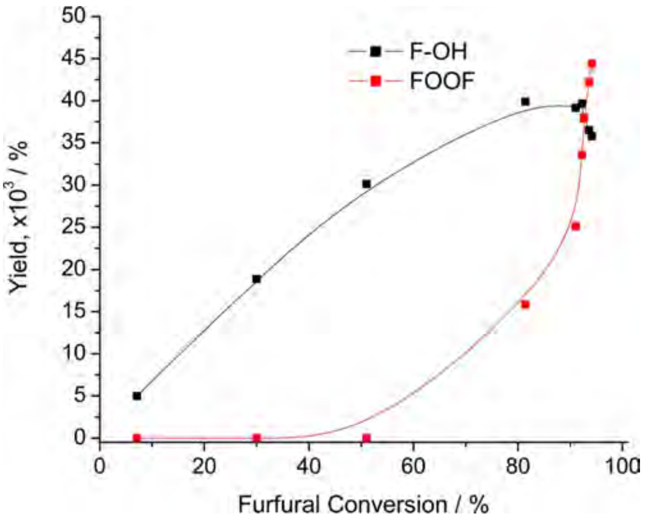

Figure 7. Furfuryl alcohol (F–OH) and furfuryl furoate (FOOF) yields observed during aldol condensation of furfural and cyclohexanone over reconstructed HTC ($T=25\,^\circ C$, CH/F molar ratio $=5$).

Reusing of the reconstructed HTC

The performance of the reconstructed HTC used in three consecutive catalytic runs at $T=25\,^\circ C$ with an intermediate catalyst separation by simple filtration (that is, without any additional steps, such as washing and calcination) is presented in Figure 8. The conversion of furfural dropped first moderately from 97% at the end of the first run to 88% after the second run. At the end of the third run, the decline of furfural conversion was already substantial and furfural conversion reached just 36% (Figure 8A). This was accompanied by a dramatic decrease in the yield of furfuryl alcohol (Figure 8B), which is an indication of the occurrence of the Cannizzaro reaction and, hence, furoic acid formation. Such a progressive loss of catalyst activity observed in consecutive runs is unequivocally concerned with a decrease in the amount of accessible active sites. In general, two different deactivation causes have been considered: the fouling of the catalyst surface with reaction products and the leaching of active compounds from the catalyst into the reaction mixture.[39] We could exclude leaching since the catalyst composition (Mg, Al) did not change after catalytic run, Mg nor Al were found in the liquid phase (as it was evidenced by ICP analysis), and after removing catalyst from the reaction mixture no further aldol condensation reaction was observed. Therefore, the spent catalysts after the first and the third cycle were analyzed by TGA and FTIR and the results were compared with those obtained for the fresh catalyst.

The weight loss of the fresh reconstructed HTC was 43.8% and it increased to 51.8–52% for the spent catalysts after the first and the third catalytic runs (Figure 9A). TGA curves also showed that the weight loss of the spent catalysts continued to grow at temperatures as high as 800 °C, in contrast to the freshly reconstructed HTC. The increase in the weight loss at temperature above about 500 °C can be attributed to heavy deposits formed in the reaction, plausibly heavy aldol condensation products that were reported previously.[40] The comparison of TGA results presented in Figure 9A suggests that the total weight loss of catalysts after either single or three catalytic runs was very similar. It means that in consecutive catalytic runs most of the heavy reaction products were formed already after the first experiment with no further accumulation of these compounds in the subsequent runs. Nonetheless, this contradicts to the steep decline in furfural conversion between the second and the third run. The yield of furfuryl alcohol (Figure 8B), on the other hand, suggests that in the second run still a significant amount of furoic acid and thus interlayer furoates was formed, while in the third run it was significantly reduced. Consequently, it can be concluded that deactivation by furoic acid that interacts with the Brønsted basic sites forming interlayer furoate species is responsible for the significant drop in the catalyst activity. Figure 9B evidences the presence of a shoulder signal in the range of $T=310–350\,^\circ C$ on DTG curve after the third run. This signal was previously attributed to decomposition of furoates.[50]

The DRIFT spectrum of the spent catalyst after catalytic runs, both the first and the third, shows the appearance of new bands compared to those observed in the spectrum of the fresh reconstructed HTC (Supporting Information, Figure S5). These were previously ascribed to furoates.[50] Thus, both the TGA/DTG and DRIFT results support catalytic data and evi-

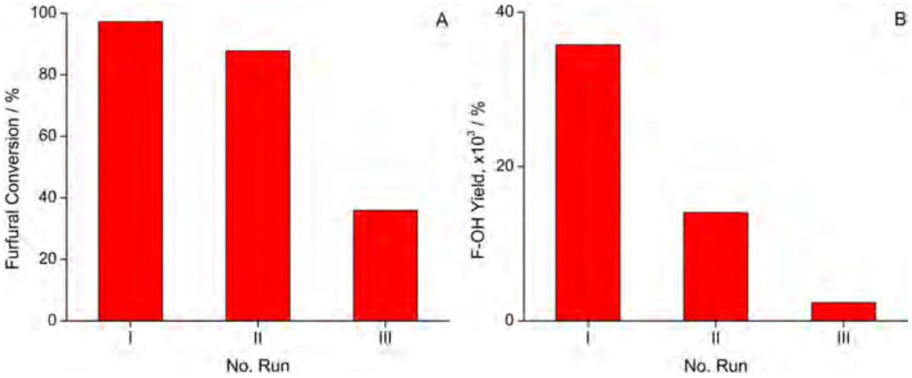

Figure 8. A) Furfural conversion and B) yield of furfuryl alcohol observed on reconstructed HTC in three consecutive catalytic runs. $T=25\,^\circ C$, CH/F $=5$, time -60 min.

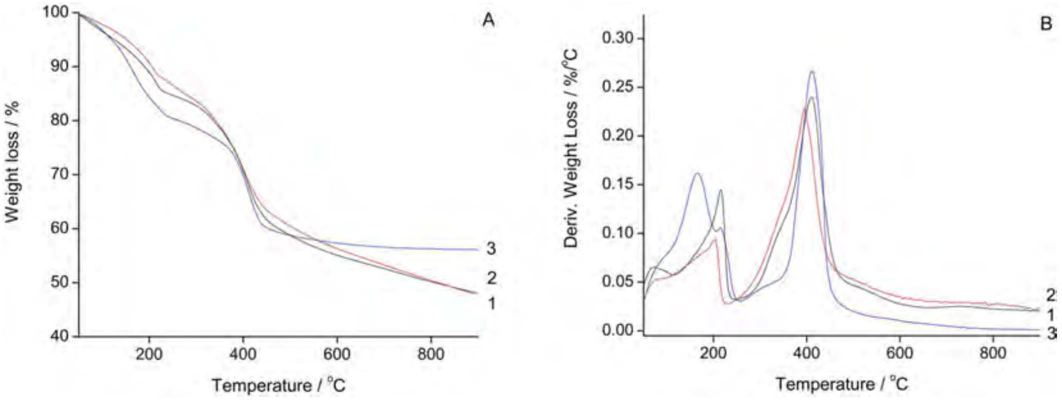

Figure 9. A) TGA and B) DTG curves for the spent reconstructed HTC catalyst after the first (1) and the third (2) catalytic run at $T=25\,^{\circ}C$. Characterization of the fresh reconstructed HTC is added as (3).

dence the formation of interlayer furoates which are formed in reconstructed HTC during aldol condensation of furfural and cyclohexanone. The formation of these species results in a decline of catalyst activity. As evidenced by TGA data, these furoates can be decomposed thermally.

Besides the accumulation of heavy deposits and the occurrence of Cannizzaro reaction, there could be also other plausible causes of the observed decrease in the activity of the reconstructed HTC in the recycling experiments. Aldol condensation on reconstructed hydrotalcites occurs with the participation of active OH-groups which are located near the edges of the platelets.[45] These groups are charge-compensating, so their properties, in terms of both basic strength and concentration, should be very sensitive to small changes in the surface properties of HTC platelets. Mechanisms of deactivation, such as surface reconstruction, pore collapse, or the destruction of the crystalline structure, which may occur during sequential catalytic runs cannot be excluded; however, this is outside the scope of the present study.

Influence of CH/F molar ratio

The results on the influence of cyclohexanone to furfural molar ratio in the range from 1 to 10 over the reconstructed Mg-Al HTC at 25 and 90 °C are shown in Figure 10. At both reaction temperatures, furfural conversion observed after 180 min. gradually increased with the growth in CH/F ratio (Figures 10 A, B). This increase is more pronounced at 25 °C what could be concerned with the effect of Cannizzaro reaction rather than the change in feed composition itself since the furfural-to-catalyst ratio was kept constant. Indeed, as Cannizzaro reaction is a bimolecular reaction of two furfural molecules, its probability in-

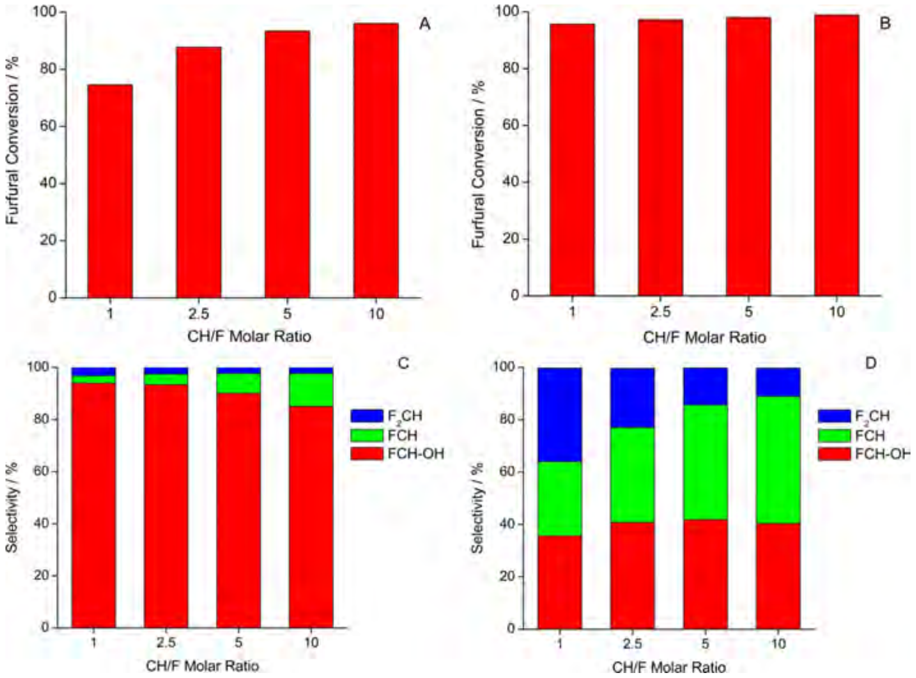

Figure 10. The influence of CH/F molar ratio on F conversion observed on reconstructed HTC after 180 min. of the reaction at A) $T=25\,^{\circ}C$ and B) after 40 min. of the reaction at $T=90\,^{\circ}C$. The composition of reaction products at C) $T=25\,^{\circ}C$ and D) 90 °C at furfural conversion of about 50 %.

creases with the increasing concentration of furfural in the reaction mixture. The deactivation caused by furoic acid is then augmented and consequently the conversion of furfural is lower. Owing to the lower reaction rate of aldol condensation at 25 °C, the effect of Cannizzaro reaction is more pronounced at this temperature (Figure 10 A). The conclusion is further corroborated by the yield of furfuryl alcohol in the reaction products that increases with the increasing CH/F molar ratio (Supporting Information, Figure S6) and by the analysis of spent catalysts by TGA and DRIFT that confirmed increased abundance of furoates on the spent catalyst at lower CH/F molar ratio (Supporting Information, Figure S7).

The composition of the reaction products as a function of the CH/F molar ratio was compared at nearly equal furfural conversion of about 50% for both temperatures (Figures 10 C, D). In all experiments at $T=25\,^{\circ}C$, the intermediate aldol FCH–OH was the most abundant reaction product and its selectivity decreased from 94 to 85% when increasing the CH/F molar ratio from 1 to 10 (Figure 10 C). At the same time, the selectivity to dehydrated FCH increased from 3 to 13% (Figure 10 C). It can be inferred that the dehydration performance of the reconstructed Mg-Al HTC is improved at lower furfural concentration in the reaction mixture, possibly due to the diminished extent of Cannizzaro reaction. Similarly, at 90 °C the selectivity to FCH also increased (from 28 to 49%) with the increasing CH/F ratio (Figure 10 D). On the contrary, the selectivity to F_2CH decreased from 36 to 10% upon increasing the CH/F molar ratio from 1 to 10 (Figure 10 D) which can be attributed to the limited availability of furfural for the second aldol condensation step, that is, for the reaction between FCH and F, at high CH/F molar ratios.

The presented results show that, by varying CH/F molar ratio, it is possible to influence the composition of obtained products. At a relatively high CH/F molar ratio (using CH excess) FCH–OH and FCH are predominantly formed, both having 11 carbon atoms, which fits well in the composition range of jet fuels. On the other hand, high furfural contents should be used if the production of F_2CH, that is, the product with 16 carbon atoms, is targeted. In both cases, HTC-derived catalysts show promising performance in aldol condensation of furfural and cyclohexanone that can be produced by the complex processing of lignocellulosic biomass. Nevertheless, the high activity of reconstructed HTC in the reaction is accompanied by the deactivation of the catalyst, what is evidenced by experiments with consecutive catalytic runs (Figure 8). The formation of compounds that block the active sites of the catalyst is a key factor that can influence the successful development of this environmentally friendly way of producing bio-derived jet fuel. Consequently, the improvement of the properties of a solid base catalyst and the optimization of reaction conditions are considered as a challenge for forthcoming studies.

Conclusions

The results of this study evidence that both Mg-Al mixed oxide and reconstructed HTC produced from an as-prepared HTC using corresponding treatments (thermal activation and rehydration), can be used as catalysts for valorization of cyclic ketones and furanics by aldol condensation. The performance of both basic catalysts in cyclohexanone self-condensation is very sensitive to moisture in the reaction mixture. Water either initially present in the feed or formed by dehydration of the produced intermediate (D1) decreases cyclohexanone conversion. Nevertheless, if water is constantly removed from a reactor, cyclohexanone conversion substantially increases up to 44% at 150 °C. Consequently, CH self-condensation does compete only to a very minor extent with the aldol condensation of CH and F.

The activity of the reconstructed HTC in aldol condensation of furfural and cyclohexanone is significantly higher than that of the Mg-Al mixed oxide, confirming that Brønsted basic sites rather than Lewis basic sites are responsible for the catalyst activity, similar to other aldol condensations. The reaction between furfural and cyclohexanone on reconstructed HTC proceeds at a high reaction rate even at $T=25\,^{\circ}C$. The increase in the reaction temperature promotes both the dehydration of the intermediate aldol to FCH and the second condensation step to F_2CH. Furthermore, the ratio between FCH and F_2CH reaction products may be changed by varying the molar ratio between furfural and cyclohexanone in the reaction mixture. The observed high conversions of the reactants together with the possibility to regulate the composition (molecular weight) of the reaction products hold substantial potential for the development of a reliable process aiming to produce bio-derived naphthenic components of jet fuel. Currently, the catalyst deactivation by side-products adsorbed on the catalysts surface poses the key challenge that needs to be further addressed. As shown in this study, it may be partially overcome by optimization of reaction parameters, for example, the cyclohexanone/furfural molar ratio. Gentle catalyst regeneration is another alternative to be further investigated.

Experimental Section

Catalyst

The details of Mg-Al HTC (Mg/Al = 3) preparation are presented elsewhere.[33] Briefly, the sample was synthesized by co-precipitation of an aqueous solution of magnesium and aluminum nitrates with a basic solution of potassium carbonate and potassium hydroxide at constant pH value of 9.5 and $T=60\,^{\circ}C$. Mg-Al mixed oxide was prepared by calcination of a dried as-prepared HTC (Mg/Al = 3) at 450 °C for 3 h. Reconstructed HTC was obtained by rehydration of the mixed oxide in pure water for 10 minutes followed by filtration and drying for 20 minutes using the method described elsewhere.[36]

Characterization

The structure of catalysts used in the study was confirmed by X-ray powder diffraction using a Philips MPD 1880 instrument with CuK_{α} irradiation ($\lambda = 0.154$ nm) in the 2θ range of 5°–70° at the 2θ scanning rate of $2.4^{\circ}\,min^{-1}$. Thermogravimetric analysis (TGA/DTG) was performed using a TA Instruments TGA Discovery series equipment operating with a heating ramp of $10\,^{\circ}C\,min^{-1}$ from room temperature to 900 °C in N_2 flow. TGA-MS experiments were performed using the same TGA unit equipped with a mass-spectrometer OmniStar GSD 320 (Pfeiffer-Vacuum) with a MID (multiple ion detection) measurement mode, a SEM (secondary electron multiplier) detector, and a quadrupole mass analyzer. DRIFT spectra were recorded on a Nicolet IS 10 FTIR spectrometer equipped with a DTGS detector and KBr beam splitter. All spectra were collected over the range of 4000–400 cm^{-1} at a spectral resolution of 4 cm^{-1} and number of scans 128 (both for the background and the sample spectra).

Catalysis

Furfural (F) (Sigma–Aldrich) and cyclohexanone (CH) (Sigma–Aldrich) used in catalytic experiments were pre-dried with a molecular sieve 3A to exclude the effect of moisture originating from the chemicals. All catalytic experiments on CH self-condensation and aldol condensation of F and CH were performed by using a 100 mL stirred batch reactor (a glass flask reactor). For these experiments, freshly calcined catalyst (0.5 g; $T=450\,^{\circ}C$) was used (0.5 g of Mg-Al mixed oxide was also used to prepare the reconstructed HTC). Furfural (6.5 g) and different amounts of cyclohexanone (6.6–66.4 g, corresponding to CH/F molar ratio in the range of 1–10) were used as a reaction mixture. The experiments were carried out at 25, 50, or 90 °C. In experiments on CH self-condensation 33.2 g of cyclohexanone was used and reaction temperature was in the range of 25–150 °C. After adjusting the desired reaction temperature, a catalyst was added to the reaction mixture, and the reaction was carried out for 180 min at 200 RPM. In experiments with changing stirring rate and catalyst particle size, it was established that the reaction is limited neither by external nor internal mass transfer under the chosen reaction conditions. Samples of liquid products were periodically withdrawn from the reactor during the experiment, diluted with excessive benzene, centrifuged, and analyzed by Agilent 7890A GC unit equipped with a flame ionization detector (FID), using a HP-5 capillary column (30 m/0.32 mm ID/0.25 μm). Each catalytic experiment was performed in parallel and the results were used only if the relative error did not exceed 2%. The composition of reaction products was determined by GC-MS by means of GC-2010 Plus (Shimadzu) unit (MS detector: GC-MS-QP 2010 Ultra; GC column: Rxi-5 Sil MS, Restek, 30 m × 0.25 mm ID *x* 0.25 μm). Catalytic results of aldol condensation of furfural and cyclohexanone were described by conversion and selectivity parameters that were calculated as follows:

reactant conversion(t) (mol%) $=100\times$ $(\text{reactant}_{t=0}-\text{reactant}_{t})/\text{reactant}_{t=0}$;

selectivity to product $i=$(mole of reactant converted to product i)/(total moles of reactant converted).

Carbon balance was monitored in all experiments as the total number of carbon atoms detected in each organic compound with Cn atoms divided by the initial number of carbon atoms in a feed, similar to the method used elsewhere.[36]

The yields of furfuryl alcohol (F–OH) and furoyl furoate (FOOF) determined in reaction products were calculated as the percentage of moles of the corresponding compound per the initial number of moles of furfural in reaction mixture.

Acknowledgements

The publication is a result of the project reg. No. GA15-21817S, which was financially supported by the Czech Science Foundation. Z. Tišler (UNICRE) is acknowledged for preparing the Mg-Al hydrotalcite sample.

Conflict of interest

The authors declare no conflict of interest.

Keywords: aldol condensation · cyclohexanone · furfural · hydrotalcite · mixed oxides

[1] G. W. Huber, S. Iborra, A. Corma, *Chem. Rev.* **2006**, *106*, 4044 – 4098.
[2] G. W. Huber, B. E. Dale, *Sci. Am.* **2009**, *301*, 52 – 59.
[3] D. Kubička, I. Kubičková, J. Čejka, *Catal. Rev. Sci. Eng.* **2013**, *55*, 1 – 78.
[4] C. Somerville, H. Youngs, C. Taylor, S. C. Davis, S. P. Long, *Science* **2010**, *329*, 790 – 792.
[5] S. Zinoviev, F. Müller-Langer, P. Das, N. Bertero, P. Fornasiero, M. Kaltschmitt, G. Centi, S. Miertus, *ChemSusChem* **2010**, *3*, 1106 – 1133.
[6] C. E. Wyman, *Appl. Biochem. Biotechnol.* **1994**, *45/46*, 897 – 915.
[7] G. W. Huber, A. Corma, *Angew. Chem. Int. Ed.* **2007**, *46*, 7184 – 7201; *Angew. Chem.* **2007**, *119*, 7320 – 7338.
[8] *Aviation and the Global Atmosphere, A special report of the Intergovernmental panel on climate change* (Eds.: E. Penner, D. H. Lister, D. J. Griggs, D. J. Dokken, M. McFarland), Cambridge University Press, Cambridge **1999**.
[9] T. Edwards, C. Moses, F. Dryer, *Evaluation of combustion performance of alternative aviation fuels*, 46th AIAA/ASME/SAE/ASEE Joint Propulsion Conference & Exhibit., Nashville, TN, USA, **2010**.
[10] L. M. Shafer, R. C. Striebich, J. Gomach, T. Edwards, *Chemical class composition of commercial jet fuels and other specialty kerosene fuels*, AIAA 2006 – 7972, **2006**.
[11] O. J. Hadaller, J. M. Johnson, *World fuel sampling program*, Coordinating research council report No. 647, **2006**.
[12] G. W. Huber, J. N. Chheda, C. J. Barret, J. A. Dumesic, *Science* **2005**, *308*, 1446 – 1450.
[13] R. Ramos, Z. Tišler, O. Kikhtyanin, D. Kubička, *Catal. Sci. Technol.* **2016**, *6*, 1829 – 1841.
[14] L. Faba, E. Díaz, S. Ordóñez, *Catal. Today* **2011**, *164*, 451 – 456.
[15] H. S. Chung, C. S. H. Chen, R. A. Kremer, J. R. Boulton, *Energy Fuels* **1999**, *13*, 641 – 649.
[16] B. G. Harvey, M. E. Wright, R. L. Quintana, *Energy Fuels* **2010**, *24*, 267 – 273.
[17] H. A. Meylemans, R. L. Quintana, B. G. Harvey, *Fuel* **2012**, *97*, 560 – 568.
[18] Q. Deng, J. Xu, P. Han, L. Pan, L. Wang, X. Zhang, J.-J. Zou, *Fuel Process. Technol.* **2016**, *148*, 361 – 366.
[19] M. Hronec, K. Fulajtárova, T. Liptaj, M. Stolcová, N. Prónayová, T. Soták, *Biomass Bioenergy* **2014**, *63*, 291 – 299.
[20] J. Cueto, L. Faba, E. Díaz, S. Ordóñez, *ChemCatChem* **2017**, *9*, 1765 – 1770.
[21] W. Wang, X. Ji, H. Ge, Z. Li, G. Tian, X. Shao, Q. Zhang, *RSC Adv.* **2017**, *7*, 16901 – 16907.
[22] H. Liu, T. Jiang, B. Han, S. Liang, Y. Zhou, *Science* **2009**, *326*, 1250 – 1252.
[23] J.-F. Zhu, G.-H. Tao, H.-Y. Liu, L. He, Q.-H. Sun, H.-C. Liu, *Green Chem.* **2014**, *16*, 2664 – 2669.
[24] M. Hronec, K. Fulajtarova, T. Liptaj, *Appl. Catal. A* **2012**, *437 – 438*, 104 – 111.
[25] M. Hronec, K. Fulajtarová, *Catal. Commun.* **2012**, *24*, 100 – 104.
[26] Y. Yang, Z. Du, Y. Huang, F. Lu, F. Wang, J. Gao, J. Xu, *Green Chem.* **2013**, *15*, 1932 – 1940.
[27] J. Yang, N. Li, G. Li, W. Wang, A. Wang, X. Wang, Y. Cong, T. Zhang, *Chem. Commun.* **2014**, *50*, 2572 – 2574.
[28] D. Lorenzo, E. Simón, A. Santos, A. Romero, *Ind. Eng. Chem. Res.* **2014**, *53*, 19117 – 19127.
[29] D. Lorenzo, A. Santos, E. Simón, A. Romero, *Ind. Eng. Chem. Res.* **2013**, *52*, 2257 – 2265.
[30] D. Liang, G. Li, Y. Liu, J. Wu, X. Zhang, *Catal. Commun.* **2016**, *81*, 33 – 36.
[31] F. Cheng, C. E. Brewer, *Renewable Sustainable Energy Rev.* **2017**, *72*, 673 – 722.
[32] P. Bi, J. Wang, Y. Zhang, P. Jiang, X. Wu, J. Liu, H. Xue, T. Wang, Q. Li, *Bioresour. Technol.* **2015**, *183*, 10 – 17.
[33] L. Hora, O. Kikhtyanin, L. Čapek, O. Bortnovskiy, D. Kubička, *Catal. Today* **2015**, *241*, 221 – 230.

[34] C. J. Barrett, J. N. Chheda, G. W. Huber, J. A. Dumesic, *Appl. Catal. B* **2006**, *66*, 111 – 118.
[35] G. J. Kelly, F. King, M. Kett, *Green Chem.* **2002**, *4*, 392 – 399.
[36] O. Kikhtyanin, Z. Tišler, R. Velvarská, D. Kubička, *Appl. Catal. A* **2017**, *536*, 85 – 96.
[37] D. Tichit, M. N. Bennani, F. Figueras, R. Tessier, J. Kervennal, *Appl. Clay Sci.* **1998**, *13*, 401 – 415.
[38] F. Figueras, *Top. Catal.* **2004**, *29*, 189 – 196.
[39] L. Faba, E. Díaz, S. Ordóñez, *Appl. Catal. B* **2012**, *113 – 114*, 201 – 211.
[40] O. Kikhtyanin, L. Hora, D. Kubička, *Catal. Commun.* **2015**, *58*, 89 – 92.
[41] *Layered double hydroxides: Present and future*, (Ed. V. Rives), Nova Science, New York, **2001**.
[42] *Layered double hydroxides, Structure and bonding series, 119*, (Eds.: X. Duan, D. G. Evans), Springer, Heidelberg, **2006**.
[43] D. P. Debecker, E. M. Gaigneaux, G. Busca, *Chem. Eur. J.* **2009**, *15*, 3920 – 3935.
[44] D. Tichit, D. Lutic, B. Coq, R. Durand, R. Teissier, *J. Catal.* **2003**, *219*, 167 – 175.
[45] S. Abelló, F. Medina, D. Tichit, J. Pérez-Ramírez, J. C. Groen, J. E. Sueiras, P. Salagre, Y. Cesteros, *Chem. Eur. J.* **2005**, *11*, 728 – 739.
[46] O. Kikhtyanin, L. Čapek, L. Smoláková, Z. Tišler, D. Kadlec, M. Lhotka, P. Diblíková, D. Kubička, *Ind. Eng. Chem. Res.* **2017**, *56*, 13411 – 13422.
[47] Y. S. Mahajan, R. S. Kamath, P. S. Kumbhar, S. M. Mahajani, *Ind. Eng. Chem. Res.* **2008**, *47*, 25 – 33.
[48] J. M. Aragón, J. M. R. Vegas, L. G. Jodra, *Ind. Eng. Chem. Res.* **1994**, *33*, 592 – 599.
[49] G. G. Podrebarac, F. T. T. Ng, G. L. Rempel, *Chem. Eng. Sci.* **1997**, *52*, 2991 – 3002.
[50] O. Kikhtyanin, E. Lesnik, D. Kubička, *Appl. Catal. A* **2016**, *525*, 215 – 225.

Manuscript received: November 24, 2017
Accepted manuscript online: December 19, 2017
Version of record online: February 19, 2018

frontiers
in Chemistry

ORIGINAL RESEARCH
published: 24 May 2018
doi: 10.3389/fchem.2018.00176

Physico-Chemical Properties of MgGa Mixed Oxides and Reconstructed Layered Double Hydroxides and Their Performance in Aldol Condensation of Furfural and Acetone

Oleg Kikhtyanin[1,2], Libor Čapek[3], Zdeněk Tišler[1], Romana Velvarská[1], Adriana Panasewicz[3], Petra Diblíková[4] and David Kubička[2]*

[1] Unipetrol Centre for Research and Education, Litvínov, Czechia, [2] Technopark Kralupy VŠCHT Praha, University of Chemistry and Technology Prague, Kralupy nad Vltavou, Czechia, [3] Department of Physical Chemistry, Faculty of Chemical Technology, University of Pardubice, Pardubice, Czechia, [4] Department of Organic Technology, University of Chemistry and Technology Prague, Prague, Czechia

OPEN ACCESS

Edited by:
*Konstantinos Triantafyllidis,
Aristotle University of Thessaloniki,
Greece*

Reviewed by:
*Jozef Mikulec,
VÚRUP (Slovakia), Slovakia
Miguel Angel Centeno,
Consejo Superior de Investigaciones
Científicas (CSIC), Spain
Ioannis N. Lykakis,
Aristotle University of Thessaloniki,
Greece*

***Correspondence:**
*David Kubička
kubickad@vscht.cz*

Specialty section:
*This article was submitted to
Green and Sustainable Chemistry,
a section of the journal
Frontiers in Chemistry*

Received: *30 January 2018*
Accepted: *03 May 2018*
Published: *24 May 2018*

Citation:
*Kikhtyanin O, Čapek L, Tišler Z,
Velvarská R, Panasewicz A,
Diblíková P and Kubička D (2018)
Physico-Chemical Properties of MgGa
Mixed Oxides and Reconstructed
Layered Double Hydroxides and Their
Performance in Aldol Condensation of
Furfural and Acetone.
Front. Chem. 6:176.
doi: 10.3389/fchem.2018.00176*

MgGa layered double hydroxides (Mg/Ga = 2–4) were synthesized and used for the preparation of MgGa mixed oxides and reconstructed hydrotalcites. The properties of the prepared materials were examined by physico-chemical methods (XRD, TGA, NH_3-TPD, CO_2-TPD, SEM, and DRIFT) and tested in aldol condensation of furfural and acetone. The as-prepared phase-pure MgGa samples possessed hydrotalcite structure, and their calcination resulted in mixed oxides with MgO structure with a small admixture phase characterized by a reflection at $2\theta \approx 36.0°$. The interaction of MgGa mixed oxides with pure water resulted in reconstruction of the HTC structure already after 15 s of the rehydration with maximum crystallinity achieved after 60 s. TGA-MS experiments proved a substantial decrease in carbonates in all rehydrated samples compared with their as-prepared counterparts. This allowed suggesting presence of interlayer hydroxyls in the samples. Acido-basic properties of MgGa mixed oxides determined by TPD technique did not correlate with Mg/Ga ratio which was explained by the specific distribution of Ga atoms on the external surface of the samples. CO_2-TPD method was also used to evaluate the basic properties of the reconstructed MgGa samples. In these experiments, an intensive peak at $T = 450°C$ on CO_2-TPD curve was attributed to the decomposition of carbonates newly formed by CO_2 interaction with interlayer carbonates rather than to CO_2 desorption from basic sites. Accordingly, CO_2-TPD method quantitatively characterized the interlayer hydroxyls only indirectly. Furfural conversion on reconstructed MgGa materials was much larger compared with MgGa mixed oxides confirming that Brønsted basic sites in MgGa catalysts, like MgAl catalysts, were active in the reaction. Mg/Ga ratio in mixed oxides influenced product selectivity which was explained by the difference in textural properties of the samples. In contrast, Mg/Ga ratio in reconstructed catalysts had practically no effect on the composition of reaction products suggesting that the basic sites in these catalysts acted similarly in aldol condensation of acetone with furfural. It was concluded that the properties of MgGa samples resembled in a great extent those of MgAl hydrotalcite-based materials and demonstrated their potential as catalysts for base-catalyzed reactions.

Keywords: MgGa layered double hydroxides, mixed oxides, reconstructed hydrotalcites, aldol condensation, acido-basic properties

INTRODUCTION

A common feature of the Layered Double Hydroxides (LDH) or Hydrotalcite-like (HTC) family, both natural and synthesized, is that they all have a structure closely related to that of the mineral hydrotalcite, that is, rhombohedral $Mg_6Al_2(OH)_{16}CO_3{\cdot}4H_2O$. All these materials are composed of two-dimensional layers of positively charged double hydroxides together with water molecules and exchangeable charge-compensating anions which located in interlayer (Cavani et al., 1991; Sels et al., 2001; Debecker et al., 2009; Takehira, 2017). The general formula of LDHs can be described as $[M^{2+}_{1-x}M^{3+}{}_{x}(OH)_2]^{x+}$ $[A_{x/n}]^{n-}{\cdot}mH_2O$, where M^{2+} is a divalent cation, M^{3+} is a trivalent cation and A is a charge-compensating anion. Mg-Al hydrotalcites, most known and well-studied among the total family, are derived from brucite $Mg(OH)_2$ as a general crystallographic structure. These brucite layers are stacked on top of each other and held together by weak interactions through hydrogen atoms (Cavani et al., 1991; Debecker et al., 2009). In the brucite layers a part of Mg^{2+} cations are substituted with Al^{3+} cations thus creating a positive charge in the layers. In synthetic MgAl HTCs, the substitution degree of Mg → Al may be different but lies in the range of $x = 0.1$–0.5 (Cavani et al., 1991). A charge resulting from this substitution is compensated by interlayer anions (CO_3^{2-}, NO_3^-, Cl^-, etc). Additionally, water molecules are in the interlayer in amounts dependent on the temperature, on the water vapor pressure and the nature of the anions present (Cavani et al., 1991; Debecker et al., 2009). The chemical composition of LDHs is not limited to Mg and Al cations, and at the present the family of these compounds consists of a large variety of synthetic materials which are composed of Mg^{2+}, Zn^{2+}, Co^{2+}, Cu^{2+}, etc., as divalent cations, and Al^{3+}, Fe^{3+}, Cr^{3+}, La^{3+}, etc., as trivalent cations (Cavani et al., 1991; Choudary et al., 2001; Sels et al., 2001; Motokura et al., 2006; Pérez-Ramírez et al., 2007a; Debecker et al., 2009; Takehira, 2017).

The most popular method of synthesizing LDHs is based on the co-precipitation of aqueous solutions of the corresponding salts (usually nitrates) with alkaline solutions (Na or K hydroxide and carbonate) at low supersaturating conditions and fixed pH values. As a consequence, carbonate groups are present as charge-compensation anions in as-prepared LDHs. The as-prepared materials exhibit low activity in catalytic applications and therefore have to be activated. Heat treatment is the main and the simple way to activate the as-prepared LDHs which results in the removal of water, the dehydroxylation of brucite-like layers and the decomposition of interlayer carbonates. Mixed oxides formed by the thermal decomposition of as-prepared LDHs exhibit much better basic properties than the starting as-prepared LDHs. The mixed oxides possess Lewis basic sites and are widely used in base-catalyzed reactions such as transesterification (Zeng et al., 2008), condensations (Kustrowski et al., 2006; Perez et al., 2009), alkylation (Cavani et al., 2005), and Michael addition (Prescott et al., 2005).

A distinctive feature of HTC-like materials is so-called "memory effect" described for the first time by Miyata (1980), i.e., the recovery of original lamellar structure by hydration of mixed oxide. Thus, the interaction of MgAl mixed oxide either with water vapor or by immersion in decarbonated water leads to the formation of meixnerite $[Mg_6Al_2(OH)_{18}{\cdot}4H_2O]$ which is a hydrotalcite analog with OH^- groups as compensating anions in the interlayer instead of the original carbonates (Climent et al., 2002b; Tichit and Coq, 2003; Abelló et al., 2005; Pérez-Ramírez et al., 2007b; Kikhtyanin et al., 2017b). The interlayer hydroxyls are Brønsted basic sites and, therefore, the reconstructed materials are widely used in a number of base-catalyzed-reactions which require Brønsted basicity, such as self- and cross-aldol condensation of aldehydes and ketones (Tichit et al., 1998, 2002; Climent et al., 2002a; Abelló et al., 2005), Michael additions (Choudary et al., 1999), Knoevenagel and Claisen-Schmidt condensation (Cavani et al., 1991; Climent et al., 1995; Guida et al., 1997; Di Cosimo et al., 1998), etc.

In a zeolite family, the substitution of aluminum atoms by gallium in a silicate matrix leads to the formation of gallium silicates of various structural types whose specific physicochemical properties are successfully used in a number of acid-catalyzed reactions (Fricke et al., 2000; Chao and Liu, 2005; Wu et al., 2010). It is therefore not surprising that a possibility to replace Al atoms by Ga atoms is also assumed in other classes of inorganic compounds. Indeed, the synthesis and the study of the physico-chemical properties of MgGa LDHs have been reported repeatedly (Rebours et al., 1994; López-Salinas et al., 1996, 1997; Aramendía et al., 1999a,b, 2000; Thomas and Vishnu Kamath, 2005; Grand et al., 2010). Similar to other LDHs, the synthesis of MgGa is performed starting from Mg and Ga salt solutions mixed with sodium hydroxide and carbonate solutions; the heat treatment of the as-prepared materials results in MgGa mixed oxides. Nevertheless, in most cases, the studies on the properties of the prepared MgGa LDHs and mixed oxides are limited to their synthesis and characterization by different physico-chemical methods, such as XRD, TGA, DRIFT, MAS, NMR. More rarely, studies on the basic properties of MgGa mixed oxides have also been documented (López-Salinas et al., 1997; Prinetto et al., 2000). In addition, the "memory effect" has been demonstrated for this type of materials. Indeed, MgGa mixed oxides restored LDH structure (i) by exposure to a water-saturated atmosphere for 18 h followed by CO_2 picked up from the ambient for this reconstruction (Thomas and Vishnu Kamath, 2005), (ii) by the dispersion of MgGa mixed oxide under vigorous magnetic stirring during 1 h into the decarbonated water at 298 K and 1×10^5 Pa (Prinetto et al., 2000), or (iii) by the treatment of MgGa mixed oxide with a carbonate-containing aqueous solution (López-Salinas et al., 1996). Despite the growing interest to Ga-containing catalysts in different applications, there is a lack of available information which reports about their catalytic performance in base-catalyzed reactions. Concerning Ga-containing MgGa LDHs, Prinetto et al. (2000) demonstrated that the substitution of Al^{3+} with Ga^{3+} slightly increased the density of the basic sites in the Mg-containing mixed oxides and slightly increased their catalytic activity in acetone self-condensation. Tabanellia et al. (2018) used MgGa mixed oxide for the gas-phase methylation of phenol to 2,4,6-trimethylphenol and attributed the outstanding performance of the catalyst to its high activity in methanol dehydrogenation to formaldehyde as well as to the moderate acidic features due to Ga sites, which enhanced the intramolecular rearrangement of O-alkylated compounds. Rousselot et al. (1999) investigated the catalytic performance of both as-prepared and calcined MgGa LDHs in Knoevenagel condensation of benzaldehyde with ethyl cyanoacetate. They explained the obtained results by a rehydration process of the calcined samples during the catalytic reaction.

Nevertheless, there is a great lack in information about the performance of catalysts based on reconstructed MgGa LDHs. Moreover, in contrast to MgAl materials (Pérez-Ramírez et al., 2007b; Kikhtyanin et al., 2017b), the effect of reconstruction time on the physico-chemical properties of MgGa LDHs and the catalytic performance of the reconstructed materials has not been reported yet.

Aldol condensation of furfural and acetone (**Scheme 1**) is an attractive object for an investigation from several points of view. First of all, this reaction has a great practical potential as it allows increasing the carbon atom chain length starting from the relatively simple ones which can be produced by biomass processing (Gámez et al., 2006; Mäki-Arvela et al., 2011). The obtained condensation products can be further hydrogenated/deoxygenated to afford hydro-carbons, namely C_8 and C_{13} alkanes (Zapata et al., 2012; Ramos et al., 2016). On the other hand, aldol condensation of furfural and acetone attracts also a scientific interest, because this reaction makes it possible to probe both the acid (Kikhtyanin et al., 2014, 2015) and basic sites (Sádaba et al., 2011; Faba et al., 2012; Thanh et al., 2016) of heterogeneous catalysts. Regularities found in preceding studies help to evaluate and understand the catalytic performance of following catalytic materials.

The purpose of this paper is to correlate the physicochemical characteristics of samples derived from MgGa LDHs varied by Mg/Ga ratio with their catalytic performance. A special attention is paid to the reconstructed MgGa materials, namely, a possibility to recover HTC structure by the interaction of MgGa mixed oxide with pure water. For this purpose, the effect of rehydration duration of MgGa mixed oxides on the properties of the obtained samples was studied in detail and the catalytic performance of both MgGa mixed oxides and reconstructed LDHs were compared in aldol condensation of furfural and acetone.

MATERIALS AND METHODS

Preparation of MgGa Mixed Oxides

MgGa layered double hydroxides varied in Mg:Ga molar ratio in reactive mixture in the range of (2–4):1 were prepared based on a method described in Hora et al. (2015). For these syntheses Ga nitrate was prepared by the dissolution of powder metallic Ga (Unimagnet) in concentrated nitric acid followed by the evaporation of the excessive acid by using vacuum evaporator. The composition of obtained salt was determined by ICP. MgGa LDH's with Mg:Ga molar ratio from 2:1 to 4:1 were synthesized by co-precipitation method at constant pH value (pH = 9.5) and constant temperature (T = 60°C). The preparation procedure involves mixing of aqueous solutions of nitrates consisting of Gallium nitrate $Ga(NO_3)_2 \cdot 6H_2O$ prepared as described above and magnesium nitrate $Mg(NO_3)_2 \cdot 6H_2O$ (Lach-ner, p.a. purity) ($c_{Mg+Ga} = 1$ mol/dm^3), and a basic solution containing potassium carbonate K_2CO_3 (Penta, p.a.

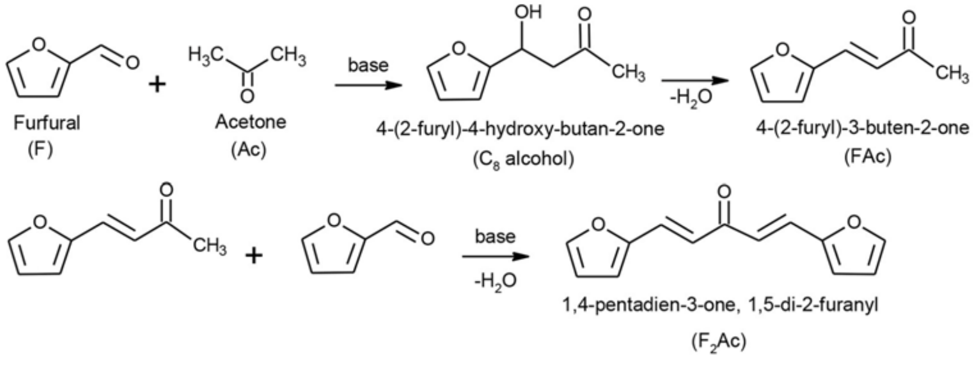

SCHEME 1 | Reaction scheme of aldol condensation between furfural and acetone.

purity) and potassium hydroxide KOH (Lach-ner, p.a. purity) ($c_{KOH} = 2$ mol/dm^3 + $c_{k_2co_3} = 0.2$ mol/dm^3). After precipitation the solids were isolated by press-filtration using paper filter plate S15N (Hobra); the filter cake was washed by demineralized water to neutral pH and dried in oven overnight at 65°C.

The MgGa mixed oxides were prepared by calcination of the dried as-prepared LDHs at 450°C for 3 h (heating rate 5°C·min^{-1}). The rehydration of the mixed oxides with deionized water was performed at room temperature and rehydrate on time in the range of 0–40 min. All samples chosen for physico-chemical characterization and catalytic runs were dried for 40 min. Other details in the preparation of the rehydrated samples are available in Kikhtyanin et al. (2017b). After preparation (rehydration+drying steps), all materials were kept in a desiccator under inert atmosphere to prevent contact of the samples with CO_2 from air during their storage. The samples were taken away from the desiccator only before performing experiments on their characterization. Further in the text, the as-prepared MgGa LDHs are denoted as MgGa-xA, calcined MgGa mixed oxides are denoted as MgGa-xC and rehydrated samples are denoted as MgGa-xR-y, where x stands for Mg/Ga molar ratio and y stands for rehydration time.

Physico-Chemical Characterization

Chemical composition was determined by ICP-OES. The phase composition of the prepared samples was determined by X-ray powder diffraction using a Philips MPD 1880 instrument with Cu K_α irradiation ($\lambda = 0.154$ nm) in the 2θ range of 5–70° at the 2θ scanning rate of 2.4°·min^{-1}. In each group of prepared catalysts, i.e., as-prepared LDHs, MgGa mixed oxides and reconstructed LDHs, the sample with the highest crystallinity was assigned relative crystallinity 100%. Textural properties were determined from N_2 physisorption isotherms at 77 K obtained by using a Quantachrome AUTOSORB unit. Prior to the analyses, the samples were outgassed at 250°C for 3 h in flowing N_2. BET equation was used to calculate the specific surface area of the samples. Thermogravimetric analysis (TGA/DTG) of the dried as-prepared LDHs, MgGa mixed oxides and rehydrated samples was performed using a TA Instruments TGA Discovery series equipment operating with a heating ramp of 10°C·min^{-1} from room temperature to 900°C in N_2 flow. TGA-MS experiments were performed using the same TGA unit equipped with a mass-spectrometer OmniStar GSD 320 (Pfeiffer-Vacuum) with a MID (Multiple Ion Detection) measurement mode, a SEM (Secondary Electron Multiplier) detector, and a quadrupole mass-analyzer. DRIFT spectra were recorded on a Nicolet IS 10 FTIR spectrometer equipped with a DTGS detector and KBr beam splitter. All spectra were collected over the range of 4,000–400 cm^{-1} at a spectral resolution of 4 cm^{-1} and number of scans 128 (both for the background and the sample spectra).

Samples for Scanning Electron Microscopy (SEM) observations were mounted on a holder and sputter-coated (Q150R ES, Quorum Technologies Ltd., United Kingdom) by 10 nm of gold to neutralize charging-effects and to increase an SE yield at final micrographs. Further, the images of coated samples were acquired using field emission scanning electron microscope (Lyra3 GMU, Tescan Orsay Holding a.s., Czech Republic) at an accelerating voltage of 12 kV and absorbed current ranging from 200 to 300 pA. For imaging, the SE detection was used to investigate the morphology of samples. The temperature-programmed desorption of carbon dioxide (CO_2-TPD) or ammonia (NH_3-TPD) was used to evaluate basic and acidic properties of MgGa mixed oxides and reconstructed LDHs. The details of the methods are presented in Kikhtyanin et al. (2017a). Maximum temperature in TPD experiments was chosen as 450°C which is temperature used for the preparation of MgGa mixed oxides.

Catalytic Test

Furfural (Sigma-Aldrich) and acetone (LachNer, Czech Republic) used for catalytic experiments were pre-dried with a molecular sieve 3A to exclude the effect of moisture originating from the chemicals.

For catalytic experiments with MgGa mixed oxides, 0.5 g of freshly calcined HTC was used. For catalytic experiments with reconstructed MgGa LDHs, 0.5 g of freshly calcined HT was pre-rehydrated according to the method described above.

Aldol condensation of furfural with acetone was carried out in a 100-ml stirred batch reactor (a glass flask reactor) at temperature of 50°C in the case of mixed oxides or 25°C in the case of reconstructed LDHs. Prior to the catalytic tests, the mixture of 19.7 g of acetone and 6.5 g of furfural (acetone to furfural molar ratio 5/1) was stirred at 200 RPM and kept at the predetermined reaction temperature. After that, a studied catalyst (grain of 0.25–0.5 mm) was added and the reaction was carried out at predetermined temperature for 120 min at 200 RPM. It was previously established that the reaction is limited neither by external nor internal mass transfer under the chosen reaction conditions (in tests with changing stirring rate and catalyst particle size; Hora et al., 2015). Samples of liquid products were periodically withdrawn from the reactor during the experiment, filtered and analyzed by Agilent 7890A GC unit equipped with a flame ionization detector (FID), using a HP-5 capillary column (30 m/0.32 mm ID/0.25 μm). Catalytic results of aldol condensation of furfural and acetone were described by conversion and selectivity parameters that were calculated as follows:

$$\text{reactant conversion (t) (mol\%)} = 100 \times (\text{reactant}_{t=0} - \text{reactant}_t)/\text{reactant}_{t=0};$$

$$\text{selectivity to product i} = (\text{mole of reactant converted to product i}) / (\text{total moles of reactant converted}).$$

Carbon balance was monitored in all experiments as the total number of carbon atoms detected in each organic compound with C_n atoms (where $n = 3, 5, 8, \ldots$, etc.) divided by the initial number of carbon atoms in F+Ac feed:

$$\text{C balance (\%)} = (3\,\text{mol}C_3 + 5\,\text{mol}C_5 + \ldots \text{nmol}C_n) / (3\,\text{mol}C_{3(t=0)} + 5\,\text{mol}C_{5(t=0)}).$$

RESULTS AND DISCUSSION

Chemical, Structural, and Textural Properties of As-Prepared LDHs and Mixed Oxides

ICP data showed that gallium content in the prepared samples was higher than the values calculated based on the composition of the chemical mixture used for the synthesis. Similar deviation from the theoretical composition was observed for MgGa LDHs repeatedly (López-Salinas et al., 1996; Aramendía et al., 1999a,b) what was explained by the considerable solubility of intermediate $Ga(OH)_3$ species in a basic solution (López-Salinas et al., 1996).

The XRD data confirmed that Ga was highly efficiently incorporated into the brucite-like layers of MgGa LDHs in a wide range of Mg/Ga molar ratios. XRD patterns of the as-prepared MgGa LDHs varying by gallium content (**Figure 1**) show the intensive symmetric lines of a pure hydrotalcite phase (similar to JCPDS Card No. 22-0700). The reflections at $2\theta \approx 11.2^\circ$, 22.8°, 36°, and 60° are characteristic for the brucite-like layers (Di Cosimo et al., 1998; Abelló et al., 2005; Kikhtyanin et al., 2017a). The absence of additional lines in the diffractograms suggests that no other crystalline phases are present in the samples thus proving the high phase purity of the as-prepared MgGa LHDs materials. The preparation of phase-pure MgGa LDHs has also been reported in other studies (Rebours et al., 1994; Aramendía et al., 1999b; Thomas and Vishnu Kamath, 2005). MgGa-3A possesses the highest crystallinity; the other two samples show crystallinity of 93–95% relative to MgGa-3A.

The diffraction peaks assigned to (003) and (110) reflections (i.e., at 11.2 and 60°) were used to calculate the basal spacing between the layers (d) and unit cell dimension a (as $a = 2d_{110}$), respectively. Both the d and a values increase with the increasing Mg/Ga molar ratio (**Table 1**), which is an usual trend observed for MgAl hydrotalcites with different Al content (Yun and Pinnavaia, 1995; Di Cosimo et al., 1998; Kikhtyanin et al., 2017a). The increase in the spacing between layers in LDH structure is unequivocally ascribed to differences in the ionic radii of Ga^{3+} and Mg^{2+} being 0.62 and 0.72 Å, respectively[1], proving the isomorphous substitution of Mg^{2+} by Ga^{3+} atoms within the brucite-like layers. The calcination of the as-prepared materials at $T = 450^\circ C$ results in total destruction of the LDH structure as evidenced by the disappearance of diffraction lines corresponding to the HTC structure. Two intensive diffraction lines observed in XRD patterns of all MgGa mixed oxides at $2\theta \approx 43.0^\circ$ and 62.5° and a smaller diffraction peak at $2\theta \approx 37.0^\circ$ are typical for MgO periclase-type structure (JCPDS card No. 45-0946). Similar XRD patterns were observed also after heat treatment of MgAl hydrotalcites (Yun and Pinnavaia, 1995; Di Cosimo et al., 1998; Kikhtyanin et al., 2017a). The relative crystallinity of the MgO phase decreased dramatically with the decline in the Mg/Ga ratio of the mixed oxides (**Table 1**) suggesting the presence of amorphous phase at high Ga content. The decrease in the MgO basal spacing, d(200), from 2.112 to 2.105 Å with the increasing Ga content (**Table 1**) indicates that Ga replaced partially Mg in the MgO crystalline framework. Besides, an additional reflection is present in XRD patterns of MgGa mixed oxides at $2\theta \approx 36.0^\circ$. It becomes more intensive with the increasing Ga content suggesting that it is originated from a Ga-containing compound. The appearance of an additional line in XRD patterns of MgGa mixed oxides after the calcination of MgGa LDHs at moderate temperatures was reported earlier in several studies (Rebours et al., 1994; Aramendía et al., 1999b; Grand et al., 2010). Rebours et al. (1994) suggested that the reflection at $2\theta \approx 36.0^\circ$ was either due to the presence of magnesium gallate, $MgGa_2O_4$, or due to the presence of Ga cations in the tetrahedral sites in magnesia lattice.

As-prepared MgGa LDHs possess BET surface area in the range of 68–82 $m^2 \cdot g^{-1}$, but the values of BET surface area for MgGa mixed oxides increases to 123–140 $m^2 \cdot g^{-1}$ (**Table 1**) what is a consequence of the collapse of lamellar HTC structure.

DRIFT spectra of the as-prepared MgGa LDH samples are presented in **Figure 2**. They agree with those published elsewhere

---

[1] *Database of Ionic Radii*. Available online at: http://abulafia.mt.ic.ac.uk/shannon/ptable.php

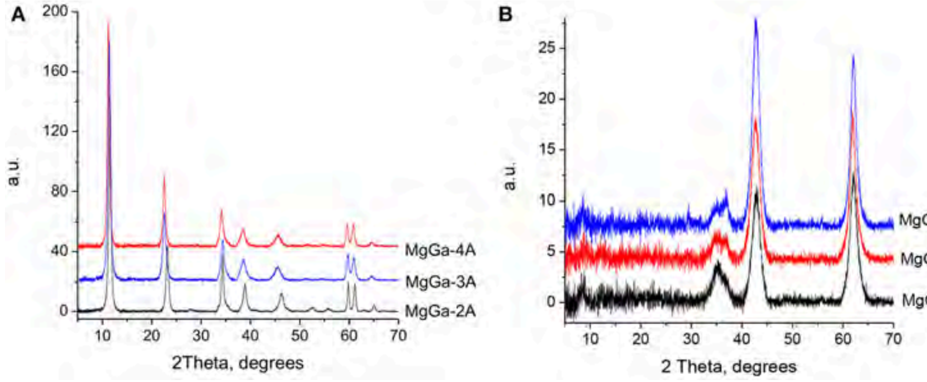

FIGURE 1 | XRD patterns of as-prepared MgGa LDHs **(A)** and mixed oxides **(B)**.

TABLE 1 | Phase composition and BET surface area of the as-prepared hydrotalcites.

Sample	Mg/Ga ratio	Phase composi-tion	HTC/MgO crystallini-ty, %	HTC basal spacing *d*, Å	HTC unit cell *a*, Å	MgO *d(200)*, Å	BET surface, $m^2 \cdot g^{-1}$
MgGa-2A	2.75	HTC	93	7.69	3.090	–	77
MgGa-3A	4.11	HTC	100	7.78	3.091	–	68
MgGa-4A	5.24	HTC	95	7.90	3.102	–	82
MgGa-2C		MgO	56	–	–	2.105	123
MgGa-3C		MgO	67	–	–	2.111	127
MgGa-4C		MgO	100	–	–	2.112	140
MgGa-2R10		HTC	83	7.86	n.d.	–	5.5
MgGa-3R10		HTC	100	7.88	n.d.	–	5.7
MgGa-4R10		HTC	91	7.96	n.d.	–	3.0

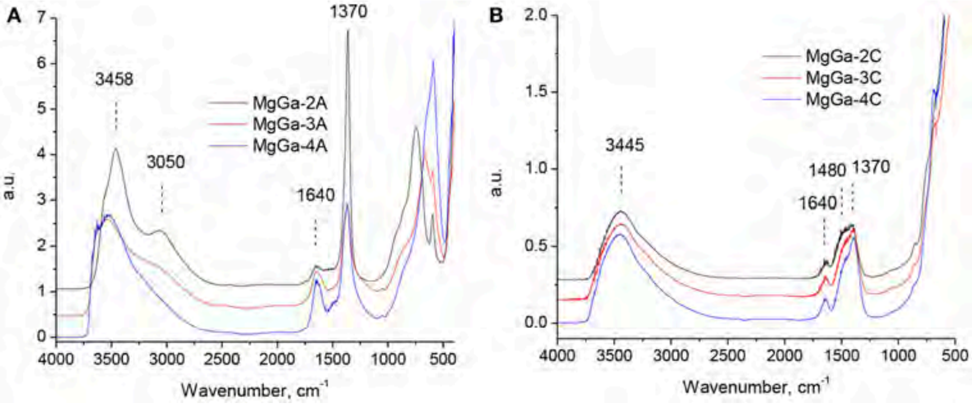

FIGURE 2 | DRIFT spectra of as-prepared MgGa LDHs **(A)** and MgGa mixed oxides **(B)**.

for MgAl (Di Cosimo et al., 1998; Abelló et al., 2005; Kikhtyanin et al., 2017b) and MgGa hydrotalcites (López-Salinas et al., 1996; Aramendía et al., 1999a,b; Thomas and Vishnu Kamath, 2005).

The broad band in the range of 2,700–3,700 cm^{-1} with the maximum at about 3,450–3,550 cm^{-1} is usually attributed to the stretching vibrations of structural hydroxyl groups in the brucite-like layer (Roy et al., 1953) and the twisting vibrations of physisorbed water (Allegra and Ronca, 1978). The shoulder at 3,050 cm^{-1} is assigned to the hydrogen bonding between water molecules and interlayer carbonate anions (López-Salinas et al., 1996). **Figure 2** shows that the intensity of this shoulder increases with increase in Ga content. It may be considered as an additional proof that Ga atoms in the composition of brucite-like layers are compensated by interlayer carbonates. The band corresponding to the vibration mode δ_{HOH} at 1,630–1,645 cm^{-1} indicates the presence of interlayer water molecules and the band at 1,370 cm^{-1} arises from the ν_3 mode of interlayer CO_3^{2-} (chelating or bridging bidentate) anions (Abelló et al., 2005). The low intensive band at 1,515 cm^{-1} is ascribed to the reduction in the symmetry caused by the presence of monodentate carbonates ($\nu_{\text{asym O–C–O}}$) interacting with Mg^{2+} (Di Cosimo et al., 1998; Abelló et al., 2005). In low frequency region the band at 870 cm^{-1} is characteristic for the out-of-plane deformation of carbonate, whereas the in-plane bending is located at 680 cm^{-1} (Abelló et al., 2005). In Mg-Al hydrotalcites, a band at about 560 cm^{-1} corresponds to the translation modes of hydroxyl groups influenced by Al^{3+} cations (Abelló et al., 2005; Pérez-Ramírez et al., 2007b). Accordingly, the band at 590 cm^{-1} observed in DRIFT spectra of MgGa samples could be attributed to the translation modes of hydroxyl groups influenced by Ga^{3+} cations. Indeed, López-Salinas et al. (1996) proposed that the appearance of this band may be related with Mg-O-Mg or Mg-O-Ga vibrations.

Calcination of the as-prepared MgGa hydrotalcites resulted in a collapse of the lamellar structure accompanied by H_2O and CO_2 removal. Correspondingly, DRIFT spectra of the resulting mixed oxides changed significantly (**Figure 2B**). The intensity of the bands in the range of 2,700–3,700 cm^{-1} substantially decreased due to dehydroxylation. Water removal can be evidenced also by the disappearance of the band at around 1,640 cm^{-1} (water bending vibrations) and of the shoulder at 3,000 cm^{-1} (H_2O–CO_3^{2-} interaction in the interlayer). Decomposition of the interlayer carbonates resulted in a decrease in the intensity of the band at 1,370 cm^{-1}. A new broad band in the range of 1,400–1,500 cm^{-1} arised from the interaction of non-interlayer carbonates with Mg^{2+} cations on the surface of mixed oxides

(Abelló et al., 2005). Additionally, the DRIFT spectra of mixed oxides show that reversible adsorption of water from air can take place during experiments as evidenced by the existence of a small band at around 1,640 cm^{-1} and re-appearance of a broad band with the maximum at 3,450 cm^{-1}.

Thermal Treatment of the As-Prepared MgGa LDHs to Mixed Oxides

Figure 3 depicts the TGA (A) and DTG (B) profiles of the as-prepared MgGa hydrotalcites affording the corresponding MgGa mixed oxides. The total weight loss of the samples is in the range of 36.1–39.1 wt.% (**Table 2**) and it corresponds well with the data reported earlier for similar materials (López-Salinas et al., 1996; Aramendía et al., 1999a; Thomas and Vishnu Kamath, 2005). The weight loss is 12.2–12.8 wt.% in the temperature range of 50–200°C (**Table 2**) and it corresponds to the removal of both physically adsorbed and interlayer water molecules. **Figure 3B** depicts that with increasing Ga content in the as-prepared MgGa LDHs the amount of physisorbed water ($T_{max.}$ = 100–120°C) constantly decreases while the amount of interlayer water ($T_{max.}$ = 170–185°C) correspondingly increases. The second weight loss of 21.0–22.6 wt.% is observed in the temperature range of 200–500°C and it originates from dehydroxylation of the brucite-like layers and decomposition of carbonates in the interlayer with the corresponding evolution of water and CO_2, respectively. **Figure 3B** evidences that the shape of DTG curve in this temperature range depends on Ga content in the samples. MgGa-3A and MgGa-4A have only one predominant signal at $T \approx 380°C$, while the DTG curve of MgGa-2A has an additional signal at $T = 270°C$. Earlier, the presence of more than one kind of OH-groups which differ in properties was suggested in MgAl hydrotalcites with low Mg/Al ratio (Kikhtyanin et al., 2017a). Similarly, the presence of the low-temperature signal in DTG curve of MgGa-2A can be attributed either to the dehydroxylation of defective Ga atoms in the composition of layered structure or to the dehydroxylation of XRD invisible Ga hydroxide phase.

Above 500°C, the DTG curve evidences the small additional weight loss of 2.8–4.3 wt.%. Aramendía et al. (1999a) suggested that the final weight loss involves the sustained release of water which results from the residual dehydroxylation of the species with results in Ga_2O_3 phase. Nevertheless, without carrying out additional TGA-MS experiments, it is impossible to uniquely assign this signal to a certain species.

MS curves from the TGA-MS experiments (**Figure 4**) demonstrate that the dehydroxylation of brucite-like layers and decomposition of charge-compensating carbonates in MgGa hydrotalcites occurs simultaneously in similar temperature range. Nevertheless, the removal of water due to dehydroxylation takes place in a broader range compared to decarbonation (**Figure 4**) and it ends at temperatures of 550–600°C. It is also seen (**Figure 4**) that the dehydroxylation of samples with high Ga content occurs in two steps which are characterized by the presence of two peaks at $T \approx 290$ and $T \approx 370°C$. It allows suggesting that these samples possess two kinds of hydroxyl groups in their composition. Additionally, a slight increase in the TGA-MS-H_2O profile at temperatures up to 800°C suggests dehydroxylation of the residual OH groups in MgGa mixed oxides, while a small peak at 590°C in TGA-MS-CO_2 profile can be attributed to the decomposition of residual carbonates. A ratio between areas under TGA-MS-H_2O and

TABLE 2 | The results of thermal analysis for the studied MgGa hydrotalcites.

Sample	Weight loss (%)				Ratio between signals TGA-MS_{H2O}/TGA-MS_{CO2} in the range of T = 200–500°C
	20–200°C	200–500°C	>500°C	Total	
MgGa-2A	12.8	21.0	4.3	36.1	4.3
MgGa-3A	12.2	21.3	2.8	36.3	4.8
MgGa-4A	12.8	22.6	3.8	39.2	5.0
MgGa-2R10				53.2	16.4
MgGa-3R10				56.8	21.2
MgGa-4R10				51.3	31.6

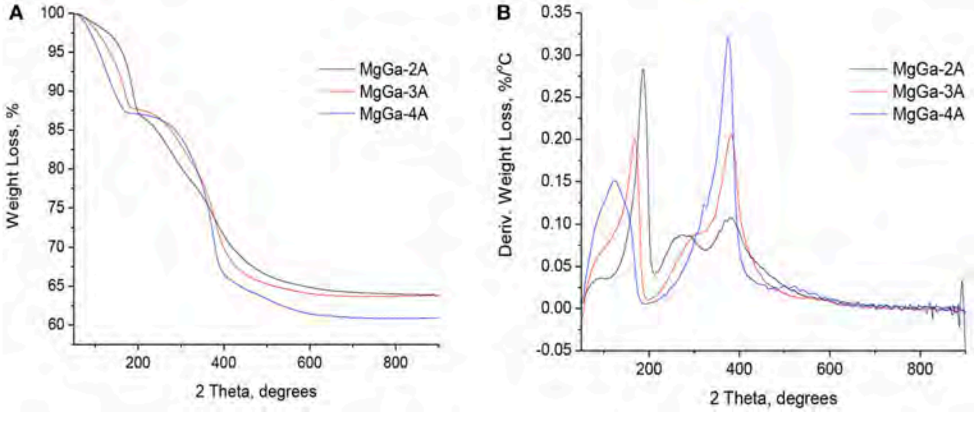

FIGURE 3 | TGA **(A)** and DTG **(B)** curves of as-prepared MgGa hydrotalcites.

TGA-MS-CO_2 curves in the temperature range from 200 to 500°C can serve as a measure of the ratio of removed H_2O and CO_2 molecules by dehydroxylation and decarbonation, respectively. This ratio increases from 4.3 to 5.0 with an increase in Mg/Ga ratio from 2 to 4 (**Table 2**) and it reflects the decrease in carbonate groups in the as-prepared samples. It seems to be logical since the theoretical Ga^{3+}/CO_3^{2-} ratio in the as-prepared hydrotalcites is constant and equal to 0.5, while the content of structural hydroxyls is independent on Mg/Ga ratio, so less carbonate groups are present in low-gallium samples.

Reconstructed MgGa LDH Materials

Figure 5A depicts XRD patterns of MgGa-3R0.25 to MgGa-3R40 samples prepared by rehydration of MgGa-3C using decarbonized water under vigorous stirring for different time ranging from 0.25 to 40 min. All prepared samples represent well-crystalline materials with hydrotalcite structure and, therefore, evidence that the prepared MgGa mixed oxides demonstrate a "memory effect" firstly described for MgAl mixed oxides (Miyata, 1980). **Figure 5B** shows the effect of the duration of the rehydration of MgGa mixed oxide on the crystallinity of the resulting reconstructed LDH. Two main conclusions can be drawn from the observed dependence. Firstly, the crystallinity exceeds 50% already after 0.25 min of rehydration and is close to 100% after 1 min without a visible change with further increase in treatment time. Secondly, **Figure 5A** shows that the intensity of the XRD reflexes at low 2θ values (<25°) are higher whereas those at higher 2θ values (>25°) are lower in comparison with the XRD patterns of the as-prepared MgGa LDHs. This difference may be due to a change in the textural characteristics of the reconstructed materials, which will be discussed further when considering SEM results.

The results suggest that the transformation of MgGa mixed oxide occurs very rapidly upon contact with water, similar to the behavior of MgAl mixed oxides (Kikhtyanin et al., 2017b). Only a few minutes of rehydration are enough to get reconstructed MgGa LDHs with maximal crystallinity. In addition, the peak at 2θ ≈ 36°, which was present in the XRD patterns of MgGa mixed oxides (attributed either to the presence of magnesium gallate, $MgGa_2O_4$, or to the presence of Ga cations in tetrahedral sites in the magnesia lattice), is not observed in the XRD patterns of the reconstructed materials. The disappearance of this line designates either the reverse transformation of such a specific MgGa compound into the HTC structure or, at least, these species become XRD-invisible because of a decrease in their size, concentration, or crystallinity during the rehydration treatment.

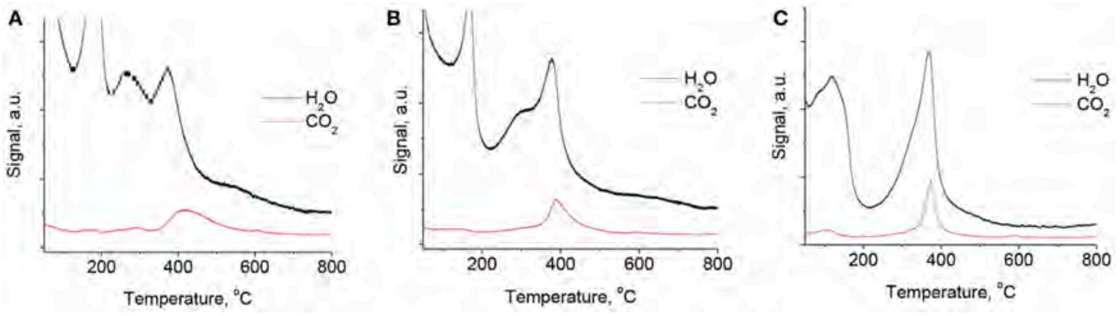

FIGURE 4 | TGA-MS spectra of evolved H_2O and CO_2 molecules for MgGa-2A **(A)**, MgGa-3A **(B)**, and MgGa-4A **(C)** samples.

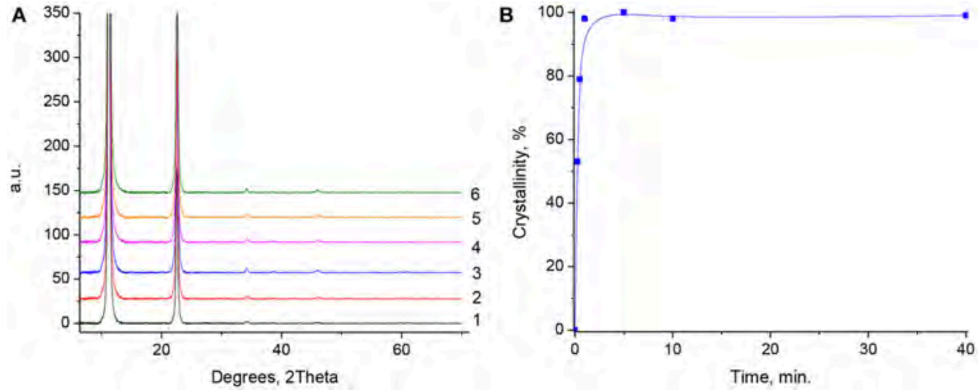

FIGURE 5 | (A) XRD patterns of reconstructed MgGa hydrotalcites at different rehydration times. 1-MgGa-3R0.25; 2-MgGa-3R0.5; 3-MgGa-3R1; 4-MgGa-3R5; 5-MgGa-3R-10; 6-MgGa-3R40. **(B)** The dependence of MgGa-3R crystallinity on the duration of MgGa mixed oxides rehydration.

The basal spacing between the layers (*d*) can be calculated from the position of the peak assigned to (003) reflection, however, the calculation of unit cell dimension (*a*) for the reconstructed samples not possible because of the very low intensity of (110) reflection. **Table 1** evidences that the *d*-value calculated for MgGa-2R10, MgGa-3R10, and MgGa-4R10 (**Table 1**) is less than that for the as-prepared samples. The basal spacing (*d*) can be considered as an indicator for the number of heteroatoms (Ga in this study) in "brucite-like" layers. Therefore, the increase in this value observed for the reconstructed samples allows suggesting that not all Ga atoms are recovered to the crystallographic sites of HTC framework after the rehydration of MgGa mixed oxide. Plausibly they are part of an amorphous phase.

DRIFT study (**Figure 6**) provides an additional proof for the existence of the "memory effect" for MgGa samples: DRIFT spectra of the reconstructed materials are very similar to those of the as-prepared materials. Moreover, the spectra do not show any dependence on the rehydration time of MgGa mixed oxides, so **Figure 6** depicts only the results for the reconstructed samples prepared by rehydration for 10 min. The recovery of the structural hydroxyl groups in the brucite-like layer is evidenced by an increase in the intensity of the wide band in the range of 2,500–3,600 cm^{-1}. The shoulder signal at 3,050 cm^{-1} and the band at 1,670 cm^{-1} re-appear in the spectra, indicating the presence of physisorbed and interlayer water in the prepared samples. The high intensity of the band at 1,370 cm^{-1} suggests the presence of a large number of interlayer compensating anions. As mentioned earlier, this band is attributed to interlayer carbonates in the case of the as-prepared samples. Abelló et al. (2005) noted that this band in the reconstructed MgAl hydrotalcites may also indicate the presence of carbonate groups in the prepared samples due to their contamination with CO_2 during the rehydration step. However, based on TGA-MS results we proposed that the band at 1,370 cm^{-1} can characterize not only carbonate, but also hydroxyl groups in the interlayer (Kikhtyanin et al., 2017b). Accordingly, we believe that the band at 1,370 cm^{-1} present in the spectra of MgGa reconstructed materials is mostly due to hydroxyl groups rather than carbonate groups. In the analysis, we considered the differences in the signals from H_2O and CO_2 in TGA-MS spectra (see below).

According to TGA results, the total weight loss of the reconstructed MgGa samples is in the range of 51–57% (**Table 2**), which is larger than expected based on the composition of these samples. As shown in Kikhtyanin et al. (2017b), this can be explained by the presence of excessive physisorbed water in the reconstructed samples, which is not removed during the drying of the samples after rehydration. In this case, the TGA method gives only general information about the increase in weight of the obtained samples. More useful information can be obtained by using the TGA-MS method, which allows estimating the relative amount of released H_2O and CO_2 molecules and, consequently, the relative content of hydroxyl and carbonate groups in the reconstructed MgGa LDHs.

There were observed approximately similar intensities of TGA-MS-H_2O and TGA-MS-CO_2 signals of reconstructed samples with different Mg/Ga molar ratios. Also, the TGA-MS-H_2O and TGA-MS-CO_2 profiles did not show a significant dependence on the rehydration duration. Therefore, **Figure 7** depicts the selected characteristic TGA-MS profiles of reconstructed samples with different Mg/Ga ratios and the same rehydration time (10 min) of the corresponding mixed oxides. **Figure 7** evidences that the intensity of the signal in TGA-MS-CO_2 profiles is substantially lower for all the rehydrated samples compared with their as-prepared MgGa LDHs counterparts (**Figure 4**).

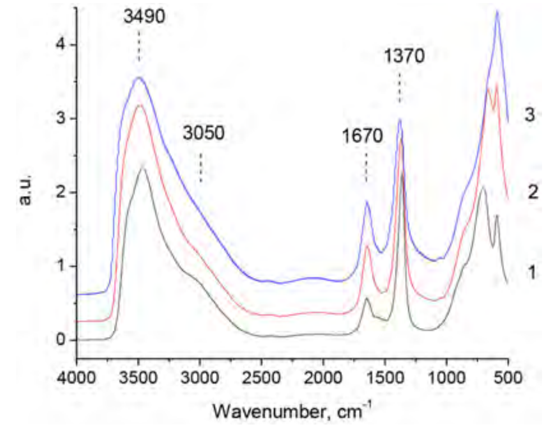

FIGURE 6 | DRIFT spectra for reconstructed MgGa-2R10 (1), MgGa-3R10 (2), and MgGa-4R10 (3).

Table 2 shows the range of ratios calculated from the areas under the TGA-MS signals of H_2O and CO_2 evolution in the range of 200–500°C. This ratio continuously increases from 16.4 to 31.6 with growing Mg/Ga ratio in the reconstructed MgGa samples. In an ideal case, carbonate groups should be completely absent in the reconstructed MgGa LDHs. In the prepared reconstructed MgGa samples, the presence of carbonates can have two causes. Firstly, MgGa mixed oxides may contain a certain amount of residual carbonates that have not be decomposed during the thermal treatment of the corresponding MgGa LDHs. Indeed, TGA-MS spectra (**Figure 4**) evidence residual CO_2 evolution at temperatures above 450°C, which is calcination temperature for the as-prepared materials. Secondly, the reconstructed LDHs can be accidentally exposed to CO_2 from air during the rehydration/drying processes involved in their preparation and/or during the TGA experiment. In any case, it is practically impossible to avoid completely the presence of carbonates in the reconstructed MgGa materials.

SEM

SEM images were recorded to investigate the morphology of MgGa materials with different Mg/Ga ratio. The micrographs of the as-synthesized LDHs with Mg/Ga molar ratio in the range of 2–4 (**Figure 8**) show a well-developed layered structure which is typical for of hydrotalcite-like materials.

MgGa-3A with the highest crystallinity was formed by well-developed large platelet aggregates with the size in the range

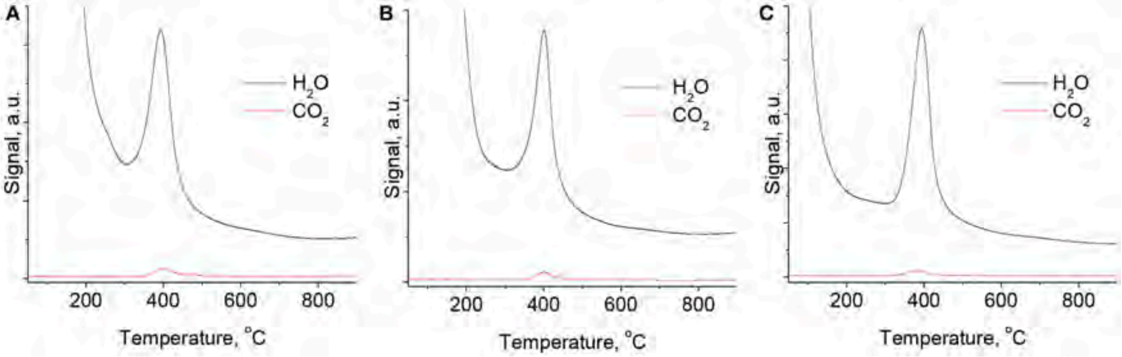

FIGURE 7 | TGA-MS spectra for reconstructed MgGa-2R10 **(A)**, MgGa-3R10 **(B)**, and MgGa-4R10 **(C)**.

of 5–10 μm consisting of thin, hexagonal, plate-like crystals of 1.5–2.5 μm in length (**Figure 8A1**). MgGa-2A with higher Ga content was formed by smaller aggregates of ≤5 μm in size (**Figure 8B1**). They were composed of plate-like crystals which were smaller in size (0.7–1.5 μm) and significantly thinner than those in Mg/Ga = 3. This tendency was observed previously also for MgAl LDHs (Kikhtyanin et al., 2017a). MgGa-4A with lower Ga content was built of large massive agglomerates where the plate-like crystals had the size of 1.7–3.5 μm (**Figure 8C1**). The SEM images of the as-prepared MgGa LDHs also evidence that MgGa-3A has the largest size of individual platelets.

MgGa mixed oxides obtained upon calcination at 450°C maintained a lamellar structure (**Figures 8A2–C2**). Moreover, the morphology and the size of plate-like crystals and agglomerates were very similar to that of the corresponding as-prepared samples. Nevertheless, the morphology of the crystals of the reconstructed MgGa LDHs was significantly different from the as-prepared materials and mixed oxides. **Figures 8A3–C3** depict the SEM images of the reconstructed MgGa materials prepared by rehydration of the corresponding MgGa mixed oxides for 10 min. First of all, separate plate-like crystals became stacked together and created large unshaped agglomerates with the size ≥20 μm in MgGa-3R10 and ≥10 μm in MgGa-2R10 and MgGa-4R10. The size of the individual platelets in the crystals of the reconstructed MgGa LDHs was noticeably smaller, but the thickness of the platelets slightly increased in comparison with the as-prepared materials and mixed oxides. The shape of these platelets became irregular and more defective after rehydration. Finally, **Figure 8B3** evidences that the surface of the platelets was cracked. It is obvious that rehydration of mixed oxides had a significant effect on the morphology of the resulting crystals of rehydrated LDHs even though their layered character was preserved. Because of these transformations, the intensity of reflexes in XRD patterns of the reconstructed MgGa LDHs also changed in comparison with the as-prepared materials.

Acid-Base Properties

Figure 9A depicts the NH_3-TPD profiles of MgGa mixed oxides with different Mg/Ga ratio while **Table 3** reports the total concentration of acid sites determined from the total amount of desorbed NH_3 from MgGa mixed oxides.

MgGa-3C possesses the largest concentration of acid sites, 190 $\mu mol \cdot g^{-1}$, while MgGa-2C and MgGa-4C have similar concentration of acid sites, 96 $\mu mol \cdot g^{-1}$. A comparison in the shapes of the obtained curves allows suggesting that the mixed oxides contain acid sites varied in their strength. Indeed, two peaks with maximums at about 160 and 250°C can be identified in the TPD profiles (**Figure 9A**). However, there is no clear dependence of the intensity of individual peaks on Mg/Ga molar ratio. Assuming that the acidity of MgGa mixed oxides should originate from Ga oxidic species, the obtained result is rather curious. Nevertheless, it allows suggesting that the acidity of mixed oxides is not only a consequence of their composition, but other factors, such as presence of admixtures, the distribution of heteroatoms throughout the crystalline framework, etc., should be considered. This implies using broader characterization methods than those used in the present study.

Figure 9B shows the CO_2-TPD profiles of MgGa mixed oxides. **Table 3** gives the total concentration of basic sites derived from the total amount of evolved CO_2. The TPD curves obtained for all three MgGa mixed oxides have a pronounced maximum between 100 and 120°C. As mentioned previously (López-Salinas et al., 1997; Aramendía et al., 1999a), the peak in the low-temperature region of CO_2-TPD curve may be assigned to weak basic sites (OH groups). In our previous work, we reported for MgAl mixed oxides that this peak also could reflect the part of medium basic sites (Mg-Al pairs) (Smoláková et al., 2017). Additionally, López-Salinas et al. (1997) observed the second peak on the CO_2-TPD curve for MgGa mixed oxides, which was present at 200–250°C as a shoulder partially overlapped with the first peak, and a small third peak present as a shoulder above 400°C. The authors ascribed these additional peaks to the appearance of medium and very strong basic sites present in MgGa mixed oxides, respectively (López-Salinas et al., 1997). Taking into account the shape of CO_2-TPD profiles obtained in the present study, we do not dare to discriminate with certainty between different peaks in the curve and, consequently, we do not provide quantitative contribution of basic sites varied by their strengths to the total basicity of MgGa mixed oxides. Similarly,

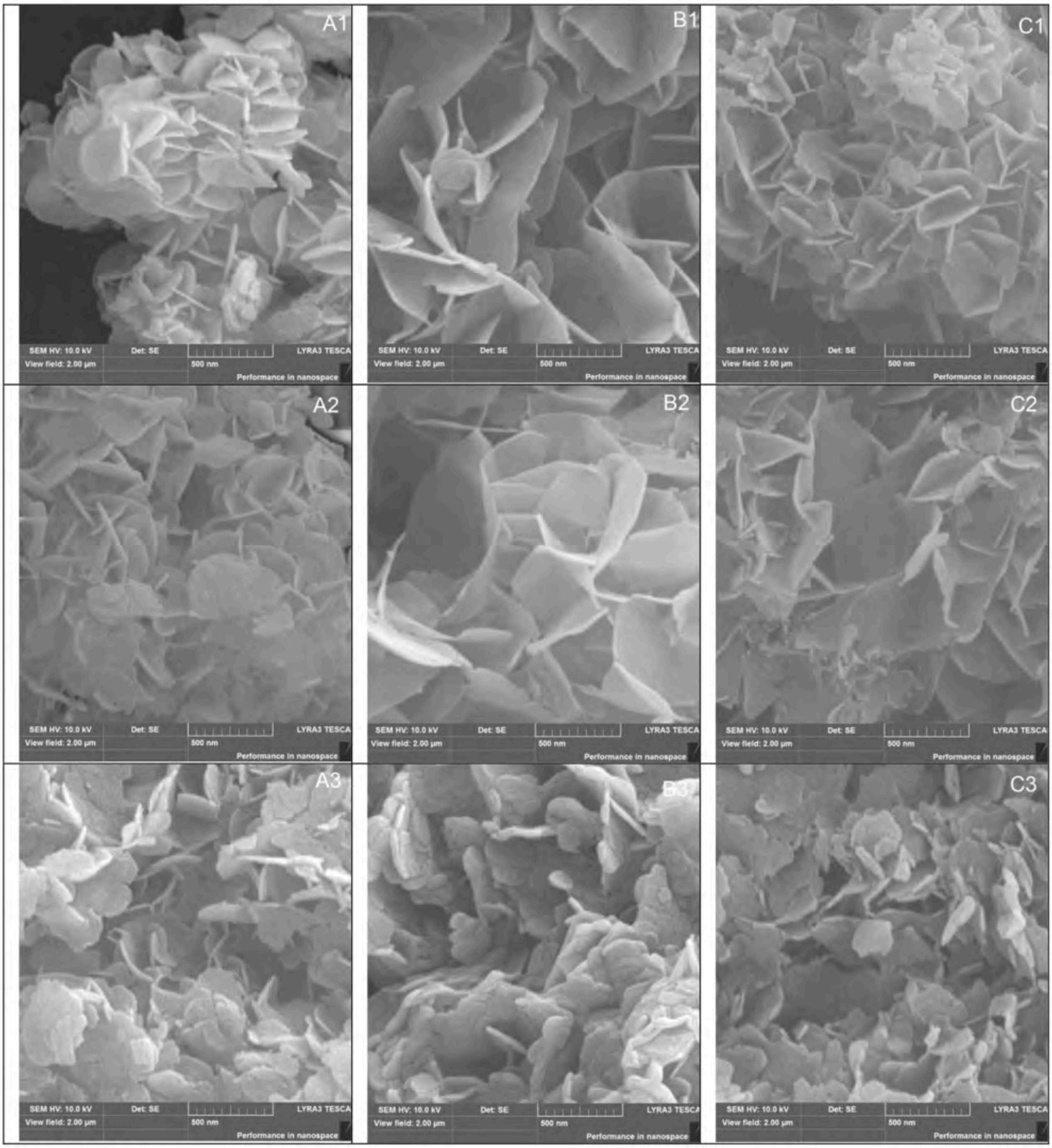

FIGURE 8 | SEM images of MgGa as-prepared materials (A1–C1), mixed oxides (A2–C2), and reconstructed LDHs rehydrated during 10 min (A3–C3). A, Mg/Ga = 2; B, Mg/Ga = 3; C, Mg/Ga = 4.

Aramendía et al. (1999a) reported it was difficult to express the strength of basic sites on an absolute scale and to quantify the number of the sites.

The total concentration of basic sites in the MgGa mixed oxides is 149 and 178 $\mu mol \cdot g^{-1}$ for MgGa-2C and MgGa-3C, respectively, but it noticeably decreases to 90 $\mu mol \cdot g^{-1}$ for MgGa-4C. MgGa-3C mixed oxide possesses both the highest amount of acid and basic sites. The dependence of the number of basic sites on Mg/Ga molar ratio follows a general trend between a chemical composition and the total basicity that was earlier

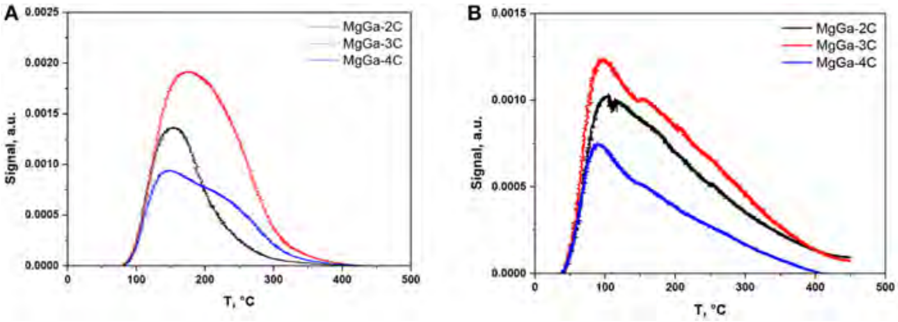

FIGURE 9 | (A) NH_3-TPD and **(B)** CO_2-TPD profiles of MgGa mixed oxides.

TABLE 3 | Concentration of acid and basic sites in MgGa mixed oxides determined by TPD of adsorbed NH_3 and CO_2, correspondingly.

Sample	Amount of desorbed NH_3, μmol·g^{-1}	Amount of desorbed CO_2, μmol·g^{-1}			Evaluated concentra-tion of interlayer hydroxyls, μmol·g^{-1}	Theoretical concentra-tion of interlayer hydroxyls, μmol·g^{-1}	Recovery of Ga atoms by reconstruct-tion process, %
		Total	L.T.	H.T.			
MgGa-2C	96	149	64	784	1,568	3,784	41
MgGa-3C	190	178	113	770	1,540	3,016	51
MgGa-4C	96	90	88	886	1,772	2,565	69
MgGa-2R10	–	848					
MgGa-3R10	–	883					
MgGa-4R10	–	974					

observed for MgAl mixed oxides (Kikhtyanin et al., 2017a). Earlier, Di Cosimo et al. (1998) explained the decrease in the basicity observed for MgAl mixed oxides with low Al content by a significant Al surface enrichment. In line with this explanation, it can be assumed that the loss of the total basicity observed for MgGa-4C compared to materials with larger Ga content can also be explained by the specific distribution of Ga atoms on the external surface of the mixed oxides.

CO_2-TPD is usually used to characterize the basic properties (in terms of both the concentration of basic sites and their distribution by strength) of mixed oxides prepared by heat treatment of LDH materials (López-Salinas et al., 1997; Aramendía et al., 1999a; Di Cosimo et al., 2000; Aramenda et al., 2003; Kikhtyanin et al., 2017a). In contrast, the basic properties of reconstructed hydrotalcites are characterized less often. Abelló et al. (2005) performed an investigation of reconstructed MgAl hydrotalcites by using CO_2-TPD and identified two peaks in their TPD profile, at around 400–420°C and at ≈550°C. They attributed the observed peaks to two types of basic sites in the rehydrated MgAl mixed oxides. The authors considered the first peak as the contribution of mainly bidentate carbonates, together with bicarbonate species, on the catalyst surface, whereas the second smaller peak was ascribed to monodentate species, similar to those observed in mixed oxides after CO_2 adsorption.

Figure 10 depicts CO_2-TPD profiles observed after the interaction of CO_2 with three reconstructed MgGa materials, MgGa-2R10, MgGa-3R10, and MgGa-4R10. A strong intensive peak with a maximum at around 400°C was observed in the CO_2-TPD profiles of all the samples. Additionally several smaller peaks can be distinguished between 50 and 230°C. The obtained profiles inevitably indicate the presence of different basic sites in the reconstructed MgGa LDHs.

Table 3 gives the amount of CO_2 desorbed up to 230°C and between 230 and 450°C. The amount of CO_2 that desorbed up to 230°C is between 64 and 113 μmol·g^{-1}. That amount of CO_2 is lower compared to the amount of CO_2 desorbed from the corresponding MgGa mixed oxides (90–178 μmol·g^{-1}). However, it has to be mentioned that the absolute amount of CO_2 desorbed from MgGa mixed oxides and reconstructed MgGa LDHs cannot be directly compared due to the higher amount of water present in the reconstructed materials. The highest amount of desorbed CO_2 in the range of $T \leq 230$°C is observed for the reconstructed MgGa-3R10 material being prepared from mixed oxide MgGa-3C having the highest number of acid and basic sites. Nonetheless, most CO_2 (between 770 and 886 μmol·g^{-1}) desorbed from the reconstructed MgGa materials between 230 and 450°C. This is considerably more than for CO_2 desorbed from MgGa mixed oxides (90–178 μmol·g^{-1}, **Table 3**).

To explain the origin of the desorption peak between 230 and 450°C in TPD profiles of reconstructed MgGa materials, we did the same experiment as in the case of TPD-CO_2, but without any adsorption of CO_2. In that case, only a marginal amount of CO_2 desorbed from MgGa-3R10 up to 230°C, but 1,186 μmol·g^{-1} of CO_2 desorbed between 230 and 450°C. The desorbed CO_2 can be either from an external or an internal source. It is worth noting that water used for rehydration can be excluded as a source of carbonates.

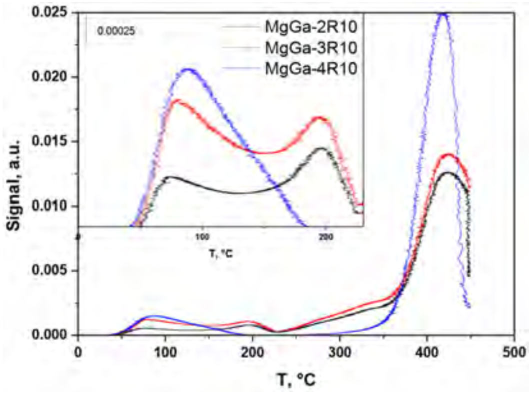

FIGURE 10 | CO_2-TPD profiles for reconstructed MgGa LDHs.

The external origin could be attributed to a dramatic increase in the number of basic sites in the reconstructed MgGa materials compared to MgGa mixed oxides, followed by the rapid interaction of interlayer hydroxyls in freshly prepared reconstructed materials with CO_2 from air during the preparations for TPD measurements.

The internal origin could be explained by redistribution of CO_2 from carbonate species that were not decomposed, i.e., that require >450°C to decompose thermally. In a special experiment we checked the amount of residual carbonate species in MgGa-3C mixed oxide and found that the amount of CO_2 desorbed during a thermal treatment of MgGa-3C from 450 to 900°C is 155 $\mu mol \cdot g^{-1}$ (not shown). Consequently, the amount of residual carbonates is too low to explain the CO_2 desorbed from the rehydrated materials between 230 and 450°C. Based on this experiment, the internal origin of carbonates in reconstructed materials can be excluded.

Accordingly, we may conclude that interlayer hydroxyl groups (i.e., charge-compensating anions) in the reconstructed materials readily interact with CO_2 from air forming interlayer carbonates similar to those present in as-prepared materials. It is evident that the interaction of hydroxyl groups with CO_2 from air is fast as TPD-CO_2 experiment with reconstructed MgGa-3R10 material without CO_2 adsorption followed the rehydration process (the contact of the sample with air could not be excluded). It seems more probable that the intensive peak at around 400°C in the CO_2-TPD profile of reconstructed MgGa LDHs originates from the decomposition of the newly-formed interlayer carbonates rather than from the decomposition of different species (bidentate or monodentate) on the surface of reconstructed MgGa LDHs, as proposed in Abelló et al. (2005).

If so, the amount of desorbed CO_2 molecules desorbed between 230 and 450°C in CO_2-TPD experiments may be considered as a quantitative characteristic of interlayer hydroxyls, which exist in freshly reconstructed LDHs after rehydration treatment. Such assumption can be valid provided that (i) MgGa mixed oxide used for rehydration treatment is substantially free from residual carbonates; and (ii) each CO_2 molecule during CO_2-TPD experiments with reconstructed LDHs interacts with two interlayer hydroxyls forming carbonate and water. Based on these assumptions, the concentration of interlayer hydroxyls should be two times larger than the concentration of desorbed CO_2, i.e., 1,540–1,772 $\mu mol \cdot g^{-1}$ (**Table 3**).

The maximum possible concentration of interlayer hydroxyls in reconstructed MgGa LDHs can be calculated from the theoretical composition of the corresponding samples, provided that all Ga are in the crystallographic sites of HTC structure (it is lower as evidenced by XRD data for the reconstructed materials). **Table 3** shows that the concentration of interlayer hydroxyls estimated from the amount of desorbed CO_2 in the range of 230–450°C is lower than the theoretically expected values. Moreover, the increasing Ga content in MgGa LDH should increase the concentration of interlayer hydroxyls. Nevertheless, the obtained results suggest a reverse trend: the evaluated concentration of hydroxyls decreases with the growth of Ga content. It should be however noted that the amount of interlayer hydroxyls in reconstructed materials may be underestimated because not all such hydroxyls in interlayer can be probed by CO_2, but those located at the edges of the platelets, as proposed by Abelló et al. (2005). Additionally, it should be considered that TPD experiments with the rehydrated materials were terminated at $T = 450°C$, and this can also contribute to the underestimation of evolved CO_2, i.e., of interlayer hydroxyls. In any case, the performed CO_2-TPD experiments give, albeit indirectly, a possibility to evaluate the amount of Brønsted basic sites in reconstructed MgGa materials.

Catalysis

Before discussing the catalytic results obtained for MgGa catalysts, several related aspects need to be considered. Firstly, on the interaction of reaction mixture with a basic catalyst, both aldol condensation of furfural and acetone self-condensation take place simultaneously. However, in the performed experiments it was found that acetone conversion by self-condensation route did not exceed 2% and therefore it was excluded from further consideration. Secondly, partial dissolution of a catalyst in a reaction mixture may occur under liquid phase conditions which could enable homogeneous reactions. To test this possibility, MgGa-3C was separated from the reaction mixture after 20 min (in a dedicated experiment) and the remaining reaction mixture was stirred for 2 h. The composition of the reaction mixture after 20 min and after the additional 2 h of the experiment was virtually unchanged and catalyst leaching could therefore be excluded. Thirdly, furfural conversion in the presence of the as-prepared MgGa materials was below 0.5% proving that aldol condensation of furfural and acetone required basic sites formed by calcination (MgGa mixed oxides) or calcination followed by rehydration (reconstructed MgGa LDHs) of the as-prepared MgGa LDHs.

Figure 11A depicts furfural conversion as a function of reaction time in presence of MgGa mixed oxides with different Mg/Ga ratio at $T = 50°C$.

Among all studied catalysts, MgGa-2C demonstrated the largest furfural conversion of 6.7% after 120 min of the reaction at $T = 50°C$ (**Figure 11A**). The increase of Mg/Ga ratio in the MgGa mixed oxides resulted in a consistent decline of furfural conversion. The observed trend in the furfural

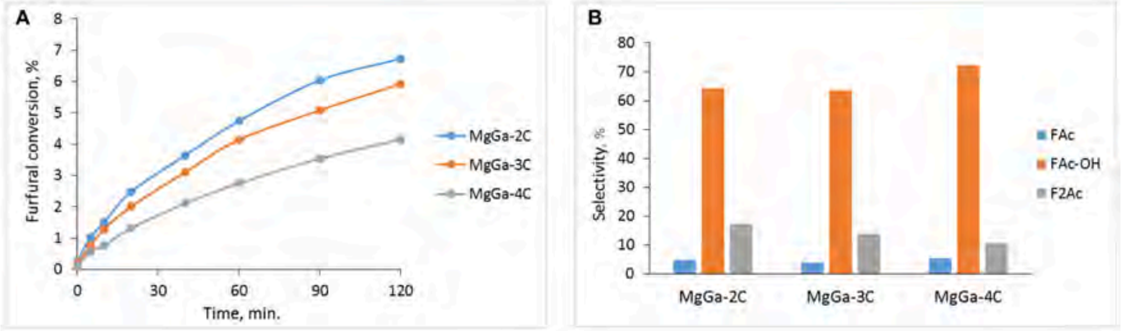

FIGURE 11 | Catalytic properties of MgGa mixed oxides. **(A)** Furfural conversion, **(B)** Selectivity to reaction products at furfural conversion ≈4%. T = 50°C, molar ratio Ac/F = 5.

conversion (**Figure 11A**) does not show a direct correlation with the concentration of neither acid nor basic sites present in these catalysts (**Table 3**), and it contrasts with what was usually observed for HTC-derived MgAl mixed oxides (Di Cosimo et al., 1998; Kustrowski et al., 2006; Kikhtyanin et al., 2017a). Therefore, other characteristics of the catalysts should be also considered. For instance, not only the number of active sites, but also their accessibility plays a key role in the observed catalyst activity. **Figure 8A2** evidences that the size of the individual platelets of MgGa-2C is lower than that of MgGa-3C. The smaller platelets of MgGa-2C could facilitate the access of reactant molecules to active sites and the removal of reaction products, thus contributing to the increase in furfural conversion. Similarly, Abelló et al. (2005) also discussed the accessibility of active sites in the reconstructed MgAl materials differing in both the size of the platelets and porosity.

Figure 11B shows the product selectivity at furfural conversion ≈4% observed for MgGa mixed oxides with different Mg/Ga ratio. For all catalysts, the selectivity toward FAc is similar (3.9–5.2%), but the selectivity to F_2Ac obviously increased with the increasing gallium content in the catalysts. In view of the smaller platelets in MgGa-2C, the favorable formation of the second (larger) condensation product seems to be reasonable.

Figure 12A demonstrates the dependence of furfural conversion on the duration of catalytic experiment at T = 25°C observed for reconstructed MgGa-3R materials varied by the rehydration time. The furfural conversion is significantly higher compared to the corresponding MgGa mixed oxides (**Figure 11A**). The observed change in the furfural conversion is in agreement with results obtained earlier for MgAl-derived materials (Kikhtyanin et al., 2017b) thus suggesting that, independently on the chemical composition of LDHs, Brønsted rather Lewis basic sites are favorable for aldol condensation of furfural and acetone. **Figure 12A** also evidences that the increase in rehydration time resulted in an increased furfural conversion. Such behavior was earlier reported for reconstructed MgAl hydrotalcites (Kikhtyanin et al., 2017b). Taken together, the catalytic performance of both MgAl and MgGa reconstructed LDHs is enabled by rehydration of the corresponding mixed oxides. Regardless of rehydration duration, all reconstructed MgGa LDHs exhibit same product distribution in dependence on furfural conversion (**Figure 12B**) with selectivity to FAc, FAc-OH, and F_2Ac being in the range of 8.7–9.8, 76.7–79.2, and 7.8–9.2%, respectively at furfural conversion ≈30%. The similarity in the composition of reaction products regardless the rehydration time allows suggesting that the acid-base characteristics of the catalysts are identical. Consequently, the incomplete reconstruction of HTC framework has no impact on the selectivity but affects the catalytic behavior of the catalysts.

Figure 12C depicts the dependence of furfural conversion on Mg/Ga ratio of reconstructed MgGa materials. The reconstructed MgGa materials with Mg/Ga ratio in the range of 2–4 exhibit the high furfural conversion of 56.6–59.7% after 120 min of the reaction at 25°C. Nevertheless, despite the observed similarity at the end of experiment, the furfural conversion over MgGa-2R10 is lower than that over the other two catalysts, particularly at the beginning of the experiment indicating a lower activity of MgGa-2R10. The observed tendency does not correlate totally with the CO_2-TPD results for the reconstructed MgGa materials (**Figure 10** and **Table 3**). Indeed, provided that the amount of CO_2 removed from the samples in CO_2-TPD experiments in the range of 230–450°C characterizes the amount of interlayer hydroxyls which are Brønsted basic sites, i.e., the active sites of the reaction, the furfural conversion for the reconstructed MgGa LDHs in the reaction should increase in the following order: MgGa-3R10 ≈ MgGa-2R10 < MgGa-4R10. Actually, furfural conversion observed on MgGa-2R10 and MgGa-3R10 differs. As with MgGa mixed oxides, also in the case of reconstructed MgGa LDHs the accessibility of active sites could play a crucial role. In this case a difference in the size of CO_2 and organic molecules which is responsible for their diffusion to Brønsted basic sites should be taken into account.

A change in Mg/Ga ratio had practically no effect on the composition of reaction products obtained on the reconstructed MgGa LDHs. At furfural conversion of about 30% MgGa-2R10 all reconstructed materials have FAc-OH selectivity of 71–73.5%, FAc selectivity of 8.1–9.3% and F_2Ac selectivity of 12.1–12.9% (**Figure 12D**). The obtained results show that, independently on chemical composition, the basic sites in the reconstructed

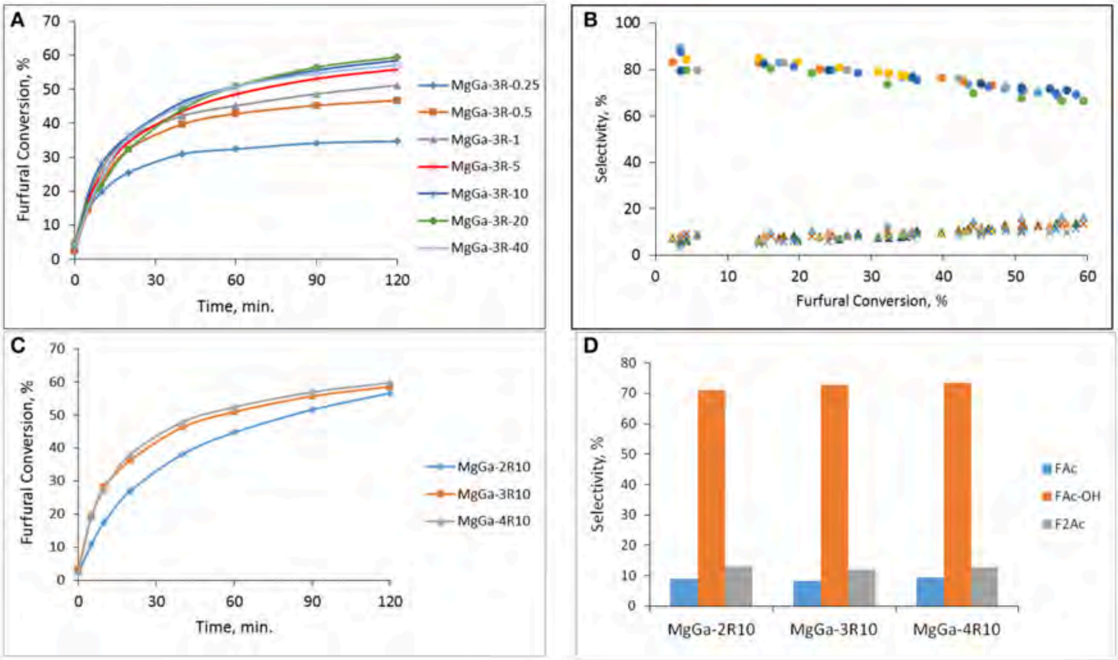

FIGURE 12 | (A) The change in furfural conversion in the course of experiment observed on MgGa-3R samples prepared by different rehydration time. **(B)** The dependence of product selectivity on furfural conversion observed on MgGa-3R-X catalysts (• – FAc-OH, Δ - FAc, x – F_2Ac). **(C)** Influence of Mg/Ga in reconstructed MgGaXR-10 samples on furfural conversion. **(D)** Influence of Mg/Ga in reconstructed MgGaXR-10 samples on product selectivity at furfural conversion ≈30%. T = 25°C, molar ratio Ac/F = 5.

MgGa LDHs act similarly in aldol condensation of acetone with furfural (**Scheme 1**). Thus, the prepared reconstructed MgGa LDHs exhibit similar trends in catalytic performance in aldol condensation reaction that have been previously observed for MgAl hydrotalcite-derived materials, i.e., the enhanced activity compared to corresponding mixed oxides and the dependence of reaction product composition on the acid-base and textural characteristics of the catalysts. Nevertheless, a direct comparison of the physico-chemical properties and the catalytic performance of MgAl and MgGa mixed oxides and reconstructed LDHs could be considered as the subject of a separate study.

CONCLUSION

The results obtained in this paper demonstrate that the synthesis and the characterization approaches developed earlier for Mg-Al LDH-derived materials can be successfully applied in the case of MgGa samples. The heat treatment of as-prepared MgGa LDHs leads to the destruction of HTC structure and the formation of MgGa mixed oxides. These oxidic materials have both acidic and basic sites and they demonstrate an intersiting values of furfural conversion in the aldol condensation of furfural and acetone. The contact of freshly calcined MgGa mixed oxides with pure water results in the fast recovery of HTC structure of MgGa materials, as it is evidenced by XRD, TGA, and DRIFT. The XRD study of the reconstructed MgGa LDHs suggests that after the rehydration process only part of Ga atoms occupy the crystallographic sites of the HTC crystal framework. Nevertheless, the reconstructed MgGa LDHs have significantly higher values of furfural conversion in the aldol condensation of furfural and acetone compared to the corresponding MgGa mixed oxides. Being catalyzed by Brønsted basic sites more effectively, the reaction proves presence of interlayer hydroxyls in the reconstructed MgGa LDHs. Nevertheless, the basic properties of the reconstructed materials cannot be properly characterized by such routine method as CO_2-TPD because during the experiment CO_2 as a probe molecule reacts with the interlayer hydroxyls forming interlayer carbonates rather than adsorbed CO_2 species on basic sites. By the combination of physico-chemical properties and catalytic performance, MgGa mixed oxides and reconstructed MgGa LDHs are analogous to the corresponding Mg-Al counterparts. However, a difference in the nature of the M^{3+} element, Al vs. Ga, which are present in HTC structure should have a significant effect in other applications of these materials, which can be identified in forthcoming studies.

AUTHOR CONTRIBUTIONS

OK performed and evaluated catalytic experiments and participated in preparing the manuscript. LC evaluated TPD data and participated in preparing the manuscript. ZT prepared MgGa samples and collected the data of physico-chemical characterization. RV carried out and evaluated TGA (TGA-MS) experiments. AP carried out and evaluated TPD experiments. PD carried out and evaluated SEM. DK focused on interpretation of data and participated in preparing manuscript.

ACKNOWLEDGMENTS

The publication is a result of the project reg. No. GA15-21817S which was financially supported by the Czech Science Foundation of the Czech Republic. AP, from Maria Curie-Sklodowska University (Lublin, Poland), thanks the ERASMUS + program for funding her internship at the University of Pardubice. The work was inspired by the discussions within the COST Action FP1306 Valorization of lignocellulosic biomass streams for sustainable production of chemicals, materials and fuels using low environmental impact technologies.

REFERENCES

Abelló, S., Medina, F., Tichit, D., Pérez-Ramírez, J., Groen, J. C., Sueiras, J. E., et al. (2005). Aldol condensations over reconstructed Mg–Al hydrotalcites: structure-activity relationships related to the rehydration method. *Chem. Eur. J.* 11, 728–739. doi: 10.1002/chem.200400409

Allegra, G., and Ronca, G. (1978). Crystal powder statistics. II. Line profiles in diffraction spectra of identical crystals and of Gaussian samples. Crystal size distributions. *Acta Crystallogr. Sect. A* 34, 1006–1013. doi: 10.1107/S0567739478002053

Aramenda, M. A., Borau, V., Jimenez, C., Marinas, J. M., Ruiz, J. R., and Urbano, F. J. (2003). Catalytic hydrogen transfer from 2-propanol to cyclohexanone over basic Mg–Al oxides. *Appl. Catal. A Gen.* 255, 301–308. doi: 10.1016/S0926-860X(03)00569-6

Aramendía, M. A., Avilés, Y., Benítez, J. A., Borau, V., Jiménez, C., Marinas, J. M., et al. (1999a). Comparative study of Mg/Al and Mg/Ga layered double hydroxides. *Micropor. Mesopor. Mater.* 29, 319–328. doi: 10.1016/S1387-1811(98)00345-X

Aramendía, M. A., Avilés, Y., Borau, V., Luque, J. M., Marinas, J. M., Ruiz, J. R., et al. (1999b). Thermal decomposition of Mg/Al and Mg/Ga layered-double hydroxides: a spectroscopic study. *J. Mater. Chem.* 9, 1603–1607. doi: 10.1039/a900535h

Aramendía, M. A., Borau, V., Jiménez, C., Marinas, J. M., Ruiz, J. R., and Urbano, F. J. (2000). XRD and ^{1}H MAS NMR spectroscopic study of mixed oxides obtained by calcination of layered-double hydroxides. *Mater. Lett.* 46, 309–314. doi: 10.1016/S0167-577X(00)00193-2

Cavani, F., Maselli, L., Scagliarini, D., Flego, C., and Perego, C. (2005). How basic properties of MgO-based mixed oxides affect the catalytic performance in gas-phase and liquid-phase methylation of m-cresol. *Stud. Surf. Sci. Catal.* 155, 167–177. doi: 10.1016/S0167-2991(05)80146-6

Cavani, F., Trifirò, F., and Vaccari, A. (1991). Hydrotalcite-type anionic clays: preparation, properties and applications. *Catal. Today* 11, 173–301. doi: 10.1016/0920-5861(91)80068-K

Chao, K.-J., and Liu, P.-H. (2005). Gallium-containing zeolites: characterization of catalytic role of gallium species in converting light paraffins to aromatics. *Catal. Surveys Asia* 9, 11–15. doi: 10.1007/s10563-005-3332-1

Choudary, B. M., Kantam, M. L., Rahman, A., Reddy, C. V., and Rao, K. K. (2001). The first example of activation of molecular oxygen by nickel in Ni-Al hydrotalcite: a novel protocol for the selective oxidation of alcohols. *Angew. Chem.* 113, 785–788. doi: 10.1002/1521-3773(20010216)40:4<763::AID-ANIE7630>3.0.CO;2-T

Choudary, B. M., Kantam, M. L., Reddy, C. R. V., Rao, K. K., and Figueras, F. (1999). The first example of Michael addition catalysed by modified Mg–Al hydrotalcite. *J. Mol. Catal. A Chem.* 146, 279–284. doi: 10.1016/S1381-1169(99)00099-0

Climent, M. J., Corma, A., Fornés, V., Guil-Lopez, R., and Iborra, S. (2002a). Aldol condensations on solid catalysts: a cooperative effect between weak acid and base sites. *Adv. Synth. Catal.* 344, 1090–1096. doi: 10.1002/1615-4169(200212)344:10<1090::AID-ADSC1090>3.0.CO;2-X

Climent, M. J., Corma, A., Iborra, S., and Primo, J. (1995). Base catalysis for fine chemicals production: Claisen-Schmidt condensation on zeolites and hydrotalcites for the production of chalcones and flavanones of pharmaceutical interest. *J. Catal.* 151, 60–66. doi: 10.1006/jcat.1995.1008

Climent, M. J., Corma, A., Iborra, S., and Velty, A. (2002b). Synthesis of methylpseudoionones by activated hydrotalcites as solid base catalysts. *Green Chem.* 4, 474–480. doi: 10.1039/b205532p

Debecker, D.P., Gaigneaux, E. M., and Busca, G. (2009). Exploring, tuning, and exploiting the basicity of hydrotalcites for applications in heterogeneous catalysis. *Chem. Eur. J.* 15, 3920–3935. doi: 10.1002/chem.200900060

Di Cosimo, J. I., Apestegua, C. R., Gines, M. J. L., and Iglesia, E. (2000). Structural requirements and reaction pathways in condensation reactions of alcohols on Mg_yAlO_x catalysts. *J. Catal.* 190, 261–275. doi: 10.1006/jcat.1999.2734

Di Cosimo, J. I., Díez, V. K., Xu, M., Iglesia, E., and Apesteguía, C. R. (1998). Structure and surface and catalytic properties of Mg-Al basic oxides. *J. Catal.* 178, 499–510. doi: 10.1006/jcat.1998.2161

Faba, L., Díaz, E., and Ordóñez, S. (2012). Aqueous-phase furfural-acetone aldol condensation over basic mixed oxides. *App. Catal. B Environ.* 113–114, 201–211. doi: 10.1016/j.apcatb.2011.11.039

Fricke, R., Kosslick, H., Lischke, G., and Richter, M. (2000). Incorporation of gallium into zeolites: syntheses, properties and catalytic application. *Chem. Rev.* 100, 2303–2406. doi: 10.1021/cr9411637

Gámez, S., González-Cabriales, J. J., Ramírez, J. A., Garrote, G., and Vázquez, M. (2006). Study of the hydrolysis of sugar cane bagasse using phosphoric acid. *J. Food Eng.* 74, 78–88. doi: 10.1016/j.jfoodeng.2005.02.005

Grand, L.-M., Palmer, S. J., and Frost, R. L. (2010). Synthesis and thermal stability of hydrotalcites based upon gallium. *J. Therm. Anal. Calorim.* 101, 195–198. doi: 10.1007/s10973-009-0456-y

Guida, A., Lhouty, M. H., Tichit, D., Figueras, F., and Geneste, P. (1997). Hydrotalcites as base catalysts. Kinetics of Claisen-Schmidt condensation, intramolecular condensation of acetonylacetone and synthesis of chalcone. *Appl. Catal. A Gen.* 164, 251–264. doi: 10.1016/S0926-860X(97)00175-0

Hora, L., Kikhtyanin, O., Čapek, L., Bortnovskiy, O., and Kubička, D. (2015). Comparative study of physico-chemical properties of laboratory and industrially prepared layered double hydroxides and their behavior in aldol condensation of furfural and acetone. *Catal. Today* 241, 221–230. doi: 10.1016/j.cattod.2014.03.010

Kikhtyanin, O., Chlubná, P., Jindrová, T., and Kubička, D. (2014). Peculiar behavior of MWW materials in aldol condensation of furfural and acetone. *Dalton Trans.* 43, 10628–10641. doi: 10.1039/c4dt00184b

Kikhtyanin, O., Kubička, D., and Cejka, J. (2015). Toward understanding of the role of Lewis acidity in aldol condensation of acetone and furfural using MOF and zeolite catalysts. *Catal. Today* 243, 158–162. doi: 10.1016/j.cattod.2014.08.016

Kikhtyanin, O., Čapek, L., Smoláková, L., Tišler, Z., Kadlec, D., Lhotka, M., et al. (2017a). Influence of Mg-Al mixed oxide compositions on their properties and performance in aldol condensation. *Ind. Eng. Chem. Res.* 56, 13411–13422. doi: 10.1021/acs.iecr.7b03367

Kikhtyanin, O., Tišler, Z., Velvarská, R., and Kubička, D. (2017b). Reconstructed Mg-Al hydrotalcites prepared by using different rehydration and drying time: physico-chemical properties and catalytic performance in aldol condensation. *Appl. Catal. A Gen.* 536, 85–96. doi: 10.1016/j.apcata.2017.02.020

Kustrowski, P., Sulkowska, D., Chmielarz, L., and Dziembaj, R. (2006). Aldol condensation of citral and acetone over mesoporous catalysts obtained by thermal and chemical activation of magnesium-aluminum hydrotalcite-like precursors. *Appl. Catal. A Gen.* 302, 317–324. doi: 10.1016/j.apcata.2006.02.003

López-Salinas, E., García-Sánchez, M., Ramon-Garcia, Ma, L., and Schifter, I. (1996). New gallium-substituted hydrotalcites:

$[Mg_{1-x}Ga_x(OH)_2](CO_3)_{x/2}\cdot mH_2O$. *J. Porous Mater*. 3, 169–174. doi: 10.1007/BF01134028

López-Salinas, E., García-Sánchez, M., Llanos-Serrano, Ma, E., and Navarrete-Bolañoz J (1997). Formation of base sites on calcined Mg-Ga hydrotalcite-like $[Mg_{1-x}Ga_x(OH)_2](CO3)_{x/2}\cdot mH_2O$. *J. Phys. Chem. B* 101, 5112–5117. doi: 10.1021/jp9702558

Mäki-Arvela, P., Salmi, T., Holmbom, B., Willfor, S., and Murzin, D. Y. (2011). Synthesis of sugars by hydrolysis of hemicelluloses - a review. *Chem. Rev*. 111, 5638–5666. doi: 10.1021/cr2000042

Miyata, S. (1980). Physico-chemical properties of synthetic hydrotalcites in relation to composition. *Clay Clay Miner*. 28, 50–56. doi: 10.1346/CCMN.1980.0280107

Motokura, K., Fujita, N., Mori, K., Mizugaki, T., Ebitani, K., Htsukawa, K., et al. (2006). Environmentally friendly one-pot synthesis of α-alkylated nitriles using hydrotalcite-supported metal species as multifunctional solid catalysts. *Chem. Eur. J*. 12, 8228–8239. doi: 10.1002/chem.200600317

Perez, C. N., Monteiro, J. L. F., Nieto, J. M. L., and Henriques, C. A. (2009). Influence of basic properties of Mg,Al-mixed oxides on their catalytic activity in knoevenagel condensation between benzaldehyde and phenylsulfonylacetonitrile. *Quim. Nova* 32, 2341–2346. doi: 10.1590/S0100-40422009000900020

Pérez-Ramírez, J., Abelló, S., and van der Pers, N. M. (2007a). Influence of the divalent cation on the thermal activation and reconstruction of hydrotalcite-like compounds. *J. Phys. Chem. C* 111, 3642–3650. doi: 10.1021/jp064972q

Pérez-Ramírez, J., Abelló, S., and van der Pers, N. M. (2007b). Memory effect of activated Mg-Al hydrotalcite: *in situ* XRD studies during decomposition and gas-phase reconstruction. *Chem. Eur. J*. 13, 870–878. doi: 10.1002/chem.200600767

Prescott, H. A., Li, Z. J., Kemnitz, E., Trunschke, A., Deutsch, J., Lieske, H., et al. (2005). Application of calcined Mg-Al hydrotalcites for Michael additions: an investigation of catalytic activity-and acid-base properties. *J. Catal*. 234, 119–130. doi: 10.1016/j.jcat.2005.06.004

Prinetto, F., Tichit, D., Teissier, R., and Coq, B. (2000). Mg- and Ni-containing layered double hydroxides as soda substitutes in the aldol condensation of acetone. *Catal. Today* 55, 103–116. doi: 10.1016/S0920-5861(99)00230-8

Ramos, R., Tišler, Z., Kikhtyanin, O., and Kubička, D. (2016). Towards understanding the hydrodeoxygenation pathways of furfural–acetone aldol condensation products over supported Pt catalysts. *Catal. Sci. Technol*. 6, 1829–1841. doi: 10.1039/C5CY01422K

Rebours, B., d'Espinose de la Caillerie, J.-B., and Clause, O. (1994). Decoration of nickel and magnesium oxide crystallites with spinel-type phases. *J. Am. Chem. Soc*. 116, 1707–1717. doi: 10.1021/ja00084a011

Rousselot, I., Taviot-Gueho, C., and Besse, J. P. (1999). Synthesis and characterization of mixed Ga/Al-containing layered double hydroxides: study of their basic properties through the Knoevenagel condensation of benzaldehyde and ethyl cyanoacetate, and comparison to other LDHs. *Int. J. Inorg. Mater*. 1, 165–174. doi: 10.1016/S1466-6049(99)00025-2

Roy, D., Roy, R., and Osborn, E. (1953). The system $MgO-Al_2O_3-H_2O$ and influence of carbonate and nitrate ions on the phase equilibria. *Am. J. Sci*. 251, 337–361. doi: 10.2475/ajs.251.5.337

Sádaba, I., Ojeda, M., Mariscal, R., Richards, R., and López Granados, M. (2011). Mg–Zr mixed oxides for aqueous aldol condensation of furfural with acetone: effect of preparation method and activation temperature. *Catal. Today* 167, 77–83. doi: 10.1016/j.cattod.2010.11.059

Sels, B. F., De Vos, D. E., and Jacobs, P. A. (2001). Hydrotalcite-like anionic clays in catalytic organic reactions. *Catal. Rev. Sci. Eng*. 43, 443–488. doi: 10.1081/CR-120001809

Smoláková, L., Frolich, K., Kocík, J., Kikhtyanin, O., and Čapek, L. (2017). Influence of acido-basic properties of Zn(Mg)Al mixed oxides on its catalytic activity in aldol condensation of furfural with acetone. *Ind. Eng. Chem. Res*. 56, 4638–4648. doi: 10.1021/acs.iecr.6b04927

Tabanellia, T., Cocchi, S., Gumina, B., Izzo, L., Mella, M., Passeri, S., et al. (2018). Mg/Ga mixed-oxide catalysts for phenol methylation: outstanding performance in 2,4,6-trimethylphenol synthesis with co-feeding of water. *Appl. Catal. A Gen*. 552, 86–97. doi: 10.1016/j.apcata.2018.01.001

Takehira, K. (2017). Recent development of layered double hydroxide-derived catalysts – Rehydration, reconstitution, and supporting, aiming at commercial application. *Appl. Clay Sci*. 136, 112–141. doi: 10.1016/j.clay.2016.11.012

Thanh, D. N., Kikhtyanin, O., Ramos, R., Kothari, M., Ulbrich, P., Munshi, T., et al. (2016). Nanosized TiO_2 - A promising catalyst for the aldol condensation offurfural with acetone in biomass upgrading. *Catal. Today* 277, 97–107. doi: 10.1016/j.cattod.2015.11.027

Thomas, G. S., and Vishnu Kamath, P. (2005). Reversible thermal behavior of the layered double hydroxides (LDHs) of Mg with Ga and In. *Mater. Res. Bull*. 40, 671–681. doi: 10.1016/j.materresbull.2004.12.011

Tichit, D., Bennani, M. N., Figueras, F., Tessier, R., and Kervennal, J. (1998). Aldol condensation of acetone over layered double hydroxides of the meixnerite type. *Appl. Clay Sci*. 13, 401–415. doi: 10.1016/S0169-1317(98)00035-0

Tichit, D., and Coq, B. (2003). Catalysis by hydrotalcites and related materials. *Cat. Tech*. 7, 206–217. doi: 10.1023/B:CATT.0000007166.65577.34

Tichit, D., Coq, B., Cerneaux, S., and Durand, R. (2002). Condensation of aldehydes for environmentally friendly synthesis of 2-methyl-3-phenyl-propanal by heterogeneous catalysis. *Catal. Today* 75, 197–202. doi: 10.1016/S0920-5861(02)00069-X

Wu, W., Wu, W., Kikhtyanin, O. V., Li, L., Toktarev, A. V., Ayupov, A. B., et al. (2010). Methylation of naphthalene on MTW-type zeolites. Influence of template origin and substitution of Al by Ga. *Appl. Catal. A Gen*. 375, 279–288. doi: 10.1016/j.apcata.2010.01.003

Yun, S. K., and Pinnavaia, T. J. (1995). Water-content and particle texture of synthetic hydrotalcite-like layered double hydroxides. *Chem. Mater*. 7, 348–354. doi: 10.1021/cm00050a017

Zapata, A., Faria, J., Pilar Ruiz, M., and Resasco, D. E. (2012). Condensation/hydrogenation of biomass-derived oxygenates in water/oil emulsions stabilized by nanohybrid catalysts. *Top. Catal*. 55, 38–52. doi: 10.1007/s11244-012-9768-4

Zeng, H. Y., Feng, Z., Deng, X., and Li, Y. Q. (2008). Activation of Mg-Al hydrotalcite catalysts for transesterification of rape oil. *Fuel* 87, 3071–3076. doi: 10.1016/j.fuel.2008.04.001

Conflict of Interest Statement: The authors declare that the research was conducted in the absence of any commercial or financial relationships that could be construed as a potential conflict of interest.

The reviewer, IL, and handling Editor declared their shared affiliation.

Catalysis Today 241 (2015) 221–230

Contents lists available at ScienceDirect

Catalysis Today

journal homepage: www.elsevier.com/locate/cattod

Comparative study of physico-chemical properties of laboratory and industrially prepared layered double hydroxides and their behavior in aldol condensation of furfural and acetone

Lukáš Hora[a], Oleg Kikhtyanin[a], Libor Čapek[b], Oleg Bortnovskiy[c], David Kubička[a,*]

[a] Research Institute of Inorganic Chemistry, UniCRE-RENTECH, Areál Chempark Záluží, 436 70 Litvínov, Czech Republic
[b] Department of Physical Chemistry, Faculty of Chemical Technology, University of Pardubice, Studentská 57, 532 10 Pardubice, Czech Republic
[c] Eurosupport Manufacturing Czechia, Areál Chempark Záluží, 436 70 Litvínov, Czech Republic

ARTICLE INFO

Article history:
Received 24 October 2013
Received in revised form 2 March 2014
Accepted 5 March 2014
Available online 8 April 2014

Keywords:
Aldol condensation
Layered double hydroxides
Hydrotalcites
Furfural
Acetone

ABSTRACT

In this article, properties of laboratory and industrially prepared Mg–Al layered double hydroxides (LDH) with Mg:Al molar ratios varied in the range from 2 to 4 were compared. Physico-chemical properties of the studied materials were investigated with XRD, SEM, N_2 physisorption, TGA and CO_2-TPD methods. Catalytic behavior of the LDH samples was examined in the liquid phase aldol condensation of furfural and acetone at 20 and 60 °C. It was found that LDH from the small-scale preparation have different physico-chemical characteristics than the LDH materials originating from the large-scale (industrial) preparation which is also reflected in their catalytic behavior. As-synthesized laboratory LDH catalysts are phase-pure crystalline samples with hydrotalcite structure while the industrial materials also possess MgO as admixture. The laboratory samples possess larger BET surface area and mesopore volume in comparison with the industrially prepared ones. Despite the similarity in basic properties of the studied materials, the samples with molar ratio Mg:Al = 3 in both groups of LDH using different method of preparation possess the best activity in aldol condensation. Generally, the calcined laboratory samples are more active than the industrial materials in the reaction. This is explained by the better textural properties of the former ones and their susceptibility to in-situ reconstruction in the presence of water formed during the reaction.

1. Introduction

Layered double hydroxides (LDH) are formed by substitution of atoms of the matrix crystalline framework on atoms of elements with different valence. Among them, hydrotalcites (HTC) are mostly known, which possess a brucite-like $[Mg(OH)_2]$ network wherein isomorphous substitution of Mg^{2+} ion by a trivalent cation M^{3+} occurs and the excess positive charge is compensated by anions which are located in the interlayer along with water molecules. Consequently, they exhibit basic properties and could be used in a number of reactions of organic synthesis, including C–C bond formation, isomerization, cyclization, etc. [1–4].

Synthesis of fine chemicals from biomass by heterogeneously catalyzed reactions is a recent topic of great importance particularly in the view of the finite reserves of fossil resources and the connected adverse environmental impacts of the use of these non-renewable resources [5,6]. Among them, aldol condensation is an important reaction as it allows obtaining compounds with larger number of C atoms starting from simple organic molecules [1,7,8] that are typical intermediates in biomass processing. Moreover, it makes possible the evaluation of the catalysts from the viewpoint of the peculiarities of their physicochemical characteristics. As a result, the attention is focused on the search of efficient catalysts for aldol condensation due to the prospect of creating new technologies for the synthesis of fine chemicals, pharmaceuticals, plasticizers and fragrances from renewable chemicals [3,9,10]. Until now the industrial aldol condensation technologies rely on the use of NaOH as a catalyst, which results in high operation costs and serious environmental problems [11,12]. Hence, the development of basic heterogeneous catalysts, for example HTC, for this field is essential. A lot of publications accessible in open literature deal with different methods of preparation of HTC materials on laboratory scale [13–16], as well as with study of their physico-chemical and catalytic properties [17,18]. Nevertheless,

---

[*] Corresponding author. Tel.: +420 476163735; fax: +420 476768476.
E-mail address: david.kubicka@vuanch.cz (D. Kubička).

http://dx.doi.org/10.1016/j.cattod.2014.03.010
0920-5861/© 2014 Elsevier B.V. All rights reserved.

an objective assessment of the prospects of a new technology is hardly possible without estimation of the possibility to move from the laboratory synthesis of catalysts to the large-scale industrial preparation. However, publications on comparing the properties of laboratory and industrially prepared HTC samples in aldol condensation are missing. Therefore, the main objective of the present study is to provide information about differences between laboratory and industrially prepared hydrotalcites with respect to their physico-chemical and catalytic properties. Both groups of the materials were characterized by a number of methods (XRD, N2 physisorption, ICP, TGA, CO_2-TPD and SEM). Their catalytic properties were compared in aldol condensation of furfural and acetone which was chosen as a commonly used test reaction for evaluating basic properties of solids.

2. Experimental

2.1. Preparation of the samples

2.1.1. Preparation of catalysts precursor

Industrially prepared Mg–Al hydrotalcites with Mg/Al molar ratio ranging from 2:1 to 4:1 were provided by Eurosupport Manufacturing Czechia (ESMC) as dried samples at temperature 150 °C. They were denoted HTC Mg/Al molar ratio-I; e.g. HTC 3:1-I denotes industrially prepared hydrotalcite sample having Mg/Al molar ratio equal approximately to 3:1.

Laboratory prepared Mg–Al hydrotalcites with Mg/Al the same molar ratio ranging from 2:1 to 4:1 were synthesized by co-precipitation at constant pH value. They were denoted HTC Mg/Al molar ratio-L; e.g. HTC 3:1-L denotes laboratory prepared hydrotalcite sample having Mg/Al molar ratio equal approximately to 3:1. The preparation procedure involves mixing of an aqueous solution of magnesium nitrate $Mg(NO_3)_2{\cdot}6H_2O$, p.a. (Lach-Ner) and aluminum nitrate $Al(NO_3)_2{\cdot}9H_2O$, p.a. (Lach-Ner), solution A, and a basic solution of potassium carbonate K_2CO_3, p.a. (Lachema) and potassium hydroxide KOH, p.a. (Lach-Ner), solution B. Solution A contained always the same concentration of $Mg(NO_3)_2$ 8.2 wt% and the appropriate amount of $Al(NO_3)_3$ in order to obtain hydrotalcite with the desired Mg/Al molar ratio. Solution B used as precipitation agent was prepared by dissolving relevant amount of K_2CO_3 and KOH in order to obtain content 5.9 wt% of K_2CO_3 and 14.4 wt% of KOH.

In the synthesis procedure, 500 ml of demineralized water was placed in a 4000 ml baker and heated to temperature 60 °C. This temperature was stayed constant for the duration of the precipitation procedure. Solution A was dropped via membrane pump (STEPDOS FEM 08) into the baker under vigorous stirring. Flow rate of solution A was 10 ml per minute. At the same time, solution B was added into the baker via membrane pump (KNF Liquidport NF 100 FT.18RC) connected with pH controller (OMEGA INFCPH PHCH-37) which set up flow rate of solution B for constant pH value 9.5 maintaining.

After that, the obtained suspension was stirred at 60 °C for 1 h. Then the solid LDH was separated by filtration, washed with demineralized water and dried at temperature 60 °C for 12 h.

2.1.2. Catalyst activation

The following calcination procedure was applied to transform the as supplied LDH materials into catalysts. As-prepared LDH materials were calcined at 450 °C in air and mixed Mg–Al oxide catalysts were obtained. The temperature during calcination was raised at the rate of 5 °C/min to reach 450 °C and maintained for 16 h. The calcined mixed oxides were used as catalysts in aldol condensation reaction directly.

2.2. Physico-chemical methods

The crystallographic structures of dried LDH catalysts were determined by X-ray powder diffraction using a Philips MPD 1880, working with the Cu-K_α line ($\lambda = 0.154$ nm) in the 2Θ range of 5–70° at a scanning rate of 2Θ of 2.4°/min. The size and shape of hydrotalcite crystals were determined by scanning electron microscopy (Jeol, JSM-5500LV). The elemental composition was determined by ICP-OES equipment (HPST, Agilent 725). The textural properties of the catalysts (specific surface area and pore volume) were measured by nitrogen physisorption at 77 K using a Micromeritics TRISTAR 3000 surface area and porosity analyzer. Thermogravimetric analysis (TGA) of dried LDH catalysts were obtained using a TA Instruments TGA Discovery series operating at heating ramp 10 °C/min from room temperature to 900 °C in flowing of nitrogen (20 ml/min, Linde 5.0). Approximately 15 mg of sample was heated in an open alumina crucible.

Temperature programmed desorption of carbon dioxide as probe molecule (TPD-CO_2) was carried out on AutoChem equipped with a TPD detector and mass spectrometry using quadrupole spectrometer (MS OmniStar). Approximately 100 mg of catalyst (grain of 0.25–0.5 mm) was placed in quartz reactor. Before TPD experiments the catalysts were outgassed at 450 °C for 4 h in a flow of helium. Subsequently the catalysts were cooled down to 0 °C and treated with a CO_2 flow (99% purity) for 30 min. Weakly adsorbed CO_2 was removed by flushing with He at 0 °C for 30 min. The desorption of CO_2 was measured by heating the catalyst from 0 to 900 °C at a heating rate of 10 °C/min in He flow. The desorbed products were analyzed by mass spectrometry. The number of basic sites was calculated from the CO_2 peaks (the molecular ion, $m/z = 44$) with help of calibration using a known amount of CO_2 desorbed from $CaCO_3$ [19].

2.3. Reaction studies

The experiments were carried out in a 100 ml stirred batch reactor (a glass flask reactor) at temperatures 20 and 50 °C. Before the start of an experiment, 2 g of catalyst was mixed together with a stirred mixture of 39.5 g acetone and 6.5 g furfural (acetone/furfural molar ratio 10:1, dried with molecular sieve 3A, pre-heated to the desired reaction temperature) and kept at this temperature for 6 h under intensive stirring. Before performing the series of experiments, it has been established that under the chosen reaction conditions the reaction is limited neither by external nor internal mass transfer by changing the stirring rate and catalyst particle size. As synthesized and calcined catalyst agglomerates with particle size less than 350 μm were used in the experiments. Samples were withdrawn from the reactor during the experiment (one sample per 1 h), filtered, and analyzed by Agilent 7890A gas chromatograph equipped with a flame ionization detector (FID), using a HP 5 capillary column (30 m/0.32 mm ID/0.25 μm). Reaction pathway of aldol condensation of furfural with acetone is shown in Scheme 1.

Catalytic results of aldol condensation of furfural and acetone have been described by conversion and selectivity parameters that have been calculated as follows:

$$\text{reactant conversion}\,(t)\,(\text{mol\%}) = 100 \times \frac{(\text{reactant}_{t=0} - \text{reactant}_t)}{\text{reactant}_{t=0}};$$

$$\frac{\text{selectivity to product } i = (\text{mole of reactant converted to product } i)}{(\text{total number of mole of reactant converted})}.$$

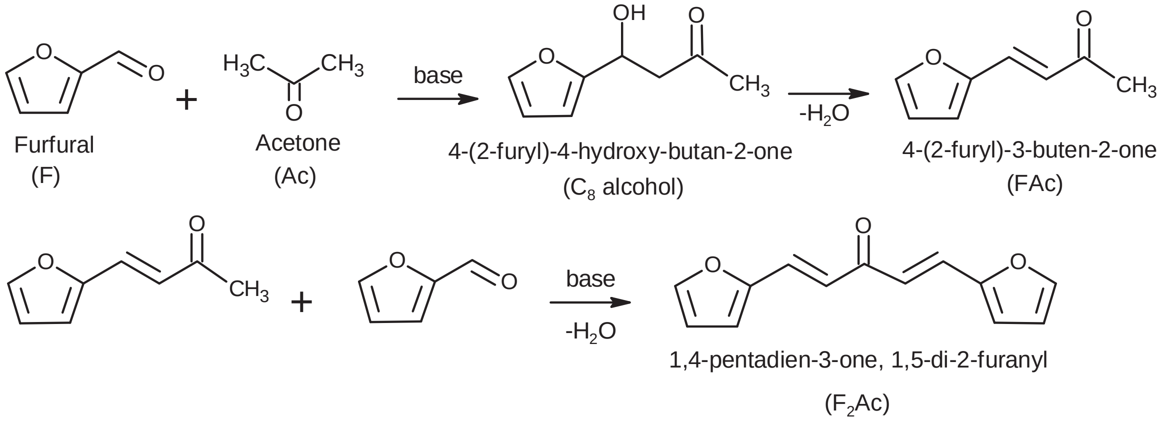

Scheme 1. Mechanism of the condensation reactions of furfural and acetone.

The carbon balance calculated as the carbon atoms detected in each sample (C_3, C_5, C_8 and C_{13}) divided by the initial carbon atoms (C_3 and C_5 fed) has been preserved during all experiments:

$$\mathrm{C\,balance\,\%} = \frac{(3\quad \mathrm{mol\,C3} + 5\quad \mathrm{mol\,C5} + 8\quad \mathrm{mol\,C8} + 13\quad \mathrm{mol\,C13})}{(3\quad \mathrm{mol\,C3}_{t=0} + 5\quad \mathrm{mol\,C5}_{t=0})}$$

3. Results and discussion

3.1. XRD study

Fig. 1 depicts XRD patterns of the samples under study. Three laboratory prepared samples, HTC 2:1-L, HTC 3:1-L and HTC 4:1-L (Fig. 1A), possess the typical diffractograms of hydrotalcite-like materials. The intensive peaks at $2\theta \approx 11°$, 23° and 34° correspond to the (0 0 3), (0 0 6) and (0 0 9) planes [14,20], indicating a well-formed crystalline layered structure. A small shift of these characteristic peaks of HTC structure toward low-angle region is observed with the increasing Mg/Al molar ratio. This shift may suggest the basal spacing expansion due to e.g. a difference in nature of the intercalated anions which are presented in the interlayer space [21]. Unlike the laboratory samples, the XRD patterns of the materials prepared in an industrial large-scale basis indicate presence of more than one crystalline phase. Along with the presence of XRD peaks corresponding to the HTC structure, there are also reflexes from magnesium oxide and magnesium hydroxide. It may be assumed that in the course of large scale preparation an incomplete interaction of the initial reactants has occurred. As a result the content of the desired HTC structure decreased at the expense of the simultaneous formation of MgO and $Mg(OH)_2$ admixture phases. It is clearly seen that the intensity of the characteristic peaks of the HTC structure is lower in the industrial samples in comparison with for the laboratory ones. Among the large-scale prepared materials, the intensity of the peaks attributed to both HTC and MgO phases is the highest for the HTC 2:1-I sample while the intensity of the peaks of $Mg(OH)_2$ phase is the highest for HTC 4:1-I and HTC 3:1-I samples.

The XRD patterns of the calcined samples (Fig. 1B) exhibit peaks at $2\theta \approx 37°$, 43° and 62° which correspond to diffraction by the (1 1 1), (2 0 0) and (2 2 0) planes of periclase MgO phase [14]. The change of diffractograms reveals that the layered HTC structure was completely transformed after the heat treatment of the samples. It is believed that after the calcination the aluminium compounds should be well-dispersed in the MgO phase or should form a separate amorphous phase [22]. It is also seen that peaks reflections of MgO structure are higher and sharper for

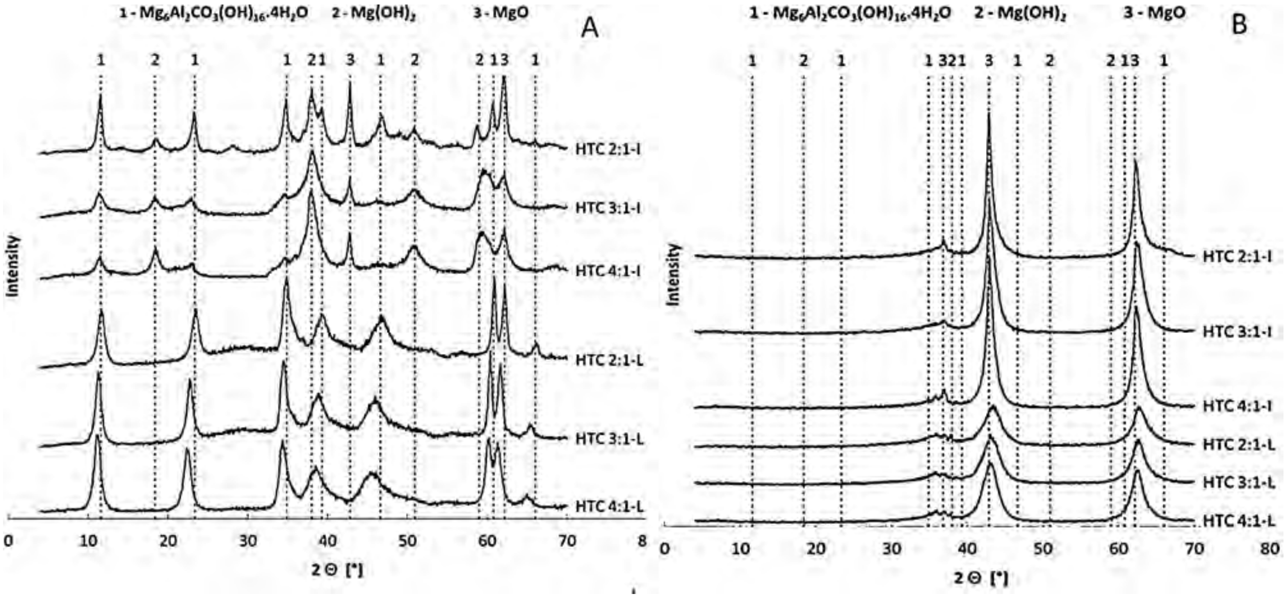

Fig. 1. XRD patterns of the laboratory and industrially prepared samples with different Mg/Al molar ratio. (A) Raw materials, (B) calcined materials.

Table 1
Chemical composition of the laboratory and industrially prepared samples and crystallite size of the calcined materials.

Parameter/sample	Unit	HTC 2:1-I	HTC 3:1-I	HTC 4:1-I	HTC 2:1-L	HTC 3:1-L	HTC 4:1-L
Mg	wt%	11.3	13.2	14.9	10.5	14.8	11.8
Al	wt%	5.6	4.5	4.0	5.7	5.4	3.2
Si	wt%	0.1	0.06	0.05	0.04	0.04	<0.02
Ca	wt%	0.12	0.08	0.11	0.02	0.02	0.01
Fe	wt%	0.05	0.03	<0.02	<0.02	<0.02	<0.02
K	wt%	<0.02	<0.02	<0.02	0.03	0.02	0.08
Mg:Al	mol/mol	2.24	3.28	4.14	2.06	3.03	4.09
L_{200}	nm	17.1	15.5	21.4	7.1	7.1	7.1

the calcined industrially prepared samples in comparison with the laboratory ones. The crystallite size of the mixed oxides was estimated from the plane (2 0 0) ($2\theta \approx 43^\circ$) using the Debye–Scherrer equation [23], and the calculated values are presented in Table 1.

3.2. SEM

Fig. 2 shows SEM images of the prepared samples. It is seen that the large-scale prepared samples represent large agglomerates of 10–15 μm, which consist of tightly compacted sheets of a layered

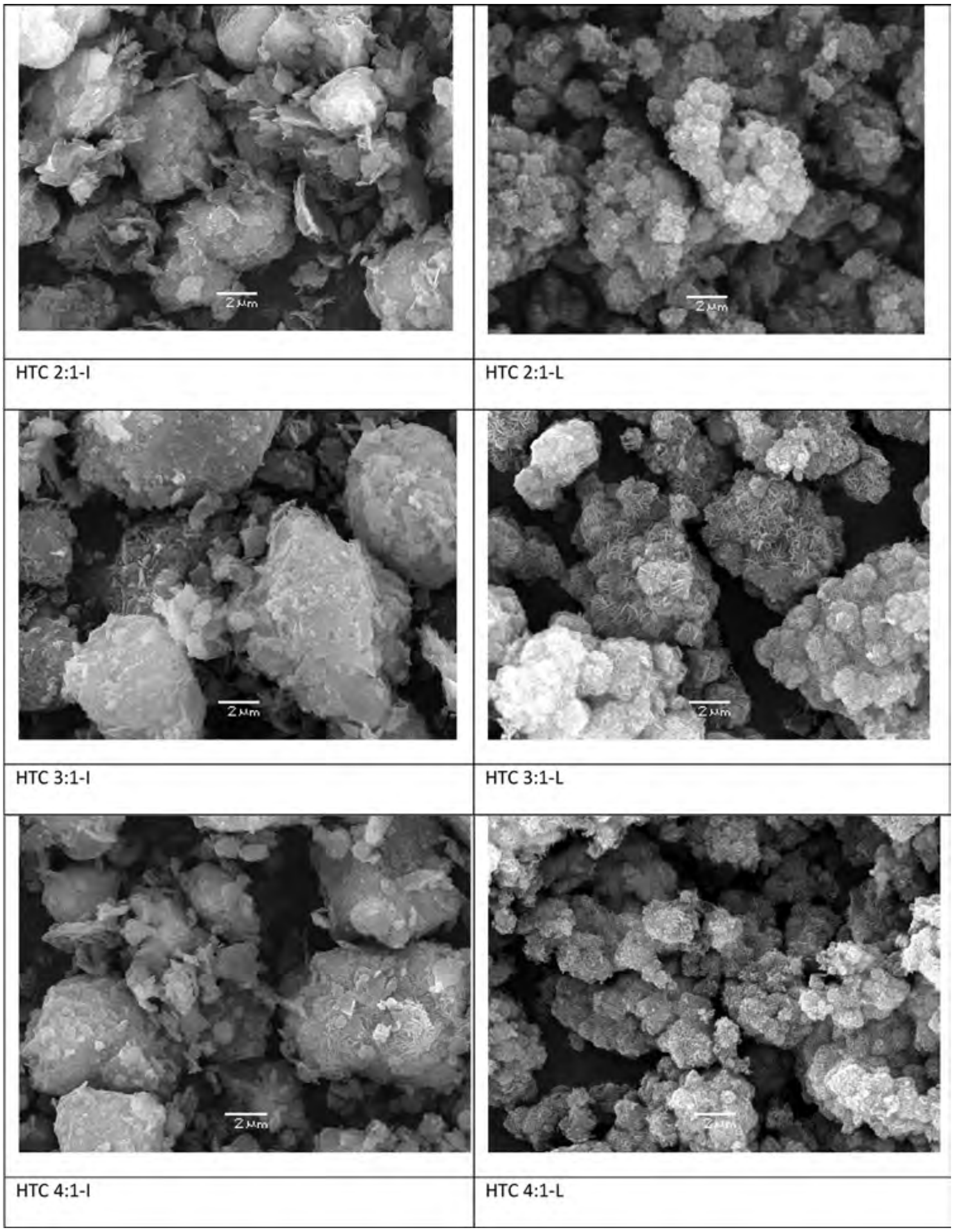

HTC 2:1-I
HTC 2:1-L
HTC 3:1-I
HTC 3:1-L
HTC 4:1-I
HTC 4:1-L

Fig. 2. SEM images of laboratory and large-scale prepared HTC samples with different Mg:Al molar ratio.

Table 2
Textural properties of laboratory and industrially prepared LDH samples.

Sample	BET surface area (m^2/g)	Pore volume* (cm^3/g)	Pore volume$_{1-4\,\text{nm}}$ (cm^3/g)	Pore volume$_{4-10\,\text{nm}}$ (cm^3/g)	Pore volume$_{10-50\,\text{nm}}$ (cm^3/g)
HTC 2:1-I	167	0.41	0.09	0.16	0.15
HTC 3:1-I	164	0.34	0.11	0.13	0.08
HTC 4:1-I	159	0.33	0.1	0.14	0.07
HTC 2:1-L	247	1.18	0.03	0.07	0.96
HTC 3:1-L	213	1.08	0.02	0.10	0.91
HTC 4:1-L	200	0.96	0.05	0.10	0.74

* BJH method.

material. At the same time, small particles of micron size also possessing a layered structure can be determined. These are likely to be fragments of the large agglomerates. Laboratory samples also represent large agglomerates up to 10 μm, which consist of small shapeless particles of 1–2 μm in size. A more detailed analysis of the images of the laboratory prepared samples reveals that these small particles possess a well-developed layered structure which is characteristic of the LDH materials [24].

3.3. *Chemical analysis*

Chemical composition of all the materials in the as-dried form was determined by the ICP method. Results presented in Table 1 show that Mg/Al molar ratio in the samples is close to the claimed content of these elements. The main impurities in the industrially prepared samples include small amounts of Fe, Ca and Si, while the laboratory samples occasionally contain a detectable amount of potassium.

3.4. *Textural properties*

Table 2 presents data on textural properties of the samples. The obtained results show that in the two groups of differently prepared samples both BET specific surface area (BET SSA) and the total pore volume increase as Mg/Al molar ratio decreases. BET SSA for the laboratory samples increases from 200 m^2/g for HTC 4:1-L to 247 m^2/g for HTC 2:1-L while the total pore volume increases in the same direction from 0.89 cm^3/g to 1.06 cm^3/g. BET SSA and the total pore volume of the industrially prepared samples are lower being in the range of 159–167 m^2/g and 0.31–0.4 cm^3/g, respectively. The pore size distribution provides additional information about the difference in the textural properties of the two groups of

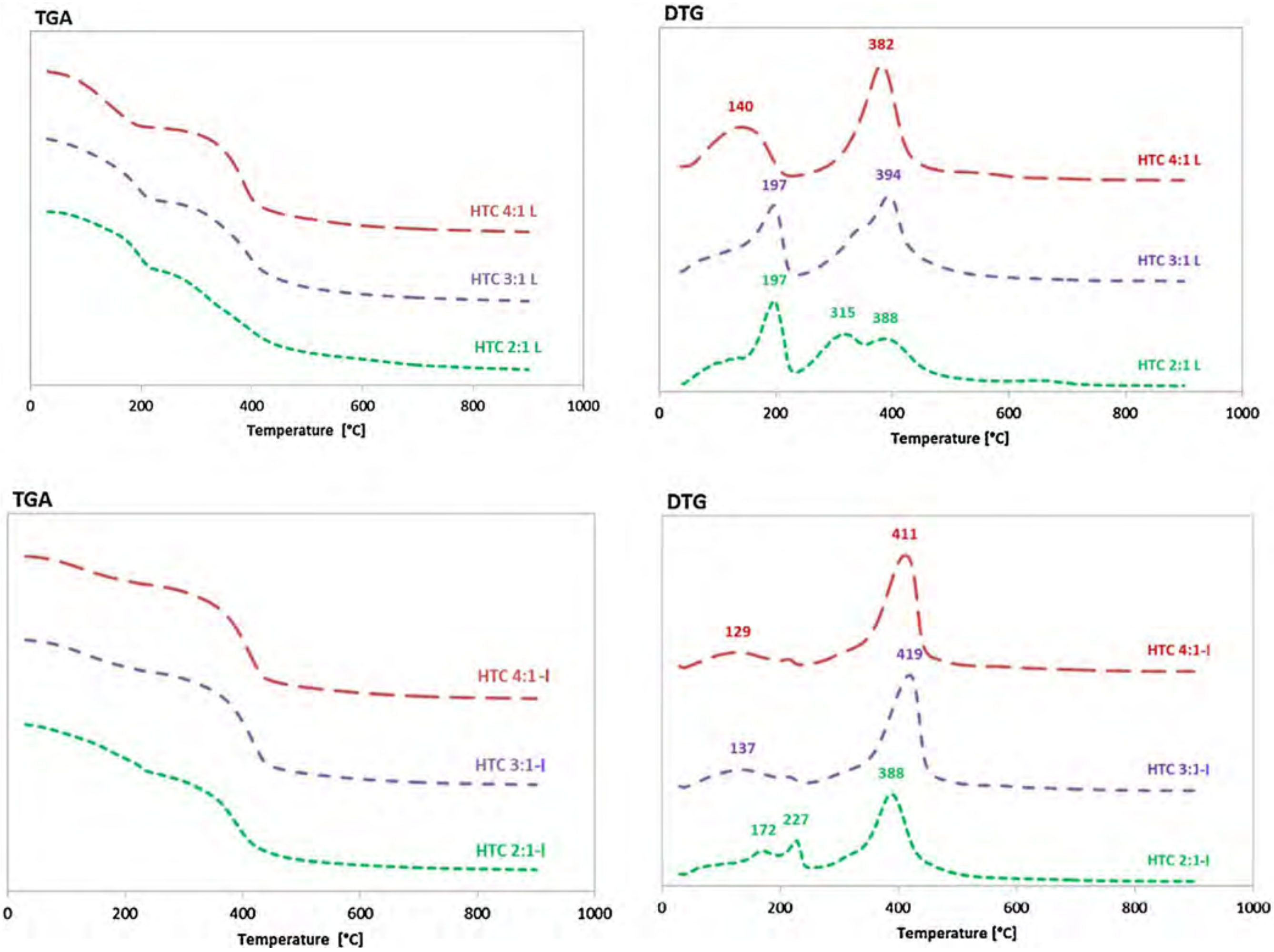

Fig. 3. TGA/DTG curves of the fresh laboratory and industrially prepared LDH catalysts.

Table 3
Weight loss at different stages of heat treatment of the laboratory and industrially prepared LDH samples.

Sample	Temperature range (°C)	Maximum of peak (°C)	Weight loss (%)
HTC 2:1-L	20–220	116, 193	16.5
	220–500	309, 379	25.1
	≥500	650	1.9
HTC 3:1-L	20–220	106, 193	17.3
	220–500	335, 390	26.3
	≥500	–	0
HTC 4:1-L	20–220	130	15.7
	220–500	375	25.7
	≥500	530	2.2
HTC 2:1-I	20–250	160, 219	11.8
	250–500	382	21.5
	≥500	–	0
HTC 3:1-I	20–240	125	7.5
	240–500	412	24.1
	≥500	555	1.8
HTC 4:1-I	20–240	117	6.7
	240–500	406	24.3
	≥500	563	1.7

HTC samples (Table 2). For the industrial materials the pore size distribution in the range of 1–50 nm is quite uniform and amounts to 0.07–0.16 cm^3/g. Apparently, a relatively large contribution of the small pores of 1–4 nm in the industrially prepared samples could be a result of close packing of the layers which make up the large agglomerates, as evidenced by the SEM images (Fig. 2–left column). In contrast, most of the pores in the laboratory samples are in the range of 10–50 nm, which is a consequence of the specific morphology of the hydrotalcite materials (Fig. 2—right column) [24].

3.5. Thermal decomposition of LDH materials

The process of the transformation of a hydrotalcite structure into mixed oxides was investigated by thermal analysis of the samples. TGA/DTG profiles of decomposition of the laboratory and industrially prepared materials are presented in Fig. 3. All of the studied samples show three general decomposition steps that are accompanied by weight loss. The first step occurs at 50–200 °C and is ascribed to the loss of physically adsorbed and interlayer water molecules [20,24]. The second step takes place in the range of 200–500 °C and corresponds to the loss of layer OH^- groups and decomposition of the interlayer carbonates [24]. Due to this stage a transformation of the layered structure to the mixed oxide takes place [25]. At temperatures above 500 °C, the DTG curves of several samples contain an additional peak which could be possibly attributed to removal of the residual interlayer species.

Table 3 summarizes the weight losses observed at each step of the thermal treatment of LDH samples. The amount of desorbed water is higher for the laboratory samples in comparison with the industrially prepared ones, 15.7–17.3% and 6.7–11.8%, respectively. The observed difference in water amount may be attributed to different HTC content in the samples what is proved by XRD data (Fig. 1A). The asymmetrical shape of the curve at this stage observed for several samples could be explained by the co-existence of two modes of the water adsorption, namely loosely surface-adsorbed and bound interlayer water. The weight loss at the second step amounts to 25.1–26.3% for the laboratory samples and 21.5–24.3% for the industrial samples. It is seen that in the case of HTC 2:1-L, and to a lesser degree, HTC 3:1-L, the signal in the range of $T = 300–400$ °C is splitted to two different peaks. According to [14], the loss of OH^- groups is observed at lower temperatures than CO_2 removal. So, the observed splitting of the signal at the second step may be attributed to the dehydroxylation of the interlayer space followed by decarbonation. On the other hand, the thermal decomposition of the industrially prepared samples (Fig. 3) as well as of the HTC 4:1-L sample exhibits only one dominant peak at the temperature in the range of 375–412 °C. When comparing the obtained results of the thermal analysis it may be concluded that the difference between the samples originates not only from the amount of the desorbed species but also from their nature.

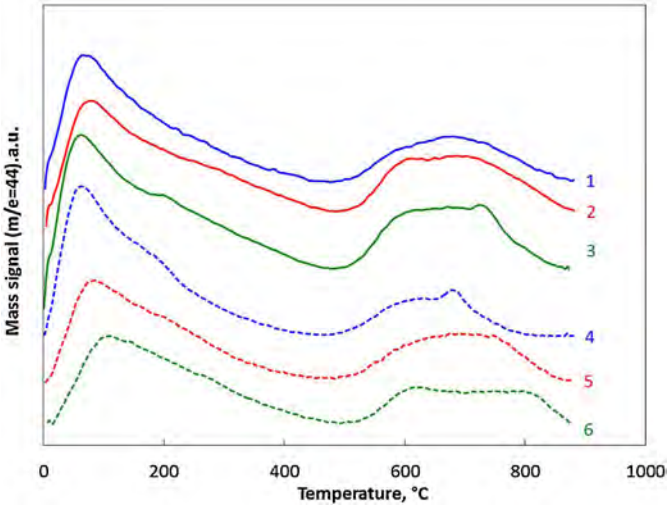

Fig. 4. CO_2-TPD spectra of laboratory (HTC 2:1-L (1), HTC 3:1-L (2), HTC 4:1-L (3)) and industrially (HTC 2:1-I (4), HTC 3:1-I (5), HTC 4:1-I (6)) prepared samples.

3.6. CO_2-TPD

The results of the investigation of basicity of the LDH samples by means of CO_2-TPD method are presented in Fig. 4 and Table 4. CO_2-TPD spectra of the samples indicate presence of at least two types of basic sites located in low temperature ($T = 20–500$ °C) and high temperature ($T \geq 500$ °C) regions. It is known that the basic sites can be classified according to their different strengths (i.e. different

Table 4
Concentration of basic sites in the samples.

Sample	CBS* 20–485 °C [$\mu mol/CO_2/g_{cat}$]
HTC 2:1-L	640
HTC 3:1-L	642
HTC 4:1-L	753
HTC 2:1-I	718
HTC 3:1-I	549
HTC 4:1-I	547

* CBS—concentration of basic sites.

carbon dioxide desorption temperature). In accordance with this dependence peaks located in the two above-mentioned temperature regions indicate presence of weak/moderate and strong basic sites, respectively. However, as pointed out in [26], information obtained from CO_2 desorbed at temperatures above the calcination temperature of the solids should be carefully considered since structural transformations could occur on the samples. Since the samples of the present work were calcined at $T = 450\,^{\circ}C$, the high temperature peak at $T \geq 500\,^{\circ}C$ in the CO_2-TPD curve was excluded from the discussion of the obtained results. CO_2-TPD spectra presented in Fig. 4 show that the shape of all the low-temperature peaks in the range of 25–485 °C is essentially the same for different samples and does not reveal any significant dependence neither on the preparation method nor on the chemical composition of the samples. Table 4 gives total amount of desorbed CO_2 detected in TPD-CO_2 profiles of Mg–Al mixed oxides in the range of 25–485 °C. The obtained results show that the highest concentration of basic sites in the laboratory samples is observed for HTC 4:1-L (753 μmol CO_2/g), while this value for HTC 2:1-L and HTC 3:1-L is approximately the same and amounts to 640–642 μmol CO_2/g. For industrially prepared samples a reverse tendency is observed. The highest concentration of basic sites is observed for HTC 2:1-I with the highest Al content (718 μmol/CO_2/g), while for HTC 3:1-I and HTC 4:1-I this value is 547–549 (μmol CO_2/g).

3.7. *Catalytic experiments*

Fig. 5 depicts catalytic behavior of the calcined laboratory and industrially prepared samples. Experiments at two different reaction temperatures, $T = 20\,^{\circ}C$ and $50\,^{\circ}C$, show that all the samples possess good activity in aldol condensation of furfural and acetone (Fig. 5A and B). Already after 1 h of the experiment furfural conversion reaches 10–17% at $T = 20\,^{\circ}C$ and 40–83% at $T = 50\,^{\circ}C$. After 6 h of the reaction furfural conversion is 17–36% and 79–100% at $T = 20^{\circ}$ C and $T = 50^{\circ}$ C, respectively. As a result of reaction between furfural and acetone the formation of C_8 alcohol, FAc and F_2Ac takes place, which is in full agreement with the commonly accepted scheme of aldol condensation of F and Ac over basic catalysts (see Scheme 1). The selectivity toward C_8 alcohol (Fig. 5C and D), FAc (Fig. 5E and F) and F_2Ac (Fig. 5G and H) shows a dependence on both furfural conversion and the type of the used catalyst. The compounds formed due to self-condensation of acetone to diacetone alcohol with its further transformation are also observed among the reaction products, but here we exclude them from the consideration as their overall concentration among all reaction products does not exceed 8 wt% and furfural is not involved in their formation.

A steep increase of FAc selectivity at high F conversion (>80%) is observed at $T_{reac.} = 50\,^{\circ}C$ (Fig. 5F). The comparison of FAc and Fac-OH selectivities indicates that with the increase of the TOS the ability of the catalyst to dehydrate the intermediate alcohol is enhanced. It can assumed that consecutive changes in the catalytic properties of the catalyst are the result of the partial reconstruction of HTC structure due to the interaction of the catalyst with water released during the reaction, as discussed below. Fig. 5 shows that at 50 °C the overall selectivity to (FAc + FAc-OH) decreases gradually with the increasing TOS, while the selectivity to F_2Ac increases showing an almost linear dependency on the F conversion.

In both groups of HTC catalysts, i.e. laboratory and industrially prepared HTC catalysts, the samples with molar ratio Mg:Al = 3:1 are the most active in aldol condensation. However, there is not any obvious dependence of the catalytic behavior of the samples on their chemical composition. For the laboratory prepared samples the conversion of furfural decreases in the order: HTC 3:1-L > HTC 2:1-L > HTC 4:1-L, whereas for the industrially prepared samples it decreases in a different order: HTC 3:1-I > HTC 4:1-I > HTC 2:1-I. Nevertheless, Fig. 5 shows that laboratory samples are clearly more active in furfural conversion than the industrially prepared ones. To explain this result it is necessary to take into account in addition to chemical composition also the collected data on the physico-chemical characterization of the samples.

The XRD patterns of the as-prepared dried laboratory samples show the characteristic peaks corresponding to HTC structure. After calcination this layered material is completely transformed into highly disordered structure of periclase (MgO) as proved by XRD. According to N_2 physisorption this disordered mixed oxide, independently on chemical composition, possesses high degree of mesoporosity. Contrary to that, the industrially prepared samples before calcination consist of a mixture of at least two crystalline phases, HTC and MgO, but after calcination the XRD patterns of these materials contain only peaks characteristic for highly-crystalline MgO phase which is made of large crystals (Table 1). As a consequence, these materials possess small mesopore volume, as proved by N_2 adsorption measurements (Table 2). Apparently, the small dimensions of the particles and high mesopores volume are very favorable for easy access of reactant molecules to the active sites of the disordered calcined LDH, i.e. the mixed oxide. Indeed, the improved textural properties of the laboratory samples show good correlation with the high activity of these samples in aldol condensation. So, generation of transport pores with dimensions ≥4 nm formed during the calcination process ensures improved transport of both reactants and reaction products, which is essential for preparing highly active catalysts. Despite this consideration, there is a disagreement between the textural characteristics of the prepared materials and their catalytic properties. Fig. 5 shows that activity of HTC 3:1-I sample is almost similar to that of HTC 4:1-L sample. At the same time, the textural data presented in Table 2 prove that BET SSA and mesopores volume is significantly higher for HTC 4:1-L when compared with HTC 3:1-I. It means that other factor(s) that affect the catalytic behavior of the studied catalysts need to be taken into account.

Among these factors basicity of the materials is an obvious parameter that might affect significantly the catalytic behavior of HTC materials in aldol condensation. It is known [27] that calcined Mg–Al hydrotalcites can contain basic sites with p*K*a values up to 16.5. These sites act, in fact, as weak Lewis acid/strong Lewis base catalysts due to the presence of O^{2-} basic sites. Indeed, Fig. 4 and Table 4 confirm the presence of basic sites in all the studied samples. Their concentration measured by CO_2-TPD is in the range of 547–753 μmol/g. Additionally, it seems that their strength is also approximately the same, as the temperature at the CO_2 desorption peak maximum as well as the shape of the signals are approximately the same and show neither dependence on the chemical composition of the samples nor the method of their preparation. By comparing the obtained CO_2-TPD data and catalytic results it is hardly possible to introduce a definite correlation between the basic properties of the mixed oxides and their behavior in aldol condensation. It may be concluded that in this case basicity of the samples is an important but not a determining factor which could unambiguously explain the obtained experimental results.

Investigating influence of basic properties of HTC materials on their catalytic behavior in aldol condensation of furfural and acetone it is necessary to consider conformity of the interlayer distance in HTC materials with dimensions of reactant molecules. A distance between layers of HTC structure is 2.9 Å [28], and kinetic diameter of CO_2 is 3.9 Å [29]. Taking into account a linearity of CO_2 molecule it could be assumed that determination of basic sites in the interlayer space of HTC with CO_2-TPD is reasonable. However, molecular diameter of acetone is larger, 6.16 Å [30], and it is hardly possible that this molecule could interact with interlayer active sites. So, concentration of basic sites measured by CO_2-TPD should be higher than amount of active sites accessible to acetone molecules. Consequently, one should be careful in finding correlation between

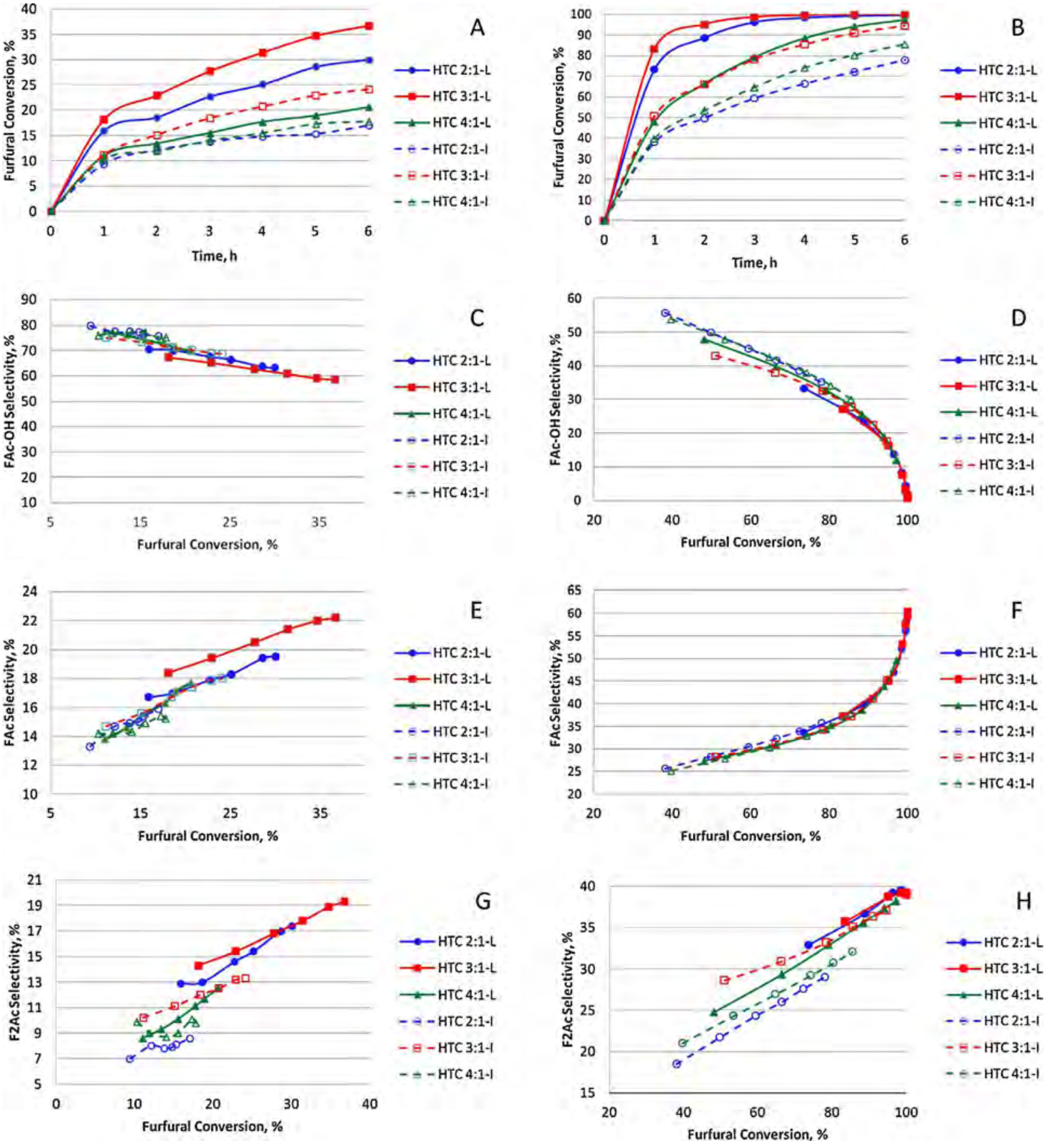

Fig. 5. Catalytic properties of calcined LDH samples at $T = 20\,^{\circ}\mathrm{C}$ (left) and $T = 50\,^{\circ}\mathrm{C}$ (right). (A) and (B) Furfural conversion in dependence on reaction time. C–H-products selectivity in dependence on furfural conversion ((C) and (D) FAc-OH, (E) and (F) FAc, (G) and (H) F_2Ac).

basic properties of HTC materials and their catalytic properties in reactions between large organic molecules.

In order to obtain additional information to explain the obtained catalytic results, we investigated the properties of the materials after the reaction. It is seen (Fig. 6) that the XRD patterns of the spent laboratory samples, HTC 2:1-L, HTC 2:1-L and HTC 4:1-L, contain very small peaks characteristic to the layered HTC structure. This observation indicates that during the reaction a partial reconstruction of the highly disordered mixed oxide to HTC phase takes place for these samples. As this can be achieved only by rehydration, the local reconstruction of the HTC structure is made possible only by water released during the reaction which reacts with the surface of the mixed oxide (as both raw materials were dried prior to the experiments using a molecular sieve). Simultaneously, the interaction of O^{2-} basic sites present in the calcined material with water formed due to aldol condensation results in the formation of OH^- Brønsted basic sites which provide higher activity to the reconstructed LDH materials in aldol condensation in comparison with the calcined ones [18,31]. Thus, the presented XRD results prove that samples HTC 2:1-L and HTC 3:1-L are the most susceptible catalytic materials to the presence of water formed during the reaction. As a result they exhibit higher catalytic activity in aldol condensation than the other studied materials.

At present it is difficult to reveal the underlying reason of the observed discrepancy. The reason could be that the aldol condensation reaction over HTC materials occurs with the participation of

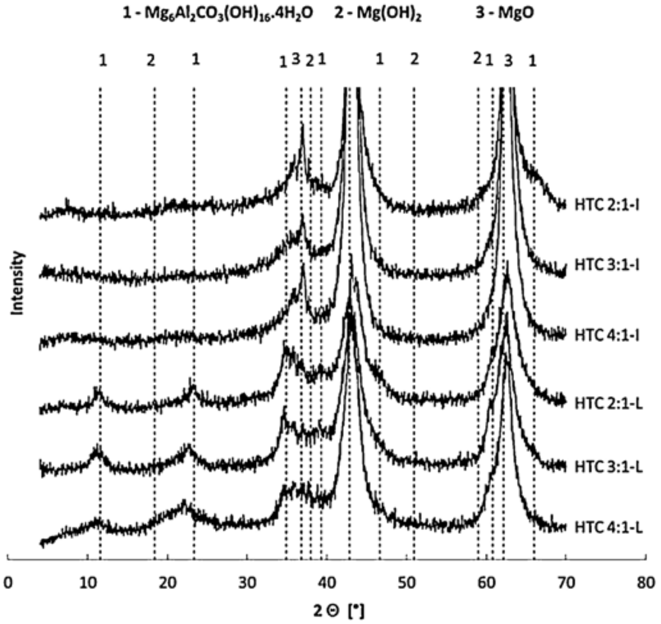

Fig. 6. XRD patterns of the laboratory and industrially prepared spent catalysts with different Mg:Al molar ratio.

those basic OH^- sites present in the reconstructed HTC which are readily accessible for the reactants, i.e. with the hydroxyl groups located at the edges of the platelets. Apparently, under the reaction conditions the water molecules interact only with the most accessible O^{2-} basic sites, i.e. with those located at the edges of the platelets. This limited interaction between these sites and water molecules may explain the observed low degree of reconstruction of the calcined material. As pointed out in [27], the amount of such accessible sites is connected with the presence of smaller and more irregular platelets which exhibit a higher proportion of the edges. Therefore, the possibility of formation of OH^- ions is determined by the degree of irregularity of the morphology of the materials. Hence, the samples 2:1-L and HTC 3:1-L should possess an increased degree of irregularity of the structure, which is indirectly confirmed by the low intensity of the reflections in the XRD patterns of the calcined laboratory prepared materials (Fig. 1). However, similar effect of the partial re-hydration is not observed for the industrially prepared samples, possibly due to decreased mesoporosity and larger crystal size of these materials, thus limiting the number of the sites available for interaction with water molecules. The laboratory sample HTC 4:1-L exhibits worse catalytic behavior than the other laboratory HTC sample which can be explained only by performing additional experiments. A detailed study of the re-hydration process in a dependence on the method of preparation of the samples and their chemical composition will be the subject of our forthcoming research.

4. Conclusions

Comparative study of properties of laboratory and industrially prepared Mg–Al LDH materials revealed that these two groups of solids differed in their physico-chemical characteristics. According to XRD study, as-synthesized laboratory samples represented phase-pure hydrotalcite structure that distinguished them from industrial samples which represented a mixture of hydrotalcite and MgO phases. Accordingly, the morphology and texture characteristics of the samples varied in the method of their preparation were also different. On the other hand, a study of the samples with CO_2-TPD showed that their basic properties did not reveal any dependence on the method of preparation. Besides, within each group of the materials no correlation between basic properties and chemical composition was observed. Catalytic experiments showed that all the samples exhibited good activity in aldol condensation of acetone and furfural. Catalysts with a molar ratio of 3:1 were the most active for both, laboratory and industrial, groups of the materials. Nevertheless, when comparing the samples of the same chemical composition, it was seen that laboratory samples possessed better properties in aldol condensation. The observed difference could be attributed to the increased mesoporosity of the laboratory samples. It was also proved by XRD method that in reaction conditions the calcined laboratory materials showed an increased susceptibility to reconstruction of mixed oxide phase back to hydrotalcite structure. As a consequence, this reconstruction resulted to a change in the structure of the active sites in the samples what could be also a reason of increased activity of the laboratory LDH materials. However, the received experimental results have showed that other factors that influence the catalytic properties of LDH materials may also exist, and elicitation of such factors is considered as a task for the forthcoming study.

Acknowledgments

Financial support from the Ministry of Industry and Trade of the Czech Republic (project FR-TI3/327) and Czech Science Foundation (P106/11/0773) is gratefully acknowledged. This publication was created in connection with the project Unipetrol research and education center Reg. CZ.1.05/2.1.00/03.0071, which is funded through the Operational Programme for Research and Innovation Development of the Structural Funds (specifically the European Regional Development Fund) and the state budget of the Czech Republic.

References

[1] S. Ordóñez, E. Díaz, M. León, L. Faba, Catal. Today 167 (2011) 71–76.
[2] M. Campanati, S. Franceschini, O. Piccolo, A. Vaccari, A. Zicmanis, Catal. Commun. 5 (2004) 145–150.
[3] S. Abelló, D. Vijaya-Shankar, J. Pérez-Ramírez, Appl. Catal., A 342 (2008) 119–125.
[4] Y. Ono, J. Catal. 216 (2003) 406–415.
[5] P. Mäki-Arvela, B. Holmbom, T. Salmi, D.Yu. Murzin, Catal. Rev. Sci. Eng. 49 (2007) 197–340.
[6] A. Corma, S. Iborra, A. Velty, Chem. Rev. 107 (2007) 2411–2502.
[7] D. Kubička, I. Kubičková, J. Čejka, Catal. Rev. Sci. Eng. 55 (2013) 1–78.
[8] L. Faba, E. Díaz, S. Ordóñez, Appl. Catal., B 113–114 (2012) 201–211.
[9] M.J. Climent, A. Corma, S. Iborra, A. Velty, Catal. Lett. 79 (2002) 157–163.
[10] J. Červený, J. Šplíchalová, P. Kačer, F. Kovanda, M. Kuzma, L. Červený, J. Mol. Catal. A: Chem. 285 (2008) 150–154.
[11] G.S. Salvapati, K.V. Ramanamurty, M.J. Janardanarao, J. Mol. Catal. 54 (1989) 9–30.
[12] G.J. Kelly, F. King, M. Kett, Green Chem. 4 (2002) 392–399.
[13] W.T. Reichle, Solid State Ionics 22 (1986) 135–141.
[14] M. León, E. Díaz, S. Bennici, A. Vega, S. Ordóñez, A. Auroux, Ind. Eng. Chem. Res. 49 (2010) 3663–3671.
[15] H. Liu, W. Xu, X. Liu, Y. Guo, G. Lu, Y. Wang, Kinet. Catal. 51 (2010) 75–80.
[16] F. Kovanda, D. Koloušek, Z. Cílová, V. Hulínksý, Appl. Clay Sci. 28 (2005) 101–109.
[17] K. Rozov, U. Berner, C. Taviot-Gueho, F. Leroux, G. Renaudin, D. Kulik, L.W. Diamond, Cem. Concr. Res. 40 (2010) 1248–1254.
[18] K.K. Rao, M. Gravelle, J.S. Valente, F. Figureas, J. Catal. 173 (1998) 115–121.
[19] L. Čapek, P. Kutálek, L. Smoláková, M. Hájek, I. Troppová, D. Kubička, Top. Catal. 56 (2013) 586–593.
[20] Xiao Ping Wang, Jun Jie Yu, Jie Cheng, Zheng Ping Hao, Zhi Ping Xu, Environ. Sci. Technol. 42 (2008) 614–618.
[21] T. Kameda, M. Saito, Y. Umetsu, Mater. Trans. 47 (2006) 923–930.
[22] D. Carriazo, M. del Arco, C. Martín, V. Rives, Appl. Clay Sci. 37 (2007) 231–239.
[23] C. Weidenthaler, Nanoscale 3 (2011) 792–810.
[24] S. Abelló, F. Medina, D. Tichit, J. Pérez-Ramírez, J.C. Groen, J.E. Sueiras, Chem. Eur. J. 11 (2005) 728–739.
[25] K. Parida, J. Das, J. Mol. Catal. A: Chem. 151 (2000) 185–192.

[26] M.A. Aramendia, V. Borau, C. Jiménez, A. Marinas, J.M. Marinas, J.R. Ruiz, F.J. Urbano, J. Mol. Catal. A: Chem. 218 (2004) 81–90.
[27] D.P. Debecker, E.M. Gaigneaux, G. Busca, Chem. Eur. J. 15 (2009) 3920–3935.
[28] J.C.A.A. Roelofs, J.A. van Bokhoven, A. Jos van Dillen, J.W. Geus, K.P. de Jong, Chem. Eur. J. 8 (2002) 5571–5579.
[29] R.V. Siriwardane, Ming-Shing Shen, E.P. Fisher, J.A. Poston, Energy Fuels 15 (2001) 279–284.
[30] A.B. Nadykto, F. Yu, J. Geophys. Res. 108 (2003) 4717–4721.
[31] M.J. Climent, A. Corma, S. Iborra, A. Velty, J. Mol. Catal. A: Chem. 182–183 (2002) 327–342.

I&EC research
Industrial & Engineering Chemistry Research

Article

Cite This: Ind. Eng. Chem. Res. 2017, 56, 13411-13422

pubs.acs.org/IECR

Influence of Mg–Al Mixed Oxide Compositions on Their Properties and Performance in Aldol Condensation

Oleg Kikhtyanin,*[†,‡] Libor Čapek,[§] Lucie Smoláková,[§] Zdeněk Tišler,[†] David Kadlec,[†] Miloslav Lhotka,[∥] Petra Diblíková,[⊥] and David Kubička[‡]

[†]Research Institute of Inorganic Chemistry, RENTECH-UniCRE, Chempark Litvínov, Záluží–Litvínov 436 70, Czech Republic

[‡]Technopark Kralupy VŠCHT Praha, University of Chemistry and Technology Prague, Žižkova 7, 278 01 Kralupy nad Vltavou, Czech Republic

[§]Department of Physical Chemistry, Faculty of Chemical Technology, University of Pardubice, Studentská 573, 532 10 Pardubice, Czech Republic

[∥]Department of Inorganic Technology, University of Chemistry and Technology Prague, Technická 5, 166 28 Praha 6 - Dejvice, Czech Republic

[⊥]Department of Organic Technology, University of Chemistry and Technology Prague, Technická 5, 166 28 Praha 6 - Dejvice, Czech Republic

Supporting Information

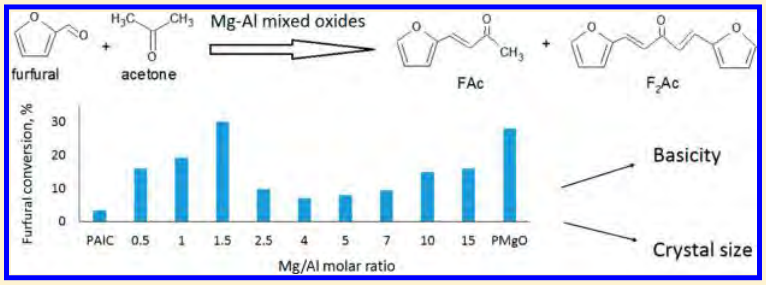

ABSTRACT: The influence of chemical composition of Mg–Al mixed oxides on their properties and catalytic performance in aldol condensation of furfural and acetone was studied. Pure alumina, Mg–Al layered double hydroxides with a wide range of Mg/Al molar ratios from 0.5 to 15, and pure magnesia were prepared by the same synthesis method, and corresponding oxides were produced by calcination of the as-prepared samples at T = 450 °C. The physicochemical properties of the samples were investigated by XRD, N_2 physisorption, SEM, CO_2-TPD, and NH_3-TPD, and their catalytic performance was evaluated in aldol condensation of furfural and acetone. SEM images revealed that the Al content in the samples influenced the size and the morphology of both large agglomerates and plate-like crystals. The CO_2-TPD measurements proved that the concentration of basic sites and the distribution of their strengths was determined by the Mg/Al molar ratio in the Mg–Al mixed oxides. However, over the whole range of Mg/Al compositions studied here, no clear correlation between the chemical composition and the number and strength of basic sites was found. Nonetheless, the change in the strength and in the density of basic sites affected the catalytic performance of calcined Mg–Al mixed oxides. Additionally, morphology and crystal size also influenced the performance of the catalysts. Finally, the composition of reaction products was affected by acid–base and textural properties of the prepared Mg–Al-mixed oxides.

1. INTRODUCTION

Hydrotalcite-like materials (HTC) are solids with a structure closely related to that of the mineral hydrotalcite which is a stoichiometric double magnesium–aluminum hydroxide with the rhombohedral structure, i.e., $Mg_6Al_2(OH)_{16}CO_3{\cdot}4H_2O$. Synthetic Mg–Al hydrotalcites have chemical compositions $[M^{2+}_{1-x}M^{3+}_{x}(OH)_2]^{b+}[A^{n-}]_{b/n}{\cdot}mH_2O$, where M^{2+} and M^{3+} are divalent and trivalent metal cations (mostly Mg^{2+} and Al^{3+}), respectively, A is interlayer anion, and b is equal to x or $2x - 1$ for n = 2 or 1, respectively. The degree of partial substitution of Mg^{2+} by Al^{3+} (denoted as x in the above formula) usually varies in the range of 0.1–0.5[1] or 0.2–0.5.[2] Nevertheless, it is suggested[1] that HTC pure phases may form only for a narrow range ($0.20 < x < 0.34$): for higher x values, the formation of $Al(OH)_3$ occurs, while lower x values result in segregation of $Mg(OH)_2$. However, these admixture phases are amorphous in most cases, therefore not detectable by XRD.

Special Issue: Tapio Salmi Festschrift

Received: August 14, 2017
Revised: October 10, 2017
Accepted: October 14, 2017
Published: October 14, 2017

DOI: 10.1021/acs.iecr.7b03367
Ind. Eng. Chem. Res. 2017, 56, 13411–13422

Scheme 1. General Reaction Pathway of Aldol Condensation of Furfural with Acetone

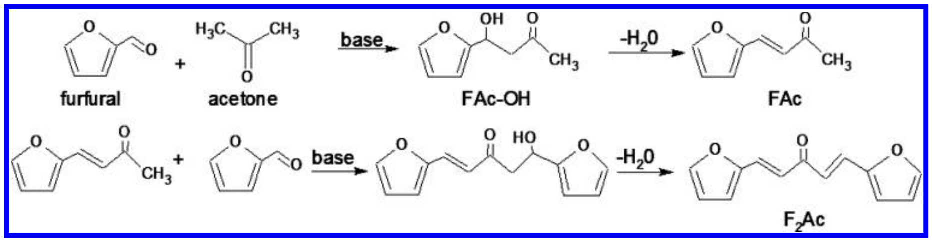

Thermal treatment of as-prepared Mg−Al HTCs produces corresponding Mg−Al mixed oxides. These mixed oxides have been reported to be active in different base-catalyzed organic reactions such as transesterification,[3] condensations,[4,5] alkylation,[6] and Michael addition.[7] They are characterized by homogeneously interdispersed oxide phases having a strong surface basicity, high surface area, and high quantity of defects that are formed due to the incorporation of Al^{3+} into the M^{2+} lattice.[8] In addition, the synthesis of mixed oxides is cheap, and they exhibit sufficiently high thermal stability.

The catalytic performance of Mg−Al mixed oxides is generally determined by the concentration and the strength of their basic sites. Hence, many studies have dealt with the characterization of basic sites of HTCs and the related mixed oxides. Several species, such as monodentate, bidentate, and bicarbonate anions, could be detected by IR spectroscopy after the CO_2 adsorption on Mg−Al mixed oxides, reflecting three different types of surface basic sites, namely, strong Lewis (low coordination O^{2-} anions), medium Lewis ($Mg^{2+}-O^{2-}$ or $Al^{3+}-O^{2-}$), and weak Brønsted (OH^- groups) basic sites.[8,9] Nevertheless, the influence of the chemical composition of Mg−Al mixed oxides on the amount and the strength of their basic/acid sites as well as their catalytic performance is still a matter of discussion.[4,5,10,11] Considering the performance of Mg−Al mixed oxides in the condensation reactions, authors have generally reported that the activity increases with increasing both the total number of basic sites and their density.[5,10,11] In contrast, some authors[4] did not observe any clear relation between the activity and the basicity of Mg−Al mixed oxide. Additionally, the performance of the Mg−Al mixed oxide catalysts in condensation reactions was attributed either to the distribution of basic and acid sites[12] or to the susceptibility of Mg−Al mixed oxides to be reconstructed into hydrotalcite structures.[13] The discrepancy in the reported results implies a dependence of the catalytic performance of Mg−Al mixed oxides in condensation reactions on a complex effect of different factors, such as crystallinity, basicity, specific surface area, particle size, and coherence length of the MgO-like phase. These factors are clearly connected with the preparation method, Mg/Al molar ratio, and postsynthesis thermal treatment of the as-prepared hydrotalcite-like materials.

Aldol condensation of aldehydes and ketones is a well-known reaction of organic synthesis aiming to prepare complex molecules starting from relatively simple ones. Among others, aldol condensation of furfural with acetone (Scheme 1) followed by the hydrogenation/deoxygenation of aldol-condensation products represents an attractive way to produce bioderived C_8 and C_{13} alkanes.[14] Furfural can be obtained by acid hydrolysis of sugar cane bagasse, a residue from sugar cane processing, followed by extraction,[15] while acetone may be obtained by ketonization of acetic acid[16] that is an important product of biomass pyrolysis. According to the general reaction scheme (Scheme 1), reaction between furfural and acetone results in the formation of C_8 aldol which undergoes dehydration to 4-(2-furyl)-3-buten-2-one (FAc). This product can react with another furfural molecule giving the C_{13} compound, 1,4-pentadien-3-one, 1,5-di-2-furanyl (F_2Ac). Besides aldol condensation with furfural, acetone is also converted by a self-condensation reaction route producing diacetone alcohol, mesityl oxide, etc. Different catalytic materials have been proposed for these reactions.[17−21] Among other catalysts, Mg−Al mixed oxides derived from hydrotalcite precursors attract a special attention since they are relatively cheap, do not contain toxic metals, and possess high activity and enhanced stability both at high temperatures and in aqueous medium.[12,22] Nevertheless, more studies are necessary to understand the correlation between their chemical composition and acido-basic properties, such as the nature and density of acid and basic sites, on the one hand, and their catalytic performance in aldol condensation, on the other hand.

This work follows our previous study,[13] where we have successfully developed Mg−Al mixed oxides active in aldol condensation of furfural and acetone from hydrotalcites. In the present study, we go beyond the generally used hydrotalcite-precursor concept of mixed oxides and focus on Mg−Al mixed oxides derived from Mg−Al layered double hydroxides (LDH) over the whole range of compositions, i.e., from pure MgO to pure Al_2O_3, and synthesized in the same way. This allows us to address the relation between the chemical composition of Mg−Al mixed oxides, their acido-basic properties, their morphology, and their activity in aldol condensation of furfural and acetone. Hence, we answer the following questions over the whole range of Mg/Al ratios: How does the concentration of basic sites and the distribution of their strengths change? How is the morphology of mixed oxides affected? How are these changes reflected in the catalytic performance of mixed oxides in aldol condensation of furfural and acetone? To the best of our knowledge, this has not been done before.

2. EXPERIMENTAL SECTION

2.1. Preparation of Mg−Al Mixed Oxides.

Mg−Al layered double hydroxides with different Mg/Al molar ratios were prepared by a coprecipitation method. An aqueous solution of $Mg(NO_3)_2\cdot 6H_2O$ and $Al(NO_3)_3\cdot 9H_2O$ (total metal ion concentration of 1 $mol\cdot l^{-1}$) was slowly added to 200 mL of redistilled water. The flow rate of a simultaneously added alkaline solution of K_2CO_3 (0.5 $mol\cdot l^{-1}$) and KOH (3 $mol\cdot l^{-1}$) was controlled to maintain the reaction pH at the desired value (9.5 ± 0.5). The coprecipitation was carried out under vigorous stirring (1400 rpm) at 75 °C. The resulting suspension was then maintained at 75 °C and pH 9.5 ± 0.5 with stirring for 1 h. The product was filtered, washed with distilled water several times until filtrate pH was 7, and dried for 12 h at room temperature. Finally, Mg−Al LDHs were grained to 0.25−0.50

Table 1. Phase Composition and BET Surface of the As-Prepared Mg−Al Materials

Sample	Phase composition	HTC crystallinity, %	HTC basal spacing *d*, Å	Unit cell *a*, Å	Crystallite size, nm	BET surface, m^2/g
PAl	Boehmite	–	–	–	–	373
MgAl-0.5-HTC	HTC+$MgAl_2(OH)_8$	7	7.57	3.015	1.8	151
MgAl-1-HTC	HTC	56	7.58	3.017	3.2	84
MgAl-1.5-HTC	HTC	70	7.58	3.032	4.2	91
MgAl-2.5-HTC	HTC	100	7.73	3.058	5.3	74
MgAl-4-HTC	HTC	64	7.92	3.075	3.6	78
MgAl-5-HTC	HTC	42	7.98	3.089	2.7	68
MgAl-7-HTC	HTC	8	–	–	–	72
MgAl-10-HTC	HTC+$Mg(OH)_2$	5	–	–	–	64
MgAl-15-HTC	HTC+$Mg(OH)_2$	–	–	–	–	70
PMg	$Mg(OH)_2$	–	–	–	–	157

mm particle size and calcined in static air at 450 °C for 4 h in a muffle oven. The calcined samples were transferred into a desiccator at the end of the calcination procedure to avoid contamination by CO_2 during cooling. As-prepared Mg−Al LDHs and Mg−Al mixed oxides with various Mg/Al molar ratios were denoted as MgAl-X-HTC and MgAl-X, respectively, where X refers to the Mg/Al molar ratio in the synthesis mixture. Pure alumina and magnesia prepared by the same synthesis method were denoted as PAl/PAlC and PMg/PMgC in as-prepared and calcined forms, respectively.

2.2. Physico-Chemical Characterization. Chemical composition was determined by using of XRF analysis (recorded with X-ray fluorescence spectrometer Philips PW1404).

X-ray diffractograms were recorded with a Bruker AXS D8-Advance diffractometer using Cu Kα radiation (λ = 0.154056 nm) with a secondary graphite monochromator. The relative crystallinity (%) of both as-prepared Mg−Al LDHs and Mg−Al mixed oxides was estimated from the area of signals at the diffraction angle $2\theta \approx 34.5°$ and 43°, respectively. In this case, the sample with the highest crystallinity was used as the reference.

Samples for scanning electron microscopy (SEM) observations were mounted on a holder and sputter-coated (Q150R ES, Quorum Technologies Ltd., UK) by 10 nm of gold to neutralize charging effects and to increase an SE yield at final micrographs. Further, the images of coated samples were acquired using a field emission scanning electron microscope (Lyra3 GMU, Tescan Orsay Holding a.s., Czech Republic) at an accelerating voltage of 12 kV and absorbed current ranging from 200 to 300 pA. For imaging, the SE detection was used to investigate the morphology of the samples.

The temperature-programmed desorption of carbon dioxide (CO_2-TPD) was performed using a Micromeritics AutoChem II 2920 (Micromeritics Instrument Corp., USA). Prior to the test, 50 mg of sample was placed in a quartz reactor heated (10 $°C\cdot min^{-1}$) to 450 °C in a flow of helium (25 $mL\cdot min^{-1}$). Subsequently, the sample was cooled to 25 °C and saturated by CO_2 using flow of a gas mixture containing 10 vol % of CO_2 in helium (25 $mL\cdot min^{-1}$) for 30 min. Then, the sample was purged by helium for 60 min to remove the physically absorbed CO_2. Finally, the TPD experiment was carried out with a linear heating rate of 10 $°C\cdot min^{-1}$ in a flow of He (25 $mL\cdot min^{-1}$). The desorbed products were analyzed by a mass spectrometer (the molecular ion m/z = 44 was analyzed). The total basicity was estimated from the area below the curve due to CO_2 desorption (the molecular ion, m/z = 44) with the help of calibration using a known amount of CO_2 desorbed from the decomposition of $NaHCO_3$ as the standard in the flow of helium (25 $mL\cdot min^{-1}$). As the position and shape of TPD-CO_2 curves are generally influenced by chosen experimental conditions, we used the same experimental conditions as in our previous works[23] and as used by other authors.[11,24]

The temperature-programmed desorption of ammonia (NH_3-TPD) was performed using the same equipment used for the CO_2-TPD experiments and similar preactivation procedure. The sample was cooled to 70 °C and saturated by ammonia using flow of a gas mixture containing 5 vol % of NH_3 in helium (15 $mL\cdot min^{-1}$) for 15 min. Then, the sample was purged by helium (25 $mL\cdot min^{-1}$) for 60 min to remove the physically absorbed NH_3, and the TPD experiment was carried out with a linear heating rate of 10 $°C\cdot min^{-1}$ in a flow of He (25 $mL\cdot min^{-1}$).

2.3. Catalytic Test. Aldol condensation of furfural with acetone was carried out in a 100-mL stirred batch reactor (a glass flask reactor) at temperature of 50 °C. Prior to the catalytic tests, the mixture of 19.7 g of acetone and 6.5 g of furfural (acetone to furfural molar ratio 5/1), both predried with molecular sieve 3A, was stirred at 200 rpm and heated to the reaction temperature of 50 °C. After that, 0.5 g of studied catalyst (grain of 0.25−0.5 mm, freshly calcined in a muffle oven at 450 °C) was added, and the reaction was carried out at 50 °C for 120 min at 200 rpm. It was previously established that the reaction is limited neither by external nor internal mass transfer under the chosen reaction conditions (in tests with changing stirring rate and catalyst particle size[25]). Samples of liquid products were periodically withdrawn from the reactor during the experiment, filtered, and analyzed by Agilent 7890A GC unit equipped with a flame ionization detector (FID), using a HP-5 capillary column (30 m/0.32 mm ID/0.25 μm). Catalytic results of aldol condensation of furfural and acetone were described by conversion and selectivity parameters that were calculated as follows:

$$\text{reactant conversion (t) (mol\%)} = 100 \times (\text{reactant}_{t=0} - \text{reactant}_{t})/\text{reactant}_{t=0}$$

$$\text{selectivity to product i} = (\text{mole of reactant converted to product i})/(\text{total moles of reactant converted})$$

Carbon balance was monitored in all experiments as the total number of carbon atoms detected in each organic compound with C_n atoms (where n = 3, 5, 8, ..., etc.) divided by the initial number of carbon atoms in F+Ac feed:

$$\text{C balance (\%)} = (3\,\text{mol}\,C_3 + 5\,\text{mol}\,C_5 + ...\text{n}\,\text{mol}\,C_n) / (3\,\text{mol}\,C_{3(t=0)} + 5\,\text{mol}\,C_{5(t=0)})$$

3. RESULTS AND DISCUSSION

3.1. Effect of Mg/Al Molar Ratio on Structure of As-Prepared Mg−Al LDHs and Mg−Al Mixed Oxides. Table 1 gives the nominal chemical composition of as-prepared Mg−Al materials, BET surface area, and crystalline phases of both as-prepared Mg−Al LDHs and Mg−Al mixed oxides. XRF proved that the experimental Mg/Al molar ratio was close to that presented in a reactive synthesis gel with Mg/Al ratios in the range of 0.5−3, while at higher Mg/Al ratios the samples had a lack of magnesium (SI, Figure 1S), suggesting the precipitation of this element was not completed during the precipitations. The potassium content was below 0.08 wt % and confirmed that K^+ cations were successfully removed by filtration and washing of the precipitates.

3.1.1. XRD Data and BET Surface of Mg−Al As-Prepared Materials. The XRD patterns of as-prepared Mg−Al materials with Mg/Al molar ratios in the range of 0.5−15 as well as pure alumina and magnesia prepared by the same synthesis procedure are presented in Figure 2S of the SI. The as-prepared pure alumina (PAl) had a low crystalline boehmite structure (JCPDS Card No. 21-1307), while the as-prepared pure magnesia (PMg) had XRD pattern of a phase-pure brucite material (JCPDS Card No. 44-1482). Most of the as-prepared Mg−Al materials in the broad range of the Mg/Al ratios can be considered as hydrotalcites with a different degree of crystallinity and phase purity. The as-prepared MgAl-0.5-HTC with the lowest Mg content is in fact a mixture of hydrotalcite with magnesium−aluminum hydroxide $MgAl_2(OH)_8$ (JCPDS card No. 35-1274). According to XRD, the as-prepared Mg−Al materials with Mg/Al molar ratios in the range of 1−7 were phase-pure hydrotalcites (JCPDS card No. 22-0700) as evidenced by the intensive diffraction lines at $2\theta \approx$ 11°, 22.5°, 34.5°, 39°, 46°, 60°, and 61.5°, which are typical for HTC layered structures.[26,27] The diffraction peaks at $2\theta \approx$ 11°, 22.5°, and 60° are ascribed to the (003), (006), and (110) reflections. The peaks assigned to (003) and (110) reflections were used to calculate the basal spacing between the layers (d) and unit cell dimension a (as $a = 2\ d_{110}$), respectively. Both the d and a values increase with increasing Mg/Al molar ratios (Table 1), which agrees with the results reported by other authors.[8,28] The observed changes in the XRD values can be attributed to a difference in the ionic radii for $A1^{3+}$ and Mg^{2+} being 0.53 and 0.72 Å, respective1y,[28] proving the isomorphous substitution of Mg^{2+} by Al^{3+} atoms within the "brucite"-like layers. The XRD patterns of Mg-rich Mg−Al materials, MgAl-10-HTC and MgAl-15-HTC, exhibited the diffraction lines of both HTC and brucite structures.

In general, Mg−Al hydrotalcites are prepared with Mg/Al molar ratio in the range of 2−4.[22] Outside this ratio, XRD patterns of synthesized materials may indicate the presence of admixture phases, for example, gibbsite, bayerite, or hydromagnesite.[8,29−31] Data from Table 1 (see also SI, Figure 2S) prove that the applied synthesis method ensures the preparation of phase-pure HTCs without XRD-detectable admixtures, i.e., without crystalline admixtures, in a broader range of Mg/Al of 1−7. Nonetheless, the presence of the amorphous phase cannot be completely excluded. The obvious variation in HTC lattice parameters suggests a change in the chemical composition of the brucite-like layers. Table 1 also shows that despite the absence of admixture crystalline phases, the relative crystallinity of HTC phase in the as-prepared Mg−Al materials with Mg/Al = 1−7 substantially varies, reaching the highest value of 100% for the as-prepared MgAl-2.5-HTC. The decrease in the relative crystallinity observed for other phase-pure as-prepared Mg−Al materials allows suggesting the growing defectiveness of the HTC crystalline framework with increasing either Al or Mg content. Additionally, part of Al atoms (at low Mg/Al molar ratio) or Mg atoms (at high Mg/Al molar ratio) in these Mg−Al hydrotalcite-like materials might be excluded from the formation of the HTC crystalline framework composing either an amorphous or a well-dispersed alumina or magnesia crystalline phases not visible by the XRD method. Average crystallite size of phase pure hydrotalcites was calculated from the half-widths of diffraction peaks at $2\theta \approx 11°$ and 22.5° using Scherrer's formula: $D = 0.9\lambda/\beta \cos \theta$.[32] The broadness of the XRD peaks indicated the smaller average size of HTC crystallites with low or high Mg/Al molar ratio, i.e., with a less ordered HTC structure (Table 1).

Pure alumina (PAl) and magnesia (PMg) as-prepared materials possessed maximum BET surface areas, 373 and 157 m^2/g, correspondingly (Table 1). The values of BET surface areas were slightly larger for as-prepared Mg−Al materials with higher Al content, while most of the rest of the samples had the values in the range of 64−78 m^2/g.

3.1.2. XRD Data and BET Surface of Mg−Al Mixed Oxides. The powder XRD patterns of Mg−Al mixed oxides prepared by calcining the corresponding as-prepared Mg−Al materials at 450 °C evidenced the disappearance of diffraction lines due to HTC and brucite structures after the heat treatment (SI, Figure 2S). Two intensive diffraction lines observed in XRD patterns of all the Mg−Al mixed oxides at $2\theta \approx 43.0°$ and 62.5° are typical for an MgO periclase-type structure (JCPDS card No. 45-0946). No crystalline AlO_x phase was observed in XRD patterns of calcined samples suggesting the formation of Mg−Al mixed oxides with extra-framework Al highly dispersed in MgO lattice.[8,33] Nevertheless, the relative crystallinity of the MgO phase exhibited a clear dependence on the chemical composition of Mg−Al mixed oxides. It had a maximum value of 90−100% for calcined PMgC and Mg−Al mixed oxides with Mg/Al ≥ 10 (Table 2) but declined with the decrease in Mg/Al molar ratio suggesting the presence of amorphous phase in Mg−Al mixed oxides with high Al content. Additionally, part of the tetrahedrally coordinated Al atoms can be present in the MgO crystalline framework after calcination, as proposed in ref

Table 2. Phase Composition and BET Surface of Mg−Al Mixed Oxides under Study

Sample	Phase composition	Crystallinity, HTC/MgO, %	MgO *d(200)*, Å	BET surface, m^2/g
PAlC	γ-Al_2O_3	–	–	344
MgAl-0.5	MgO	6	–	376
MgAl-1	MgO	16	2.073	275
MgAl-1.5	MgO	25	2.084	269
MgAl-2.5	MgO	38	2.090	219
MgAl-4	MgO	55	2.097	239
MgAl-5	MgO	74	2.101	207
MgAl-7	MgO	87	2.104	215
MgAl-10	MgO	92	2.108	243
MgAl-15	MgO	96	2.109	201
PMgC	MgO	100	2.114	234

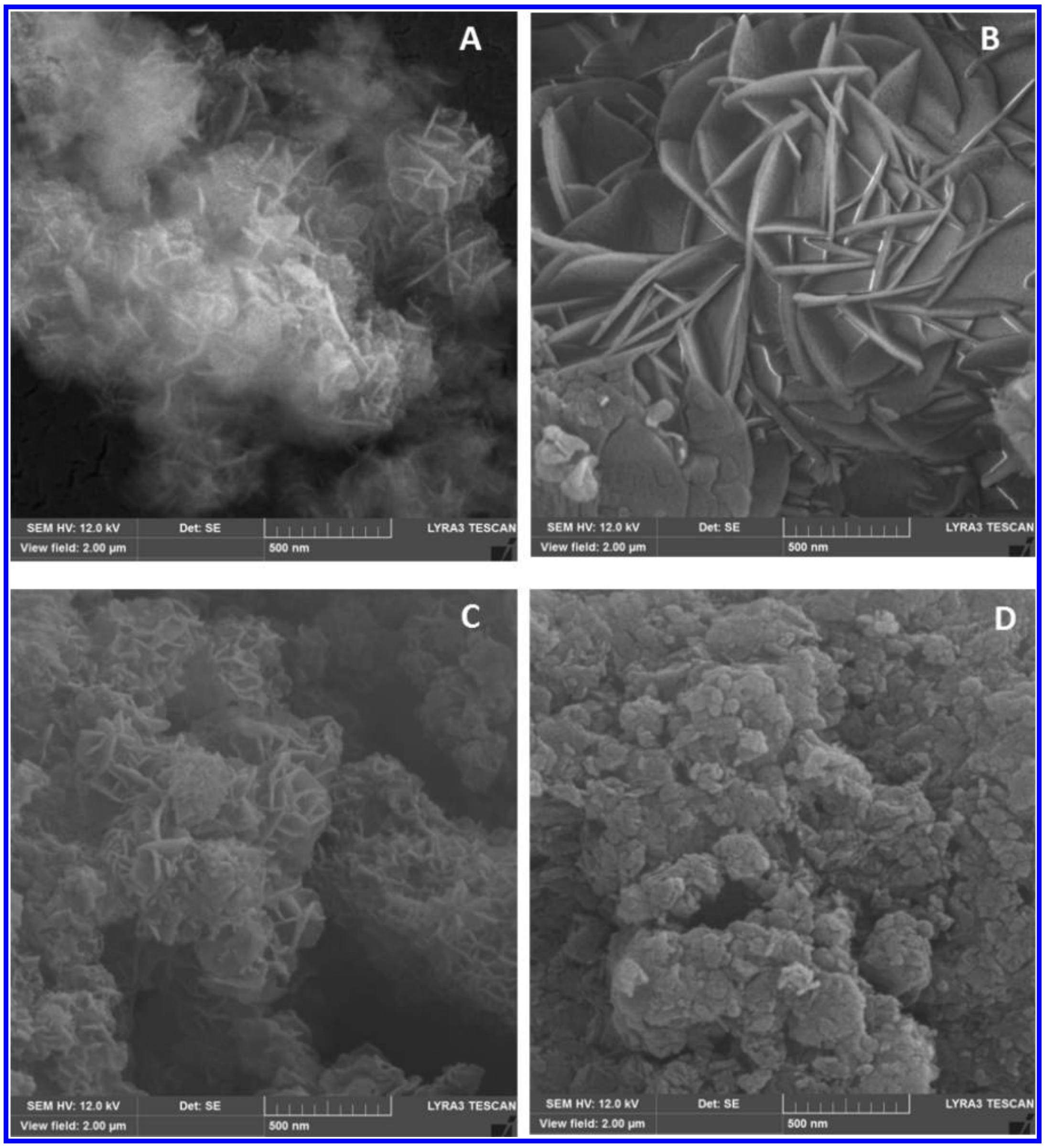

Figure 1. Scanning electron micrographs of the as-synthesized samples: (A) MgAl-1.5-HTC, (B) MgAl-2.5-HTC, (C) MgAl-7-HTC, and (D) PMg.

34. It was evidenced by a change in the position of a diffraction (200) peak at $2\theta \approx 43.0°$. At decreasing Al content in the Mg−Al mixed oxides, it shifted to a lower angles range, while the corresponding *d* spacing increased (Table 2). Derouane et al.[35] also showed that both the crystallinity and the unit cell of pure MgO decreased with the Al content. They attributed the observed trends to the migration of Al^{3+} cations into the MgO framework.

The BET surface area of Mg−Al mixed oxides increased in comparison with the as-prepared Mg−Al materials. It was 234 m^2/g for pure PMgC and 243 m^2/g for the MgAl-10 mixed oxide, but it increased to 343−376 m^2/g with the growth of Al content and declining crystallinity. The trends observed in the present study agree well with results from ref 8 where higher surface areas and decreased crystallinity also correlated with increasing Al content in the Mg−Al mixed oxide.

3.2. Scanning Electron Microscopy. SEM images were recorded to investigate the morphology of as-prepared and calcined samples with different Mg/Al ratios. The micrographs of the as-synthesized Mg−Al materials with Mg/Al molar ratios in the range of 1−7 (Figure 1) showed a well-developed layered structure; however, the Al content in the samples influenced the size and the morphology of the particles. MgAl-2.5-HTC with the highest crystallinity possessed a well-developed platelet structure typical of layered materials. It was formed by aggregates with the size in the range of 5−10 μm consisting of thin, hexagonal, plate-like crystals 0.3−0.6 μm in size (Figure 1B). MgAl-1.5-HTC with a higher Al content was formed by smaller aggregates of ≤5 μm in size (Figure 1A). They were composed of plate-like crystals which were smaller in size (0.1−0.3 μm) and significantly thinner than those in Mg/Al = 2.5. Besides, the micrograph of MgAl-1.5-HTC allows assuming the presence of an amorphous constituent in this sample. The

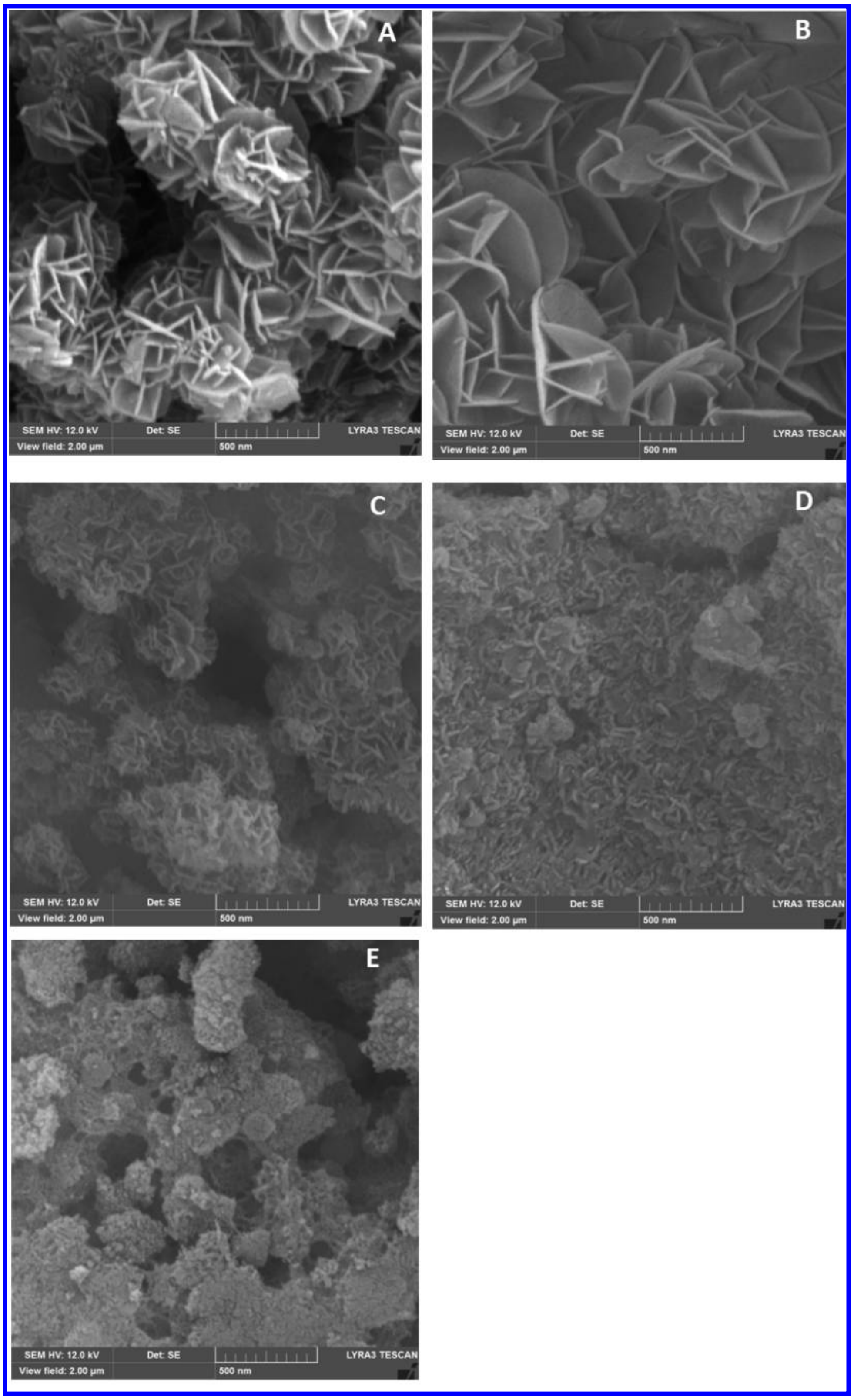

Figure 2. Scanning electron micrographs of the calcined samples: (A) MgAl-1.5, (B) MgAl-2.5, (C) MgAl-7, and (D) PMgC, E-PAlC.

increase in Mg/Al molar ratio also influenced the size and the morphology of the particles. Mg/Al = 7 was built of agglomerates with the size of 0.5−3 μm, while constituent plate-like crystals had the size of 0.1−0.2 μm (Figure 1C).

Table 3. Concentration and Density of Basic and Acid Sites in Prepared Mg−Al Mixed Oxides Determined by TPD of Adsorbed CO_2 and NH_3, Correspondingly

Sample	Concentration of basic sites, μmol/g	Density of basic sites, μmol/m²				Concentration of acid sites, μmol/g	Density of acid sites, μmol/m²
		Total	Weak (l.t.p)	Medium (m.t.p.)	Strong (h.t.p.)		
PAlC	156	0.453	0.134	0.302	0.017	272	0.791
MgAl-0.5	329	0.875	0.234	0.463	0.178	203	0.540
MgAl-1.5	247	0.918	0.190	0.416	0.312	215	0.629
MgAl-2.5	197	0.900	0.178	0.484	0.238	106	0.484
MgAl-4	164	0.686	0.167	0.326	0.193	99	0.414
MgAl-7	134	0.623	0.158	0.302	0.163	96	0.447
MgAl-10	130	0.535	0.124	0.259	0.152	73	0.300
PMgC	267	1.141	0.209	0.445	0.487	4	0.017

Taken together, the morphology of the as-prepared Mg−Al materials determined by SEM correlates well with XRD data: the higher the crystallinity of hydrotalcite phase is, the larger the sizes of the agglomerates and the constituent platelets are. The micrograph of as-prepared PMg showed the absence of a layered structure. It was formed by particles with an irregular surface and without a well-defined shape with the size of 5−10 μm (Figure 1D). Because of the irregularity, PMg was X-ray amorphous and possessed the highest BET surface among all as-prepared samples except PAl.

The mixed oxides with Mg/Al ratios in the range of 1−7 obtained upon calcination at 450 °C maintained a lamellar structure (Figure 2A−C). Moreover, the morphology and the size of plate-like crystals and agglomerates were similar to that of the as-prepared samples. In contrast, the morphology of calcined PMg changed compared to its as-prepared counterpart (Figure 2D). PMgC was formed by large agglomerates with the size of ≥5 μm consisting of very small plate-like crystals with the size of 50−100 nm. Additionally, the scanning electron micrograph of the calcined PAl indicated that this sample was composed of irregular particles without a well-defined size and shape (Figure 2E).

3.3. Basicity of Mg−Al Mixed Oxides Determined by CO_2-TPD.

The total concentration of basic sites and their distribution by their relative strength in Mg−Al mixed oxides with different Mg/Al molar ratios were determined by CO_2-TPD measurements. The profiles of CO_2 temperature-programmed desorption from PAlC, MgAl-X, and PMgC are shown in Figure 3S of the SI. The total evolved CO_2 (per catalyst weight) was obtained by integration of areas under the curves, and the resulting values as well as the density of basic sites (per unit surface area) are reported in Table 3. The total concentration of basic sites in PMgC was 267 μmol/g giving the highest basic sites density among all samples of 1.14 μmol/m². This value is slightly lower than that determined for MgO by Di Cosimo et al.[8] in the range of 1.63−2.33 μmol/m². The difference is possibly concerned with the differences in sample preparation procedures and measuring techniques. Both the total evolved CO_2 and the density of basic sites notably decreased when small amounts of Al were present in the samples (Table 3). Basic site densities on MgAl-7 and MgAl-10 with values in the range of 0.54−0.56 μmol/m² were less than half of the corresponding values measured on pure MgO. A similar trend in the basicity of Mg−Al mixed oxides with the change of Al content was observed by Di Cosimo et al.[8] and Fishel et al.[36] who observed that basic site density in MgO decreased when small amounts of Al were added, but it increased for higher Al contents. Based on XPS results, Di Cosimo et al.[8] explained the decrease in basic site density observed on the samples with low Al content by a significant Al surface enrichment. They suggested the presence of more electronegative amorphous AlO_y structures or isolated Al centers on MgO surface blocks CO_2 chemisorption sites.

The consistent increase in Al content in Mg−Al mixed oxides resulted in the growth of the total evolved CO_2, from 197 to 329 μmol/g in MgAl-2.5 and MgAl-0.5, respectively. Correspondingly, the density of basic sites attained the high value of 0.875−0.918 μmol/m² for samples with Mg/Al molar ratios in the range of 0.5−2.5, but it did not exceed the value observed for PMgC. Based on XPS data, Di Cosimo et al.[8] suggested that at higher Al contents the surface segregation of Al is less likely to occur; thus, the solid solution displays higher basicity concurrently with an increase in surface oxygen concentrations. A decrease in the crystallinity of high alumina mixed oxides could be an additional factor which influences the basicity of these samples. Indeed, the structural defects in the MgO crystalline framework may contribute to the increased accessibility of basic sites in the Mg−Al mixed oxides for CO_2. In contrast, PAlC had low values for both the total evolved CO_2 and basic sites density, 156 μmol/g and 0.45 μmol/m², respectively, indicating a change in the chemical and phase composition of this sample.

As evidenced by FTIR, adsorption of CO_2 on Mg−Al mixed oxides results in several forms of carbonate species, namely, monodentate carbonates, bidentate carbonates, and bicarbonates, which are generally described as strong (surface O^{2-} ions) and medium (Mg^{2+}−O^{2-}) pairs and weak (OH groups) basic sites, correspondingly.[5,8,37−39] Accordingly, the CO_2-TPD profiles are usually deconvoluted in three (arbitrary) desorption peaks to evaluate their relative contribution and, consequently, to characterize basic sites varied in their strength.[5,8,11] These desorption peaks have their maxima at about 100, 170, and 270 °C, and their appearance in the TPD curve is the most obvious for PMgC (SI, Figure 3S). The density of basic sites calculated from the amount of evolved CO_2 for each individual desorption peak obtained by deconvolution of the overall TPD signal is presented in Table 3. The general observation is that the density of all basic sites independently on their strength demonstrates two maximums: for PMgC and for Mg−Al mixed oxides with high Al content. The density of strong basic sites was more expressed on PMgC; it amounted to 0.487 μmol/m². The density of the strong basic sites sharply decreased to 0.152−0.163 μmol/m² for low-alumina mixed oxides. It showed that surface amorphous AlOy structures or isolated Al centers on the MgO surfaces of low-alumina Mg−Al mixed oxides decreased the population of the strongest basic sites, as proposed by Di Cosimo et al.[8] Further growth in Al content resulted in the gradual increase in the density of strong basic sites, and it reached the second maximum of 0.312 μmol/m^2 in MgAl-1.5. This can be attributed to the increased number of surface defects and the high concentration of surface oxygen atoms in high-Al mixed oxides due to incorporation of Al^{3+} ions into the MgO matrix along with the less pronounced surface segregation of Al atoms.[8] The density of medium strength basic sites was in the range of 0.416−0.484 μmol/m^2 for PMgC and high-Al mixed oxides with Mg/Al of 0.5−2.5 with a decrease to 0.259−0.326 μmol/m^2 for samples with Mg/Al = 4−10. The density of weak basic sites gradually decreased from 0.234 to 0.124 μmol/m^2 as the Mg/Al ratio increased from 0.5 to 10 followed by a sharp increase to 0.209 μmol/m^2 for PMgC. At last, the density of strong basic sites in PAlC was as low as 0.017 μmol/m^2, and this sample predominantly contained weakly basic OH-groups and Al^{3+}−O^{2-} pairs with medium strength, as proposed in ref 8.

3.4. Acidity of Mg−Al Mixed Oxides Determined by NH$_3$-TPD.

The NH$_3$-TPD profiles of the calcined samples with a different Mg/Al ratio are shown in Figure 4S of the SI, while Table 3 reports the values of the total evolved NH$_3$. The total concentration of acid sites gradually decreased with declining Al content in the samples from 272 to 4 μmol/g in PAlC and PMgC, correspondingly. Accordingly, the density of the total acid sites decreased from 0.791 to 0.017 μmol/m^2. The shape of the NH$_3$-TPD profile for PAlC allows suggesting the existence of several constituent peaks with maxima at about 180 and 280 °C (SI, Figure 4S), which implies the presence of acid sites with different strengths. The contribution of the high-temperature peak may be detected in the NH$_3$-TPD profile of MgAl-0.5 with the largest Al content, but it is negligible for other samples. The NH$_3$-TPD results indicate that PAlC is the most acidic among all prepared samples, while PMgC is the least acidic both in the total concentration and in the strength of acid sites.

3.5. Catalysis.

Two parallel reactions take place when contacting a mixture of furfural and acetone with a catalyst: aldol condensation of furfural and acetone and acetone self-condensation. Acetone conversion by self-condensation affording mainly diacetone alcohol was very low (below 2%) and was therefore not considered further. The carbon balance was estimated to be close to 100% based on the carbon balance including only reactants, the main acetone self-condensation products (diacetone alcohol and mesityl oxide), and the main aldol condensation products (FAcOH, FAc, and F2Ac) that exceeded always 92%. In addition to these products, heavier aldol condensation products were observed as well but could not be quantified precisely due to their low concentration and poor chromatographic resolution and thus used in carbon balance calculation.

Additionally, special experiments with MgAl-1.5 and MgAl-10 were performed to evaluate the possibility of leaching, i.e., the partial dissolution of catalysts in a reaction medium and, as a consequence, the occurrence of a homogeneous reaction. The comparison of Mg/Al molar ratio in the mixed oxides before and after catalytic run by XRF method proved a similarity in their chemical compositions. Then, the analysis of the reaction mixture at the end of a catalytic run and catalyst separation showed the absence of Mg and Al elements in the organic phase. Finally, in a special experiment, a catalyst was separated from the reaction mixture after 20 min of the run followed by the stirring of the mixture for additional 2 h. The composition of the mixture determined by GC after 20 and after 2 h of the experiment was similar, thus proving the absence of leaching effect. Based on these results, it was concluded that furfural conversion and the composition of reaction products determined in the performed catalytic experiments were exclusively due to the physicochemical characteristics of the solid Mg−Al mixed oxides.

Figure 3 depicts furfural conversion observed on Mg−Al mixed oxides with a different Mg/Al molar ratio in aldol condensation of furfural and acetone after 120 min (the dependence of furfural conversion on reaction time is presented in Figure 5S of the SI). Furfural conversion did significantly vary in the range of 3.4−30%, and it did not show any certain dependence on the chemical composition of Mg−Al mixed oxides. Among all studied catalysts, PAlC demonstrated the lowest activity in the reaction with furfural conversion of 3.4%. Even a small amount of Mg in the composition of Mg−Al mixed oxides induced a significant growth in the furfural conversion. It gradually increased from 16% for MgAl-0.5 to 30% for MgAl-1.5. Further increase in Mg content in the catalysts resulted in a sharp decline in furfural conversion with the minimum value of 6.9% observed for MgAl-4. The next and gradual increase in the catalyst activity was observed for mixed oxides with Mg/Al ≥ 5, and PMgC afforded the furfural conversion of 27.9% (Figure 3).

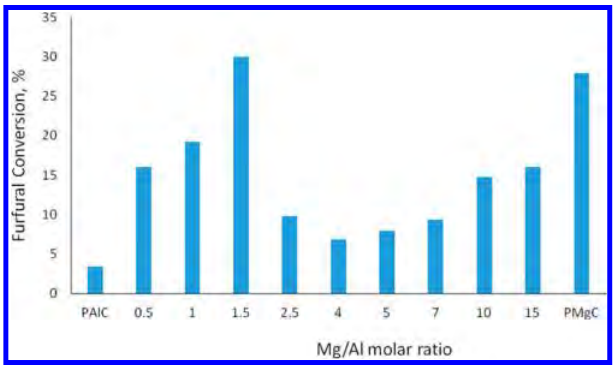

Figure 3. Furfural conversion as a function of a Mg/Al molar ratio in mixed oxides (A) and the density of basic sites (B) in Mg−Al mixed oxides. $T_{reac.}$ = 50 °C, time = 120 min.

Usually the catalytic performance of HTC-derived mixed oxide materials in aldol condensation is correlated with their acido-basic properties,[4,5,10,11] more particularly, with the density of basic sites.[8,11,39,40] Our results are partially also in agreement with these findings; a high furfural conversion was observed for Mg−Al-0.5, Mg−Al-1.5, and PMgC (Figure 3) which possessed the highest density of basic sites, while pure alumina (PAlC) with the lowest density of basic sites exhibited small activity in aldol condensation reaction compared with the other catalysts (Table 3). The latter result proves that neither Al^{3+} Lewis acid sites nor basic sites associated with Al atoms (weak OH-hydroxyls and medium Al^{3+}-O^{2-} pairs) are able to initiate aldol condensation by abstracting proton from an acetone molecule. In contrast, furfural conversion over all Mg−Al mixed oxides and PMgC was substantially higher, suggesting that the catalytic activity of these samples originated from basicity associated with Mg atoms, i.e., weak OH-hydroxyls, medium Mg^{2+}−O^{2-} pairs, and isolated O^{2-} basic centers. Nevertheless, despite a general tendency for the growth of

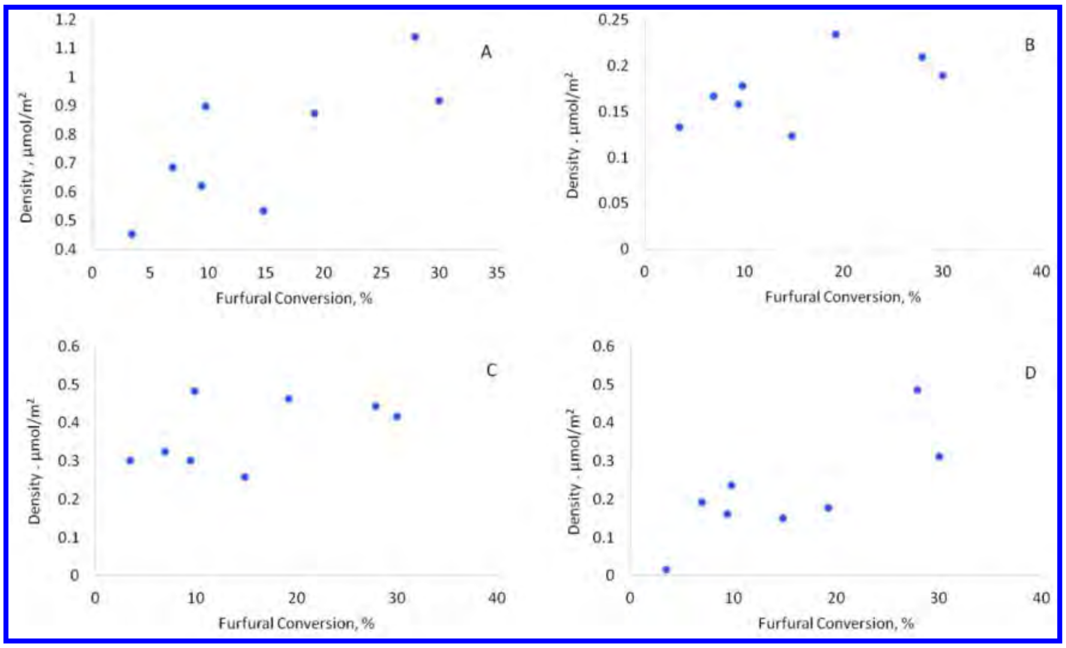

Figure 4. Furfural conversion in dependence on the density of total (A), weak (B), medium (C), and strong (D) basic sites. $T_{reac.}$ = 50 °C, time = 120 min.

furfural conversion with the increasing density of basic sites, a linear correlation between these parameters in the whole range of chemical compositions is not quite apparent (Figure 4A). Hence, we compared the catalysts activity data of Figure 3 with the density of weak, medium, and strong basic sites, obtained by deconvolution of the CO_2-TPD signal and given in Table 3.

A very weak increasing trend was observed when furfural conversion was plotted versus the density of weak or medium basic sites (Figure 4B and C). It is worth noting that desorption peaks in the medium temperature range (at ≈170 °C) represents a superposition of two peaks which characterize basic sites associated with both Al and Mg atoms. As is shown from the catalytic performance of PAlC, the medium basic sites associated with Al ($Al^{3+}-O^{2-}$ pairs) have a poor activity in the reaction. Consequently, an accurate correlation between the density of medium basic sites which are active in the reaction ($Mg^{2+}-O^{2-}$ pairs) and furfural conversion is difficult to establish for samples with high Al content. The dependence of furfural conversion on the density of strong basic sites is more straightforward (Figure 4D) suggesting that these sites mostly contribute to the activity of Mg−Al mixed oxides in aldol condensation of furfural and acetone. A similar conclusion was made by Díez et al.[40] who suggested that the rate-limiting step of aldol condensation is the abstraction of proton from the acetone molecule that is essentially promoted by strong basic sites. Ordóñez et al.[12] also suggested that aldol condensation of furfural and acetone required both acid−base pair sites and high density of strong basic sites. Nevertheless, the contribution of basic sites with medium strength (i.e., Mg^{2+}-O^{2-} pairs) to the activity of Mg−Al catalysts in aldol condensation of furfural and acetone cannot be totally excluded. Faba et al.[41] proposed that the rate-determining step of the reaction is promoted by medium-strength base sites. A similar conclusion was recently made by us[42] for Zn(Mg)Al mixed oxides with a constant M^{2+}/Al^{3+} molar ratio, when higher furfural conversion was observed for mixed oxides with higher population of $Mg^{2+}-O^{2-}$ pairs (sites with medium strength) that represented a dominant type of basic sites in all that catalysts. Considering catalytic results of the present study indicating an increase in furfural conversion with the growth of the density of medium (a weaker correlation, Figure 4C) and strong basic sites (a stronger correlation, Figure 4D) as well as suggestions from the above-mentioned references, both medium and strong basic sites can contribute to the occurrence of aldol condensation.

The obtained results allow suggesting that a specific correlation between the basicity of catalysts and their activity can be additionally influenced by other factors related to the preparation method. Our results suggest that the morphology and the size of the plate-like crystals which form Mg−Al mixed oxides should be taken into account when evaluating their catalytic performance. Indeed, MgAl-2.5 and MgAl-7 demonstrate similar activity in aldol condensation with furfural conversion in the range of 9.4−9.8%, although the density of strong basic sites in these catalysts varies 1.5 times, 0.15 and 0.10 μmol/m², respectively (additionally, the density of medium basic sites in these catalysts varies as well, 0.31 and 0.19 μmol/m², respectively). At the same time, MgAl-2.5 is formed of plate-like crystals of 0.3−0.6 μm in size, while the crystals present in MgAl-7 have only 0.1−0.2 μm (Figure 3). The similar activity of both materials, despite the lack in the basicity of the latter catalyst, can be therefore explained by the morphology and size of the crystals in MgAl-7. Similarly, Abello et al.[43] correlated the catalytic performance of differently prepared hydrotalcites with their textural properties and concluded that crystal size of the catalysts is the activity-directing factor in aldol condensation reactions.

The composition of the reaction products provides additional information on the effect of the properties of Mg−Al mixed oxides with different chemical composition on the occurrence of aldol condensation. At similar furfural conversion of 5%, the ratio between the selectivity to aldol (FAcOH, i.e., a primary product of furfural−acetone interaction) and the

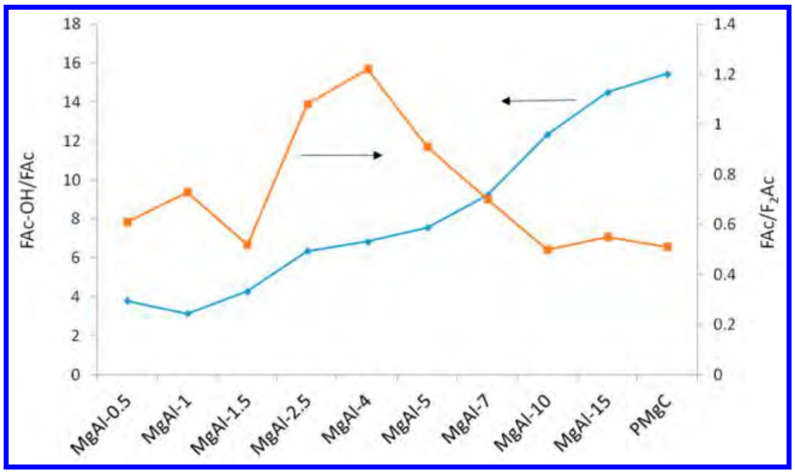

Figure 5. Influence of a Mg/Al ratio in mixed oxides on FAc−OH/FAc and FAc/F_2Ac selectivity ratio observed in aldol condensation at furfural conversion of ≈5%. T = 50 °C, F:Ac = 1:5 (mol.).

selectivity to FAc, which is the product of the aldol dehydration, gradually increased with the growth in the Mg/Al molar ratio of the samples (Figure 5). The obtained results agree well with the conclusion of Tichit et al.[44] that acidic sites of Mg−Al mixed oxides were not strong enough to catalyze the aldol condensation, but they were responsible for the dehydrating activity of the catalysts. Indeed, the density of acid sites in the prepared samples decreased successively with the increasing Mg/Al ratio (Table 3) and did not contribute to the catalysts activity. Simultaneously, it resulted in a decrease in the dehydrating ability of the catalysts and, correspondingly, to an increase in the FAc−OH/FAc selectivity ratio.

Figure 5 depicts that the selectivity to the second condensation step which resulted in the formation of F_2Ac did not correlate unambiguously with the chemical composition of Mg−Al mixed oxides. The FAc/F_2Ac selectivity ratio reached its maximum value for MgAl-2.5 and MgAl-4, but declined with either increasing or decreasing aluminum content in the samples. The observed trend can hardly be explained by the acid−base characteristics of the prepared catalysts because it does not follow a change in the density of either acidic or basic sites. The second step of aldol condensation results in the formation of F_2Ac which is a more voluminous molecule compared to FAc. Therefore, the existence of diffusion limitations associated with the access of the reactants to the active sites followed by the formation of the bulkier molecule may be assumed. In contrast to the acido-base characteristics, the FAc/F_2Ac selectivity ratio (Figure 5) correlated well with the size of the plate-like crystals determined by SEM (Figure 3): the smaller the size of plate-like crystals is, the higher the ability of catalysts to form F_2Ac is. Thus, when evaluating the catalytic performance of Mg−Al mixed oxides in aldol condensation of furfural and acetone, both acid−base and textural properties of the prepared materials have to be taken into account.

■ CONCLUSIONS

The results of the study show that Mg−Al mixed oxides prepared from layered double hydroxides over a wide range of Mg/Al compositions differ in a great extent in their textural and basic properties. This difference is reflected in their catalytic performance in aldol condensation of furfural and acetone. In general, the catalytic activity of the Mg−Al mixed oxides in the condensation reaction correlates with the density of basic sites, in particular, strong (surface O^{2-} ions) basic sites. Nevertheless, the contribution of medium strength (Mg^{2+}−O^{2-} pairs) to the occurrence of aldol condensation cannot be excluded. Besides, morphology and the size of crystals affect the activity of Mg−Al mixed oxides and the composition of reaction products. More specifically, the existence of small-size crystals diminishes the influence of diffusion limitations and favors the access of the reactants to the active sites and, thus, the formation of bulkier compounds, such as F2Ac. Finally, the presence of acid sites in the Mg−Al mixed oxides determines their dehydrating properties and, consequently, also influences the composition of the reaction products. Hence, the understanding of the catalytic performance of Mg−Al mixed oxides in aldol condensation reactions requires to assess not only their basic properties but also their acidic and textural properties and morphology.

■ ASSOCIATED CONTENT

Ⓢ Supporting Information

The Supporting Information is available free of charge on the ACS Publications website at DOI: 10.1021/acs.iecr.7b03367.

Information as mentioned in the text. (PDF)

■ AUTHOR INFORMATION

Corresponding Author

*Oleg Kikhtyanin. E-mail: oleg.kikhtyanin@vscht.cz. Tel.: (+420) 775527919.

ORCID

David Kubička: 0000-0003-2996-7824

Notes

The authors declare no competing financial interest.

■ ACKNOWLEDGMENTS

The authors gratefully thank the Czech Science Foundation (Project No. 15-21817S).

■ REFERENCES

(1) Vaccari, A. Preparation and catalytic properties of cationic and anionic clays. *Catal. Today* **1998**, *41*, 53.

(2) Sels, B. F.; De Vos, D. E.; Jacobs, P. A. Hydrotalcite-like anionic clays in catalytic organic reactions. *Catal. Rev.: Sci. Eng.* **2001**, *43*, 443.

(3) Zeng, H. Y.; Feng, Z.; Deng, X.; Li, Y. Q. Activation of Mg-Al hydrotalcite catalysts for transesterification of rape oil. *Fuel* **2008**, *87*, 3071.

(4) Kustrowski, P.; Sulkowska, D.; Chmielarz, L.; Dziembaj, R. Aldol condensation of citral and acetone over mesoporous catalysts obtained by thermal and chemical activation of magnesium-aluminum hydrotalcite-like precursors. *Appl. Catal., A* **2006**, *302*, 317.

(5) Perez, C. N.; Monteiro, J. L. F.; Lopez Nieto, J. M.; Henriques, C. A. Influence of basic properties of Mg,Al-mixed oxides on their catalytic activity in knoevenagel condensation between benzaldehyde and phenylsulfonylacetonitrile. *Quim. Nova* **2009**, *32*, 2341.

(6) Cavani, F.; Maselli, L.; Scagliarini, D.; Flego, C.; Perego, C. How basic properties of MgO-based mixed oxides affect the catalytic performance in gas-phase and liquid-phase methylation of m-cresol. *Stud. Surf. Sci. Catal.* **2005**, *155*, 167.

(7) Prescott, H. A.; Li, Z. J.; Kemnitz, E.; Trunschke, A.; Deutsch, J.; Lieske, H.; Auroux, A. Application of calcined Mg-Al hydrotalcites for Michael additions: an investigation of catalytic activity-and acid-base properties. *J. Catal.* **2005**, *234*, 119.

(8) Di Cosimo, J. I.; Díez, V. K.; Xu, M.; Iglesia, E.; Apesteguia, C. R. Structure and surface and catalytic properties of Mg-Al basic oxides. *J. Catal.* **1998**, *178*, 499.

(9) Abello, S.; Medina, F.; Tichit, D.; Perez-Ramirez, J.; Rodriguez, X.; Sueiras, J. E.; Salagre, P.; Cesteros, Y. Study of alkaline-doping agents on the performance of reconstructed Mg−Al hydrotalcites in aldol condensations. *Appl. Catal., A* **2005**, *281*, 191.

(10) Sharma, S. K.; Parikh, P. A.; Jasra, R. V. Solvent free aldol condensation of propanal to 2-methylpentenal using solid base catalysts. *J. Mol. Catal. A: Chem.* **2007**, *278*, 135.

(11) Veloso, C. O.; Perez, C. N.; de Souza, B. M.; Lima, E. C.; Dias, A. G.; Monteiro, J. L. F.; Henriques, C. A. Condensation of glyceraldehyde over Mg,Al-mixed oxides derived from hydrotalcites. *Microporous Mesoporous Mater.* **2008**, *107*, 23.

(12) Ordóñez, S.; Díaz, E.; León, M.; Faba, L. Hydrotalcite-derived mixed oxides as catalysts for different C−C bond formation reactions from bioorganic materials. *Catal. Today* **2011**, *167*, 71.

(13) Hora, L.; Kikhtyanin, O.; Čapek, L.; Bortnovskiy, O.; Kubička, D. Comparative study of physico-chemical properties of laboratory and industrially prepared layered double hydroxides and their behavior in aldol condensation of furfural and acetone. *Catal. Today* **2015**, *241*, 221.

(14) Alonso, D. M.; Bond, J. Q.; Dumesic, J. A. Catalytic conversion of biomass to biofuel. *Green Chem.* **2010**, *12*, 1493.

(15) Gamez, S.; Gonzalez-Cabriales, J. J.; Ramirez, J. A.; Garrote, G.; Vazquez, M. Study of the hydrolysis of sugar cane bagasse using phosphoric acid. *J. Food Eng.* **2006**, *74*, 78.

(16) Pham, T. N.; Shi, D.; Resasco, D. E. Evaluating strategies for catalytic upgrading of pyrolysis oil in liquid phase. *Appl. Catal., B* **2014**, *145*, 10.

(17) Barrett, C. J.; Chheda, J. N.; Huber, G. W.; Dumesic, J. A. Single-reactor process for sequential aldol-condensation and hydrogenation of biomass-derived compounds in water. *Appl. Catal., B* **2006**, *66*, 111.

(18) Kikhtyanin, O.; Kubička, D.; Čejka, J. Toward understanding of the role of Lewis acidity in aldol condensation of acetone and furfural using MOF and zeolite catalysts. *Catal. Today* **2015**, *243*, 158.

(19) Nguyen Thanh, D.; Kikhtyanin, O.; Ramos, R.; Kothari, M.; Ulbrich, P.; Munshi, T.; Kubička, D. Nanosized TiO2—A promising catalyst for the aldol condensation of furfural with acetone in biomass upgrading. *Catal. Today* **2016**, *277*, 97.

(20) Sádaba, I.; Ojeda, M.; Mariscal, R.; Fierro, J. L. G.; López Granados, M. Catalytic and structural properties of co-precipitated Mg−Zr mixed oxides for furfural valorization via aqueous aldol condensation with acetone. *Appl. Catal., B* **2011**, *101*, 638.

(21) Xu, W.; Liu, X.; Ren, J.; Liu, H.; Ma, Y.; Wang, Y.; Lu, G. Synthesis of nanosized mesoporous Co−Al spinel and its application as solid base catalyst. *Microporous Mesoporous Mater.* **2011**, *142*, 251.

(22) Cavani, F.; Trifiro, F.; Vaccari, A. Hydrotalcite-Type Anionic Clays: Preparation, Properties and Applications. *Catal. Today* **1991**, *11*, 173.

(23) Čapek, L.; Kutalek, P.; Smoláková, L.; Hajek, M.; Troppova, I.; Kubička, D. The Effect of Thermal Pre-Treatment on Structure, Composition, Basicity and Catalytic Activity of Mg/Al Mixed Oxides. *Top. Catal.* **2013**, *56*, 586.

(24) Grabowska, H.; Zawadzki, M.; Syper, L.; Mista, W. Mg,Al-mixed oxide system: Synthesis under hydrothermal conditions, physico-chemical characterisation and application as an efficient catalyst for imidazole methylation. *Appl. Catal., A* **2005**, *292*, 208.

(25) Hora, L.; Kelbichová, V.; Kikhtyanin, O.; Bortnovskiy, O.; Kubička, D. Aldol condensation of furfural and acetone over Mg Al layered double hydroxides and mixed oxides. *Catal. Today* **2014**, *223*, 138.

(26) Cantrell, D. G.; Gillie, L. J.; Lee, A. F.; Wilson, K. Structure-reactivity correlations in MgAl hydrotalcite catalysts for biodiesel synthesis. *Appl. Catal., A* **2005**, *287*, 183.

(27) Teng, G. Y.; Gao, L. J.; Xiao, G. M.; Liu, H.; Lv, J. H. Biodiesel Preparation from Jatropha curcas Oil Catalyzed by Hydrotalcite Loaded With K_2CO_3. *Appl. Biochem. Biotechnol.* **2010**, *162*, 1725.

(28) Yun, S. K.; Pinnavaia, T. J. Water-Content and Particle Texture of Synthetic Hydrotalcite-Like Layered Double Hydroxides. *Chem. Mater.* **1995**, *7*, 348.

(29) Albuquerque, M. C. G.; Santamaria-Gonzalez, J.; Merida-Robles, J. M.; Moreno-Tost, R.; Rodriguez-Castellon, E.; Jimenez-Lopez, A.; Azevedo, D. C. S.; Cavalcante, C. L.; Maireles-Torres, P. MgM (M = Al and Ca) oxides as basic catalysts in transesterification processes. *Appl. Catal., A* **2008**, *347*, 162.

(30) Di Serio, M.; Tesser, R.; Ferrara, A.; Santacesaria, E. Heterogeneous basic catalysts for the transesterification and the polycondensation reactions in PET production from DMT. *J. Mol. Catal. A: Chem.* **2004**, *212*, 251.

(31) Miyata, S. Physicochemical Properties of Synthetic Hydrotalcites in Relation to Composition. *Clays Clay Miner.* **1980**, *28*, 50.

(32) Cullity, B. D.; Stock, S. R. *Elements of X-Ray Diffraction*, third ed.; Prentice-Hall, Inc. 2001; pp 167−171.

(33) Constantino, V. R. L.; Pinnavaia, T. J. Basic Properties of Mg1-X(2+)Alx(3+) Layered Double Hydroxides Intercalated by Carbonate, Hydroxide Chloride and Sulfate Anions. *Inorg. Chem.* **1995**, *34*, 883.

(34) Sato, T.; Fujita, H.; Endo, T.; Shimada, M.; Tsunashima, A. Synthesis of hydrotalcite-like compounds and their physico-chemical properties. *React. Solids* **1988**, *5*, 219.

(35) Derouane, E. G.; Jullien-Lardot, V.; Davis, R. J.; Blom, N.; Hojlund-Nielsen, P. E. Aromatization of n-Hexane by Aluminium-Stabilized Magnesium Oxide-Supported Noble Metal Catalysts. *Stud. Surf. Sci. Catal.* **1993**, *75*, 1031.

(36) Fishel, C. T.; Davis, R. Characterization of magnesium-aluminum mixed oxides by temperature-programmed reaction of 2-propanol. *Langmuir* **1994**, *10*, 159.

(37) Bolognini, M.; Cavani, F.; Scagliarini, D.; Flego, C.; Perego, C.; Saba, M. Heterogeneous basic catalysts as alternatives to homogeneous catalysts: reactivity of Mg/Al mixed oxides in the alkylation of m-cresol with methanol. *Catal. Today* **2002**, *75*, 103.

(38) Carvalho, D. L.; de Avillez, R. R.; Rodrigues, M. T.; Borges, L. E. P.; Appel, L. G. Mg and Al mixed oxides and the synthesis of n-butanol from ethanol. *Appl. Catal., A* **2012**, *415-416*, 96.

(39) Díez, V. K.; Apesteguia, C. R.; Di Cosimo, J. I. Effect of the chemical composition on the catalytic performance of MgyAlOx catalysts for alcohol elimination reactions. *J. Catal.* **2003**, *215*, 220.

(40) Díez, V. K.; Apesteguía, C. R.; Di Cosimo, J. I. Aldol condensation of citral with acetone on MgO and alkali-promoted MgO catalysts. *J. Catal.* **2006**, *240*, 235.

(41) Faba, L.; Díaz, E.; Ordóñez, S. Aqueous-phase furfural-acetone aldol condensation over basic mixed oxides. *Appl. Catal., B* **2012**, *113−114*, 201.

(42) Smoláková, L.; Frolich, K.; Kocík, J.; Kikhtyanin, O.; Čapek, L. Surface Properties of Hydrotalcite-Based Zn(Mg)Al Oxides and Their

Catalytic Activity in Aldol Condensation of Furfural with Acetone. *Ind. Eng. Chem. Res.* **2017**, *56*, 4638.

(43) Abelló, S.; Medina, F.; Tichit, D.; Pérez-Ramírez, J.; Groen, J. C.; Sueiras, J. E.; Salagre, P.; Cesteros, Y. Aldol Condensations Over Reconstructed Mg−Al Hydrotalcites: Structure−Activity Relationships Related to the Rehydration Method. *Chem. - Eur. J.* **2005**, *11*, 728.

(44) Tichit, D.; Lhouty, M. H.; Guida, A.; Chiche, B. H.; Figueras, F.; Auroux, A.; Bartalini, D.; Garrone, E. Textural Properties and Catalytic Activity of Hydrotalcites. *J. Catal.* **1995**, *151*, 50.

Applied Catalysis A: General 525 (2016) 215–225

Contents lists available at ScienceDirect

Applied Catalysis A: General

journal homepage: www.elsevier.com/locate/apcata

The occurrence of Cannizzaro reaction over Mg-Al hydrotalcites

Oleg Kikhtyanin[a,*], Estera Lesnik[a], David Kubička[b]

[a] Unipetrol Centre of Research and Education, Block 2838, Záluží 1, 436 70 Litvínov, Czech Republic
[b] Technopark Kralupy VŠCHT Praha, University of Chemistry and Technology, Prague, Žižkova 7, 278 01 Kralupy nad Vltavou, Czech Republic

ARTICLE INFO

Article history:
Received 26 May 2016
Received in revised form 14 July 2016
Accepted 5 August 2016
Available online 5 August 2016

Keywords:
Basic catalysis
Cannizzaro reaction
Mg-Al hydrotalcite
Mixed oxide rehydration
Aldol condensation

ABSTRACT

Mg-Al mixed oxides and reconstructed hydrotalcites prepared from mixed oxides by rehydration attract much attention as solid basic catalysts for organic reactions, such as aldol condensation. Therefore, the understanding of parameters that govern their catalytic performance is of great importance. Cannizzaro reaction in the presence of mixed oxide and reconstructed HTC as basic catalysts was used as a model reaction to characterize both catalytic systems and to understand their behavior in aldol condensation. The performance of the samples was investigated in the conversion of aqueous furfural mixture using stirred batch reactor operating at T = 50 °C. The properties of both initial samples and catalysts after reaction were studied by different physico-chemical methods, such as XRD, DRIFT and TGA. It was shown that both mixed oxide and reconstructed HTC possessed poor activity in the conversion of dried furfural proving the importance of water presence for the reaction to take place. Addition of water to the reaction mixture resulted in growth of the yield of both furfuryl alcohol and furoyl furoate as reaction products. Furoic acid was not identified by GC analysis, but the interaction of the acid with the basic sites of catalysts was confirmed by DRIFT and TGA analyses indicating that at optimum reaction conditions, most of the basic sites were involved in the formation of furoate species. The formation of the surface furoate species influenced the behavior of the basic catalysts in aldol condensation of furfural and acetone. It allows concluding that the occurrence of Cannizzaro reaction should be taken into account when considering the behavior of basic catalysts in organic reactions with furfural as a reactant.

1. Introduction

In recent years hydrotalcites (HTCs) have found numerous applications as adsorbents or ion exchangers, catalyst precursors or supports, etc. [1–4]. These materials represent a class of hydrated double hydroxides with a general formula $[M^{2+}{}_{n}M^{3+}{}_{m}(OH)_{2(n+m)}]^{m+}(A^{x-})_{m/x}\cdot yH_2O$. The most commonly used Mg-Al HTCs consist of a brucite-like $[Mg(OH)_2]$ network wherein isomorphous substitution of Mg^{2+} ion by a trivalent Al^{3+} occurs and the excess positive charge of the framework is compensated by gallery anions which are located in the interlayer along with water molecules [4–6]. As-prepared HTCs typically contain carbonates as compensating anions which makes these materials inactive in base-catalyzed reactions [7]. Thermal treatment of Mg–Al HTCs results in decomposition of carbonate groups accompanied by the release of CO_2 and the formation of a well-dispersed mixture of magnesium and aluminum oxides (MgAlO). The calcined mixed oxides act as weak Lewis acid/strong base catalysts and find various applications as effective catalysts in transesterification [8,9], alcohol elimination [10] and condensation [11,12] reactions. A distinctive feature of MgAlO materials is their ability to reconstruct the lamellar HTC structure (so-called memory effect) when contacted with water vapor or liquid water in absence of carbon dioxide. This leads to meixnerite (magnesium aluminium hydroxide hydrate), that is HTC intercalated with OH^- as compensating anions in the interlayer [11,12]. In addition, the treatment of MgAlO with aqueous reaction mixture (*in situ* rehydration) leading to reconstructed HTCs is also known [12–14]. These rehydrated materials have been applied to a number of base-catalyzed reactions which require Brønsted basic character, including different self- and cross-condensations [12–15] Michael additions [16], etc.

Condensation reactions attract much attention because they allow obtaining more complex compounds with more carbon atoms starting from relatively simple molecules. The interest in these reactions stems from the fact that many of the initial molecules for the syntheses can be obtained by biomass processing. For example, furfural can be obtained by acid hydrolysis of sugar cane bagasse, a residue from sugar cane processing, followed by extraction [17]. The needed acetone may be obtained by ketonization of acetic acid [18] that is an important product

---

* Corresponding author.
E-mail address: oleg.kikhtyanin@unicre.cz (O. Kikhtyanin).

http://dx.doi.org/10.1016/j.apcata.2016.08.007

of biomass pyrolysis. Aldol condensation of these relatively simple molecules allows increasing chain length to 8+ carbon atoms. This route has attracted significant interest, because hydrogenation/hydrodeoxygenation of these aldol condensation products leads to various hydrocarbons suitable for blending in conventional diesel fuel and kerosene [19]. A comprehensive study of aldol condensation over solid catalysts is thus necessary for designing the pathway to components of motor fuels from renewable natural resources.

Aldol condensation of furfural (F) and acetone (Ac) in the presence of a basic catalyst begins with the initial abstraction of the α-proton from acetone, forming a carbanion that consecutively attacks the carbonyl group of the nearby adsorbed furfural molecule [20,21]. Additionally, acetone can be transformed on basic (or acidic as well) sites by its own reaction pathway which is acetone self-condensation resulting to the formation of diacetone alcohol, mesityl oxide, etc [11,13]. Both aldol condensation of furfural with acetone and acetone self-condensation can proceed simultaneously; in this case the rate-determining step should be shared by both reaction pathways and involve basic sites with similar strength [20].

Much less attention is paid to the transformation of furfural on basic sites of a solid catalyst in absence of acetone, or generally in absence of carbonyl compounds having no α-hydrogen atoms. Nevertheless, furfural can hardly be considered as an inert component when contacted with basic sites and a specific parallel reaction route has to be considered. Cannizzaro reaction (CR) is a well-known base-induced redox reaction of an aldehyde lacking a hydrogen atom in the alpha position. It represents the disproportionation of an aldehyde into a carboxylic acid and an alcohol catalyzed by a strong aqueous base, i.e. it takes two aldehydes to produce one acid and one alcohol. In case of furfural, two furfural molecules would produce furfuryl alcohol (F-OH) and furoic acid (F-OOH) according to the reaction scheme below (Scheme 1).

The mechanism of the CR is well postulated. The reaction begins with the attack of hydroxide from basic NaOH on the carbonyl carbon followed by deprotonation to give a dianion. This unstable intermediate releases a hydride anion which attacks another molecule of aldehyde. In this process the dianion converts to a carboxylate anion and the aldehyde to an alkoxide. The alkoxide then picks up a proton from water to provide the alcohol final product, while the caboxylate is converted to the carboxylic acid product after acid work-up [22]. It should be mentioned that in aqueous basic solution carboxylic acid produced by CR can hardly be detected in pure form as it immediately reacts with the base to form a corresponding salt.

Taking into account the scheme of furfural transformation by CR the occurrence of this reaction on a basic solid can also be assumed provided that the catalyst possesses hydroxides of sufficient strength as active sites and the reaction proceeds in aqueous medium. Indeed, this reaction was proposed among others when considering all possible reactions occurring during aqueous furfural aldol condensation with acetone using base solid catalysts [23]. Additionally, it was mentioned that MgO in aqueous media could catalyze the formation of the intermediate species for the Cannizzaro reaction (furfuryl alcohol and furoic acid) resulting in the formation of esterification product, 2-furancarboxylic 2-furanmethyl ester (furoyl furoate, FF) [24]. Nevertheless, there is no information available on the effect of CR on the physico-chemical properties of a solid basic catalyst as well as on its impact on the behavior of the catalyst in aldol condensation.

The scope of the present work is thus to understand the behavior of calcined Mg-Al mixed oxide as a catalyst for converting aqueous furfural mixture and to provide information on the extent of CR and its impact on the catalyst performance in aldol condensation.

2. Experimental

Mg–Al layered double hydrotalcite (HTC) with a Mg:Al molar ratio of 3:1 was prepared according to a procedure described in [25]. The Mg-Al mixed oxide was prepared by calcination of the dried as-prepared HTC at 450 °C for 3 h (heating rate 5 °C/min). The rehydration of the mixed oxide was performed by its stirring in water (2 g of freshly calcined material per 30 mL of water) at room temperature for 30 min, followed by the filtration of resulting solid with a vacuum pump and drying in a rotary evaporator in N_2 flow during 40 min. The calcined HTC is further on referred to as Mg-Al mixed oxide while the fully rehydrated mixed oxide is denoted as reconstructed HTC.

The crystallographic structures of the dried as-prepared HTC sample, Mg-Al mixed oxide and materials obtained during rehydration experiments were determined by X-ray powder diffraction using a Philips MPD 1880 instrument with Cu Kα irradiation (λ = 0.154 nm) in the 2θ range of 5°–70° at the 2θ scanning rate of 2.4°/min. The relative content of present crystalline phases in the solids was evaluated using the areas of diffraction peaks at 2θ = 11.4 and 22.8° for the HTC phase and at 2θ = 43.1° for the MgO phase, wherein the relative content of the respective phases in as-synthesized HTC and Mg-Al mixed oxide were taken as 100%. The textural properties of the samples (specific surface area and pore volume) were measured by nitrogen physisorption at −196 °C using an Autosorb surface area and porosity analyzer. The basic properties of as-prepared HTC were evaluated by temperature programmed desorption (TPD) of carbon dioxide in a Micromeritics Autochem 2950 apparatus. Before reduction, the sample was outgassed under a He flow of 25 $cm^3\ min^{-1}$ with a heating ramp of 10 °C min^{-1} up to 500 °C. The sample was cooled down to 50 °C and saturated under a CO_2 flow (10 vol.% in He) of 50 $cm^3\ min^{-1}$ for 30 min. Subsequently, the physically adsorbed carbon dioxide was removed by flowing He (25 $cm^3\ min^{-1}$) at 50 °C for 60 min. Finally, the chemically absorbed CO_2 was desorbed by heating up the sample to 850 °C (heating rate of 15 °C min^{-1}) in flowing He (25 $cm^3\ min^{-1}$) and maintaining this temperature for 30 min. The amounts of desorbed species were quantified using calibration standards. Thermogravimetric analysis of the dried as-prepared HTC catalysts was performed using a TA Instruments TGA Discovery series equipment operating with a heating ramp of 10 °C/min from room temperature to 900 °C in N_2 flow. TGA-MS experiments were performed on the same TGA unit equipped with mass-spectrometer OmniStar GSD 320 (Pfeiffer-Vacuum) with MID (Multiple Ion Detection) measurement mode, SEM (Secondary Electron Multiplier) detector and quadrupole mass analyzer. The DRIFT spectra were recorded on a Nicolet IS 10 FTIR spectrometer equipped with DTGS detector and KBr beam splitter. All spectra were collected over the range of 4000–400 cm^{-1} at a spectral resolution of 4 cm^{-1} and number of scans 128 (both for the background and the sample spectra).

Furfural (Sigma-Aldrich) used for the study was pre-dried with a molecular sieve 3A to exclude the influence of moisture originating from the chemicals. All catalytic experiments on furfural conversion using either water-free conditions or aqueous furfural mixture were carried out in a 100 mL stirred batch reactor (a glass flask reactor) operating at T = 50 °C. Furfural conversion as a function of reaction time was studied in experiments using 2 g of freshly calcined HTC (or rehydrated HTC prepared from the same amount of Mg-Al mixed oxide) and 30 g of furfural. To prepare aqueous furfural mixtures, different amount of water (ranging from 0 to 33%wt.) was added to furfural. As the solubility of water and F in each other is limited [26], aqueous furfural mixtures with water content ≤6 wt.% were monophasic solutions while higher water amounts resulted in the formation of a biphasic (water and organic phases) mixtures if no stirring was used. To ensure

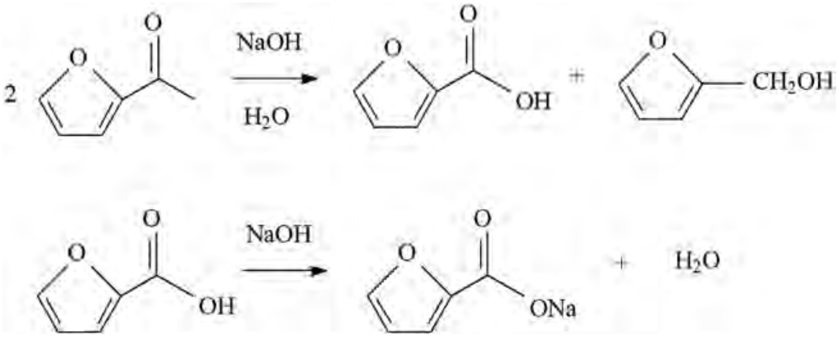

Scheme 1. Cannizzaro reaction in the presence of sodium hydroxide as a basic catalyst.

a "quasi-constant" reaction conditions, the reaction mixture was stirred at 300 RPM to afford aqueous organic emulsion. After adding the catalyst to the reaction mixture, the reaction was carried out at T = 50 °C for 180 min at 300 RPM. Samples were periodically withdrawn from the reactor during the experiment, filtered, and analyzed by Agilent 7890A GC unit equipped with a flame ionization detector (FID), using a HP-5 capillary column (30 m/0.32 mm ID/0.25 μm). The obtained products were identified based on standard reference compounds as well as additional GC–MS analyses. The catalytic results of furfural transformation over basic catalysts were described in terms of product yield that was calculated as follows:

$$\text{Yield of producti(t)(mol\%)} = 100 \times (\text{mole of reactant converted to product i})_{t/reactant\,t=0}.$$

After the reaction the catalysts were separated from aqueous furfural mixture by filtration, washed with ethanol, dried in N_2 flow at room temperature and characterized by different methods. Catalysts obtained from experiments with aqueous furfural mixtures having different water content are denoted HTC-xx where xx stands for the wt.% of water in the mixture, i.e. HTC-23 is a catalyst obtained from reaction in which aqueous furfural containing 23 wt.% of water was used as feedstock.

Aldol condensation of furfural and acetone was performed by using the same stirred batch reactor operating at T = 50 °C. For these experiments 0.5 g of freshly calcined HTC, 6.5 g of furfural and 19.7 g of acetone (Ac:F = 5 mol/mol) were used. After adding the catalyst to the reaction mixture, the reaction was carried out at T = 50 °C for 180 min under intensive stirring. Samples were periodically withdrawn from the reactor during the experiment, filtered and analyzed by the same GC method. Catalytic results of aldol condensation of furfural and acetone were described by conversion parameter that was calculated from the corresponding molar concentrations as follows:

$$\text{Reactant conversion (t)(mol\%)} = 100 \times (\text{reactant}_{t=0} - \text{reactant}_t)/\text{reactant}_{t=0}.$$

3. Results

3.1. Catalyst characterization

The physico-chemical properties of as-prepared HTC, calcined HTC (Mg-Al mixed oxide) and rehydrated HTCs investigated by XRD, TGA/DTG and DRIFT are presented in Table 1 and the *Supplementary information* (SI).

The XRD pattern of the freshly synthesized sample used in this study (see *SI*) shows a pure hydrotalcite phase (JCPDS 22-700) with intensive symmetrical peaks at $2\theta \approx 11°$, 22.8°, 36° and 60°, which are characteristic for the brucite-like layers. No additional crystalline phases could be identified in the diffractogram proving the high phase purity of the as-prepared hydrotalcite material. The XRD pattern of the sample calcined at 450 °C (Mg-Al mixed oxide) confirms the disappearance of the layered HTC structure. The only reflections observed in the XRD pattern (see SI) correspond to the MgO phase proving the formation of Mg-Al mixed oxide with the MgO periclase-type structure (JCPDS 87-0653). XRD pattern of a sample obtained after interaction of the Mg-Al mixed oxide with liquid water evidences the presence of a reconstructed HTC phase (meixnerite, JCPDS 35-0965) (see SI). It is worth noting that the XRD patterns of totally rehydrated samples shows neither a significant loss in intensity nor broadening of XRD peaks in comparison with the as-prepared HTC., i.e. these samples can be considered to be reconstructed HTCs. It also means that upon mechanical stirring during the rehydration process in liquid phase the hydrotalcite-like platelets were not broken or exfoliated which would result in a decrease in their particle size and in a change in their textural properties.

The textural properties of the as-prepared and Mg-Al mixed oxide (Table 1) are similar to those obtained for similar materials in our other studies [25]. According to chemical analysis, Mg/Al molar ratio in as-prepared material is 3.8 (Table 1), i.e. slightly higher when compared with the starting concentration of the elements in reactive synthesis gel. Assuming that each Al atom in the solid should produce one basic site, the theoretically possible concentration of basic sites in the sample with Mg/Al = 3.8 (with respect to bulk Al content) is 4.9 mmol/g for calcined sample, i.e. Mg-Al mixed oxide, (Table 1) or 2.7 mmol/g for dried as-prepared HTC taking into account its general formula and weight loss upon calcination (TGA data see below).

The actual concentration of basic sites was measured by CO_2-TPD technique. The uptake of CO_2 was 0.85 mmol per one gram of dried as-prepared HTC sample used in the experiment, hence the total concentration of basic sites determined by CO_2-TPD was 0.85 mmol/g based on the as-prepared HTC or 1.54 mmol/g if recalculated for Mg-Al mixed oxide, i.e. nearly 31.5% of theoretical value (Table 1).

The TGA profile for the as-prepared HTC sample (see SI) is in good agreement with the profiles reported in literature for HTC-like materials [27,28]. The total weight loss for this sample amounts to 45.8 wt.% (Table 2) which is in accordance with previous results [27,28]. The low temperature weight loss of 16.7 wt.% occurs in the range of 20–200 °C due to the removal of water molecules. It is clearly seen (see SI) that the signal in this range could be deconvoluted in two peaks with maxima at ca. 100 and 200 °C which are generally attributed to the loss of physically adsorbed and interlayer water molecules, correspondingly [27]. The high tem-

Table 1
Physico-chemical characteristics of Mg-Al samples used in the present study.

Sample	Phase composi-tion	BET area (m^2/g)	Mg/Al in synthesis gel (mol/mol)	Mg/Al by XRF (mol/mol)	Theoretical amount of basic sites (mmol/g)	Concentration of basic sites by CO_2-TPD (mmol/g)
$HTC_{as\text{-}prep.}$	HTC	–	3	3.8	2.7	0.85
$Mg\text{-}Al_{calc.}$	MgO	180			4.9	1.54
$HTC_{reconstr.}$	HTC	–			2.7	

Table 2
Results on the thermal analysis of the samples and their formula calculated from TGA-MS data.

Sample	Weight loss (TGA), %			Calculated formula (using TGA-MS)
	Total	20–250 °C	250–800 °C	
$HTC_{as\text{-}prep.}$	45.8	16.7	29.1	$Mg_{7.6}Al_2CO_{3(1.08)}OH_{19.6}\cdot 6.2H_2O$
$Mg\text{-}Al_{calc.}$	10.2	4	6.2	–
$HTC_{reconstr.}$	45.4	17.1	28.3	$Mg_{7.6}Al_2CO_{3(0.16)}OH_{21}\cdot 8.2H_2O$

perature weight loss of 29.1 wt.% is observed at temperature above 200 °C and originated from the dehydroxylation of the brucite-like sheets and the decomposition of carbonates in the interlayer [27]. To quantify the ratio between hydroxyl and carbonate groups in the as-prepared HTC, TGA-MS technique was used to determine H_2O and CO_2 evolution from the sample. Above 250 °C, the MS spectra show the presence of signals of H_2O and CO_2 (see *SI*) with the maxima at similar temperature, i.e. 395 and 404 °C, correspondingly, which prevents their differentiation by a routine TGA analysis. Using data from chemical and thermal analysis, the composition of the as-prepared hydrotalcite was calculated being very close to expectations from theory (Table 2).

In comparison with the as-prepared HTC, the weight loss of the calcined material (i.e. Mg-Al mixed oxide) is, as expected, much lower (only 10.2 wt.%) (Table 1). It corresponds to the loss of the physically adsorbed water below 100 °C (4.0 wt.%) and the removal of residual hydroxyls and carbonate groups at $T \geq 500$ °C remained present after the sample calcination at $T = 450$ °C (see SI). Total weight loss in the rehydrated sample is 45.4 wt.% (Table 1), i.e. very close to the value determined for the as-prepared HTC material. The distribution and intensity of the signals observed in the DTG spectra for the as-prepared and the reconstructed samples are also similar. Nevertheless, the performed TGA-MS study of both samples evidences a substantial decrease in the intensity of the signal corresponding to the evolved CO_2 (see SI). It proves that as a result of the calcination-rehydration procedure most of the carbonate groups are replaced by hydroxyls in the reconstructed HTC as evidenced by the calculated formula of the reconstructed HTC (Table 2). The observed presence of carbonate groups in the reconstructed HTC results most probably from the interaction of the rehydrated sample with CO_2 from air before the TGA analysis.

The DRIFT spectrum of the as-synthesized HTC material (see SI) is similar to the spectra published elsewhere [1,12,29,30]. A typical broad band at about 3460–3500 cm^{-1} is attributed to the stretching vibrations of structural hydroxyl groups in the brucite-like layer. A shoulder at 3000 cm^{-1} is assigned to hydrogen bonding between water molecules and the interlayer carbonate anions. The bands at around 1640 and 1370 cm^{-1} confirms the expected presence of interlayer water molecules and carbonate (chelating or bridging bidentate) anions, respectively. The vibration at 1515 cm^{-1} is ascribed to a reduction in the symmetry caused by the presence of monodentate carbonates ($\gamma_{asymO-C-O}$) interacting with Mg^{2+}, as reported elsewhere [1,12,29,30]. The low frequency region shows a band at about 560 cm^{-1}, corresponding to the translation modes of hydroxyl groups, influenced by Al^{3+} cations [12,31,32]. The band at 870 cm^{-1} is characteristic for the out-of-plane deformation of carbonate, whereas the in-plane bending is located at 680 cm^{-1} [12].

Calcination of the as-prepared HTC results in water removal that is evidenced by the disappearance of the band at around 1640 cm^{-1} (water bending vibrations) and of the shoulder at 3000 cm^{-1} (interaction of H_2O—$CO_3{}^{2-}$ in the interlayer) (see *SI*). The intensity of the bands at around 3460–3500 cm^{-1} also decreases due to the surface dehydroxylation upon calcination. The band at 1370 cm^{-1} (interlayer carbonates) decreases in intensity and the two peaks at about 1515 and about 1400 cm^{-1} evidencing the interaction between $CO_3{}^{2-}$ and Mg^{2+} [12] are also present, but their intensity decreases as well. The obtained FTIR spectrum proves that residual carbonate and hydroxyls anions as well as small amount of water (band at around 1640 cm^{-1}) are still present in HTC sample calcined at $T = 450$ °C, i.e. in the Mg-Al mixed oxide sample, most likely due the adsorption of CO_2 and moisture from air during the DRIFT experiment.

The spectrum of the reconstructed HTC is substantially similar to that of the as-prepared HTC (see SI). The broad band at 3460–3500 cm^{-1} evidences the recovery of the structural hydroxyl groups in the brucite-like layers. The bands at 3050 and 1640 cm^{-1} also reappears in the spectra of this sample, indicating a significant amount of adsorbed water molecules in the reconstructed material. The band at 1370 cm^{-1} which also reappears in the spectra as a symmetric peak is usually attributed to the presence of carbonates in reconstructed materials, even after rehydration step [12,32]. In the latter case, the existence of these groups in the rehydrated samples is explained by a probable introduction of $(CO_3)^{2-}$ from air during the reconstruction process [12]. However, the performed TGA-MS analysis of the reconstructed HTC proves low concentration of carbonates in the reconstructed HTC, so the band at 1370 cm^{-1} in DRIFT spectrum cannot be unequivocally attributed to carbonate groups. Moreover, anionic OH-groups should be inevitably identified in the DRIFT spectra of the reconstructed HTC material as well. It is known that anionic groups other than carbonates could be characterized by absorption bands in the FTIR region close to 1370 cm^{-1}. For example, a band at 1364 cm^{-1} was previously ascribed to the anti-symmetrical stretching mode of nitrate ions [33] and a band observed at 1390 cm^{-1} was attributed to the symmetric stretching of the carboxylate group [34]. Hence, hydroxyl groups formed due to the rehydration of Mg-Al mixed oxide (calcined HTC), which compensate the positive charge of the layers, could be also responsible for the observed band lying in the same FTIR-region. This makes us to conclude that the band at 1370 cm^{-1} could in fact signify the presence of any extra-framework functional anionic groups, including OH^-, which compensate the positive charge of the inorganic framework originating from the Mg-Al isomorphous substitution.

3.2. Interaction of Mg-Al mixed oxide with aqueous furfural mixture

According to the reaction scheme (Scheme 1), water is a necessary participant of Cannizzaro reaction donating a proton for an intermediate alkoxide to be converted to a final alcohol. In other words, the absence of water makes the disproportionation of furfural to furfuryl alcohol (F-OH) and furoic acid (F-OOH) in the presence of a basic catalyst impossible. Accordingly, in our experiments we have studied the behavior of Mg-Al mixed oxide in CR of aqueous furfural solutions having different water content.

The main reaction products obtained by reaction of aqueous furfural feedstock over calcined HTC, i.e. over Mg-Al mixed oxide, are F-OH and furoyl furoate (FF). Despite no F-OOH is found in reaction products, the formation of F-OH and FF, a product of esterification reaction between F-OH and F-OOH, provides an indirect evidence that furfural undergoes CR over the solid base catalyst. One-stage alcohol formation from aldehyde is only possible by using hydrogen atmosphere and a hydrogenation catalyst which is not the case in our experiment. Moreover, due to the basic nature of the catalyst used it is highly likely that F-OOH will react immediately with the basic sites forming either salts, e.g. sodium furoate when NaOH would be used as catalyst, or surface furoates in case of solid base catalysts. This is confirmed by a titration experiment (see *SI*) in which F-OOH is successively added to Mg-Al mixed oxide (calcined HTC) catalyst immersed in acetone followed by GC analysis of the liquid phase. A signal on the GC diagram belonging to F-OOH appears only when the amount of acid added to the catalyst exceed 0.3 g/g_{cat}. The only plausible explanation of the performed titration experiment is that the acid remains adsorbed on the catalyst. It is worth noting that the concentration of basic sites in the calcined sample titrated with F-OOH is ≈2.7 mmol/g, which is higher than that determined by CO_2-TPD (based on Mg-Al mixed oxide). Presumably, furoic acid could additionally adsorb on weak basic sites which do not interact with CO_2 in the CO_2-TPD experiment. Assuming the formation of surface furoates, we have introduced the yield of F-OH as the measure of catalyst activity in Cannizzaro reaction.

Fig. 1A depicts F-OH yield observed during reaction of aqueous furfural mixtures having different water content on Mg-Al mixed oxide in dependence on experiment duration. A clear dependence of catalyst activity on water content in the mixture is observed. At water-free conditions, F-OH yield is as low as 0.11 wt.% after 180 min of the reaction. This result confirms the necessity of water presence in the reaction mixture to facilitate the Cannizzaro reaction, which is in accordance with the reaction scheme (Scheme 1). The catalyst activity observed in the water-free experiment can be explained by the traces of moisture in the sample due to adsorption from air during the transfer of the calcined catalyst into the reactor. This explanation is also supported by TGA results. The observed alcohol yield corresponds to 0.15 mmol of F-OH produced per 1 g of Mg-Al mixed oxide. Taking into account the reaction stoichiometry, i.e. the equimolar formation of F-OH and F-OOH, and assuming acid-base interaction between the formed F-OOH and basic sites of the catalyst, it can be inferred that about 10% of the basic sites in the catalyst probed by CO_2 (Table 1) participate in the reaction and react with the produced acid forming furoate species.

Fig. 1A shows that the increase in water content in the mixture results in the growth of F-OH yield proving thus the importance of water in the reaction (Scheme 1). For monophasic reaction conditions (water content in the range of 0–6 wt.%) the F-OH yield is below 0.5 wt.% after 180 min of the reaction. Under biphasic reaction conditions (water content >12 wt.%) the F-OH yield substantially increases to 1.8-2.3 wt.% (Fig. 1A). The maximum alcohol yield of 2.3 wt.% is observed for water content of 23 wt.% in the mixture while further increase in water content up to 33% results in a slight decrease of F-OH yield to 1.9 wt.%.

The maximum F-OH yield of 2.3 wt.% (Fig. 1A) corresponds to 3.6 mmol of produced F-OH per 1 g of calcined catalyst. Hence, the amount of the produced acid should also correspond to 3.6 $mmol_{F\text{-}OOH}/g_{cat}$. Since F-OOH is not identified by GC among reaction products, the concentration of basic sites that interacted with the acid should also be equal to 3.6 $mmol/g_{cat}$. This value is larger than that determined by the direct titration of Mg-Al mixed oxide with furoic acid (see SI) and substantially exceeds the value determined by CO_2-TPD (Table 1). On the other hand, the concentration of basic sites in the catalyst evaluated from its activity in CR is still lower than the theoretical basicity derived from its chemical composition. It allows concluding that not all basic sites in the catalyst are involved in the reaction and the formation of surface furoates. Nevertheless, the concentration of basic sites as high as 3.6 mmol/g determined by the *in-situ* "titration" with furoic acid proves that physico-chemical characteristics of basic catalysts including the amount of basic sites can change during the rehydration step as discussed below.

Besides F-OH, furoyl furoate is observed as a reaction product (Fig. 1B), apparently as a result of esterification reaction between furfuryl alcohol and furoic acid. In contrast to F-OH, the yield of the FF ester exhibits a less pronounced dependence on water content. Fig. 1B shows that after 180 min of the reaction, the ester yield is 0.16 wt.% for monophasic aqueous furfural mixture (≤6 wt.% of water) and only small increase to 0.18–0.2 wt.% is observed for higher water contents (biphasic reaction mixture). The observed poor dependence of the ester yield on water content allows assuming that the formation of this compound could be more preferable in water-free reaction conditions. Obviously, as water is a product of the esterification reaction, an increase in water content will favor hydrolysis over esterification, i.e. shift the reaction equilibrium towards the reactants.

3.3. The properties of Mg-Al catalysts after reaction

The experimental results provide a strong indication that furfural is converted by Cannizzaro reaction over Mg-Al mixed oxide when water is present. Whereas F-OH is observed in the reaction products by GC, it is highly probable that F-OOH forms furoate species on the catalyst surface, i.e. remains adsorbed on the basic sites of the catalyst. The formation of such species would definitely change physico-chemical properties of a basic catalyst and these have been monitored by different techniques.

3.3.1. XRD

Fig. 2A depicts XRD patterns of catalysts after reaction in dependence on water content in aqueous furfural mixture. XRD patterns of samples after experiments using a monophasic reaction mixture (water content of 0–6 wt.%) contain predominantly reflections characteristic for MgO phase. As soon as the furfural mixture becomes biphasic (water content ≥12 wt.%), the intensity of the reflections due to the MgO phase noticeably decreases while the intensity of reflections corresponding to the HTC phase increases. The calculated relative content of the crystalline phases (Fig. 2B) evidences that a dramatic step change in the phase composition of the catalysts occurs when the monophasic reaction mixture turns into a biphasic one due to the increase in water concentration. In the monophasic aqueous-organic mixture the probability for the inorganic solid to interact with water molecules (a necessary step for rehydration to take place) is low because of high furfural concentration because both molecules compete for the same adsorption places. As a consequence, the rehydration of the mixed oxide to a reconstructed HTC is slow. In contrast, when the reaction mixture is biphasic, the catalyst is in contact with both organic (mostly furfural) and aqueous (mostly water) phases. The XRD data evidence (Fig. 2) that such intermittent interaction of Mg-Al mixed

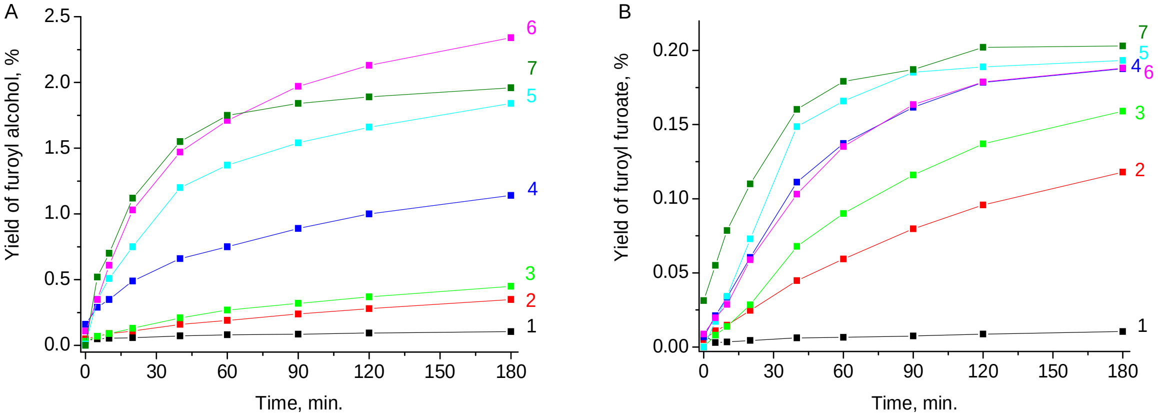

Fig. 1. Yields of furfuryl alcohol (A) and furoyl furoate (B) observed during reaction of aqueous furfural mixture on Mg-Al mixed oxide in dependence on water content (in wt.%): 1–0%, 2–3%, 3–6%, 4–12%, 5–18%, 6–23%, 7–33%. $T_{reac.} = 50\,°C$, $m_{furfural} = 30\,g$, $m_{calc.cat.} = 2\,g$.

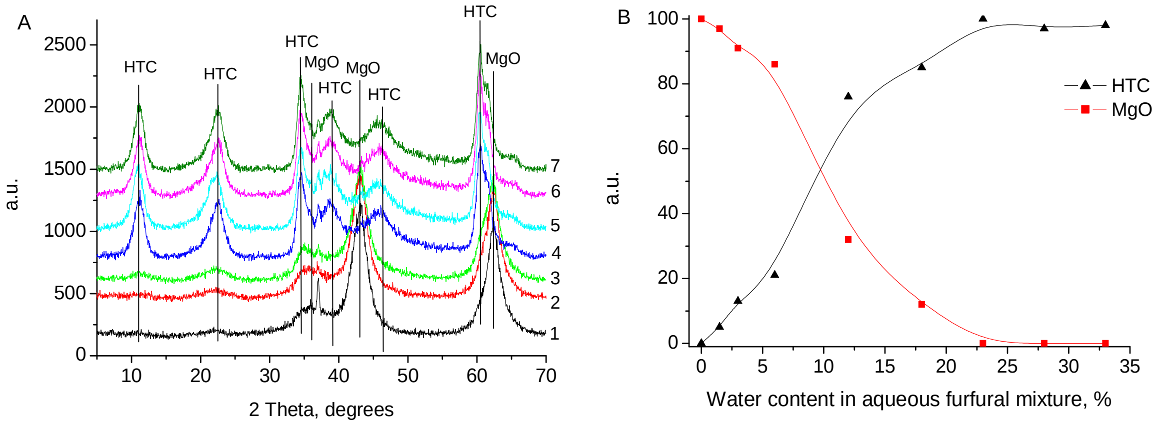

Fig. 2. XRD patterns (A) and the relative content of HTC and MgO phases (B) in catalysts after reaction in dependence on concentration of water in aqueous furfural mixture: 1–HTC-0, 2–HTC-3, 3–HTC-6, 4–HTC-12, 5–HTC-18, 6–HTC-23, 7–HTC-33 where the numbers denote wt.% of water in the mixture.

oxide with either organic or aqueous phase under intensive stirring ensures the transformation of the solid mixed oxide into reconstructed HTC. The comparison of the catalytic results with the XRD data allows concluding that the observed high activity of the catalysts in CR is connected with the high rehydration degree of Mg-Al mixed oxide to a reconstructed HTC. This conclusion is in agreement with the reaction scheme of CR: the disproportionation of furfural to F-OH and F-OOH takes place with the participation of hydroxyls which are Brønsted basic sites of the rehydrated HTC catalyst rather than with the Lewis basic sites of Mg-Al mixed oxide.

3.3.2. TGA

Fig. 3A depicts TGA curves of the catalyst samples after Cannizzaro reaction of furfural aqueous mixtures having variable water content. The catalysts were separated from reaction mixtures by filtration followed by washing with ethanol and drying at 80 °C for 4 h before TGA experiments to exclude the contribution of any physisorbed organic species to the results. The increase in water content results in a progressive increase in the total weight loss of the samples (Fig. 3A) which correlates with the transformation of the Mg-Al mixed oxide to reconstructed HTC materials as proved by XRD (Fig. 2). The samples obtained from the reaction of monophasic furfural-water mixtures possess low-to-moderate weight loss in the range of 21–30 wt.%, due to the small rehydration degree of the Mg-Al mixed oxide (<20%). In contrast, the weight loss of the sample HTC-23 obtained after reaction of biphasic furfural-water mixture amounts to 49 wt.% which is close to the values for as-prepared or water-reconstructed HTC samples (Table 1). In agreement with these results, the sample HTC-23 affords a nearly fully reconstructed HTC after the reaction as evidenced by the XRD results (Fig. 2).

The DTG curves of the samples after reaction (Fig. 3B) show two ranges of weight losses in accordance with the results for as-prepared or reconstructed HTC samples. The low-temperature region consists of two signals at T = 80–100 °C and 180–200 °C attributed to physically adsorbed and interlayer water, respectively, the latter exhibiting a clear dependence on the reconstruction degree of the rehydrated samples. In fact, the change in phase composition is linearly proportional to the water content in the aqueous furfural mixture. In agreement with the XRD data (Fig. 2A) an obvious difference is observed between the TGA/DTG curves for samples obtained from monophasic or biphasic reaction mixture experiments.

In the high-temperature region of DTG curves, the presence of two well-distinguished signals at ∼320 and ∼400 °C can be observed. The signal at T = 385–400 °C is similar to those observed in both as-prepared and reconstructed HTC samples and corresponds to the removal of carbonate and/or hydroxyl groups from the samples [27]. For the catalysts after reaction the intensity of this peak increases with the growth in water content in the reaction mixture and, as a consequence, it is in line with the increase in the rehydration degree of Mg-Al mixed oxide proved by XRD (Fig. 2). Nevertheless, the signal with maximum at T = 320 °C was not previously observed in DTG curves for as-prepared and water-reconstructed HTC materials (see SI). Therefore, this signal has to originate from other compounds than water, CO_2 or contaminants

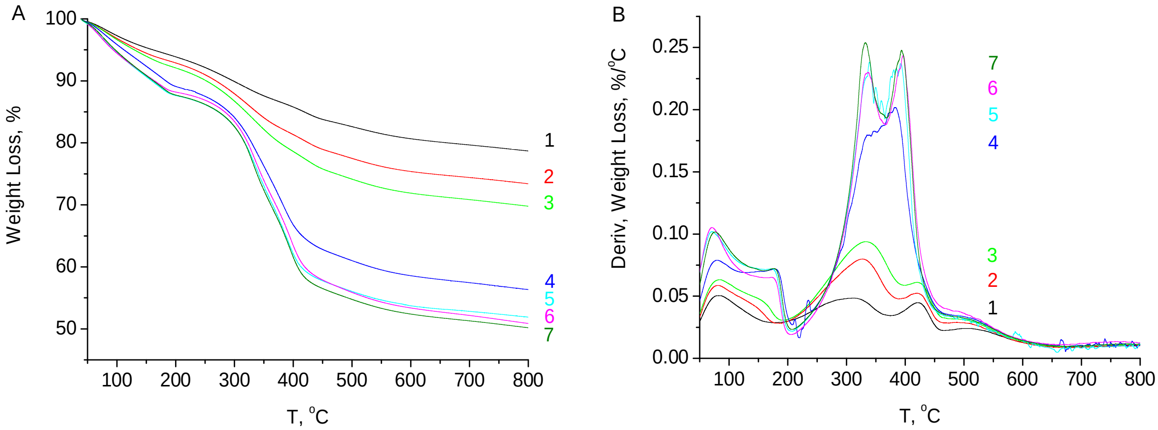

Fig. 3. TGA (A) and DTG (B) curves of catalysts obtained after reaction with aqueous furfural mixture with different water content. 1–HTC-0, 2–HTC-3, 3–HTC-6, 4–HTC-12, 5–HTC-18, 6–HTC-23, 7–HTC-33.

from ambient air, i.e. from furfural or reaction products of furfural transformation including F-OH, F-OOH and FF. The intensity of this signal also increases with the increasing concentration of water in the reaction mixture. As the increase in the water content resulted in an increase in the furfuryl alcohol yield (Fig. 1A), it can be deduced that the signal at T = 320 °C is due to furfuryl alcohol or, more likely, due to surface furoates formed by adsorption of furoic acid that is produced from furfural by Cannizzaro reaction in equimolar yields as furfuryl alcohol, but unlike F-OH is not detected among reaction products.

3.3.3. DRIFT

DRIFT spectra obtained after contacting Mg-Al mixed oxide with aqueous furfural mixtures having different water content are shown in Fig. 4 (reconstructed HTC rehydrated with pure water is shown as a reference). With increasing water content, a broad band in the range of 2700–3700 cm^{-1} reappears in the spectra proving the recovery of structural hydroxyl groups in the brucite-like layers of the rehydrated samples (Fig. 4A). The bands in the range of 1300–1700 cm^{-1} which characterize the presence of interlayer water molecules and compensating extra-framework anions also appear in the spectra (Fig. 4B). The change of the DRIFT spectra for Mg-Al mixed oxide sample after its contact with aqueous medium can be attributed to the HTC structure recovery and is thus in agreement with XRD and TGA results. However, comparing the DRIFT spectra for catalysts after reaction with the spectra for both as-prepared and rehydrated HTC samples, it can be concluded that the composition of the functional groups in the samples after reaction is different than in the fresh samples. First, shoulder at 3000 cm^{-1} usually observed in the DRIFT spectra of both as-prepared and reconstructed HTC rehydrated with pure water is absent in the DRIFT spectra of the spent catalysts. The absence of this shoulder suggests that the $H_2O—CO_3^{2-}$ interaction in the interlayer is weakened. Furthermore, the character of the bands in the range of 1300–1700 cm^{-1} differs: it becomes more complex for the samples after reaction as additional bands appeared in the spectra (Fig. 4B). Instead of a single band at 1640 cm^{-1} which characterizes the presence of water molecules in interlayer (Fig. 2) several bands at 1561 and 1591 are present in the DRIFT spectra of catalysts after reaction. These bands suggest that other molecules than water are present in the interlayer of the rehydrated catalysts. Moreover, two new bands at 1363 and 1390 cm^{-1} are also present in the spectra. For as-prepared and reconstructed HTC rehydrated with pure water the band at 1370 cm^{-1} characterizes the presence of compensating anions, as discussed above. The appearance of the new bands at 1363 and 1390 cm^{-1} can be related with the presence of new kind of compensating anions, such as furoates. Besides, a well-expressed band at 1479 cm^{-1} not observed previously in the DRIFT spectra for neither as-prepared nor rehydrated HTC samples is found in the spectra of spent catalysts. Finally, several new bands appeared also in the range of 900–1250 cm^{-1} (Fig. 4B) which could be caused by the presence of new surface species in the catalysts after reaction.

In summary, the characterization data prove that the increase in water content in the aqueous furfural mixture promotes the rehydration of the Mg-Al mixed oxide and facilitates the formation of reconstructed HTC. As soon as Brønsted basic sites are formed in the reconstructed material, its activity in furfural conversion increases as demonstrated by the increase in both F-OH and furoyl furoate yield. After the reaction, the catalyst contains additional species which differ from carbonate or OH$^-$ anions as well as from water molecules. Taking into account the concentration of F-OH in the liquid reaction products together with the absence of furoic acid among these products, it is highly probable that these newly formed species found in the catalysts after reaction are surface furoate species. To support this claim, a specific study of furoic acid interaction with the rehydrated catalysts was undertaken.

3.4. The study of interaction between rehydrated HTC and furoic acid

Different amounts of furoic acid were added to the mixture of water and reconstructed HTC after the completion of the rehydration procedure (see the *Experimental*), and the resulting mixture was stirred for 10 min. The solids treated with furoic acid were then separated by filtration using a vacuum pump, dried in N_2 flow at room temperature and investigated by TGA and DRIFT.

A gradual growth in the DTG signal with the maximum at T = 330–340 °C is observed for rehydrated HTC after its treatment with furoic acid as the ratio of m_{FOOH}/m_{sample} increases from 0 to 0.5 (Fig. 5). The filtrate solution was analyzed by GC, but no furoic acid was detected. This strongly suggests that it was adsorbed on the catalyst and hence the signal at T = 330–340 °C may be unequivocally attributed to the surface furoate species. The position of this signal agrees well with the observed unknown signal in the DTG curves obtained for spent catalysts after their treatment with aqueous furfural mixture (Fig. 3). Consequently, it can be concluded that furoate species are indeed present in the spent rehydrated HTC after Cannizzaro reaction.

Additionally, the observed increase in the signal intensity at T = 330–340 °C is in line with a gradual decrease in the intensity of signals at T = 200–210 °C and T = 390–410 °C. The signal at T = 200–210 °C characterizes interlayer water molecules which are

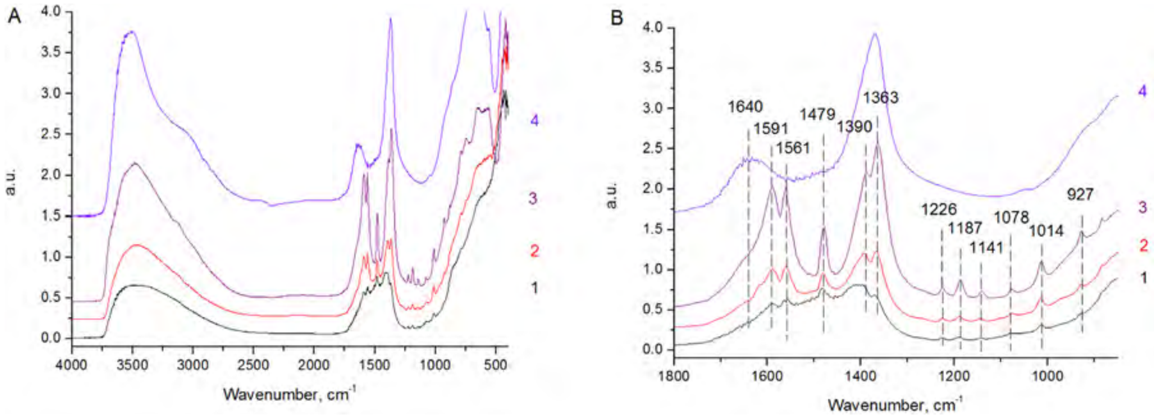

Fig. 4. DRIFT spectra of calcined Mg-Al mixed oxide after its interaction with aqueous furfural mixture in the range of 400–4000 cm^{-1} (A) and 800–1800 cm^{-1} (B). 1–HTC-0; 2–HTC-6; 3–HTC-23; 4–reconstructed HTC rehydrated with pure water (reference material).

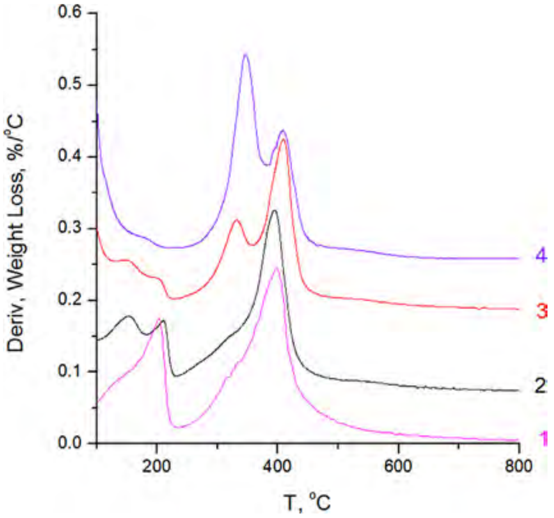

Fig. 5. DTG curves for rehydrated HTC treated with different amounts of Furoic acid. $m_{FOOH}/m_{calcinedsample}$ = 0 (1); 0.1 (2); 0.3 (3) and 0.5 (4).

stabilized in interlayer due to hydrogen bonding between them and interlayer compensating anions while the signal at 390–410 °C is characteristic for the removal of structural hydroxyls and compensating anions [12]. The interaction of furoic acid with basic sites and the generation of furoic species should in fact decrease the total amount of structural hydroxyls and compensating anions and thus result in weakened hydrogen bonding between the anions and water molecules. As a consequence, the amount of interlayer water would decrease as would the corresponding signal in DTG data, which is apparent in the experimental data (Fig. 5).

Fig. 6 depicts total DRIFT spectra for rehydrated HTC samples treated with furoic acid in the range of 500–4000 cm^{-1} (A) and in the specific range of 800–1800 cm^{-1} (B). The intensity of a shoulder signal at 2700–3200 cm^{-1} assigned to hydrogen bonding between water molecules and the interlayer anions decreases in intensity with the increase in acid content from 0 to 0.5 g_{acid}/g_{cat}. (Fig. 6A). The behavior of this band correlates well with the decrease in the intensity of the DTG signal in the range of T = 100–200 °C and proves the loss of water (including interlayer water) in the samples as a consequence of the formed furoate species. A large difference in the DRIFT spectra between the untreated rehydrated HTC and the samples treated with furoic acid (Fig. 6) is observed in the range of 1300–1700 cm^{-1}. The peak at 1640 cm^{-1} attributed to the presence of interlayer water has very low intensity in the spectra of F-OOH-treated rehydrated samples suggesting low water content in the interlayer. Instead, two peaks appear in this range at 1594 and 1563 cm^{-1} (Fig. 6B). A peak at 1365 cm^{-1} which is usually attributed to carbonate cations [12] or, as supposed in the present study, to compensating OH^{-}-groups decreases in intensity with the increase in acid content in the mixture while a new band at 1390 cm^{-1} has appeared. Finally, a very distinctive band at 1481 cm^{-1} is observed in the samples, and its intensity correlates well with the amount of acid in the treatment solution. In summary, the observed changes and the appearance of new bands in the DRIFT spectra of HTC samples treated with F-OOH can be unequivocally attributed to the surface furoate species formed by adsorption of furoic acid on the basic sites. The formation of furoate species in the treated materials could be also related with the appearance of new small bands in DRIFT spectra in the range of 900–1250 cm^{-1}. In total, the similarity in the positions of the bands observed in DRIFT spectra of samples either treated with furoic acid or those obtained after reaction with aqueous furfural mixture (Figs. 4 and 6B) allows concluding that the formed surface species on the catalysts are indeed furoates.

3.5. *Reconstructed HTC as a catalyst for Cannizzaro reaction*

Catalytic results presented above indicate that the increased catalyst activity in CR is observed when reconstructed HTC is formed as a result of complete rehydration of the Mg-Al mixed oxide. This reconstruction is achieved provided large water amount is present in the reaction mixture. On the other hand, the catalytic results indicate that water could have a negative effect on the reaction resulting in a decrease in furfural conversion (Fig. 1). Using a reconstructed HTC prepared by a pre-treatment of mixed oxide with liquid water allows avoiding large water content in the reaction mixture. In addition, these experiments reveal more accurately the effect of water on the course of Cannizzaro reaction, i.e. it allows decoupling the influence of water on catalyst reconstruction (and its activity) from its influence on the reaction.

In these sets of experiments 2 g of freshly calcined HTC was used in rehydration procedure as described in the *Experimental* to prepare reconstructed HTC sample as a catalyst for the reaction. It allows making an accurate comparison between the catalytic activity of mixed oxide and reconstructed samples based on their calcined form. Fig. 7 depicts F-OH yield obtained during the interaction of reconstructed HTC with aqueous furfural mixture. The catalyst possesses poor activity in the conversion of water-free furfural evidencing the necessity of water for the Cannizzaro reaction to take place. In this experiment F-OH yield of ~0.1 wt.% could be attributed to the residual water in the dried reconstructed HTC catalyst. Addition of water to furfural promotes

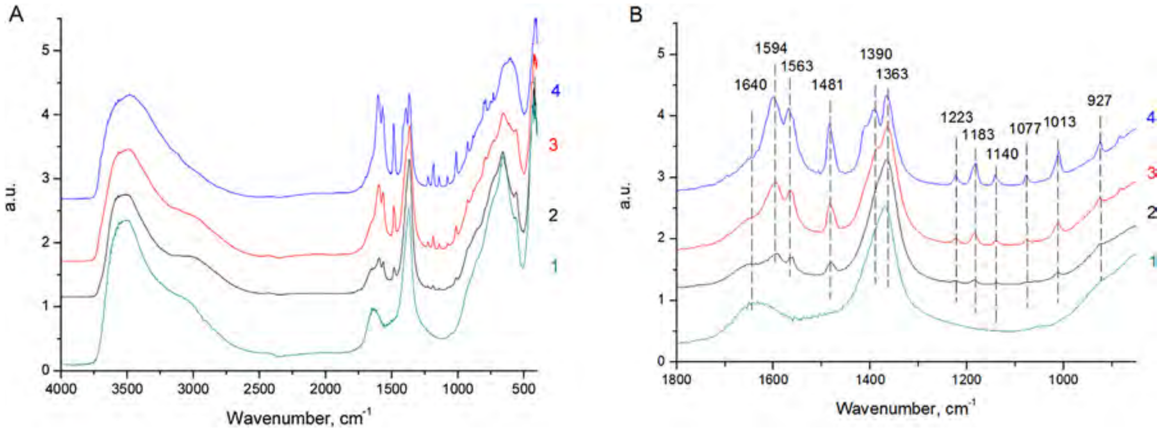

Fig. 6. DRIFT spectra of rehydrated HTC treated with different amounts of Furoic acid. m_{FOOH}/m_{sample} = 0 (1); 0.1 (2); 0.3 (3); 0.5 (4). A – the range of 400–4000 cm^{-1}, B – the range of 800–1800 cm^{-1}.

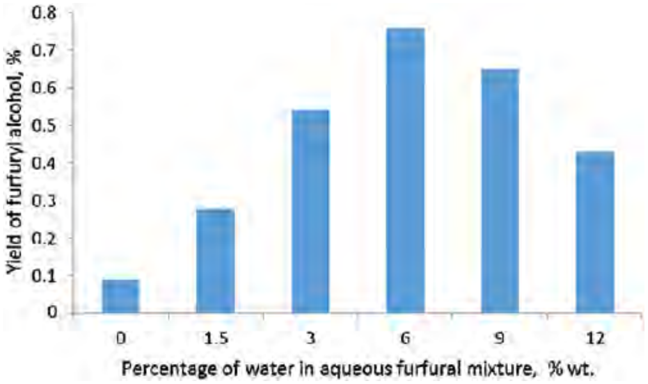

Fig. 7. The yield of furfuryl alcohol in experiments with aqueous furfural solution having different water content using dried reconstructed HTC as catalyst. Treac. = 50 °C, t = 3 h, $m_{cat.}$ = 2 g (calcined base), m_F = 30 g.

the activity of the reconstructed HTC: alcohol yield increases from 0.28 wt.% to 0.76 wt.% as the water content in aqueous furfural mixture grows from 1.5% to 6%, respectively. Nevertheless, further increase in water content in the mixture does not result in a corresponding growth in the furfuryl alcohol yield (Fig. 7). It is worth noting that the maximum F-OH yield observed in experiments with the reconstructed HTC (Fig. 7) is significantly lower than that for Mg-Al mixed oxide (calcined HTC) treated with aqueous reaction mixture (Fig. 1). The observed difference in catalytic behavior suggests that the number of basic sites which are accessible to furfural molecules in the catalyst rehydrated with pure water is lower compared with the catalyst rehydrated *in situ* with biphasic aqueous-organic mixture. Indeed, calculations show that the maximum alcohol yield of 0.76 wt.% produced on reconstructed HTC corresponds to 1.19 mmol of alcohol per 1 g of the catalyst (calcined base). Consequently, 1.19 mmol/g of furoic acid produced by CR is bound with 1.19 mmol/g of basic sites in the catalyst, which is 24.3 wt.% with respect to the bulk Al content. This concentration of basic sites titrated with the acid is much lower than that evaluated from the results of catalytic experiments with Mg-Al mixed oxide. Moreover, it is also slightly lower than that determined by CO_2-TPD (1.57 mmol/g, calcined base, Table 1). On the other hand, the concentration of basic sites evaluated in rehydrated HTC by means of Cannizzaro reaction agrees well with the results from [12] that 24.5% of the OH^- sites with respect to the bulk Al content in HTC rehydrated in liquid water are evaluated by CO_2-TPD. In summary, the obtained catalytic results make us suggest that the concentration of basic sites in the reconstructed HTC depends on the properties of a liquid medium used for rehydration of Mg-Al mixed oxide, i.e. calcined HTC. Nonetheless, further fundamental studies are necessary to understand the relationship between the basic sites formation and the properties of the media used.

3.6. *The impact of CR on aldol condensation of furfural and acetone*

Aldol condensation (AC) of furfural and acetone takes place in the presence of basic catalysts, for example activated HTC. In general, any of the two components of the reaction mixture interacts with the active centers of the catalyst. Basic sites promote the activation of acetone which is necessary for AC to take place [20,21], while furfural is also transformed by CR, as shown in the present study. Both reactions, AC and CR, proceed simultaneously and share the same active centers; therefore, the deactivation of basic sites with furoic acid formed by CR should influence the conversion of reactants by AC. The following model experiments represent examples aimed to demonstrate the degree of this influence. Three series of catalytic runs with Mg-Al mixed oxide were carried out:

Example I. Mg-Al mixed oxide is added at once to prepared F + Ac mixture (a reference run).

Example II. Mg-Al mixed oxide is initially stirred in acetone for 0–90 min and then furfural is added.

Example III. Mg-Al mixed oxide is initially stirred in furfural for 0–90 min and then acetone is added.

The results of these experiments are presented in Fig. 8. In the reference run (Fig. 8A, Example I) furfural conversion is 20.7% after 3 h of the reaction. Along with compounds formed by aldol condensation, the formation of furfuryl alcohol with the yield of 0.06 wt.% after 3 h is observed. Its presence among other products evidences the simultaneous occurrence of AC and CR, i.e. the formation of furoic acid. As shown above, furoic acid interacts with the basic sites of the catalyst resulting in the formation of surface furoate species. As a consequence, the amount of active sites which are able to participate in both reactions is reduced thus leading to a loss of activity.

The initial stirring of catalyst in acetone for 0, 30, 60 and 90 min, respectively, (Example II) does not introduce any significant effect on its performance in either AC or CR reaction routes. Regardless of the duration of the initial step, the conversion of furfural after 3 h of its addition to the acetone + catalyst mixture is in the range of 18.6-21% while the yield of F-OH is 0.05-0.06 wt.%. These experiments (Example II) evidence that the contact between acetone and catalyst does not contribute to any change in the catalytic activ-

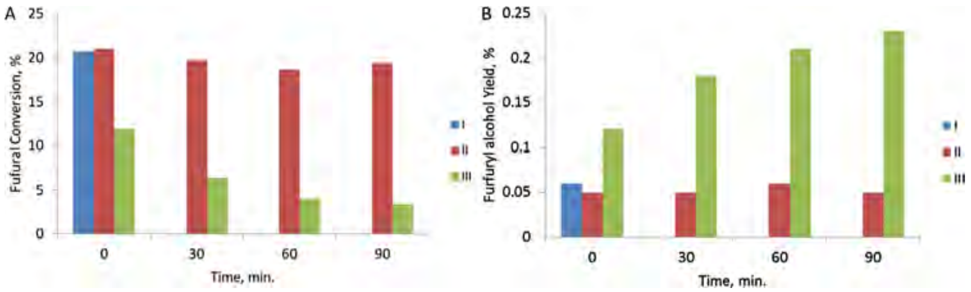

Fig. 8. Furfural conversion (A) and the yield of F-OH (B) observed after 3 h of the aldol condensation of furfural and acetone over Mg-Al mixed oxide. I – Catalyst is added to the mixture of acetone and furfural (Reference run); II – Catalyst is stirred in acetone for 0, 30, 60, 90 min followed by furfural addition; III – Catalyst is stirred in furfural for 0, 30, 60, 90 min followed by acetone addition. Reaction conditions: $m_{cat.}$ = 0.5 g, F:Ac = 6.5/19.7 g/g (1/5 mol/mol), $T_{reac.}$ = 50 °C.

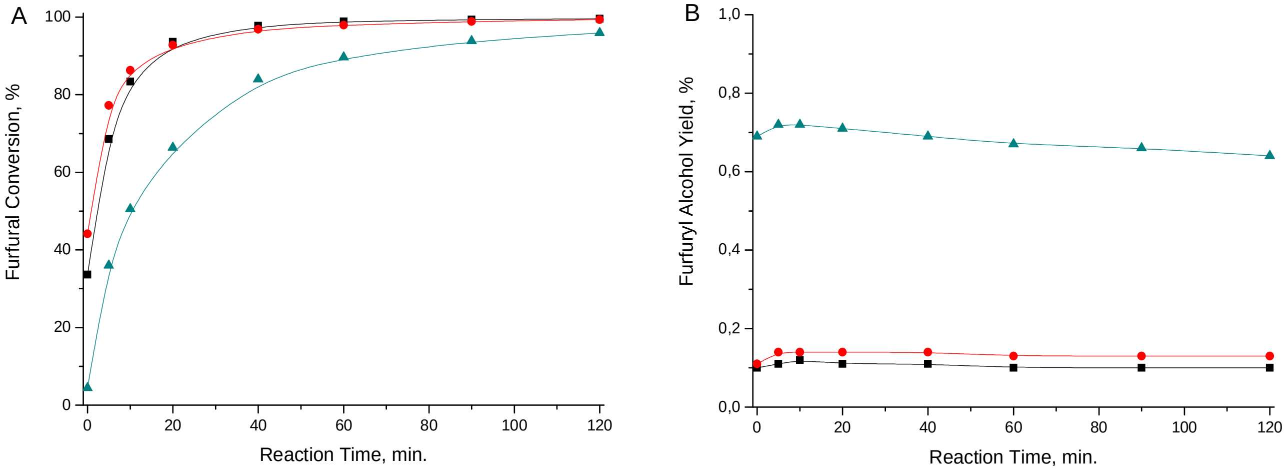

Fig. 9. Furfural conversion (A) and the yield of F-OH (B) observed during the aldol condensation of furfural and acetone over reconstructed HTC. I – Catalyst is added to the mixture of acetone and furfural (Squares); II – Catalyst is stirred in acetone for 30 min followed by furfural addition (Circles); III – Catalyst is stirred in furfural for 30 min followed by acetone addition (Triangles). Reaction conditions: $m_{cat.}$ = 0.5 g (calcined base), F:Ac = 6.5/19.7/ g/g (1/5 mol/mol), $T_{reac.}$ = 25 °C. Prior to catalyst addition the reaction mixtures (I–III) are mixed with 0.4 g of water to promote CR.

ity in AC, so the behavior of the catalyst is comparable with that observed in the reference run (Example I).

In contrast, the initial stirring of catalyst in furfural (Example III) leads to unique results (Fig. 8A). Even a brief contact between furfural and catalyst decreases the activity of the catalyst in aldol condensation which is evidenced by furfural conversion of 11.9% after 3 h of the reaction (Fig. 6A). When increasing the time of the initial stirring of the catalyst in furfural up to 90 min, a further decrease in furfural conversion in aldol condensation down to 3.4% is observed. Simultaneously with the decline in the overall activity of the catalyst, the increase in the yield of furfuryl alcohol from 0.12 to 0.23 wt.% is observed as the duration of the first stage of the experiment increases from 0 to 90 min, respectively (Fig. 8B). As postulated above, the presence of F-OH indicates that F-OOH is formed because these two compounds are related with each other by the stoichiometry of Cannizzaro reaction. Being produced by Cannizzaro reaction, F-OOH generates surface furoate species by reacting with the basic sites and, consequently, the basic sites become catalytically inactive. It could be also assumed that the organic salts being formed on the catalyst surface would result in selective leaching of the corresponding catalyst components. To evaluate the plausible leaching, we have analyzed the reaction mixture after catalytic experiment (Example III) by ICP. However, we did not detect any traces of Mg or Al in the solution after reaction. It allows concluding that the catalyst is chemically stable and the organic salts, if formed, stay bound on the catalyst surface. Therefore, the decrease in furfural conversion observed in these experiments (Example III), can be explained by the gradual poisoning of the catalyst with products formed by CR.

Similar experiments investigating the influence of mixing order of reactants during aldol condensation on furfural conversion were performed with reconstructed HTC (Fig. 9). As expected, the activity of the reconstructed HTC in the reaction was higher in comparison with Mg-Al mixed oxide, so to observe any differences in conversion the catalytic experiments were carried out at T = 25 °C

In agreement with the results obtained for Mg-Al mixed oxide, furfural conversion is similar when the rehydrated catalyst is either added to the mixture of acetone and furfural (Example I) or stirred in acetone for 30 min followed by furfural addition (Example II) (Fig. 9A). In contrast, the activity of the reconstructed HTC in aldol condensation is significantly lower when the rehydrated catalyst is initially in contact with furfural (Example III). In all three cases F-OH is detected among reaction products proving the occurrence of CR, as discussed above. Nevertheless, its yield is much lower in Examples I and II being 0.10–0.14 wt.% in comparison with Example III (0.64–0.72 wt.%). These experiments give an additional evidence that CR proceeds simultaneously with AC and definitely influences the performance of a basic catalyst in the latter reaction.

CR may contribute not only to the observed activity of basic catalysts in aldol condensation reaction involving furfural but may also affect re-using of the catalysts. The loss of the activity of hydrotalcites and mixed oxides in several successive catalytic runs of condensation reactions has been reported repeatedly. In general, two different deactivation causes have been considered: fouling caused by subsequent aldol condensations and leaching of active compounds from the catalyst in the aqueous medium [20]. The results presented in this study evidence that other reasons could explain the loss of catalyst activity in condensation reactions, for example, the occurrence of Cannizzaro reaction. Under the real experimental conditions of AC, a catalyst is in contact with both components of the reaction mixture (acetone and furfural) and the reaction is usually carried out in excess of acetone. Therefore, the probability of furfural interacting with basic sites that is necessary for CR to take place is low under high Ac to F molar ratio in reaction mixture. As a consequence, the influence of CR on catalyst performance in AC is not pronounced and conventional solid basic catalysts exhibit good activity in AC. Nevertheless, it is not possible to avoid a contact between furfural and basic sites, so the AC and CR take place simultaneously, as evidenced by the formation of furfuryl alcohol even at conventional reaction conditions (Figs. 8 and 9B, Example I). Even the small contribution of CR would result in the progressive deactivation of the catalyst thus decreasing its activity in AC and making it difficult to recycle/reuse the catalyst without an oxidative regeneration step. Therefore, the optimization of catalytic properties and the determination of optimum reaction conditions to perform AC which would allow reducing the influence of CR on catalyst behavior are important objectives of forthcoming studies.

4. Conclusions

The rehydration of Mg-Al mixed oxide (calcined as-prepared hydrotalcite) using pure water results in the formation of reconstructed hydrotalcite that possesses OH^- groups rather than carbonates in interlayer as proved by TGA-MS results. The comparison of DRIFT spectra of the as-prepared and the reconstructed materials allowed concluding that these newly formed hydroxyls are characterized by the band at $1370\,cm^{-1}$ which is usually considered as a characteristic band of carbonate groups. The results also show that Mg-Al mixed oxide can be successively rehydrated with aqueous furfural mixture resulting in the formation of reconstructed hydrotalcite structure. The amount of water in the mixture influences the rehydration degree and the total reconstruction of the hydrotalcite structure is observed only when using biphasic (water-organic) reaction conditions. The catalytic data allow concluding unequivocally that Brønsted basic sites of the reconstructed HTC catalyze furfural transformation by Cannizzaro reaction. Both furfuryl alcohol and furfuryl furoate formed during the reaction are evidenced by GC analysis. On the contrary, furoic acid is not detected among reaction products by routine GC analysis because it remains adsorbed on the basic sites of the catalyst forming surface furoates. These species can be detected by both TGA (a peak in the range of $T = 320\,^{\circ}C$) and DRIFT (characteristic band at $1481\,cm^{-1}$) methods. The formation of the surface furoates leads to a gradual catalyst deactivation, as evidenced by the time dependency of furfural conversion and yield of furfuryl alcohol.

The rehydration of Mg-Al mixed oxide (calcined HTC) with aqueous furfural mixture affords a reconstructed HTC possessing a higher amount of basic sites in comparison with a reconstructed HTC prepared by rehydration of the same Mg-Al mixed oxide with pure water. This is demonstrated by the yield of reaction products formed by CR. It can thus be inferred that the rehydration procedure has a significant influence on the basic properties of the resulting reconstructed material.

The performed comparative experiments show that the Cannizzaro reaction also influences aldol condensation of furfural and acetone. The longer is the contact time between furfural molecules and the basic sites of a catalyst, the lower is the furfural conversion in aldol condensation. Consequently, Cannizzaro reaction would result in the gradual deactivation of the catalyst thus making it difficult to recycle/reuse the catalyst without an oxidative regeneration step.

Acknowledgements

The publication is a result of the project reg. No. GA15-21817S which was financially supported by the Czech Science Foundation of the Czech Republic. The project has been integrated into the National Program for Sustainability of the Ministry of Education, Youth and Sports of the Czech Republic through the project Development of the UniCRE Centre, project code LO1606.

Appendix A. Supplementary data

Supplementary data associated with this article can be found, in the online version, at http://dx.doi.org/10.1016/j.apcata.2016.08.007.

References

[1] J.I. Di Cosimo, V.K. Díez, M. Xu, E. Iglesia, C.R. Apesteguía, J. Catal. 178 (1998) 499–510.
[2] R.K. Allada, A. Navrotsky, H.T. Berbeco, W.H. Casey, Science 296 (2002) 721–723.
[3] A. Corma, S. Iborra, Adv. Catal. 49 (2006) 239–302.
[4] X. Duan, D.G. Evans (Eds.), Layered Double Hydroxides, Structure and Bonding Series, vol. 119, Springer, Berlin, 2006.
[5] D. Tichit, D. Lutic, B. Coq, R. Durand, R. Teissier, J. Catal. 219 (2003) 167–175.
[6] H. Liu, W. Xu, X. Liu, Y. Guo, Y. Guo, G. Lu, Y. Wang, Kinet. Catal. 51 (2010) 75–80.
[7] D.P. Debecker, E.M. Gaigneaux, G. Busca, Chem. Eur. J. 15 (2009) 3920–3935.
[8] A. Corma, S. Iborra, S. Miquel, J. Primo, J. Catal. 173 (1998) 315–321.
[9] Y. Xi, R.J. Davis, J. Catal. 254 (2008) 190–197.
[10] V.K. Diez, C.R. Apesteguia, J.I. Di Cosimo, J. Catal. 215 (2003) 220–233.
[11] D. Tichit, B. Coq, Cattech 7 (2003) 206–217.
[12] S. Abelló, F. Medina, D. Tichit, J. Pérez-Ramírez, J.C. Groen, J.E. Sueiras, P. Salagre, Y. Cesteros, Chem. Eur. J. 11 (2005) 728–739.
[13] D. Tichit, M.N. Bennani, F. Figueras, R. Tessier, J. Kervennal, Appl. Clay Sci. 13 (1998) 401–415.
[14] C. Xu, Y. Gao, X. Liu, R. Xin, Z. Wang, RSC Adv. 3 (2013) 793–801.
[15] K.K. Rao, M. Gravelle, J. Sánchez-Valente, F. Figueras, J. Catal. 173 (1998) 115–121.
[16] B.M. Choudary, M.L. Kantam, C.R.V. Reddy, K.K. Rao, F. Figueras, J. Mol. Catal. A: Chem. 146 (1999) 279–284.
[17] S. Gámez, J.J. González-Cabriales, J.A. Ramírez, G. Garrote, M. Vázquez, J. Food Eng. 74 (2006) 78–88.
[18] T.N. Pham, D. Shi, D.E. Resasco, Appl. Catal. B 145 (2014) 10–23.
[19] C.J. Barrett, J.N. Chheda, G.W. Huber, J.A. Dumesic, Appl. Catal. B: Environ. 66 (2006) 111–118.
[20] L. Faba, E. Díaz, S. Ordóñez, Appl. Catal. B: Environ. 113–114 (2012) 201–211.
[21] S. Abelló, F. Medina, D. Tichit, J. Pérez-Ramírez, J.E. Sueiras, P. Salagre, Y. Cesteros, Appl. Catal. B: Environ. 70 (2007) 577–584.
[22] S. Cannizzaro, Ann. Chem. Pharm. 88 (1853) 129–130.
[23] I. Sádaba, M. Ojeda, R. Mariscal, J.L.G. Fierro, M. López Granados, Appl. Catal. B: Environ. 101 (2011) 638–648.
[24] P.A. Zapata, J. Faria, M. Pilar Ruiz, D.E. Resasco, Top. Catal. 55 (2012) 38–52.
[25] L. Hora, V. Kelbichová, O. Kikhtyanin, O. Bortnovskiy, D. Kubička, Catal. Today 223 (2014) 138–147.
[26] W.V. Evans, M.B. Aylesworth, Ind. Eng. Chem. 18 (1926) 24–27.
[27] A. Morato, C. Alonso, F. Medina, Y. Cesteros, P. Salagre, J.E. Sueiras, D. Tichit, B. Coq, Appl. Catal. B: Environ. 32 (2001) 167–179.
[28] F. Prinetto, G. Ghiotti, P. Graffin, D. Tichit, Microporous Mesoporous Mater. 39 (2000) 229–247.
[29] J.T. Kloprogge, R.L. Frost, Phys. Chem. Chem. Phys. 1 (1999) 1641–1647.
[30] F. Prinetto, G. Ghiotti, R. Durand, D. Tichit, J. Phys. Chem. B 104 (2000) 11117–11126.
[31] F. Millange, R.I. Walton, D. O'Hare, J. Mater. Chem. 10 (2000) 1713–1720.
[32] S.K. Sharma, P.A. Parikh, R.V. Jasra, Appl. Catal. A: Gen. 386 (2010) 34–42.
[33] M.D. Ureña-Amate, N.D. Boutarbouch, M. del Mar Socias-Viciana, E. González-Pradas, Appl. Clay Sci. 52 (2011) 368–373.
[34] M.F. Beegum, L.U. Kumari, B. Harikumar, H.T. Varghese, C.Y. Panicker, J. Rasayan, Chemistry 1 (2008) 117–124.

Catalysis Communications 58 (2015) 89–92

Contents lists available at ScienceDirect

Catalysis Communications

journal homepage: www.elsevier.com/locate/catcom

Short Communication

Unprecedented selectivities in aldol condensation over Mg–Al hydrotalcite in a fixed bed reactor setup

Oleg Kikhtyanin, Lukáš Hora, David Kubička *

Research Institute of Inorganic Chemistry, UniCRE-RENTECH, Areál Chempark Záluží, 436 70 Litvínov, Czech Republic

ARTICLE INFO

Article history:
Received 23 May 2014
Received in revised form 15 August 2014
Accepted 1 September 2014
Available online 16 September 2014

Keywords:
Aldol condensation
Hydrotalcites
Furfural
Acetone

ABSTRACT

Aldol condensation of furfural with acetone (molar ratio 1:10) was carried out in a flow fixed bed setup at 50 °C using calcined hydrotalcite with Mg/Al of 3 as a catalyst. Complete conversion of furfural and stable catalyst performance was obtained during the initial 50 h on stream. This period was followed by a rapid catalyst deactivation. In contrast to previous reports, higher molecular weight products that were identified as products of successive aldol condensation of acetone with furfural were observed. Their concentration was time-dependent with a maximum formation after 10 to 30 h on stream.

1. Introduction

Biomass-derived short-chain aldehydes and ketones originating from pyrolysis of lignocellulosic biomass have rather limited direct applicability. Aldol condensation has been proposed to valorize these primary products by combining them into more complex reaction products with higher molecular weight. The reaction between furfural and acetone, which are suitable model compounds, results in the formation of ketones with 8 or 13 carbon atoms [1] (Scheme 1). Moreover, acetone molecule can interact not only with aldehydes (e.g. furfural) but also with ketones, hence also with another acetone molecule. This acetone self-condensation produces compounds with 6 or 9 carbon atoms [2]. Both acetone self-condensation and aldol condensation of furfural and acetone can be competitive reactions and proceed over the same catalyst at the same reaction conditions [1]. Industrially, homogenous base catalysts, such as sodium and calcium hydroxide, are used for aldol condensation. However, due to ecological and economic considerations the introduction of heterogeneous basic catalysts becomes very relevant [3]. Among these catalysts, layered double oxides, for example hydrotalcites (HTC), seem to be the most promising [4]. Calcined Mg–Al hydrotalcites possess high activity in the aldol condensation of furfural and acetone even at reaction temperatures below 100 °C [1]. Aldol condensation over heterogeneous basic catalysts, similar to a homogeneous process, is usually investigated in a batch reactor (a glass reactor or an autoclave) equipped with a stirring system. Nevertheless, to our best knowledge no information has been provided to date on the behavior of HTC as a catalyst for the aldol condensation between furfural and acetone in flow reaction systems which are more favorable from a practical point of view. Moreover, only the application of a flow reactor system makes it possible to investigate the long-term stability (durability) of HTC materials in aldol condensation, which is essential for evaluating their prospects in industrial applications. In the present work we have studied aldol condensation of furfural and acetone using a flow reactor system with a fixed bed of a catalyst, a Mg–Al hydrotalcite with a molar ratio of Mg:Al = 3:1 calcined at 450 °C.

2. Experimental

Mg–Al layered double HTC with a Mg:Al molar ratio of 3:1 was prepared according to a procedure described in [1]. The crystallographic structure of the dried HTC catalyst was determined by X-ray powder diffraction using a Philips MPD 1880 instrument. Aldol condensation of furfural and acetone was carried out in a fixed-bed continuous-flow reactor with a catalyst loading of 10 g. The catalyst with a particle size of 0.125–0.150 mm was placed in the isothermal zone of the reactor, activated at 450 °C for 16 h under nitrogen flow, and then cooled down to 50 °C. The liquid feed, consisting of furfural (Acros Organics, 99%) and acetone (Lach:Ner, p.a.) in the molar ratio of 1:10 was fed into the reactor by a micro-metering pump at weight hourly space velocity (WHSV) of the total reaction feed equal to 2 h^{-1}. The reaction conditions were $T = 50$ °C and $P = 0.5$ MPa. During the experiment, liquid reaction products were withdrawn from a cooler-condenser ($T = 0$ °C) every 2 h, weighed and analyzed by an Agilent 7890A GC equipped with a flame ionization detector and an HP-5 capillary column (30 m/0.32 mm ID/0.25 μm). The yield of liquid products during the experiment was 98% which can be explained by losses due to acetone evaporation. Finally, the carbon balance in GC analyses was calculated

---

* Corresponding author. Tel.: +420 476163735; fax: +420 475 212 079.
E-mail address: david.kubicka@vuanch.cz (D. Kubička).

http://dx.doi.org/10.1016/j.catcom.2014.09.002
1566-7367/© 2014 Elsevier B.V. All rights reserved.

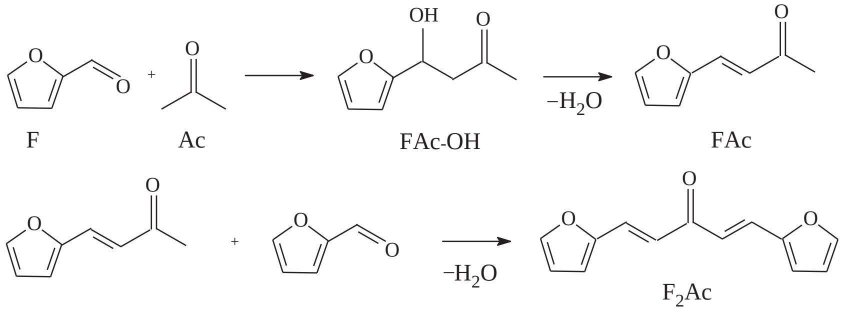

Scheme 1. Reaction pathways of aldol condensation of furfural and acetone showing only the main products.

as the number of carbon atoms analyzed in each GC sample (C3, C5, C8, C13, etc.) divided by the number of carbon atoms (C3 and C5) in the feedstock.

3. Results and discussion

In accordance with the generally accepted reaction route, aldol condensation of furfural and acetone over basic catalysts results in the successive formation of the following reaction products: FAc-OH, FAc and F_2Ac (Scheme 1). GC analyses of mixtures obtained under flow reaction conditions revealed, however, the presence of additional reaction products. Their combined selectivity was as high as 35%. Using GC-MS analysis the following molecular weights (MWs) of the unknown products were established: 176, 218, 254, 272, 312 and 350. By combining the MWs of acetone and furfural while taking into account that furfural and acetone can interact not only with each other, but also with the products of acetone self-condensation and the main aldol condensation products, i.e. FAc-OH, FAc and F_2Ac, it was possible to identify plausible until now unknown reaction products. The classical products of the aldol condensation of furfural and acetone (FAc-OH, FAc and F_2Ac) can participate in the successive condensation reactions either with furfural or with acetone owing to the presence of α-H atoms in their structure. Based on the GC-MS results, the formation of the following products can be deduced: FAc_2 (MW 176), FAc_3 (MW 218), F_2Ac_2-OH (MW 272), F_2Ac_2 (MW 254), F_2Ac_3 (MW 312) and F_3Ac_2 (MW350). Moreover, the involvement of acetone self-condensation products in aldol condensation with furfural is probable as well as these by-products were found in the reaction products too. The reaction between furfural and Ac_2 or Ac_3 would yield FAc_2 (MW 176) and FAc_3 (MW 218), respectively. The verification of both the exact molecular structure of these products and the proposed reaction pathways leading to their formation is an objective of our forthcoming study. There is no doubt, however, that aldol condensation of acetone and furfural is more complex than the reaction route presented in Scheme 1, resulting in a large number of products having high molecular weight that have not yet been reported and that could be attractive as automotive fuel components or their precursors. A tentative simplified reaction network leading to the formation of these products is depicted in Scheme 2. As it will be shown further, these products might affect the long-term stability of the catalytic activity of HTC catalysts.

Fig. 1 shows that complete furfural conversion was obtained during the initial 45 h of TOS (Fig. 1(A)). The observed high activity of the HTC sample during a long period proves that aldol condensation can be successfully carried out using a flow reactor with a fixed catalyst bed. Nevertheless, after TOS = 45 h furfural conversion has rapidly decreased and reached ca. 50% after 64 h. This indicates a rapid HTC catalyst deactivation. Fig. 1 also shows changes in selectivity to the reaction products with the increasing TOS. These changes reflect the alteration of the catalyst performance with TOS. At the very beginning, the composition of reaction products is limited to two compounds, FAc and F_2Ac (Fig. 1), which is in accordance with the commonly accepted reaction scheme. The primary reaction product, FAc-OH, is completely absent during the initial 45 h of TOS indicating good dehydrating properties of fresh HTC catalyst. FAc is the main reaction product of aldol condensation of furfural and acetone, and selectivity to this compound exhibits an intricate dependence on TOS. At the beginning of the experiment the selectivity to FAc is 62–63%; it decreases to 54% at TOS = 20 h but reaches a maximum value of 73–74% at TOS = 42–44 h, i.e. at the very end of the range of total furfural conversion. Further, as the conversion of furfural rapidly drops, FAc selectivity tends to decrease to 66–67%. Fig. 1(A) shows that this decrease is accompanied by an increase in selectivity to primary reaction product, FAc-OH, proving a weakening of the dehydrating properties of the catalyst and, accordingly, a reduction of its total activity. A consecutive interaction of FAc with furfural results in F_2Ac formation. Fig. 1(A) shows that the selectivity to this product is equal to 33% at the start of experiment, but decreases to 5.6% after 20 h of TOS. As TOS further grows, the selectivity to F_2Ac also increases followed by a stabilization at 16–18%.

The peculiar selectivity dependence can be attributed to the formation of heavier condensation products. Fig. 1(B) shows that the group of heavier condensation products, i.e. F_2Ac_2-OH, F_2Ac_2, F_2Ac_3 and F_3Ac_2, is almost absent in the reaction mixture at low TOS. Their selectivity increases with the increasing TOS and reaches a maximum value at TOS = 10–30 h followed by a continuous decrease. Finally, these compounds totally disappear in reaction products at TOS > 60 h. Fig. 1 shows that the selectivities to FAc and F_2Ac, on the one hand, and to F_2Ac_2-OH, F_2Ac_2, F_2Ac_3 and F_3Ac_2, on the other hand, can be described as "inverse volcano" and "volcano" curves, respectively. Apparently, the increase in F_2Ac_2-OH, F_2Ac_2, F_2Ac_3 and F_3Ac_2 formation takes place at the expense of FAc and F_2Ac formation in the range of TOS = 10–30 h.

The observed variation in the composition of the reaction products during the experiment clearly has to reflect a change in the properties of the catalyst. At the initial phase (0–4 h), the pre-calcined HTC sample promotes the formation of FAc and F_2Ac in accordance with the commonly accepted reaction route of the aldol condensation of furfural

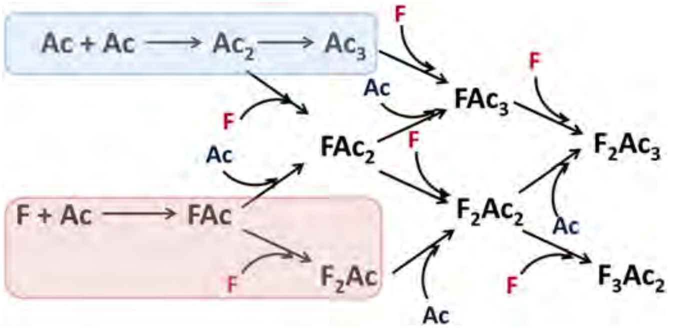

Scheme 2. Tentative reaction network leading to the formation of heavier condensation products of furfural (F) and acetone (Ac). The shaded areas correspond to acetone self-condensation (blue) and the main reactions of furfural and acetone condensation (pink). For the sake of clarity, only dehydrated products are shown.

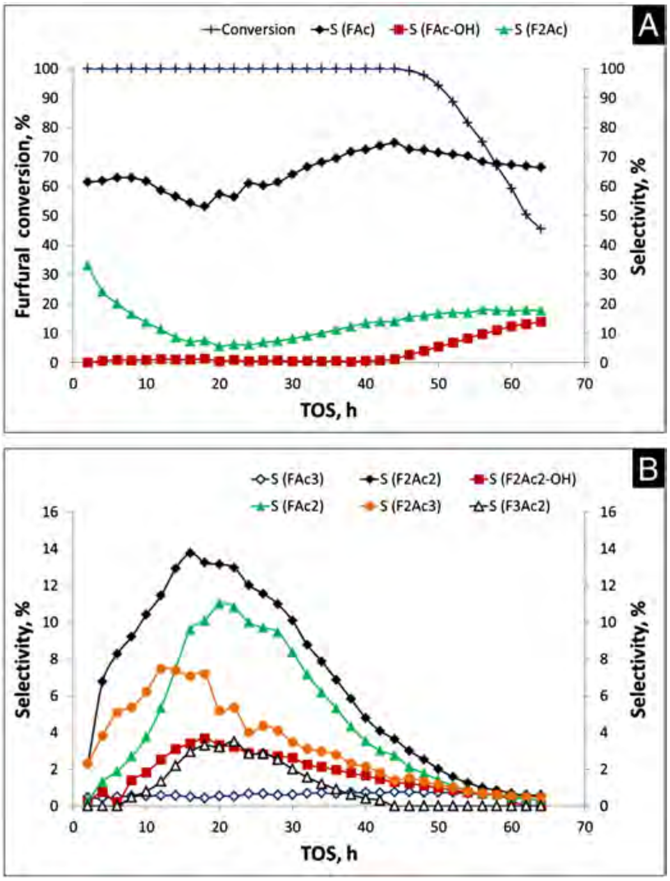

Fig. 1. A—Furfural conversion and selectivity to main reaction -FAc, FAc-OH and F_2Ac. B—Selectivity to heavier reaction products.

and acetone (Scheme 1). In the course of the reaction water is formed as one of the products of dehydration of a reaction intermediate, FAc-OH.

According to [5], calcined hydrotalcites can be reconstructed back to a layered structure if put in contact with water and appropriate anions. A comparison of the XRD patterns of as-synthesized HTC, the material calcined at 450 °C and the catalyst after long-term run (Fig. 2), proves that during the reaction the reconstruction of MgO phase which is characteristic of the calcined material to the layered HTC structure really takes place. Also, rehydration enhances the catalytic activity of reconstructed HTC materials in base-catalyzed reactions, including aldol condensation [1,6–8]. Thus, water formed due to FAc-OH dehydration could induce the reconstruction of HTC and cause a Lewis-to-Brønsted site transformation resulting from the reaction of O^{2-} basic sites with H_2O [9]. This process results in the enhancement of the catalytic activity of base-catalyzed reactions, for which OH^- sites act as active Brønsted base sites [4,6,8,10]. Our results show that these Brønsted basic sites in the reconstructed material have a pronounced ability to activate α-H atoms in ketones thus promoting an additional formation of bulky compounds and changing the product selectivity. However, these strong basic sites have been recently suggested to be responsible for catalyst deactivation in this kind of reactions [2]. The formation of bulkier compounds than F_3Ac_2 and F_2Ac_3 determined by GC may be also expected due to the further interaction of reaction products. These bulkier compounds would be less prone to desorption from the HTC surface resulting in the gradual deactivation of the catalyst as the one observed here, i.e. due to restricting/preventing the access of reactants to active sites. Nonetheless, further investigations of the formation of the heavier compounds and particularly of their interaction with the catalyst surface are needed.

Important supporting information for the conclusions presented above can be obtained from detailed analysis of acetone transformation. Acetone conversion and selectivity to the products of acetone self-condensation observed during the long-term run are shown in Fig. 3. The initial conversion of acetone is ≈15% with its slight increase to 17% after 12–14 h of the experiment. This increase in catalyst activity can be again explained by HTC reconstruction due to its re-hydration and the formation of Brønsted basic sites, which appear to have an increased ability to the abstract the α-proton in acetone molecule. Acetone conversion remains constant during the next ca. 30 h followed by its sharp decrease, which is in line with the trend observed for furfural conversion. Moreover, as the acetone conversion is stable for about 40–45 h at around 15–17% it can be unequivocally concluded that under the selected reaction conditions the HTC catalyst exhibits stable activity followed by a sharp deterioration of the catalyst performance. This conclusion is supported by the comparison of the reported thermodynamic equilibrium of acetone self-condensation to mesityl oxide, which is ca. 20% at 120 °C [11], and the conversion to mesityl oxide and diacetone alcohol reported here, which is about 5% (Fig. 3). As a result, it is concluded that the acetone conversion is not limited by the thermodynamical equilibrium.

Ac_2-OH is the main product of acetone self-condensation with a selectivity of 23–27%, and this compound gives Ac_2 upon dehydration (the remaining converted acetone yields condensation products with furfural described above). Fig. 3 depicts the complex behavior of Ac_2 selectivity during the experiment. At the beginning of the run Ac_2 selectivity exceeds 5%, followed by a sharp decrease to <1% at TOS = 8–10 h. This drop in selectivity may be explained by the increased affinity of the freshly calcined HTC catalyst to interaction with water resulting in the formation of the reconstructed HTC material as proved by XRD (Fig. 2). As a consequence, at the initial time the equilibrium

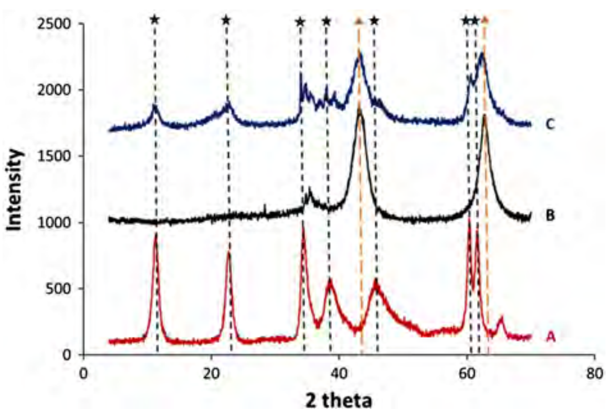

Fig. 2. XRD patterns of the initial as-synthesized hydrotalcite (A), calcined material (B) and catalyst after long-run test (C). ★—HTC phase, ▲—MgO phase.

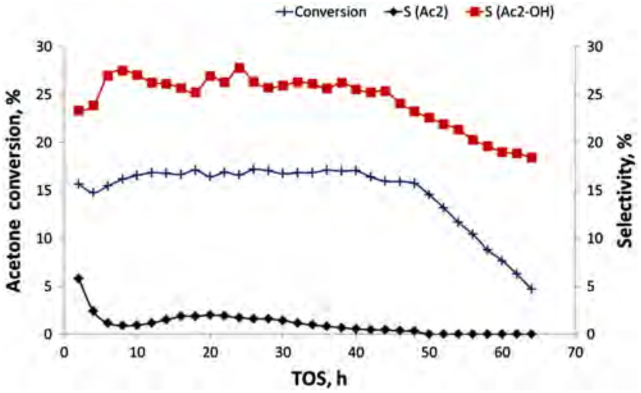

Fig. 3. Acetone conversion and selectivity to the reaction products of acetone self-condensation (the rest of selectivity is due to the formation of compounds of F + Ac interaction).

$Ac_2OH \leftrightarrow Ac_2 + H_2O$ is shifted to the right. As the process of HTC reconstruction is completed, the formed material does not react with water as easily thus resulting in the drop of Ac_2 selectivity.

However, with the further increase of TOS Ac_2 selectivity starts to increase and attains 2% at TOS = 20 h. The observed increase in the dehydration ability of the catalyst reflects the gradual changes in the properties of the active sites in reconstructed HTC, possibly, due to the increase of their strength. Obviously, a detailed investigation of the change of the properties of calcined hydrotalcite during the reaction under flow reaction conditions requires a separate study.

The results presented in Figs. 1 and 2 show that the behavior of Ac_2 selectivity and selectivities to bulky products of acetone/furfural aldol condensation observed at TOS = 10–50 h is very similar. It could be concluded that the formation of these compounds takes place on the strong sites which are responsible for both Ac_2-OH dehydration and α-proton activation in ketones. However, the same sites could be also responsible for the formation of non-desorbed reaction products which result in catalyst deactivation and the sharp decrease of its activity after 50 h of TOS.

4. Conclusions

It has been demonstrated for the first time that aldol condensation of furfural and acetone under flow conditions over calcined hydrotalcite catalyst results in the formation on a much wider variety of products than those typically reported for aldol condensation in a batch setup. While total furfural conversion could be obtained over the initial 40 h on stream, this period was followed by sharp decrease in activity due to rapid catalyst deactivation. The heavier products were identified as successive condensation products of acetone and furfural and they could be plausibly exploited as valuable diesel fuel components, particularly after deoxygenation.

Acknowledgments

This publication is a result of project no. P106/12/G015 supported by the Czech Science Foundation which is being carried out in the UniCRE center (CZ.1.05/2.1.00/03.0071) whose infrastructure was supported by the European Regional Development Fund and the state budget of the Czech Republic.

References

[1] L. Hora, V. Kelbichová, O. Kikhtyanin, O. Bortnovskiy, D. Kubička, Catal. Today 223 (2014) 138.

[2] L. Faba, E. Díaz, S. Ordóñez, Appl. Catal. B Environ. 142–143 (2013) 387.

[3] W. Shen, G.A. Tompsett, K.D. Hammond, R. Xing, F. Dogan, C.P. Grey, W.C. Conner Jr., S.M. Auerbacha, G.W. Huber, Appl. Catal. A Gen. 392 (2011) 57.

[4] D.P. Debecker, E.M. Gaigneaux, G. Busca, Chem. Eur. J. 15 (2009) 3920.

[5] D. Tichit, B. Coq, Cattech 7 (2003) 206.

[6] S. Abello, F. Medina, D. Tichit, J. Perez-Ramirez, X. Rodriguez, J.E. Sueiras, P. Salagre, Y. Cesteros, Appl. Catal. A 281 (2005) 191.

[7] S. Abello, F. Medina, D. Tichit, J. Perez-Ramirez, J.C. Groen, J.E. Sueiras, P. Salagre, Y. Cesteros, Chem. Eur. J. 11 (2005) 728.

[8] Y. Xi, R.J. Davis, J. Catal. 254 (2008) 190.

[9] Y. Liu, E. Lotero, J.G. Goodwin, X. Mo, Appl. Catal. A Gen. 331 (2007) 138.

[10] R.J. Chimentao, S. Abello, F. Medina, J. Llorca, J.E. Sueiras, Y. Cesteros, P. Salagre, J. Catal. 252 (2007) 249.

[11] A.A. Nikolopoulos, G.B. Howe, B.W.-L. Jang, R. Subremanian, J.J. Spivey, D.J. Olsen, T.J. Devon, R.D. Culp, Catalysis of organic reactions", in: M.E. Ford (Ed.), Marcel Dekker, Inc, NY, 2001, pp. 533–543.

Applied Catalysis A: General 525 (2016) 215–225

Contents lists available at ScienceDirect

Applied Catalysis A: General

journal homepage: www.elsevier.com/locate/apcata

The occurrence of Cannizzaro reaction over Mg-Al hydrotalcites

Oleg Kikhtyanin[a,*], Estera Lesnik[a], David Kubička[b]

[a] Unipetrol Centre of Research and Education, Block 2838, Záluží 1, 436 70 Litvínov, Czech Republic
[b] Technopark Kralupy VŠCHT Praha, University of Chemistry and Technology, Prague, Žižkova 7, 278 01 Kralupy nad Vltavou, Czech Republic

ARTICLE INFO

Article history:
Received 26 May 2016
Received in revised form 14 July 2016
Accepted 5 August 2016
Available online 5 August 2016

Keywords:
Basic catalysis
Cannizzaro reaction
Mg-Al hydrotalcite
Mixed oxide rehydration
Aldol condensation

ABSTRACT

Mg-Al mixed oxides and reconstructed hydrotalcites prepared from mixed oxides by rehydration attract much attention as solid basic catalysts for organic reactions, such as aldol condensation. Therefore, the understanding of parameters that govern their catalytic performance is of great importance. Cannizzaro reaction in the presence of mixed oxide and reconstructed HTC as basic catalysts was used as a model reaction to characterize both catalytic systems and to understand their behavior in aldol condensation. The performance of the samples was investigated in the conversion of aqueous furfural mixture using stirred batch reactor operating at $T = 50\,^{\circ}C$. The properties of both initial samples and catalysts after reaction were studied by different physico-chemical methods, such as XRD, DRIFT and TGA. It was shown that both mixed oxide and reconstructed HTC possessed poor activity in the conversion of dried furfural proving the importance of water presence for the reaction to take place. Addition of water to the reaction mixture resulted in growth of the yield of both furfuryl alcohol and furoyl furoate as reaction products. Furoic acid was not identified by GC analysis, but the interaction of the acid with the basic sites of catalysts was confirmed by DRIFT and TGA analyses indicating that at optimum reaction conditions, most of the basic sites were involved in the formation of furoate species. The formation of the surface furoate species influenced the behavior of the basic catalysts in aldol condensation of furfural and acetone. It allows concluding that the occurrence of Cannizzaro reaction should be taken into account when considering the behavior of basic catalysts in organic reactions with furfural as a reactant.

1. Introduction

In recent years hydrotalcites (HTCs) have found numerous applications as adsorbents or ion exchangers, catalyst precursors or supports, etc. [1–4]. These materials represent a class of hydrated double hydroxides with a general formula $[M^{2+}{}_{n}M^{3+}{}_{m}(OH)_{2(n+m)}]^{m+}\,(A^{x-})_{m/x}\cdot yH_2O$. The most commonly used Mg-Al HTCs consist of a brucite-like $[Mg(OH)_2]$ network wherein isomorphous substitution of Mg^{2+} ion by a trivalent Al^{3+} occurs and the excess positive charge of the framework is compensated by gallery anions which are located in the interlayer along with water molecules [4–6]. As-prepared HTCs typically contain carbonates as compensating anions which makes these materials inactive in base-catalyzed reactions [7]. Thermal treatment of Mg–Al HTCs results in decomposition of carbonate groups accompanied by the release of CO_2 and the formation of a well-dispersed mixture of magnesium and aluminum oxides (MgAlO). The calcined mixed oxides act as weak Lewis acid/strong base catalysts and find various applications as effective catalysts in transesterification [8,9], alcohol elimination [10] and condensation [11,12] reactions. A distinctive feature of MgAlO materials is their ability to reconstruct the lamellar HTC structure (so-called memory effect) when contacted with water vapor or liquid water in absence of carbon dioxide. This leads to meixnerite (magnesium aluminium hydroxide hydrate), that is HTC intercalated with OH^- as compensating anions in the interlayer [11,12]. In addition, the treatment of MgAlO with aqueous reaction mixture (*in situ* rehydration) leading to reconstructed HTCs is also known [12–14]. These rehydrated materials have been applied to a number of base-catalyzed reactions which require Brønsted basic character, including different self- and cross-condensations [12–15] Michael additions [16], etc.

Condensation reactions attract much attention because they allow obtaining more complex compounds with more carbon atoms starting from relatively simple molecules. The interest in these reactions stems from the fact that many of the initial molecules for the syntheses can be obtained by biomass processing. For example, furfural can be obtained by acid hydrolysis of sugar cane bagasse, a residue from sugar cane processing, followed by extraction [17]. The needed acetone may be obtained by ketonization of acetic acid [18] that is an important product

---

[*] Corresponding author.
E-mail address: oleg.kikhtyanin@unicre.cz (O. Kikhtyanin).

http://dx.doi.org/10.1016/j.apcata.2016.08.007
0926-860X/© 2016 Elsevier B.V. All rights reserved.

of biomass pyrolysis. Aldol condensation of these relatively simple molecules allows increasing chain length to 8+ carbon atoms. This route has attracted significant interest, because hydrogenation/hydrodeoxygenation of these aldol condensation products leads to various hydrocarbons suitable for blending in conventional diesel fuel and kerosene [19]. A comprehensive study of aldol condensation over solid catalysts is thus necessary for designing the pathway to components of motor fuels from renewable natural resources.

Aldol condensation of furfural (F) and acetone (Ac) in the presence of a basic catalyst begins with the initial abstraction of the α-proton from acetone, forming a carbanion that consecutively attacks the carbonyl group of the nearby adsorbed furfural molecule [20,21]. Additionally, acetone can be transformed on basic (or acidic as well) sites by its own reaction pathway which is acetone self-condensation resulting to the formation of diacetone alcohol, mesityl oxide, etc [11,13]. Both aldol condensation of furfural with acetone and acetone self-condensation can proceed simultaneously; in this case the rate-determining step should be shared by both reaction pathways and involve basic sites with similar strength [20].

Much less attention is paid to the transformation of furfural on basic sites of a solid catalyst in absence of acetone, or generally in absence of carbonyl compounds having no α-hydrogen atoms. Nevertheless, furfural can hardly be considered as an inert component when contacted with basic sites and a specific parallel reaction route has to be considered. Cannizzaro reaction (CR) is a well-known base-induced redox reaction of an aldehyde lacking a hydrogen atom in the alpha position. It represents the disproportionation of an aldehyde into a carboxylic acid and an alcohol catalyzed by a strong aqueous base, i.e. it takes two aldehydes to produce one acid and one alcohol. In case of furfural, two furfural molecules would produce furfuryl alcohol (F-OH) and furoic acid (F-OOH) according to the reaction scheme below (Scheme 1).

The mechanism of the CR is well postulated. The reaction begins with the attack of hydroxide from basic NaOH on the carbonyl carbon followed by deprotonation to give a dianion. This unstable intermediate releases a hydride anion which attacks another molecule of aldehyde. In this process the dianion converts to a carboxylate anion and the aldehyde to an alkoxide. The alkoxide then picks up a proton from water to provide the alcohol final product, while the caboxylate is converted to the carboxylic acid product after acid work-up [22]. It should be mentioned that in aqueous basic solution carboxylic acid produced by CR can hardly be detected in pure form as it immediately reacts with the base to form a corresponding salt.

Taking into account the scheme of furfural transformation by CR the occurrence of this reaction on a basic solid can also be assumed provided that the catalyst possesses hydroxides of sufficient strength as active sites and the reaction proceeds in aqueous medium. Indeed, this reaction was proposed among others when considering all possible reactions occurring during aqueous furfural aldol condensation with acetone using base solid catalysts [23]. Additionally, it was mentioned that MgO in aqueous media could catalyze the formation of the intermediate species for the Cannizzaro reaction (furfuryl alcohol and furoic acid) resulting in the formation of esterification product, 2-furancarboxylic 2-furanmethyl ester (furoyl furoate, FF) [24]. Nevertheless, there is no information available on the effect of CR on the physico-chemical properties of a solid basic catalyst as well as on its impact on the behavior of the catalyst in aldol condensation.

The scope of the present work is thus to understand the behavior of calcined Mg-Al mixed oxide as a catalyst for converting aqueous furfural mixture and to provide information on the extent of CR and its impact on the catalyst performance in aldol condensation.

2. Experimental

Mg–Al layered double hydrotalcite (HTC) with a Mg:Al molar ratio of 3:1 was prepared according to a procedure described in [25]. The Mg-Al mixed oxide was prepared by calcination of the dried as-prepared HTC at 450 °C for 3 h (heating rate 5 °C/min). The rehydration of the mixed oxide was performed by its stirring in water (2 g of freshly calcined material per 30 mL of water) at room temperature for 30 min, followed by the filtration of resulting solid with a vacuum pump and drying in a rotary evaporator in N_2 flow during 40 min. The calcined HTC is further on referred to as Mg-Al mixed oxide while the fully rehydrated mixed oxide is denoted as reconstructed HTC.

The crystallographic structures of the dried as-prepared HTC sample, Mg-Al mixed oxide and materials obtained during rehydration experiments were determined by X-ray powder diffraction using a Philips MPD 1880 instrument with Cu Kα irradiation ($\lambda = 0.154$ nm) in the 2θ range of 5°–70° at the 2θ scanning rate of 2.4°/min. The relative content of present crystalline phases in the solids was evaluated using the areas of diffraction peaks at $2\theta = 11.4$ and 22.8° for the HTC phase and at $2\theta = 43.1°$ for the MgO phase, wherein the relative content of the respective phases in as-synthesized HTC and Mg-Al mixed oxide were taken as 100%. The textural properties of the samples (specific surface area and pore volume) were measured by nitrogen physisorption at −196 °C using an Autosorb surface area and porosity analyzer. The basic properties of as-prepared HTC were evaluated by temperature programmed desorption (TPD) of carbon dioxide in a Micromeritics Autochem 2950 apparatus. Before reduction, the sample was outgassed under a He flow of 25 $cm^3\,min^{-1}$ with a heating ramp of 10 °C min^{-1} up to 500 °C. The sample was cooled down to 50 °C and saturated under a CO_2 flow (10 vol.% in He) of 50 $cm^3\,min^{-1}$ for 30 min. Subsequently, the physically adsorbed carbon dioxide was removed by flowing He (25 $cm^3\,min^{-1}$) at 50 °C for 60 min. Finally, the chemically absorbed CO_2 was desorbed by heating up the sample to 850 °C (heating rate of 15 °C min^{-1}) in flowing He (25 $cm^3\,min^{-1}$) and maintaining this temperature for 30 min. The amounts of desorbed species were quantified using calibration standards. Thermogravimetric analysis of the dried as-prepared HTC catalysts was performed using a TA Instruments TGA Discovery series equipment operating with a heating ramp of 10 °C/min from room temperature to 900 °C in N_2 flow. TGA-MS experiments were performed on the same TGA unit equipped with mass-spectrometer OmniStar GSD 320 (Pfeiffer-Vacuum) with MID (Multiple Ion Detection) measurement mode, SEM (Secondary Electron Multiplier) detector and quadrupole mass analyzer. The DRIFT spectra were recorded on a Nicolet IS 10 FTIR spectrometer equipped with DTGS detector and KBr beam splitter. All spectra were collected over the range of 4000–400 cm^{-1} at a spectral resolution of 4 cm^{-1} and number of scans 128 (both for the background and the sample spectra).

Furfural (Sigma-Aldrich) used for the study was pre-dried with a molecular sieve 3A to exclude the influence of moisture originating from the chemicals. All catalytic experiments on furfural conversion using either water-free conditions or aqueous furfural mixture were carried out in a 100 mL stirred batch reactor (a glass flask reactor) operating at T = 50 °C. Furfural conversion as a function of reaction time was studied in experiments using 2 g of freshly calcined HTC (or rehydrated HTC prepared from the same amount of Mg-Al mixed oxide) and 30 g of furfural. To prepare aqueous furfural mixtures, different amount of water (ranging from 0 to 33%wt.) was added to furfural. As the solubility of water and F in each other is limited [26], aqueous furfural mixtures with water content ≤6 wt.% were monophasic solutions while higher water amounts resulted in the formation of a biphasic (water and organic phases) mixtures if no stirring was used. To ensure

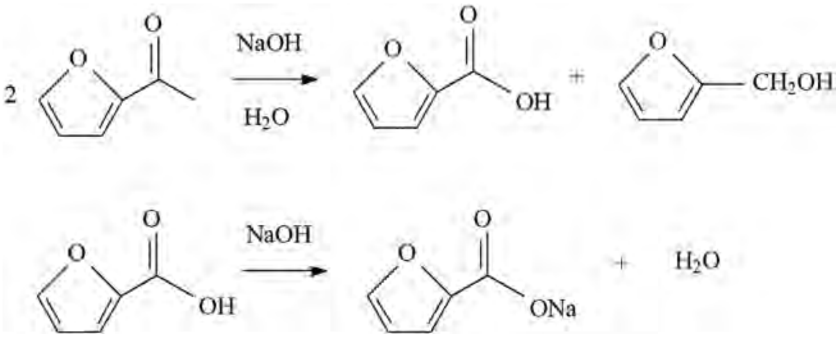

Scheme 1. Cannizzaro reaction in the presence of sodium hydroxide as a basic catalyst.

a "quasi-constant" reaction conditions, the reaction mixture was stirred at 300 RPM to afford aqueous organic emulsion. After adding the catalyst to the reaction mixture, the reaction was carried out at T = 50 °C for 180 min at 300 RPM. Samples were periodically withdrawn from the reactor during the experiment, filtered, and analyzed by Agilent 7890A GC unit equipped with a flame ionization detector (FID), using a HP-5 capillary column (30 m/0.32 mm ID/0.25 μm). The obtained products were identified based on standard reference compounds as well as additional GC–MS analyses. The catalytic results of furfural transformation over basic catalysts were described in terms of product yield that was calculated as follows:

$$\text{Yield of product}i(t)(\text{mol\%}) = 100 \times (\text{mole of reactant converted to product i})_{t/reactant\,t=0}.$$

After the reaction the catalysts were separated from aqueous furfural mixture by filtration, washed with ethanol, dried in N_2 flow at room temperature and characterized by different methods. Catalysts obtained from experiments with aqueous furfural mixtures having different water content are denoted HTC-xx where xx stands for the wt.% of water in the mixture, i.e. HTC-23 is a catalyst obtained from reaction in which aqueous furfural containing 23 wt.% of water was used as feedstock.

Aldol condensation of furfural and acetone was performed by using the same stirred batch reactor operating at T = 50 °C. For these experiments 0.5 g of freshly calcined HTC, 6.5 g of furfural and 19.7 g of acetone (Ac:F = 5 mol/mol) were used. After adding the catalyst to the reaction mixture, the reaction was carried out at T = 50 °C for 180 min under intensive stirring. Samples were periodically withdrawn from the reactor during the experiment, filtered and analyzed by the same GC method. Catalytic results of aldol condensation of furfural and acetone were described by conversion parameter that was calculated from the corresponding molar concentrations as follows:

$$\text{Reactant conversion }(t)(\text{mol\%}) = 100 \times (\text{reactant}_{t=0} - \text{reactant}_t)/\text{reactant}_{t=0}.$$

3. Results

3.1. Catalyst characterization

The physico-chemical properties of as-prepared HTC, calcined HTC (Mg-Al mixed oxide) and rehydrated HTCs investigated by XRD, TGA/DTG and DRIFT are presented in Table 1 and the *Supplementary information* (SI).

The XRD pattern of the freshly synthesized sample used in this study (see *SI*) shows a pure hydrotalcite phase (JCPDS 22-700) with intensive symmetrical peaks at $2\theta \approx 11°$, 22.8°, 36° and 60°, which are characteristic for the brucite-like layers. No additional crystalline phases could be identified in the diffractogram proving the high phase purity of the as-prepared hydrotalcite material. The XRD pattern of the sample calcined at 450 °C (Mg-Al mixed oxide) confirms the disappearance of the layered HTC structure. The only reflections observed in the XRD pattern (see SI) correspond to the MgO phase proving the formation of Mg-Al mixed oxide with the MgO periclase-type structure (JCPDS 87-0653). XRD pattern of a sample obtained after interaction of the Mg-Al mixed oxide with liquid water evidences the presence of a reconstructed HTC phase (meixnerite, JCPDS 35-0965) (see SI). It is worth noting that the XRD patterns of totally rehydrated samples shows neither a significant loss in intensity nor broadening of XRD peaks in comparison with the as-prepared HTC., i.e. these samples can be considered to be reconstructed HTCs. It also means that upon mechanical stirring during the rehydration process in liquid phase the hydrotalcite-like platelets were not broken or exfoliated which would result in a decrease in their particle size and in a change in their textural properties.

The textural properties of the as-prepared and Mg-Al mixed oxide (Table 1) are similar to those obtained for similar materials in our other studies [25]. According to chemical analysis, Mg/Al molar ratio in as-prepared material is 3.8 (Table 1), i.e. slightly higher when compared with the starting concentration of the elements in reactive synthesis gel. Assuming that each Al atom in the solid should produce one basic site, the theoretically possible concentration of basic sites in the sample with Mg/Al = 3.8 (with respect to bulk Al content) is 4.9 mmol/g for calcined sample, i.e. Mg-Al mixed oxide, (Table 1) or 2.7 mmol/g for dried as-prepared HTC taking into account its general formula and weight loss upon calcination (TGA data see below).

The actual concentration of basic sites was measured by CO_2-TPD technique. The uptake of CO_2 was 0.85 mmol per one gram of dried as-prepared HTC sample used in the experiment, hence the total concentration of basic sites determined by CO_2-TPD was 0.85 mmol/g based on the as-prepared HTC or 1.54 mmol/g if recalculated for Mg-Al mixed oxide, i.e. nearly 31.5% of theoretical value (Table 1).

The TGA profile for the as-prepared HTC sample (see SI) is in good agreement with the profiles reported in literature for HTC-like materials [27,28]. The total weight loss for this sample amounts to 45.8 wt.% (Table 2) which is in accordance with previous results [27,28]. The low temperature weight loss of 16.7 wt.% occurs in the range of 20–200 °C due to the removal of water molecules. It is clearly seen (see SI) that the signal in this range could be deconvoluted in two peaks with maxima at ca. 100 and 200 °C which are generally attributed to the loss of physically adsorbed and interlayer water molecules, correspondingly [27]. The high tem-

Table 1
Physico-chemical characteristics of Mg-Al samples used in the present study.

Sample	Phase composi-tion	BET area (m^2/g)	Mg/Al in synthesis gel (mol/mol)	Mg/Al by XRF (mol/mol)	Theoretical amount of basic sites (mmol/g)	Concentration of basic sites by CO_2-TPD (mmol/g)
$HTC_{as\text{-}prep.}$	HTC	–	3	3.8	2.7	0.85
$Mg\text{-}Al_{calc.}$	MgO	180			4.9	1.54
$HTC_{reconstr.}$	HTC	–			2.7	

Table 2
Results on the thermal analysis of the samples and their formula calculated from TGA-MS data.

Sample	Weight loss (TGA), %			Calculated formula (using TGA-MS)
	Total	20–250 °C	250–800 °C	
$HTC_{as\text{-}prep.}$	45.8	16.7	29.1	$Mg_{7.6}Al_2CO_{3(1.08)}OH_{19.6}\cdot 6.2H_2O$
$Mg\text{-}Al_{calc.}$	10.2	4	6.2	–
$HTC_{reconstr.}$	45.4	17.1	28.3	$Mg_{7.6}Al_2CO_{3(0.16)}OH_{21}\cdot 8.2H_2O$

perature weight loss of 29.1 wt.% is observed at temperature above 200 °C and originated from the dehydroxylation of the brucite-like sheets and the decomposition of carbonates in the interlayer [27]. To quantify the ratio between hydroxyl and carbonate groups in the as-prepared HTC, TGA-MS technique was used to determine H_2O and CO_2 evolution from the sample. Above 250 °C, the MS spectra show the presence of signals of H_2O and CO_2 (see *SI*) with the maxima at similar temperature, i.e. 395 and 404 °C, correspondingly, which prevents their differentiation by a routine TGA analysis. Using data from chemical and thermal analysis, the composition of the as-prepared hydrotalcite was calculated being very close to expectations from theory (Table 2).

In comparison with the as-prepared HTC, the weight loss of the calcined material (i.e. Mg-Al mixed oxide) is, as expected, much lower (only 10.2 wt.%) (Table 1). It corresponds to the loss of the physically adsorbed water below 100 °C (4.0 wt.%) and the removal of residual hydroxyls and carbonate groups at $T \geq 500$ °C remained present after the sample calcination at $T = 450$ °C (see SI). Total weight loss in the rehydrated sample is 45.4 wt.% (Table 1), i.e. very close to the value determined for the as-prepared HTC material. The distribution and intensity of the signals observed in the DTG spectra for the as-prepared and the reconstructed samples are also similar. Nevertheless, the performed TGA-MS study of both samples evidences a substantial decrease in the intensity of the signal corresponding to the evolved CO_2 (see SI). It proves that as a result of the calcination-rehydration procedure most of the carbonate groups are replaced by hydroxyls in the reconstructed HTC as evidenced by the calculated formula of the reconstructed HTC (Table 2). The observed presence of carbonate groups in the reconstructed HTC results most probably from the interaction of the rehydrated sample with CO_2 from air before the TGA analysis.

The DRIFT spectrum of the as-synthesized HTC material (see SI) is similar to the spectra published elsewhere [1,12,29,30]. A typical broad band at about 3460–3500 cm^{-1} is attributed to the stretching vibrations of structural hydroxyl groups in the brucite-like layer. A shoulder at 3000 cm^{-1} is assigned to hydrogen bonding between water molecules and the interlayer carbonate anions. The bands at around 1640 and 1370 cm^{-1} confirms the expected presence of interlayer water molecules and carbonate (chelating or bridging bidentate) anions, respectively. The vibration at 1515 cm^{-1} is ascribed to a reduction in the symmetry caused by the presence of monodentate carbonates ($\gamma_{asymO-C-O}$) interacting with Mg^{2+}, as reported elsewhere [1,12,29,30]. The low frequency region shows a band at about 560 cm^{-1}, corresponding to the translation modes of hydroxyl groups, influenced by Al^{3+} cations [12,31,32]. The band at 870 cm^{-1} is characteristic for the out-of-plane deformation of carbonate, whereas the in-plane bending is located at 680 cm^{-1} [12].

Calcination of the as-prepared HTC results in water removal that is evidenced by the disappearance of the band at around 1640 cm^{-1} (water bending vibrations) and of the shoulder at 3000 cm^{-1} (interaction of $H_2O—CO_3{}^{2-}$ in the interlayer) (see *SI*). The intensity of the bands at around 3460–3500 cm^{-1} also decreases due to the surface dehydroxylation upon calcination. The band at 1370 cm^{-1} (interlayer carbonates) decreases in intensity and the two peaks at about 1515 and about 1400 cm^{-1} evidencing the interaction between $CO_3{}^{2-}$ and Mg^{2+} [12] are also present, but their intensity decreases as well. The obtained FTIR spectrum proves that residual carbonate and hydroxyls anions as well as small amount of water (band at around 1640 cm^{-1}) are still present in HTC sample calcined at $T = 450$ °C, i.e. in the Mg-Al mixed oxide sample, most likely due the adsorption of CO_2 and moisture from air during the DRIFT experiment.

The spectrum of the reconstructed HTC is substantially similar to that of the as-prepared HTC (see SI). The broad band at 3460–3500 cm^{-1} evidences the recovery of the structural hydroxyl groups in the brucite-like layers. The bands at 3050 and 1640 cm^{-1} also reappears in the spectra of this sample, indicating a significant amount of adsorbed water molecules in the reconstructed material. The band at 1370 cm^{-1} which also reappears in the spectra as a symmetric peak is usually attributed to the presence of carbonates in reconstructed materials, even after rehydration step [12,32]. In the latter case, the existence of these groups in the rehydrated samples is explained by a probable introduction of $(CO_3)^{2-}$ from air during the reconstruction process [12]. However, the performed TGA-MS analysis of the reconstructed HTC proves low concentration of carbonates in the reconstructed HTC, so the band at 1370 cm^{-1} in DRIFT spectrum cannot be unequivocally attributed to carbonate groups. Moreover, anionic OH-groups should be inevitably identified in the DRIFT spectra of the reconstructed HTC material as well. It is known that anionic groups other than carbonates could be characterized by absorption bands in the FTIR region close to 1370 cm^{-1}. For example, a band at 1364 cm^{-1} was previously ascribed to the anti-symmetrical stretching mode of nitrate ions [33] and a band observed at 1390 cm^{-1} was attributed to the symmetric stretching of the carboxylate group [34]. Hence, hydroxyl groups formed due to the rehydration of Mg-Al mixed oxide (calcined HTC), which compensate the positive charge of the layers, could be also responsible for the observed band lying in the same FTIR-region. This makes us to conclude that the band at 1370 cm^{-1} could in fact signify the presence of any extra-framework functional anionic groups, including OH^-, which compensate the positive charge of the inorganic framework originating from the Mg-Al isomorphous substitution.

3.2. Interaction of Mg-Al mixed oxide with aqueous furfural mixture

According to the reaction scheme (Scheme 1), water is a necessary participant of Cannizzaro reaction donating a proton for an intermediate alkoxide to be converted to a final alcohol. In other words, the absence of water makes the disproportionation of furfural to furfuryl alcohol (F-OH) and furoic acid (F-OOH) in the presence of a basic catalyst impossible. Accordingly, in our experiments we have studied the behavior of Mg-Al mixed oxide in CR of aqueous furfural solutions having different water content.

The main reaction products obtained by reaction of aqueous furfural feedstock over calcined HTC, i.e. over Mg-Al mixed oxide, are F-OH and furoyl furoate (FF). Despite no F-OOH is found in reaction products, the formation of F-OH and FF, a product of esterification reaction between F-OH and F-OOH, provides an indirect evidence that furfural undergoes CR over the solid base catalyst. One-stage alcohol formation from aldehyde is only possible by using hydrogen atmosphere and a hydrogenation catalyst which is not the case in our experiment. Moreover, due to the basic nature of the catalyst used it is highly likely that F-OOH will react immediately with the basic sites forming either salts, e.g. sodium furoate when NaOH would be used as catalyst, or surface furoates in case of solid base catalysts. This is confirmed by a titration experiment (see *SI*) in which F-OOH is successively added to Mg-Al mixed oxide (calcined HTC) catalyst immersed in acetone followed by GC analysis of the liquid phase. A signal on the GC diagram belonging to F-OOH appears only when the amount of acid added to the catalyst exceed 0.3 g/g_{cat}. The only plausible explanation of the performed titration experiment is that the acid remains adsorbed on the catalyst. It is worth noting that the concentration of basic sites in the calcined sample titrated with F-OOH is ≈2.7 mmol/g, which is higher than that determined by CO_2-TPD (based on Mg-Al mixed oxide). Presumably, furoic acid could additionally adsorb on weak basic sites which do not interact with CO_2 in the CO_2-TPD experiment. Assuming the formation of surface furoates, we have introduced the yield of F-OH as the measure of catalyst activity in Cannizzaro reaction.

Fig. 1A depicts F-OH yield observed during reaction of aqueous furfural mixtures having different water content on Mg-Al mixed oxide in dependence on experiment duration. A clear dependence of catalyst activity on water content in the mixture is observed. At water-free conditions, F-OH yield is as low as 0.11 wt.% after 180 min of the reaction. This result confirms the necessity of water presence in the reaction mixture to facilitate the Cannizzaro reaction, which is in accordance with the reaction scheme (Scheme 1). The catalyst activity observed in the water-free experiment can be explained by the traces of moisture in the sample due to adsorption from air during the transfer of the calcined catalyst into the reactor. This explanation is also supported by TGA results. The observed alcohol yield corresponds to 0.15 mmol of F-OH produced per 1 g of Mg-Al mixed oxide. Taking into account the reaction stoichiometry, i.e. the equimolar formation of F-OH and F-OOH, and assuming acid-base interaction between the formed F-OOH and basic sites of the catalyst, it can be inferred that about 10% of the basic sites in the catalyst probed by CO_2 (Table 1) participate in the reaction and react with the produced acid forming furoate species.

Fig. 1A shows that the increase in water content in the mixture results in the growth of F-OH yield proving thus the importance of water in the reaction (Scheme 1). For monophasic reaction conditions (water content in the range of 0–6 wt.%) the F-OH yield is below 0.5 wt.% after 180 min of the reaction. Under biphasic reaction conditions (water content > 12 wt.%) the F-OH yield substantially increases to 1.8-2.3 wt.% (Fig. 1A). The maximum alcohol yield of 2.3 wt.% is observed for water content of 23 wt.% in the mixture while further increase in water content up to 33% results in a slight decrease of F-OH yield to 1.9 wt.%.

The maximum F-OH yield of 2.3 wt.% (Fig. 1A) corresponds to 3.6 mmol of produced F-OH per 1 g of calcined catalyst. Hence, the amount of the produced acid should also correspond to 3.6 $mmol_{F\text{-}OOH}/g_{cat}$. Since F-OOH is not identified by GC among reaction products, the concentration of basic sites that interacted with the acid should also be equal to 3.6 $mmol/g_{cat}$. This value is larger than that determined by the direct titration of Mg-Al mixed oxide with furoic acid (see SI) and substantially exceeds the value determined by CO_2-TPD (Table 1). On the other hand, the concentration of basic sites in the catalyst evaluated from its activity in CR is still lower than the theoretical basicity derived from its chemical composition. It allows concluding that not all basic sites in the catalyst are involved in the reaction and the formation of surface furoates. Nevertheless, the concentration of basic sites as high as 3.6 mmol/g determined by the *in-situ* "titration" with furoic acid proves that physico-chemical characteristics of basic catalysts including the amount of basic sites can change during the rehydration step as discussed below.

Besides F-OH, furoyl furoate is observed as a reaction product (Fig. 1B), apparently as a result of esterification reaction between furfuryl alcohol and furoic acid. In contrast to F-OH, the yield of the FF ester exhibits a less pronounced dependence on water content. Fig. 1B shows that after 180 min of the reaction, the ester yield is 0.16 wt.% for monophasic aqueous furfural mixture (≤6 wt.% of water) and only small increase to 0.18–0.2 wt.% is observed for higher water contents (biphasic reaction mixture). The observed poor dependence of the ester yield on water content allows assuming that the formation of this compound could be more preferable in water-free reaction conditions. Obviously, as water is a product of the esterification reaction, an increase in water content will favor hydrolysis over esterification, i.e. shift the reaction equilibrium towards the reactants.

3.3. The properties of Mg-Al catalysts after reaction

The experimental results provide a strong indication that furfural is converted by Cannizzaro reaction over Mg-Al mixed oxide when water is present. Whereas F-OH is observed in the reaction products by GC, it is highly probable that F-OOH forms furoate species on the catalyst surface, i.e. remains adsorbed on the basic sites of the catalyst. The formation of such species would definitely change physico-chemical properties of a basic catalyst and these have been monitored by different techniques.

3.3.1. XRD

Fig. 2A depicts XRD patterns of catalysts after reaction in dependence on water content in aqueous furfural mixture. XRD patterns of samples after experiments using a monophasic reaction mixture (water content of 0–6 wt.%) contain predominantly reflections characteristic for MgO phase. As soon as the furfural mixture becomes biphasic (water content ≥ 12 wt.%), the intensity of the reflections due to the MgO phase noticeably decreases while the intensity of reflections corresponding to the HTC phase increases. The calculated relative content of the crystalline phases (Fig. 2B) evidences that a dramatic step change in the phase composition of the catalysts occurs when the monophasic reaction mixture turns into a biphasic one due to the increase in water concentration. In the monophasic aqueous-organic mixture the probability for the inorganic solid to interact with water molecules (a necessary step for rehydration to take place) is low because of high furfural concentration because both molecules compete for the same adsorption places. As a consequence, the rehydration of the mixed oxide to a reconstructed HTC is slow. In contrast, when the reaction mixture is biphasic, the catalyst is in contact with both organic (mostly furfural) and aqueous (mostly water) phases. The XRD data evidence (Fig. 2) that such intermittent interaction of Mg-Al mixed

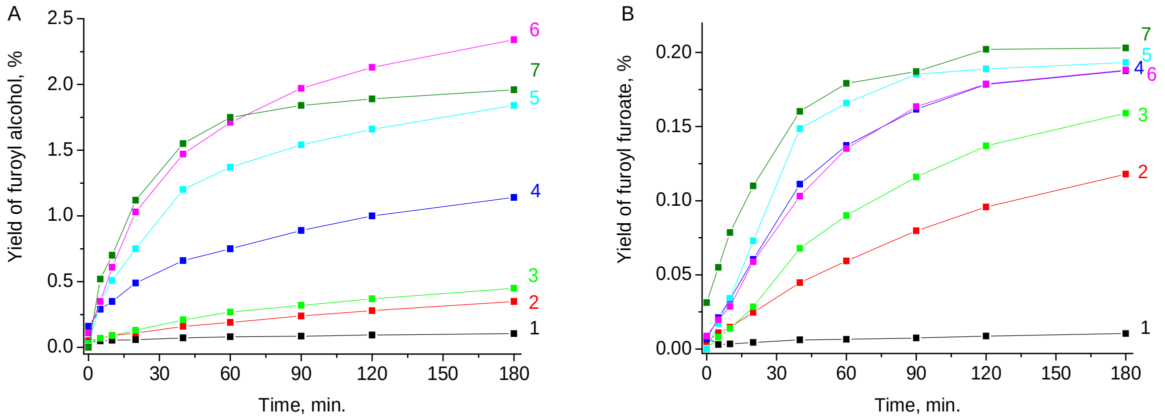

Fig. 1. Yields of furfuryl alcohol (A) and furoyl furoate (B) observed during reaction of aqueous furfural mixture on Mg-Al mixed oxide in dependence on water content (in wt.%): 1–0%, 2–3%, 3–6%, 4–12%, 5–18%, 6–23%, 7–33%. $T_{reac.} = 50\,°C$, $m_{furfural} = 30\,g$, $m_{calc.cat.} = 2\,g$.

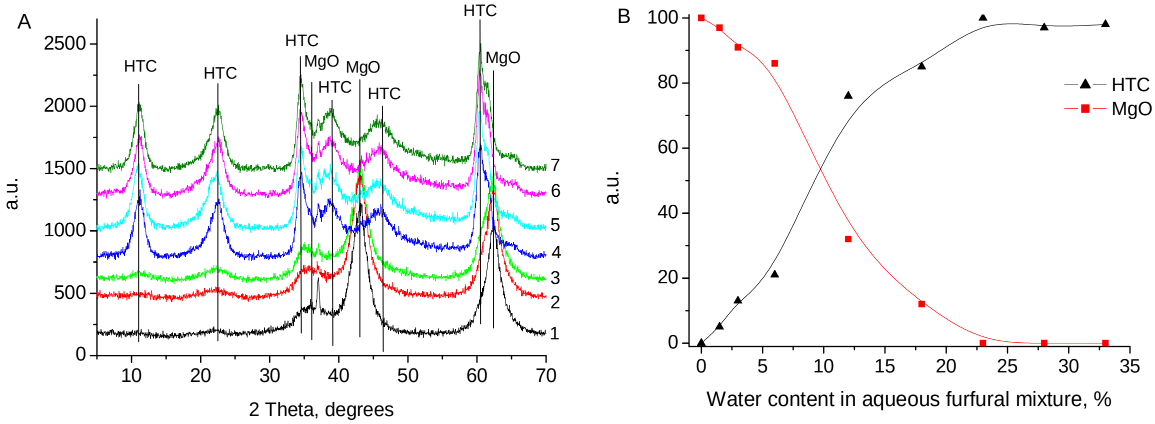

Fig. 2. XRD patterns (A) and the relative content of HTC and MgO phases (B) in catalysts after reaction in dependence on concentration of water in aqueous furfural mixture: 1–HTC-0, 2–HTC-3, 3–HTC-6, 4–HTC-12, 5–HTC-18, 6–HTC-23, 7–HTC-33 where the numbers denote wt.% of water in the mixture.

oxide with either organic or aqueous phase under intensive stirring ensures the transformation of the solid mixed oxide into reconstructed HTC. The comparison of the catalytic results with the XRD data allows concluding that the observed high activity of the catalysts in CR is connected with the high rehydration degree of Mg-Al mixed oxide to a reconstructed HTC. This conclusion is in agreement with the reaction scheme of CR: the disproportionation of furfural to F-OH and F-OOH takes place with the participation of hydroxyls which are Brønsted basic sites of the rehydrated HTC catalyst rather than with the Lewis basic sites of Mg-Al mixed oxide.

3.3.2. TGA

Fig. 3A depicts TGA curves of the catalyst samples after Cannizzaro reaction of furfural aqueous mixtures having variable water content. The catalysts were separated from reaction mixtures by filtration followed by washing with ethanol and drying at 80 °C for 4 h before TGA experiments to exclude the contribution of any physisorbed organic species to the results. The increase in water content results in a progressive increase in the total weight loss of the samples (Fig. 3A) which correlates with the transformation of the Mg-Al mixed oxide to reconstructed HTC materials as proved by XRD (Fig. 2). The samples obtained from the reaction of monophasic furfural-water mixtures possess low-to-moderate weight loss in the range of 21–30 wt.%, due to the small rehydration degree of the Mg-Al mixed oxide (<20%). In contrast, the weight loss of the sample HTC-23 obtained after reaction of biphasic furfural-water mixture amounts to 49 wt.% which is close to the values for as-prepared or water-reconstructed HTC samples (Table 1). In agreement with these results, the sample HTC-23 affords a nearly fully reconstructed HTC after the reaction as evidenced by the XRD results (Fig. 2).

The DTG curves of the samples after reaction (Fig. 3B) show two ranges of weight losses in accordance with the results for as-prepared or reconstructed HTC samples. The low-temperature region consists of two signals at T = 80–100 °C and 180–200 °C attributed to physically adsorbed and interlayer water, respectively, the latter exhibiting a clear dependence on the reconstruction degree of the rehydrated samples. In fact, the change in phase composition is linearly proportional to the water content in the aqueous furfural mixture. In agreement with the XRD data (Fig. 2A) an obvious difference is observed between the TGA/DTG curves for samples obtained from monophasic or biphasic reaction mixture experiments.

In the high-temperature region of DTG curves, the presence of two well-distinguished signals at ~320 and ~400 °C can be observed. The signal at T = 385–400 °C is similar to those observed in both as-prepared and reconstructed HTC samples and corresponds to the removal of carbonate and/or hydroxyl groups from the samples [27]. For the catalysts after reaction the intensity of this peak increases with the growth in water content in the reaction mixture and, as a consequence, it is in line with the increase in the rehydration degree of Mg-Al mixed oxide proved by XRD (Fig. 2). Nevertheless, the signal with maximum at T = 320 °C was not previously observed in DTG curves for as-prepared and water-reconstructed HTC materials (see SI). Therefore, this signal has to originate from other compounds than water, CO_2 or contaminants

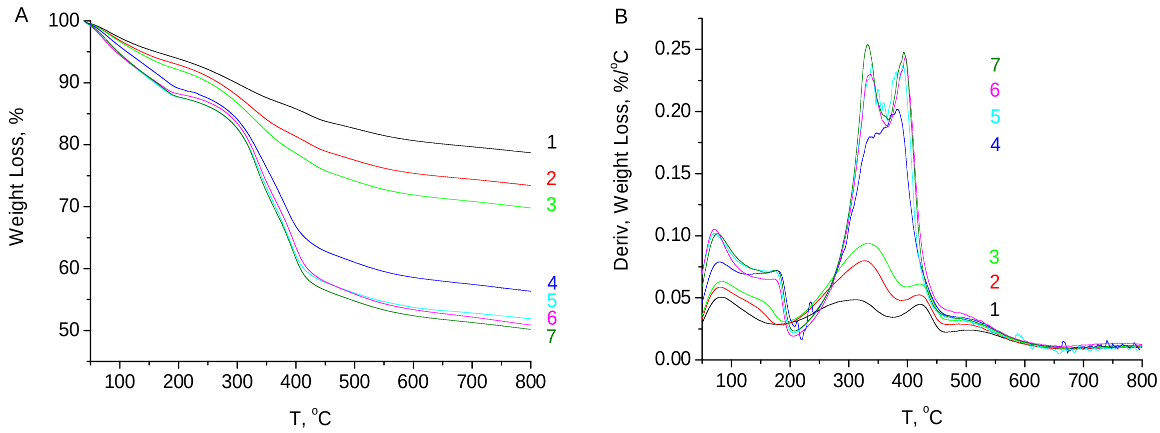

Fig. 3. TGA (A) and DTG (B) curves of catalysts obtained after reaction with aqueous furfural mixture with different water content. 1–HTC-0, 2–HTC-3, 3–HTC-6, 4–HTC-12, 5–HTC-18, 6–HTC-23, 7–HTC-33.

from ambient air, i.e. from furfural or reaction products of furfural transformation including F-OH, F-OOH and FF. The intensity of this signal also increases with the increasing concentration of water in the reaction mixture. As the increase in the water content resulted in an increase in the furfuryl alcohol yield (Fig. 1A), it can be deduced that the signal at T = 320 °C is due to furfuryl alcohol or, more likely, due to surface furoates formed by adsorption of furoic acid that is produced from furfural by Cannizzaro reaction in equimolar yields as furfuryl alcohol, but unlike F-OH is not detected among reaction products.

3.3.3. DRIFT

DRIFT spectra obtained after contacting Mg-Al mixed oxide with aqueous furfural mixtures having different water content are shown in Fig. 4 (reconstructed HTC rehydrated with pure water is shown as a reference). With increasing water content, a broad band in the range of 2700–3700 cm^{-1} reappears in the spectra proving the recovery of structural hydroxyl groups in the brucite-like layers of the rehydrated samples (Fig. 4A). The bands in the range of 1300–1700 cm^{-1} which characterize the presence of interlayer water molecules and compensating extra-framework anions also appear in the spectra (Fig. 4B). The change of the DRIFT spectra for Mg-Al mixed oxide sample after its contact with aqueous medium can be attributed to the HTC structure recovery and is thus in agreement with XRD and TGA results. However, comparing the DRIFT spectra for catalysts after reaction with the spectra for both as-prepared and rehydrated HTC samples, it can be concluded that the composition of the functional groups in the samples after reaction is different than in the fresh samples. First, shoulder at 3000 cm^{-1} usually observed in the DRIFT spectra of both as-prepared and reconstructed HTC rehydrated with pure water is absent in the DRIFT spectra of the spent catalysts. The absence of this shoulder suggests that the $H_2O—CO_3^{2-}$ interaction in the interlayer is weakened. Furthermore, the character of the bands in the range of 1300–1700 cm^{-1} differs: it becomes more complex for the samples after reaction as additional bands appeared in the spectra (Fig. 4B). Instead of a single band at 1640 cm^{-1} which characterizes the presence of water molecules in interlayer (Fig. 2) several bands at 1561 and 1591 are present in the DRIFT spectra of catalysts after reaction. These bands suggest that other molecules than water are present in the interlayer of the rehydrated catalysts. Moreover, two new bands at 1363 and 1390 cm^{-1} are also present in the spectra. For as-prepared and reconstructed HTC rehydrated with pure water the band at 1370 cm^{-1} characterizes the presence of compensating anions, as discussed above. The appearance of the new bands at 1363 and 1390 cm^{-1} can be related with the presence of new kind of compensating anions, such as furoates. Besides, a well-expressed band at 1479 cm^{-1} not observed previously in the DRIFT spectra for neither as-prepared nor rehydrated HTC samples is found in the spectra of spent catalysts. Finally, several new bands appeared also in the range of 900–1250 cm^{-1} (Fig. 4B) which could be caused by the presence of new surface species in the catalysts after reaction.

In summary, the characterization data prove that the increase in water content in the aqueous furfural mixture promotes the rehydration of the Mg-Al mixed oxide and facilitates the formation of reconstructed HTC. As soon as Brønsted basic sites are formed in the reconstructed material, its activity in furfural conversion increases as demonstrated by the increase in both F-OH and furoyl furoate yield. After the reaction, the catalyst contains additional species which differ from carbonate or OH$^-$ anions as well as from water molecules. Taking into account the concentration of F-OH in the liquid reaction products together with the absence of furoic acid among these products, it is highly probable that these newly formed species found in the catalysts after reaction are surface furoate species. To support this claim, a specific study of furoic acid interaction with the rehydrated catalysts was undertaken.

3.4. The study of interaction between rehydrated HTC and furoic acid

Different amounts of furoic acid were added to the mixture of water and reconstructed HTC after the completion of the rehydration procedure (see the *Experimental*), and the resulting mixture was stirred for 10 min. The solids treated with furoic acid were then separated by filtration using a vacuum pump, dried in N_2 flow at room temperature and investigated by TGA and DRIFT.

A gradual growth in the DTG signal with the maximum at T = 330–340 °C is observed for rehydrated HTC after its treatment with furoic acid as the ratio of m_{FOOH}/m_{sample} increases from 0 to 0.5 (Fig. 5). The filtrate solution was analyzed by GC, but no furoic acid was detected. This strongly suggests that it was adsorbed on the catalyst and hence the signal at T = 330–340 °C may be unequivocally attributed to the surface furoate species. The position of this signal agrees well with the observed unknown signal in the DTG curves obtained for spent catalysts after their treatment with aqueous furfural mixture (Fig. 3). Consequently, it can be concluded that furoate species are indeed present in the spent rehydrated HTC after Cannizzaro reaction.

Additionally, the observed increase in the signal intensity at T = 330–340 °C is in line with a gradual decrease in the intensity of signals at T = 200–210 °C and T = 390–410 °C. The signal at T = 200–210 °C characterizes interlayer water molecules which are

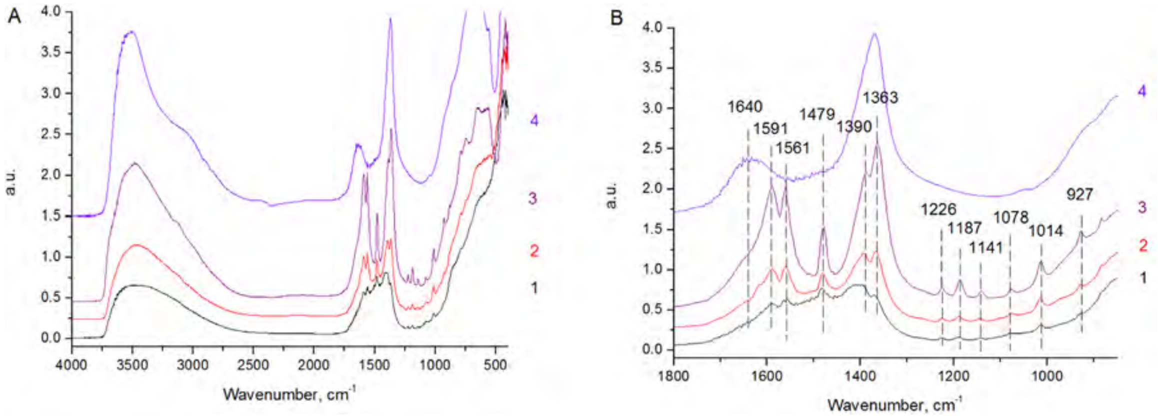

Fig. 4. DRIFT spectra of calcined Mg-Al mixed oxide after its interaction with aqueous furfural mixture in the range of 400–4000 cm^{-1} (A) and 800–1800 cm^{-1} (B). 1–HTC-0; 2–HTC-6; 3–HTC-23; 4–reconstructed HTC rehydrated with pure water (reference material).

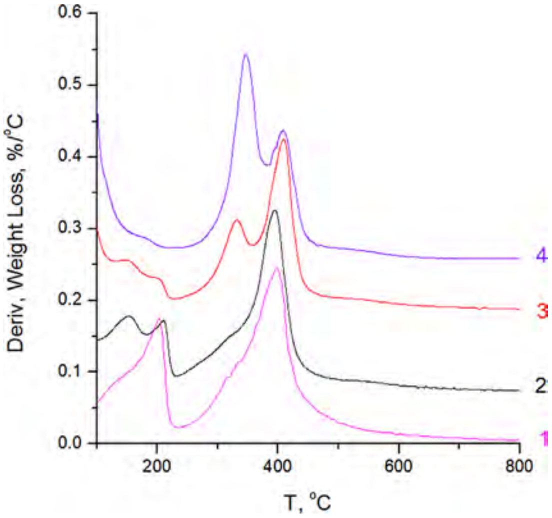

Fig. 5. DTG curves for rehydrated HTC treated with different amounts of Furoic acid. $m_{FOOH}/m_{calcinedsample}$ = 0 (1); 0.1 (2); 0.3 (3) and 0.5 (4).

stabilized in interlayer due to hydrogen bonding between them and interlayer compensating anions while the signal at 390–410 °C is characteristic for the removal of structural hydroxyls and compensating anions [12]. The interaction of furoic acid with basic sites and the generation of furoic species should in fact decrease the total amount of structural hydroxyls and compensating anions and thus result in weakened hydrogen bonding between the anions and water molecules. As a consequence, the amount of interlayer water would decrease as would the corresponding signal in DTG data, which is apparent in the experimental data (Fig. 5).

Fig. 6 depicts total DRIFT spectra for rehydrated HTC samples treated with furoic acid in the range of 500–4000 cm^{-1} (A) and in the specific range of 800–1800 cm^{-1} (B). The intensity of a shoulder signal at 2700–3200 cm^{-1} assigned to hydrogen bonding between water molecules and the interlayer anions decreases in intensity with the increase in acid content from 0 to 0.5 g_{acid}/g_{cat}. (Fig. 6A). The behavior of this band correlates well with the decrease in the intensity of the DTG signal in the range of T = 100–200 °C and proves the loss of water (including interlayer water) in the samples as a consequence of the formed furoate species. A large difference in the DRIFT spectra between the untreated rehydrated HTC and the samples treated with furoic acid (Fig. 6) is observed in the range of 1300–1700 cm^{-1}. The peak at 1640 cm^{-1} attributed to the presence of interlayer water has very low intensity in the spectra of F-OOH-treated rehydrated samples suggesting low water content in the interlayer. Instead, two peaks appear in this range at 1594 and 1563 cm^{-1} (Fig. 6B). A peak at 1365 cm^{-1} which is usually attributed to carbonate cations [12] or, as supposed in the present study, to compensating OH^--groups decreases in intensity with the increase in acid content in the mixture while a new band at 1390 cm^{-1} has appeared. Finally, a very distinctive band at 1481 cm^{-1} is observed in the samples, and its intensity correlates well with the amount of acid in the treatment solution. In summary, the observed changes and the appearance of new bands in the DRIFT spectra of HTC samples treated with F-OOH can be unequivocally attributed to the surface furoate species formed by adsorption of furoic acid on the basic sites. The formation of furoate species in the treated materials could be also related with the appearance of new small bands in DRIFT spectra in the range of 900–1250 cm^{-1}. In total, the similarity in the positions of the bands observed in DRIFT spectra of samples either treated with furoic acid or those obtained after reaction with aqueous furfural mixture (Figs. 4 and 6B) allows concluding that the formed surface species on the catalysts are indeed furoates.

3.5. *Reconstructed HTC as a catalyst for Cannizzaro reaction*

Catalytic results presented above indicate that the increased catalyst activity in CR is observed when reconstructed HTC is formed as a result of complete rehydration of the Mg-Al mixed oxide. This reconstruction is achieved provided large water amount is present in the reaction mixture. On the other hand, the catalytic results indicate that water could have a negative effect on the reaction resulting in a decrease in furfural conversion (Fig. 1). Using a reconstructed HTC prepared by a pre-treatment of mixed oxide with liquid water allows avoiding large water content in the reaction mixture. In addition, these experiments reveal more accurately the effect of water on the course of Cannizzaro reaction, i.e. it allows decoupling the influence of water on catalyst reconstruction (and its activity) from its influence on the reaction.

In these sets of experiments 2 g of freshly calcined HTC was used in rehydration procedure as described in the *Experimental* to prepare reconstructed HTC sample as a catalyst for the reaction. It allows making an accurate comparison between the catalytic activity of mixed oxide and reconstructed samples based on their calcined form. Fig. 7 depicts F-OH yield obtained during the interaction of reconstructed HTC with aqueous furfural mixture. The catalyst possesses poor activity in the conversion of water-free furfural evidencing the necessity of water for the Cannizzaro reaction to take place. In this experiment F-OH yield of ~0.1 wt.% could be attributed to the residual water in the dried reconstructed HTC catalyst. Addition of water to furfural promotes

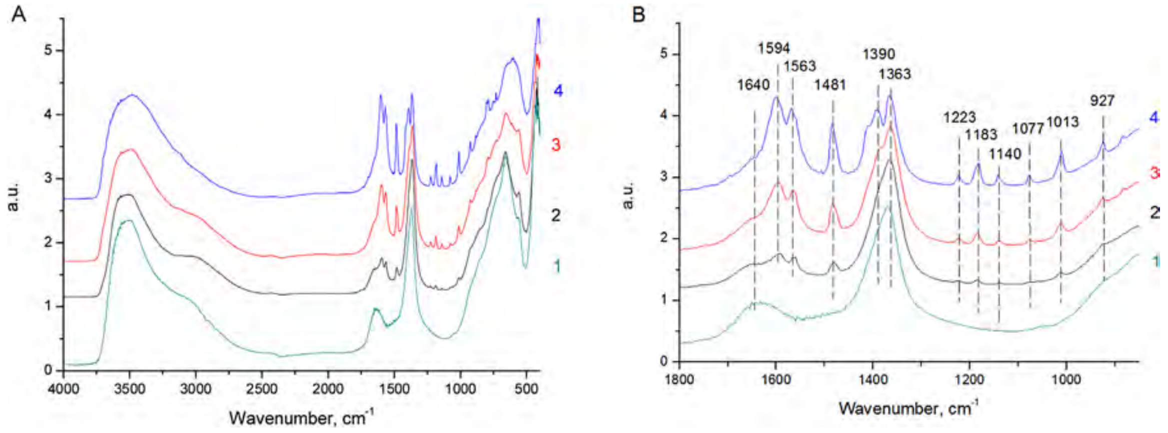

Fig. 6. DRIFT spectra of rehydrated HTC treated with different amounts of Furoic acid. m_{FOOH}/m_{sample} = 0 (1); 0.1 (2); 0.3 (3); 0.5 (4). A – the range of 400–4000 cm^{-1}, B – the range of 800–1800 cm^{-1}.

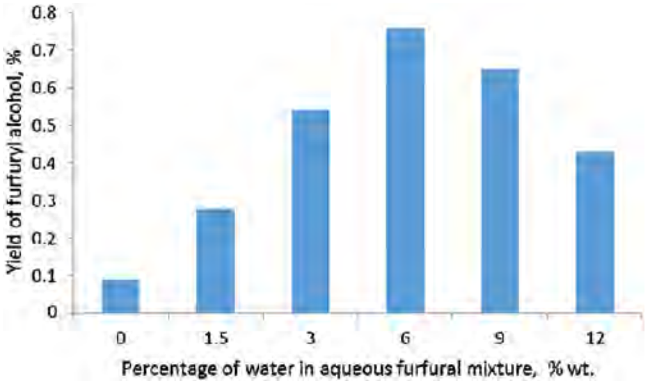

Fig. 7. The yield of furfuryl alcohol in experiments with aqueous furfural solution having different water content using dried reconstructed HTC as catalyst. Treac. = 50 °C, t = 3 h, $m_{cat.}$ = 2 g (calcined base), m_F = 30 g.

the activity of the reconstructed HTC: alcohol yield increases from 0.28 wt.% to 0.76 wt.% as the water content in aqueous furfural mixture grows from 1.5% to 6%, respectively. Nevertheless, further increase in water content in the mixture does not result in a corresponding growth in the furfuryl alcohol yield (Fig. 7). It is worth noting that the maximum F-OH yield observed in experiments with the reconstructed HTC (Fig. 7) is significantly lower than that for Mg-Al mixed oxide (calcined HTC) treated with aqueous reaction mixture (Fig. 1). The observed difference in catalytic behavior suggests that the number of basic sites which are accessible to furfural molecules in the catalyst rehydrated with pure water is lower compared with the catalyst rehydrated *in situ* with biphasic aqueous-organic mixture. Indeed, calculations show that the maximum alcohol yield of 0.76 wt.% produced on reconstructed HTC corresponds to 1.19 mmol of alcohol per 1 g of the catalyst (calcined base). Consequently, 1.19 mmol/g of furoic acid produced by CR is bound with 1.19 mmol/g of basic sites in the catalyst, which is 24.3 wt.% with respect to the bulk Al content. This concentration of basic sites titrated with the acid is much lower than that evaluated from the results of catalytic experiments with Mg-Al mixed oxide. Moreover, it is also slightly lower than that determined by CO_2-TPD (1.57 mmol/g, calcined base, Table 1). On the other hand, the concentration of basic sites evaluated in rehydrated HTC by means of Cannizzaro reaction agrees well with the results from [12] that 24.5% of the OH^- sites with respect to the bulk Al content in HTC rehydrated in liquid water are evaluated by CO_2-TPD. In summary, the obtained catalytic results make us suggest that the concentration of basic sites in the reconstructed HTC depends on the properties of a liquid medium used for rehydration of Mg-Al mixed oxide, i.e. calcined HTC. Nonetheless, further fundamental studies are necessary to understand the relationship between the basic sites formation and the properties of the media used.

3.6. *The impact of CR on aldol condensation of furfural and acetone*

Aldol condensation (AC) of furfural and acetone takes place in the presence of basic catalysts, for example activated HTC. In general, any of the two components of the reaction mixture interacts with the active centers of the catalyst. Basic sites promote the activation of acetone which is necessary for AC to take place [20,21], while furfural is also transformed by CR, as shown in the present study. Both reactions, AC and CR, proceed simultaneously and share the same active centers; therefore, the deactivation of basic sites with furoic acid formed by CR should influence the conversion of reactants by AC. The following model experiments represent examples aimed to demonstrate the degree of this influence. Three series of catalytic runs with Mg-Al mixed oxide were carried out:

Example I. Mg-Al mixed oxide is added at once to prepared F + Ac mixture (a reference run).

Example II. Mg-Al mixed oxide is initially stirred in acetone for 0–90 min and then furfural is added.

Example III. Mg-Al mixed oxide is initially stirred in furfural for 0–90 min and then acetone is added.

The results of these experiments are presented in Fig. 8. In the reference run (Fig. 8A, Example I) furfural conversion is 20.7% after 3 h of the reaction. Along with compounds formed by aldol condensation, the formation of furfuryl alcohol with the yield of 0.06 wt.% after 3 h is observed. Its presence among other products evidences the simultaneous occurrence of AC and CR, i.e. the formation of furoic acid. As shown above, furoic acid interacts with the basic sites of the catalyst resulting in the formation of surface furoate species. As a consequence, the amount of active sites which are able to participate in both reactions is reduced thus leading to a loss of activity.

The initial stirring of catalyst in acetone for 0, 30, 60 and 90 min, respectively, (Example II) does not introduce any significant effect on its performance in either AC or CR reaction routes. Regardless of the duration of the initial step, the conversion of furfural after 3 h of its addition to the acetone + catalyst mixture is in the range of 18.6-21% while the yield of F-OH is 0.05-0.06 wt.%. These experiments (Example II) evidence that the contact between acetone and catalyst does not contribute to any change in the catalytic activ-

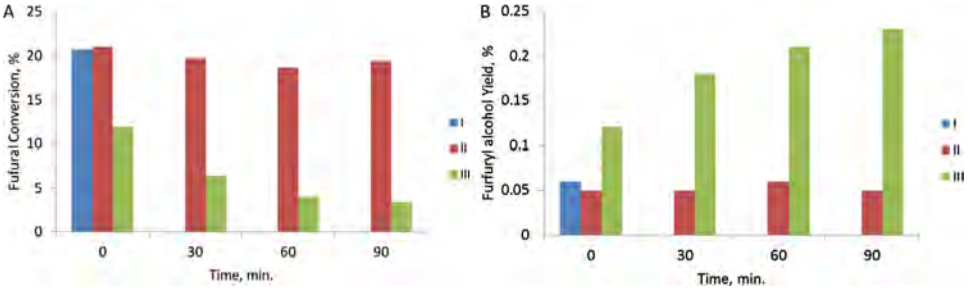

Fig. 8. Furfural conversion (A) and the yield of F-OH (B) observed after 3 h of the aldol condensation of furfural and acetone over Mg-Al mixed oxide. I – Catalyst is added to the mixture of acetone and furfural (Reference run); II – Catalyst is stirred in acetone for 0, 30, 60, 90 min followed by furfural addition; III – Catalyst is stirred in furfural for 0, 30, 60, 90 min followed by acetone addition. Reaction conditions: $m_{cat.} = 0.5$ g, F:Ac = 6.5/19.7 g/g (1/5 mol/mol), $T_{reac.} = 50\,°C$.

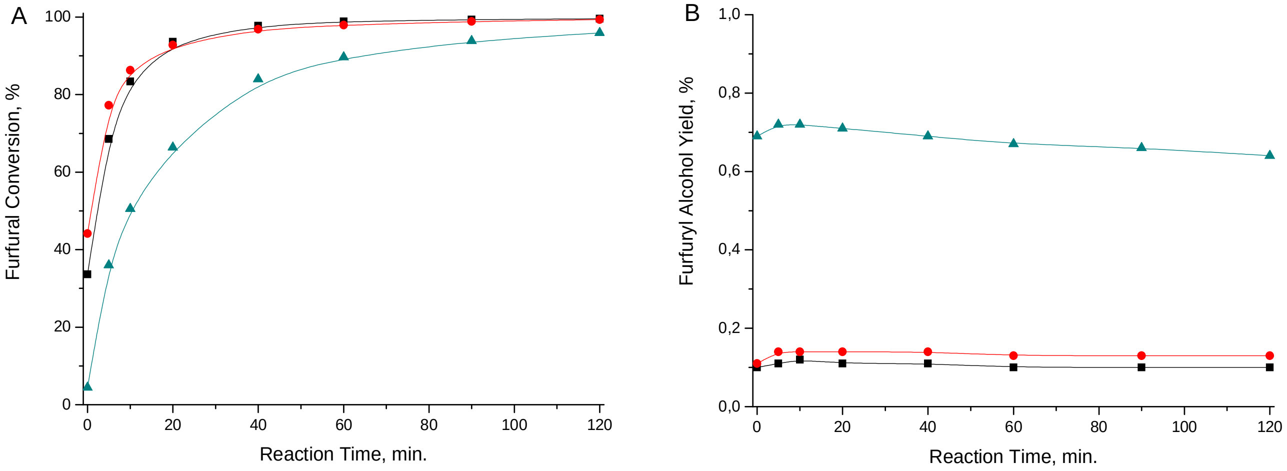

Fig. 9. Furfural conversion (A) and the yield of F-OH (B) observed during the aldol condensation of furfural and acetone over reconstructed HTC. I – Catalyst is added to the mixture of acetone and furfural (Squares); II – Catalyst is stirred in acetone for 30 min followed by furfural addition (Circles); III – Catalyst is stirred in furfural for 30 min followed by acetone addition (Triangles). Reaction conditions: $m_{cat.} = 0.5$ g (calcined base), F:Ac = 6.5/19.7/ g/g (1/5 mol/mol), $T_{reac.} = 25\,°C$. Prior to catalyst addition the reaction mixtures (I–III) are mixed with 0.4 g of water to promote CR.

ity in AC, so the behavior of the catalyst is comparable with that observed in the reference run (Example I).

In contrast, the initial stirring of catalyst in furfural (Example III) leads to unique results (Fig. 8A). Even a brief contact between furfural and catalyst decreases the activity of the catalyst in aldol condensation which is evidenced by furfural conversion of 11.9% after 3 h of the reaction (Fig. 6A). When increasing the time of the initial stirring of the catalyst in furfural up to 90 min, a further decrease in furfural conversion in aldol condensation down to 3.4% is observed. Simultaneously with the decline in the overall activity of the catalyst, the increase in the yield of furfuryl alcohol from 0.12 to 0.23 wt.% is observed as the duration of the first stage of the experiment increases from 0 to 90 min, respectively (Fig. 8B). As postulated above, the presence of F-OH indicates that F-OOH is formed because these two compounds are related with each other by the stoichiometry of Cannizzaro reaction. Being produced by Cannizzaro reaction, F-OOH generates surface furoate species by reacting with the basic sites and, consequently, the basic sites become catalytically inactive. It could be also assumed that the organic salts being formed on the catalyst surface would result in selective leaching of the corresponding catalyst components. To evaluate the plausible leaching, we have analyzed the reaction mixture after catalytic experiment (Example III) by ICP. However, we did not detect any traces of Mg or Al in the solution after reaction. It allows concluding that the catalyst is chemically stable and the organic salts, if formed, stay bound on the catalyst surface. Therefore, the decrease in furfural conversion observed in these experiments (Example III), can be explained by the gradual poisoning of the catalyst with products formed by CR.

Similar experiments investigating the influence of mixing order of reactants during aldol condensation on furfural conversion were performed with reconstructed HTC (Fig. 9). As expected, the activity of the reconstructed HTC in the reaction was higher in comparison with Mg-Al mixed oxide, so to observe any differences in conversion the catalytic experiments were carried out at T = 25 °C

In agreement with the results obtained for Mg-Al mixed oxide, furfural conversion is similar when the rehydrated catalyst is either added to the mixture of acetone and furfural (Example I) or stirred in acetone for 30 min followed by furfural addition (Example II) (Fig. 9A). In contrast, the activity of the reconstructed HTC in aldol condensation is significantly lower when the rehydrated catalyst is initially in contact with furfural (Example III). In all three cases F-OH is detected among reaction products proving the occurrence of CR, as discussed above. Nevertheless, its yield is much lower in Examples I and II being 0.10–0.14 wt.% in comparison with Example III (0.64–0.72 wt.%). These experiments give an additional evidence that CR proceeds simultaneously with AC and definitely influences the performance of a basic catalyst in the latter reaction.

CR may contribute not only to the observed activity of basic catalysts in aldol condensation reaction involving furfural but may also affect re-using of the catalysts. The loss of the activity of hydrotalcites and mixed oxides in several successive catalytic runs of condensation reactions has been reported repeatedly. In general, two different deactivation causes have been considered: fouling caused by subsequent aldol condensations and leaching of active compounds from the catalyst in the aqueous medium [20]. The results presented in this study evidence that other reasons could explain the loss of catalyst activity in condensation reactions, for example, the occurrence of Cannizzaro reaction. Under the real experimental conditions of AC, a catalyst is in contact with both components of the reaction mixture (acetone and furfural) and the reaction is usually carried out in excess of acetone. Therefore, the probability of furfural interacting with basic sites that is necessary for CR to take place is low under high Ac to F molar ratio in reaction mixture. As a consequence, the influence of CR on catalyst performance in AC is not pronounced and conventional solid basic catalysts exhibit good activity in AC. Nevertheless, it is not possible to avoid a contact between furfural and basic sites, so the AC and CR take place simultaneously, as evidenced by the formation of furfuryl alcohol even at conventional reaction conditions (Figs. 8 and 9B, Example I). Even the small contribution of CR would result in the progressive deactivation of the catalyst thus decreasing its activity in AC and making it difficult to recycle/reuse the catalyst without an oxidative regeneration step. Therefore, the optimization of catalytic properties and the determination of optimum reaction conditions to perform AC which would allow reducing the influence of CR on catalyst behavior are important objectives of forthcoming studies.

4. Conclusions

The rehydration of Mg-Al mixed oxide (calcined as-prepared hydrotalcite) using pure water results in the formation of reconstructed hydrotalcite that possesses OH^- groups rather than carbonates in interlayer as proved by TGA-MS results. The comparison of DRIFT spectra of the as-prepared and the reconstructed materials allowed concluding that these newly formed hydroxyls are characterized by the band at $1370\,cm^{-1}$ which is usually considered as a characteristic band of carbonate groups. The results also show that Mg-Al mixed oxide can be successively rehydrated with aqueous furfural mixture resulting in the formation of reconstructed hydrotalcite structure. The amount of water in the mixture influences the rehydration degree and the total reconstruction of the hydrotalcite structure is observed only when using biphasic (water-organic) reaction conditions. The catalytic data allow concluding unequivocally that Brønsted basic sites of the reconstructed HTC catalyze furfural transformation by Cannizzaro reaction. Both furfuryl alcohol and furfuryl furoate formed during the reaction are evidenced by GC analysis. On the contrary, furoic acid is not detected among reaction products by routine GC analysis because it remains adsorbed on the basic sites of the catalyst forming surface furoates. These species can be detected by both TGA (a peak in the range of $T = 320\,^{\circ}C$) and DRIFT (characteristic band at $1481\,cm^{-1}$) methods. The formation of the surface furoates leads to a gradual catalyst deactivation, as evidenced by the time dependency of furfural conversion and yield of furfuryl alcohol.

The rehydration of Mg-Al mixed oxide (calcined HTC) with aqueous furfural mixture affords a reconstructed HTC possessing a higher amount of basic sites in comparison with a reconstructed HTC prepared by rehydration of the same Mg-Al mixed oxide with pure water. This is demonstrated by the yield of reaction products formed by CR. It can thus be inferred that the rehydration procedure has a significant influence on the basic properties of the resulting reconstructed material.

The performed comparative experiments show that the Cannizzaro reaction also influences aldol condensation of furfural and acetone. The longer is the contact time between furfural molecules and the basic sites of a catalyst, the lower is the furfural conversion in aldol condensation. Consequently, Cannizzaro reaction would result in the gradual deactivation of the catalyst thus making it difficult to recycle/reuse the catalyst without an oxidative regeneration step.

Acknowledgements

The publication is a result of the project reg. No. GA15-21817S which was financially supported by the Czech Science Foundation of the Czech Republic. The project has been integrated into the National Program for Sustainability of the Ministry of Education, Youth and Sports of the Czech Republic through the project Development of the UniCRE Centre, project code LO1606.

Appendix A. Supplementary data

Supplementary data associated with this article can be found, in the online version, at http://dx.doi.org/10.1016/j.apcata.2016.08.007.

References

[1] J.I. Di Cosimo, V.K. Díez, M. Xu, E. Iglesia, C.R. Apesteguía, J. Catal. 178 (1998) 499–510.
[2] R.K. Allada, A. Navrotsky, H.T. Berbeco, W.H. Casey, Science 296 (2002) 721–723.
[3] A. Corma, S. Iborra, Adv. Catal. 49 (2006) 239–302.
[4] X. Duan, D.G. Evans (Eds.), Layered Double Hydroxides, Structure and Bonding Series, vol. 119, Springer, Berlin, 2006.
[5] D. Tichit, D. Lutic, B. Coq, R. Durand, R. Teissier, J. Catal. 219 (2003) 167–175.
[6] H. Liu, W. Xu, X. Liu, Y. Guo, Y. Guo, G. Lu, Y. Wang, Kinet. Catal. 51 (2010) 75–80.
[7] D.P. Debecker, E.M. Gaigneaux, G. Busca, Chem. Eur. J. 15 (2009) 3920–3935.
[8] A. Corma, S. Iborra, S. Miquel, J. Primo, J. Catal. 173 (1998) 315–321.
[9] Y. Xi, R.J. Davis, J. Catal. 254 (2008) 190–197.
[10] V.K. Diez, C.R. Apesteguia, J.I. Di Cosimo, J. Catal. 215 (2003) 220–233.
[11] D. Tichit, B. Coq, Cattech 7 (2003) 206–217.
[12] S. Abelló, F. Medina, D. Tichit, J. Pérez-Ramírez, J.C. Groen, J.E. Sueiras, P. Salagre, Y. Cesteros, Chem. Eur. J. 11 (2005) 728–739.
[13] D. Tichit, M.N. Bennani, F. Figueras, R. Tessier, J. Kervennal, Appl. Clay Sci. 13 (1998) 401–415.
[14] C. Xu, Y. Gao, X. Liu, R. Xin, Z. Wang, RSC Adv. 3 (2013) 793–801.
[15] K.K. Rao, M. Gravelle, J. Sánchez-Valente, F. Figueras, J. Catal. 173 (1998) 115–121.
[16] B.M. Choudary, M.L. Kantam, C.R.V. Reddy, K.K. Rao, F. Figueras, J. Mol. Catal. A: Chem. 146 (1999) 279–284.
[17] S. Gámez, J.J. González-Cabriales, J.A. Ramírez, G. Garrote, M. Vázquez, J. Food Eng. 74 (2006) 78–88.
[18] T.N. Pham, D. Shi, D.E. Resasco, Appl. Catal. B 145 (2014) 10–23.
[19] C.J. Barrett, J.N. Chheda, G.W. Huber, J.A. Dumesic, Appl. Catal. B: Environ. 66 (2006) 111–118.
[20] L. Faba, E. Díaz, S. Ordóñez, Appl. Catal. B: Environ. 113–114 (2012) 201–211.
[21] S. Abelló, F. Medina, D. Tichit, J. Pérez-Ramírez, J.E. Sueiras, P. Salagre, Y. Cesteros, Appl. Catal. B: Environ. 70 (2007) 577–584.
[22] S. Cannizzaro, Ann. Chem. Pharm. 88 (1853) 129–130.
[23] I. Sádaba, M. Ojeda, R. Mariscal, J.L.G. Fierro, M. López Granados, Appl. Catal. B: Environ. 101 (2011) 638–648.
[24] P.A. Zapata, J. Faria, M. Pilar Ruiz, D.E. Resasco, Top. Catal. 55 (2012) 38–52.
[25] L. Hora, V. Kelbichová, O. Kikhtyanin, O. Bortnovskiy, D. Kubička, Catal. Today 223 (2014) 138–147.
[26] W.V. Evans, M.B. Aylesworth, Ind. Eng. Chem. 18 (1926) 24–27.
[27] A. Morato, C. Alonso, F. Medina, Y. Cesteros, P. Salagre, J.E. Sueiras, D. Tichit, B. Coq, Appl. Catal. B: Environ. 32 (2001) 167–179.
[28] F. Prinetto, G. Ghiotti, P. Graffin, D. Tichit, Microporous Mesoporous Mater. 39 (2000) 229–247.
[29] J.T. Kloprogge, R.L. Frost, Phys. Chem. Chem. Phys. 1 (1999) 1641–1647.
[30] F. Prinetto, G. Ghiotti, R. Durand, D. Tichit, J. Phys. Chem. B 104 (2000) 11117–11126.
[31] F. Millange, R.I. Walton, D. O'Hare, J. Mater. Chem. 10 (2000) 1713–1720.
[32] S.K. Sharma, P.A. Parikh, R.V. Jasra, Appl. Catal. A: Gen. 386 (2010) 34–42.
[33] M.D. Ureña-Amate, N.D. Boutarbouch, M. del Mar Socias-Viciana, E. González-Pradas, Appl. Clay Sci. 52 (2011) 368–373.
[34] M.F. Beegum, L.U. Kumari, B. Harikumar, H.T. Varghese, C.Y. Panicker, J. Rasayan, Chemistry 1 (2008) 117–124.

Waste Biomass Valor (2010) 1:293–308
DOI 10.1007/s12649-010-9032-8

Utilization of Triglycerides and Related Feedstocks for Production of Clean Hydrocarbon Fuels and Petrochemicals: A Review

Iva Kubičková · David Kubička

Received: 28 February 2010 / Accepted: 20 July 2010 / Published online: 5 August 2010

Abstract Catalytic deoxygenation of triglycerides and related feedstocks for production of biofuels is reviewed in this paper. Green diesel, triglyceride-based hydrocarbons in diesel boiling range, is an attractive alternative to biodiesel—a product of transesterification of vegetable oils, particularly due to its superior fuel properties and full compatibility with current diesel fuels. Two basic approaches to production of green diesel—(i) hydrodeoxygenation of triglycerides and related compounds over metal sulfide catalysts and (ii) deoxygenation over supported noble metal catalysts are thoroughly discussed from the point of view of reaction conditions, catalyst composition and reaction pathways and products. Furthermore, catalytic cracking of triglycerides and related feedstocks over microporous and mesoporous catalysts is reviewed as well. It constitutes an interesting alternative to deoxygenation using hydrotreating and noble metal catalysts as it does not consume hydrogen. It provides a wide spectrum of products reaching from olefins to green gasoline and diesel.

Keywords Biofuels · Vegetable oils · Triglycerides · Deoxygenation · Decarboxylation · Hydrodeoxygenation · Noble metal catalysts · Sulfided metal catalysts · Zeolites

Introduction

Biofuels and their production and consumption have become an inherent part of everyday life worldwide. Any fuel of biological origin can be in principle called biofuel. For the sake of clarity, we shall use the term biofuel exclusively for liquid transportation fuels produced from renewable (biological) feedstocks in this review.

The use of biofuels has been promoted and supported in the recent years, as it can contribute to (i) decreasing of CO_2 emissions from fossil energy sources, (ii) (renewed) development of rural areas and (iii) partial reduction of the complete dependence of world economy on the ever declining fossil energy resources, particularly petroleum and natural gas [1–7], the main feedstocks used for production of transportation fuels. Due to the dispersed nature of emissions originating from transportation and their increasing amount [8], as a result of the continually wider spread of road as well as air transport [3, 4], these emissions are difficult to tackle. In addition to increasing the efficiency of the internal combustion engines, constant enhancing of the fuel quality is an indispensable tool. Biofuels play an important role in the fuel quality improvement, as they can be denoted clean fuels since they do not usually contain aromatics and sulfur [2] and may improve some performance characteristics of automotive fuels, e.g. octane number (bioethanol) and cetane index (biodiesel) [1, 7].

Biofuels are currently classified as the first generation and the second generation biofuels [1, 3, 4, 7, 8]. Typical first generation biofuels are bioethanol obtained by fermentation of sugars (i.e. either from sugarcane or from corn, sugar beet, wheat etc.) and biodiesel produced by transesterification of vegetable oils with methanol [3, 7, 8]. Lignocellulosic bioethanol and fuels produced from biomass-derived synthesis gas, i.e. mixture of CO and H_2, are usually called second generation biofuels [4, 7, 8]. Nevertheless, the definition of the second generation biofuels is not strict. Rather than to technological development/maturity, it should refer to environmental benefits and

---

I. Kubičková · D. Kubička (✉)
Department of Refinery and Petrochemical Research, Research Institute of Inorganic Chemistry (VUANCH, a.s.), Areál Chempark, Záluží 1, 436 70 Litvinov, Czech Republic
e-mail: david.kubicka@vuanch.cz

sustainability of different biofuels, i.e. to their greenhouse gas emissions and cumulative energy-demand (fossil) savings over the whole life cycle. Consequently, the same biofuel, e.g. bioethanol, produced at two different locations could be considered as second generation biofuel in one of them and first generation biofuel in the other.

Owing to their chemical composition and physico-chemical properties, triglycerides were used to fuel the first diesel engines (soybean oil in 1920s) [7]. After decades dominated by the cheaper hydrocarbon-based fuels derived mainly from petroleum and to a lesser extent from coal, a renewed interest in alternative (renewable) feedstocks for fuel production led inevitably to development of triglyceride-based fuels and fuel components [1]. Since the high density and viscosity prevent the direct use of triglycerides as fuels for the modern diesel engines [7, 9], alternative approaches have been sought. Until now, two basic concepts have been applied industrially—transesterification and hydrotreating [10].

The product of transesterification of vegetable oils (Fig. 1), typically rapeseed, soybean and palm oil, with methanol that complies with the appropriate quality standard (e.g. EN 14214 [11]) is called biodiesel or FAME (fatty acid methyl esters). Biodiesel is along with bioethanol the most important biofuel of the so-called first generation and it is mostly popular in Europe due to the suitable climatic conditions for production of rapeseed and the highest share of diesel-engine-driven cars in the world. The production of biodiesel has been extensively reviewed over the past years [12–14]. The main advantages of this process are its simplicity and mild reaction conditions allowing small-scale production practically anywhere. On the other hand, it suffers from several drawbacks, the most important being the use of a homogenous catalyst and the need of its neutralization and separation and production of glycerol of a rather low quality as a by-product. The newly developed process that uses a heterogeneous solid catalyst can tackle these disadvantages as there is no need to neutralize and separate the catalyst and consequently high purity glycerol is obtained [15].

However, there exist other disadvantages of biodiesel related to its fuel properties that cannot be easily dealt with. The main drawbacks include low thermal and oxidation stability in comparison with ordinary diesel fuel, which limit the use of biodiesel in the modern diesel engines to low concentration biodiesel-diesel mixtures (up to 7 vol%, [11]). The efforts aimed at increasing efficiency of the diesel engines led to application of higher injections pressures and smaller injection nozzles diameters. Under these conditions biodiesel tends to polymerize and form deposits on the nozzles that can cause their plugging. Consequently, the safe use of neat biodiesel or high concentration biodiesel–diesel blends requires approval of the engine manufacturer [16].

The chemical nature of biodiesel has to be changed to deal efficiently with the stability issues discussed above. Upgrading of triglycerides into hydrocarbons constitutes a promising alternative to transesterification. Even though the product of this upgrading could be in principle called biodiesel, we shall call it green diesel in this review to stress its different chemical nature and avoid confusion as the term biodiesel is widely accepted as a synonym for fatty acid methyl esters.

Conversion of triglycerides into hydrocarbons necessitates elimination of oxygen from the feedstock, i.e. deoxygenation. Deoxygenation, as a general term for oxygen elimination, can refer to different chemical reactions. In the case of triglycerides, these include hydrodeoxygenation and hydrodecarboxylation (Fig. 1) [17, 18]. Hydrodeoxygenation consists of several consecutive reaction steps, in which oxygen is removed in the form of water and the resulting *n*-alkane has the same number of carbon atoms as the corresponding fatty acid bound in the original triglyceride. Hydrodecarboxylation refers to a process where oxygen is removed as CO_2 by decarboxylation of fatty acid reaction intermediate formed by hydrotreating of the corresponding triglyceride. Consequently, the resulting *n*-alkane has one carbon atom less than the corresponding fatty acid bound in the original triglyceride [17, 18]. In contrast to hydrodecarboxylation, decarboxylation proceeds only in carboxylic

Fig. 1 A simplified scheme of the main reaction paths in transformation of triglycerides into biofuels via catalytic processes; (*1*) transesterification, (*2*) hydrodeoxygenation, (*3*) hydrodecarboxylation, (*4*) decarbonylation

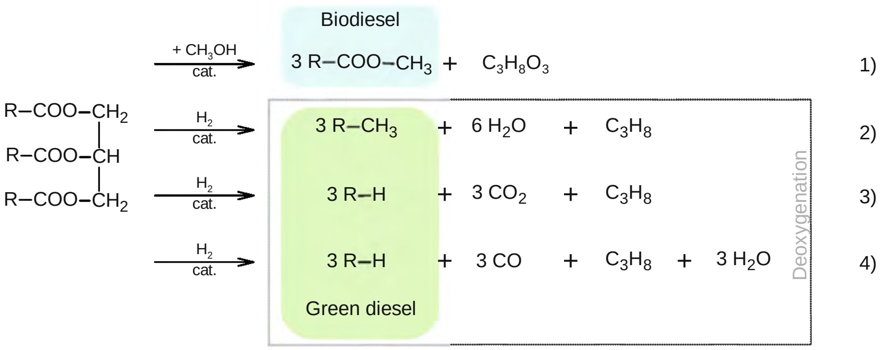

acids and does not involve reaction with hydrogen [17, 18]. Moreover, decarbonylation has been proposed as a plausible reaction in transformation of triglycerides into hydrocarbons (Fig. 1) [19]. In general, these reactions could be denoted as selective deoxygenation since oxygen is eliminated either in form of water or CO_2 and the molecular weight of the product corresponds to that of the alkyl chains of fatty acids bound in triglycerides. In addition to selective deoxygenation, oxygen can be eliminated from triglycerides by non-selective deoxygenation, i.e. by their cracking that results in formation of shorter chain oxygenates, hydrocarbons and CO_2. The hydrocarbons obtained in non-selective deoxygenation consist, besides alkanes, of naphthenes and aromatics, formed by secondary reactions.

Production of hydrocarbons from triglycerides is now accomplished also commercially [20, 21] in a process called NexBTL (Neste Oil, Porvoo, 2 × 170 kt/a) and other production units have been announced [21]. Other companies (e.g. Petrobras, Eni + UOP) have announced or patented production of green diesel (hydrocarbons) from triglycerides [22–26]. Nevertheless, the production capacity of biodiesel (ca. 21 Mt/a in Europe, with production ca. 7.7 Mt/a in 2008 [27]) is currently significantly larger than the production of green diesel (0.34 Mt/a [28]), i.e. the product of hydrotreating of triglycerides.

Recently, several reviews dealing with upgrading of biomass to fuels and chemicals [1, 29–32] and specific reviews focusing primarily on biodiesel production [12, 13], deoxygenation in general [33] and upgrading of triglycerides into biodiesel and/or green hydrocarbons [10, 34] have been published. In this contribution, we aim at reviewing of deoxygenation chemistry and processes used for upgrading of triglycerides and related feedstocks, such as fatty acids, into green hydrocarbons (e.g. green diesel). The review will be divided into three main sections based on the nature of catalysts used. In the first part, deoxygenation of triglycerides and related feedstocks, mainly fatty acids and their monoesters, over supported noble metal catalysts, particularly Pd and Pt, will be discussed. The second section will focus on the use of conventional hydrotreating catalysts, i.e. NiMo, CoMo, NiW sulfides, in triglycerides upgrading to hydrocarbons and the activity and selectivity of these catalysts. The final part will review the performance of micro- and mesoporous molecular sieves in cracking of triglycerides to hydrocarbon fractions.

Supported Noble Metal Catalysts

Supported noble metals, such as Pt, Pd, Ru, are a versatile class of catalysts that are applied in different industrial processes, the most important being various hydrogenations, including selective hydrogenations of oxygenated intermediates to produce fine chemicals [31], and isomerization, hydrocracking, cyclization and dehydrogenation of hydrocarbons [35, 36]. The supported noble metal catalysts were proposed to be efficient deoxygenation catalysts [37] and their activity and selectivity were studied comprehensively by Murzin et al. [34, 38–46]. The group was even awarded a patent covering the method of hydrocarbon production by using noble metal catalysts [47, 48].

Stearic acid was used as the principle model compound to study deoxygenation using noble metal catalysts [38, 39, 41] as it is a typical reaction intermediate in deoxygenation of triglycerides [10, 17, 18, 38, 41] (Table 1). A wide variety of supported metal catalysts was investigated to find the most promising metal-support combinations active in deoxygenation of stearic acid [39]. Pt and Pd supported on active carbon were the only catalysts providing significant yield of desired deoxygenation products. These consisted almost exclusively of a mixture of C_{17} hydrocarbons among which *n*-heptadecane was the most abundant product. It was accompanied by 1-heptadecene and other C_{17} isomers [38, 39]. In addition to Pt/C and Pd/C, Ru supported on MgO exhibited under the same reaction conditions (N_2, 300°C, 0.6 MPa) almost complete conversion of stearic acid, however, formation of C_{17} hydrocarbons was not observed. Instead, a condensation product of two stearic acid molecules (a symmetrical ketone C_{35}) was formed (Fig. 2) [39]. Besides Pd/C, Pd supported on SBA-15 was shown to be active and selective in stearic acid deoxygenation, in fact TOF on Pd/SBA-15 was higher than that on Pd/C (0.72 vs. 0.13 s^{-1}) [45], however in the case of Pd/C the TOF is based on Pd loading rather than on exposed Pd atoms. The other tested supported metal catalysts gave much lower conversion of stearic acid (<50%) under the above-mentioned reaction conditions [39].

Interestingly, formation of the symmetric ketone (Fig. 2) was observed on Pt and Pd supported on alumina, suggesting that the support plays a crucial role in determining the selectivity as Ru/C provided predominantly C_{17} hydrocarbons [39]. The formation of the ketone was observed also in presence of hydrogen over Pt/Al_2O_3 and Pt/TiO_2 where it was accompanied by formation of an ester (octadecyl stearate, Fig. 2) [49]. The formation of condensation products was ascribed to the catalytic role of the oxide support under hydrogen-deficient environment, i.e. when hydrogen spill-over could occur thanks to the presence of Pt, the formation of condensation products was greatly suppressed [49]. Presence of vacancy oxygen sites plays an important role in determining the selectivity towards condensation products. It was shown that Pt supported on TiO_2, i.e. a support having more oxygen vacancy sites than Al_2O_3, favors the formation of symmetrical ketones from acids and esters in comparison with Pt/Al_2O_3.

Table 1 An overview of reaction conditions and catalysts used for deoxygenation of triglycerides and related feedstocks over supported noble metal catalysts

Model compound	Catalyst	Reaction conditions	Reference
Fatty acids			
Stearic acid	Pd/C	He, H_2–Ar, H_2; 300°C; 1.7 MPa; SBR	[38, 41]
Caprylic acid	Pd/C ($NiMo/Al_2O_3$)	H_2–He; 300–400°C; 2.1 MPa; FBR	[50]
Various acids (i.e. heptanoic, octanoic)	Pd/SiO_2 (Ni/Al_2O_3)	H_2, N_2; 330°C, atm.; FBR	[37]
Stearic, oleic, linoleic acids	Pd/C	He, H_2–He; 300°C; 1.5 MPa; SBR	[51]
Stearic acid	Various catalysts	N_2; 300°C; 0.6 bar; SBR	[39]
Oleic, linoleic acids	Pd/C	Ar, H_2–Ar; 300–360°C; 1.5–4.2 MPa; SBR	[43]
Esters			
Ethyl stearate	Pd/C	He, H_2–Ar, H_2; 300–360°C; 1.7–4 MPa; SBR	[38, 41]
		He, N_2, H_2–Ar, H_2; 300–320°C; 0.6–1.7 MPa; SBR	[38, 41]
Methyl octanoate	Pt/Al_2O_3; Pt/TiO_2	H_2–He; 330°C, atm.; FBR	[49]
Methyl stearate	Pt/Al_2O_3	H_2–He; 300–350°C; 0.7 MPa; SBR	[49]
Triglycerides			
Tristearin	Pd/C,	He, H_2–Ar, H_2; 300–360°C; 1.7–4 MPa; SBR	[38]
Tricaprylin	Pd/C, ($NiMo/Al_2O_3$)	H_2–He, 300–400°C, 2.1 MPa, FBR	[50]

SBR semi-batch reactor, *FBR* fixed bed reactor

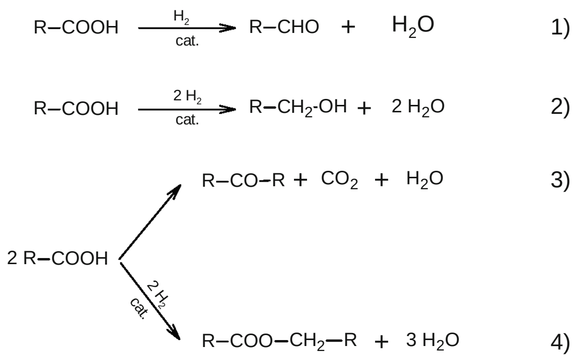

Fig. 2 A simplified scheme of partial deoxygenation reactions of fatty acids; (*1*, *2*) partial hydrogenation (deoxygenation), (*3*) condensation, (*4*) esterification

Moreover, these vacancies were reported to be responsible for the significantly higher formation of C_8 hydrocarbons in methyl octanoate deoxygenation over Pt/TiO_2 in comparison with Pt/Al_2O_3. This is a consequence of higher C–O cleavage activity of Pt/TiO_2 [49]. Further evidence of the role of catalytically active oxide phase was provided, when a commercial $NiMo/Al_2O_3$, i.e. non-sulfided oxide-phase catalyst, was used in hydrogen-rich environment. Hydrogenation products were formed at the expense of decarboxylation/decarbonylation products [50].

Owing to the low acidity of the used supports (C, SiO_2, Al_2O_3), cracking was negligible with Pt, Pd, Rh, Ir (selectivity <5%), but it was pronounced when Ni catalysts were used (selectivity >15%) [39]. Similarly, cracking was virtually absent in deoxygenation of methyl stearate over Pt/Al_2O_3 [49]. It can be hence concluded that supported Pt and Pd catalysts are efficient deoxygenation catalysts yielding with high selectivity hydrocarbons that have one carbon atom less than the corresponding fatty acid or fatty acid part of an ester, i.e. the feed undergoes either decarboxylation or decarbonylation.

The effect of Pd dispersion on deoxygenation of a mixture consisting of palmitic (59 mol%) and stearic acid (40 mol%) was investigated using four 1 wt% Pd/C (sibunit) catalysts under standard deoxygenation conditions (300°C, 1.7 MPa, dodecane solvent). Their Pd dispersions were in the range 18–72% [46]. The effect of Pd dispersion was significant. The catalysts with the lowest and highest dispersion showed the lowest initial deoxygenation rate (TOF = 30 and 12 s^{-1}, respectively) while the catalysts with medium dispersion exhibited significantly higher initial reaction rates (TOF = 76 and 109 s^{-1} for Pd dispersions 47 and 65%, respectively) [46]. These results suggest that there is an optimum Pd crystallite size. The low activity of highly dispersed Pd was attributed to strong interaction of Pd crystallites with the support [46]. Furthermore, the acidity/basicity of Pd/C catalysts (determined by the pH measurement of catalyst slurry) was reported to affect deoxygenation of ethyl stearate [41].

The important consequence of the decarboxylation/decarbonylation reaction route proposed for supported noble metal catalysts is that deoxygenation of fatty acids and/or esters (including triglycerides) does, in principle, not require presence of hydrogen atmosphere [38, 39]. This constitutes a significant advantage over hydrogenation-based processes, such as those using hydrotreating catalysts, due to the suppressed hydrogen consumption. On the other hand, the elimination of one carbon atom per one fatty acid in order to form CO or CO_2 results, however, in lower hydrocarbon yield, on weight basis, as compared with the hydrogenation processes. Even though high conversion of stearic acid and its esters was observed under inert atmosphere (N_2, He), presence of hydrogen was found to be beneficial for catalyst stability [38, 49, 51].

It was demonstrated that when inert atmosphere (He) was replaced by hydrogen atmosphere, the conversion of methyl octanoate immediately increased to the levels observed during deoxygenation carried out under hydrogen atmosphere [49]. The fast deactivation in inert atmosphere was ascribed to formation of heavy products and unsaturated hydrocarbons that took part in oligomerization reactions leading eventually to coke formation. Owing to fast saturation of unsaturated intermediates under hydrogen atmosphere, the fast catalyst deactivation was greatly diminished [49]. Similar results were reported also for fixed-bed deoxygenation of stearic acid over Pd/C (360°C, 1 MPa, Ar or 5% H_2 in Ar) where stable conversion was achieved only in presence of H_2 [52].The effect of hydrogen concentration in the reaction atmosphere was studied in ethyl stearate deoxygenation [41]. With decreasing H_2 concentration (different H_2/He mixtures) the initial reaction rate decreased as did the selectivity to *n*-heptadecane. At the same time, the selectivity to stearic acid, i.e. an intermediate in ethyl stearate deoxygenation, was increasing [41]. This suggests that ethyl stearate yields primarily stearic acid which is subsequently deoxygenated and that higher partial pressure of hydrogen is beneficial for the subsequent reaction step. Since ethyl stearate was reported to decompose to ethylene and stearic acid in absence of catalyst at temperatures around 300°C [53], the positive effect of hydrogen could be attributed to preservation of the catalyst activity due to hydrogenation of unsaturated reaction intermediates as observed in methyl octanoate deoxygenation [49].

In contrast to studies performed with esters of saturated fatty acids, an optimum hydrogen concentration in the reaction gas was reported for fatty acids [38, 51]. In semi-batch operation the conversion of stearic acid increased when instead of pure hydrogen atmosphere a mixture containing 5% H_2 in Ar [38] or 10% H_2 in He [51] was used. Furthermore, the initial reaction rate of stearic acid conversion was higher in He then in 10% H_2 in He. Nevertheless, under inert atmosphere the reaction rate dropped significantly after ca. 10 min [51], presumably due to catalyst deactivation as observed in the case of fatty esters deoxygenation discussed above. It was proposed that the inhibition of stearic acid deoxygenation at high hydrogen partial pressure may be a consequence of competitive dissociative adsorption of stearic acid and hydrogen [51]. The presence of adsorbed hydrogen leads to fast hydrogenation of the adsorbed carboxylate, a product of carboxylic acid dissociative adsorption, before it can undergo decarboxylation [54].

The importance of hydrogen on deoxygenation of carboxylic acids was further confirmed by studies using different solvents [41, 51]. It was proposed that some solvents may act as hydrogen donors and consequently affect deoxygenation. Dodecane was found to undergo dehydrogenation (conversion ca. 2%) over Pd/C under typical deoxygenation conditions (300°C, 1.5 MPa) and hydrogen was formed [51]. Analogously, the initial rate of formation of stearic acid from ethyl stearate in inert atmosphere was higher in dodecane than in mesitylene [41]. The difference could be explained by the different nature of the solvents used. While dodecane can act as hydrogen-donor solvent, mesitylene cannot. The initial rate of *n*-heptadecane formation remained, however, unaltered by the solvent change [41] suggesting that the initial deoxygenation was not affected by hydrogen availability.

Unsaturated fatty acids and their esters are relevant probe molecules for deoxygenation (Table 1) since majority of fatty acids bound in naturally occurring triglycerides have at least one double bond [55]. As expected, hydrogen plays an important role in their transformation to hydrocarbons. It was demonstrated that the double bond hydrogenation of oleic and linoleic acid precedes their deoxygenation in hydrogen-rich atmosphere [43, 51]. Consequently, *n*-heptadecane was the main reaction product. While the kinetics of stearic and oleic acid deoxygenation were indistinguishable under 10% H_2 in He, under He atmosphere deoxygenation of oleic acid was significantly slower [51]. The authors propose that the lower deoxygenation rate in absence of hydrogen is due to *cis*-C–C double bond adsorption [51], which may compete with carboxylic group adsorption. Moreover, under hydrogen-deficient conditions, dehydrogenation of fatty acids occurs yielding polyunsaturated acids and aromatics and consequently resulting in faster catalyst deactivation [43]. The reported high selectivity to methyl stearate in methyl oleate deoxygenation (300°C, 1.5 MPa, Pd/C) under different atmospheres (Ar, 5% H_2 in Ar, H_2) suggests that hydrogen transfer plays an important role as well [43].

Deoxygenation of different fatty acids (C_{17}–C_{22}) in dodecane under argon (300°C, 1.7 MPa, Pd/C) was shown to be independent of their chain length; the initial deoxygenation rate of C_{17}, C_{18} and C_{20} fatty acids was virtually identical [56]. Same conclusion was reached also for deoxygenation of palmitic and stearic acid under 5% H_2 in Ar [46]. The different rate of deoxygenation observed in the case of the C_{19} and C_{22} fatty acids was attributed to their impurities, i.e. unsaturated fatty acids and phosphorus, respectively. The final conversion dropped from about 90% to approximately 20% when the mentioned impurities were present [56].

Gaseous products formed and detected during deoxygenation of fatty acids could provide essential information about its reaction mechanism over noble metal catalysts. Nevertheless, due to facile reactions of CO, CO_2, H_2 and H_2O on catalyst surface, the observed composition of gas phase is difficult to interpret unambiguously and several proposals have been put forward [37, 39, 50, 51]. Moreover, the mechanism may be strongly affected by catalyst choice and reaction conditions, particularly reaction atmosphere (inert or H_2). The fundamental and yet not fully understood issue concerns formation of hydrocarbons having one carbon atom less than the original fatty acid. Both decarboxylation and decarbonylation have been proposed to explain formation of these hydrocarbons [37, 39, 49–51]. On the other hand, it is widely accepted that hydrocarbons with the same carbon atom number as the original fatty acids are produced by consecutive hydrogenation steps where the formation of reaction intermediates (aldehydes and alcohols) is accompanied by formation of water [39, 49–51].

Carbon dioxide was detected as a major gaseous product in deoxygenation of several carboxylic acids on Pd/SiO_2. Its formation was explained by α–β adsorption of primary and secondary acids followed by the adsorbed C–C bond hydrogenolysis and hydrogen-assisted desorption of the corresponding hydrocarbon and CO_2 [37]. In contrast, no significant amount of CO_2 was obtained in deoxygenation of caprylic acid under H_2 atmosphere [50]. Bimolecular reaction between adsorbed caprylic acid and hydrogen yielding *n*-heptane, CO and water was proposed. It was suggested that the initial hydrogenolysis of caprylic acid to adsorbed *n*-heptane and formic acid is followed by fast decomposition of formic acid to CO and water [50]. Parallel formation of CO_2 and CO was observed in deoxygenation of oleic and stearic acids with CO_2 being the predominant gaseous product both under He and 10% H_2 in He atmosphere ($CO_2/CO = 8$–9) [51]. The CO_2 yield (in He) was higher than expected from the yield of *n*-heptadecane. It was hence suggested that part of the primarily formed CO underwent reaction with adsorbed water (formed in decarbonylation) yielding CO_2 and H_2 [51]. When 10% H_2 in He was used as reaction atmosphere, only *n*-heptadecane was observed in the liquid phase, i.e. no heptadecenes were detected. However, the gas phase contained both CO and CO_2 [51]. This could be explained either by hydrogenation of heptadecenes from decarbonylation [51] or by partial hydrogenation of CO_2 from decarboxylation [52].

Composition of gaseous products from triglyceride deoxygenation is similar to that of fatty acid deoxygenation as a facile hydrogenolysis of triglycerides yielding fatty acids and propane precedes the actual deoxygenation [50]. In addition to hydrogenolysis, direct decarboxylation/decarbonylation of methyl octanoate was suggested for its gas-phase deoxygenation [49].

Supported Metal Sulfides Catalysts

Supported metal sulfides catalysts belong to the most important industrial catalysts as they are used in hydrotreating and hydrocracking applications to remove sulfur and nitrogen from petroleum fractions [57]. Moreover, the first hydrotreating catalysts were developed for upgrading of coal-derived liquids that contain, in contrast to petroleum feedstock, significant amounts of oxygenated compounds [58]. It is therefore not surprising that they have been suggested to be suitable catalysts for deoxygenation of renewable feedstocks (Table 2) [10, 17, 19, 59, 60]. In fact, the up-to-date the only industrial application of triglyceride deoxygenation relies on the use of supported metal sulfide catalyst [20].

The reactivity of oxygenated compounds in deoxygenation over sulfided catalysts differs significantly. The most challenging is deoxygenation of heterocyclic compounds (furanes) and phenols that usually require reaction temperatures above 350°C [33, 61]. On the other hand, alcohols, aldehydes and ketones can be deoxygenated rather easily, typically at temperatures below 250°C [33, 61]. All these types of oxygenated compounds are present in bio-oils and their different reactivity/stability makes the deoxygenation of bio-oils very demanding [61, 62]. On the contrary, feedstocks containing triglycerides and fatty acids are characterized by a rather uniform composition and intermediate reactivity among oxygenated compounds. Temperatures just below 300°C are sufficient to accomplish their complete deoxygenation [61].

Early studies with model compounds (diethyl sebacate, ethyl decanoate, decanoic acid) indicated that esters of carboxylic acids are more prone to deoxygenation than acids [17]. It was shown that deoxygenation of acids and their esters involve two parallel reaction pathways—(i) hydrodeoxygenation and (ii) hydrodecarboxylation of esters or decarboxylation of acids [17]. Similar product distribution has been observed also for deoxygenation of triglycerides [18, 19, 63] as well as other esters and acids [63–65]. The main products were, in all cases, *n*-alkanes having either the same number of carbon atoms (hydrodeoxygenation) as or one carbon atom less (hydrodecarboxylation/decarboxylation) than the original acid, regardless whether it was a free acid or acid bound in an ester [17–19, 63]. The origin of triglycerides, in particular their degree of unsaturation, has been shown to influence significantly the product distribution; with increasing degree of unsaturation the products contained higher concentrations of cyclic hydrocarbons, mainly alkylnaphthenes

Table 2 An overview of reaction conditions and catalysts used for deoxygenation of triglycerides and related feedstocks over supported metal sulfide catalysts

Model compound	Catalyst	Reaction conditions	Reference
Fatty acids			
Decanoic acid	NiMo/Al_2O_3	H_2; 280°C; 7 MPa; FBR	[84]
Esters			
Methyl laurate	NiMoP/Al_2O_3	H_2; 300°C; 5 MPa; FBR	[63]
Diethyl sebacate	NiMo/Al_2O_3, CoMo/Al_2O_3	H_2; 260–300°C; 7 MPa; FBR	[84]
Methyl heptanoate	NiMo/Al_2O_3, CoMo/Al_2O_3	H_2; 250°C; 1.5 MPa; FBR	[64, 65]
	NiMo/Al_2O_3	H_2; 250°C; 7.5 MPa; BR	
Vegetable oils			
Rapeseed oil/gas oil mixture	NiMo/Al_2O_3	H_2; 350°C; 4.5 MPa; FBR	[63]
Rapeseed oil	NiMo/Al_2O_3, CoMo/Al_2O_3, Ni/Al_2O_3, Co/Al_2O_3	H_2; 250–310°C; 0.7–7 MPa; FBR	[18, 67, 74]
	NiMo/Al_2O_3	H_2; 310–360°C; 7–15 MPa; FBR	[28]

BR batch reactor, *FBR* fixed bed reactor

[66]. The reaction conditions as well as the nature of the catalyst were found to affect the product distribution, i.e. the extent of hydrodeoxygenation and hydrodecarboxylation/decarboxylation [17, 18].

Under identical reaction conditions (280–310°C) an increase in overall hydrogen pressure (from 0.7 to 7 MPa) suppressed hydrodecarboxylation of triglycerides at the expense of their hydrodeoxygenation [10, 67]. On the other hand, increasing reaction temperature (from 280 to 310°C) promoted hydrodecarboxylation over hydrodeoxygenation at constant pressure (7 MPa) [10, 17, 18]. These findings were also supported by thermodynamic calculations [68]. However, the influence of reaction conditions is greatly affected by the choice of the catalyst. The effect of temperature increase, i.e. promotion of hydrodecarboxylation over hydrodeoxygenation, has been found to be more pronounced over NiMo than CoMo catalysts [17] while NiW catalyst has shown significantly higher sensitivity to reaction pressure changes than NiMo and CoMo catalysts [10]. Moreover, it was demonstrated that the yield of decarboxylation products from carboxylic acids exceeds that of hydrodecarboxylation products from esters of the corresponding acid [17].

In the case of triglycerides, fatty acids and alcohols were observed as reaction intermediates [18] while in the case of shorter chain esters, e.g. methyl heptanoate, in addition to acids and alcohols, traces of aldehydes were found as well [64, 65]. The formation of aldehydes is not surprising since they are plausible reaction intermediates of carboxylic acids hydrogenation to alcohols. Nonetheless, it does not confirm the decarbonylation pathway in deoxygenation of carboxylic acids and their esters, which has been proposed by several researchers [19, 69]. Under reaction conditions of triglycerides deoxygenation (ca. 260–300°C, 1–7 MPa, NiMo) the main oxygenated reaction intermediates, fatty alcohols and acids, tend to undergo esterification, a competing reaction to deoxygenation, and form corresponding esters and water (Fig. 2) [18, 70]. As water is released during this reaction, it could be considered as a partial deoxygenation reaction since the ester undergoes subsequently deoxygenation as any other ester.

Formation of *n*-alkanes in deoxygenation reactions is accompanied by formation of water and CO_2/CO, the primary products of hydrodeoxygenation and hydrodecarboxylation/decarboxylation, respectively [18, 60, 63]. However, CO_2 can undergo subsequent hydrogenation under typical hydrotreating conditions leading to carbon monoxide and ultimately methane [63], which increases hydrogen consumption. In the specific case of triglycerides, propane is formed during deoxygenation from the glycerol backbone [18, 63].

In addition to standard hydrotreating catalysts (NiMo, CoMo sulfides), the performance of individual sulfides (Ni, Mo) has been investigated to understand in more detail the role of individual components of hydrotreating catalysts on their selectivity [18]. Salient differences in activity and selectivity have been observed. The monometallic sulfide catalysts were less active than the bimetallic ones, with Ni sulfide catalyst being the least active. This is in agreement with the activity trends reported for hydrodesulfurization [57, 58]. Hence, Ni acts as a promoter in the NiMo sulfide catalysts during deoxygenation [18]. While NiMo sulfide catalyst yielded both hydrodeoxygenation and hydrodecarboxylation products in conversion of rapeseed oil, Ni sulfide catalyst yielded exclusively hydrodecarboxylation products and Mo sulfide catalyst almost exclusively hydrodeoxygenation products [18]. A higher selectivity of Ni and Co sulfides to decarboxylation in comparison with MoS_2 was reported previously also by Landa and Weisser [58]. This suggests that the different electronic properties of the individual metal sulfides [71, 72] affect the adsorption of triglycerides and consequently the preferred deoxygenation pathway [18]. Moreover, unsupported MoS_2 catalysts with different degree of stacking, i.e. with different morphology, were shown to affect the selectivity in hydrodeoxygenation of phenols. Hydrogenation was favored by higher degree of stacking (exfoliated MoS_2) while lower degree of stacking favored hydrogenolysis. The exfoliated MoS_2 catalyst exhibited also the highest activity (per edge Mo site) [73].

The activity of hydrotreating catalysts is affected by the nature of the support and its properties [57]. Several efforts to understand the role of support on the activity and selectivity metal sulfides catalysts used for deoxygenation of triglycerides were reported [67, 74]. Specifically, mesoporous materials have shown great potential as catalyst supports [75, 76] and have been reported to provide some advantages over conventional alumina support in hydrotreating applications [77, 78]. Organized-mesoporous-alumina-supported CoMo sulfided catalysts gave higher conversion of triglycerides than industrial-alumina-supported CoMo under the same reaction conditions (250–310°C, 7 MPa) [74]. In contrast, Si–MCM-41-supported CoMo sulfided catalyst showed significantly worse performance than any of the alumina-based catalysts. The yield of hydrocarbons was only ca. 40% for CoMo/Si–MCM-41 at 290°C, while yields over >90% were achieved when alumina-supported catalysts were used. It was suggested that this is due to the differences in interactions between the active phase and support originating from the differences in support composition [67, 74]. Incorporation of Al in MCM-41 support enhanced the activity of the CoMo sulfided catalyst in comparison with Si–MCM-41-supported CoMo catalyst; however the deoxygenation activity remained lower than that of alumina supports [67].

Deactivation of the metal sulfide catalysts during deoxygenation of triglycerides and related feedstocks is of vast importance, particularly because these catalysts strive for sulfur, which is in the typical triglyceride feedstocks virtually absent, to avoid reduction of the sulfide phase and hence to keep their activity [57, 58]. Indeed, the conversion of rapeseed oil over a $NiMo/Al_2O_3$ sulfided catalyst decreased rapidly (from 100% to ca. 85% after 144 h time-on-stream) in absence of hydrogen sulfide source [79]. On the other hand, when dimethyldisulfide was added to rapeseed oil, complete conversion and full selectivity to hydrocarbons was preserved over long time-on-stream (ca. 250 h) [79]. Alternatively, mixing of triglyceride-rich feedstock in a primary petroleum-derived feedstock, i.e. sulfur containing fraction such as straight-run gas oil, could be used to avoid the addition of dimethyldisulfide or another hydrogen sulfide source. Despite co-processing, i.e. upgrading of triglycerides together with petroleum fractions, was demonstrated to be feasible [19, 80, 81], it was argued that there are drawbacks that make it inferior to stand-alone processing of triglycerides followed by their blending to petroleum-derived diesel fuels [82, 83]. These include mainly reduced process flexibility as additional issues have to be dealt with (e.g. sulfur content of the final product, effect of water and carbon oxides on the catalyst lifetime, separation of carbon oxides from the recycle gas, etc.) [82, 83]. Consequently, most refiners seem to favor stand-alone triglyceride processing [20, 21, 23, 82, 83].

The stand-alone processing of triglycerides into diesel-fuel-range hydrocarbons allows enhancing the fuel quality as the primary green diesel has poor cold flow properties [28] and cannot be therefore used directly in diesel fuel blending, but in low blending concentrations. It has been demonstrated that cold-flow-properties additives are inefficient at as low concentration of *n*-alkanes (obtained by triglyceride hydrotreating) in diesel fuel as 5% [28]. Other properties of the green diesel, such as density, cetane index, sulfur and aromatics content, are superior to those of conventional diesel fuel [28, 80, 81]. Consequently, mild isomerization would suffice to convert the triglyceride-hydrotreating product into an excellent diesel-fuel blending fraction. In fact, this is implemented in the NexBTL and Ecofining processes [20, 21, 23, 26].

While hydrogen sulfide helps in preserving the activity of hydrotreating catalysts during deoxygenation, it may also interfere with deoxygenation itself. The effects of hydrogen sulfide, ammonia and water on deoxygenation of various oxygenated compounds were studied in detail [64, 84–86]. Water inhibited the rate of hydrodeoxygenation and hydrodecarboxylation of esters only slightly, but it supported hydrolysis of esters to corresponding acids. Consequently, the overall conversion of diethylsebacate was not increased due to water addition [84]. In contrast, the addition of water was reported to decrease conversion of methyl and ethyl heptanoate (ca. 5–10% decrease in conversion as a result of addition of 5000 ppm H_2O) [85]. Interestingly, inhibition of hydrogenation reactions by water, as showed by the decrease of the molar ratio of saturated-to-unsaturated hydrocarbons, was observed for NiMo, but not for CoMo catalyst [85]. Ammonia exhibited a strong inhibition effect both on hydrodeoxygenation as well as hydrodecarboxylation, but the inhibition of the hydrodecarboxylation was more pronounced [84]. In contrast to ammonia and water, hydrogen sulfide promoted deoxygenation of esters over both NiMo and CoMo catalysts [64, 84, 86]. From the two principal deoxygenation pathways, primarily hydrodecarboxylation was promoted by hydrogen sulfide [84, 86]; the hydrodeoxygenation route was affected only slightly [84]. These observations were explained by the increase in density of Brønsted acid sites of the sulfide phase as a consequence of H_2S addition [84]. Furthermore, the addition of hydrogen sulfide resulted in the formation of sulfur containing products, namely thiols and sulfides, during deoxygenation of alkyl heptanoates [64]. It is obvious that particularly the involvement of hydrogen sulfide in deoxygenation is rather complex as it takes part in the reactions, affects the catalyst acidity and hence its selectivity, and protects the catalyst from desulfurization and its subsequent deactivation.

Having covered the main aspects of triglycerides and related feedstocks transformation into hydrocarbons over sulfided hydrotreating catalysts, the issue of the mechanism of this transformation remains to be addressed. There is agreement that two parallel pathways play an important role in deoxygenation of fatty acids and their esters over sulfided catalysts, namely hydrodeoxygenation and decarboxylation/decarbonylation [10, 17–19, 63, 65, 66, 69]. However, their details are not fully understood, particularly the formation of fatty acids that have been identified as reaction intermediates [17, 18, 66, 69]. Gusmão has proposed initial degradation of triglyceride to two fatty acid molecules, a ketene and acrolein. The latter two intermediates are, however, very reactive under hydrotreating conditions and undergo fast hydrogenation [69]. Consequently, the proposed mechanism is hard to prove.

In deoxygenation of methyl heptanoate, hydrolysis was proposed to be responsible for formation of carboxylic acid as reaction intermediate since formation of methanol was observed [65]. Due to absence of water in the feedstock and rapid formation of heptanoic acid, occurrence of acid-catalyzed hydrolysis is questionable. It was therefore suggested that alkaline hydrolysis could take place as a result of attack of OH^- or SH^- group on the carboxylic group of the ester [65]. Nevertheless, glycerol formation, which should be an intermediate in this reaction route, has not been reported in deoxygenation of triglycerides. On the other hand, fatty alcohols have been found to be reaction intermediates of triglycerides transformation [18], i.e. it is plausible that glycerol or other C_3 alcohols could exist under hydrotreating conditions. In fact, propyl esters of fatty acids have been identified among triglyceride deoxygenation products [18].

Alternatively, fatty acids could be also formed by hydrogenolysis of C–O bond, which has been recently reported in deoxygenation of tricaprylin over Pd/C and, more importantly, over $NiMo/Al_2O_3$ (even though non-sulfided) [50].

The fatty acid intermediates undergo hydrodeoxygenation (total hydrogenation) yielding water and decarboxylation/decarbonylation resulting in formation of CO_2 and CO [10, 17–19, 63, 65, 66, 69]. Under typical hydrotreating conditions, subsequent reactions involving CO_2 hydrogenation to CO (reversed water–gas-shift reaction), CO_2 or CO hydrogenation to methane (methanization) and reaction of CO with water to CO_2 and H_2 (water–gas-shift reaction) have to be considered. Consequently, it is difficult to determine whether carbon oxides are formed via decarboxylation or decarbonylation of fatty acids [63] or both. Furthermore, the origin of hydrodeoxygenation and decarboxylation activity of hydrotreating catalysts is also not fully understood. Some results suggest that it could be a consequence of different properties of individual metal sulfides since NiS was found to yield selectively hydrodecarboxylation products while MoS_2 yielded almost exclusively products of total hydrogenation (hydrodeoxygenation) [18].

Acidic micro- and mesoporous molecular sieves catalysts

Zeolites belong to the most important industrial catalysts, particularly for production of clean fuels [35, 36, 87, 88]. In particular, tunable acid–basic properties, easy modification by ion-exchange and molecular sieving properties have contributed to wide-spread industrial use of zeolites [88]. Moreover, extensive research of zeolites and related materials leads to discoveries of new structures and new potential commercial applications [88]. It is hence not surprising that they were suggested for upgrading of vegetable oils into biofuels [89–93]. Catalytic cracking using zeolites resulting in oxygen elimination from the products can be considered as unselective deoxygenation. It does not require hydrogen, which is significant advantage over deoxygenation using hydrotreating catalysts. Furthermore, unselective deoxygenation differs from the selective processes using supported noble metals or hydrotreating catalysts by the nature of products. While the selective deoxygenation processes provide almost exclusively *n*-alkanes with minimum loss of carbon atoms, products of the unselective deoxygenation include, in addition to *n*-alkanes, aromatics, naphthenes and iso-alkanes having a broad distribution of molecular weights. The broad molecular-weight distribution of products can be regarded as a disadvantage in comparison with the selective processes since more complex downstream treatment of the products is necessary in order to use all products efficiently.

Catalytic cracking of vegetable oils and related feedstocks was usually investigated at temperatures in the range 350–550°C (Table 3) under atmospheric pressure in the presence of alumina [94–96], zeolites [89, 91, 96–104], amorphous aluminosilicates [91, 96, 101], mesoporous molecular sieves [92, 102, 105, 106], micro/mesoporous materials [93, 103, 107], aluminophosphates [101, 108] and sulfated zirconia [109, 110]. In addition to acidic catalysts, the performance of basic oxides, such as MgO and CaO was studied as well [94, 96]. The use of basic catalysts is together with thermal cracking and pyrolysis of triglycerides out of the scope of this paper. Main products of acidic catalytic cracking of vegetable oils are hydrocarbon gases

Table 3 An overview of reaction conditions and catalysts used for deoxygenation of triglycerides and related feedstocks over microporous and mesoporous catalysts

Model compound	Catalyst	Reaction conditions	Reference
Fatty acids			
C_{12}–C_{24} fatty acid mixture	HZSM-5, composite MCM-41/HZSM-5	400–450°C, atm.; FBR	[93]
Esters			
Methyl octanoate	Zn–HZSM-5, HZSM-5	H_2, 400–500°C, atm., FBR	[111, 112]
	CsNaX, NaX, MgO	Methanol, 425°C, atm., FBR	[113]
Vegetable oils			
Soybean oil	Al_2O_3, MgO	300–500°C, atm.; FBR	[94]
Canola oil	SAPO 5, SAPO-11, HZSM-5, MgAPO-36	330–550°C, atm.; FBR	[101]
	HZSM-5, HY, silica–alumina[a]	400–550°C, atm.; FBR	[98]
	K–HZSM-5	400–550°C, atm.; FBR	[96]
	Pt–HZSM-5	400–550°C, atm.; FBR	[100]
Palm oil (incl. palm kernel oil, palm olein oil)	HZSM-5, USY, zeolite β, K–HZSM-5[a]	350–450°C, atm.; FBR	[105]
	MCM-41 (various Si/Al)	450°C, atm.; FBR	[92, 105]
Used vegetable oil	HZSM-5, S–ZrO_2[a]	H_2; 280–430°C; BR	[110]

BR batch reactor, *FBR* fixed bed reactor

[a] Used either neat or in physical mixtures of given materials

(C_3–C_5), so-called organic liquid product (OLP, i.e. mixture of aliphatic and aromatic hydrocarbons with traces of oxygenates) and coke [89, 91]. Oxygen is typically eliminated as carbon oxides and water [89, 91, 96]. The organic liquid product (OLP) consists mainly of gasoline and diesel fractions [89, 91, 96]. The yield of OLP, which is desired for potential biofuel applications, depends predominantly on the density and strength of Brønsted acid sites of the cracking catalysts.

Typically, the yield of OLP decreases with increasing concentration and strength of acid sites that support overcracking leading to gaseous products [98]. For example, enhanced yields of gasoline and kerosene at the expense of gases and diesel were achieved while increasing of Si/Al ratio of H–ZSM-5 from 50 to 400. Concurrently, the aromatics content of OLP decreased from about 52 to 35 wt% and only small yields of coke (<2 wt%) were formed [102]. Analogously, amorphous silica–alumina and MCM-41 gave high yield of OLP (up to 65 wt%), which was however accompanied by coke formation (9–12 wt%) [98, 102]. The formation of coke contributing to lower yields of OLP could be suppressed by addition of zeolites [98]. Owing to their pore dimensions, large molecules cannot enter their pore system and, more importantly, cannot be formed in the pores and cause thus their blockage. Furthermore, the yield of OLP can be affected by reaction conditions, i.e. with increasing reaction temperature and residence time the yield of OLP for a given catalyst decreases, e.g. due to an increase in temperature from 450 to 500°C the yield of OLP dropped from 54 to 40 wt% over H–ZSM-5 [98].

H–ZSM-5 zeolite has been the most extensively investigated zeolite for application in catalytic cracking of triglycerides [89, 91, 97, 98, 102, 104]. It is more active than zeolites USY and Beta that deactivate much faster [89]. Similarly, silico–alumino-phosphates, i.e. another group of microporous solids, exhibited significantly lower activity than H–ZSM-5 [108]. For example, the yield of OLP was 54 wt% at 450°C and 3.6 h^{-1} over H–ZSM-5, but only 36 wt% over SAPO-5. This was assigned to the fast deactivation of SAPO materials by coking [108] but could be also caused by the lower density and strength of Brønsted acid sites in these catalysts. Modification of H–ZSM-5 by potassium [99] and platinum [100] led to lower density of acid sites in ZSM-5 and consequently lower activity in cracking of triglycerides.

As a result of strong acidity and unique pore dimensions and architecture of H–ZSM-5, high yields of aromatic hydrocarbons (80–95 wt% of OLP), mainly benzene and toluene, were obtained in the organic liquid product (OLP). In contrast, mildly acidic amorphous silica–alumina provided OLP containing significant concentrations of aliphatic hydrocarbons (10–30 wt% of OLP) in addition to aromatics (25–50 wt% of OLP) [98]. However, C_6–C_9 aromatics were also the main hydrocarbons present in OLP when SAPO-5 and SAPO-11, i.e. mildly acidic microporous silico–alumino-phosphates, were used. In contrast, Mg–APO-36, i.e. a non-acidic alumino-phosphate, provided aliphatic hydrocarbons in concentrations similar to those of aromatics [91]. It clearly shows the importance of density of acid sites as well as of their strength. This was also demonstrated by studies using potassium-loaded ZSM-5 [99]. Apart from decreased conversion of triglycerides, the impregnation of H–ZSM-5 with potassium resulted in decreased yields of gasoline-range hydrocarbons, particularly aromatics. This change can be attributed to the decreased density of Brønsted acid sites, which is responsible for the lower yields of aromatics that are formed over strong acid sites [99]. Based on the differences in product distribution over H–ZSM-5 and K–ZSM-5 it can be suggested that the catalyst acidity plays a crucial role in the reactions consecutive to deoxygenation, namely aromatization and oligomerization, but does not affect the initial deoxygenation so severely.

The other investigated zeolites, Beta and USY, provided a different product distribution within OLP. In contrast to ZSM-5 favoring formation of gasoline-range hydrocarbons and gaseous products, formation of diesel-like product was prominent particularly over USY and to a lesser extent over Beta [89]. The difference can be attributed mainly to pore dimensions and architecture of the zeolites, as the dimensions of ZSM-5 pores restrict the formation of diesel-like products. The rate of coke formation increased in the order H–ZSM-5 < H-Beta < H–USY [89]. This corresponds well with the increasing pore diameter of these zeolites and presence of cavities in USY allowing the formation of coke precursors inside zeolite pores.

In addition to type and modification of microporous solids used as catalysts in triglyceride cracking, co-feeding of steam affects the product distribution within organic liquid products. Particularly, the formation of aromatics was suppressed in presence of steam. In the case of H–ZSM-5 the total yield of aromatics decreased from 80–95 to 74–87 wt%. It was proposed that the hydride transfer reactions were inhibited due to presence of steam [98]. In contrast, catalyst lifetime was prolonged as a result of steam addition [98, 100], which was explained by possible competitive adsorption of coke and water molecules [98]. Alternatively, the prolonged catalyst lifetime could be explained by the suppressed formation of aromatics and hence the suppressed formation of coke precursors. Finally, the formation of light olefins was promoted by steam, e.g. the gas yield over H–ZSM-5 increased from 25 to 34 wt% due to steam addition at 450°C and 3.6 h^{-1} [98], which is in line with the other observations, i.e. the suppressed aromatization.

Besides catalytic cracking of triglycerides, cracking of fatty acids and their mixtures with triglycerides is of high importance, as these mixtures generated in oleochemical industry cannot be directly used as a feed for base-catalyzed transesterification. During cracking over H–ZSM-5 (Si/Al = 50) temperature and weight-hourly space velocity were identified as the most important process variables affecting the gasoline yield. A maximum yield of gasoline (44 wt%) was obtained at 440°C and 3.7 h^{-1} [103].

Methyl octanoate was used as a model component representing esters (Table 3), i.e. triglycerides, to understand the influence of catalyst acidity/basicity on deoxygenation of esters in more detail [111–113]. Methyl octanoate underwent condensation reactions yielding C_{15}-symmetrical ketone (8-pentadecanone) and hydrolysis producing octanoic acid (at 500°C, 0.1 MPa) (Fig. 1). Through cracking and decarboxylation/decarbonylation of these intermediates, olefins, and subsequently aromatics were formed [111]. The aromatization of methyl octanoate on H–ZSM-5 was more effective than aromatization of *n*-octane that occurred by its cracking to olefins and their subsequent oligomerization and aromatization [111]. Modification of H–ZSM-5 by Zn (0.3 wt%) increased significantly aromatization of *n*-octane, but did not influence aromatization of methyl octanoate, i.e. Zn does not affect the reaction steps leading to formation of aromatics from methyl octanoate [112]. Moreover, high selectivity to *o*-xylene at low conversions of methyl octanoate over both H–ZSM-5 and Zn/H–ZSM-5 indicates that direct ring closure occurs, possibly before deoxygenation. On the contrary, *o*-xylene was not observed at low conversions of *n*-octane. Hence, the aromatization pathways differ for methyl octanoate (direct ring closure) and *n*-octane (cracking and subsequent oligomerization and cyclization) [112].

Methyl octanoate conversion (420°C, 0.1 MPa) over basic zeolites, such as CsNaX and NaX, is strongly affected by solvent choice (10% methyl octanoate in solvent). While in a non-polar solvent (nonane) fast deactivation within 300 min time-on-stream (TOS) was observed, in a polar solvent (methanol) the conversion remained stable during the same (TOS). The difference was explained by strong adsorption of methyl octanoate and subsequent condensation reactions in nonane. On the contrary, methanol competed for adsorption sites with methyl octanoate by forming adsorbed formate and carbonate species that led to lower methyl octanoate coverage and, in turn, to suppression of condensation reactions and to better catalytic stability [113]. Owing to the strong adsorption on the basic sites of CsNaX, methyl octanoate cannot be desorbed before decomposing. The direct decomposition routes involve decarbonylation and deacetylation yielding heptenes and hexenes, respectively. Moreover, octenes and other hydrogenated products are formed by hydrogenation/dehydration. The formation of these products is assisted by the surface hydrogen produced from methanol decomposition [113]. Moreover, the poor performance of MgO indicates that apart from catalyst basicity, the polar environment in zeolite micropores plays an essential role [113].

Aiming at higher yields of OLP, particularly in the diesel range, mesoporous and composite (micro/mesoporous) catalysts have been studied in detail by the group of Bhatia [93, 102, 103]. The possible advantages of the composite catalysts over both microporous and mesoporous materials were discussed in detail by Čejka and Mintova [76, 114].

The key issues, in connection with triglyceride cracking, appear to be the adjustment between strong and weak acid sites, and improvements in the molecular traffic. Several composite microporous/mesoporous materials (H–ZSM-5/MCM-41, H–ZSM-5/SBA-15) have been shown to give higher conversion and enhanced yields of the organic liquid products as compared with the parent materials [93, 102].

A comparison of catalytic cracking of a fatty acid mixture (FAM) and used palm oil (UPO) over H–ZSM-5 and H–ZSM-5/MCM-41 composite catalyst at 400–450°C and 2.5–4.5 h^{-1} clearly demonstrated significantly enhanced conversion of UPO when using the composite catalyst (from 50 to 70% at 400°C). The UPO conversion enhancement decreased with increasing cracking temperature. On the other hand, only slight increase in conversion of FAM was observed. The enhancement of conversion during cracking was hence attributed to reduced diffusional constrains when composite catalyst was used [107]. Most of the composite catalysts (H–ZSM-5/MCM-41, H–ZSM-5/SBA-15) having different content of the mesoporous phase gave slightly higher conversion of FAM (90–98% at 450°C) than the parent H–ZSM-5 (90%). As expected, the conversion over the neat mesoporous materials was significantly lower (60–70%) owing to their lower density and strength of acid sites [93]. Consequently, the yield of gasoline increased in comparison with mesoporous catalysts when composite catalysts and H–ZSM-5 were used. In fact, the yield of gasoline fraction was the highest (44 wt%) for composite catalysts having 10–30% of mesoporous phase [93], presumably due to better molecular traffic control to and from Brønsted acid sites located in the micropores of H–ZSM-5. Similar optimum range for maximizing gasoline yield was found also for cracking of palm oil over H–ZSM-5/MCM-41 composite catalysts [102].

Fluid catalytic cracking (FCC) of hydrocarbons is the largest refining catalytic process [87]. As a catalytic cracking process, FCC constitutes an interesting industrial possibility for upgrading of triglycerides into hydrocarbon fuel components without hydrogen consumption and with minimum capital cost investment [115]. The addition of rapeseed oil (up to 30%) to vacuum gas oil (VGO), a typical FCC feedstock, was shown to result in decreasing yield of liquid hydrocarbon product and in increasing yield of C_3/C_4 olefins with increasing rapeseed oil concentration [116, 117]. At the same time, the amount of gasoline fraction in the liquid products increased. The oxygen originating from triglycerides was eliminated mainly as water a partially as CO and CO_2. Moreover, traces of phenols and carboxylic acids were identified in the liquid products [116]. The yield of light olefins and of aromatics in gasoline increased with increasing reaction temperature in the range 450–520°C during these micro-activity test (MAT) experiments [116]. MAT is a standardized test for evaluation of FCC catalysts performance (ASTM D-3907). Similar results were obtained when rapeseed oil was replaced by animal fats (5–10% in VGO). Cracking of neat animal fat over dealuminated zeolites yielded predominantly aliphatic hydrocarbons at 400°C, while at 550°C alkyl aromatics were the prevailing products [118]. The impurities present in triglycerides have a detrimental effect on catalyst activity. In particular, Ca and P, i.e. typical impurities of vegetable oils, were found to deteriorate the catalyst cracking activity. Their negative impact was larger than that of water formed during cracking of triglycerides that could plausibly cause hydrothermal damage of zeolites [116].

The reaction pathways of triglyceride cracking over acidic zeolites have been recently studied by Benson [119]. Propylbenzene and phenylbutene have been suggested to be the primary aromatic intermediates in cracking of unsaturated mono-, di- and triglycerides. They are formed by cyclization of intermediates originating from cracking of the acid moiety after its double bond protonation [119]. As an alternative, initial cracking along the glycerol backbone (cleavage of C–O bonds) was proposed [119]. Moreover, an overview of reaction pathways in catalytic cracking of triglycerides was provided by Kloprogge [55]. There is general agreement that cracking of triglycerides includes deoxygenation, cracking (via β-elimination and γ-hydrogen transfer), oligomerization and aromatization. Details of the proposed reaction pathways are beyond the scope of this review and can be found in the review [55] and the original papers [91, 95, 96, 98, 101, 120].

Conclusions and outlook

Production of biofuels can help in tackling the ever increasing greenhouse gas emissions from transportation. Deoxygenation of triglycerides and related feedstocks, both selective and non-selective, has a potential to become a key process for the production of biofuels since it provides high-quality hydrocarbon-based fuels. Selective deoxygenation provides green diesel as the main product and relies on the use of supported noble metal catalysts and metal sulfide catalysts. Unselective deoxygenation, on the other hand, uses zeolite-based catalysts and yields a wide spectrum of products ranging from gases to diesel-like products. The present paper reviews the main aspects of the three deoxygenation systems.

Supported noble metal catalysts show an enormous potential, particularly thanks to their high selectivity and moderate hydrogen consumption. Owing to the fact that decarboxylation/decarbonylation is favored over supported noble metal catalysts, majority of oxygen is eliminated in the form of carbon oxides and hydrogen is ideally needed only to saturate olefinic compounds present in the feedstock and to stabilize catalyst activity. Pd supported on active carbon has been found to be a very promising catalyst for an industrial application. The origin of its high activity and selectivity, as compared with Pt and other supports, is not yet fully understood.

Supported metal sulfide catalysts have been used as hydrotreating catalysts over several decades. Development of deoxygenation processes based on these catalysts can thus use the vast experience gathered during application of these catalysts. In fact, the first commercial deoxygenation process (NexBTL) relies on a hydrotreating catalyst [121]. Nevertheless, significant differences among conventional hydrotreating catalysts have been found, particularly in their selectivity to hydrodeoxygenation and hydrodecarboxylation. This is of immense importance since hydrogen consumption that is typically much larger than over supported noble metal catalysts could be reduced by fine tuning of catalyst composition and properties.

Microporous and mesoporous molecular sieves transform triglycerides and related feedstocks into hydrocarbons in absence of hydrogen. Consequently, gaseous olefins and rather highly aromatic liquid products are formed. These can be used for production of green gasoline components and for chemical syntheses. The main drawback of this approach is, apart from need of upgrading of the primary cracking products, the fast deactivation of the catalysts.

Owing to the increasing environmental awareness, biofuels will play an important role in future transportation fuels. This will create a strong demand for development of new sustainable processes for their production. The inherently high oxygen content of biomass-derived feedstocks, as compared with fossil raw materials, predetermines deoxygenation to become a key process in production of biofuels. We can also expect intensive research efforts to tackle the fundamental mechanistic aspects of deoxygenation as their understanding is crucial for development of more efficient deoxygenation catalysts.

Acknowledgments The financial support from the Czech Science Foundation (GAČR, P106/10/1733) is gratefully acknowledged.

References

1. Naik, S.N., Goud, V.V., Rout, P.K., Dalai, A.K.: Production of first and second generation biofuels: a comprehensive review. Renew. Sustain. Energy Rev. **14**, 578–597 (2010)
2. Demirbas, A.: Progress and recent trends in biofuels. Prog. Energy Combust. Sci. **33**, 1–18 (2007)
3. Schaub, G.: Synthetic fuels and biofuels for the transportation sector—principles and perspectives. Erdoel Erdgas Kohle **122**, 34–38 (2006)
4. Schaub, G., Vetter, A.: Biokraftstoffe–Eine Übersicht. Chem. Ing. Tech. **79**, 569–578 (2005)
5. European Biofuels Technology Plattform: Strategic Research Agenda & Strategy Deployment Document. CPL Press (2008). www.biofuelstp.eu
6. Anon: Sustainable Biofuels: Prospects and Challenges. The Royal Society, London (2008). http://royalsociety.org/sustainable-biofuels-prospects-and-challenges/. Accessed 2 Aug 2010
7. Demirbas, A.: Biofuels—Securing the Planet's Future Energy Needs. Springer-Verlag London Limited, London (2009)
8. Lüke, H.W.: BTL fuels—a promising option for the future. Erdol Erdgas Kohle **121**, 3–5 (2005)
9. Van Gerpen, J.H., Peterson C.L., Goering C.E.: Biodiesel: an alternative fuel for compression ignition engines. ASAE distinguished lecture no. 31, pp 1–22 (2007)
10. Kubička, D.: Future refining catalysis—introduction of biomass feedstocks. Collect. Czech. Chem. Commun. **73**, 1015–1044 (2008)
11. The European standards organization (CEN): European fuel standards—EN 590 (diesel), EN 14 214 (biodiesel). European Committee for Standardization (CEN), Brussels 2008(EN14214) 2004 (EN590)
12. Ma, F., Hanna, M.A.: Biodiesel production: a review. Bioresour. Technol. **70**, 1–15 (1999)
13. Meher, L.C., Sagar, D.V., Naik, S.N.: Technical aspects of biodiesel production by transesterification—a review. Renew. Sustain. Energy Rev. **10**, 248–268 (2006)
14. Knothe, G., Krahl, J., van Gerpen, J.: The Biodiesel Handbook. AOCS Press, Champaign (2005)
15. Bournay, L., Casanave, D., Delfort, B., Hillion, G., Chodorge, J.A.: New heterogeneous process for biodiesel production: a way to improve the quality and the value of the crude glycerin produced by biodiesel plants. Catal. Today **106**, 190–192 (2005)
16. European Automobile Manufacturers Association (ACEA), Alliance of Automobile Manufacturers (AAM), Engine Manufacturers Association (EMA), Japan Automobile Manufacturers Association (JAMA): Worldwide Fuel Charter, 4th edn. (2006). http://www.jama.or.jp/wwfc/pdf/WWFC_Sep2006_Brochure.pdf/. Accessed 2 Aug 2010
17. Laurent, E., Delmon, B.: Study of the hydrodeoxygenation of carbonyl, carboxylic and guaiacyl groups over sulfided CoMo/γ-Al_2O_3 and NiMo/γ-Al_2O_3 catalysts. I. Catalytic reaction schemes. Appl. Catal. A **109**, 77–96 (1994)
18. Kubička, D., Kaluža, L.: Deoxygenation of vegetable oils over sulfided Ni, Mo and NiMo catalysts. Appl. Catal. A **372**, 199–208 (2010)
19. Huber, G.W., O'Connor, P., Corma, A.: Processing biomass in conventional oil refineries: production of high quality diesel by hydrotreating vegetable oils in heavy vacuum oil mixtures. Appl. Catal. A **329**, 120–129 (2007)
20. Jakkula, J., Niemi, V., Nikkonen, J., Purola, V.-M., Myllyoja, J., Aalto, P., Lehtonen, J., Alopaeus, V.: Process for producing hydrocarbon component of biological origin. United States Patent, US 7,232,935 (2007)
21. Maula, H.: Neste commissions second NExBTL plant. http://www.biodieselmagazine.com/article.jsp?article_id=3632 (2009). Accessed 5 Feb 2010
22. H-Bio process. http://www2.petrobras.com.br/tecnologia/ing/hbio.asp (2010). Accessed 5 Feb 2010
23. Gross, S.: UOP and Italy's ENI s.p.a. announce plans for facility to produce diesel fuel from vegetable oil (2007). http://www.uop.com/pr/releases/PR.EniEcofiningFacility.pdf. Accessed 5 Feb 2010
24. Craig, W.K., Soveran, D.W.: Production of hydrocarbons with relatively high cetane rating. United States Patent, US 4,992,605 (1991)

25. Pinho, A.R., Silva, M., Silva Neto, A.P., Cabral, J.A.R.: Catalytic cracking process for the production of diesel from vegetable oils. United States Patent, US 7,540,952 B2 (2009)
26. Petri, J.A., Marker, T.L.: Production of diesel fuel from biorenewable feedstocks. United States Patent, US 7,511,181 B2 (2009)
27. The EU biodiesel industry—statistics. http://www.ebb-eu.org/stats.php (2010). Accessed 25 Feb 2010
28. Šimáček, P., Kubička, D., Šebor, G., Pospíšil, M.: Fuel properties of hydroprocessed rapeseed oil. Fuel **89**, 611–615 (2010)
29. Huber, G.W., Iborra, S., Corma, A.: Synthesis of transportation fuels from biomass: chemistry, catalysts, and engineering. Chem. Rev. **106**, 4044–4098 (2006)
30. Corma, A., Iborra, S., Velty, A.: Chemical routes for the transformation of biomass into chemicals. Chem. Rev. **107**, 2411–2502 (2007)
31. Mäki-Arvela, P., Holmbom, B., Salmi, T., Murzin, D.Yu.: Recent progress in synthesis of fine and specialty chemicals from wood and other biomass by heterogeneous catalytic processes. Catal. Rev. Sci. Eng. **49**, 197–340 (2007)
32. Gallezot, P.: Catalytic routes from renewables to fine chemicals. Catal. Today **121**, 76–91 (2007)
33. Furimsky, E.: Catalytic hydrodeoxygenation. Appl. Catal. A **199**, 147–190 (2000)
34. Lestari, S., Mäki-Arvela, P., Beltramini, J., Max Lu, G.Q., Murzin, D.Yu.: Transforming triglycerides and fatty acids into biofuels. ChemSusChem **2**, 1109–1119 (2009)
35. Rigutto, M.S., van Veen, R., Huve, L.: Zeolites in hydrocarbon processing. Stud. Surf. Sci. Catal. **168**, 855–913 (2007)
36. Corma, A., Martinez, A.: Zeolites in refining and petrochemistry. Stud. Surf. Sci. Catal. **157**, 337–366 (2005)
37. Maier, W.F., Roth, W., Thies, I., Rague Schleyer, P.v.: Gas phase decarboxylation of carboxylic acids. Chem. Ber. **115**, 808–812 (1982)
38. Kubičková, I., Snåre, M., Eränen, K., Mäki-Arvela, P., Murzin, D.Yu.: Hydrocarbons for diesel fuel via decarboxylation of vegetable oils. Catal. Today **106**, 197–200 (2005)
39. Snåre, M., Kubičková, I., Mäki-Arvela, P., Eränen, K., Murzin, D.Yu.: Heterogeneous catalytic deoxygenation of stearic acid for production of biodiesel. Ind. Eng. Chem. Res. **45**, 5708–5715 (2006)
40. Snåre, M., Kubičková, I., Mäki-Arvela, P., Eränen, K., Wärnå, J., Murzin, D.Yu.: Production of diesel fuel from renewable feeds: Kinetics of ethyl stearate decarboxylation. Chem. Eng. J. **134**, 29–34 (2007)
41. Mäki-Arvela, P., Kubičková, I., Snåre, M., Eränen, K., Murzin, D.Yu.: Catalytic deoxygenation of fatty acids and their derivatives. Energy Fuels **21**, 30–41 (2007)
42. Lestari, S., Simakova, I., Tokarev, A., Mäki-Arvela, P., Eränen, K., Murzin, D.Yu.: Synthesis of biodiesel via deoxygenation of stearic acid over supported Pd/C catalyst. Catal. Lett. **122**, 247–251 (2008)
43. Snåre, M., Kubičková, I., Mäki-Arvela, P., Chichova, D., Eränen, K., Murzin, D.Yu.: Catalytic deoxygenation of unsaturated renewable feedstocks for production of diesel fuel hydrocarbons. Fuel **87**, 933–945 (2008)
44. Simakova, I., Simakova, O., Romanenko, A.V., Murzin, D.Yu.: Hydrogenation of vegetable oils over Pd on nanocomposite carbon catalysts. Ind. Eng. Chem. Res. **47**, 7219–7225 (2008)
45. Lestari, S., Mäki-Arvela, P., Eränen, K., Beltramini, J., Max Lu, G.Q., Murzin, D.Yu.: Diesel-like hydrocarbons from catalytic deoxygenation of stearic acid over supported Pd nanoparticles on SBA-15 catalysts. Catal. Lett. **130**, 48–51 (2009)
46. Simakova, I., Simakova, O., Mäki-Arvela, P., Simakov, A., Estrada, M., Murzin, D.Yu.: Deoxygenation of palmitic and stearic acid over supported Pd catalysts: effect of metal dispersion. Appl. Catal. A **355**, 100–108 (2009)
47. Murzin, D.Yu., Kubičková, I., Snåre, M., Mäki-Arvela, P., Myllyoja, J.: Method for manufacture of hydrocarbons. United States Patent, US 7,491,858 (2009)
48. Murzin, D.Yu., Kubičková, I., Snåre, M., Mäki-Arvela, P., Myllyoja, J.: Method for the manufacture of hydrocarbons. PCT International Application WO 2006/075057 A2 (2006)
49. Do, P.T., Chiappero, M., Lobban, L.L., Resasco, D.E.: Catalytic deoxygenation of methyl-octanoate and methyl-stearate on Pt/Al_2O_3. Catal. Lett. **130**, 9–18 (2009)
50. Boda, L., Onyestyák, G., Solt, H., Lónyi, F., Valyon, J., Thernesz, A.: Catalytic hydroconversion of tricaprylin and caprylic acid as model reaction for biofuel production from triglycerides. Appl. Catal. A **374**, 158–169 (2010)
51. Immer, J.G., Kelly, M.J., Lamb, H.H.: Catalytic reaction pathways in liquid-phase deoxygenation of C_{18} free fatty acids. Appl. Catal. A **375**, 134–139 (2010)
52. Lestari, S., Mäki-Arvela, P., Bernas, H., Simakova, O., Sjöholm, R., Beltramini, J., Max Lu, G.Q., Myllyoja, J., Simakova, I., Murzin, D.Yu.: Catalytic deoxygenation of stearic acid in a continuous reactor over a mesoporous carbon-supported Pd catalyst. Energy Fuel **23**, 3842–3845 (2009)
53. Colson, A.: Formation of ethylene hydrocarbon from esters. C. R. Acad. Sci. Ser. IIc Chim. **147**, 1054–1057 (1999)
54. Davis, J.L., Barteau, M.A.: Hydrogen bonding in carboxylic acid adlayers on Pd(111): evidence for catemer formation. Langmuir **5**, 1299–1309 (1989)
55. Kloprogge, J.T., Duong, L.V., Frost, R.L.: A review of the synthesis and characterisation of pillared clays and related porous materials for cracking of vegetable oils to produce biofuels. Environ. Geol. **47**, 967–981 (2005)
56. Simakova, I., Simakova, O., Mäki-Arvela, P., Murzin, D.Yu.: Decarboxylation of fatty acids over Pd supported on mesoporous carbon. Catal. Today **150**, 28–31 (2010)
57. Topsoe, H., Clausen, B.S., Masoth, F.E.: Hydrotreating Catalysis. Springer-Verlag, Berlin (1996)
58. Weisser, O., Landa, S.: Sulphide Catalysts, Their Properties and Applications. Pergamon, Oxford (1973)
59. Şenol, O.I., Viljava, T.R., Krause, A.O.I.: Hydrodeoxygenation of methyl esters on sulphided NiMo/γ-Al_2O_3 and CoMo/γ-Al_2O_3 catalysts. Catal. Today **100**, 331–335 (2005)
60. Šimáček, P., Kubička, D., Šebor, G., Pospíšil, M.: Hydroprocessed rapeseed oil as a source of hydrocarbon-based biodiesel. Fuel **88**, 456–460 (2009)
61. Elliott, D.C.: Historical developments in hydroprocessing bio-oils. Energy Fuel **21**, 1792–1815 (2007)
62. Bridgwater, A.V.: Catalysis in thermal biomass conversion. Appl. Catal. A **116**, 5–47 (1994)
63. Donnis, B., Egeberg, R.G., Blom, P., Knudsen, K.G.: Hydroprocessing of bio-oils and oxygenates to hydrocarbons. understanding the reaction routes. Top. Catal. **52**, 229–240 (2009)
64. Şenol, O.I., Viljava, T.R., Krause, A.O.I.: Effect of sulphiding agents on the hydrodeoxygenation of aliphatic esters on sulphided catalysts. Appl. Catal. A **326**, 236–244 (2007)
65. Ryymin, E.M., Honkela, M.L., Viljava, T.R., Krause, A.O.I.: Insight to sulfur species in the hydrodeoxygenation of aliphatic esters over sulfided NiMo/γ-Al_2O_3 catalyst. Appl. Catal. A **358**, 42–48 (2009)
66. Rocha Filho, G.N.d., Brodzki, D., Djega-Mariadassou, G.: Formation of alkanes alkylcycloalkanes and alkylbenzenes during catalytic hydrocracking of vegetable oils. Fuel **72**, 543–549 (1993)
67. Kubička, D., Bejblová, M., Vlk, J.: Conversion of vegetable oils into hydrocarbons over CoMo/MCM-41 catalysts. Top. Catal. **53**, 168–178 (2010)

68. Smejkal, Q., Smejkalová, L., Kubička, D.: Thermodynamic balance in reaction system of total vegetable oil hydrogenation. Chem. Eng. J. **146**, 155–160 (2009)
69. Gusmão, J., Brodzki, D., Djega-Mariadassou, G., Frety, R.: Utilization of vegetable oils as an alternative source for diesel-type fuel: hydrocracking on reduced Ni/SiO_2 and sulphided Ni-Mo/γ-Al_2O_3. Catal. Today **5**, 533–544 (1989)
70. Landa, S., Andrzejak, A., Weisser, O.: Über die Eigenschaften von Sulfidkatalysatoren XIV. Zur Hydrierung von Säuren. Collect. Czech. Chem. Commun. **27**, 979–986 (1962)
71. Thakur, D.S., Delmon, B.: The role of group VIII metal promoter in MoS_2 and WS_2 hydrotreating catalysts: I. ESR studies of CoMo, NiMo, and NiW catalysts. J. Catal. **91**, 308–317 (1985)
72. Zakharov, I.I., Startsev, A.N., Zhidomirov, G.M.: Quantum chemical study of the electronic structure of the Ni/MoS_2 hydrodesulfurization catalysts. J. Mol. Catal. A **119**, 437–447 (1997)
73. Yang, Y.Q., Tye, C.T., Smith, K.J.: Influence of MoS_2 catalyst morphology on the hydrodeoxygenation of phenols. Catal. Commun. **9**, 1364–1368 (2008)
74. Kubička, D., Šimáček, P., Žilková, N.: Transformation of vegetable oils into hydrocarbons over organized-mesoporous-alumina-supported CoMo catalysts. Top. Catal. **52**, 161–168 (2009)
75. Čejka, J.: Organized mesoporous alumina: synthesis, structure and potential in catalysis. Appl. Catal. A **254**, 327–338 (2003)
76. Čejka, J., Mintova, S.: Perspectives of micro/mesoporous composites in catalysis. Catal. Rev. Sci. Eng. **49**, 457–509 (2007)
77. Čejka, J., Žilková, N., Kaluža, L., Zdražil, M.: Mesoporous alumina as a support for hydrodesulfurization catalysts. Stud. Surf. Sci. Catal. **141**, 243–250 (2002)
78. Kaluža, L., Gulková, D., Šolcová, O., Žilková, N., Čejka, J.: Hydrotreating catalysts supported on organized mesoporous alumina: optimization of Mo deposition and promotional effects of Co and Ni. Appl. Catal. A **351**, 93–101 (2008)
79. Kubička, D., Horáček, J., Kaluža, L.: Catalytic Transformation of Triglycerides: Influence of Catalyst and Feedstock Compositions. Europacat-IX, Salamanca (2009)
80. Sebos, I., Matsoukas, A., Apostolopoulos, V., Papayannakos, N.: Catalytic hydroprocessing of cottonseed oil in petroleum diesel mixtures for production of renewable diesel. Fuel **88**, 145–149 (2009)
81. Šimáček, P., Kubička, D.: Hydrocracking of petroleum vacuum distillate containing rapeseed oil: evaluation of diesel fuel. Fuel **89**, 1508–1513 (2010).
82. Holmgren, J., Gosling, C., Couch, K., Kalnes, T., Marker, T., McCall, M., Marinangeli, R.: Refining biofeedstock innovations. Pet. Technol. Q. **3**, 119–125 (2007)
83. Holmgren, J., Gosling, C., Marinangeli, R., Marker, T., Faraci, G., Perego, C.: New developments in renewable fuels offer more choices. Hydrocarb. Process. **9**, 67–71 (2007)
84. Laurent, E., Delmon, B.: Study of the hydrodeoxygenation of carbonyl, carboxylic and guaiacyl groups over sulfided CoMo/γ-Al_2O_3 and NiMo/γ-Al_2O_3 catalysts. II. Influence of water, ammonia and hydrogen sulfide. Appl. Catal. **109**, 97–115 (1994)
85. Şenol, O.İ., Viljava, T.-R., Krause, A.O.I.: Hydrodeoxygenation of aliphatic esters on sulphided NiMo/γ-Al_2O_3 and CoMo/γ-Al_2O_3 catalyst: the effect of water. Catal. Today **106**, 186–189 (2005)
86. Şenol, O.İ., Ryymin, E.-M., Viljava, T.-R., Krause, A.O.I.: Effect of hydrogen sulphide on the hydrodeoxygenation of aromatic and aliphatic oxygenates on sulphided catalysts. J. Mol. Catal. A **277**, 107–112 (2007)
87. Degnan, T.F.: Applications of zeolites in petroleum refining. Top. Catal. **13**, 349–356 (2000)
88. Di Renzo, F., Fajula, F.: Introduction to molecular sieves: trends of evolution of the zeolite community. Stud. Surf. Sci. Catal. **157**, 1–12 (2005)
89. Twaiq, F.A., Zabidi, N.A.M., Bhatia, S.: Catalytic conversion of palm oil to hydrocarbons: performance of various zeolite catalysts. Ind. Eng. Chem. Res. **38**, 3230–3237 (1999)
90. Adjaye, J.D., Katikaneni, S.P.R., Bakhshi, N.N.: Catalytic conversion of a biofuel to hydrocarbons: effect of mixtures of HZSM-5 and silica-alumina catalysts on product distribution. Fuel Process. Technol. **48**, 115–143 (1996)
91. Katikaneni, S.P.R., Adjaye, J.D., Bakhshi, N.N.: Catalytic conversion of canola oil to fuels and chemicals over various cracking catalysts. Can. J. Chem. Eng. **73**, 484–497 (1995)
92. Twaiq, F.A., Zabidi, N.A.M., Bhatia, S.: Liquid hydrocarbon fuels from palm oil by catalytic cracking over aluminosilicate mesoporous catalysts with various Si/Al ratios. Microporous Mesoporous Mater. **64**, 95–107 (2003)
93. Ooi, Y.-S., Zakaria, R., Mohamed, A.R., Bhatia, S.: Catalytic conversion of fatty acids mixture to liquid fuel and chemicals over composite microporous/mesoporous catalysts. Energy Fuel **19**, 736–743 (2005)
94. Anjos, J.R.S., Gonzales, W.A., Lam, Y.L., Frety, R.: Catalytic decomposition of vegetable oil. Appl. Catal. A **5**, 299–308 (1983)
95. Leung, A., Boocock, D.G.B., Konar, S.K.: Pathway for the catalytic conversion of carboxylic acids to hydrocarbons over activated alumina. Energy Fuels **9**, 913–920 (1995)
96. Idem, R.O., Katikaneni, S.P.R., Bakhshi, N.N.: Catalytic conversion of canola oil to fuels and chemicals: roles of catalyst acidity, basicity and shape selectivity on product distribution. Fuel Process. Technol. **51**, 101–125 (1997)
97. Yarlagadda, P.S., Yaollang, H., Bakhshi, N.N.: Effect of hydrothermal treatment of HZSM-5 catalyst on its performance for the conversion of canola and mustard oils to hydrocarbons. Ind. Eng. Chem. Prod. Res. Dev. **25**, 251–257 (1988)
98. Katikaneni, S.P.R., Adjaye, J.D., Bakhshi, N.N.: Studies on the catalytic conversion of canola oil to hydrocarbons: influence of hybrid catalysts and steam. Energy Fuel **9**, 599–609 (1995)
99. Katikaneni, S.P.R., Adjaye, J.D., Idem, R.O., Bakhshi, N.N.: Catalytic conversion of canola oil over potassium-impregnated HZSM-5 catalysts: C2–C4 olefin production and model reaction studies. Ind. Eng. Chem. Res. **35**, 3332–3346 (1996)
100. Katikaneni, S.P.R., Adjaye, J.D., Bakhshi, N.N.: Conversion of canola oil to various hydrocarbons over Pt/HZSM-5 bifunctional catalyst. Can. J. Chem. Eng. **75**, 391–401 (1997)
101. Katikaneni, S.P.R., Adjaye, J.D., Idem, R.O., Bakhshi, N.N.: Performance studies of various cracking catalysts in the conversion of canola oil to fuels and chemicals in a fluidized-bed reactor. JAOCS **75**, 381–391 (1998)
102. Twaiq, F.A., Mohamad, A.R., Bhatia, S.: Performance of composite catalysts in palm oil cracking for the production of liquid fuels and chemicals. Fuel Process. Technol. **85**, 1283–1300 (2004)
103. Ooi, Y.-S., Zakaria, R., Mohamed, A.R., Bhatia, S.: Catalytic conversion of palm oil-based fatty acid mixture to liquid fuel. Biomass Bioenergy **27**, 477–488 (2004)
104. Dandik, L., Aksoy, H.A., Erdem-Senatalar, A.: Catalytic conversion of used oil to hydrocarbon fuels in a fractionating pyrolysis reactor. Energy Fuel **12**, 1148–1152 (1998)
105. Twaiq, F.A., Zabidi, N.A.M., Mohamad, A.R., Bhatia, S.: Catalytic conversion of palm oil over mesoporous aluminosilicate MCM-41 for the production of liquid hydrocarbon fuels. Fuel Process. Technol. **84**, 105–120 (2003)
106. Mbaraka, I.K., Shanks, B.H.: Conversion of oils and fats using advanced mesoporous heterogeneous catalysts. JAOCS **83**, 79–91 (2006)
107. Ooi, Y.-S., Zakaria, R., Mohamed, A.R., Bhatia, S.: Catalytic cracking of used palm oil and palm oil fatty acids mixture for the production of liquid fuel: kinetic modeling. Energy Fuel **18**, 1555–1561 (2004)

108. Katikaneni, S.P.R., Adjaye, J.D., Bakhshi, N.N.: Performance of aluminophosphate molecular sieve catalysts for the production of hydrocarbons from wood-derived and vegetable oils. Energy Fuel **9**, 1065–1078 (1995)
109. Charusiri, W., Vitidsant, T.: Kinetic study of used vegetable oil to liquid fuels over sulfated zirkonia. Energy Fuel **19**, 1783–1789 (2005)
110. Charusiri, W., Yongchareon, W., Vitidsant, T.: Conversion of used vegetable oils to liquid fuels and chemicals over HZSM-5, sulfated zirconia and hybrid catalysts. Korean J. Chem. Eng. **23**, 349–355 (2006)
111. Danuthai, T., Jongpatiwut, S., Rirksomboon, T., Osman, S., Resasco, D.E.: Conversion of methylesters to hydrocarbons over an H-ZSM-5 zeolite catalyst. Appl. Catal. A **361**, 99–105 (2009)
112. Danuthai, T., Jongpatiwut, S., Rirksomboon, T., Osman, S., Resasco, D.E.: Conversion of methylesters to hydrocarbons over Zn-modified H-ZSM-5 zeolite catalyst. Catal. Lett. **132**, 197–204 (2009)
113. Sooknoi, T., Danuthai, T., Lobban, L.L., Mallinson, R.G., Resasco, D.E.: Deoxygenation of methylesters over CsNaX. J. Catal. **258**, 199–209 (2008)
114. Prokešová, P., Mintova, S., Čejka, J.: Preparation of nanosized micro/mesoporous composites. Mater. Sci. Eng. C **23**, 1001–1005 (2003)
115. Corma, A., Huber, G.W., Sauvanaud, L., O'Connor, P.: Processing biomass-derived oxygenates in the oil refinery: catalytic cracking (FCC) reaction pathways and role of catalyst. J. Catal. **247**, 307–327 (2007)
116. Bormann, K., Tilgner, H., Moll, H.J.: Rape seed oil as a feed component for the catalytic cracking process. Erdol Erdgas Kohle **109**, 172–176 (1993)
117. Bormann, K., Tilgner, H.: On the influence of rape seed oil triglycerides on the catalytic cracking of petroleum distillate. Erdol Erdgas Kohle **110**, 75–77 (1994)
118. Stadlbauer, E.A., Altensen, R., Bojanowski, S., Donnevert, S., Fiedler, A., Hossain, S., Rossmanith, J., Schilling, G.: Production of hydrocarbons from animal fat by thermocatalytic cracking. Erdol Erdgas Kohle **122**, 64–69 (2006)
119. Benson, T.J., Hernandez, R., French, W.T., Alley, E.G., Holmes, W.E.: Elucidation of the catalytic cracking pathway for unsaturated mono-, di-, and triacylglycerides on solid acid catalysts. J. Mol. Catal. A **303**, 117–123 (2009)
120. Vonghia, E., Boocock, D.G.B., Konar, S.K., Leung, A.: Pathways for the deoxygenation of triglycerides to aliphatic hydrocarbons over activated alumina. Energy Fuel **9**, 1090–1096 (1995)
121. Schmidt, S.: Albemarle to supply catalysts for NExBTL plant (2008). http://www.biomassmagazine.com/article.jsp?article_id=1862. Accessed 5 Feb 2010

FUTURE REFINING CATALYSIS – INTRODUCTION OF BIOMASS FEEDSTOCKS

David KUBIČKA
Department of Refinery and Petrochemical Research, Research Institute of Inorganic Chemistry, Záluží 1, 436 70 Litvínov, Czech Republic; e-mail: david.kubicka@vuanch.cz

Received April 30, 2008
Accepted August 18, 2008

Refining catalysis has been developing over many years to satisfy the demand for high-quality and environmentally-acceptable automotive fuels. Biomass-derived feedstocks have been recently introduced into refineries posing thus new challenges for refining processes and catalysis. The manuscript focuses on three prominent biomass-derived feedstocks: triglycerides, bio-oils and Fischer–Tropsch products from gasified biomass. Due to high oxygen content in biomass feedstocks, deoxygenation processes play an important role in upgrading of these feedstocks. Thus, first peculiarities of deoxygenation are discussed in detail in the context of hydrotreatment processes. Different possibilities of triglycerides and bio-oils deoxygenation including their coprocessing with crude-oil-derived fractions are described. Since biomass-to-liquid processes are very important for the conversion of general biomass into liquid products, the second part deals with the aspects of biomass conversion to synthesis gas, Fischer–Tropsch synthesis and introduction of new co-catalysts.
Keywords: Refining catalysis; Biomass feedstocks; Triglycerides; Bio-oils; Hydrodeoxygenation; Fischer–Tropsch synthesis.

Crude-oil refining is one of the most important industries of our time. It supplies the society mainly with automotive fuels covering thus one third of its energy consumption[1]. At the same time it is an exclusive supplier of feedstocks for the petrochemical industry which produces a wide variety of base chemicals (ethene, propene, benzene, ammonia, sulfuric acid) which are essential for the production of polymers and other products. Since the crude-oil reserves are finite and decreasing, new resources for the production of fuels and chemicals have to be sought.

As far as transportation fuels and base chemicals are concerned, our economy is almost completely carbon-based (hydrocarbon-based), i.e. the transportation fuels and base chemicals have a carbon chain backbone. The only sustainable (renewable) source of organic carbon is currently the plant biomass[2]. Consequently, the efficient use of this source is the only feasible way

Collect. Czech. Chem. Commun. 2008, Vol. 73, Nos. 8–9, pp. 1015–1044

doi:10.1135/cccc20081015

forward in order to decrease the impact of human activities on the environment (climate) on the one hand, and to facilitate a transition from crude-oil-dependent society (i.e. an unsustainable one) to a renewable-energy-dependent society on the other. The estimated worldwide biomass energy potential in 2050 is[3] between 150–450 EJ/year. For comparison, the current annual worldwide total energy consumption is about 470 EJ and has been predicted[4] to rise to 740 EJ/year in 2030.

The crude-oil refining relies completely on catalysis. The fractional composition of crude oil deviates substantially from the desired product slate and catalytic processes, such as fluid catalytic cracking (FCC) and hydrocracking have to be used to satisfy the demand for gasoline and diesel. Additionally, the composition of the primary gasoline and diesel fractions is altered by subsequent catalytic processes to optimize their properties (e.g. by catalytic reforming, isomerization) and to minimize their environmental impacts (e.g. hydrodesulfurization). Despite the maturity of these technologies, they continue to develop intensively. Apart from the economics the main development drivers in the refining catalysis are environmental and social issues, development of refinery processes and feedstock changes. The mutual interactions between these drivers are schematically depicted in Fig. 1.

Environmental concerns and growing public awareness have successfully contributed to a substantial decrease in pollutants emitted due to combus-

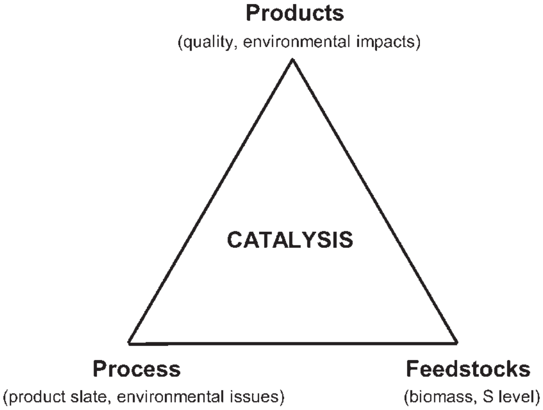

FIG. 1
Schematic representation of development drivers in the refining catalysis (for details, see the text)

tion of automotive fuels; e.g. Pb-based octane boosters were completely abandoned in the developed countries[5], the sulfur level in transportation fuels has been drastically reduced, ultralow sulfur fuels (10 ppm S) have been introduced in the developed countries[5–7] and the concentration of aromatics has been cut as well[5,6,8]. The role of catalysis in the achieved environmental benefits is indispensable, as will be shown later using the example of hydrodesulfurization. Catalysis plays a vital role in development of refining processes as well; let the prime objective be the product-slate modification or the environmental aspects. New catalytic processes have been developed (e.g. production of octane boosters, such as methyl or ethyl *tert*-butyl ethers[9]) or are being developed (e.g. alkylation using heterogeneous catalysts)[10]. Processes have been (and are being) modified to satisfy the changing demands: the increasing demands for middle distillates (diesel fuel) and propene have given rise to new hydrocracking[11] and FCC catalysts[12,13], respectively.

Finally, catalysis has to deal with the challenge of new and ever-changing feedstocks. On the one hand, the crude oils are getting heavier and more sour (i.e. have higher density and sulfur content)[14] and, at the same time, lighter products with ultralow sulfur contents are demanded[15]. On the other hand, the limited reserves of fossil fuels and the increasing concentrations of atmospheric CO_2 that is generally accepted to be caused by combustion of fossil fuels and to contribute to global warming have led to introduction of biomass, a renewable source of carbon, into the liquid fuels production scheme[16,17].

The biomass-based fuels may help diminish the impact of human activities on the environment, provided that they are produced in a sustainable way (based on their life cycle analysis). Other possible benefits are decreasing the dependence of fuel production on crude oil and development of rural areas. As the price of crude oil is predicted to continue growing (the crude-oil price will climb to a record average price above 90 \$/barrel and possibly even above 100 \$/barrel in 2011)[18], biomass-derived fuels (biofuels) may even become price-competitive. (The crude-oil prices predicted for 2011 have become reality already in February 2008.) The gasoline and diesel engines will remain the dominating powertrains[16,19] until 2030 and biofuels should thus be compatible with these engine technologies as well as with the corresponding fuels. Moreover, the compatibility of biofuels with fossil automotive fuels is important also from the distribution point of view. Processing of biomass feedstocks in crude-oil refineries to produce biofuels offers a wide range of advantages from both technological and economical point of view – availability of up- and down-stream processes for automotive fuels, experience in catalytic processes for fuel production, existing technologies to be used for coprocessing biomass and crude-oil feedstocks, availability of utilities and possibility of synergies.

Besides biofuels there are other alternatives to conventional transportation fuels such as methane (compressed or liquefied), hydrogen and fuel cells. Nevertheless, the state-of-art of these alternatives indicates that they will cover only a small share of the energy demand in the transport sector[16,19] by 2030 and therefore they cannot be, in contrast to biofuels, used immediately. In the short term, biofuels are thus the only alternative to reduce the impact of fossil fuels on the environment. In the long term, the energy efficiency, distribution infrastructure and sustainability of the individual alternatives will determine which will predominate beyond 2030. The perspective of biofuels is in the use of the abundant lignocellulosic biomass, which can be converted by (i) pyrolysis into a mixture of oxygen-containing compounds (bio-oil) or by (ii) gasification into synthesis gas (a mixture of H_2 and CO). The main advantages of lignocellulosic biomass are its availability and independence on food-supply chain; the main disadvantages being the high degree of complexity and variability of composition, which make its use technologically and energetically demanding.

The objective of this contribution is to address the possibilities of processing or coprocessing biomass-derived feedstocks in existing oil refineries. Two principal catalytic approaches will be discussed – deoxygenation of liquid biomass feedstocks, such as vegetable oils and bio-oils, and synthesis of fuels and chemicals from gasified biomass.

FROM HYDRODESULFURIZATION (HDS) TO HYDRODEOXYGENATION (HDO) – GOING BEYOND BIODIESEL

A typical feature of biomass is that it contains large quantities of heteroatoms, mainly oxygen. The elimination of heteroatoms is vital for the quality of the final fuels, as these should contain only hydrocarbons in the optimal case. The presence of heteroatom-containing compounds is usually a source of problems – combustion of sulfur-containing compounds contributes significantly to air pollution, oxygenates lower the higher heating value (HHV) of the fuel, may be miscible with water and suffer from decreased oxidation stability as compared with hydrocarbons. In spite of these drawbacks, ethers and lower alcohols have found their use in gasoline and methyl esters of fatty acids (FAME, also called biodiesel) are blended in diesel.

Sulfur is the main heteroatom present in fossil fuels and is removed by hydrodesulfurization (HDS), which is the prominent reaction in hydrotreatment, hydroprocessing and hydrocracking. Analogously, oxygen can be removed from fuels by hydrodeoxygenation (HDO) using, e.g., hydrotreatment or hydrocracking processes. Biomass feedstocks that are rich in oxygen could be thus upgraded by HDO to obtain high-quality automotive fuels. Obviously, HDO would challenge the existing production of biodiesel as both technologies would compete for the same feedstocks, namely triglycerides.

Conventional Biodiesel

Biodiesel is currently the most important biofuel for diesel engines. Unlike vegetable oils it has a suitable viscosity and boiling point range. Depending on the local climate, rapeseed, soybean and palm oils are used for biodiesel production in Europe, U.S.A. and South Asia, respectively. Biodiesel production is based on the reaction of triglycerides of fatty acids with methanol in the presence of basic catalysts that yield methyl esters of the fatty acids (biodiesel) and glycerol (Fig. 2). Several detailed reviews can be found in the literature[20–22] and, thus, only the aspects of biodiesel production that are pertinent to this review will be briefly highlighted.

Glycerol is a byproduct of biodiesel production and its production corresponds to roughly 10 wt.% of the starting vegetable oil. Consequently, its utilization for making value-added chemicals is essential for the economics of biodiesel manufacture. Due to a sharp increase in biodiesel production in recent years[23], there is an excess of glycerol[24] on the market pushing down its prices and decreasing the profitability of biodiesel units. New applications of glycerol are, thus, required and developed[24]. The profitability is

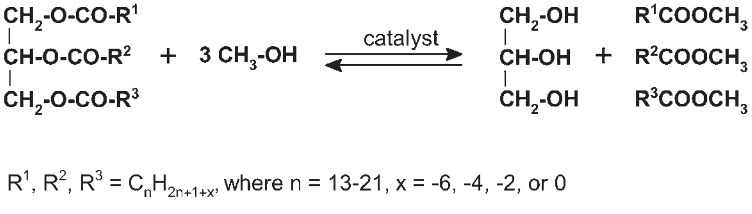

FIG. 2

Simplified scheme of transesterificatition of vegetable oils with methanol. Typical reaction conditions: 60 °C, 101 kPa, CH_3OH/oil = 5–6 mol/mol further affected by high prices of the raw materials, and new suitable feedstocks are intensively sought[25,26]. In order to meet the biodiesel legislative specifications, the starting vegetable oils have to be of high quality and the feedstock flexibility is, thus, rather low. The main limiting quality factor from the production point of view is the content of free fatty acids, which, if present at high concentrations (>2%), prevent the use of the conventional process[20,21].

The industrial processes rely on homogenous catalysts (NaOH, KOH, or the corresponding methoxides) and are one of the few large-scale processes using homogeneous catalysts. The homogeneous catalyst exhibits high activity, but its inherent drawback is separation from products. Consequently, large quantities of waste waters need to be treated and, moreover, the produced glycerol contains impurities and water (its concentration is usually >20%). This severely limits glycerol application in synthesis of value-added chemicals and hence has a negative impact on the whole process economy. Recently, Axens has developed a heterogeneously-catalyzed process that is claimed to have higher yields of biodiesel and, more importantly, a glycerol purity >98% without need for its separation[27] making it suitable for the production of specialty chemicals. Nevertheless, the homogenous process still predominates.

Biodiesel can be easily blended into crude-oil-derived diesel. In Europe, it is allowed to sell diesel fuel containing up to 5% (v/v) of biodiesel as a conventional diesel[6]. The mixtures containing a higher percentage of biodiesel have to be distributed separately because they do not meet the specifications of diesel engine manufacturers. Due to the stricter CO_2/km emission requirements[28] set for the modern vehicles, the lower oxidation stability of biodiesel (as compared with diesel) becomes a liability. To achieve the CO_2 emission standards, higher injection pressures and, consequently, temperatures are used. Under these conditions, biodiesel is prone to polymerization reactions which form deposits in the injection nozzles and lead ultimately to engine failure[29]. The long-term storage of biodiesel is problematic as well since oxidation and biodegradation (by microorganisms) can take place. The cold-flow properties of biodiesel are acceptable for mild climate regions, but not for the cold climate ones.

The use of vegetable oils for production of biodiesel (fatty acid methyl esters (FAME)) is associated with the socio-economic and technical problems discussed above. Some of them could be tackled by converting triglycerides, in particular those not suitable for food production, to hydrocarbons in the diesel fuel range, so-called green or renewable diesel. This can be achieved by selectively removing oxygen atoms while keeping the carbon–carbon bonds intact, i.e. by hydrodeoxygenation (HDO).

Apart from the technical problems discussed above, the use of triglycerides is connected with the fundamental questions of the sustainability of their production and of the competition with food production. To address these issues, non-food triglyceride sources such as algae oils, trap greases, waste vegetable oils and animal fats, non-edible oils from marginal lands should be primarily used for production of fuels from triglycerides. Some of these feedstocks are not suitable for conventional biodiesel production (trap greases, animal fats); nevertheless they could be conveniently upgraded to transportation fuels by deoxygenation.

Lessons from Hydrodesulfurization (HDS)

Hydrodesulfurization (HDS) is a mature and wide-spread process and the reaction itself has been studied in meticulous detail, due to its industrial significance, for several decades[7,15,30–32]. It can thus provide useful insights into the considerably less investigated hydrodeoxygenation (HDO) which is in principle an analogous reaction. In addition, the competition between HDO and HDS during hydroprocessing mixtures containing both organic sulfur and oxygen compounds may be detrimental for common hydrotreatment of crude-oil- and biomass-derived feedstocks.

Hydrotreatment is an indispensable refinery process and the hydrotreatment catalysts are, together with the cracking and three-way exhaust gas catalysts, the most important industrial catalysts[7]. The Mo and W transition metal sulfides promoted with Co and/or Ni metal sulfides have been the active components of hydrotreatment catalysts from the very beginning of the process. They are usually supported on γ-Al_2O_3 doped sometimes with SiO_2, phosphorus and boron[7]. Despite the fact that the active components of the hydrotreatment catalysts have not really changed over the years, they have undergone substantial development and innovations in order to cope with the ever-growing requirements for their performance. The main development drivers have been the need to process sourer and heavier crude oils including new synthetic crude oils produced from tar sands, the increasing demand for transportation fuels and the changing product slate demand, the production of ultralow sulfur transportation fuels (environmental concerns), the innovations in the engine and automotive industry and the efforts to increase the refinery throughput[15].

In order to increase the performance of hydrotreatment catalysts it is essential to understand in detail the hydrotreatment chemistry, particularly the inhibition effects involved, and the active sites. The inhibition in hydrotreatment originates from the competitive adsorption of possible reactants (S-, N- and O-containing organics and aromatics) and from hydrogen availability at the active sites, i.e. from hydrogen diffusion limitations. It has been observed that trace concentrations of organic nitrogen compounds (<30 ppm) deteriorate the HDS activity by strong adsorption on active sites and their inhibition[31,33–38]. While there is an agreement on the inhibition by N-containing species, the inhibition by aromatics has been a matter of disputes[33,39–41]. Recently, Choudhary et al.[39] have reported that in hydrotreatment of heavy oils the extent of sulfur removal is determined by the content of aromatics having three or more rings and not by the nature and content of sulfur species. The inhibition effect of aromatics seems to depend on their adsorption strength as compared with that of sulfur species. Due to the strong adsorption of the aromatics containing three and more rings, they inhibit the HDS reactions[39,40] while the effect of aromatics having one or two rings on HDS is negligible[33,40]. Using model feedstocks, Egorova et al.[37] have observed inhibition of HDS by naphthalene, but not by toluene. Hence, HDS of heavy oils is more demanding than HDS of naphtha and middle distillates due to higher concentrations of polyaromatic hydrocarbons in heavy oils. However, only little is known about the effects of oxygenates on HDS and of S- and N-species and aromatics on HDO. Organic nitrogen compounds, in particular the basic ones, and H_2S cause strong to moderate inhibition of HDO [31]. It has been reported that the efficiency of a typical HDS process can be expected to decrease when S- and O-containing compounds are present simultaneously[42].

The importance of the inhibition effects has grown significantly with the advent of ultralow sulfur fuels in the recent years, as even the most refractory S-containing species (e.g. dimethyldibenzothiophenes) have to be eliminated to achieve <10 ppm S in the final product. Any loss of HDS activity is thus detrimental. As a result, much attention has been focused on revealing the reaction pathways of HDS [31,32,43–48]. Out of a great variety of organic S-containing species, benzothiophenes and dibenzothiophenes (DBT) are the most difficult to desulfurize. Generally, it is agreed that their desulfurization follows two parallel reaction pathways: hydrogenolysis (direct elimination of S) and hydrogenation followed by extraction of sulfur in the form of hydrogen sulfide[32,46,47] (Fig. 3). In desulfurization of DBT, the direct elimination of sulfur by hydrogenolysis is preferred[32]. The rate of direct sulfur elimination, however, decreases significantly, when alkyl- or dialkylbenzothiophenes (in particular those substituted at the carbon atoms adjacent to the sulfur atom) have to be desulfurized, whereas the hydrogenation pathway is practically unaffected[32,46]. Consequently, $CoMoS/Al_2O_3$ is outperformed in HDS of 4,6-dimethyldibenzothiophene (DMDBT) by $NiMoS/Al_2O_3$, which is a superior hydrogenation and HDN catalyst as compared with $CoMoS/Al_2O_3$ (ref.[46]). However, the sulfur removal via the hydrogenation pathway is accompanied by a significant increase in hydrogen consumption due to aromatics hydrogenation and, thus, the isomerization of DMDBT to facilitate the direct HDS (hydrogenolysis) to save hydrogen has been proposed and investigated[43,44,48–50] (Fig. 3).

The fundamental knowledge of the desulfurization reaction pathways, their inhibition mechanisms and the active sites involved is therefore of paramount importance for the selection of the most efficient catalyst and of the optimum operating conditions. As biomass-derived raw materials (oxygenated feedstocks) are close to being introduced into refinery streams for hydroprocessing, deoxygenation (hydrodeoxygenation) has to be taken into account. Particularly, the plausible inhibition effects have to be studied in detail together with HDS, HDN and hydrogenation reactions to optimize the performance of the current hydrotreatment catalysts with respect to the new, oxygen-containing, refinery feedstocks.

Removing Oxygen – Hydrodeoxygenation (HDO) and Hydrodecarboxylation (HDC)

A wide variety of raw materials suitable for the production of fuels can be derived from biomass – synthesis gas or hydrogen (by gasification), ethanol

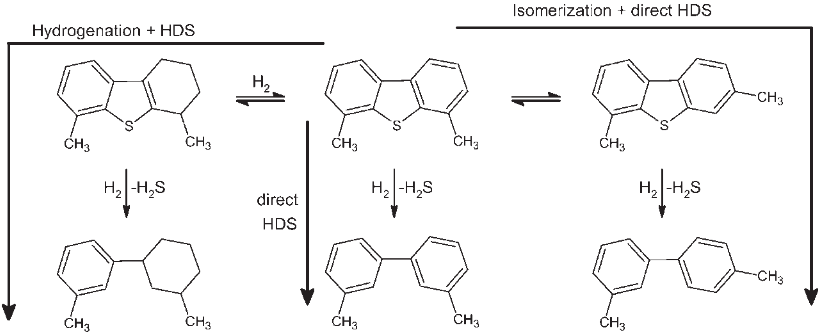

FIG. 3
A general scheme of 4,6-dimethyldibenzothiophene hydrodesulfurization[43–45]

or butanol (by fermentation), sugars (by hydrolysis), bio-oil (by pyrolysis) and triglycerides (by extraction and/or pressing). The production and use of alcohols and sugars for fuels fall outside the scope of this paper and will not be discussed here; the use of synthesis gas will be discussed in a separate chapter. This chapter will be devoted to deoxygenation of biomass-derived liquid feedstocks, i.e. to elimination of oxygen from vegetable oils and bio-oils.

Vegetable oils (i.e. triglycerides of fatty acids) obtained from suitable plants are currently used as food and raw material for biodiesel production (see above). In contrast to biodiesel production, low quality oils (e.g. used frying oils), yellow and trap greases, tallow and lard, i.e. resources that can not be used for food production, can be used as a starting material for production of fuels by deoxygenation as well. Typical oxygen content is about 10 wt.%.

Bio-oils, on the other hand, are manufactured from non-food biomass (wood, straw, etc.) by pyrolysis (usually without a catalyst) in the absence of oxygen or by high pressure liquefaction. Although the high pressure liquefaction yields better-quality bio-oil product (lower content of moisture and oxygen, Table I), the lower yield of bio-oil and higher price, in comparison with pyrolysis, favor the biomass pyrolysis processes for industrial

TABLE I
Elemental composition (in wt.%), moisture content (in wt.%) and properties of biomass- and crude-oil-derived feedstocks[2,59]

Composition, %	Heavy fuel oil	Vegetable oil[a]	Bio-oil	
			pyrolysed[b]	liquefied
Carbon	85.2	77.5	45.3	74.8
Hydrogen	12.8	11.6	7.5	8.0
Sulfur	1.8	<0.1	<0.1	<0.1
Nitrogen	0.1	<0.1	<0.1	<0.1
Oxygen	0.1	10.9	46.9	16.6
Moisture	<0.1	<0.1	44.8	5.1
HHV[c], MJ/kg	41.2	39.7	22.6	35.7
Viscosity, cP	12 (40 °C)	38 (40 °C)	59 (40 °C)	15000 (61 °C)

[a] Rape-seed oil. [b] Flash pyrolysis of wood. [c] Higher heating value.

application[51]. The highest yields of bio-oil (up to 70% on dry basis) are obtained by flash pyrolysis which is typically carried out at 500 °C, at very high heating rates and short contact times (typically <1 s)[52,53]. The main benefits of bio-oil in comparison with raw biomass are high energy density and easy transportability[53]. Consequently, pyrolysis processes are studied intensively[52–58] and several demonstration units using different concepts of pyrolysis (fluid bed, rotating cone, twin screw) have been constructed[54].

The composition of both discussed feedstocks differs enormously and will undoubtedly affect the mechanism of their deoxygenation. Whereas bio-oils are formed by very complex mixtures of oxygenates (phenols, ketones, aldehydes, carboxylic acids, esters, alcohols and ethers)[59], vegetable oils are formed almost exclusively by triglycerides of fatty acids, i.e. esters, accompanied in some cases by free fatty acids. Moreover, the high content of moisture in bio-oil, its immiscibility with crude-oil fractions and chemical instability pose a further challenge to their processing. Therefore, both the direct conversion to fuels by deoxygenation and gasification (steam reforming) to synthesis gas has been proposed for bio-oil upgrading[2,54,57,58,60,61]. On the other hand, direct deoxygenation of vegetable oils to fuels is the preferred upgrading technology in addition to their transesterification yielding biodiesel (see above).

Mechanistic Aspects of HDO

Deoxygenation of biomass-derived feedstocks can be achieved by several reactions – hydrodeoxygenation, decarboxylation, decarbonylation and dehydration[59]. Various combinations of these reactions can take place, depending on the feedstock composition, catalyst choice and reaction conditions. The most common and universal is hydrodeoxygenation (HDO), in which oxygen-containing materials are reduced with hydrogen, and hydrocarbons and water are formed. Decarboxylation is restricted only to carboxylic acids and their esters; the formation of hydrocarbons is accompanied by the release of CO_2. In the presence of hydrogen, the alkene resulting from CO_2 elimination is hydrogenated to the corresponding alkane and the reaction is then called hydrodecarboxylation (HDC). Decarbonylation and dehydration are reactions of ketones or aldehydes and alcohols, respectively. In line with the composition of biomass-derived feedstocks, hydrodeoxygenation is the most important deoxygenation reaction.

The catalytic hydrodeoxygenation has been reviewed by Furimsky[59] and the following order of reactivity of O-containing groups has been put forward: alcohols > ketones > alkyl ethers > carboxylic acids ≈ *m*- and *p*-alkyl-substituted phenols ≈ naphthol > phenol > diaryl ethers ≈ *o*-alkyl-substituted phenols ≈ alkylfurans > benzofurans > dibenzofurans[59,62,63]. In view of biomass feedstocks available, the reactivities of phenols, acids and esters are the most relevant. Phenols, which may account for up to 25% of liquids obtained by pyrolysis of lignocellulosic materials[59], are refractory oxygenates. Moreover, HDO of phenols depends on the position and type of other substituents; e.g., the reactivity of methylphenol (MP) decreases in the order *m*-MP > *p*-MP > *o*-MP [59,64]. HDO of phenols and furans (including benzo- and dibenzofurans) follows two parallel reaction pathways – direct (through hydrogenolysis) and indirect which proceeds by hydrogenation of aromatic ring[59,62,65].

On the other hand, carboxylic acids and their esters are more reactive than phenols[66,67]; carboxylic acids are less reactive than their esters[66]. Furthermore, there are two reaction pathways responsible for the conversion of carboxylic acids and their esters to hydrocarbons – hydrogenation of the carboxylic group and decarboxylation[66–69]. The origin of the decarboxylation activity of the sulfidized metal catalysts (NiMo, CoMo) has not been yet satisfactorily explained. It was, however, reported by Weisser and Landa[70] that sulfides of the promoters, i.e. Ni and Co, are more active in decarboxylation than molybdenum sulfide.

HDO is a reaction analogous to the other hydrotreatment reactions, namely hydrodesulfurization (HDS) and hydrodenitrogenation (HDN); the same types of catalysts, i.e. NiMo and CoMo sulfides, have been extensively studied[59,66–69]. HDO, HDS, HDN and hydrogenation of aromatics are competing reactions and this has to be kept in mind when studying real reaction systems. It has been established that the hydrotreatment rate decreases generally in the order HDS > HDO > HDN [59]. Nevertheless, deviations from the established order exist due to the complexities of a given feedstock, choice of catalyst and due to the inhibition of HDS, HDO and HDN by S-, O- and N-containing compounds and aromatics, including self-inhibition, i.e. inhibition by the reactant molecules[59].

Hydrogen sulfide, ammonia and water, i.e. the products of HDS, HDN and HDO, respectively, inhibit HDO of different O-containing compounds. For instance, in HDO of 4-ethylphenol the inhibition increases in the order H_2O << 2-ethylphenol < H_2S < NH_3 [65]. Ammonia inhibits the conversion of carboxylic esters and methoxy groups, but does not affect conversion of ketones[68]. H_2S, on the other hand, suppresses the conversion of ketones and phenols (by inhibiting their direct hydrogenolysis) and enhances the conversion of carboxylic esters by promoting their decarboxylation[63,67,68,71]. It was suggested[68,72] that the promotional effect is due to an increase in concentration of Bronsted acid sites in the sulfide phase caused by H_2S. Moreover, addition of H_2S to a feed containing oxygen compounds does not prevent the sulfidized catalyst deactivation[71,72]. In contrast to H_2S and NH_3, water has only a very weak inhibiting effect on the HDO reactions[68], but it dramatically lowers the overall catalyst activity[73,74]. The loss of the activity was ascribed to partial re-crystallization of the support γ-Al_2O_3 into the hydrated boehmite phase and partial oxidation of the NiS promoter; oxidation of the MoS_2 phase, however, was not observed[74]. Addition of H_2S was reported to compensate the loss of activity caused by water[73].

Apart from the inhibition by hydrotreatment products, heteroatoms-containing compounds can cause inhibition of hydrotreating reactions as well[42]. Interactions between sulfenyl and methoxy groups affecting the HDS and HDO rates have been observed. It has been suggested that the efficiency of a typical HDS process can be expected to decrease as a result of interactions between sulfenyl and methoxy groups[42].

HDO of Real Feeds – Conversion of Vegetable Oils

The experiments using probe compounds are undeniably crucial for revealing the underlying mechanisms of HDO, studying the inhibition effects and developing more active and selective catalysts. Nevertheless, experiments using real feedstocks under real conditions cannot be omitted as they provide invaluable information for process development. Cracking and hydrotreating approaches were suggested for upgrading vegetable oils (or, more generally, triglycerides) to hydrocarbons. Zeolites, mesoporous materials and composite materials have been studied extensively in the conversion of vegetable oils or fatty acids to hydrocarbon fuels[75–79]. Main products of catalytic cracking of vegetable oils are hydrocarbon gases and gasoline fraction; however, the yield of the most desired fuel fraction, i.e. diesel, is low[75–79]. Moreover, the liquid products contain rather high concentrations of aromatics[75–79] which are in conflict with the newest fuel specifications. Addition of vegetable oil to fluid-catalytic-cracking (FCC) feedstock led to an increased formation of coke[80]. Nonetheless, co-processing of vegetable oils with vacuum gas oil (VGO) has been proposed for production of gasoline and olefins[81–83] and has been planned for commercial demonstration[84].

The hydrogenation processes (hydrocracking, hydrotreatment), on the other hand, facilitate direct conversion of vegetable oils to hydrocarbons in the diesel fuel boiling range and seem thus to be more promising technologies even though they consume hydrogen[83–95]. Apart from academic research activities, hydrodeoxygenation of triglycerides attracts attention of the industrial research as well[83,89–95]. The Finnish company Neste Oil has developed and commercialized a process, called NexBTL [89–91], for diesel production from vegetable oils and greases and other oil companies are developing their own solutions as well[92–95]. Diesel fuel obtained by HDO of vegetable oils (green diesel) is fully compatible with crude-oil based diesel. As it contains no aromatics and sulfur, it is even superior from the environmental point of view. The poor cold-flow properties of the primary HDO product have been solved by its mild isomerization[91]. Moreover, it has been demonstrated that NexBTL diesel, i.e. product of HDO of triglycerides, shows environmental benefits (in terms of emissions and energy consumption) over both conventional diesel and biodiesel (FAME)[96,97].

The experimental results of hydrotreatment (hydrodeoxygenation) of rapeseed oil over sulfidized catalysts are in a good agreement with the results of HDO of relevant simpler probe compounds[66–69]; two main reaction pathways – direct hydrodeoxygenation (total hydrogenation, HDO) and decarboxylation (hydrodecarboxylation, HDC) – have been identified[87,88]. The extent of both reactions, at a complete conversion of rapeseed oil, is sensitive to the reaction temperature, pressure and choice of the catalyst. With increasing reaction temperature the yield of the HDC products rises at the expense of the HDO products[87,88]. On the other hand, augmenting hydrogen partial pressure results in the enhanced formation of HDO products[87,88] (Fig. 4). The extent of HDO and HDC reactions can be quite easily determined at complete conversion by using the concentration of hydrocarbons with an even and odd number of carbon atoms, respectively (see Fig. 4).

A simplified reaction network is depicted for triolein, a representative abundant triglyceride in vegetable oils, in Fig. 5. The initial reaction is the hydrogenation of double bonds which proceeds at milder conditions (<250 °C) than those needed for deoxygenation. Depending on the reaction conditions and catalyst choice, the saturated triglyceride undergoes direct hydrodecarboxylation or direct hydrodeoxygenation. Apart from propane, the main products are straight-chain alkanes with an even number of carbon atoms (n-octadecane for triolein) and water in the case of hydrodeoxygenation (HDO) and n-alkanes with an odd number of carbon atoms (n-heptadecane for triolein) and CO_2 in the case of hydrodecarboxylation (HDC). Alternatively, the triglycerides are hydrogenolyzed to the corresponding fatty acids (stearic acid for triolein) which can undergo either HDO or HDC or be hydrogenated to yield the corresponding fatty alcohols. As alcohols are deoxygenated more easily than acids and esters[59], they are seldom found among the reaction products. However, fatty alcohol esters of fatty acids have been identified in the products as a result of esterification reactions[98]. The formation of alkyl esters of fatty acids under the hydrotreatment conditions has been reported by Landa et al.[99]. Besides

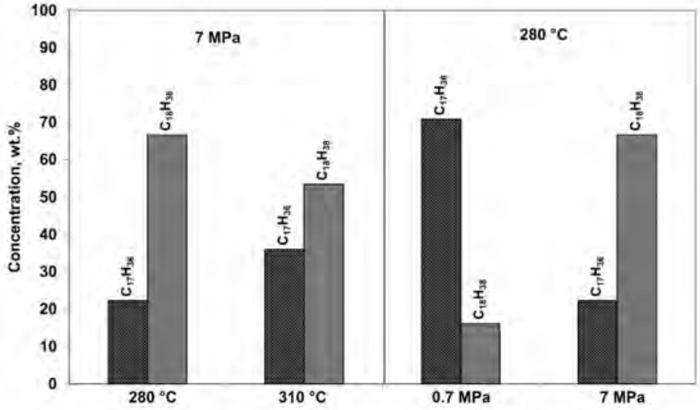

FIG. 4
Effect of temperature and pressure on the distribution of hydrodeoxygenation ($C_{18}H_{38}$) and hydrodecarboxylation ($C_{17}H_{36}$) products

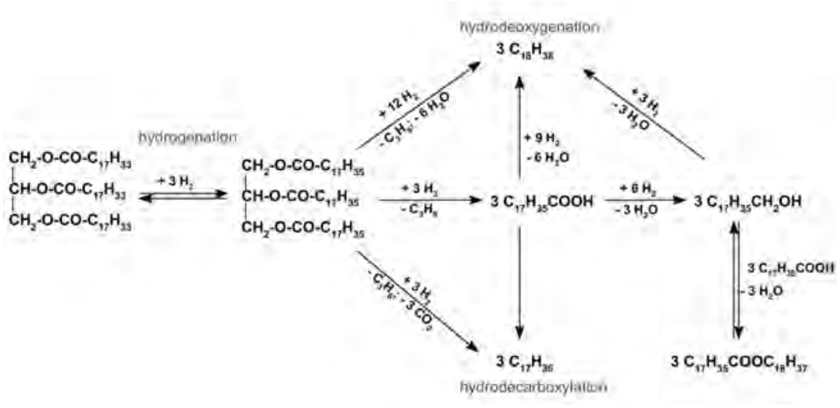

FIG. 5
Scheme of deoxygenation of triolein (the most abundant triglyceride in rapeseed oil)

HDO and HDC, decarbonylation has been proposed to take place as well[85,100]. Nevertheless, there is not enough conclusive evidence for the decarbonylation pathway as CO can originate from partial hydrogenation of CO_2.

The proportion of HDO and HDC at the total conversion of triglycerides to hydrocarbons is decisive for the overall hydrogen consumption of the process. Based on the stoichiometry of both reaction pathways, it is clear that in an ideal case the hydrogen consumption is four times higher for HDO than for HDC of a saturated triglyceride (Fig. 5). However, when sulfidized hydrotreatment catalysts are used, carbon dioxide is partially converted to CO and methane[88,98]; the extent of these reactions depends once again on the catalyst and reaction conditions. Nevertheless, if all CO_2 was converted to methane, the consumption of hydrogen for HDC would be higher than that for HDO. Therefore, selective decarboxylation catalysts having negligible selectivity for the total hydrogenation of CO_2 are sought[101,102].

Hydrotreatment of triglycerides for production of hydrocarbons on an industrial scale can be implemented either by HDO of triglycerides in stand-alone units or by coprocessing of triglyceride feedstocks with crude-oil-derived fractions, e.g. atmospheric gas oil (AGO). Coprocessing offers the advantage of low implementation costs due to the possibility of using the existing hydrotreatment equipment[95]. However, several potential risks have been identified and it has been concluded that processing of vegetable oils in dedicated units was more cost-efficient. The drawbacks of coprocessing include (i) the potential need for a pretreatment reactor to remove contaminants, such as phosphorus and alkali metals; (ii) revamp of the recycle gas systems to deal with the deoxygenation products (CO_2, CO, H_2O); (iii) need for an increase in the quenching capacity as HDO is highly exothermic and (iv) the expected competition of HDO reactions with HDS leading to lower desulfurization efficiency[95]. The suggested negative impact of HDO on HDS reactions[42] has been recently confirmed in coprocessing of AGO with used frying oil (UFO). HDS of a mixture consisting of 90% AGO and 10% UFO required an increase of 4 °C in the HDS temperature as compared with pure AGO in order to obtain 10 ppm S in the final product[103] (Fig. 6).

Conversion of Bio-Oils into Fuels

The upgrading of bio-oils into transportation fuels by deoxygenation is not as advanced as production of fuels from vegetable oils. The main obstacles of bio-oil upgrading are its high moisture content (up to 30%, Table I) and chemical instability. Moreover, the oxygen content is substantially higher than that of triglycerides (Table I) and, consequently, the hydrogen consumption could be prohibitively high. The quality of bio-oil varies significantly depending on the raw material used for pyrolysis and on the severity of reaction conditions and, therefore, the deoxygenation process is more difficult to optimize as compared with triglycerides deoxygenation. Bio-oils can be used for production of fuels either directly by using hydrotreatment[52,53,104] or zeolite upgrading[52,53,77,105–107], or indirectly by converting it first to synthesis gas and subsequently to fuels[2,58] (see next chapter). Hydrotreatment and upgrading of bio-oil over zeolites have been studied intensively using suitable probe compounds to reveal the underlying chemical mechanisms and to identify suitable catalysts[59,65–69,71–74]. Studies using bio-oil as feedstock are less common[52,53,77,104–107].

Hydrotreatment of bio-oils (hydrodeoxygenation) can be performed using conventional hydrotreatment catalysts, i.e. supported sulfidized metals, giving a naphtha-like product[52,53]. Due to chemical instability of the bio-oil it is necessary to treat it in a two-stage process. In the first step, bio-oil is stabilized under mild reaction conditions (250–275 °C) by hydrogenation of the most reactive double bonds to prevent its polymerization and fouling of the catalyst under typical hydrotreatment conditions. Only in the second step, the standard hydrotreatment temperatures (350–400 °C) can

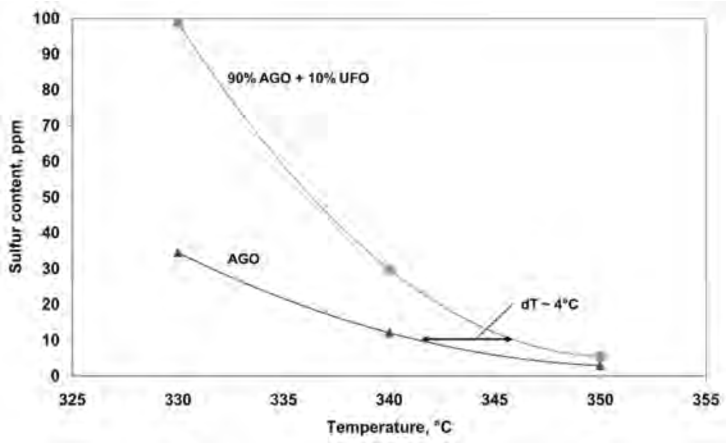

FIG. 6
The effect of addition of used frying oil (UFO) to atmospheric gas oil (AGO) on its hydrodesulfurization[103]

be used to deoxygenate bio-oil[52,53]. The hydrotreatment pressures may vary in a wide range (7–20 MPa)[52,53] depending on the composition of bio-oil on the one hand, and on the desired level of deoxygenation on the other. Oxygenated compounds are generally more resistant to hydrotreatment than sulfur-containing compounds[59] and require thus more severe reaction conditions[52] and optimization of the catalyst as well as optimization of the process conditions for a particular bio-oil feedstock[52]. Some applications of bio-oil do not necessitate full deoxygenation, e.g. fuels for stationary engines, and only partial hydrotreatment has been suggested for them[52]. This approach has the benefit of lower hydrogen consumption which is fairly high for complete hydrodeoxygenation (600–1000 $l_{H2}/kg_{bio\text{-}oil}$)[52] and is, therefore, the major inhibiting factor of its commercialization. The progress in hydroprocessing of bio-oils over the past 25 years has been recently reviewed by Elliot[104].

Upgrading of bio-oils over zeolites is a promising alternative to hydrotreatment, as this can be achieved at low-pressures (even atmospheric) and at temperatures similar to those used for bio-oil production. Thus it offers the advantage of combining the pyrolysis of biomass to produce bio-oil with its subsequent catalytic upgrading[52]. Oxygen is eliminated in the form of water (by dehydration) or in the form of carbon oxides (by decarboxylation or decarbonylation). As external hydrogen is not supplied, hydrogen necessary for partial hydrogenation (saturation, stabilization) of the unsaturated reaction intermediates originates from the hydrogen transfer reactions. Consequently, the product is highly aromatic and large amounts of hydrogen-deficient products, such as coke, tar and char, are formed[77]. The mechanism, however, is not yet fully understood. Due to the recent developments in transportation fuel specifications, the aromatics content has to be decreased and therefore it will become increasingly more difficult to use the highly aromatic product from bio-oil upgrading for blending of automotive fuels. Nonetheless, it could be utilized in the petrochemical sector as a raw material for production of aromatics and derived polymers.

Bio-oil is well-suited for production of specialty chemicals thanks to its complex chemical composition. In this case, the presence of oxygenated compounds becomes an advantage as they may be used directly in synthesis and, therefore, deoxygenation is not desired. The production of chemicals from biomass feedstocks, however, is out of the scope of traditional refineries and will not be, thus, discussed in this paper. The topic has been recently reviewed by several research groups[24,108,109].

BIOMASS TO GAS – A ROUTE TO TAILOR-MADE PRODUCTS

Biomass gasification is a universal tool for conversion of biomass to fuels and chemicals. While hydrodeoxygenation is limited to a special type of liquid feedstocks, such as vegetable oils (triglycerides) or bio-oils, gasification can be used basically for any biomass feedstock. This provides gasification with the inherent advantage of cheaper and more abundant raw materials as compared with HDO.

Gasification can be defined as partial combustion using air or oxygen to produce fuel gas or synthesis gas. Steam is often added to the feed to increase the heating value of the final product gas[52]. Its composition depends on the reaction temperature. Low-temperature gasification (800–1000 °C) yields, in the case of oxygen gasification, the so-called product gas consisting of CO, CO_2, H_2, H_2O, CH_4, hydrocarbons and tars, which is suitable mainly for direct power and heat generation[110]. On the other hand, the product of high-temperature gasification (1200–1400 °C) consists of CO and H_2 (so called biosyngas)[110]. In air gasification, nitrogen is present in addition to the above-mentioned compounds. Biosyngas can be alternatively obtained by catalytic gasification or by removing tar and hydrocarbons from the product gas by thermal cracking or reforming; it is chemically similar to syngas derived from fossil fuel sources[52,110]. When fuels and chemicals are desired, the product gas has to be processed to contain only CO and H_2 in a suitable molar ratio (the usage ratio); for some applications CO_2 may be present as well.

Gasification Challenges

The high diversity of biomass composition makes the production of fuels and chemicals a complex and demanding task as the final products need to have rather well-defined and uniform composition. Gasification enables to convert practically any carbon- and hydrogen-containing feedstock into synthesis gas with a desired usage ratio for a particular application. Nevertheless, the biomass feedstock diversity makes the production of synthesis gas more complex and sophisticated as compared with gasification of fossil fuels (mainly methane and coal)[111]. The main challenge lies in the scattered occurrence of biomass and its low volume energy density in comparison with fossil fuels (e.g. straw bales and diesel fuel have about 2 and 36 GJ/m^3, respectively)[111]. Therefore, collection of biomass from large areas and its transportation over long distances that affects negatively the total costs and energy inputs is necessary. Moreover, gasification, particularly purification and conditioning of synthesis gas, and conversion technologies of syngas are technically demanding and require intensive investment and, hence, large-scale units are preferred. Regional fast pyrolysis of biomass to obtain pyrolysis oil and char has been proposed[111]. The char is then suspended in the pyrolysis oil and the resulting slurry holds up to 90% of the original biomass energy content[111]. More importantly, the volume energy density increases from about 2 to ca. 25 GJ/m^3 and the intermediate can be thus transported over larger distances to central gasification units.

From the view point of crude-oil refinery, the slurry could become one of the raw materials for manufacturing biofuels. Conceptually, the slurry could be either coprocessed by gasification or partial oxidation together with liquid hydrocarbon feedstocks or the synthesis gas could be produced in a separate gasification reactor and then purified and conditioned together with the fossil-based syngas. The use of the existing gas purification and conditioning equipment would decrease the investment intensity of biomass-to-syngas units and biosyngas would get access to downstream conversion processes at the same time. The integration of bio-oil slurry or biosyngas into refineries is an opportunity that needs to be further studied.

Synthesis gas resulting from biomass gasification has typically the C/H ratio equal to about unity[111] and cannot be directly used for synthesis of hydrocarbons as a C/H ratio of less than 0.25 is needed. The concentration of hydrogen can be increased either by addition of hydrogen-rich gas or by partial conversion of CO by water-gas-shift reaction (WGS). Once again, if integrated into a refinery, the existing WGS capacities and excesses of refinery hydrogen could be used. Alternatively, direct removal of CO_2 during gasification resulting in an increased hydrogen concentration in the synthesis gas has been proposed[112]. It relies on addition of a heat carrier capable of forming carbonates, which are then decomposed in a regeneration unit and CO_2 is released during burning off the deposited tar[112].

From the viewpoint of production of fuels, synthesis gas with an adjusted usage ratio (UR) can be converted to fuels either directly by Fischer–Tropsch synthesis (FTS, UR = 2.05–2.15) or methanation (UR = 3) or indirectly via methanol synthesis (UR = 2) and its subsequent conversion into hydrocarbons or dimethyl ether (DME)[113]. In addition to fuels, a broad spectrum of chemicals can be obtained from syngas. The main conversion pathways of syngas[113] are depicted in Fig. 7. The thermal efficiency of liquid fuels production from methane (via syngas) is the highest for methanol, followed by FTS diesel and gasoline from the methanol-to-gasoline (MTG) process[114]. The liquid fuels offer several advantages over methanol, such as high energy density, low vapor pressure, insolubility in water, and compatibility with existing engines and fuel infrastructure[114].

Fischer–Tropsch Synthesis

The importance of Fischer–Tropsch synthesis (FTS) will grow in the years to come, as crude-oil reserves will be depleted and alternative feedstocks for the production of fuels and base chemicals will be used. The traditional synthesis gas sources, natural gas and coal, will be accompanied by biomass as a result of public awareness of the adverse environmental effects of CO_2 emissions. FTS has been developed with varying intensity over the past 80 years. As FTS competes with crude oil for the fuel market, its economic viability depends on the price of crude oil[115]. The FTS technology has been industrially proven in coal-based FTS plants in Germany in 1930's and currently both coal-based (Sasol, South Africa) and methane-based FTS plants (Mossgas, South Africa; Bintuli, Malaysia) are operated[114,115].

FTS can be operated in high-temperature (HTFTS) and low-temperature (LTFTS) mode. The HTFTS uses iron-based catalysts at temperatures 300–350 °C and yields low-molecular-weight olefins and gasoline[114,115]. The

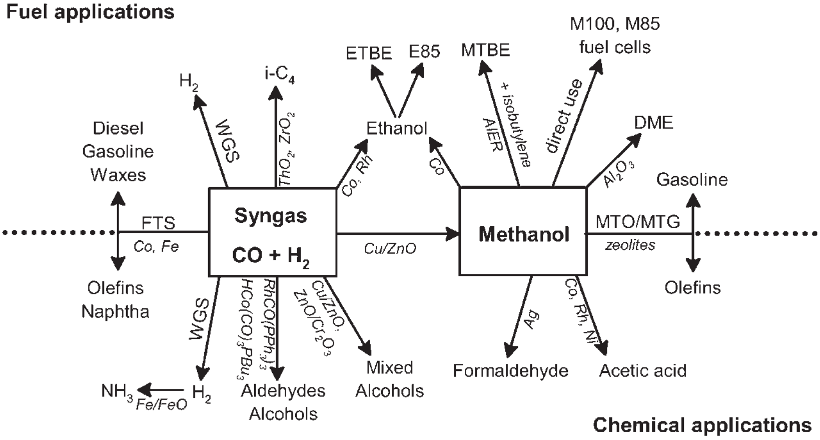

FIG. 7
Synthesis options from synthesis gas[113]. FTS, Fischer–Tropsch synthesis; WGS, water-gas shift; AIER, acid ion-exchange resins; MTO/G, methanol-to-olefins/gasoline; DME, dimethyl ether; E/MTBE, ethyl/methyl *tert*-butyl ether; E85/M100, the fuel containing 85% ethanol/ 100% methanol

LTFTS is operated at temperatures 200–240 °C to produce high-molecular-weight linear waxes and either cobalt- or iron-based catalysts are employed[114,115]. In both operating modes, it is crucial to ensure high heat-exchange rates as FTS reactions are highly exothermic (ΔH = –165 kJ/mol). These are achieved by a suitable reactor setup – fluidized-bed reactors are used in HTFTS and slurry-bed reactors or multitubular fixed-bed reactors and high gas velocities are used in LTFTS [114,115].

Just four metals – Co, Fe, Ni, Ru – have been found to be active FTS catalysts. However, nickel and ruthenium are disqualified from the industrial use, Ni due to its high selectivity for methane and Ru because of its very high price and limited availability[115]. Iron-based catalysts without support can be used both in LTFTS and HTFTS. Catalysts for LTFTS are prepared by precipitation and for HTFTS by fusing magnetite; their main promoter is K_2O [114,115]. On the other hand, cobalt-based catalysts are used only in LTFTS as they have too high selectivity for methane at high temperatures. Since Co is significantly more expensive than Fe, it is used on high surface-area supports, such as Al_2O_3, SiO_2 or TiO_2, with a loading 10–30% (ref.[115]). To improve the reducibility of dispersed Co crystallites, the cobalt-based catalysts are promoted with small quantities noble metals such as Pt, Re or Ru [115].

As a result of the different reaction conditions and catalytic systems employed, products from LTFTS differ from those obtained in HTFTS. HTFTS products contain several per cent of oxygenates and are rich in olefins, particularly α-olefins[114], being suitable for production of chemicals rather than fuels. Moreover, due to the lower chain growth probability (see below) at high temperatures, the product distribution is shifted towards light hydrocarbons[114]. On the other hand, an LTFTS product consists mainly of linear paraffins with smaller amounts of olefins and oxygenates[114]. The product distribution is shifted towards middle distillates and waxes (i.e. high-molecular-weight paraffins) as a result of a higher chain growth probability.

An inherent advantage of FTS is that the products are virtually sulfur-free and aromatics-free. The FTS follows a polymerization-type kinetics resulting in a statistical distribution of hydrocarbons determined by Anderson–Schulz–Flory distribution (ASF). The key parameter of ASF is the chain growth probability α; by changing α the product distribution can be manipulated (Fig. 8). However, with the exception of the two extremes (when $\alpha = 0$ only methane is formed, when $\alpha = 1$ an infinite paraffin chain is formed) the product will consist always of a wide range of hydrocarbons. For wax production by FTS α has a value of about 0.9, this means that the

C-atom selectivity for C_{10+} products is about 74% [116]. It has been calculated and experimentally verified that the maximum attainable gasoline and diesel yields are about 42 and 20%, respectively[114]. The achievable product distribution, hence, differs significantly from the demanded product slate as the yield of the desired fuel products (gasoline and diesel) cannot exceed 60%. Moreover, the yield of gasoline is higher than that of diesel, which is in contrast with the current as well as the expected fuel demands[16].

Apart from the unsuitable product slate, the properties of FTS gasoline and diesel do not meet the respective fuel specifications and need to be further upgraded. As the FTS products are n-alkanes and n-alkenes, they have a high cetane number and are well-suited for diesel fuel blending except for their poor cold-flow properties. Conversely, high concentrations of straight-chain paraffins make the FTS products unsuitable for direct gasoline blending due to their low octane number. The mismatch between the demands for automotive fuels (both in terms of their yields and properties) and the yields and quality of FTS products initiated recently numerous research efforts in this area[114,117–132]. Generally, two basic concepts have been followed: (1) production of FTS waxes (at $\alpha = 0.95$) as these can be obtained in very high yields and their subsequent conversion into desired products by hydrocracking technologies[114,117–122] and (2) use of acid supports or acid co-catalysts (e.g. zeolites) for partial cracking and isomerization of longer paraffins to enhance the yield of gasoline fraction[114,123–132].

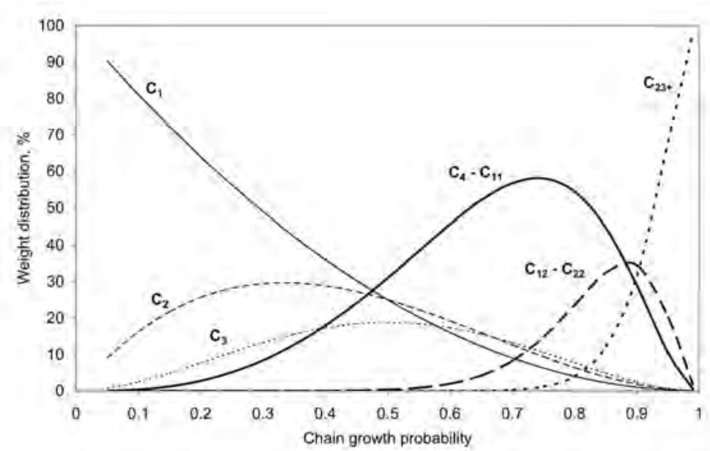

FIG. 8
ASF distribution in FTS

Mild hydrocracking and hydrotreating processes have been applied to convert FTS products in the diesel fuel and wax range into high quality diesel fuel[114,117–122]. The main objectives of the upgrading, apart from increasing diesel yield, are saturation of olefins, removal oxygenates and partial isomerization of n-alkanes into isoalkanes. Traditional refinery hydrotreatment and hydrocracking catalysts can be used[114,118]. Alternatively, modified catalysts containing noble metals (Pt) have been used[119]. Oxygenates, i.e. alcohols and carboxylic acids, have been shown to influence the hydrocracking selectivity for diesel and hydrocracking conversion[120]. It has been proposed that oxygenates present in the feed affected the balance of acid- and metal-active sites in hydrocracking catalysts, thereby modifying the catalyst selectivity[120]. As FTS products are virtually sulfur-free, noble metal catalysts could replace the traditional sulfides (e.g. NiMo, CoMo) for hydrogenation; however, in the case of significant concentration of oxygenates (in particular from HTFTS), the hydrotreatment (hydrodeoxygenation) activity of NiMo or CoMo catalysts is a benefit (see above – HDO section).

Due to the limited number of FTS installations, FTS products are usually processed on-site to final products which are then blended with crude-oil-based products. In the future, however, a tighter bond between crude-oil refineries and FTS units can be expected. Consequently, the straight-run FTS products will be upgraded in crude-oil refineries together with crude-oil streams. Therefore, optimization of refinery processes including the catalysts employed will be crucial to obtain the desired product slate. The key aspects will be the introduction of long-chain paraffins (waxes) and their selective conversion into diesel fuel by hydrocracking and isomerization. Moreover, oxygenates will have to be deoxygenated and their inhibition effects on hydrogenation and hydrodesulfurization will have to be dealt with as well (see chapter on HDO).

Production of gasoline from FTS requires a more severe upgrading than FTS diesel production[114]. Due to the paraffinic nature and absence of aromatics the straight-run FTS naphtha is an excellent steam cracker feed (for production of ethene and propene) and its transformation into gasoline (fuel) calls for catalytic reforming or aromatization and isomerization to achieve sufficient octane number values. Zeolites and mesoporous materials have been investigated either as co-catalysts (in hybrid catalysts)[126,127,131] or as support materials[123,124] to obtain higher yields and higher degrees of branching of the FTS products in the gasoline boiling range. In the case of hybrid catalysts, two-stage catalyst beds are used –

a conventional FTS catalyst, e.g. Co/SiO_2, is placed in the upper bed and a zeolite catalyst is placed in the lower bed where it can crack the high-molecular-weight FTS products. The two-bed concept makes it possible to use, at the same time, the optimum reaction temperature for the FTS catalyst and for the zeolite catalyst since they are in separate beds[131]. H-zeolites of various topologies (USY, Beta, Mordenite, ZSM-5) have been found to increase the yield of gasoline range products, the highest gasoline selectivity has been observed for ZSM-5, followed by H-Mordenite and H-Beta[126]. Similarly, an increase in selectivity for gasoline-range products together with an increase in the isoalkane/n-alkane ratio has been achieved by using Pt- or Pd-Beta catalysts in the second catalyst bed[127]. The investigations of various combinations of the composition of the first and the second catalysts have indicated that the product selectivity in FTS, particularly concerning the yield of gasoline and its degree of branching, can be adjusted[131]. It has been shown that zeolites can improve the quality of gasoline-range FTS products. However, important issues such as the detrimental effect of water formed during FTS and hydrocarbon deposits on the activity and selectivity of zeolite catalysts have to be yet solved.

CONCLUSIONS AND OUTLOOK

The crude-oil refineries will remain the unrivaled producer of automotive fuels in the years to come. Nevertheless, they will face changes in the feedstock supply. The gradually deteriorating quality of crude oil (higher density and S content) will be newly accompanied by introduction of synthetic crudes (from tar sands upgrading), biomass feedstocks (such as triglycerides and bio-oils) and FTS-derived products (based on gasification of biomass, methane and coal) into the refinery feedstock portfolio. The environmental and health concerns together with public awareness will dictate deeper upgrading of fuels (lower S and aromatics contents) and higher share of renewable resources. Consequently, the refinery upgrading processes will have to be further developed to keep up with the new challenges.

The new biomass-derived feedstocks will bring oxygen-containing compounds into refineries. Due to the interference of deoxygenation reactions and their products with other hydrotreatment reactions (mainly HDS), hydrotreatment catalysts will be further developed to cope both with increasing heteroatom levels in the feeds and, at the same time, with the ever-lower levels of heteroatoms required in the products. Moreover, advanced support materials will be sought to (1) enable better dispersion and thus more efficient use of active components, (2) resist new refining by-products, such as water and CO_2 and (3) accommodate feeds with larger molecules, such as triglycerides and waxes.

The current refining catalysts will undergo changes to satisfy the need for higher isomerization and mild cracking activity which will be required for upgrading of FTS waxes into the demanded fuel product slate. Particularly, the production of high-quality gasoline will be difficult in comparison with the production of diesel fuel and feedstocks for steam cracking to produce light olefins. Moreover, improvements in conventional FTS catalysts can be expected to be accompanied by efforts aimed at development of modified catalyst systems, such as hybrid catalysts, to achieve deviations from ASF distribution and, thus, to increase the yields of gasoline- and diesel-range products at the expense of FTS waxes.

LIST OF ABBREVIATIONS USED

AIER	acid ion-exchange resin
AGO	atmospheric gas oil
ASF	Anderson–Schulz–Flory
DME	dimethyl ether
ETBE	ethyl *tert*-butyl ether
FAME	fatty acid methyl esters
FCC	fluid catalytic cracking
FTS	Fischer–Tropsch synthesis
HDC	hydrodecarboxylation
HDN	hydrodenitrogenation
HDO	hydrodeoxygenation
HDS	hydrodesulfurization
HHV	higher heating value
HTFTS	high-temperature Fischer–Tropsch synthesis
LTFTS	low-temperature Fischer–Tropsch synthesis
MP	methylphenol
MTBE	methyl *tert*-butyl ether
MTG	methanol to gasoline
MTO	methanol to olefins
UFO	used frying oil
UR	usage ratio
VGO	vacuum gas oil
WGS	water-gas shift

The financial support from the Ministry of Industry and Trade of the Czech Republic (projects FT-TA3/074, FT-TA4/066 and 2A-3TP1/063) is gratefully acknowledged.

REFERENCES

1. *BP Statistical Review of World Energy, June 2007*; www.bp.com.
2. Huber G. W., Iborra S., Corma A.: *Chem. Rev.* **2006**, *106*, 4044.
3. International Energy Agency: *Biofuels for Transport: An International Perspective*, Paris, France 2004.
4. Energy Information Administration: *International Energy Outlook 2007*; www.eia.doe.gov/oiaf/ieo/index.html.
5. *Worlwide Fuel Charter*, 4th ed., September 2006.
6. *European Fuel Standards* – EN 229 (gasoline), EN 590 (diesel).
7. Reschetilowski W.: *Chem.-Ing.-Tech.* **2007**, *79*, 729.
8. Cooper B. H., Donnis B. B. L.: *Appl. Catal., A* **1996**, *137*, 203.
9. Ancillotti F., Fattore V.: *Fuel Process. Technol.* **1998**, *57*, 163.
10. Feller A., Lercher J. A.: *Adv. Catal.* **2004**, *48*, 229.
11. Scherzer J., Gruia A. J.: *Hydrocracking Science and Technology*. Marcel Dekker, New York 1996.
12. Corma A., Melo F. V., Sauvanaud L., Ortega F. J.: *Appl. Catal., A* **2004**, *265*, 195.
13. Degnan T. F., Chitnis G. K., Schipper P. H.: *Microporous Mesopororous Mater.* **2000**, *35–36*, 245.
14. International Energy Agency: *Oil Gas J.* **2006**, *104*, 10.
15. Leliveld R. G., Eijsbouts S. E.: *Catal. Today* **2008**, *130*, 183.
16. European Biofuels Technology Plattform: *Strategic Research Agenda & Strategy Deployment Document*. CPL Press, 2008; www.biofuelstp.eu.
17. *Sustainable Biofuels: Prospects and Challenges*. The Royal Society, London 2008.
18. Kao I.: *Crude-Oil Prices Poll*. Reuters, 31. 3. 2008.
19. Eucar, Concawe, JRC: *Well-to-Wheels Analysis of Future Automotive Fuels and Powertrains in the European Context*, Version 2c, 2002; http://ies.jrc.ec.europa.eu/wtw.html.
20. Ma F., Hanna M. A.: *Bioresour. Technol.* **1999**, *70*, 1.
21. Meher L. C., Sagar D. V, Naik S. N.: *Renew. Sustain. Energy Rev.* **2006**, *10*, 248.
22. Knothe G., Krahl J., Gerpen J. V.: *The Biodiesel Handbook*. AOCS Press, Champaign, Illinois 2005.
23. European Biodiesel Board, www.ebb-eu.org; National Biodiesel Board, www.biodiesel.org.
24. Corma A., Iborra S., Velty A.: *Chem. Rev.* **2007**, *107*, 2411.
25. Das L. M.: *FITT Forum* **2007**, *13*, 3; http://www.fitt-iitd.org/pub/.
26. Dorado M. P., Cruz F., Palomar J. M., López F. J.: *Renew. Energy* **2006**, *31*, 1231.
27. Bournay L., Casanave D., Delfort B., Hillion G., Chodorge J. A.: *Catal. Today* **2005**, *106*, 190.
28. http://ec.europa.eu/environment/co2/pdf/cars_ia_final_report.pdf.
29. Van Gerpen J. H., Peterson C. L., Goering C. E.: *ASAE Distinguished Lect.* **2007**, *31*, 1.
30. Grange P., Vanhaeren X.: *Catal. Today* **1997**, *36*, 375.
31. Topsoe H., Clausen B. S., Masoth F. E.: *Hydrotreating Catalysis*. Springer-Verlag, Berlin, Heidelberg 1996.
32. Knudsen K. G., Cooper B. H., Topsoe H.: *Appl. Catal., A* **1999**, *189*, 205.
33. van Looij F., van der Laan P., DiCamillo D. J., Swain J.: *Appl. Catal., A* **1998**, *170*, 1.
34. Song C.: *Catal. Today* **2003**, *86*, 211.
35. La Vopa V., Satterfield C. N.: *J. Catal.* **1988**, *110*, 375.
36. Zeuthen P., Knudsen K. G., Whistehurst D. D.: *Catal. Today* **2001**, *65*, 307.

37. Egorova M., Prins R.: *J. Catal.* **2004**, *224*, 278.
38. Egorova M., Prins R.: *J. Catal.* **2004**, *221*, 11.
39. Choudhary T. V., Parrott S., Johnson B.: *Environ. Sci. Technol.* **2008**, *42*, 1944.
40. Song T., Zhang Z., Chen J., Ring Z., Yang H., Zheng Y.: *Energy Fuels* **2006**, *20*, 2349.
41. Ho T. C.: *Catal. Today* **2004**, *98*, 3.
42. Viljava T.-R., Komulainen R. S., Krause A. O. I.: *Appl. Catal., A* **2001**, *209*, 33.
43. Pérot G.: *Catal. Today* **2003**, *86*, 111.
44. Richard F., Boita T., Pérot G.: *Appl. Catal., A* **2007**, *320*, 69.
45. Prins R., Egorova M., Röthlisberger A., Zhao Y., Sivasankar N., Kukula P.: *Catal. Today* **2006**, *111*, 84.
46. Gates B. S., Topsoe H.: *Polyhedron* **1997**, *16*, 3213.
47. Egorova M., Prins R.: *J. Catal.* **2004**, *225*, 417.
48. Breysse M., Djega-Mariadassou G., Pessayre S., Geantet C., Vrinat M., Pérot G., Lemaire M.: *Catal. Today* **2003**, *84*, 129.
49. Boita T., Moreau M., Richard F., Pérot G.: *Appl. Catal., A* **2006**, *305*, 90.
50. Solís D., Agudo A. L., Ramírez J., Klimova T.: *Catal. Today* **2006**, *116*, 469.
51. Viljava T.-R.: *Ph.D. Thesis*. Helsinki University of Technology, Espoo, Finland 2001; lib.tkk.fi/Diss/2001/isbn9512259125/isbn9512259125.pdf.
52. Bridgwater A. V.: *Appl. Catal., A* **1994**, *116*, 5.
53. Bridgwater A. V.: *Catal. Today* **1996**, *29*, 285.
54. Bridgwater A. V., Peacocke G. V. C.: *Renew. Sustain. Energy Rev.* **2000**, *4*, 1.
55. Bridgwater A. V., Meier D., Radlein D.: *Org. Geochem.* **1999**, *30*, 1479.
56. Bridgwater A. V.: *J. Anal. Appl. Pyrolysis* **1999**, *51*, 3.
57. Bridgwater A. V.: *Chem. Eng. J.* **2003**, *91*, 87.
58. Mohan D., Pittman C. U., Steele P. H.: *Energy Fuels* **2006**, *20*, 848.
59. Furimsky E.: *Appl. Catal., A* **2000**, *199*, 147.
60. Czernik S., Bridgwater A. V.: *Energy Fuels* **2004**, *18*, 590.
61. Ringer M., Putsche V., Scahill J.: *Technical Report NREL/TP-510-37779*, 2006; www.nrel.gov/docs/fy07osti/37779.pdf.
62. Furimsky E.: *Catal. Rev.-Sci. Eng.* **1983**, *25*, 421.
63. Grange P., Laurent E., Maggi R., Centeno A., Delmon B.: *Catal. Today* **1996**, *29*, 297.
64. Weigold H.: *Fuel* **1982**, *61*, 1021.
65. Laurent E., Delmon B.: *Ind. Eng. Chem. Res.* **1993**, *32*, 2516.
66. Laurent E., Delmon B.: *Appl. Catal., A* **1994**, *109*, 77.
67. Senol O. I., Ryymin E.-M., Viljava T.-R., Krause A. O. I.: *J. Mol. Catal. A: Chem.* **2007**, *277*, 107.
68. Laurent E., Delmon B.: *Appl. Catal., A* **1994**, *109*, 97.
69. Senol O. I., Viljava T.-R., Krause A. O. I.: *Catal. Today* **2005**, *100*, 331.
70. Weisser O., Landa S.: *Sulphide Catalysts, Their Properties and Applications*. Pergamon, Oxford 1973.
71. Viljava T.-R., Saari E. R. M., Krause A. O. I.: *Catal. Today* **2000**, *60*, 83.
72. Senol O. I., Viljava T.-R., Krause A. O. I.: *Appl. Catal., A* **2007**, *326*, 236.
73. Senol O. I., Viljava T.-R., Krause A. O. I.: *Catal. Today* **2005**, *106*, 186.
74. Laurent E., Delmon B.: *J. Catal.* **1994**, *146*, 281.
75. Twaiq F. A., Zabidi N. A. M., Bhatia S.: *Ind. Eng. Chem. Res.* **1999**, *38*, 3230.
76. Adjaye J. D., Katikaneni S. P. R., Bakhshi N. N.: *Fuel Process. Technol.* **1996**, *48*, 161.
77. Katikaneni S. P. R., Adjaye J. D., Bakhshi N. N.: *Energy Fuel* **1995**, *9*, 1065.

78. Twaiq F. A., Zabidi N. A. M., Bhatia S.: *Microporous Mesoporous Mater*. **2003**, *64*, 95.
79. Ooi Y.-S., Zakaria R., Mohamed A. R., Bhatia S.: *Energy Fuels* **2005**, *19*, 736.
80. Dupain X., Costa D., Schaverien C. J., Makkee M., Moulijn J. A.: *Europacat VIII, Turku, Finland, August 26–31, 2007*; http://www.europacat.org/.
81. Bormann K., Tilgner H., Moll H. J.: *Erdol Erdgas Kohle* **1993**, *109*, 172.
82. Bormann K., Tilgner H.: *Erdol Erdgas Kohle* **1994**, *110*, 75.
83. Holmgren J., Gosling C., Couch K., Kalnes T., Marker T., McCall M., Marinangeli R.: *Petroleum Techn. Q*. **2007**, *3*, 119.
84. Chynoweth E.: *ICIS Chemical Business, November 13–19, 2006*, p. 30.
85. Gusmao J., Brodzki D., Djega-Mariadassou G., Frety R.: *Catal. Today* **1989**, *5*, 533.
86. Rocha Filho G. N. D., Brodzki D., Djega-Mariadassou G.: *Fuel* **1993**, *72*, 543.
87. Šimáček P., Kubička D.: *Fuel*, submitted.
88. Kubička D., Chudoba J., Šimáček P.: *Europacat VIII, Turku, Finland, August 26–31, 2007*; http://www.europacat.org/.
89. Jakkula J., Aalto P., Niemi V., Kiiski U., Nikkonen J., Mikkonen S., Piirainen O.: a) WO 022674 A1 (2004); b) Eur. 1 396 531 A2; c) U.S. 0055209 A1 (2004).
90. Jakkula J., Niemi V., Nikkonen J., Purola V.-M., Myllyoja J., Aalto P., Lehtonen J., Alopaeus V.: U.S. 7 232 935 B2 (2007).
91. NesteOil: http://www.nesteoil.com/default.asp?path=1,41,539,7516,7522.
92. ConocoPhillips: http://www.conocophillips.com/Tech/emerging/index.htm.
93. Petrobras: http://www2.petrobras.com.br/tecnologia/ing/hbio.asp.
94. Syntroleum: http://www.syntroleum.com/proj_rba_biofining.aspx.
95. Holmgren J., Gosling C., Marinangeli R., Marker T., Faraci G., Perego C.: *Hydrocarbon Process*. **2007**, *9*, 67.
96. Hodge C.: *California Energy Commission, Workshop on Bioenergy, March 9, 2006*; http://www.energy.ca.gov/bioenergy_action_plan/documents/2006-03-09_workshop/2006-03-09_NESTE_OIL.PDF.
97. Reinhardt G.: *An Assessment of Energy and Greenhouse Gases of NExBTL, IFEU, Heidelberg, June 2006*; http://nesteoil.com/binary.asp?GUID=75672FE1-6375-424D-B188-17868732307E.
98. Kubička D., Chudoba J., Šimáček P.: *DGMK-Fachbereichstagung, Energetische Nutzung von Biomassen, Velen, Germany, April 14–16, 2008*, p. 101; http://www.dgmk.de/kohle/fbk.html#tagberichte_kohle
99. Landa S., Andrzejak A., Weisser O.: *Collect. Czech. Chem. Commun*. **1962**, *27*, 979.
100. Huber G. W., O'Connor P., Corma A.: *Appl. Catal., A* **2007**, *329*, 120.
101. Kubičková I., Snåre M., Mäki-Arvela P., Eränen K., Murzin D. Yu.: *Catal. Today* **2005**, *106*, 197.
102. Murzin D. Yu., Kubičková I., Snåre M., Mäki-Arvela P.: Eur. 1 681 337 A1 (2006).
103. Kubička D.: Unpublished results.
104. Elliott D. C.: *Energy Fuel* **2007**, *21*, 1792.
105. Qi Z., Jie C., Tiejun W., Ying X.: *Energy Conversion Management* **2007**, *48*, 87.
106. Yaman S.: *Energy Conversion Management* **2004**, *45*, 87.
107. Vitolo S., Bresci B., Seggiani M., Gallo M. G.: *Fuel* **2001**, *80*, 17.
108. Mäki-Arvela P., Holmbom B., Salmi T., Murzin D. Yu.: *Catal. Rev. Sci. Eng*. **2007**, *49*, 197.
109. Murzin D. Yu., Mäki-Arvela P., Salmi T., Holmbom B.: *Chem. Eng. Technol*. **2007**, *30*, 569.

110. Boerrigter H., Rauch R. in: *Handbook Biomass Gasification* (H. A. M. Knoef, Ed.). BTG Biomass Technology Group, The Netherlands 2005.
111. Dahmen N., Dinjus E., Heinrich H.: *Oil Gas Eur. Mag.* **2007**, *1*, 31.
112. Marquard-Moellenstedt T., Specht M., Zuberbühler U., Pfeifer C., Rauch R., Hofbauer Y., Koch M.: *DGMK-Fachbereichstagung, Energetische Nutzung von Biomassen, Velen, Germany, April 14–16, 2008*, p. 149; http://www.dgmk.de/kohle/fbk.html#tagberichte_kohle.
113. Spath P. L., Dayton D. C.: *Preliminary Screening – Technical and Economic Assessment of Synthesis Gas to Fuels and Chemicals with Emphasis on the Potential for Biomass-Derived Syngas*. NREL/TP-510-34929, 2003; www.nrel.gov/docs/fy04osti/34929.pdf.
114. Steynberg A. P., Dry M. E.: *Fischer–Tropsch Technology*. Elsevier B. V., The Netherlands 2004.
115. Dry M. E.: *Catal. Today* **2002**, *71*, 227.
116. Lögdberg S.: *Licenciate Thesis*. KTH, Stockholm 2007; www.diva-portal.org/diva/getDocument?urn_nbn_se_kth_diva-4440-2__fulltext.pdf.
117. de Klerk A.: *Ind. Eng. Chem. Res.* **2007**, *46*, 5516.
118. Fernandes F. A. N., Teles U. M.: *Fuel Process. Technol.* **2007**, *88*, 207.
119. Leckel D., Liwanga-Ehumbu M.: *Energy Fuels* **2006**, *20*, 2330.
120. Leckel D.: *Energy Fuels* **2007**, *21*, 662.
121. Bolder F. H. A.: *Energy Fuels* **2007**, *21*, 1396.
122. Lamprecht D.: *Energy Fuels* **2007**, *21*, 2509.
123. Martínez A., Lopéz C., Márquez F., Díaz I.: *J. Catal.* **2003**, *220*, 486.
124. Concepción P., Lopéz C., Martínez A., Puntes V. F.: *J. Catal.* **2004**, *228*, 321.
125. Martínez A., Lopéz C., Corma A.: *Stud. Surf. Sci. Catal.* **2005**, *158*, 1327.
126. Martínez A., Rollán J., Arribas M. A., Cerqueira H. S., Costa A. F., Aguiar E. F. S.: *J. Catal.* **2007**, *249*, 162.
127. Liu Z. W., Li X. H., Asami K., Fujimoto K.: *Catal. Today* **2005**, *104*, 41.
128. Liu Z. W., Li X. H., Fujimoto K.: *Ind. Eng. Chem. Res.* **2005**, *44*, 7329.
129. Liu Z. W., Li X. H., Asami K., Fujimoto K.: *Appl. Catal., A* **2006**, *300*, 162.
130. Mysov V. M., Reshetnikov S. I., Stepanov V. G., Ione K. G.: *Chem. Eng. J.* **2005**, *107*, 63.
131. Zhao T. S., Chang J., Yoneyama Y., Tsubaki N.: *Ind. Eng. Chem. Res.* **2005**, *44*, 769.
132. Cowley M.: *Energy Fuels* **2006**, *20*, 1771.

Top Catal (2010) 53:168–178
DOI 10.1007/s11244-009-9421-z

ORIGINAL PAPER

Conversion of Vegetable Oils into Hydrocarbons over CoMo/MCM-41 Catalysts

David Kubička · Martina Bejblová · Josef Vlk

Abstract Deoxygenation of triglycerides over Co and Mo sulfides supported on a series of mesoporous molecular sieves (MCM-41) with varying Si/Al ratio has been investigated in this contribution. The catalysts were tested in a flow reactor at reaction temperatures 300 and 320 °C, hydrogen pressures 2–11 MPa and space velocities 1–4 h^{-1} using refined rapeseed oil as a feedstock. Incorporation of Al into the framework of MCM-41 led to an increase of both conversion of triglycerides and selectivity to hydrocarbons, namely *n*-heptadecane and *n*-octadecane. However, the conversion of triglycerides was lower than that achieved over alumina supported CoMo. Moreover, the rather high selectivity to oxygenated products, as compared with alumina supports, has made possible a detailed description of the reaction intermediates and their dependence on the reaction conditions.

Keywords Hydrodeoxygenation · Hydrodecarboxylation · CoMo catalysts · MCM-41 · Biofuels

D. Kubička (✉)
Department of Refinery and Petrochemical Research, Research Institute of Inorganic Chemistry, Záluží 1, D.S. 458, 436 70 Litvínov, Czech Republic
e-mail: david.kubicka@vuanch.cz

M. Bejblová · J. Vlk
J. Heyrovský Institute of Physical Chemistry, v.v.i, Academy of Sciences of the Czech Republic, Dolejškova 3, 182 23 Prague, Czech Republic

1 Introduction

A part of current fossil transportation fuels could be replaced by biofuels contributing thus to the reduction of CO_2 emissions [1, 2]. In order to minimize the impact of biofuel production on the environment, the research activities have been focused on the development of advanced biofuel technologies, so called 2nd generation biofuels. The main characteristics of 2nd generation biofuels are: (i) higher greenhouse gas (GHG) emission reduction in the complete life cycle in comparison with current biofuels and (ii) non-food biomass raw materials.

Vegetable oils have a suitable composition for production of fuels and have been therefore exploited for the production of biodiesel (fatty acids methyl esters). However, biodiesel suffers from several drawbacks such as limited compatibility with conventional diesel engines, use of high quality food feedstocks, etc. Therefore, direct upgrading of vegetable oils into hydrocarbons has been proposed and commercially demonstrated [3, 4]. Apart from the excellent compatibility with conventional diesel, the diesel components obtained from triglycerides outperform the conventional biodiesel in terms of both fossil cumulative energy demand (CED, GJ/t) and greenhouse gas emissions savings ($t_{CO2eq.}$/t) [5]. Moreover, in contrast to the conventional biodiesel production, lower quality triglyceride feedstocks such as used frying oils, animal fats, trap greases, and non-food vegetable oils, e.g., from algae or jathropha, can be used to lower the cost and dependency on food grade vegetable oils.

Refined vegetable oils require the removal of oxygen, the sole heteroatom present, to obtain hydrocarbons. Conventional hydrodesulfurization catalysts, such as CoMo, NiMo, NiW supported on alumina, have been reported to be active in deoxygenation of biomass-derived oxygenated feedstocks [6–10]. In addition to direct hydrotreating of neat vegetable oils [3, 11, 12], hydrotreating of vegetable oils in refineries by co-processing of vegetable oils with crude-oil-based refinery fractions has been proposed [11–14]. Due to the stringent limits for diesel fuel quality and the need to isomerize the obtained hydrocarbons owing to their poor cold-flow properties, the former technological option is preferred by the refiners [3, 12].

Deoxygenation can be studied by using a wide range of probe molecules [6, 7, 15–20]. The reaction mechanism and reaction rate depend on the type of oxygen compound. Therefore, the most appropriate reactants to study deoxygenation of vegetable oils are fatty acids and their esters [15–20] or triglycerides, i.e., the main components of vegetable oils [6, 7, 21]. Three basic reaction pathways have been reported for deoxygenation of triglycerides: hydrodeoxygenation, decarbonylation, and decarboxylation [6]. Moreover, the rate of deoxygenation is affected by presence of other heteroatoms, e.g., inhibition of deoxygenation has been reported when the feed contained both S- and O-containing compounds [22].

Recently, mesoporous materials have been investigated as potential supports for hydrodeoxygenation of triglycerides [21]. Similarly to conventional supports (Al_2O_3), selective conversion of triglycerides into hydrocarbons was achieved at 310 °C and 7 MPa over CoMo supported on organized mesoporous alumina supports showing a better performance than the industrial-alumina-based catalyst. On the other hand, the performance of MCM-41 (all-silica-based) was worse compared with alumina-based catalysts [21].

CoMo modified MCM-41 catalysts with different Al content were therefore synthesized and investigated in deoxygenation of triglycerides with the aim to better understand the effect of catalyst support and its interaction with the active phase (CoMo) on catalyst activity and selectivity. The effects of reaction temperature, residence time and hydrogen pressure on the product distribution are discussed as well.

2 Experimental

2.1 Catalyst Preparation and Characterization

2.1.1 Synthesis of Mesoporous Molecular Sieves MCM-41

The following raw materials were used for the synthesis of MCM-41 supports: sodium silicate, hexadecyltrimethylammonium bromide (template), ethyl acetate, and aluminium isopropoxide (only for (Al)MCM-41 materials, i.e., A02 and A03). In a typical synthesis, 9.81 g of hexadecyltrimethylammonium bromide was dissolved in 500 mL of distilled water in an autoclavable polypropylene bottle and stirred for 10 min at 35 °C, then corresponding amount of aluminium isopropoxide (only in the case of (Al)MCM-41 materials) was added and this mixture was stirred for 10 min at 35 °C. At the same time, 10 g of Na_2SiO_3 was dissolved in 450 mL of distilled water and stirred for 10 min at 35 °C in the second bottle. Then the contents of both bottles were mixed together and the mixture was stirred for 10 min at 35 °C. Finally, 15 mL of ethyl acetate was added and stirred for 10 min at 35 °C. The mixture then was aged for 2 days in an oven at 95 °C. The product was then filtered, washed, and dried. The obtained solid was calcined at a heating rate of 1 °C/min from room temperature to 540 °C. The temperature was then kept constant for 6 h. The targeted Si/Al values of the synthesized MCM-41 materials are given in Table 1 together with the bulk values of Si/Al ratio determined by XRF [23].

Table 1 Intended and real Si/Al ratios of the MCM-41 supports

Catalyst		Si/Al	Si/Al by XRF
(Si)MCM-41	A01	–	318
(Al)MCM-41	A02	15	12
(Al)MCM-41	A03	30	23

2.2 Synthesis of $MoO_3/CoO/MCM\text{-}41$

The catalysts MoO_3/CoO/MCM-41 containing 15 wt% of MoO_3 and 3.3 wt% of CoO were prepared by thermal spreading method. The mixture of the MCM-41 materials (A01, A02 or A03), obtained as described above, with corresponding amounts of crystalline MoO_3 and CoO were ground intensively in an agate mortar for approximately 1.5 h. The ground mixture was then calcined in an oven at a heating rate of 1 °C/min from room temperature to 550 °C.

2.3 Characterization

The crystallinity of mesoporous molecular sieves in their parent and modified forms were determined by X-ray powder diffraction with a Bruker D8 X-ray powder diffractometer equipped with a graphite monochromator and position-sensitive detector using Cu Kα radiation in the Bragg–Brentano geometry. The size and shape of MCM-41 crystals, both unmodified and modified, were determined by scanning electron microscopy (Jeol, JSM-5500LV). Textural parameters of catalysts and supports were determined with a Micromeritics ASAP 2020 volumetric instrument at −196 °C. The concentration of Lewis and Brønsted acid sites were determined by adsorption of pyridine as probe molecule followed by FTIR spectroscopy (Nicolet Protégé 460) using self-supported wafer technique. A thin powder wafer was activated prior to the experiment under a high vacuum at the temperature of 450 °C overnight. The total

Si/Al ratio was determined by X-ray fluorescence technique Philips PW 1404 using the analytical software UniQuant.

2.4 Catalytic Activity Measurements

Refined rapeseed oil (food grade) was used as a starting material. The distribution of fatty acids in the oil was determined by gas chromatography and is given in Table 2. Refinery hydrogen gas with >99% of H_2 was used in the experiments. The main impurities were methane (0.6%) and nitrogen (0.3%). The experiments were performed in an electrically-heated fixed-bed reactor of inner diameter equal to 17 mm. The reactor was loaded prior to the experiments with 8 g of catalyst diluted by an inert (SiC) to ensure sufficient catalyst-bed length and to improve the reaction-heat transfer. A layer of the inert material was placed above the catalyst bed to preheat rapeseed oil and hydrogen and to guarantee a good feed flow distribution prior to entering the catalyst bed. The particle sizes of the catalyst and SiC were 0.1–0.25 mm and <0.1 mm, respectively. In the vertical axis of the reactor, there was a thermo-well of the outer diameter equal to 5 mm, in which three adjustable thermocouples, used to determine the reaction temperature, were placed. The catalysts were activated (sulfided) in situ prior to the experiments by means of a solution of dimethyl disulfide (DMDS) in isooctane (5 wt% DMDS) at 320 °C. The reaction temperature and hydrogen pressure were varied during the experiments in the range of 300–320 °C and 2–11 MPa, respectively. The liquid feed rate was adjusted in the range of 1–4 h^{-1}. The hydrogen-to-rapeseed oil molar ratio was kept constant at 50. The liquid and gaseous products were separated at the reactor outlet in a heated gas–liquid separator as some of the products are solid at ambient temperatures.

The liquid products (collected and separated at 80 °C) were withdrawn after stabilization of reaction conditions (6 h) in 2-h intervals and analyzed by off-line gas chromatography (Shimadzu 2010) after separation of the water phase. Due to the presence of triglycerides in the products, on-column injection had to be used. Trikaprin (Fluka, >99%) was used as an internal standard in order to quantify the concentration of triglycerides. Moreover, the reaction intermediates included fatty acids and alcohols and silylation of reaction products by MSTFA (Acros, 97%) was applied to enhance their volatility and to improve the shapes of the peaks. The products were separated on a Restek MTX-Biodiesel TGw/Int-GAP column (14 m × 0.53 mm × 0.16 µm) and detected using a flame ionization detector (FID). The following temperature program was used: initial temperature 50 °C for 3 min, heating first 11 °C/min to 180 °C, then 5 °C/min to 230 °C, and finally 15 °C/min to 390 °C with dwelling time of 7 min at 390 °C. The individual products were identified using GC standards and the identification was further confirmed by GC-MS analysis (HP 6890). The gas-phase products were collected once under every reaction conditions and analyzed using a standard three-column GC setup (Agilent) with flame ionization and thermal conductivity detectors enabling the detection of both permanent gases and hydrocarbons at the same time.

Table 2 Distribution of fatty acids in rapeseed oil (raw material)

Fatty acid (X:Y)[a]	Wt%
Myristic acid (14:0)	0.1
Palmitic acid (16:0)	4.8
Palmitoleic acid (16:1)	0.3
Stearic acid (18:0)	1.9
Oleic acid (18:1)	61.9
Linoleic acid (18:2)	19.8
Linolenic acid (18:3)	9.2
Arachidic acid (20:0)	0.6
Gadoleic acid (20:1)	1.4

[a] X:Y = carbon number:number of double bonds

3 Results and Discussion

3.1 Catalyst Characterization

X-ray diffraction patterns of all samples provided clear evidence of the good crystallinity and phase purity of mesoporous sieves under investigation. MCM-41 materials before modification (Fig. 1a) exhibit a main peak at 2θ–2° assigned to hexagonal array of parallel mesoporous tubes. The two lower intensity peaks in the range of $2\theta = 3$–6° indicate the long range hexagonal ordered pores. The XRD patterns of MCM-41 modified by oxides MoO_3 and CoO (Fig. 1b) indicate, except A01 material, only one well distinguished peak at 2θ–2°. Moreover, the intensity of this peak decreases after modification with oxides. In the case of A01 material, i.e., (Si)MCM-41, peaks in the range of $2\theta = 3$–6° are still evident after thermal spreading with MoO_3 and CoO.

The particle size of the materials after solid state ion-exchange was determined from SEM images (Fig. 2). MoO_3/CoO/A01 material (Fig. 2a) exhibited size of the particles about 1–6 µm, MoO_3/CoO/A02 material (Fig. 2b) had size approximately 5 µm and MoO_3/CoO/A03 material (Fig. 2c) about 4 µm. Moreover, the shape of the particles of materials A02 and A03 with oxides was more oblong.

FTIR spectra of all tested catalysts contain a band at 3,745 cm^{-1} in the OH regions corresponding to the terminal silanol groups. After adsorption of pyridine, new bands in the region between 1,650 and 1,400 cm^{-1}

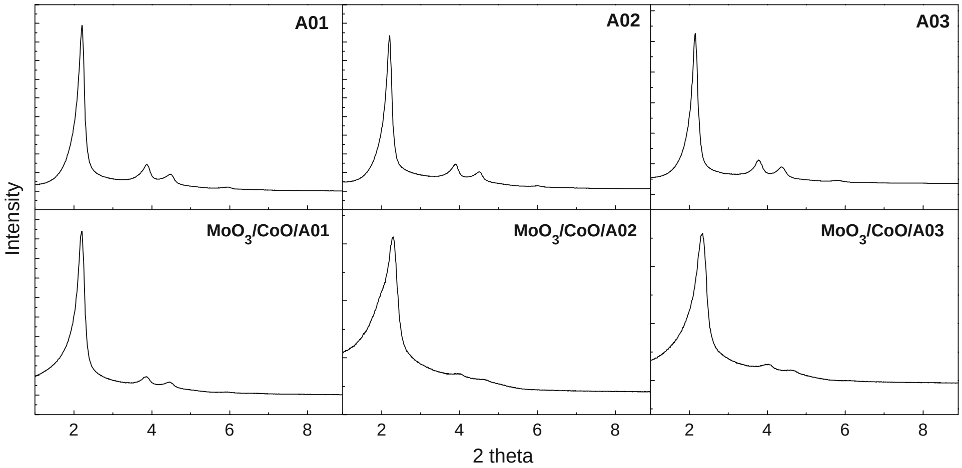

Fig. 1 X-ray powder diffraction patterns of parent MCM-41 materials (A01, A02, A03) and MoO_3/CoO/MCM-41 catalysts, A01 = (Si)MCM-41, A02, A03 = (Al)MCM-41

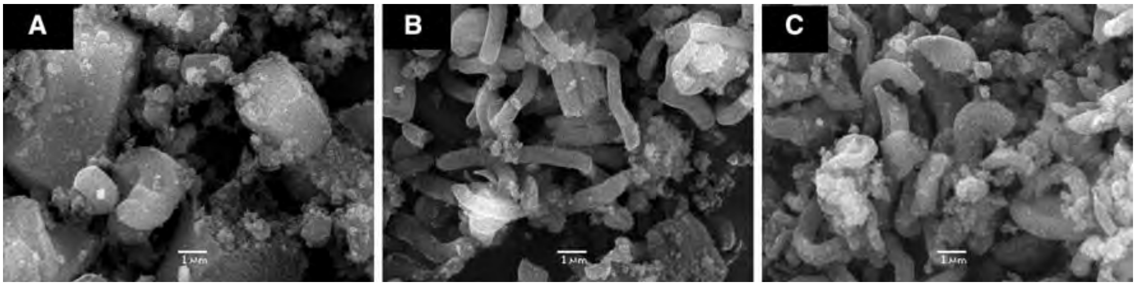

Fig. 2 SEM images of MoO_3/CoO/MCM-41 catalysts. **a** MoO_3/CoO/A01, **b** MoO_3/CoO/A02, **c** MoO_3/CoO/A03, A01 = (Si)MCM-41, A02, A03 = (Al)MCM-41

appeared (Fig. 3). Pyridine adsorption resulted in the formation of a new band at 1,455 cm^{-1} corresponding to the interaction between pyridine and Lewis acid (this band is slightly shifted to 1,452 cm^{-1} for materials modified by MoO_3/CoO). Only a negligible band at 1,550–45 cm^{-1} attributable to pyridinium ion (PyH^+) was found in the samples. This indicates that practically no acid OH groups are present in the mesoporous catalysts under investigation. The band at 1,445 cm^{-1} was observed only in the case of parent materials and corresponds to the interaction of pyridine with silanols [24]. The concentrations of Brønsted and Lewis acid sites were calculated from integral intensities of individual bands characteristic of pyridine on Brønsted acid sites and band of pyridine on Lewis acid sites and molar absorption coefficients [25] of $\varepsilon(B) = 1.67 \pm 0.1$ cm μmol^{-1} and $\varepsilon(L) = 2.22 \pm 0.1$ cm μmol^{-1}, respectively (Table 3). The parent (Al)MCM-41 support has a very low concentrations Brønsted and Lewis acid sites while in (Si)MCM-41 these acid sites are virtually absent. The concentration of Lewis acid sites, however, increased in all supports after their modification with MoO_3 and CoO. Hence, the acidity of the catalyst samples can be attributed to the active phase with only a minor contribution from the support in the case of (Al)MCM-41.

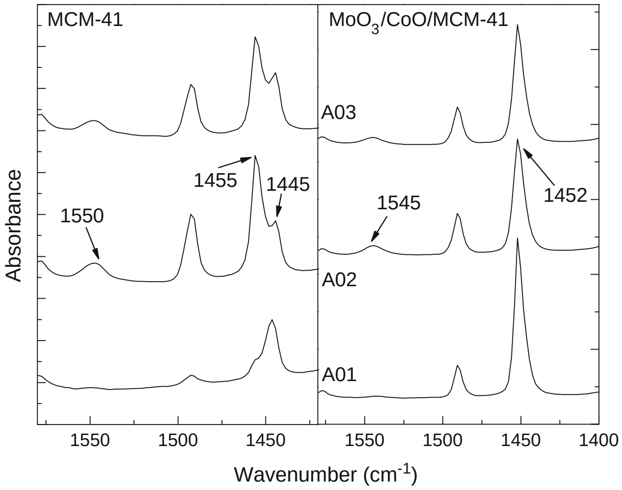

Fig. 3 FTIR spectra of pyridine adsorbed on parent materials (*left*) and MoO_3/CoO modified materials (*right*)-spectra after 20 min desorption at 150 °C. A01 = (Si)MCM-41, A02, A03 = (Al)MCM-41

The nitrogen isotherms obtained for modified catalysts are shown in Fig. 4. All samples exhibited adsorption isotherms typical for mesoporous materials. The textural properties such as surface area, pore volume and pore size

Table 3 Concentrations of Broensted (BC) and Lewis (LC) acid sites determined from pyridine adsorption followed by FTIR spectroscopy

	MCM-41		MoO$_3$/CoO/MCM-41	
	c_{LC} (mmol/g)	c_{BC} (mmol/g)	c_{LC} (mmol/g)	c_{BC} (mmol/g)
A01	0.01	–	0.37	–
A02	0.06	0.04	0.29	0.05
A03	0.08	0.03	0.28	0.04

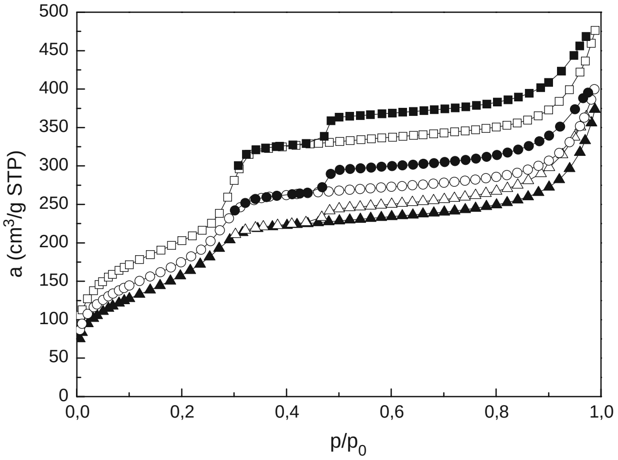

Fig. 4 Nitrogen adsorption isotherms of MoO$_3$/CoO/MCM-41 materials. *Open square*, *filled square* MoO$_3$/CoO/A01; *open triangle*, *filled triangle* MoO$_3$/CoO/A02; *open circle*, *filled circle* MoO$_3$/CoO/A03. A01 = (Si)MCM-41, A02, A03 = (Al)MCM-41

of the parent and modified materials are summarized in Table 4. It is clearly seen from Table 4 that after modification with oxides the surface area and pore volume decreased. A negligible decrease can be also observed in the case of pore size. This can be due to a presence of some surface roughness in the walls of mesoporous MCM-41 although of lower extent as reported recently for SBA-15 [26, 27].

3.2 Reaction Products and their Analysis

Transformation of rapeseed oil over CoMo-modified catalysts yielded three main product groups—gaseous products, liquid, and solid organic products and water. The gaseous products consisted of propane, propene (only at low reaction pressures), methane, carbon monoxide and carbon dioxide (each in the range 0.05–0.5 vol%). Other hydrocarbons were present only in trace amounts. The liquid and solid organic products contained hydrocarbons, mainly in the range C$_{15}$–C$_{18}$, saturated triglycerides, fatty acids, alcohols, and fatty esters of fatty acids. Hydrocarbons consisted predominantly of *n*-alkanes, only minor amounts of *iso*-alkanes and olefins have been found. Short chain hydrocarbons that would indicate hydrocarbon cracking reactions have not been detected in the products. The short chain hydrocarbons present in the gaseous products, i.e., methane and propane and propylene, are formed by hydrogenation of carbon oxides and from the glycerol backbone of triglycerides, respectively. Fatty acids and alcohols were saturated and their carbon chain lengths corresponded to those of fatty acids present in triglycerides making up rapeseed oil, i.e., stearic acid, palmitic acid and octadecanol. Significant amounts of esters formed by esterification of fatty acids, i.e., reaction intermediates, by alcohols, i.e., another reaction intermediates, were identified in the products by GC/MS. Stearyl-stearate was identified as the dominant ester.

Table 4 Textural properties of parent materials and after their modification with MoO$_3$ and CoO

	MCM-41			MoO$_3$/CoO/MCM-41		
	S_{BET} (m^2/g)	V (cm^3/g)	D (nm)	S_{BET} (m^2/g)	V (cm^3/g)	D (nm)
A01	920	0.596	3.7	734.0	0.519	3.6
A02	832	0.515	3.7	584.5	0.356	3.3
A03	957	0.618	3.7	653.3	0.413	3.4

V total volume in pores, *D* pore width (DFT pore size)

Even though the triglycerides found in the products were formed by hydrogenation of double bonds of the original triglycerides, they were considered, for the purpose of conversion determination, as raw materials since the main objective was to describe deoxygenation of triglycerides. Hydrogenation of double bonds in triglycerides usually precedes deoxygenation, since olefinic bonds can be saturated already at low temperatures (100–180 °C) over hydrogenation or hydrotreating catalysts [10], i.e., at temperatures too low for deoxygenation to take place.

3.3 Catalytic Activity of CoMo/MCM-41 Catalysts

Total conversion of triglycerides was obtained at space velocity 1 h^{-1} and temperatures 300 and 320 °C (Fig. 5) for all investigated CoMo/MCM-41 catalysts. The conversion decreased for all tested catalysts with increasing space velocity, i.e., with decreasing the contact time and the reaction temperature (Fig. 5). All CoMo/MCM-41 catalysts exhibited rather similar conversion of triglycerides, nevertheless some consistent differences among the catalysts were observed at both reaction temperatures at higher space velocities (2 and 4 h^{-1}). The conversion increased in the order A01 < A02 < A03, i.e., the CoMo supported on (Si)MCM-41 showed the lowest conversion of triglycerides and the CoMo supported on (Al)MCM-41 with nominal Si/Al equal to 30 showed the highest activity. This means that incorporation of Al contributed to an

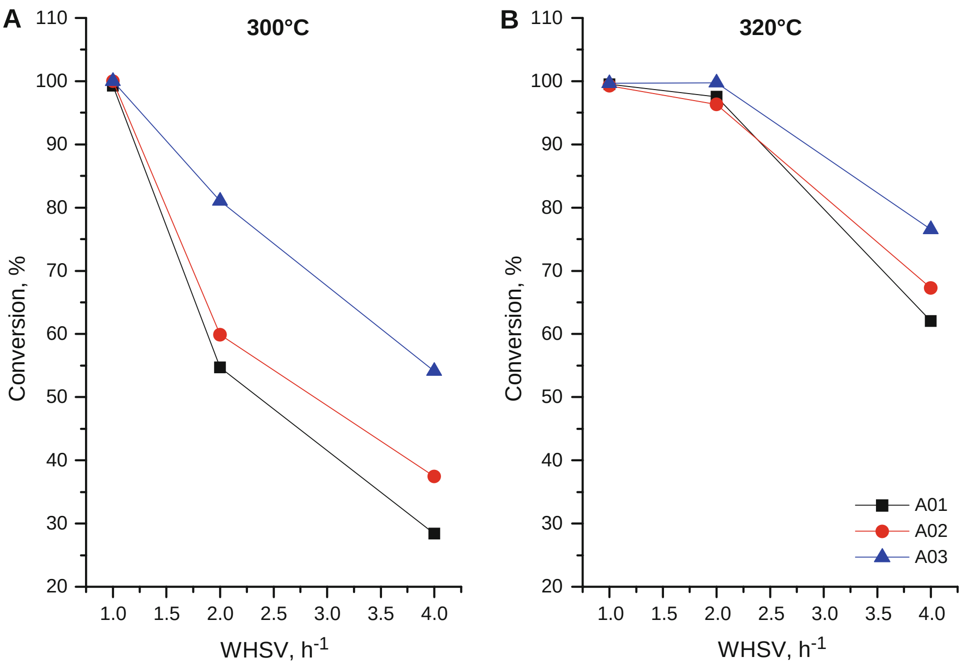

Fig. 5 Conversion of triglycerides over CoMo/MCM-41 catalysts at 3.5 MPa

increase in the catalyst acidity, but the change in the conversion of triglycerides could not be directly correlated with the increase in the Al content of MCM-41. A comparison with textural properties of the catalysts (Table 4) suggests that, in addition to the positive effect of Al, the larger pore volume and specific surface area of A03 as compared with A02 catalyst could plausibly lead to a better dispersion of the active components and hence a slightly higher conversion. Moreover, the acidity measurements suggest that approximately the same amount of Al is accessible in A02 and A03 catalysts as their acidic properties are almost identical. It has been reported previously that with decreasing Si/Al ratio Al atoms are incorporated not only on the wall surface but also inside the channel walls and are thus being inaccessible for reactants, e.g., at Si/Al = 11 only 55% of Al were placed on the MCM-41 surface [28]. The positive effect of Al incorporation is in agreement with a previous study [21], where lower deoxygenation activity of CoMo/(Si)MCM-41 in comparison with CoMo supported on organized mesoporous alumina (OMA) has been observed. Moreover, an improvement of CoMo catalyst activity has been reported for substitution of ordinary Al_2O_3 support by OMA [21], i.e., a support with higher specific surface area.

As triglycerides are rather easily converted over hydrotreating catalysts both to oxygenated intermediates (mainly fatty acids, fatty alcohols, and their esters) and hydrocarbons, i.e., the ultimate deoxygenation products, the selectivity to these two major product groups is an important parameter for determination of the overall performance of the catalysts. A comparison of the most and least active catalysts (A03 and A01, respectively) is given in Fig. 6 at both reaction temperatures. It can be clearly seen that with increasing space velocity, i.e., with decreasing contact time, the selectivity to hydrocarbons decreases (Fig. 6a) while the selectivity to oxygenated products increases (Fig. 6b). Hence, the oxygenated products can be in fact described as reaction intermediates. As the conversion of triglycerides over MCM-41 supported catalysts is lower than that of mesoporous alumina and conventional alumina supported ones [21, 29], the concentrations of reaction intermediates are substantially higher and allow thus for a more detailed view on the deoxygenation mechanism. The differences in selectivity between the catalysts are more pronounced at higher reaction temperature, 320 °C (Fig. 6). It can be observed that the more active catalyst (A03) is also more selective to hydrocarbons than A01. This conclusion is particularly valid at space velocities 1 and 2 h^{-1} at 320 °C, as under these reaction conditions a practically identical conversion is obtained over both catalysts (Fig. 5). This further confirms that the presence of Al support is beneficial for improvement of deoxygenation performance of CoMo catalysts.

As mentioned above, the high selectivity to reaction intermediates provides a unique possibility for a more detailed investigation of reaction steps involved in deoxygenation of triglycerides. Three major groups of reaction oxygenated intermediates have been identified in the reaction product mixtures: fatty acids (mainly stearic acid), fatty alcohols (mainly stearyl alcohol), and their esters (mainly stearylstearate). While fatty acids and their esters

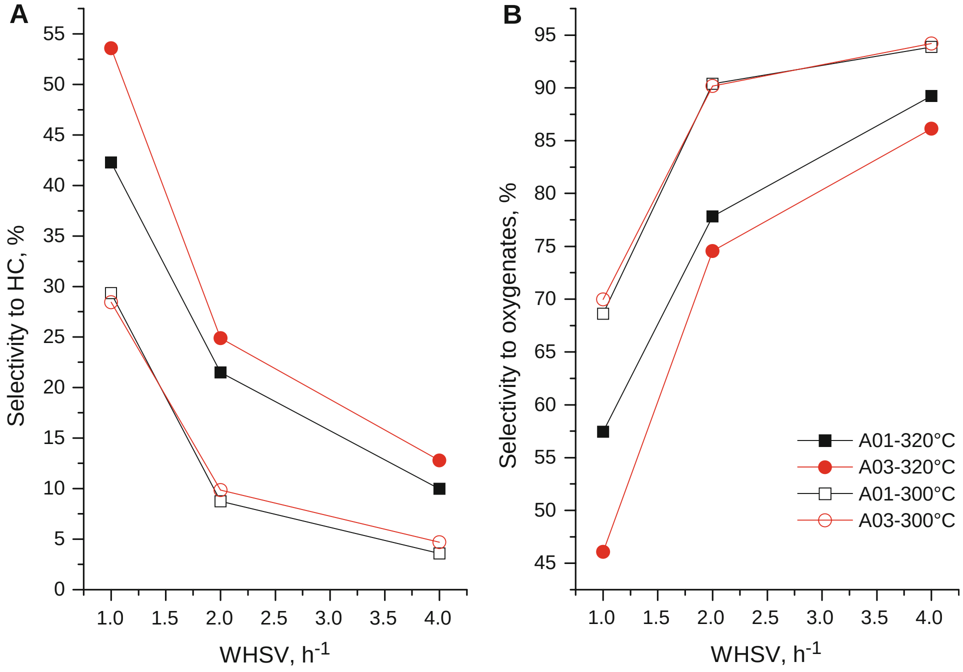

Fig. 6 Selectivity to hydrocarbons (**a**) and oxygenated reaction intermediates (**b**) as a function of space velocity for A01 and A03 catalysts at 300 and 320 °C and 3.5 MPa

with fatty alcohols could be observed over the whole range of reaction conditions (Fig. 7), fatty alcohols were present in concentrations exceeding 1 wt% only at complete conversion of triglycerides, i.e., at 1 h^{-1} and 300 and 320 °C, and were strongly favored over Al-containing catalysts (Fig. 8). In addition to these major oxygenated components that have been also reported previously [21], other oxygenated compounds have been identified by GC/MS, namely propylstearate and stearolactone. The presence of propyl ester of stearic acid is particularly significant, as it suggests that the triglyceride molecule is attacked at the oxygen-carbon bonds between the glycerol backbone and fatty acid chains. Hence, glycerol is not formed during the process as the corresponding carbon chain is saturated after releasing the fatty acid and yields a propyl chain (i.e., after releasing two fatty acid chains) and ultimately propane.

Figure 7 also indicates that there are differences among the catalysts as formation of fatty acids and their fatty esters is concerned. In general, the CoMo/(Si)MCM-41 exhibits a higher formation of esters at the expense of fatty acids formation. The differences are more clearly visible at 300 °C (Fig. 7a, c). The amount of fatty esters is fairly similar at both reaction temperatures and decreases with the decreasing contact time (Fig. 7a, b). As it will be demonstrated below (Fig. 9), fatty esters are secondary products formed by reaction of fatty acids and fatty alcohols. The more flat curves of yields of fatty esters at 320 °C are the result of fatty esters being deoxygenated to form hydrocarbons, as witnessed by the increasing selectivity to hydrocarbons at lower space velocities (Fig. 6). The peculiar behavior of fatty acids concentration as a function of space velocity (Fig. 7c, d) is due to the fact that they are the primary products being consumed to form either fatty esters or alcohols and ultimately hydrocarbons, i.e., there is a balance between their rate of formation and their rate of consumption. While only minor differences among the catalysts can be seen at 320 °C, there is a significant variation in fatty acids concentrations at 300 °C corresponding to the differences in overall activity of the catalysts (Fig. 5).

Fatty alcohols are important reaction intermediates, but they can be only seldom found among reaction products. This is apparently a consequence of their high reactivity in comparison with acids and esters [15]; they are either dehydrated to form olefins being subsequently hydrogenated to produce *n*-alkanes or they react with the present fatty acids to form fatty esters. The results indicate that the formation of fatty esters is a fast reaction, as alcohols can be found in the products only when the rate of their formation from fatty acids is greater than the sum of their consumption rates in dehydration (deoxygenation) and etherification. As it can be seen in Fig. 8, alcohols were found in the reaction products only at longer contact time (WHSV = 1 h^{-1}). At shorter contact times, they were observed only at 320 °C with CoMo/(Al)MCM-41 catalysts (Fig. 8). The data thus support the abovementioned conclusions.

The experimental data cover a wide range of triglycerides conversions, namely 20–100% (Fig. 9) and they hence provide a good basis for analysis of the sequence of individual reaction steps. Hydrocarbons are clearly the secondary products, as their concentrations are below 10% up

Fig. 7 Effect of the reaction temperature on the production of reaction intermediates—fatty esters (**a**, **b**) and fatty acids (**c**, **d**) at 3.5 MPa

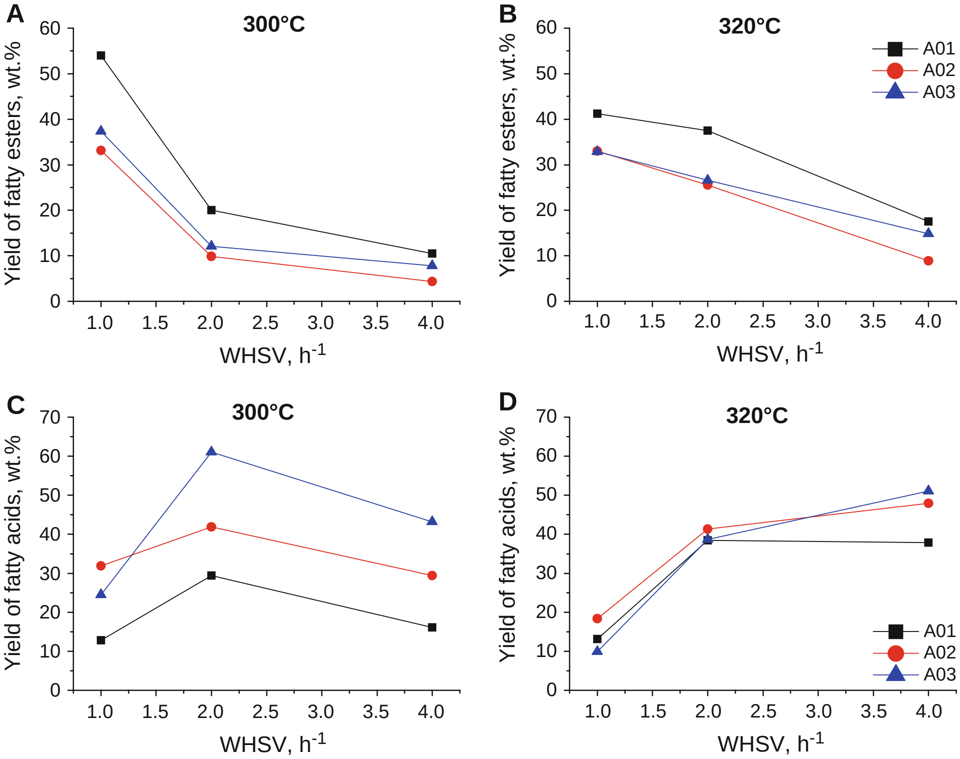

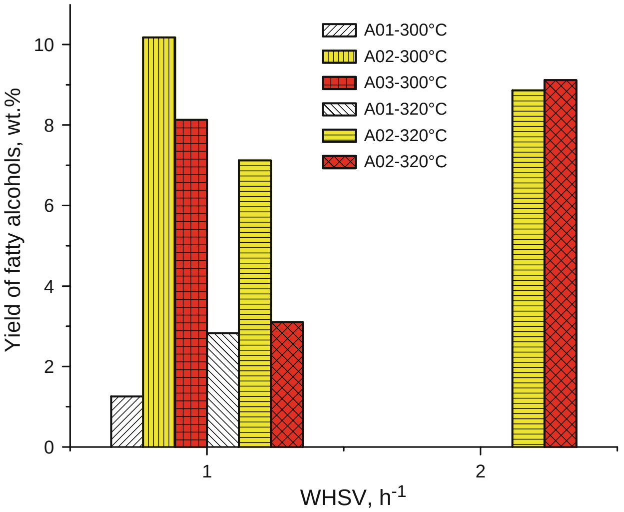

Fig. 8 Effect of the reaction temperature on the production of fatty alcohols at 3.5 MPa

to conversions levels of 60–70% (Fig. 9a). Moreover, there is no difference among the catalysts in total yield of hydrocarbons. Oxygenated products, on the other hand, can be clearly seen as primary products (Fig. 9b). A closer look on the results reveals that from the main oxygenated products fatty acids are the true primary products, while alcohols and fatty esters are secondary products (Fig. 9c, d). The sharp decrease of fatty acids concentrations in products (Fig. 9d) at high conversion levels is then due to their consumption in alcohol formation and fatty esters formation. While there is no apparent difference among the catalysts when formation of oxygenates is considered, differences can be found among the individual groups of oxygenates. The CoMo/(Si)MCM-41 catalyst (A01) can be observed to yield more fatty esters than the CoMo/(Al)MCM-41 catalysts (A02 and A03) at comparable conversions (Fig. 9c).

Generally, it can be concluded that the data provide new evidence for the previously proposed reaction scheme of triglycerides conversion into hydrocarbons (Scheme 1) [10, 21]. The initial reaction step is hydrogenation of unsaturated triglycerides, which are the predominant components in vegetable oils, to saturated ones. This reaction is here, however, not considered as reaction contributing to conversion of triglycerides. The saturated triglycerides then undergo conversion to fatty acids that are subsequently converted either by hydrodeoxygenation or decarboxylation. The reaction rate of these reaction steps is strongly dependent on the reaction pressure, as discussed below. In the process of hydrodeoxygenation, fatty acids can be partially hydrogenated to fatty alcohols. Fatty alcohols are subsequently dehydrated and hydrogenated to yield hydrocarbons with even number of carbon atoms in molecule. They can, however, also react with fatty acids to yield fatty esters that have been also found in the products (see above). Fatty aldehydes, the other plausible reaction intermediates, have not been detected. Corresponding to

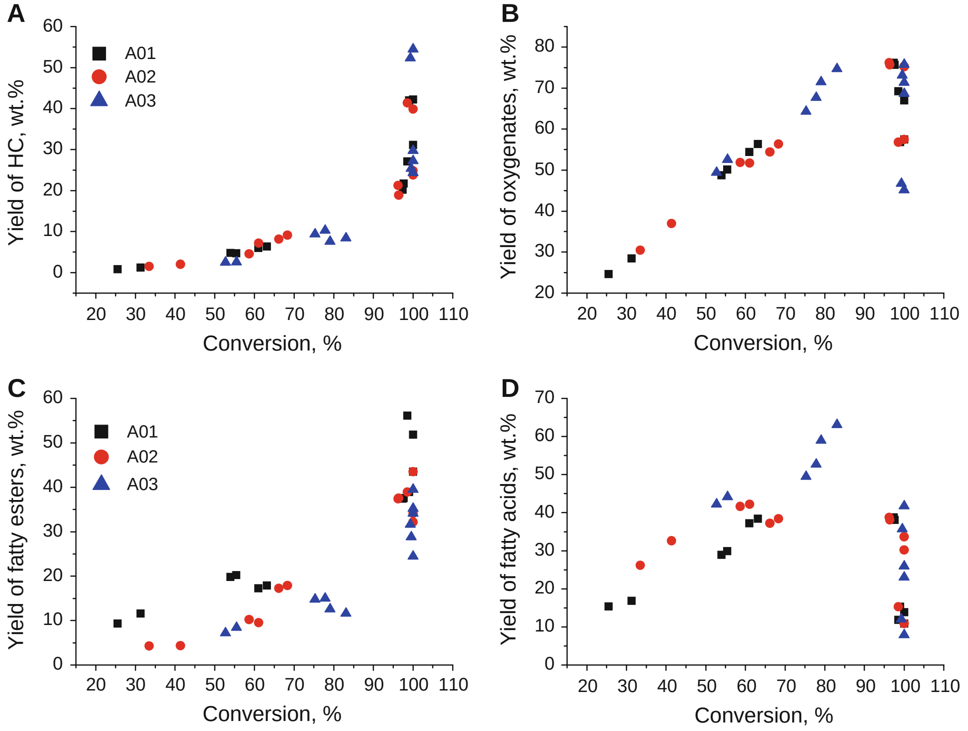

Fig. 9 The dependence of the concentration of different deoxygenation products—sum of hydrocarbons (**a**), sum of oxygenates (**b**), sum of fatty esters (**c**) and sum of fatty acids (**d**)—as a function of total conversion for CoMo/MCM-41 catalysts at 3.5 MPa

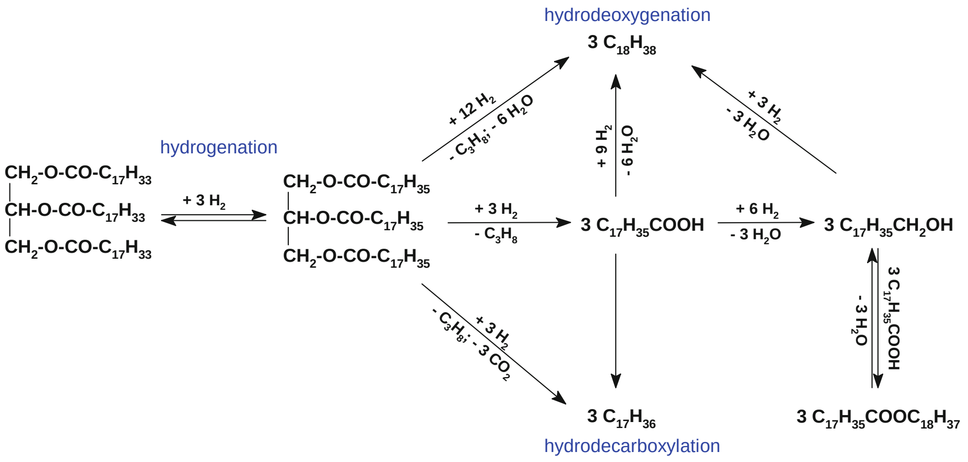

Scheme 1 Reaction scheme of triglyceride conversion into hydrocarbons [10]

the reactions in the liquid phase, water, and gaseous products are formed. The analyses of gaseous products confirmed the conclusion drawn and as the data are consistent with the data reported previously [21], they are not given here.

Reaction pressure is also known to affect the rate of deoxygenation as well as its selectivity [10, 21, 30]. The data shown in Fig. 10 clearly demonstrate that at a given contact time between the feedstock and catalyst the selectivity to hydrocarbons increases with increasing hydrogen pressure (Fig. 10a). The effect is more pronounced at longer contact times (see Fig. 10a, pressure 3.5 and 7 MPa at space velocities 1, 2, and 4 h^{-1}). Moreover, the selectivity to deoxygenation products increases at a given pressure with a decreasing space velocity, which is in agreement with conclusions made above. It has been previously suggested that the fatty acids that are reaction intermediates of triglycerides transformation can undergo either decarboxylation or hydrodeoxygenation to yield hydrocarbons [9, 21, 29]. As the products of these two parallel reactions have different number of carbon atoms in molecule (it is an odd carbon number in the case of decarboxylation and an even carbon number in the case of hydrodeoxygenation), the composition of the hydrocarbon mixtures can be used as a tool for describing the changes in the reaction pathway. Since a majority (ca. 90%) of the

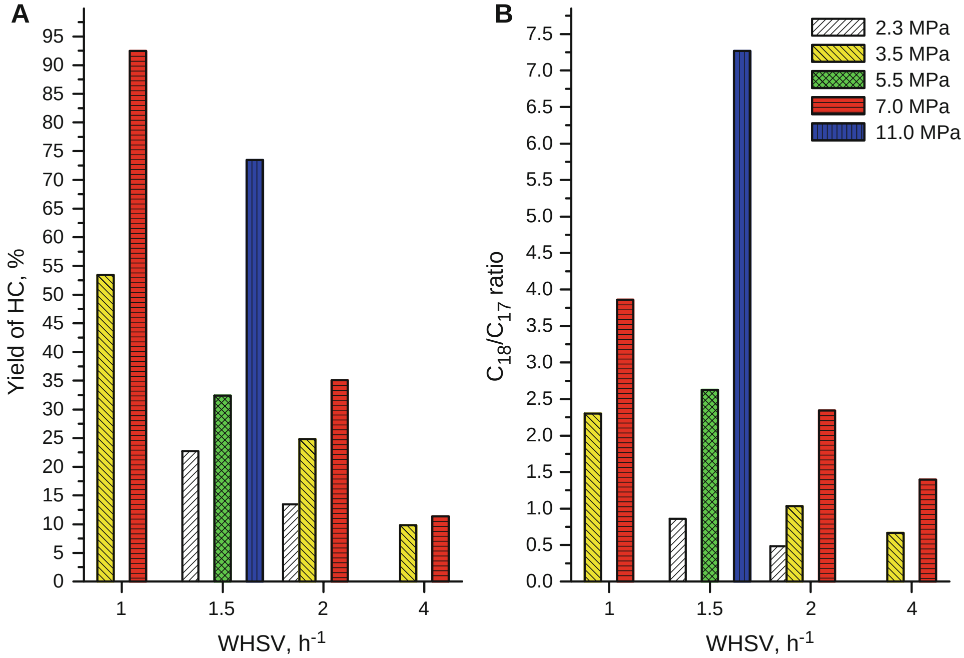

Fig. 10 Effect of reaction pressure on the production of hydrocarbons from triglycerides (**a**) and deoxygenation reaction pathway (**b**) at 320 °C over A03

fatty acid chains of triglycerides in rapeseed oil has 18 carbon atoms, the ratio of C_{18}/C_{17} has been used as a measure of quantification of changes in the final deoxygenation pathway. A strong dependence on reaction pressure is again obvious from Fig. 10b. For a given contact time, the ratio C_{18}/C_{17} increases substantially with hydrogen pressure, i.e., the hydrodeoxygenation pathway is preferred to the decarboxylation pathway. Only at low hydrogen pressure, e.g., 2.3 MPa, decarboxylation is the main reaction-ratio $C_{18}/C_{17} < 1$ (Fig. 10b). It is interesting to observe that at constant hydrogen pressure the ratio C_{18}/C_{17} decreases with increasing space velocity, i.e., with shorter contact time. The plausible explanation is the formation fatty esters. The esters are formed by reaction of a fatty alcohol with a fatty acid and while the fatty acid can undergo either decarboxylation or hydrodeoxygenation, the fatty alcohol can undergo only hydrodeoxygenation (dehydration). Hence, the selectivity to hydrocarbons with even carbon number is higher in the case of fatty esters than in the case of fatty acids. Since the fatty esters are secondary products, their subsequent transformation to hydrocarbons is favored by longer contact times as it can be seen from the changes in C_{18}/C_{17} ratio (Fig. 10b).

4 Conclusions

Hydrodeoxygenation catalysts were prepared by modification of synthesized MCM-41 catalyst supports having different Si/Al ratio with molybdenum and cobalt and their performance in deoxygenation of rapeseed oil was investigated. These catalysts are significantly less active in complete deoxygenation of triglycerides into hydrocarbons than alumina catalysts. This difference can be attributed to differences in interactions between the support and active phase (CoMo) due to different composition of supports (Si versus Al). A partial improvement of catalyst performance has been achieved when Al was incorporated in the MCM-41 support.

Reaction temperature and pressure determine the selectivity not only to hydrocarbons and oxygenated products but also within these product groups. An increase in hydrogen pressure favors strongly hydrodeoxygenation over decarboxylation. Incorporation of aluminium into the framework of MCM-41 as well as higher reaction temperature results in better selectivity to hydrocarbons. Interestingly, MCM-41 without aluminium, i.e., CoMo/(Si)MCM-41, promotes, in comparison with CoMo/(Al)MCM-41 catalysts, the formation of fatty esters at the expense of formation of fatty acids. The effect of the support composition on the reaction pathway has not been, however, fully clarified yet. Hence further research is needed to understand fully the influence of the catalyst-related properties (support type and its properties, active phase type and its properties, active-phase-support interactions) on the product distribution.

Acknowledgements The financial support by the Ministry of Industry and Trade of the Czech Republic (project FT-TA3/074) is gratefully acknowledged. The authors thank to Mr. Josef Chudoba (Institute of Chemical Technology Prague) for the GC/MS analyses of deoxygenation products.

References

1. Huber GW, Iborra S, Corma A (2006) Chem Rev 106:4044
2. Huber GW, Corma A (2007) Angew Chem Int Ed 46:7184
3. Jakkula J, Aalto P, Niemi V, Kiiski U, Nikkonen J, Mikkonen S, Piirainen O, WO 2004/022674 A1, EP 1 396 531 A2, US 2004/0055209 A1
4. NesteOil. http://www.nesteoil.com/default.asp?path=1,41,539,7516,7522
5. UOP, 1st alternative fuels technology conference, 18 Feb 2008, Prague, Czech Republic
6. Gusmao J, Brodzki D, Djega-Mariadassou G, Frety R (1989) Catal Today 5:533
7. Rocha Filho GND, Brodzki D, Djega-Mariadassou G (1993) Fuel 72:543
8. Huber GW, O'Connor P, Corma A (2007) Appl Catal A 329:120
9. Šimáček P, Kubička D, Šebor G, Pospíšil M (2009) Fuel 88:456
10. Kubička D (2008) Collect Czech Chem Commun 73:1015
11. Holmgren J, Gosling C, Couch K, Kalnes T, Marker T, McCall M, Marinangeli R (2007) Petrol Technol Q 3:119
12. Holmgren J, Gosling C, Marinangeli R, Marker T, Faraci G, Perego C (2007) Hydrocarb Process 9:67
13. ConocoPhillips. http://www.conocophillips.com/Tech/emerging/index.htm
14. Petrobras. http://www2.petrobras.com.br/tecnologia/ing/hbio.asp
15. Furimsky E (2000) Appl Catal A 199:147
16. Laurent E, Delmon B (1994) Appl Catal 109:77
17. Laurent E, Delmon B (1994) Appl Catal 109:97
18. Senol OI, Viljava T-R, Krause AOI (2005) Catal Today 100:331
19. Kubičková I, Snåre M, Eränen K, Mäki-Arvela P, DYu Murzin (2005) Catal Today 106:197
20. Snåre M, Kubičková I, Mäki-Arvela P, Eränen K, DYu Murzin (2006) Ind Eng Chem Res 45:5708
21. Kubička D, Šimáček P, Žilková N (2009) Top Catal 52:161
22. Viljava T-R, Komulainen RS, Krause AOI (2001) Appl Catal A 209:33
23. Zukal A, Thommes M, Čejka J (2007) Microporous Mesoporous Mater 104:52
24. Gil B, Zones SI, Hwang SJ, Bejblová M, Čejka J (2008) J Phys Chem C 112:2997
25. Emeis CA (1993) J Catal 141:347
26. Zukal A, Šiklová H, Čejka J (2008) Langmuir 24:9837
27. Gommes CJ, Friedrich H, Wolters M, de Jongh PE, de Jong KP (2009) Chem Mater 21:1311
28. Dědeček J, Žilková N, Čejka J (2001) Microporous Mesoporous Mater 44–45:259
29. Kubička D, Lederer J, Bělohlav Z (2009) Oil Gas Eur Mag 35:40
30. Smejkal Q, Smejkalová L, Kubička D (2009) Chem Eng J 146:155

Fuel 121 (2014) 57–64

Contents lists available at ScienceDirect

Fuel

journal homepage: www.elsevier.com/locate/fuel

HDO catalysts for triglycerides conversion into pyrolysis and isomerization feedstock

Jan Horáček [*], Zdeněk Tišler, Vlastimil Rubáš, David Kubička

Research Institute of Inorganic Chemistry, RENTECH-UniCRE, Chempark Litvínov, Záluží, Litvínov 436 70, Czech Republic

HIGHLIGHTS

- NiMo is the most active composition for deoxygenation.
- Co promotes hydrodeoxygenation over decarboxylation.
- Hydrotalcite support favors hydrodeoxygenation.
- Si-SBA-15 is significantly more active than ordinary silica support.

GRAPHICAL ABSTRACT

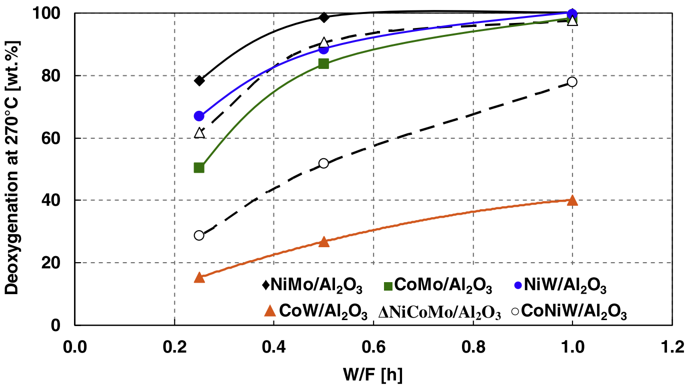

ARTICLE INFO

Article history:
Received 28 October 2013
Received in revised form 7 December 2013
Accepted 10 December 2013
Available online 25 December 2013

Keywords:
Deoxygenation
Triglycerides
Effect of promoters
Effect of supports

ABSTRACT

The effects of promoters, active metals and catalyst support material on deoxygenation of rapeseed oil were investigated. At 250 and 270 °C and various flow rates (W/F = 0.25, 0.50, 1.00 h), Ni-promoted catalysts were found more active than Co-promoted ones. NiMo catalyst was found as the most active metal combination, while CoW was the least active one. High selectivity for hydrodeoxygenation reaction pathway (total hydrogenation) was observed for CoMo type catalysts. Co addition into NiMo type catalyst resulted in conversion decrease, nevertheless selectivity was not affected. From the support-type point of view, alumina-supported NiMo was identified as the most active. SBA-15 support modified the product selectivity to increased formation of the hydrodeoxygenation products in comparison with the ordinary SiO_2 support.

1. Introduction

The sustainable utilization of renewable feedstocks for the production of fuels and chemicals is one of the great challenges of our time. Heterogeneous catalysis offers various possibilities to achieve the transformation of biomass-derived feedstocks into the desired products in an energy and raw material efficient way [1,2]. Triglycerides belong to biomass-related feedstocks that are the easiest to convert into fuels [3,4]. The traditional way relies on their transesterification with methanol yielding into fatty acids methyl esters (FAME) that are used as a diesel fuel component or even neat diesel fuel [3]. However, there are several deficiencies, such as lower thermal and chemical stability or lower heating value in comparison with petroleum-derived diesel fuel that limit the usage of FAME [3]. As a result alternative conversion pathways have been looked for in the past decade or so [3–13].

Deoxygenation of triglycerides by their hydrogenation has been demonstrated as an efficient way of their utilization [14,15]. It allows also processing of lower quality oils and fats that can be converted to FAME only with difficulties. In fact, hydrogenation-based processes using HDS and hydrotreating catalysts were already

---

[*] Corresponding author. Tel.: +420 476163735; fax: +420 476768476.
E-mail address: jan.horacek@vuanch.cz (J. Horáček).

http://dx.doi.org/10.1016/j.fuel.2013.12.014

applied industrially for the conversion of non-food quality oils and fats into fuels and petrochemicals (NExBTL, Ecofining, Bio-synfining, Agtane/Supercetane). Typical product of simple deoxygenation is mixture of n-alkanes [8]. The reaction mechanism consists of two reaction pathways: (i) hydrodeoxygenation (HDO) producing even-numbered hydrocarbon chains and (ii) (hydro)decarboxylation (DC) yielding odd-numbered hydrocarbon chains [8]. The reaction mechanism is depicted in Fig. 1. The other products of deoxygenation include propane, water, carbon dioxide and its hydrogenation products: carbon monoxide and methane [8].

Potential utilizations of n-alkanes formed by triglyceride hydrodeoxygenation are steam cracking (ethylene and propylene production) [16] and diesel fuel production [6,7,11,13,17–19]. Steam cracking of linear hydrocarbon chains typically produces excellent yields of ethylene (about 40 wt.%) and propylene (17–18 wt.%) [16]. Direct utilization of deoxygenation products as diesel fuel is limited by their high melting points and thus unsuitable cold-flow properties [17–19].

The economic viability of the production of hydrocarbons from triglycerides is determined apart from the price of the feedstock by the hydrogen consumption, which depends strongly on the reaction pathway (Fig. 1). As both pathways (HDO and DC) take place over sulfided catalysts, it is important to control the extent of HDO and DC reactions during deoxygenation. This work is focused on the elucidation of the effect of promoters (Ni or Co), active phase metals (Mo or W) as well as the support materials (alumina, silica, titania, SBA-15 and hydrotalcite) on the activity and selectivity of the catalysts in deoxygenation of rapeseed oil.

2. Experimental

2.1. Catalysts

A series of deoxygenation metal-sulfide-based catalysts using different supports and active components were prepared to investigate the role of the support material and active components on the catalytic deoxygenation of triglycerides. The studied supports included commercially available supports – alumina (Sasol), silica (Cherox) and titania (Cherox) – as well as an in-house synthesized support – mesoporous silica with the SBA-15 structure. The active phase of the catalysts consisted of molybdenum or tungsten sulfides promoted by nickel or cobalt sulfides. In addition to bimetallic catalysts, tri-metallic catalysts were studied as well.

The bimetallic catalysts were denoted as follows: PA/S where P stands for the promoter (Ni or Co), A for the active phase (Mo or W) and S for the support (Al_2O_3, TiO_2, SiO_2, SBA-15). Similarly, the tri-metallic catalysts were denoted as PRA/S where P and R stand for the promoter and A for the active phase. The composition of the prepared catalysts and their basic characteristics are summarized in Table 1.

Two or three step (according to number of loaded metals) incipient wetness impregnation was used to introduce the metal oxides on the support. The metal oxides were loaded in the following sequence: MoO3 or WO_3 followed by NiO or CoO. In the case of catalysts with both NiO and CoO, NiO was introduced prior to CoO. Nickel nitrate hexahydrate (Sigma Aldrich), cobalt chloride (Sigma Aldrich), ammonium molybdate (Sigma Aldrich) and, ammonium metatungstate (Sigma Aldrich) were used as the precursors of the respective supported metal oxides/sulfides. Precursors were loaded to obtain 4 wt.% of the promoter (Ni or Co) and 15 wt.% of the active phase metal (Mo or W) in the final catalyst. Every impregnation step was followed by calcination at 550 °C. Mesoporous silica was prepared using SBA-15 preparative method described in [20]. The other supports were commercially produced supports.

2.2. Catalyst testing

Catalytic tests were performed in stainless steel tubular reactor with internal diameter of 17 mm. Reactor was equipped by a three-zone electric furnace and integrated thermo-well for thermocouple insertion Fig. 2. The experiments were carried out at temperatures 250 and 270 °C and overall pressure 5 MPa. F/W ratios, i.e. space velocities tested were 1, 2, 4 h^{-1} (F = mass flow rate (g/h); W = amount of oxide form catalyst (g)). The reaction products were collected in a heated gas–liquid separator and sampled in defined times on stream (see below).

Before each test, the reactor was loaded with 5 g of fractionated catalyst (particle size 0.25–0.50 mm). Catalysts were mixed with fine inert (SiC, particle size 0.1 mm) in volume ratios 1–5:1 (SiC: catalyst) to enable better removal of released reaction heat and thus better temperature control along the catalyst bed. Catalyst activation/sulfiding was carried out using 5 vol.% dimethyldisulfide (DMDS) solution in isooctane in presence of hydrogen at temperatures up to 340 °C and pressure 5.1 MPa. After activation, the feedstock was exchanged and rapeseed oil (food quality) containing 0.3 wt.% of DMDS was pumped into the reactor. DMDS addition into the vegetable oil is needed to protect the sulfided active sites from desulfiding and losing activity. The amount of DMDS was selected based on a previous work [21] and additional experiments using gradually decreasing amount of DMDS in feedstock (rapeseed oil) in which the minimum addition of DMDS that ensured a stable conversion of triglycerides was determined. Sulfur presence in the reaction mixture and the gas phase inside reactor, respectively stabilizes the hypothetical surface sites equilibria [22]. The constant

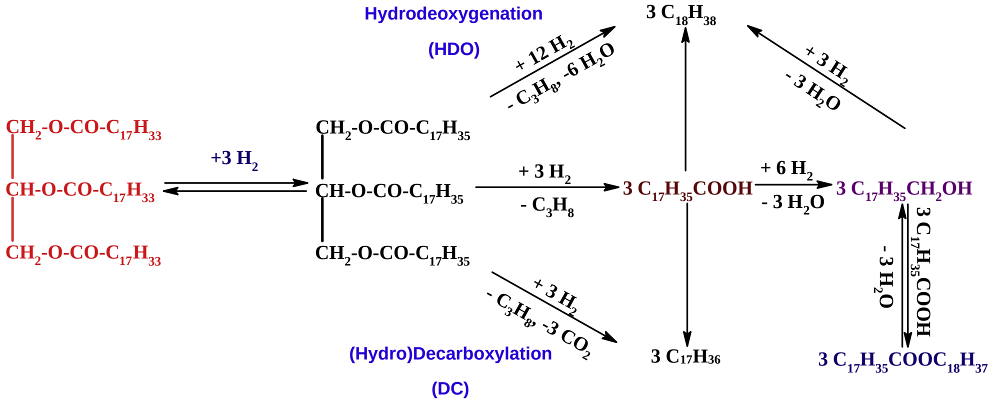

Fig. 1. Reaction scheme of triolein deoxygenation [8].

Table 1
The basic catalyst characterization.

Catalyst type	Metal content (wt.%) (XRF)				Support surface area (m^2/g)
	Co	Ni	W	Mo	
$NiMo/Al_2O_3$	0.0	3.9	0.0	16.3	198
NiW/Al_2O_3	0.0	3.7	15.4	0.0	
$CoMo/Al_2O_3$	3.9	0.0	0.0	13.2	
CoW/Al_2O_3	3.7	0.0	15.9	0.0	
$NiMo/SiO_2$	0.0	3.3	0.0	11.9	57
$NiMo/TiO_2$	0.0	3.0	0.0	15.5	109
NiMo/SBA-15	0.0	3.7	0.0	9.7	650
NiMo/HTC	0.0	4.0	0.0	15.4	171
$NiCoMo/Al_2O_3$	3.7	3.7	0.0	13.8	198
$CoNiW/Al_2O_3$	3.6	3.6	15.5	0.0	198

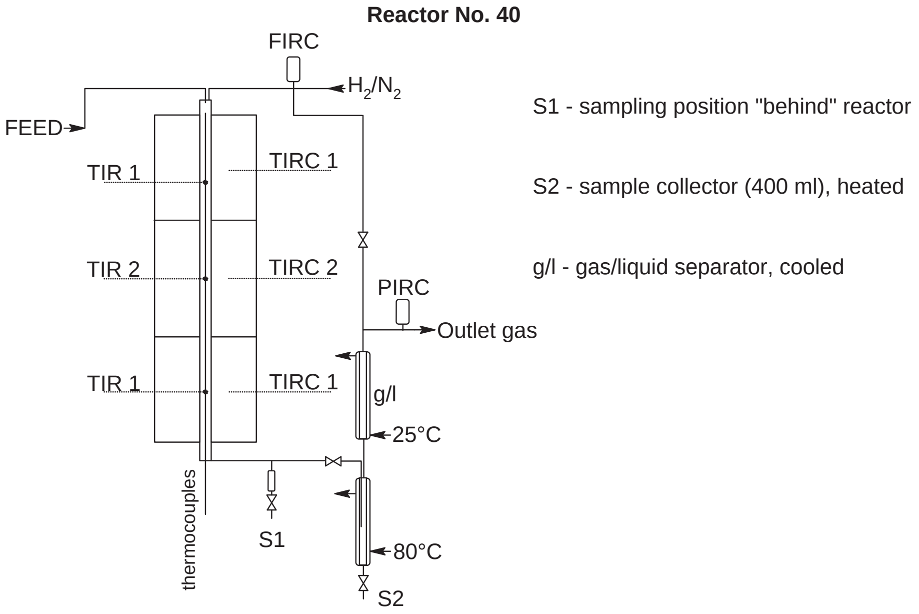

Fig. 2. Scheme of the reactor used in the deoxygenation experiments.

sulfur content in the active phase results in a more stable catalytic system and reduces catalyst deactivation [21]. The reactor was cooled down to the reaction temperature from the activation temperature in presence of the feedstock. The collected liquid phase samples were separated into organic and aqueous phase. The organic phase was analyzed as described previously [21]. In brief, the composition of the organic phase was determined by on-column gas chromatography using an Agilent 7890 A instrumentation and "Select Biodiesel for Glycerides" column with a retention gap. The temperature profile is described below in Table 2. Helium was used as carrier gas with inlet pressure of 15 kPa.

The description of the catalytic results is based on conversion of triglycerides and selectivity to hydrocarbons. The conversion is defined as the difference between the amount of triglycerides entering and exiting the reactor divided by the amount of triglycerides entering the reactor. It follows that hydrogenation of the original rapeseed oil triglycerides to saturated ones is not considered as conversion here. The selectivity to C_{17} and C_{18} hydrocarbons is defined as the amount of n-heptadecane and n-octadecane, respectively, formed per the amount of converted (consumed) triglycerides.

Table 2
Temperature program of the GC analysis method.

Rate (°C/min)	Set point (°C)	Hold time (min)
–	50	1.00
5	120	0.00
15	230	0.00
10	395	1.67

3. Results and discussion

3.1. Catalytic test optimization

Deoxygenation of triglycerides was performed in a wide range of conversions by varying the reaction conditions (temperature and feed rate). Consequently, the time needed to achieve steady state operation varies significantly as well. The reaction conditions and the sampling of the reaction products thus had to be optimized to ensure reproducible results of the catalytic tests obtained under the steady state conditions while minimizing the overall length of the catalytic test. To achieve this, a preliminary test with 1 h sampling interval was carried out to establish the time needed for the stabilization of the reactor after changing the reaction conditions. A commercial $NiMo/Al_2O_3$ catalyst was used as a model catalyst for the optimization. Based on the experimental data (conversion of triglycerides, yield of hydrocarbons) depicted in Fig. 3, the optimum duration of each of the reaction conditions and the time window for sampling under the steady state conditions was

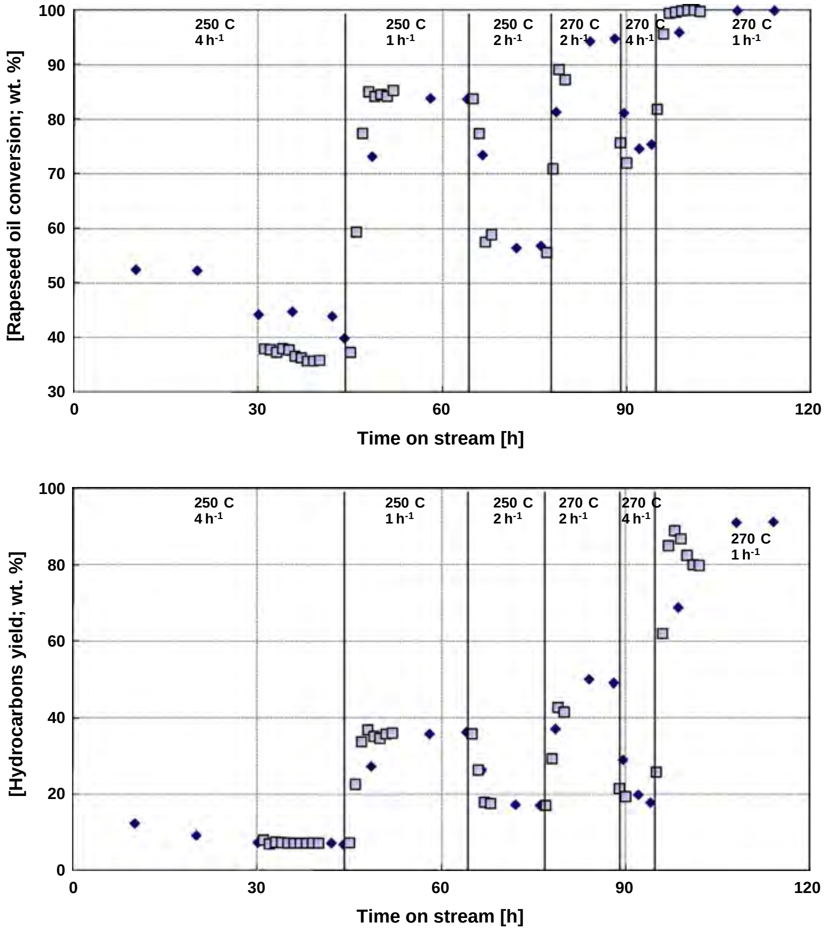

Fig. 3. The rapeseed oil conversion and hydrocarbon yields over model commercial catalyst, data used for time on stream optimization (□ sampling each 1 h; ♦ sampling during the stabilization and under the steady state conditions for F/W = 1, 2 and 4 h^{-1}).

determined. Finally, the overall time on stream was optimized to 108 h.

3.2. The effect of active metals and promoters on the course of the deoxygenation

The catalysts were prepared using the same preparation method to compare the catalytic role of the active metals and precursors at defined reaction conditions and to find the effect of the various catalyst support materials on the activity and selectivity of the catalysts.

3.2.1. Bimetallic catalysts

The direct comparison of the promoters, i.e. Ni and Co, in the bimetallic combinations (NiMo, CoMo, NiW and CoW) showed a higher promoting effect of nickel in comparison with cobalt. The highest conversions (extent of deoxygenation) and hydrocarbons yields at 250 and 270 °C were obtained over NiMo/alumina followed by NiW/alumina catalyst. A significantly lower conversion was observed over CoMo/alumina and CoW/alumina catalyst. While the conversion and more importantly deoxygenation of triglycerides over the CoMo/alumina catalyst could be increased to the values observed for the Ni-promoted catalysts by increasing the reaction temperature and contact time, the deoxygenation of triglycerides over CoW/alumina remained low (<40%) even at 270 °C (Fig. 4).

Apart from the clear effect of promoters one can also observe differences in the function of the active metals. When comparing the active phase metals (Mo and W), tungsten was found to be active in triglyceride structure decomposition, but its activity for deoxygenation was lower than that of molybdenum, e.g. at approximately 85% conversion level the yield of hydrocarbons was nearly 60% over NiMo/alumina, but only slightly over 20% over NiW/alumina (Fig. 4). This behavior resulted in enhanced formation of fatty carboxylic acids and fatty esters over the tungsten-based catalyst (not shown). Although almost complete rapeseed oil conversion was observed over CoW/alumina, it can be described as inactive due its low deoxygenation activity and consequently low hydrocarbons formation. For instance, the yield of hydrocarbons was below 20% over CoW/alumina at the conversion of triglycerides >95% (Fig. 4).

Although lower yields of hydrocarbons were obtained over the Co-promoted catalyst, the promoting effect of cobalt is still very interesting from the selectivity point of view. Hydrodeoxygenation is preferred over all tested catalysts (Fig. 5, $C_{18}/C_{17} > 1$), but Co as a promoter induced important selectivity changes leading to the dominant formation of hydrodeoxygenation (HDO) products (Fig. 5, $C_{18}/C_{17} > 20$). This behavior can be attributed to the fact that nickel is promoting C–C bond cleavage in carboxylic acids, specifically splitting off the carboxylic group and releasing CO_2, i.e. decarboxylation. The selectivity to hydrocarbon products is important for several reasons, like hydrogen consumption, catalyst deactivation and byproduct formation. Decarboxylation is directly connected with the shortening of the hydrocarbon chains of hydrocarbons and decreasing thus the hydrocarbons yields (in comparison with the hydrodeoxygenation pathway). Carbon dioxide produced by decarboxylation is being typically partially reduced

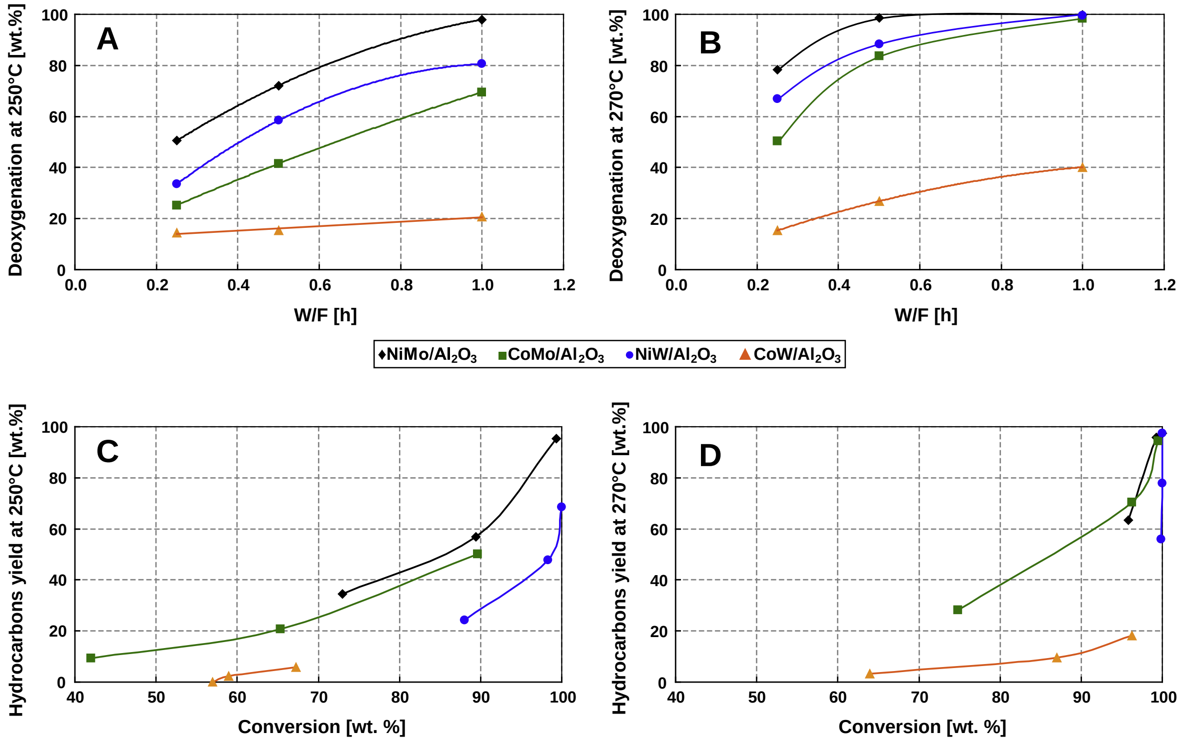

Fig. 4. Comparison of alumina-supported bimetallic catalysts activity; deoxygenation extent at 250 (A) and 270 °C (B) and yield of hydrocarbons in the organic phase at 250 (C) and 270 °C (D).

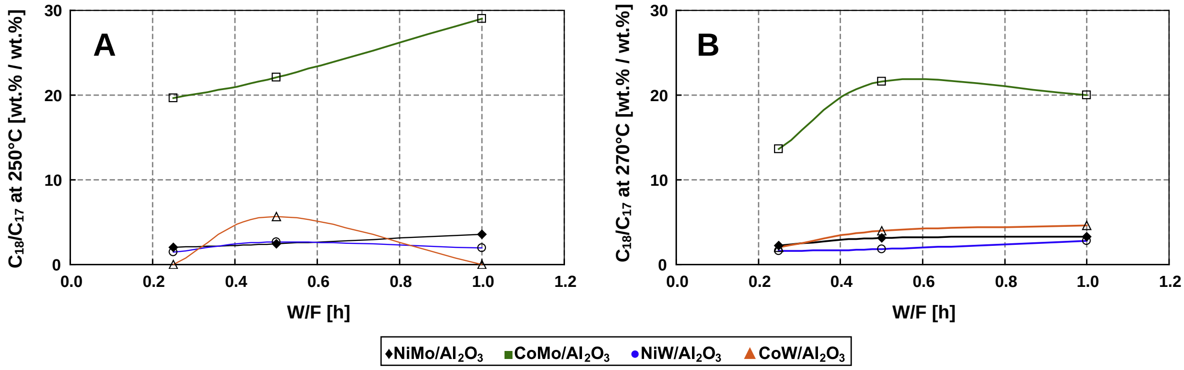

Fig. 5. Selectivity comparison of the bimetallic catalysts; the effect of reaction conditions on the hydrodeoxygenation/decarboxylation products ratio (C_{18}/C_{17}).

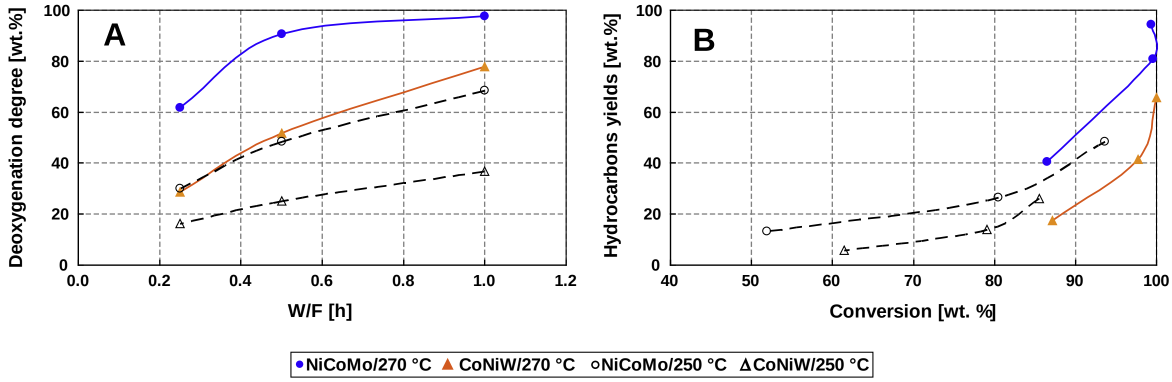

Fig. 6. The basic comparison of tri-metallic catalysts activity at 250 and 270 °C; deoxygenation extent over trimetallic catalysts (A) and yield of hydrocarbons in organic phase (B).

into CO that is responsible for catalyst activity inhibition. Except catalyst inhibition (by CO), decarboxylation reaction pathway also rapidly increases hydrogen consumption due to the complete reduction of CO_2 into methane and water.

3.2.2. Tri-metallic catalysts

The effect of both promoters on the alumina-supported Mo and W catalysts was investigated as well. The comparison of these tri-metallic catalysts (NiCoMo/alumina and NiCoW/alumina) is depicted in Fig. 6. The addition of Ni into the inactive CoW/alumina type (see Fig. 6) resulted in a conversion increase at both reaction temperatures and promoted deoxygenation reactions and hydrocarbons formation respectively. As depicted in Fig. 6 A CoNiMo/alumina catalyst is very sensitive to the change in the reaction temperature. It is caused by the Co presence which results in the activity increase in comparison with NiMo/alumina catalyst and significant selectivity changes (Fig. 7). It can be inferred that Co as a promoter requires higher reaction temperature in comparison with Ni. This conclusion is in good agreement with results obtained from comparison of bimetallic catalysts (Fig. 4 A and B).

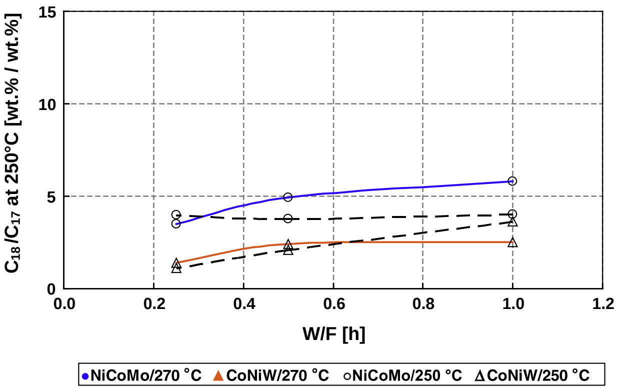

Fig. 7. Product selectivities over tri-metallic catalysts; the effect of reaction conditions on the hydrodeoxygenation/decarboxylation products ratio (C_{18}/C_{17}).

3.3. Role of catalyst support

Five catalyst supports (alumina, titania, silica, SBA-15 and hydrotalcite) were compared to study their role in triglycerides deoxygenation. For all the materials, NiMo bimetallic combination was applied and the same nominal loadings of promoter and active metal (3 wt.% Ni and 15 wt.% Mo, respectively) were used.

At temperatures 250 and 270 °C, alumina and SBA-15 were found to be very good supports for NiMo catalyst. Rapeseed oil was completely deoxygenated at the contact time of 1 h (Fig. 8) when catalysts supported on alumina and highly porous silica was used. Moreover, over alumina supported catalyst complete oil deoxygenation was achieved in 30 min at 270 °C (Fig. 8B). Silica and titania together with hydrotalcite were not found as good choice for the low temperature conversion of triglycerides into hydrocarbons. Based on previous experience [23], temperature increase promotes catalytic activity of these materials and behavior of catalyst might even be better than in case of alumina-based type. Hydrotalcite supported NiMo was found little less active at 250 °C than silica and titania, but the increase of reaction temperature by 20 °C promoted its activity more, than in the case of silica- and titania-based NiMo catalysts. In Fig. 8, the promoting effect of the support specific surface area is clearly depicted, the increase of the specific surface area from approximately 57 m^2/g (Silica, Cherox) to 650 m^2/g (SBA-15) results in higher deoxygenation degree. This effect can be attributed to the plausibly better dispersion of the active sulfide phase on the support surface as the active-phase-support interactions can be expected to be very similar due to the similar chemical nature of both supports. In addition to SBA-15, the hydrodeoxygenation reaction mechanism is promoted over the hydrotalcite support as well. The increased selectivity for decarboxylation (Fig. 9) in the case of silica and titania supports is in good agreement with previous work [23]. The selectivity of NiMo/SBA-15 for HDO reaction mechanism can be attrib-

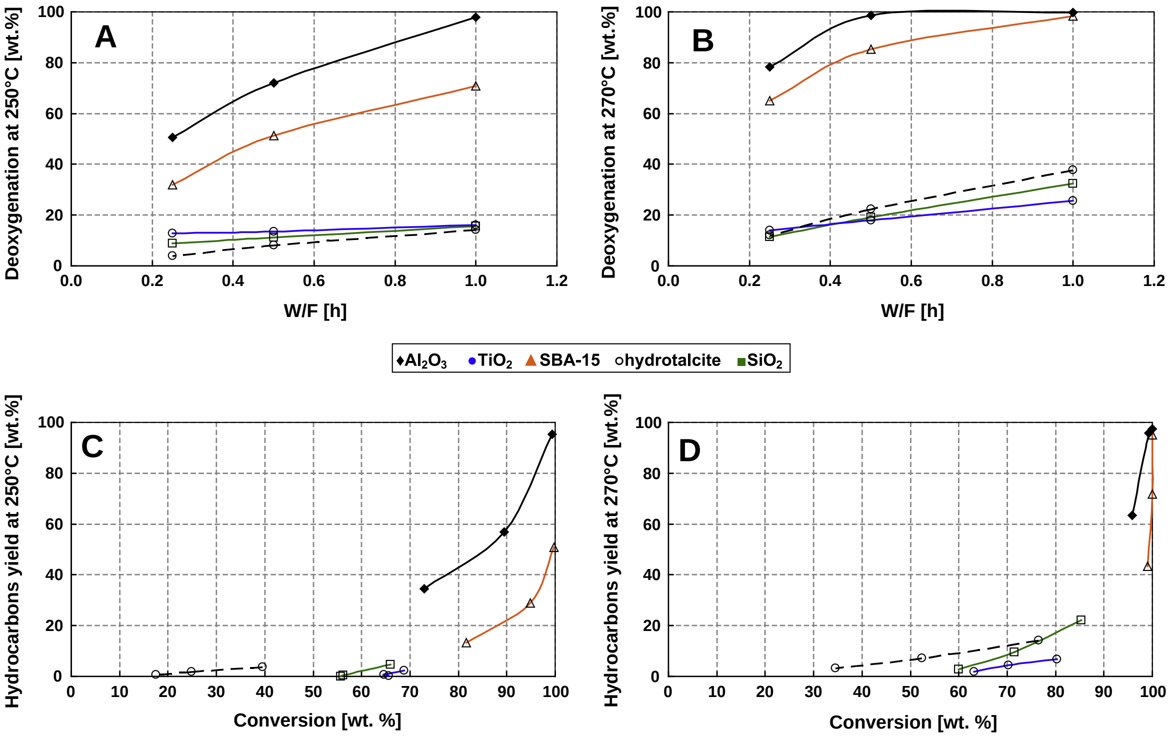

Fig. 8. The comparison of support materials (alumina, titania, SBA-15, hydrotalcite and silica) loaded with NiMo; the comparison of the deoxygenation extent as a function of the residence time, W/F (h), (A and B) and yields of hydrocarbons as a function of triglycerides conversion.

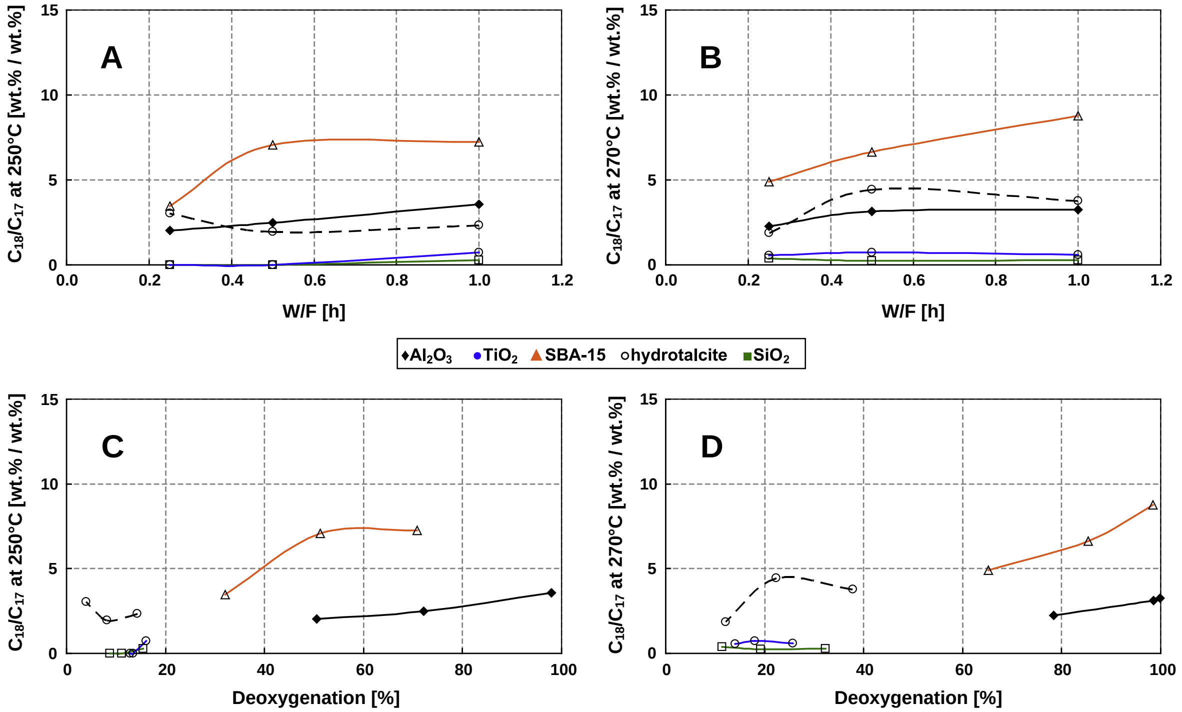

Fig. 9. Comparison of reaction pathways based on the hydrodeoxygenation/decarboxylation products ratio (C_{18}/C_{17}) for various support materials presented as a function of residence time, W/F (h) (A and B) and extent of deoxygenation (C and D).

uted to its high specific surface area, organized structure improving transport parameters avoiding C–C bond cleavage of decarboxylation. Increased selectivity to hydrodeoxygenation of hydrotalcite-based NiMo catalysts is given by its typical basicity (specific for this type of materials) that results in lower acidity of the catalyst and thus to the reduced C–C bond cleavage activity (see Fig. 9).

4. Conclusions

Alumina-supported NiMo bimetallic promoter-active metal combination was found as most active catalyst type at 250 and 270 °C. Co presence in the catalyst strongly affected the deoxygenation mechanism; it was found that promoting effect of Co starts to work at higher temperatures in comparison with Ni as promoter. CoW was identified as the least active metal combination at the investigated reaction conditions. The lower activity of silica- and titania-supported catalysts and their higher selectivity to decarboxylation pathway are in good agreement with previous work [23]. The high specific surface of an in-laboratory-prepared SBA-15 support resulted in significantly higher deoxygenation degrees in comparison with silica- and titania-supported catalysts. The hydrotalcite-based NiMo catalyst was little less active than silica- and titania-based types at 250 °C, but the increase of the reaction temperature resulted in a more pronounced activity increase than in the case of silica- and titania-supported NiMo.

Acknowledgements

The financial support by the Czech Science Foundation – project P106/12/G015 – is highly acknowledged. The project (P106/12/G015) is being carried out in the UniCRE centre (CZ.1.05/2.1.00/03.0071) using its research infrastructure.

References

[1] Huber G, Iborra S. Corma, synthesis of transportation fuels from biomass: chemistry, catalysts, and engineering. A. Chem. Rev. 2006;106(9):4044–98.
[2] Kubička D, Kubičková I, Čejka J. Application of molecular sieves in transformations of biomass and biomass-derived feedstocks. Catal. Rev. Sci. Eng. 2013;55:1–78.
[3] Kubičková I, Kubička D. Utilization of triglycerides and related feedstocks for production of clean hydrocarbon fuels and petrochemicals: a review. Waste Biomass Valorization 2010;1:293–310.
[4] Lestari S, Mäki-Arvela P, Beltramini J, Max Lu, Murzin GQ, Yu D. Transforming triglycerides and fatty acids into biofuels. ChemSusChem 2009;2:1109–19.
[5] Donnis B, Egeberg RG, Blom P, Knudsen KG. Hydroprocessing of bio-oils and oxygenates to hydrocarbons. Understanding the reaction routes. Top. Catal. 2009;52:229–40.
[6] Bezergianni S, Dimitriadis A, Kalogianni A, Pilavachi P. Hydrotreating of waste cooking oil for biodiesel production. Part I: effect of temperature on product yields and heteroatom removal. Bioresour Technol 2010;101:6651.
[7] Bezergianni S, Dimitriadis A, Sfetsas T, Kalogianni A. Hydrotreating of waste cooking oil for biodiesel production. Part II: effect of temperature on hydrocarbon composition. Bioresour Technol 2010;101:7658.
[8] Kubička D. Future refining catalysis-introduction of biomass feedstocks. Collect Czech Chem Commun 2008;73:1015–44.
[9] Kubička D, Bejblová M, Vlk J. Conversion of vegetable oils into hydrocarbons over CoMo/MCM-41 catalysts. Top Catal 2010;53:168–78.
[10] Melis S, Mayo S, Leliveld B: Vegetable oil co-processing in diesel hydrotreaters, PTQ Biofuels, 2009, p. 43.
[11] Mikulec J, Cvengroš J, Joríková L, Banič M, Kleinová A. Second generation diesel fuel from renewable sources. Chem Eng Trans 2009;18:475.
[12] Kubičková I, Snare M, Eranen K, Maki-Arvela P, Murzin. Hydrocarbons for diesel fuel via decarboxylation of vegetable oils. D: Catal Today 2005;106:197–200.
[13] Sebos I, Matsoukas A, Apostolopoulos A, Papayannakos N. Catalytic hydroprocessing of cottonseed oil in petroleum diesel mixtures for production of renewable diesel. Fuel 2009;88:145–9.
[14] Neste Oil, <http://www.nesteoil.com/default.asp?path¼1,41,11991,12243,13565>. Accessed April, 2013.
[15] UOP, www.uop.com, UOP/ENI Ecofining Process.pdf. Accessed April, 2013.
[16] Kubička D, Lederer J, Bělohlav Z. Catalytic transformation of triglycerides in refineries – a promising route to clean fuels and feedstocks for petrochemicals. Oil Gas Eur Mag 2009;35:40–3.
[17] Šimáček P, Kubička D. Hydrocracking of petroleum vacuum distillate containing rapeseed oil: evaluation of diesel fuel. Fuel 2010;89:1508–13.

[18] Šimáček P, Kubička D, Šebor G, Pospíšil M. Fuel properties of hydroprocessed rapeseed oil. Fuel 2010;89:611.
[19] Šimáček P, Kubička D, Kubičková I, Homola F, Chudoba J, Pospíšil M. Premium quality renewable diesel fuel by hydroprocessing of sunflower oil. Fuel 2011;90:2473.
[20] Zhao D, Huo Q, Feng J, Chmelka BF, Stucky GD. Nonionic triblock and star diblock copolymer and oligomeric surfactant syntheses of highly ordered, hydrothermally stable, mesoporous silica structures. J. Am. Chem. Soc. 1998;120:6024–36.
[21] Kubička D, Horáček J. Deactivation of HDS catalysts in deoxygenation of vegetable oils. Appl Catal A: Gen 2011;394:9–17.
[22] Furimsky E, Massoth FE. Introduction. Catal Today 1993;17:537–660.
[23] Kubička D, Horáček J, Setnička M, Bulánek R, Kubičková I. Effect of support-active phase interactions on the catalyst activity and selectivity in deoxygenation of triglycerides. Appl Catal B Environ 2014;145:101–7.

Applied Catalysis A: General 372 (2010) 199–208

Contents lists available at ScienceDirect

Applied Catalysis A: General

journal homepage: www.elsevier.com/locate/apcata

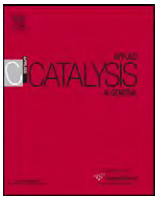

Deoxygenation of vegetable oils over sulfided Ni, Mo and NiMo catalysts

David Kubička [a,*], Luděk Kaluža [b]

[a] Department of Refinery and Petrochemical Research, Research Institute of Inorganic Chemistry, Záluží 1, D.S. 458, 436 70 Litvínov, Czech Republic
[b] Institute of Chemical Process Fundamentals of the Academy of Sciences of the Czech Republic, v.v.i., Rozvojová 2, 165 02 Prague, Czech Republic

ARTICLE INFO

Article history:
Received 20 August 2009
Received in revised form 13 October 2009
Accepted 21 October 2009
Available online 30 October 2009

Keywords:
Deoxygenation
Decarboxylation
Hydrodeoxygenation
Ni/Al_2O_3
Mo/Al_2O_3
$NiMo/Al_2O_3$
Biofuels
Vegetable oils

ABSTRACT

Deoxygenation of vegetable oils has a potential to become an important process for production of biofuels. The present work focuses on investigation of Ni, Mo, and NiMo sulfided catalysts prepared by impregnation in deoxygenation of rapeseed oil at 260–280 °C, 3.5 MPa and 0.25–4 h^{-1} in a fixed-bed reactor. The activity of the catalysts decreased in the order $NiMo/Al_2O_3 > Mo/Al_2O_3 > Ni/Al_2O_3$. The catalysts exhibited significantly different product distributions. The bimetallic NiMo catalysts showed higher yields of hydrocarbons than the monometallic catalysts at a given conversion. Apart from the various oxygenated product intermediates, $NiMo/Al_2O_3$ yielded a mixture of decarboxylation and hydrodeoxygenation hydrocarbon products while Ni/Al_2O_3 yielded only decarboxylation hydrocarbon products and Mo/Al_2O_3 yielded almost exclusively hydrodeoxygenation hydrocarbon products. The effect of Ni/(Ni + Mo) atomic ratio in the range 0.2–0.4 on the activity and selectivity was not significant.

1. Introduction

Sustainable production of biofuels is an important scientific challenge with a potential to tackle, at least partially, the environmental problems resulting from the extensive use of fossil fuels [1–3]. Hence, a lot of attention is paid to research and development of advanced biofuel technologies – so-called 2nd generation biofuels. The main characteristics of 2nd generation biofuels are: (i) higher greenhouse gas (GHG) emission reduction in the complete life cycle in comparison with current biofuels and (ii) non-food biomass raw materials [4].

Common vegetable oils consist of triglycerides that have bound in their molecules fatty acids with 14 to 22 carbon atoms in their chain. Due to a rather low degree of functionalization and its simplicity (the carboxylic group is the only functional group present in triglycerides) as compared with other types of biomass-based raw materials and suitable chain length, direct upgrading of triglycerides into hydrocarbons has been patented by several companies [5–8] and already commercially demonstrated by Neste Oil [9]. Moreover, several environmental advantages of direct transformation of triglycerides to hydrocarbons over their conversion to fatty acid methyl esters, known also as biodiesel, have been reported [10,11].

Refined vegetable oils require the removal of oxygen, the sole heteroatom present, to obtain hydrocarbons. Due to the nature of oxygen bonding in triglycerides, there are two possible deoxygenation approaches: (i) hydrodeoxygenation and (ii) decarboxylation. In the first approach, oxygen is removed in the form of water while in the latter one it is removed as CO_2 [3,12]. Hence suitable probe molecules are either fatty acids or their esters, including triglycerides.

Investigations of conventional hydrodesulfurization catalysts, such as CoMo, NiMo, NiW supported on alumina, have revealed that complete conversion of triglycerides can be achieved over these catalysts [10–15]. Moreover, the studies have shown that both reaction pathways, *i.e.* hydrodeoxygenation and decarboxylation, are responsible for hydrocarbons formation. The extent of the pathways depended on the catalyst choice and reaction conditions [3,12–14]. The effect of reaction parameters, namely temperature and pressure, has been recently described by a basic thermodynamic model [16]. It has confirmed the experimental observations showing that higher hydrogen pressure and lower reaction temperature favour the hydrodeoxygenation pathway over the decarboxylation one. In comparison with hydrodeoxygenation pathway decarboxylation offers the advantage of lower hydrogen consumption. Thus, decarboxylation of fatty acids and their methyl esters has been studied extensively over Pd/C [17–21]

---

[*] Corresponding author.
E-mail address: david.kubicka@vuanch.cz (D. Kubička).

0926-860X/$ – see front matter © 2009 Elsevier B.V. All rights reserved.
doi:10.1016/j.apcata.2009.10.034

and Pt/Al_2O_3 [22] catalysts, which have shown quite selective propensity to formation of hydrocarbons and carbon oxides. It is, however, essential to avoid subsequent reactions of CO_2 that consume hydrogen, such as methanization, otherwise the increased hydrogen consumption together with the decreased diesel yield will make this route less attractive than hydrodeoxygenation [12].

In addition to studies using neat vegetable oils or probe molecules such as fatty acids or their methyl esters, attention has been paid to co-processing of vegetable oils with crude-oil-derived fractions and detailed characterization of the products [15,23–25]. The advantages of the co-processing would be lower investments and use of already existing infrastructure. However, due to the stringent limits for diesel fuel quality and the need to isomerize the obtained hydrocarbons owing to their poor cold-flow properties, the separate processing of vegetable oils followed by blending of the products seems to be preferred by the refiners [7–11]. The possible negative impact of co-processing on the diesel fuel quality is due to mutual inhibition effects. Not only the rate of deoxygenation is affected by presence of other heteroatoms, *e.g.* inhibition of deoxygenation has been reported when the feed contained both S- and O-containing compounds [26], desulfurization can be inhibited by O-containing compounds as well [27].

It is obvious that sulfided hydrotreating catalysts are suitable candidates for deoxygenation of triglycerides. Nevertheless, relatively little is known about their activity and the activity of their individual active components. The present work is, therefore, focused on investigation of the activity and selectivity of sulfided Ni/Al_2O_3, Mo/Al_2O_3 and $NiMo/Al_2O_3$ and aims at description of the differences among their catalytic functions. Such knowledge is essential for further optimization of hydrotreating catalysts to become efficient deoxygenation catalysts. Moreover, the presented results make it possible to shed light on the effect of the individual active components, *i.e.* Ni and Mo sulfide phases, on the deoxygenation pathways of triglyceride deoxygenation.

2. Experimental

2.1. Catalyst preparation and characterization

The support Al_2O_3 (Eurosupport Manufacturing Czechia), was crushed and sieved to a 0.25–0.50 mm particle size fraction. The catalysts were prepared by conventional impregnation of the support grain using an aqueous solution of $(NH_4)_6Mo_7O_{24}$ and $Ni(NO_3)_2$ (Purum, Lachema, the Czech Republic). The support was mixed with the impregnation solution and after stirring for 1 h it was dried in a rotary vacuum evaporator and calcined in an air stream at 400 °C for 1 h. The loadings of MoO_3 and NiO in the monometallic catalysts were 21.8 and 12.7 wt.%, respectively, which represent 3.4 atoms of Mo or Ni per nm^2. The catalysts were labelled Mo/Al_2O_3 and Ni/Al_2O_3.

The Mo/Al_2O_3 catalyst was also used in preparation of bimetallic NiMo catalysts. It was mixed with an appropriate amount of $Ni(NO_3)_2$ solution to achieve the required atomic ratio Ni/(Ni + Mo) and after stirring for 1 h it was dried in a rotary vacuum evaporator. The solid was calcined at 400 °C for 1 h in a fixed-bed reactor in an air stream. Three bimetallic catalysts with the atomic ratio Ni/(Ni + Mo) equal to 0.2, 0.3 and 0.4 were prepared by this procedure. The bimetallic catalysts were named as follows: $0.3NiMo/Al_2O_3$, for instance, is the NiMo sample having the atomic ratio of Ni/(Ni + Mo) equal to 0.3.

N_2 adsorption–desorption isotherms were measured using a Micromeritics ASAP 2010 M instrument over samples evacuated at 350 °C for 4 h. Specific surface area (S_{BET}) was determined by the common Brunauer, Emmett and Teller (BET) procedure. The specific surface area of the mesopores (S_M) and the volume of the micropores (V_{Micro}), were determined by the t-plot method. The total pore volume (V_{Total}) was calculated from the volume of N_2 adsorbed at the relative pressure p/p_0 0.97. Pore size distribution was calculated from the desorption branch of the adsorption–desorption isotherms by the Barrett–Joyner–Halenda (BJH) method. All textural parameters were normalized also per gram of support.

2.2. Catalytic activity measurements

Refined rapeseed oil (food grade) with the following mass distribution of fatty acids was used as a starting material: palmitic acid: 4.8%, stearic acid: 1.9%, oleic acid: 61.9%, linoleic acid: 19.8% and linolenic acid: 9.2% [15]. The content of metals and other heteroatoms in refined rapeseed oil was low (S: 7 mg kg^{-1}; N: 15 mg kg^{-1}, P: <1 mg kg^{-1}; Na: <1 mg kg^{-1}; K: <1 mg kg^{-1}; Ca: 2 mg kg^{-1}; Mg: 3 mg kg^{-1}) [24]. Refinery hydrogen gas with >99% of H_2 was used in the experiments. The main impurities were methane (0.6%) and nitrogen (0.3%). The experiments were performed in an electrically heated fixed-bed reactor of inner diameter equal to 17 mm. The reactor was loaded prior to the experiments with catalyst diluted by an inert (SiC) to ensure sufficient catalyst-bed length and to improve the reaction-heat transfer. A layer of the inert material was placed above the catalyst bed to preheat rapeseed oil and hydrogen and to guarantee a good feed flow distribution prior to entering the catalyst bed. The particle sizes of the catalyst and SiC were 0.25–0.5 mm and <0.1 mm, respectively. In the vertical axis of the reactor, there was a thermo-well of the outer diameter equal to 5 mm, in which three adjustable thermocouples, used to determine the reaction temperature, were placed. The catalysts were activated (sulfided) in situ prior to the experiments by means of a mixture of dimethyl disulfide (DMDS) in isooctane (5 wt.% DMDS) at 320 °C. The reaction temperature was varied during the experiments in the range of 260–280 °C. The contact time of the liquid feed with the catalyst (V/F) was varied in the range of 0.25–4 h by varying the catalyst mass (V) and rapeseed oil feed rate (F) within the range 10–16 g and 4–40 g h^{-1}, respectively. The hydrogen-to-rapeseed-oil molar ratio and hydrogen pressure were constant at 50 and 3.5 MPa, respectively. The approximate apparent bulk densities of the NiMo, Mo and Ni catalysts were 0.80, 0.84 and 0.76 g/cm^3; the density of rapeseed oil at 15 °C was 0.92 g/cm^3. The liquid and gaseous products were separated at the reactor outlet in a heated gas–liquid separator as some of the products are solid at ambient temperatures.

The liquid products (collected and separated at 80 °C) were withdrawn after stabilization of reaction conditions (6 h) in two-hour intervals and analyzed by off-line gas chromatography after separation of the water phase. Due to the presence of triglycerides in the products, on-column injection had to be used. Trikaprin (Fluka, >99%) was used as an internal standard in order to quantify the concentration of triglycerides. Moreover, the reaction intermediates included fatty acids and alcohols and silylation of reaction products by MSTFA (Acros, 97%) was applied to enhance their volatility and to improve the shapes of the peaks. The products were separated on a Restek MTX-Biodiesel TGw/Int-GAP column (14 m × 0.53 mm × 0.16 μm) and detected using a flame ionization detector (FID). The following temperature program was used: initial temperature 50 °C for 3 min, heating first 11 °C/min to 180 °C, then 5 °C/min to 230 °C and finally 15 °C/min to 390 °C with dwelling time of 7 min at 390 °C. The individual products were identified using GC standards and the identification was further confirmed by GC–MS analysis. The gas-phase products were collected once at every reaction condition and analyzed off-line using a standard three-column GC setup with flame ionization and thermal conductivity detectors enabling the detection of both permanent gases and hydrocarbons at the same time.

Table 1
Textural parameters of Al_2O_3 support and Ni, Mo and NiMo catalyst.

	Al_2O_3	Ni/Al_2O_3		Mo/Al_2O_3		$0.3NiMo/Al_2O_3$	
		Per gram of catalyst	Per gram of Al_2O_3	Per gram of catalyst	Per gram of Al_2O_3	Per gram of catalyst	Per gram of Al_2O_3
S_{BET}, m^2g^{-1}	344	220	252	274	351	259	348
S_{MESO}, m^2g^{-1}	243	160	183	174	223	168	225
V_{Total}, cm^3g^{-1}	0.405	0.291	0.333	0.306	0.392	0.277	0.372
V_{Micro}, cm^3g^{-1}	0.070	0.043	0.049	0.063	0.081	0.058	0.078

3. Results and discussion

3.1. Catalyst characterization

The textural parameters of the Al_2O_3 support and the selected catalysts are summarized in Table 1. The impregnation of the support with Ni species resulted in about 25% decrease of all textural parameters studied probably because of partial over-loading of the Al_2O_3 support surface with three-dimensional Ni oxide phase, which blocked the porous system. This assumption was supported by powder XRD (not shown) where a broad weak peak corresponding to NiO crystalline phase was detected. In contrast, the support texture remains practically unaffected after Mo and NiMo deposition and their powder XRD spectra did not show any crystalline phase except a week signal from the Al_2O_3 support. The average pore radiuses taking from the pore size distributions of the support and the catalysts were the same in the range 1.9–2.5 nm.

The loading of Mo in Mo/Al_2O_3 and of Ni in Ni/Al_2O_3 catalyst were 21.85 and 12.67 wt.%, respectively. These loadings correspond to the surface concentration of active metals approximately 3.4 atoms/nm^2. The bimetallic catalysts were prepared by impregnation of the Mo/Al_2O_3 catalyst by Ni to obtain Ni/(Ni + Mo) atomic ratios equal to 0.2, 0.3 and 0.4. The resulting concentrations of Ni and Mo in the 0.2NiMo, 0.3NiMo and 0.4 NiMo were 2.76 and 21.24 wt.%, 4.63 and 20.84 wt.%, and 7.03 and 20.31 wt.%, in that order. Owing to the chosen catalyst synthesis method the given nominal loading values can be considered as the actual loadings because all dissolved species deposited onto the support during vacuum impregnation.

3.2. Conversion of rapeseed oil

Conversion of rapeseed oil, *i.e.* of triglycerides that make up rapeseed oil, was determined in order to compare the performances Ni/Al_2O_3, Mo/Al_2O_3 and $0.3NiMo/Al_2O_3$ catalysts. The catalysts contained the same total amount of active sites (*i.e.* Ni and Mo atoms) to allow a fair comparison of their performance. The concentration of active sites was about 3.4 atoms/nm^2. The conversion of triglycerides over these catalysts as a function of contact time (V/F) is depicted in Fig. 1. The conversion decreased in the following order at all investigated reaction temperatures: 0.3NiMo > Mo > Ni. The contact time, at a given reaction temperature, had to be doubled and quadrupled for Mo and Ni catalyst, respectively, to achieve same conversion as over 0.3NiMo catalyst (Fig. 1). These results are in qualitative agreement with the results obtained during hydrodesulfurization [28]. It can be concluded that, similarly to desulfurization, Ni functions as an activity promoter of Mo catalysts in deoxygenation of triglycerides. Furthermore, it can be seen that the conversion over all three catalysts increases with increasing reaction temperature and that complete conversion of triglycerides can be obtained already at 270 °C (Fig. 1). These results suggest that the deoxygenation reactions of triglycerides are irreversible at the selected reaction conditions.

The concentration of Ni, *i.e.* of the promoter, was varied to obtain different Ni/(Ni + Mo) atomic ratios. It is known that the optimum ratio Ni/(Ni + Mo) for desulfurization is about 0.3 [28,29]. Therefore, a series of the deoxygenation catalysts with the Ni/(Ni + Mo) ratio equal to 0.2, 0.3 and 0.4 was synthesized to assess its influence on deoxygenation of triglycerides. Fig. 2 shows that the effect of Ni/(Ni + Mo) ratio on triglycerides conversion is rather minor at all three tested reaction temperatures. Largest differences can be observed at short contact times (0.25 h) at which the

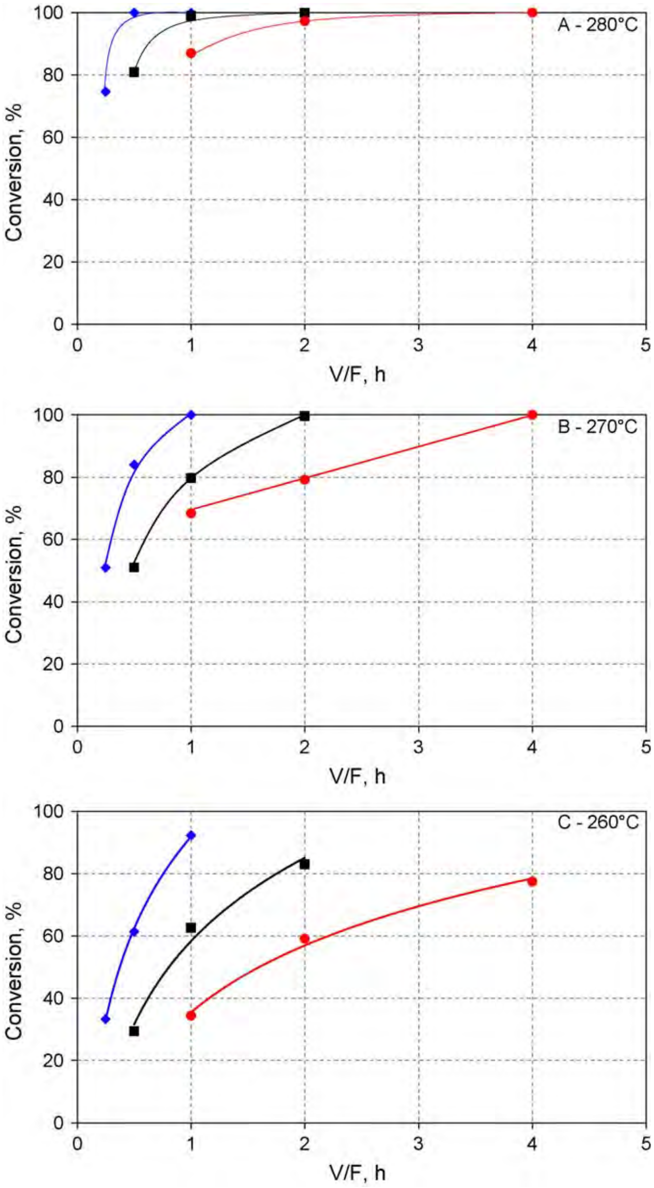

Fig. 1. Conversion of triglycerides over NiMo (◆ – Ni/(Ni + Mo) = 0.3); Mo (■) and Ni (●) catalysts at different reaction temperatures; T = 260–280 °C, p = 3.5 MPa.

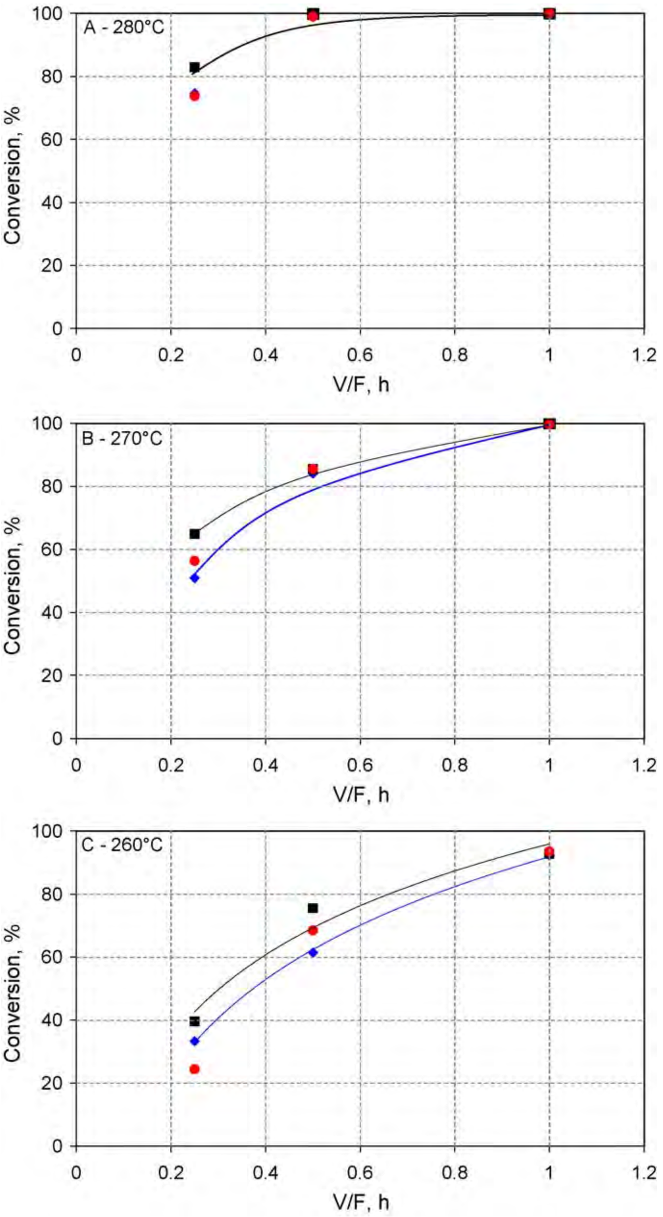

Fig. 2. Conversion of triglycerides over NiMo catalysts with different Ni/(Ni + Mo) atomic ratio at different reaction temperatures (■ – Ni/(Ni + Mo) = 0.2; ◆ – Ni/(Ni + Mo) = 0.3; ● – Ni/(Ni + Mo) = 0.4); T = 260–280 °C, p = 3.5 MPa.

catalyst with Ni/(Ni + Mo) ratio of 0.2 gives the highest conversion at all three reaction temperatures. However, the differences among the three NiMo catalysts (Fig. 2) are not as considerable as they were in the case Ni, Mo and NiMo catalysts (Fig. 1).

The activity of the catalysts in deoxygenation can be described either by looking at the conversion of triglycerides, *i.e.* evaluating the rate of disappearance of triglycerides, or by looking at the concentration of oxygen in liquid products at the reactor outlet, *i.e.* evaluating the rate of disappearance of oxygen from liquid products. Both dependencies have been obtained by using the pseudo-first-order kinetics to fit the relevant experimental data for 0.3NiMo, Mo and Ni catalysts at three reaction temperatures. The results are depicted in Fig. 3, where it is seen that the experimental data followed the empiric pseudo-first-order-kinetics. A comparison of the concentration profiles of triglycerides, on the one hand, and oxygen, on the other hand, reveals significant differences among the catalysts. These are most obvious in the case of Ni catalyst. In order to quantify these differences, the relative pseudo-first order rate constants have been calculated at 270 °C (Table 2).

The rate of disappearance of triglycerides is the highest over the bifunctional catalyst being approximately two and three times higher than that over Mo and Ni catalysts, respectively (Table 2). In the case of the rate of oxygen disappearance, it is again the highest over 0.3NiMo catalyst with the rates over Mo and Ni catalysts being 3.5 and 19 times slower. The difference between the rates of disappearance of triglycerides and of oxygen clearly shows that conversion of triglycerides leads at first to oxygen-containing intermediates that are subsequently converted into hydrocarbons. Moreover, it can be also inferred from the data that the Ni catalyst is significantly less efficient in the subsequent deoxygenation step, probably due to a different mechanism as it is discussed bellow based on the organic liquid products distributions. While the relative rate constant of consumption of the organically bound oxygen is about 63% of the relative rate constant of triglycerides disappearance in the case of 0.3NiMo catalyst, it corresponds to only 10% and 40% of the relative rate constant of triglycerides disappearance in the case of Ni and Mo catalysts, correspondingly (Table 2).

The very low activity of Ni catalyst in comparison with Mo and in particular with NiMo catalysts (Table 2) cannot be explained only by its lower surface area (Table 1) since addition of Ni to Mo phase results in 3.5 higher activity of the promoted catalyst. Furthermore, the NiMo is ca. 19 times more active in deoxygenation than the Ni catalyst and an implausible increase in Ni dispersion on NiMo catalyst in comparison with Ni catalyst would be needed. Hence in can be concluded that similarly to hydrodesulfurization NiS phase acts in synergy with MoS_2 increasing thus the catalyst deoxygenation activity [28].

3.3. Overall product distribution

Deoxygenation of triglycerides over all investigated catalyst yielded two main classes of organic liquid reaction products and intermediates – hydrocarbons and oxygenates. The ultimate products of deoxygenation were hydrocarbons, oxygenates were the reaction intermediates, in particular fatty acids (*e.g.* stearic acid), fatty alcohols (*e.g.* *n*-octadecanol) and their fatty esters (*e.g.* stearylstearate). The shape of the selectivity curves of the two main reaction product classes confirms that hydrocarbons are the final reaction products and that their formation is preceded by the formation of oxygenated intermediates (Fig. 4). The hydrocarbons consisted mainly of *n*-octadecane, *n*-heptadecane, *n*-hexadecane and *n*-pentadecane. In addition to the organic liquid products, water and gaseous products, such as propane, carbon oxides and methane, were formed during deoxygenation of triglycerides. This is in agreement with previous studies on deoxygenation [12,13,15,22,30]. However, in contrast to Craig [30] no organic liquid products with boiling point below 210 °C (*i.e.* cracking products) were obtained in this study. This difference can be attributed to the different reaction temperature ranges used in both studies, the reaction temperatures used by Craig (350–420 °C) favour cracking of the primary n-alkanes considerably more than the temperatures used here (260–280 °C).

It can be seen that oxygen is principally eliminated in two forms – water and carbon oxides. It has been shown previously that formation of carbon oxides is connected with decarboxylation and formation of hydrocarbons with odd number of carbon atoms in their molecule, *i.e.* predominantly *n*-heptadecane and *n*-pentadecane in the case of rapeseed oil. On the other hand the production of water is related to (i) reduction of triglycerides yielding hydrocarbons with an even number of carbon atoms in their molecule, *i.e.* predominantly *n*-octadecane and *n*-hexadecane in the case of rapeseed oil, and to (ii) reduction of carbon oxides. The

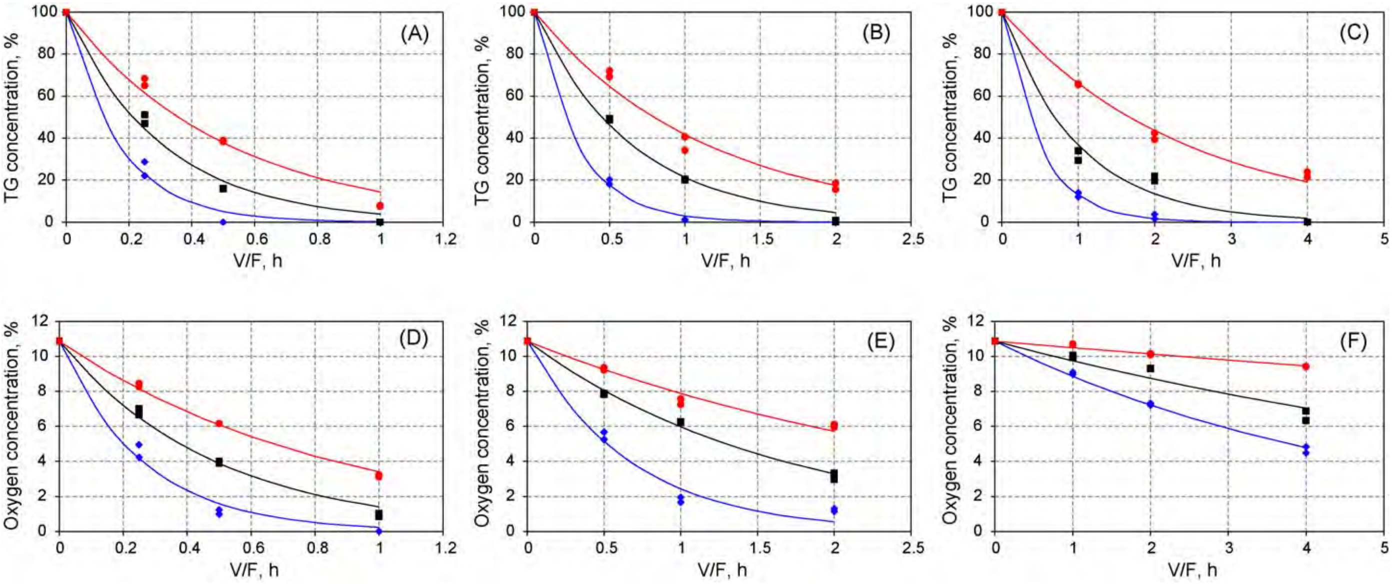

Fig. 3. The change in concentration of triglycerides (A–C) and oxygen (D–F) as a function of contact time for 0.3NiMo (A and D), Mo (B and E) and Ni (C and F) catalysts at three temperatures (◆ – 280 °C; ■ – 270 °C; ● – 260 °C). Solid points = experimental data, solid lines = concentrations based on the pseudo-first-order kinetics approximation of experimental data. Oxygen concentration corresponds to the concentration of organically bound oxygen and was calculated by using the composition of the products and their corresponding oxygen fraction.

primarily formed carbon dioxide is at first reduced to carbon monoxide, which can be further reduced to methane. The reduction of triglycerides to hydrocarbons and water, *i.e.* without formation of carbon oxides, is called hydrodeoxygenation. The last gaseous product, propane, originates from the glycerol part of triglycerides.

The cracking activity of the tested catalysts was very low under the experimental conditions since no other gaseous products or short chain liquid hydrocarbons were found in reaction products. Moreover, the extent of isomerization was also negligible under the investigated conditions since only traces of skeletal isomers were identified in the organic liquid reaction products. On the other hand, all tested catalysts exhibited a good hydrogenation activity as olefinic products, such as propene and C_{15}–C_{18} alkenes, were not present in the reaction products.

The selectivities of the two main organic liquid reaction products, based on the total yield of organic liquid products are depicted in Figs. 4 and 5 for Ni, Mo and 0.3NiMo catalysts and for the series of NiMo catalysts with different Ni/(Ni + Mo) atomic ratio, respectively. The selectivity to hydrocarbons increases for all tested catalysts with increasing conversion, which reveals that hydrocarbons are formed, at least partially, from the oxygenated intermediates. It is also interesting to note that while in the case of monometallic catalysts oxygenates appear to be the exclusive primary products (Fig. 4), in the case of bimetallic catalysts even hydrocarbons appear to be formed as primary products. This might be a consequence of the higher activity of bimetallic catalysts that results in deoxygenation of deoxygenation intermediates before they can desorb and be found as reaction intermediates in the liquid phase.

Table 2
Relative pseudo-first order rate constants for triglycerides and oxygen disappearance over 0.3NiMo, Mo and Ni catalysts at 270 °C.

Catalyst/reaction	Triglycerides disappearance	Oxygen disappearance
0.3NiMo/Al_2O_3	2.08	1.31
Mo/Al_2O_3	1.00	0.38
Ni/Al_2O_3	0.65	0.06

Furthermore, there is a clear difference in selectivity between the monometallic catalysts (Ni, Mo) on the one hand, and bimetallic 0.3NiMo catalyst on the other hand (Fig. 4). The selectivity to hydrocarbons of 0.3NiMo catalyst is, at a comparable conversion, substantially larger than that of Ni and Mo catalysts. Correspondingly, 0.3 NiMo catalyst exhibits lower selectivity to oxygenates than

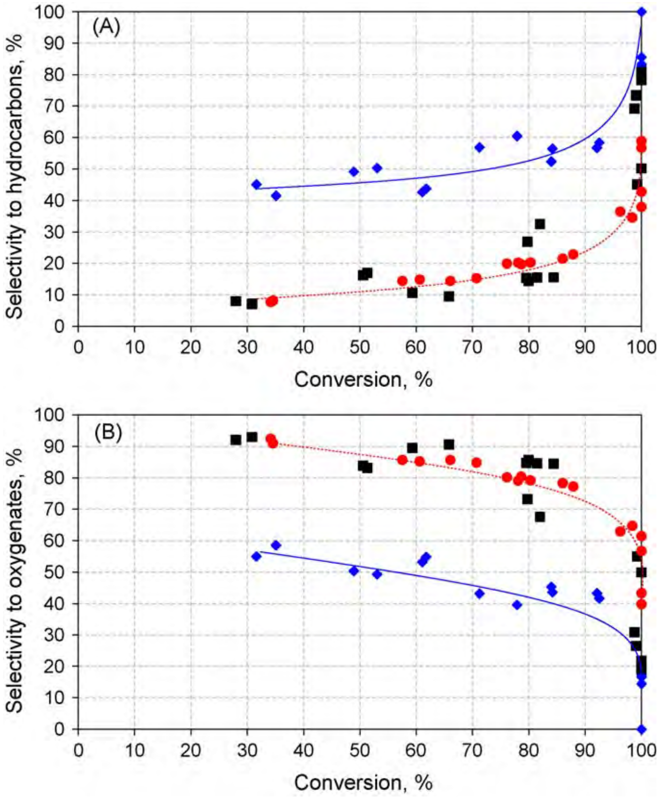

Fig. 4. Selectivity to the main product types – hydrocarbons (A) and oxygenates (B) – as a function of conversion for NiMo (◆ – Ni/(Ni + Mo) = 0.3); Mo (■) and Ni (●) catalysts; *T* = 260–280 °C, *p* = 3.5 MPa, *V*/*F* = 0.25–4 h.

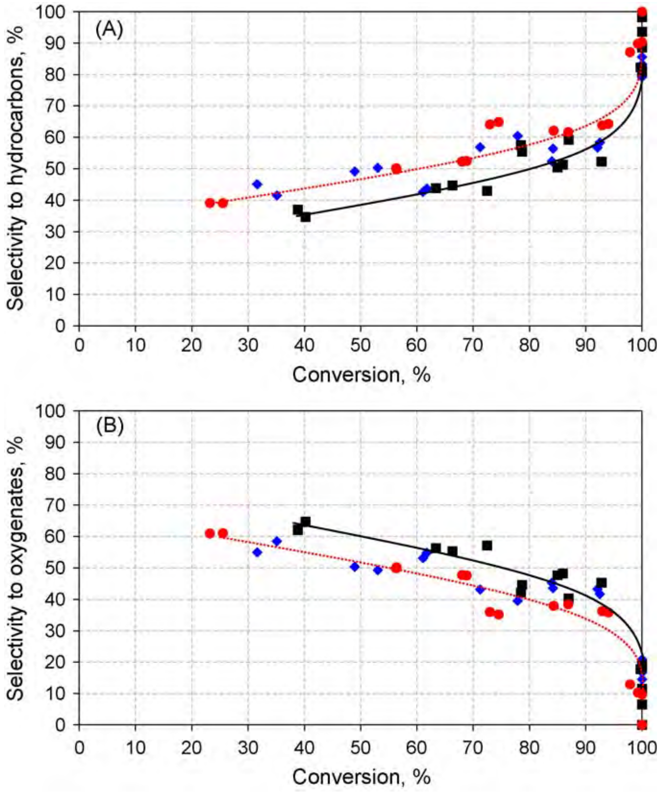

Fig. 5. Selectivity to the main product types – hydrocarbons (A) and oxygenates (B) – as a function of conversion for NiMo catalysts with different Ni/(Ni + Mo) atomic ratio (■ – Ni/(Ni + Mo) = 0.2; ◆ – Ni/(Ni + Mo) = 0.3; ● – Ni/(Ni + Mo) = 0.4); T = 260–280 °C, p = 3.5 MPa, V/F = 0.25–1 h.

the monometallic catalysts (Ni, Mo). It can be thus inferred that the overall deoxygenation activity of the NiMo catalysts is larger than that of monometallic catalysts, *i.e.* that at a given conversion of triglycerides the oxygenated intermediates are converted faster into the ultimate reaction products (hydrocarbons) over the 0.3NiMo/Al_2O_3 catalyst than over Ni/Al_2O_3 and Mo/Al_2O_3. Interestingly, the selectivities to hydrocarbons are virtually the same for Ni and Mo catalysts over the whole range of triglyceride conversions (Fig. 4) even though the Mo catalyst gave higher conversion of triglycerides than Ni catalyst under comparable reaction conditions (Fig. 1) and thus seemed to have a higher deoxygenation activity. The same holds also for the selectivities to oxygenates over these catalysts. These results further support the suggestion that there is a synergetic effect between the NiS and MoS_2 phase.

A comparison of the three NiMo catalysts with different Ni/(Ni + Mo) atomic ratio is shown on Fig. 5. The differences in selectivities among the catalysts are just minor. Nevertheless, a careful inspection of the data reveals that the catalyst with the lowest Ni concentration, *i.e.* 0.2NiMo (Ni/(Ni + Mo) = 0.2) gives slightly lower selectivity to hydrocarbons and consequently slightly higher selectivity to oxygenates than the other two NiMo catalysts at comparable conversions. It suggests that the promoting effect of Ni in the 0.2NiMo catalyst is lower than in the other two catalysts and that the Mo character of the catalysts begins to prevail. However, the deoxygenation activity of the 0.2NiMo catalysts is still much closer to that of the other two NiMo catalysts than to that of monometallic Mo catalyst (Figs. 4 and 5).

3.4. Product distribution of oxygenates

A deeper understanding of the deoxygenation of triglycerides can be obtained from a detailed analysis of the both main product groups, *i.e.* from selectivities to different types of oxygenates and hydrocarbons. The oxygenated products and intermediates consist of three main types of products – fatty acids (almost exclusively stearic and palmitic acids), fatty alcohols (almost exclusively *n*-octadecanol and *n*-hexadecanol) and their fatty esters, *i.e.* the esters that are formed by the reaction of fatty acids with fatty alcohols that are both reaction intermediates in deoxygenation of triglycerides. The other plausible reaction intermediates – fatty aldehydes – were not found among reaction products most probably due to their high reactivity.

The selectivity curves of the three main classes of oxygenated products confirm that fatty acids and fatty alcohols are formed prior to the formation of fatty esters (Fig. 6). A striking difference can be seen between catalysts containing Mo, *i.e.* Mo/Al_2O_3 and NiMo/Al_2O_3, on the one hand, and those without any Mo, *i.e.* Ni/Al_2O_3 (Fig. 6), on the other hand. There are virtually no alcohols formed over the Ni catalyst and, consequently, fatty esters cannot

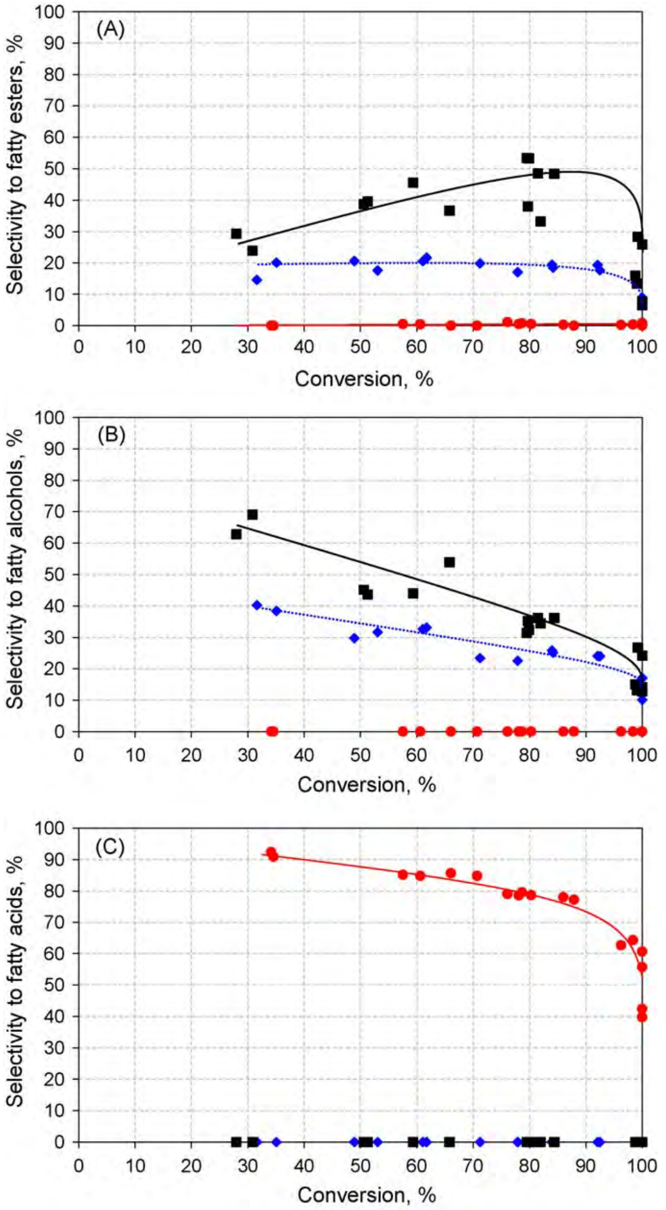

Fig. 6. Selectivity to different types of oxygenated products – fatty esters (A), fatty alcohols (B) and fatty acids (C) as a function of conversion of triglycerides for NiMo (◆ – Ni/(Ni + Mo) = 0.3); Mo (■) and Ni (●) catalysts; T = 260–280 °C, p = 3.5 MPa, V/F = 0.25–4 h.

be formed either (Fig. 6). Subsequently, the only oxygenates formed over Ni/Al_2O_3 are fatty acids. In contrast, high selectivities to fatty esters and fatty alcohols are obtained when deoxygenation is catalyzed by Mo/Al_2O_3 or NiMo catalysts. The absence of fatty acids, which have to be formed prior to the formation of fatty alcohols and fatty esters, in the reaction products over the Mo containing catalysts is due to their subsequent reaction with fatty alcohols to form fatty esters. It can be inferred that esterification is, under the experimental conditions over Mo containing catalysts, faster then the formation of fatty acids from triglycerides and fatty acids are thus not detected in the reaction products. Moreover, esterification competes with the final deoxygenation step, *i.e.* with deoxygenation of fatty alcohols. In accordance with the higher selectivity to oxygenates over Mo/Al_2O_3 in comparison with $0.3NiMo/Al_2O_3$ (Fig. 4), the selectivity to fatty esters and fatty alcohols is significantly higher over the Mo/Al_2O_3 catalyst (Fig. 6).

These results indicate that there is a major difference between Ni and Mo catalysts. While the oxygenates obtained over Mo catalyst correspond to the sequence of stepwise reduction, *i.e.* of fatty acids to fatty alcohols, this step is completely missing over the monometallic Ni catalyst. It can be explained either by insufficient hydrogenation activity of the Ni catalyst or by the involvement of a competing reaction pathway. The overall hydrocarbons and oxygenates selectivities (Fig. 4) strongly suggest that fatty acids are converted directly into hydrocarbons by decarboxylation, *i.e.* there is a different prevailing deoxygenation pathway for monometallic Ni catalyst (decarboxylation) than for monometallic Mo catalyst (hydrodeoxygenation), as will shown by the hydrocarbon products distribution which is discussed below. This difference can be attributed, most probably, to differences in electronic properties of these catalysts.

The differences among the three NiMo catalysts with different Ni/(Ni + Mo) atomic ratio are not very significant (Fig. 7). Free fatty acids were not found in the products of any of these three catalysts. The main products were fatty esters and fatty alcohols. In agreement with the overall selectivity to oxygenates (Fig. 5), the selectivity to fatty esters is slightly higher over 0.2NiMo catalyst than over the other two NiMo catalysts. The selectivities to fatty alcohols are virtually identical for all three NiMo catalysts (Fig. 7). It can be thus concluded that the 0.2NiMo catalyst, *i.e.* the catalyst with lowest Ni concentration, shows more prominently its Mo character than the other two NiMo catalysts. However, the difference in the selectivity to fatty esters between the monometallic Mo catalyst and 0.3NiMo catalyst is more pronounced than the difference in the selectivity to fatty alcohols for these two catalysts (Fig. 6). Therefore, the slightly lower promoter efficiency of the 0.2NiMo catalyst in comparison with the other two NiMo catalysts can be seen only in the selectivity to fatty esters and not in the selectivity to fatty alcohols.

3.5. Product distribution of liquid-phase hydrocarbons

The selectivities to *n*-heptadecane and *n*-octadecane were calculated based on the total yield of liquid-phase hydrocarbons, *i.e.* the sum of selectivities to individual hydrocarbons is 100% and the sum of selectivities to *n*-heptadecane and *n*-octadecane is >90%, which is the consequence of the rapeseed oil composition and of the absence of cracking reactions. These selectivities provide valuable information about the final reaction step in deoxygenation of triglycerides. The striking difference in the product distribution observed for the oxygenated products is reflected in the distribution of hydrocarbons as well (Fig. 8). The selectivities to the two major hydrocarbons formed, *i.e.* *n*-heptadecane and *n*-octadecane, are in this case plotted as a function of the total yield of hydrocarbons to achieve better visualization. The other hydrocarbons, mainly *n*-pentadecane and *n*-hexadecane, were formed in quantities corresponding to the concentrations of respective fatty acids bound in triglycerides. As their concentrations are low and the trends are the same as those determined for *n*-octadecane and *n*-heptadecane, the discussion will focus, for the sake of clarity, only on these two major hydrocarbons. Furthermore, *n*-heptadecane and *n*-octadecane can be used as indicators of the decarboxylation and hydrodeoxygenation pathways, respectively.

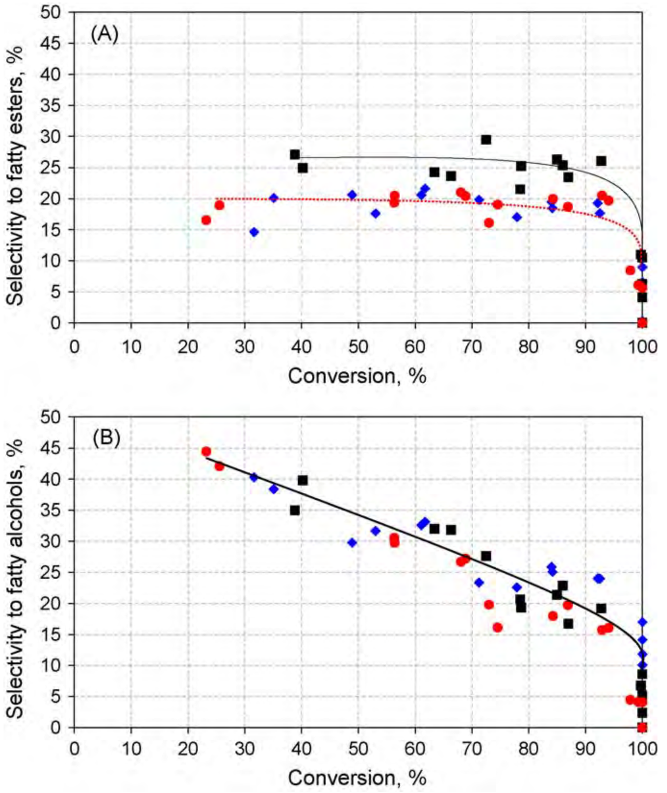

Fig. 7. Selectivity to different types of oxygenated products – fatty esters (A) and fatty alcohols (B) as a function of conversion of triglycerides for NiMo catalysts with different Ni/(Ni + Mo) atomic ratio (■ – Ni/(Ni + Mo) = 0.2; ◆ – Ni/(Ni + Mo) = 0.3; ● – Ni/(Ni + Mo) = 0.4); T = 260–280 °C, p = 3.5 MPa, V/F = 0.25–1 h. Only traces of fatty acids have been found in the products.

The inspection of Fig. 8 reveals that *n*-heptadecane is formed selectively over Ni/Al_2O_3 while *n*-octadecane is formed almost exclusively over Mo/Al_2O_3. The 0.3NiMo catalyst yields both hydrocarbons with *n*-octadecane being the favoured hydrocarbon product with selectivity in the range 50–70%. The complete selectivity to *n*-heptadecane over the Ni/Al_2O_3 catalyst is the result of fatty acids decarboxylation as fatty acids were the virtually exclusive oxygenates (Fig. 6). It can be thus concluded that over Ni/Al_2O_3 the deoxygenation is achieved by decarboxylation of fatty acids that are formed from triglycerides. Furthermore, it can be inferred that the decarboxylation step over Ni catalyst is significantly faster than the hydrogenation step as neither fatty alcohols nor *n*-octadecane were found in the reaction products. On the other hand, there is virtually no *n*-heptadecane formed over the Mo catalysts, which means that hydrogenation is significantly faster than decarboxylation over Mo catalyst. These results suggest that both metals are very specific either in promoting decarboxylation or in favouring a sequence of hydrogenation steps of hydrodeoxygenation. This difference can be attributed to the inherently different electronic properties of the Ni and Mo sulfided phases. The behaviour of the 0.3NiMo catalysts reflects this specificity and the final hydrocarbon products contained both *n*-heptadecane and *n*-octadecane. Since Ni is a promoter and is

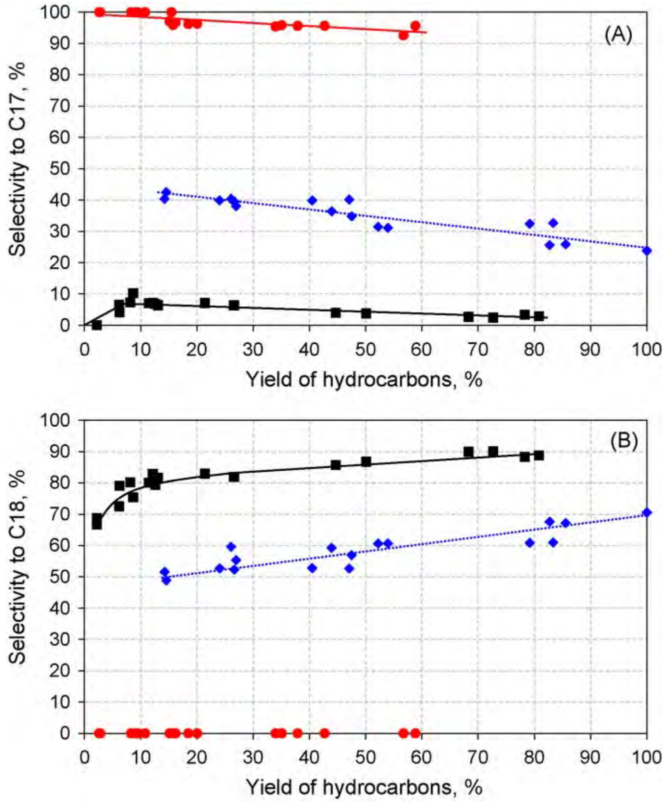

Fig. 8. Selectivity within the hydrocarbon products group to main hydrocarbons – *n*-heptadecane (A) and *n*-octadecane (B) as a function of total yield of hydrocarbons for NiMo (◆ – Ni/(Ni + Mo) = 0.3); Mo (■) and Ni (●) catalysts; T = 260–280 °C, p = 3.5 MPa, V/F = 0.25–4 h.

present in a lower concentration than Mo, *n*-octadecane is the main hydrocarbon formed over 0.3NiMo catalyst (Fig. 8).

Similar selectivities to hydrodecarboxylation products, to those shown here for the sulfided monometallic Ni catalyst, were previously reported also on various Pd/C catalysts under similar reaction temperatures (260–300 °C) and lower H_2 partial pressures [17–20] using stearic acid as a probe molecule. However, a Pd/C catalyst was also shown to yield *n*-pentadecane from stearic acid with high selectivity [21]. Decarboxylation has been recently shown to be the preferred reaction pathway for deoxygenation of methylstearate over Pt/Al_2O_3 catalyst at 325 °C [22]. On the contrary, bimetallic catalysts containing MoS_2 phase yield, in addition to decarboxylation products, also hydrodeoxygenation products [12,13,15], *e.g.* *n*-octadecane as discussed above, that were not observed over Pd/C or Pt/Al_2O_3 catalysts.

A mixture of *n*-heptadecane and *n*-octadecane was obtained over all three NiMo catalysts. Once again the lower promoting effect of Ni in the 0.2NiMo catalyst is reflected by the slightly higher selectivity to *n*-octadecane which is achieved at the expense of the selectivity to *n*-heptadecane (Fig. 9). The selectivity to *n*-octadecane increases with increasing conversion from the initial value of about 50% to ca 70% (Fig. 9). This peculiar behaviour can be explained by the fact that with increasing conversion, hydrocarbons are formed from oxygenated intermediates (fatty acids, alcohols and esters) rather than from triglycerides. Deoxygenation of *n*-octadecanol yields selectively *n*-octadecane (it cannot undergo decarboxylation) while deoxygenation of stearic acid yields over NiMo catalysts both *n*-heptadecane, *i.e.* a hydrodecarboxylation (HDC) product and *n*-octadecane, *i.e.* a hydrodeoxygenation (HDO) product, in ratios that are affected by reaction temperature and pressure [3]. As fatty esters are products of reaction between fatty acids and fatty alcohols, they are bound to give over NiMo catalysts higher yields of HDO products than triglycerides or fatty acids and hence the selectivity to *n*-octadecane increases with increasing yield of hydrocarbons.

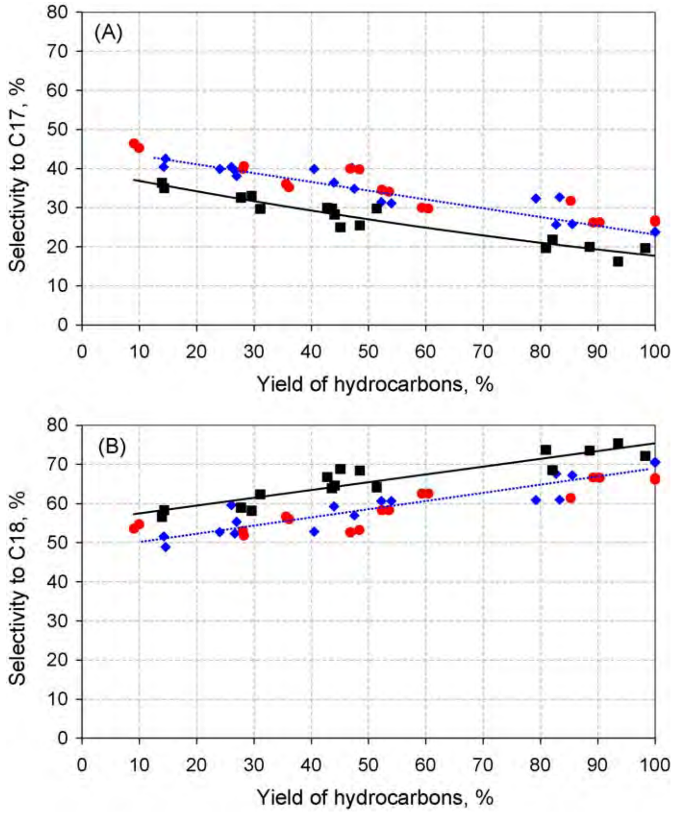

Fig. 9. Selectivity within the hydrocarbon products group to main hydrocarbons – *n*-heptadecane (A) and *n*-octadecane (B) as a function of total yield of hydrocarbons for for NiMo catalysts with different Ni/(Ni + Mo) atomic ratio (■ – Ni/(Ni + Mo) = 0.2; ◆ – Ni/(Ni + Mo) = 0.3; ● – Ni/(Ni + Mo) = 0.4); T = 260–280 °C, p = 3.5 MPa, V/F = 0.25–1 h.

3.6. *Gas-phase product distribution*

The gas-phase products consisted of propane, CO, CO_2 and methane. Other gaseous products were present only in negligible concentrations. The concentration of the main gaseous products was usually lower than 1 mol% as the reaction was carried out in a large excess of hydrogen (the molar ratio of hydrogen-to-rapeseed oil was equal to 50). Due to the low concentration of products in the gaseous phase as well as the off-line analysis, which was performed once per an experimental condition, the results have mainly supporting character. As the composition of the gaseous products suggest, they reflect the decarboxylation performance of the catalyst and the overall conversion of triglycerides. It can be clearly seen from the data collected in Fig. 10 for Ni/Al_2O_3, Mo/Al_2O_3 and $0.3NiMo/Al_2O_3$ that highest concentrations of carbon oxides, *i.e.* decarboxylation products, were observed for Ni/Al_2O_3. On the contrary, the lowest concentration of decarboxylation products was found over Mo/Al_2O_3. These findings are in line with the conclusions resulting from the analysis of organic liquid products (see above) – the Ni catalyst exhibits the highest decarboxylation selectivity from the investigated catalysts while the Mo catalyst shows the lowest decarboxylation selectivity. Furthermore, propane concentration is a partial indicator of triglyceride conversion and it increases with increasing triglyceride conversion. It has to be kept in mind, however, that due to the stepwise elimination of fatty acid chains from a triglyceride

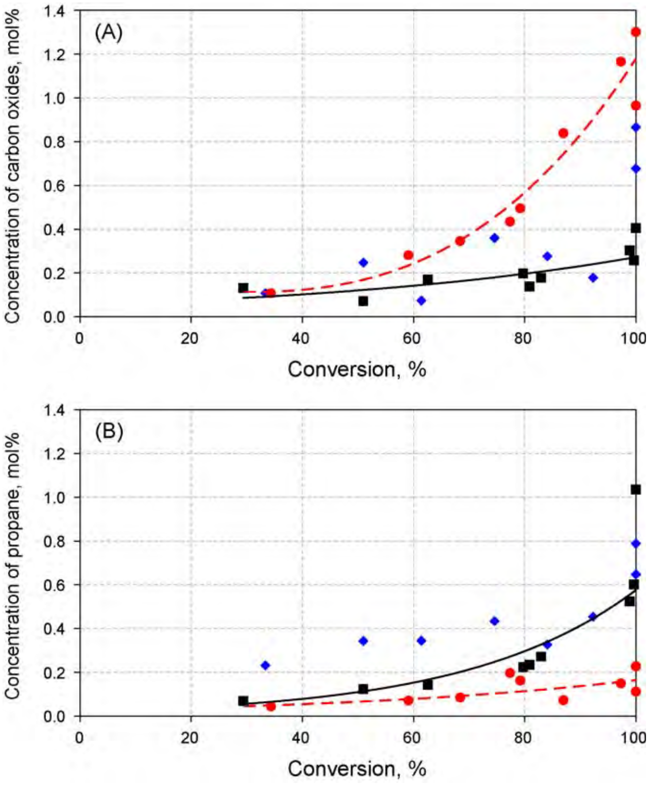

Fig. 10. Concentrations of main gaseous products at reactor outlet in hydrogen – carbon oxides (A) and propane (B) as a function of conversion of triglycerides for NiMo (◆ – Ni/(Ni + Mo) = 0.3); Mo (■) and Ni (●) catalysts; T = 260–280 °C, p = 3.5 MPa, V/F = 0.25–4 h.

molecule, propane can be released only when all three fatty acid chains had been cleaved off, *i.e.* even at complete conversion of triglycerides propane can be still bound in some reaction intermediates. In fact, GC–MS analysis of reaction products has revealed that propylstearate (propyl octadecanoate) is a reaction intermediate in deoxygenation of rapeseed oil, the other plausible intermediates being diglycerides and monoglycerides identified mainly over deactivated catalysts and 1,2- or 1,3-propanediyl dioctanedecanoate (not yet confirmed experimentally). The concentration of propane also indicates higher efficiency of 0.3NiMo in hydrocarbon formation as compared with the monometallic catalysts since it is higher over 0.3NiMo than over the monometallic catalysts (Fig. 10), particularly in the region of low conversions (40–80%). Nevertheless, due to the abovementioned limitations of the analysis of gas-phase products the results should be used only as further evidence supporting the conclusions based on the analysis of organic liquid products.

3.7. Deoxygenation pathways

The experimental data collected over three sulfided catalysts, namely Ni/Al_2O_3, Mo/Al_2O_3 and $0.3NiMo/Al_2O_3$ are very helpful in shedding light on the reaction pathways involved in transformation of triglycerides into hydrocarbons. Moreover, the results also imply possible strategies for further development of deoxygenation of triglycerides with respect to hydrogen consumption, which is an important issue for the petroleum refinery point of view.

The discussed results provide additional experimental evidence for the reaction scheme of triglyceride deoxygenation proposed previously without experimental support [3]. The scheme is schematically depicted in Fig. 11. The double bonds in triglycerides, the main components of vegetable oils, are at first saturated. Then they are converted into fatty acids that can either (i) undergo further hydrogenation steps to yield fatty alcohols and ultimately saturated *n*-alkanes with an even carbon atoms number (hydrodeoxygenation) or (ii) undergo decarboxylation to yield hydrocarbons directly, *i.e.* hydrocarbons with an odd number of carbon atoms (hydrodecarboxylation). Hydrodeoxygenation (HDO) leads to elimination of water from triglycerides, fatty acids, fatty alcohols and fatty esters as a result of reaction with hydrogen. It has been proposed that this reaction occurs via adsorbed enol intermediate [12]. Hydrodecarboxylation (HDC) consists of decarboxylation (CO_2 elimination) of compounds containing carboxylic functional group and hydrogenation of the unsaturated intermediates of CO_2 elimination. CO_2 is a primary product of this reaction and it may undergo further reactions, particularly hydrogenation, which is undesired since it causes significant increase in hydrogen consumption. Consequently, there are numerous efforts to achieve selective decarboxylation without CO_2 hydrogenation [19–21].

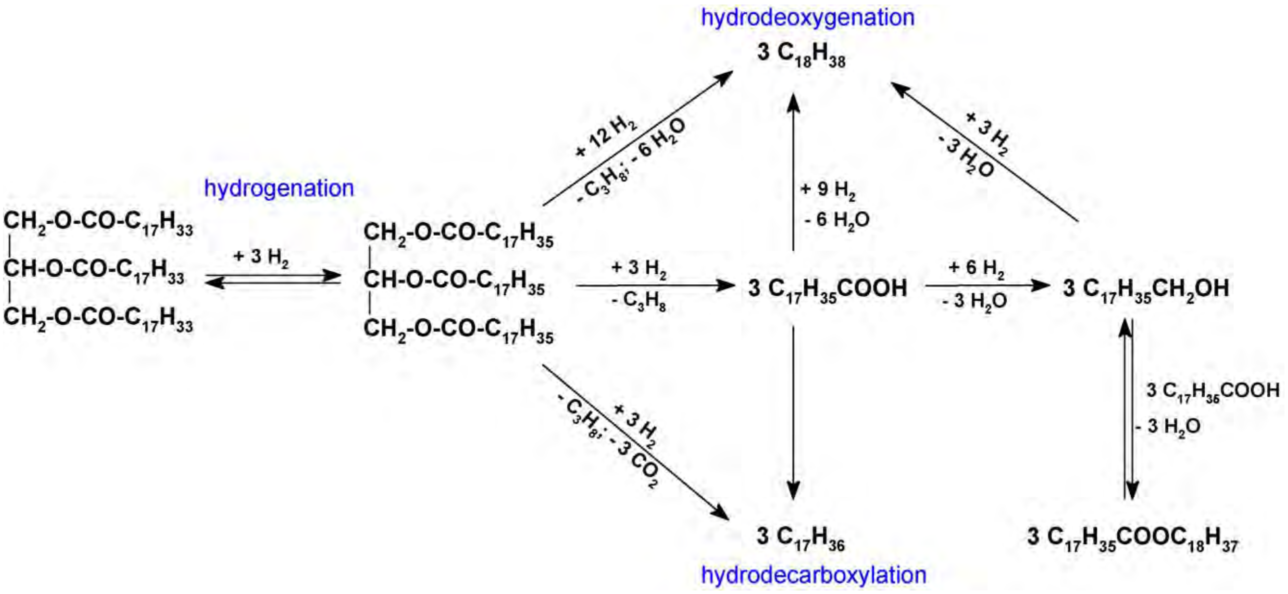

Fig. 11. The reaction pathways involved in conversion of triglycerides into hydrocarbons.

The simultaneous presence of both fatty acids and alcohols leads to formation of fatty esters thanks to esterification of fatty acids with fatty alcohols. These esters are, nevertheless, subsequently converted into hydrocarbons. There are two possible initial steps of triglycerides conversion: (i) hydrolysis yielding fatty acids and glycerol or (ii) hydrogenolysis yielding fatty acids and propane. Since neither the feed contains water nor the conversion of triglycerides increases with due to deoxygenation increasing concentration of water in the product mixture, it is plausible to assume that the reaction is initiated by hydrogenolysis of the C–O bond between the fatty acid chain and the propane (glycerol) backbone of triglycerides.

The decarboxylation pathway seems to be more interesting from the industrial point of view since it requires less hydrogen. However, it has to be kept in mind that under the reaction conditions of deoxygenation the hydrotreating catalysts are active also in CO_2 hydrogenation. Should CO_2 be completely reduced to methane, the consumption of hydrogen would be even higher than in the case of hydrodeoxygenation.

The significant differences in reaction pathway and consequently in the product distribution between monometallic Ni catalyst, on the one hand, and monometallic Mo catalyst on the other hand require further studies to explain them. It can be proposed they originate from differences in electronic properties of NiS and MoS_2 [31–33] that might lead to different adsorption of triglycerides and fatty acids on the surface of different sulfides and consequently to either reaction of adsorbed hydrogen with oxygen atoms (HDO) or cleavage of carbon–carbon bond at the carboxylic group resulting in elimination of CO_2 (HDC).

4. Conclusions

Reaction pathways in deoxygenation of rapeseed oil were investigated over sulfided Ni/Al_2O_3, Mo/Al_2O_3, and a series of $NiMo/Al_2O_3$ with atomic ratio of Ni/(Ni + Mo) in the range 0.2–0.4. The catalysts were prepared by impregnation of commercial Al_2O_3 support having specific surface area equal to 344 m^2/g. Its textural properties were not significantly affected by the impregnation process. The experiments were carried out in a fixed-bed reactor at 260–280 °C, 3.5 MPa and 0.25–4 h^{-1} and the conversion of triglycerides was hence varied in the range of 30–100%.

The activity of the catalysts decreased in the order $NiMo/Al_2O_3 > Mo/Al_2O_3 > Ni/Al_2O_3$ showing hence the synergy between Ni and Mo. The rate of disappearance of triglycerides was larger, at least by almost 40%, than the rate of oxygen disappearance for all investigated catalysts, which indicated that oxygenated intermediates were formed. Moreover, the difference between the rates of triglycerides and oxygen disappearance increased in the order $NiMo/Al_2O_3 < Mo/Al_2O_3 \ll Ni/Al_2O_3$ demonstrating thus the lowest overall deoxygenation efficiency of Ni/Al_2O_3 and suggesting that a different reaction pathway as compared with Mo and NiMo catalysts plays an important role.

Organic-liquid-phase analysis provided evidence of the differences in reaction pathways over the studied catalysts. Ni/Al_2O_3 was found to catalyze selectively decarboxylation of fatty acids that are reaction intermediates of triglycerides deoxygenation. There were not found any products of hydrogenation of fatty acids, *i.e.* fatty alcohols or hydrocarbons with an even number of carbon atoms. Over Mo/Al_2O_3, on the other hand, there were only minor concentrations of decarboxylation products and consequently the hydrogenation (hydrodeoxygenation) pathway was nearly the exclusive one. $NiMo/Al_2O_3$ catalysts yielded both hydrogenation and decarboxylation products. The molar ratio of hydrodeoxygenation and decarboxylation products was in the range 1–3.5 and it increased with increasing conversion. The increase was caused by formation of fatty esters, *i.e.* intermediates formed by esterification of fatty acids with fatty alcohols, which were formed at lower conversions of triglycerides and were transformed into hydrocarbons at higher conversion levels. The reason is that while the fatty acid part of such ester may yield decarboxylation as well as hydrodeoxygenation products, the fatty alcohol part of the ester yields only hydrodeoxygenation products.

Acknowledgements

The financial support by the Ministry of Industry and Trade of the Czech Republic (project FT-TA3/074) is gratefully acknowledged. The authors thank to Mr. Josef Chudoba (Institute of Chemical Technology Prague) for the GC/MS analyses of deoxygenation products.

References

[1] G.W. Huber, S. Iborra, A. Corma, Chem. Rev. 106 (2006) 4044–4098.
[2] G.W. Huber, A. Corma, Angew. Chem. Int. Ed. 46 (2007) 7184–7201.
[3] D. Kubička, Collect. Czech. Chem. Commun. 73 (2008) 1015–1044.
[4] D. Kubička, P. Šimáček, N. Žilková, Top. Catal. 52 (2009) 161–168.
[5] A.R. Pinho, M. Silva, A.P. Silva Neto, J.A.R. Cabral, Catalytic cracking process for the production of diesel from vegetable oils, United States Patent, US 7,540,952 B2, 2009.
[6] J.A. Petri, T.L. Marker, Production of diesel fuel from biorenewable feedstocks, United States Patent, US 7,511,181 B2, 2009.
[7] D.Y. Murzin, I. Kubičková, M. Snåre, P. Mäki-Arvela, J. Myllyoja, Method for the manufacture of hydrocarbons. United States Patent, US 7,491,858 B2, 2009.
[8] D.Y. Murzin, I. Kubičková, M. Snåre, P. Mäki-Arvela, J. Myllyoja, Method for the manufacture of hydrocarbons. PCT International Application WO 2006/075057 A2, 2006.
[9] J. Jakkula, V. Niemi, J. Nikkonen, V.-M. Purola, J. Myllyoja, P. Aalto, J. Lehtonen, V. Alopaeus, Process for producing hydrocarbon component of biological origin, United States Patent, US 7,232,935, 2007.
[10] J. Holmgren, C. Gosling, K. Couch, T. Kalnes, T. Marker, M. McCall, R. Marinangeli, Petrol. Technol. Quart. 3 (2007) 119–125.
[11] J. Holmgren, C. Gosling, R. Marinangeli, T. Marker, G. Faraci, C. Perego, Hydrocarbon Process. 9 (2007) 67–71.
[12] B. Donnis, R.G. Egeberg, P. Blom, K.G. Knudsen, Top. Catal. 52 (2009) 229–240.
[13] E. Laurent, B. Delmon, Appl. Catal. 109 (1994) 77–96.
[14] E. Laurent, B. Delmon, Appl. Catal. 109 (1994) 97–115.
[15] P. Šimáček, D. Kubička, G. Šebor, M. Pospíšil, Fuel 88 (2009) 456–460.
[16] Q. Smejkal, L. Smejkalová, D. Kubička, Chem. Eng. J. 146 (2009) 155–160.
[17] I. Kubičková, M. Snåre, K. Eränen, P. Mäki-Arvela, D.Y. Murzin, Catal. Today 106 (2005) 197–200.
[18] M. Snåre, I. Kubičková, P. Mäki-Arvela, K. Eränen, D.Y. Murzin, Ind. Eng. Chem. Res. 45 (2006) 5708–5715.
[19] I. Simakova, O. Simakova, P. Mäki-Arvela, A. Simakov, M. Estrada, D.Y. Murzin, Appl. Catal. A: Gen. 355 (2009) 100–108.
[20] M. Snåre, I. Kubičková, P. Mäki-Arvela, D. Chichova, K. Eränen, D.Y. Murzin, Fuel 87 (2008) 933–945.
[21] S. Lestari, I. Simakova, A. Tokarev, P. Mäki-Arvela, K. Eränen, D.Y. Murzin, Catal. Lett. 122 (2008) 247–251.
[22] P.T. Do, M. Chiappero, L.L. Lobban, D.E. Resasco, Catal. Lett. 130 (2009) 9–18.
[23] G.W. Huber, P. O'Connor, A. Corma, Appl. Catal. A: Gen. 329 (2007) 120–129.
[24] P. Šimáček, D. Kubička, G. Šebor, M. Pospíšil, Fuel, in press, doi:10.1016/j.fuel.2009.09.017.
[25] P. Šimáček, D. Kubička, Fuel, in press, doi:10.1016/j.fuel.2009.09.029
[26] T.-R. Viljava, E.R.M. Saari, A.O.I. Krause, Appl. Catal. A: Gen. 209 (2001) 33–43.
[27] E. Furimsky, Appl. Catal. A: Gen. 199 (2000) 147–190.
[28] H. Topsoe, B.S. Clausen, F.E. Massoth, Hydrotreating Catalysis, Springer-Verlag, 1996,, p. 164.
[29] L. Kaluža, D. Gulková, Z. Vít, M. Zdražil, Appl. Catal. A: Gen. 324 (2007) 30–35.
[30] W.K. Craig, D.W. Soveran, Production of hydrocarbons with relatively high cetane rating, United States Patent, US 4,992,605, 1991.
[31] D.S. Thakur, B. Delmon, J. Catal. 91 (1985) 308–317.
[32] D.S. Thakur, P. Grange, B. Delmon, J. Catal. 91 (1985) 318–326.
[33] I.I. Zakharov, A.N. Startsev, G.M. Zhidomirov, J. Mol. Catal. A: Chem. 119 (1997) 437–447.

Applied Catalysis A: General 397 (2011) 127–137

Contents lists available at ScienceDirect

Applied Catalysis A: General

journal homepage: www.elsevier.com/locate/apcata

The role of Ni species in the deoxygenation of rapeseed oil over NiMo-alumina catalysts

Peter Priecel[a], David Kubička[b,*], Libor Čapek[a], Zdeněk Bastl[c], Petr Ryšánek[b]

[a] Department of Physical Chemistry, Faculty of Chemical Technology, University of Pardubice, Studentská 573, 532 10 Pardubice, Czech Republic
[b] Department of Refinery and Petrochemical Research, Research Institute of Inorganic Chemistry, Záluží 1, 436 70 Litvínov, Czech Republic
[c] J. Heyrovský Institute of Physical Chemistry, Academy of Sciences of the Czech Republic, 18223 Prague, Czech Republic

ARTICLE INFO

Article history:
Received 20 September 2010
Received in revised form 15 February 2011
Accepted 19 February 2011
Available online 24 February 2011

Keywords:
Deoxygenation
NiMo-alumina
UV–vis
XRD
XPS
Ni species
Temperature pretreatment
Hydrotreating

ABSTRACT

The deoxygenation of rapeseed oil has been studied over sulfided NiMo-alumina catalysts (NiMoS-alumina). The main focus has been on the preparation of catalyst precursors (oxide form of sulfided NiMo-alumina catalysts – NiMoO-alumina) with a different distribution of Ni species in order to contribute to the understanding of the effect of catalyst preparation on the activity/selectivity of NiMoS-alumina catalysts in the deoxygenation of rapeseed oil. To analyze the state of Ni species the NiMoO-alumina catalysts have been characterized by UV–vis diffuse reflectance spectrometry (DRS), X-ray diffraction (XRD) and XPS. It has been found out that the NiMoO-alumina catalysts with higher population of octahedral nickel species resulted in more active NiMoS-alumina catalysts than those containing higher population of tetrahedral nickel species.

1. Introduction

Nowadays, liquid biofuels are becoming more and more important, mainly because of their application as transportation fuels. Many countries worldwide have been increasing the amount of biofuels blended with regular petroleum-derived fuels in an attempt to decrease the greenhouse gases emissions. Two types of biofuels, namely biodiesel and so called green or renewable diesel, are being produced as alternatives to the conventional diesel fuel [1]. Biodiesel as fatty acids methyl esters (FAME) is produced by transesterification of triglycerides with methanol, while renewable diesel is produced by hydrotreating of vegetable oils. The latter alternative has several advantages over the biodiesel made by transesterification – its production can be implemented in the present refineries and the products are straight-chain alkanes consisting of 15–20 carbons, which after isomerization are much alike the hydrocarbons found in conventional diesel. The conventional catalysts employed in deoxygenation are sulfided forms of Mo or W supported on alumina, promoted with Ni or Co. These catalysts have been used for many decades as hydrodesulfurization catalysts for sulfur removal from crude oil streams.

Many effects, such as type of the support, preparation procedure and additives (phosphorus, potassium or fluorine) [2–6], sulfur species [7–12], water [13,14] or other reaction variables, i.e. temperature, pressure and type of the catalyst [15–19] have been studied for deoxygenation of various oxygenated compounds, such as rapeseed oil [17–19], various esters and fatty acids [2,3,7–9,11,13,20] or aromatic and cyclic oxygenates [2–8,10,12,21,22]. Upgrading of triglycerides and related feedstocks has been recently reviewed by several authors [1,23,24].

The identification of active sites or their precursors is much desired information in heterogeneous catalytic reactions. This approach is a matter of discussion in many reactions, but a complex analysis of active sites is very challenging. Due to the complexity of hydrotreating catalysts, there is a lack of information about the nature of active sites in the deoxygenation of rapeseed oil over NiMoS-alumina catalysts. The activity and selectivity of hydrotreating catalysts in the deoxygenation of vegetable oils can be expected to be affected by (i) *total amount, distribution and crystallite size of Ni and Mo species*, (ii) *nature and specific surface area of the support* and (iii) *Ni and Mo precursors and their impregnation order*.

---

* Corresponding author. Tel.: +420 47616 3735.
E-mail addresses: david.kubicka@vuanch.cz (D. Kubička), libor.capek@upce.cz (L. Čapek).

0926-860X/$ – see front matter © 2011 Elsevier B.V. All rights reserved.
doi:10.1016/j.apcata.2011.02.022

Table 1
The list of prepared NiMoO-alumina catalysts and their properties.

Catalyst[a]	Ni-alumina	Mo-alumina	NiO450	NiO800	NiMoO450	NiMoO600	NiMoO800
Ni calcination temp., °C	600	–	450	800	450	600	800
Mo calcination temp., °C	–	600	–	–	600	600	600
Ni, % – XRF	3.1	–	11.2	11.4	3.0	3.0	2.8
Ni, % – XPS[b]	–	–	–	–	3.6 (O), 2.7 (S)	–	1.8 (O), 1.7 (S)
Mo, % – XRF	–	6.0	–	–	5.7	5.8	6.4
Mo, % – XPS[b]	–	–	–	–	7.9 (O), 6.8 (S)	–	10.7 (O), 10.7 (S)
Impregnation order	–	–	–	–	Mo, Ni	Mo, Ni	Ni, Mo
Catalyst color	Azure blue	White	Blue gray	Azure blue	Light green	Light green blue	Light blue
S(BET), $m^2 g^{-1}$	–	–	–	–	129	153	137
d (37.6°), nm	–	–	1.72	3.28	3.34	4.85	5.70

[a] The catalysts are denoted NiMoX where X is either S or O; S – sulfide form of the catalyst, O – oxide form of the catalyst.

[b] The metal concentrations calculated from XP spectra in oxide (O) and sulfide (S) catalysts forms are surface concentrations, while the concentrations by XRF are bulk concentrations.

Several authors have investigated the influence of the impregnation order of hydrotreating catalysts on their catalytic activity in hydrotreating reactions, either as NiMoS on alumina [25], on Al-pillared clays [26], on AlMCM-41 [27] or as CoMoS on activated carbon [3]. The results of these studies are rather inconclusive. Nonetheless, impregnation with the promoter (Ni, Co) prior to impregnation with Mo yields typically a more active catalyst.

The distribution of Ni sites and their structure can be affected by catalyst pretreatment temperature. It has been studied with respect to catalyst characterization using TPR [28], electron spectroscopy [29], XRD [29], Raman spectroscopy [30], UV–vis DRS [30], XPS [30] and HRTEM [30] and also with respect to its catalytic activity in various chemical reactions, such as thiophene hydrodesulfurization [31–34], acrylonitrile hydrogenation [35] or oxidative dehydrogenation of ethane [36].

In this manuscript the attention is aimed at identification of the structure of Ni species in the precursors of hydrotreating catalysts (i.e. as-prepared NiMoO-alumina catalysts) that can be transformed by sulfidation into highly active hydrotreating catalysts for deoxygenation reactions (NiMoS-alumina catalysts). In order to investigate solely the effect of Ni species, NiMoO-alumina catalysts with the different distribution of Ni species and constant distribution of Mo species were prepared. The change in the distribution of Ni species was achieved by varying the pretreatment temperature as reported previously [28–38]. The NiMoO-alumina catalysts were characterized with respect to the amount of metal species deposited on the support (XRF), the structure of the catalysts (XRD), coordination states of metal species (diffuse reflectance UV–vis), homogeneity of metals surface distribution (SEM-EDX), the specific surface area of catalysts (N_2-adsorption) and surface composition and coordination of the NiMoO phase (XPS). In addition, fresh NiMoS-alumina catalysts were characterized by XPS as well in order to describe any changes in the catalyst structure (NiMo coordination) resulting from the sulfidation procedure.

2. Experimental

2.1. Preparation of catalysts

γ-Alumina, supplied by Eurosupport Manufacturing Czechia, was used as a support for NiMo-based deoxygenation catalysts. Table 1 shows notation of Ni- and NiMoO-alumina catalysts, concentration of Ni and Mo, the pretreatment temperatures of catalysts, impregnation order of Ni and Mo species, catalysts color, their specific surface area and average particle size of alumina.

NiO and MoO_3 were supplied by Sigma–Aldrich. Ni- and NiMo-alumina catalysts were prepared by impregnating alumina with an ethanol solution of nickel acetonate tetrahydrate ($(CH_3COO)_2Ni{\cdot}4H_2O$, Sigma–Aldrich) and molybdenyl acetylacetonate ($C_{10}H_{14}MoO_6$, Acros Organics). After impregnation, the materials were dried overnight at 120 °C, followed by calcination in the air flow for 5 h. NiO450 and NiO800 were prepared by impregnation of Ni and calcined at 450 and 800 °C, respectively. NiMoO450 was first impregnated with Mo and calcined at 600 °C, followed by the impregnation of Ni with subsequent calcination at 450 °C. NiMoO600 was impregnated with Mo, followed by the impregnation of Ni and the calcination at 600 °C. NiMoO800 was first impregnated with Ni and calcined at 800 °C, followed by the impregnation of Mo with subsequent calcination at 600 °C.

To discuss the UV–vis spectra of NiMoO-alumina catalysts, the Ni- and Mo-alumina were prepared with the same amount of Ni (ca 3.1 wt.%) and Mo (ca 6.0 wt.%) as dual NiMoO-alumina catalysts. The calcinations of these catalysts were carried out at 600 °C.

2.2. XRF

Concentration of the Ni and Mo species in the catalysts was determined with Elvatech desktop energy-dispersive XRF spectrometer Elva X equipped with a Ti anode X-ray tube.

2.3. XRD

X-ray diffractograms were recorded with Bruker AXE D8-Advance diffractometer using Cu Kα radiation with a secondary graphite monochromator.

2.4. SEM-EDX

Electron microscopy images of samples were taken with JEOL JSM-5500LV scanning electron microscope equipped with X-ray energy-dispersive (EDX) microanalyzer (IXRF Systems, detector GRESHAM Sirius 10).

2.5. UV–vis DRS

UV–vis diffuse reflectance spectra of granulated (0.25–0.50 mm diameter) catalysts were recorded using GBC CINTRA 303 spectrometer equipped with a spectralon-coated integrating sphere against a spectralon reference. Kubelka–Munk function was calculated from reflectance by formula: $F(R) = (1 - R)^2/2R$, where $F(R)$ is the Kubelka–Munk function and R is reflectance.

2.6. XPS

The catalyst samples were measured at room temperature using a VG ESCA3 MkII (VG Scientific, UK) electron spectrometer with a base pressure 2×10^{-9} mbar. Al Kα radiation was used for excitation of electrons. The hemispheric electron analyzer was operated in the fixed analyzer transmission mode at constant pass energy of 20 eV. The spectra of Al 2p, O 1s, Mo 3d, Mo 3p, Ni 2p and S 2p

Table 2
Catalytic testing conditions.

Variable, unit	Range
Hydrogen pressure, MPa	3.5
H_2/rapeseed oil molar ratio, –	50
Hydrogen flow, $Nl\,h^{-1}$	12.9–51.4
Temperature, °C	260–280
WHSV, $g_{feed}\,g_{cat}{}^{-1}\,h^{-1}$	1–4
Rapeseed oil flow, $g\,h^{-1}$	10–40

(for the sulfided catalysts) were measured. The overlapping spectral lines were resolved into individual components using the lines of Gaussian–Lorentzian shape and damped nonlinear least squares method. The spectra were calibrated using Al 2p core level binding energy at 74.4 eV. Quantification of elemental surface concentrations was accomplished by correcting the photoelectron peak areas for their cross-sections.

2.7. N_2-adsorption

Specific surface areas of the catalysts were measured at the boiling point of the liquid nitrogen (77 K) on flow BET apparatus equipped with TCD detection. The nitrogen relative pressure was varied in the 0.02–0.34 range. The specific surface area (S_{BET}) was determined by the fitting of the experimental data to the BET isotherm.

2.8. Catalytic testing

Catalytic tests were performed in a bench-scale catalytic apparatus equipped with electrically heated fixed-bed reactor of 17 mm inner diameter. Food grade rapeseed oil (distribution of fatty acids: oleic acid 62%, linoleic acid 20%, linolenic acid 9%, stearic acid 2%, palmitic acid 5%, gondoic acid 2%) was used as a liquid feed and refinery hydrogen gas (>99% purity) was used as a gas feed. The main impurities of hydrogen gas were methane (ca. 0.6%) and nitrogen (ca. 0.3%). Prior to the catalytic testing, catalysts mixed with silicon carbide were introduced into the reactor and sulfide (S-form of catalysts). Sulfidation included several steps as follows. The reactor was heated to the 200 °C in hydrogen (5 MPa, 50 $Nl\,h^{-1}$). Once the temperature of 200 °C was reached, sulfiding agent (5 vol.% dimethyl disulfide in *iso*-octane) was introduced (1.17 $ml\,min^{-1}$). The temperature gradient was set to 10 $°C\,h^{-1}$. After reaching 220 °C, the slope was increased to 30 $°C\,h^{-1}$ until achieving final temperature of 340 °C, at which the catalyst was sulfided for the next 4 h. Reaction conditions used in catalytic tests are specified in Table 2.

2.9. Products analysis

Liquid products were analyzed after separation of water by gas chromatography. Analysis was performed with Shimadzu GC-2010 gas chromatograph equipped with RESTEK MTX® Biodiesel TG film-coated column ($l = 10$ m, $d = 0.32$ mm, $t_f = 0.1$ μm). Conversion of rapeseed oil was calculated as: $X = 100 - c(\text{TG})$, where $c(\text{TG})$ is sum of the concentrations of triglycerides determined by GC analysis (%). The sum of triglycerides consists of both original triglycerides and triglycerides formed by double bond saturation of the original triglycerides. Selectivity was calculated as: $S(i) = c(i)/X \times 100$, where $c(i)$ is concentration of the product (%) determined by GC analysis. The reaction scheme including the main products of triglyceride deoxygenation can be found in the previous studies [1,17,23].

3. Results

3.1. Catalysts characterization

3.1.1. N_2-adsorption

Impregnation of Ni and Mo on alumina support leads to a decrease in the specific surface area. The decrease in specific surface area is approximately 30% in comparison with alumina support (181 $m^2\,g^{-1}$). It can be seen (Table 1) that the decrease in the specific surface area of NiMoO450, NiMoO600 and NiMoO800 is comparable and it is not affected by the change in the temperature pretreatment

3.1.2. SEM-EDX

Fig. 1 shows the Ni and Mo species distributed on the alumina surface as it is evidenced from SEM-EDX images of NiMoO600 catalyst. The light dots represent Ni and Mo, while alumina surface is depicted in dark color. It can be seen that Ni and Mo species are homogeneously distributed on the alumina surface evenly and no aggregates can be observed.

3.1.3. XRD

Fig. 2 depicts XRD patterns of alumina support, Ni-alumina and NiMoO-alumina catalysts. It also shows the XRD patterns of NiO, MoO_3 and $NiAl_2O_4$ as reference materials. The alumina support exhibits poorly resolved diffraction peaks at 14.4°, 37.6°, 45.8° and 67°, which can be attributed to the γ-alumina phase [39–43]. The peak at 28.2° is assigned with Al(O)OH phase [41]. The maxima in diffraction patterns for Ni- and NiMoO-alumina catalysts can be seen at 2θ angles of 19.2°, 37.5°, 45.8° and 67°, where the peak at 19.2° is ascribed to $NiAl_2O_4$ structure [44], while the latter three peaks correspond to the γ-alumina phase [39–43]. However, the peak at 19.2° is only visible in the XRD pattern of NiO800, NiMoO600 and NiMoO800 catalysts. No signs of crys-

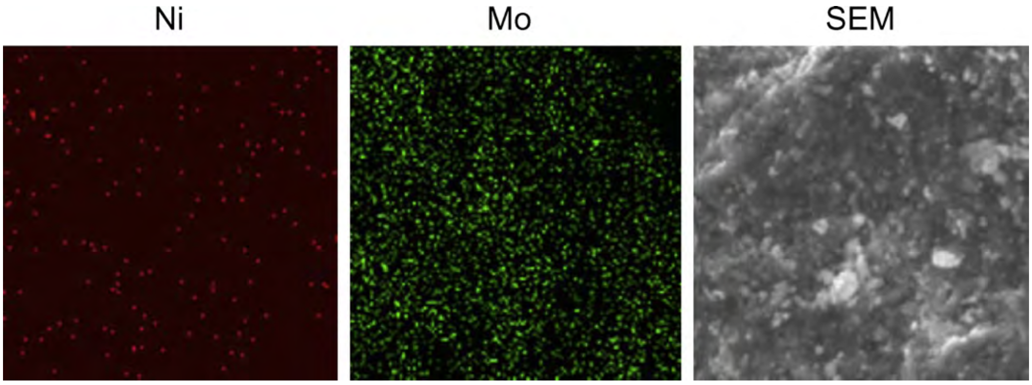

Fig. 1. SEM-EDX images of NiMoO-alumina catalysts (NiMoO600).

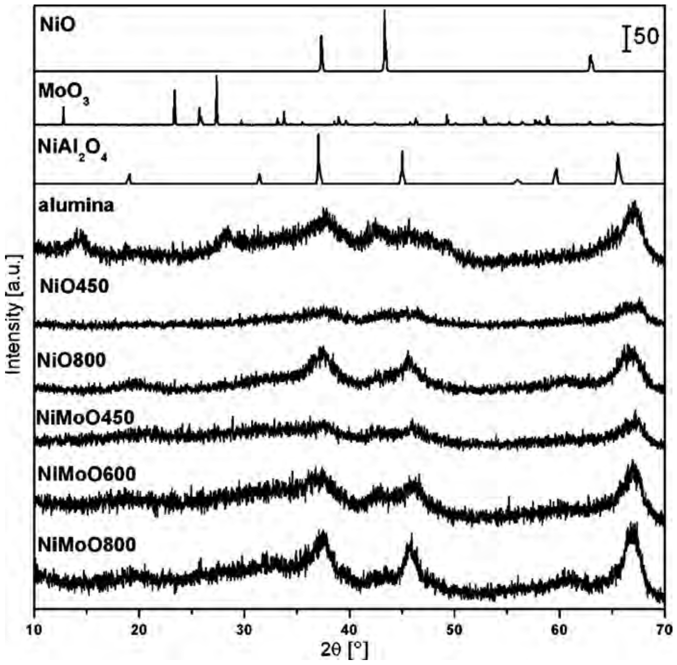

Fig. 2. XRD patterns of NiO, NiAl$_2$O$_4$, MoO$_3$, alumina support and NiMoO-alumina catalysts.

talline NiO or MoO$_3$ formation can be found in the XRD patterns of NiMoO-alumina catalysts. This is evidenced from the absence of NiO characteristic peaks at 37.3°, 43.3°, 63° and of MoO$_3$ main characteristic peaks at 12.8°, 23.3°, 25.7° and 27.3°.

Many authors [45–50] discussed the change of material crystallite size based on the broadening of the characteristic diffraction maxima in the XRD patterns. We have adopted this approach to discuss the effect of the alumina crystallite size change in the Ni- and NiMoO-alumina catalysts (Table 1). XRD maxima at 37.6° characteristic for γ-alumina phase were used in the calculations based on the Scherrer's formula for the determination of the alumina crystallite size: $d = K\lambda/\beta\cos\theta$, where d is the crystallite size [nm], K is Scherrer constant, which depends on the crystal shape, diffraction line indices and the dispersion of particle sizes of powder [45] (value 0.9 is used), λ is the X-ray wavelength [nm] (0.154056 nm), β is the full width of the peak at half maximum [rad] and θ is the Bragg angle [rad]. The values calculated for the above mentioned diffraction maxima are displayed in Table 1. Several authors compared crystallite sizes obtained from XRD and TEM [18,51,52], but our main concern in this matter is to show the change of the alumina crystallite size itself in the Ni- and NiMo-alumina catalysts. It can be seen (Table 1) that the alumina crystallite size is increasing with increasing calcination temperature of the catalysts. This might be caused by the aggregation of small crystallites at elevated temperatures.

3.1.4. UV–vis DRS

Seven UV–vis bands can be seen in the spectra of NiMoO450, NiMoO600 and NiMoO800 catalysts at 15,970, 16,860, 24,130, 33,480, 36,230, 40,270 and 46,750 cm^{-1} (Fig. 3A). The identification and discussion of the presence of individual Ni and Mo species in NiMoO-alumina catalysts based on the UV–vis spectra is difficult. Thus, the UV–vis spectra of single Ni- and Mo-alumina catalysts with the same amount of Ni and Mo as in dual NiMoO-alumina catalysts are shown in Fig. 3B. The UV–vis spectra of Ni-alumina exhibit the diffuse reflectance (DR) bands at 13,000–14,000, 15,970–16,860, 24,000–26,000, 34,300, 38,400 and 46,750 cm^{-1}. The UV–vis spectra of Mo-alumina exhibit the DR bands at 33,800, 35,970, 37,700, 40,300 and 46,750 cm^{-1}.

The identification of the Ni and Mo transitions to individual DR bands, based on the literature, is presented in Table 3. The doublet at 15,970–16,860 cm^{-1} is attributed to the transition characteristic for tetrahedral Ni^{2+}(Td) ions [53–56]. The shoulder at 24,130 cm^{-1} is ascribed with the transition of the octahedral Ni^{2+}(Oh) ions [53,54,57]. The band at 33,480 cm^{-1} is characteristic for Mo^{6+}(Oh) species [30,58–61] and unspecified Ni^{2+}-O charge transfer transition. Absorptions typical for transitions of Mo^{6+}(Td) ions can be found at 36,230 cm^{-1} [30,58,59,61], 40,270 cm^{-1} [58,61] and 46,750 cm^{-1} [60,62,63]. The UV–vis band at 36,230 cm^{-1} is also connected with transition of the three-coordinated Ni$_{3c}{}^{2+}$ ions [55]. Finally, Yang and Xia [57] and Oetliker et al. [64] calculated wavenumbers for the absorptions of the Ni^{2+}(Oh) ions, which correspond with absorption bands at 40,270 cm^{-1} and 46,750 cm^{-1}, respectively.

3.1.5. XPS

The obtained XP spectra of all samples confirmed that only expected elements (Ni, Mo, Al, O and in the case of NiMoS also S) are present in the surface layer of the NiMoO and NiMoS catalysts. The determined surface concentrations of Mo exceed the bulk values determined by XRF (Table 1) due to the fact that the Mo precursor deposits preferentially in the surface layer. The difference between bulk and surface concentration is larger when Ni impregnation and calcination at 800 °C preceded Mo impregnation. On the contrary, Ni surface concentration is lower than the Ni bulk concentration (NiMoO800) or similar to the Ni bulk concentration (NiMoO450) as shown in Table 1. This reflects the order of impregnation (Table 1).

The binding energies of Mo 3d$_{5/2}$ as well Mo 3p$_{3/2}$ electrons in the NiMoO-alumina catalysts correspond to those reported for Mo^{6+} in molybdenum oxide [65,66]. The binding energy of the predominant Mo 3d$_{5/2}$ component in the spectra of Mo 3d–S 2s electrons in the NiMoS samples (229.1 eV) is consistent with the value reported for Mo^{4+} in molybdenum sulfide [66,67] (Fig. 4).

The measured binding energy of Ni 2p$_{3/2}$ electrons (856.2 ± 0.2 eV) in NiMoO samples is in agreement with the binding energy published for NiMo catalysts [65,67]. After sulfidation, an additional component appeared in the spectra of Ni 2p$_{3/2}$ electrons with binding energy corresponding to sulfided nickel [65,67] (Fig. 5). It can be seen from the comparison of Figs. 4 and 5 that the extent of sulfidation of Mo is higher than the extent of Ni sulfidation. Moreover, the extent of sulfidation of Ni in NiMoS800 is only 25% while it is about 55% in NiMoS450 (Fig. 5).

3.2. Catalytic activity of NiMoS-alumina catalysts in the deoxygenation of rapeseed oil

Fig. 6 shows the dependence of the conversion of rapeseed oil on temperature during its deoxygenation over NiMoS-alumina catalysts at WHSV = 4 h^{-1}. The values of the conversion of rapeseed oil decrease in order NiMoS450 > NiMoS600 ~ NiMoS800. Fig. 7 shows the dependence of the conversion of vegetable oil on the WHSV at 260 °C. The decreasing trend in the conversion of rapeseed oil can be also seen in order NiMoS450 > NiMoS600 ~ NiMoS800.

Summarized selectivities for NiMoS450, NiMoS600 and NiMoS800 catalysts to oxygenated products (sum of fatty acids, fatty alcohols and their esters) and hydrocarbons (typically C$_{15}$–C$_{18}$ n-alkanes) are shown in Fig. 8 as a function of the conversion. All three catalysts (NiMoS450, NiMoS600 and NiMoS800) exhibit one selectivity-conversion behavior. Oxygenates prevail in the product mixtures at low conversions of rapeseed oil. On the other hand, with increasing conversion of rapeseed oil, composition of the

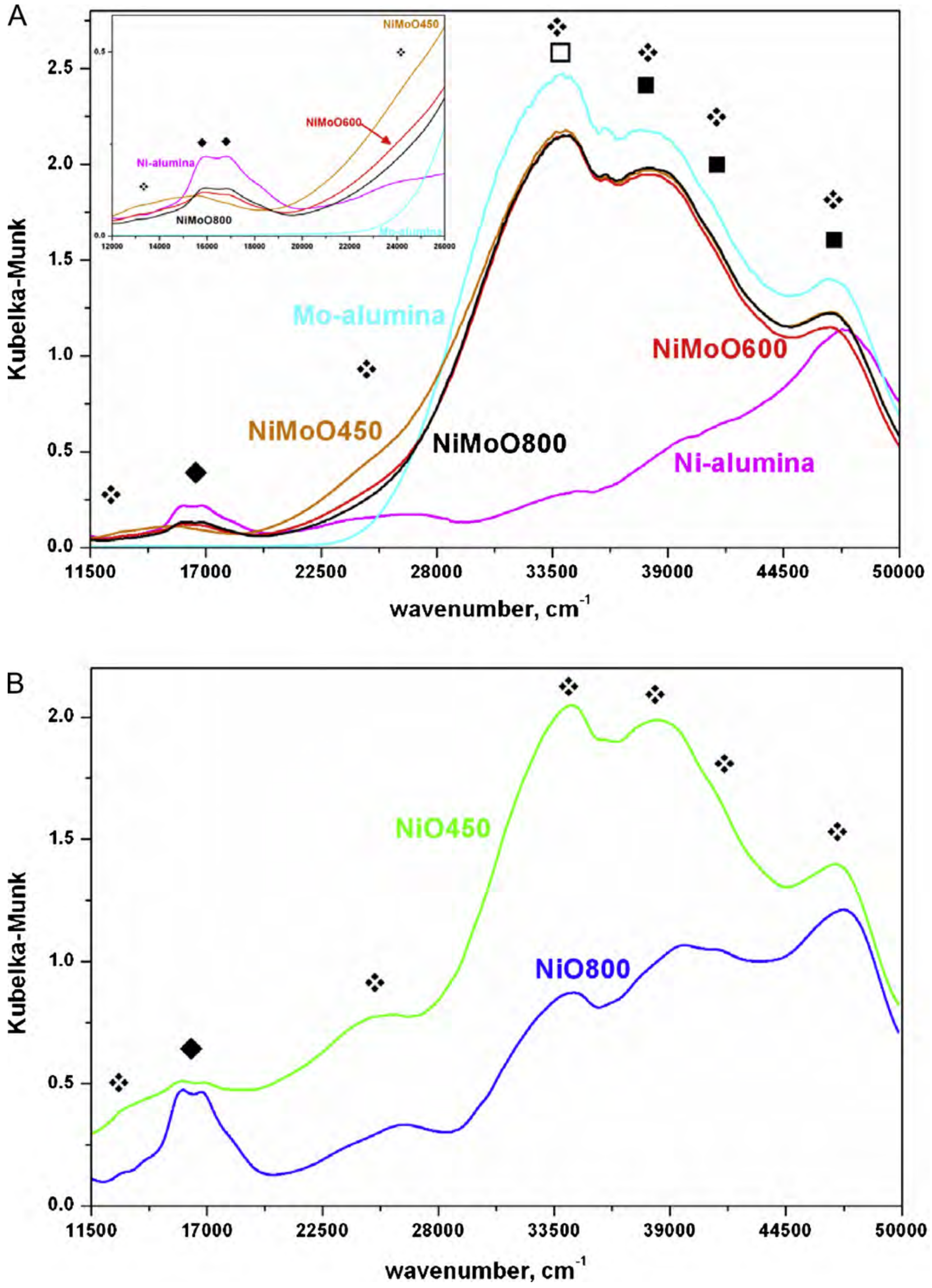

Fig. 3. (A) UV–vis DR spectra of oxide forms of NiMoO-alumina catalysts. Legend: (❖) Ni(Oh), (♦)Ni(Td), (□) Mo(Oh) and (■) Mo(Td). (B) UV–vis DR spectra of oxide forms of NiO450 and NiO800 catalysts. Legend: (❖) Ni(Oh) and (♦) Ni(Td).

mixture is changed towards the domination of the main desired products of the reaction, i.e. hydrocarbons.

Ratio of the selectivity to C_{18} and C_{17} hydrocarbons (S_{18}/S_{17}), i.e. the main hydrocarbon products, is shown in Fig. 9 as a function of the conversion of rapeseed oil. It describes the relative rates of the two main deoxygenation reactions, namely hydrodeoxygenation yielding C_{18} alkanes and hydrodecarboxylation resulting in formation of C_{17} alkanes. S_{18}/S_{17} decreases in order NiMoS800 > NiMoS600 ~ NiMoS450.

To understand better the role of Ni species in NiMo-alumina catalysts, NiS450 and NiS800 catalysts were tested in the deoxygenation of rapeseed oil as well. The NiS-catalysts exhibited lower deoxygenation activity than the NiMoS-catalysts as it is documented in Fig. 10 by plotting oxygen elimination as a function of WHSV. In comparison with NiMoS-catalysts NiS-catalysts favor formation of fatty acids from triglycerides, which is reflected in conversion of triglycerides. However, this reaction does not contribute to deoxygenation and therefore a fair comparison of NiS-catalysts is possible only when conversion is replaced by oxygen elimination. It should be also noted that no hydrocarbons having even number of carbon atoms in their molecule (e.g. C_{18}), i.e. hydrodeoxygenation products, were formed. The comparison of the two Ni catalysts

Table 3
Assignment of the UV–vis bands for NiMoO-alumina catalysts from literature.

Wavenumber, cm^{-1}	Wavelength, nm	Metal coordination	Transition	References
13,000–14,000	714–769	Ni^{2+} (Oh)	${}^3A_{2g} \rightarrow {}^1T_{2g}(P)$	[53–55]
15,970	626	Ni^{2+} (Td)	${}^3T_1 \rightarrow {}^3T_1(F)$	[53–56]
16,860	593	Ni^{2+} (Td)	${}^3T_1 \rightarrow {}^3T_1(F)$	[53,56]
24,130	414	Ni^{2+} (Oh)	${}^3A_{2g} \rightarrow {}^3T_{1g}(P)$	[53,54,57]
33,480	298	Ni^{2+} (–)	Ni^{2+}-O CT	[36]
		Mo^{6+} (Oh)	$O^{2-} \rightarrow Mo^{6+}$	[30,58–61]
36230	276	$Ni_{3c}{}^{2+}$ (D_{3h} symmetry)	${}^3A_2'(F) \rightarrow {}^3E''(P)$	[55]
		Mo^{6+} (Td)	$O^{2-} \rightarrow Mo^{6+}$	[30,58,59,61]
40,270	248	Ni^{2+} (Oh)	${}^3A_{2g}(F) \rightarrow {}^1T_{2g}(G)$	[57]
		Mo^{6+} (Td)	$O^{2-} \rightarrow Mo^{6+}$	[58,61]
46,750	213	Ni^{2+} (Oh)	${}^3A_{2g} \rightarrow {}^1A_{1g}(2)$	[64]
		Mo^{6+} (Td)	–	[60,62,63]

shows that NiS450 exhibited higher deoxygenation activity than NiS800 (Fig. 10).

4. Discussion

4.1. Factors that could cause the observed change in the activity and selectivity of NiMoS-alumina catalysts

The observed changes in the activity and selectivity of NiMoS-alumina catalysts could be plausibly attributed to variations of the following catalyst related parameters (i) concentration of Ni, Mo, (ii) distribution of Ni species (iii) distribution of Mo species, (iv) catalyst specific surface area, (v) crystallite size of Ni, Mo, Al_2O_3, and (vi) impregnation order of Ni and Mo precursors.

The variations in Ni and Mo concentrations in the NiMoO-alumina catalysts as well as in their specific surface areas are only small (Table 1) and Ni and Mo species are homogeneously distributed on the support (Fig. 1). As these parameters are not affected by the sulfidation of NiMoO-alumina to provide the active NiMoS-alumina catalysts used in the deoxygenation experiments, the contribution of the differences in these parameters to the observed changes in the activity and selectivity of NiMoS-alumina catalysts can be considered to be insignificant.

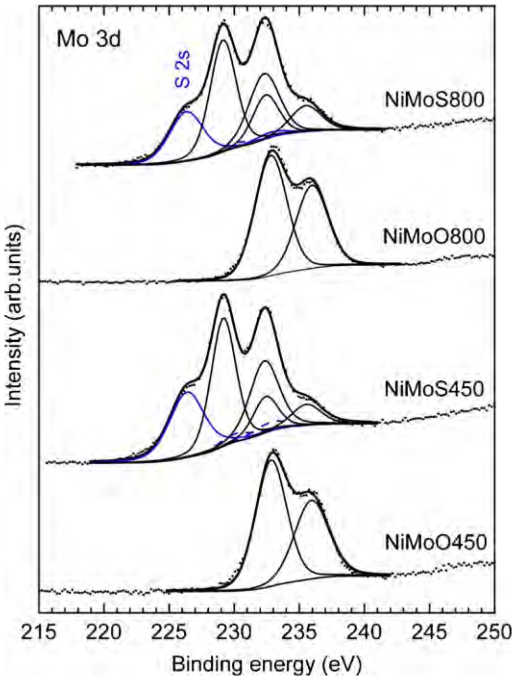

Fig. 4. Fitted spectra of S 2s and Mo 3d photoelectrons for NiMo450 and NiMo800 catalysts.

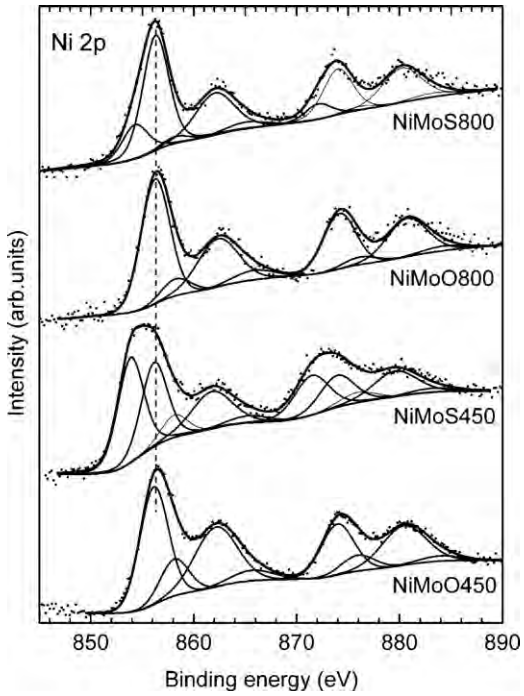

Fig. 5. Fitted spectra of Ni 2p photoelectrons for NiMo450 and NiMo800 catalysts.

The NiMoO450 and NiMoO600 catalysts were prepared in the same impregnation order (Mo impregnated first), while for NiMoO800 the impregnation order had to be reversed in order to keep the constant pretreatment temperature of Mo. As there can be

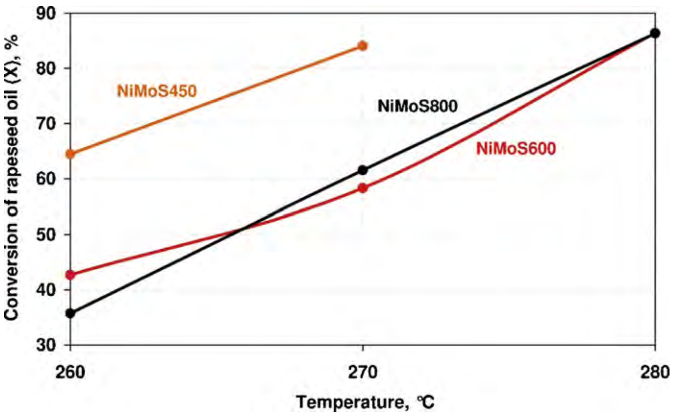

Fig. 6. Conversion of vegetable oil as a function of the temperature ($p(H_2) = 3.5$ MPa, H_2/rapeseed oil molar ratio = 50, $F(H_2) = 51.4$ Nl h^{-1}, F(rapeseed oil) = 40 g h^{-1}, WHSV = 4 h^{-1}).

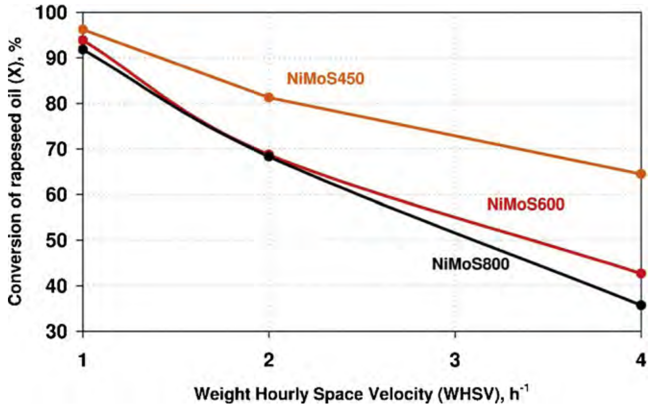

Fig. 7. Conversion of vegetable oil as a function of WHSV ($p(H_2)$ = 3.5 MPa, H_2/rapeseed oil molar ratio = 50, $F(H_2)$ = 12.9–51.4 Nl h^{-1}, F(rapeseed oil) = 10–40 g h^{-1}, T = 260 °C).

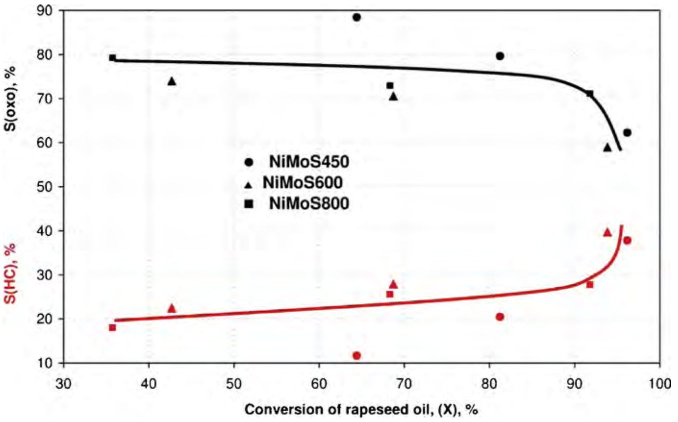

Fig. 8. Selectivity to oxygenates (S(oxo)) and hydrocarbons (S(HC)) as a function of the conversion ($p(H_2)$ = 3.5 MPa, H_2/rapeseed oil molar ratio = 50, $F(H_2)$ = 12.9–51.4 Nl h^{-1}, F(rapeseed oil) = 10–40 g h^{-1}, T = 260 °C).

observed significant differences in activity and, to a lesser extent, in selectivity of NiMoS450 and NiMoS600 catalysts, it can be inferred that the change of impregnation order is not the main cause of the observed differences. Nonetheless, there can be observed differences in Ni and Mo distribution in the catalyst (Table 1). The catalyst impregnated first with Ni, then calcined at 800 °C and subsequently impregnated with Mo (NiMoO800) exhibits higher surface concentration of Mo and lower surface concentration of Ni than NiMoO450. The same is observed also for the sulfided forms of these catalysts (NiMoS800 and NiMoS450). These differences might then contribute to the observed differences in catalytic activity and selectivity.

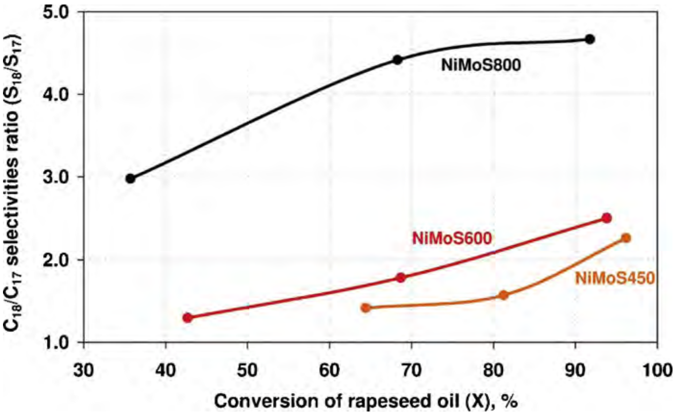

Fig. 9. Selectivity to octadecane (S_{18}) and selectivity to heptadecane (S_{17}) ratio as a function of the conversion ($p(H_2)$ = 3.5 MPa, H_2/rapeseed oil molar ratio = 50, $F(H_2)$ = 12.9–51.4 Nl h^{-1}, F(rapeseed oil) = 10–40 g h^{-1}, T = 260 °C).

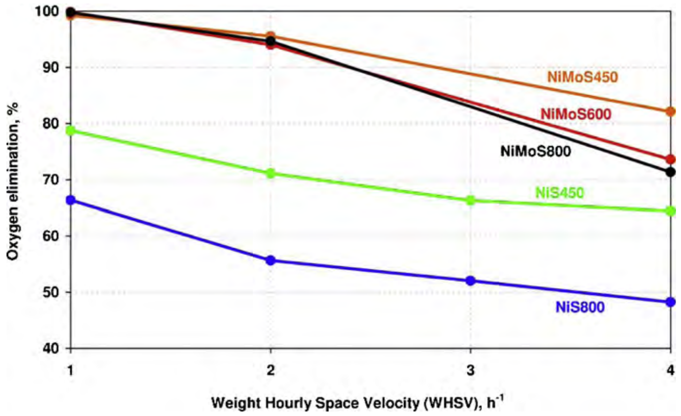

Fig. 10. Oxygen elimination as a function of the WHSV ($p(H_2)$ = 3.5 MPa, H_2/rapeseed oil molar ratio = 50, $F(H_2)$ = 12.9–51.4 Nl h^{-1}, F(rapeseed oil) = 10–40 g h^{-1}, T = 280 °C).

As the impregnation with Mo precursor was carried out in the same way for all three NiMoO-alumina catalysts (only the support was already modified with Ni and calcined at 800 °C prior to impregnation with Mo in NiMoO800) and they were all calcined at 600 °C, it can be assumed that there are no significant differences in the distribution of Mo species. This assumption is further supported by the fact that no significant difference in the UV–vis spectra of NiMoO-alumina catalysts was found with respect to the characteristic bands of Mo^{6+} species between 28,000 and 50,000 cm^{-1} (Fig. 3A).

Consequently, due to the elimination of most of the catalyst variables, two important parameters relating to Ni that could affect the catalyst performance remain – namely distribution of Ni species in the NiMoO-alumina catalysts and crystallite size of Ni species. Unfortunately, there is not sufficient information on Ni crystallite size as the crystallites could not be observed by XRD (due to either their small size or amorphous nature, Fig. 2). Nevertheless, the alumina particle size increased with the increasing pretreatment temperature. With respect to the reported results [68,69], it can however be proposed that, similarly to alumina particle size, the nickel particle size increased with the increasing pretreatment temperature.

The observed differences in the catalytic performance of the NiMoS-alumina catalysts can be, hence, related to the variation in the calcination temperature of Ni species that affects the distribution of Ni species in the NiMoO-alumina catalysts. The changes in Ni distribution in NiMoO-alumina catalysts are discussed in detail in Section 4.2. However, it is very difficult to relate the observed changes in Ni species distribution on NiMoO-alumina catalysts, i.e. in the structure of the active sites, to the structure of their working NiMoS-alumina catalysts counterparts. Nonetheless, based on the comparison of XPS analysis of NiMoO-alumina and NiMoS-alumina catalysts it can be inferred that the different calcination temperature affects the extent of Ni sulfidation, which in turn may play an important role in the catalyst activity and selectivity.

4.2. Distribution of Ni species

Ni species can be present as surface Ni^{2+} in the form of stoichiometric or non-stoichiometric NiO and Ni^{2+} as stoichiometric or non-stoichiometric $NiAl_2O_4$, which can be present at the surface or in the bulk [70]. There was also reported presence of surface reduced nickel [70] and Ni_2O_3 [25]. These species can be present either in octahedral or in tetrahedral coordination.

In order to discuss the change in the distribution of Ni species in NiMoO-alumina catalysts, the attention has been focused firstly on the distribution of Ni species in a simpler system, namely in Ni-alumina catalysts (NiO450 and NiO800) that were specifically prepared for this purpose.

4.2.1. NiO450 and NiO800 catalysts.

The first hint about the distribution of the Ni species in NiO450 and NiO800 catalysts is given by the catalysts color (Table 1). NiO450 catalyst is gray with blue touch. The greyish color is an indication of non-stoichiometric NiO formation [71], while the bluish touch indicates the formation of small amount of nickel aluminate ($NiAl_2O_4$) [70,72,73]. The formation of non-stoichiometric NiO in NiO450 could be the reason why it is not seen in XRD pattern (Fig. 2) and it can be also evidenced by elevated background of the UV–vis spectra (Fig. 3) [71]. In contrast, the color of the NiO800 is bright azure blue, which is the evidence of the nickel aluminate presence [70,72].

Nickel aluminate is partially inverse spinel $NiAl_2O_4$ [71,74–76]. Its inversion is given by the calcination temperature and it is an indication of how many Ni(II) and Al(III) ions occupy tetrahedral (Td) and octahedral (Oh) sites. In normal spinel, Ni(II) ions occupy Td sites and Al(III) ions occupy Oh sites. In inverse spinel, Ni(II) ions occupy Oh sites and Al(III) ions occupy Td and Oh sites [77]. Dufresne et al. [76] reported that Ni(Td) should have higher binding energy with support and, thus, be more stable at elevated temperatures. However, the presence of $NiAl_2O_4$ having close to the inverse spinel structure was also reported [74–76].

Regarding the UV–vis spectra of NiO450 and NiO800 catalysts, several differences can be seen (Fig. 3B). The spectrum of NiO450 shows intensive DR bands at 34,300 and 38,400 cm^{-1}. It is known that Ni ions in nickel oxide are in octahedral coordination. Thus, it is possible that Ni^{2+}-O charge-transfer band at 34,300 cm^{-1} along with bands at 13,000–14,000, 27,000 and 38,400 cm^{-1} could be assigned in the spectra of the NiO450 catalyst to the Ni(Oh) ions in NiO lattice. In agreement with the visual observations, these bands are significantly weaker in the spectrum of NiO800.

Furthermore, a low-intensity doublet at 15,970–16,860 cm^{-1} can be observed in the spectrum of NiO450, while it is rather prominent in the spectrum of NiO800. This doublet is characteristic for Ni species with tetrahedral coordination. Here it reflects elevated diffusion of the Ni species into the alumina lattice, where Ni ions are located in tetrahedral coordination [78]. Moreover, presence of the Ni(Td) in $NiAl_2O_4$ was also reported [25].

Based on the visual observations and UV–vis spectra it can be concluded that at increased calcination temperature the primarily formed NiO having Ni in exclusively octahedral coordination is transformed into the $NiAl_2O_4$ with Ni in both octahedral as well as tetrahedral coordination.

4.2.2. NiMo450, NiMo600 and NiMo800 catalysts

In agreement with Ni catalysts, the formation of the $NiAl_2O_4$ surface spinel structure is observed also in NiMoO-alumina catalysts at high Ni calcination temperatures. It is evidenced particularly in the XRD pattern of NiMoO800 (Fig. 2) by the increased signal at 2θ of 19.2°, which is attributed to the $NiAl_2O_4$ surface spinel structure. In the XRD pattern of NiMoO600, peak at 19.2° is only poorly notable, meaning lower $NiAl_2O_4$ concentration and for NiMoO450, this peak is not visible at all, meaning that calcination temperature as low as 450 °C does not allow for Ni to create appreciable concentration of $NiAl_2O_4$ in NiMoO-alumina system. This can be also evidenced by the absence of bluish color in NiMoO450 (Table 1). Many authors reported that in $NiAl_2O_4$ as a mostly inverse spinel Ni is found mainly in octahedral coordination [74–76], however also presence of the $NiAl_2O_4$ in a tetrahedral Ni arrangement was reported [25,76].

UV–vis spectra of the NiMoO-alumina catalysts exhibit DR bands of the transitions of tetrahedral (Td), octahedral (Oh) and some other unspecified Ni^{2+} species (Fig. 3A). The main objective here is not to discuss the individual DR bands, but rather investigate the changes in the distribution between the octahedral and tetrahedral Ni species. UV–vis bands of the Ni(Td) are present as a doublet at 15,970–16,860 cm^{-1}, while Ni(Oh) can be seen at 24,130, 34,300, 38,400, 40,270 and 46,750 cm^{-1}. However, the bands of Ni(Oh) at 34,300, 38,400, 40,270 and 46,750 cm^{-1} in the spectra of NiMoO-alumina catalysts are overlapped by the DR bands of the molybdenum (Fig. 3A). Therefore, only bands of Ni(Td) at 15,970–16,860 cm^{-1} and band of Ni(Oh) at 24,130 cm^{-1} can be discussed.

From UV–vis spectra shown in Fig. 3A, it can be clearly seen, that the intensity of the DR band at 24130 cm^{-1}, which we attributed to the Ni(Oh), is the highest for NiMoO450 catalyst and its intensity decreases in order: NiMoO450 ≫ NiMoO600 > NiMoO800. Based on the intensities of the DR doublet at 15,970–16,860 cm^{-1}, which is attributed to the Ni(Td), relative concentration of the Ni(Td) species is increasing in the order: NiMoO450 ≪ NiMoO600 < NiMoO800. Thus, the most pronounced difference in the distribution of Ni(Oh) and Ni(Td) species is observed for NiMoO450 and NiMoO600. On the other hand, the NiMoO600 and NiMoO800 exhibited small difference in the population of Ni(Oh) and Ni(Td) species. However, the difference between NiMoO600 and NiMoO800 can be observed mainly in the population of $NiAl_2O_4$ spinel.

According to the literature, Ni in tetrahedral coordination is hardly reducible [25,79], because it is incorporated in and strongly interacts with the alumina lattice [25,29]. It could be therefore assumed that the increasing calcination temperature enables part of the Ni species to diffuse preferably into the alumina lattice, in which Ni is present in the tetrahedral coordination. There is also possible creation of Ni(Td) in $NiAl_2O_4$ spinel [25]. Therefore, we assign the lowest intensity of Ni(Td) doublet to the effect of the low calcination temperature in terms of low diffusion of Ni into the alumina lattice. This finding is in agreement with the results presented above for NiO450 and NiO800 catalysts and it is also in agreement with a previous study of the behavior of Ni-alumina catalysts pretreated at 600 and 800 °C, where the increase in the calcination temperature led to the increase of the relative population of Ni(Td) and the decrease in the relative population of Ni(Oh) [36].

There are several explanations possible for the relative increase in the population of Ni(Td) arising from the increase of the pretreatment temperature: (i) some of the Ni(Oh) species in the NiO lattice (characteristic by the decrease of the intensity of transition at 24,130 cm^{-1}) are diminished and Ni diffuses into the alumina lattice and also creates $NiAl_2O_4$ (increase at 15,970–16,860 cm^{-1}), both in a tetrahedral coordination, (ii) more of the Ni(Oh) species in the NiO lattice are diminished and Ni diffuses into the alumina lattice and it is in tetrahedral coordination (increase at 15,970–16,860 cm^{-1}) and also creates $NiAl_2O_4$, however in octahedral coordination, which could be poorly visible, because of the nickel aluminate location under the surface of the alumina support.

Nevertheless, it is obvious that due to increased calcinations temperature of Ni precursors, NiMoO-alumina catalysts with increasing population of Ni in tetrahedral coordination are obtained. As discussed in the following section, the NiMoS-alumina catalysts, prepared by sulfidation of NiMoO-alumina catalysts, exhibit different catalytic performance. While it is impossible to make a direct link between the structure of NiMoO-alumina catalysts, on the one hand, and of NiMoS-alumina catalysts, on the other hand, the XPS investigations of both catalyst forms (i.e. oxide and sulfide) clearly demonstrate that there is a difference in the extent of sulfidation of NiMoS450 and NiMoS800 (Fig. 5).

The catalyst with the highest concentration of Ni(Td), i.e. NiMoO800, exhibits significantly lower extent of Ni sulfidation than the catalyst that has predominantly octahedral coordination of Ni, i.e. NiMoO450 (Fig. 5). It has been previously reported [67] that sulfidation of Ni in tetrahedral coordination in nickel aluminate is more difficult than sulfidation of Ni(Oh). It can be thus concluded that higher calcination temperature of Ni precursor leads to formation of Ni(Td) species that are more difficult to transform into sulfide form that is active in deoxygenation.

4.3. Structure vs. catalytic activity of NiMo-alumina (HDO)

The above-reported catalyst characterization results indicate differences in the structure of the NiMoO-alumina catalysts and are here combined with the performance of the NiMoS-alumina catalysts in an attempt to reveal a link between catalyst preparation and its performance in the deoxygenation of triglycerides. Even though the coordination of Ni species has been determined for NiMoO-alumina catalysts and the experiments have been carried out using NiMoS-alumina catalysts, the differences in the catalysts activities and selectivities suggest that the structural differences of NiMoO-alumina catalysts have been propagated into the working NiMoS-alumina catalysts. This is confirmed by the XPS results that indicate a lower extent of Ni sulfidation in catalyst with higher concentration of Ni in tetrahedral coordination. Moreover, if the differences in the structure of the NiMoO-alumina catalysts were not significant, the working NiMoS-alumina catalysts should exhibit the same catalytic performance.

The catalytic performance of the NiMoS-alumina catalysts in the deoxygenation of rapeseed oil is described by three basic parameters (i) conversion (or oxygen elimination that describes the real deoxygenation efficiency [17,80]), (ii) selectivity towards hydrocarbons (non-oxygenated products) and oxygenated products (sum of fatty acids, fatty alcohols, and their esters) and (iii) selectivity to the hydrodeoxygenation (HDO) and hydrodecarboxylation (HDC) reaction pathway that is expressed as the ratio of C_{18}/C_{17} hydrocarbons, i.e. products of HDO and HDC, respectively.

4.3.1. Conversion

Conversion of the rapeseed oil (Figs. 6 and 7) as well as oxygen elimination (Fig. 10) is the highest for the NiMoS450 catalyst. The NiMoS600 and NiMoS800 catalysts exhibit similar conversion (Figs. 6 and 7) and oxygen elimination (Fig. 10), respectively, but visibly lower than NiMoS450. The deoxygenation activity seems to correlate with the relative population of Ni(Oh) species that is also the highest in NiMoO450. Moreover, NiMoO600 and NiMoO800 catalysts exhibit almost similar relative population of Ni(Oh) species (Section 4.2) and similar conversion of rapeseed oil (Figs. 6 and 7). Therefore, it can be concluded that Ni(Oh) in NiMoO-alumina catalysts could be the precursors of the active Ni species in the hydrotreating NiMoS-alumina catalysts. This conclusion is further supported by the performance of Ni catalysts calcined at 450 and 800 °C, respectively (Fig. 10) and is in line with previous reports discussing that the active form of the promoter metal (Ni, Co) in the alumina supported hydrotreating catalysts exhibits octahedral coordination [81,82]. Moreover, the XPS measurements reveal differences in the extent of sulfidation of Ni species that can be related to their nature (Ni(Td) *vs.* Ni(Oh) as discussed above).

4.3.2. Oxygenates vs. hydrocarbons

At low conversion levels of rapeseed oil, the products of triglyceride transformation consist almost exclusively of oxygenates (fatty acids, fatty alcohols and their esters). This is in agreement with previous studies [14–17] that have established that formation of oxygenates precedes that of hydrocarbons. Consequently, with increasing conversion of rapeseed oil the amount of desired hydrocarbons is increasing, while the amount of oxygenates is decreasing. In contrast to the activity of NiMoS-alumina catalysts, there are no discernible differences in selectivity to hydrocarbons and oxygenates among the catalysts, i.e. when the selectivity to both main product groups is plotted as a function of conversion (Fig. 8).

4.3.3. C_{17} vs. C_{18}

There are two major deoxygenation reaction routes over NiMoS-alumina catalysts [17] – hydrodeoxygenation (HDO) yielding hydrocarbons with even carbon number and hydrodecarboxylation (HDC) yielding hydrocarbons with odd carbon number. As over 90% of fatty acids bound in triglycerides present in rapeseed oil have 18 carbon atoms in their molecule, provides the ratio of selectivities to C_{18}/C_{17} (S_{18}/S_{17}) a useful tool for describing the relative importance of HDO and HDC. Despite the product distribution between oxygenates and hydrocarbons was not affected by the catalyst structure, significant differences can be found in selectivities to C_{18} and C_{17} hydrocarbons that reflect the differences in deoxygenation mechanism. S_{18}/S_{17} ratio for the tested catalysts is decreasing in order: NiMoS800 ≫ NiMoS600 > NiMoS450 (Fig. 9).

Sulfided Mo-alumina catalyst has been shown to deoxygenate rapeseed oil selectively by HDO, while sulfided Ni-alumina catalyst yielded almost exclusively HDC products [17]. The difference in S_{18}/S_{17} between NiMoS450 and NiMoS600 can be hence attributed to the higher population of the more active Ni(Oh) in NiMoO450 that results in higher HDC activity and, in turn, in lower S_{18}/S_{17} ratio (Fig. 9). The significantly higher S_{18}/S_{17} ratio observed for NiMoS800 can be caused by two factors (i) increased population of Ni(Td) that lead to Ni sites in NiMoS catalysts with low HDC activity or (ii) impregnation order. In contrast to NiMoO450 and NiMoO600, NiMoO800 was prepared by impregnating the alumina support first with Ni and then with Mo, and Mo sites could be thus more readily accessible and HDO route preferred. This explanation is supported by the surface concentration of Ni and Mo obtained from XPS (Table 1).

5. Conclusions

NiMoS-alumina catalysts are highly active in the deoxygenation of rapeseed oil. In order to obtain information about the role of Ni species and their effect on the activity of NiMoS-alumina catalysts in the deoxygenation of rapeseed oil, the NiO- and NiMoO-alumina catalysts with a different distribution of Ni species were prepared. The change in the distribution of Ni species has been achieved by various temperature pretreatments of Ni species, while keeping the total amount of Ni and Mo species and the pretreatment procedure of Mo species constant.

The prepared NiMoO-alumina catalysts mainly differed in the population of octahedral and tetrahedral nickel species. However, there was not found any significant difference in the distribution of Mo species. This was determined for NiMoO450 and NiMoO600 catalysts, where the Ni species were impregnated on the Mo-alumina catalyst prepared by the same procedure. Although NiMoO800 catalyst was prepared by reversed impregnation order of Ni and Mo species, there was not observed any difference in the population of the UV–vis bands characteristic for Mo species in comparison with NiMoO450 and NiMoO600 catalysts. All NiMo-alumina catalysts had similar specific surface area and did not contain any bulk NiO and MoO_3 like species.

A change in pretreatment temperature led to changes in the population of Ni species. With increasing pretreatment temperature of Ni species, the Ni(Oh) concentration decreased and Ni(Td) increased in NiO- and NiMoO-alumina catalysts. Thus, the Ni(Oh) species in the NiO lattice were diminished and Ni diffused into the alumina lattice in a tetrahedral coordination and also created $NiAl_2O_4$ in Ni(Oh) and/or Ni(Td) coordination. This conclusion was further supported by XPS measurements that revealed that Ni was more difficult to convert into its sulfide form in the catalyst with higher Ni(Td) concentration.

The activity of NiMoS-alumina catalysts in the deoxygenation of rapeseed oil was discussed with respect to the conversion of rapeseed oil, selectivity to oxygenates and hydrocarbons and selectivity to C_{17} and C_{18} hydrocarbons.

Conversion. Conversion of rapeseed oil was affected by the population of the octahedral and tetrahedral nickel species in NiMoO-alumina catalysts. It has been found that the catalysts with higher population of octahedral nickel species are more active than those containing higher population of tetrahedral nickel species. This was attributed to the lower sulfidation of Ni(Td) species in comparison with Ni(Oh) species.

Oxygenates vs. hydrocarbons. Selectivities to oxygenates and hydrocarbons were not affected by the population of Ni species, but by the conversion of rapeseed oil. Oxygenates were mainly formed at low conversion of rapeseed oil, while hydrocarbons prevailed at high conversion of rapeseed oil.

C_{17} vs. C_{18}. Based on previous measurements [17], single Ni-alumina catalysts favor almost exclusively deoxygenation through the hydrodecarboxylation pathway (the formation of the C_{17} hydrocarbons) whereas single Mo-alumina catalysts favor the hydrodeoxygenation pathway (the formation of C_{18} hydrocarbons). Here, it has been found that due to the lower surface concentration of Ni in NiMoS800 (a consequence of a different impregnation order in comparison with the other tested catalysts) and lower extent of Ni sulfidation (a consequence of higher concentration of Ni species in tetrahedral coordination), NiMoS800 favors the hydrodeoxygenation pathway more prominently than NiMoS450 and NiMoS600 catalysts.

Acknowledgments

The authors gratefully thank to the Ministry of Industry and Trade of the Czech Republic (project FT-TA3/074) and Ministry of Education, Youth and Sports (no. MSM0021627501). This work is part of the UniCRE project (CZ.1.05/2.1.00/03.0071).

References

[1] I. Kubičková, D. Kubička, Waste Biomass Valor. 1 (2010) 293–308.
[2] M. Ferrari, B. Delmon, P. Grange, Microporous Mesoporous Mater. 56 (2002) 279–290.
[3] M. Ferrari, B. Delmon, P. Grange, Carbon 40 (2002) 497–511.
[4] W.-Y. Wang, Y.-Q. Yang, J.-G. Bao, Z. Chen, J. Fuel Chem. Technol. 37 (2009) 701–706.
[5] W.-Y. Wang, Y.-Q. Yang, H.-A. Luo, W.-Y. Liu, Catal. Commun. 11 (2010) 803–807.
[6] A. Centeno, E. Laurent, B. Delmon, J. Catal. 154 (1995) 288–298.
[7] M. Ferrari, S. Bosmans, R. Maggi, B. Delmon, P. Grange, Catal. Today 65 (2001) 257–264.
[8] M. Ferrari, R. Maggi, B. Delmon, P. Grange, J. Catal. 198 (2001) 47–55.
[9] O.I. Senol, T.R. Viljava, A.O.I. Krause, Appl. Catal. A: Gen. 326 (2007) 236–244.
[10] O.I. Senol, E.M. Ryymin, T.R. Viljava, A.O.I. Krause, J. Mol. Catal. A 277 (2007) 107–112.
[11] E.M. Ryymin, M.L. Honkela, T.R. Viljava, A.O.I. Krause, Appl. Catal. A: Gen. 358 (2009) 42–48.
[12] T.R. Viljava, R.S. Komulainen, A.O.I. Krause, Catal. Today 60 (2000) 83–92.
[13] O.I. Senol, T.R. Viljava, A.O.I. Krause, Catal. Today 106 (2005) 186–189.
[14] E. Laurent, B. Delmon, J. Catal. 146 (1994) 281–291.
[15] D. Kubička, P. Šimáček, N. Žilková, Top. Catal. 52 (2009) 161–168.
[16] D. Kubička, M. Bejblová, J. Vlk, Top. Catal. 53 (2010) 168–178.
[17] D. Kubička, L. Kaluža, Appl. Catal. A: Gen. 372 (2010) 199–208.
[18] T. Morgan, D. Grubb, E. Santillan-Jimenez, M. Crocker, Top. Catal. 53 (11–12) (2010) 820–829.
[19] P. Šimáček, D. Kubička, G. Šebor, M. Pospíšil, Fuel 88 (2009) 456–460.
[20] M. Snare, I. Kubičková, P. Maki-Arvela, D. Chichova, K. Eranen, D.Y. Murzin, Fuel 87 (2008) 933–945.
[21] Y.Q. Yang, H. Luo, G.S. Tong, J.S. Kevin, C.T. Tye, Chin. J. Chem. Eng. 16 (2008) 733–739.
[22] E. Furimsky, Ind. Eng. Chem. Prod. Res. Dev. 22 (1983) 31–34.
[23] D. Kubička, Collect. Czech. Chem. Commun. 73 (2008) 1015–1044.
[24] S. Lestari, P. Mäki-Arvela, J. Beltramini, G.M. Lu, D. Murzin, ChemSusChem 2 (2009) 1109–1119.
[25] S.T. Hong, D.R. Park, S.J. Yoo, J.D. Kim, H.S. Park, Res. Chem. Intermed. 32 (2006) 857–870.
[26] P. Salerno, S. Mendioroz, A.L. Agudo, Appl. Catal. A: Gen. 259 (2004) 17–28.
[27] S.J.S. Basha, P. Vijayan, C. Suresh, D. Santhanaraj, K. Shanthi, Ind. Eng. Chem. Res. 48 (2009) 2774–2780.
[28] J.L. Brito, J. Laine, J. Catal. 139 (1993) 540–550.
[29] B. Scheffer, J.J. Heijeinga, J.A. Moulijn, J. Phys. Chem. 91 (1987) 4752–4759.
[30] A. Guevara-Lara, R. Bacaud, M. Vrinat, Appl. Catal. A: Gen. 328 (2007) 99–108.
[31] H.R. Reinhoudt, A.D. van Langeveld, P.J. Kooyman, R.M. Stockman, R. Prins, H.W. Zandbergen, J.A. Moulijn, J. Catal. 179 (1998) 443–450.
[32] H.R. Reinhoudt, E. Crezee, A.D. van Langeveld, P.J. Kooyman, J.A.R. van Veen, J.A. Moulijn, J. Catal. 196 (2000) 315–329.
[33] H.R. Reinhoudt, R. Troost, A.D. van Langeveld, J.A.R. van Veen, S. Sie, J.A. Moulijn, J. Catal. 203 (2001) 509–515.
[34] M.J. Vissenberg, Y. van der Meer, E.J.M. Hensen, V.H.J. de Beer, A.M. van der Kraan, R.A. van Santen, J.A.R. van Veen, J. Catal. 198 (2001) 151–163.
[35] H. Li, H.X. Li, W.L. Dai, J.F. Deng, Appl. Catal. A: Gen. 207 (2001) 151–157.
[36] L. Čapek, L. Vaněk, L. Smoláková, R. Bulánek, J. Adam, Collect. Czech. Chem. Commun. 73 (2008) 1177–1191.
[37] O.S. Joo, K.D. Jung, B Kor. Chem. Soc. 23 (2002) 1149–1153.
[38] J. Juan-Juan, M.C. Roman-Martinez, M.J. Illan-Gomez, Appl. Catal. A: Gen. 355 (2009) 27–32.
[39] A. Boumaza, L. Favaro, J. Ledion, G. Sattonnay, J.B. Brubach, P. Berthet, A.M. Huntz, P. Roy, R. Tetot, J. Solid State Chem. 182 (2009) 1171–1176.
[40] Q. Liu, A.Q. Wang, X.D. Wang, T. Zhang, Microporous Mesoporous Mater. 92 (2006) 10–21.
[41] Z.X. Sun, T.T. Zheng, Q.B. Bo, M. Du, W. Forsling, J. Colloid Interface Sci. 319 (2008) 247–251.
[42] T. Seki, S. Ikeda, M. Onaka, Microporous Mesoporous Mater. 96 (2006) 121–126.
[43] C. Lesaint, G. Kleppa, D. Arla, W.R. Glomm, G. Oye, Microporous Mesoporous Mater. 119 (2009) 245–251.
[44] E. Heracleous, A.F. Lee, K. Wilson, A.A. Lemonidou, J. Catal. 231 (2005) 159–171.
[45] V. Uvarov, I. Popov, Mater. Charact. 58 (2007) 883–891.
[46] S. Cava, S.M. Tebcherani, S.A. Pianaro, C.A. Paskocimas, E. Longo, J.A. Varela, Mater. Chem. Phys. 97 (2006) 102–108.
[47] M.H. Jellinek, I. Fankuchen, Ind. Eng. Chem. 37 (1945) 158–163.
[48] U.J. Kim, S.H. Eom, M. Wada, Polym. Degrad. Stab. 95 (2010) 778–781.
[49] J.I. Langford, A.J.C. Wilson, J. Appl. Crystallogr. 11 (1978) 102–113.
[50] A. Majhi, G. Pugazhenthi, A. Shukla, Ind. Eng. Chem. Res. 49 (2010) 4710–4719.
[51] D.G. Mustard, C.H. Bartholomew, J. Catal. 67 (1981) 186–206.
[52] X. Shen, L.J. Garces, Y. Ding, K. Laubernds, R.P. Zerger, M. Aindow, E.J. Neth, S.L. Suib, Appl. Catal. A: Gen. 335 (2008) 187–195.
[53] D. Nikolova, R. Edreva-Kardjieva, M. Glurginca, A. Meghea, J. Vakros, G.A. Voyiatzis, C. Kordulis, Vib. Spectrosc. 44 (2007) 343–350.
[54] M.A. Zanjanchi, A. Ebrahimian, J. Mol. Struct. 693 (2004) 211–216.
[55] C. Lepetit, M. Che, J. Phys. Chem. 100 (1996) 3137–3143.
[56] R.A. Schoonheydt, D. Roodhooft, H. Leeman, Zeolites 7 (1987) 412–417.
[57] L. Yang, K.H. Xia, Solid State Commun. 90 (1994) 737–739.
[58] O.Y. Gutierrez, D. Valencia, G.A. Fuentes, T. Klimova, J. Catal. 249 (2007) 140–153.
[59] H. Jeziorowski, H. Knozinger, J. Phys. Chem. 83 (1979) 1166–1173.
[60] Y.V. Plyuto, I.V. Babich, I.V. Plyuto, A.D. VanLangeveld, J.A. Moulijn, Colloids Surf., A 125 (1997) 225–230.
[61] G.M.S. El Shafei, N.A. Moussa, C.A. Philip, J. Colloid Interface Sci. 228 (2000) 105–113.
[62] A. Bartecki, D. Dembicka, J. Inorg. Nucl. Chem. 29 (1967) 2907–2916.
[63] M.J. Cheng, F. Kumata, T. Saito, T. Komatsu, T. Yashima, Appl. Catal. A: Gen. 183 (1999) 199–208.
[64] U. Oetliker, M.J. Riley, H.U. Gudel, J. Lumin. 63 (1995) 63–73.
[65] S.T. Hong, D.R. Park, S.J. Yoo, J.-D. Kim, H.S. Park, Res. Chem. Intermed. 32 (2006) 857–870.
[66] http://srdata.nist.gov/xps/.
[67] S. Houssenbay, S. Kazstelan, H. Toulhoat, J.P. Bonnelle, J. Grimblot, J. Phys. Chem. 93 (1989) 7176–7180.
[68] M. Chareonpanich, N. Teabpinyok, S. Kaewtaweesub, Wcecs 2008: World Congress on Engineering and Computer Science, 2008, pp. 98–102.
[69] J.H. Kim, D.J. Suh, T.J. Park, K.L. Kim, Appl. Catal. A: Gen. 197 (2000) 191–200.
[70] P. Salagre, J.L.G. Fierro, F. Medina, J.E. Sueiras, J. Mol. Catal. A 106 (1996) 125–134.
[71] M. Jitianu, A. Jitianu, M. Zaharescu, D. Crisan, R. Marchidan, Vib. Spectrosc. 22 (2000) 75–86.
[72] S. Ummartyotin, N. Koonsaeng, B. Ksapabutr, N. Yoswathananont, M. Sato, A. Laobuthee, 32nd Congress on Science and Technology of Thailand, Thailand, 2006.
[73] K.M. Lee, W.Y. Lee, Catal. Lett. 83 (2002) 65–70.
[74] K. Mocala, A. Navrotsky, J. Am. Ceram. Soc. 72 (1989) 826–832.

[75] E. Kis, R. Marinkovic-Neducin, G. Lomic, G. Boskovic, D.Z. Obadovic, J. Kiurski, P. Putanov, Polyhedron 17 (1998) 27–34.
[76] P. Dufresne, E. Payen, J. Grimblot, J.P. Bonnelle, J. Phys. Chem. 85 (1981) 2344–2351.
[77] M. Rotan, J. Tolchard, E. Rytter, M.A. Einarsrud, T. Grande, J. Solid State Chem. 182 (2009) 3412–3415.
[78] F. Iova, A. Trutia, Opt. Mater. 13 (2000) 455–458.
[79] G. Poncelet, M.A. Centeno, R. Molina, Appl. Catal. A: Gen. 288 (2005) 232–242.
[80] D. Kubička, J. Horáček, Appl. Catal. A: Gen. 394 (2011) 9–17.
[81] C. Leyva, J. Ancheyta, M.S. Rana, G. Marroquin, Fuel 86 (2007) 1232–1239.
[82] J.T. Richardson, Ind. Eng. Chem. Fundam. 3 (1964) 154–158.

Applied Catalysis B: Environmental 145 (2014) 101–107

Contents lists available at ScienceDirect

Applied Catalysis B: Environmental

journal homepage: www.elsevier.com/locate/apcatb

Effect of support-active phase interactions on the catalyst activity and selectivity in deoxygenation of triglycerides

David Kubička[a,*], Jan Horáček[a], Michal Setnička[b], Roman Bulánek[b], Arnošt Zukal[c], Iva Kubičková[a]

[a] *Research Institute of Inorganic Chemistry, RENTECH-UniCRE, Chempark Litvínov, Záluží – Litvínov, 436 70, Czech Republic*
[b] *Department of Physical Chemistry, Faculty of Chemical Technology, University of Pardubice, Studentská 573, 532 10 Pardubice, Czech Republic*
[c] *J. Heyrovský Institute of Physical Chemistry, Academy of Sciences of the Czech Republic, v.v.i., Dolejškova 3, 182 23 Prague, Czech Republic*

ARTICLE INFO

Article history:
Received 14 October 2012
Received in revised form
25 December 2012
Accepted 11 January 2013
Available online 18 January 2013

Keywords:
Deoxygenation
Vegetable oils
Effect of support
Supported NiMo catalysts

ABSTRACT

Three industrially important supports, SiO_2, TiO_2 and Al_2O_3, were used for preparation of NiMo catalysts (3.3 wt.% Ni and 15.0 wt.% Mo) and used in deoxygenation of rapeseed oil in presence of hydrogen (3.5 MPa) at 260–300 °C and liquid feed weight-hourly space velocity in the range 2–8 h^{-1}. Due to the same method of preparation and activation (sulfidation) of the catalysts, the final properties were affected mainly by the differences in the nature of supports as well as their properties, such as specific surface area, pore size distribution or acidity. Most notably the dispersion of the active phase decreased in the following order $SiO_2 > Al_2O_3 > TiO_2$. As a result, the SiO_2-supported NiMo catalyst exhibited smaller extent of hydrogenation reactions and a larger extent of decarboxylation. On the other hand, the TiO_2-supported NiMo catalyst exhibited increased selectivity to hydrodeoxygenation products, plausible due to the larger active phase cluster size and broad pore size distribution. The results provide clear evidence that even with the conventional hydrotreating active phase, such as sulfided NiMo, the selectivity can be fine-tuned by support selection and modification.

1. Introduction

Deoxygenation of triglycerides is one of key processes making possible a convenient production of high quality automotive fuels components (sulfur-, oxygen- and aromatics-free). Various alternative routes for upgrading of triglycerides and related feedstocks, such as free fatty acids, into hydrocarbons have been reported in the literature [1–3]. Three most promising options include (i) catalytic cracking of triglycerides [4–11] under conditions similar to those of fluid catalytic cracking, (ii) decarboxylation using supported Pd catalysts [12–19] and (iii) hydrotreating using conventional hydrotreating catalysts, i.e. supported sulfides of Mo or W promoted by Ni or Co [20–32].

The advantage of catalytic cracking is that deoxygenation can be accomplished without hydrogen consumption. However, the process exhibits rather low selectivity towards diesel fuel components as gaseous and gasoline-range products are formed. The yields vary significantly depending on the catalyst type [4,7–9,11]. The highest yield of diesel cut products were obtained when using hierarchical zeolites (micro-mesoporous materials, such as ZSM-5–MCM-41) [8,33]. Moreover, due to the acid nature of cracking catalysts, cyclization and hydrogen transfer reactions resulting in formation of aromatics take place in addition to cracking and deoxygenation reactions. Consequently, the diesel fuel properties (cetane number, aromatics content) are worse as compared with hydrodeoxygenation products.

The alternative approach using noble metal catalysts, particularly palladium on carbon, is highly selective, as fatty acids undergo virtually exclusively decarboxylation [12]. Moreover, the reaction does not per se consume hydrogen [12], nonetheless, it has been demonstrated that hydrogen helps in preventing rapid catalyst deactivation by side reactions [14,17,19]. Hydrogen is also needed to saturate any double bonds in the fatty acid moieties to be deoxygenated in order to obtain deoxygenated product having good thermal and oxidation stability. From the industrial perspective point of view, long-term stability and activity of Pd/C catalysts for deoxygenation was not yet demonstrated hindering their widespread application. Recently, another alternative class of catalytic materials has attracted attention for deoxygenation of triglycerides, namely carbides, nitrides and phosphides of molybdenum or nickel [34–36]. These materials offer several advantages for processing of neat triglycerides as these catalysts are stable with time-on-stream [36] and co-feeding of sulfur-containing compounds, which is required for sulfided catalysts to maintain their activity, can be avoided. Since these catalysts are sulfur resistant, co-processing of refinery feeds with triglycerides is possible as well [36].

In contrast to the previous two alternatives, sulfided hydrotreating catalysts have been shown as active and selective catalysts and

---

[*] Corresponding author.
E-mail address: david.kubicka@vuanch.cz (D. Kubička).

0926-3373/$ – see front matter © 2013 Elsevier B.V. All rights reserved.
http://dx.doi.org/10.1016/j.apcatb.2013.01.012

have been also employed commercially [37,38]. While diesel fuel components are obtained selectively, the only by-products being water, carbon oxides and propane, even at total conversion, and the catalysts are well-known and widely used in the industry, there are several disadvantages to this approach. They include higher consumption of hydrogen than in decarboxylation or cracking [1], need of an external sulfur source to keep the sulfided catalyst in active state [30] and possible formation of sulfur species in the final product [39]. Generally, the formation of new sulfur-containing species is rather limited not threatening the diesel fuel specification limits and hydrogen-sulfide-containing hydrogen streams are readily available in conventional refineries. Hence, the most significant challenge, both from the environmental as well as economical point of view, is the high hydrogen consumption caused by the high oxygen content of triglycerides and fatty acids (ca. 11 wt.%).

The issue can be, in principal, tackled by varying the selectivity of the two main reaction pathways, namely hydrodeoxygenation (HDO) and decarboxylation (HDC). Assuming a model triglyceride consisting exclusively of C_{18} fatty acids moieties, then in HDO is oxygen eliminated as water and *n*-octadecane (*n*-C_{18}) is formed while in HDC oxygen is removed primarily as CO_2 and *n*-heptadecane (*n*-C_{17}) is formed. Looking at the different stoichiometric requirements for hydrogen consumption in the just described reaction pathways, it becomes obvious that hydrogen consumption could be reduced if one could steer the selectivity towards the HDC pathway. Another aspect that needs to be noted is that by favoring decarboxylation pathway, the yield of diesel fuel range products will be decreased (approximately by 5–6%), as there will be one carbon atom less in the final products than in the case of HDO reaction pathway.

The aim of the work is to investigate the effect of catalyst support on its deoxygenation performance, in particular on the selectivity towards HDO and HDC, respectively. Hence three NiMo catalysts having the same active phase composition were prepared using different industrially relevant supports (Al_2O_3, SiO_2, TiO_2). The deoxygenation performance focusing on deoxygenation products distribution was investigated under typical deoxygenation conditions reported previously [24,32] using rapeseed oil as model feedstock.

2. Experimental

2.1. Catalyst preparation and characterization

NiMo catalysts having the same loading of active components (Ni–3.3 wt.% and Mo–15 wt.%) and different support (Al_2O_3, SiO_2 and TiO_2) were prepared by incipient wetness. The commercial supports were crushed and the fraction 0.25–0.50 mm was used in catalyst preparation. Aqueous solutions of $Ni(NO_3)_2{\cdot}6H_2O$ and $(NH_4)_6Mo_7O_{24}{\cdot}4H_2O$ were used as the source of nickel and molybdenum, respectively. A two-step procedure was applied. At first the catalyst was impregnated with $(NH_4)_6Mo_7O_{24}{\cdot}4H_2O$ to contain 15 wt.% Mo and dried at 95–100 °C. Then it was calcined in an oven at 400 °C. Subsequently, the Mo-containing support was impregnated with $Ni(NO_3)_2{\cdot}6H_2O$ to contain 3.3 wt.% of Ni and dried again at 95–100 °C. Finally, the catalyst was calcined at 400 °C. The same procedure was used for all three supports.

The catalysts were characterized by several physico-chemical methods to assess their relevant catalytic properties. The methods included N_2 physisorption isotherm, DR UV–vis and FTIR spectroscopy, H_2 TPR and NH_3 TPD, and elemental composition (C, S). Nitrogen physisorption method was used to determine textural properties of catalysts (specific surface area and pore size distribution) using a Micromeritics ASAP 2020 volumetric instrument at −196 °C, for details see [40]. The BET surface area was evaluated using adsorption data in a relative pressure range from 0.05 to 0.25 and mesopore size distributions were calculated using BJH algorithm using Harkins–Jura equation calibrated to accurately determine the pore diameter and volume.

The UV–vis diffuse reflectance spectra of dehydrated samples were measured using Cintra 303 spectrometer (GBC Scientific Equipment, Australia) equipped with a Spectralon-coated integrating sphere using a Spectralon coated discs as a standard. The spectra were recorded in the range of the wavelength 190–850 nm. Before the spectra measurement the samples were dehydrated and oxidized in the glass apparatus under static oxygen atmosphere (15 kPa) in two steps: 120 °C for 30 min and 450 °C for 60 min and subsequently cooled down to 250 °C and evacuated for 30 min. After the evacuation the samples were transferred into the quartz optical cuvette 5 mm thick and sealed under vacuum. This procedure guaranteed complete dehydration and defined oxidation state of all $NiMoO_x$ particles on the catalyst surface. The obtained reflectance spectra were transformed into the dependencies of Kubelka–Munk function $F(R_\infty)$ on the wavenumber [41].

Redox behavior and dispersion of $NiMoO_x$ surface species was investigated by the temperature programmed reduction by hydrogen (H_2-TPR) using the AutoChem 2920 (Micromeritics, USA). A 100 mg sample in a quartz U-tube microreactor was oxidized in oxygen flow at 450 °C for 60 min prior the TPR measurement. The reduction was carried out from 50 °C to 1 050 °C with a temperature gradient of 10 °C/min in flow (25 ml/min) of reducing gas (5 vol% H_2 in Ar). The changes of hydrogen concentration were monitored by the TCD detector and simultaneously hydrogen consumption and water formation was also detected on a quadrupole mass spectrometer OmniStar^{TM} GDS 300 (Pfeiffer vacuum, Germany).

Acidity of supported NiMoO catalysts was investigated by the temperature programmed desorption of ammonia (NH_3-TPD). NH_3-TPD experiments were carried out on the same instrument as H_2-TPR. Before each experiment a 100 mg of sample were pretreated in a flow of dry oxygen at 450 °C for 60 min and after that the sample was exposed to NH_3 (5 vol% NH_3 in He) at 75 °C for 30 min. The physically adsorbed ammonia was removed by purging with a helium flow for 30 min. Then the TPD was performed in He flow (25 ml/min) with a temperature gradient of 10 °C/min and the desorbed NH_3 was monitored by a TCD detector and by mass spectrometer which allow a monitoring other products of desorption as well.

2.2. Catalytic experiments

The catalytic experiments were carried out in an electrically-heated fixed bed reactor (inner diameter 17 mm) using rapeseed oil as a feedstock (food grade quality, without addition of sulfiding agent) in presence of hydrogen (3.5 MPa) at 260–300 °C. The sulfiding agent was not used to have a clear view on the effect of support only. The liquid feed weight-hourly space velocity was varied in the range 2–8 h^{-1}, while the hydrogen to liquid feed ratio was kept constant at 50 mol/mol. A wide range of LHSV was used in order to evaluate the selectivity changes over a wide range of conversions and degrees of deoxygenation. The conversion and degree of deoxygenation is defined in Eqs. (1) and (2), respectively:

$$\text{Conversion} = \frac{C_{TG_0} - C_{TG}}{C_{TG_0}} \times 100 \tag{1}$$

$$\text{Degree of deoxygenation} = \frac{C_{OX_0} - C_{OX}}{C_{OX_0}} \times 100 \tag{2}$$

where C_{TG_0} and C_{OX_0} are the concentration of triglycerides and oxygen, respectively, in the feedstock, and C_{TG} and C_{OX} are the concentration of triglycerides and oxygen in products.

Table 1
Basic physico-chemical properties of studied catalysts.

	BET (m^2/g)	S (wt.%)	C (wt.%)
NiMo/SiO_2	343 (524)[a]	15.6	5.6
NiMo/Al_2O_3	177 (198)[a]	9.8	5.9
NiMo/TiO_2	117 (203)[a]	7.1	5.5

[a] The number in parentheses gives the BET surface area of the support.

The NiMo catalysts (particle size 0.25–0.50 mm) were loaded in the reactor and were diluted with silicon carbide (particle size 0.1 mm) to improve the temperature profile along the catalyst bed. The profile was monitored by three adjustable thermocouples placed in a thermowell located in the axis of the reactor. The void space above the catalyst bed was filled with silicon carbide and in this part of the reactor the feed and hydrogen were preheated, mixed and distributed over the reactor cross-section. The catalyst was activated (sulfided) in situ prior to each experiment using dimethyldisulfide (DMDS) in isooctane. The sulfiding procedure lasted 10 hours including a dwell at 340 °C.

Several samples from each reaction condition were collected and analyzed by GC equipped with an on-column injection system and a flame ionization detector. Details of the analytical method were reported previously elsewhere [24,32].

3. Results and discussion

3.1. Catalyst characterization

The catalysts were prepared by incipient wetness impregnation to contain the same concentration of active components, i.e. 3.3 wt.% Ni and 15.0 wt.% Mo. The final catalysts differed in their specific surface area as shown in Table 1. The sulfur content of the catalysts, measured after reaction, exhibited a linear correlation with the catalyst specific surface area as it increased from 7.1 wt.% for NiMo/TiO_2 to 15.6 wt.% for NiMo/SiO_2 (Table 1). Since the metal content and preparation and pre-treatment methods were identical, it can be concluded that the dispersion of the active NiMo phase increased in the order $TiO_2 < Al_2O_3 < SiO_2$ which can also be associated with the available specific surface area that increased in the same order. At the same time, the content of carbon, reflecting the amount of carbonaceous deposits on the catalyst surface, was virtually the same for all three catalysts regardless their total specific surface area (Table 1). This indicates that the deactivation reactions proceeded approximately at the same rate. Moreover, TiO_2-supported catalyst exhibited a rather broad pore size distribution, while SiO_2 and Al_2O_3-supported catalysts showed a narrow and unimodal pore size distribution centered around 6 and 9 nm, respectively (Fig. 1). In all three cases the pore sizes are sufficient for triglycerides to enter them.

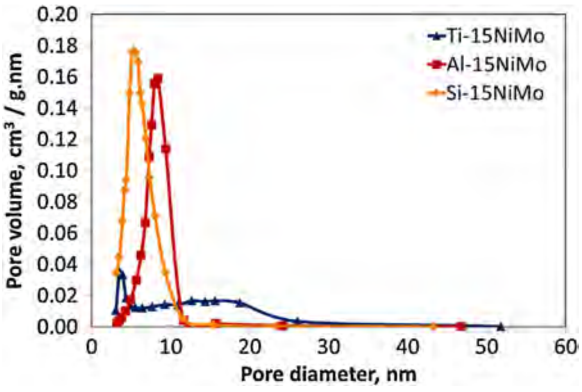

Fig. 1. Pore size distribution of the catalysts determined by BJH method.

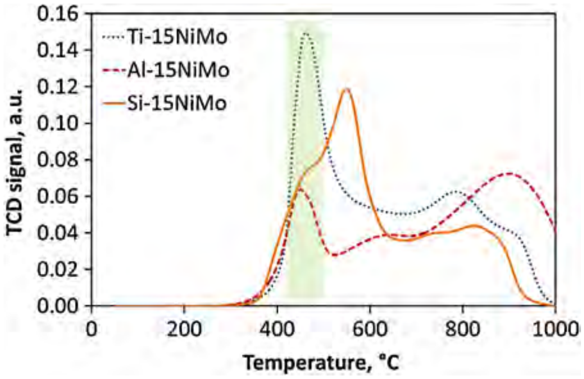

Fig. 2. Temperature programmed reduction (H_2-TPR) of catalysts. The shaded area (420–500 °C) shows the position of the first reduction peak.

The catalysts exhibited different temperature programmed reduction profiles (H_2-TPR, Fig. 2) indicating that there were differences in the active phase-support interaction. The main reduction peak corresponding to the active phase reduction was located approximately between 350 and 600 °C (Fig. 2). As the active phase composition was identical, these differences could be explained by different strength of active phase-support interaction reflecting the support nature and active phase cluster size. The TiO_2-supported catalyst was the most easily reduced (reduction maximum at 460 °C) probably due to the largest active phase cluster size (as indicated by the lowest sulfur content in the sulfided catalyst) weakening the active phase-support interaction, whereas the SiO_2-supported catalyst showed a clear shift to higher reduction temperature (ca. 550 °C). It could be attributed to the smaller active phase cluster size (as indicated by the catalyst sulfur content, Table 1) and hence more intimate contact with the support (Fig. 2, Table 2). Finally, it was seen that alumina-supported catalyst was the most difficult to reduce suggesting a strong interaction of the intermediate clusters of active phase.

The UV–vis spectra of the catalysts did not exhibit any surprising features (Fig. 3). It could be seen that the nickel in tetrahedral coordination Ni(Td), typically recognizable by a band around 17000 cm^{-1}, was absent (Fig. 3, compare with [32]). A close inspection of the bands corresponding to nickel in octahedral coordination Ni(Oh) revealed though that there was an important difference in the intensity and hence in population of the Ni(Oh) species at ca. 22500 cm^{-1} in different catalysts (Fig. 3). While a very intense band was found in the case of SiO_2-supported catalyst, this band was absent in the case of alumina-supported catalyst and only a shoulder was visible (taking into account the shift of the edge) in the case of TiO_2-supported catalyst (Fig. 3). It might be speculated that this band could be connected with shift in H_2-TPR to higher reduction temperature and, in turn, with the differences in selectivity as discussed later. Obviously, further fundamental investigations are needed to prove or disprove this conclusion.

The measurements of temperature programmed desorption of ammonia demonstrated differences among the catalysts in the

Table 2
H_2-TPR and NH_3-TPD characteristic data.

	H_2-TPR		NH_3-TPD	
	H_2 consumption mmol	T_{max} (°C)	Desorbed NH_3 mmol	T_{max} (°C)
NiMo/SiO_2	3.0	549	108.1	160
NiMo/Al_2O_3	3.1	896	98.3	167
NiMo/TiO_2	3.7	461	54.1	195

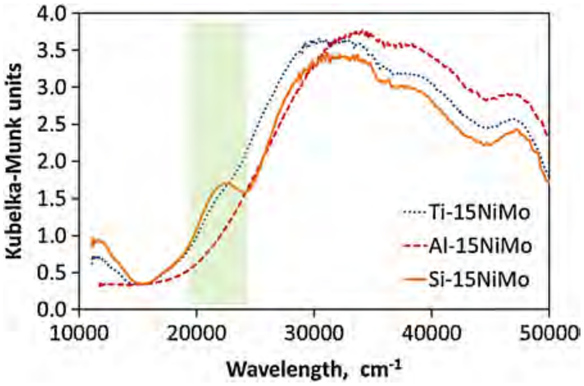

Fig. 3. UV–vis spectra of catalysts (in oxide form). The shade area shows the Ni(Oh) region exhibiting difference among the catalysts.

amount of acid sites interacting with ammonia as well as in their strength. The highest amount of acid sites contained the SiO_2-supported catalyst, which could be explained by the largest surface area and the best dispersion of the active phase resulting in high number of Lewis acid sites originating from dispersed $MoNiO_x$ phase and alternatively remaining silanols, as the desorption peak was at low temperature (ca. 160 °C, Fig. 4). A desorption peak at a similar position (desorption temperature) could be also seen in the remaining two catalysts. In contrast to SiO_2-supported catalyst, TiO_2- and Al_2O_3-supported catalysts had a second desorption peak with a maximum around 300 °C (Fig. 4). It was thus clear that there was another type of acid sites in these two catalysts and that these sites were stronger than the acid sites found in the SiO_2-supported catalyst. The population of these sites was the largest in the case of Al_2O_3-supported catalyst and it could be one of the reasons for stronger interaction between the active phase and support and consequently for the lower reducibility of the alumina-supported catalyst.

The catalyst characterization results showed rather convincingly that the SiO_2-supported NiMo catalyst exhibited, in spite of the same composition of the active phase and catalyst preparation and activation procedures, different properties than the other two catalysts (TiO_2- and Al_2O_3-NiMo supported catalysts). The above-discussed differences could be related to one common denominator, namely the interaction between the active phase and the support.

3.2. *Catalytic experiments*

Sulfided NiMo active phase supported on three different industrially relevant supports – Al_2O_3, SiO_2 and TiO_2 – had the ability to convert triglycerides completely into products at 300 °C (Fig. 5A). This is in line with previous reports [20,24,32]. With decreasing reaction temperature the conversion decreased and at 260 °C it was in the range 52–62% for all three catalysts (Fig. 5A). Despite the large conversion achieved, it can be clearly seen that the degree of deoxygenation (defined as reduction in oxygen content as compared to the feedstock, Eq. (2)) was significantly lower than conversion (Fig. 5B). The information about oxygen content was calculated from concentration of individual products determined by GC analysis of products. It can be observed that within the range of temperature ca. 250–300 °C, at WHSV of 4 h^{-1}, hydrogen pressure 3.5 MPa and hydrogen to feed ratio of 50 mol_{H2}/mol_{feed} the deoxygenation degree varied from 0 to 100%, i.e. from exclusive formation of oxygenated products to sole formation of hydrocarbons. It can be concluded that oxygenates are reaction intermediates.

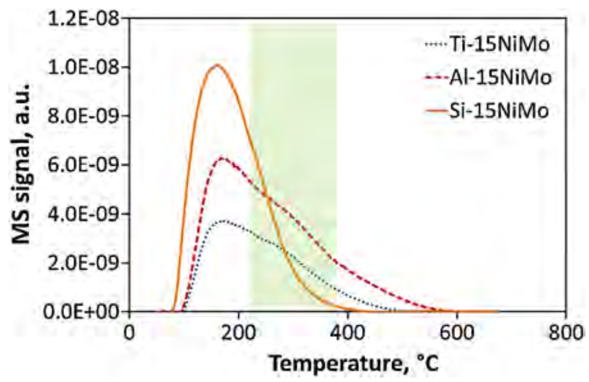

Fig. 4. Temperature-programmed desorption (TPD) of NH_3 of catalysts (in oxide form). The shaded area shows the second desorption peak of ammonia.

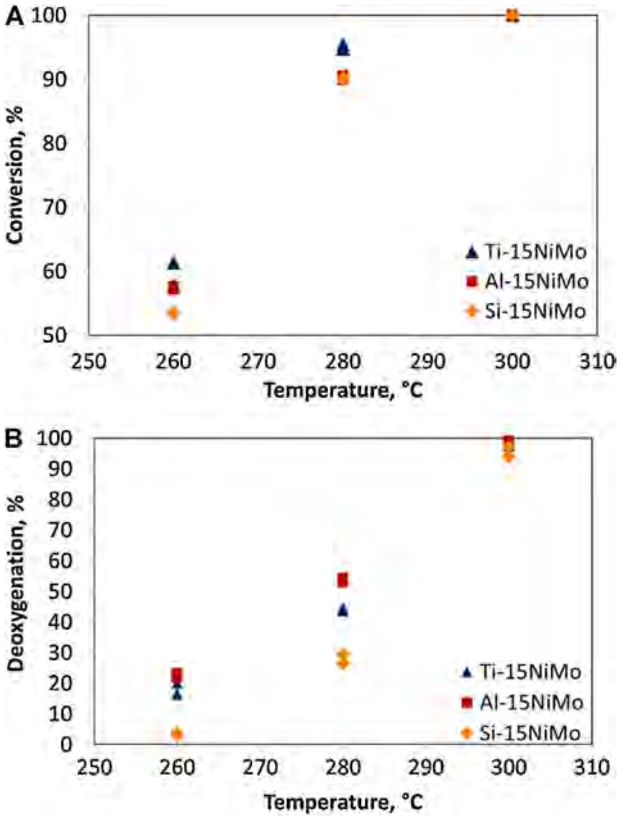

Fig. 5. Conversion, A, and deoxygenation, B of rapeseed oil as a function of reaction temperature (260–300 °C) at 4 h^{-1}, 3.5 MPa and 50 mol_{H_2}/mol_{feed}.

This conclusion is valid in the entire experimental range, i.e. at 260–300 °C and 2–8 h^{-1} (Fig. 6) where yields of oxygenated products and hydrocarbons are plotted as a function of degree of deoxygenation. While the general trend in the dependence of the yields of oxygenated products on the degree of deoxygenation is an expected one, there are obvious differences among the studied supports. At the same degree of deoxygenation, the highest yield of hydrocarbons is obtained over SiO_2-supported catalyst and the lowest over TiO_2-supported catalyst (Fig. 6B). This is also reflected in the shift of the maximum on the yield curve of oxygenates towards higher deoxygenation degree from SiO_2 to TiO_2-supported catalyst (Fig. 6A). The difference among the supports stems from different relative reaction rates of hydrodeoxygenation (HDO) and decarboxylation (HDC) reactions over sulfided NiMo active phase supported on these supports. This can be clearly seen from analysis of yield curves of the main product groups that were denoted as oxygenated products, namely fatty acids, fatty alcohols and fatty esters.

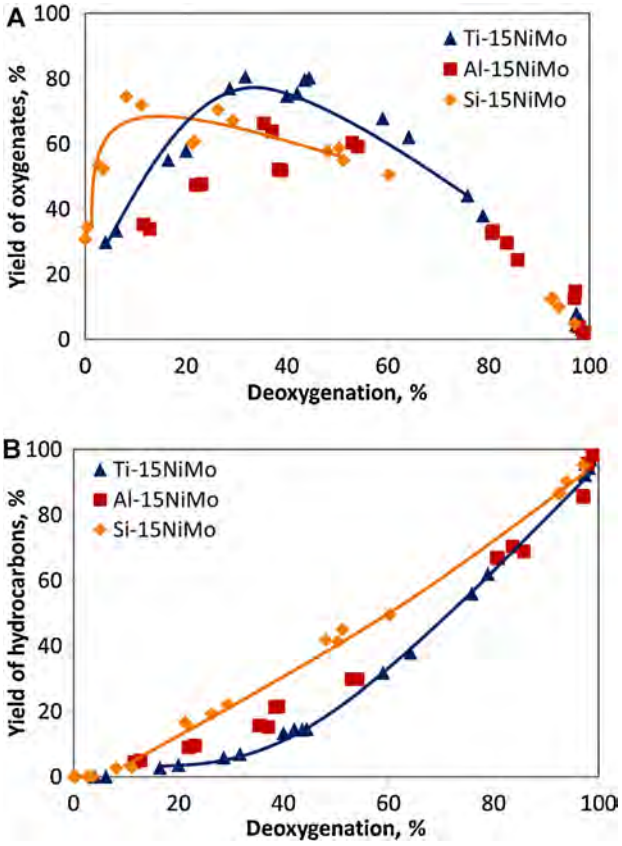

Fig. 6. Yields of the main product groups (oxygenated products (A) and hydrocarbons (B)) as a function of deoxygenation performance of the catalysts at 260–300 °C, 2–8 h^{-1}, 3.5 MPa and 50 mol_{H_2}/mol_{feed}.

The mutual interdependence (inter-conversion) of these products including formation of byproducts is schematically depicted in Fig. 7. Generally speaking, fatty acids originate from hydrogenolysis of triglycerides, fatty alcohols are products of reduction (hydrogenation) of carboxylic group in fatty acids and fatty esters are products of reaction between the former two groups of products. The yield curves support this claim as fatty acids can be seen as the primary products followed by fatty alcohols and fatty esters (Fig. 8A). The less pronounced yield curve of fatty alcohols (Fig. 8B) is a consequence of their higher reactivity in comparison with fatty acids or esters [42]. As a result, the concentration of fatty alcohols appears to be the rate-limiting step for the formation of fatty esters (Fig. 8C). The general scheme is in agreement with previous investigations [24].

An inspection of the Fig. 8 reveals that there is a significant difference among the supports. The high yield of fatty acids over SiO_2-supported NiMo catalyst in comparison with the remaining two supports (50 vs. ca. 20% at deoxygenation degree of ca. 25%, Fig. 8A) combined with the significantly lower yield of fatty esters (ca. 20% for SiO_2 vs. ca. 50% for TiO_2 at deoxygenation degree of ca. 25%, Fig. 8C) can be attributed to lack of fatty alcohols (Fig. 8B) in the product mixture. As the active phase and its composition is the same for all studied catalysts, it can be inferred that the differences are due to the involvement of the support, i.e. that the support affects the performance of the catalyst in other way than just influencing the active phase dispersion. The experimental data indicate that in the case of SiO_2-supported catalyst, fatty alcohols are not formed (Fig. 8B) rather than they are immediately consumed by deoxygenation. If it was the case, the fatty acids should have been consumed faster, as it is seen in the case of TiO_2 and Al_2O_3-supported catalysts (Fig. 8A). It can be thus concluded the catalyst hydrogenation performance in deoxygenation is affected by the support type. The performance of TiO_2 and Al_2O_3-supported catalysts is in this respect more similar to each other (Fig. 8), the main difference being the yield of fatty esters that is substantially lower in the case of Al_2O_3-supported catalyst (Fig. 8C). As the yield

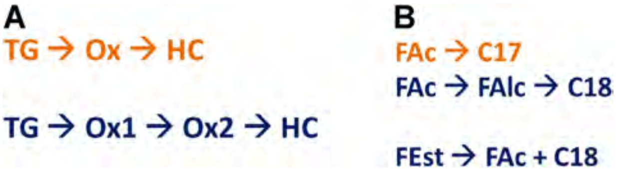

Fig. 7. Schematic representation of (A) triglycerides (TG) deoxygenation to oxygenated products (Ox) and hydrocarbons (HC) and of (B) fatty acid (FAc) intermediates deoxygenation to decarboxylation products (C17) or to fatty alcohols (FAlc) and hydrodeoxygenation products (C18). Fatty esters (FEst) deoxygenation is captured as well.

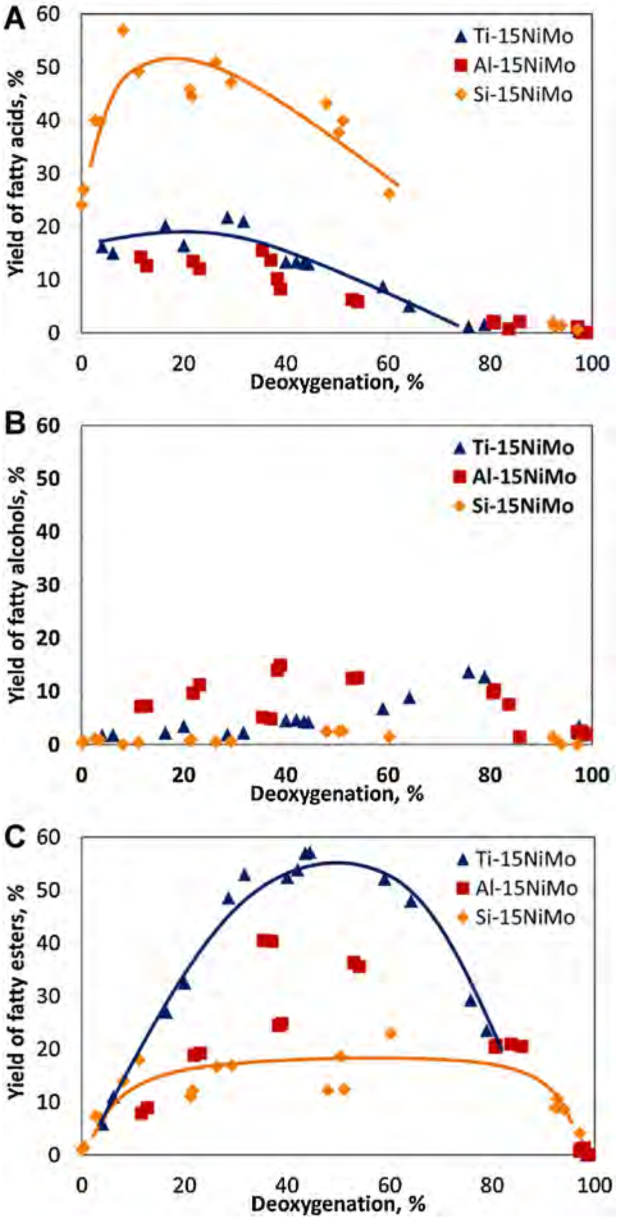

Fig. 8. Yields of fatty acid (A) fatty alcohols (B) and fatty esters (C) as a function of deoxygenation performance of the catalysts at 260–300 °C, 2–8 h^{-1}, 3.5 MPa and 50 mol_{H_2}/mol_{feed}.

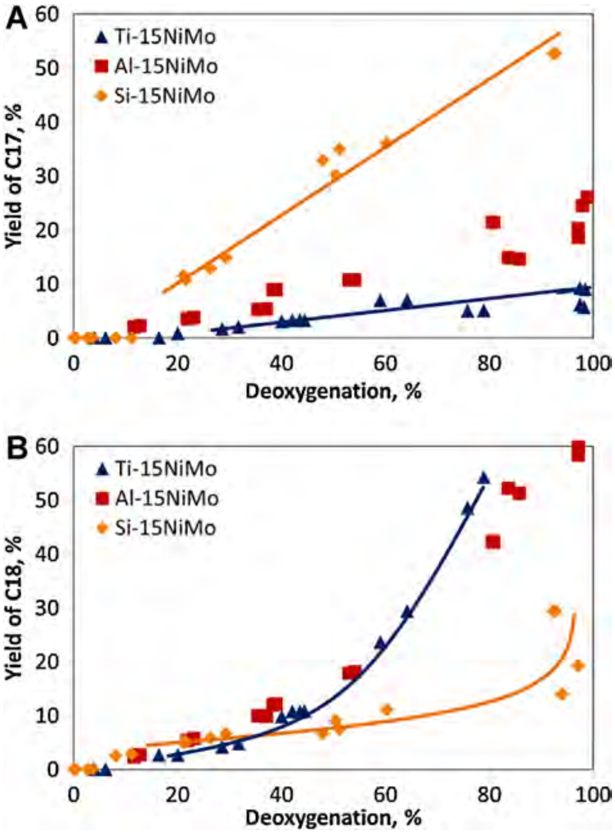

Fig. 9. Yields of *n*-heptadecane (A) and *n*-octadecane (B) as a function of deoxygenation performance of the catalysts at 260–300 °C, 2–8 h^{-1}, 3.5 MPa and 50 mol_{H_2}/mol_{feed}.

of fatty alcohols is at the same time slightly higher than in the case of TiO_2-supported catalyst, it can be suggested that the Al_2O_3 catalyst is more efficient in hydrogenation.

The observed differences in oxygenated products distribution are further propagated in the distribution of the ultimate deoxygenation products, hydrocarbons (Fig. 9). The SiO_2-supported NiMo catalyst yielded *n*-heptadecane as the main deoxygenation product, while Al_2O_3- and particularly TiO_2-supported catalysts afforded *n*-octadecane as the main deoxygenation product (Fig. 9). This means that over SiO_2-supported NiMo catalyst decarboxylation was preferred to hydrodeoxygenation. In contrast, over Al_2O_3 and above all TiO_2-supported NiMo catalysts hydrodeoxygenation was the predominant reaction pathway. The differences are summarized in Fig. 10 depicting the value of C_{18}/C_{17} ratio as a function of the overall deoxygenation degree. If equal to unity, there is the same extent of hydrodeoxygenation and decarboxylation. It can be seen that for SiO_2-supported catalyst the C_{18}/C_{17} ratio is less than one at complete deoxygenation, while over TiO_2-supported NiMo catalyst as high value as ten is achieved at complete deoxygenation (Fig. 10). With Al_2O_3-supported NiMo catalyst the final C_{18}/C_{17} ratio is about four (Fig. 10).

It is known that the preferred deoxygenation pathway can be related to catalyst composition. Alumina-supported Ni sulfided catalysts were shown to act virtually exclusively as decarboxylation catalysts whereas Mo sulfided catalysts exhibited a strong preference towards hydrodeoxygenation [24]. Variations in the yield of C_{17} and C_{18} hydrocarbons have been reported also for differently pretreated NiMo catalysts supported on Al_2O_3 [32]. It has been shown that with increasing content of NiO having tetrahedral coordination (result of high calcination temperature) the C_{18}/C_{17} ratio increased, i.e. that hydrodeoxygenation was preferred over decarboxylation [32].

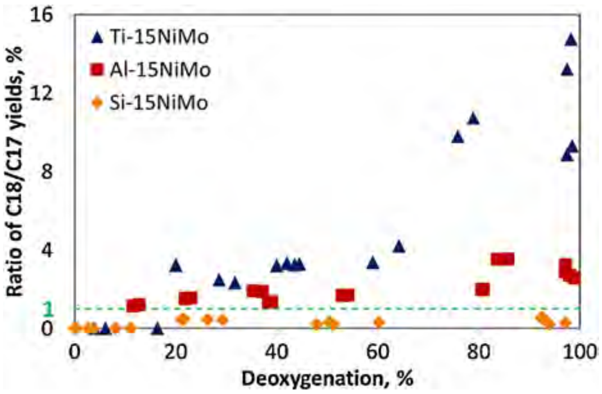

Fig. 10. Molar ratio of *n*-octadecane to *n*-heptadecane (C_{18}/C_{17}) as a function of deoxygenation performance of the catalysts at 260–300 °C, 2–8 h^{-1}, 3.5 MPa and 50 mol_{H_2}/mol_{feed}.

As all the catalysts investigated here were pre-treated using the same procedure and the UV–vis spectra indicate that NiO is present only in octahedral coordination (Fig. 3), the noteworthy difference in C_{18}/C_{17} ratio (Fig. 10) among the investigated supports can be attributed to a role of the support. The SiO_2-supported NiMo catalyst affording mostly decarboxylation products, it can be inferred that it is a consequence of its different properties, namely higher dispersion giving rise to stronger active phase-support interaction. This can be observed not only in the shift in TPR profile to higher reduction temperature, but also plausibly by a specific Ni(Oh) band present in the UV–vis spectra at 22500 cm^{-1}. A plausible reason for the exceptional hydrodeoxygenation selectivity of the TiO_2-supported NiMo catalyst is not fully understood. The characterization results though indicate that the broad pore size distribution together with the largest active phase clusters among the tested catalyst might be the cause.

The differences in catalyst performance might originate not only from different interaction between the support and sulfide phase, but they can be plausibly related also to the differences in interaction between the oxides and the different supports. As seen from TPR, there is the formation of different types of metal oxide phase which could result in (after sulfiding) MoS_2 slabs having different stacking thus explaining the observed differences in deoxygenation selectivity. While the effects of promotion and structure (brim or edge sites, vacancies) of MoS_2 slabs and their influence on activity and selectivity of hydrotreating catalysts have been studied in great detail [43], there is still lack of knowledge regarding the relationship between deoxygenation activity/selectivity and catalyst structure although some theoretical and experimental attempts have been recently done [44].

4. Conclusions

Three different industrially important supports, SiO_2, TiO_2 and Al_2O_3, were used for preparation of NiMo catalysts to be used in deoxygenation of rapeseed oil. The catalysts were prepared using the same method and activation (sulfidation) procedure and had the same concentration of active components (3.3 wt.% Ni and 15.0 wt.% Mo). Due to the differences in the nature of supports as well as their properties, such as specific surface area, pore size distribution or acidity, the final properties differed as well. Most notably the dispersion of the active phase decreased in the following order $SiO_2 > Al_2O_3 > TiO_2$. Moreover, the different active phase cluster size and support nature were reflected in differences in active phase reducibility and in the character of Ni(Oh) species that were the only NiO coordination type. These changes could be connected with the observed differences in catalyst selectivity as their overall activity was affected only to a lesser extent. The SiO_2-supported NiMo catalyst exhibited smaller extent of hydrogenation reactions and a larger extent of decarboxylation. As a result, *n*-heptadecane was the main product and at a given deoxygenation level less oxygenated products were yielded in comparison with the other two catalysts. On the other hand, the TiO_2-supported NiMo catalyst exhibited increased selectivity to hydrodeoxygenation products, plausible due to the larger active phase cluster size and broad pore size distribution. The results provide clear evidence that even with the conventional hydrotreating active phase, such as sulfided NiMo, the selectivity can be fine-tuned by support selection and modification.

Acknowledgements

The authors thank the Czech Science Foundation for financial support (Centre of Excellence–P106/12/G015). The project (P106/12/G015) is being carried out in the UniCRE centre (CZ.1.05/2.1.00/03.0071) in the Research Institute of Inorganic Chemistry.

References

[1] I. Kubičková, D. Kubička, Waste Biomass Valorization 1 (2010) 293.
[2] S. Lestari, P. Mäki-Arvela, J. Beltramini, G.Q. Max Lu, D.Yu. Murzin, ChemSusChem 2 (2009) 1109–1119.
[3] D. Kubička, I. Kubičková, J. Čejka, Catal. Rev. Sci. Eng. 55 (2013) 1–78.
[4] F.A. Twaiq, N.A.M. Zabidi, S. Bhatia, Industrial and Engineering Chemistry Research 38 (1999) 3230–3237.
[5] J.D. Adjaye, S.P.R. Katikaneni, N.N. Bakhshi, Fuel Processing Technology 48 (1996) 115–143.
[6] S.P.R. Katikaneni, J.D. Adjaye, N.N. Bakhshi, Canadian Journal of Chemical Engineering 73 (1995) 484–497.
[7] F.A. Twaiq, N.A.M. Zabidi, S. Bhatia, Microporous and Mesoporous Materials 64 (2003) 95–107.
[8] Y.-S. Ooi, R. Zakaria, A.R. Mohamed, S. Bhatia, Energy Fuels 19 (2005) 736–743.
[9] T. Danuthai, S. Jongpatiwut, T. Rirksomboon, S. Osman, D.E. Resasco, Applied Catalysis A: General 361 (2009) 99–105.
[10] T. Danuthai, S. Jongpatiwut, T. Rirksomboon, S. Osman, D.E. Resasco, Catalysis Letters 132 (2009) 197–204.
[11] T. Sooknoi, T. Danuthai, L.L. Lobban, R.G. Mallinson, D.E. Resasco, Journal of Catalysis 258 (2008) 199–209.
[12] I. Kubičková, M. Snåre, K. Eränen, P. Mäki-Arvela, D.Yu. Murzin, Catalysis Today 106 (2005) 197–200.
[13] I. Simakova, O. Simakova, P. Mäki-Arvela, A. Simakov, M. Estrada, D.Yu. Murzin, Applied Catalysis A: General 355 (2009) 100–108.
[14] P.T. Do, M. Chiappero, L.L. Lobban, D.E. Resasco, Catalysis Letters 130 (2009) 9–18.
[15] M. Snåre, I. Kubičková, P. Mäki-Arvela, K. Eränen, D.Yu. Murzin, Industrial and Engineering Chemistry Research 45 (2006) 5708–5715.
[16] P. Mäki-Arvela, I. Kubičková, M. Snåre, K. Eränen, D.Yu. Murzin, Energy Fuels 21 (2007) 30–41.
[17] B. Rozmyslowicz, P. Mäki-Arvela, A. Tokarev, A.-R. Leino, K. Eränen, D.Yu Murzin, Industrial and Engineering Chemistry Research 51 (2012) 8922–8927.
[18] L. Boda, G. Onyestyák, H. Solt, F. Lónyi, J. Valyon, A. Thernesz, Applied Catalysis A: General 374 (2010) 158–169.
[19] J.G. Immer, M.J. Kelly, H.H. Lamb, Applied Catalysis A: General 375 (2010) 134–139.
[20] B. Donnis, R.G. Egeberg, P. Blom, K.G. Knudsen, Topics in Catalysis 52 (2009) 229–240.
[21] G.N.d. Rocha Filho, D. Brodzki, G. Djega-Mariadassou, Fuel 72 (1993) 543–549.
[22] J. Gusmão, D. Brodzki, G. Djega-Mariadassou, R. Frety, Catalysis Today 5 (1989) 533–544.
[23] E. Laurent, B. Delmon, Applied Catalysis 109 (1994) 77–96.
[24] D. Kubička, L. Kaluža, Applied Catalysis A: General 372 (2010) 199–208.
[25] G.W. Huber, P. O'Connor, A. Corma, Applied Catalysis A: General 329 (2007) 120–129.
[26] D. Kubička, Collection of Czechoslovak Chemical Communications 73 (2008) 1015–1044.
[27] S. Bezergianni, A. Dimitriadis, A. Kalogianni, P. Pilavachi, Bioresource Technology 101 (2010) 6651.
[28] S. Bezergianni, A. Dimitriadis, T. Sfetsas, A. Kalogianni, Bioresource Technology 101 (2010) 7658.
[29] D. Kubička, M. Bejblová, J. Vlk, Topics in Catalysis 53 (2010) 168.
[30] D. Kubička, J. Horáček, Applied Catalysis A: General 394 (2011) 9.
[31] J. Mikulec, J. Cvengroš, L. Joríková, M. Banič, A. Kleinová, Chemical Engineering Transactions 18 (2009) 475.
[32] P. Priecel, D. Kubička, L. Čapek, Z. Bastl, P. Ryšánek, Applied Catalysis A: General 397 (2011) 127.
[33] F.A. Twaiq, A.R. Mohamad, S.P. Bhatia, Fuel Processing Technology 85 (2004) 1283.
[34] J. Monnier, H. Sulimma, A. Dalay, G. Caravaggio, Applied Catalysis A: General 382 (2010) 176.
[35] Y. Yang, C. Ochoa-Hernández, V.A.P. O'Shea, J.M. Coronado, D.P. Serrano, American Chemical Society Catalysis 2 (2012) 592.
[36] L.A. Sousa, J.L. Zotin, V. Teixeira da Silva, Applied Catalysis A: General 449 (2012) 105.
[37] Neste Oil, http://www.nesteoil.com/default.asp?path=1,41,11991,12243,13565, 2012 (accessed October, 2012).
[38] UOP, www.uop.com, UOP/ENI Ecofining Process.pdf, 2012 (accessed October 2012).
[39] T.-R. Viljava, E.R.M. Saari, A.O.I. Krause, Applied Catalysis A: General 209 (2001) 33.
[40] A. Zukal, H. Šiklová, J. Čejka, Langmuir 24 (2008) 9837.
[41] P. Kubelka, F. Munk, Zeitschrift Technical Physics 12 (1931) 593.
[42] E. Furimsky, Applied Catalysis A: General 199 147 (2000).
[43] A. Stanislaus, A. Marafi, M.S. Rana, Catalysis Today 153 (2010) 1.
[44] M. Ruinart de Brimont, C. Dupont, A. Daudin, C. Geantet, P. Raybaud, Journal of Catalysis 286 (2012) 153.

Catalysis Today 176 (2011) 409–412

Contents lists available at ScienceDirect

Catalysis Today

journal homepage: www.elsevier.com/locate/cattod

The role of alumina support in the deoxygenation of rapeseed oil over NiMo–alumina catalysts

Peter Priecel[a], Libor Čapek[a,*], David Kubička[b], František Homola[b], Petr Ryšánek[b], Miloslav Pouzar[a]

[a] Faculty of Chemical Technology, University of Pardubice, Studentská 573, 532 10 Pardubice, Czech Republic
[b] Department of Refinery and Petrochemical Research, Research Institute of Inorganic Chemistry, Záluží 1, 436 70 Litvínov, Czech Republic

ARTICLE INFO

Article history:
Received 19 September 2010
Received in revised form 4 November 2010
Accepted 5 November 2010
Available online 16 December 2010

Keywords:
Deoxygenation
NiMo–alumina
UV–vis
Mesoporous alumina

ABSTRACT

Deoxygenation of rapeseed oil was studied over NiMo–alumina catalysts. The research was focused on supporting of Ni and Mo species on a conventional alumina ($255\,m^2\,g^{-1}$) and a commercially available mesoporous alumina ($520\,m^2\,g^{-1}$) supports and on establishing their catalytic performance. The NiMo–alumina/meso catalyst showed significantly better performance than the NiMo–alumina catalyst in deoxygenation of rapeseed oil. The better performance was attributed to the significantly higher specific surface area and the total pore volume of NiMo–alumina/meso in comparison with the NiMo–alumina.

1. Introduction

Transesterification, thermal and catalytic cracking and deoxygenation have been developed to produce the renewable fuels from vegetable oils [1]. In general, the term deoxygenation can refer to several reactions, mainly decarboxylation, decarbonylation, dehydration and hydrodeoxygenation, and is often accompanied by hydrogenation of double bonds [1,2]. The advantage of deoxygenation over transesterification and cracking is that it yields straight-chain alkanes having 15–20 carbon atoms, which, after isomerisation, are much alike the hydrocarbons found in conventional diesel. Different types of catalysts have been investigated in deoxygenation reactions with particular focus on CoMo–alumina [3], NiMo–alumina [4–6] and NiMoP–alumina [5] catalysts.

It is generally accepted that mesoporous materials offer a great potential as support for the active species in the catalytic processes [7,8]. Mesoporous alumina supports offer several advantages over conventional alumina supports, such as high specific surface area resulting in a possibility to achieve high dispersion and loading of active species on the support and narrow pore size distribution with pore size ranging from 2 to more than 10 nm [7] enabling the access of large organic molecules to the active sites situated inside the pores.

Previously, Kubička et al. [9] showed high potential of CoMo species supported on the organized mesoporous materials synthesized in a laboratory. In the present work, the attention is focused on supporting of Ni and Mo species on commercially available mesoporous and conventional alumina supports and the comparison of the activity/selectivity of NiMo–alumina/meso and NiMo–alumina catalysts in the deoxygenation of rapeseed oil.

2. Experimental

Alumina (denoted as alumina, $255\,m^2\,g^{-1}$) and mesoporous alumina (denoted as alumina/meso, $520\,m^2\,g^{-1}$) were supplied by Eurosupport Manufacturing Czechia and NanoScale Corporation, respectively. NiMo–alumina catalysts were prepared by impregnating the alumina supports with an ethanol solution of nickel acetonate tetrahydrate and molybdenyl acetylacetonate followed by calcination at 600 °C in the air flow for 5 h. NiMo–alumina and NiMo–alumina/meso catalysts were prepared with the same amount of Ni (3.0 wt.%) and Mo (6.0 wt.%). The concentration of the Ni and Mo species in the catalysts was determined with Elvatech desktop energy-dispersive XRF spectrometer Elva X equipped with a Ti anode X-ray tube. X-ray diffractograms were recorded with Bruker AXE D8-Advance diffractometer using Cu Kα radiation with a secondary graphite monochromator. UV–vis diffuse reflectance spectra of granulated catalysts (particle size 0.25–0.50 mm) were recorded using GBC CINTRA 303 spectrometer equipped with a spectralon-coated integrating sphere against a spectralon reference. The specific surface areas and the pore size distributions of the catalysts were obtained by Coulter SA 3100 Surface Area and

---

* Corresponding author.
E-mail addresses: libor.capek@upce.cz (L. Čapek), david.kubicka@vuanch.cz (D. Kubička).

0920-5861/$ – see front matter © 2010 Elsevier B.V. All rights reserved.
doi:10.1016/j.cattod.2010.11.022

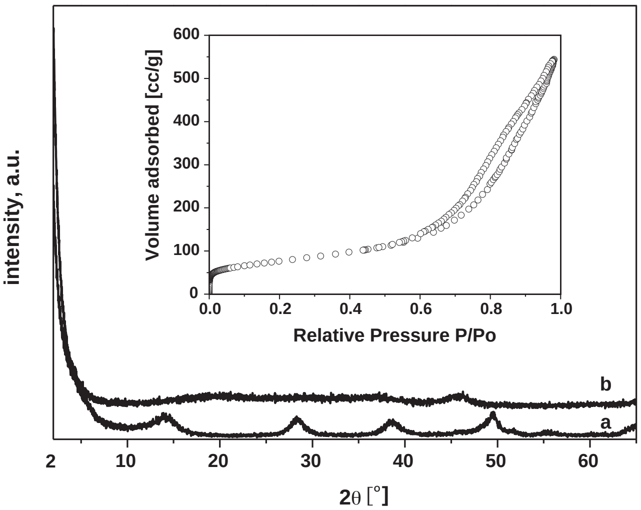

Fig. 1. (A) XRD patterns of alumina–meso (a) and NiMo–alumina–meso materials (b) and (B) adsorption/desorption isotherms of NiMo–alumina–meso catalyst.

Pore Size Analyzer. Specific surface area was calculated by the BET method and the pore size distribution (pore diameter and pore volume) was determined by the BJH method. Deoxygenation of rapeseed oil was performed in a bench-scale fixed-bed reactor of 17 mm inner diameter. Firstly, catalysts were mixed with silicon carbide and sulfided with 5 vol.% dimethyl disulfide in iso-octane at 340 °C. Secondly, the deoxygenation of rapeseed oil was studied under hydrogen (3.5 MPa and H2/rapeseed oil molar ratio 50) at 260–280 °C and *W/F* 0.25–1 h^{-1} [9].

3. Results and discussion

The specific surface area of conventional alumina support was 255 $m^2\,g^{-1}$, while the specific surface area of alumina/meso was 520 $m^2\,g^{-1}$. The mesoporous alumina structure of alumina/meso material was confirmed by XRD (Fig. 1) and sorption isotherm of nitrogen. The diffraction pattern of alumina/meso (Fig. 1) showed the intensive diffraction peak at 2–3°, typical for organized mesoporous aluminas [7]. Nevertheless, it should be mentioned that the low angle diffraction peak corresponds to the mesopores with high pores diameter and long distance atom ordering [10].

Fig. 2 shows the pore size distribution and the physicochemical properties of the NiMo–alumina and NiMo–alumina/meso catalysts. NiMo–alumina/meso catalyst exhibited a broad pore size distribution (Fig. 2B) owing to the commercially available mesoporous alumina properties. On the other hand, the pore size distribution of mesoporous alumina materials synthesized at lab was reported to have narrow pore size distribution [7]. The specific surface area of NiMo–alumina/meso (273 $m^2\,g^{-1}$) was significantly higher in comparison with NiMo–alumina catalyst (193 $m^2\,g^{-1}$). The decrease in the specific surface area was higher after the impregnation of Ni and Mo species on the alumina/meso support (48%) in comparison with the impregnation of Ni and Mo species on alumina support (25%). Addition of Ni and Mo species on the alumina/meso support decreased the specific surface area (from 520 $m^2\,g^{-1}$ to 272 $m^2\,g^{-1}$) and total pore volume (from 1.3032 $cm^3\,g^{-1}$ to 0.8402 $cm^3\,g^{-1}$) suggesting that the impregnated Ni and Mo species blocked some pores in the alumina–meso support.

Fig. 3 shows the normalized UV–vis spectra of NiMo–alumina and NiMo–alumina/meso catalysts. Seven bands were observed in the spectra of NiMo–alumina and NiMo–alumina/meso catalysts with a maximum at 15 970, 16 860, 24 130, 33 480, 36 230, 40 270 and 46 750 cm^{-1}. The identification of the individual bands to the corresponding types of Ni and Mo species was based on the literature. The doublet at 15,970–16,860 cm^{-1} and the shoulder at 24,130 cm^{-1} was attributed to the transition characteristic for tetrahedral Ni^{II}(Td) ions [11–14] and the octahedral Ni^{II}(Oh) ions [11,12,15], respectively. The bands at 33 480 cm^{-1} and 36 230 cm^{-1} were characteristic for Mo^{VI}(Oh) and Mo^{VI}(Td) species, respectively [16–19]. Unfortunately, the bands above 30,000 cm^{-1} characteristic for Mo species were also affected by Ni^{II}–O charge transfer transitions. The spectra of NiMo–alumina/meso contained slightly

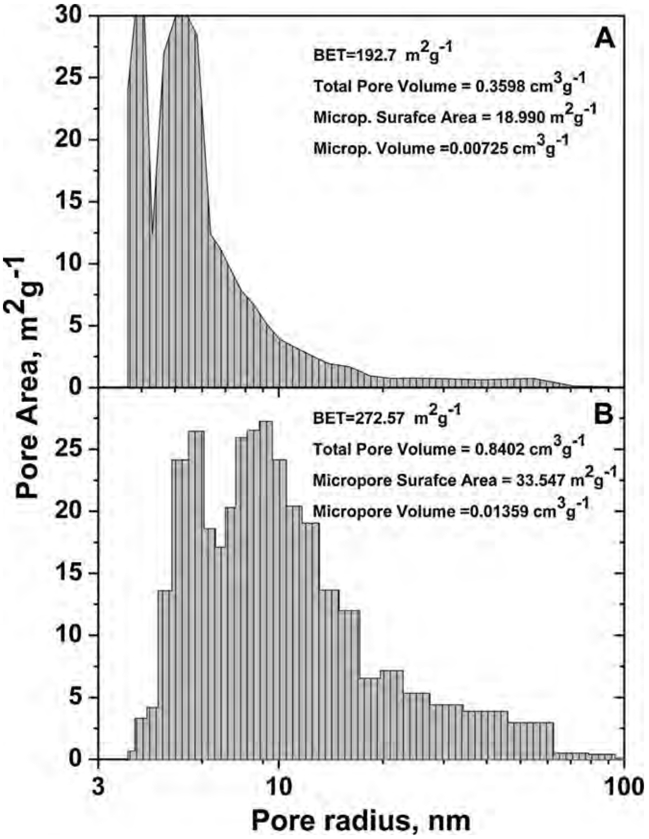

Fig. 2. Specific surfaces area, porosity and BJH pores size distribution plots of micropore surface area versus pore radius of the (A) NiMo–alumina and (B) NiMo–alumina/meso catalysts.

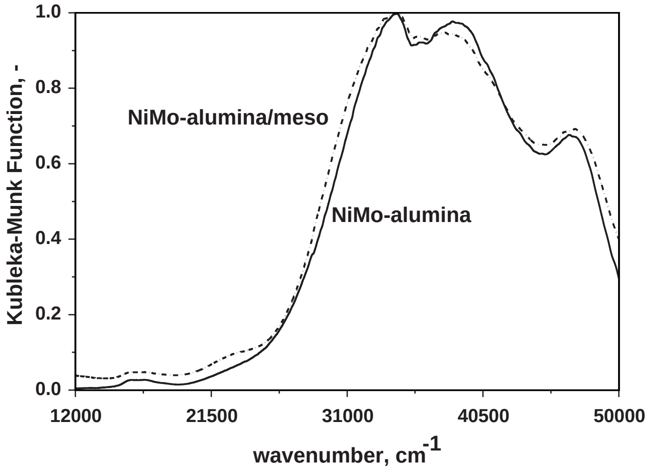

Fig. 3. Normalized UV–vis spectra of NiMo–alumina/meso (dashed-line) and NiMo–alumina (solid-line) catalysts.

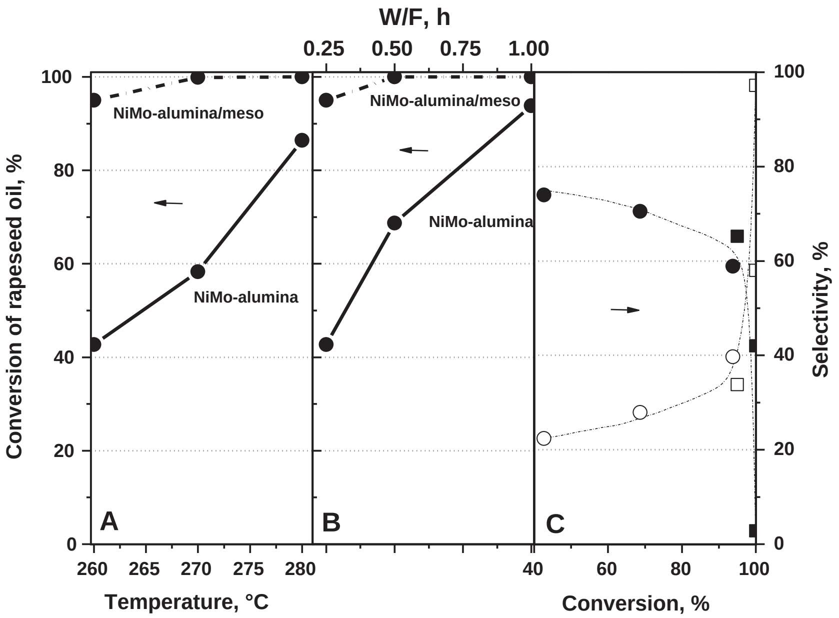

Fig. 4. (A) Dependence of the conversion of rapeseed oil on temperature in the deoxygenation of rapeseed oil at *W*/*F* 0.25 h over NiMo–alumina/meso (dashed line) and NiMo–alumina (solid line) catalysts; (B) dependence of the conversion of rapeseed oil on catalyst weight/total flow (*W*/*F*) ratio in the deoxygenation of rapeseed oil at 260 °C over NiMo–alumina/meso (dashed line) and NiMo–alumina (solid line) catalysts; and (C) dependence of the selectivity of oxygenates (solid symbols) and hydrocarbons (open symbols) as a function of the conversion of rapeseed oil at 260 °C over NiMo–alumina/meso (squares) and NiMo–alumina (circles) catalysts.

higher intensity of the bands at 24,130 cm^{-1} and 33,480 cm^{-1} representing the presence of the Ni^{II}(Oh) species and the Mo^{VI}(Oh) species, respectively, and slightly lower intensity of the band at 36,230 cm^{-1} characteristic for the Mo^{VI}(Td) species. Thus, it was concluded that the difference in the distribution of the bands characteristic for Ni and Mo species in the spectra of NiMo–alumina and NiMo–alumina/meso catalysts was insignificant, suggesting that a similar distribution of the Ni and Mo species was achieved on the alumina and alumina/meso materials.

Fig. 4A shows the dependence of the conversion of rapeseed oil on the reaction temperature in its deoxygenation over NiMo–alumina and NiMo–alumina/meso catalysts at *W*/*F* = 0.25 h. Fig. 4B shows the dependence of the conversion of rapeseed oil as a function of *W*/*F* (the ratio of catalyst mass (*W*, g) and rapeseed oil feed rate (*F*, g/h), *i.e.* contact time, in deoxygenation over NiMo–alumina and NiMo–alumina/meso catalysts at 260 °C. It is clearly seen that the conversion is higher for NiMo–alumina/meso in comparison with NiMo–alumina.

Oxygenates and hydrocarbons are the most important products of triglyceride deoxygenation. Previously, several authors suggested that the formation of oxygenates precedes that of hydrocarbons [9,20]. The selectivity-conversion behaviour (the dependence of the selectivity to oxygenates and hydrocarbons on the conversion of rapeseed oil) of NiMo–alumina/meso and NiMo–alumina catalysts was difficult to compare due to the high activity of NiMo–alumina/meso catalyst (Fig. 4C). Nevertheless, no significant difference was observed in the selectivity-conversion behaviour at around 90% conversion. To analyse the selectivity-conversion behaviour in more detail, further experiments would be needed in the future to obtain data at lower conversion levels and for more catalysts.

NiMo–alumina and NiMo–alumina/meso catalysts were prepared with the same amount of Ni (3.0 wt.%) and Mo (6.0 wt.%) and by the same preparation procedure. Moreover, the impregnation of Ni and Mo species also led to catalysts with similar distribution of metal species (Fig. 3). Thus, the main difference between NiMo–alumina/meso and NiMo–alumina catalysts was the specific surface area and the pore size distribution (Fig. 2). NiMo–alumina/meso exhibited significantly higher specific surface area and the total pore volume than the NiMo–alumina catalyst, which originated from the conventional alumina support.

On the other hand, the industrially available alumina/meso support exhibited a broad pore-size distribution (Fig. 2B), while organized mesoporous alumina could be synthesized in a laboratory with a narrow pore-size distribution [7]. Thus, it could be expected that the defined small-scale synthesis of organized mesoporous alumina could lead to a better structural properties and thus result in the further enhancement of the catalytic properties of NiMo–alumina/meso catalysts.

The NiMo–alumina and NiMo–alumina/meso exhibited relatively stable activity in the deoxygenation of rapeseed oil. The decrease in deoxygenation activity is estimated to be less than 5% during the 100 h catalytic run based on the previous results [21]. Moreover, the XRF analysis proved that the amount of Ni and Mo species in the spent catalysts was approximately the same as in the fresh ones.

It is generally accepted that the impregnation of metal species on the support with higher specific surface area leads to the higher dispersion of metal species on the support. However, only a minimum difference was observed in the distribution of Ni and Mo species in NiMo–alumina and NiMo–alumina/meso catalysts. Neither NiO- nor MoO_3-like species were present in the prepared catalysts, as evidenced from the absence of their characteristic UV–vis bands (Fig. 3) and XRD (Fig. 1) diffraction peaks.

Thus, the better performance of NiMo–alumina/meso, as evidenced by the higher conversion of rapeseed oil, was attributed to the significantly higher specific surface area and the total pore volume of NiMo–alumina/meso in comparison with the NiMo–alumina.

4. Conclusions

The NiMo–alumina/meso and NiMo–alumina catalysts were prepared using commercially available mesoporous alumina support and the conventional alumina support, respectively. The NiMo–alumina/meso catalyst showed significantly better performance than the NiMo–alumina catalyst in the deoxygenation of rapeseed oil. As both catalysts were prepared with the same amount of Ni and Mo species, by the same procedure and they also exhibited the similar population of Ni and Mo species, the type of alumina support played the critical role in the reaction. The better deoxygenation performance of NiMo–alumina/meso could be explained by the significantly higher specific surface area and the total pore volume of NiMo–alumina/meso in comparison with the NiMo–alumina.

Acknowledgments

The authors gratefully thank the Ministry of Industry and Trade of the Czech Republic (project FT-TA3/074) and Ministry of Education, Youth and Sports (No. MSM0021627501).

References

[1] I. Kubičková, D. Kubička, Waste Biomass Valor., in press, doi:10.1007/s12649-010r-r9032-8.
[2] J. Gusmão, D. Brodzki, G. Djega-Mariadassou, R. Frety, Catal. Today 5 (1989) 533–544.
[3] I. Sebos, A. Matsoukas, V. Apostolopoulos, N. Papayannakos, Fuel 88 (2009) 145–149.
[4] J. Walendziewski, M. Stolarski, R. Luzny, B. Klimek, Fuel Process. Technol. 90 (2009) 686–691.
[5] D. Kubička, L. Kaluža, Appl. Catal. A 372 (2010) 199–208.
[6] P. Šimáček, D. Kubička, G. Šebor, M. Pospíšil, Fuel 88 (2009) 456–460.
[7] J. Čejka, Appl. Catal. A 254 (2003) 327–338.
[8] A. Taguchi, F. Schüth, Microporous Mesoporous Mater. 77 (2005) 1–45.
[9] D. Kubička, P. Šimáček, Žilková.F N., Top. Catal. 52 (2009) 161–168.
[10] J. Sanchez-Valente, X. Bokhimi, J.A. Toledo, Appl. Catal. A 264 (2004) 175–181.
[11] D. Nikolova, R. Edreva-Kardjieva, M. Giurginca, A. Meghea, J. Vakros, G.A. Voyiatzis, Ch. Kordulis, Vib. Spectrosc. 44 (2007) 343–350.
[12] M.A. Zanjanchi, A. Ebrahimian, J. Mol. Struct. 693 (2004) 211–216.
[13] Ch. Lepetit, M. Che, J. Phys. Chem. 100 (1996) 3137–3143.
[14] R.A. Schoonheydt, D. Roodhooft, H. Leeman, Zeolites 7 (1987) 412–417.
[15] L. Yang, K. Xia, Solid State Commun. 90 (1994) 737–739.
[16] A. Guevara-Lara, R. Bacaud, M. Vrinat, Appl. Catal. A 328 (2007) 99–108.
[17] H. Jeziorowski, H. Knoezinger, J. Phys. Chem. 83 (1979) 1166–1173.
[18] Y.V. Plyuto, I.V. Babich, I.V. Plyuto, A.D. Van Langeveld, J.A. Moulijn, Colloids Surf., A 125 (1997) 225–230.
[19] G.M.S. El Shafei, N.A. Moussa, Ch.A. Philip, J. Colloid Interface Sci. 228 (2000) 105–113.
[20] G.W. Huber, P. O'Connor, A. Corma, Appl. Catal. A 329 (2007) 120–129.
[21] D. Kubička, J. Horáček, Appl. Catal. A, doi:10.1016/j.apcata.2010.10.034, in press.

Top Catal (2009) 52:161–168
DOI 10.1007/s11244-008-9145-5

ORIGINAL PAPER

Transformation of Vegetable Oils into Hydrocarbons over Mesoporous-Alumina-Supported CoMo Catalysts

David Kubička · Pavel Šimáček · Naděžda Žilková

Abstract Deoxygenation of triglycerides over organized-mesoporous-alumina-supported CoMo catalysts (CoMo/OMA) has been investigated in this work. CoMo/OMA catalysts exhibited higher activity for deoxygenation of triglycerides than CoMo supported on MCM-41 (silica) and ordinary alumina supports. Two main deoxygenation pathways were found: hydrodeoxygenation and hydrodecarboxylation. Their extent was affected by reaction temperature, pressure and the support used. Hydrodeoxygenation was the main reaction under the studied conditions. The extent of hydrodecarboxylation increased with increasing reaction temperature and decreasing reaction pressure.

Keywords Organized mesoporous alumina · CoMo catalysts · Hydrodeoxygenation · Hydrodecarboxylation · Triglycerides

1 Introduction

Biofuels have a potential to replace a part of fossil transportation fuels and to contribute thus to the reduction of CO_2 emission [1, 2]. In order to minimize the impacts of biofuel production on the environment, the research activities have been focused on the development of advanced biofuel technologies, so called second generation biofuels. The main characteristics of second generation biofuels are: (i) higher greenhouse gas (GHG) emission reduction in the complete life cycle in comparison with current biofuels and (ii) non-food biomass raw materials.

Vegetable oils have a suitable composition for production of fuels and have been therefore exploited for the production of biodiesel. However, biodiesel suffers from several drawbacks such as limited compatibility with conventional diesel engines, use of high quality food feedstocks, etc. Therefore, direct upgrading of vegetable oils into hydrocarbons have been proposed and commercially demonstrated [3, 4]. Apart from the excellent compatibility with conventional diesel, the diesel components from triglycerides outperform the conventional biodiesel in terms of both fossil cumulative energy demand (CED, GJ/t) and GHG savings $\left(t_{CO_{2eq.}}/t\right)$ [5]. Moreover, in contrast to the conventional biodiesel production, lower quality triglyceride feedstocks such as used frying oils, animal fats and trap greases can be used lowering the cost and dependency on food grade vegetable oils.

Transformation of triglycerides into hydrocarbons requires elimination of oxygen. It has been found that conventional hydrotreating catalysts, such as CoMo or NiMo, are suitable for deoxygenation of triglycerides [6–10]. Two general approaches have been proposed: hydrotreating of neat vegetable oils [3, 11, 12] and co-processing of vegetable oils with crude-oil-based refinery fractions

D. Kubička (✉)
Department of Refinery and Petrochemical Research,
Research Institute of Inorganic Chemistry,
Záluží 1, D.S. 458, 436 70 Litvínov, Czech Republic
e-mail: david.kubicka@vuanch.cz

P. Šimáček
Department of Petroleum Technology and Alternative Fuels,
Institute of Chemical Technology Prague, Technická 5,
166 05 Prague, Czech Republic

N. Žilková
J. Heyrovský Institute of Physical Chemistry, v.v.i.,
Academy of Sciences of the Czech Republic,
Dolejškova 3, 182 23 Prague, Czech Republic

[11–14]. The first approach offers the advantage of high process flexibility, but it requires high investments. In the latter one, the existing apparatus and utilities can be utilized reducing the investments needed. However, the flexibility is reduced as additional issues have to be dealt with (e.g. sulfur content of the final product, effect of water and carbon oxides on the catalyst lifetime, separation of carbon oxides from the recycle gas, etc.). As a result of these issues, the refiners seem to favor the former option [3, 12].

Deoxygenation has been studied using a wide range of probe molecules [6, 7, 15–20]. As the reaction mechanism and the reaction rate depend on the type of oxygen compounds, studies using fatty acids and their esters as model reactants [15–20] or directly triglycerides [6, 7] are the most relevant ones. It has been reported that deoxygenation of these compounds can follow three different reaction pathways—hydrodeoxygenation, decarbonylation and decarboxylation [6]. Moreover, inhibition of deoxygenation and desulfurization may occur when both types of compounds (S- and O-containing compounds) are present at the same time [20].

Mesoporous materials show a great potential as catalyst supports [21]. Their synthesis and application have been reviewed recently [22–24]. Moreover, mesoporous supports, such as mesoporous molecular sieves (MCM-41, SBA-15) or organized mesoporous alumina (OMA) offer several advantages over alumina support used in traditional hydrodesulfurization catalysts [25, 26]. In contrast to standard alumina supports and similarly to microporous molecular sieves (zeolites), organized mesoporous aluminas have very high specific surface areas that can be used to achieve very high dispersions of the supported active phase [23] and high loadings of active phase. Moreover, larger pore diameters as compared with zeolites make mesoporous supports excellent candidates for applications where large organic molecules have to access the well-dispersed active sites located inside the pores. This is of a high importance for instance in the case of hydrodesulfurization of heavy crude oil fractions. The molecular size of triglycerides suggests that mesoporous supports could be used advantageously in catalytic transformations of triglycerides as well.

The application of several mesoporous supports modified with cobalt and molybdenum for the catalytic deoxygenation of rapeseed oil into hydrocarbons has been investigated in the present work. The conversion and selectivity over mesoporous supports are compared with those obtained over industrial alumina support. The effects of reaction temperature and hydrogen pressure on the product distribution are discussed and a possible reaction network of rapeseed oil transformation into hydrocarbons is proposed.

2 Experimental

2.1 Catalyst Preparation and Characterization

Four different support materials were used to prepare cobalt–molybdenum modified hydrodeoxygenation catalysts. Three mesoporous supports—two different organized mesoporous aluminas (OMA) and MCM-41 silica were synthesized while the ordinary γ-alumina was purchased from Eurosupport Manufacturing Czechia (CZ).

MCM-41 was synthesized by homogeneous precipitation [27]. The reaction mixture was prepared in a polypropylene screw-cap bottle by dissolution of 9.8 g of cetyltrimethylammonium bromide (CTABr, Aldrich) in 950 mL of warm water. The solution was cooled to room temperature (RT) and 10 g of solid Na_2SiO_3 (Aldrich) was added. After dissolution of Na_2SiO_3 15 mL of ethyl acetate was added, mixture was intensively shaken and left to stand for 8 h. Then the bottle was placed in an oven heated to 90 °C and kept at that temperature for 48 h. The product was filtered off from the hot solution, washed by water and ethanol, dried at RT and calcined at 600 °C for 20 h. (temperature ramp 5 °C/min).

The first OMA (OMA1) was prepared as follows. 100 g of PE 10400 (BASF) was dissolved in 600 mL of acetonitrile (Riedel-de-Haen) and 100 g of aluminum-tri-sec-butoxide (97%, Aldrich 20,107-3) was added to the solution. Then 60 mL of ammonium hydroxide solution (25%, Lachema) was added slowly. The resulting gel was stirred 24 h at RT, until white precipitate was formed. The product was filtered off, dried at room temperature and calcined in muffle oven using following temperature program: 1 °C/min to 120 °C–120 min hold, 1 °C/min to 240 °C–240 min hold, 1 °C/min to 540 °C–360 min hold.

The second OMA was synthesized according to the following procedure. 17 g of stearic acid (Aldrich, 17,536-6) were dissolved in 200 mL of 2-butanol (Lachema). 50 g of aluminum-tri-sec-butoxide (97%, Aldrich 20,107-3) in 150 mL of 2-butanol were hydrolyzed by 20 mL of distilled water. Both solutions were mixed together and stirred at RT for 24 h. The reaction mixture was then poured into 1,000 mL polypropylene screw-cap bottle and was heated at 95 °C for 48 h. Solid product was collected by centrifugation, dried at 60 °C overnight and calcined in muffle oven using following temperature program: 1 °C/min to 120 °C–120 min hold, 1 °C/min to 240 °C–240 min hold, 1 °C/min to 475 °C–360 min hold.

Metal modification of all supports was carried out using the following procedure. First, the supports were mixed with a specific amount of MoO_3 (Lachema) corresponding to a loading 15 wt% Mo on the support. The mixtures were then calcined in a shallow layer in air at 550 °C for 6 h. After calcination the Mo-containing catalysts were impregnated by $Co(NO_3)_2 \cdot 6H_2O$ (Fluka, pa.) in methanol (Fluka, HPLC grade) to obtain Co loading equal to 3 wt%. The impregnated catalysts were first dried at 60 °C and subsequently calcined in a shallow layer in air at 400 °C for 3 h. Finally, the structural catalyst properties were characterized by means of N_2 physisorption (Micromeritics ASAP 2020), XRD (Bruker D8) and SEM (Jeol), for details see [28].

2.2 Catalytic Activity Measurements

Refined rapeseed oil (food grade) was used as a starting material. The distribution of fatty acids in the oil was determined by gas chromatography and is given in Table 1. Refinery hydrogen gas with >99% of H_2 was used in the experiments. The main impurities were methane (0.6%) and nitrogen (0.3%). The experiments were performed in an electrically-heated fixed-bed reactor of inner diameter equal to 17 mm. The reactor was loaded prior to the experiments with 10–15 g of catalyst diluted by an inert (SiC) to ensure sufficient catalyst-bed length and to improve the reaction-heat transfer. A layer of the inert material was placed above the catalyst bed to preheat rapeseed oil and hydrogen and to guarantee a good feed flow distribution prior to entering the catalyst bed. The particle sizes of the catalyst and SiC were 0.1–0.25 mm and <0.1 mm, respectively. In the vertical axis of the reactor was a thermo-well of the outer diameter equal to 5 mm, in which three adjustable thermocouples, used to determine the reaction temperature, were located. The catalysts were activated (sulfided) in-situ prior to the experiments by means of a solution of dimethyl disulfide (DMDS) in isooctane (5 wt% DMDS) at 320 °C. The reaction temperature and hydrogen pressure were varied during the experiments in the range of 250–350 °C and 0.7–7 MPa, respectively. The liquid feed rate and the hydrogen-to-rapeseed oil molar ratio were kept constant at 1.5 h^{-1} and 100, correspondingly. The liquid and gaseous products were separated at the reactor outlet in a heated gas–liquid separator as some of the products are solid at ambient temperatures.

Table 1 Distribution of fatty acids in rapeseed oil (raw material)

Fatty acid (X:Y)[a]	Wt%
Myristic acid (14:0)	0.1
Palmitic acid (16:0)	4.8
Palmitoleic acid (16:1)	0.3
Stearic acid (18:0)	1.9
Oleic acid (18:1)	61.9
Linoleic acid (18:2)	19.8
Linolenic acid (18:3)	9.2
Arachidic acid (20:0)	0.6
Gadoleic acid (20:1)	1.4

[a] X:Y = carbon number: number of double bonds

The liquid products (collected and separated at 80 °C) were withdrawn after reaction-condition stabilization (6 h) in 2-h intervals and analyzed by off-line gas chromatography after separation of the water phase. Due to the presence of triglycerides in the products, on-column injection had to be used. Trikaprin (Fluka, >99%) was used as an internal standard in order to quantify the concentration of triglycerides. Moreover, the reaction intermediates included fatty acids and alcohols and silylation of reaction products by MSTFA (Acros, 97%) was applied to enhance their volatility and to improve the shapes of the peaks. The products were separated on a Restek MTX-Biodiesel TGw/Int-GAP column (14 m × 0.53 mm × 0.16 μm) and detected using a flame ionization detector (FID). The following temperature program was used: initial temperature 50 °C for 3 min, heating first 11 °C/min to 180 °C, then 5 °C/min to 230 °C and finally 15 °C/min to 390 °C with dwelling time of 7 min at 390 °C. The individual products were identified using GC standards and the identification was further confirmed by GC-MS analysis. The gas-phase products were collected once at every reaction condition and analyzed using a standard three-column GC setup with flame ionization and thermal conductivity detectors enabling the detection of both permanent gases and hydrocarbons at the same time.

3 Results and Discussion

3.1 Catalyst Characterization

Basic characterization of the mesoporous supports synthesized and of the industrial alumina support was performed. The structure of the supports was determined by XRD. The diffractograms are displayed in Fig. 1. The observed patterns are in good agreement with literature data [22, 27]. The specific surface area and mean pore diameters were obtained from nitrogen physisorption using the BET method. The results are summarized in Table 2. The industrial support has a typical broad pore-size distribution whereas the mesoporous catalysts have a very narrow pore-size distribution. The mean pore diameter of MCM-41 is about 3 nm and of OMAs between 5 and 6 nm (Table 2). Due to the different synthesis procedure slight differences can be found between the OMAs. The procedure using stearic acid as a structuring agent (OMA2) led to a mesoporous alumina with larger surface area and wider pores in comparison with OMA1. The difference between OMA1 and OMA2 is about 10% (Table 2). More importantly, both OMAs have significantly larger surface area

Fig. 1 XRD patterns of Al_2O_3 (**a**), MCM-41 (**b**), OMA1 (**c**) and OMA2 (**d**)

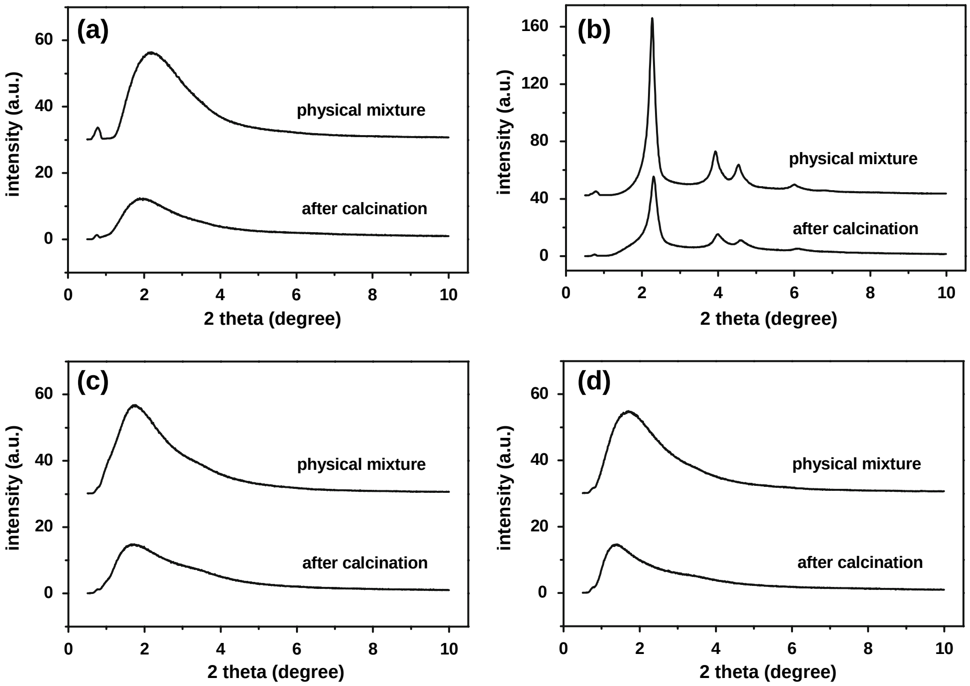

Table 2 Specific surface area (BET), volume and average diameter of mesopores

Catalyst	S_{BET} (m^2/g)	V_{ME} (cm^3/g)	D_{ME} (nm)
CoMo/Al_2O_3	159.5	0.233	4–10
CoMo/MCM-41	662.3	0.443	3.0
CoMo/OMA1	219.5	0.344	5.2
CoMo/OMA2	234.5	0.459	5.7

and pore volumes than the industrial alumina support (Table 2).

3.2 Reaction Products and their Analysis

Transformation of rapeseed oil over CoMo-modified catalysts yielded three main product groups—gaseous products, liquid and solid organic products and water. The gaseous products consisted of propane, propene (only at low reaction pressures), methane, carbon monoxide and carbon dioxide. Other hydrocarbons were present only in trace amounts. The liquid and solid organic products contained hydrocarbons, mainly in the range C_{15}–C_{18}, saturated triglycerides, fatty acids, alcohols, and fatty esters of fatty acids. Hydrocarbons consisted predominantly of *n*-alkanes, only minor amounts of iso-alkanes and olefins have been found. Short chain hydrocarbons that would indicate hydrocarbon cracking reactions have not been detected in the products. Fatty acids and alcohols were saturated and their carbon chain length corresponded to that of fatty acids present in triglycerides making up rapeseed oil, i.e. stearic acid, palmitic acid and octadecanol. Significant amounts of esters formed by esterification of fatty acids, i.e. reaction intermediates, by alcohols, i.e. another reaction intermediates, were identified in the products by GC/MS. Stearylstearate was identified as the dominant ester.

Even though the triglycerides found in the products were formed by hydrogenation of double bonds of the original triglycerides, they were considered, for the purpose of conversion determination, as raw materials since the main objective was description of triglyceride deoxygenation. Hydrogenation of double bonds in triglycerides always precedes deoxygenation, since C=C double bonds can be saturated already at low temperatures (100–180 °C) over hydrogenation or hydrotreating catalysts [29], i.e. at temperatures too low for deoxygenation to take place.

3.3 Catalytic Activity of Mesoporous Catalysts

The investigated CoMo-modified catalysts were active in conversion of triglycerides into hydrocarbons. Complete conversion of triglycerides was achieved at temperatures equal to 280 °C or higher (Fig. 2a). It should be noted that conversion is based on triglyceride disappearance from the reaction mixture. Complete hydrogenation of rapeseed oil triglycerides to their saturated counterparts, mainly tristearin, was found in the whole studied range of reaction conditions.

Differences in conversion among the individual catalysts could be observed only at lower temperatures, where a significant difference between the two studied mesoporous alumina supports was found. OMA1 exhibited high activity

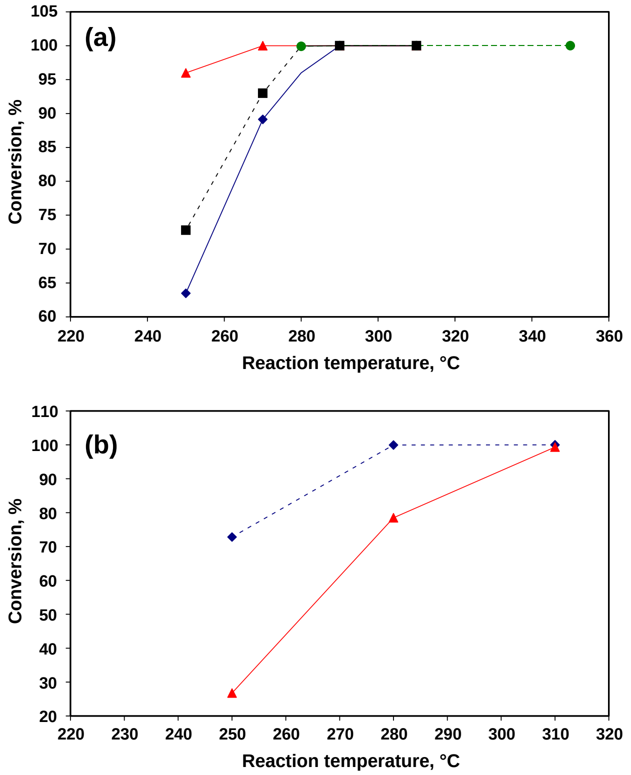

Fig. 2 Conversion of triglycerides as a function of reaction temperature: **a** comparison of the supports (*diamond* Al_2O_3, *circle* MCM-41, *triangle* OMA1, *square* OMA2); **b** the effect of reaction pressure over OMA2 (*diamond* 7 MPa, *triangle* 0.7 MPa), WHSV = 1.5 h^{-1} for Al_2O_3 and 2 h^{-1} for the other supports

even at 250 °C (conversion of 95%), while the conversion over OMA2 dropped below 75%. This is surprising as their surface areas and pore volumes were similar; in fact those of OMA2 were even slightly higher (Table 2). The commercial alumina supported CoMo catalyst showed the lowest conversion; however, the experiment was carried out at a higher WHSV than the experiments using OMAs and MCM-41 (2 h^{-1} vs. 1.5 h^{-1}).

The conversion was affected considerably by the hydrogen partial pressure (Fig. 2b). When the total reaction pressure was reduced from 7 to 0.7 MPa, the conversion dropped by 20% at 280 °C and by 45% at 250 °C (Fig. 2b). This can be ascribed to the lower reaction (deoxygenation) rate due to the decreased reaction temperature and the reduced availability of hydrogen at the active sites, which is caused by the hydrogen-mass-transfer limitations through the liquid film on catalyst–particle surface. On the other hand, at 310 °C the reaction proceeds with such speed that the effect of hydrogen-pressure reduction is compensated by the temperature effect and thus could not be observed at 1.5 h^{-1} (Fig. 2b).

Commercial catalysts have been studied previously in the transformation of vegetable oils into hydrocarbons. It has been found that approximately above 300 °C complete conversion of triglycerides can be obtained [6, 7, 9, 10]. This has been further confirmed in this study by using a commercial CoMo catalyst that showed complete conversion of triglycerides in the same temperature range as the mesoporous catalysts. It can thus be concluded that mesoporous supports supported CoMo catalysts are suitable for deoxygenation of triglycerides.

3.4 Selectivity of Mesoporous Catalysts

The selectivity in deoxygenation of triglycerides can be looked at from two different angles: (i) as selectivity to hydrocarbons and oxygenated reaction intermediates, on the one hand, and (ii) as selectivity to individual hydrocarbons, on the other hand. Both views are equally important as they provide useful insights into the chemistry of deoxygenation and may help in selecting a good catalyst.

The objective of triglyceride transformation into hydrocarbons is to eliminate oxygen from the liquid products. Hence selectivity to oxygenated compounds is yet another measure of the catalyst activity, in addition to conversion of triglycerides, as it describes the relative rate of formation of intermediates and of their consumption (i.e. the rate of formation of hydrocarbons). The plausible reaction intermediates are corresponding fatty acids, aldehydes and alcohols. While the reactivity of hydroxyl- and aldehyde group is higher than that of esters, the reactivity of carboxyl group is lower [15]. Therefore, it is not surprising that carboxylic acids were found in the reaction mixture as reaction intermediates in large quantities whereas only traces of alcohols were detected. Moreover, aldehydes were not found at all. The most abundant oxygenated reaction intermediates were identified as esters of fatty acids, e.g. stearyl stearate. These compounds are formed by esterification of fatty acids with fatty alcohols and their presence further substantiates the virtual absence of free fatty alcohols. Their formation over hydrotreating catalysts was previously reported in hydrogenation of fatty acids by Landa and Weiser [30].

The selectivity to oxygenated products (here presented as sum of acids, alcohols and esters) increased over the studied catalysts with the decreasing conversion of triglycerides and with the decreasing reaction temperature (Fig. 3a). Whereas at temperatures above 300 °C were these intermediates virtually absent, large quantities of oxygenates (selectivity >50%), particularly of esters and stearic acid, were observed below 280 °C (Fig. 3a). Among the mesoporous catalysts stood out the performance of MCM-41 with its significant concentrations of oxygenates found already at 280 °C. This indicates that alumina supports are superior to silica supports. Since the surface area of MCM-41 is substantially higher than that of

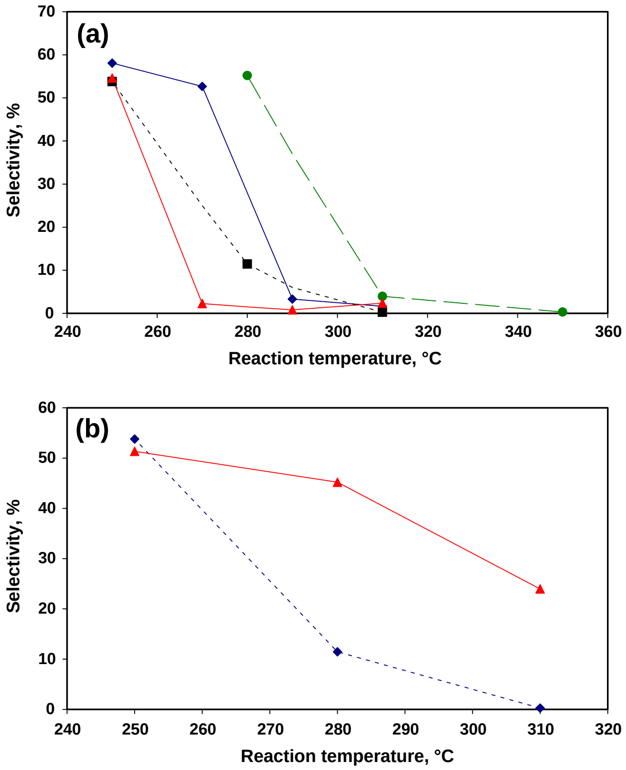

Fig. 3 Selectivity to oxygenated products as a function of reaction temperature: **a** comparison of the supports (*diamond* Al_2O_3, *circle* MCM-41, *triangle* OMA1, *square* OMA2); **b** the effect of reaction pressure over OMA2 (*diamond* 7 MPa, *triangle* 0.7 MPa)

alumina supports (Table 2), it can be expected that better dispersion of the active phase is achieved. Therefore, the differences could be attributed to the active-phase–support interactions, as different surface groups are present in MCM-41 (silica) than in alumina supports, or to diffusion limitations of the bulky triglyceride molecules in the pores of MCM-41 that are much narrower than those of the alumina supports investigated (Table 2). However, the latter reason is less likely since in previous studies using MCM-41 and triglycerides no diffusion limitations of triglyceride molecules in the pores of MCM-41 were observed [31, 32]. Among the alumina supports, both OMAs exhibit lower selectivity to the oxygenated products and higher selectivity to hydrocarbons at comparable reaction conditions. This can be ascribed to the differences in their surface areas and consequently in the dispersion of the active phase. However, this cannot be the only reason, since the performance of both OMAs varies, even though their structural parameters are not very different from each other (Table 2).

The selectivity to oxygenated products is also appreciably affected by the reaction pressure (Fig. 3b). This can be seen predominantly at reaction temperatures 280 and 310 °C, where relatively comparable conversions were obtained (Fig. 2b). Similarly to conversion of triglycerides, the consecutive reactions of oxygenated intermediates are inhibited by the lower availability of hydrogen and thus increased selectivity to oxygenated products (e.g. from 10 to 45% at 280 °C, see Fig. 3b) is found at reduced reaction pressure.

The distribution of hydrocarbons in the products is affected by the way of oxygen elimination. Two principal deoxygenation pathways can be proposed based on the experimental results: hydrodeoxygenation (HDO) and hydrodecarboxylation (HDC). These are in line with the previously published data [6–10]. In contrast to the previous works [6, 8], the suggested decarbonylation pathway could not be confirmed or ruled out, as the origin of CO found in the products could not be conclusively determined. Moreover, the formation of other hydrocarbon products (such as naphthenes and aromatics) that was reported previously [7] was not observed in this study. The reason is most probably the lower reaction temperature used in the present study (310 vs. 360 °C).

Hydrodeoxygenation (HDO) yields generally two principal products: a hydrocarbon and water. The hydrocarbon has the same number of carbon atoms in the molecule as the corresponding fatty acid chain, from which it was formed. This means that hydrocarbons formed by HDO have exclusively even number of carbon atoms. On the other hand, the principal products from hydrodecarboxylation (HDC) are a hydrocarbon and carbon dioxide. Therefore, hydrocarbons resulting from HDC have odd carbon number, i.e. they have one carbon atom less than the original fatty acid chain. Additionally, the glycerol backbone of triglycerides is converted in both pathways into propane.

The extent of both pathways and the effect of reaction conditions on them can be consequently elucidated from the liquid hydrocarbon distributions. The results for the most abundant hydrocarbons, i.e. *n*-octadecane and *n*-heptadecane that are formed by HDO and HDC, respectively, of C_{18} fatty acid chains [they make up >90% of total fatty acid chains (Table 1)], are presented in Fig. 4a for all catalysts as a function of temperature. In the region where complete or nearly complete conversion was obtained ($T > 270$ °C), the selectivity towards C_{17} hydrocarbons increased with the increasing conversion (Fig. 4a), i.e. the ratio C_{18}/C_{17} decreased. The ratio is substantially affected by the nature of the support. Once again, the behavior of MCM-41 (silica) clearly deviates from the alumina supports. However, even among the three alumina supports significant differences can be observed. The differences could be plausibly explained by different adsorption mode of triglycerides induced by the active phase–support interactions and by the differences in dispersion of the active phase. However, further experimental work and detailed catalyst characterization is needed to

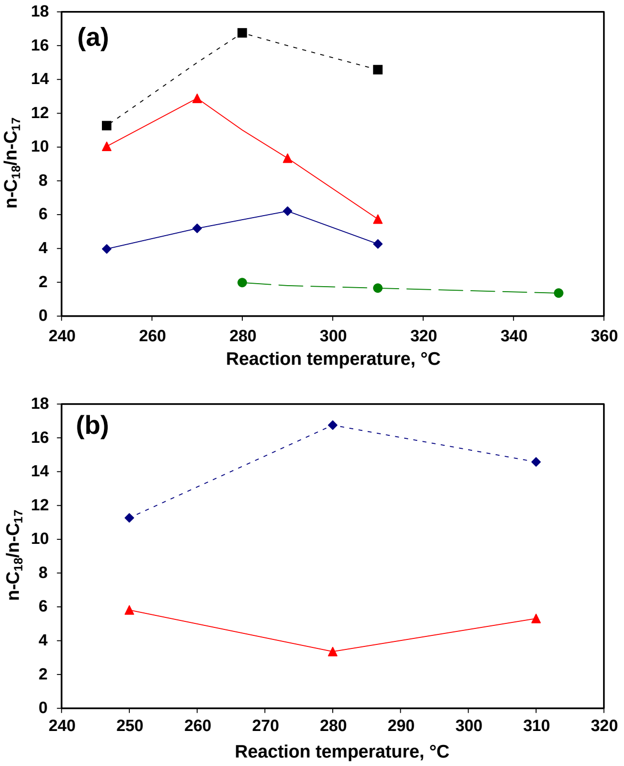

Fig. 4 Ratio of selectivity to *n*-octadecane to selectivity to *n*-heptadecane as a function of reaction temperature: **a** comparison of the supports (*diamond* Al_2O_3, *circle* MCM-41, *triangle* OMA1, *square* OMA2); **b** the effect of reaction pressure over OMA2 (*diamond* 7 MPa, *triangle* 0.7 MPa)

justify these assumptions. Previously, different extents of HDO and HDC pathways were observed as a result of the active phase used (NiMo, Ni) [10].

Both reaction pathways are affected by the reaction pressure as well (Fig. 4b). When reaction pressure was decreased, the selectivity towards *n*-heptadecane increased at the expense of *n*-octadecane formation (e.g. the C_{18}/C_{17} ratio dropped from 14 to 6 as a result of decreasing the reaction pressure from 7 to 0.7 MPa at 310 °C, see Fig. 4b). This behavior is apparently connected to the hydrogen availability. In terms of hydrogen consumption, HDO is more demanding than HDC and is therefore preferred at higher hydrogen pressures. Moreover, more gaseous products are formed during HDC and it is consequently favored at lower reaction pressure. The hydrogen consumption is an important issue from the industrial point of view; a process with lower hydrogen demands has a better chance to succeed.

The product distributions in the liquid phase can be summarized in the following reaction scheme (Fig. 5). The two main reaction pathways are affected by the reaction conditions (temperature, pressure) as well as by the catalyst employed (active phase, support) as discussed above. The conclusions drawn here, based on the liquid-phase–product distributions, concerning the main reaction pathways and their dependence on the reaction temperature and pressure, are further supported by the gas-phase composition.

3.5 Gas-Phase Selectivity

Gas-phase analyses were performed only once per each reaction condition and have, thus, a supporting character. Nevertheless, the data are in good agreement with the liquid-phase analysis. The gas-phase composition for OMA2 is given in Table 3. The balance to 100% is hydrogen that was used in a large excess in all experiments (100:1 mol/mol). Propane, the main gas-phase product, is a partial indication of triglyceride conversion and its concentration in the gas-phase products decreases with decreasing reaction temperature (Table 3), which is in agreement with the triglyceride conversion trend (Fig. 2a). Furthermore, at decreased pressure larger quantities of C_1 gases are formed coinciding with the higher extent of HDC pathway (Fig. 4b). Similarly, the share of C_1 gases increases with increasing reaction temperature, which is

Fig. 5 Reaction scheme of triglyceride conversion into hydrocarbons [33]

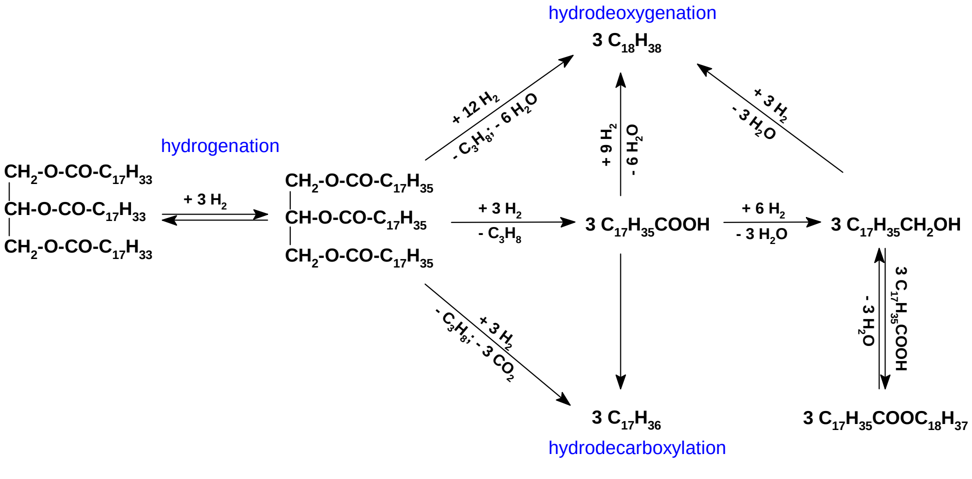

Table 3 Composition of gas-phase products over OMA2 (WHSV = 1.5 h^{-1})

Pressure (MPa)	7.0			0.7		
Temperature (°C)	310	280	250	310	280	250
Composition (vol. %)						
CH_4	0.09	0.03	0.01	0.02	0.00	0.00
CO	0.04	0.05	0.01	0.22	0.07	0.00
CO_2	0.12	0.11	0.05	0.11	0.05	0.04
C_3H_8	0.81	0.76	0.21	0.09	0.03	0.01
C_3H_6	0.00	0.01	0.06	0.43	0.17	0.06

again the consequence of the promotion of HDC pathway with increasing temperature (Fig. 4b). It is important to note that CO_2 is accompanied by CO and CH_4 (for concentrations of these products at specific reaction conditions see Table 3), which strongly suggests that under the chosen reaction conditions CO_2 is hydrogenated to CO and CH_4. Additionally, propane is accompanied by propene; at decreased pressure propene is even more abundant than propane (Table 3). This clearly shows that hydrogen availability at the active-phase surface is limited. It can be thus concluded that the gas-phase data support the conclusions drawn from the analysis of liquid product distribution.

4 Conclusions

Hydrodeoxygenation catalysts consisting of mesoporous support (organized mesoporous alumina and MCM-41), modified with molybdenum and cobalt were synthesized and their performance in deoxygenation of rapeseed oil was investigated. Selective conversion of triglycerides into hydrocarbons was achieved at 310 °C and 7 MPa. The OMA catalysts showed better performance than the industrial-alumina-based catalyst. The performance of MCM-41 (silica) was worse than that of alumina-based catalysts. Two main reaction pathways were observed: hydrodeoxygenation and hydrodecarboxylation. The extent of these reaction pathways is very important from the industrial point of view since it determines the hydrogen consumption. It is affected by reaction parameters (temperature, pressure) as well as support choice. Further research is needed to understand fully the influence of the catalyst related properties (support type and its properties, active phase type and its properties, active-phase–support interactions) on the product distribution.

Acknowledgements The financial support by the Ministry of Industry and Trade of the Czech Republic (project FT-TA3/074) is gratefully acknowledged.

References

1. Huber GW, Iborra S, Corma A (2006) Chem Rev 106:4044
2. Huber GW, Corma A (2007) Angew Chem Int Ed 46:7184
3. Jakkula J, Aalto P, Niemi V, Kiiski U, Nikkonen J, Mikkonen S, Piirainen O (2004) WO 2004/022674 A1, EP 1 396 531 A2, US 2004/0055209 A1
4. NesteOil, http://www.nesteoil.com/default.asp?path=1,41,539,7516,7522
5. UOP (2008) In: 1st alternative fuels technology conference, February 18, 2008, Prague, Czech Republic
6. Gusmao J, Brodzki D, Djega-Mariadassou G, Frety R (1989) Catal Today 5:533
7. da Rocha Filho GN, Brodzki D, Djega-Mariadassou G (1993) Fuel 72:543
8. Huber GW, O'Connor P, Corma A (2007) Appl Catal A Gen 329:120
9. Kubička D, Chudoba J, Šimáček P (2007) In: Europacat VIII, Turku, Finland, August 26–31, 2007
10. Šimáèek P, Kubièka D, Šebor G, Pospíšil M (2008) Fuel (in press). doi:10.1016/j.fuel.2008.10.022
11. Holmgren J, Gosling C, Couch K, Kalnes T, Marker T, McCall M, Marinangeli R (2007) Petroleum Technol Q 3:119
12. Holmgren J, Gosling C, Marinangeli R, Marker T, Faraci G, Perego C (2007) Hydrocarbon Process 9:67
13. ConocoPhillips, http://www.conocophillips.com/Tech/emerging/index.htm
14. Petrobras, http://www2.petrobras.com.br/tecnologia/ing/hbio.asp
15. Furimsky E (2000) Appl Catal A Gen 199:147
16. Laurent E, Delmon B (1994) Appl Catal 109:77
17. Laurent E, Delmon B (1994) Appl Catal 109:97
18. Senol OI, Viljava T-R, Krause AOI (2005) Catal Today 100:331
19. Senol OI, Ryymin E-M, Viljava T-R, Krause AOI (2007) J Mol Catal A Chem 277:107
20. Viljava T-R, Komulainen RS, Krause AOI (2001) Appl Catal A Gen 209:33
21. Taguchi A, Schüth F (2005) Microporous Mesoporous Mater 77:1
22. Čejka J (2003) Appl Catal A Gen 254:327
23. Corma A (1997) Chem Rev 97:2373
24. Márques-Alvarez C, Žilková N, Pérez-Pariente J, Čejka J (2008) Catal Rev 50:222
25. Čejka J, Žilková N, Kaluža L, Zdražil M (2002) Stud Surf Sci Catal 141:243
26. Kaluža L, Zdražil M, Žilková N, Čejka J (2002) Catal Commun 3:151
27. Schulz-Ekloff G, Rathouský J, Zukal A (1999) Int J Inorg Mater 1:97
28. Čejka J, Žilková N, Rathouský J, Zukal A (2001) Phys Chem Chem Phys 3:5076
29. Wiley-VCH (ed) (2003) Ullmann's encyclopedia of industrial chemistry, vol 13, 6th edn. Wiley-VCH Verlag GmbH & Co., Weinheim
30. Landa S, Andrzejak A, Weisser O (1962) Collect Czech Chem Commun 27:979
31. Corma A, Iborra S, Miquel S, Primo J (1998) J Catal 173:315
32. Díaz I, Mohino F, Pérez-Pariente J, Sastre E (2003) Appl Catal A Gen 242:161
33. Kubièka D (2008) Collect Czech Chem Commun 73:1015

Applied Catalysis A: General 394 (2011) 9–17

Contents lists available at ScienceDirect

Applied Catalysis A: General

journal homepage: www.elsevier.com/locate/apcata

Deactivation of HDS catalysts in deoxygenation of vegetable oils

David Kubička*, Jan Horáček

Research Institute of Inorganic Chemistry, Department of Refinery and Petrochemical Research, Záluží 1, 436 70 Litvínov, Czech Republic

ARTICLE INFO

Article history:
Received 26 August 2010
Received in revised form 13 October 2010
Accepted 31 October 2010
Available online 5 November 2010

Keywords:
Deoxygenation
Deactivation
Hydrotreating catalysts
Biofuels
Vegetable oils

ABSTRACT

Several rapeseed oils with different degree of upgrading were used as feedstocks for deoxygenation over sulfided CoMo/γ-Al_2O_3 catalyst. The rapeseed oil samples differed in the concentration of inorganic impurities, water, free fatty acids and phospholipids. The catalytic experiments were carried out in a fixed bed reactor at constant reaction conditions (310 °C, WHSV = 2 h^{-1}, hydrogen pressure 3.5 MPa). Refined rapeseed oils were converted to hydrocarbons more efficiently than neat rapeseed oil, trap grease and waste oil. The high concentration of phospholipids in trap grease was the most likely cause of catalyst deactivation by coking. Decomposition of phospholipids as well as oligomerization of rapeseed oil by phosphoric acid at 310 °C was confirmed by separate laboratory experiments. The high concentration of alkalis in waste rapeseed oil was the main reason for increased deactivation in comparison with neat rapeseed oil. Sulfur removal from catalyst active sites affected adversely the deoxygenation of triglycerides. The catalyst deoxygenation activity was partially restored by pulse addition of dimethyldisulfide (DMDS) to the feedstock, however the degradation of active sites by loss of sulfur was not fully reversible. In contrast, continually added sulfur agent (DMDS) ensured significantly slower catalyst deactivation. Moreover, presence of H_2S lowered considerably hydrodeoxygenation/decarboxylation ratio.

1. Introduction

Triglycerides are one of the most versatile and easily exploitable renewable feedstocks for production of fuels and chemicals. By deoxygenation, they can be rather easily converted into hydrocarbons and provide an excellent feedstock for production of ethylene by steam cracking [1] or diesel fuel [2–6]. Owing to its topicality, deoxygenation of triglycerides and related feedstocks has been recently reviewed by several authors [7–9]. Fatty acids and their esters as well as triglycerides, usually vegetable oils, have been used extensively as feedstocks in catalytic deoxygenation yielding hydrocarbons [10–18]. The primary aim of these studies has been to understand the fundamental (mechanistic) aspects of catalytic deoxygenation [10,15,16,18–20], to develop/design suitable active and selective catalysts [15–18,21–23] and to demonstrate the properties of deoxygenation products and their industrial applicability [24–28].

Triglycerides can be converted into hydrocarbons either by using acidic catalysts, such as zeolites and mesoporous molecular sieves [9,29–34], or by using supported metal catalysts in reduced or sulfided state [3,4,9,11]. The former approach can be described as non-selective one as wide variety of hydrocarbons having a broad distribution of molecular weight is obtained. On the other hand, the latter approach can be denoted as selective one since either only oxygen atoms or oxygen atoms together with one carbon atom are removed per each fatty acid moiety. Consequently, the final liquid product has a rather narrow distribution of molecular weights that corresponds almost exclusively to diesel fuel range.

Supported metal catalysts in reduced state, such as Pd/C [8,16,17,21], have been shown to transform fatty acids, their esters and triglycerides into hydrocarbons by decarboxylation, *i.e.* n-alkanes containing an odd number carbon atoms in molecule and carbon dioxide were the main deoxygenation products. On the other hand, sulfided metal catalysts, *e.g.* conventional hydrotreating catalysts, yield more complex hydrocarbon mixtures consisting of n-alkanes having both odd and even carbon atom numbers. It has been demonstrated [10,11,15] that these hydrocarbons are formed by decarboxylation/hydrodecarboxylation and hydrodeoxygenation, respectively. While decarboxylation/hydrodecarboxylation yield CO_2 as the primary oxygenated product of deoxygenation, in hydrodeoxygenation oxygen is removed as water [9].

Hydrotreating catalysts are already applied industrially to produce diesel blending feedstocks from triglycerides [4] and hence investigation of their deactivation behavior is of utmost importance. Several studies have analyzed the impact of hydrotreating products originating from heteroatoms, mainly H_2S, NH_3 and water, on the catalyst activity and selectivity [35–37]. It has been shown that ammonia strongly inhibits both hydrodeoxygenation and (hydro)decarboxylation reactions [35]. The inhibition effect of water was reported to be less than the effect of ammonia [35].

---

* Corresponding author. Tel.: +420 47616 3735.
E-mail address: david.kubicka@vuanch.cz (D. Kubička).

0926-860X/$ – see front matter © 2010 Elsevier B.V. All rights reserved.
doi:10.1016/j.apcata.2010.10.034

Table 1
Concentration of main impurities in processed vegetable oils.

Feed	Acid number (mg/g)[a]	Ca (mg/kg)	Mg (mg/kg)	Na (mg/kg)	K (mg/kg)	P (mg/kg)	M eq. (mmol/kg)[b]	P (mmol/kg)
RRO	0.08	3.80	0.40	4.70	1.80	<0.5	0.237	<0.016
PRO	0.82	3.50	0.45	3.30	1.50	0.71	0.197	0.023
NRO	0.70	146.00	45.90	7.20	24.60	188.00	6.003	6.070
WRO	49.02	74.10	0.91	4.50	4.00	37.90	2.035	1.224
Trap grease	61.00	6.60	2.60	4.80	5.30	310.00	0.444	10.010

[a] mg/g of KOH.

[b] $\text{M eq.} = \frac{\sum(\text{cation charge} \times \text{cation concentration})/\text{cation atomic weight}}{|\text{anion charge}|}$, where anion charge was equal to −2, as the phosphate group is bound to the glycerol backbone in phospholipids.

For example, addition 5000 wt. ppm of water reduced conversion of methyl- and ethylheptanoate by ca. 5–10% [36]. In contrast to ammonia and water, hydrogen sulfide promoted deoxygenation of esters over both NiMo and CoMo catalysts [35,37].

A key economic aspect of triglycerides conversion to hydrocarbons is the price of raw materials, which depends strongly on the required upgrading level of triglycerides-containing feedstocks to prevent catalyst deactivation. Therefore, lower quality feedstocks, such as waste cooking or frying oils, have been investigated as alternative source of triglycerides [38,39]. It has been demonstrated that despite their lower quality, waste cooking oils can be converted over conventional hydrotreating catalysts into diesel-like products, *i.e.* hydrocarbons. The thermal changes in vegetable (cooking) oils may, however, negatively influence the quality of the diesel-like products as it is obvious from the distillation curves of these products [38].

The effects of naturally occurring impurities of vegetable oils, or triglycerides in general, on deactivation of deoxygenation catalysts have not been discussed in detail as yet. Hence the main objective of this contribution is to address the issue of deactivation of hydrotreating catalysts used for catalytic deoxygenation of triglycerides. In particular, the effects of phosphorus, alkalis (*i.e.* alkali and alkaline-earth metals are referred to as alkalis for the sake of brevity) and sulfur on catalyst deactivation will be discussed in detail. The underlying cause of deactivation, such as coking or poisoning, due to presence of different feedstock impurities will be identified.

2. Experimental

Samples of vegetable oils originated from rapeseed refining for food and biodiesel production and were obtained from Setuza a.s. The following feeds were used in the hydrotreating experiments: refined rapeseed oil (RRO, *i.e.* food quality oil), primary refined rapeseed oil (PRO, *i.e.* oil after degumming), neat rapeseed oil (NRO, *i.e.* fresh oil after pressing and extraction from seeds), trap grease (TG, *i.e.* oil collected from washing the tanks *etc.*), oleic acid (Fluka, *p.a.*) and waste rapeseed oil (WRO, *i.e.* oil separated during water treatment process). An overview of the feedstocks together with their main impurities, namely alkalis and phosphorus, is given in Table 1. A general process of rapeseed refining to yield food quality rapeseed oil is shown in Fig. 1. The concentrations of major impurities (Table 1) were determined by ICP (inductively coupled plasma). In addition, the value acid number (mg_{KOH}/g_{oil}) of the feedstocks that reflects the concentration of free fatty acids is reported as well. Standard refinery hydrogen (>99%, v/v) was used as hydrogen source in the catalytic experiments. Its main impurities were methane (ca. 0.7%, v/v) and nitrogen (ca.0.3%, v/v).

All hydrotreating experiments were carried out in an electrically heated fixed bed tubular reactor. The reaction temperature, hydrogen pressure, hydrogen-to-oil molar ratio and WHSV were kept constant at 310 °C, 3.5 MPa, 100 mol/mol and $2\ h^{-1}$, in that order. The selection of the reaction conditions was based on previous experience [7,15] in order to follow the catalyst activity decrease. A commercial $CoMo/\gamma\text{-}Al_2O_3$ catalyst was used containing 3.0 wt.% CoO and 13.5 wt.% MoO_3 was used in the experiments. The original extrudates (1 mm) were diluted with SiC (0.1 mm) to achieve good heat and mass transfer and avoid feed channeling. Fresh catalyst was used for each experiment and it was sulfided prior to the experiments to obtain its active sulfide form by in-situ activation using dimethyldisulfide (DMDS). The experimental procedure was described previously in detail elsewhere [7,15]. The specific surface area (BET) of the fresh catalyst in oxide state was $188\ m^2/g$ as determined by nitrogen physisorption (Carlo Erba Instruments Sorptomatic 1900). Moreover, carbon and sulfur content on the spent catalyst was determined as well.

As the main objective of the experiments was to establish the role of vegetable oil impurities in catalyst deactivation, the experiments were performed under constant conditions for ca. 100–150 h. In addition, a set of experiments aimed at determination of the effect of added sulfur on catalyst activity was carried out. In these tests two feedstocks were used: refined rapeseed oil

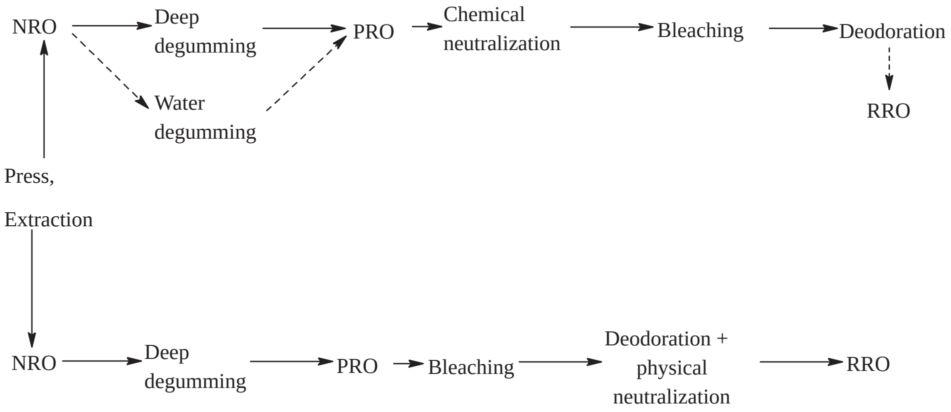

Fig. 1. Scheme of rapeseed refining alternatives.

(RRO) and RRO containing 0.5 wt.% DMDS (RRO-SC). In this case the experiment lasted >250 h. Finally an experiment was carried out where two feedstocks, sulfur-free RRO and RRO containing 1 wt.% S in the form of DMDS (RRO-SP), were alternated—after feeding RRO for 120 h, RRO-SP was fed for 12 h. Then once again RRO was fed for 42 h followed by feeding RRO-S for 8 h. Finally, feeding RRO for 48 h concluded the test.

In each experiment, samples of liquid phase products were collected in high-pressure gas/liquid separator and withdrawn every four hours. The temperature of the separator was kept constant at 80 °C to keep saturated triglycerides, fatty esters and fatty acids above their melting point. The collected samples were first separated into organic and water layer. The organic layer was then analyzed off-line by GC technique using on-column injection. Due to the complex nature of the reaction products, the organic layer samples had to be silylated prior to their analysis. N-methyl-N-(trimethylsilyl)trifluoroacetamide (MSTFA) was used as the silylation agent. 66.8 μl of MSTFA was added to 6.8 μl of each sample dissolved in 4 ml of cyclohexane before analysis. For GC analysis, RESTEK MTX Biodiesel TG w/2 m column was used; column dimensions were 10 m length, 0.32 mm inner diameter and 0.32 μm stationary phase thickness.

A tendency of different feeds to yield carbonaceous deposits (coke) was tested by aging of the raw materials. RRO and RRO with addition of H_3PO_4 equivalent to 310 ppm phosphorus (the same concentration as in trap grease) were heated at 290 or 310 °C for 4 h. The products were characterized visually and by means of density, viscosity and color (ASTM D 1500).

3. Results and discussion

3.1. General product distribution

Catalytic deoxygenation of rapeseed oil over $CoMo/Al_2O_3$ sulfided catalyst results under suitable reaction conditions, *e.g.* 310 °C, 3.5 MPa, 2 h^{-1}, in complete deoxygenation. Consequently, mixture of n-alkanes is formed alongside with water and carbon oxides. While fatty acids bound in triglycerides have exclusively even number of carbon atoms in their molecules, n-alkanes both with even as well as odd carbon number were formed. As reported previously [7,10,11,15], this is a consequence of at least two parallel reaction pathways taking place during deoxygenation, namely hydrodeoxygenation (full hydrogenation, HDO) and hydrodecarboxylation yielding n-alkanes with even and odd carbon number, respectively. The other primary deoxygenation products of these pathways are water and carbon dioxide, correspondingly. In addition, decarbonylation was suggested as plausible reaction pathway as well [10,14].

Due to the complex nature of reactions between water, hydrogen, CO and CO_2, it is virtually impossible to determine whether CO is formed by decarbonylation, *i.e.* as a primary deoxygenation product, or whether it is created in secondary reactions of CO_2. The reaction mechanism has a significant impact on the practical side of deoxygenation as well. On the one hand, if the secondary hydrogenation of CO_2 can be avoided, the hydrogen consumption is lower in decarboxylation than in hydrodeoxygenation. On the other hand, part of feedstock that would be in HDO converted into liquid hydrocarbons is lost as CO_2 or worse as methane unless the subsequent hydrogenation of CO_2 can be controlled.

As the time-on-stream increases, the activity of the catalyst decreases and formation of reaction intermediates can be observed. In agreement with previous studies [10,11,15,22,23] these include fatty acids, fatty alcohols and a product of esterification fatty acids with fatty alcohols, *i.e.* fatty esters. Under severe deactivation mono- and diglycerides have been also detected in the reaction products. The reaction products containing oxygen are referred to as oxygenates or oxygenated products. As the main objective is deoxygenation, saturation of double bonds in triglycerides is not considered as their conversion. As demonstrated below, the changes within intermediates reflect the gradual deterioration of catalyst activity.

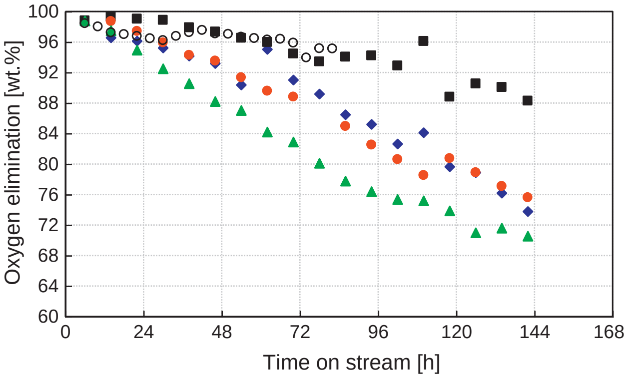

Fig. 2. Deoxygenation of rapeseed oil obtained from different stage of its processing as a function of time-on-stream: (●) RRO – refined rapeseed oil (food grade), (■) PRO – primary refined rapeseed oil (after degumming, without bleaching and desodoration), (♦) NRO – neat rapeseed oil (oil before degumming), (▲) WRO – waste rapeseed oil; (●) oleic acid.

3.2. Effect of alkalis

Rapeseed oil obtained from different stages of its processing was used to study the effect its natural impurities on deactivation of $CoMo/Al_2O_3$ catalyst. An overview of the samples including description of their origin and composition is given in Table 1. The reaction parameters (310 °C, 3.5 MPa, 2 h^{-1}) were set up so that complete deoxygenation of rapeseed oil was achieved at the beginning of the test run and that the decrease of the catalyst activity with increasing time-on-stream could be observed. Elimination of oxygen rather than conversion of triglycerides was selected to describe the catalyst performance as conversion does not always describe the deoxygenation performance of a catalyst. For example, when triglycerides are converted to fatty acids oxygen is not consumed and hence deoxygenation does not occur even though conversion of triglycerides can be, depending on the catalyst, fairly high.

The comparison of deoxygenation of four different rapeseed oils is depicted in Fig. 2. For all investigated grades of rapeseed oils, there is a clear decline in deoxygenation of the feedstock with prolonging time-on-stream. However, the results are somewhat surprising as the lowest quality oil—neat rapeseed oil (NRO), *i.e.* the one with the highest concentration of impurities, was deoxygenated virtually to the same extent as the refined rapeseed oil (RRO), *i.e.* the oil with the lowest concentration of impurities (Fig. 2). Furthermore, the oil that underwent only the first treatment stage (PRO) and had slightly higher concentration of impurities than RRO exhibited the best performance while the waste rapeseed oil showed clearly the poorest performance (Fig. 2). In order to understand these peculiarities it is necessary to study not only the absolute concentrations of impurities, but also their balance, *i.e.* the balance between the cations (alkalis) and anions represented by the phosphate anion originating from phospholipids. It can be seen (Table 1) that except NRO there is imbalance between alkalis cations, on the one hand, and phosphate anion on the other hand in the waste and refined oils. The most pronounced imbalance was observed for WRO that in turn showed the worst performance (Fig. 2), *i.e.* the most pronounced deactivation presumably due to the alkalis. Nonetheless, the absolute concentration of the impurities is essential in both cases. In the case of imbalance between cations and anions the deactivation rate will increase with the increasing concentration of impurities. In the specific case when the concentration of cations of alkalis and phosphate anion are in balance, deposits will be formed that will cause plugging of the reactor.

The striking behavior of NRO has a rather simple explanation. The phospholipids tend to decompose under the reaction conditions, as discussed below, and in the case of NRO alkalis phosphates were formed and deposited before and at the very beginning of the catalyst bed. Consequently, the feedstock entering the catalyst bed was virtually free of impurities and hence it performed similarly to RRO (Fig. 2). Obviously, a longer time-on-stream would result in build up of phosphate deposits, increased pressure drop and ultimately in plugging of the reactor.

The differences in composition of RRO and PRO are almost negligible (Table 1) and can be thus hardly the reason for the systematic difference in deoxygenation of these oils (Fig. 2). Nonetheless, it is not a matter of the repeatability of the catalytic tests as will be shown later when discussing the effect of H_2S on the catalyst performance (see Fig. 6). A plausible explanation is lower susceptibility of PRO to thermal degradation in comparison with RRO that has undergone more extensive treatment and some of its natural antioxidants were destroyed in the process. NRO should be, however, the best oil in this regard as it did not undergo any thermal or chemical treatment. Hence, it has to be concluded that the nature of the differences in deoxygenation of RRO and PRO is not yet satisfactorily explained. On the other hand, the effect of alkalis seems to be detrimental for the catalyst activity (WRO) as would ultimately be the phosphate deposits originating from decomposition of phospholipids (NRO) present in neat vegetable oils.

The damaging effect of alkalis on catalyst performance can be understood more clearly when comparing the yields of hydrocarbons or oxygenated products (Fig. 3a and b). While the final elimination of oxygen (defined as ratio of the following mass fractions: (oxygen in feedstock—oxygen in products)/(oxygen in feedstock) multiplied by 100) *i.e.* after 144 h, was about 70% for WRO and ca. 75% for RRO (Fig. 2), the yield of hydrocarbons dropped to ca. 62% for RRO and to about 45% for WRO (Fig. 3a). Similarly, the yield of oxygenated intermediates is significantly higher for WRO (ca. 50%) in comparison with RRO (ca. 20%), see Fig. 3b. These differences can be attributed primarily to deterioration of catalyst activity that can be evidenced by a significant increase in formation of fatty ester, *i.e.* secondary reaction intermediates, in the experiment where WRO was used as feedstock (Fig. 3c). It should be noted that in contrast to the other oils WRO contains significant amount of free fatty acids. Their concentration was based on the determined acid number (Table 1) ca. 20–25%. Nonetheless, experiments carried out with neat oleic acid (Fluka, p.a.) clearly demonstrated that under the selected reaction conditions oleic acid was converted to hydrocarbons at similar deoxygenation rate as refined rapeseed oil, PRO (Fig. 2). Therefore, any deviations between WRO and the other oils cannot be ascribed to its higher concentration of fatty acids, but rather to the feedstock quality, *i.e.* low concentration of impurities such as alkalis and phosphorus is of the utmost importance.

The gradual loss of catalyst activity when feedstock contains alkalis cations without charge-compensating inorganic anion can be explained by deposition of alkalis (*i.e.* alkali and alkaline-earth metals) on catalyst surface inducing electronic effects limiting hydrogenation [40]. Consequently, the hydrodeoxygenation pathway as well as hydrogenation of double bonds would be suppressed. Alkalis were observed to deposit on the external surface of catalyst particles [41] and calcium was reported to cause deactivation in hydrogenation, hydrocracking, hydrodesulfurization and hydrodeoxygenation. [42]. Moreover, various alkalis molybdates, tungstates and aluminates were indicated as thermodynamically probable compounds formed on hydroprocessing catalysts in presence of alkalis particles. However, their stability and behavior under hydroprocessing conditions is unknown [41].

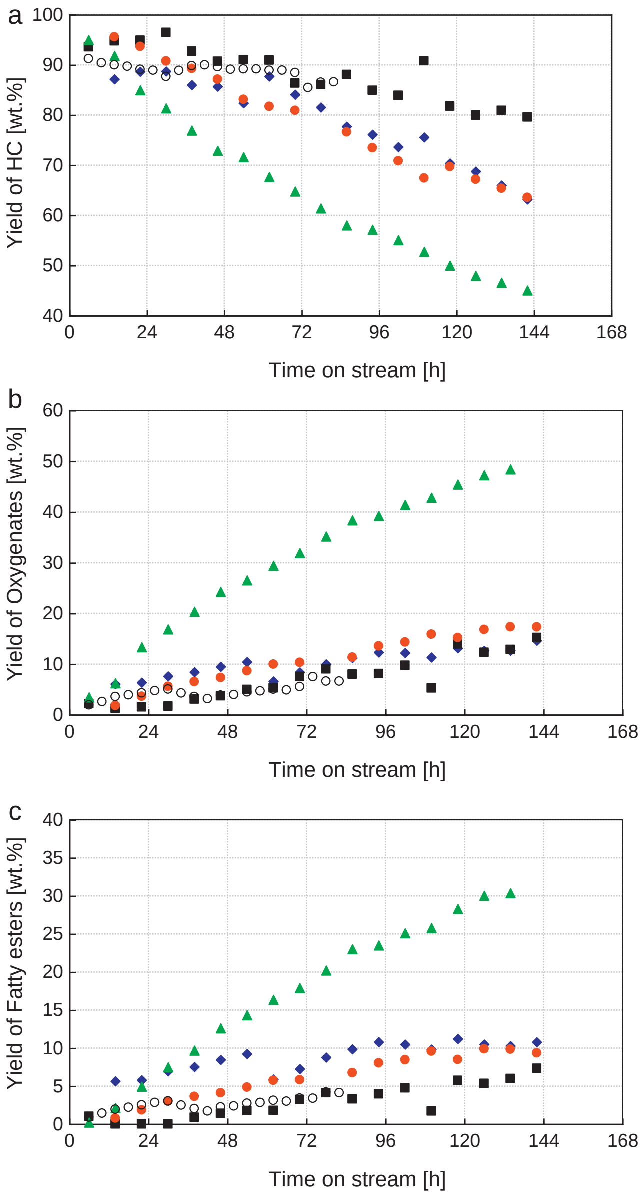

Fig. 3. Hydrocarbons (a), oxygenates (b) and fatty esters (c) content in deoxygenation products as function of time on stream: (●) RRO – refined rapeseed oil (food grade), (■) PRO – primary refined rapeseed oil (after degumming, without bleaching and desodoration), (♦) NRO – neat rapeseed oil (oil before degumming), (▲) WRO – waste rapeseed oil; (●) oleic acid.

3.3. *Effect of phosphorus*

While the rapeseed-oil-based feedstocks have shown low to moderate rate of deactivation (Fig. 3) depending on the degree of their upgrading and the residual level of impurities, trap grease, a very specific waste stream from vegetable oils processing, caused severe catalyst deactivation (Fig. 4a and b). Virtually all deoxygenation activity was lost within the first 48 h on stream (Fig. 4a and b). The trap grease contains significant amounts of phosphorus together with free fatty acids (Table 1). In the case of vegetable-oils-based feedstock it means that phospholipids are present. In contrast to neat (not refined) vegetable oils (*e.g.* NRO in Table 1) that contain alkalis and hence the phosphate group is neutral, the phosphate group in trap grease is acidic as there is only low concentration of alkalis (Table 1). Consequently, upon decomposition of phospholipids phosphoric acid is released and it acts as an oligomerization/polymerization catalyst [43,44]. The high-

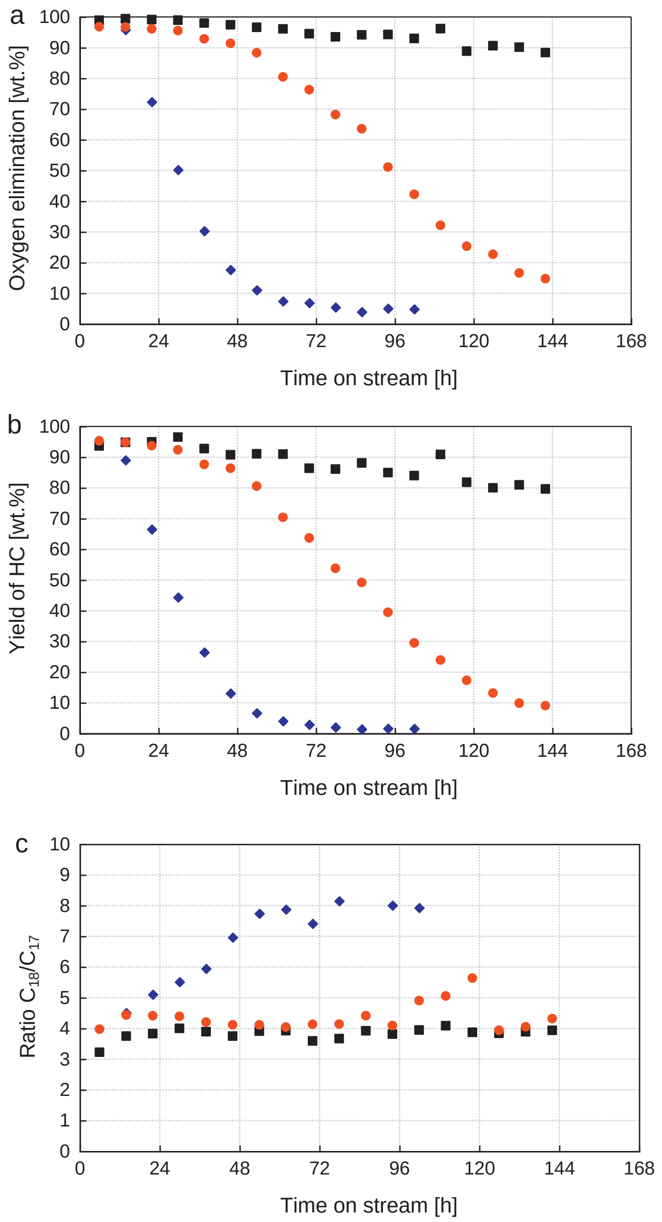

Fig. 4. Deoxygenation of rapeseed oil obtained from different stage of its processing as a function of time-on-stream (a); hydrocarbons production as function of time on stream (b); weight ratio of C_{18} and C_{17} hydrocarbons as function of of time on stream (c): (♦) TG-Trap Grease; (■) PRO-Primary refined oil; (●) mixture of TG and PRO (1:2).

molecular-weight oligomers tend to deposit on catalyst surface leading ultimately to formation of carbonaceous deposits and catalyst deactivation. In fact, the deactivation was so severe that it caused reactor plugging and the experiment had to be stopped just after 100 h on stream (Fig. 4a and b). It should be noted that the observed yield of oxygenated products, mainly fatty acids, originates predominantly from the feedstock and not from the conversion of triglycerides (Fig. 5a). Unfortunately, it was not possible to determine the content of fatty acids in trap grease chromatographically due to the high content of triglycerides that prevented any reliable analysis. However, based on the determined acid number of trap grease (Table 1), it can be roughly estimated that neat trap grease contained about 30 wt.% of free fatty acids.

The formation of oligomers was confirmed in laboratory experiments using refined rapeseed oil (RRO) and phosphoric acid. When RRO was heated up to 290 or 310 °C in presence of phosphoric acid a dark sludge was formed and the density, viscosity a color (ASTM D1500) increased in comparison with the fresh (unheated) RRO (Table 2). Heating RRO in absence of phosphoric acid resulted also in increased density, viscosity and color of the oil (Table 2). However, no sludge was formed and particularly the change in color was significantly less in absence of phosphoric acid. The changes in density and viscosity after heating the oil to 310 °C with and without phosphoric acid, respectively, were larger when phosphoric acid was present, but the differences were not too significant (Table 2). Similar changes were also observed for the trap grease. The formation of sludge was hence attributed to oligomerization reactions catalyzed by phosphoric acids and the sludge was suggested to be a precursor of the carbonaceous deposits formed on the catalyst during the course of trap grease deoxygenation.

To investigate the course of deactivation by coking during deoxygenation of vegetable-oil-based feedstocks, the neat trap grease (TG) was diluted by refined rapeseed oil (PRO) to contain

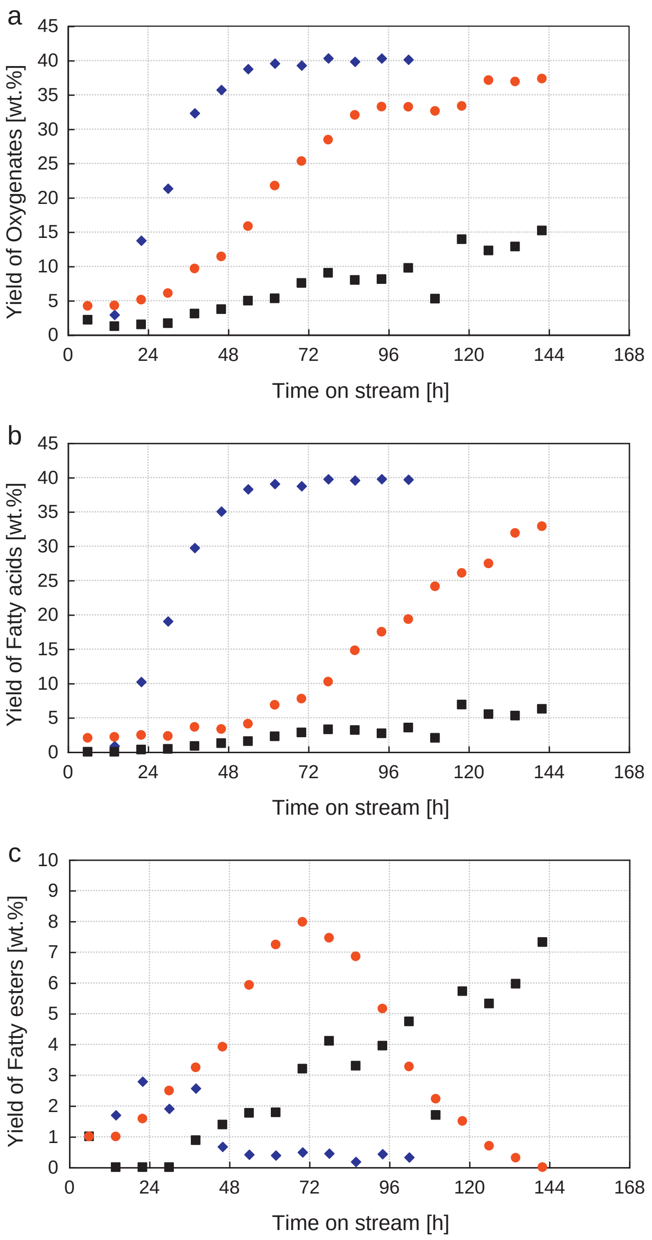

Fig. 5. Oxygenates (a), acids (b) and fatty esters(c) content in deoxygenation products as function of time on stream: (♦) TG-Trap Grease; (■) PRO-Primary refined oil; (●) mixture of TG and PRO (1:2).

Table 2
Physical parameters of fresh and aged oils.

Raw material	Temperature (°C)	Density (g/cm^3)$_{(15\,°C)}$	Viscosity (CSt)$_{(40\,°C)}$	Index of color
RRO	a	0.9201	35.93	0.6
	310	0.9295	101.32	1.5
RRO + H_3PO_4	290	0.9251	53.61	2.2
	310	0.9302	102.47	2.5
Trap grease	a	0.9200	33.08	6.3
	290	0.9178	45.05	7.0
	310	0.9253	69.15	b

(a) Represents fresh oil and (b) not analyzed.

3.35 mmol P/g (*i.e.* ca. one third of the original phosphorus concentration). As a result, the catalyst deactivation was slowed down (Fig. 4a and b) and it was possible to follow the development of individual reaction products and intermediates with time-on-stream (Fig. 5a–c). It can be clearly seen that the yield of hydrocarbons closely followed the elimination of oxygen (Fig. 4a and b), *i.e.* there were not formed significant quantities of partially deoxygenated products, such as alcohols. The yields of oxygenated products confirmed this conclusion; the only organic-phase products of partial deoxygenation observed are fatty esters (Fig. 5c). The overall yield of oxygenated products increased with time-on-stream (Fig. 5a); the higher the concentration of phosphorus in the feed the faster the increase of oxygenates. The oxygenated products consisted of fatty acids and fatty esters, *i.e.* products of esterification reaction between fatty acids and fatty alcohols (Fig. 5c). Other oxygenates namely fatty alcohols, diglycerides, monoglycerides and propylesters, were present only in negligible amounts.

Valuable insight into the course of deoxygenation can be gained from the changes of yields of fatty esters with time-on-stream (Fig. 5c). On a fresh catalyst with slowly-deactivating feedstocks (PRO), fatty esters were virtually absent and their concentration increased with time-on-stream as a result of catalyst deactivation. When a feedstock more prone to deactivating the catalyst (TG+PRO) was used, the concentration of fatty esters increased at first showing that not all intermediates could be converted to hydrocarbons under the chosen reaction conditions (Fig. 5c). The increase was, however, followed by a decrease of fatty esters concentration that was accompanied by a pronounced increase in concentration of fatty acids approximately after 72 h TOS (Fig. 5c). This can be attributed to further deactivation resulting in suppressed hydrogenation activity of the catalyst. Fatty alcohols were thus not formed and consequently fatty esters could not be formed either and the concentration of fatty acids started increasing (Fig. 5c). The increase of fatty acids also suggests that the relative decarboxylation activity of the catalyst was not increased. This conclusion is confirmed by the ratio of C_{18}/C_{17} hydrocarbons, *i.e.* ratio of hydrodeoxygenation/hydrodecarboxylation reactions (Fig. 4c). The results indicated that the decarboxylation activity was suppressed more than the hydrodeoxygenation activity. However, as the yield of hydrocarbons was close to zero, the accuracy of the ratio is rather low (division of two very small numbers in the range of tenths of a percent) and the result should thus not be overestimated.

Table 3
Amounts of sulfur and carbon in spent catalysts.

Feedstock	C on catalyst (wt.%)	S on catalyst (wt.%)	Time on stream (h)
NRO	12.60	8.99	176
RRO	14.60	8.86	154
PRO	13.12	8.53	154
TG	10.90	9.52	114
TG + PRO	10.01	8.72	154
RRO-SP	14.50	9.19	240
RRO-SC	13.23	9.47	266
WRO	12.44	8.96	130
Oleic acid	12.80	8.36	84

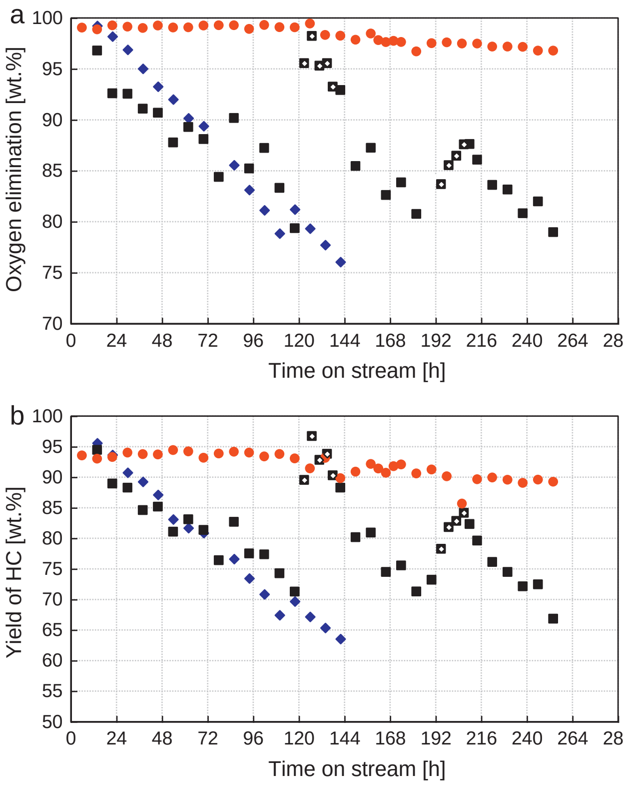

Fig. 6. Deoxygenation (a) of refined rapeseed oil (RRO): pure and sulfured RRO and hydrocarbons yields (b) as function of time on stream: (♦) RRO-refined rapeseed oil; (■) RRO-SP pulses-refined rapeseed oil with pulses of sulfured RRO; (●) RRO-SC.

3.4. *Effect of sulfur*

The gradual catalyst activity decrease when refined rapeseed oils (NRO, PRO) were used as feedstock can be ascribed neither to alkalis nor phosphorus, as these were virtually absent in these feedstocks. There are two plausible explanations for this deactivation: (i) formation of carbonaceous deposits blocking the active sites and (ii) depletion of active sites by gradual sulfur removal from the catalyst surface due to absence of sulfur in the feedstock. Addition of dimethyldisulfide (DMDS) to refined rapeseed oil (RRO), 0.5 wt.% DMDS in RRO (RRO-SC), resulted in significantly improved stability of the catalyst activity over long TOS (Fig. 6a). When neat RRO was used the elimination of oxygen dropped to ca. 75% after 144 h TOS, whereas it remained above 95% when the feedstock contained DMDS (Fig. 6a). It can be therefore inferred that the main reason for the gradual deactivation during vegetable oils deoxygenation was the depletion of sulfur. Obviously, sulfur depletion will play a role in deoxygenation of other investigated feedstocks as well. Nevertheless, it can be expected that the effect of sulfur depletion on catalyst deactivation will not be affected by feed impurities.

Previously, the loss of catalyst activity was attributed to loss of incompletely coordinated sulfur in sulfided CoMo catalyst during tetrahydrofuran hydrogenation [45]. The changes in catalyst active phase are partially reversible, as demonstrated on Figs. 6a and b. When neat RRO was replaced with sulfur-containing feedstock (RRO-SP), elimination of oxygen improved significantly (Fig. 6a). However, under the sulfur-free conditions the loss of deoxygenation activity continued and the next introduction of RRO-SP led only to partial recovery of the catalyst activity. It can be concluded that some of the changes leading to catalyst deactivation

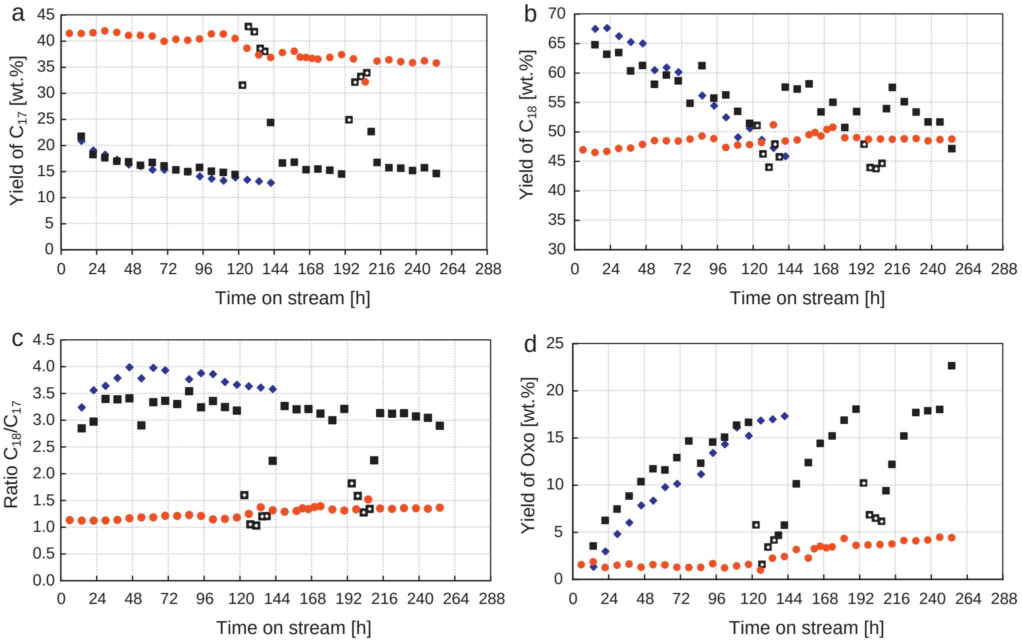

Fig. 7. Yields of C_{17} (a) and C_{18} (b) hydrocarbons, hydrodeoxygenation/decarboxylation ratio (c) and oxygenates yields (d) as functions of time on stream: (♦) RRO-refined rapeseed oil; (■) RRO-SP pulses-refined rapeseed oil with pulses of sulfured RRO; (●) RRO-SC.

are irreversible. These changes can be plausibly attributed to partial reduction of the sulfide phase (*i.e.* loss of sulfur) under reaction conditions due to insufficient quantities of sulfur in the feedstock to maintain catalyst in sulfided form [46,47]. Alternatively, the active phase may undergo oxidation changes (sulfur to sulfate, Mo^{4+} to Mo^{6+}) due to the presence of oxygen-containing compounds [46]. A comparison of DMDS pulses with continuous feeding of sulfur-doped oil (RRO-SC) showed that continuous catalyst reactivation with sulfur-containing feed is more effective than reactivation by pulses (Fig. 6). This can be also observed from the characterization of spent catalysts (Table 3). The concentration of sulfur in the catalyst decreases in the order RRO-SC > RRO-SP > RRO and correlates with the catalyst performance (the oxygen elimination decreases in the same order). Moreover, the amount of carbonaceous deposits (expressed in wt.% of carbon) decreases in the same order as well (Table 3). Except the experiments with TG, the contents of carbon and sulfur on the catalyst were rather comparable. The deviation can be explained by rapid deactivation and blocking of the initial part of the catalyst bed that resulted in reactor plugging, which prevented further formation of carbonaceous deposits and depletion sulfur.

Apart from improving the stability of catalyst deoxygenation activity, DMDS affected considerably product selectivity and hence the preferred reaction pathway (Figs. 7 and 8a and b). Hydrodeoxygenation (HDO) is the predominant reaction pathway in the absence of DMDS, *i.e.* in the absence of H_2S as DMDS decomposes under the reaction conditions and yields H_2S and methane. Consequently, the C_{18}/C_{17} ratio was in the range 3–4 which means that formation of HDO products was 3–4 times faster than formation of hydrodecarboxylation (HDC) products (Fig. 7c). However, when the feedstock contained DMDS, the ratio C_{18}/C_{17} was close to 1 (in the range 1–1.5), which means that HDC reaction pathway played a more significant role. This is clearly visible from the yields of C_{17} hydrocarbons that were higher in presence of DMDS than in its absence (Fig. 7a). At the same time the yield of C_{18} hydrocarbons was suppressed (Fig. 7b). If the main impact of H_2S was only suppression of catalyst hydrogenation activity, the catalyst deoxygenation activity should be deteriorated as a result of DMDS addition. The experimental results showed the opposite (Fig. 6a), *i.e.* enhanced oxygen elimination, and it can be hence inferred that the main consequence of DMDS (H_2S) addition was the promotion of its hydrodecarboxylation activity as suggested also by the changes in C_{18}/C_{17} ratio (Fig. 7c). The pulses of RRO-SP caused an increase in C_{17} hydrocarbons yield while the yield of C_{18} hydrocarbons was enhanced significantly less (Fig. 7b). These changes can be attributed to the increased hydrogenolysis activity, which is a consequence of dissociative adsorption of H_2S on coordinatively unsaturated sites leading to formation of Brønsted acid sites [47,48].

Addition of DMDS in the feedstock influenced significantly also distribution in the group of oxygenates. As a result of better stability of the active phase and hence of the catalyst activity in presence of H_2S, only low yields of fatty esters, fatty acids and fatty alcohols were observed over the whole range of TOS (Fig. 8a and b). Nonetheless, their concentration increased slightly with TOS, *i.e.* some deactivation of the catalyst occurred (Fig. 8a and b). When DMDS was not added (RRO), fatty esters and alcohols were the main oxygenated products and their yield increased gradually with TOS (Fig. 8b and c). Substitution of sulfur-free by sulfur-containing feedstock (*i.e.* of RRO by RRO-SP) resulted in dramatic changes. The yield of fatty esters as well as of fatty alcohols dropped immediately virtually to zero (Fig. 8a and b). Since fatty esters are tertiary reaction intermediates formed by esterification of fatty acids (primary reaction intermediates) by fatty alcohols (secondary reaction intermediates), their disappearance can be explained by disappearance of fatty alcohols. Since fatty alcohols are formed by hydrogenation of fatty acids, the sudden decrease in the yield of fatty alcohols after introduction of DMDS can be attributed plausibly to either decreased hydrogenation rate of fatty acids to fatty alcohols or to increased consumption rate of fatty acids by a competing reaction, in this case by decarboxylation. As discussed above, if decreased hydrogenation rate was the main cause of the decreased fatty alcohols yield, the yield of fatty acids should increase dramatically. Even though there can be observed some increase in the yield of fatty acids as a result of DMDS introduction, it is significantly less than the decrease of fatty alcohols and fatty esters. This implies

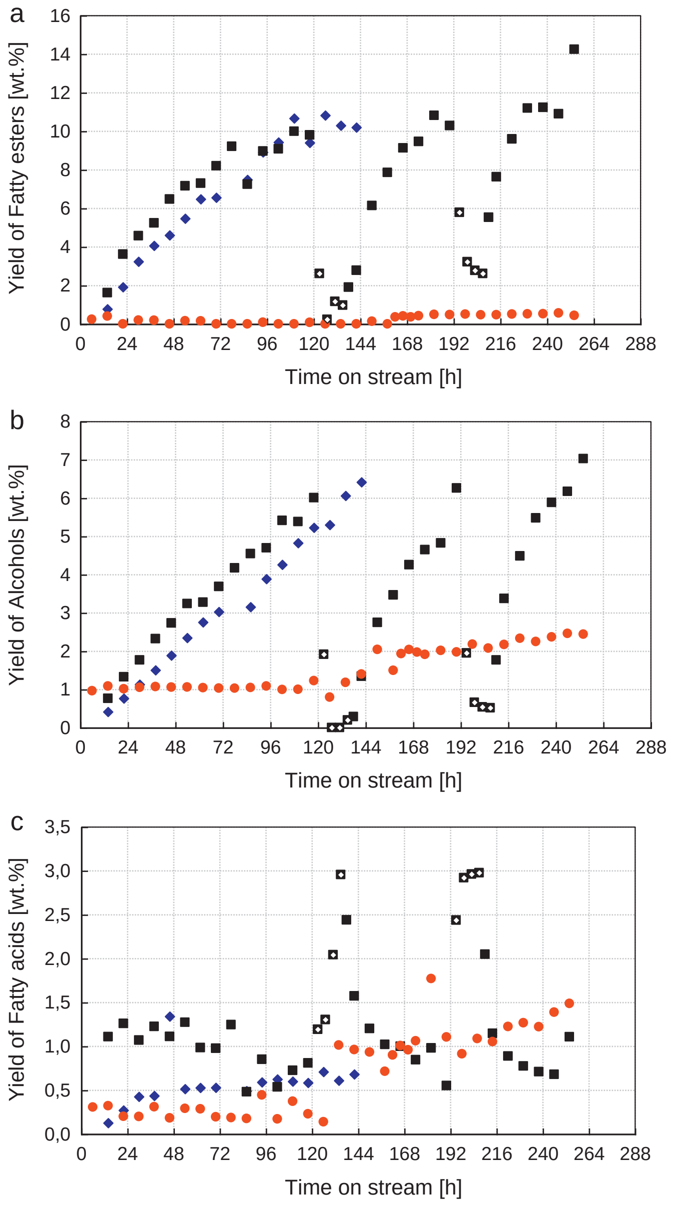

Fig. 8. Fatty esters (a), alcohols (b) and acids (c) yields obtained from pure and sulfured RRO as function of time on stream: (♦) RRO-refined rapeseed oil; (■) RRO-SP pulses-refined rapeseed oil with pulses of sulfured RRO; (●) RRO-SC.

that the main cause for the decrease in the yield of fatty alcohols is the increased consumption of fatty acids by a competing reaction. Based on the hydrocarbon product distribution it can be concluded that the competing reaction is decarboxylation of fatty acid intermediates or hydrodecarboxylation of triglycerides.

4. Conclusions

Catalytic deoxygenation of different rapeseed-oil-derived feedstocks over sulfided CoMo catalyst was carried out at 310 °C and 3.5 MPa (H_2 pressure) in a fixed-bed reactor aiming at description of parameters affecting the catalyst deactivation. Three main feedstock-related parameters were identified to play an important role in deoxygenation catalyst deactivation, namely the concentrations of phosphorus, alkalis and sulfur.

Presence of alkalis promoted catalyst deactivation due to their deposition on catalyst surface leading to blockage/poisoning of active sites. The effect of phosphorus was two-fold. When charge-compensating alkalis were present, corresponding phosphates were deposited above and at the beginning of catalyst bed leading to gradual build-up of deposits. On the other hand, in absence of alkalis decomposition of phospholipids yielded phosphoric acid that catalyzed oligomerization reactions leading to rapid catalyst deactivation by carbonaceous deposits.

Presence of sulfur compounds, here demonstrated by addition of dimethyldisulfide (DMDS), was shown to be beneficial for the catalyst deoxygenation performance. While in absence of DMDS gradual deactivation was observed, addition of DMDS resulted in a stable catalyst performance. The changes in active sites structure caused by their desulfurization under hydrogen atmosphere were shown to be partially reversible. Nonetheless, part of the active sites was irreversibly lost. In addition to modifying catalyst activity, H_2S formed by DMDS decomposition, influenced significantly the selectivity of deoxygenation reactions. The presence of H_2S resulted in an augmented (hydro)decarboxylation catalyst selectivity plausibly owing to the increased catalyst acidity.

Acknowledgements

The financial support from the Ministry of Industry and Trade of the Czech Republic (project No. FT-TA3/074) is gratefully acknowledged.

References

[1] D. Kubička, J. Lederer, Z. Bělohlav, Oil Gas Eur. Mag. 35 (2009) 40–43.
[2] W.K. Craig, D.W. Soveran, Production of hydrocarbons with relatively high cetane rating, United States Patent, US 4,992,605 (1991).
[3] D.Yu. Murzin, I. Kubičková, M. Snåre, P. Mäki-Arvela, J. Myllyoja, Method for the manufacture of hydrocarbons, PCT International Application WO 2006/075057 A2 (2006).
[4] J. Jakkula, V. Niemi, J. Nikkonen, V.-M. Purola, J. Myllyoja, P. Aalto, J.Lehtonen, V. Alopaeus, Process for producing hydrocarbon component of biological origin, United States Patent, US 7,232,935 (2007).
[5] A. R. Pinho, M. Silva, A. P. Silva Neto, J. A. R. Cabral, Catalytic cracking process for the production of diesel from vegetable oils, United States Patent, US 7,540,952 B2 (2009).
[6] J. A. Petri, T. L. Marker, Production of diesel fuel from biorenewable feedstocks, United States Patent, US 7,511,181 B2 (2009).
[7] D. Kubička, Collect. Czech. Chem. Commun. 73 (2008) 1015–1044.
[8] S. Lestari, P. Mäki-Arvela, J. Beltramini, G.Q. Max Lu, D.Yu. Murzin, ChemSusChem 2 (2009) 1109–1119.
[9] I. Kubičková, D. Kubička, Waste Biomass Valor 1 (2010) 293–308.
[10] B. Donnis, R.G. Egeberg, P. Blom, K.G. Knudsen, Top. Catal. 52 (2009) 229–240.
[11] E. Laurent, B. Delmon, Appl. Catal. 109 (1994) 77–96.
[12] O.I. Şenol, T.R. Viljava, A.O.I. Krause, Catal. Today 100 (2005) 331–335.
[13] G.N.d. Rocha Filho, D. Brodzki, G. Djega-Mariadassou, Fuel 72 (1993) 543–549.
[14] J. Gusmão, D. Brodzki, G. Djega-Mariadassou, R. Frety, Catal. Today 5 (1989) 533–544.
[15] D. Kubička, L. Kaluža, Appl. Catal. A: Gen. 372 (2010) 199–208.
[16] I. Kubičková, M. Snåre, K. Eränen, P. Mäki-Arvela, D.Yu. Murzin, Catal. Today 106 (2005) 197–200.
[17] M. Snåre, I. Kubičková, P. Mäki-Arvela, K. Eränen, D. Yu, Murzin Ind. Eng. Chem. Res. 45 (2006) 5708–5715.
[18] P.T. Do, M. Chiappero, L.L. Lobban, D.E. Resasco, Catal. Lett. 130 (2009) 9–18.
[19] L. Boda, G. Onyestyák, H. Solt, F. Lónyi, J. Valyon, A. Thernesz, Appl. Catal. A: Gen. 374 (2010) 158–169.
[20] J.G. Immer, M.J. Kelly, H.H. Lamb, Appl. Catal. A: Gen. 375 (2010) 134–139.
[21] M. Snåre, I. Kubičková, P. Mäki-Arvela, D. Chichova, K. Eränen, D.Yu. Murzin, Fuel 87 (2008) 933–945.
[22] D. Kubička, M. Bejblová, J. Vlk, Top. Catal. 53 (2010) 168–178.
[23] D. Kubička, P. Šimáček, N. Žilková, Top. Catal. 52 (2009) 161–168.
[24] P. Šimáček, D. Kubička, G. Šebor, M. Pospíšil, Fuel 88 (2009) 456–460.
[25] P. Šimáček, D. Kubička, G. Šebor, M. Pospíšil, Fuel 89 (2010) 611–615.
[26] P. Šimáček, D. Kubička, Fuel 89 (2010) 1508–1513.
[27] I. Sebos, A. Matsoukas, V. Apostolopoulos, N. Papayannakos, Fuel 88 (2009) 145–149.
[28] J. Mikulec, J. Cvengroš, Ľ. Joríková, M. Banič, A. Kleinová, J. Clean. Prod. 18 (2010) 917–926.
[29] F.A. Twaiq, N.A.M. Zabidi, S. Bhatia, Ind. Eng. Chem. Res. 38 (1999) 3230–3237.
[30] J.D. Adjaye, S.P.R. Katikaneni, N.N. Bakhshi, Fuel Process. Technol. 48 (1996) 115–143.
[31] S.P.R. Katikaneni, J.D. Adjaye, N.N. Bakhshi, Can. J. Chem. Eng. 73 (1995) 484–497.
[32] T. Danuthai, S. Jongpatiwut, T. Rirksomboon, S. Osman, D.E. Resasco, Appl. Catal. A: Gen. 361 (2009) 99–105.

[33] T. Danuthai, S. Jongpatiwut, T. Rirksomboon, S. Osman, D.E. Resasco, Catal. Lett. 132 (2009) 197–204.
[34] T. Sooknoi, T. Danuthai, L.L. Lobban, R.G. Mallinson, D.E. Resasco, J. Catal. 258 (2008) 199–209.
[35] E. Laurent, B. Delmon, Appl. Catal. 109 (1994) 97–115.
[36] O.İ. Şenol, T.-R. Viljava, A.O.I. Krause, Catal. Today 106 (2005) 186–189.
[37] O.İ. Şenol, E.-M. Ryymin, T.-R. Viljava, A.O.I. Krause, J. Mol. Catal. A: Chem. 277 (2007) 107–112.
[38] S. Bezergianni, A. Dimitriadis, A. Kalogianni, P.A. Pilavachi, Bioresour. Technol. 101 (2010) 6651–6656.
[39] S. Bezergianni, A. Dimitriadis, T. Sfetsas, A. Kalogianni, Bioresour. Technol. 101 (2010) 7658–7660.
[40] S. Brunet, D. Mey, G. Perot, C. Bouchy, F. Diehl, Appl. Cat. A: Gen. 278 (2005) 143–172.
[41] E. Furimsky, F.E. Massoth, Catal. Today 52 (1999) 381–495.
[42] T.L. Cable, F.E. Massoth, M.G. Thomas, Fuel Process. Technol. 10 (1985) 105.
[43] F. Cavani, G. Girotti, G. Terzoni, Appl. Cat. A: Gen. 97 (1993) 177–196.
[44] A. De Klerk, Ind. Eng. Chem. Res. 44 (2005) 3887–3893.
[45] E. Furimsky, Ind. Eng. Chem. Prod. Res. Dev. 22 (1983) 34.
[46] E. Furimsky, F.E. Massoth, Catal. Today 17 (1993) 537–660.
[47] A. Stanislaus, A. Marafi, M.S. Rana, Catal. Today 153 (2010) 1–68.
[48] H. Topsoe, B.S. Clausen, F.E. Massoth, Hydrotreating Catalysis, Science and Technology, Springer Verlag, Berlin, 1996.

CHAPTER THREE

Hydrotreating of Triglyceride-Based Feedstocks in Refineries

David Kubička[*], **Vratislav Tukač**[†]
[*]Department of Renewable and Environmental Technologies (UniCRE-RENTECH), Research Institute of Inorganic Chemistry (VUANCH), Chempark Litvínov, Litvínov, Czech Republic
[†]Department of Organic Technology, Institute of Chemical Technology Prague, Technická 5, Praha, Czech Republic

Contents

Abstract

This chapter deals with some important aspects of deoxygenation of triglycerides that has become a new refining technology. After the introduction of basics of deoxygenation chemistry, the thermodynamic aspects of deoxygenation are discussed. Then hydrodynamics in conventional hydrotreaters is compared with the deoxygenation system, and predictions on the vegetable oils deoxygenation are made. Kinetics of triglyceride deoxygenation reactions including kinetics of the individual reaction steps

Advances in Chemical Engineering, Volume 42
ISSN 0065-2377
http://dx.doi.org/10.1016/B978-0-12-386505-2.00003-1

involved are discussed for the system CoMo on alumina. Next factors influencing catalyst deactivation, particularly those related to feedstock, are analyzed. Finally, commercial, available deoxygenation technologies are overviewed. The attention is focused on both stand-alone and coprocessing technologies.

LIST OF SYMBOLS

A. LATIN LETTERS

A pre-exponential factor of reaction, dimension depends on the reaction
Bo Bodenstein number
c concentration, mol/m^3
c_p specific heat capacity, J/kg/K
C_{H_2} concentration of hydrogen, kmol/m^3
C_S concentration of liquid substrate, kmol/m^3
C concentration, wt%
d_p diameter of the catalyst particles, mm
d_{pi} diameter of inert fines, mm
D diameter of the reactor, m
D_j substance diffusivity, m^2/s
E activation energy of reaction, J/mol
ΔH_r heat of reaction, kJ/mol
k kinetic constant of reaction, dimension depends on the reaction
kc mass transfer coefficient, m/s
L length of the bed, m
n reaction order to substrate, 1
P pressure, MPa
Q volumetric flow rate, m^3/s
Q_m mass flow rate, kg/h
r reaction rate, mol/s/m^3
R universal gas constant, 8.31434 J/mol/K
t time, s
T temperature, K
U linear velocity of the fluid, m/s
V volume, m^3
W mass of catalyst, kg
X conversion level, 1

B. GREEK LETTERS

ε bed voidage, 1
λ heat conductivity, J/m/K/s
μ dynamic viscosity, Pa s
ν kinematic viscosity, mm^2/s
ρ density, kg/m^3
σ surface tension, mN/m

C. SUBSCRIPTS AND SUPERSCRIPTS

calc calculation
cat catalyst
exp experimental
G gas
i index of reaction
j index of substance
L liquid
s solid phase
wt weight

ABBREVIATIONS

AGO atmospheric gas oil
LGO lite gas oil
RO rapeseed oil

1. INTRODUCTION

Several reasons can be identified for the recent interest in automotive fuels derived from renewable energy resources. The major ones include (i) the limited reserves of petroleum that could be replaced, at least partially, by renewable feedstocks; (ii) the national security, as the main petroleum reserves are found in politically unstable regions; (iii) the increased awareness of climate changes that have been attributed to the increasing atmospheric concentrations of CO_2 due to the ever-increasing consumption of fossil fuels; and (iv) the support of rural areas in Western countries aimed at supporting employment and cultural landscape in the areas (Kubičková and Kubička, 2010; Schaub and Vetter, 2008).

Consequently, a fast development and commercialization of two large-scale biofuel production technologies, namely, bioethanol and fatty acid methyl esters (FAME) production, have followed to satisfy the current demand for biofuels, that is, automotive fuels derived from renewable energy resources. Bioethanol is produced typically from sugar cane (Brazil), corn (United States), and wheat and sugar beet (Europe) and is consumed in gasoline-driven cars. There are two common alternatives: (i) gasoline–bioethanol blends with up to 10 vol.% of ethanol that can be used in the standard spark-ignition engines and (ii) ethanol-based fuels containing typically 70–90 vol.% of ethanol, which require specially modified engines (the so-called flexi fuel vehicles; Kubičková and Kubička, 2011).

FAME (biodiesel) is produced by transesterification of vegetable oils (VOs) with methanol as an alternative fuel for compression-ignition engines. It is used either as a blending component of the standard diesel (in volumetric concentrations up to 7% or 10%) or as a stand-alone fuel that requires that a car is equipped with a modified compression-ignition engine. The recognition that transesterification of VOs yields a diesel fuel having significantly better fuel properties than neat VOs led to the spread of this technology. Biodiesel provides some benefits in comparison with conventional diesel fuel. These include its biodegradability and better lubricity that allows reducing the amount of added diesel lubricity additives. On the other hand, there are some disadvantages connected to the use of biodiesel (Kubičková and Kubička, 2011).

From the refining perspective, both technologies are rather agriculturally based technologies and the refiners have to purchase these products to blend them as it is required by the legislation in many European countries. Moreover, neither bioethanol nor biodiesel is fully compatible with the current hydrocarbon fuels and existing engine technologies. It seems, thus, only logical that there is a demand for alternative refining technologies. As a result, renewable (green) diesel has become, in the recent years, a viable alternative to the conventional biodiesel. The renewable diesel concept is based on a fundamentally different approach than production of biodiesel even though it uses the same feedstock. In contrast to biodiesel production, which is based on mere reduction of the molecular weight of triglycerides due to their transesterification with methanol and leads to modification of physical properties while keeping chemical properties intact, renewable diesel production is based on modification of chemical as well as physical properties. Consequently, the renewable diesel is much closer in terms of chemical composition as well as fuel properties to the conventional diesel fuel than biodiesel.

The relevant issues pertaining, in particular, to the accomplishment of catalytic transformation of triglycerides into a mixture of hydrocarbons being suitable as diesel fuel blending components have been addressed by several authors over the past 5 years (Kubička, 2008; Kubičková and Kubička, 2010, 2011; Lestari et al., 2009; Murzin et al., 2012). While the fundamental aspects of deoxygenation chemistry have been covered in these reviews in detail, a view focused on chemical engineering aspects of deoxygenation including an overview of commercial applications is still missing. Thus, the aim of this review is to address the most important issues relevant to commercialization of deoxygenation technologies. After a brief summary of the main aspects of deoxygenation chemistry, the next chapters will be devoted to thermodynamics, hydrodynamics, and kinetics of triglyceride deoxygenation. Then deactivation aspects will be discussed, and the final part will be focused on the existing commercial technologies and their most salient features. In particular, the advantages and disadvantages of the two basic concepts, namely, stand-alone processing of triglycerides and coprocessing of triglycerides with petroleum fractions in existing or modified hydrotreating units, will be analyzed.

2. BASICS OF DEOXYGENATION CHEMISTRY

The production of renewable diesel is based on the conversion of triglycerides into hydrocarbons, that is, on the complete deoxygenation. Reflecting the nature of carbon–oxygen bonds in triglycerides, deoxygenation can proceed via several different reaction routes which take place either in the presence or in the absence of hydrogen. The method utilizing hydrogen is, in fact, more common. It secures a stable catalytic activity, and it is hence used in the commercialized deoxygenation technologies. Several deoxygenation pathways have been reported in the presence of hydrogen (Huber et al., 2007; Kubička and Kaluža, 2010; Kubičková and Kubička, 2010; Laurent and Delmon, 1994a). They have been classified as hydrodeoxygenation (HDO), (hydro)decarboxylation, and decarbonylation.

HDO can be described as a total hydrogenation that yields hydrocarbons and water as the only reaction products. All oxygen atoms are eliminated during HDO in the form of water. As all naturally occurring fatty acid moieties of triglycerides have an even number of carbon atoms, the resulting hydrocarbons, except propane that originates from the glycerol backbone of triglycerides, have an even carbon number too (Kubička and Kaluža, 2010). In contrast, in (hydro)decarboxylation (HDC), any oxygen atom in triglycerides is eliminated as carbon dioxide. Consequently, only hydrocarbons with odd carbon atom numbers are formed from the fatty acid moieties. The prefix hydro- is sometimes used to stress that hydrogen is involved in the reaction. It has been proposed that hydrogen is needed to break the fatty acid moiety loose from the triglyceride. The released fatty acids undergo subsequent decarboxylation to yield hydrocarbon and CO_2 (Kubička and Kaluža, 2010). Both reaction pathways are schematically depicted in Fig. 3.1.

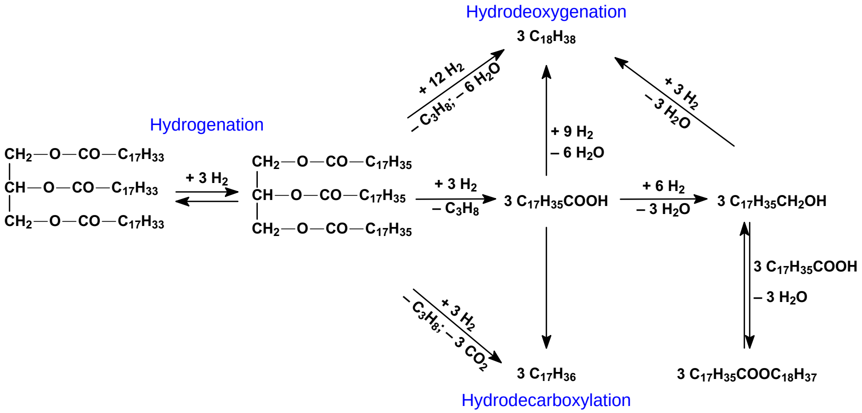

Figure 3.1 A schematic view on the transformation of triglycerides into hydrocarbons under hydrotreating conditions. *Based on Kubička (2008).*

In addition, decarbonylation has been proposed as a plausible reaction pathway as well (Huber et al., 2007). Unfortunately, the complex reaction network involving hydrogen, CO, CO_2, water, and methane under typical deoxygenation reaction conditions makes it difficult, if not impossible, to provide an unequivocal evidence whether carbon oxides found in reaction products originate from decarboxylation and subsequent hydrogenation of carbon dioxide or decarbonylation or whether both decarboxylation and decarbonylation take place in parallel.

The understanding of the deoxygenation reaction pathway is of immense practical importance as it determines the theoretical hydrogen consumption which is extremely important for any refining process. The reaction scheme (Fig. 3.1) indicates that hydrodecarboxylation should be the preferred course of deoxygenation if hydrogen consumption was the only criterion. However, this would be true only if the secondary reactions, in particular, carbon dioxide hydrogenation to carbon monoxide and even methane, could be avoided. It can be easily seen that if all carbon dioxide formed was to be hydrogenated to afford methane the total hydrogen consumption of the HDC route would be larger than the total hydrogen consumption of the HDO path. Moreover, both reaction pathways differ in the carbon atom efficiency. While in HDO theoretically, only three carbon atoms per each triglyceride molecule are not recovered as liquid hydrocarbons, in HDC it is six carbon atoms.

The occurrence of both reaction pathways is affected by catalytic system used as well as by the reaction conditions. For example, palladium on carbon catalysts was shown to catalyze virtually and exclusively the hydro(decarboxylation) pathway (Immer et al., 2010; Kubičková et al., 2005; Maier et al., 1982; Snåre et al., 2006), while typical hydrotreating catalysts (sulfided NiMo, CoMo) provide both HDO and HDC products, that is, *n*-octadecane and *n*-heptadecane, respectively (Bezergianni et al., 2010a,b; Donnis et al., 2009; Kubička, 2008; Kubička and Kaluža, 2010; Kubička et al., 2009, 2010; Mikulec et al., 2009; Priecel et al., 2011). The extent to which each of the pathways contributes to the overall deoxygenation depends on reaction conditions and catalyst composition. HDO was shown to be preferred over HDC at higher hydrogen pressures and lower reaction temperatures (Kubička, 2008). The origin of this selectivity dependence will be discussed in Section 3. The role of the sulfided catalyst is an interesting one, too. It has been recently observed by Kubička and Kaluža (2010) that sulfided nickel catalyst provided virtually and exclusively the HDC products, while sulfided molybdenum catalyst yielded almost solely HDO products. However, both sulfided catalysts were significantly less active than the sulfided NiMo catalyst that afforded both HDC and HDO products.

The experimental studies have demonstrated that milder reactions that typically used in hydrotreating of petroleum middle distillate fractions are sufficient to achieve complete deoxygenation of triglycerides. Over fresh sulfided catalysts, total conversion of triglycerides was obtained at as low temperatures as 280 °C at moderate hydrogen pressures (1–5 MPa; Donnis et al., 2009; Kubička and Kaluža, 2010; Kubička et al., 2010; Priecel et al., 2011). Similar reaction conditions were applied successfully also in the case of palladium catalysts (Immer et al., 2010; Kubičková et al., 2005; Simakova et al., 2009; Snåre et al., 2006, 2008). As the aim of this chapter is to describe upgrading of triglycerides in a refinery, the discussion will be focused mostly on sulfided hydrotreating catalysts that are the most likely ones to be used commercially. In fact, the available data on the already commercialized technologies indicate the use of hydrotreating catalysts.

3. THERMODYNAMIC ASPECTS OF DEOXYGENATION

Thermodynamic assessment of any reaction system is essential prior to any industrial application. While, nowadays, there are many different databases containing relevant thermodynamic data for a wide variety of reaction systems, the relevant data for deoxygenation of triglycerides have been until recently missing. Smejkal et al. (2009) have applied Joback's contribution method for the assessment of the relevant thermodynamic data of tristearate, which was chosen as a model compound representing triglycerides. Considering that the majority of triglycerides in VOs are composed of C_{18} fatty acid moieties and that hydrogenation of their double bonds is very facile at deoxygenation reaction conditions, tristearate seems to be an ideal model component to describe triglycerides. The applicability of Joback's contribution method for estimating thermodynamic properties of tristearate was verified on butyl stearate for which there are available data in commercial databases. Based on the very good agreement between these data and data estimated by Joback's contribution method, it was argued that the method is suitable for the assessment of thermodynamic data of tristearate (Smejkal et al., 2009).

The thermodynamic prediction for 7 MPa indicated that in the temperature range of 270–350 °C, which is relevant for total deoxygenation of triglycerides, *n*-octadecane is the thermodynamically preferred product. Its concentration was predicted to be in the range of 70–80%. This means that, at an elevated pressure of 7 MPa and high temperature, the HDO reaction is preferred over hydrodecarboxylation resulting in the formation of hydrocarbons having the same number of carbon atoms in their molecules as there were in the original fatty acid moieties (in case of tristearate it means *n*-octadecane). On the other hand, the relative importance of hydrodecarboxylation increases with the decreasing reaction pressure. For example, the decrease in reaction pressure from 7 to 0.7 MPa at a constant temperature of 310 °C results in a change in the predicted composition (based on thermodynamic data) from ca. 80/20 (C_{18}/C_{17}) to about 55/45 (C_{18}/C_{17}; Smejkal et al., 2009). This can be attributed to the mole changes in the reaction system—during hydrodecarboxylation, the total number of moles in the system increases from 4 to 7, while during HDO, the total number of moles in the system decreases from 13 to 10 (transformation of 1 mol of tristearate is considered). These results are in line with experimental observations (Kubička, 2008).

The thermodynamic predictions showed that, in excess of hydrogen, *n*-octadecane should be the exclusive hydrocarbon product, which was not found experimentally. In order to account for the observed formation of *n*-heptadecane, the H_2/oil ratio was varied until reasonable agreement with the experimental data was found, which was at the value of H_2/oil ratio equal to 7. It was thus suggested that under the reaction conditions, the reaction was limited by hydrogen diffusion to the active sites, that is, by hydrogen mass transfer through the stagnant liquid film formed by reactants and/or products on the outer surface of catalyst particles (Smejkal et al., 2009). Apart from the mass transfer limitations itself, the availability of hydrogen is negatively affected by the low solubility of hydrogen in VOs (Piqueras et al., 2008; Santacesaria et al., 1994; Schmidt and Schomacker, 2007). A calculation confirming these previous reports is given below.

From the practical point of view, heat of reaction is key information obtainable from thermodynamic data. Heat effects of chemical reactions influence both reaction rates in the catalytic bed and operation conditions and engineering process design. Industrial high-capacity trickle-bed reactors which are preferentially used for hydrodesulphurization (HDS) treatment of crude oil distillates, as well as promising HDO of VOs, are considered to be adiabatic. This is due to the bad radial heat conductivity by contact points among particles of catalyst. Overheating of the catalytic bed that would follow could result in catalyst deactivation by excessive coking, undesired cracking of VO, and vaporization of reaction mixture. The most important parameter that characterizes the heat effect during the reactor operation is the adiabatic temperature rise defined by the following equation:

$$\Delta T_{\mathrm{ad}} = c_0(-\Delta H_r)/(\rho c_p) \qquad [3.1]$$

The practical meaning of this parameter is that it makes possible the assessment of the increase in temperature of the reaction mixture caused by chemical reaction carried out with 100% conversion. These conditions are common for both HDS and HDO processes. The most important parameter of Eq. (3.1) is the value of reaction enthalpy at reaction temperature.

There is a brief list of the main reactions relevant for deoxygenation and HDS, and their respective heats of reaction are given in Table 3.1. Heat of reaction was computed here at 280 °C using the process simulator Aspen Plus (AspenTech, 2011).

From the comparison of the reaction heats of some reactions which can occur in HDO and HDS processes, presented in Table 3.1, it follows that all important reactions, except decarboxylation, produce thermal energy, that is, exothermic. Magnitudes of reaction heats are comparable for both HDO and HDS, but very high concentration of triglycerides in VOs in conjunction with high heat of possible triglyceride hydrolysis poses an insuperable problem to operate HDO of pure VO in industrial scale trickle-bed reactors. The only practicable arrangement is to dilute VO to get proper adiabatic temperature rise, and/or to coprocess VO together with crude oil fractions by HDS process.

Table 3.1 Heat of selected reactions characteristic for deoxygenation and hydrodesulphurization at 280 °C

Reaction ID	Reaction path	$(\Delta H_r)_{280\,°C}$ (kJ/mol)
Hydrolysis	Glyceryl oleate → oleic acid and glycerol	−176.3
Saturation	Oleic acid → stearic acid	−53.8
HDO	Stearic acid → *n*-octadecanol and water	−65.8
HDO	Stearic acid → *n*-octadecane and water	−178.5
Decarboxylation	Stearic acid → *n*-heptadecane and carbon dioxide	+18.8
HDS	Thiophene → *n*-butane and hydrogen sulfide	−262.3
HDS	Benzothiophene → ethylbenzene and hydrogen sulfide	−159.1
HDS	Dibenzothiophene → biphenyl and hydrogen sulfide	−124.8
HDN	Quinoline → *n*-propylbenzene and ammonia	−245.5

4. HYDRODYNAMICS ASPECTS

Catalytic deoxygenation of VOs in refineries resembles much catalytic hydroprocessing of middle distillates obtained by crude oil fractionation, namely, atmospheric gas oil (AGO) HDS. The principal issue that needs to be addressed is focused on scale-up of laboratory kinetic data to full industrial scale process. The crucial task in evaluation of reaction kinetics parameters is to eliminate the influence of both internal and external mass and heat transfer on kinetic results. On the other hand, productivity and selectivity of industrial hydroprocessing reactors are frequently determined by hydrodynamics of flowing fluids. It is well known (Levenspiel, 1999) that reactor behavior is governed by four interrelated quantities. In process design, it is necessary to specify the input—known kinetics and flow pattern, and based on these data, it is possible to predict the output results. Mass transfer limitations caused by both internal diffusion in catalyst particles and external transport of hydrogen to surface of the catalyst can also be the reaction rate constraining features, that is, limiting the reactor productivity.

To evaluate hydrodynamics and mass transfer conditions in a trickle-bed reactor, information about physical properties of used fluids needs to be available in order to calculate flow and mass transfer criteria. Also the type of flow regime, such as trickling, pulsing, or spray flow, determines deviations from the plug flow caused by axial dispersion of fluids in fixed catalytic bed. Moreover, maldistribution of liquid velocities in the cross-section of the catalytic bed, catalyst bypassing as a result of wall flow, and uneven wetting of the outer surface of catalyst particles are important for trickle-bed reactor behavior. All these phenomena have a profound influence on the overall effectiveness of the catalytic reactor. Therefore, in Section 4.1, the key hydrodynamic parameters of VOs and middle distillates will be compared in order to allow an assessment of VO deoxygenation in conventional hydrotreating reactors using hydrodesulfurization reactors as a benchmark.

4.1. Flow characteristic of VOs and middle distillates

A comparison of key physical properties (viscosity, density, and surface tension) of VO (rapeseed oil) with petroleum middle distillates (AGO) is given in Table 3.2. It can be clearly seen that the main difference is in viscosity, which is 4–10 times higher for rapeseed oil than for AGO. The other parameters are also higher in the case of rapeseed oil, but only by 10% for density and 20–30% for surface tension. The presented values are at temperatures where they can be obtained experimentally, which are significantly lower than the typical temperatures used during HDS and deoxygenation. Hence, the usual (Reid et al., 2001) physical approximations of temperature dependence of physical properties were used to estimate these important physical properties under relevant reaction temperatures. Due to the difference between common temperatures needed for deoxygenation (temperatures less than 300 °C are generally sufficient to achieve complete conversion) and for HDS process, which is operated at around 350 °C,

Table 3.2 Comparison of important properties of middle distillate (AGO) and rapeseed oil (RSO)

Physical property	Unit	Middle distillate	Rapeseed oil
Density, $\rho(15\ ^\circ\mathrm{C})$	$\mathrm{kg/m^3}$	844	920
Density, $\rho(70\ ^\circ\mathrm{C})$	$\mathrm{kg/m^3}$	806	883
Kin. viscosity, $\nu(25\ ^\circ\mathrm{C})$	$\mathrm{mm^2/s}$	6.84	62.14
Kin. viscosity, $\nu(150\ ^\circ\mathrm{C})$	$\mathrm{mm^2/s}$	0.95	3.98
Surface tension, $\sigma(40\ ^\circ\mathrm{C})$	mN/m	27	33
Surface tension, $\sigma(85\ ^\circ\mathrm{C})$	mN/m	22.5	29

the physical properties of middle distillate and rapeseed oil were extrapolated up to temperature of 300 °C. The approximations and the resulting estimates of physical properties calculated here for both feedstocks are presented in Table 3.2.

The temperature dependence of kinematic viscosity can be approximated by Eq. (3.2), using the values of the coefficients of the equation presented in Table 3.3 that were determined here by fitting measured viscosities in the range of 25–150 °C (Fig. 3.2).

$$\ln(v) = b_1 + \frac{b_2}{T} + \frac{b_3}{T^2} \qquad [3.2]$$

Table 3.3 The temperature dependence of kinematic viscosity: coefficients of Eq. (3.2)

Liquid	b_1	b_2	b_3
AGO	1.1526	−2299.4	7.5524×10^5
Rapeseed oil	3.7084	−3678	1.1363×10^6

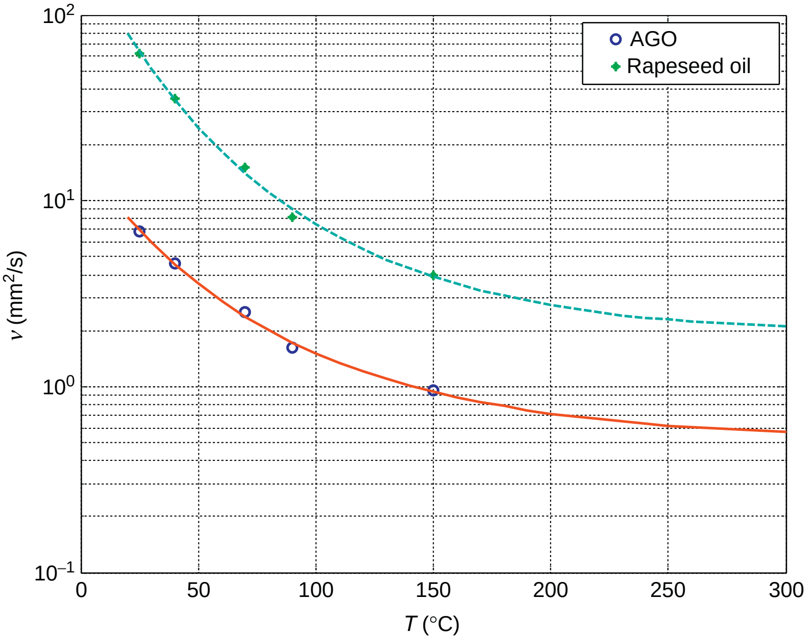

Figure 3.2 Temperature dependence of kinematic viscosity of rapeseed oil (RSO) and middle distillate (AGO).

A comparison of the solution of Eq. (3.2) with experimental data is presented in Fig. 3.2. Rapeseed oil has almost an order of magnitude higher viscosity than middle distillate in the experimental region which is also predicted for the extrapolated region. As a consequence, it can be expected that the flowing features of rapeseed oil will be worse in comparison with AGO.

The temperature dependence of density can also be described by a polynomial expression given by Eq. (3.3). The coefficients of this equation are presented in Table 3.4 and were estimated by fitting the experimentally measured values in the range of 15–70 °C. The graphical comparison of experimental data and prediction based on Eq. (3.3) for rapeseed oil and AGO is shown in Fig. 3.3. The higher density of rapeseed oil by approximately 10 % in

Table 3.4 The temperature dependence of density: coefficients of Eq. (3.3)

Liquid	a_1 (g/dm^3)	a_2 (g/dm^3 K)	a_3 (g/dm^3 K^2)
AGO	0.85442	−0.00068484	0
Rapeseed oil	0.93052	−0.00069805	2.3377×10^{-7}

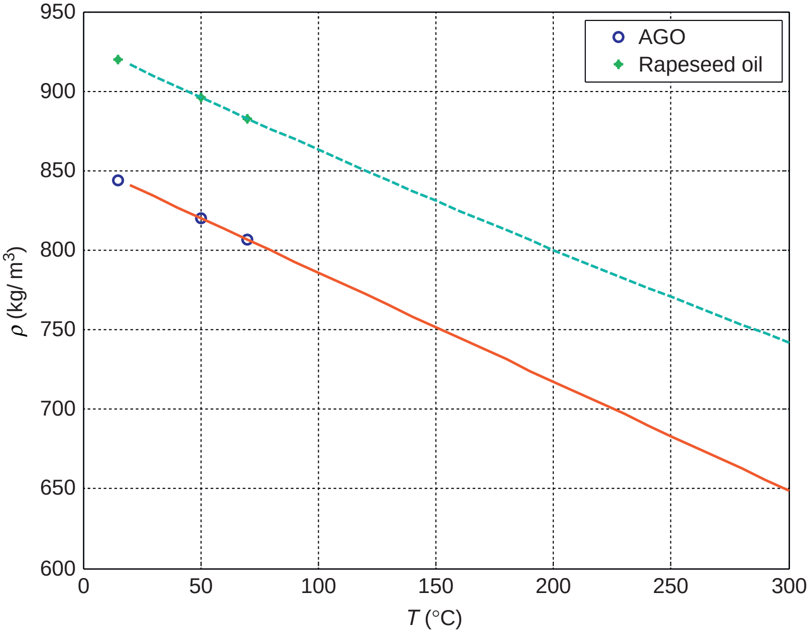

Figure 3.3 Temperature dependence of density of rapeseed oil and middle distillate (AGO).

comparison with AGO, which was found at temperatures below 100 °C was also predicted by the Eq. (3.3) for 300 °C. Once again this will have an impact on the hydrodynamics of the hydrotreating system.

$$\rho = a_1 + a_2\,T + a_3 T^2 \qquad [3.3]$$

The surface tension data were adopted from the literature (Lüft and Spicher, 2007) and subsequently were approximated using Eq. (3.4) proposed by Macleod (1923). This equation can be simplified into Eq. (3.5) with parameter $k' = 2.7354$ for AGO and 2.6586 for rapeseed oil. The graphical representation of the surface tension temperature dependence is then given in Fig. 3.4. It demonstrates that similar to the other investigated physical properties, also estimated surface tension of rapeseed oil at 300 °C is higher than the surface tension of AGO.

$$\text{const.} = \frac{M\sigma^{1/4}}{\rho^L - \rho^G} \qquad [3.4]$$

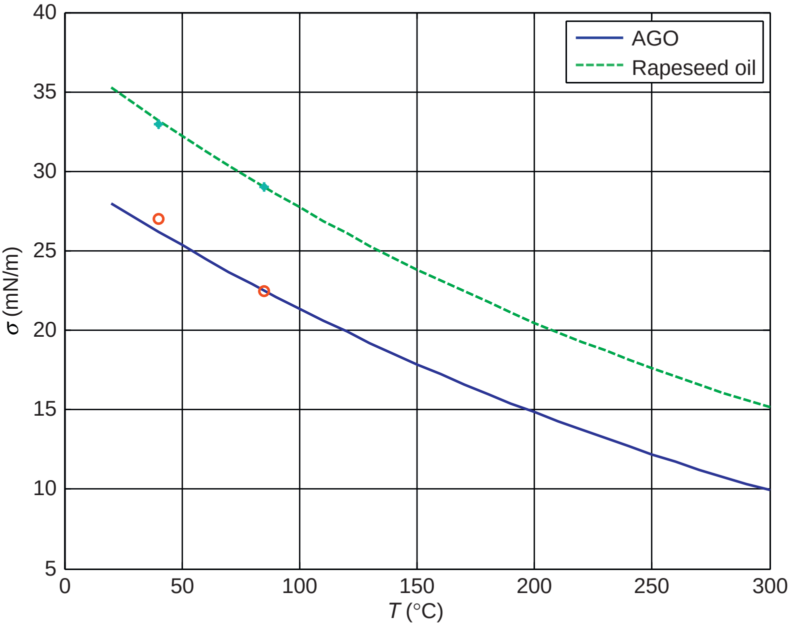

Figure 3.4 Temperature dependence of surface tension of rapeseed oil and middle distillate (AGO).

$$k' = \frac{\sigma^{1/4}}{\rho^L} \qquad [3.5]$$

In summary, the flow characteristics determining properties of rapeseed oil such as viscosity, density, and surface tension are less convenient in comparison with those of middle distillate and hence more energy needs to be spent to transport VOs into the reactor. Furthermore, higher pressure drop along the trickle-bed reactor can also be expected for VOs deoxygenation in comparison with AGO hydrotreating.

The driving force of the hydrogen liquid–solid mass transfer as well as of the reaction rate in porous catalysts is the concentration of hydrogen dissolved in the liquid phase reactants, here AGO and VO, respectively. Some data for hydrogen solubility in triglycerides could be found in the literature. For example, hydrogen solubility in soybean oil was reported by Fillion to follow Eq. (3.6) with parameters $H_0 = 8.84$ MPa m^3/kmol and $\Delta E = -5000$ kJ/kmol (Fillion and Morsi, 2000):

$$\mathrm{He}_{\mathrm{H}_2} = H_0 \exp\left(\frac{-\Delta E}{RT}\right) \qquad [3.6]$$

The equilibrium hydrogen concentration (kmol/m^3) in rapeseed oil was given by Bern et al. (1975) and can be calculated according to Eq. (3.7) with P(MPa), T(K). Hydrogen solubility in light vacuum gas oil was reported in the literature (Cai et al., 2001) and allows to estimate hydrogen solubility in a petroleum fraction to be hydrotreated:

$$C^* = 0.203 \exp\left(\frac{-5900}{RT}\right) P \qquad [3.7]$$

Using the available data, solubility of hydrogen in both VOs and a petroleum fraction as a function of temperature was calculated here. The results are summarized in Fig. 3.5. It can be observed that while similar hydrogen solubility is predicted for petroleum distillate and rapeseed oil, lower hydrogen solubility is predicted for soybean oil at 300 °C, which is the temperature used here to represent reaction conditions.

Apart from hydrogen solubility which is comparable for VOs and gas oil fractions, hydrogen diffusivity in those liquids can play an important role as well. Hydrogen diffusivity in soybean oil was taken from the literature (Fillion and Morsi, 2000), while diffusivity in diesel was calculated using Wilke Chang equation for benzene as a model compound. The results are reported as a function of temperature in Fig. 3.6. Moreover, comparison

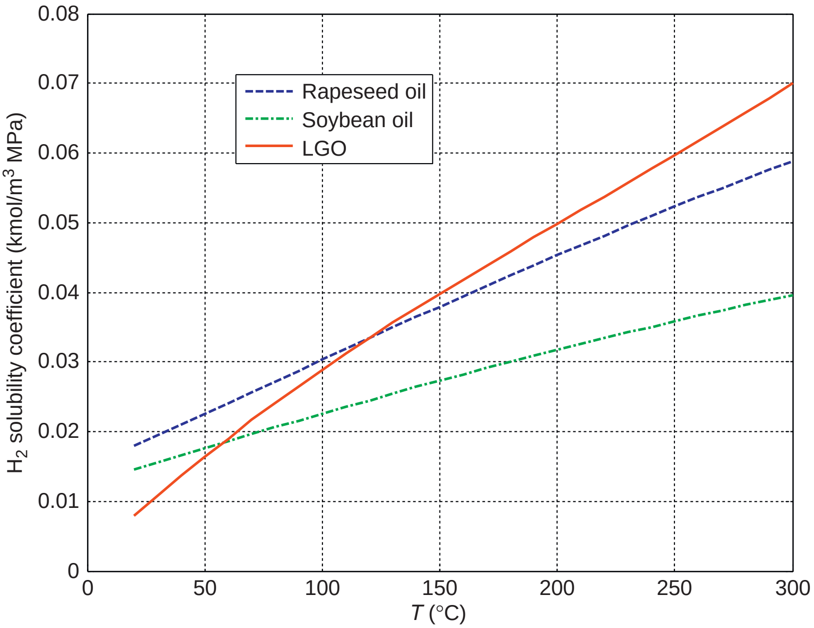

Figure 3.5 Temperature dependence of hydrogen solubility in rapeseed and soybean oil and light vacuum gas oil.

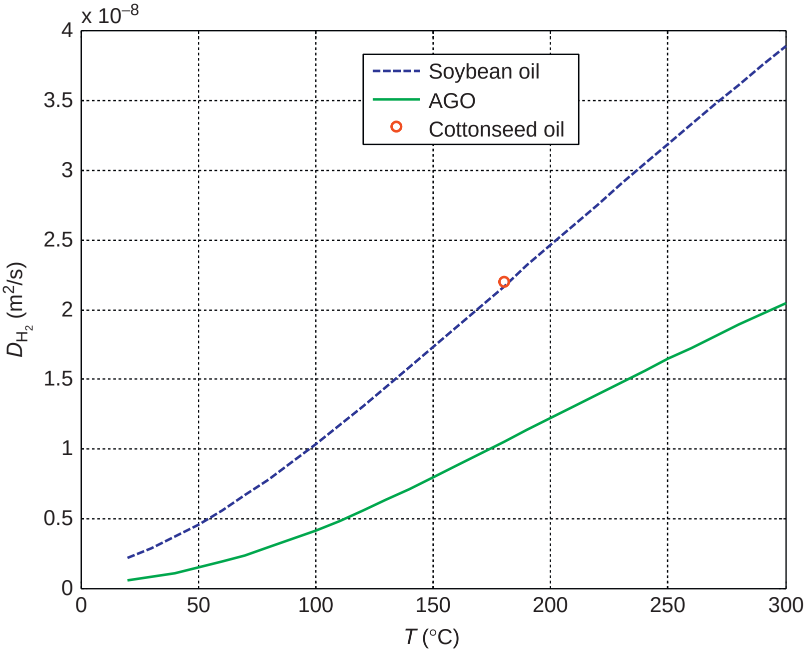

Figure 3.6 Temperature dependence of hydrogen diffusivity in soybean oil and middle distillate (AGO).

of triglyceride and hydrogen diffusivity in VO is also available in the literature (Andersson et al., 1974). Hydrogen diffusivity in cottonseed oil at 180 °C was 2.2×10^{-8} m^2/s, whereas triglyceride diffusivity in the same oil was 100 times slower (1.8×10^{-10} to 4.2×10^{-10} m^2/s at 131–192 °C, respectively). The higher hydrogen diffusivity in VOs as compared with middle distillate (Fig. 3.6) compensates its lower solubility in the same liquid, and the transport phenomena in VO and AGO can be estimated to be approximately the same.

4.2. Hydrodynamics and mass transfer in HDO and HDS reactors

Continuous catalytic deoxygenation of VOs in trickle-bed reactors to the mixture of hydrocarbons (alkanes) is still performed and investigated more in laboratory and pilot scale than in industrial scale, which is contrary to HDS process with capacities exceeding 100 tons of fuel per hour in one reactor. This was the reason to compare transport properties of laboratory HDO trickle-bed reactor with an industry scale HDS reactor.

Parameters of the industrial trickle-bed reactor in Tables 3.5 and 3.6 were adopted from the literature (Mary et al., 2009). Parameters and conditions of the laboratory HDO reactor were calculated here and correspond to the laboratory reactor conditions at 280 °C, used for HDO kinetics evaluation.

A comparison of hydrodynamic conditions in a laboratory HDO reactor and an industry scale HDS trickle-bed reactor is presented in Table 3.6. The elimination of both external and internal mass transfer diffusion resistance is the key assumption to measure intrinsic kinetics in a laboratory reactor. Among the most important hydrodynamic phenomena, which strongly depend on the operating conditions, are catalyst wetting, liquid maldistribution, axial dispersion, and gaseous reactant transfer.

Incomplete catalyst utilization in a pilot reactor may occur especially in the trickle flow regime and can have two main causes. First is due to reactor-scale liquid maldistribution that may leave certain portions of the bed poorly irrigated by channeling and wall flow. A proper design of liquid distributors and/or sufficient layer of packing to reach equilibrium liquid distribution solve this obstacle. The other cause of incomplete catalyst utilization is particle-scale incomplete external wetting. This occurs at sufficiently low liquid mass velocity when the available liquid flow is insufficient to cover all the external surface of the catalyst particles with a continuous liquid film. Solution is to fill void space among catalyst particles by fine inert material to

Table 3.5 Operation parameters of trickle-bed reactors

Parameter	**Reactor** **Laboratory**	**Industrial (Mary et al., 2009)**
L, length of the bed (m)	0.34	5
D, diameter of the reactor (m)	0.017	1.5
d_p, diameter of the catalyst particles (mm)	0.25–0.5	1.5
d_{pi}, diameter of inert fines (mm)	0.1	–
Dilution of catalyst by inert ratio (mL_{in}/mL_{cat})	1.5	0
U_L, velocity of the liquid (m/s)	4×10^{-5}	1×10^{-3}
U_G, velocity of the gas (m/s)	5.5×10^{-2}	5×10^{-2}
Reaction type	HDO	HDS
Flow regime	Trickling downflow	Trickling/ pulsing flow
Type of catalyst	$NiMo/\gamma Al_2O_3$	$NiMo/\gamma Al_2O_3$
Inert	Silicon carbide	–
ε, bed voidage	0.3	0.4
T, temperature (°C)	280	327
P, pressure (MPa)	3.5	3.5
n, reaction order to substrate	1	1
X, conversion level	0.999	0.999
C_{H_2}, concentration of hydrogen (mol/m^3)	197	230
C_S, concentration of liquid substrate (kmol/m^3)	2.68	0.235
ρ_L, density of the liquid (kg/m^3)	753	750
ρ_G, density of the hydrogen (kg/m^3)	5	5
η_L, dynamic viscosity of the liquid (Pa/s)	16×10^{-4}	5×10^{-4}
η_G, dynamic viscosity of gas (Pa/s)	1×10^{-4}	1×10^{-4}
E, activation energy (kJ/mol)	75	100
ΔH_r, heat of reaction (kJ/mol)	–	250
D_{H_2}, molar diffusivity in oil (m^2/s)	3.6×10^{-8}	1×10^{-8}
D_{TG}, molar diffusivity in oil (m^2/s)	3.6×10^{-10}	–

Table 3.6 Comparison of hydrodynamic conditions of HDO and HDS (Mary et al., 2009)

Conditions	Criteria	HDO	HDS
Catalyst-bed dilution	$V_{\text{inert}}/V_{\text{cat}}$	1	0
Liquid maldistribution	Wall effects $\frac{D}{d_\text{p}} \geq 25$	170–85	500–25
	Channeling (mm) $d_{\text{pi}} \geq \frac{d_\text{p}}{10}$	0.04	0–0.3
Axial dispersion	$\frac{L}{d_\text{p}} \geq \frac{20n}{\text{Bo}_\text{L}}\ln\left(\frac{C_0}{C_\text{f}}\right)$	1771	1667–789
Wetting efficiency	$\frac{\eta_\text{L} U_\text{L}}{\rho_\text{L} d_\text{p}^2 g} \geq 5\times10^{-6}$	7.07×10^{-5}	7.55×10^{-6}–5×10^{-6}
Limiting reactant gas	$\frac{D_{\text{eB}}C_{\text{Bi}}}{bD_{\text{eA}}C_\text{A}^*} \gg 1$	0.14	0.014
Mass transfer	Internal $\frac{r(1-\varepsilon)\left(\frac{d_\text{p}}{2}\right)^3}{D_c C} \leq 1$	6×10^{-5}– 1×10^{-5}	1–0.315
	External $k_{\text{ext}} \geq \left(\frac{10d_\text{p}}{C}\right) r(1-\varepsilon)$	4×10^{-3}	1×10^{-3}–4.2×10^{-5}

decrease the bed porosity and increase liquid holdup by pseudostatic liquid lenses at particles contact points.

The most reaction systems could be classified (Wu et al., 1996) as being liquid- or gas reactant limited. The value of the ratio of the liquid reactant flux to the catalyst particle to the gas reactant flux to the catalyst particle delineates two categories. For value $\gg 1$, the reaction can be considered as gas reactant rate limited, while values $\ll 1$ mean that it is the liquid reactant that is rate limiting. For liquid-limited reactions, an upflow reactor should be preferred as it provides for complete catalyst wetting and for the fastest transport of the liquid reactant to the catalyst. For gas-limited reactions, a downflow reactor, especially at partially wetted conditions, is to be preferred as it facilitates the direct transport of the gaseous reactant to the catalyst by unwetted surface of catalyst particles.

Magnitudes of parameters presented in Table 3.6 give evidence on fulfilling of criteria allowing to neglect external effects in the HDO kinetic results, such as wall effects and channeling, axial dispersion and catalyst wetting, and both external and internal mass transfer. Due to the low triglyceride diffusivity in VOs and/or low sulphur compound concentration in middle distillates, both reactions HDO and HDS are liquid reactant limited. This means that complete wetting of catalyst surface is key presumption of full catalyst utilization. To guarantee it, dilution of catalyst by fine inert or high linear liquid flow velocity has to be used.

5. KINETICS ASPECTS

Deoxygenation of triglycerides involves a very complex set of reactions carried out in liquid phase on heterogeneous catalysts by gaseous hydrogen. In contrast to HDS, the concentration of liquid substrate is very high, due to the fact that the feed liquid consists almost exclusively of triglycerides. Consequently, also the necessary amount of hydrogen exceeds the amount needed for HDS. At high capacity operations in trickle-bed reactors, kinetic models like Langmuir–Hinshelwood and Hougen–Watson are overshadowed by uncertainties in hydrodynamics, mass transfer effects and frequent catalyst deactivation. As a result, simple power law kinetics is often more useful to predict reactor behavior (Levenspiel, 1999). Moreover, the underlying reaction network is developed on the basis of presumed reaction pathways.

To evaluate a set of chemical reactions which represent only important changes in chemical composition, experiments with different intermediates were carried out. The above is the reason for choosing the first-order kinetic model to evaluate reaction rates of triglycerides deoxygenation and also to use oleyl alcohol, oleic acid, and oleyl oleate as original substrates in HDO experiments. Detailed description of catalytic activity measurements is presented elsewhere (Kubička and Kaluža, 2010).

Catalytic tests were performed in a bench-scale trickle-bed reactor of 17 mm inner diameter. Food grade rapeseed oil with the following concentration of important fatty acid moieties, oleic acid 62%; linoleic acid 20%; linolenic acid 9%; and stearic acid 3%, was used as a liquid feed, and refinery hydrogen gas (>99% purity) was used as a gas feed. The reactor was loaded prior to the experiments with catalyst diluted by an inert (SiC) to ensure sufficient catalyst-bed length and to improve the reaction-heat transfer, liquid distribution, and catalyst wetting. The particle sizes of the catalyst and SiC were 0.25–0.5 mm and <0.1 mm, respectively. In the vertical axis of the reactor, a thermo-well of the outer diameter equal to 5 mm was located to ensure axial temperature profile measurement. The reaction temperature was set during the experiments in the range of 260–280 °C. The contact time of the liquid feed with the catalyst (V/F) was varied in the range of 0.2–5 h by varying the catalyst mass (W) and rapeseed oil feed rate (Q_m). The hydrogen-to-rapeseed oil molar ratio and hydrogen pressure were constant at 50 and 3.5 MPa, respectively. The liquid products (collected and separated at 80 °C) were withdrawn after stabilization of reaction conditions (6 h) in 2-h intervals and analyzed by off-line gas chromatography after separation of the water phase. The gas-phase products were collected once at every reaction condition and analyzed off-line using a standard three-column GC setup with flame ionization and thermal conductivity detectors enabling the detection of both permanent gases and hydrocarbons at the same time.

5.1. Mechanism of triglycerides deoxygenation

General lumped reaction pathway (Kubička and Kaluža, 2010) incorporates hydrogenation of olefinic bond to saturated triglycerides and parallel hydrogenolysis and decarboxylation to alkanes and to stearic acid. Stearic acid also reacts to yield C_{17} and C_{18} alkanes and stearyl alcohol and also by consecutive way to stearyl stearate. The following part of chapter on kinetics of rapeseed oil transformations and HDO of intermediates is adapted from the published data (Tukač et al., 2012). In Fig. 3.7, the reaction scheme of triglyceride deoxygenation (both unsaturated and saturated) to C_{18} and C_{17} alkanes, acids, and esters is presented.

Chemical compounds involved in HDO reactions are specified in more detail in Table 3.7, together with their IUPAC name and CAS number.

The activity of the catalysts in deoxygenation can be described by considering at the conversion of triglycerides, that is, evaluating the rate of disappearance of triglycerides. The dependencies have been obtained by using the pseudo-first-order kinetics to fit the relevant experimental data for catalysts at three reaction temperatures. The results are depicted in Fig. 3.8, where it is seen that the experimental data followed the empirical pseudo-first-order-kinetics rather well.

Furthermore, it can be seen that the conversion increases with increasing reaction temperature and that complete conversion of triglycerides can be

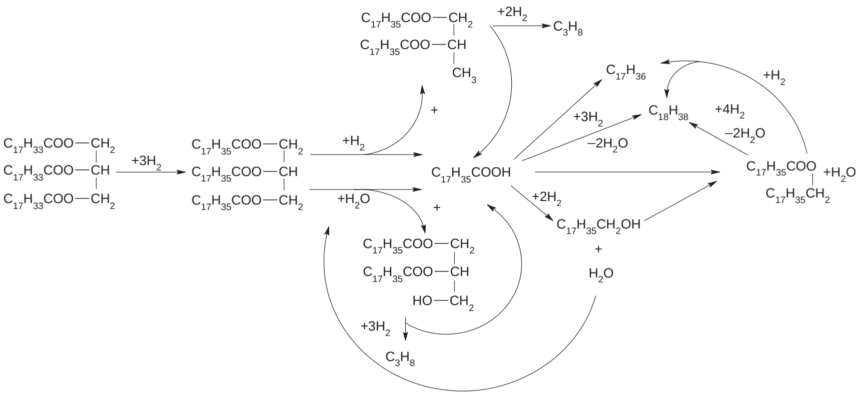

Figure 3.7 The reaction pathways involved in conversion of triglycerides into hydrocarbons.

Table 3.7 Chemical compounds important in vegetable oil deoxygenation

Name	**IUPAC name**	**Formula**	**CAS No.**
Glyceryl trioleate	2,3-Bis[[(*Z*)-octadec-9-enoyl]oxy]propyl (*Z*)-octadec-9-enoate	$(C_{17}H_{33}COO)_3C_3H_5$	122-32-7
Glyceryl tristearate	1,3-Di(octadecanoyloxy) propan-2-yl octadecanoate	$(C_{17}H_{35}COO)_3C_3H_5$	555-43-1
Glyceryl distearate	(2-Hydroxy-3-octadecanoyloxypropyl) octadecanoate	$(C_{17}H_{35}COO)_2C_3H_5OH$	504-40-5
Propanediol distearate	1,3-Propanediol distearate	$(C_{17}H_{35}COO)_2C_3H_6$	17367-44-1
Oleyl oleate	[(*Z*)-Octadec-9-enyl] (*Z*)-octadec-8-enoate	$C_{17}H_{33}COOCH_2C_{17}H_{33}$	3687-45-4
Oleyl stearate	[(*Z*)-Octadec-9-enyl] octadecanoate	$C_{17}H_{35}COOCH_2C_{17}H_{33}$	17673-50-6
Stearyl stearate	Octadecyl octadecanoate	$C_{17}H_{35}COOCH_2C_{17}H_{35}$	2778-96-3
Oleic acid	(*Z*)-Octadec-9-enoic acid	$C_{17}H_{33}COOH$	112-80-1
Stearic acid	Octadecanoic acid	$C_{17}H_{35}COOH$	57-11-4

Table 3.7 Chemical compounds important in vegetable oil deoxygenation—cont'd

Name	**IUPAC name**	**Formula**	**CAS No.**
Oleyl alcohol	(*Z*)-Octadec-9-en-1-ol	$C_{17}H_{33}CH_2OH$	143-28-2
Stearyl alcohol	Octadecan-1-ol	$C_{17}H_{35}CH_2OH$	112-92-5
Glycerol	Propane-1,2,3-triol	$C_3H_5(OH)_3$	56-81-5
Heptadecene	Heptadec-1-ene	$C_{17}H_{34}$	6765-39-5
Octadecene	Octadec-1-ene	$C_{18}H_{36}$	112-88-9
Heptadecane	Heptadecane	$C_{17}H_{36}$	629-78-7
Octadecane	Octadecane	$C_{18}H_{38}$	593-45-3
Propane	Propane	C_3H_8	74-98-6

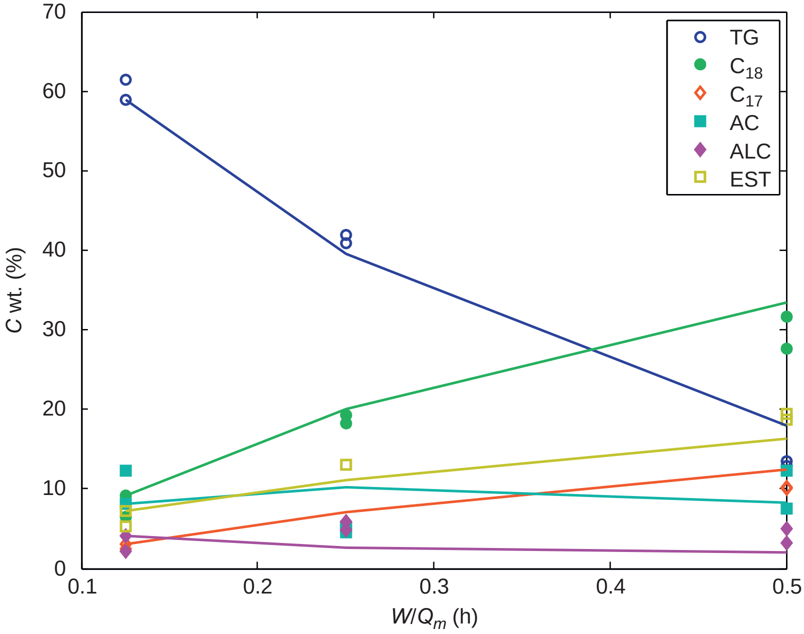

Figure 3.8 Concentrations of representative group of compounds for rapeseed oil deoxygenation. The solid lines represent the solution of the first-order pseudo-homogeneous plug flow isothermal model of the reactor and the points are the experimentally measured data. CoMo catalyst, 300 °C and 3.5 MPa. (TG, triglycerides; C_{17} C_{18}, alkanes; AC, fatty acids; ALC, fatty alcohols; EST, esters).

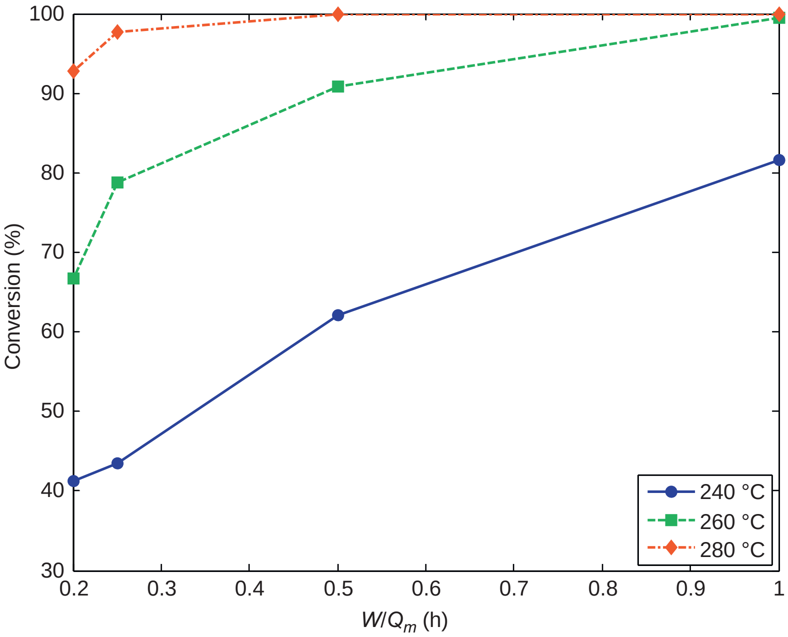

Figure 3.9 Conversion of triglycerides over the CoMo catalyst at different temperature as a function of contact time.

obtained already at 280 °C (Fig. 3.9). These results suggest that the deoxygenation reactions of triglycerides are, in fact, irreversible at the selected reaction conditions.

Deoxygenation of triglycerides over the investigated catalyst yielded two main classes of organic liquid reaction products and intermediates—hydrocarbons and oxygenates. The ultimate products of deoxygenation were hydrocarbons and oxygenates were the reaction intermediates, in particular, fatty acids (e.g., stearic acid), fatty alcohols (e.g., *n*-octadecanol), and their fatty esters (e.g., stearyl stearate). The shape of the selectivity curves of the two main reaction product classes confirms that hydrocarbons (Fig. 3.10) are the final reaction products and that their formation is preceded by the formation of oxygenated intermediates (Fig. 3.11). The hydrocarbons consisted mainly of *n*-octadecane, *n*-heptadecane, *n*-hexadecane, and *n*-pentadecane. In addition to the organic liquid products, water and gaseous products, such as propane, carbon oxides, and methane, were formed during deoxygenation of triglycerides. The cracking activity of the CoMo catalyst was very low under the experimental conditions since no other gaseous

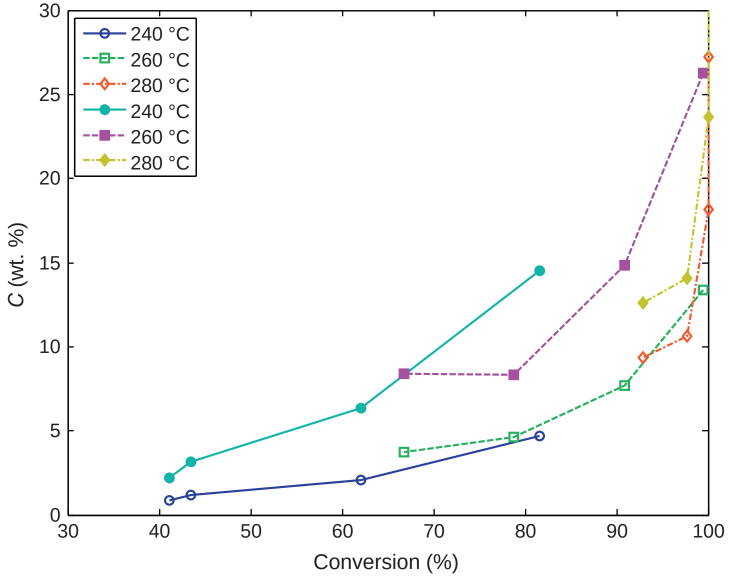

Figure 3.10 Selectivity of alkanes as a function of conversion for the CoMo catalyst at different temperatures. $p = 3.5$ MPa, $W/Q_m = 0.2$–1 h. (Open points belong to C_{17} and filled to C_{18} hydrocarbons.)

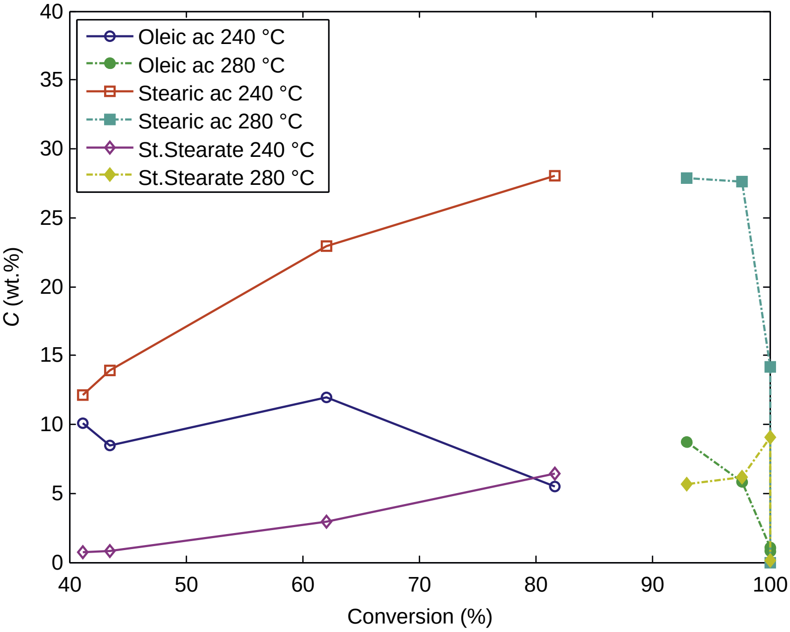

Figure 3.11 Selectivity to oxygenates as a function of conversion for the CoMo catalyst at different temperatures. $p = 3.5$ MPa, $W/Q_m = 0.2$–1 h.

products or short chain liquid hydrocarbons were found in the reaction products. Moreover, the extent of isomerization was also negligible under the investigated conditions since only traces of skeletal isomers were identified in the organic liquid reaction products.

A deeper understanding of the deoxygenation of triglycerides can be obtained from a detailed analysis of both the main product groups, that is, from selectivities to different types of oxygenates and hydrocarbons. The selectivities to *n*-heptadecane and *n*-octadecane provide valuable information about the final reaction step in deoxygenation of triglycerides. Their selectivities are in this case plotted as a function of the total triglyceride conversion (Fig. 3.10). The other hydrocarbons, mainly *n*-pentadecane and *n*-hexadecane, were formed also in the system, but in negligible concentration.

The oxygenated products and intermediates consist of three main types of products—fatty acids (almost exclusively stearic and palmitic acids), fatty alcohols (almost exclusively *n*-octadecanol and *n*-hexadecanol), and their fatty esters, that is, the esters that are formed by the reaction of fatty acids with fatty alcohols that are both reaction intermediates in deoxygenation of triglycerides. The selectivity curves of the three main classes of oxygenated products confirm that fatty acids and fatty alcohols are formed prior to the formation of fatty esters (Fig. 3.11). Fatty alcohols are not depicted here as their measured concentration was very low, presumably due to their quick consumption either by deoxygenation (resulting in formation of hydrocarbons) or by esterification reaction with fatty acids as evidenced by the significant concentration of stearyl stearate (Fig. 3.11).

The overall reaction pathway is schematically depicted in Fig. 3.7. The double bonds in triglycerides, the main components of VOs, are first saturated. Then they are converted into fatty acids that can either (i) undergo further hydrogenation steps to yield fatty alcohols and ultimately saturated *n*-alkanes with an even carbon atoms number (HDO) or (ii) undergo decarboxylation to yield hydrocarbons directly, that is, hydrocarbons with an odd number of carbon atoms (hydrodecarboxylation). HDO leads to elimination of water from triglycerides, fatty acids, fatty alcohols, and fatty esters as a result of reaction with hydrogen. It has been proposed that this reaction occurs via adsorbed enol intermediate (Donnis et al., 2009). HDC consists of decarboxylation (CO_2 elimination) of compounds containing carboxylic functional group and hydrogenation of the unsaturated intermediates of CO_2 elimination. Carbon dioxide is a primary product of this reaction, and it may undergo further reactions, particularly hydrogenation, which is undesired since it causes significant increase in hydrogen consumption. Consequently, there are numerous efforts to achieve selective decarboxylation without CO_2 hydrogenation (Lestari et al., 2008, Simakova et al., 2009, Snåre et al., 2008). The simultaneous presence of both fatty acids and alcohols leads to formation of fatty esters thanks to esterification of fatty acids with fatty alcohols. These esters are, nevertheless, subsequently converted into hydrocarbons. There are two possible initial steps of triglycerides conversion: (i) hydrolysis yielding fatty acids and glycerol and (ii) hydrogenolysis yielding fatty acids and propane. As neither the feed contains water nor the rate of triglycerides conversion increases due to deoxygenation with increasing concentration of water in the product mixture, it is plausible to assume that the reaction is initiated by hydrogenolysis of the C—O bond between the fatty acid chain and the propane (glycerol) backbone of triglycerides.

To evaluate the extent of reactions presented in Fig. 3.7, a set of separate experiments starting with the identified important intermediates was carried out. These experiments included deoxygenation of oleyl alcohol, oleic acid, and oleyl oleate that was synthesized for this purpose.

5.2. Deoxygenation of oleyl alcohol

The simplest reaction pathway of oleyl alcohol hydrogenation implies consecutive hydrogenation to stearyl alcohol followed by its deoxygenation to yield the final product, *n*-octadecane. Alternatively, oleyl alcohol can be deoxygenated first followed by hydrogenation of the unsaturated reaction intermediate to *n*-octadecane. In an attempt to understand the issue of olefin formation, an alternative scheme was tested as well. It involves consecutive hydrogenation of oleyl alcohol to stearyl alcohol, followed by its dehydration to *n*-octadecene and final hydrogenation of *n*-octadecane to *n*-octadecane. As a parallel reaction of oleyl alcohol, direct hydrogenation to *n*-octadecane was used. The second scheme describes the dependence of *n*-octadecane–*n*-octadecene concentration as a function of contact time better (see Fig. 3.12). Arrhenius plot of the corresponding rate constants of the pseudo-first-order kinetics is given in Fig. 3.13. Due to the high reactivity of oleyl alcohol, the experiments were conducted in the temperature range of 220–240 °C in order to distinguish the individual reaction steps involved in transformation of oleyl alcohol into the ultimate product, *n*-octadecane. At the higher temperatures used for rapeseed oil hydrogenation, the scheme presented in Fig. 3.7 is sufficient and, therefore, it was used for the general kinetic model.

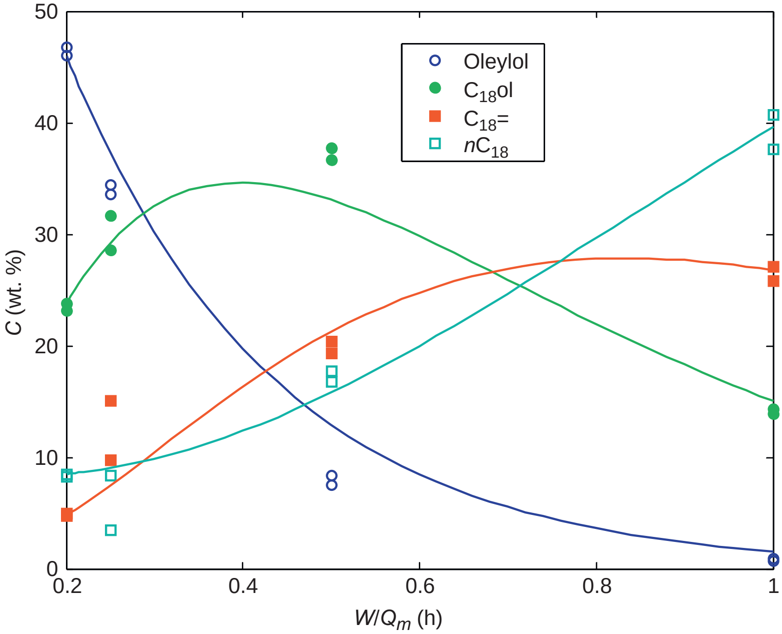

Figure 3.12 Concentration of compounds for oleyl alcohol hydrodeoxygenation at 230 °C and 3.5 MPa (*n*-octadecene formation by dehydration of stearyl alcohol assumed).

5.3. Oleic acid deoxygenation

The reaction scheme of oleic acid deoxygenation includes consecutive hydrogenation of oleic acid to stearic acid followed by several parallel reactions: hydrogenation to stearyl alcohol and its subsequent hydrogenation affording *n*-octadecane. Stearic acid produces together with stearyl alcohol an ester (stearyl stearate), which also reacts to hydrocarbons. Moreover, direct decarboxylation of stearic acid is also possible.

From the point of view of selectivity to hydrocarbons and oxygenates like in rapeseed oil deoxygenation, the formation of *n*-octadecane is preferred over HDC to *n*-heptadecane. Temperature enhances very much the formation of the fully hydrogenated product, *n*-octadecane.

5.4. Oleyl oleate HDO

Deoxygenation of oleyl oleate is preceded similar to triglycerides by total saturation of double bonds, that is, by formation of stearyl stearate via either stearyl oleate or oleyl stearate. This fully saturated ester is then split by

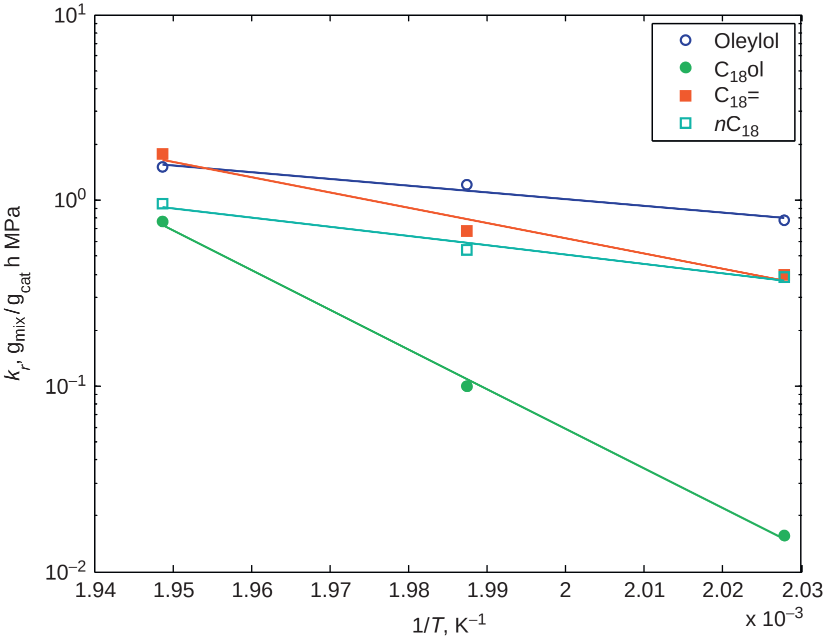

Figure 3.13 Arrhenius plot of oleyl alcohol deoxygenation in the temperature range of 220–240 °C and 3.5 MPa.

hydrogenolysis to afford *n*-octadecane and stearic acid that might undergo either further HDO to *n*-octadecane or HDC to *n*-heptadecane. Both results of experiments and kinetic modeling do not support the concept of the possible reversible reaction (hydrolysis) of stearyl stearate to stearic acid and alcohol.

5.5. HDO of rapeseed oil

The complete reaction scheme of deoxygenation of rapeseed oil is presented in Fig. 3.7. As it is not possible to distinguish unsaturated and saturated triglycerides and as it is widely accepted that hydrogenation of olefinic bonds of triglycerides is very fast and thus preceding their deoxygenation, kinetic evaluation starts with the sum of triglycerides. The estimated first-order kinetic parameters are presented in Table 3.8.

5.6. Evaluation of kinetic parameters

The experimental data measured by the method described above in a laboratory trickle-bed reactor using crushed catalyst particles diluted by fine inert SiC particles were processed by a program formulated in Matlab. Simplex

Table 3.8 Pseudo-first-order kinetic parameters for rapeseed oil HDO (Tukač et al., 2012)

Reaction No.	**Reaction (initial compound → product)**	***k* (280 °C) (g_L/g_{cat} h MPa)**	***E* (kJ/mol)**	***A* (g_L/g_{cat} h^{-} MPa)**
1	$TGC_{18} \rightarrow (C_{17}H_{35}COO)_2C_3H_6$	0.987	89.4	2.55×10^8
2	$C_{17}H_{35}COOH \rightarrow C_{17}H_{35}CH_2OH$	1.52	95.7	2.04×10^9
3	$C_{17}H_{35}COOH \rightarrow C_{17}H_{36}$	0.433	47.4	13,000
4	$C_{17}H_{35}COOH \rightarrow C_{18}H_{38}$	2.70	219.2	1.28×10^{21}
5	$C_{17}H_{35}COOH + C_{17}H_{35}CH_2OH \rightarrow C_{17}H_{35}COOC_{18}H_{37}$	3.33	323.1	2.00×10^{31}
8	$C_{17}H_{35}COOC_{18}H_{37} \rightarrow C_{18}H_{38}$	1.36	72.7	1.06×10^7
9	$C_{17}H_{35}COOC_{18}H_{37} \rightarrow C_{17}H_{36}$	0.0574	268.2	5.12×10^{24}
10	$TGC_{18} \rightarrow (C_{17}H_{35}COO)_2C_3H_5OH$	1.43	154.3	7.81×10^{14}
11	$(C_{17}H_{35}COO)_2C_3H_6 \rightarrow C_{17}H_{35}COOH$	2.23	36.8	6695
12	$(C_{17}H_{35}COO)_2C_3H_5OH \rightarrow C_{17}H_{35}COOH$	3.32	41.9	29,100

Nelder–Mead optimization based on minimization of sum of squared deviation of experimental and computed concentration was applied. The kinetic model of reactions supposed the first-order power law rate equations and the reactor differential balance presumed plug flow and pseudo-homogeneous mass and heat transfer conditions without external and internal mass transfer resistance. The differential balance for each compound was solved by the Runge–Kutta method. The parity plot demonstrating the rather good agreement between the experimental and calculated concentrations (Tukač et al., 2012) is shown in Fig. 3.14.

The differential balance of each substrate is introduced in Eq. (3.8), and rate equation depending on concentration and pressure is presented in Eq. (3.9).

$$\frac{dC_i}{d(W/Q_m)} = -r_i \tag{3.8}$$

$$r_i = k_i C_i P \tag{3.9}$$

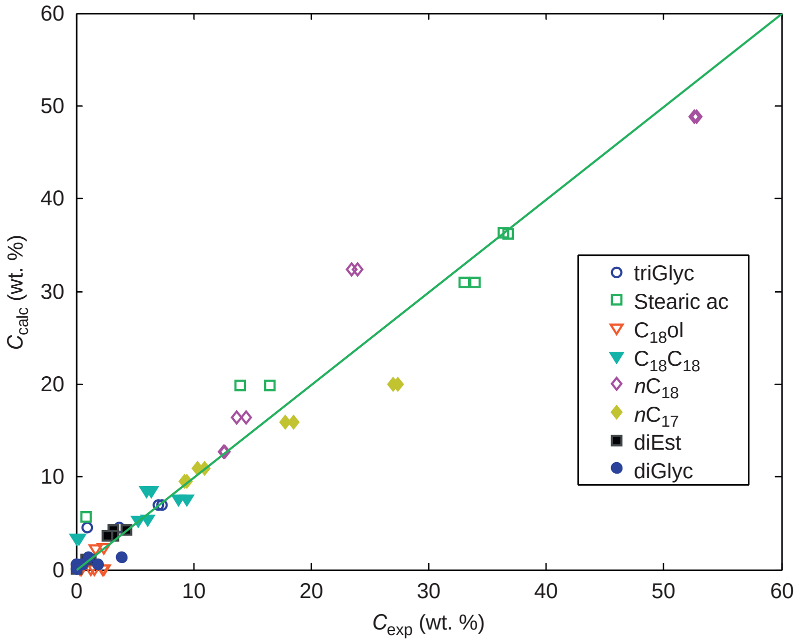

Figure 3.14 Parity plot of experimental and computed concentration of rapeseed oil hydrodeoxygenation at 280 °C, 3.5 MPa and contact time 0.2–1 h (Tukač et al., 2012).

The results of kinetic data evaluation are presented in Table 3.8. Chemical reactions are briefly identified by the principal reactant and product. The other columns provide rate constant at 280 °C, apparent energy of activation, and frequency factor of Arrhenius equation for each of the reactions in the model.

Reactions with apparent activation energy lower than 30 kJ/mol are probably influenced by external mass transfer resistance. Also internal mass transfer limitation is possibly of importance if the value of apparent activation energy is below 70 kJ/mol.

The chemical reactions involved in triglycerides deoxygenation can be classified into several groups according to their reaction rate constants. The fastest reactions include the formation of C_{18} alkanes from saturated and unsaturated alcohols, followed by saturation (hydrogenation) of double bonds in unsaturated acids, alcohols, and esters. These are followed by reactions involved esterification and in di- and triglyceride hydrogenolysis. Decarboxylation of acids seems to be the slowest reaction in the system.

6. DEACTIVATION ASPECTS

Long-term stability of catalytic activity is essential for any commercial catalytic process that does not involve continuous catalyst regeneration. From a practical point of view, the cycle length of HDO catalyst should be similar to that of conventional hydrotreating, that is, in the case of stand-alone technology, it should be in the range of 12–24 months that is the typical cycle length of middle distillate hydrotreating units. More importantly, in the case of VO (or generally triglycerides) coprocessing with petroleum-derived feedstocks, typically AGO, the impact on AGO hydrotreating cycle length should be minimized as to not affect the schedule of a given refinery shut-down/maintenance plan. The lifecycle length of a catalyst depends primarily on three factors, namely, feedstock properties, operating conditions, and catalyst properties including its composition. As the focus here is on refinery processing of triglycerides, either stand-alone or coprocessing the obvious choice for coprocessing units is conventional hydrotreating catalyst, while stand-alone units could utilize either conventional hydrotreating catalysts or other types of catalysts, for example, supported noble metals such as Pd on carbon that has been demonstrated to be an efficient deoxygenation catalyst (Kubičková et al., 2005; Murzin et al., 2006; Snåre et al., 2006).

As the triglyceride feedstock is concerned, the catalyst activity regardless of the catalyst type discussed above is affected primarily by the feedstock composition. The main issue to be addressed is the concentration of contaminants originating from VO production. The naturally occurring components having potentially a negative effect on catalyst activity include generally phosphorus, sodium, potassium, calcium, and magnesium. Some other impurities can also be found depending on the oil origin; for example, algae oils often viewed as the bio-feedstock of future are rich in nitrogen compounds. The concentration of the impurities depends not only on the VO origin but also on its processing prior to its hydrotreating. Typically, the highest concentration of impurities is in raw oils, that is, after their pressing and/or extraction from oil seeds. The presence of these impurities is connected to phospholipids, that is, triglycerides in which one of the fatty acid moieties is replaced by phosphoric acid. The additional charge of phosphoric acid moiety in phospholipids is compensated by the alkali metal cations and/or cations of the alkaline earths metals. For example, in neat rapeseed oil, the concentrations were in the range from tens to hundreds of ppm, which are significant amounts for any catalytic process.

The effect of these impurities on catalytic activity of the CoMo catalyst used in hydrotreating of rapeseed oil (310 °C, 3.5 MPa, 2 h^{-1}) has been investigated recently (Kubička and Horáček, 2011). Different rapeseed oil-derived feedstocks available from a rapeseed oil producer were processed. The concentration of impurities ranged from unit ppm or sub-ppm levels found in refined food grade rapeseed oil up to tens to hundreds ppm in neat rapeseed oil or the so-called trap grease. Thanks to using triglyceride streams in different stages of processing, the proportions of phosphorus, on the one hand, and alkali and/or alkaline earths metals, on the other hand, varied making it possible to elucidate the effect of phosphorus and alkali and/or alkaline earths metals, respectively.

The tested feedstocks can be classified into three groups: (i) feedstock with cations–anions charge balance, (ii) feedstocks with excess of phosphoric acid moiety in respect to alkali and/or alkaline earths metals cations, and (iii) feedstock with excess of alkali and/or alkaline earths metals cations in respect to phosphoric acid moiety (Kubička and Horáček, 2011). The slowest deactivation was observed for the first type of feedstock and feedstocks with very low concentration of impurities, that is, units of ppm or even sub-ppm level, despite being of type (iii). On the other hand, the fastest and most severe deactivation was observed when the feedstock with large excess of phosphorus with respect to the available cations was used (type (ii)). In this case, the catalyst was completely deactivated within the first 48 h on stream. The origin of this behavior lied in the large concentration of phosphoric acid moiety which was not compensated by alkali and/or alkaline earths metals cations and was hence acidic. The present phospholipids decomposed under the reaction conditions and phosphoric acid were created and acted as an oligomerization/polymerization catalyst of the unsaturated fatty acid moieties in triglycerides (Kubička and Horáček, 2011). Consequently, very fast coking of the catalyst occurred leading to virtually complete loss of catalyst activity.

On the other hand, the large concentration of phosphoric acid moiety, the charge of which was compensated by alkali and/or alkaline earths metals cations, did not lead to fast deactivation. In fact, the catalyst performance with this feedstock was similar to the performance of the same catalyst using food grade rapeseed oil over the test period that lasted nearly 150 h on stream. Nonetheless, the analyses of the catalyst bed revealed that phospholipids decomposed as well and phosphates of the corresponding alkali and/or alkaline earths metals were deposited just upstream the catalytic bed. As these were not acidic, they could not catalyze the oligomerization reaction.

Nevertheless, it could be anticipated that the reactor would get plugged due to a gradual buildup of phosphates originating from alkali and/or alkaline earths metals containing phospholipids (Kubička and Horáček, 2011). It can be, hence, concluded that the presence of phosphorus is detrimental for the deoxygenation technology regardless of the type of phospholipids and phosphorus has to be eliminated from the feedstock. This process is indeed the first step in upgrading of VOs obtained by pressing and/or extraction to produce food grade product and is called degumming.

Alkali and/or alkaline earths metals present in the feedstock in excess were also shown to deteriorate the catalyst performance in comparison with high-quality food grade VO. A plausible explanation provided suggested that deposition of these metals on catalyst surface induced electronic effects limiting hydrogenation (Kubička and Horáček, 2011). Moreover, deactivation of hydrotreating and hydrocracking catalysts has also been reported previously (Cable et al., 1985). In addition, alkali and/or alkaline earths metals molybdates, tungstanates, and aluminates were indicated by thermodynamic calculations as compounds that could be formed under hydrotreating conditions. Unfortunately, neither their stabilities nor their activities under hydrotreating conditions are known (Furimsky and Massoth, 1999). It can be speculated that if these compounds are indeed formed, their activity will be lower than that of the active components of hydrotreating catalysts, that is, metal sulfides.

The importance of the impurities can be further inferred from the description of the NexBTL technology developed and commercialized by the Finish Company Neste Oil. Any feedstock that is processed in a NeBTL unit undergoes pretreatment in order to ensure suitable quality feedstock. The pretreatment consists of degumming using phosphoric acid to eliminate phospholipids and alkali metals and/or alkaline earths metals cations. Furthermore, sodium hydroxide is used in the pretreatment, plausibly to neutralize free acids that could cause corrosion problems upstream in the technology. The soaps formed as a consequence of neutralization are removed by washing using demineralized water (Hodge, 2006).

In addition, the degree of unsaturation of the triglycerides is of importance not only because it is directly connected to the hydrogen consumption but also because the high degree of unsaturation, that is, two or more double bonds per fatty acid chain, makes the fatty acid chains prone to cyclization reactions. This has been demonstrated by da Rocha Filho et al. (1993), who have used a series of variously unsaturated VOs in hydrocracking experiments (NiMo/Al_2O_3 catalyst, 360 °C, 14 MPa, hydrogen, 2 h). The oils containing linoleic and linolenic fatty acid moieties in large concentration (it totals above 60 wt.%) yielded significant amounts of cycloalkanes ($\sim$15 wt.%) and also some alkylaromatics (about 4 wt.%) while oils consisting of saturated fatty acid moieties afforded almost exclusively alkanes. The concentration of cyclic compounds (both cycloalkanes and aromatics) was less than 3 wt.%. When monounsaturated fatty acid moieties (typically oleic acid) prevailed in the feedstock, a moderate yield of cycloalkanes was observed (ca. 8 wt.%; da Rocha Filho et al., 1993).

These conditions might seem too extreme and hence irrelevant for hydrotreating applications. However, the authors (da Rocha Filho et al., 1993) have investigated also the effects of reaction temperature and pressure on formation of cyclic products in hydrocracking of buriti oil (consisting of 80 wt.% oleic acid and 17 wt.% palmitic acid moieties). When pressure was decreased from 14 to 7 MPa at a reaction temperature of 360 °C, which is a common hydrotreating temperature in hydrotreating of middle distillates, the formation of cycloalkanes increased by nearly 40%. The formation of alkylaromatics remained low (it increased from 0.2 to 0.3 wt.%). The increase in reaction temperature had a more profound effect. At 14 MPa and 1-h reaction time, the concentration of cycloalkanes increased from 5 wt.% to more than 20 wt.% upon increase in temperature from 360 to 395 °C, which can be in some hydrotreating units the maximum operating temperature. At the same time, the concentration of aromatics increased from 0.1 to 0.8 wt.% (da Rocha Filho et al., 1993).

To provide more fundamental information reflecting the formation of cycloalkanes and aromatics as a function of the degree of unsaturation, a series of C_{18} fatty acids was also used in hydrocracking (NiMo/Al_2O_3 catalyst, 360 °C, 14 MPa, H_2, 2 h; da Rocha Filho et al., 1993). The concentration of alkylcycloalkanes afforded by hydrocracking of stearic, oleic, linoleic, and linolenic acid, that is, of fatty acid with 0, 1, 2, and 3 double bonds in their molecule, increased from $<$1 wt.% found for stearic acid to ca. 12, 19, and 30 wt.% for oleic, linoleic, and linolenic acid, respectively. For the same sequence of fatty acids, the concentration of alkyl aromatics was increased in the following order: zero, traces, 0.8 and 6.8 wt.%.

Thus, it can be inferred from these observations that with the increasing degree of unsaturation of the triglycerides in an HDO feedstock, the propensity of the feedstock to formation of carbonaceous deposits will increase depending on the operating conditions. The significant formation of cycloalkanes and alkylaromatics from linolenic acid (ca. 30 and 6.8 wt.%, respectively) indicates that the concentration of fatty acid moieties with more than two double bonds needs to be monitored closely in any incoming feedstock as a measure to avoid increased carbonaceous deposits formation. Moreover, the high degree of unsaturation of triglycerides might plausibly cause problems in the feedstock preheating section due to their lower thermal stability as compared with saturated triglycerides.

Apart from the possible adverse effect of significant degree of unsaturation, catalyst deactivation may originate also from deoxygenation products, particularly water and carbon oxides. In this context, a specific problem relates to the use of sulfided catalysts. It is well known that these catalysts are used under reductive conditions. Consequently, the catalysts are susceptible to reduction and loss of their catalytic activity. When treating sulfur-containing feedstocks, this is generally not an issue as the concentration of hydrogen sulfide, the product of hydrodesulfurization, in gas phase is sufficient to keep the catalyst in sulfided form, that is, prevent its desulfidation/reduction. However, the sulfur content of majority of triglyceride feedstocks is very low. For example, rapeseed oil contains approximately 2–3 ppm of sulfur, which is not sufficient to keep a hydrotreating catalyst in its active form. As a result, gradual catalyst reduction and loss of hydrogenation activity occur. This has been demonstrated in long-term experiments focused on deoxygenation of rapeseed oil (Kubička and Horáček, 2011).

The deoxygenation activity of the CoMo catalyst, expressed as the extent of oxygen atom elimination from liquid phase products, dropped from 100% (complete deoxygenation) to ca. 75–80% after the first 144 h on stream when refined sulfur-free rapeseed oil was processed. However, when sulfur was introduced in the feedstock (in the form of dimethyl disulfide) to ensure suitable concentration of hydrogen sulfide in the gas phase, the deoxygenation activity of the CoMo catalyst was stable over the whole test length (ca. 260 h). At the end of the test, the extent of oxygenation was still above 96% (Kubička and Horáček, 2011). Moreover, there were periodic changes in the delivery of hydrogen sulfide source, that is, between short periods (2 h) when rapeseed oil containing dimethyl disulfide was fed in the reactor, and there were longer periods (ca. 50–100 h) when sulfur-free rapeseed oil feedstock was used. These experiments indicated that the loss of activity when sulfur-free feedstock was used was partially reversible, that is, that the deoxygenation activity decrease due to processing sulfur-free rapeseed oil can be stopped by adding dimethyl disulfide in the feedstock and the activity can be even temporarily restored (Kubička and Horáček, 2011).

Obviously, this is an issue only in stand-alone HDO units as during coprocessing of triglycerides with petroleum feedstocks, such as AGO, there is a sufficient amount of sulfur presents to ensure stable catalyst performance. The technology scheme of the NexBTL process (Hodge, 2006) indicates that hydrogen sulfide exits the hydrotreater where only pretreated feedstock consisting of VOs is fed. The origin of hydrogen sulfide is not given. Owing to the readily available hydrogen streams containing hydrogen sulfide (any gas outlet of a conventional hydrotreater), it can be speculated that for hydrotreating/deoxygenation of triglycerides, such a stream is used before it is scrubbed to remove hydrogen sulfide. It is a much simpler alternative than addition of dimethyl disulfide. Alternatively, one could imagine that even in a stand-alone unit, VO is hydrotreated together with a petroleum fraction containing sulfur that is easily hydrotreated. As the NexBTL scheme suggests that the liquid product is directly fed into an isomerization unit, it seems more plausible that the option with hydrogen sulfide containing hydrogen is used. It is also clear that if the stand-alone unit was to use a noble metal type of catalyst, the question of sulfur addition would be redundant.

On the other hand, water and carbon oxides as the ultimate deoxygenation products apart from the desired hydrocarbons can affect negatively the catalytic activity of both noble metal and metal sulfide catalysts. For example, deactivation of hydrogenation catalysts by carbon monoxide is well known. However, its effect is greatly dependent on the type of catalyst and in particular on reaction conditions. From the mechanistic point of view, carbon monoxide is a reaction intermediate that is either formed by hydrogenation of carbon dioxide, that is, the primary product of the decarboxylation reaction pathway, or as a product of decarbonylation that has also been proposed as a viable reaction route in deoxygenation of triglycerides and fatty acids (Donnis et al., 2009; Kubičková and Kubička, 2010). The options that are applied in the commercialized technologies to deal with the inhibition effect of carbon monoxide are discussed in detail in Section 7 that covers the commercial technologies. Apart from purging, pressure swing adsorption (PSA) or methanation can be applied to eliminate carbon monoxide from the recycle hydrogen stream.

Carbon dioxide does not constitute a major problem as it is scrubbed together with hydrogen sulfide from the hydrogen stream. It is also hydrogenated in the deoxygenation reactor which leads to increased hydrogen consumption and formation of undesired carbon monoxide. Several studies have focused on the effect of water formed in course of the deoxygenation reaction on the deoxygenation activity of sulfided catalysts (Laurent and Delmon, 1994b,c). Laurent and Delmon (1994c) reported that water had only a very weak inhibiting effect on majority of various reactions taking place during deoxygenation of phenols and ketones. An exception was hydrolysis of carboxylic esters that was favored by water addition (Laurent and Delmon, 1994c). In another study, the same authors have found that water caused a two-thirds of decrease (in less than 60 h on stream) of the catalytic activity during deoxygenation, but the hydrogenation–hydrogenolysis selectivity remained unaltered (Laurent and Delmon, 1994b). Water caused a small loss of catalyst (NiMo/γAl_2O_3)-specific surface area which was connected with a recrystallization of γ-alumina supported into hydrated boehmite phase. More importantly, water caused partial oxidation of nickel sulfide species which was suggested to be the reason behind the observed loss of catalytic activity (Laurent and Delmon, 1994b). Two plausible interpretations were put forward by the authors: (i) nickel sulfide is oxidized to nickel sulfate species that form an inactive layer on the nickel sulfide particles and (ii) water favors migration of nickel in the alumina lattice where the inactive nickel aluminate species are formed (Laurent and Delmon, 1994b). Nonetheless, the effect was not observed when water in the feed was replaced by oxygenated organic compounds. It should be noted here that the treatment was rather severe (360 °C, 7 MPa, dodecane/water = 170/10 ml/ml, 1–5 days) which might be the reason why there was no effect of organic oxygenates that were hydrotreated only for 150 min (13.6 wt.% of dibenzofuran or 4-methylphenol in dodecane). In contrast, the molybdenum sulfide phase was virtually unaffected (not oxidized) by the water or oxygenates treatment (Laurent and Delmon, 1994b).

7. COMMERCIAL STATUS OF HDO

The intensive interest in renewable fuels that are fully compatible with the current automotive fuels as well as with the modern combustion engine technology resulted in fast development and commercialization of several deoxygenation technologies by several companies. In principle, they can be divided into two major categories, namely, stand-alone units and coprocessing units. Stand-alone units are such technologies that process neat VOs (or, in general, triglyceride feedstocks), and their product is renewable (or green) diesel fuel, which can then be used for blending with diesel fuel fulfilling the legislative requirements. As it will be discussed later on, due to isomerization, the renewable diesel outperforms conventional diesel as it is sulfur- and aromatics-free. On the other hand, coprocessing technology refers to hydrotreating of mixtures containing AGO and VOs. The product is then a mixture of conventional diesel and renewable diesel fuel. From the economic point of view, the stand-alone units are definitely more investment intensive, while the coprocessing units require significantly less investments to be made to adapt the existing units to operate efficiently with the new feedstock. The trade-off is connected with the process flexibility. While the stand-alone units are very flexible in terms of feedstock type and quality, and the product properties can be rather easily adjusted, the coprocessing units lack this flexibility as they need to take into account also the HDS process (with the aim to achieve diesel fuel with less than 10 ppm S) and it might be difficult to obtain suitable low-temperature properties of the final product as will be discussed also in this section.

7.1. Stand-alone deoxygenation technologies

The most advanced stand-alone deoxygenation technologies include processes NexBTL be Neste Oil and Ecofining by UOP and ENI. The main features of these will be discussed in the following paragraphs followed by the assessment of the main challenges in coprocessing.

The NexBTL process consists of three essential stages: feedstock pretreatment, hydrotreating, and isomerization (Fig. 3.15). The pretreatment stage is an indispensable part of the process as it ensures high quality of feedstock that can be fed into the catalytic units, particularly the hydrotreating unit which precedes isomerization. As a result, any contaminants of renewable triglyceride-based or -related feedstocks that could affect catalyst performance are removed. Typical contaminants that are being removed in the NexBTL process include phosphorus and metals (Ca, Mg). The processes involved in feedstock pretreatment consist of degumming by H_3PO_4, neutralization by NaOH, and washing by demineralized water. The pretreated (refined) oil is fed in the hydrotreating unit where the

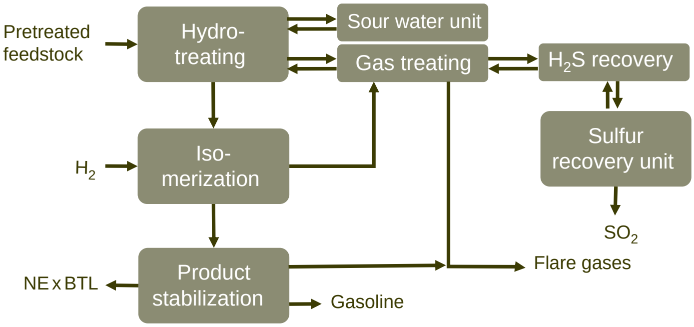

Figure 3.15 Schematic flow scheme of the NexBTL process (Hodge, 2006).

deoxygenation takes place. The catalyst is supplied by Albemarle (Green Car Congress, 2012a), and it is the most probably a sulfided NiMo or CoMo catalyst.

The deoxygenation step of the NexBTL process is followed by isomerization, which is an essential part of the technology as it modifies the chemical structure of the deoxygenation product. The ultimate deoxygenation products, *n*-alkanes, are mildly isomerized to afford a mixture of iso-alkanes that have far better cold flow properties than the original *n*-alkanes. Without this modification, the renewable diesel fuel would not be suitable for use in diesel engines in mild or cold climates as it will be demonstrated later in this chapter when the fuel properties of renewable diesel will be discussed.

Neste Oil has actually pioneered the renewable diesel technology, and currently, four units with the total combined nominal capacity of nearly 2 million tons per year are operated worldwide.

The feedstock portfolio of NexBTL process consists of crude palm oil (<50%); waste and side streams, such as waste animal fat, palm oil fatty acid distillate, and stearin (ca. 40%); and other VOs, such as rapeseed, soybean, and camelina oils (ca. 10%). The given shares of the individual feedstocks were the targets for Neste Oil's procurement of renewable raw materials in 2011. Owing to the sustainability issues that have been raised in connection with production of fuels from renewable raw materials, Neste Oil prioritizes suppliers that follow sustainable cultivation and production practices and have a good greenhouse gas (GHG) balance (Neste Oil, 2012b). Apart from the currently used renewable raw materials, Neste Oil also pays attention to alternative raw materials for production of renewable diesel fuel. These include forest industry by-products, waste fat from fish-processing industry, microalgae oil, and microbial oil (Neste Oil, 2012c).

UOP has developed together with Eni a process called Ecofining that they have been successfully demonstrating since 2008 in 12-kt/yr-demonstration unit in the USA. Commercial units are either completed and awaiting for approval (640 kt/yr in total) or under construction (810 kt/yr), see Table 3.9 for details. The feedstock requirements have evolved similar to Neste Oil—prior to the sustainability question being raised, palm, soybean, and canola oils were considered. Since 2007, however, the focus was shifted toward nonfood and more sustainable sources, such as camelina, jatropha, and algal oils, and cheaper oils and fats, including tallow, yellow grease, and tall oil. The cheaper triglyceride alternatives have the advantage of the lower feedstock price and sustainability since they are typically derived from waste streams in food and wood and forest industries.

Table 3.9 Commercial deoxygenation units and their current status (Frey, 2011; Neste Oil, 2012a)
Technology

Name	Technology developer	Location	Company	Capacity (kt/a)	Status
NexBTL	NesteOil	Finland	NesteOil	190,000	2007
		Finland	NesteOil	190,000	2009
		Singapore		800,000	2010
		Netherlands		800,000	2011
Ecofining	UOP/Eni	UOP	USA	12,000	2008
		Italy	ENI	320,000	Awaiting approval
		Portugal	GALP	320,000	Awaiting approval
		North America	Diamond Green Diesel	490,000	2012—expected
		North America	Undisclosed	320,000	2013—expected
		North America	AltAir Fuels	320,000	Pending

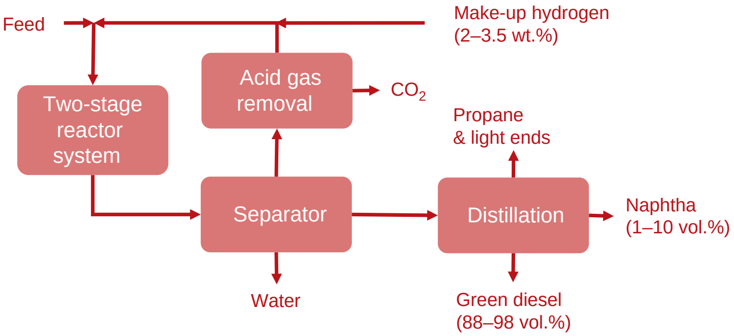

Figure 3.16 Schematic depiction of the Ecofining process (Frey, 2011; UOP, 2012).

Their inherent disadvantage is the higher concentration of undesired contaminants and with it connected more demanding preprocessing.

The Ecofining process relies on a two-stage fixed-bed reactor system (Fig. 3.16). Due to the schematic depiction in the available materials, it is not clear whether the reactor system consists of two reactors (a HDO reactor and a hydroisomerization reactor) or a single reactor with a HDO and hydroisomerization stage. The placement of a separator after the reactor system to remove water, an inevitable reaction by-product, indicates that the latter option is most probably used. On the other hand, information provided elsewhere (Kalnes et al., 2008) suggests that the system includes in fact two reactors. In the first one, the feedstock is completely deoxygenated and the light products (water, light hydrocarbons, and carbon dioxide) are immediately separated at reactor pressure. The main product, mixture of *n*-alkanes, is then mixed with additional hydrogen and fed into an integrated catalytic hydroisomerization reactor to afford branched-paraffin-rich diesel (Kalnes et al., 2008). In this way, diesel having suitable cold flow properties is obtained and both reaction steps (deoxygenation and isomerization) are kept at their maximum selectivity. The hydrogen needed can be obtained, for example, by steam reforming of a portion of the light hydrocarbons (Kalnes et al., 2008). Deoxygenation and isomerization catalysts supplied by UOP are employed in the Ecofining process. According to the technical information leaflet, the typical inside battery limits erected costs are between 40 and 60 million USD per a unit with production capacity of ca. 250 kt/yr (UOP, 2012). In order to reduce significantly the capital investment, an existing distillate hydrotreater could be revamped into the Ecofining process.

Depending on the feedstock and the calculation method used, the green diesel offers GHG saving in an excess of 50% relative to petroleum-derived diesel fuel. In addition to GHG savings, the renewable diesel offers further advantages over conventional diesel owing to its superior properties (low aromaticity, low sulfur). As an example, the green diesel from the NexBTL process (100% NexBTL diesel) has been tested extensively. These tests included a 3-year test in buses in the city of Helsinki, Finland; Mercedes Benz trucks tests in Germany; and an arctic trial in Canada. Data on emissions collected in Helsinki showed reduction of particulate matter and nitrogen oxides (NO_x) emissions by 30% and 10%, respectively. The test in Germany confirmed that emissions were reduced significantly in comparison with standard-diesel-driven trucks (Neste Oil, 2012d).

In addition to renewable diesel, renewable jet production is targeted as well. For example, UOP and Eni have announced that they will construct a unit for renewable jet production for AltAir fuels with a capacity of 320,000 t/a (Frey, 2011), and UOP has already performed several successful tests of renewable jet fuel with the major aircraft producers (Boeing, Airbus) and US military demonstrating that replacement of standard jet fuel by renewable jet fuel is feasible. Neste Oil claims that it produces renewable aviation fuel using its NexBTL technology (Neste Oil, 2012e) as a commitment to the European Aviation Biofuels Flightpath that is aimed at increasing the use of aviation biofuels to 2 million tons annually by 2020.

Besides NexBTL and Ecofining, another stand-alone deoxygenation technology, Vegan, was introduced by Axens. The principle of the technology seems to be similar to the discussed technologies. After the hydrotreating step in which VOs are completely deoxygenated follows the second step, which is in this case not called isomerization, but rather mild hydrocracking/dewaxing. Nonetheless, the purpose is the same, that is, to convert *n*-alkanes into iso-alkanes in order to improve the cold flow properties of the final renewable diesel product. However, no information was found whether and where the process is commercially used.

The advantages of renewable (green) diesel in comparison with the traditional biodiesel (FAME), from the application point of view, are rather significant. Apart from the full compatibility with conventional diesel and compliance with the strictest fuel, improved emission characteristics and fossil CO_2 savings have been reported. An overview is given in Table 3.10 (Neste Oil, 2012f).

7.2. Coprocessing deoxygenation technologies

Owing to the apparent simplicity and low investments needed, the coprocessing deoxygenation technology seems to be a popular one. It has been addressed not only by refining companies, such as Petrobras and ConocoPhillips, but also by catalyst manufactures, mainly Haldor Topsoe and Albemarle. As a revamp of existing hydrotreater is sufficient, it is not easy

Table 3.10 Comparison of renewable diesel and biodiesel

NExBTL renewable diesel (HVO)	Traditional biodiesel (FAME)
Can be used in blends in any concentration, that is, 0–100% of the content	Can only be used in blends upto 5–7% of the content[a]
Complies with the strictest quality standards	Biofuel usage requirements cannot be met without compromising fuel quality specifications
Reduces greenhouse gas and tailpipe emissions (PM, NO_x, CO, HC)	Increases NO_x emissions
Offers excellent storability	Must be used before a specific “best before” date
Does not require engine modifications or changes in logistical system	Can cause engine problems

[a] Maximum allowed under the European diesel standard.

to quantify the real extent to which renewable diesel is produced by coprocessing. For example, ConocoPhillips has been produced renewable diesel fuel at its refinery in Whitegate, Cork, Ireland, since 2006, but detailed information about real capacity, content of VO in the hydrotreated feedstock, is not available.

Another example of a coprocessing technology is process H-BIO. It has been developed by the Petrobras research and development center (CENPES). The technology is schematically depicted in Fig. 3.17. The core of the process is catalytic hydrotreatment of diesel fuel blending components, such as straight run diesel, light cycle oil from fluid catalytic cracking (FCC), coker gas oil, and VOs in an existing hydrotreating reactor under controlled reaction temperature and hydrogen pressure (Costa, 2007). Triglycerides in VOs are converted into linear hydrocarbons at very high yields—at least 95% (v/v) to diesel. Owing to the product originating from triglycerides, the quality of refinery diesel gets improved, mainly by increasing the cetane number and decreasing the density and sulfur content (Costa, 2007). The plan of Petrobras was to have the process implemented in at least three of its refineries by the end of 2007. The total VO consumption was about 256,000 m^3/yr, that is, ca. 230,000 t/yr. After implementation of two other refineries, the VO consumption should rise to 425,000 m^3/yr, that is, ca. 390,000 t/yr. The required investment to adjust the production and logistics was estimated to be in the range of USD 23–38 million (Costa, 2007).

However, the implementation was put on hold in 2008 due to high soybean oil prices that should have been the main feedstock. At that time, the refined soy oil price of $180 per barrel by far exceeded a regular diesel price

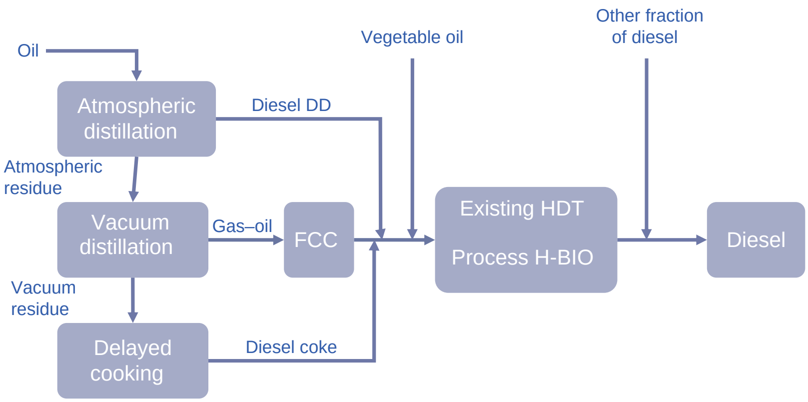

Figure 3.17 A schematic depiction of the H-Bio process (Costa, 2007).

of $104 a barrel (Green Car Congress, 2012b). It has been reported that the capacities were planned to be put into operation during late 2009 (World Fuels, 2012). However, no additional information about the current status of the technology and its commercial use was published since the news it was being put on hold due to high soybean oil prices.

Recently, some aspects of coprocessing were discussed in publications by major catalyst manufacturers including general information on the use of their catalysts in refineries for coprocessing. For example, Haldor Topsoe supplies its deoxygenation catalyst to three undisclosed refineries in Australia, Europe, and the USA coprocessing bio-feedstocks in the range of 0–5%, 2–5%, and 10–20%, respectively (Gabrielsen et al., 2011). The feedstocks include typically animal fats, for example, chicken fat in the USA, and other unspecified bio-feedstocks. In Preem, Sweden, Haldor Topsoe has supplied its deoxygenation catalyst for coprocessing of raw tall oil (20–30% of the feed). Apart from coprocessing, Haldor Topsoe catalyst is used by Cetane Energy, USA, to process neat animal fat and algae oil.

The possible pitfalls of revamping industrial hydrotreating or mild hydrocracking units to coprocess renewable feedstocks in significant amounts (up to 30% as in the case of Preem refinery, Sweden) have been discussed by Egeberg et al. (2011). The feed consisted of raw tall oil diesel (RTD) which is produced by esterification of tall oil, a wood processing by-product. There are about 500 kt of tall oil processed every year in Scandinavia (Gabrielsen et al., 2011). The main challenges identified included reaction heat evolution (exotherm, which is a consequence of high oxygen content of bio-feedstocks and also of their often unsaturated nature), corrosion (both up- and downstream of the reactor being consequences of the presence of free fatty acids), hydrogen consumption, and catalyst selection.

The corrosion problem is a consequence of the presence of rosin acids (they are not converted in the tall oil esterification) and unconverted free fatty acids in the RTD. In the process design, the possible problems were minimized by feeding RTD partly into AGO after the heater and partly as a liquid quench after the first catalyst bed. Consequently, the material needed to be changed only in small part of the technology. The liquid quench together with additional hydrogen quenches after second and third catalyst beds helps in controlling the exotherm (see Fig. 3.18). Moreover, due to the liquid quench between the first and second catalyst beds, a higher hydrogen partial pressure can be maintained in the upper part of the reactor (as it is not used for quenching after the first catalyst bed), thus preventing/suppressing condensation and coking reactions leading to catalyst deactivation. Besides, corrosion is suppressed as well (Egeberg et al., 2011).

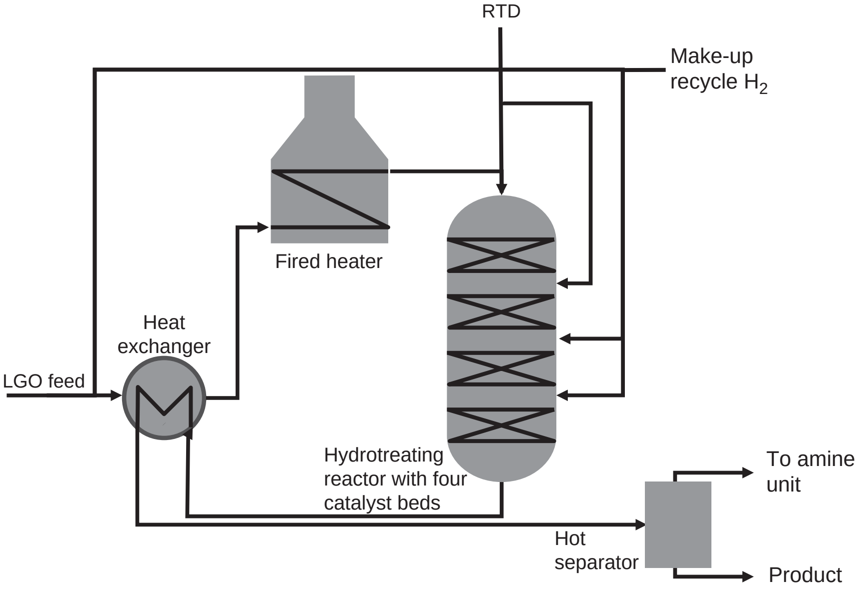

Figure 3.18 Coprocessing of tall oil with LGO in Preem refinery (Egeberg et al., 2011).

Due to the high concentration of oxygen to be removed by hydrotreating, which is significantly higher than typical sulfur concentration in petroleum-derived feeds (typically by an order of magnitude), hydrogen consumption for hydrotreating of bio-feedstocks is significantly higher than in the case of conventional hydrotreating. Obviously, this is also the cause of the increased exotherm when coprocessing bio-feedstocks with conventional petroleum-derived feedstocks. The correct balance between catalyst stability and activity is of the utmost importance (Egeberg et al., 2011). Hence, Haldor Topsoe has designed the catalyst system in the Preem refinery in such a way that RTD is converted in the upper two catalyst beds using catalysts with lower catalyst activity than their latest generation Brim catalysts. Brim NiMo catalyst is then used in the bottom two catalyst beds to ensure final product quality, that is, sulfur content below 10 ppm (Egeberg et al., 2011). The approach is based on the knowledge that deoxygenation reactions are significantly faster than the majority of hydrodesulfurization reactions.

Carbon oxides and methane are typical deoxygenation by-products causing problems in coprocessing units. Although majority of CO_2 from decarboxylation is removed in the amine wash used for H_2S scrubbing.

Downstream CO_2 can form carbonic acid in the presence of liquid water and hence cause corrosion unless the downstream equipment is modified accordingly (Egeberg et al., 2011). CO and methane will build up in the recycle gas, and a substantial purge is necessary to avoid this (Egeberg et al., 2011). Apart from reducing hydrogen partial pressure in the recycle gas loop, CO can act also as catalyst inhibitor. The purge hydrogen-rich gas has to be then treated according to its application. Removal of methane and CO in PSA is one option (Egeberg et al., 2011).

The operating experience in Preem Gothenburg refinery has shown that the reaction exotherm increased, as expected, with the increasing concentration of RTD. While in the absence of RTD the delta T was about 30 °C, it was around 60 °C when the feed contained 30% of RTD. At the same time, the hydrogen consumption increased from ca. 80 to about 140 nm^3/m^3. When the content of RTD was increased further to 50–55%, hydrogen consumption increased to ca. 200–220 nm^3/m^3 (Egeberg et al., 2011). Based on the comparison of different modes of operation (light cut gas oil mode vs. renewable mode), it was concluded that the catalyst was not inhibited either by the renewable feed components or by their products (Egeberg et al., 2011). Unfortunately, no information about the different feedstocks and their products was provided. It has been, however, reported (Gabrielsen et al., 2011) that the renewable diesel product of Preem refinery meets all the requirements of EN 590.

According to Albemarle, coprocessing of VOs in existing hydrotreaters is a straightforward alternative of introducing bio-feedstocks in the diesel fuel range in refineries. Similar issues to those identified in the Preem coprocessing case study have been discussed as well. Despite the relatively simple chemistry and high catalytic activity of the conventional hydrotreating catalyst, coprocessing gives rise to several technological and operational issues including (i) possible formation of CO having an inhibiting effect on the catalyst; (ii) accumulation of CO in recycle gas as it is not removed in scrubbers; (iii) high hydrogen consumption during triglyceride deoxygenation in comparison with HDS of AGO connected with a significant heat release; (iv) formation of *n*-alkanes that affect negatively the cold flow properties of the final diesel fuel; and (v) formation of free fatty acids, reaction intermediates in triglyceride deoxygenation, that can cause local corrosion problems (Melis et al., 2009). Albemarle has proposed a so-called BioSTAX system that is a solution consisting of several different commercial catalysts loaded at a specific place in the reactor and taking into account the constraints of the unit, such as H_2/oil ratio, outlet pressure, capacity of quenching, and intended VO addition (type and amount). The distribution (placement) of catalysts in the reactor reflects the main factors affecting the kinetics of individual feed components conversion. For instance, the requirements of a triglyceride and a dibenzothiophene vary significantly, and their conversion takes place at different positions along the catalyst bed in the reactor, that is, under different reaction conditions (e.g., hydrogen partial pressure). Consequently, different catalysts give optimum performance at a different place in the reactor with respect to the actual feed composition and reaction conditions.

If large guard beds are not available, the inherent impurities of VOs, such as phospholipids and metals, should be removed by refining, bleaching, and deodorization. On the other hand, the absence of sulfur, nitrogen, and aromatics has a positive dilution effect when coprocessed with AGO. An increase in WABT (weighted average bed temperature) of ca. 20 °C has been reported for the CoMo catalyst when coprocessing rapeseed oil (10 wt%) in AGO. When H_2/oil and pressure were increased from 300 Nm^3/m^3 and 40 bar, respectively, to 500 Nm^3/m^3 and 60 bar, the WABT increase dropped to ca. 11 °C in order to reach 10 ppm S at the outlet. The observed phenomenon was attributed to the inhibiting effect of CO, a deoxygenation by-product originating from fatty acids decarbonylation and/or from CO_2 hydrogenation (Melis et al., 2009). The inhibition is particularly severe for the direct desulfurization pathway, that is, it is more pronounced with CoMo than with NiMo catalysts. The lower impact on NiMo catalysts was verified experimentally; at 50 bar and H_2/oil of 200, an WABT increase of less than 5 °C was reported. Moreover, the large WABT increase observed for CoMo catalysts might be detrimental for the stability of catalytic activity due to considerable faster deactivation rates (Melis et al., 2009). The issue of CO-induced inhibition could be augmented with time since it is not removed by scrubbing and can be eliminated in a typical setup only by purging. This may be a limiting factor decisive for the maximum concentration of VO to be coprocessed. For higher VO concentrations, different solutions might be necessary, for example, use of selective membranes or passing of scrubbed, that is, H_2S free, recycle gas through a PSA unit. Due to the significant extent of hydrogenation reactions during deoxygenation of VOs, including double-bond hydrogenation, hydrogenation of the carboxylic group, and CO and CO_2 hydrogenation to methane, the reaction is highly exothermic leading to an increase in temperature along the catalyst bed (increase in Delta *T*). For instance, Albemarle reported an additional hydrogen consumption of 10–20 Nm^3/m^3 and a further Delta *T* increase of 12–21 °C in comparison with typical operations when coprocessing 5% of rapeseed oil. It follows that hydrogen consumption and quenching capacities are of crucial importance and optimum catalyst design is essential for limiting hydrogen consumption and affording acceptable hydrotreater cycle lengths (Melis et al., 2009).

In conclusion, to achieve the optimum performance, the extent of different deoxygenation reactions (HDO, decarboxylation/decarbonylation, methanation) needs to be optimized as well. This can be accomplished by selection of a suitable catalyst combination. The main products, *n*-alkanes, are another limiting factor for the amount of VO to be coprocessed. Their increasing concentration worsens the cold flow properties which might be an issue. For instance, coprocessing of 5% rapeseed oil can result in a decrease in cloud point of 5–6 °C, which is unacceptable typically for the winter diesel fuel grades (Melis et al., 2009).

7.3. Deoxygenation product quality

The final deoxygenation product quality is critical for its end use, that is, either for its blending in the diesel fuel pool in the case of stand-alone deoxygenation units or for the quality of the product of VO and AGO coprocessing. Obviously, the stand-alone option offers a better flexibility as the coprocessing alternative is limited by additional constraints, such as sulfur content of the final product. As discussed in the section describing different technologies, there are ways how to minimize the negative impacts of VOs on AGO hydrotreating during coprocessing. To meet specific fuel targets, the solutions can be either based on technology selection, improvements, and modifications, or on product treatment/modification. A conventional product treatment used for refinery products is the application of various additives enhancing diesel fuel properties. In the case of deoxygenation that affords as primary products *n*-alkanes having poor cold flow properties, the use of depressants might tackle the issue. The application of two industrially, widely used flow improvers (Infineum R-288 and Keroflux® 3566, BASF) for blends consisting of conventional petroleum diesel, having properties in accordance with EN 590, and mixture of hydrocarbons obtained by deoxygenation of rapeseed oil was investigated by Šimáček et al. (2010).

The results clearly demonstrated that neither of the two investigated flow improvers was able to improve the cold flow properties sufficiently. While the sensitivity of conventional diesel was high—the cold flow plugging point (CFPP) dropped from −12 °C to below −25 °C already when 200 mg/kg of flow improver (either Infineum R-288 or Keroflux® 3566) was added, there was hardly any response when the diesel fuel contained 5 wt.% of hydrocarbons from deoxygenation—the CFPP dropped from −12 to ca. −15 °C. The CFPP of diesel fuels containing 10–30 wt.% of hydrocarbons from deoxygenation did not decrease with addition of flow improvers in the range of 100–500 mg/kg more than by 1–2 °C (Šimáček et al., 2010). This clearly demonstrates that a technological solution affecting the composition of deoxygenation products, namely, shifting it from *n*-alkanes to a mixture of *n*- and iso-alkanes, is crucial.

There are several options; the most important being selective hydroisomerization of *n*-alkanes that is used in the NexBTL and Ecofining processes (Frey, 2011; Neste Oil, 2012a) and has also been the topic of recent research activities (Sebos et al., 2009). Another option, mild hydrocracking/dewaxing, was proposed by Axens (process Vegan) and Haldor Topsoe and also investigated experimentally (Šimáček and Kubička, 2010; Šimáček et al., 2011). The beneficial effect of hydrocracking of VOs on the cold flow properties of hydrocarbon mixtures afforded by this process was demonstrated by Šimáček et al. (2011). Hydrocracking of sunflower oil of 18 MPa yielded liquid hydrocarbons with *n*-alkane concentration decreasing from 67 to 20 wt.% as a result of reaction temperature increase from 360 to 420 °C. The concentration of iso-alkanes and cycloalkanes in the products obtained at reaction temperature above 400 °C exceeded 60 wt.%. Consequently, their cold flow properties were considerably improved. For instance, the cloud point of the hydrocarbon product obtained at 360 °C (*n*-alkanes/(iso-alkanes + cycloalkanes)—65/31 wt.%) decreased from 19 to −11 °C when the reaction temperature was increased to 420 °C (*n*-alkanes/(iso-alkanes + cycloalkanes)—20/74 wt.%; Šimáček et al., 2011). At the same time, the distillation curve remained within the EN 590 specification requirements and the cetane index dropped from 91 at 360 °C to 65 at 420 °C which is well above the requirements for diesel fuel (>46 units; Šimáček et al., 2011).

When the products obtained at 420 °C were blended in conventional diesel fuel in concentrations in the range of 10–50 wt.%, the CFPP values were in the range of −15 to −12 °C. As a result of commercial flow improvers (Infineum R-288 and Infineum R-291), the CFPP dropped below −20 °C and there were no differences between neat diesel fuel and diesel fuel blends containing product of sunflower oil hydrocracking. The results indicate that the sensitivity of these diesel fuel blends depends on the total content of long-chain *n*-alkanes (>C_{17}); when it exceeds a certain concentration, the commercial flow improvers become ineffective. On the basis of the results reported by Šimáček et al. (2011), this threshold can be estimated to be around 6–7 wt.% of long-chain *n*-alkanes (>C_{17}) in the final diesel fuel blend.

8. CONCLUSION

While deoxygenation of VOs is a new technology to the refining industry, it can build on the experiences gathered during operation of hydrotreating (HDS) units. Analysis of the thermodynamic, hydrodynamic, and kinetics aspects points out the differences between HDS and deoxygenation technologies that have to be taken into account when developing further deoxygenation technology. The successful examples from both stand-alone as well as coprocessing technologies demonstrate that the technology has a future in the portfolio of refining technologies.

The future development should be focused on two particular directions: further catalyst development and utilization of more sustainable feedstocks. From the point of view of catalyst development, it would be certainly beneficial if more selective catalysts, for example, decarboxylation catalysts, found their application in the stand-alone units limiting, thus, the need for catalyst sulphiding. Moreover, the industry would certainly benefit from catalysts facilitating both deoxygenation and isomerization in one step (reactor). From the point of view of feedstock, the technology has to be focused on nonfood sources of triglycerides that are produced in a sustainable way. Moreover, the need for their preprocessing (purification) should be minimized as this would result in a more cost-effective production, which is a key to avoiding too large dependence on legislation and subsidies.

ACKNOWLEDGMENTS

This publication was created in connection with the project "Unipetrol research and education center" Reg. No. CZ.1.05/2.1.00/03.0071, which is funded through the Operational Program for Research and Innovation Development of the Structural Funds (specifically the European Regional Development Fund) and the state budget of the Czech Republic.

REFERENCES

Andersson K, Hell M, Löwendahl L, Schöön NHJ: Diffusivities of hydrogen and glyceryl trioleate in cottonseed oil at elevated temperature, *J Am Oil Chem Soc* 51:171, 1974.
AspenTech, aspenONE V7.3, Process Engineering Products, 2011.
Bern L, Hell M, Schöön NH: Kinetics of hydrogenation of rapeseed oil: I. Influence of transport steps in kinetic study, *J Am Chem Oil Soc* 52:182, 1975.

Bezergianni S, Dimitriadis A, Kalogianni A, Pilavachi P: Hydrotreating of waste cooking oil for biodiesel production. Part I: Effect of temperature on product yields and heteroatom removal, *Bioresour Technol* 101:6651, 2010a.

Bezergianni S, Dimitriadis A, Sfetsas T, Kalogianni A: Hydrotreating of waste cooking oil for biodiesel production. Part II: effect of temperature on hydrocarbon composition, *Bioresour Technol* 101:7658, 2010b.

Cable TL, Massoth FE, Thomas MG: A basic study of catalyst aging in the H-coal process, *Fuel Process Technol* 10:105, 1985.

Cai HY, Shaw JM, Chung KH: Hydrogen solubility measurements in heavy oil and bitumen cuts, *Fuel* 80:1055, 2001.

Costa PR: Increasing biodiesel production, *PTQ-Biofuels* 2007:32, 2007.

da Rocha Filho GN, Brodzki D, Djega-Mariadassau G: Formation of alkanes, alkylcycloalkanes and alkylbenzenes during the catalytic hydrocracking of vegetable oils, *Fuel* 72:543, 1993.

Donnis B, Egeberg RG, Blom P, Knudsen KG: Hydroprocessing of bio-oils and oxygenates to hydrocarbons. Understanding the reaction routes, *Top Catal* 52:229, 2009.

Egeberg R, Knudsen K, Nystrom S, Grennfelt EL, Efraimsson K: Industrial-scale production of renewable diesel, *Petroleum Technol Q* Q3:59, 2011.

Fillion B, Morsi BI: Gas–liquid mass-transfer and hydrodynamic parameters in a soybean oil hydrogenation process under industrial conditions, *Ind Eng Chem Res* 39:2157, 2000.

Frey, S. 2011. Honeywell development of green jet fuel technology. IAE Bioenergy ExCo67 meeting, paper 08, Helsinki.

Furimsky E, Massoth FE: Deactivation of hydroprocessing catalysts, *Catal Today* 52:381, 1999.

Gabrielsen J, Egeberg RG, Knudsen KG: *Hydrotreating of triglycerides to make aviation fuels, Biomass 2011*, Maryland, 2011, National Harbor.

Green car congress, 2012. http://www.greencarcongress.com/2008/01/petrobras-h-bio.html. Accessed February.

Green car congress, 2012. http://www.greencarcongress.com/2008/08/albemarle-to-pr.html. Accessed February.

Hodge, C. 2006. California Energy Commission, Workshop on bioenergy. http://www.energy.ca.gov/bioenergy_action_plan/documents/2006-03-09_workshop/2006-03-09_NESTE_OIL.PDF. Accessed March 9.

Huber G, O'Connor P, Corma A: Processing biomass in conventional oil refineries: production of high quality diesel by hydrotreating vegetable oils in heavy vacuum oil mixtures, *Appl Catal A Gen* 329:120, 2007.

Immer J, Kelly M, Lamb H: Catalytic reaction pathways in liquid-phase deoxygenation of C18 free fatty acids, *Appl Catal A Gen* 375:134, 2010.

Kalnes TN, Marker T, Shonnard D, Koers KP: Green diesel production by hydrorefining renewable feestocks, *PTQ-Biofuels* 2008:7, 2008.

Kubička D: Future refining catalysis—introduction of biomass feedstocks, *Collect Czech Chem Commun* 73:1015, 2008.

Kubička D, Horáček J: Deactivation of HDS catalysts in deoxygenation of vegetable oils, *Appl Catal A Gen* 394:9, 2011.

Kubička D, Kaluža L: Deoxygenation of vegetable oils over sulfided Ni, Mo and NiMo catalysts, *Appl Catal A Gen* 372:199, 2010.

Kubička D, Šimáček P, Žilková N: Transformation of vegetable oils into hydrocarbons over mesoporous-alumina-supported CoMo catalysts, *Top Catal* 52:161, 2009.

Kubička D, Bejblová M, Vlk J: Conversion of vegetable oils into hydrocarbons over CoMo/MCM-41 catalysts, *Top Catal* 53:168, 2010.

Kubičková I, Kubička D: Utilization of triglycerides and related feedstocks for production of clean hydrocarbon fuels and petrochemicals: a review, *Waste Biomass Valor* 1:293, 2010.

Kubičková I, Kubička D: Heterogeneous catalysts for production of renewable fuels from triglycerides. In Kubičková I, Kubička D, editors: *Heterogeneous catalysis in biomass to chemicals and fuels*, Kerala, India, 2011, Research Signpost, 978-81-308-0462-0.

Kubičková I, Snåre M, Eränen K, Mäki-Arvela P, Murzin D: Hydrocarbons for diesel fuel via decarboxylation of vegetable oils, *Catal Today* 106:197, 2005.

Laurent E, Delmon B: Study of the hydrodeoxygenation of carbonyl, carboxylic and guaiacyl groups over sulfided CoMo/gamma-Al2O3 and NiMo/gamma-Al2O3 catalysts. I. Catalytic reaction schemes, *Appl Catal A Gen* 109:77, 1994a.

Laurent E, Delmon B: Influence of water in the deactivation of a sulfided NiMo gamma-Al2O3 catalyst during hydrodeoxygenation, *J Catal* 146:281, 1994b.

Laurent E, Delmon B: Study of the hydrodeoxygenation of carbonyl, carboxylic and guaiacyl groups over sulfided CoMo/gamma-Al2O3 and NiMo/gamma-Al2O3 catalyst. II. Influence of water, ammonia and hydrogen sulfide, *Appl Catal A Gen* 109:97, 1994c.

Lestari S, Simakova I, Tokarev A, Mäki-Arvela P, Eränen K, Murzin D: Synthesis of biodiesel via deoxygenation of stearic acid over supported Pd/C catalyst, *Catal Lett* 122:247, 2008.

Lestari S, Mäki-Arvela P, Beltramini J, Lu G, Murzin D: Transforming triglycerides and fatty acids into biofuels, *ChemSusChem* 2:1109, 2009.

Levenspiel O: Chemical reaction engineering, *Ind Eng Chem Res* 38:4140, 1999.

Lüft, M., Spicher, U. 2007. *Optimierung von Kraftstoffstrahlausbreitung für Pflanzenöl. insbesondere natürliches Rapsöl. bei der Verwendung moderner Diesel Einspritzsysteme. BWK 25002—Study,* Germany.

Macleod DB: On a relation between surface tension and density, *Trans Faraday Soc* 19:38, 1923.

Maier WF, Roth W, Thies I, Rague Schleyer PV: Hydrogenolysis, IV. Gas phase decarboxylation of carboxylic acids, *Chem Ber* 115:808, 1982.

Mary G, Chaouki J, Luck F: Trickle-bed laboratory reactors for kinetic studies, *Int J Chem Reactor Eng* 7 R2:1, 2009.

Melis S, Mayo S, Leliveld B: Vegetable oil co-processing in diesel hydrotreaters, *PTQ-Biofuels* 2009:43, 2009.

Mikulec J, Cvengroš J, Joríková L, Banič M, Kleinová A: Diesel production technology from renewable sources—second generation biofuels, *Chem Eng Trans* 18:475, 2009.

Murzin, D., Kubičková, I., Snåre, M., Mäki-Arvela, P., Myllyoja, J. 2006. Method for the manufacture of hydrocarbons, PCT International Application 2006/075057 A2, 2006.

Murzin, D.Y., Mäki-Arvela, P., Simakova, I.L. 2012. Triglycerides and oils for biofuels, Kirk-Othmer encyclopedia of chemical technology, Published Online: 13 January, 2012. http://dx.doi.org/10.1002/0471238961.trigmurz.a01.

Neste Oil, 2012. http://www.nesteoil.com/default.asp?path=1,41,11991,12243,13565. Accessed February, 2012.

Neste Oil, 2012. http://www.nesteoil.com/default.asp?path=1,41,11991,12243,15658. Accessed February, 2012.

Neste Oil, 2012. http://www.nesteoil.com/default.asp?path=1,41,11991,12243,15658,12139. Accessed February, 2012.

Neste Oil, 2012. http://www.nesteoil.com/default.asp?path=1,41,11991,12243,12335,14116. Accessed February, 2012.

Neste Oil, 2012. http://www.nesteoil.com/default.asp?path=1,41,11991,12243,17555. Accessed February, 2012.

Neste Oil, 2012. http://www.nesteoil.com/default.asp?path=1,41,11991,12243,12335. Accessed February, 2012.

Piqueras CM, Tonetto G, Bottini S, Damiani DE: Sunflower oil hydrogenation on Pt catalysts: comparison between conventional process and homogeneous phaseoperation using supercritical propane, *Catal Today* 133–135:836, 2008.

Priecel P, Kubička D, Čapek L, Bastl Z, Ryšánek P: The role of Ni species in the deoxygenation of rapeseed oil over NiMo-alumina catalysts, *Appl Catal A Gen* 397:127, 2011.

Reid R, Poling BE, Prausnitz JM: *The properties of gases and liquids,* ed 5, New York, 2001, McGraw-Hill Co., Inc.

Santacesaria E, Parrella P, Di Serio SNM, Borrelli M: Role of mass transfer and kinetics in the hydrogenation of rapeseed oil on a supported palladium catalyst, *Appl Catal A Gen* 116:269, 1994.

Schaub G, Vetter A: Biofuels for automobiles—an overview, *Chem Eng Technol* 31(5):721, 2008.

Schmidt A, Schomacker R: Partial hydrogenation of sunflower oil in a membrane reactor, *J Mol Catal A Chem* 271:192, 2007.

Sebos I, Matsoukas A, Apostolopoulos A, Papayannakos N: Catalytic hydroprocessing of cottonseed oil in petroleum diesel mixtures for production of renewable diesel, *Fuel* 88:145, 2009.

Šimáček P, Kubička D: Hydrocracking of petroleum vacuum distillate containing rapeseed oil: evaluation of diesel fuel, *Fuel* 89:1508, 2010.

Šimáček P, Kubička D, Šebor G, Pospíšil M: Fuel properties of hydroprocessed rapeseed oil, *Fuel* 89:611, 2010.

Šimáček P, Kubička D, Kubičková I, Homola F, Chudoba J, Pospíšil M: Premium quality renewable diesel fuel by hydroprocessing of sunflower oil, *Fuel* 90:2473, 2011.

Simakova I, Simakova O, Mäki-Arvela P, Simakov A, Estrada M, Murzin D: Deoxygenation of palmitic and stearic acid over supported Pd catalysts: Effect of metal dispersion, *Appl Catal A Gen* 355:100, 2009.

Smejkal Q, Smejkalová L, Kubička D: Thermodynamic balance in reaction system of total vegetable oil hydrogenation, *Chem Eng J* 146:155, 2009.

Snåre M, Kubičková I, Mäki-Arvela P, Eränen K, Murzin D: Heterogeneous catalytic deoxygenation of stearic acid for production of biodiesel, *Ind Eng Chem Res* 45:5708, 2006.

Snåre M, Kubičková I, Mäki-Arvela P, Chichova D, Eränen K, Murzin D: Catalytic deoxygenation of unsaturated renewable feedstocks for production of diesel fuel hydrocarbons, *Fuel* 87:933, 2008.

Tukač, V., Kubička, D., Horáček, J. 2012. Manuscript under preparation.

UOP, 2012. www.uop.com, UOP/ENI Ecofining Process.pdf. Accessed February, 2012.

World Fuels, 2012. http://www.worldfuels.com/wfExtract/exports/Content/e0daa202-f81c-4ff2-c5-ca0aba8.html. Accessed February, 2012.

Wu Y, Khadilkar MR, Al-Dahhan MH, Dudukovic´ MP: Comparison of upflow and downflow two-phase flow packed-bed reactors with and without fines: experimental observations, *Ind Eng Chem Res* 35:397, 1996.

Fuel 90 (2011) 2473–2479

Contents lists available at ScienceDirect

Fuel

journal homepage: www.elsevier.com/locate/fuel

Premium quality renewable diesel fuel by hydroprocessing of sunflower oil

Pavel Šimáček [a,*,1], David Kubička [b,2], Iva Kubičková [b,2], František Homola [b,2], Milan Pospíšil [a,1], Josef Chudoba [a,1]

[a] Institute of Chemical Technology, Prague, Department of Petroleum Technology and Alternative Fuels, Technická 5, 166 28 Prague 6, Czech Republic
[b] Research Institute of Inorganic Chemistry, Department of Refining and Petrochemical Research, 436 70 Litvínov – Záluží 1, Czech Republic

ARTICLE INFO

Article history:
Received 9 August 2010
Received in revised form 8 February 2011
Accepted 10 March 2011
Available online 6 April 2011

Keywords:
Hydroprocessing
Hydrodeoxygenation
Vegetable oil
Sunflower oil
Biodiesel

ABSTRACT

Hydroprocessing of neat sunflower oil was carried out at 360–420 °C and 18 MPa over a commercial hydrocracking catalyst in a bench scale fixed bed reactor. In the studied experimental range, products consisted exclusively of hydrocarbons that differed significantly in composition. While the concentration of *n*-alkanes exceeded 67 wt.% in the reaction products collected at 360 °C, it decreased to just 20 wt.% in the product obtained at 420 °C. Consequently, the fuel properties of the latter product were very similar to those of standard (petroleum-derived) diesel fuel. Particularly, it exhibited excellent low-temperature properties (cloud point −11 °C; CFPP −14 °C). Reaction products obtained at 400 and 420 °C were blended into petroleum-derived diesel fuel in three concentration levels ranging from 10 to 50 wt.% and the fuel properties of these mixtures were evaluated. Diesel fuel mixtures containing the product of sunflower oil hydrocracking at 420 °C showed very good low-temperature properties including cloud point (−8 °C) and CFPP (−15 °C) that was further lowered to −25 °C due to addition of flow improvers.

1. Introduction

Traditional biodiesel (fatty acid methyl esters – FAME) is produced from vegetable oils by homogeneously-catalyzed transesterification with methanol [1]. Even though FAME is suitable for blending with petroleum-derived diesel fuels, it suffers from some drawbacks, the main being low oxidation stability that limits (i) its long-term storage and (ii) the use of biodiesel–diesel blends containing more than 20–30 vol.% of FAME. Hydroprocessing of vegetable oils, i.e. their conversion into hydrocarbons resulting from their reaction with hydrogen at elevated temperature and pressure in the presence of heterogeneous catalysts, provides an alternative for diesel fuel production from renewable resources [2]. In contrast to FAME, hydrocarbons obtained by vegetable oil hydroprocessing are significantly more resistant to oxidation than FAME. Although the composition of products of vegetable oil hydroprocessing depends on several factors (reaction conditions, catalyst used), they can be in general characterized as low-aromatic sulfur-free hydrocarbon mixtures containing neither alkenes nor heteroatoms [2–9].

The fatty acids bound in vegetable oils have exclusively straight chains with an even number of carbon atoms. Consequently, their hydroprocessing yields *n*-alkanes as primary products. Two kinds of *n*-alkanes are formed: (i) *n*-alkanes that have the same carbon atom number or (ii) *n*-alkanes that have one carbon atom less than the original fatty acids present in vegetable oil [4,10–16]. Since fatty acids in natural vegetable oils have predominantly 18 carbon atoms in their chain, hydroprocessed vegetable oil often yields *n*-alkanes with high concentration of *n*-heptadecane and *n*-octadecane. The sum of these two hydrocarbons commonly reaches 70–90 wt.% [6–8]. These hydrocarbons have an excellent cetane rating, but their low-temperature properties are poor and prevent their direct use as a diesel fuel blending component in concentrations higher than 5–10%.

The subsequent reactions of primary hydrocarbon products, *n*-alkanes, lead to formation of other hydrocarbons: *i*-alkanes, cycloalkanes and aromatics. While the formation of aromatics is limited, several studies have demonstrated that with increasing reaction temperature the yield of *i*-alkanes increased significantly [6,17–20]. Higher reaction temperature favored also cracking reactions leading to the formation of light hydrocarbons in gasoline range [9] or even gases [14].

As mentioned above, the hydroprocessed vegetable oil has generally poor low-temperature properties. Cloud point and cold filter plugging point (CFPP) values of the products are usually higher than +20 °C [5,7,18]. Utilization of such fuel in moderate climate is impossible. It has been found that diesel fuel containing hydroprocessed rapeseed oil (5–30 wt.%) had significantly worse low-temperature properties than neat petroleum-derived diesel fuel. Moreover, the addition of flow improvers to these blends was inefficient, as it virtually did not affect their cold flow properties [7].

---

[*] Corresponding author. Tel.: +420 220 444 236; fax: +420 220 444 321.
E-mail addresses: pavel.simacek@vscht.cz (P. Šimáček), david.kubicka@vuanch.cz (D. Kubička).

[1] Tel.: +420 220 444 236; fax: +420 220 444 321.

[2] Tel.: +420 476 163 735; fax: +420 476 768 476.

0016-2361/$ - see front matter © 2011 Elsevier Ltd. All rights reserved.
doi:10.1016/j.fuel.2011.03.013

The low-temperature properties of hydroprocessed vegetable oil can be upgraded by subsequent catalytic isomerization of *n*-alkanes. Hancsók et al. [18] have isomerized hydroprocessed sunflower oil using Pt/HZSM-22/Al_2O_3 catalyst. While the original CFPP of hydroprocessed sunflower oil was +23 °C, it dropped down to −23 °C after isomerization. Isomerization of the primary hydrocarbon products allowed commercial utilization of hydroprocessed vegetable oil as a new kind of renewable diesel fuel. At present, Neste Oil uses its product called NExBTL [19] not only as a component for diesel fuel blending, but even as a premium 100% renewable diesel fuel under the name Neste Green 100 diesel [20].

This paper focuses on determination of the composition and physicochemical properties of hydroprocessed sunflower oil obtained at four temperature levels. In contrast to the recent work concerning rapeseed oil hydroprocessing [7], different type of catalyst and more severe reaction conditions have been used in an attempt to prepare a hydrocarbon-based product having more favorable low-temperature properties. The properties of fuel blends consisting of petroleum-derived diesel (50–90 wt.%) and 10–50 wt.% of two selected hydroprocessing products are reported as well.

2. Experimental

2.1. Hydroprocessing

Hydroprocessing of sunflower oil was carried out in a bench scale fixed bed reactor equipped with a salt bath heating system. Dimensions of the reactor were 900 mm (length) and 40 mm (inner diameter). A commercial hydrocracking catalyst consisting of supported metal sulfides was used in the experiments. The catalyst was activated prior to the experiments using refinery recycle gas, i.e. hydrogen gas containing H_2S, at 360 °C and 18 MPa. The catalyst bed consisted of 70 g of the catalyst and 100 ml of silicon carbide that was used for catalyst bed dilution to minimize the wall effects and feedstock channeling. All experiments were performed under the hydrogen pressure of 18 MPa. The reaction products were collected at four temperature levels: 360, 380, 400 and 420 °C. The temperature range was chosen to convert triacylglycerides exclusively to hydrocarbons and to minimize their overcracking to light products. Liquid feed flow (sunflower oil) and hydrogen flow was 49 g h^{-1} and 0.049 N m^3 h^{-1}, respectively. Food grade sunflower oil was used as raw material.

2.2. Analysis of products

Organic liquid products and water were separated after pressure reduction from gas stream in a low pressure separator. After liquid sample collection, the organic liquid product was separated from water formed due to deoxygenation of the sunflower oil, i.e. due to its hydrodeoxygenation or due to hydrogenation of CO_2 originating from sunflower oil (hydro)decarboxylation. The gaseous products and water were not further analyzed. The composition of the organic products was then determined using gas chromatography (GC) and high performance liquid chromatography (HPLC). Simulated distillation and a conventional GC method were used for determination of distillation range and *n*-alkane content in the products, respectively. The detailed description of both GC methods has been reported recently elsewhere [16]. The content of aromatic hydrocarbons was determined using a standard HPLC method designated for diesel fuels (European standard EN 12916). These measurements were performed using a chromatographic set Shimadzu consisting of a pump (LC-10A), a control module (CBM-10A), a refractometric detector (RID-10A) and an oven (CTO-10AC) equipped with the column Supelcosil LC-NH2-NP (25 cm × 4.6 mm i.d.; particle size 5 μm). The flow rate of the mobile phase (*n*-heptane) was 1 cm^3 min^{-1}. The concentration of the sum of *i*-alkanes and cycloalkanes was balanced to 100%. Physicochemical properties of the neat hydroprocessing products as well as the properties of all prepared fuel blends were determined using the standard test procedures designated for diesel fuels (as defined by the European standard EN 590) or petroleum products (standards EN 12634 and EN ISO 3016). The cold filter plugging point (CFPP) of the hydroprocessing product obtained at 420 °C was measured also after treatment using flow improvers Infineum R288 and Infineum R591 in the concentration range of 200–800 mg kg^{-1}.

2.3. Preparation of fuel blends

The hydroprocessing products obtained at 400 and 420 °C were used for preparation of their fuel blends with petroleum-derived diesel fuel. FAME- and additive-free diesel was prepared in the laboratory by blending hydrotreated gas oil and kerosene in a weight ratio of 65:35. Low-temperature properties of the resulting diesel fuel corresponded to those of a commercial diesel fuel before the final addition of additives. The prepared petroleum-derived diesel was then blended with the hydroprocessing products in order to prepare six blends containing 10, 30 and 50 wt.% of the product obtained at 400 and 420 °C, respectively. The properties of these fuel blends were evaluated as a commercial diesel fuel according to the European standard EN 590. Finally, the fuel blends were separately treated with flow improvers Infineum R288 and Infineum R591 in the concentration range of 100–400 mg kg^{-1} to evaluate the efficiency of these flow improvers.

3. Results and discussion

3.1. Composition of reaction products

The chromatographic fingerprints of all products obtained by hydroprocessing of sunflower oil are presented in Fig. 1. There were not detected any oxygenated intermediates (such as fatty acids or fatty esters) in the reaction products. This observation is in agreement with previous findings [7]. Moreover, the absence of free fatty acids was indirectly confirmed by the low values of acid number of all products (see below). All products of sunflower oil hydroprocessing can be thus considered as neat hydrocarbon mixtures. It can be also clearly seen that the content of *n*-alkanes in the products decreased with the increasing reaction temperature (Fig. 1 and Table 1). Besides isomerization and cyclization, the higher reaction temperature also resulted in higher yields of lower hydrocarbons due to the more intensive cracking of the primary hydrocarbon products (mainly C_{15}–C_{18} *n*-alkanes). Two primary products of hydroprocessing, *n*-heptadecane and *n*-octadecane, represented more than 50 wt.% of the product obtained at 360 °C (Table 1). The increase of the reaction temperature by 20 °C caused a relative decrease of their concentration in the hydroprocessing products by more than 50%. Consequently, the product obtained at 420 °C contained only 2.8 and 1.8 wt.% of *n*-heptadecane and *n*-octadecane, respectively (Table 1). The total concentration of *n*-alkanes in this product is fully comparable with the content of *n*-alkanes in petroleum-derived diesel used for preparation of the fuels blends (see Table 1). On the other hand, the content of other saturated hydrocarbons (*i*-alkanes and cycloalkanes) increased with the increasing reaction temperature. The yield of aromatics increased also with the increasing reaction temperature as a result of the enhanced rate of the cyclization reactions. The dehydrogenation reactions proceeded in spite of the high hydrogen pressure (18 MPa). While the content of aromatics in the hydroprocessing

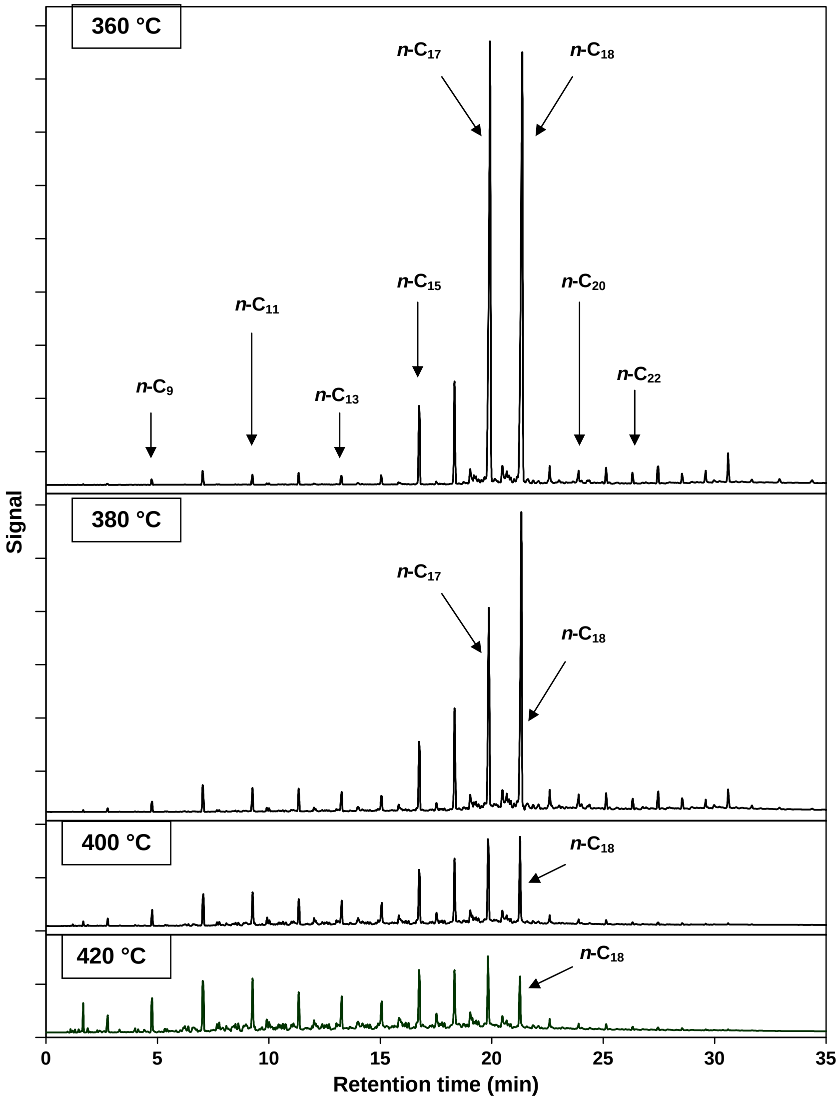

Fig. 1. The gas chromatograms of the sunflower oil hydroprocessing products obtained at various reaction temperatures (the chromatograms are presented in the same scale).

Table 1
The composition (wt.%) of the sunflower oil hydroprocessing products obtained at various reaction temperatures.

Component	Reaction conditions				Petroleum-derived diesel
	360 °C	380 °C	400 °C	420 °C	
n-alkanes < n-C$_{15}$	2.0	4.6	9.1	9.8	11.7
n-C$_{15}$	3.2	3.1	3.6	2.4	1.8
n-C$_{16}$	3.5	4.0	3.7	2.1	1.5
n-C$_{17}$	**24.7**	**10.0**	**5.7**	**2.8**	**1.4**
n-C$_{18}$	**26.5**	**13.7**	**5.1**	**1.8**	**1.1**
n-C$_{19}$	0.5	0.5	0.4	0.3	1.0
n-C$_{20}$	0.5	0.5	0.3	0.2	0.7
n-C$_{20}$ to n-C$_{33}$	3.9	3.6	0.8	0.6	1.4
Total *n*-alkanes	**64.7**	**40.0**	**28.7**	**19.8**	**20.6**
Total aromatics	0.1	0.5	2.0	5.2	19.1
i-alkanes + cycloalkanes	31.2	50.5	63.3	73.5	60.3
Other hydrocarbons[a]	4.0	9.0	6.0	1.5	0.0

[a] Not specified hydrocarbons of heavy fraction (boiling point > 470 °C).

product obtained at 360 °C was negligible, the product obtained at 380 °C contained 0.5 wt.% of aromatics. The concentration of aromatics in the products obtained at 400 and 420 °C was more than three and ten times higher, respectively (Table 1). Monoaromatics formed more than 90% of all aromatic hydrocarbons in all hydroprocessing products. The distribution of aromatic hydrocarbons among mono-, di- and polyaromatics in the products of sunflower oil hydroprocessing is illustrated in Fig. 2.

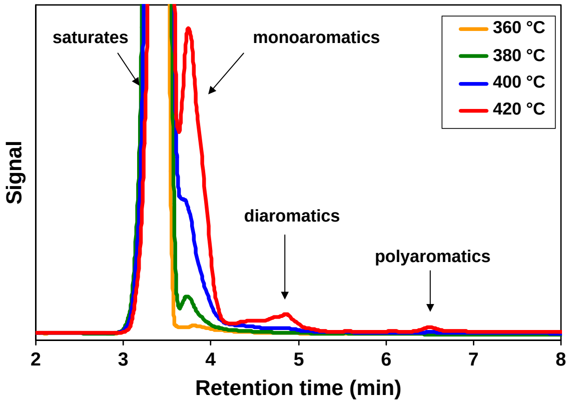

Fig. 2. The HPLC chromatograms of the sunflower oil hydroprocessing products obtained at various reaction temperatures.

3.2. Fuel properties of neat hydroprocessing products

The profiles of the distillation curves of the neat hydroprocessing products were strongly influenced by the reaction temperature of the sunflower oil hydroprocessing (Fig. 3a). The product obtained at 360 °C had a very flat distillation curve owing to the presence of only a few chemical individuals (mainly C_{17} and C_{18} hydrocarbons). As the reaction temperature rose, the distillation curves of the respective products had a more uniform distribution. The distillation curve of the product obtained at 420 °C was already very similar to the distillation curve of a common petroleum-derived diesel. Unfortunately, some products contained a relatively large amount of heavier fractions. The worst in this respect was the product obtained at 380 °C having only 87 vol.% recovered at the final boiling point. The presence of the heavy fractions was confirmed by the simulated distillation (Fig. 3b), but no additional analysis was performed for their closer identification. Since the products did not contain any triacylglycerides (as confirmed by the simulated distillation), the heavy fractions were most probably formed as a result of the condensation and oligomerization reactions. It is plausible to assume that oligomerization can occur owing to the high degree of unsaturation of sunflower oil (more than four double bonds per an average molecule of triglyceride), catalyst acidity and the high reaction temperature. In fact, the high degree of unsaturation has previously been reported to cause an increased formation of aromatics [4].

All hydroprocessing products had a lower density than the standard diesel fuel (Table 2), which was caused by the low concentration of aromatics and the high concentration of alkanes (Table 1). The relatively high viscosity of the hydroprocessing products obtained at reaction temperatures lower than 420 °C was attributed to the high concentration of *n*-alkanes and the low concentration of low-boiling fractions. Moreover, the high viscosity of the product obtained at 380 °C can be also connected with the higher concentration of the heavy fractions. On the other hand, the viscosity of the product obtained at 420 °C (2.65 mm^2 s^{-1}) was fully comparable with the viscosity of a standard diesel fuel. The flash point of the hydroprocessing products naturally decreased with the increasing content of the light fractions and thus with the increasing reaction temperature. The flash point of the product obtained at 420 °C was even lower than the lower limit specified for diesel fuel. The value 49 °C is, however, still acceptable for diesel fuel blending. Although the cetane index of the products decreased with the increasing reaction temperature significantly (Table 2), the lowest achieved value, 65 units, is still excellent. Similar values of the cetane number can be expected. The very low values of the acid number indicate that the products did not contain any free fatty acids (the reaction intermediates).

The low-temperature properties (cloud point, CFPP and pour point) of the products obtained at 360 and 380 °C were poor. All these parameters had higher values than +10 °C. The cloud point of the product obtained at 400 °C was still rather high (+8 °C), but the CFPP was already much more favorable (−5 °C). On the other hand, the product obtained at 420 °C showed excellent values of the cloud point (−11 °C) and CFPP (−14 °C). This product thus overcomes the main disadvantage of hydroprocessed vegetable oils – the unacceptable low-temperature properties. While the cloud point and the CFPP of the hydroprocessing product obtained at 420° C were comparable with a standard winter diesel fuel (for the temperate climate) before addition of flow improvers, the other qualitative parameters, particularly the concentration of aromatics and cetane rating, were superior to those of any standard diesel fuel. Unfortunately, the neat hydroprocessing product was less sensitive to the addition of flow improvers (Fig. 4) than the standard diesel fuel. The CFPP of the hydroprocessing product dropped from the original −14 °C to −20 °C for an additive concentration of 400 mg kg^{-1}. A further increase in the concentration of the additive did not improve the cold flow properties any more.

3.3. Fuel blends

The products obtained by hydroprocessing of sunflower oil at 400 and 420 °C, respectively (P400 and P420, respectively), were chosen for blending with petroleum-derived diesel fuel. The distillation curves of all six blends are presented in Fig. 5. With the increasing concentration of the hydroprocessing products in

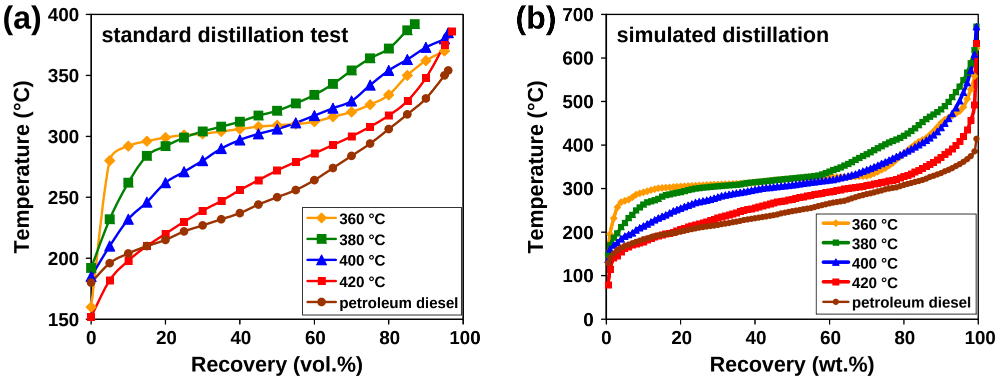

Fig. 3. The distillation curves of the products of sunflower oil hydroprocessing obtained at various reaction temperatures – (a) standard distillation test and (b) simulated distillation test.

Table 2
The physicochemical properties of the products obtained at various reaction temperatures.

Parameter	Reaction conditions				EN 590 (temperate climate)
	360 °C	380 °C	400 °C	420 °C	
Density at 15 °C (kg m^{-3})	799.5[a]	814.5[a]	813.7	805.8	820–845
Kin. viscosity at 40 °C (mm^2 s^{-1})	4.92	6.06	4.51	2.65	2.00–4.50
Distillation					
at 250 °C recovered (vol.%)	3	7	16	32	<65
at 350 °C recovered (vol.%)	85	63	78	91	>85
95 vol.% recovered at (°C)	370	–	380	375	<360
Flash point in closed cup (°C)	>100	99	78	49	>55
Cetane index	91	78	72	65	>46
Sulfur (mg kg^{-1})	20	8	9	10	<10
Nitrogen (mg kg^{-1})	5	3	2	7	–
Water (mg kg^{-1})	56	50	46	30	<200
Acid number (mg KOH g^{-1})	0.02	0.03	0.03	0.03	–
Low-temperature properties					
Cloud point (°C)	19	18	8	−11	<−8[b]
CFPP (°C)	>15	11	−5	−14	[c]
Pour point (°C)	17	11	−7	−18	–

[a] Heterogeneous nature of the samples did not allow to measure their standard density at 15 °C. Density at 15 °C was calculated from the density at 40 °C at which the liquid samples were homogenous.
[b] Grade F diesel.
[c] Maximum values for grades A, B, C, D, E and F are +5, 0, −5, −10, −15 and −20 °C resp.

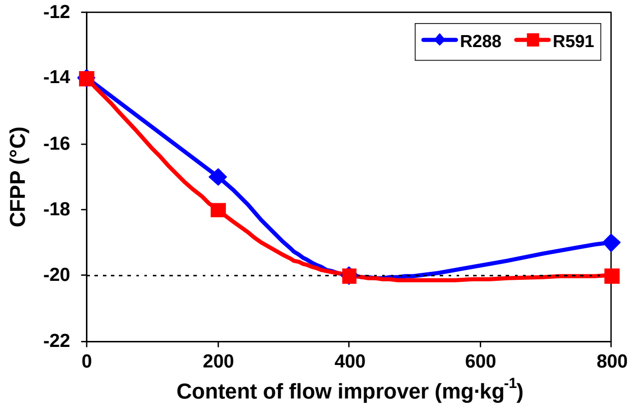

Fig. 4. The cold filter plugging point (CFPP) values of the hydroprocessing product obtained at 420 °C treated with flow improvers Infineum R288 and Infineum R591, respectively.

the blends the distillation curves of the blends shifted toward higher boiling points in all cases, however the differences between the curves of the blends containing the product P420 were very small. It means that the distillation characteristics of the product P420 were very close to those of the petroleum-derived diesel fuel. The fuel blend containing 50 wt.% of the product P420 showed a little higher distillation parameter T95 (367 °C). A deviation of this parameter was observed also for the blends containing 30 and 50 wt.%. of the product P400. This was a consequence of the higher concentration of the heavier products that originated plausibly from the oligomerization reactions. From an industrial refinery point of view, it is not a significant problem since the initial and final boiling points are commonly adjusted by distillation. All the other distillation parameters were in line with the EN 590 standard requirements (Table 3).

The other monitored fuel properties of all fuel blends were favorable (Table 3) in comparison with the standard diesel fuel. The observed deviations in the density did not play an important role. The flash point of the blend containing 50 wt.% of the product P420 was relatively low (57 °C), however, it still fulfilled the specified requirements. All fuel blends had a higher cetane index in comparison with the neat petroleum-derived diesel fuel. The increase in the cetane index was approximately 3–10 units for the blends containing the product P400 and 1–7 units for the blends containing the product P420.

The presence of the hydroprocessing products in the fuel blends affected their low-temperature properties differently (see Table 3). The cloud point increased from −8 °C (the neat petroleum-derived

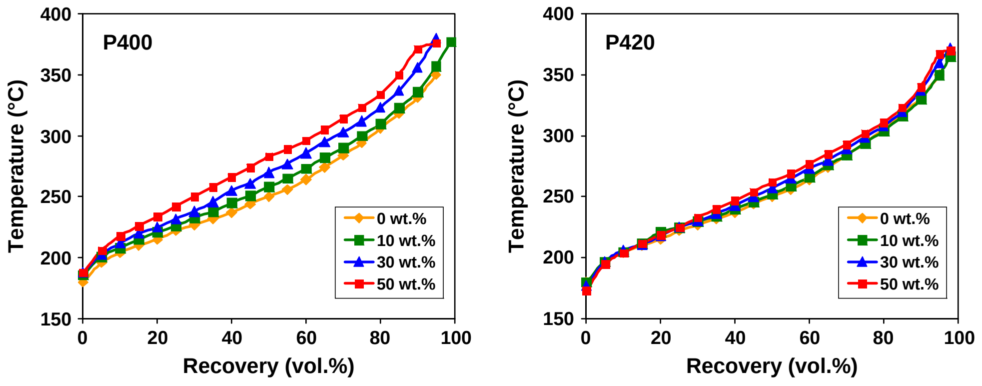

Fig. 5. The distillation curves of the fuel blends containing various amounts of the product P400 and P420 respectively (products of sunflower oil hydroprocessing at 400 and 420 °C, respectively).

Table 3
The physicochemical properties of the fuel blends containing various amounts of the products P400 and P420 respectively (products of sunflower oil hydroprocessing at 400 and 420 °C, respectively).

Parameter	Content of the product (wt.%)							EN 590 (temperate climate)
	0	Product obtained at 400 °C			Product obtained at 420 °C			
		10	30	50	10	30	50	
Density at 15 °C (kg m^{-3})	825.0	823.8	821.5	819.1	823.1	819.3	815.1	820–845
Kin. viscosity at 40 °C (mm^2 s^{-1})	2.32	2.47	2.81	3.21	2.35	2.41	2.47	2.00–4.50
Distillation								
at 250 °C recovered (vol.%)	50	44	37	30	49	45	42	<65
at 350 °C recovered (vol.%)	95	93	88	85	95	93	92	>85
95 vol.% recovered at (°C)	350	357	370	380	350	360	367	<360
Flash point in closed cup (°C)	69	68	71	72	66	60	57	>55
Cetane index	52.5	55.0	58.4	62.3	53.8	56.4	59.2	>46
Sulfur (mg kg^{-1})	65	59	48	37	60	49	38	<10
Nitrogen (mg kg^{-1})	16	15	12	9	15	13	12	–
Water (mg kg^{-1})	14	17	24	30	16	19	22	<200
Low-temperature properties								
Cloud point (°C)	−8	−4	3	4	−8	−8	−8	<−8[a]
CFPP (°C)	−12	−16	−14	−10	−12	−14	−15	[b]
Pour point (°C)	−25	−12	−9	−7	−22	−19	−19	–

[a] Grade F diesel.

[b] Maximum values for grades A, B, C, D, E and F is +5, 0, −5, −10, −15 and −20 °C resp.

diesel fuel) up to +4 °C for the blend containing 50 wt.% of the product P400. A similarly significant increase in the pour point was also observed. However, the differences in the CFPP values of the above-mentioned samples were not so significant. The CFPP values of the blends containing 10 and 30 wt.% of the product P400 were even lower than the CFPP values of the neat petroleum-derived diesel fuel. In contrast, the cloud point of all fuel blends containing the product P420 was the same as the cloud point of the neat petroleum-derived diesel fuel (−8 °C) and the pour point of these blends did not virtually change either. On the other hand, the CFPP values decreased slightly with the increasing concentration of the product P420 in the fuel blends. In general, the low-temperature properties of all six fuel blends corresponded to the diesel fuel grade D or E (according to EN 590).

In addition to the evaluation of the fuel blends without additives, the performance of two different flow improvers (Infineum R288 and Infineum R2591) was investigated as well. The results of the CFPP measurements of three fuel blends containing the product P400 are presented in Fig. 6. Both additives improved the CFPP values of the blend containing 10 wt.% of the product P400. The initial decrease in the CFPP was smaller than that observed for neat petroleum-derived diesel fuel, but it was possible to reach values lower than −20 °C. However, while both additives were slightly efficient as the cloud point depressants in this case (decrease by 2 °C), the final cloud point did not drop below −6 °C. On the other hand, the efficiency of both flow improvers in the fuel blends containing more than 10 wt.% of the product P400 was negligible.

The results of the CFPP measurements of three fuel blends containing the product P420 are presented in Fig. 7. The CFPP values of all blends dropped to −20 °C or lower for the additive concentration equal to 100 mg kg^{-1}. The flow improver Infineum 288 showed a better efficiency for the blends with a high concentration of the product P420 (30 and 50 wt.%) than for the neat petroleum-derived diesel fuel and the blend containing only 10 wt.% of P420. The CFPP of the two last mentioned fuels did not improve after addition of another 100 mg kg^{-1}. All other blends had the CFPP values −23 or −24 °C after addition of either of the tested flow improvers in a concentration of 200 mg kg^{-1}. The flow improver Infineum 591 showed a comparable efficiency for each of the tested fuels including the neat petroleum-derived diesel fuel and the blend containing 10 wt.% of the product P420. The measurements of the low-temperature properties thus proved that all investigated fuel blends could be labeled as F-grade diesel fuels after the addition of a suitable flow improver. The results also demonstrated that when the nature of the hydroprocessing

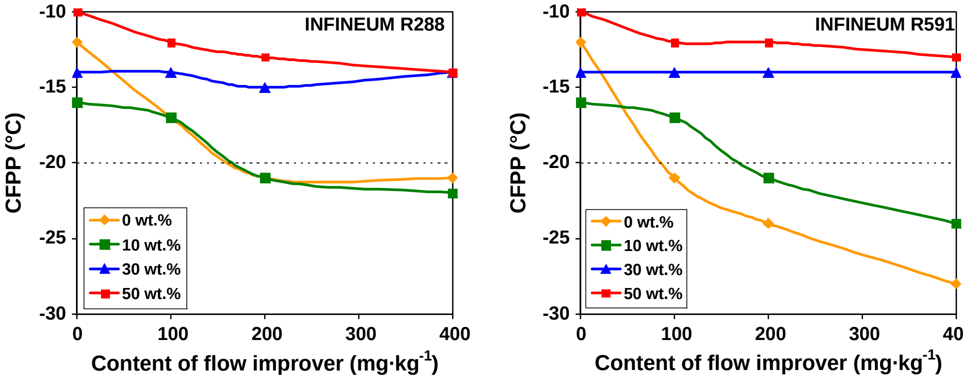

Fig. 6. The cold filter plugging point (CFPP) values of the diesel fuels containing various amounts of the product P400 (product of sunflower oil hydroprocessing at 400 °C) treated with the flow improver Infineum R288 and Infineum R591, respectively.

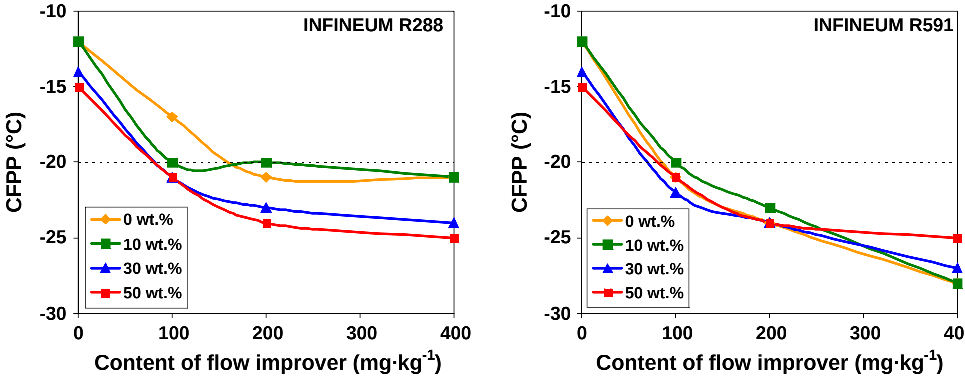

Fig. 7. The cold filter plugging point (CFPP) values of the diesel fuels containing various amounts of the product P420 (product of sunflower oil hydroprocessing at 420 °C) treated with the flow improver Infineum R288 and Infineum R591, respectively.

products changed from *n*-alkanes to *i*-alkanes and cycloalkanes, the efficiency of the flow improvers increased significantly.

4. Conclusions

Hydroprocessing of sunflower oil in the temperature range 360–420 °C yielded hydrocarbon mixtures containing saturated hydrocarbons with a low concentration of aromatics. The composition of the products was strongly influenced by the reaction temperature. The concentration of the primary hydrocarbon products of sunflower oil hydroprocessing, *n*-alkanes C_{17} and C_{18}, decreased from 53 to 5 wt.%, when the reaction temperature was increased from 360 °C to 420 °C. While the concentration of aromatics in the product obtained at 360 °C was negligible, the product of hydroprocessing at 420 °C contained more than 5 wt.% of aromatic hydrocarbons.

The distillation characteristics and physicochemical properties of the product obtained at 420 °C were very close to those of a standard neat petroleum-derived diesel fuel. The product showed also excellent low-temperature properties (cloud point −11 °C; CFPP −14 °C) that were further improved by applying flow improvers (CFPP down to−20 °C). It should be emphasized that the superior low-temperature properties were reached without any separate isomerization process. Moreover, the cetane index of this “biodiesel” was still very high – 65 units.

The diesel fuel blends containing from 10 to 50 wt.% of the product of sunflower oil hydroprocessing at 420 °C met the diesel fuel specifications. Most importantly, all fuel blends met the winter diesel specification for grade F after treatment by flow improvers. The product obtained at 420 °C can thus be considered as an excellent bio-component for the diesel fuel blending.

Acknowledgements

This work was supported by the Ministry of Education, Youth and Sports of the Czech Republic under the agreement No. MSM 6046137304 and by the Ministry of Industry and Trade of the Czech Republic (Project FT-TA4/066).

References

[1] Ma F, Hanna MA. Biodiesel production: a review. Bioresour Technol 1999;70:1–15.
[2] Kubičková I, Kubička D. Utilization of triglycerides and related feedstocks for production of clean hydrocarbon fuels and petrochemicals – a review. Waste Biomass Valor 2010;1:293–308.
[3] Gusmao J, Brodzki D, Djéga-Mariadassou G, Frety R. Utilization of vegetable oils as an alternative source for diesel-type fuel: hydrocracking on reduced Ni/SiO_2 and sulphided Ni-Mo/γ-Al_2O_3. Catal Today 1989;5:533–44.
[4] da Rocha Filho GN, Brodzki D, Djéga-Mariadassou G. Formation of alkanes alkylcykloalkanes and alkylbenzenes during the catalytic hydrocracking of vegetable oils. Fuel 1993;72:543–9.
[5] Stumborg M, Wong A, Hogan E. Hydroprocessed vegetable oils for diesel fuel improvement. Bioresour Technol 1996;56:13–8.
[6] Šimáček P, Kubička D, Šebor G, Pospíšil M. Hydroprocessed rapeseed oil as a source of hydrocarbon-based biodiesel. Fuel 2009;88:456–60.
[7] Šimáček P, Kubička D, Šebor G, Pospíšil M. Fuel properties of hydroprocessed rapeseed oil. Fuel 2010;89:611–5.
[8] Mikulec J, Cvengroš J, Joríková Ľ, Banič M, Kleinová A. Second generation diesel fuel from renewable resources. J Clean Prod 2010;18:917–26.
[9] Bezergianni S, Dimitriadis A, Kalogianni A, Pilavachi PA. Hydrotreating of waste cooking oil for biodiesel production. Part I: effect of temperature on product yields and heteroatom removal. Bioresour Technol 2010;101:6651–6.
[10] Kubička D, Šimáček P, Žilková N. Transformation of vegetable oils into hydrocarbons over organized-mesoporous-alumina-supported CoMo catalysts. Top Catal 2009;52:161–8.
[11] Kubička D. Future refining catalysis – introduction of biomass feedstocks. Collect Czech Chem Commun 2008;73:1015–44.
[12] Laurent E, Delmon B. Study of the hydrodeoxygenation of carbonyl, carboxylic and guaiacyl groups over sulfided CoMo/γ-Al_20_3 and NiMo/γ-Al_20_3 catalysts. I. Catalytic reaction schemes. Appl Catal 1994;109:77–96.
[13] Kubička D, Kaluža L. Deoxygenation of vegetable oils over sulfided Ni, Mo and NiMo catalysts. Appl Catal A-Gen 2010;372:199–208.
[14] Kubička D, Bejblová M, Vlk J. Conversion of vegetable oils into hydrocarbons over CoMo/MCM-41 catalysts. Top Catal 2010;53:168–78.
[15] Huber GW, O'Connor P, Corma A. Processing biomass in conventional oil refineries: production of high quality diesel by hydrotreating vegetable oils in heavy vacuum oil mixtures. Appl Catal A-Gen 2007;329:120–9.
[16] Šimáček P, Kubička D. Hydrocracking of petroleum vacuum distillate containing rapeseed oil: evaluation of diesel fuel. Fuel 2010;89:1508–13.
[17] Bezergianni S, Dimitriadis A, Sfetsas T, Kalogianni A. Hydrotreating of waste cooking oil for biodiesel production. Part II: effect of temperature on hydrocarbon composition. Bioresour Technol 2010;101:7658–60.
[18] Hancsók J, Krár M, Magyar S, Boda L, Holló A, Kalló D. Investigation of the production of high cetane number bio gas oil from pre-hydrogenated vegetable oils over Pt/HZSM-22/Al_2O_3. Micropor Mesopor Mater 2007;101:148–52.
[19] Neste oil cleans up in biofuels. Focus Catal 2006;7:6.
[20] Neste oil. <http://www.nesteoil.com> [access year 2010].

Fuel 89 (2010) 1508–1513

Contents lists available at ScienceDirect

Fuel

journal homepage: www.elsevier.com/locate/fuel

Hydrocracking of petroleum vacuum distillate containing rapeseed oil: Evaluation of diesel fuel

Pavel Šimáček [a,1], David Kubička [b,*]

[a] Institute of Chemical Technology Prague, Department of Petroleum Technology and Alternative Fuels, Technická 5, 166 28 Prague 6, Czech Republic
[b] Research Institute of Inorganic Chemistry, Department of Refining and Petrochemical Research, 436 70 Litvínov – Záluží 1, Czech Republic

ARTICLE INFO

Article history:
Received 19 August 2009
Received in revised form 23 September 2009
Accepted 24 September 2009
Available online 27 October 2009

Keywords:
Hydrocracking
Rapeseed oil
Biodiesel

ABSTRACT

Hydrocracking of pure petroleum vacuum distillate and the same fraction containing 5 wt.% of rapeseed oil was carried out at 400 and 420 °C and under a hydrogen pressure of 18 MPa over commercial Ni–Mo catalyst. Reaction products were separated by distillation into kerosene, gas oil and the residue. Fuel properties of fractions suitable for diesel production were evaluated (gas oils and remixed blends of kerosene and gas oil). Gas oils obtained from co-processing showed very good fuel properties as the remixed distillates did. Gas oil obtained from co-processing at 420 °C showed also reasonable key low-temperature properties (cloud point: −23 °C, CFPP: −24 °C) similar to those of gas oil obtained from pure petroleum raw material processing.

1. Introduction

Transformation of vegetable oils into hydrocarbons via hydroprocessing is a promising way for production of renewable hydrocarbons. They can be used either for production of oxygen-free biodiesel or as a raw material for petrochemistry [1]. The composition of hydroprocessed vegetable oil depends on reaction conditions and the catalyst used. Hydroprocessing of vegetable oils is usually carried out in the temperature range of 300–400 °C and under the hydrogen pressure of 6–20 MPa [2–7]. Traditional hydrogenation catalysts of the type Ni/Al_2O_3, $Ni–Mo/Al_2O_3$, $Co–Mo/Al_2O_3$ or Ni/SiO_2 are used [2,3,6,9] for vegetable oil hydroprocessing, but other types of catalysts have been also proposed [4,5]. The product generally contains acyclic saturated hydrocarbons having most often 15–18 carbon atoms in the molecule. The content of cycloalkanes is usually not significant and the content of aromatic hydrocarbons is generally negligible. It is common that the product contains large amount of C_{17} and C_{18} *n*-alkanes having excellent cetane number. Thanks to that, such product is to be called as super cetane diesel [9]. On the other hand, poor low-temperature properties limit its utilization as a diesel fuel.

There are several ways how to improve low-temperature properties of hydroprocessed vegetable oil. It seems that routine treating with ordinary flow-improvers is ineffective [10]. Another option is a two-stage upgrading. The first stage includes hydroprocessing of vegetable oil into *n*-alkane-rich hydrocarbon mixture. The mixture is subsequently isomerized to increase the concentration of *i*-alkanes in the second stage. Hancsók et al. [11] carried out hydroprocessing of sunflower oil over conventional hydrotreating catalyst. Obtained hydrocarbon mixture contained about 90% of *n*-octadecane. CFPP of the product was +23 °C. This product was isomerized over $Pt/HZSM-22/Al_2O_3$ catalyst at temperatures 280–370 °C and under the pressure of 3.5–8 MPa. Optimized final product of this two-stage processing contained <30% of *n*-alkanes. The product kept its excellent cetane number (>80) and had very favourable low-temperature properties (CFPP < −15 °C). Two-stage production of hydrocarbon-based biodiesel has been already commercialized. Finnish company Neste Oil produces such biodiesel under the commercial name NExBTL [12–14].

Beside separate hydroprocessing of vegetable oil in order to produce diesel-range hydrocarbons, there is an option of vegetable oil co-processing with petroleum-derived raw materials. This solution allows utilization of existing refinery technologies and equipment. On the other hand, the optimization of mixed feed processing can be difficult. Sebos et al. [15] hydroprocessed desulphurized (S < 50 ppm) mineral diesel containing 10 wt.% of cottonseed oil. Hydroprocessing was carried out over a commercial $CoMo/Al_2O_3$ and under common hydrotreating conditions (305–355 °C, 3 MPa). The feed was artificially sulphurized by adding DMDS. The obtained product containing renewable diesel had a benefit of +3 cetane units compared to the pure mineral diesel used as a matrix. The cloud point of the product was the same as cloud point of the summer-type diesel matrix (0 °C).

---

[*] Corresponding author. Tel.: +420 476 163 735; fax: +420 476 768 476.
E-mail addresses: pavel.simacek@vscht.cz (P. Šimáček), david.kubicka@vuanch.cz (D. Kubička).
[1] Tel.: +420 220 444 236; fax: +420 220 444 321.

0016-2361/$ - see front matter © 2009 Elsevier Ltd. All rights reserved.
doi:10.1016/j.fuel.2009.09.029

Huber et al. [16] studied hydroprocessing of sunflower oil and heavy vacuum oil–sunflower oil mixtures (5–50 wt.% of sunflower oil) over a wide range of reaction temperatures (300–450 °C). Their experiments were carried out over a $NiMo/Al_2O_3$ and under the pressure of 5 MPa. The total conversion of sunflower oil into hydrocarbons was observed at a reaction temperature of 350 °C and above, at which no acidity was detected. Thanks to the wide range of reaction temperatures general trends of increasing *n*-alkane isomerization and cracking at higher reaction temperatures were well illustrated as was the increasing decarbonylation/decarboxylation selectivity. It was found, that desulfurization of petroleum-derived feed component is significantly slower than hydrocarbon formation from vegetable oil. However, mixing the sunflower oil with petroleum-derived feed did not decrease the rate of desulfurization. Co-processing vegetable oil with conventional petroleum fractions on an industrial scale has been reported by Petrobras. The process is known under the name H-Bio [17,18].

Refinery hydroprocessing technologies, thus, seem to be applicable for co-processing of petroleum-derived feeds with vegetable oils. The vegetable oil component increases firstly the yield of diesel fuel. Hydrocracking technologies may be more suitable due to more severe reaction conditions (firstly higher reaction temperature) that help producing diesel fuel with better low-temperature properties. The scope of the present work is evaluation of fuel properties of diesel obtained by hydrocracking of vacuum distillate containing 5 wt.% of rapeseed oil.

2. Experimental

2.1. Raw materials

Straight-run vacuum distillate obtained from a petroleum refinery was used as a raw material for hydrocracking experiments. Distillation characteristics together with some other parameters are presented in Fig. 1. Pure vacuum distillate was used as a feed for comparison purposes and for preparation of rapeseed oil/vacuum distillate mixture. The mixture used as a feed contained 95 wt.% of vacuum distillate and 5 wt.% of rapeseed oil (food grade, Brokelmann & Co. GmbH, Germany). It contained ~90 wt.% of unsaturated C_{18} fatty acids chains, 5 wt.% of palmitic acid chains and 5 wt.% of other acids chains (detailed composition is given elsewhere [8]). The water content was 460 mg kg^{-1}. The content of metals and other heteroatoms in refined rapeseed oil was low (S: 7 mg kg^{-1}; N: 15 mg kg^{-1}, P: <1 mg kg^{-1}; Na: <1 mg kg^{-1}; K: <1 mg kg^{-1}; Ca: 2 mg kg^{-1}; Mg: 3 mg kg^{-1}).

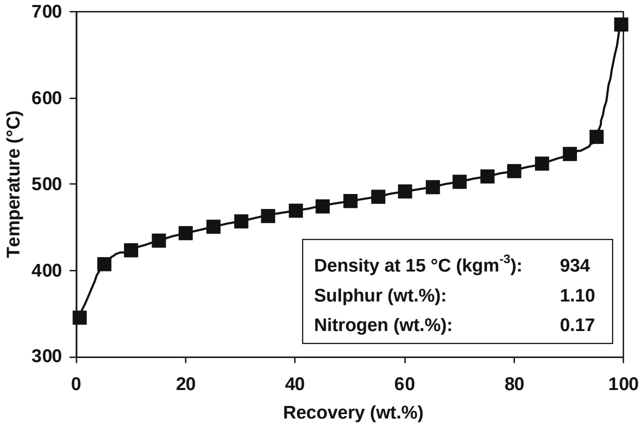

Fig. 1. Simulated distillation and other selected parameters of straight-run vacuum distillate (raw material for hydrocracking).

2.2. Hydrocracking

Hydrocracking of petroleum vacuum distillate and its mixture with rapeseed oil was performed in a bench-scale flow reactor equipped with a salt bath heating system. The dimensions of the reactor were 900 mm (length) and 40 mm (inner diameter). The total amount of the commercial Ni–Mo catalyst used was 100 g. The experiments were carried out at 400 and 420 °C under a hydrogen pressure of 18 MPa. The weight-hourly-space velocity and hydrogen-to-liquid feed ratio were 1 h^{-1} and 1000:1, respectively. The products were stripped with hydrogen prior to their further processing.

2.3. Analysis of products

The products of hydrocracking were separated by distillation into three fractions (two distillates and the residue) in order to obtain fractions suitable for diesel blending. Remixed middle distillates were prepared from kerosene and gas oil in the ratio corresponding to distillation yield in order to extend the number of diesel fuels evaluated.

All obtained primary middle distillates were characterized using simulated distillation performed on the gas chromatograph TRACE GC 2000 (ThermoQuest, CE Instruments). The chromatograph was equipped with an on-column injector, oven cryogenic cooling and a capillary column Varian WCOT Ulti-metal (5 m × 0.53 mm i.d.; film thickness 0.17 μm). Helium was used as the carrier gas (flow: 5 cm^3 min^{-1}). The temperature program was as follows: 2 min at −30 °C, followed by a linear increase at 15 °C min^{-1}–410 °C (5 min). The second distillates (gas oils) were in addition analyzed by other GC method in order to monitor the approximate content of *n*-alkanes. These measurements were carried out on a gas chromatograph HP-6890 equipped with a split-type injector, FID detector and a J&W capillary column HP-ULTRA 1 (12 m × 0.32 mm i.d.; film thickness 0.52 μm). Nitrogen was used as the carrier gas in this case (flow: 1 cm^3 min^{-1}). The following temperature profile was used: 3 min at 60 °C, followed by a linear increase at 8 °C min^{-1}–280 °C (5 min). Approximate values of *n*-alkanes content were calculated from area of the respective *n*-alkane peak and the total area of the chromatogram. Physicochemical properties of all analyzed fractions were determined using the standard test procedures designated for diesel fuel and petroleum products.

3. Results and discussion

3.1. Kerosene fractions

The product of hydrocracking was distilled in order to isolate diesel fraction from naphtha fraction and from high-boiling hydrocarbons designated as residue. The yields of distillation are presented in Table 1. The products contained only a small amount of light volatile hydrocarbons and the majority of them thus escaped

Table 1
Distillation yields of the products obtained by hydrocracking (at 400 and 420 °C) of vacuum distillate (VD) and vacuum distillate containing 5 wt.% of rapeseed oil (RO).

Parameter	Yield (wt.%)			
	VD (400 °C)	VD + RO (400 °C)	VD (420 °C)	VD + RO (420 °C)
Kerosene (1st distillate)	5.3	6.4	18.1	19.8
Gas oil (2nd distillate)	41.9	45.6	53.9	55.4
Residue	52.4	47.2	26.6	23.2
Losses	0.4	0.9	1.4	1.6

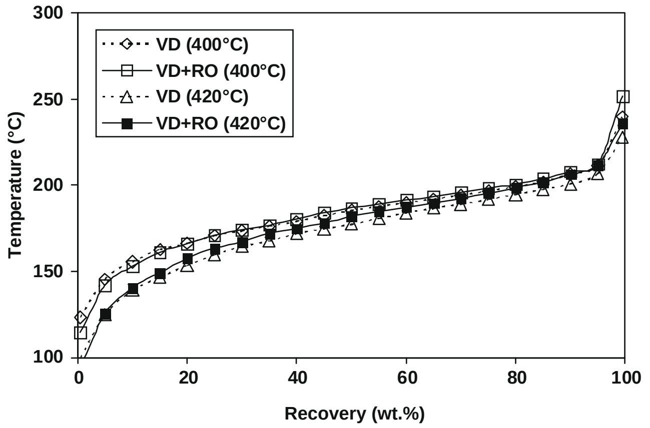

Fig. 2. Simulated distillation of kerosene fractions obtained by hydrocracking (at 400 and 420 °C) of vacuum distillate (VD) and vacuum distillate containing 5 wt.% of rapeseed oil (RO).

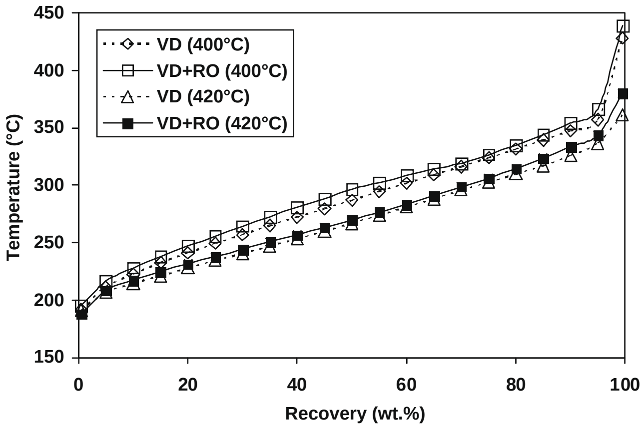

Fig. 3. Simulated distillation of gas oils obtained by hydrocracking (at 400 and 420 °C) of vacuum distillate (VD) and vacuum distillate containing 5 wt.% of rapeseed oil (RO).

as distillation loss (from 0.4 to 1.6 wt.%). The first distillate obtained can be consequently denoted as kerosene rather than naphtha (see Fig. 2). As expected, the distillation profile of kerosene fractions was not influenced by the presence of rapeseed oil in the feed for hydrocracking as the extent of cracking reactions of *n*-alkanes formed by rapeseed oil deoxygenation was limited. This can be seen from only minor increase of the distillate fractions content when 5% of vacuum distillate was replaced by rapeseed oil. The reaction temperature plays, on the other hand, more important role, as can be seen by the dramatic increase of the kerosene yield when the reaction temperature was increased from 400 to 420 °C. Similar trend is also visible for the gas-oil yield. The physicochemical properties of the obtained kerosene fractions are in agreement with physicochemical properties typical for hydrocracking products – high-quality low-sulphur low-aromatic distillates (see Table 2).

3.2. Gas oils (diesel fuels)

The second distillates (gas oils) obtained from the products of hydrocracking are typical petroleum middle distillates. Their fraction composition matches gas oil having a slightly lower distillation end point in some cases (Fig. 3). It is obvious that the reaction temperature influenced, once again, the distillation profile of the gas oils much more than the presence of rapeseed oil in the feed for hydrocracking. Nevertheless, it is possible to observe a slight shift towards higher boiling points in the case of gas oils originating from the feedstock containing rapeseed oil.

The presence of products of rapeseed oil transformation is clearly visible on chromatograms (Fig. 4). Rapeseed oil present in the feedstock was transformed into saturated hydrocarbons having mainly 17 and 18 carbon atoms. This can be seen from the increase of *n*-heptadecane and *n*-octadecane content in the gas oils, which

Table 2
Physicochemical properties of "kerosene fractions" obtained by hydrocracking of vacuum distillate (VD) and vacuum distillate containing 5 wt.% of rapeseed oil (RO).

Parameter	Row material for hydrocracking (reaction temperature)			
	VD (400 °C)	VD + RO (400 °C)	VD (420 °C)	VD + RO (420 °C)
Density at 15 °C (kg m^{-3})	804	803	790	786
Kin. viscosity at 40 °C (mm^2 s^{-1})	1.15	1.14	1.02	0.98
Distillation[a]				
Initial boiling point (°C)	123	114	94	100
10 wt.% recovered at (°C)	156	153	141	139
50 wt.% recovered at (°C)	185	187	182	177
90 wt.% recovered at (°C)	206	208	206	201
final boiling point (°C)	240	251	236	228
Sulphur (mg kg^{-1})	4	3	4	4
Nitrogen (mg kg^{-1})	7	9	1	4
Group-type composition (wt.%)				
Saturated hydrocarbons	97.4	98.1	98.0	98.6
Monoaromatics	2.6	1.9	2.0	1.4
Diaromatics	<0.1	<0.1	<0.1	<0.1
Polyaromatics (tri +)	<0.1	<0.1	<0.1	<0.1

[a] Data originated from simulated distillation due to the small amount available.

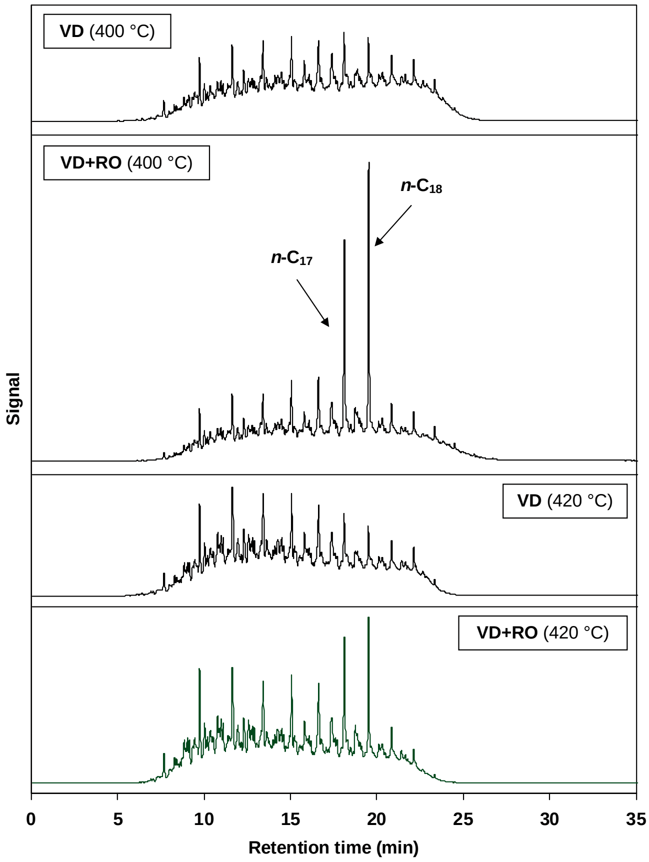

Fig. 4. Chromatograms of gas oils obtained by hydrocracking (at 400 and 420 °C) of vacuum distillate (VD) and vacuum distillate containing 5 wt.% of rapeseed oil (RO).

Table 3
Approximate content of key *n*-alkanes (wt.%) in gas oils obtained by hydrocracking (at 400 and 420 °C) of vacuum distillate (VD) and vacuum distillate containing 5 wt.% of rapeseed oil (RO).

n-alkane	Content (wt.%)			
	VD (400 °C)	VD + RO (400 °C)	VD (420 °C)	VD + RO (420 °C)
n-C_{15}	0.5	0.7	0.7	0.8
n-C_{16}	0.5	0.7	0.5	0.6
***n*-C_{17}**[a]	**0.6**	**2.8**	**0.5**	**1.5**
***n*-C_{18}**[a]	**0.6**	**3.7**	**0.5**	**1.6**
n-C_{19}	0.3	0.3	0.3	0.4
n-C_{20}	0.3	0.3	0.3	0.2

[a] Main products of rapeseed oil hydroprocessing.

is particularly significant at the reaction temperature of 400 °C where cracking and isomerization reactions are not as abundant as at 420 °C. Due to larger production of *i*-alkanes at 420 °C, the increase of C_{17} and C_{18} *n*-alkanes content is not so significant, but still evident. This fact can be also observed in Table 3. Although the GC determination of *n*-alkanes in gas oil is not very accurate, it provides sufficient information for comparison purposes. The increase of reaction temperature by 20 °C not only increased the total yield of middle distillates (Table 1), but it simultaneously caused decrease of *n*-alkanes content in gas oil originating from the feed containing rapeseed oil (Table 3). This is desirable, because low content of *n*-alkanes is very important for good low-temperature properties, which are the weak point of hydroprocessed vegetable oils.

The content of rapeseed oil and its intermediates (mono- and diglycerides, alcohols, free fatty acids) could not be determined due to peak overlapping. Earlier experience with rapeseed oil hydroprocessing suggests that the most refractory species are triglycerides and free fatty acids [6]. The presence of triglycerides in the distillation residue is not probable due to high reaction temperature. The same assumption can be applied for free fatty acids that could be theoretically present in the evaluated gas oils. The validity of this assumption is supported by low acid numbers of obtained gas oils (see Table 4), which indicates that there are no free fatty acids in the products. One of the gas oils showed a slightly higher acid number, but this fact could not be related to presence of free fatty acids since the feed for hydrocracking did not contain rapeseed oil in this case. Physicochemical properties (Table 4) of gas oils predetermine their utilization as diesel fuel or as a high-quality diesel fuel component. Their density and viscosity meet European quality requirements except one negligible deviation in density (815 kg m^{-3}). Raw materials hydrocracked at 420 °C yielded low-aromatic gas oils that fulfilled the current requirement for sulphur-free diesel. The differences among different gas oils in sulphur content and content of aromatics are not too significant. The cetane index of all gas oils was higher than 60, but gas oils obtained from feedstock containing rapeseed oil had higher cetane index than those obtained from pure mineral oil by 2–3 cetane index units. The relatively high flash point of all samples was due to their higher beginning of distillation.

In contrast to the other parameters, the low-temperature properties were strongly influenced by the presence of rapeseed oil in the feed. The gas oils obtained from raw material containing rapeseed oil had significantly worse low-temperature properties than those prepared from rapeseed oil-free feed (Table 4) in all cases, which can be attributed to the higher content of *n*-alkanes in these products. The reaction temperature played an important role particularly in gas oils originating from rapeseed oil containing feed; higher reaction temperature (420 °C) improved cloud point, pour point and CFPP of the gas oil by 9–13 °C in comparison with gas oil obtained at 400 °C. The favourable influence of higher reaction temperature is probably caused by larger formation of *i*-alkanes from dominant *n*-alkanes (*n*-heptadecane an *n*-octadecane) originating from rapeseed oil. On the other hand, the difference in low-temperature properties of gas oils obtained from rapeseed oil-free feed was less significant (from 1 to 6 °C).

Table 4
Physicochemical properties of gas oils obtained by hydrocracking of vacuum distillate (VD) and vacuum distillate containing 5 wt.% of rapeseed oil (RO).

Parameter	Row material for hydrocracking (reaction temperature)				EN 590 (temperate climate)
	VD (400 °C)	VD + RO (400 °C)	VD (420 °C)	VD + RO (420 °C)	
Density at 15 °C (kg m^{-3})	833	830	821	815	820–845
Kin. viscosity at 40 °C (mm^2 s^{-1})	3.62	3.85	2.94	2.78	2.00–4.50
Distillation					
At 250 °C recovered (vol.%)	13	9	30	26	<65
At 350 °C recovered (vol.%)	98.5	98.4	99.0	99.0	>85
95 vol.% recovered at (°C)	339	346	318	326	<360
Flash point in closed cup (°C)	101	105	97	95	>55
Cetane index	60.5	63.9	61.2	63.6	>46
Sulphur (mg kg^{-1})	15	13	8	10	<10
Nitrogen (mg kg^{-1})	9	11	6	10	–
Water (mg kg^{-1})	20	10	20	10	<200
Group-type composition (wt.%)					
Saturated hydrocarbons	93.8	96.0	94.6	95.7	–
Monoaromatics	5.5	3.5	4.8	3.9	–
Diaromatics	0.6	0.5	0.6	0.4	<11
Polyaromatics (tri +)	<0.1	<0.1	<0.1	<0.1	
Acid number (mg KOH g^{-1})	0.14	0.02	0.01	0.01	–
Copper corrosion	Class 1	Class 1	Class 1	Class 1	Class 1
Low-temperature properties					
Cloud point (°C)	−24	−10	−23	−23	<−8[a]
CFPP (°C)	−25	−13	−29	−24	<(+5 to −20)[b]
Pour point (°C)	−41	−17	−47	−26	–

[a] F grade diesel.
[b] Maximum values for grade A, B, C, D, E and F are +5, 0, −5, −10, −15 and −20 °C, respectively.

Table 5
Physicochemical properties of remixed middle distillate obtained by hydrocracking of vacuum distillate (VD) and vacuum distillate containing 5 wt.% of rapeseed oil (RO).

Parameter	Row material for hydrocracking (reaction temperature)				EN 590 (temperate climate)
	VD (400 °C)	VD + RO (400 °C)	VD (420 °C)	VD + RO (420 °C)	
Density at 15 °C (kg m^{-3})	830	827	813	807	820–845
Kin. viscosity at 40 °C (mm^2 s^{-1})	3.08	3.21	2.17	2.02	2.00–4.50
Distillation					
At 250 °C recovered (vol.%)	31	26	54	50	<65
At 350 °C recovered (vol.%)	99	99	99	99	>85
95 vol.% recovered at (°C)	338	343	324	316	<360
Flash point in closed cup (°C)	79	79	58	57	>55
Cetane index	57.6	60.3	57.2	57.6	>46
Sulphur (mg kg^{-1})	14	12	7	9	<10
Nitrogen (mg kg^{-1})	9	11	5	8	–
Water (mg kg^{-1})	19	11	20	12	<200
Group-type composition (wt.%)					
Saturated hydrocarbons	94.2	96.2	95.5	96.4	–
Monoaromatics	5.2	3.3	4.1	3.3	–
Diaromatics	0.6	0.4	0.4	0.3	<11
Polyaromatics (tri +)	<0.1	<0.1	<0.1	<0.1	
Acid number (mg KOH g^{-1})	0.12	0.01	0.01	0.01	–
Copper corrosion	Class 1	Class 1	Class 1	Class 1	Class 1
Low-temperature properties					
Cloud point (°C)	−23	−14	−30	−24	<−8[a]
CFPP (°C)	−24	−19	−31	−27	<(+5 to −20)[b]
Pour point (°C)	−44	−20	<−50	−29	–

[a] F grade diesel.
[b] Maximum values for grade A, B, C, D, E and F are + 5, 0, −5, −10, −15 and −20 °C, respectively.

As the kerosene fraction is also a middle distillate used for diesel production, remixed middle distillates were prepared and evaluated as a diesel fuel too. The remixed distillates were blended from the appropriate kerosene and gas oil in the ratio corresponding to the distillation yields. The physicochemical properties of remixed distillates are presented in Table 5. Addition of kerosene caused, as expected, decrease of flash point, which was still within the limits specified by the European standard for diesel fuel, increase of the volume recovered at 250 °C (satisfactory) and slight decrease of density and cetane index. On the other hand the low-temperature properties were improved.

Providing that more than 80% of rapeseed oil mass is transformed into hydrocarbons from gas oil range (gas oil formed about 50 wt.% of the product), gas oil obtained at reaction temperature 420 °C contains about 8 wt.% of “full-energy” hydrocarbon-based biodiesel. In fact, a part of rapeseed oil mass is transformed also into lighter hydrocarbons due to cracking reactions. Nevertheless, remixed middle distillate obtained at 420 °C still contained more than 5 wt.% of “biohydrocarbons”. The low-temperature properties of gas oil and remixed middle distillate seem to be reasonable if evaluated as diesel fuel.

4. Conclusions

Hydrocracking of petroleum vacuum distillate containing 5 wt.% of rapeseed oil yielded high-quality hydrocarbon middle distillates suitable for diesel fuel production. Obtained gas oils contained more than 5 wt.% of hydrocarbon-based biodiesel. The products contained neither free fatty acids nor triglycerides (products of incomplete transformation of rapeseed oil into hydrocarbons). The product of co-processing obtained at 400 °C (18 MPa) contained significantly larger amount of *n*-alkanes C_{17} and C_{18} than the product obtained from rapeseed-oil-free raw material. The high concentration of *n*-alkanes resulted in worse low-temperature properties of co-processed product. Larger formation of *i*-alkanes at 420 °C decreased the content of *n*-heptadecane and *n*-octadecane in the co-processed product. Consequently, the key low-temperature properties of this product were significantly improved (cloud point: −23 °C, CFPP: −24 °C). It seems that joint hydrocracking of petroleum raw material and vegetable oil can be a promising alternative to produce green diesel using existing refinery technologies. There was not observed any significant deactivation of the catalyst used in this study, however, a more detailed investigation of hydrocracking catalyst deactivation during co-processing of petroleum fractions with vegetable oils is needed.

Acknowledgement

This work was supported by Ministry of Education, Youth and Sports of the Czech Republic under the Agreement No. MSM 6046137304 and by the Ministry of Industry and Trade of the Czech Republic (Project FT-TA3/074).

References

[1] Kubička D, Lederer J, Bělohlav Z. Catalytic transformation of triglycerides in refineries – a promising route to clean fuels and feedstocks for petrochemicals. Oil Gas Eur Mag 2009;35(/1):40–3.
[2] Gusmao J, Brodzki D, Djéga-Mariadassou G, Frety R. Utilization of vegetable oils as an alternative source for diesel-type fuel: hydrocracking on reduced Ni/SiO_2 and sulphided Ni–Mo/γ–Al_2O_3. Cat Today 1989;5:533–44.
[3] da Rocha Filho GN, Brodzki D, Djéga-Mariadassou G. Formation of alkanes alkylcycloalkanes and alkylbenzenes during the catalytic hydrocracking of vegetable oils. Fuel 1993;72:543–9.
[4] Kubičková I, Snåre M, Eränen K, Mäki-Arvela P, Murzin DYu. Hydrocarbons for diesel fuel via decarboxylation of vegetable oils. Cat Today 2005;106:197–200.
[5] Snåre M, Kubičková I, Mäki-Arvela P, Chichova D, Eränen K, Murzin DYu. Catalytic deoxygenation of unsaturated renewable feedstocks for production of diesel fuel hydrocarbons. Fuel 2008;87:933–45.
[6] Šimáček P, Kubička D, Šebor G, Pospíšil M. Hydroprocessed rapeseed oil as a source of hydrocarbon-based biodiesel. Fuel 2009;88:456–60.
[7] Kubička D. Future refining catalysis – introduction of biomass feedstocks. Collect Czech Chem Commun 2008;73:1015–44.
[8] Kubička D, Šimáček P, Žilková N. Transformation of vegetable oils into hydrocarbons over organized-mesoporous-alumina-supported CoMo catalysts. Topics Cat 2009;52(/1):161–8.
[9] Stumborg M, Wong A, Hogan E. Hydroprocessed vegetable oils for diesel fuel improvemnent. Bioresour Technol 1996;56:13–8.

[10] Šimáček P, Kubička D, Šebor G, Pospíšil M. Fuel properties of hydroprocessed rapeseed oil. Fuel 2010;89:611–5.

[11] Hancsók J, Krár M, Magyar S, Boda L, Holló A, Kalló D. Investigation of the production of high cetane number bio gas oil from pre-hydrogenated vegetable oils over Pt/HZSM-22/Al_2O_3. Micropor Mesopor Mater 2007;101:148–52.

[12] Hodge C. California Energy Commission. Workshop on Bioenergy, 2006 (9 March).

[13] Neste Oil. <http://www.nesteoil.com> [accessed 2009].

[14] Jakkula J, Aalto P, Niemi V, Kiiski U, Nikkonen J, Mikkonen S, et al., WO 2004/022674 A1, EP 1 396 531 A2, US 2004/0055209 A1.

[15] Sebos I, Matsoukas A, Apostolopoulos V, Papayannakos N. Catalytic hydroprocessing of cottonseed oil in petroleum diesel mixtures for production of renewable diesel. Fuel 2009;88:145–9.

[16] Huber GW, O'Connor P, Corma A. Processing biomass in conventional oil refineries: production of high quality diesel by hydrotreating vegetable oils in heavy vacuum oil mixtures. Appl Catal A – Gen 2007;329:120–9.

[17] Petrobras. <http://www2.petrobras.com.br/ingles/ads/ads_Tecnologia.html> [accessed 2009].

[18] Petrobras. <http://www2.petrobras.com.br/ri/pdf/Petrobras_Biofuels_May2007.pdf> [accessed 2009].

Fuel 89 (2010) 611–615

Contents lists available at ScienceDirect

Fuel

journal homepage: www.elsevier.com/locate/fuel

Fuel properties of hydroprocessed rapeseed oil

Pavel Šimáček [a,*], David Kubička [b,1], Gustav Šebor [a], Milan Pospíšil [a]

[a] Institute of Chemical Technology, Prague Department of Petroleum Technology and Alternative Fuels, Technická 5, 166 28 Prague 6, Czech Republic
[b] Research Institute of Inorganic Chemistry, Department of Refining and Petrochemical Research, 436 70 Litvínov – Záluží 1, Czech Republic

ARTICLE INFO

Article history:
Received 2 March 2009
Received in revised form 16 September 2009
Accepted 17 September 2009
Available online 1 October 2009

Keywords:
Hydroprocessing
Rapeseed oil
Biodiesel
Hydrodeoxygenation

ABSTRACT

This paper deals with the hydroprocessing of rapeseed oil as a source of hydrocarbon-based biodiesel. Rapeseed oil was hydroprocessed in a laboratory flow reactor under four combinations of reaction conditions at temperatures 310 and 360 °C and under hydrogen pressure of 7 and 15 MPa. A commercial hydrotreating Ni–Mo/alumina catalyst was used. Reaction products contained mostly *n*-heptadecane and *n*-octadecane accompanied by low concentrations of other *n*-alkanes and *i*-alkanes. Reaction product obtained at 360 °C and 7 MPa was blended into mineral diesel fuel in several concentration levels ranging from 5 to 30 wt.%. It was found, that most of the standard parameters were similar to or better than those of pure mineral diesel. On the other hand, low-temperature properties were worse, even after addition of high concentrations of flow improvers.

1. Introduction

Hydroprocessing of vegetable oils allows easy transformation of fatty acid triglycerides into hydrocarbons. Three most important reactions take place during hydroprocessing of vegetable oil [1]:

(i) Hydrogenation of double bonds present in unsaturated chains of bonded fatty acids.
(ii) Hydrodeoxygenation (HDO), which results in removal of oxygen atoms from carboxylic group in the form of water.
(iii) Hydrodecarboxylation (HDC), which leads to elimination of carboxylic group in the form of carbon dioxide.

It was found that hydrogenation of double bonds precedes HDO and HDC reactions [1]. HDO and HDC of saturated triglycerides proceed at different reaction rates, which depend on reaction conditions and type of catalyst used. The changes in the respective reaction rates can be observed by the changing ratio of the principal products, *i.e.* *n*-octadecane in the case of HDO and *n*-heptadecane in the case of HDC. In general, the main reaction products of vegetable oil hydroprocessing are thus *n*-alkanes having the same carbon atom number as fatty acids present in the original vegetable oil (HDO) and *n*-alkanes with the carbon atom number lower by one as compared to the carbon atom number of fatty acids in the original vegetable oil (HDC). Hydroprocessing of common vegetable oils (rapeseed, sunflower, soybean and palm oil) leads to hydrocarbon mixtures, in which *n*-alkanes C_{15} to C_{18} are predominant [2–4].

Reaction conditions and type of catalyst also influence the extent of side reactions leading to formation of *i*-alkanes, cycloalkanes and aromatics [2,4]. Cracking of the hydrocarbon chains is usually negligible. The vegetable oil hydroprocessing [5] is sometimes referred to as hydrogenation [6] or hydrocracking [2,3]. However, the term hydrogenation can be misleading, because it has a different meaning in food industry. During this process the unsaturated chains of fatty acids are hydrogenated and become saturated while the structure of triglycerides remains unchanged. The term hydrocracking may also not be completely exact, because cracking of carbon–carbon bonds occurs only in some cases (HDC) and generally at the carbon atom carrying oxygen-functional group. Therefore, we will denote the set of reactions in this reaction system as hydroprocessing and the individual reactions will be referred to as hydrodeoxygenation (HDO) and hydrodecarboxylation (HDC) throughout the article.

From the refinery point of view, all hydrocarbons present in hydroprocessed vegetable oil belong to middle distillates and are thus suitable for production of diesel fuel. Hydroprocessed vegetable oil can be, hence, called hydrocarbon-based or oxygen-free biodiesel. Oxygen-free biodiesel eliminates some drawbacks of the traditional FAME-type biodiesel relating mostly to fuel stability. Car manufacturers would probably also prefer hydrocarbon-based biodiesel to FAME as it offers full compatibility with current diesel fuel for which the diesel engine systems are optimized. Moreover, the content of such bio-component in diesel fuel could be much higher than 5 vol.% permitted currently for FAME concentration

---

[*] Corresponding author. Tel.: +420 220 444 236; fax: +420 220 444 321.
E-mail addresses: pavel.simacek@vscht.cz (P. Šimáček), david.kubicka@vuanch.cz (D. Kubička).
[1] Tel.: +420 476 163 735; fax: +420 476 768 476.

0016-2361/$ - see front matter © 2009 Elsevier Ltd. All rights reserved.
doi:10.1016/j.fuel.2009.09.017

in diesel in Europe without negative impacts on engine operation. Thanks to its high content of *n*-alkanes, oxygen-free biodiesel has an excellent cetane number ranging from 55 to 90 [5] depending on degree of branching. The worsened low-temperature properties seem to be the only disadvantage in comparison with FAME-type biodiesel. Low-temperature properties can be improved either by choice of proper catalyst and reaction conditions or by isomerisation [7,8] following the hydroprocessing. It is also possible to use existing refinery technologies for co-processing of vegetable oil and petroleum feedstock. The most promising way is perhaps the addition of vegetable oil into feedstock for hydrocracking or hydrotreating [9,10].

Commercial production of hydrocarbon-based biodiesel from vegetable oil has been recently incorporated in petroleum refinery. Finnish company Neste Oil operates two vegetable oil hydroprocessing units with capacity 170 kt/y each in its refinery in Porvoo. Two world-scale plants, in Singapore and Rotterdam, with capacity 800 kt/y each are under construction [8,11,12]. The production of biodiesel takes place in two stages. Product of vegetable oil hydroprocessing (stage 1) proceeds to an isomerisation unit (stage 2) where its low-temperature properties are improved. The final product called NExBTL is used as renewable component for production of diesel fuel. Neste Oil guarantees that its Neste Green diesel, which suits all diesel engines, contains at least 10% of NExBTL.

The paper summarizes some fuel properties of hydroprocessed rapeseed oil obtained at various reaction conditions using commercial Ni–Mo catalyst. Furthermore, fuel properties of mixed fuels containing the selected hydroprocessed rapeseed oil (5–30 wt.%) and mineral diesel are reported and discussed. This work is a logical continuation of the recent experiments aimed at reaction mechanism description and determination of detailed composition of reaction products [4,13].

2. Experimental

2.1. Hydroprocessing

Hydroprocessing of rapeseed oil was performed in a bench scale flow reactor equipped with a salt bath heating system. The experimental set-up is schematically depicted in Fig. 1. All the feed and product lines were heated to prevent feed and product solidification in the lines. The liquid products were stripped with hydrogen prior to sample collection (not shown in Fig. 1). The dimensions of the reactor were 900 mm (length) and 40 mm (inner diameter). The total amount of the catalyst used was 100 g. The composition of the commercial hydrotreating Ni–Mo/alumina catalyst was as follows: NiO – 3.8 wt.%, MoO_3 – 17.3 wt.% and P_2O_5 – 6.7 wt.%. Rapeseed oil used as raw material had food quality (S: 3 mg kg^{-1}; P: <0.5 mg kg^{-1}; Na: 5 mg kg^{-1}; K: 2 mg kg^{-1}; Ca: 4 mg kg^{-1}; Mg: <0.5 mg kg^{-1}). The liquid feed flow and hydrogen flow was 100 g h^{-1} and 0.1 Nm^3 h^{-1}, respectively. The WHSV and gas-to-oil ratio were thus 1 h^{-1} and 920 Nm^3/Nm^3, respectively. The reaction products were collected during the hydroprocessing of rapeseed oil at two temperature levels, 310 and 360 °C, and at two hydrogen pressure levels, 7 and 15 MPa.

2.2. Analysis of products

After separation of aqueous and organic phases, the reaction products were analyzed by gas chromatography. A gas chromatograph, model HP-6890 (Agilent), was used for all chromatographic measurements. Gaseous products and all organic liquid products were analyzed by gas-chromatographic methods proposed in recent work [4]. Physiochemical properties of the organic liquid products and mixed fuels were determined using standard test procedures designated for diesel fuel or petroleum products.

2.3. Mixing of product with mineral diesel fuel

Organic liquid product (OLP) obtained by hydroprocessing of rapeseed oil at 360 °C and 7 MPa was chosen for preparation of blends with mineral diesel fuel. The mineral diesel fuel was obtained from a refinery and it had low sulfur content (10 mg kg^{-1}). Furthermore, it did not contain FAME or any additives. All monitored physiochemical properties of this basic mineral diesel corresponded to the properties of a commercial diesel fuel before final additivation. Four diesel blends containing 5, 10, 20 and 30 wt.% of OLP, respectively, were prepared and evaluated as commercial diesel fuel according to the European standard EN 590. These mixed fuels were then separately treated with flow improvers Keroflux® 3566 (BASF) and Infineum R 288 (Infineum) in concentration ranges of 10–500 mg kg^{-1} to evaluate their impact on low-temperature properties of the blends.

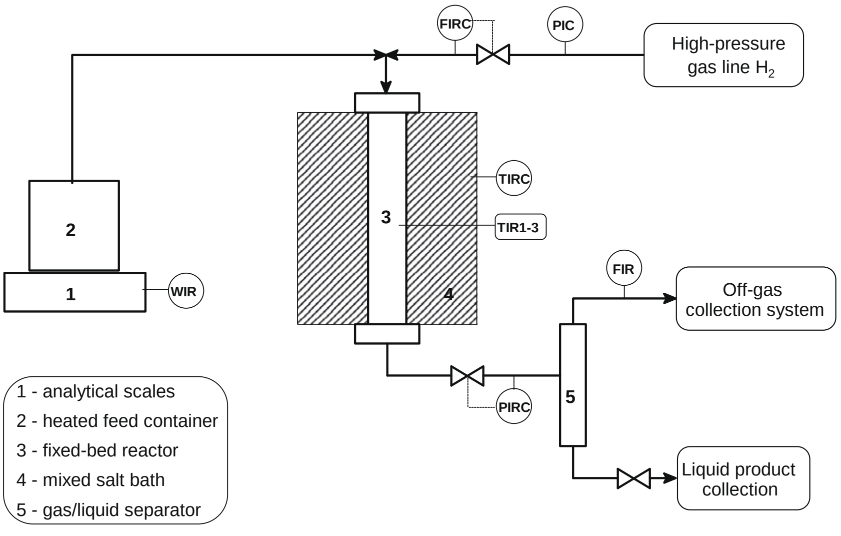

Fig. 1. A schematic figure of the bench scale reactor.

3. Results and discussion

3.1. Composition of reaction products

Hydroprocessing of rapeseed oil yielded water, gaseous hydrocarbons and organic liquid product (OLP). The conversion of rapeseed oil was >99% at 310 °C and complete conversion was achieved at 360 °C. The yields of the main products were as follows: OLP – 83 wt.%, water – 11 wt.% and gaseous hydrocarbons 6 wt.%. Beside hydrogen, the reaction gas contained mainly propane (0.8–2.5 vol.%) and small amounts of carbon dioxide (0.05–0.3 vol.%), carbon monoxide (up to 0.5 vol.%) and methane.

All OLPs were colourless or slightly yellowish liquids with density around 770 kg m^{-3} at 40 °C. However, in the temperature range of 20–30 °C they became solids. The composition of OLPs is presented in Table 1. It is evident, that OLP is a mixture of saturated, in particular non-branched, hydrocarbons. Two hydrocarbons – *n*-heptadecane and *n*-octadecane – represent more than 75 wt.% of OLP in all cases. Besides other *n*-alkanes, the OLPs contained also *i*-alkanes and smaller amounts of cycloalkanes. Formation of *i*-alkanes was observed to increase with increasing reaction temperature and pressure. Aromatics were found in OLPs only in trace amounts (<0.1 wt.%) in some cases. The OLPs obtained at 310 °C contained small amounts (up to 2 wt.%) of reaction intermediates (mainly stearic acid) and reactants. Traces of *n*-octadecanol, another reaction intermediate, was also observed, but only in one of the products. On contrary, the OLPs obtained at 360 °C contained no oxygenated compounds and they can be, thus, denoted as oxygen-free hydrocarbon mixtures.

3.2. Physiochemical properties

The composition of OLPs determines their boiling point range. Narrow range of carbon atom numbers of dominant hydrocarbons causes the flat shape of distillation curve. Approximately 80% of each product distilled at a boiling point of about 300–310 °C (see Fig. 2), which is the boiling point falling into the diesel fuel distillation range. Density and kinematic viscosity of OLPs showed also values acceptable for diesel fuel although the density of OLPs was a little lower than that of diesel (see Table 2). However, this issue can be easily solved by blending with a suitable heavier fraction. Typical composition of hydroprocessed rapeseed oil leads to high calculated cetane index of all prepared OLPs. It is expected that cetane number can reach or even exceed the value of 100, as the calculated cetane index does. Other monitored parameters (sulfur, water and flash point) also satisfied the demands for diesel fuel. Products obtained at 310 °C showed increased acid number, probably due to carboxylic acid content (see Table 1 and 2).

Table 1
Composition (wt.%) of organic liquid products obtained under various reaction conditions (temperature and pressure).

Component	Reaction conditions			
	310 °C, 7 MPa	310 °C, 15 MPa	360 °C, 7 MPa	360 °C, 15 MPa
n-alkanes $\leqslant$ *n*-C_{16}	5.0	4.9	5.8	6.3
n-heptadecane	18.4	10.5	24.9	24.9
n-octadecane	70.6	78.2	58.1	51.8
n-alkanes > *n*-C_{18}	3.3	3.2	4.5	3.6
Other hydrocarbons[a]	1.1	2.3	6.7	13.4
Palmitic acid (C16:0)	–	–	–	–
Stearic acid (C18:0)	0.6	0.6	–	–
n-octadecanol	–	0.1	–	–
Monoglycerides	0.1	0.1	–	–
Diglycerides	0.1	–	–	–
Triglycerides	0.8	0.1	–	–

[a] This group includes all hydrocarbons except *n*-alkanes (contains more than 90% *i*-alkanes C_{16}–C_{18}).

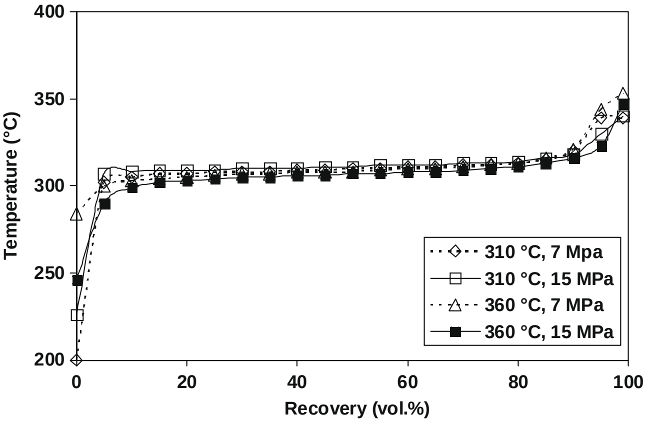

Fig. 2. Distillation curves of organic liquid products obtained under various reaction conditions.

The main disadvantage of OLPs as a potential component of diesel fuel consists in their poor low-temperature properties. All low-temperature parameters (cloud point, pour point and cold filter plugging point) fell into the range of +20 to +30 °C (Table 2). Utilization of such a kind of diesel fuel in the pure form would be very problematic even in countries with hot climate.

3.3. Mixed diesel fuels

The product obtained by hydroprocessing of rapeseed oil at 360 °C and 7 MPa was chosen for mixing with mineral diesel fuel. Neither reactants nor intermediates were detected in OLPs

Table 2
Physiochemical properties of organic liquid products obtained under various reaction conditions.

Parameter	Reaction conditions			
	310 °C, 7 MPa	310 °C, 15 MPa	360 °C, 7 MPa	360 °C, 15 MPa
Density at 40 °C (kg m^{-3})[a]	772 (788[b])	771 (787[b])	771 (787[b])	770 (786[b])
Kin. viscosity at 40 °C (mm^2 s^{-1})	4.15	4.11	3.92	3.82
Distillation				
At 250 °C recovered (vol.%)	<5	<5	<5	<5
At 350 °C recovered (vol.%)	>95	>95	>95	>95
95 vol.% recovered at (°C)	339	330	344	323
Flash point in closed cup (°C)	>128	>128	125	120
Cetane index[c]	103	105	103	103
Sulfur (mg kg^{-1})	9	9	10	10
Nitrogen (mg kg^{-1})	11	11	11	11
Water (mg kg^{-1})	95	95	66	42
Acid number (mg KOH g^{-1})	0.54	0.65	0.06	0.05
Low-temperature properties				
Cloud point (°C)	26–28	28–30	25–27	23–25
CFPP (°C)	>20	>20	>20	>20
Pour point (°C)	28	29	25	23

[a] Solid nature of the sample did not allow to measure its standard density at 15 °C.

[b] Approximate values (density at 15 °C was calculated from density at 40 °C taking the sample as homogenous liquid).

[c] Cetane index calculated with the estimated density at 15 °C.

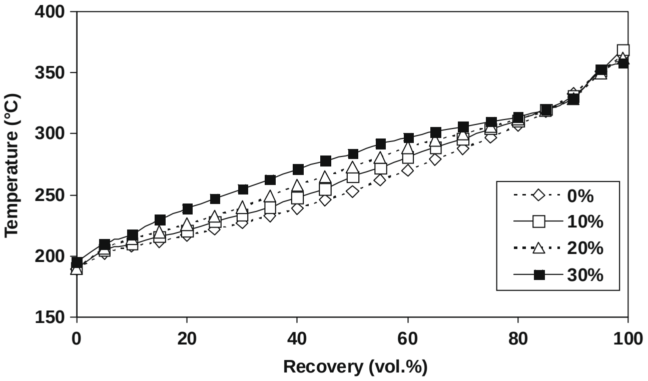

Fig. 3. Distillation curves of mixed fuels containing various amount of organic liquid product (hydroprocessed rapeseed oil processed at 360 °C and 7 MPa).

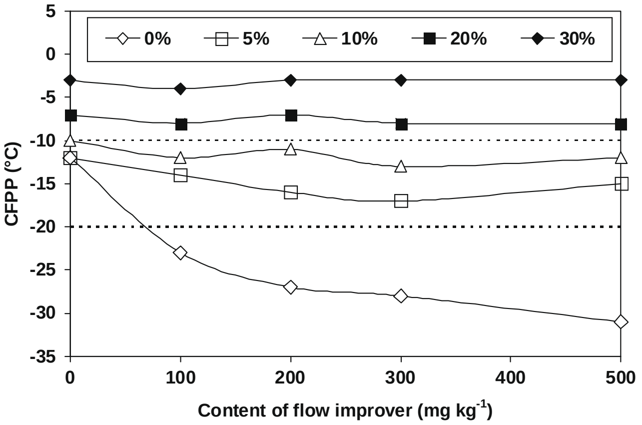

Fig. 4. Cold filter plugging point (CFPP) of diesel fuels containing various amount of organic liquid product (hydroprocessed rapeseed oil processed at 360 °C and 7 MPa) treated with flow improver Keroflux® 3566 (BASF).

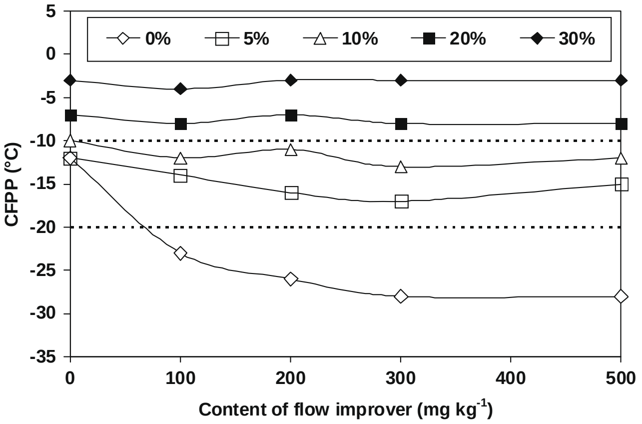

Fig. 5. Cold filter plugging point (CFPP) of diesel fuels containing various amount of organic liquid product (hydroprocessed rapeseed oil processed at 360 °C and under the pressure of 7 MPa) treated with flow improver Infineum R 288.

processed at 360 °C. While the low-temperature properties of the products processed at 7 and 15 MPa were comparable, hydroprocessing at the lower pressure would be the preferable technological solution. Addition of OLP into mineral diesel results in a shift of the distillation curve toward to higher boiling points (see Fig. 3). The shift is in the middle part of the curve and therefore it does not influence negatively the key points of distillation curve. All measured physiochemical properties of mixed fuels containing various amount of hydroprocessed rapeseed oil are presented in Table 3. Viscosity and density of mixed fuels corresponded to EN 590 standard requirements with one exception of a little deviation in density (for the mixed fuel containing 30 wt.% of OLP). Flash points of mixed fuels were comparable or slightly higher than that of basic mineral diesel. Mixed fuels had, however, significant benefit in the calculated cetane index, which linearly increased from 52 (pure basic mineral diesel) up to 66 units (mixed fuel containing 30 wt.% of OLP). Similar increase of cetane number can be expected.

As expected, the addition of OLP worsened the low-temperature properties of the mixed fuels in comparison with the basic mineral diesel. The increase of cloud point and CFPP seems to be negligible (not more than 2 °C) for fuels containing up to 10 wt.% of OLP. However, higher concentration of OLP in the mixed fuel caused a more significant increase (5–12 °C) of all key low-temperature parameters. After evaluation of the fuels without additives, the performance of two different flow improvers (Keroflux 3566 by BASF and Infineum R 288 by Infineum) was investigated. The results of CFPP measurements of the mixed fuels treated with various concentrations of additive Keroflux® 3566 (BASF) are presented in Fig. 4. While CFPP of pure basic mineral diesel dropped according to expectations, the additive showed negligible efficiency in mixed fuels. While CFPP of the basic mineral diesel dropped from original −12 to −27 °C for additive concentration

Table 3
Physiochemical properties of mixed fuels containing various amount of organic liquid product (hydroprocessed rapeseed oil processed at 360 °C and 7 MPa).

Parameter	Content of the product (wt.%)					EN 590 (temperate climate)
	0	5	10	20	30	
Density at 15 °C (kg m^{-3})	829	826	824	820	816	820–845
Kin. viscosity at 40 °C (mm^2 s^{-1})	2.35	2.44	2.50	2.63	2.76	2.00–4.50
Distillation						
At 250 °C recovered (vol.%)	48	45	42	36	27	<65
At 350 °C recovered (vol.%)	95	95	95	95	95	>85
95 vol.% recovered at (°C)	351	350	352	350	352	<360
Flash point in closed cup (°C)	72	72	73	74	76	>55
Cetane index	52.1	54.3	56.7	60.6	65.7	>46
Sulfur (mg kg^{-1})	10	10	10	10	10	<10
Nitrogen (mg kg^{-1})	37	36	34	32	29	–
Water (mg kg^{-1})	40	41	43	45	48	<200
Low-temperature properties						
Cloud point (°C)	−9	−8	−7	−1	+3	<−8[a]
CFPP (°C)	−12	−12	−10	−7	−3	<(+5 to −20) [b]
Pour point (°C)	−12	−12	−9	−9	−3	–

[a] Grade F diesel.
[b] Maximum values for grades A, B, C, D, E and F is +5, 0, −5, −10, −15 and −20 °C, respectively.

200 mg kg^{-1}, the same concentration of additive in mixed fuels did not improve CFPP more than by 5 °C. Although CFPP of untreated mineral diesel and mixed fuel containing 5 wt.% of OLP were the same, basic mineral diesel became F-grade diesel after addition of 100 mg kg^{-1} of flow improver. On the other hand, not even 500 mg kg^{-1} changed the grade of mixed fuels. Mixed fuels containing from 5 to 30 wt.% of OLP could be labeled only as E-grade to B-grade diesel. Hence, there is no benefit in treating the mixed fuels with ordinary commercial flow improvers, as similar results were obtained when using additive Infineum R 288 (see Fig. 5). Nevertheless, it is possible that some kind of tailored flow improver could be more effective.

4. Conclusions

Hydroprocessing of rapeseed oil at 360 °C and 7 and 15 MPa yielded oxygen-free hydrocarbon mixtures. Only trace amounts of reactants and intermediates were observed in products obtained at 310 °C. The organic liquid products (OLPs) contained acyclic saturated hydrocarbons having carbon atom number ranging from about 14 to 20, where *n*-alkanes C_{17} and C_{18} formed more than 75 wt.% of the product. The composition and physiochemical properties of hydroprocessed rapeseed oil predetermine this product as a high cetane diesel fuel, but its poor low-temperature properties (pour point higher than +20 °C) prevents its utilization in the pure form.

Mixed diesel fuels containing from 5 to 30 wt.% of OLP (obtained at 360 °C and 7 MPa) met the European diesel fuel specification EN 590. The greatest benefit of the mixed fuels is probably the increase of the cetane index (by 2–14 units). On the other hand, the flow improvers used were shown to be ineffective in lowering CFPP. The mixed fuels thus met only diesel grade specifications B, C, D and E, respectively, while the basic mineral diesel treated with flow improvers met F-grade specification (EN 590) easily.

Acknowledgement

This work was supported by the Ministry of Industry and Trade of the Czech Republic (project FT-TA3/074) and by the Ministry of Education, Youth and Sports of the Czech Republic (agreement No. MSM 6046137304).

References

[1] Kubička D. Future refining catalysis – introduction of biomass feedstocks. Collect Czech Chem Commun 2008;73:1015–44.
[2] da Rocha Filho GN, Brodzki D, Djéga-Mariadassou G. Formation of alkanes alkylcycloalkanes and alkylbenzenes during the catalytic hydrocracking of vegetable oils. Fuel 1993;72:543–9.
[3] Gusmao J, Brodzki D, Djéga-Mariadassou G, Frety R. Utilization of vegetable oils as an alternative source for diesel-type fuel: hydrocracking on reduced Ni/SiO_2 and sulphided Ni–Mo/γ-Al_2O_3. Catal Today 1989;5:533–44.
[4] Šimáček P, Kubička D, Šebor G, Pospíšil M. Hydroprocessed rapeseed oil as a source of hydrocarbon-based biodiesel. Fuel 2009;88:456–60.
[5] Stumborg M, Wong A, Hogan E. Hydroprocessed vegetable oils for diesel fuel improvement. Bioresource Technol 1996;56:13–8.
[6] Smejkal Q, Smejkalová L, Kubička D. Thermodynamic balance in reaction system of total vegetable oil hydrogenation. Chem Eng J 2009;146:155–60.
[7] Hancsók J, Krár M, Magyar S, Boda L, Holló A, Kalló D. Investigation of the production of high cetane number bio gas oil from pre-hydrogenated vegetable oils over Pt/HZSM-22/Al_2O_3. Micropor Mesopor Mater 2007;101:148–52.
[8] Hodge C. California Energy Commission, workshop on bioenergy, 9 March 2006.
[9] Huber GW, O'Connor P, Corma A. Processing biomass in conventional oil refineries: production of high quality diesel by hydrotreating vegetable oils in heavy vacuum oil mixtures. Appl Catal A Gen 2007;329:120–9.
[10] Sebos I, Matsoukas A, Apostolopoulos V, Papayannakos N. Catalytic hydroprocessing of cottonseed oil in petroleum diesel mixtures for production of renewable diesel. Fuel 2009;88:145–9.
[11] NesteOil, <http://www.nesteoil.com> [accessed 2009].
[12] Jakkula J, Aalto P, Niemi V, Kiiski U, Nikkonen J, Mikkonen S, et al. WO 2004/022674 A1, EP 1 396 531 A2, US 2004/0055209 A1.
[13] Kubička D, Šimáček P, Žilková N. Transformation of vegetable oils into hydrocarbons over organized-mesoporous-alumina-supported CoMo catalysts. Top Catal 2009;52:161–8.

Fuel 88 (2009) 456–460

Contents lists available at ScienceDirect

Fuel

journal homepage: www.elsevier.com/locate/fuel

Hydroprocessed rapeseed oil as a source of hydrocarbon-based biodiesel

Pavel Šimáček [a,1], David Kubička [b,*], Gustav Šebor [a], Milan Pospíšil [a]

[a] Institute of Chemical Technology, Prague, Department of Petroleum Technology and Alternative Fuels, Technická 5, 166 28 Prague 6, Czech Republic
[b] Research Institute of Inorganic Chemistry, Department of Refining and Petrochemical Research, 436 70 Litvínov-Záluží 1, Czech Republic

ARTICLE INFO

Article history:
Received 8 February 2008
Received in revised form 13 October 2008
Accepted 14 October 2008
Available online 7 November 2008

Keywords:
Hydroprocessing
Hydrocracking
Rapeseed oil
Biodiesel

ABSTRACT

This paper deals with the hydroprocessing of rapeseed oil representing a perspective technological way for production of biocomponents in diesel fuel range. Rapeseed oil was hydroprocessed at various temperatures (260–340 °C) under a pressure of 7 MPa in a laboratory flow reactor. Three Ni–Mo/alumina hydrorefining catalysts were used. Reaction products were analyzed using several gas-chromatographic methods. Reaction products contained water, hydrogen-rich gas and organic liquid product (OLP). The main components of OLP were identified as C_{17} and C_{18} *n*-alkanes and *i*-alkanes. At a low reaction temperature, OLP contained also free fatty acids and triglycerides. At reaction temperatures higher than 310 °C, OLP contained only hydrocarbons of the same nature as hydrocarbons present in diesel fuel. Influence of reaction temperature and catalyst on the composition of reaction products is discussed.

1. Introduction

There are only a few types of liquid fuels produced from biomass, which are commercially used as motor fuels. Bioethanol is used either as a component of motor gasoline (up to 5 or 10 vol.%) or as special gasoline–ethanol blends (E85). Bioethanol is also used in the form of ethyl tert-butyl ether (ETBE) as a component of motor gasoline (up to 15 vol.%). Strongly additived ethanol is also used as fuel for special designed diesel engines. Several recent studies also deal with idea of large production of biobutanol instead of bioethanol.

Fatty acid methyl esters (FAME), or biodiesel, are the other group of widely used biofuels. FAME is produced by transesterification of vegetable oils with methanol. Besides rapeseed oil used in Europe, there are other oils used for production of FAME (soybean oil, sunflower oil, palm oil, etc.). In principle, it is possible to use also waste cooking oil or animal fats. All fats mentioned above are chemically based on triglycerides of fatty acids, which can be transesterified to FAME. FAME is used either in pure form, or in mixtures with mineral diesel or as a component of ordinary commercial diesel fuel according to EN 590 (FAME content up to 5 vol.%). Furthermore, biodiesel can be produced from oils and fats also by transesterification using bioethanol. Obtained product, fatty acid ethyl esters (FAEE), have similar properties like FAME. Production of FAEE was commercialized in Brasil [1] where FAEE is produced from waste feedstock (tallow, free fatty acids).

Although FAME has been used as diesel fuel for many years, the use of FAME is connected with some problems as compared to the use of petroleum-based diesel fuel. FAME damages some construction materials of the fuel system (seals). Detergent properties of FAME cause elution of impurities and plugging of some parts of the fuel system. This phenomenon is significant especially when changing mineral diesel fuel for diesel fuel containing FAME. FAME also tends to form sludge and deposits, especially during long-term storage no matter whether pure FAME or diesel fuel containing FAME are stored. High content of FAME in diesel fuel or combustion of pure biodiesel usually leads to faster degradation of motor oil. Relatively high solubility of water in FAME can cause larger corrosion of metal parts in comparison to mineral diesel fuel. Majority of the negative effects of FAME usage can be minimizing the content of FAME in diesel fuel. On the other hand, small content of FAME inhibits its larger utilization. Beside FAME production, there are other possibilities of vegetable oil processing for motor fuel production.

The beginning of thermo-catalytic processing of vegetable oil dates back to twenties of 20th century. The first catalysts used for cracking in gas phase were MgO, Al_2O_3, CaO and Cu. Chlorides of Zn, Cu and Ba were used for cracking in liquid phase. The processes were carried out at temperatures 400–450 °C [2–4]. Vegetable oil was cracked in large scale in China during world war II. Acidic ($AlCl_3$) and basic (MgO, CaO, NaOH) catalysts were used in batch reactors [5]. Catalysts based on silica–alumina and zeolites (e.g. HZSM 5, Pd/HZSM 5, H-Y) have been used in more recent works aimed at development of new catalysts [6–9]. Some modern

---

[*] Corresponding author. Tel.: +420 476 163 735; fax: +420 476 768 476.
E-mail addresses: pavel.simacek@vscht.cz (P. Šimáček), david.kubicka@vuanch.cz (D. Kubička).
[1] Tel.: +420 220 444 236; fax: +420 220 444 321.

0016-2361/$ - see front matter © 2008 Elsevier Ltd. All rights reserved.
doi:10.1016/j.fuel.2008.10.022

technologies use also catalytic hydroprocessing. All thermo-catalytic processing of vegetable oil has been carried out with the intention to produce alternative motor fuels, namely gasoline and diesel.

Three main concepts are described in the literature: hydroprocessing (hydrogenolysis), catalytic cracking and thermal cracking. With respect to the fractional composition, products of thermo-catalytic cracking represent a suitable alternative to gasoline rather than to diesel. Even if the catalytic cracking process is optimized the yields of "biodiesel" are relatively low. Furthermore, these products often contain carboxylic acids and other oxygenates, which could complicate their use both with respect to their storage and distribution and also with respect to their combustion in engines [10–14]. On the other hand, hydroprocessing provides high conversion of vegetable oils as well as high yields of hydrocarbon middle distillates, which can be used as an alternative diesel fuel. Due to high cetane number in the range from 55 to 90 [15] are such fuels sometimes called "super cetane diesel". Possible drawback of such fuels is their somewhat worse low-temperature properties.

Papers discussing hydroprocessing of vegetable oils agree on the composition of the relatively simple mixture of reaction products. The main product of hydroprocessing of vegetable oils is a mixture of *n*-alkanes and the most represented ones are those from n-C_{15} up to n-C_{18} [16,17]. There is also small amount of free carboxylic acids in reaction products in some cases. Several reactions take place during vegetable oil hydroprocessing: hydrogenation of double bonds in alkyl chains of fatty acids, decarboxylation and decarbonylation or reduction of carboxylic acids. Besides main reactions mentioned above, cyclization and aromatization reactions can take place [16].

Gusmao et al. [17] and da Rocha Filho et al. [16] studied extensively the transformation of vegetable oils on sulfide catalysts under hydrogen pressure. Gusmao et al. investigated hydrocracking of soy and babassu oils in a batch reactor at temperatures 350–400 °C and at hydrogen partial pressures 1–20 MPa. They used sulfided Ni–Mo/γ-Al_2O_3 and reduced Ni/SiO_2 catalysts. They found that only double bonds were hydrogenated in soy oil at low reaction temperatures (less than 200 °C) and corresponding saturated triglycerides, i.e., tristearin and tripalmitin, were formed. The decomposition of triglycerides accompanied by the hydrogenation of the decomposition products was observed at temperatures above 290 °C. In contrast to reduced Ni catalyst, sulfided Ni–Mo catalysts requires higher reaction temperatures (in the range of 230–280 °C) to achieve double bond hydrogenation. On the other hand, the transformation of the carboxylic groups is achieved under similar reaction temperatures (around 300 °C) on both catalysts [17]. The main reaction products are, for both catalysts, aliphatic hydrocarbons that correspond either to products of total hydrogenation, i.e. they have the same carbon number as the acids, or hydrodecarboxylation, i.e. their carbon atom number is smaller by one than the corresponding carboxylic acid. If the reaction conditions are enough severe, all carboxylic acids (reaction intermediates) converted into the hydrocarbons. Almost no cracking of the hydrocarbon chains was observed.

Da Rocha Filha et al. [16] studied hydrogenation of vegetable oils on Ni–Mo/γ-Al_2O_3. In addition to decomposition of soy oil, the authors investigated hydrogenolysis of special vegetable oils, such as maracuja, buritim tucha and babassu oils. The main reaction products were corresponding *n*-alkanes (66–76 wt.%) after 2 h at 360 °C and 14 MPa (filling pressure of hydrogen at room temperature) in a batch reactor. The yields of gaseous products and water were 9–13 and 5 wt.%, respectively. The main gaseous product was CO_2 (80 wt.%). The rest was formed by CO and C_1–C_4 hydrocarbons. The main reaction product, *n*-alkanes were accompanied in substantial amounts by cycloalkanes (up to 13 wt.%) and alkylaromatics (up to 4 wt.%). The experimental results suggest that cycloalkanes and aromatics are formed due to the presence of polyunsaturated fatty acids in the triglycerides, mainly linoleic acid that is found particularly in soy and maracuja oils. The identified cycloalkanes have 18 carbon atoms in the molecule, which further confirms the theory of aromatics and cycloalkanes formation. The concentration of free fatty acid was low (less than 1 wt.%).

Hydroprocessing of vegetable oil could become a regular part of an oil refinery in the future. For example Finland's company NesteOil [18–21] has completed the construction of a unit for vegetable oil hydroprocessing in Porvoo (Finland). The unit with capacity 170 kt/year has two stages: hydroprocessing of vegetable oils and isomerisation of obtained hydrocarbon product to improve its low-temperature properties. NesteOil also declared that the emissions of CO_2 in this process are lower than emissions coming from production of FAME [22]. Other oil companies are developing their own solutions as well [23–26].

The paper presents the results of hydroprocessing of rapeseed oil under wide range of reaction temperature using three Ni–Mo commercial hydrorefining catalysts. The aim is to describe in detail the effect of reaction temperature on product distributions in the organic liquid product (OLP) as well as in its hydrocarbon fraction.

2. Experimental

2.1. Catalysts

Three commercial hydrorefining catalysts with alumina as carrier were used. List of the catalysts is in Table 1. The catalysts were activated before experiments via sulfidation using 5% solution of dimethyldisulfide (DMDS) in isooctane. During sulfidation, reaction temperature was gradually increased from 210 to 340 °C. This temperature was kept constant for 4 h. During sulfidation, pressure and hydrogen flow were kept constant at 5 MPa and 30 $Ndm^3\,h^{-1}$, respectively. The sulfidation process was followed directly by the experiments. Pressure was increased to 7 MPa and injection of raw material was initiated.

2.2. Hydroprocessing

Hydroprocessing of rapeseed oil was performed in a laboratory flow reactor equipped with electric heating. The inner diameter of the reactor was 17 mm and the length of the isothermal catalyst bed was about 100 mm. Due to the absence of heated reaction products tank, rapeseed oil (row material) was diluted with an inert solvent – isooctane (the volume ratio 1:1) before feed introduction. The reaction was performed with a high surplus of hydrogen to the raw material (1000:1) in the temperature range of 260–340 °C and at pressure 7 MPa. The feed flow (isooctane/rapeseed oil mixture) was 22 g h^{-1} at weight hour space velocity of 1 h^{-1}.

A typical experiment with one catalyst took from 70 to 90 h. During this time, reaction temperature was decreased from initial 340 to 260 °C in 20 °C steps. Unless the reactor was fouled up, temperature was increased again in two steps to 340 °C. Samples of reaction products were collected in 2 h intervals. Three samples were collected at each reaction temperature level.

Table 1
The list of the catalysts used.

Content (wt.%)	Catalyst		
	A[a]	B	C
NiO	3.8	2.6	2.6
MoO_3	17.3	15.7	8.8

[a] Catalyst A contained 6.1 wt.% of P_2O_5.

2.3. Analysis of products

After separation of the aqueous and organic phases, determination of volume, density and the composition of organic phase as well as dissolved-water content were determined. At each temperature level, a representative sample of gas products was also collected.

All gaseous and organic liquid samples were analyzed using HP-6890 chromatographs. Gaseous products were analyzed by gas chromatography using CP Carbobond column (50 m × 0.53 mm i.d.; film thickness 5 μm) and thermal conductivity and flame ionization detectors. Helium was used as the carrier gas ($8\ \mathrm{cm^3\ min^{-1}}$). The following temperature profile was used: 5 min at 30 °C, followed by a linear increase at $30\ \mathrm{°C\ min^{-1}}$ to 180 °C (30 min).

Three different gas-chromatographic (GC) methods were used to evaluate the liquid organic product (OLP) composition:

1. Products containing only hydrocarbons were analyzed by simple GC method using split injector and non-polar J&W capillary column HP-ULTRA 1 (12 m × 0.32 mm i.d.; film thickness 0.52 μm). Nitrogen was used as the carrier gas ($1\ \mathrm{cm^3\ min^{-1}}$). The following temperature profile was used: 3 min at 60 °C, followed by a linear increase at $8\ \mathrm{°C\ min^{-1}}$ to 280 °C (5 min).
2. The second GC method was selected for samples containing also other substances than hydrocarbons. The method uses silylation of substances containing the OH group. Beside hydrocarbons, the method also allows to determine carboxylic acids and alcohols. The procedure is slightly modified method EN 14105 dedicated primarily for determination of free and bound glycerol in fatty acid methyl esters (FAME). The method uses derivatization of *N*-methyl-*N*-trimethylsilyltrifluoracetamide (MSTFA) in the presence of pyridine. After silylation and addition of the internal standard, the sample was dissolved in *n*-heptane and analyzed using gas chromatography equipped with on-column injection (1 μl) and a non-polar J&W capillary column HP-5 (10 m × 0.25 mm i.d.; film thickness 0.1 μm). Nitrogen was used as the carrier gas ($2.5\ \mathrm{cm^3\ min^{-1}}$). The following three-ramp temperature profile was used: 1 min at 50 °C, followed by a linear increase at $15\ \mathrm{°C\ min^{-1}}$ to 180 °C, next linear increase at $7\ \mathrm{°C\ min^{-1}}$ to 230 °C; the last ramp at $10\ \mathrm{°C\ min^{-1}}$ (5 min).

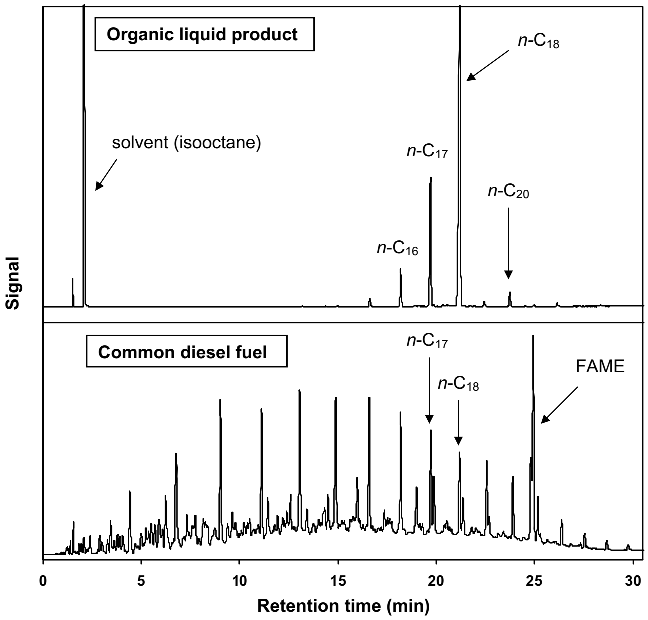

Fig. 1. Typical chromatograms of organic liquid product (OLP) and common diesel fuel containing 5 wt.% of fatty acid methyl esters (FAME).

3. In order to obtain more detailed information about composition of identified free and bound fatty acids, the method of esterification with subsequent GC analysis was used. Samples were processed in two steps in a special flask. First, the sample was hydrolyzed (80 °C, 5 min) by methanolic solution of NaOH. After hydrolysis the sample was esterified (80 °C, 2 min) using methanolic solution of BF_3. Finally, saturated NaCl solution was added and the sample was centrifuged. A sample of the separated top layer was withdrawn and injected into chromatograph equipped with split injector and polar (PEG) capillary SGE column BP-20 (25 m x 0.53 mm i.d.; film thickness 1 μm). The following temperature profile was used: 1 min at 150 °C, followed by a linear increase at $5\ \mathrm{°C\ min^{-1}}$ to 220 °C (10 min). Nitrogen was used as the carrier gas ($2\ \mathrm{cm^3\ min^{-1}}$).

3. Results and discussion

3.1. Composition of reaction products

Basic properties and composition of rapeseed oil hydroprocessing products are similar for all catalysts used. Reaction gas always contained propane (0.8–2.5 vol.%). Traces of methane were detected in some cases only. Other hydrocarbons were not detected in the reaction gas. As permanent gases are concerned, small amounts of carbon dioxide (0.05–0.3 vol.%) and carbon monoxide (0–0.5 vol.%) were detected.

Beside gaseous products and water, the reaction yields an organic liquid product (OLP). Character of this OLP depended on the reaction temperature. At low reaction temperatures (260–300 °C depending on the catalyst used), the products were either cloudy, or they have a heterogeneous nature of a suspension of white crystals in liquid. On contrary, the products obtained at reaction temperatures above 300 °C were clear colourless liquids with density ranging from 730 to 750 $\mathrm{kg\ m^{-3}}$.

The analyses showed that the clear homogenous OLP represents a relatively simple mixture containing, beside the inert solvent (about 50 wt.%), predominantly *n*-alkanes C_{15}–C_{18}. This suggests that the solvent is really inert; however it can plausibly suppress the catalyst deactivation due to the dilution effects. Moreover, the selectivity to hydrocarbons and oxygenated products was not affected by the presence of the solvent. Content of individual *n*-alkanes increased in the given line, i.e. the dominant hydrocarbon was *n*-octadecane. The main products of rapeseed oil hydroprocessing are thus the natural components of conventional diesel fuel (see Fig. 1). These hydrocarbons, *n*-alkanes C_{15}–C_{18}, are present in diesel fuel in the concentration about 0.5–2.5 wt.% each. Selected properties of the discussed *n*-alkanes as well as "classic biodiesel"

Table 2
Selected properties of dominant components of rapeseed oil hydroprocessing together with parameters of diesel fuel and rapeseed oil methyl esters.

Parameter	Main components of OLP[a]				Diesel	RME[b]
	n-C_{15}	*n*-C_{16}	*n*-C_{17}	*n*-C_{18}		
Density ($\mathrm{kg\ m^{-3}}$) at temp. (°C)	769 (20)	774 (20)	775 (20)	776 (28)	820–845 (15)	820–845 (15)
Boiling point (°C)	271	287	302	316	180–360	320-350
Cetane number	95	100	105	110	51–60	>51
Melting point (°C)	10	18	19	28	−25–0[c]	−20–5[c]

[a] Organic liquid product.
[b] Rapeseed oil methyl esters.
[c] Common values of CFPP (cold filter plugging point).

Table 3
Distribution of fatty acids in rapeseed oil (raw material).

Acid	Number of carbon atoms: number of double bonds									
	C14:0	C16:0	C16:1	C18:0	C18:1	C18:2	C18:3	C20:0	C20:1	>C20
Content (wt.%)	0.1	4.8	0.2	1.9	61.9	19.8	9.2	0.6	1.5	0.1

(rapeseed oil methyl esters) are presented in Table 2 along with properties of ordinary commercial diesel fuel. Besides *n*-alkanes, the OLPs contained also *i*-alkanes and small amounts of cycloalkanes. Aromatics were found in OLP only in trace amounts (<0.2%) and only at high reaction temperature.

Furthermore, the GC analysis of heterogeneous samples revealed the presence of triglycerides (especially tristearin) and free carboxylic acids (especially stearic acid). These samples contained also a small amount of mono- and diglycerides and trace of *n*-octadecanol. It is an important finding that molecules of glycerides and free fatty acids contained in principle only saturated hydrocarbon chains. This is in contrast to the raw material for hydroprocessing (rapeseed oil) that contained more than 90% of unsaturated fatty acids (see Table 3). This clearly shows that hydrogenation of double bonds is the primary reaction. Other reactions, leading to formation of hydrocarbons, follow hydrogenation of triglycerides. Composition of selected OLP obtained at the two temperature extremes is presented in Table 4.

3.2. Influence of reaction temperature and catalyst

As expected, the content of reactants and intermediates (mainly triglycerides and free fatty acids) decreased with increasing reaction temperature. This relation is graphically expressed in Fig. 2 for catalyst A. At temperatures higher than about 310 °C, the mentioned reactants and intermediates were not detected in the reaction mixture. As to the other catalysts (B and C), similar trends were observed. However the absence of triglycerides and free fatty acids was observed already at lower reaction temperatures (290–300 °C).

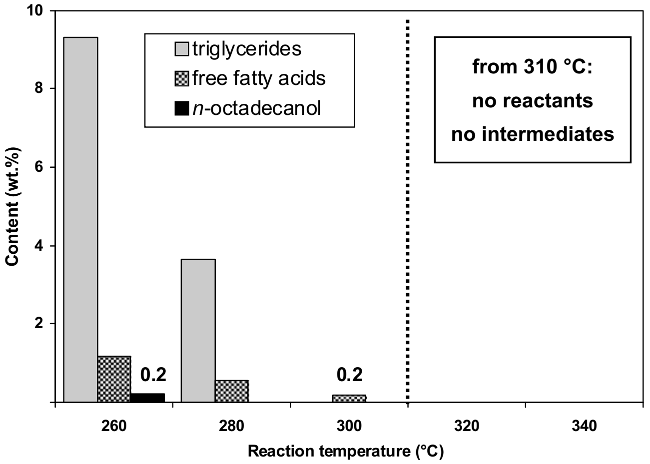

Fig. 2. Content of reactants and intermediates in dependence on reaction temperature catalyst A (content is calculated on OLP without inert solvent – isooctane).

Reaction temperature has a relatively strong influence on the ratio of *n*-alkanes with even and odd carbon atom number. This fact is well documented in Fig. 3, which shows a dependence of the content of alkanes *n*-C_{18} and *n*-C_{17} on reaction temperature. It is apparent that as the reaction temperature is increased the content of *n*-heptadecane increases at the expense of *n*-octadecane. The content of *n*-heptadecane linearly increases with temperature and the trend seems to be very similar for all the catalysts used. On the other hand, there are larger differences in *n*-octadecane content between the catalysts used, especially at the highest reaction temperature (340 °C).

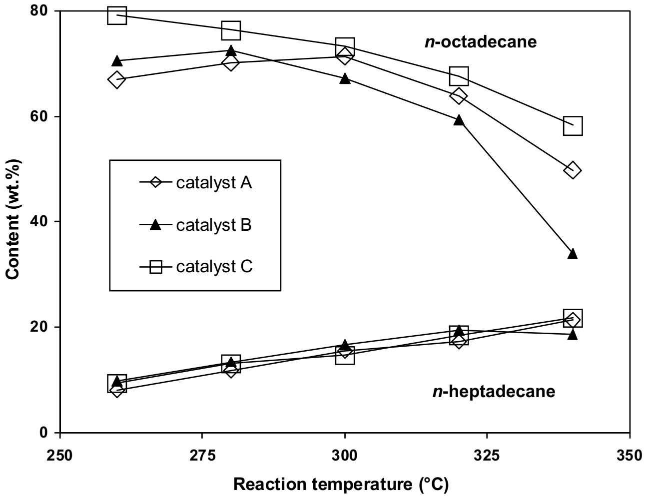

Fig. 3. Content of *n*-octadecane and *n*-heptadecane in OLP in dependence on reaction temperature and the catalyst used (content is calculated on OLP without inert solvent – isooctane).

Table 4
Composition of selected OLPs (organic liquid products) – catalyst A.

Reaction temperature Nature of OLP Component	260 °C Heterogeneous Content (wt.%)	340 °C Homogeneous Content (wt.%)
i-Octane (inert solvent used for feed dilution)	41.9	45.6
n-Alkanes ⩽ *n*-C_{14}	1.0	1.2
n-Pentadecane	0.7	0.2
n-Hexadecane	1.8	2.1
n-Heptadecane	4.7	11.6
n-Octadecane	39.6	27.1
n-Alkanes ⩾ *n*-C_{18}	1.2	1.4
i-Alkanes [a]	2.5	10.7
Palmitic acid (C16:0)	0.1	<0.05
Stearic acid (C18:0)	0.6	<0.05
n-Hexadecanol	<0.05	<0.05
n-Octadecanol	0.1	<0.05
Monoglycerides	0.1	<0.05
Diglycerides	0.2	<0.05
Triglycerides	5.5	<0.05
Acid number (mg KOH g^{-1})	0.7	<0.1

[a] GC–MS analysis proved that they are especially C_{16} up to C_{18} *i*-alkanes and a small or trace amounts of cycloalkanes and aromatics, respectively.

Similar dependencies can be observed also with respect to pair of alkanes *n*-C_{16}/*n*-C_{15}, but differences between the catalysts are not as prominent. This is probably the result of lower accuracy of *n*-alkane determination resulting from a smaller absolute amount of substances that are being determined (0.2–2.4 wt.%). Nevertheless, the trend of increasing content of *n*-C_{15} and decreasing content of *n*-C_{16} can be well seen in Fig. 4. From the composition of

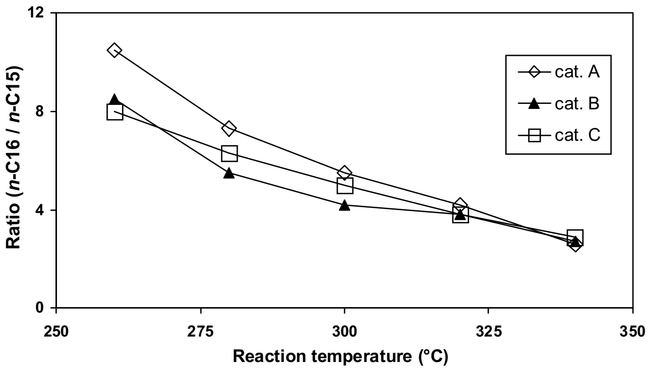

Fig. 4. Ratio of content of *n*-hexadecane and *n*-pentadecane in OLP in dependence on reaction temperature and the catalyst used.

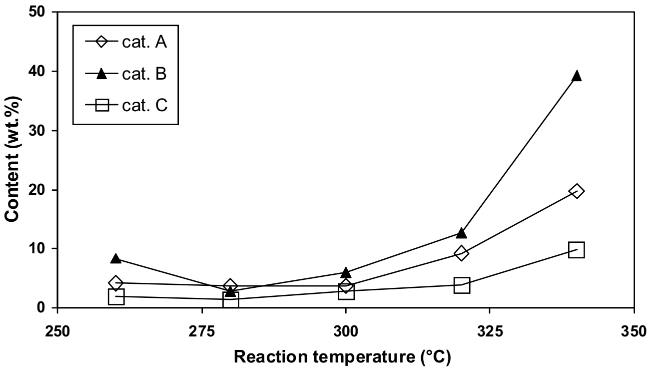

Fig. 5. Dependence of *i*-alkanes content (mostly C_{16}–C_{18}) in OLP on reaction temperature and the catalyst used (content is calculated on OLP without inert solvent – isooctane).

the reaction products, it can be deduced that splitting of saturated triglycerides takes place via two routes. The first one represents hydrogenation and a breakdown of triglycerides to respective *n*-alkanes with the same carbon atom number as the fatty acids in triglycerides. The second one involves hydrogenation and decarboxylation of fatty acids resulting in formation of *n*-alkanes having one carbon atom less than the respective carboxylic acids. From Figs. 3 and 4, it is apparent that with increasing reaction temperature decarboxylation comes into play more prominently. Reaction temperature has also a significant influence on the formation of *i*-alkanes. On Fig. 5, there is an obvious increase of the *i*-alkane content with increasing temperature for all tested catalysts; the formation of these hydrocarbons was most prominent in the case of catalyst B. The higher content of *i*-alkanes is advantageous from the fuel-use point of view because it could improve low-temperature properties of the product.

4. Conclusions

It follows from the preliminary experiments of rapeseed oil hydroprocessing that at a sufficiently high reaction temperature (above about 310 °C), the obtained organic liquid product (OLP) does not contain basically any intermediates nor any remaining raw material. It was determined that OLP contained mostly *n*-alkanes *n*-C_{18}, *n*-C_{17}. Depending on the type of the used catalyst and reaction temperature, OLP can also contain a significant amount of *i*-alkanes C_{16}–C_{18} (up to 40 wt.%). Taking into account the composition of the product, it can be concluded that it is suitable as a component for diesel fuel blending. However, further studies are necessary to verify and possibly adjust some of its fuel properties such as low-temperature properties, oxidation stability and corrosion properties, so it could be applied on an industrial scale.

Acknowledgement

This work was carried out as part of the research project MPO CR No. FT-TA3/074.

References

[1] Agropalma. <http://www.agropalma.com> [Accesed 2008].
[2] Mailhe MA. Sur la décomposition catalytique de l'huile de requin. Bull Soc Chim France 1922;31:249–52.
[3] Mailhe A. Action des chlorures métalliques sur les corps gras. J des Usines a Gaz 1923;47:321–4.
[4] Kobayashi K, Yamaguchi E. Artificial petroleum from fish oils. J Chem Ind Japan 1921;24:1399–420.
[5] Chang CC, Wan SW. China's motor fuels from tung oil. Ind Eng Chem 1947;39:1543–8.
[6] U.S. Patent 4,102,938; 1978.
[7] British Patent 2,039,943 A; 1980.
[8] Weisz PB, Haag WO, Rodewald PG. Catalytic production of high-grade fuel (gasoline) from biomass compounds by shape-selective catalysis. Science 1979;206:57–8.
[9] Katikaneni Sai PR, Adjaye JD, Bakhshi NN. Studies on the catalytic conversion of canola oil to hydrocarbons: influence of hybrid catalysts and steam. Energ Fuel 1995;9:599–609.
[10] Katikaneni Sai PR, Adjaye JD, Bakhshi NN. Catalytic conversion of canola oil to fuels and chemicals over various cracking catalysts. Can J Chem Eng 1995;73:484–97.
[11] Idem RO, Katikaneni Sai PR, Bakhshi NN. Thermal cracking of canola oil: reaction products in the presence and absence of steam. Energ Fuel 1996;10:1150–62.
[12] Twaiq FA, Zabidi Noor AM, Bhatia S. Catalytic Conversion of palm oil to hydrocarbons: performance of various zeolite catalysts. Ind Eng Chem Res 1999;38:3230–7.
[13] Twaiq FA, Mohamed AR, Bhatia S. Liquid hydrocarbon fuels from palm oil by catalytic cracking over aluminosilicate mesoporous catalysts with various Si/Al ratios. Micropor Mesopor Mater 2003;64:95–107.
[14] Twaig FA, Mohamed AR, Bhatia S. Performance of composite catalysts in palm oil cracking for the production of liquid fuels and chemicals. Fuel Proc Tech 2004;85:1283–300.
[15] Stumborg M, Wong A, Hogan E. Hydroprocessed vegetable oils for diesel fuel improvement. Bioresour Technol 1996;56:13–8.
[16] da Rocha Filho GN, Brodzki D, Djéga-Mariadassou G. Formation of alkanes alkylcykloalkanes and alkylbenzenes during the catalytic hydrocracking of vegetable oils. Fuel 1993;72:543–9.
[17] Gusmao J, Brodzki D, Djéga-Mariadassou G, Frety R. Utilization of vegetable oils as an alternative source for diesel-type fuel: Hydrocracking on reduced Ni/SiO_2 and sulphided Ni–Mo/γ-Al_2O_3. Cat Today 1989;5:533–44.
[18] Carmichael H. ICIS chemical business 2006; 15–24 May, 2006. p. 21.
[19] Anon. Hydrocarbon Processing 2006. Design Diesel: 27–28.
[20] NesteOil. <http://www.nesteoil.com> [Accesed 2008].
[21] Jakkula J, Aalto P, Niemi V, Kiiski U, Nikkonen J, Mikkonen S et al. WO 2004/022674 A1, EP 1 396 531 A2, US 2004/0055209 A1.
[22] Hodge C. California Energy Comission. Workshop on Bioenergy; 9 March 2006.
[23] ConocoPhillips. <http://www.conocophillips.com/Tech/emerging/index.htm> [Accesed 2008].
[24] Petrobras. <http://www2.petrobras.com.br/tecnologia/ing/hbio.asp> [Accesed 2008].
[25] Syntroleum. <http://www.syntroleum.com/proj_rba_biofining.aspx> [Accesed 2008].
[26] Holmgren J, Gosling C, Marinangeli R, Marker T, Faraci G, et al. New developments in renewable fuels offer more choice. Hydrocarbon Process. 2007;9:67–72.

Catalytic Transformation of Triglycerides in Refineries – a Promising Route to Clean Fuels and Feedstocks for Petrochemicals

*VON D. KUBIČKA, J. LEDERER, Z. BĚLOHLAV**

Abstract

Direct conversion of vegetable oil to hydrocarbons is a suitable technology not only for the production of automotive fuels. The article discusses the basic aspects of rapeseed-oil hydrotreatment to produce hydrocarbons and the possibilities to use them as a feedstock for the production of light olefins, namely ethene and propene.

Introduction

The use of renewable energy sources including biomass has been at the center of scientific attention for many years. It is the result of the efforts to slow down the rate of accumulation of carbon dioxide in the atmosphere and to ensure further sustainable development of the rural areas. Despite the heated discussion on the sustainability of biomass exploitation to cover the energetic needs of the society, it seems that biomass will become an indispensable supplementary raw material for production of energy and chemicals. While electric energy can be produced from a wide variety of sources besides biomass (e. g. solar, wind, geothermal and water energy), the only renewable alternative for the production of transportation fuels and chemicals is currently biomass.

It has been previously reported that hydrotreatment of rapeseed oil over a sulfided NiMo catalyst yields hydrocarbons quantitatively at a hydrogen pressure 0.7 MPa and reaction temperatures above 310 °C [1–3]. The main reaction products were n-heptadecane and n-octadecane. Their concentrations in the final product were influenced by reaction conditions – the concentration of n-heptadecane increased at the expense of n-octadecane concentration as a result of the increasing reaction temperature and the decreasing reaction pressure. Nevertheless, n-octadecane was the main product over the whole range of investigated experimental conditions. Based on the composition of the liquid and gaseous products, which consisted predominantly of propane, methane and carbon oxides, the following reaction mechanism was proposed (Fig. 1). The formation of n-C_{17} and n-C_{18} is explained by two parallel competing reactions – hydrodeoxygenation in which oxygen is eliminated in the form of water and octadecane is formed, and hydrodecarboxylation which is characterized by elimination of CO_2 and formation of heptadecane. Prior to both reactions the double bonds present in vegetable oil are saturated. Formed CO_2 undergoes subsequent hydrogenation yielding CO and methane.

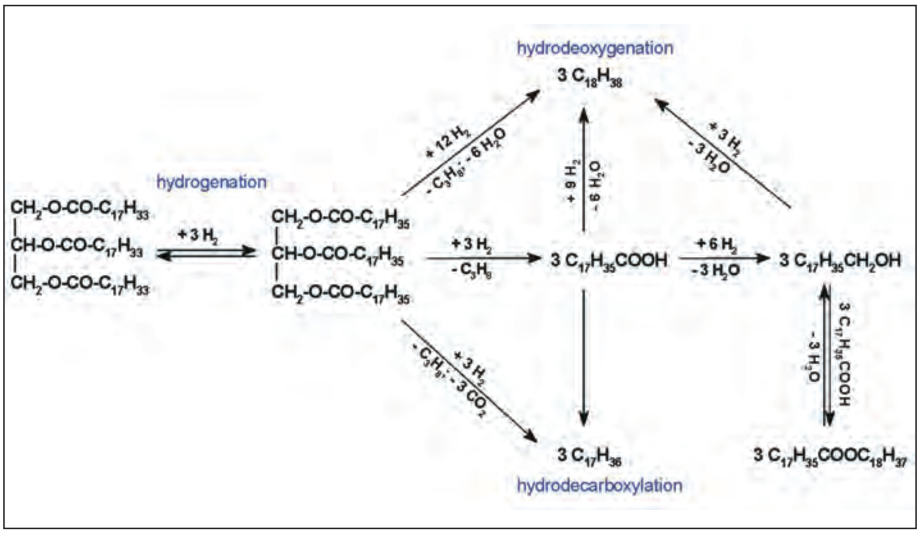

Fig. 1 Reaction mechanism of rapeseed oil hydrotreatment [1]

The aim of the present work is to investigate the conversion of rapeseed oil over a NiW hydrotreatment catalyst, particularly the effects of reaction temperature and pressure on rapeseed oil conversion and on distribution of hydrocarbon products. With regard to the potential industrial application of the process, the work focuses on upgrading of the neat hydrocarbons and their mixtures with crude-oil fractions by steam cracking to light olefins.

Experimental

The catalytic conversion of rapeseed oil to hydrocarbons was studied in a bench-scale experimental unit. The unit consists of an electrically heated flow reactor of inner diameter equal to 17 mm. There is a thermowell (outer diameter 5 mm) placed along the axis of the reactor containing three thermocouples. The position of the thermocouples is adjustable and they are usually located at positions corresponding to the inlet, middle and outlet of the catalyst bed. The outlet from the reactor can be heated to prevent solidification of reaction products. The experimental unit is equipped with measurement and control of temperature, pressure and feed flows (both liquid and gaseous feeds).

Refined rapeseed oil and hydrogen (99 vol.%) were used as feedstocks. The reaction was carried under a large molar excess of hydrogen (100:1) and constant WHSV equal to 1 h^{-1}. Reaction temperature was varied in the range of 250–310 °C at two pressure levels (0.7 and 7 MPa). A commercial hydrotreatment NiW catalyst placed in the isothermal zone of the reactor was employed in the experiments. The catalyst bed consisted of a mixture of the catalyst and silicon carbide (1:1 vol./vol.) in order to improve reaction heat removal and liquid flow distribution. There was a layer of silicon carbide above and below the catalyst bed. The catalyst was activated in-situ prior to the experiments by sulfidation using dimethyl disulfide dissolved in isooctane (5 vol.%) at 350 °C. The sulfidation temperature was reached by gradually increasing temperature at a heating rate less than 30 °C/h under a hydrogen flow.

---

* D. Kubička, J. Lederer, VUAnCH, Department of Refining and Petrochemical Research, Litvínov, Czech Republic, (E-Mail: David.Kubicka@vuanch.CZ); Z. Bělohlav, Institute of Chemical Technology Prague, Department of Organic Chemistry, Prague, Czech Republic. Paper, presented at the DGMK Conference “Future Feedstocks for Fuels and Chemicals”, September 29 – October 1, 2008, Berlin, Germany.

0179-3187/09/I

The liquid products were periodically withdrawn from the liquid-gas phase separator that was kept at 80 °C to prevent solidification of the products (n-alkanes) and reaction intermediates (stearic acid, saturated triglycerides) in the separator. These products were analyzed by gas chromatography after separation of the water phase. The gaseous products were analyzed off-line by using a GC equipped with a three-column system and two detectors – flame-ionization detector for hydrocarbons and thermal-conductivity detector for permanent gases.

Pyrolysis (steam cracking) of hydrocarbons obtained by hydrogenating rapeseed oil and of their mixtures with traditional crude-oil-derived steam-cracking feedstocks was studied by pyrolysis gas chromatography. The key feature of this method is the direct connection of the pulse flow reactor to a chromatographic column [4]. The pyrolysis of hydrocarbons takes place in the pyrolysis reactor that consists of a thin silica glass tube filled with fine inert silicon carbide powder (particle size – 0.1 mm). The reactor can be heated up to 810 °C by the electrical furnace equipped with precise temperature control. There is a dosing unit in the upper part of the reactor that makes it possible to inject gaseous, liquid or solid samples together with a carrier gas. Products and unconverted hydrocarbons are then analyzed in two sequential gas chromatographs allowing separate analysis of pyrolysis gas (hydrogen and C_1–C_4 hydrocarbons), pyrolysis gasoline (C_5–C_{11} hydrocarbons) and pyrolysis oil (hydrocarbons C_{12+}).

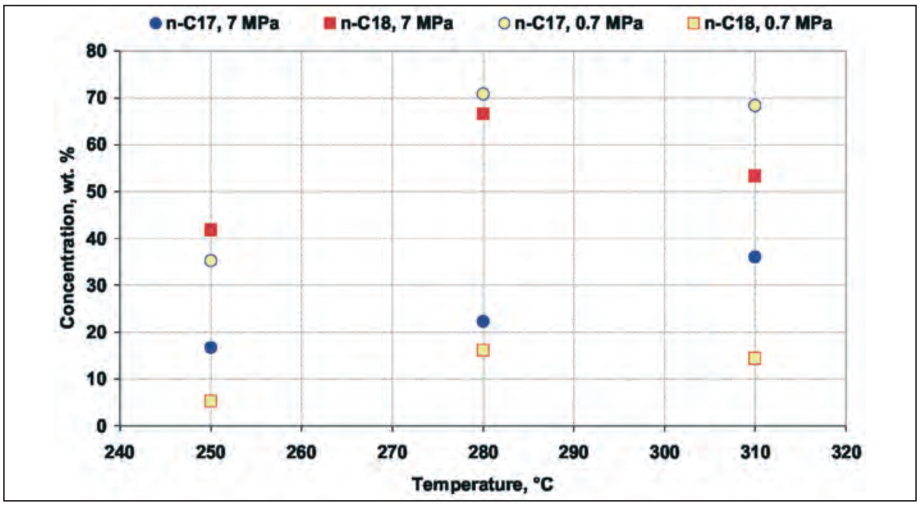

Fig. 2 Distribution of n-alkanes in the products of rapeseed oil hydrotreatment at 310 °C, 7.0 MPa. WHSV = 1 h^{-1}, H_2/RO = 102 mol·mol^{-1}

Results and Discussion

Total or nearly complete conversion of rapeseed oil was achieved over NiW catalyst at reaction temperatures of 280 °C and higher. The liquid products consisted almost exclusively of n-heptadecane and n-octadecane (Table 1). On the other hand, lower conversion of triglycerides was observed at 250 °C. In addition to hydrocarbons, the liquid-phase products included stearic acid, its esters and other oxygenates. The concentration of n-octadecane and n-heptadecane (ca. 90 wt.%) corresponds well with the concentration of C_{18} fatty acids making up triglycerides of rapeseed oil (ca. 93 wt.%). Similarly, the concentration of n-pentadecane and n-hexadecane (ca. 5 wt.%) is in good agreement with the concentration of C_{16} fatty acid chains in the triglycerides (ca. 6 wt.%). This agreement suggests indirectly that C_{16} and C_{18} hydrocarbons originate from total hydrogenation (hydrodeoxygenation) of corresponding fatty acid chains and that C_{15} and C_{17} are formed via a different reaction pathway which includes the loss of one carbon atom, e. g. decarboxylation. n-Alkanes were, however, not the only hydrocarbon products found. Small amounts of isomers (< 1 wt.%) of C_{15}–C_{18} n-alkanes were observed at 310 °C. Moreover, at 0.7 MPa and 310 °C alkenes were found in the products as well (ca 1 wt.%).

These results are in a good agreement with the hydrotreatment of rapeseed oil over NiMo catalyst [1–3], where the formation of hydrocarbons was ascribed to hydrodeoxygenation (hydrocarbons with even number of carbon atoms) and to hydrodecarboxylation (hydrocarbons with odd number of carbon atoms). The formation of hydrocarbons is accompanied by formation of water, in the former case, and of carbon dioxide, in the latter case. The share of these reactions is significantly influenced by reaction temperature as well as pressure (Fig. 2). A fair comparison of the temperature and pressure effects on the selectivity can be obtained particularly at 280 and 310 °C since the conversion is the same, namely 100%.It can be seen that the concentration of n-octadecane increases with decreasing reaction temperature and increasing reaction pressure at the expense of n-heptadecane concentration. In other words, the hydrodeoxygenation is favored by lower reaction temperature and higher hydrogen pressure, while hydrodecarboxylation is promoted by higher reaction temperature and lower hydrogen pressure. Similar conclusions were reached previously for NiMo catalysts [1–3].

Table 1 **Composition of liquid products of rapeseed oil (RO) hydrotreatment at 250–310 °C and 0.7 and 7 MPa. WHSV = 1 h^{-1}, H_2/RO = 102 mol·mol^{-1}**

Reaction conditions						
Temperature, °C	310	280	250	310	280	250
Pressure, MPa	7.0	7.0	7.0	0.7	0.7	0.7
Liquid products composition, wt. %						
n-Pentadecane	2.00	1.26	0.92	4.12	3.83	1.80
n-Hexadecane	3.20	3.87	2.47	1.38	1.12	0.32
n-Heptadecane	36.02	22.29	16.65	68.34	70.82	35.29
n-Octadecane	53.39	66.60	41.85	14.41	16.15	5.27
Stearic acid	0.00	0.12	4.14	0.01	0.13	13.47
Unknown oxygenates	0.59	0.47	2.41	0.77	1.44	1.13
Esters of fatty acids	0.01	0.59	17.77	0.01	0.03	13.98
Triglycerides	0.01	0.00	3.17	0.00	0.00	11.35
Total	95.23	95.20	89.39	89.04	93.52	82.62

Particularly the effect of hydrogen pressure on the selectivity is significant. The main hydrocarbon product obtained at 7 MPa is n-octadecane whereas at 0.7 MPa the predominant product is n-heptadecane (Fig. 2). This is in contrast to NiMo catalyst [1–3] where n-octadecane was always the main hydrocarbon produced, even though its concentration decreased with decreasing hydrogen pressure. The distribution of n-alkanes is affected by the catalyst deactivation as well. The mass ratio of C_{18}/C_{17} increased from 1.2 (a value found for a fresh catalyst) to 2.4 after streaming for 90 hours under constant reaction conditions (Fig. 3). The most significant changes were observed during the first 20 hours of streaming, after that only a minor increase of the C_{18}/C_{17} mass ratio could be seen (Fig. 3).

Useful information about the course of the hydrotreatment reactions can be obtained from experiments under only partial conversion of triglycerides, e. g. at 250 °C, since they allow the following and identification of key reaction intermediates. Two major

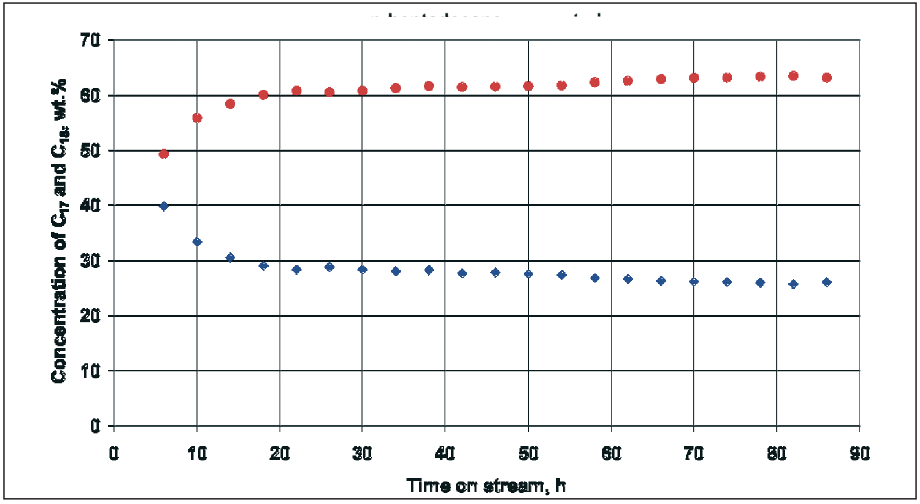

Fig. 3 Change in n-alkane concentration in the products of rapeseed oil (RO) hydrotreatment at 310 °C, 7.0 MPa, WHSV = 1 h^{-1}, H_2/RO = 102 mol·mol^{-1}

groups of intermediates were observed at 250 °C – fatty acids and alkyl esters of fatty acids. The group of fatty acids was almost exclusively composed of stearic acid and palmitic acid, i. e. of saturated fatty acids. The alkyl esters were, in contrast to fatty acids, unexpected intermediates and they were identified as stearylstearate and stearylpalmitate. Their presence can be explained by esterification of fatty acids by fatty alcohols as these are plausible intermediates in hydrogenation of fatty acids to hydrocarbons and were found in small concentrations in the reaction products. Reduced hydrogen pressure led to the increase in the concentration of stearic acid and esters (Table 1). It seems that the lower hydrogen pressure suppresses the consecutive hydrogenation of fatty acids to alcohols and thus results in a higher concentration of fatty acids and a lower concentration of their esters.

It is very well known that n-alkanes are the best feedstock for production of light olefins, i. e. ethene and propene, by steam cracking of hydrocarbons. The high concentrations of n-alkanes in the products of rapeseed oil hydrotreatment make these products viable as an alternative renewable feedstock for these basic petrochemicals. Besides neat hydrocarbon product obtained by hydrotreatment of rapeseed oil at 310 °C and 7 MPa, mixtures of these hydrocarbons with heavy naphtha and distillation residue from hydrocracking, i. e. with typical feedstocks of the steam cracker unit in Litvinov, were prepared. The concentration of hydrocarbons obtained by rapeseed oil hydrotreatment in these mixtures ranged from 5–20 wt.%.

The results of laboratory pyrolysis experiments are summarized in Table 2. Very high yields of ethene (43 wt.%) and propene (19 wt.%), in comparison with the traditional feedstocks, were obtained in pyrolysis of rapeseed-oil-hydrotreatment products (Table 2). Furthermore, addition of these hydrocarbons into the traditional crude-oil-derived feedstocks resulted in increased formation of ethene and propene. The concentration of ethene and propene increased linearly with the increasing concentration of the hydrocarbons obtained by hydrotreatment of rapeseed oil (Table 2). This increase was accompanied by reduced formation of the undesired and less valuable pyrolysis oils (Table 2).

A comparison of the results of pyrolysis of naphtha and distillation residue from hydrocracking with added hydrocarbons originating from rapeseed oil hydrotreatment reveals that the addition of hydrocarbons from rapeseed oil hydrotreatment has an analogous effect on the yield vectors of both crude-oil-derived fractions. This suggests that hydrocarbons obtained by hydrotreatment of rapeseed oil could be added to a wide variety of steam cracking feedstocks.

Conclusions

The performance of hydrotreatment NiW catalyst is in general in accordance with the catalytic performance of other hydrotreatment catalysts (NiMo, CoMo). The main reaction products are hydrocarbons, mainly octadecane and heptadecane. They are formed by hydrodeoxygenation and hydrodecarboxylation, respectively, of C_{18} fatty acids that make up the triglycerides of rapeseed oil. The complete conversion of these triglycerides is achieved already at 280 °C. The extent of the principal reactions depends on reaction temperature and pressure. Particularly, the dependence on reaction pressure is very strong – n-octadecane is the main product at 7 MPa while n-heptadecane prevails at 0.7 MPa.

The synthesized hydrocarbons were pyrolyzed both neat and mixed with hydrocarbon fractions. The pyrolysis of neat hydrocarbons resulted in very high yields of ethene and propene, 43 and 19 wt.%, respectively. The yield of light olefins from the pyrolysis of mixtures depended on the concentration of hydrocarbons prepared from rapeseed oil and corresponded to a linear combination of yields obtained by pyrolysis of individual feedstocks. Moreover, the yields of less valuable heavy products decreased as a result of addition of hydrocarbons obtained from vegetable oil hydrotreatment.

The financial support given by the Ministry of Industry and Trade of the Czech Republic (project FT-TA3/074) is gratefully acknowledged.

Literature

[1] Kubička D.: Future Refining Catalysis – Introduc-

Table 2 **Yield of laboratory pyrolysis of mixtures of crude-oil fractions and products of rapeseed oil hydrotreatment.** N – naphtha, H – distillation residue from hydrocracking, R – products of rapeseed oil hydrotreatment (composition: n-C18 – 63 wt.%, n-C17 – 26 wt.%, see Fig. 3 – reaction time 86 h)

Sample	R	N	H	N + 5% R	N + 10% R	N + 20% R	H + 5% R	H + 10% R	H + 20% R
Methane	8.0	9.2	7.2	8.9	8.8	9.0	7.2	7.8	7.6
Ethane	3.3	2.2	1.7	2.1	2.1	2.8	1.7	2.1	2.0
Ethene	43.4	19.2	31.3	20.6	21.6	23.1	33.4	32.3	34.3
Propane	0.6	0.3	0.4	0.3	0.3	0.4	0.4	0.5	0.5
Propene	19.0	13.5	15.5	13.7	13.8	14.6	16.0	16.1	16.4
Acetylene	0.3	0.3	0.6	0.3	0.3	0.3	0.6	0.5	0.5
2-Butene	0.9	1.1	0.9	1.1	1.1	1.1	0.9	0.9	0.9
1-Butene	4.8	2.2	3.7	2.3	2.4	2.6	4.1	3.6	4.0
iso-Butene	0.2	2.2	1.7	2.1	2.0	1.8	1.5	1.5	1.3
1,3-Butadiene	8.3	6.4	8.3	6.6	6.6	6.2	8.4	8.2	8.4
Fraction C_{5-6}	4.5	10.5	6.0	10.3	10.1	9.1	5.6	6.1	5.7
Benzene	2.8	5.8	5.3	5.7	5.7	5.3	4.9	5.5	5.0
Toluene	0.9	7.7	2.8	7.4	7.2	6.5	2.5	2.9	2.6
Ethylbenzene	0.1	1.3	0.4	1.3	1.3	1.0	0.4	0.4	0.4
Xylenes	0.1	4.1	0.7	3.9	4.0	3.3	0.6	0.7	0.6
Styrene	0.3	1.5	0.7	1.4	1.4	1.3	0.7	0.8	0.7
Naphthalene	0.1	0.5	0.6	0.4	0.4	0.5	0.5	0.6	0.5
Other C_{7-12}	0.8	8.7	3.4	8.6	8.2	7.4	3.0	3.3	2.9
Pyrolysis oils	1.2	2.5	7.6	2.3	2.2	3.0	6.6	5.4	4.7

tion of Biomass Feedstocks. Collect. Czech. Chem. Commun. 73 (2008) 1015.

[2] Kubička, D.; Chudoba, J.; Šimáček, P.: Catalytic conversion of vegetable oils into transport fuels. Europacat-VIII, 26–31.8. 2007; Turku, Finland.

[3] Šimáček, P.; Kubička, D.; Šebor, G.; Pospíšil, M.: Hydroprocessed rapeseed oil as a source of hydrocarbon-based biodiesel. Fuel 2008, in press (http://dx.doi.org/10.1016/j.fuel.2008.10.022).

[4] Bělohlav, Z.; Herink, T.; Lederer, J.; Marek, J.; Rachová, N.; Svoboda, P.; Zámostný, P., Vojtová, D.: Evaluation of pyrolysis feedstock by pyrolysis gas chromatography. Petrol. Chem. 45 (2005) 118.

__David Kubička__ works as a researcher at the Research Institute of Inorganic Chemistry (VÚAnCh), Department of Refining and Petrochemical Research, in Litvínov (Czech Republic). He graduated at the Institute of Chemical Technology Prague (Czech Republic) in 1999 and obtained his Ph.D. in Chemical Engineering and Catalysis from the Laboratory of Industrial Chemistry, Åbo Akademi in Turku (Finland) in 2005. His main research interests are catalytic transformations of biomass-derived feedstocks into automotive fuels and petrochemicals.

__Jaromír Lederer__ is the head of the Department of Refining and Petrochemical Research at Unipetrol's R&D organization – VÚAnCh. In addition he is the associated professor at the Prague Institute of Chemical Technology. He is involved in basic petrochemical processes especially in olefins and aromatics chemistry. His main attention is given to the simulation and optimization of processes installed in a steam cracker including processes for the utilization of steam cracking by-products.

__Zdenìk Bìlohlav__ is a professor at the Institute of Chemical Technology and an editor of the Association journal "Chemické listy". He is involved in chemical reactors and pharmaceutical processes mathematical modeling, optimization and scale-up. He especially attends to the design of experiments and laboratory or industrial data handling and mining.

Fuel 238 (2019) 98–110

Contents lists available at ScienceDirect

Fuel

journal homepage: www.elsevier.com/locate/fuel

Full Length Article

Hydrotreatment of straw bio-oil from ablative fast pyrolysis to produce suitable refinery intermediates

Miloš Auersvald, Bogdan Shumeiko, Dan Vrtiška, Petr Straka, Martin Staš, Pavel Šimáček, Josef Blažek, David Kubička*

University of Chemistry and Technology Prague, Department of Petroleum Technology and Alternative Fuels, Technická 5, 166 28 Prague, Czech Republic

GRAPHICAL ABSTRACT

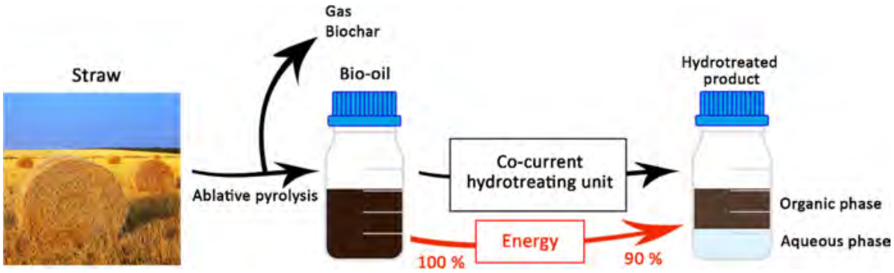

ARTICLE INFO

Keywords:
Hydrotreatment
Straw bio-oil
Ablative fast pyrolysis (AFP)
Biofuels
Sulphided catalysts

ABSTRACT

To meet the expected requirements of the proposed EU Renewable Energy Directive for the next decade (RED II), it is necessary to increase the availability of second-generation biofuels. One promising way of doing this involves using ablative fast pyrolysis units to transform an agricultural by-product, for example straw, into bio-oil. To obtain straw bio-oil suitable for processing in a typical refinery, we optimized the key parameters of its hydrotreatment. For the upgrading, a continuous flow reactor with a fixed bed of a commercial sulphide NiMo/Al_2O_3 catalyst was used. The reaction temperature and pressure were tested at 240–360 °C and 2–8 MPa, respectively. The reaction off-gas was analysed by GC-FID/TCD. A detailed physicochemical analysis of the products was carried out. Under most conditions tested, the product was separated into an aqueous and an organic phase. For the best products, > 85% of the feed energy content remained in the organic phase and a significant decrease in viscosity and acidity was achieved. The product prepared at 360 °C and 8 MPa was the only one completely miscible with straight-run gas oil and, thus, appears to be the most suitable for co-processing in a refinery.

1. Introduction

Fossil fuels are currently used to cover about 78% of our global energy demand [1]. Their reserves are, however, finite and their use has adverse environmental impacts as their combustion contributes to a gradual increase in CO_2 concentration in the atmosphere. Apart from CO_2 itself, biomass is the only renewable feedstock containing carbon that can be converted to liquid fuels [2]. Considering the ever-growing human population and the associated growing demand for food and water, it follows that a further increase in the production of the first-generation biofuels is not sustainable and thus not acceptable. Consequently, the EU Commission proposal for the new EU Directive (RED II)

---

* Corresponding author.
E-mail address: david.kubicka@vscht.cz (D. Kubička).

https://doi.org/10.1016/j.fuel.2018.10.090
Received 25 June 2018; Received in revised form 4 October 2018; Accepted 15 October 2018

demands a decrease in the food-based biofuels from 7% (energy content) in 2021 down to 3.8% by 2030. In addition, the EU COM draft for RED II proposes a sub-target of 3.6% (energy content) blending for advanced biofuels originating from residues either directly from agriculture or indirectly as a by-product from food/feed production. An example of acceptable feedstock for advanced biofuels production is lignocellulosic biomass, such as straw, also listed in Annex IX of the drafted EU directive [3]. The final RED II directive is expected to be available in Q3 or Q4 of 2018 and is currently getting developed in a joint consultation ("trilogue") between EU Commission, EU Council and EU Parliament.

A variety of biomass-upgrading technologies was investigated, such as pyrolysis, gasification, hydrothermal upgrading, depolymerisation, *etc.* [4]. Among them, pyrolysis stands out as one of the few biofuel technologies that can handle a range of biomass feedstocks (agri-residues, forest residues, energy crops, municipal solid wastes). Hence, it is an attractive option for expanding the biomass availability by using less desirable biomass. In this context, ablative fast pyrolysis (AFP) is of particular interest as it does not require reducing the particle size of biomass, which is a significant advantage over fluidized bed pyrolysis requiring energy-intensive grinding when it comes to straw pyrolysis [5]. Also, the possible mobility of AFP unit would be beneficial for straw upgrading as it would allow avoiding the inefficient transport of straw biomass over long distances (80% of straw cost are logistic cost) [5]. Finally, AFP is also characterized by low construction and operational costs [6].

From the liquid biofuels point of view, the key product of pyrolysis is the liquid called bio-oil or pyrolysis oil whose yield is typically up to 75 wt% [7]. The yields of by-products, *i.e.* gases and char, are typically 13 and 12 wt%, respectively [7]. An efficient use of these by-products, *i.e.* gases to heat, *e.g.* the spinning hot rotor of the pyrolysis device and char for rejuvenation of tired soils, also reduce the bio-oil production prices [8]. Thanks to its composition, bio-oil could become one of the alternative sources of renewable energy which could provide liquid biofuels in future. However, crude bio-oil has due to its high oxygen content and degree of unsaturation some undesirable properties such as (i) low thermal and oxidation stability, (ii) high acidity and thus high corrosiveness and (iii) immiscibility with non-polar petroleum fractions. These properties prevent direct upgrading of bio-oils in refineries and appropriate upgrading (stabilization) of bio-oil is necessary prior to its upgrading or co-processing in a conventional refinery.

The possible co-processing of partially upgraded bio-oils seems especially advantageous in a situation when there are overcapacities in the EU refining sector [9] as it would promote employment in the sector and its further development while securing second-generation biofuels. When considering available refinery processes for bio-oil co-processing, hydrotreatment appears to be more beneficial than catalytic cracking as it affords higher yields and better quality of the upgraded product. This is a consequence of deeper deoxygenation and suppressed formation of gaseous and solid by-products [10]. In addition, refinery overcapacities could also be used for the primary bio-oil upgrading (stabilization) by their revamping to satisfy (meet) the specific requirements of bio-oil treatment.

Numerous detailed studies [11–14] deal with a wide variety of catalysts and process conditions for hydrotreatment/deoxygenation of lignocellulosic bio-oils to fuels and other valuable products. With respect to their active phase, the catalysts for bio-oil hydrotreatment can be divided into the following groups: (i) noble metals, (ii) transition metals and (iii) metal sulphides. Many of them are used in crude oil refining processes [15].

Among noble metals, mainly Pt, Pd, Ru and Rh were tested for bio-oil upgrading [11,16,17]. They have shown outstanding results in the conversion of oxygen-containing compounds present in bio-oils [18–20]. Unfortunately, their very high hydrogenation activity leads to increased hydrogen consumption and operating costs [21,22]. Another disadvantage of noble metal catalysts is that they can be poisoned by even small contents of sulphur present in lignocellulosic bio-oils. Due to the high acidity and water content in bio-oils, carbon supports that would not deteriorate too fast like, *e.g.* alumina supports have attracted considerable attention [23].

Transition metals have been studied as a possible alternative, the focus being on Ni, Mo, Co, Fe and Cu based catalysts [24,25] due to their good catalytic performance. In addition to metallic catalysts also phosphides, carbides and nitrides of transition metals have been investigated [13,14,26,27]. Zhao et al. [28] found that metal phosphide catalysts were more active in deoxygenation than the traditional $CoMoS/Al_2O_3$ and the commercial 5% Pd/Al_2O_3 catalysts.

Despite the promising performance of metallic catalysts, the sulphided catalysts, predominantly alumina-supported NiMo and CoMo catalysts, remain the preferred choice for bio-oil hydrotreatment thanks to being well-established and robust [29]. Their performance has been reviewed extensively by Patel et al. [30] and Mortensen et al. [10]. A wide range of experimental conditions have been covered in studies using sulphided catalysts in hydrotreatment of bio-oils originating from different feedstocks, but straw. Temperature and hydrogen pressure were varied between 200 and 450 °C and 1–29 MPa, respectively [23,25,31,32]. Due to the thermal instability of bio-oils, two-stage upgrading was often applied [11,23] with mild conditions in the first stage to remove the most reactive compounds and with more severe conditions in the second stage to eliminate recalcitrant oxygenates. The sulphur content of bio-oils is, compared to petroleum fractions, low, typically several hundred ppm [21,30]. Consequently, sulphided catalysts tend to lose their activity during hydrotreatment of bio-oils, unless a source of H_2S is added to protect the active sulphided phase of the catalyst from reduction [33]. The effects of H_2S and water on the deoxygenation of carbonyl, carboxylic, and guaiacyl groups over alumina-supported sulphided NiMo/CoMo catalysts were studied by Laurent et al. [34]. They concluded that H_2S increased the Bronsted acidity of the catalysts which promoted decarboxylation reactions, but it suppressed the deoxygenation of the carbonyl groups [34].

Nonetheless, sulphided catalysts showed good activity and selectivity in bio-oil hydrotreating [12,35] and if the stabilized (partially deoxygenated) bio-oil would be further upgraded in a refinery, the slightly increased sulphur content in comparison with the raw bio-oil would not cause any problems. Commercial hydrotreating catalysts (sulphided NiMo and CoMo) were investigated in a three-heating-zone reactor (170–250, 250–350, 350–450 °C) for converting a wood-derived bio-oil into renewable hydrocarbons by Horáček et al. [36]. The alumina-supported sulphided CoMo catalyst showed better selectivity to diesel-like products and deeper hydrogenation of gaseous intermediates (CO_x) than the sulphided NiMo catalyst. In contrast, the sulphided NiMo catalyst was found to be more active in decarboxylation and it was possible to reach a steady state production of hydrocarbons having a comparable boiling point distribution as petroleum-derived middle distillates [36]. However, the catalysts suffered from low stability of the alumina support material at high temperatures in the presence of water [33]. Similarly, Gholizadeh et al. [35] reported hydrotreating of palm bio-oil in a fixed bed flow reactor over $NiMo/Al_2O_3$ catalyst at 7 MPa hydrogen pressure and 370–450 °C. When increasing the temperature, the oxygen content in the upgraded product was reduced below 2 wt% [35].

Despite being a valuable sustainable renewable feedstock that could be abundantly available in the Europe, upgrading of bio-oil obtained from ablative fast pyrolysis of wheat/barley straw by its hydrotreatment has received only very little attention so far. Therefore, we report here the effect of key reaction parameters on the yields and properties of the hydrotreated products originating from straw bio-oil from ablative fast pyrolysis with the aim to obtain a product upgradeable in a conventional refinery rather than a fully-deoxygenated product. To the best of our knowledge, this has not been attempted in the previous studies. In addition, we propose for the first time the use of principal component analysis (PCA) classification of products to assess the degree

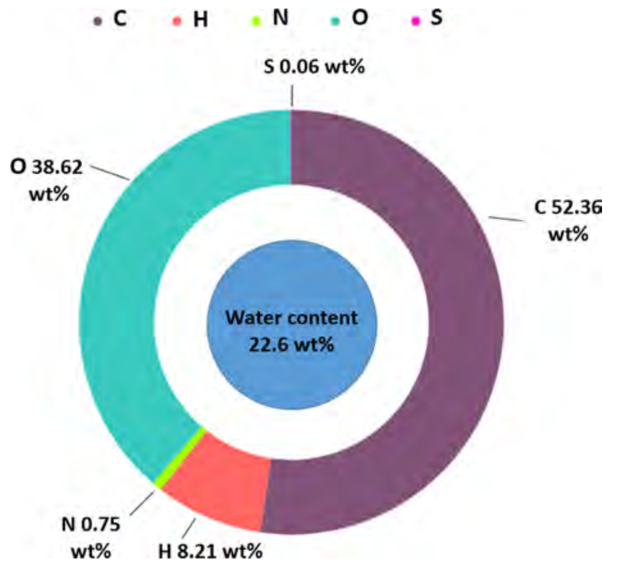

Fig. 1. Elemental composition and water content in bio-oil.

of deoxygenation of hydrotreated bio-oils allowing real time analysis of products and adjustment of reaction conditions.

2. Experimental

2.1. Materials

Straw bio-oil was produced at Fraunhofer UMSICHT by ablative fast pyrolysis of straw (wheat and barley straw, 1:1 w/w). The straw pellets were pressed onto a hot rotating disc and pyrolyzed at 550 °C with vapour residence time less than 1 s. After condensation at 2–5 °C, the liquid product spontaneously separated into an aqueous and an organic phase (bio-oil). For more details, see [37]. The bio-oil was filtered to remove any residual solids, doped with dimethyl disulphide (DMDS, ≥99.0%) supplied by Sigma-Aldrich to contain 0.5 wt% of DMDS to maintain the catalyst activity and used in the experiments. The basic properties of the straw bio-oil are summarized in Fig. 1 and Table 1. A conventional commercial sulphided NiMo/Al_2O_3 catalyst (5.5 wt% NiO and 28.3 wt% MoO_3) and hydrogen (99.9 vol%) supplied by SIAD (Czech Republic) were used in the experiments.

2.2. Bio-oil hydrotreating

Bio-oil was hydrotreated in an electrically heated fixed bed reactor (inner diameter 23 mm) having a thermo-well (outer diameter 4 mm) in its axis with 10 thermocouples. The reactor was loaded with 55 g of a NiMo catalyst. The catalyst particle sizes 0.25–0.42 in lower part and 0.85–1.5 mm in upper part of reactor were used. A metallic preheater was placed above the catalyst bed. Prior to the experiments, the catalyst was *in-situ* sulphided at 345 °C and 4 MPa using a mixture of hydrotreated gas oil and DMDS containing 3.8 wt% DMDS. The catalyst activation was followed by its stabilization using straight-run gas oil (0.23 wt% S) for 24 h at 340 °C, 4 MPa and WHSV ca 1·h^{-1}. Then, the temperature in the reactor was adjusted to the first tested temperature (240 °C) and bio-oil feeding in the reactor was started. The experiments were carried out at WHSV of approximately 1 h^{-1} and hydrogen flowrate of 90 l·h^{-1}. The reaction temperature and pressure were varied in the range 240–360 °C and 2–8 MPa, respectively. Liquid samples were collected for 2 h at each reaction condition from the moment when all reaction parameters were stabilized. Water phase was separated from organic phase that was analysed as described below by an array of analytical methods. During of each sampling period, the reaction offgas was also collected into a sampling bag and analysed by GC-FID/TCD. An overview of the experimental reaction conditions, products samples and corresponding times on stream is given in Results and Discussion section (Table 2).

Table 1
The properties of the bio-oil.

Parameter	Value
Density at 15 °C [g·cm^{-3}]	1.13
Kinematic viscosity at 40 °C [mm^2·s^{-1}]	140
Higher heating value [MJ·kg^{-1}]	23.3
Lower heating value [MJ·kg^{-1}]	21.5
Total acid number [mg KOH·g^{-1}]	98.9
Carboxylic acid number [mg KOH·g^{-1}]	54.3
Micro Conradson residue [wt%]	15

Table 2
An overview of experimental conditions, product samples and times on streams (TOS).

Sample	Average temperature in catalytic zone [°C]	TOS [h]	Sample	Average temperature in catalytic zone [°C]	TOS [h]
240/4	242	19	300/2	298	45
260/4	261	23	320/2	320	69
280/4	280	29	340/2	341	60
300/4	300	36	300/4	297	36
320/4	315	42	320/4	318	26
340/4	338	74	340/4	339	31
360/4	358	81	300/8	297	11
			320/8	319	7
			340/8	339	21
			360/8	361	52

2.3. Analyses of feed and products

Elemental composition (C, H, N, S) was determined using a Vario EL Cube analyser (Elementar). A Merck stearic acid standard and a standard by Elementar Analysensysteme GmbH (C: 67.68 wt%, H: 4.95 wt %, N: 0.69 wt%, S: 0.81 wt%) were used for the instrument calibration. The sample (5–15 mg) was burned in a pure oxygen atmosphere. Gaseous combustion products were separated after reduction in a purge and trap chromatographic system and finally detected by a thermal conductivity detector (TCD). The oxygen content was calculated by difference.

The water content was determined by a Karl Fischer volumetric titration according to the ASTM E203 using a METTLER TOLEDO DL38 device. A small amount of sample (0.02–0.05 g) was injected into a glass chamber containing HYDRANAL™-KetoSolver (Karl Fischer solvent, Honeywell). Titration was carried out by Karl Fischer titrant Composite 5 K (Riedel-de Haën).

Density at 15 °C and kinematic viscosity at 40 °C were determined by an SVM 3000 Stabinger Viscometer (Anton Paar). Micro Conradson carbon residue (MCR) was determined according to the ASTM D4530 standard method, by an NMC 420 device (NORMALAB ANALIS).

The higher heating value (HHV) was determined by an IKA 2000 device (Merci). Sample (0.5–1.0 g) was weighed into a crucible for reaching an ideal temperature increase of 3–5 °C·min^{-1}. The lower heating value (LHV) was calculated from the HHV reduced by the evaporation heat of the water in the sample and the water produced by the combustion of hydrogen.

Total acid number (TAN) and carboxylic acid number (CAN) were determined by a 716 DMS Titrino instrument (Metrohm AG). TAN was determined according to the ASTM D664, with KOH as a titrant, LiCl as an electrolyte and a mixture of toluene:isopropanol:water (100:99:1 V/V) as a solvent were used. CAN was determined by a titration method

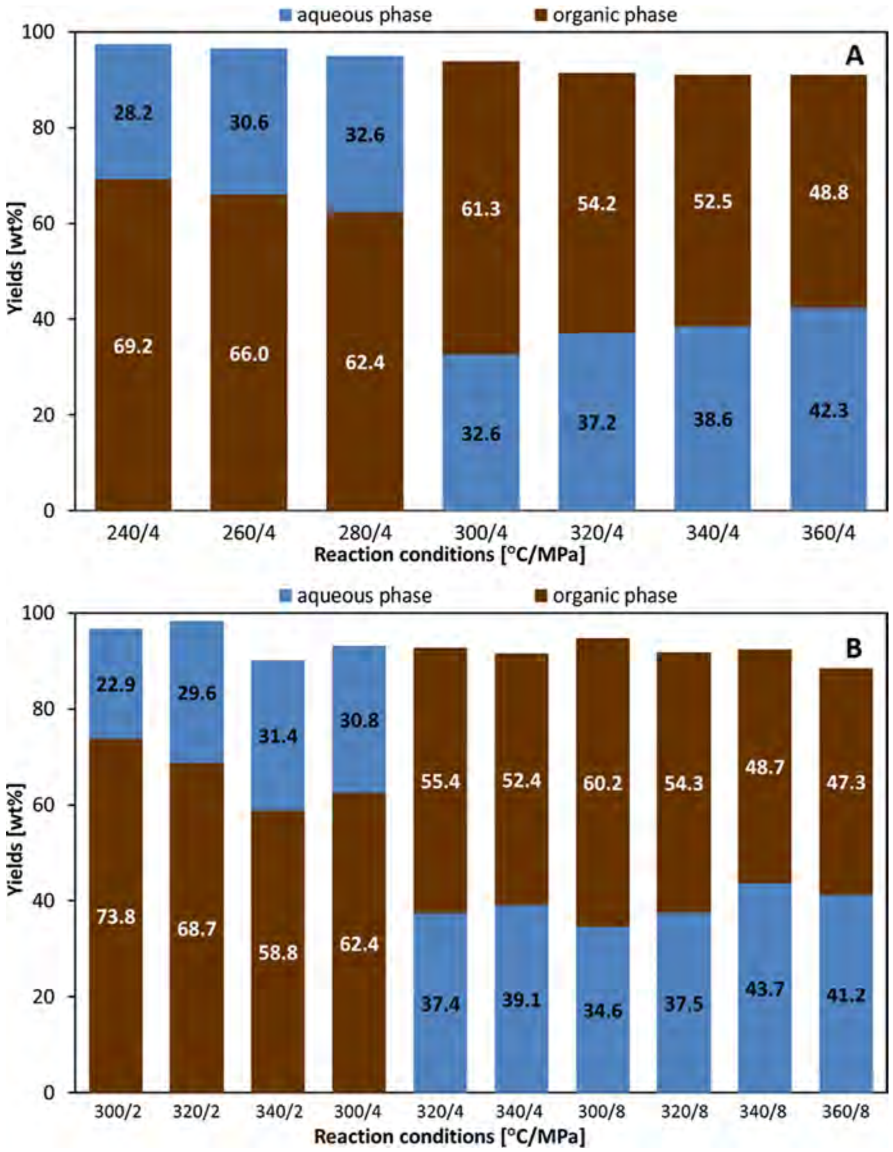

Fig. 2. Yields of organic and aqueous phases under different reaction temperatures at pressures (A) 4 MPa and (B) 2; 4 and 8 MPa.

[38], with tetrabutyl ammonium hydroxide as a titrant, tetraethyl ammonium bromide as an electrolyte, and isopropanol as a solvent were used.

Bio-oil and all liquid organic products were characterized by simulated distillation. Samples were dissolved in carbon disulphide (1 wt % solution) and introduced to a TRACE ULTRA gas chromatograph (Thermo Scientific) equipped with an on-column injector, Agilent J&W CP-SimDist UltiMetal (10 m × 0.53 mm × 0.17 µm) column, an FID detector and an oven cryogenic cooling system. The absolute accuracy of the simulated distillation was negatively affected by the presence of oxygenates in the samples, and thus a “recovery” parameter was calculated from the concentration and total chromatogram area for all samples to allow a comparison of samples. This parameter expresses the percentage of sample response related to the response of completely eluted hydrocarbons, which have, *per definition*, the “recovery” parameter equal to 100%.

All liquid samples (both organic and aqueous phases) were characterized by FTIR-ATR (Attenuated Total Reflection) technique. An infrared spectrometer IRAffinity-1 (Shimadzu, Japan) with Quest ATR accessory with a diamond crystal (Specac, USA) was used to record the FTIR spectra. LabSolution IR software (Shimadzu, Japan) was used as an interface between the spectrometer and the control computer. The spectra were recorded in the 4000–650 cm^{-1} region using the spectral resolution of 4 cm^{-1} and 128 scans.

Due to the complexity of the spectra, principal component analysis (PCA) was employed as a tool allowing a direct comparison of individual samples. PCA is a method used for a reduction of usually large data sets [39]. The original variables (*e.g.* spectroscopic data) are replaced by new variables called principal components (PCs) which are linear combinations of the original variables. The new variables are mutually orthogonal and uncorrelated. The first few principal components usually explain most of the relevant variability of the original dataset. Each sample gets its own set of values (scores) for each principal component, so it is possible to create plots of the score values and compare the samples based on their position in the plots.

Two analytical methods were used for analysis of gaseous products collected in 10 L Tedlar sampling bags: (i) determination of permanent gases and lighter hydrocarbons and (ii) determination of higher hydrocarbons and other organic compounds. The determination of permanent gases (H_2, CO, and CO_2) and light hydrocarbons and oxygenates

(C_1–C_5) was performed using a Hewlett Packard HP 6890 gas chromatograph equipped with a CP-Carbobond fused silica column (50 m × 0.53 mm × 5 µm) and two detectors; a flame ionization detector (FID) for detection of the hydrocarbons (C_1–C_5) and a thermal conductivity detector (TCD) for detection of the permanent gases. The effluent flowing out of the column was split into the detectors using a Y-piece Siltek MXT Connector (Restek). The content of higher hydrocarbons and other organic compounds was determined using an Agilent 6890 gas chromatograph equipped with an HP-PONA column (50 m × 0.2 mm × 0.5 µm) and an FID detector. Major higher hydrocarbons and other selected organic compounds were identified based on the retention times of pure substances and previous GC–MS analysis of biooil. The content of "other organic substances" including oxygenates and C_{6+} hydrocarbons was expressed as a sum using an estimated response factor of 1.2.

3. Results and discussion

3.1. Experiments performed

Two sets of experiments were performed, each with fresh catalyst at the beginning of the experiment. The first set was performed at a pressure of 4 MPa, the second set at pressures 2, 4 and 8 MPa. An overview of experimental conditions, designation of the gained product and times on stream in which they were obtained is listed in Table 2.

3.2. Mass and energy balance

The yields of liquids from bio-oil hydrotreating exceeded 90 wt% in the full range of experimental conditions (Fig. 2A and B), except product obtained at 360 °C and 8 MPa, where it attained 88.5 wt%. When considering the yield of gaseous products, the mass balance was almost completely closed. The observed slight differences in mass balance can be attributed mainly to losses during manipulation with samples and to a much smaller extent due to the formation of carbonaceous deposits on catalyst.

Reaction temperature had a pronounced effect on the yield of aqueous and organic phase. Under mild temperatures (< 300 °C), the yield of the aqueous phase was < 33 wt% (Fig. 2A), which indicates a low degree of deoxygenation (taking into account that water present in bio-oil was 22.6 wt%). As a result of (partial) deoxygenation especially at higher temperatures (> 300 °C), the yield of organic phase decreased, and its density became lower. Consequently, the order of the phases changed as indicated in Fig. 2A. At the same time, the yield of aqueous phase increased up to ca. 42 wt%.

Similarly, hydrogen pressure affected the yields of both liquid phases as well. The deoxygenation degree was lower at lower hydrogen pressures (particularly at 2 MPa) and hence less aqueous phase was formed and separated. Due to the higher density of the organic phase at these conditions, the aqueous phase was the top layer. A comparison between Fig. 2A and B reveals that the yields of liquid phases obtained at 340 °C and 4 MPa were similar in both tests despite the different time-on-stream (TOS), at which these samples were collected (TOS: 74 h in Fig. 2A and 31 h in Fig. 2B), and of different history of the catalysts. The yields of the organic and aqueous phases as a function of the hydrotreating severity demonstrate that the yields of gaseous phases (typically 2–10 wt%) increased slightly with the increased hydrotreating severity. However, extensive cracking was not observed (as discussed below).

In addition to maximizing the mass yield of the liquid organic fraction suitable for further refinery upgrading into fuel components, it is critical to ensure that most of the energy contained in the bio-oil feed is kept in the liquid organic phase. The share of the initial energy content that is transferred in the organic liquid phase, *i.e.* the energy content of the organic phase divided by the energy content of the fed bio-oil multiplied by the yield of this phase and by 100 is denoted as "energy recovery" (based on lower heating value) and reported in Fig. 3 as a function of reaction conditions. The values above 100 (Fig. 3B) thus indicate that more energy was incorporated in the liquid organic products than lost to other product streams. Specifically, hydrogenation of unsaturated bonds and reduction of aldehydes and ketones to corresponding alcohols were the main reactions at mild reaction conditions, while deoxygenation and hydrogenolysis reactions occurred mainly at more severe conditions (> 320 °C and pressures 4 or 8 MPa). Due to these reactions, some of the energy was lost from the organic liquid phase to the gas phase and the energy carried in by hydrogen was lost as water. Nonetheless, it is positive that $> 85\%$ of the initial energy content of bio-oil can be kept in the organic liquid phase, *i.e.* in the targeted product.

4. Liquid products

4.1. Composition

The composition of hydrotreated products changes gradually and reflects well the changes in the experimental conditions. At 300 °C and 2 MPa, some of the reactive groups, such as double bonds and carbonyls, were saturated, and deoxygenation, *e.g.* by dehydration, decarbonylation or decarboxylation took place although it was not very significant. This explains also the observed increase in the energy recovery to values $> 100\%$ (Fig. 3) and is as well reflected in the calculated degree of deoxygenation (DOD, a difference of the organically-bound oxygen in bio-oil and products divided by the organically-bound oxygen in bio-oil). An increase in the reaction temperature (from 240 to 360 °C) led to a continuous increase in the H/C atomic ratio and at the same time a significant decrease in the O/C atomic ratio (from ca. 0.18 to about 0.04, Fig. 4A). This confirms that in this temperature range deoxygenation reactions accompanied by hydrogenation reactions, *e.g.* saturation of double bonds after dehydration, took place. These trends were the same also in the full range of hydrogen pressure (2–8 MPa). In addition, it is also obvious that the increase in the hydrogen pressure promoted hydrogenation reactions, as indicated by the increase in the H/C atomic ratio from ca. 1.4 at 320–340 °C and 2 MPa to ca. 1.6 at 320–340 °C and 8 MPa (Fig. 4B). At the same time, deoxygenation reactions were promoted as well since for a constant temperature, *e.g.* 320 or 340 °C, there was a significant drop in the O/C atomic ratio (Fig. 4B) when hydrogen pressure was increased.

Raw bio-oils, as well as products of their hydrotreating, are very complex mixtures of many compounds, which render the analysis of their composition very difficult. Nonetheless, it is important to extract at least qualitative information about the composition in "real time" to steer the conversion process efficiently, *i.e.* to adapt reaction parameters to compensate the loss of catalyst activity and to maintain product quality. Therefore, we propose two methods, one chromatographic and one spectroscopic that enable a quick characterization of the obtained products.

The chromatographic method is based on the simulated distillation (SIMDIS) analysis. Applied to bio-oils and products of their hydrotreating, it allows estimating the "hydrocarbon-likeliness" of the product and its approximate fractional composition. The analysis relies on the different response factor of hydrocarbons (here by definition set to 100%) and that of the oxygenates which is always lower, nonetheless related to the oxygen content of the compounds. As shown in Fig. 5A, already hydrotreating at 240 °C resulted in an increase in the SIMDIS recovery from 32 to 42%. The data further evidence that deoxygenation extent increases with the increasing reaction temperature. It has to be noted that the data are reported yields related to the feed, *i.e.* the sum of the yields is less than 100% due to formation of water and gases. The fractional composition suggests (Fig. 5B) that majority of the products is within the diesel fuel range (about 30%, which corresponds to ca. 50% of the fractions). Interestingly, the amount of the heaviest products increased from 8% determined in the feed to 16% found in the products

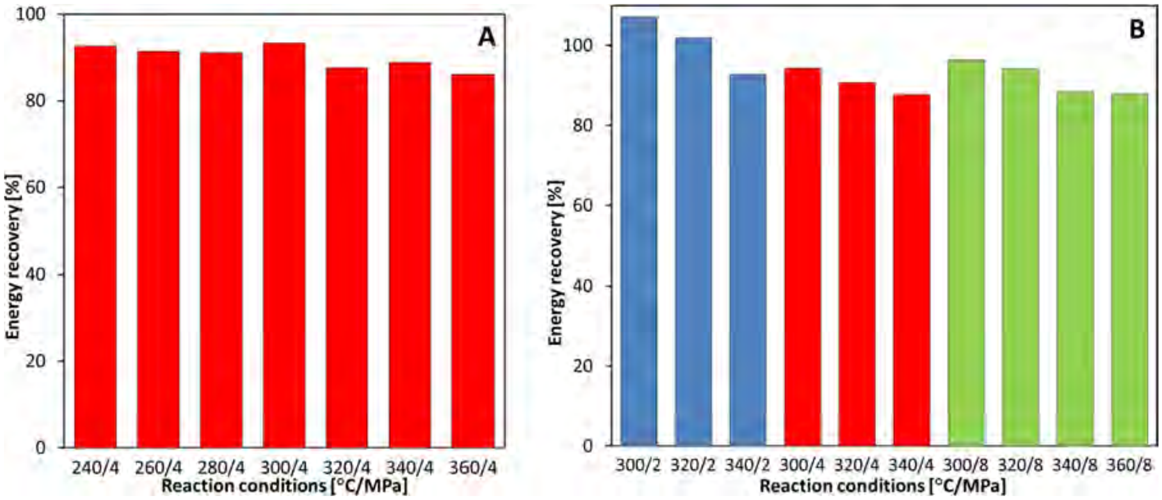

Fig. 3. Energy recovery at different reaction conditions (A) 4 MPa and (B) 2; 4 and 8 MPa.

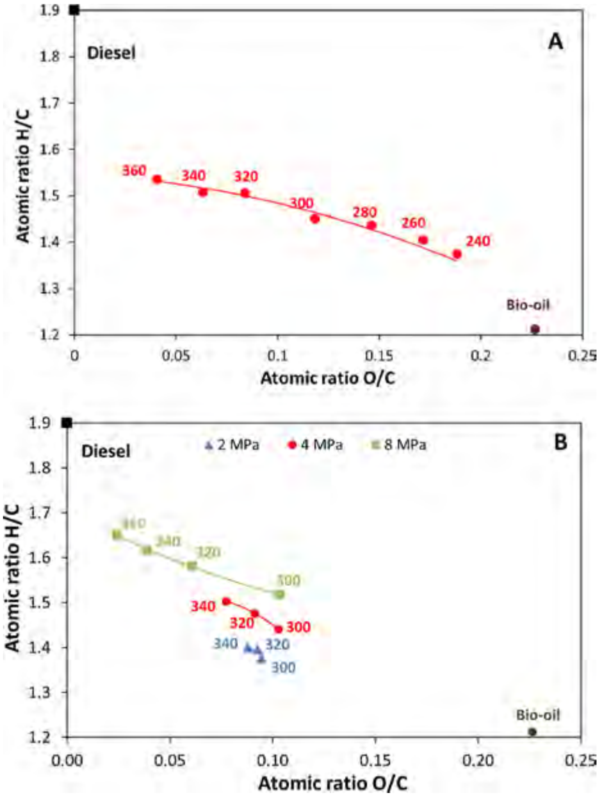

Fig. 4. Van Krevelen diagram of diesel fuel, feed bio-oil and hydrogenated products under different reaction temperatures at pressure (A) 4 MPa and (B) 2; 4 and 8 MPa.

at 280 °C. This significant increase (Fig. 5B) cannot be explained simply by the formation of gaseous products due to deoxygenation of short-chain oxygenates and has to be attributed to the occurrence of condensation reactions. However, further increase in reaction temperature resulted in a dramatic reduction of the heaviest products down to 5% at 360 °C (Fig. 5B) due to significant deoxygenation as evidenced by the increasing SIMDIS recovery (Fig. 5A) and the calculated deoxygenation degree (Fig. 8C). At the same time, the yields of gasoline- and diesel-like fractions increased (Fig. 5B) together with the increasing yield of gaseous products (Fig. 10A).

The effects of both reaction temperature and pressure on the SIMDIS recovery are presented in

Fig. 5C. As expected, both parameters have a positive effect, although the increase in SIMDIS recovery when increasing hydrogen pressure from 4 to 8 MPa is rather modest, especially at lower temperatures. Interestingly, the combination of high temperature and pressure (360 °C and 8 MPa) resulted in almost complete deoxygenation and the SIMDIS recovery reached 96%, *i.e.* the product consisted almost exclusively of hydrocarbons (Fig. 5C). The effect of pressure on the fractional composition is demonstrated in Fig. 5d. In line with the effects described for reaction temperature, the more severe reaction conditions promoted (hydro) cracking reactions affording thus more gasoline-like products and less heavy products. Also, at lower hydrogen pressure it could be confirmed that condensation reactions resulting in the formation of heavier products took place and their yield increased from 8% found in bio-oil to ca. 12% formed in the products obtained at 2 MPa and 340 °C (Fig. 5D).

4.2. FTIR spectra and principal component analysis

A complementary method for rapid screening of the character of bio-oil and products of its hydrotreating (in terms of composition) was based on FTIR.

As seen in Fig. 6, the spectra are rather complex and the changes are only subtle to allow elucidating in detail the changes in composition.

Fig. 6A shows the entire spectrum of the bio-oil and the spectra of selected products obtained by bio-oil hydrotreating. To analyse the changes, three spectral regions (B, C and D) containing the most important spectral features have been displayed in Fig. 6B–D and will be discussed separately. The broad band occurring in the region of approximately 3700–3000 cm^{-1} (Fig. 6B) can be attributed to the stretching of the OH group, which is typical for alcohols, phenols, carboxylic acids and water [40]. Signal intensity of this band in all products spectra was lower than in the feed spectrum. Moreover, the increase in the reaction temperature and pressure always led to a decrease in the signal intensity of the OH band. It can be mainly attributed to the water content decrease which was confirmed using KF titration (Figs. 8C and 9D). Nevertheless, a decrease in other OH group-containing compounds, whose other absorption bands can be found in the region 1300–1000 cm^{-1}, was observed as well. On the other hand, the bands in the region 3000–2800 cm^{-1} (Fig. 6B), which can be attributed to the asymmetrical and symmetrical stretching of the C—H bonds originating from the methyl and methylene groups, were stronger in the products spectra. As expected, the highest signal intensity of these

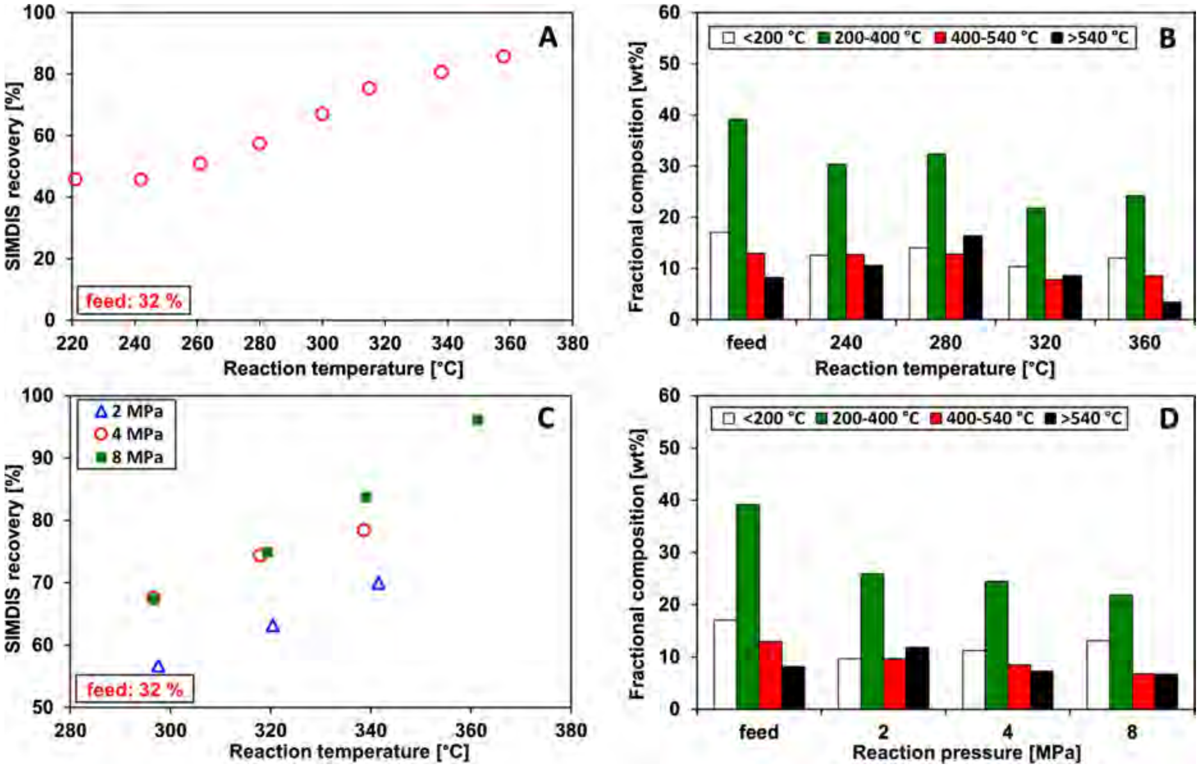

Fig. 5. SIMDIS recovery as a function of reaction temperature at 4 MPa (A), yield of fractions (on water-free basis) obtained at different temperatures at 4 MPa (B), SIMDIS recovery as a function of reaction temperature at different pressures (C) and yield of fractions (on water-free basis) obtained at 340 °C at 2–8 MPa (D).

bands was observed in the spectrum of the product obtained at the most severe conditions.

The spectral region 1820–1320 cm^{-1} (Fig. 6C) consists of signals belonging to the stretching of the C=O groups and the stretching of the C=C bonds from aromatics or alkenes. Moreover, scissoring vibration of water molecule occurs in this region. An evident change in the absorption intensity of the feed and products can be seen. Most importantly, the band with the maximum signal intensity at 1697 cm^{-1}, which can be attributed to the C=O groups (*e.g.*, ketones, aldehydes and carboxylic acids), was eliminated at the most severe reaction conditions. The intensity of the bands in the region 1630–1570 cm^{-1} and at 1514 cm^{-1} belonging to the stretching of the C=C bonds in aromatics (*e.g.*, phenols) decreased as well.

The spectra of the spectral region 1320–650 cm^{-1} are shown in Fig. 6D. The overlapped bands in the 1320–1000 cm^{-1} region can be attributed to the oxygen-containing groups present for example in phenolic compounds with hydroxyl and methoxy groups, aldehydes, carboxylic acids, glycosides, *etc.* It should be noted that the content of these compounds decreased with the increasing severity of reaction conditions. Moreover, some bands (*e.g.*, alkyl-aryl ethers and glycosides) disappeared almost completely when the highest temperature was applied. The bands in the 900–650 cm^{-1} region can be mainly attributed to the out-of-plane deformation vibrations of aromatic =C—H groups. Besides these bands, the out-of-plane deformation of O—H groups of phenols occurs in this region. Signal intensities in this region are strongly influenced by the broad band caused by deformation vibrations of water.

Although significant changes in the FTIR-ATR spectra can be observed upon careful visual inspection of the spectra, only qualitative conclusions can be drawn. Thus, to extract more valuable information and to enable a comparison of individual products, principal component analysis (PCA) of the spectra was applied. In addition to the spectra of the bio-oil hydrotreating products, *i.e.*, organic and aqueous phases, and the feed, *i.e.*, bio-oil, a spectrum of water and spectra of other batches of straw bio-oil were added to the data set. The first two principal components (PC1 and PC2) captured 99.4% of the variability of the original data. The plot of PC scores is shown in Fig. 7A. As can be seen, there are four distinct clusters of points. On the right side of the plot, aqueous phases and water can be found. Organic phases of the products and feeds are situated on the left side of the plot. Moreover, the variable chemical composition of the organic products was confirmed by moving position of the points from the top to the bottom of the plot. The most deoxygenated product is situated at the left bottom corner of the plot. On the other hand, the product treated using the mildest reaction conditions is the closest one to feeds. It follows, that while the PC1 is highly related to water content, PC2 is highly related to the carbonyl groups, aromatics and alkyl-aryl ethers.

To obtain more insight in the composition of the targeted organic products, a separate PCA model was built just for the organic products and feeds (Fig. 7B). The first two principal components (PC1 and PC2) captured 99.1% of the variability of the spectra. Since the variability caused by the large differences between the organic and aqueous phases (and water) was eliminated, *i.e.*, a new model without water and aqueous phases spectra was built, other spectral features became more important. Although the new first principal component is still related to the water content, the effect of the carbonyl groups, aromatics, alkyl-aryl ethers and other compounds increased. On the other side, the PC2 is positively correlated, *inter alia*, with the content of methylene groups. Nevertheless, since the PC2 is also positively correlated to the other types of compounds (*e.g.* glycosides) and the signal intensities of the methylene groups are influenced by the other bands, PC2 score values of the products do not have just an increasing trend. In other words, decreasing content of glycosides (and other compounds) prevailed the influence of the increasing methylene group content which caused that PC2 score values of the products obtained at the lowest temperatures have decreasing trend. As can be seen in the Fig. 7B, the products

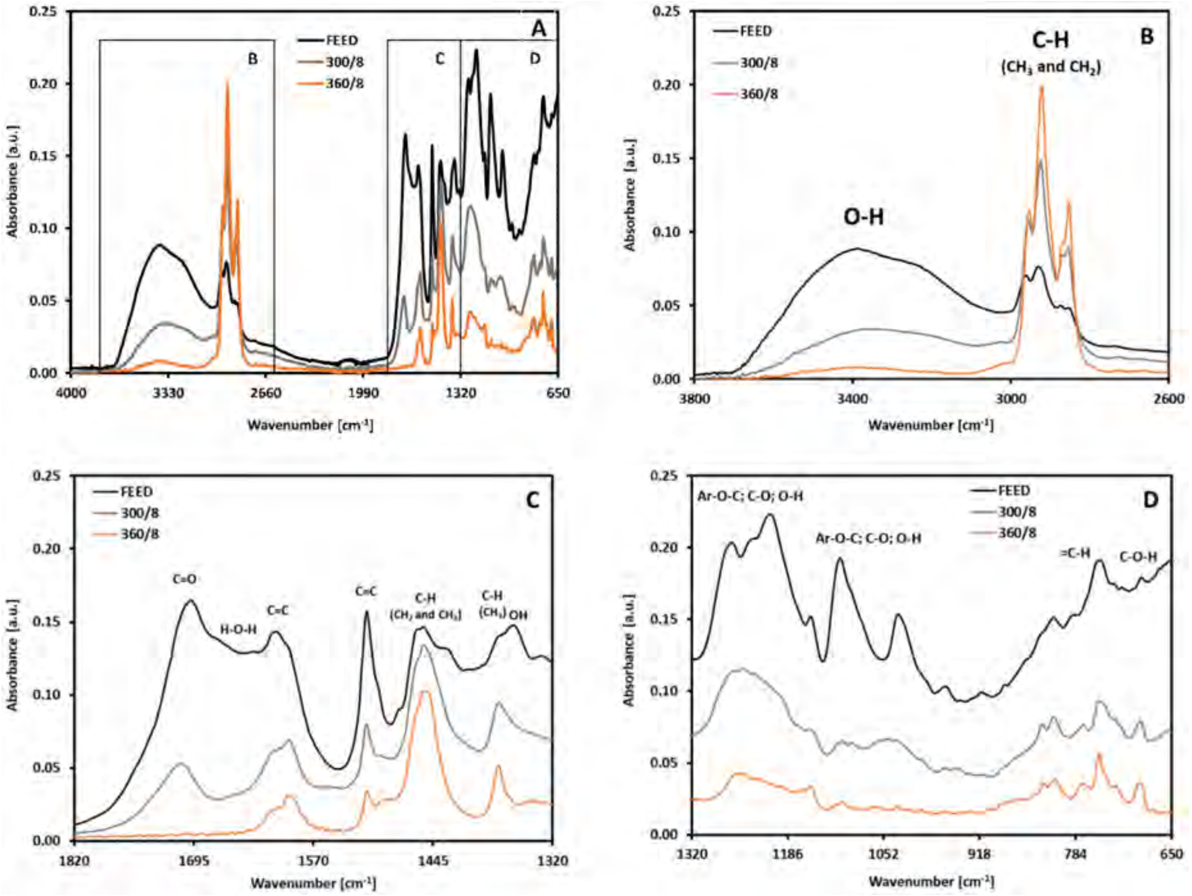

Fig. 6. Entire FTIR-ATR spectra (A), spectral region 3800–2600 cm^{-1} (B), spectral region 1820–1320 cm^{-1} (C) and spectral region 1320–650 cm^{-1} (D) of the feed and two products of the catalytic hydrotreating of the bio-oil.

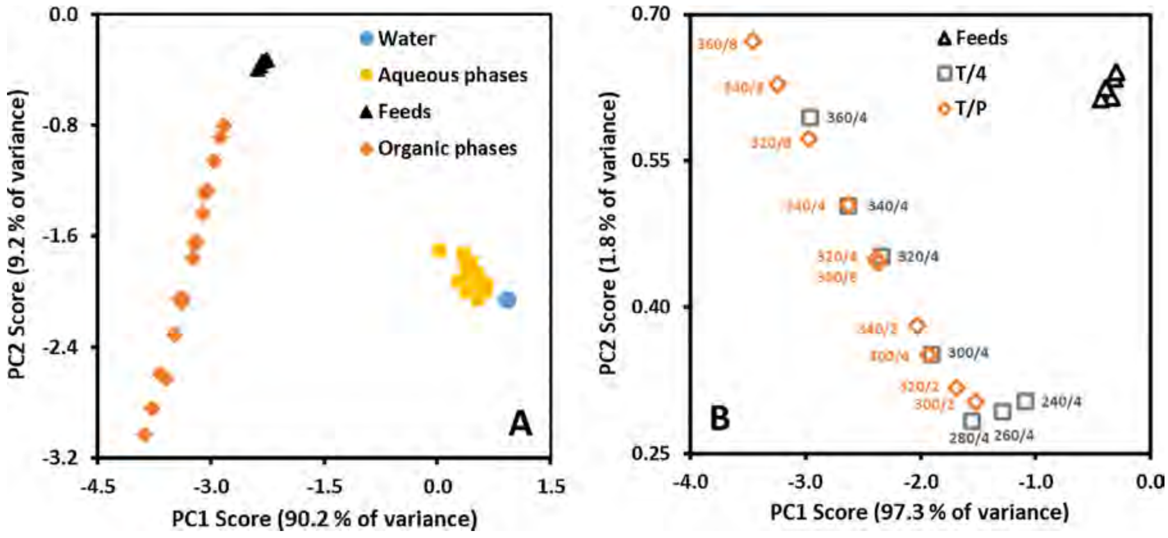

Fig. 7. PCA score plot (PC1 vs. PC2) of feeds, organic and aqueous phases and water (A) and of the organic phases of the products (denoted by T/P, *i.e.*, reaction temperature/reaction pressure) and feeds (B).

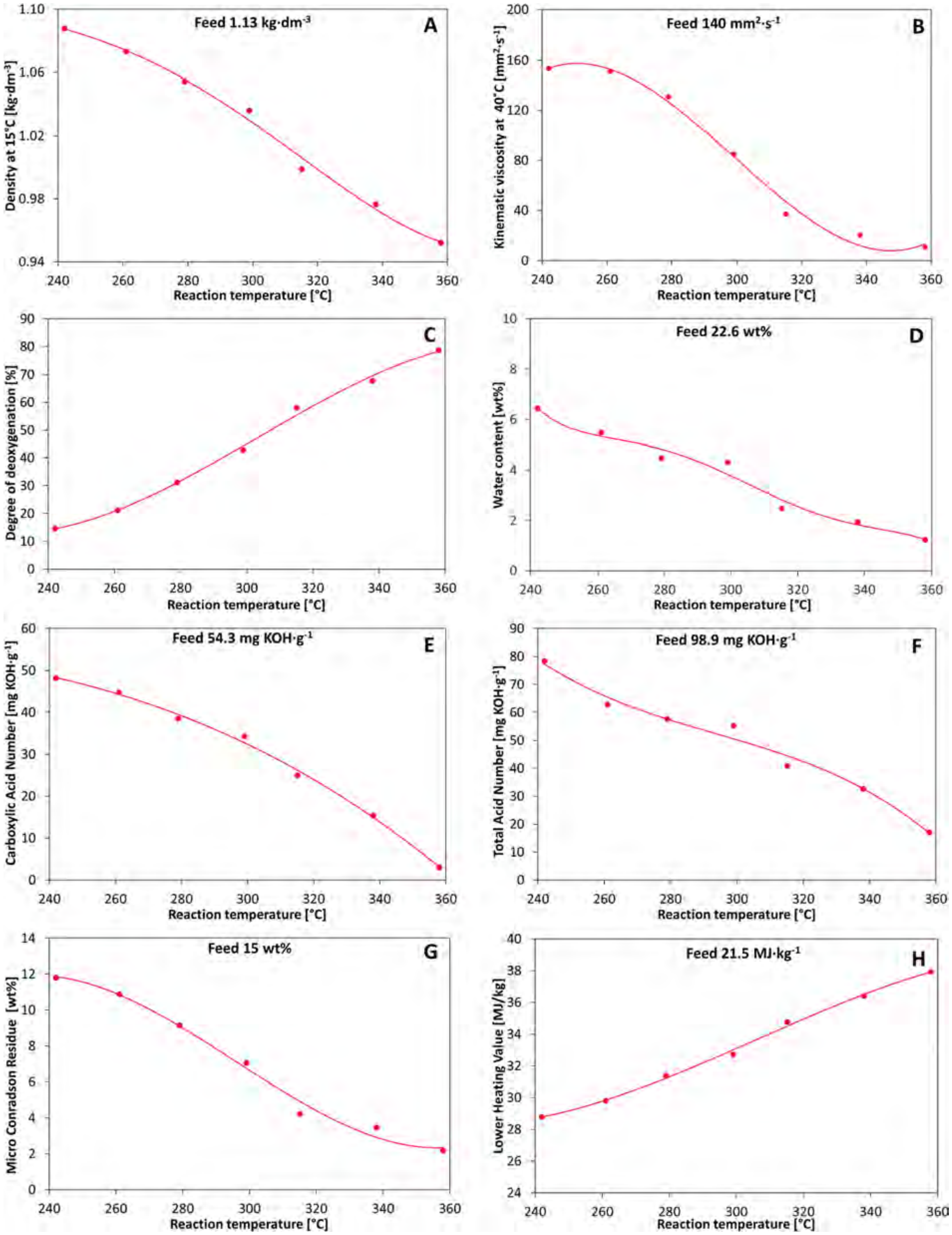

Fig. 8. Effect of temperature on physico-chemical properties of organic phase of products: density (A), kinematic viscosity (B), degree of deoxygenation, (DOD) (C), water content (D), carboxylic acid number (CAN) (E), total acid number (TAN) (F), micro Conradson carbonization residue (MCR) (G), lower heating value (H) at 4 MPa.

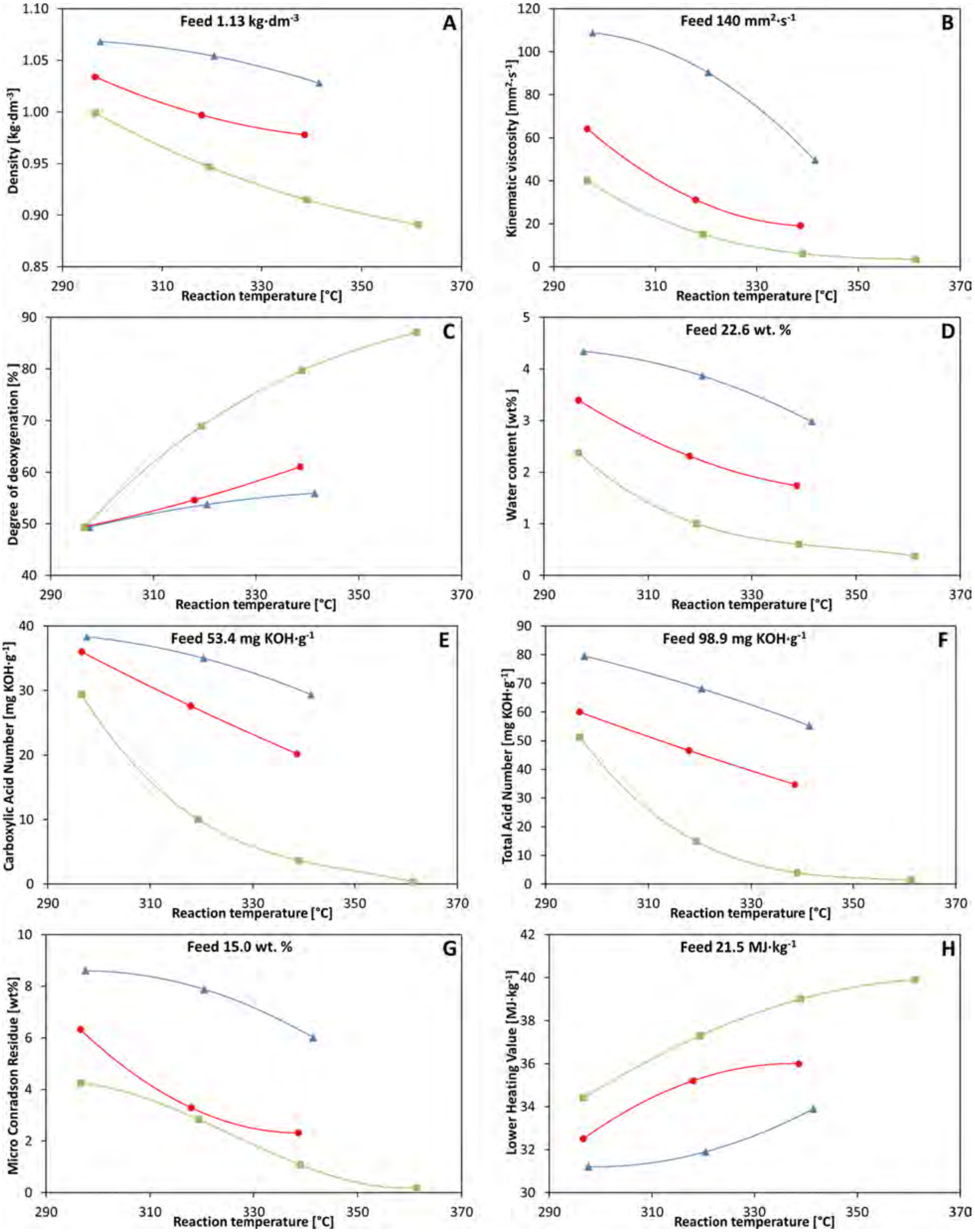

Fig. 9. Effect of temperature and pressure on physico-chemical properties of organic phase of products: density (A), kinematic viscosity (B), degree of deoxygenation (DOD) (C), water content (D), carboxylic acid number (CAN) (E), total acid number (TAN) (F), micro Conradson carbonization residue (MCR) (G), lower heating value (H); blue triangle – 2 MPa, red circle – 4 MPa, green square – 8 MPa. (For interpretation of the references to colour in this figure legend, the reader is referred to the web version of this article.)

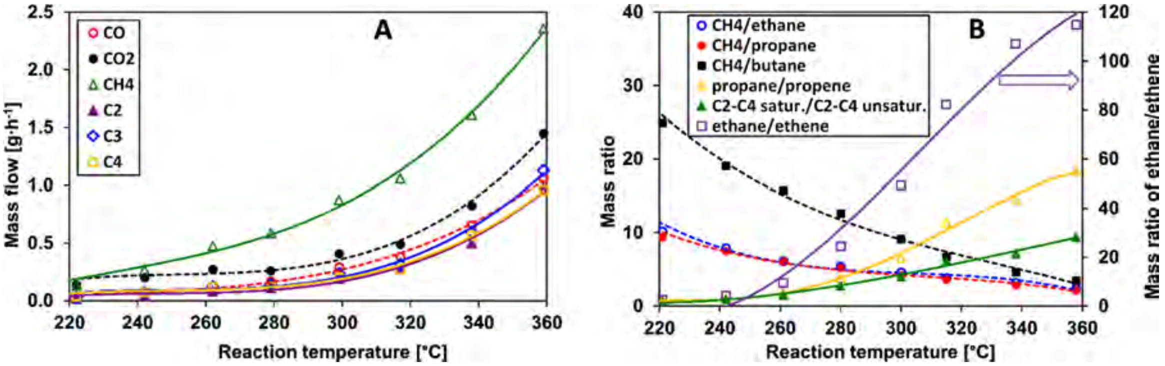

Fig. 10. Mass flow of gaseous products from bio-oil hydrotreating as a function of reaction temperature at 4 MPa (A) and selected concentration ratios (B).

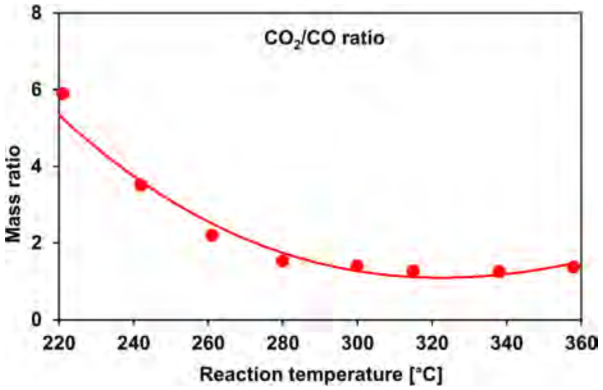

Fig. 11. Ratio CO/CO_2 in gaseous products as a function of reaction temperature at 4 MPa.

obtained in different experiments but using the same process conditions are situated very close to each other.

The results of the principal component analysis applied to the FTIR spectra of bio-oil and hydrotreated products clearly demonstrate that the method allows assessing rapidly the character of the products. This feature can be used to control the bio-oil hydrotreating by adjusting the hydrotreating process conditions to produce organic products having desired properties.

4.3. Properties of organic phases from hydrotreating

The changes in the properties of the hydrotreated products due to the increase in reaction temperature at 4 MPa are rather straightforward (Fig. 8). The increase in temperature resulted in a gradual decrease in density, kinematic viscosity, acid numbers, propensity to coking (expressed by the value of micro Conradson carbon residue, MCR) and water content. In line with the changes in elemental

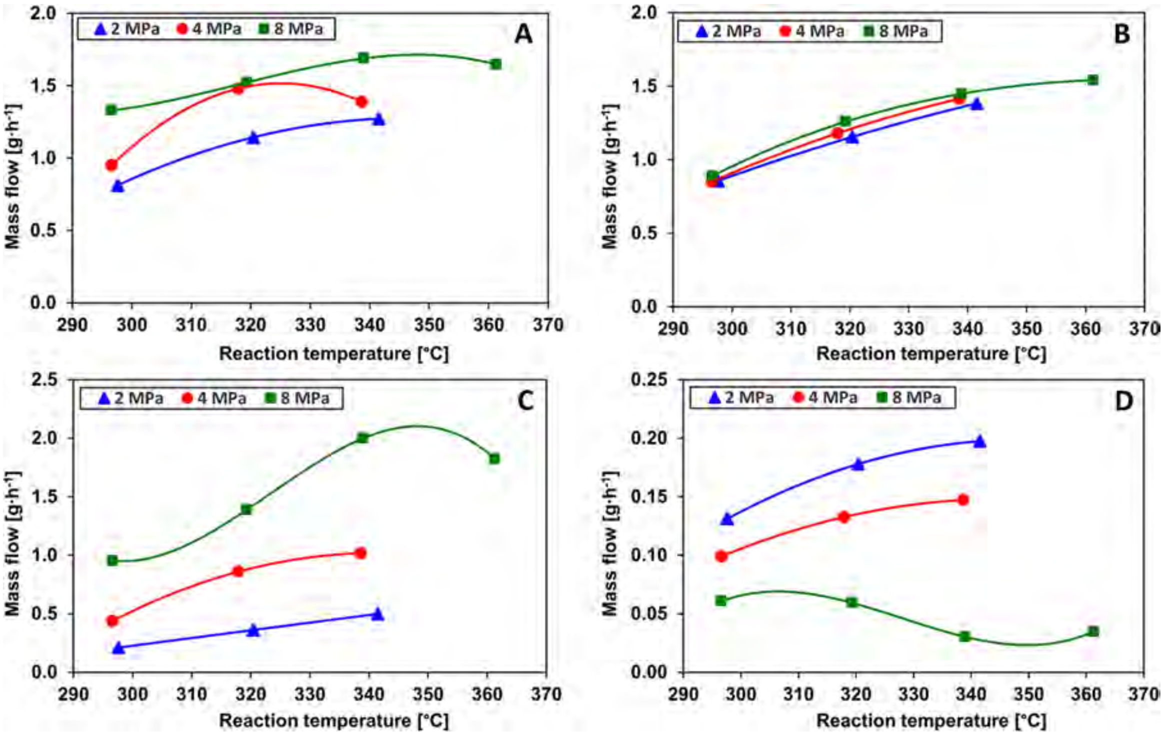

Fig. 12. Mass flow of gaseous products from bio-oil hydrotreating at different temperatures and hydrogen pressures – methane (A), CO and CO_2 (B), saturated C_2–C_4 (C) and unsaturated C_2–C_4 (D).

composition, degree of deoxygenation (DOD) and the lower heating value (LHV) increased with the increase in reaction temperature (Fig. 8). Analogous behaviour can be observed also for the set of experiments carried out over a wider range of hydrogen pressures (Fig. 9). As expected, deeper hydrogenation and deoxygenation observed at higher hydrogen pressure was reflected by a more pronounced decrease in the values of density, kinematic viscosity, acid numbers (TAN and CAN), MCR and water content. More interesting are, however, the different profiles characterizing the changes in the properties of hydrotreated products as a function of the reaction temperature.

All analysed properties change almost linearly over the studied range of temperature, LHV increases while other properties decrease. The changes in acid numbers (Fig. 8E and F), *i.e.* carboxylic and total acid number, disclose information about the type of acidic oxygenates present as well as about the extent of deoxygenation of these compounds. Whereas carboxylic acid number provides information about the concentration of carboxylic acids, the total acid number informs not only about the presence of carboxylic acids, but also about other acidic oxygenates, such as phenolics. At temperatures < 260 °C, the decrease in a CAN is slower than the decrease in TAN suggesting thus that other acidic organic compounds than carboxylic acids are predominantly hydrogenated in this range. The difference between TAN and CAN dropped from ca. 44 $mg \cdot g^{-1}$ obtained for the feed to about 18 $mg \cdot g^{-1}$ found at 260 °C (Fig. 8E and F). The difference remained constant while the temperature was increased from 260 to 340 °C, suggesting that in this range the observed deoxygenation was driven mainly by deoxygenation of carboxylic acids either by hydrodeoxygenation or decarboxylation. Finally, at 360 °C, the CAN was only 3 $mg \cdot g^{-1}$ and the difference between TAN and CAN decreased to 14 $mg \cdot g^{-1}$ indicating that also deoxygenation of some of the phenolics took place at the highest temperature. Nonetheless, it has to be kept in mind that phenol and some of the acids could have been extracted in the aqueous phase. The difference between TAN and CAN was also affected by the reaction pressure (Figs. 9E and 7F). Whereas at 2 MPa, the difference between TAN and CAN is 26 $mg \cdot g^{-1}$ at 340 °C or higher at lower temperatures, which is in line with the limited extent of deoxygenation reactions, at 8 MPa, the difference between TAN and CAN dropped to less than 5 $mg \cdot g^{-1}$ in the temperature range 320–360 °C, which proves that apart from carboxylic acids also other oxygenates, such as phenolics, were deoxygenated. Also, the TAN dropped to < 1.5 mg $KOH \cdot g^{-1}$, *i.e.* to < 2% of the original acidity, showing that the acidic compounds can be virtually completely removed under these conditions (*i.e.* at 360 °C and 8 MPa).

Keeping in mind the envisioned co-processing of the partially deoxygenated bio-oil with conventional refinery streams in a refinery, a simple preliminary blending test was carried out by blending the organic phases of the hydrotreated bio-oil products with straight run gasoil (SRGO). Among the hydrotreated bio-oil products obtained here, only the organic phase of the product obtained at 360 °C and 8 MPa was fully miscible with the SRGO.

4.4. Gaseous products

The composition of gaseous products is an additional indicator that reflects the reactions that occur in the liquid phase. The changes in the concentration of gaseous products clearly show that there were virtually no cracking and/or hydrogenolytic reactions involving carbon-carbon bonds below 260 °C (Fig. 10a). An appreciable formation of gaseous products started only when reaction temperature exceeded 280 °C (Fig. 10A). Methane was the most abundant gaseous product formed by hydrogenolysis of methoxy compounds and by hydrogenation of carbon oxides (CO and CO_2) that were produced by decarboxylation and decarbonylation reactions. Altogether, C_1 gases constitute the majority of gaseous products, which supports the interpretation of the observed changes in the acid numbers as discussed above. The formation of C_1 gases was accompanied by the formation of C_2–C_4 hydrocarbons that originate from cracking reactions of larger molecules and from deoxygenation of short-chain alcohols, aldehydes, ketones and acids. In addition, several oxygenates were identified in the gas phase as well including acetone, methylacetate, butanone, methylfuran and dimethylfuran. Their concentrations were, however, low amounting to several tens to a few hundred mg/m^3.

A closer inspection of the gas phase composition reveals (Fig. 10B) that the relative share of particularly ethane and propane increases at the expense of methane (the concentration ratio of methane to ethane or propane drops from ca. 12 to about 2) confirming thus the importance of cracking and deoxygenation reactions at higher reaction temperatures. At the same time, the hydrogenation of alkenes is significantly favoured at higher reaction temperatures, as, *e.g.* the ethane-to-ethene ratio increased from about 2 to > 100 (Fig. 10B). It is also noteworthy that the CO_2/CO ratio decreased from 3.5 at 240 °C to ca. 1.4, a value that was constant in the range 280–360 °C (Fig. 11).

The composition of gaseous products obtained at 2–8 MPa and 300–360 °C is reported in Fig. 12. In line with the above-discussed results, the increase in reaction temperature resulted in the enhanced formation of all gaseous products but the differences between 320 and 340 °C were not very significant. It can be also seen (Fig. 12) that the formation of all products except alkenes is enhanced by higher hydrogen pressure. Again, this is in agreement with the observed deeper deoxygenation particularly at 8 MPa (Fig. 9C) resulting in more pronounced hydrogenolytic and deoxygenation activity of the catalyst.

5. Conclusions

The effect of reaction conditions on the composition and properties of products obtained by hydrotreating of bio-oil originating from ablative fast pyrolysis of straw was studied over a commercial sulphided $NiMo/Al_2O_3$ catalyst in a fixed bed reactor. The effect of temperature and hydrogen pressure was investigated in the range 240–360 °C and 2–8 MPa, respectively. The experiments have shown that the degree of deoxygenation increased and the properties of the products were improved with the increasing hydrotreating severity. In particular, the acidity expressed by total and carboxylic acid number (TAN and CAN) decreased to less than 2 mg $KOH \cdot g^{-1}$ and water content dropped to less than 1 wt% in products obtained at 360 °C and 8 MPa. This would allow processing of the products obtained by hydrotreating of straw-based bio-oil in a conventional refinery. At the same time, these products contained > 85% of the initial bio-oil energy content.

Considering the complex composition of bio-oil and products of its hydrotreating, it is important to be able to characterize their overall quality in a simple yet reliable way. Therefore, two methods were proposed and verified in this study. The first one is based on simulated distillation (SIMDIS) method and allows estimating the degree of deoxygenation relying on the different response of oxygenated and non-oxygenated compounds in this chromatographic technique. The second method is based on the principal component analysis (PCA) of the infrared spectra of bio-oils and products of their hydrotreatment. The method allows classify the products according to their structural composition that is accented by the PCA method. Consequently, the depth of hydrotreatment can be estimated reliably within a few minutes.

Acknowledgements

The results were obtained in the BioMates project. This project has received funding from the European Union's Horizon 2020 research and innovation program under grant agreement no. 727463. The publication reflects only the authors' view and the Commission is not responsible for any use that may be made of the information it contains. The authors are grateful to Tim Schulzke and Stefan Conrad (Fraunhofer UMSICHT) for providing the straw bio-oil used in the hydrotreating experiments.

References

[1] REN21. Renewables 2016 Global Status Report. Paris: REN21 Secretariat; 2016.

[2] Venderbosch RH, Ardiyanti AR, Wildschut J, Oasmaa A, Heeres HJ. Stabilization of biomass-derived pyrolysis oils. J Chem Technol Biotechnol 2010;85:674–86.

[3] REDII; Available from: https://eur-lex.europa.eu/legal-content/CS/ALL/?uri=CELEX%3A52016PC0767R%2801%29.

[4] Abbasi T, Abbasi SA. Biomass energy and the environmental impacts associated with its production and utilization. Renew Sustain Energy Rev 2010;14(3):919–37.

[5] Conrad S, Apfelbacher A, Schulzke T. Fractionated condensation of pyrolysis vapours from ablative flash pyrolysis. In: Hamburg, Germany Proceedings of 22rd European Biomass Conference & Exhibition (June 23rd–26th 2014). 2014:1127–33.

[6] Peacocke G, Bridgwater A. Ablative plate pyrolysis of biomass for liquids. Biomass Bioenergy 1994;7(1–6):147–54.

[7] Bridgwater AV. Review of fast pyrolysis of biomass and product upgrading. Biomass Bioenergy 2012;38:68–94.

[8] Lee H, Kim Y-M, Lee I-G, Jeon J-K, Jung S-C, Chung JD, et al. Recent advances in the catalytic hydrodeoxygenation of bio-oil. Korean J Chem Eng 2016;33(12):3299–315.

[9] Białek M, Gross-Gołacka E, Kaliski M. Rationalization process in the refining sector of the European Union in the context of activities aimed at restoring the competitiveness of refineries. AGH Drilling Oil, Gas 2014;31(1).

[10] Mortensen PM, Grunwaldt JD, Jensen PA, Knudsen KG, Jensen AD. A review of catalytic upgrading of bio-oil to engine fuels. Appl Catal A 2011;407:1–19.

[11] Wildschut J, Mahfud FH, Venderbosch RH, Heeres HJ. Hydrotreatment of fast pyrolysis oil using heterogeneous noble-metal catalyst. Ind Eng Chem Res 2009;48:10324–34.

[12] Baldauf W, Balfanz U, Rupp M. Upgrading of flash pyrolysis oil and utilization in refineries. Biomass Bioenergy 1994;7:237–44.

[13] Ly HV, Im K, Go Y, Galiwango E, Kim S-S, Kim J, et al. Spray pyrolysis synthesis of γ-Al_2O_3 supported metal and metal phosphide catalysts and their activity in the hydrodeoxygenation of a bio-oil model compound. Energy Convers Manage 2016;127:545–53.

[14] Rodríguez-Aguado E, Infantes-Molina A, Ballesteros-Plata D, Cecilia J, Barroso-Martín I, Rodríguez-Castellón E. Ni and Fe mixed phosphides catalysts for O-removal of a bio-oil model molecule from lignocellulosic biomass. Mol Catal 2017;437:130–9.

[15] Olarte MV, Padmaperuma AB, Ferrell JR, Christensen ED, Hallen RT, Lucke RB, et al. Characterization of upgraded fast pyrolysis oak oil distillate fractions from sulfided and non-sulfided catalytic hydrotreating. Fuel 2017;202(Supplement C):620–30.

[16] Mahfud FH. Exploratory studies on fast pyrolysis oil upgrading Ph.D. Wiskunde en Natuurwetenschappen, Rijksuniversiteit Groningen; 2007. p. 158.

[17] Mercader FDM, Koehorst PJJ, Heeres HJ, Kersten SRA, Hogendoorn JA. Competition between hydrotreating and polymerization reactions during pyrolysis oil hydrodeoxygenation. Am Instit Chem Eng J 2011;57:3160–70.

[18] Zanuttini M, Lago C, Querini C, Peralta M. Deoxygenation of m-cresol on Pt/γ-Al 2 O 3 catalysts. Catal Today 2013;213:9–17.

[19] Griffin MB, Baddour FG, Habas SE, Nash CP, Ruddy DA, Schaidle JA. An investigation into support cooperativity for the deoxygenation of guaiacol over nanoparticle Ni and Rh Catalysis. Sci Technol 2017;2:P.

[20] Echeandia S, Pawelec B, Barrio V, Arias P, Cambra J, Loricera C, et al. Enhancement of phenol hydrodeoxygenation over Pd catalysts supported on mixed HY zeolite and Al_2O_3. An approach to O-removal from bio-oils. Fuel 2014;117:1061–73.

[21] Elliott DC, Hart TR, Neuenschwander GG, Rotness LJ, Zacher AH. Catalytic hydroprocessing of biomass fast pyrolysis bio-oil to produce hydrocarbon products. Am Instit Chem Eng J 2009;28:441–9.

[22] Wildschut J. Pyrolysis oil upgrading to transportation fuels by catalytic hydrotreatment Ph.D Wiskunde en Natuurwetenschappen, Rijksuniversiteit Groningen; 2009. p. 190.

[23] French RJ, Stunkel J, Black S, Myers M, Yung MM, Iisa K. Evaluate impact of catalyst type on oil yield and hydrogen consumption from mild hydrotreating. Energy Fuels 2014;28:3086–95.

[24] Steele PH, Gajjela S, Yu F, Hassan E, Gresham G. Hydrocarbon production via biomas pyrolysis and hydrodeoxygenation. NSTI-Nanotech; 2009. p. 3.

[25] Novel Guo C. Carbon-supported transition metal phosphide catalysts for hydrodeoxygenation of fast pyrolysis oil MSc The University of Western Ontario; 2015. p. 128.

[26] Lup ANK, Abnisa F, Daud WMAW, Aroua MK. A review on reaction mechanisms of metal-catalyzed deoxygenation process in bio-oil model compounds. Appl Catal A: General 2017.

[27] Boullosa-Eiras S, Lødeng R, Bergem H, Stöcker M, Hannevold L, Blekkan EA. Catalytic hydrodeoxygenation (HDO) of phenol over supported molybdenum carbide, nitride, phosphide and oxide catalysts. Catal Today 2014;223:44–53.

[28] Zhao H, Li D, Bui P, Oyama S. Hydrodeoxygenation of guaiacol as model compound for pyrolysis oil on transition metal phosphide hydroprocessing catalysts. Appl Catal A 2011;391(1):305–10.

[29] Romero Y, Richard F, Brunet S. Hydrodeoxygenation of 2-ethylphenol as a model compound of bio-crude over sulfided Mo-based catalysts: promoting effect and reaction mechanism. Appl Catal B 2010;98(3):213–23.

[30] Patel M, Kumar A. Production of renewable diesel through the hydroprocessing of lignocellulosic biomass-derived bio-oil: a review. Renew Sustain Energy Rev 2016;58:1293–307.

[31] Ardiyanti AR, Khromova SA, Venderbosch RH, Yakovlev VA, Melián-Cabrera I, Heeres HJ. Catalytic hydrotreatment of fast pyrolysis oil using bimetallic Ni–Cu catalysts on various supports. Appl Catal A 2012;449:121–30.

[32] Mercader FDM, Groneveld MJ, Kersten SRA, Way NWJ, Schaverien CJ, Hogendoorn JA. Production of advanced biofuels: co-processing of upgraded pyrolysis oil in standard refinery units. Appl Catal A 2010;96:57–66.

[33] Yoshimura Y, Sato T, Shimada H, Matsubayashi N, Nishijima A. Influences of oxygen-containing substances on deactivation of sulfided molybdate catalysts. Appl Catal 1991;73(1):55–63.

[34] Laurent E, Delmon B. Influence of water in the deactivation of a sulfided NiMo/γ-Al_2O_3 catalyst during hydrodeoxygenation. J Catal 1994;146:281–91.

[35] Gholizadeh M, Gunawan R, Hu X, de Miguel Mercader F, Westerhof R, Chaitwat W, et al. Effects of temperature on the hydrotreatment behaviour of pyrolysis bio-oil and coke formation in a continuous hydrotreatment reactor. Fuel Process Technol 2016;148:175–83.

[36] Horáček J, Kubička D. Bio-oil hydrotreating over conventional CoMo & NiMo catalysts: the role of reaction conditions and additives. Fuel 2017;198:49–57.

[37] Schulzke T, Conrad S, Westermeyer J. Ablative flash pyrolysis of straw – conversion process and valorization options for solid and liquid products. Biorefinery for food & fuels & materials. Montpellier, France; 2015.

[38] Christensen E, Ferrell J, Olarte MV, Padmaperuma AB, Lemmon T. Acid number determination of pyrolysis bio-oils using potentiometric titration. Report No: NREL/TP-5100-65890. Washington, DC: US Department of Energy; 2016.

[39] Næs T, Isaksson T, Fearn T, Davies T. A user friendly guide to multivariate calibration and classification. NIR Publications; 2002.

[40] Socrates G. Infrared and Raman characteristic group frequencies: tables and charts. John Wiley & Sons; 2001.

Fuel 198 (2017) 49–57

Contents lists available at ScienceDirect

Fuel

journal homepage: www.elsevier.com/locate/fuel

Full Length Article

Bio-oil hydrotreating over conventional CoMo & NiMo catalysts: The role of reaction conditions and additives

Jan Horáček [a,*], David Kubička [b]

[a] Unipetrol Centre of Research and Education, Block 2838, 436 70 Litvínov-Záluží 1, Czech Republic
[b] Technopark Kralupy VŠCHT Praha, University of Chemistry and Technology Prague, Žižkova 7, 278 01 Kralupy nad Vltavou, Czech Republic

ARTICLE INFO

Article history:
Received 15 May 2016
Received in revised form 25 August 2016
Accepted 2 October 2016
Available online 8 October 2016

Keywords:
Bio-oil
Deoxygenation
Hydrotreating

ABSTRACT

Wood-derived bio-oil was investigated as a feedstock for the production of renewable hydrocarbons over commercial hydrotreating CoMoS and NiMoS catalysts. Alumina-supported CoMoS active phase showed better selectivity to diesel-like products than NiMoS phase and higher activity in removal of gaseous intermediates (CO_x) by hydrogenation. This reaction can play an important role in the reduction of corrosivity at the reactor outlet and determine the process economy. The disadvantage of alumina as a support material was its low stability at high temperatures in presence of water. NiMoS catalyst was found to be more active in decarboxylation and it was possible to reach a steady state production of hydrocarbons having a comparable boiling point distribution with crude oil middle distillates. A test performed with a combination of NiMoS (at the top of the catalyst bed) and CoMoS (at the bottom of the reactor) revealed the key role of the catalyst type and reaction conditions in the first zone of the reactor. The experiments with elevated feeding rates showed the undesirable presence of the not-stabilized reactants behind the first reactor zone. Reaction conditions, catalyst selection and presence of additives (methanol to modify viscosity, DMDS/H_2S to stabilize active centers) were combined and optimized to tune the product composition and properties. The catalyst low-temperature activity in the first reactor zone was the limiting factor for the maximum feed rate and reactor capacity. The reaction temperature in this zone strongly affects the boiling point distribution of the product. In case of NiMo catalyst, the reaction temperature above 360 °C in the 3rd zone can reduce molecular weight of the product due to mild cracking. In contrast, temperatures above 400 °C result in fast deactivation preventing thus the establishment of the steady state operating regime.

1. Introduction

Bio-oil is an important and intensively studied topic in the field of renewable chemicals and fuels. The definition of the fast pyrolysis bio-oil by FPBO (Fast pyrolysis bio-oil) consortium is: "Liquid condensate recovered by thermal treatment of lignocellulose biomass, at short hot vapor residence time (typically less than about 10 s) typically at between 450 and 600 °C at near atmospheric pressure or below, in the absence of oxygen [1]". In general, these conditions allow maximizing the yield of the liquid product. The pyrolysis process can be accomplished in several reactor setups. Typically, the commercially offered reactors are downdraft fixed bed reactors with horizontally transported feed to the reaction zone, and fluidized bed reactors [2].

There are several reasons, why to produce bio-oils. One of them is the possibility to extract valuable compounds that find application in fine chemicals production generating thus bio-based high added value products. Another main direction of bio-oil investigations is energy and fuels production. The motivation for using bio-oil as an energy source instead of lignocellulosic biomass (wood chips, straw etc.) is the enhanced energy density. From the transportation point of view, it would be highly inefficient to transport straw-like lignocellulose (having typically higher heating value of about 17 MJ/t and low density of about 200 kg/m^3) to a distant place for processing. Moreover, the manipulation with bio-oil is significantly easier when compared with handling lignocellulose by crane or any other carrying machine. As mentioned before, a large interest is being paid to developing processes for upgrading bio-oil to liquid fuels for internal combustion engines. Due to its properties, such as low thermal stability (aging), corrosivity related to content of water (up to 30 wt.%) and acidic compounds (for example acetic acid, formic acid) bio-oil is not

---

* Corresponding author at: Areál Chempark, St. 2838, 436 70 Litvínov-Záluží 1, Czech Republic.
E-mail address: jan.horacek@unicre.cz (J. Horáček).

http://dx.doi.org/10.1016/j.fuel.2016.10.003

suitable for direct use in automotive engines. Basic bio-oil characterization and studies on blending fossil fuels with bio-oil revealed a decrease in engine performance and its irregular running. Moreover, the poor low temperature stability of bio-oil is problematic for coking in the injection system of diesel engines [3,4]. Hence, successful utilization of bio-oil in automotive engines requires chemical transformation of bio-oil to hydrocarbons, which can be readily integrated to refinery processes as their properties are much closer to those oil fractions. As shown below (Table 1), the main difference between bio-oil and crude-oil fractions is in the much higher content of heteroatoms in bio-oils as compared with fuel oil fraction. The high content of oxygen in form of dissolved water together with the low pH (caused by the presence of carboxylic acids) results in high corrosivity of bio-oil, particularly at elevated temperatures.

Two main routes for converting bio-oils into hydrocarbons include catalytic cracking using zeolites and hydrodeoxygenation (HDO) using metals- or metal-sulfides-based catalysts. The former reaction is being operated at near atmospheric pressure and temperatures 350–500 °C. Presence of hydrogen is not required. Oil yields are typically only about 20 wt.% related to feedstock. Catalysts introduced in published papers are based on HZSM-5 [6], aluminosilicates [7], SAPO-5, SAPO-11, Mg-APO-36 [8] and some others. The most problematic by-product is coke, which decreases the yield of liquids. HDO is an interesting alternative due to the higher yields of organic and high deoxygenation degrees. Advantageous is also the possibility of using a simpler reactor setup (such as fixed bed reactor). As mentioned in published papers, long-term activity and high deoxygenation degrees can be reached when using non-isothermal reactor profile and commercial hydrotreating catalysts (NiMoS, CoMoS types combined with Ru/C type in the first reactor zone [9]).

The character of Bio-oil hydrodeoxygenation products strongly depends on experimental conditions used (catalyst type, reaction temperature, reaction pressure and relative flow rate selection). Elliott and coworkers [9] reported as the main product practically oxygen-free hydrocarbon mixture, with initially dominant yield of diesel fraction in organic phase (53 wt.%) and large yields of gasoline over non-isothermal combined catalyst bed (RuS/C, NiMoS). After approximately 68–76 h of time on stream, the yields of fractions decreased in the following order diesel > gasoline > vacuum gas oil. The reported end of experiment was typically accompanied either by an increase in reactor pressure drop or reactor plugging by coking. Oxygen was removed as water in aqueous phase or carbon oxides in reaction outgas.

Table 1
Comparison of bio-oil and REB (Russian export blend) derived fuel oil.

Parameter	Bio-oil	Fuel oil	Rapeseed oil
Moisture (water) [wt.%]	30[a]	<0.1[b]	0[b]
pH	2.5[c]	–	–
Density [g/cm^3]	1.2[a]	0.91[b]	0.92[b]
Elemental analysis [wt.%]			
C	45.7[a]	86.3[b]	77.4[d]
H	6.4[a]	11.4[b]	11.8[d]
O	48.9[a]	0.00[b]	10.9[d]
N	<0.05[a]	0.00[b]	0.00[d]
S [wt.%]	<0.05[a]	2.3[b]	0.00[d]
Ash [wt.%]	0–0.2	0.1	–
Heat of combustion [MJ/kg]	16.47[a]	43.21[b]	38.48[b]
Viscosity (50 °C) [cP]	40–100	180	34.9[b]
Solids [wt.%]	0.2–1	1[c]	–
Distillation residue [wt.%]	Up to 50[c]	1[c]	100[d]

[a] Data for BTG bio-oil MSDS.
[b] Data measured for fuel oil by vacuum REB distillation and food quality rapeseed oil (RSO).
[c] Data by Huber and co-workers [5].
[d] Calculated for triolein as RSO model compound.

The application of exclusively carbon-supported noble metal catalysts can result in yields of organics around 36 wt.% in case of Pd/C type [10]. Ru/C catalyst was reported to provide a deoxygenation degree up to 64%. The deoxygenation degree was enhanced mainly due to an e increase in reaction temperature and residence time [10].

Bio-oil HDO can be performed also in batch reactors using bio-oil and its fractions as feedstock. Using palladium and ruthenium as active metals supported on active carbon shows high deoxygenation degrees [11].

The basic problem in use of noble metals is their sensitivity to sulfur, which is presented in bio-oil in tens to hundreds of ppm. The initial high activity can be consequently significantly reduced when operating HDO in continuous system over these metals.

Although competitive product price of HDO product calculated per ton of oil equivalent was reported [12] and this price is in the range of prices for HDO of triglycerides and is lower than in case of bio-ethanol produced from biomass, the production is less beneficial. The reason is in the high capital costs for building this technology, typically high amounts of hydrogen needed and especially in the high pressure setup of all process parts.

The aim of this study is to investigate in detail the effect of reaction conditions on the product distribution. DMDS was selected as a hydrogen sulfide source, which can be in an industrial application partially replaced by H_2S recovery from the off-gas from conventional hydrotreating processes. Methanol was selected as an additive due its reported ability to stabilize bio-oil during storage and to reduce the viscosity of bio-oil [13].

2. Experimental

2.1. Materials

BTG fast pyrolysis bio-oil supplied by BTG-BTL was used as a reference feedstock for the hydrotreating tests. The BTG-BTL technology uses a “cone rotating” reactor type [14]. Methanol (analytical grade; Lach Ner), was used to improve flow properties of the feedstock for hydrotreating. Dimethyl disulfide (DMDS; Sigma Aldrich) was used as a sulfur donor agent improving the catalyst stability. Commercial hydrotreating NiMoS and CoMoS catalysts were tested. Catalysts composition and their surface area are given in Table 2.

2.2. Methods

Simulated distillation (SIMDIS; Agilent 7890 A, ASTM D2887) was used to determine the boiling point distribution of the organic product mixture obtained prepared by bio-oil hydrotreating. Gaseous products were analyzed off-line using a gas chromatograph equipped with FID and TCD detectors. Elemental analysis was performed by ICP. The density and the refractive index of products was measured by an Anton Parr DMA 4100 M instrument and by an Anton Parr Abemat 200 instrument, respectively.

Table 2
Catalytic material characterization.

Parameter\catalyst	CoMo	NiMo
Co [wt.%]	2.9	0.0
Ni [wt.%]	13.9	3.8
Mo [wt.%]	0.0	9.5
sS [m^2/g]	133	120
Cat. support	γ-alumina	γ-alumina
Particle size [mm][a]	0.25–0.50	0.25–0.50

[a] Fraction used in the tests. It was obtained by crushing and sieving the original 3.2 mm extrudates.

Spruce bio-oil for the experiments was supplied by BTG (Netherlands). The oil was stored in fridge at temperature about 0 °C. Before a catalytic experiment, bio-oil was blended with defined amounts of additives and stored in a fridge. Experiments were carried out in a stainless steel reactor equipped with a three-zone electric heating unit. The reactor had internal diameter of 17 mm and an integrated thermowell where thermocouples are placed to control temperature (outer diameter 5.0 mm). Bio-oil was pumped into the reactor by an HPLC pump (ECOM, KAPPA 10). Hydrogen flow was controlled by an MFC Bronkhorst with a maximal flow of 720 Nl/h. The reactor set-up is depicted in Fig. 1. Before a catalytic test, the catalyst was first crushed and sieved to obtain catalyst particles of required size (0.25–0.50 mm). The fractionated catalyst was loaded into the reactor on top of a layer of inert silicon carbide. The top layer of catalyst was covered by fine SiC inert to facilitate feed distribution and to avoid feed wall flow., Glass wool was placed in the bottom and the top of the reactor to prevent SiC flushing out of the catalyst bed. CoMoS and NiMoS commercial catalysts were used to study bio-oil hydrotreating conversion.

First, a reference test (Nr. 1) using CoMoS catalyst was performed. The experimental conditions were selected based on the publication by Elliott and co-workers [9] dealing with the investigation of bio-oil continuous hydrotreating. The reactor was divided into three reaction zones having different reaction temperature set-point. In the first zone, the temperature was kept in the range 170–250 °C, in the second zone, the reaction temperature was kept in the range 250–350 °C and in the third zone, the temperature was in the range 350–450 °C. Based on [9], 0.01 wt.% addition of DMDS was added into the feedstock to protect the sulfided active sites of the catalyst. The reaction conditions and reaction mixture composition was changed in each test to investigate the roles of these parameters. The results will be described and discussed in detail in the next section. Under reaction conditions, DMDS affords H_2S the concentration of which plays an important role in equilibrium state of active phase as described by Furimski and Massoth [15], and significantly affects competitive adsorption of oxygen heteroatom. Based on the test Nr.1 results, the catalyst was changed to NiMoS type and the concentration of DMDS was increased to 0.2 wt.% (test Nr. 2). To avoid coking observed in the previous tests, 4 wt.% of methanol was added in the reaction mixture (test Nr. 3) to improve feedstock-catalyst contact. In addition, hydrogen flow was doubled (i.e. the gas-to-liquid ratio was increased). To optimize the middle distillate yield, the final reaction temperature was reduced to suppress hydrocracking reactions (Nr. 3). In this test, the role of feeding rate was investigated at reduced reaction temperatures (220, 240, 320 °C) to limit coking and extend the catalyst lifetime. WHSV was investigated in the range 0.2–0.4 h^{-1}. The following experiment (Nr. 4) was focused on extending the catalyst lifetime. Hence, the reaction temperatures were changed to 230, 320 and 350 in the top, middle and bottom zone of reactor respectively. Moreover, methanol dosing was increased from 4 to 5 wt.% and DMDS addition from 0.4 to 1.0 wt.% in the test Nr. 4. The last test (Nr. 5) was performed at similar conditions as the test Nr. 4, but the catalyst bed in the bottom part of the reactor was changed from NiMoS to CoMoS (resulting in 5:4 w/w ration of the catalysts). This test was focused on decreasing the CO_x concentration in the off-gas to reduce the corrosiveness of this stream. Summary of experimental setup for all experiments shows Table 3.

The catalysts were activated at ramped temperature profile by dimethyl disulfide solution (10 vol.% of DMDS) in isooctane in presence of hydrogen flow. The final temperature of the activation

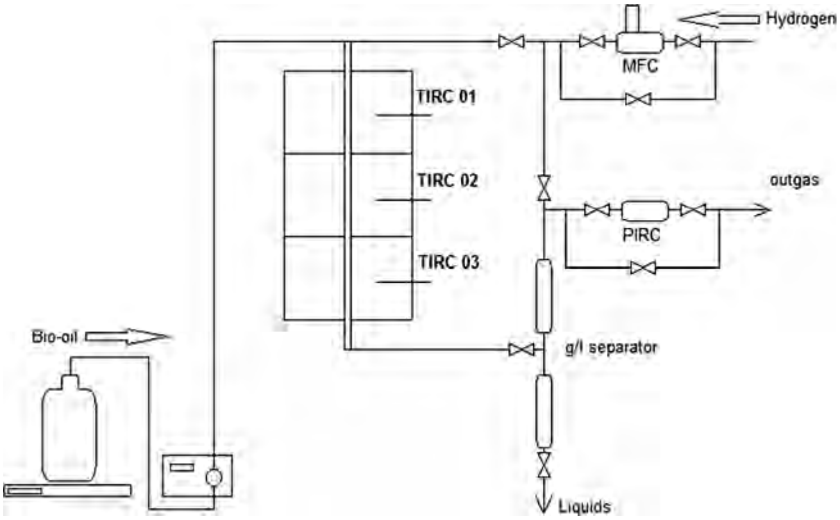

Fig. 1. Scheme of hydrotreating reactor setup.

Table 3
List of tests performed and reaction conditions, all the experiments were carried at 13 MPa.

Test[a] Nr.	Active phase	Additives [wt.%]		WHSV	Temperature			Catalyst loading
		DMDS	MeOH	[h^{-1}]	Top	Middle	Bottom	[g]
1	CoMoS	0.01	0.0	0.2	170	250–350	450	75
2	NiMoS	0.20	0.0	0.2	230	250–350	450	73.6
3	NiMoS	0.40	4.0	0.2–0.4	220	240	320	85
4	NiMoS	1.00	5.0	0.2	230	320	350	85
5	NiMoS + CoMoS	1.00	5.0	0.2	230	320	350	50 + 40

[a] Chronological order.

method was 340 °C. This temperature was held for 9 h. After the activation, the reactor was cooled down to temperature set-points of each heating zone under reduced sulfiding agent and hydrogen flow. After reaching the temperature set-points, pumping of bio-oil was started with a weight hourly space velocity (WHSV) equal to 0.2 h^{-1}. Material used as feed was BTG spruce wood bio-oil with different percentage of additives. Liquid samples and outgas samples were collected typically each 4 h from the heated and cooled (two stages) gas-liquid separator. Aqueous phase was quantitatively separated and analyzed by SPME/GC–MS in the case of low bio-oil conversion and unusual look. Typically, only some traces of hydrocarbons were detected. The absence of organics in aqueous phase indicates total deoxygenation degree. Organic phase was analyzed by simulated distillation (Agilent 7890 A, ASTM D2887). Gaseous products were analyzed by gas chromatography (RGA – refinery gas analysis) to identify and quantify gaseous products which were produced.

3. Results and discussion

The reference test (Nr. 1) performed with a CoMoS/Al_2O_3 commercial hydrotreating catalyst showed severe catalyst deactivation after only 30 h on stream. The catalyst deactivation was indicated by change in the color and physical properties of the reaction products. The color of the reaction products changed from bright/colorless to yellow, red and black during the 40 h on stream when the reference test was ended. Also, reactor plugging was indicated by a rapid increase in pressure difference between the top and the bottom of reactor (dP over 1 MPa) after 40 h on stream. The analysis of the reactor content showed massive plugging by coke formed from the unstable bio-oil, and catalyst decomposition into dust. Catalyst decomposition was observed in catalyst bed between 20 and 100% of length from the top of the catalyst layer. Coke formation was observed also in the guarding bed above catalyst layer, its formation is an indication of approaching reactor plugging. Apart from coke, the reaction products typically consisted of reaction off-gas, aqueous phase and organics. The gaseous products contained mainly carbon monoxide, carbon dioxide and methane (C_1), ethane, propane and butanes. The C_1 products originated from formic acid reduction and from decarboxylation of other acids (present in concentration of several wt.% units according to the bio-oil MSDS) and hydrogenation of the primarily formed CO_2. Ethane and propane are expected to be products of acetic acid deoxygenation/hydrogenation and lignin phenyl propanoid monomeric units decomposition, respectively.

The low feeding rate (WHSV = 0.2 h$^{-1)}$ used in all experiments caused a delay of 16 h to get a fully saturated catalyst bed and to stabilize yields of the liquid fraction (Fig. 2). The overall stabilized yield of liquids was about 85 wt.% related to the bio-oil amount fed. The overall organic phase yield (related to amount of bio-oil injected) was between 32 and 37 wt.%. This is in good agreement with results of experiments with sulfided catalysts producing fully deoxygenated hydrocarbons yielding around 33 wt.% of organics [16]. Yields of organics are in general higher in comparison with catalytic cracking [12], which is an alternative route of bio-oil conversion into hydrocarbons for fuel production. A closer inspection of Fig. 2 reveals that the overall liquids yield was slightly increasing as well as the yield of organic liquids. It was caused by a steady catalyst deactivation resulting in a gradual increase in oxygen content in the product. The catalyst possessed a high cracking activity and, as a result, nearly full selectivity to low molecular hydrocarbon liquids and gaseous hydrocarbons was observed at the very beginning of the test (in the initial 16 h). After complete catalyst layer saturation with the feed/products (i.e. ca. after 16 h), the hydrocarbon products in the boiling-point range of diesel (Bp > 200 °C; Fig. 3a) tended to slowly increase. The yield of diesel fraction increased at the expense of the yield of the petrol-like hydrocarbons.

Despite the gaseous and liquid fraction yields were stabilized, the rapid catalyst deactivation and decomposition together with the low feed rate resulted in a steady increase in density and refractive index of the organic liquid product (Fig. 3c). The catalyst deactivation and the destruction of active centers was reflected by the increasing content of heteroatoms in liquid products with time on stream. The detected nitrogen (Fig. 3b) originated from the bio-oil feedstock and the fast increase in its content pointed to the fast reduction of HDN capacity of the catalyst, i.e. due to inhibition or destruction of the active centers. The increase in sulfur content confirmed the destruction of the active centers and decrease in HDS activity and probably also leaching of sulfur bound in the catalyst active phase into the organic phase (Fig. 3b). Sulfur leaching was confirmed by elemental analysis, as just 122 ppm sulfur were detected in raw bio-oil.

The significant increase in DMDS dosing (from 0.01 wt.% to 0.2 wt.%; test Nr. 2) together with the use of NiMoS catalyst

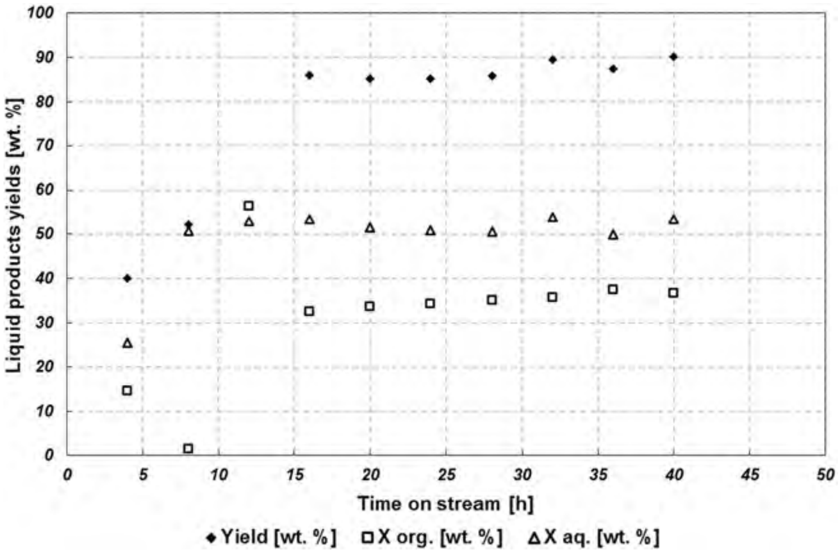

Fig. 2. Percentage of liquid products related to liquid feed.

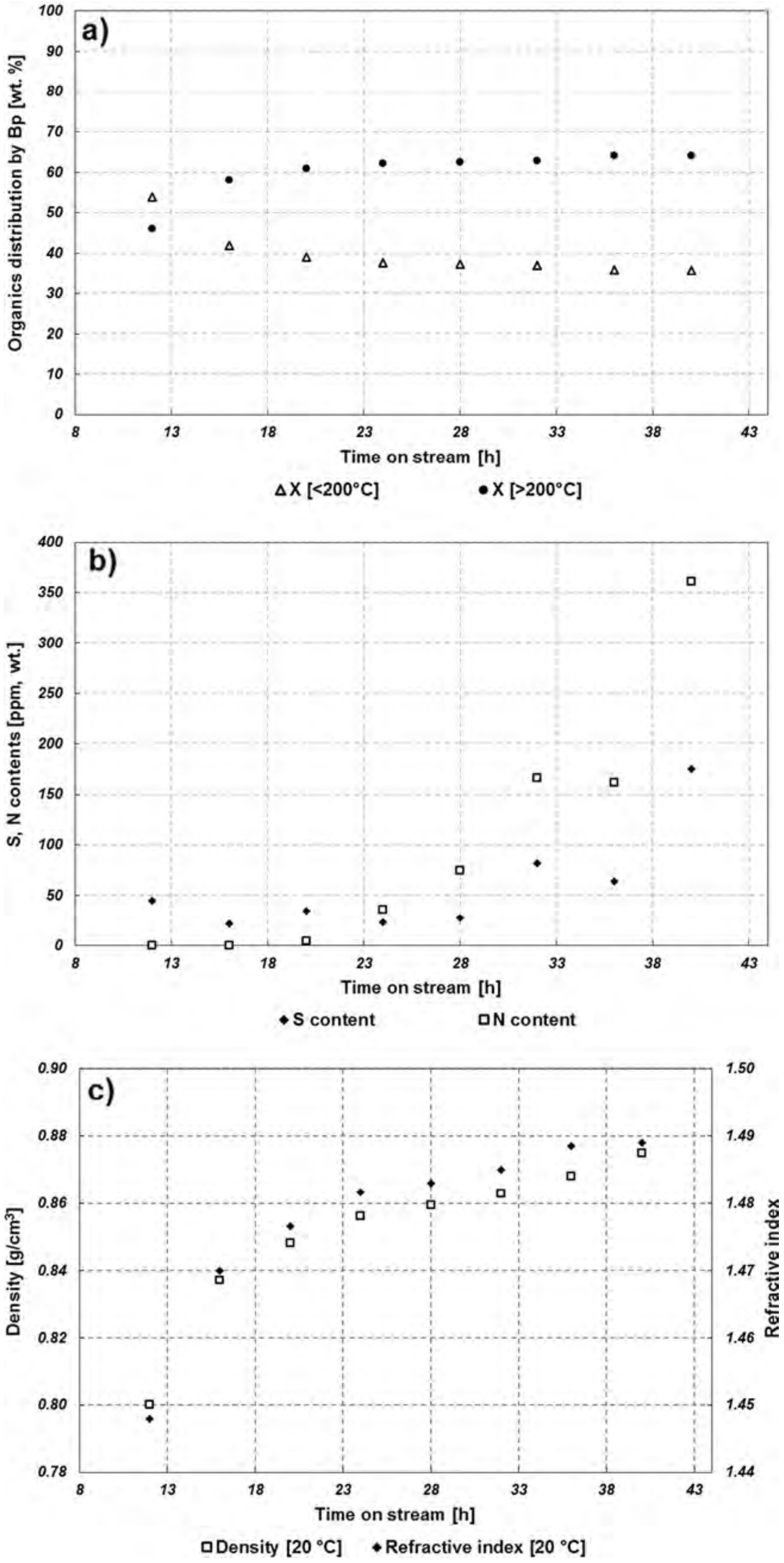

Fig. 3. Test Nr. 1 yields of organic fractions with boiling point <200 °C and >200 °C (a), content of heteroatoms in organic layer (b), changes in density and refractive index (c) as function of time on stream.

reduced the rapid decline in catalytic activity. Ni promoted catalyst was selected to speed up the decarboxylation of carboxylic acids. Moreover, the concentration of DMDS, which is responsible for establishing sufficient H_2S partial pressure and thus playing the key role in stabilizing the anionic vacancies of active centers, was increased from 0.01 wt.% to 0.2 wt.% DMDS addition. While the test length was not affected in general, important changes in products quality were observed. All product samples were colorless with slightly higher portion of lighter fraction (Fig. 4). Middle distillate yields were lower when compared with the CoMoS reference test (Fig. 3a), where middle distillates yield was typically over 60 wt.% of organic fraction. The strong effect of the low feed rate on feedstock axial dispersion (resulting in cross contamination of deoxygenated liquid samples in reactor bottom and gas-liquid separators) prevented us from checking the reactor operation stability by liquid products characterization. For this purpose, the gaseous phase was analyzed periodically to check changes in the reaction requiring a high catalyst activity (CO_x reduction, cracking; Fig. 5). As depicted, the main reaction gases are CO_2 and methane, CO was detected as a minor compound. Based on trends of the C_1 gases yields, the reactor was stabilized after ca. 20 h on stream. The main gaseous hydrocarbon products were ethane and propane.

Due to the high reactivity of bio-oil, the reactor plugging occurred in the top layer of the catalytic bed. To prevent this plugging, two methods could be applied - either lowering the temperature in the first catalytic zone, which is related with the undesirable decrease in the rate of hydrotreating, or improving the bio-oil flow properties. To investigate the effect of solvents, methanol was used to dilute the bio-oil feedstock. Apart from reducing the viscosity, the addition of small amount of methanol (5 wt.%, test Nr. 3) can significantly reduce coke formation in the reactor. Methanol presence can also slightly reduce corrosivity of the feedstock by reacting with carboxylic groups and affording respective esters. Methanol has been selected as a solvent for its oxygen content, which is nearly the same as that of neat bio-oil (ca 48.5 wt.%). 4 wt.% of methanol and 0.4 wt.% of DMDS were added into bio-oil and the homogenized feedstock was used for catalytic tests. To reduce the cleavage of C—C bonds in hydrocarbons, reaction temperatures in the middle and the last zone were reduced from 350 to 240 °C and 450 to 320 °C, respectively. The changes in experimental design resulted in production of heavier hydrocarbons (i.e. hydrocarbons with higher boiling point) and the reactor tended to reach steady state in about 40–60 h (estimation based on previous work with this reactor setup and hydrotreating reactions). Having just limited catalyst lifetime due to rapid coking, the flow rate increase from 0.2 to 0.3 h^{-1} was done before reaching the steady state (gas/liquid ratio was kept constant for all cases) and significantly changed the properties of the liquid products. However, as apparent from Fig. 6, the yields of liquids were not affected by the increase in feed rate at all.

As depicted (Fig. 7a), the higher flow rate led immediately to an increase in the density and refractive index of the products. Also, the nature of products has changed significantly: the main product fraction, naphtha, obtained at lower feeding rate, became a minor product. The influence of WHSV on the distribution of gaseous products was found to be negligible (Fig. 7b). Only carbon dioxide content has increased and methane content decreased as a result of the limited capacity of the active centers responsible for methanation. The lower content of C_4 and C_5 can be explained by the limited cracking activity at higher feed rate and partially also by catalyst deactivation due to coke formation (Fig. 7b). The middle distillate production raised to about 35 wt.% and important yield (about 25 wt.% in organic fraction) of fuel oil fraction, which could be still introduced to oil refinery system as feedstock, was obtained. The naphtha fraction has typically nature of a mixture of relatively low number of compounds present in high concentrations when compared to crude oil petrol (Fig. 7c). As can be seen in Fig. 7d, the overall distillation curve of the low-feeding-rate product has little higher final boiling point than naphtha (about 20 wt.% of middle distillate). As mentioned before, the final boiling point and overall boiling point distribution has changed: at WHSV = 0.3 h^{-1} significant yields of heavier fractions were formed. An important change was detected in the aqueous phase, where phenolic compounds were detected after 40 h on stream (SPME GC–MS: phenol, cresols, xylenols and C_3 alkylphenols) at 0.3 h^{-1}. This shows that the limiting feed rate for full deoxygenation of bio-oil was reached. A further increase in the feeding rate from 0.3 to 0.4 h^{-1} resulted in an uncontrolled temperature increase (240 ⇒ ~263 °C) in the middle (2nd) catalyst layer and after 3 h the reactor was plugged as detected by the rapid pressure difference increase. The observed spontaneous temperature increase in the middle catalyst zone followed by the reactor plugging was caused by overloading of the first (low temperature) catalyst bed. This resulted in a breakthrough of the highly reactive compounds to the second catalyst bed, i.e. the feed reached the second reaction zone without the required stabilization and due to the

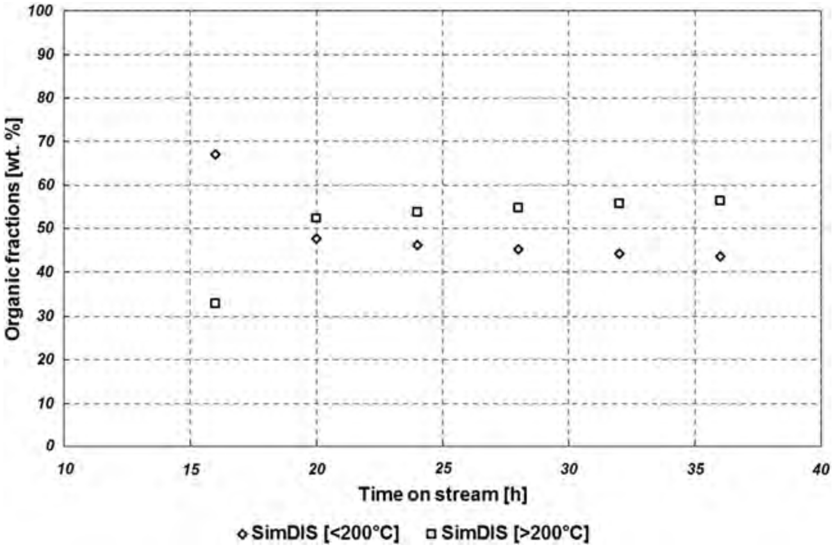

Fig. 4. Yields of organic fractions with boiling point <200 °C and >200 °C (NiMoS, test Nr. 2, 230, 250–350, 450 °C).

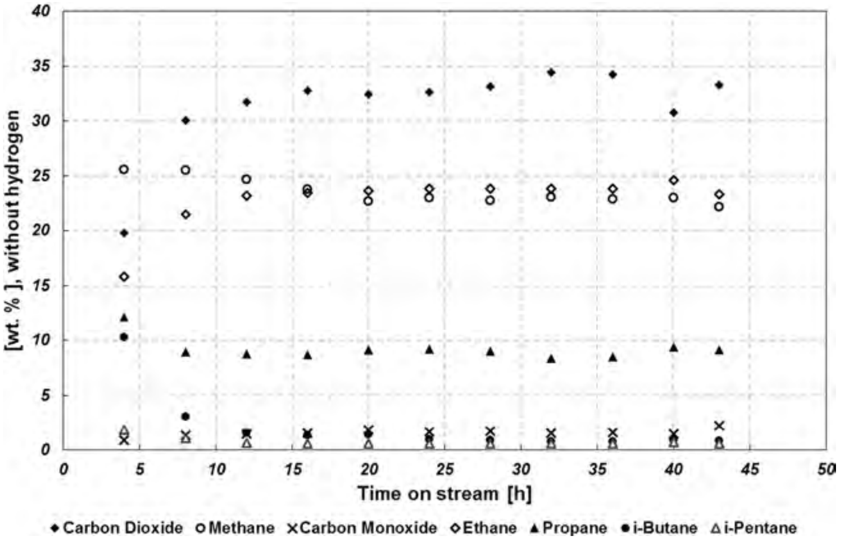

Fig. 5. Gaseous products distributions, elevated dosing of DMDS from 0.01 to 0.2 wt.% (NiMoS, test Nr. 2, 230, 250–350, 450 °C).

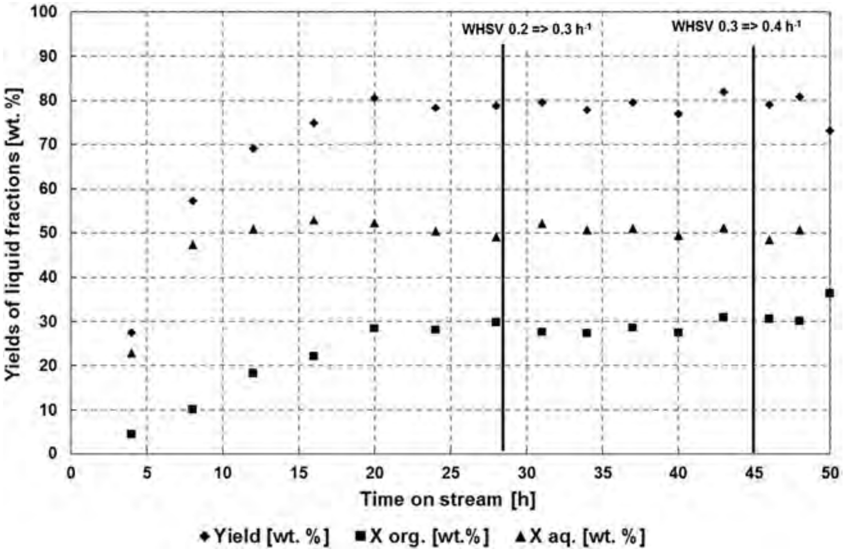

Fig. 6. Liquids fraction yields at various feeding rate (NiMoS, test Nr. 3, 230, 240, 320 °C).

deoxygenation reaction exothermicity a high increase in temperature was observed. Moreover, at higher reaction temperatures, the coking rate of the unstable feedstock significantly increased and resulted in an early test termination.

The following optimization step was focused on reaching steady state operation of the reactor and maximizing the yield of diesel and fuel oil like fraction. These "heavy" fractions (products with boiling point above 350 °C, i.e. above the final boiling point of diesel) are preferred as materials to be co-processed with crude oil without any significant changes in refinery technologies. In this case, bio-oil was modified with 5 wt.% of methanol and 1 wt.% of DMDS. The sulfur donor agent content was increased after the previous experience with the elevated feeding rate, where physical properties of products did not tend to get stabilized. Based on experience with triglycerides deoxygenation, decarboxylation is sensitive to H_2S concentration. The aim was to promote decarboxylation to speed up oxygen removal in the first two catalytic zones. To promote decarboxylation, the reaction temperatures of 2nd and 3rd zones were increased to 320 and 350 °C, respectively. As a result of these changes, steady state operation was reached in 50 h on stream. The selectivity to naphtha fraction (ca 25 wt.% in organic phase) and the average hydrocarbon yields (30 wt.% related to bio-oil fed; Fig. 8) was reduced as well. The rest of the organics was in the boiling point ranges of diesel and fuel oil. Unfortunately, the experiment had to be stopped early because of malfunctioning of the manometer on the gas liquid separator due to corrosion. The corrosiveness of the off-gas stems from its composition. It contains 50 wt.% water and high amount of H_2S and CO_2, respectively, and due to water vapor condensation in the presence of CO_2 corrosive carbonic acid is formed.

To reduce the corrosiveness, two different catalysts were loaded into the reactor based on results of previous experiments discussed above. Off-gases obtained during experiments with CoMoS catalyst contained lower concentrations of CO_x when compared with the off-gases from "NiMoS" experiments. It is explained by the lower decarboxylation activity of Co promoted catalysts and their preference in hydrodeoxygenation mechanism in oxygen removal [17,18]. CoMoS catalyst used for the initial reference test was loaded into the third (bottom) catalyst layer. The first two zones were loaded with NiMoS type catalyst used for the optimization

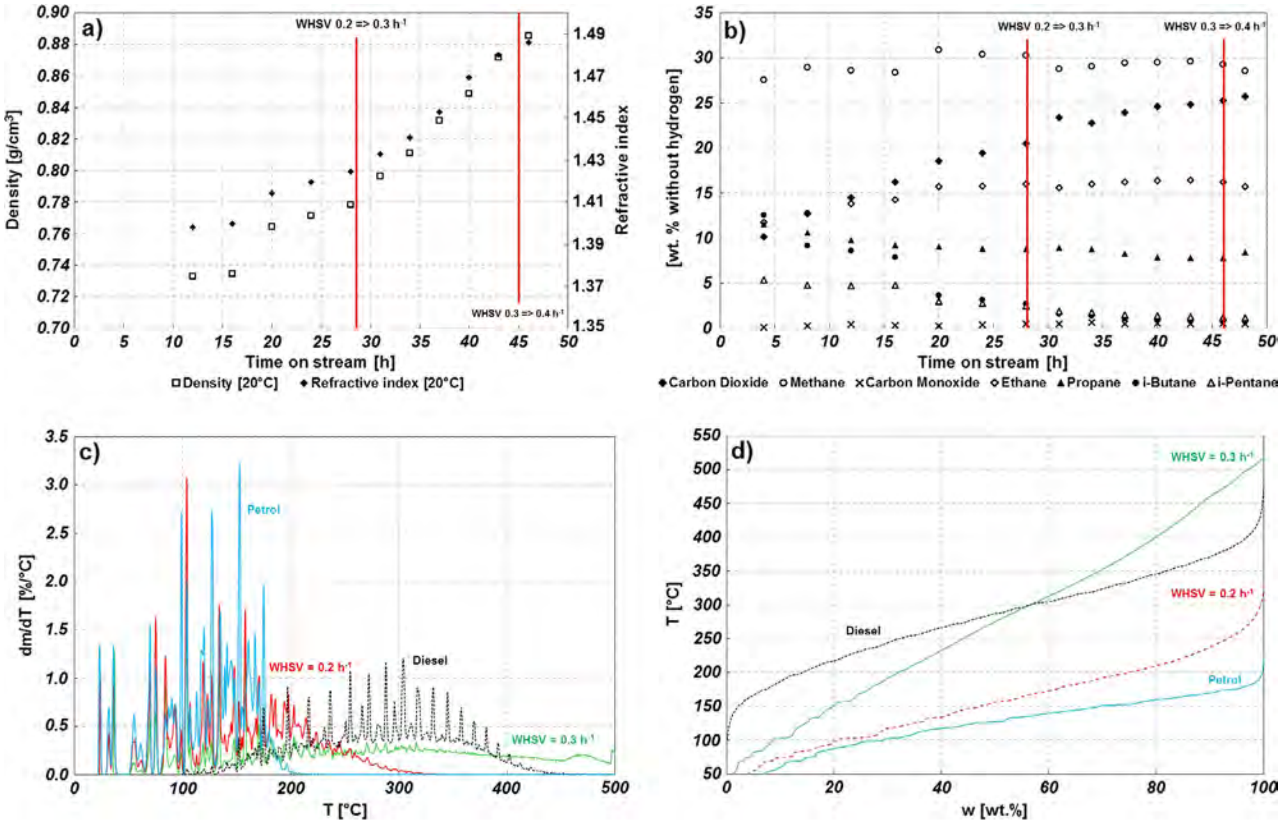

Fig. 7. Physical properties of organic layer during test (a); distribution of gaseous products (b); GC (Simdis) of products obtained over different flow rates and crude oil gasoline – Petrol (c); and distillation curves of these products (d) by Simdis, ASTM D2887.

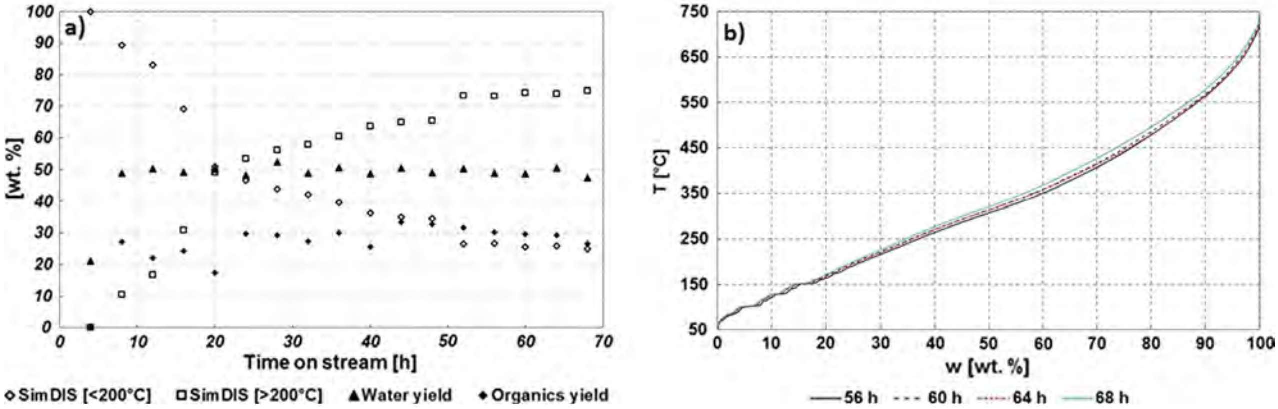

Fig. 8. Products yields from optimized test (a) and product boiling point distribution of products of steady state period (b).

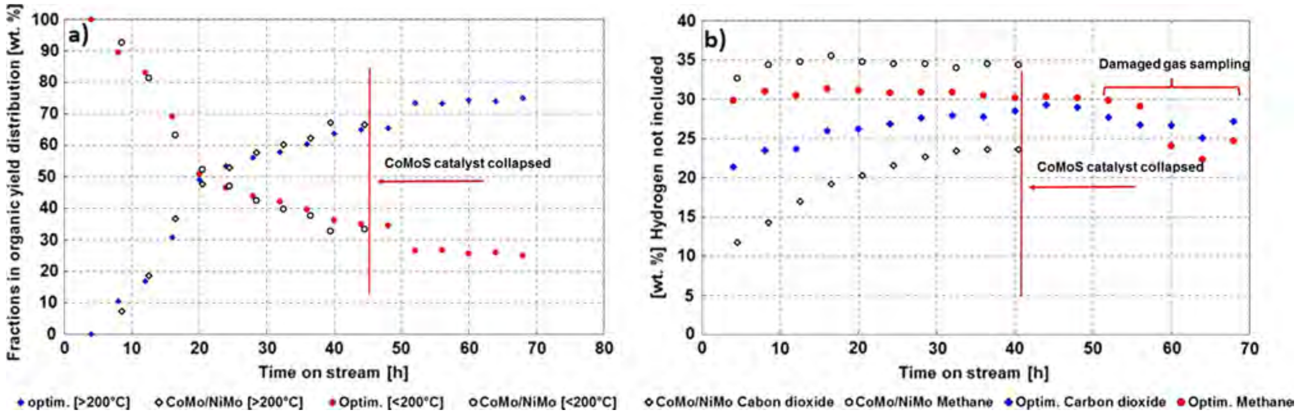

Fig. 9. Effect of CoMoS on properties of reactor outcome, role in hydrocarbon fraction composition (a), effect on CO_2 reduction (b) (NiMoS, test Nr. 4 and 5, 230, 320, 350 °C).

of feedstock composition and reaction conditions. The reaction setup was similar to that of the optimized test. No changes were observed in yields of boiling point distribution – naphtha/middle distillate yields, while gaseous product composition has changed significantly. The comparison of results pointed to near identical hydrocarbons yields with identical hydrocarbon boiling point distribution (Fig. 9a) as in the optimized test with NiMoS catalyst. It clearly shows, that the initial reaction parameters and catalyst properties are playing the key role in process of the bio-oil stabilization. The role of CoMoS active phase was reduction of CO_2 at the outlet of the reactor as it is well known that CoMoS catalysts are more active under low hydrogen partial pressure than NiMoS catalysts. Fig. 9b shows the difference between test with single NiMoS catalyst ("Optim.") and test with CoMoS type in the bottom. The presence of the CoMoS active phase resulted indeed in deeper deoxygenation/reduction of CO_2. The reduction of CO_x is a matter of economic optimization, because it reduces requirements for corrosiveness resistance of the reactor/separator parts, but also significantly increases hydrogen consumption.

4. Conclusions

A series of bio-oil hydrotreating experiments with two commercial hydrotreating catalysts and different experimental arrangements, in particular the use of additives and non-isothermal temperature profile, provided valuable information about bio-oil stabilization and its upgrading to automotive fuels fractions. In the first reactor zone, condensation reactions affording high molecular weight compounds with boiling point in the range typical for diesel fuel can be achieved by optimizing reaction temperature and feed flow rate. It results in partial deoxygenation and hydrogenation (saturation) of the most reactive compounds. This leads to the formation of two liquid phases, an organic and an aqueous one. The extent of condensation and coking in the first reactor zone is an important factor determining the overall bio-oil upgrading efficiency. The addition of methanol (up to 5 wt.%) facilitates accessibility of active centers by bio-oil compounds in the top part of the reactor. Consequently, the optimization of the reactor top zone is a key point of bio-oil stabilization. Moreover, due to the demanding conditions, a lot of attention must be paid to catalyst properties (e.g. resistance to acids in the feed, high oxygen elimination activity, coke formation reduction). The second reaction zone is responsible mainly for multiple double bonds and aromatics saturation. In the third reactor zone, the final high-temperature deoxygenation, saturation and hydrocracking take place. Hence, the optimization of the last reaction-zone temperature determines the organic-product boiling point distribution and the nature of the obtained fuel fraction. The active phase selection can help to change the product selectivity and as a result naphtha-, diesel- or fuel-oil-like products can be obtained. Moreover, the corrosiveness of the effluents from the reactor can be minimized by optimizing the catalyst composition in the last reactor zone.

Acknowledgements

The publication is a result of the project Development of the UniCRE Centre (project code LO1606) which was financially supported by the Ministry of Education, Youth and Sports of the Czech Republic under the National Programme for Sustainability I.

References

[1] European Biofuels Technology Platform web page: <http://biofuelstp.eu/bio-oil.html> [accessed on 23. 8. 2016].
[2] Bridgwater AV, Meier D, Radlein D. An overview of fast pyrolysis of biomass. Org Geochem 1999;30:1479–93.
[3] Hossain AK, Davies PA. Pyrolysis liquids and gases as alternative fuels in internal combustion engines – a review. Renew Sustain Energy Rev 2013;21:165–89.
[4] Prakash R, Singh RK, Murugan S. Experimental investigation on a diesel engine fueled with bio-oil derived from waste wood–biodiesel emulsions. Energy 2013;55:610–8.
[5] Huber GW, Iborra S, Corma A. Synthesis of transportation fuels from biomass: chemistry, catalysts, and engineering. Chem Rev 2006;106:4044–98.
[6] Guo X, Yan Y, Li T. Influence of catalyst type and regeneration on upgrading of crude bio-oil through catalytical thermal cracking. Chin. J. Process Eng. 2004;4:53–8.
[7] Adjaye JD, Bakhshi NN. Production of hydrocarbons by catalytic upgrading of a fast pyrolysis bio-oil. Part II: Comparative catalyst performance and reaction pathways. Fuel Process Technol 1995;45:185–202.
[8] Katikaneni SPR, Adjaye JD, Bakhshi NN. Performance of aluminophosphate molecular sieve catalysts for the production of hydrocarbons from wood-derived and vegetable oils. Energy Fuels 1995;9:1065–78.
[9] Elliott DC, Hart TR, Neuenschwander GG, Rotness LJ, Olarte MV, Zacher AH, et al. Catalytic hydroprocessing of fast pyrolysis bio-oil from pine sawdust. Energy Fuels 2012;26:3891–6.
[10] Zacher AH, Olarte MV, Santosa DM, Elliiott DC, Jones SB. A review and perspective of recent bio-oil hydrotreating research. Green Chem 2014;16:491–515.
[11] Capunitan JA, Capareda SC. Hydrotreatment of corn stower bio-oil using noble metal catalysts. Fuel Process Technol 2014;125:190–9.
[12] Mortensen PM, Grunwaldt J-D, Jensen PA, Knudsen KG, Jensen AD. A review of catalytic upgrading of bio-oil to engine fuels. Appl Catal A 2011;407:1–19.
[13] Diebold J, Czernik S. Additives to lower and stabilize the viscosity of pyrolysis oils during storage. Energy Fuels 1997;11:1081–91.
[14] BTG-BTL pyrolysis process web: <https://www.btg-btl.com/en/technology> [accessed on 23.8.2016].
[15] Furimsky E, Massoth FE. Deactivation of hydroprocessing catalysts. Catal Today 1993;17:537–660.
[16] Elliott DC, Baker EG, Beckman D, Solantausta Y, Tolenhiemo V, Gevert S, et al. Technoeconomic assessment of direct biomass liquefaction to transportation fuels. Biomass 1990;22:251–69.
[17] Furimsky E. Catalytic hydrodeoxygenation. Appl Catal A: Gener 2000;199:147–90.
[18] Horáček J, Tišler Z, Rubáš V, Kubička D. HDO catalysts for triglycerides conversion into pyrolysis and isomerization feedstock. Fuel 2014;121:57–64.

ACS Sustainable Chemistry & Engineering

Research Article

Cite This: *ACS Sustainable Chem. Eng.* 2019, 7, 7080−7093

pubs.acs.org/journal/ascecg

Quantitative Study of Straw Bio-oil Hydrodeoxygenation over a Sulfided NiMo Catalyst

Miloš Auersvald,*[†] Bogdan Shumeiko,[†] Martin Staš,[†] David Kubička,[†] Josef Chudoba,[‡] and Pavel Šimáček[†]

[†]University of Chemistry and Technology Prague, Department of Petroleum Technology and Alternative Fuels, Technická 5, 166 28 Prague 6, Czech Republic

[‡]Central Laboratories, University of Chemistry and Technology Prague, Technická 5, 166 28 Prague 6, Czech Republic

Supporting Information

ABSTRACT: Bio-oil upgrading through its hydrodeoxygenation (HDO) using sulfided catalysts has attracted significant attention because of its potential to provide advanced biofuels. Although many studies have been undertaken, a detailed understanding of the changes in the chemical composition on the molecular level that would allow the better design of catalysts for bio-oil upgrading is still insufficient. Therefore, we have subjected straw bio-oil and products obtained from its hydrotreatment over a broad range of experimental conditions to a detailed quantitative chemical analysis. Most of the volatile compounds were quantified by GC-MS. Among them, 115 compounds were quantified directly (i.e., using the appropriate standards) and more than 100 indirectly (i.e., based on their structural similarity with corresponding standards). Moreover, the total concentrations of carboxylic acids, carbonyls and phenols were quantified by the carboxylic acid number (CAN), Faix, and Folin−Ciocalteu methods, respectively, to obtain complementary and supporting information on the chemical composition to the GC-MS data. The detailed quantification of most volatile compounds in the feed and the products allowed us to create a reactivity order of the oxygen-containing functional groups present and to understand the origin of some of the compounds. On the basis of the results, the upgrading of straw bio-oil from ablative fast pyrolysis at 340 °C and 4 MPa seems to be optimal when evaluating the severity of the reaction conditions and hydrogen consumption, on the one hand, and the products quality, on the other hand. This provides a good starting point for further catalyst development and optimization allowing the long-term upgrading of the bio-oil for obtaining petroleum-refinery-compatible feedstock.

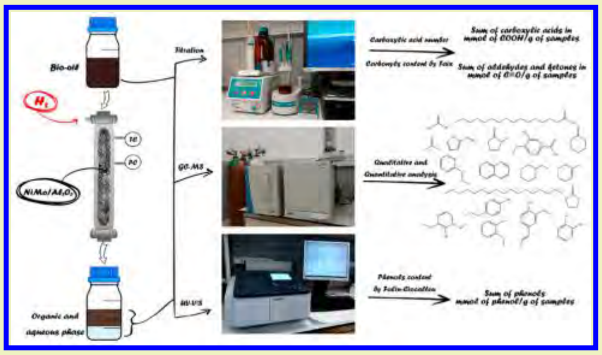

KEYWORDS: *Ablative flash pyrolysis, Hydrodeoxygenation, Quantitative analysis, GC-MS, Carboxylic acids, Carbonyls, Phenols*

INTRODUCTION

Fast pyrolysis is one of the simplest and most cost-effective options for the conversion of a lignocellulosic biomass into a bio-oil, achieving yields of up to 75 wt %.[1] Despite its undesirable properties (thermal lability, high acidity, high water/oxygen content),[2] the bio-oil has the potential to be used for the production of advanced biofuels. For this purpose, it is necessary to reduce the oxygen content of the bio-oil and to improve its properties in general. Despite its high operating expenditures, hydrotreatment is one of the most promising methods for bio-oil upgrading, producing higher yields of upgraded products with an acceptable quality.[3] Thus, it is desirable to optimize the bio-oil hydrotreatment process. For this purpose, a quantitative characterization of the chemical composition of the bio-oil and its upgraded products is crucial.[4]

A bio-oil is a complex mixture of hundreds to thousands of oxygenates.[5] Together with the fact that its chemical composition is strongly dependent on the original biomass,[2] this makes a detailed quantitative characterization very difficult and time-consuming. Probably, for this reason, some papers studying bio-oil hydrodeoxygenation (HDO) only focused on the characterization of the physicochemical properties of the HDO products.[6−8] To simplify the determination of the bio-oil composition, some researchers used the percentage of the total peak area obtained from GC-MS to estimate the content of the individual chemical compounds.[4,9−11] However, such an approach can be misleading due to the different response factors of the different oxygenates.

To our best knowledge, just three papers focused on the detailed quantification of the chemical changes occurring during the bio-oil HDO.[12−14] Routary et al.[12] used GC-FID and HPLC-RI to quantify oxygenates and a special GC-MS

Received: December 30, 2018
Revised: February 27, 2019
Published: March 11, 2019

DOI: 10.1021/acssuschemeng.8b06860

technique (nitric oxide ionization spectroscopy evaluation) to quantify the hydrocarbons formed. Sanna et al.[14] used GC-MS for the quantification of 28 different compounds and HPLC for the quantification of saccharides. Nevertheless, the most detailed study up to now was apparently carried out by Stankovikj et al.[13] from the National Renewable Energy Laboratory (NREL). This team developed, validated,[15] and recently published several methods for quantifying the most important chemical groups in bio-oils, such as carboxylic acids (CAN method),[16] carbonyls (Faix method),[17] and phenols (Folin−Ciocalteu method).[18] Stankovikj et al.[13] applied these methods to study the changes that occur in the nonvolatile oligomeric fractions during the bio-oil HDO. To quantify the changes in the volatile fraction, they used GC-MS. All of these works were focused on the hydrotreatment of wood bio-oil over noble metal catalysts. Because of their very high catalytic activity, the hydrogen consumption in the bio-oil HDO over these nonsulfided catalysts is higher than that over the sulfided catalysts, thereby increasing the processing costs and reducing product sustainability.[19] Moreover, the noble metals can be poisoned by the presence of even small amounts of sulfur compounds in the bio-oil,[19] which is why the well-established and robust sulfided catalysts remain the preferred choice for bio-oil HDO.[20]

Compared with noble metal catalysts, where HDO is often preceded by saturation of the aromatic rings, HDO preferably takes place over sulfided catalysts.[21] Often, only model compounds representing the typical compounds present in bio-oil have been hydrodeoxygenated over sulfided catalysts.[22] Typically, the reactivity of such compounds has been assessed individually, but their reactivity can be quite different in complex mixtures, such as bio-oils. The HDO of real bio-oils over sulfided catalysts has been studied as well[9,23,24] but with the main focus on the qualitative changes in the physicochemical properties, that is, none of the studies quantified the changes that take place in the chemical composition of bio-oils.

In our previous paper, we tested a sulfided NiMo/Al_2O_3 catalyst for the HDO of a straw bio-oil (as an alternative to the wood bio-oil generally used) from the ablative fast pyrolysis and analyzed the physicochemical properties of the resulting HDO products.[25] To provide a deeper understanding of the whole straw bio-oil HDO process over the sulfided catalysts, we have built upon our previous work and present what, to our best knowledge, is the first such detailed quantitative study of this process including analysis of both the aqueous and organic phases formed. Low-molecular compounds were quantified by GC-MS, 115 of them were quantified directly and the other more than 100 indirectly. The total concentrations of the carboxylic acids, carbonyls and phenols were quantified by the carboxylic acid number (CAN), Faix, and Folin−Ciocalteu methods, respectively. Thanks to the detailed analysis of the volatile compounds, we were able to consider the reactivity of the respective groups in the nonvolatile fractions of the samples. All of this allowed us to understand the complexity of the bio-oil HDO and to decide about the most favorable conditions for maximizing deoxygenation while minimizing hydrogenation of the aromatic rings. Moreover, the manuscript can serve as an overview of the HDO of oxygenates present in a real bio-oil over a sulfided catalyst. This quantitative description contributes to a better understanding of the whole process that is necessary for further advances in bio-oil hydrotreatment.

EXPERIMENTAL SECTION

Bio-oil and Hydrotreatment. Straw bio-oil was produced at Fraunhofer UMSICHT by the ablative fast pyrolysis of straw (wheat and barley, 1:1 w/w). The straw in the form of pellets was pressed onto a hot rotating disc and pyrolyzed at 550 °C with a vapor residence time of less than 1 s. After condensation at 2−5 °C, the liquid product spontaneously separated into an aqueous and organic phase (bio-oil used as feed for the hydrotreatment). More details are given in the literature by Schulzke et al.[26]

Before the hydrotreatment experiments, the bio-oil was first filtered to remove residual solids and then doped with 0.5 wt % dimethyl disulfide (Sigma-Aldrich, DMDS $\geq$ 99.0%) to maintain the catalyst activity as suggested by Yoshimura et al.[27] A commercial sulfided NiMo/Al_2O_3 catalyst (5.5 wt % of NiO and 28.3 wt % of MoO_3) and hydrogen (SIAD, 99.9 vol %) were used in the continuous fixed-bed hydrotreatment experiments. Two sets of experiments were carried out. In the first one (further labeled as $T/4$), the temperature (T) was increased from 240 to 350 °C at a constant hydrogen pressure of 4 MPa. The second experiment set was labeled as T/P; the temperature (T) and hydrogen pressure (P) varied between 300−360 °C and 2−8 MPa, respectively. Compared to our previous paper,[25] the $T/4$ experiment was repeated with a greater emphasis on the reaction conditions around 300 °C and 4 MPa, where the density of the organic phase became lower than that of water for the first time. Therefore, the temperature change step between 280−330 °C was only 10 °C.

The reaction products were labeled as follows: T/P = desired average temperature (°C)/pressure (MPa), the real average temperature in the catalyst bed and the time on stream of each reaction condition are summarized in Tables S1 and S2. The other reaction parameters were kept constant: WHSV was 1 h^{-1} (feed flow 50 $g \cdot h^{-1}$) and hydrogen flow rate at standard conditions was 90 $L \cdot h^{-1}$. The reactor configuration, catalyst activation, and other details of the hydrotreatment process are described in detail elsewhere.[25]

Analysis of the Feed and Products. The detailed description of the analytic measurement procedures for the elemental composition and water content analyses, commented on in this manuscript, was given elsewhere.[25]

GC-MS Analysis. A gas chromatograph Focus GC equipped with an autoinjector AI 3000, connected to a DSQ mass spectrometer (all Thermo-Fisher Scientific) was used for the GC-MS analyses. The instrument control, data acquisition, and processing were performed using Xcalibur 2.2 software (Thermo-Fisher Scientific). The conditions of the GC-MS analysis are given in Table 1. All samples (~80 mg) were dissolved in about 1.7 mL of acetone (Penta, p.a.) for the GC-MS analysis. Compounds with retention lower than or equal to that of acetone were analyzed in an *n*-butanol (Penta, p.a.) solution prepared at the same concentration level. The exact weight concentration obtained was finally used for the calculation of the wt % in a real sample. Ten microliters of an internal standard stock solution was added into each sample. The internal standard solution contained 1-butoxypropan-2-ol (Sigma-Aldrich) and 2-naphthalde-

Table 1. Conditions of the GC-MS Analysis

parameter	description
injection	250 °C, 1 μL, split 1:20
carrier gas	helium, (5.5), 1 $mL \cdot min^{-1}$
temperature program	32 °C (8 min), then 5 $°C \cdot min^{-1}$ to 300 °C (10 min)
column	ZB-5MSi, W/Guardian, 30 m (+5 m Guardian end) × 0.25 mm × 0.25 μm
interface	280 °C
MS ionization	EI^+, 70 eV
solvent delay	3.0 min (only for analysis of acetone solutions)
data acquisition	full scan, 20−500 Da
scanning frequency	5 $scans \cdot s^{-1}$
analyzer	quadrupole

hyde (Koch Light) dissolved in ethanol (Penta, absolute for UV spectroscopy). The concentration of each internal standard in the stock solution was 34 mg·mL^{-1}. The prepared samples were homogenized in an ultrasonic bath and filtered using a 0.45 μm syringe filter. Identification of the detected compounds was performed using a NIST 14 mass spectra library, standard compounds, or Kovats indices; only the peaks with a match factor above 700 were further quantified.

Four mixtures containing 115 standard compounds (each approximately 1 mg·mL^{-1}) were used for the direct quantification: (i) most of the oxygenates were dissolved in acetonitrile (Merck, LC grade), (ii) acids and some other oxygenates were dissolved in ethanol (Penta, absolute for UV spectroscopy) to avoid coelution with the compounds present in the first mixture, (iii) low-boiling-point oxygenates were dissolved in *n*-butanol (Penta, p.a.), and (iv) hydrocarbons were dissolved in *n*-hexane (Penta, 99%, p.a.). For each compound, a six-point calibration curve covering the concentrations from 25 to 1000 μg·mL^{-1} was created (measured from the lowest to the highest concentration). The quantification was performed using the Xcalibur 2.2 Quan Browser tool; all calibration curves were obtained with an R^2 value of ≥0.995 from at least 4 points. For a more precise quantification, the areas of the peaks from the selected extracted ions specific to each compound (instead of the total ion current (TIC)) were used. Usually, one up to three ions with the highest intensity specific for the compound concerned were selected. Other compounds were quantified indirectly based on the response factor of the most structurally similar compounds,[28] using eqs 1 and 2. The list of standards, suppliers, purity, ions for quantification, relevant oxygenates group, and other quantified compounds are given in Tables S3−S6. The primary results of the quantification expressed in μg·mL^{-1} were recalculated to wt %. For a better comparison between the product samples and the feed, the cumulative changes in wt % for each compound were calculated as the wt % of a compound divided by the yield of the relevant product, that is, as the yield of the compound. To compare between the GC-MS results and the results obtained from other applied methods (see below), the yield of each compound (cumulative wt %) was recalculated to mmol·g^{-1} using the molecular weight of relevant compound and further multiplied by the number of relevant oxygen functional groups for CAN and Faix methods.

$$C_i = A_{m/z}(i)/k(i) \times k(\mathrm{STD})/A_{m/z}(\mathrm{STD}) \times C_{\mathrm{STD}} \quad (1)$$

where C = concentration, A = peak area, k = ratio of ions area, i = similar compound to STD, and STD = standard compound.

$$k(i) = \frac{A_{m/z}(i)}{A_{\mathrm{TIC}}(i)} \quad (2)$$

where k (i) is the ratio of the area of ions for the quantification and total TIC area, determined from the NIST library.

Carboxylic Acid Number. The carboxylic acid number (CAN) was determined by a 716 DMS Titrino instrument (Metrohm AG) equipped with LabX titration software using a titration method described in detail elsewhere.[16] The electrode system consisted of combined glass, silver chloride and platinum electrodes (Metrohm AG). The sample (0.2−3.0 g, the amount used increased with its decreasing acidity) was titrated by a 0.1 M solution of tetrabutylammonium hydroxide (86854 Sigma-Aldrich) dissolved in a 10:1 V/V mixture of isopropyl alcohol and methanol (Penta, p.a.) standardized by a known amount of potassium hydrogen phthalate (Sigma-Aldrich). A 0.4 M solution of tetraethylammonium bromide (Sigma-Aldrich, 98%) dissolved in ethylene glycol (Penta) was used as an electrolyte in the silver chloride electrode and isopropanol (Penta, p.a.) was used as a sample solvent. Each sample (feed or HDO product) was analyzed in triplicate.

Carbonyls Content by Faix. The total carbonyls content was determined by the Faix method based on the oximation of the carbonyl group and further by the reverse titration of the released HCl, described in detail elsewhere.[17] The sample (0.2 g for the feed, up to 1.0 g for the best, that is, the most deoxygenated product 360/8) was weighed into an 8 mL vial. Then, (i) 1 mL of dimethyl sulfoxide (DMSO; Penta, p.a.), (ii) 2 mL of hydroxylamine hydrochloride ($NH_2OH·HCl$, Sigma-Aldrich, ≥99.9995%) solution (0.3 M in 80% ethanol), and (iii) 2 mL of triethanolamine (TEA, Sigma-Aldrich, ≥ 99.0%) solution (0.5 M in ethanol) were added in the given order. The vial was tightly closed and placed into a preheated bath (80 °C), where it was stirred for 2 h to complete the reaction. In addition, each sample group included three blank samples (consisting of a mixture of the DMSO, $NH_2OH·HCl$, and TEA solutions). After it was cooled down to ambient temperature, the sample was quantitatively transferred into a titration vessel using distilled water and ethanol to create an 80% ethanol solution and titrated. Each sample (feed or HDO product) was prepared, oximated, and analyzed in triplicate.

Phenols by Folin−Ciocalteu. The total content of the phenols was measured by the Folin−Ciocalteu method optimized for bio-oils.[18] The bio-oil and products were dissolved in ethanol (Penta, absolute for UV spectroscopy) to obtain samples with a concentration of ~500 mg·L^{-1}. The sample was homogenized in an ultrasound bath and then 20 μL of this solution was weighed into a 1 cm path-length polystyrene cuvette. Then, 1.58 mL of distilled water and 100 μL of the Folin−Ciocalteu reagent (Sigma-Aldrich, 2 N) were added, and the content of the cuvette was properly mixed. After ~5 min, 300 μL of a 20% aqueous solution of sodium carbonate was added in to the cuvette. The mixture was again properly mixed and allowed to develop the color for 2 h at ambient temperature. Gallic acid (Sigma-Aldrich, 97.5−102.5%) was used as a calibration standard to create a four-point calibration curve between the concentrations of 50 and 500 mg·L^{-1}. The absorbance of all the samples was measured after a final homogenization against a blank (20 μL of ethanol instead of a sample) at 765 nm using a UV-1800 spectrophotometer (Shimadzu, Japan). The average of three measurements was recalculated to mmol of phenols per gram assuming phenol as the surrogate structure[29] to allow a direct comparison with the GC-MS results.

■ RESULTS AND DISCUSSION

Physicochemical Properties. The physicochemical properties of the organic phases were discussed in our previous paper.[25] Regarding the aqueous phase (AP), only the elemental composition and water content were measured. We found that the AP contained 8.7 and 7.3 wt % of carbon for the mildest reaction conditions of 240 °C at 4 MPa and 300 °C at 2 MPa, respectively. The carbon content gradually decreased with the increasing severity of the reaction conditions (and, thus, the lower content of the polar oxygenates in the reaction system) to 2.4 and 1.0 wt % for the most severe conditions tested, that is, 350 °C at 4 MPa and 360 °C at 8 MPa, respectively (Tables S1 and S2). The carbon content in the AP evidence the presence of organics in the aqueous phase, which consequently contained between 85 to 98 wt % of water only (Tables S1 and S2).

GC-MS Analysis. First, the temperature program of the GC-MS analysis was optimized to obtain the optimum separation of all the samples. Then, two internal standards, which did not coelute with any peak in all of the samples, were selected. The first one (1-butoxypropan-2-ol) eluted in the first quarter of the chromatogram (retention time 16.45 min) was used for the quantification of all the compounds with the retention time (RT) of up to 24.50 min. The second one (2-naphthaldehyde RT 33.50 min) was used for the quantification of all the compounds with the RT of 24.51 min and higher. In total, 115 compounds were quantified directly and almost 140 other ones indirectly; most of them were present in the product organic phase and in the feed. Only some compounds were unique for the product aqueous phase, such as cyclohexanediols.

The feed (being the least homogeneous sample) was used, after homogenization, to prepare five samples for further analysis. Each of them was analyzed three times using the same calibration curve. We found that for the most of the oxygenates

DOI: 10.1021/acssuschemeng.8b06860
ACS Sustainable Chem. Eng. 2019, 7, 7080−7093

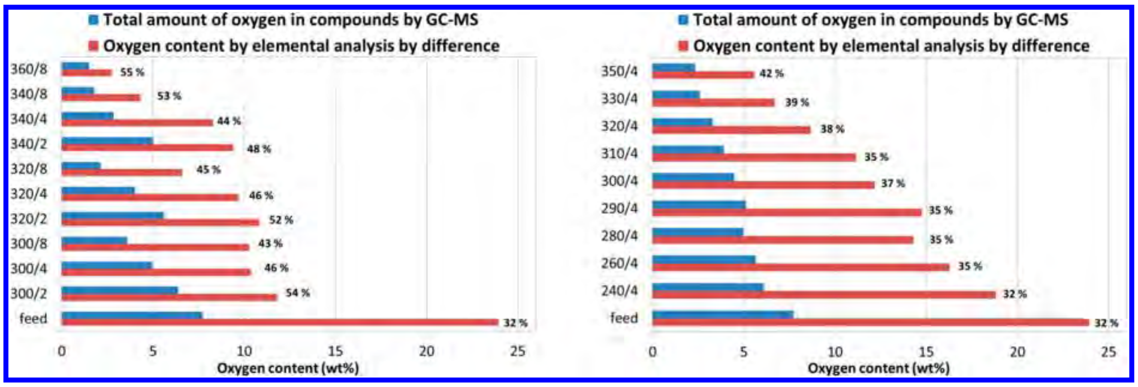

Figure 1. Total amount of oxygen in oxygenates determined by GC-MS vs the total amount of oxygen determined by elemental analysis in organic phase of bio-oil and products. The number on the right side of the red column is the share of the blue/red column.

in the standard mixtures (Tables S3−S5), the calibration curve was very stable with an R^2 value significantly higher than 0.995, and the relative standard deviation (RSD) was up to 5% for the 15 results obtained for each compound in the feed, see Table S7. There were only a few compounds with an RSD between 5−6%, such as pentan-3-one, 2,6-dimethylphenol, 2-propylphenol, 2,4,5-trimethylphenol, and 2,3-dimethylphenol (Table S7). The slightly higher RSD for these compounds was mainly caused by their low concentrations in the feed (below 0.1 wt %). For 2-ethyl-4-methylphenol, *cis*-methylisoeugenol, and 3-/4-propylphenol, the RSD was higher than 6% (Table S7), and this was caused by even lower concentrations of these compounds (below 0.05 wt %). The only compounds with a poorly stable calibration curve (RSD above 6%) were carboxylic acids (vanillic, isovanillic, palmitic, and stearic), pyrocatechol, and levoglucosan (Table S7); all of these compounds had tailing peaks. Excluding pyrocatechol, the higher RSD was probably caused also by high boiling points of these compounds leading to their discrimination in the injector.

Quantification of Oxygenates in the Aqueous Phase by GC-MS. As mentioned in previous section, the aqueous phase contained less than 9 wt % of carbon. We were only able to quantify 44 different oxygenates in the aqueous phases (APs) in total. They included predominantly low-molecular-weight alcohols, ketones, and acids up to valeric acid with acetic acid amounting to at least 40% of all the organic compounds present. All quantified compounds and their calculated amounts are given in Tables S8 and S9. The directly quantified compounds constituted more than 80% from all the quantified compounds in the AP. Except for the mentioned compounds, benzenediols, phenols, and lactones were present in the AP. The quantified compounds accounted from 50 wt % up to almost 90 wt % of the total carbon content determined by elemental analysis in the APs (Tables S8 and S9). We observed very low oxidation stability of the APs except those from the 340/8 and 360/8 products, which contained a very low amount of organic matter. After the removal of the APs from the samples and enabling access to the air, solid dark particles were formed after a few days, see Figure S1. This implies that most of the unidentified carbon was probably constituted by unstable compounds probably of saccharides or lignin origin that were soluble in water and not detectable by GC-MS.

Quantification of Oxygenates in the Organic Phase by GC-MS. We were able to identify and determine 32% of the volatile oxygenates in the feed. For the best, that is, the most deoxygenated product (360/8), it was more than 50 wt % (Tables S10 and S11). The total amount of oxygen (determined by elemental analysis by difference) in the *T*/*P* experiment sharply decreased to one-half compared to the feed already in the 300/2 product. This step change was definitely caused by the removal of water from the product by the separation of the HDO products into an aqueous and organic phase. Another reason could be the decomposition of the high-boiling pyrolytic lignin molecules and the subsequent deoxygenation of the aldehyde and aliphatic hydroxyl groups. An increase in pressure at 300 and 320 °C led to a gradual decrease in the ratio of volatile oxygenate compounds (Figure 1). As the decrease in volatile fractions was sharper than the decrease in the total oxygen content in the whole sample, we think (based on GC-MS chromatogram) that this difference was caused by the occurrence of many intermediates volatile products that were not identified and, thus, quantified due to coelution and/or unavailability of the spectra in the MS library. The decomposition of the pyrolytic lignin molecules further increased at 340 °C and 8 MPa, and thus, the share of oxygen in the volatile compounds (mainly with propyl substituent) has again increased (Figure 1). In the course of all the subsequent reactions (Figure S2), the main product of this decomposition, 4-propylphenol, reached its maximum content at 350 °C and 4 MPa (Figure 2G). Unfortunately, the results from *T*/*P* and *T*/4 experiments at the same reaction conditions (300 and 320 °C at 4 MPa) are not directly comparable. It is a consequence of a significant difference in the time-on-stream (Tables S1 and S2) and, hence, the different extent of the catalyst deactivation.

The total amount of the compounds quantified in the organic phases by GC-MS varied between 23 and 38 wt % (Tables S10 and S11). The highest amount of the compounds was determined as expected (based on the significant decrease in the MCR) in the sample prepared at 360 °C and 8 MPa (i.e., 360/8). The total fraction of the sample that was identified can be obtained by adding the water content in the relevant sample to the total concentration of all the organic compounds identified and quantified by GC-MS. For example, 48.4 wt % of the feed was determined in detail (Table S10). A change in temperature as well as in the pressure only had a minimal influence on the share of the quantified compounds in the volatile fractions, the only exceptions were the conditions ≥340 °C at 8 MPa (Table S11), caused by the increase in the extent of the pyrolytic lignin decomposition as was discussed above.

Nonquantified compounds formed approximately 5% of total TIC peak area of feed, to less than 15% in the case of the HDO products. This slightly higher abundance of the nonquantified

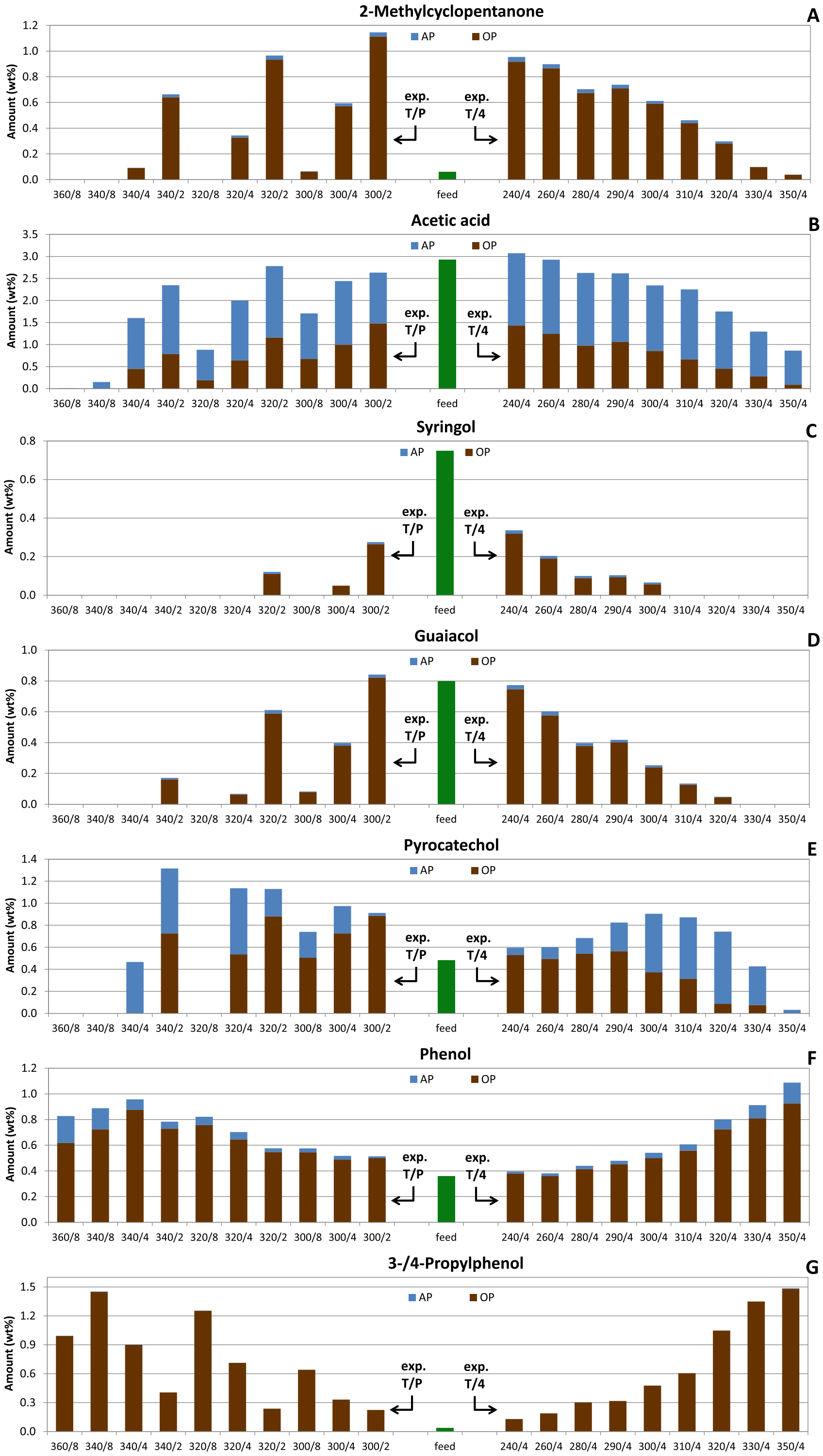

Figure 2. Cumulative changes in wt % of the compounds representing each group of oxygenates and their distributions between the aqueous and organic phase.

compounds was due to several reasons: (i) the increase in the number of compounds with a very low concentration that could not be identified with sufficient precision (and thus quantified); (ii) the increase in the peak coelution and then impossible identification; and (iii) more compounds with high-boiling-point that could not be identified and quantified were also present. Nonetheless, the majority of the volatile compounds was reliably identified and thus quantified.

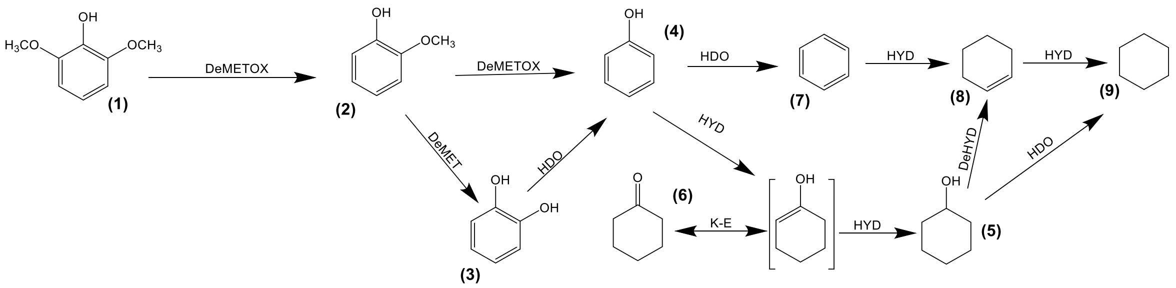

Figure 3. Reaction scheme of the nonalkyl monocyclic compounds. Compounds: (1) syringol; (2) guaiacol; (3) pyrocatechol; (4) phenol; (5) cyclohexanol; (6) cyclohexanone; (7) benzene; (8) cyclohexene; (9) cyclohexane. Reactions: HYD, hydrogenation; DeMEOX, demethoxylation; DeMET, demethylation; HDO, hydrodeoxygenation; K-E, ketone/enol isomerization.

Distribution of the Selected Compounds between the Organic and Aqueous Phase. During the bio-oil hydrotreatment, the single-phase bio-oil separated into an organic and aqueous phase as a result of the changes in its polarity. Consequently, some of the oxygenates were present in both the organic and aqueous phases which makes rigorous quantification of these compounds challenging. Significant elution into the aqueous phases was observed particularly for acids and benzenediols (Figure 2B and E) and at elevated reaction temperatures (>320 °C) for phenol also (Figure 2 F). The elution of these compounds into the aqueous phase was favored by the increased hydrotreatment severity that resulted in the decreasing of the organic phase polarity. The elution of other compounds into the aqueous phase was very limited (Figure 2). As expected, the presence and the increasing length of the alkyl chain in the phenolic compounds decreased their solubility in the aqueous phase. Thus, 3-/4-propylphenol was present in the aqueous phase in a very small concentration only at the most severe hydrotreatment conditions, that is, when the least polar organic phase product was obtained (Figure 2G, Tables S8 and S9). These findings are supported by the solubility of these compounds in water (Table S12). These results also show the necessity of analyzing both the aqueous and organic phases to obtain the complete information about the products formed. This can be demonstrated on pyrocatechol and acetic acid. Without the aqueous phase analysis, one would erroneously concluded that pyrocatechol and acetic acid were completely removed already from the reaction mixture at 340 °C and 4 MPa and 340 °C and 8 MPa, respectively. However, under these conditions, the unconverted pyrocatechol and acetic acid were present exclusively in the aqueous phase (Figure 2B and E).

For 2-methylcyclopentanone, as a ketone with the highest concentration in the HDO products, only very low elution into the aqueous phase was observed. More interestingly, its concentration increased dramatically in the products, particularly those obtained at the mildest reaction conditions, that is, at 300/2 and 240/4 (Figure 2A). On the basis of the detailed quantitative GC-MS analysis, we suggest that 2-methylcyclopentanone was created, in addition to hydrogenation of 2-methylcyclopent-2-enone (0.30 wt % in the feed) as also reported by Gunawan et al.,[30] by partial deoxygenation of 3-methylcyclopenta-1,2-dione (0.60 wt % in the feed).

Deoxygenation of Typical Oxygenates Groups. In this section, we will discuss the reactivity of all the typical oxygenate groups present in the bio-oils. We start with compounds created predominantly by the pyrolysis of cellulose and hemicellulose. Then, we will describe the reactivity of the typical aromatic compounds produced by lignin pyrolysis. We focused on nonalkylated ones and those with a propyl substituent. For those two groups, the reaction schemes were created.

The most reactive oxygenates were aldehydes that completely disappeared under both mildest conditions tested, see Tables S13 and S14. These results are in line with those presented by Elliott[31] for sulfided catalyst. On the contrary, we observed a lower reactivity of the ketones and alcohols that were completely removed only at 320 °C and 8 MPa, and at 340 °C and 8 MPa, respectively, compared to the temperatures below 200 °C reported by Elliott.[31] The main reason was probably their formation from other compounds (by consecutive reactions) and higher space velocity (1 h^{-1}) than usually used for the bio-oil hydrotreatment (~0.3 h^{-1}),[32] which did not allow their complete deoxygenation. The starting temperature of the reactivity of acetic acid in our experiments was close to that reported by Elliott[31] for acids in general (>260 °C vs ca. 290 °C). Only at 240 °C and 4 MPa, we observed a little bit higher concentration of acetic acid in the reaction system (Figure 2 B), which was caused probably by its creation from other compounds by consecutive reactions. Butyric acid was the only quantified acid for which we observed the significant increase in concentration in the products (Tables S7 and S15). The significant creation of butyric acid during hydrotreatment (the deoxygenation exceeds creation at 300 °C and 4 MPa for the first time) is in line with the results published by Chaiwat et al.[33] Although, the deoxygenation (conversion) of carboxylic acids started at temperatures below 300 °C, it was completely finished only at the conditions of 360 °C and 8 MPa, as obvious better from Figure 2 B, mainly due to the distribution of acids between the aqueous and organic phase. The reactivity of esters and lactones was slightly higher than that of acids (Tables S13 and S14), which is in accordance with the conclusions of Laurent and Delmon.[34]

However, dihydrobenzofuran completely disappeared from the reaction mixture already at the mildest conditions tested; furfurals and acetylfuran were removed at 240 °C and 4 MPa and at 290 °C and 4 MPa, respectively (Tables S7 and S15). Moreover, 2-methylfuran and 2,5-dimethylfuran were completely removed from the reaction mixture only at the conditions of 360 °C and 8 MPa (the only detected furans since acetyl furan was removed, see the content of furans in Tables S13 and S14). The presence of these furans at these conditions was probably caused because of the steric hindrance of furanic oxygen by the methyl group. Alternatively, these furans could be formed by the decomposition of the pyrolytic lignin macromolecules, where the furanic units could be present.[35] On the basis of the similar increasing trend in

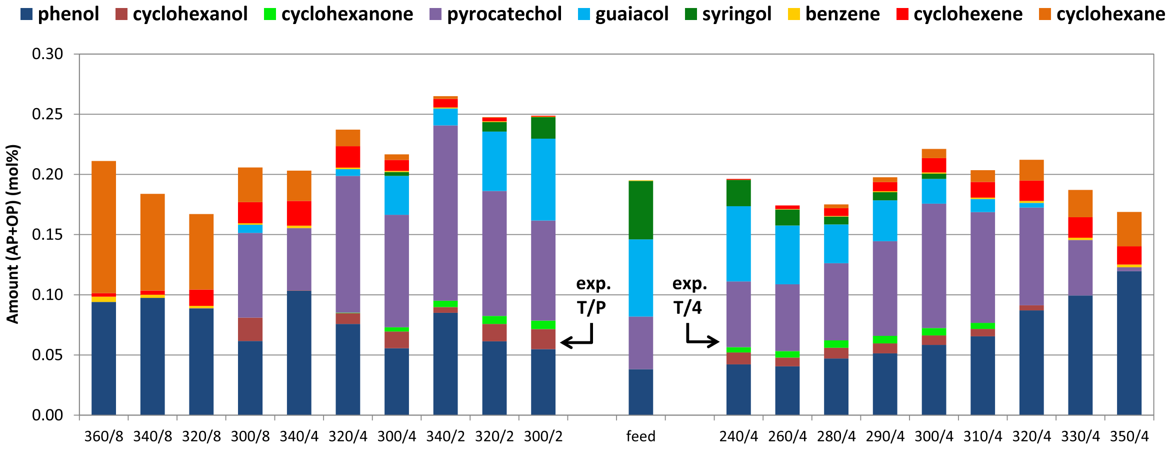

Figure 4. Cumulative changes of the nonalkyl monocyclic compounds in the feed and all products.

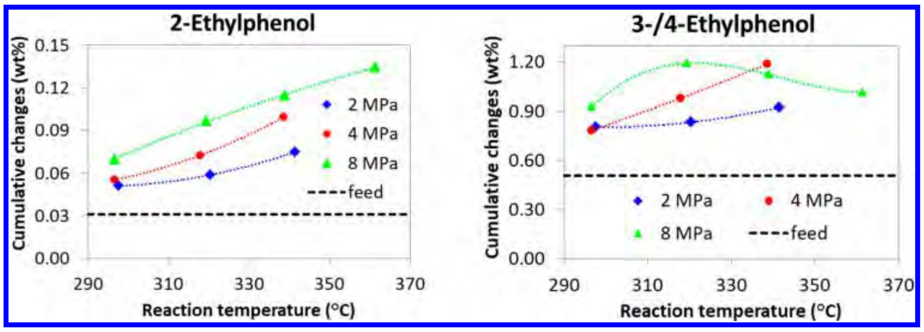

Figure 5. Content of 2-ethylphenol and 3-/4-ethylphenol in the feed and all the organic phases of products from the *T*/*P* experiment.

content of furans and monohydroxybenzenes during the increasing pressure at 300 °C (Table S14), we think that the formation of furans from the pyrolytic lignin could be possible.

The reaction scheme of the nonalkyl monocyclic compounds is shown in Figure 3. The yields of these compounds in the feed and all the products are shown in Figure 4 as the sum for the whole group of the related reaction products in molar % to allow a good comparison between the different compounds. The observed fluctuation in the content of the nonalkyl monocyclic compounds (Figure 4) can be attributed to the measurement errors and the necessary recalculations. This indicates that these compounds were formed neither by pyrolytic lignin decomposition that occurred nor by the dealkylation of alkyl monocyclic compounds.

Syringol started to deoxygenate at the mildest condition tested. On the basis of Figure 4, we can propose several reaction routes for syringol (Figure 3): (i) both methoxy groups were removed to create phenol (the concentration of guaiacol did not rise), (ii) only one methoxy group was removed and approximately the same amount of created guaiacol was deoxygenated through demethoxylation, or (iii) one methoxy group was demethoxylated and the other one was demethylated to create pyrocatechol, whose concentration increased up to the condition of 300 °C and 4 MPa and 340 °C and 2 MPa, respectively (Figure 2 E). When both methoxy groups were removed, phenol was formed and underwent further hydrogenation to yield some intermediate products such as cyclohexanone and cyclohexanol (Figure 3). These intermediates were completely removed from the reaction mixture for the *T*/4 experiment at temperatures 320 °C and for *T*/*P* experiment at all temperatures at a pressure of 8 MPa (Figure 4). It is obvious that also small amount of phenolic hydroxyl group (probably due the subsequent demethoxylation of methoxy phenols) was already deoxygenated to benzene, cyclohexane, and cyclohexene at both mildest conditions (Figure 4, Tables S16 and S17).

Assuming that guaiacol was first formed by the demethoxylation of syringol, then its demethoxylation rate was higher than that of syringol at 260 °C and 4 MPa, and 320 °C and 2 MPa, respectively, since its yield did not increase (Figure 2 D). Although benzene-di/triols were quantified with a larger measurement error (as already explained), it is obvious from the GC-MS results that their deoxygenation rate was lower than their rate of formation by guaiacol demethylation up to 300 °C at 4 MPa and for 340 °C at 2 MPa (Tables S13 and S14 and Figure 2 E).

Monohydroxylbenzenes were the least reactive compounds. Their rate of deoxygenation exceeded their rate of formation (by demethoxylation of methoxy phenols and pyrolytic lignin decomposition) at 360 °C and 8 MPa only. These results are also in line with those presented by Elliott.[31]

The presence of the alkyl chain in the ortho position of phenols could reduce the accessibility of the hydroxyl group to the catalyst active site, as was discussed by Gevert et al.[36] Therefore, compounds, such as *o*-cresol, 2-propylphenol, and 2-ethylphenol, were not deoxygenated significantly at 340 and 360 °C and 8 MPa. The concentration of 2-ethylphenol even continued to rise, which could be attributed to its significant presence and formation from pyrolytic lignin, alternatively, 2-

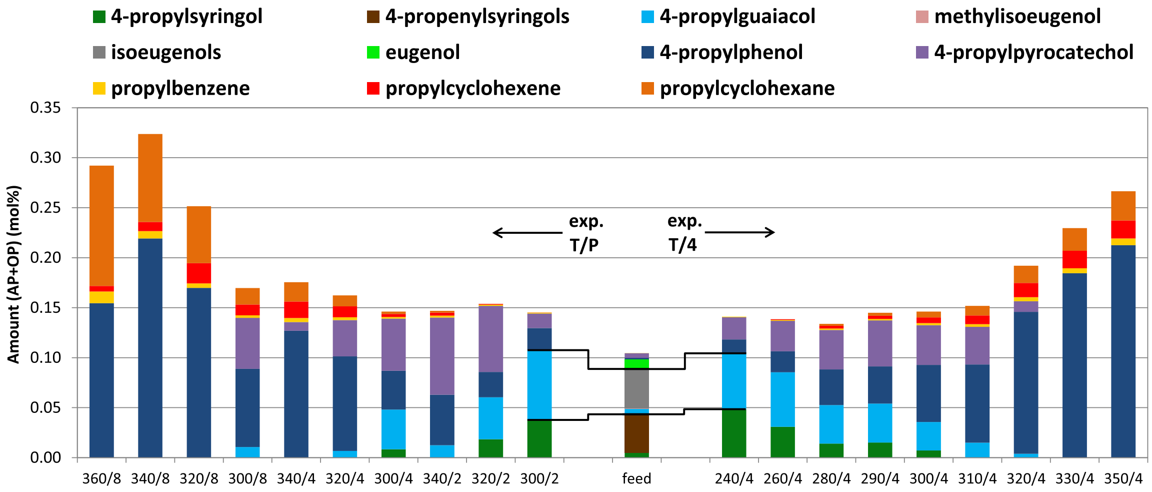

Figure 6. Cumulative changes of the compounds with one ring substituted with propyl chain (propyl monocyclic compounds); the black lines separate the compounds that were transformed to 4-propylguaiacol (gray and light blue row) and 4-propylsyringol (brown and dark green row) through hydrogenation of the double bound in the propyl substituent.

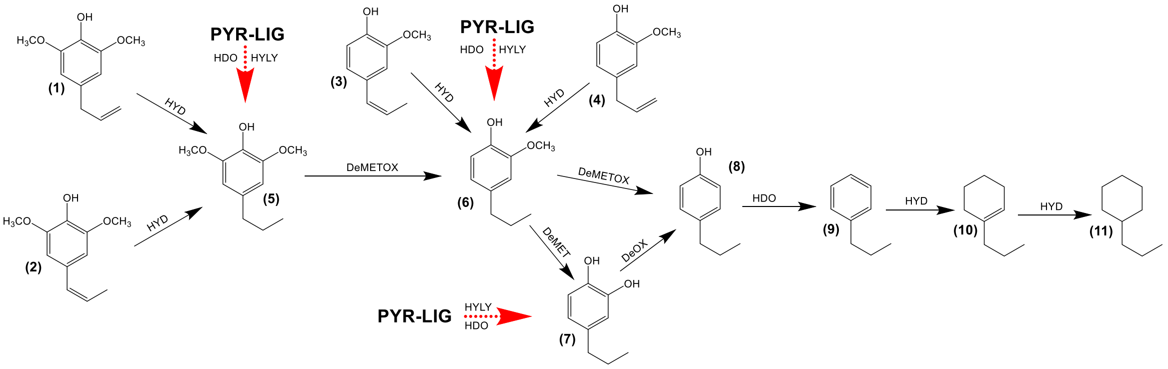

Figure 7. Reaction scheme of the propyl monocyclic compounds: (1) 4-allyl-syringol, (2) 4-(1-propenyl)syringol, (3) isoeugenol, (4) eugenol, (5) 4-propylsyringol, (6) 4-propylguaiacol, (7) 4-propylpyrocatechol, (8) 4-propylphenol, (9) propylbenzene, (10) 1-propylcyclohexene, (11) propylcyclohexane. Reactions: HYD, hydrogenation; DeMEOX, demethoxylation; DeMET, demethylation; HDO, hydrodeoxygenation; HYLY, hydrogenolysis. The compounds whose concentration is affected by the decomposition (hydrolysis) of pyrolytic lignin followed by subsequent deoxygenation of aldehydes and free hydroxyl groups are marked by red arrows.

ethylphenol could be created from benzofuran[37] possibly released from pyrolytic lignin, see Figure 5 and Table S15.

In contrast to nonalkylated monocyclic compounds, whose overall concentration was virtually constant in the range of the tested experimental conditions, the concentration of the propyl monocyclic compounds, as well as other alkylated phenols clearly increased with the increasing severity of the hydrotreatment. The increase can be attributed to the decomposition of pyrolytic lignin as indicated in Figure 7.

The hydrogenation of the double bonds in the alkyl substituents on the aromatic ring already took place at the mildest reaction conditions of both the experiments, which resulted in the complete hydrogenation of eugenol and isoeugenols to 4-propylguaiacol. The yield of 4-propylguaiacol in the product was higher than the sum of the molar yields of all the propenylguaiacols (Figure 6). This can be explained by the partial decomposition of the pyrolytic lignin molecule, where 4-propyl(enyl)guaiacols could be present, at the mildest condition of both the experiments, as assumed in previous section. For the condition of 300 °C and 2 MPa, the increase in 4-propylguaiacol could be caused by the partial demethoxylation of 4-propylsyringol. Methoxyeugenol and 4-propenylsyringols were hydrogenated to 4-propylsyringol, whose concentration slightly increased at 240 °C and 4 MPa probably because of the formation of 4-propylsyringol from pyrolytic lignin. But at 300 °C and 2 MPa, 4-propylsyringol was already partially deoxygenated to 4-propylguaiacol or to 4-propylpyrocatechol, 4-propylphenol or even completely to propylbenzene, propylcyclohexene, or propylcyclohexane (Figure 7). The same reactivity of a double bound conjugated to an aromatic ring was observed in case of 4-vinylguaiacol that was fully hydrogenated to 4-ethylguaiacol under both the mildest conditions, see Tables S7 and S15. All the aromatic oxygenates with an alkyl substituent could in principle be pyrolytic lignin decomposition products as shown in Figure 7.

The concentration of 4-propylphenol increased six times and ten times compared to the feed and products 240/4 and 300/2, respectively (Figure 2 G). At these products, the sum of all propyl monocyclic compounds increased by one-third which is further confirmation of the suggested pyrolytic lignin decomposition. Until the conditions of 310 °C at 4 MPa, the total content of propyl monocyclic compounds was almost

Table 2. Reactivity of the Compounds during the Bio-oil Hydrodeoxygenation over the Sulfided NiMo Catalyst

Decreasing reactivity

Group of compounds	Rate of removing exceeds rate of formation* (°C/MPa)	Complete disappearance from reaction mixture* (°C/MPa)
Aldehydes	ND	<240/4; <300/2
Syringols	<240/4; <300/2	340/2; 310/4
Guaiacols	240/4; 320/2	330/4; 320/8
Benzenediols	310/4	320/8
Esters/Lactones	<240/4; <300/2	350/4; 340/8
Ketones	<240/4; <300/2	340/8
Alcohols	<240/4; <300/2	360/8
Furans	<240/4; <300/2	360/8
Carboxylic acids	260/4	360/8
Mono-hydroxy-benzenes	360/8	ND

*The mildest conditions when the one of these two states was reached. The table was created based on the cumulative sum of each group. The individual compounds could have slightly different reactivity, and hence, different temperature when a change in their concentration is observed.

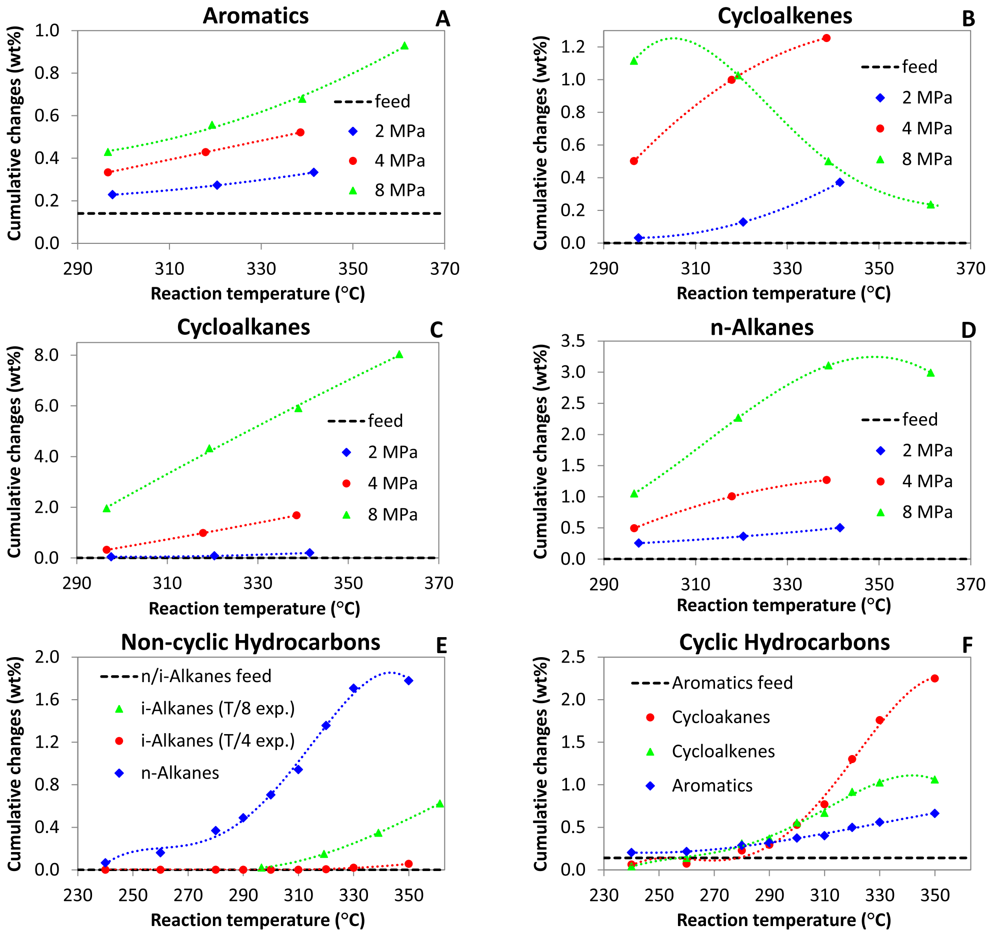

Figure 8. Cumulative changes in wt % by hydrocarbon groups A–D for the T/P and E–F for the T/4 experiment. *i*-Alkanes represent the sum of C5–C9 *i*-alkanes.

constant (Figure 6). Above 310 °C at 4 MPa, the concentration of propyl monocyclic compounds increased dramatically (Figure 6), most likely due to the further decomposition of pyrolytic lignin. The reactivity of the propyl monocyclic compounds was almost the same as that of the nonalkylated monocyclic ones. The only noteworthy difference was that no significant concentration of intermediates products, such as 4-propylcyclohexanol or 4-propylcyclohexanone, was observed. This could be attributed to the significant creation of the propyl monocyclic compounds from pyrolytic lignin and, thus, their short residence time in the reactor.

On the basis of the overall yields of the individual chemical groups over the studied range of experimental conditions (Tables S13 and S14), the order of apparent reactivity of the compounds present in the bio-oil during its hydrodeoxygenation over the sulfided catalyst at WHSV of 1 h^{-1} was established and is reported in Table 2. As the conclusions are drawn based on the bio-oil hydrotreatment, competitive adsorption or

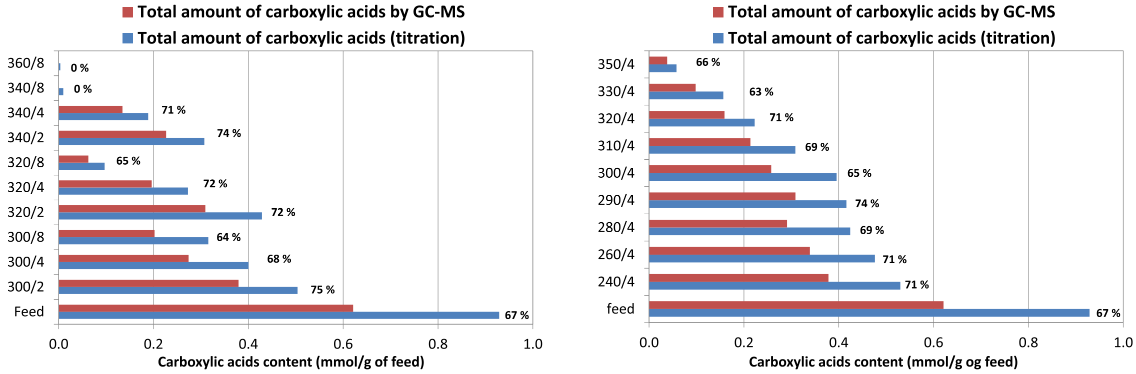

Figure 9. Amount of carboxylic acids in the organic phase (GC-MS vs CAN). The number on the right side of the blue row is the ratio of the red/blue row.

mutual inhibition effects may play a significant role in these observations.

The Quantification of Hydrocarbons by GC-MS. Only the aromatic compounds like benzene, toluene, xylenes, and naphthalene were found above the limit of quantification (LOQ) in the feed (crude bio-oil). However, their total concentration was only 0.14 wt % (Table S13). The content of all the detected hydrocarbons (except cycloalkenes in the experiments at 8 MPa) increased significantly with the hydrotreatment severity.

Compared to the double bound in alkyl substituent of phenolics, such as eugenols present in bio-oil, cycloalkenes (created by the consecutives reactions of phenolics deoxygenation) were observed even in the hydrotreatment product prepared at 360 °C and 8 MPa (Figure 8 B). The content of cycloalkenes (as sum) significantly decreased first at 340 °C and 8 MPa. According to us the main reason for the presence of cycloalkenes even at 360 °C and 8 MPa was just their creation during bio-oil hydrotreatment and not sufficient time for their hydrogenation at the used space velocity (1 h^{-1}) as they are products of consecutive reactions formed most likely at the end of the catalyst bed. Most of the detected alkylated cycloalkenes had an alkyl substituent in the position one and thus steric hindrance by the alkyl group could contribute to the lower reactivity of the double bond. Compared to 1-alkylcycloalkenes, the content of cyclohexene and 3-methylcyclohexene (i.e., compounds with not sterically hindered double bound) started to decrease at milder conditions (Table S15). There is no doubt regarding the cycloalkenes identification as it was based on the known retention time of the standards (in addition to the standards we used also 1-ethylcyclohexene), on their mass spectrum and Kovats indices.

Complete bio-oil hydrodeoxygenation to hydrocarbons could be reached by multiple step hydrotreatment, but this process is cost unattractive as it consumes too much hydrogen. The hydrogen cost constitutes up to 85% of the total bio-oil upgrading cost.[38] From the hydrogen consumption and thus sustainability point of view, it is advantageous to deoxygenate phenolic compounds in bio-oil without saturation of the aromatic rings. However, already at 320 °C and 8 MPa, a significant increase in the saturation of the aromatic ring was observed (Figure 8C). Consequently, the combination of maximal deoxygenation and minimal saturation of aromatic rings is fulfilled at conditions 340 °C and 4 MPa (Figures 1 and 8).

The yield of *n*-alkanes reached a maximum at 340 °C and 8 MPa; *n*-alkanes with an odd number of carbon atoms predominated. C15 and C17 *n*-alkanes were formed predominantly from C16 and C18 fatty acids through decarbonylation and decarboxylation reactions. On the basis of the cumulative molar yields of the possible sources of these *n*-alkanes, it is obvious that only 55% or 21% of acids and ketones were converted to C15–16 and C17–18 *n*-alkanes, respectively (Tables S18 and S19). The rest of the acids contributed to the creation of higher *n*-alkanes, by used GC-MS conditions, visible up to the n-C32 hydrocarbon. Complete deoxygenation of the acids and relevant ket-2-ones was achieved at 330 °C and 4 MPa and 320 °C and 8 MPa, respectively (Tables S7 and S15). In contrast, the *n*-alkane contents did not yet reach their maximum under these conditions (Tables S16 and S17). It is, therefore, obvious that these *n*-alkanes must also be produced from other sources than the corresponding fatty acids and ket-2-ones, probably by the cracking of longer the *n*-alkanes. The changes in the nonvolatile high-molecular-weight compounds during hydrodeoxygenation at molecular level will be studied in future work. Further, we observed that *n*-alkanes started to crack and isomerize at 360 °C and 8 MPa. The isomerization and cracking were confirmed by an increase in the concentration of the hydrocarbons in the distillation range of gasoline (Figure 8E, Tables S16 and S17). Among the C6–C12 *n*-alkanes whose content increased in the samples with the increasing severity (Tables S16 and S17), compounds with six carbons in the molecule were those mostly formed by cracking (the content of *n*-hexane in the best product 360/8 was 1.09 wt %).

Carboxylic Acid Number (CAN) in the Organic Liquid Phase. Carboxylic acids belong to the most problematic substances in bio-oils because of their corrosiveness and lower reactivity in HDO. Hence, it is also important to quantify acids in the nonvolatile bio-oil fractions in addition to the volatile fraction, where mainly acetic acid is present. We found that the concentration of carboxylic acids was below the LOQ in the products obtained at 340 and 360 °C and 8 MPa, although low acid number values were determined (~3.7 and 0.4 mg KOH·g^{-1} respectively[25]). On the basis of the evaluation of the titration curve profile, we are convinced that acids are not present in the organic phase under these conditions. The measured titration curves resemble those of phenols as a strong equivalence point is missing. We also did not detect any carbonyl group by IR in the sample 360/8, so the carboxylic acid content could be expected to be close to zero as measured

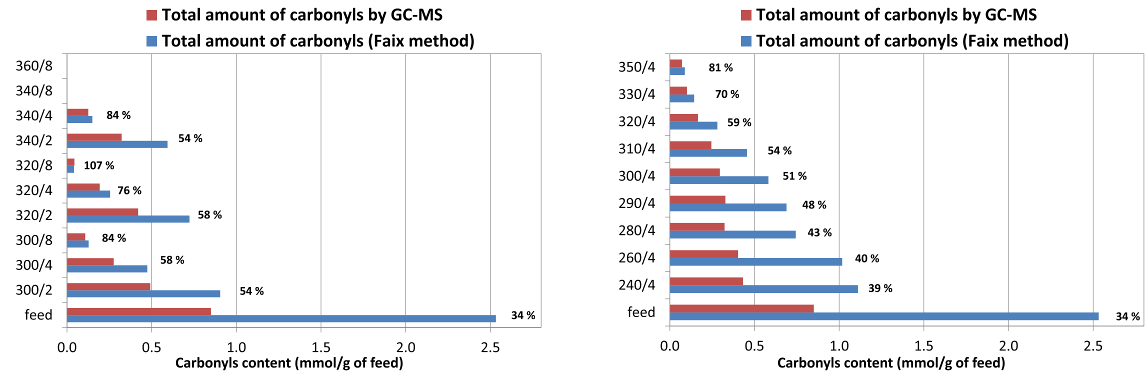

Figure 10. Amount of carbonyls in the organic phase (GC-MS vs Faix method). The number on the right side of the blue row is the ratio of the red/blue row.

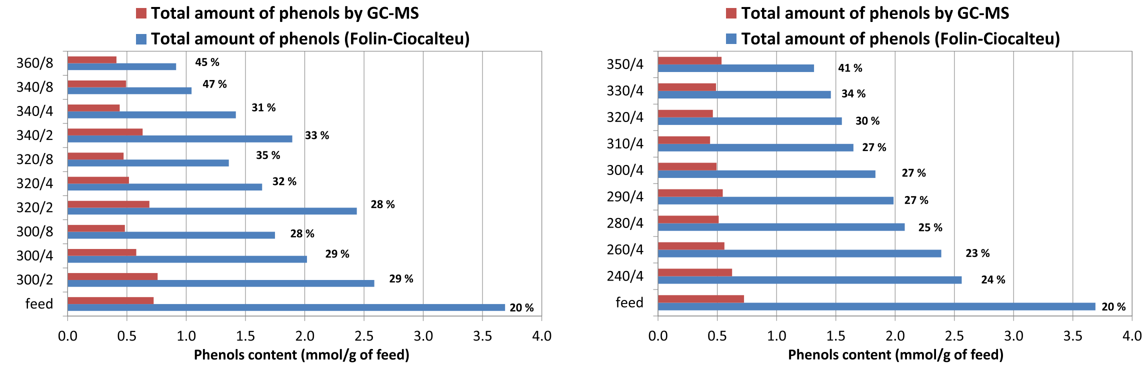

Figure 11. Amount of phenols in the organic phase (GC-MS vs Folin−Ciocalteu method). The number on the right side of the blue row is the ratio of the red/blue row.

by the CAN method. For a more precise measurement, we would need to increase the sample amount for CAN analysis that would exceed the total amount of the hydrotreated product sample. The GC-MS detectable acids were already removed from the organic phase at 340 °C and 8 MPa, where the acids were also below the limit of detection (LOD) of the CAN method.

A significant decrease in CAN (by almost 50%), between the feed on the one hand and the 300/2 and 240/4 products on the other, was probably caused by the elution of carboxylic acids (mainly acetic acid) into the aqueous phase (Figure 2 B). Thanks to the detailed GC-MS analysis, we quantified more than 64% of all the acids present, assuming that the CAN method reliably detected all the acids present. If the C6−C13 acids appeared in the samples (mainly in the feed) they were probably present in very small concentrations below the LOQ, probably even below the LOD. So, based on the assumption that we quantified almost all the volatile acids, the other undetected acid groups were probably present in high-molecular-weight compounds, for example in the pyrolytic lignin molecules. The presence of carboxylic groups in pyrolytic lignin was published by Stankovikj et al.[29]

We found the ratio of C2 + C3 versus C16 + C18 acids was almost constant for all the products (Tables S7 and S15), which implies that the reactivity of the low- and high-molecular-weight carboxylic acid was probably almost the same. This conclusion is further supported by the almost constant ratio of the volatile acids vs CAN for the feed and all the products (being in the range 65−75%, see Figure 9). Because of the low reactivity of the acids, it is necessary to optimize the catalyst composition and type of support, not only in terms of its resistance to acids, but also for its selectivity for the removal of acids.

Carbonyls in the Organic Liquid Phase by the Faix Method. Carbonyl compounds, especially aldehydes, are among the most reactive compounds and cause the low thermo-oxidative stability of bio-oils.[39] The determination of the content of the carbonyl compounds in both the volatile and nonvolatile fractions of the bio-oils and its HDO products is, therefore, important information. All the detected aldehydes were already removed under the mildest conditions of 300 °C and 2 MPa and 240 °C and 4 MPa. Thus, the carbonyl compounds detected by the Faix method were predominantly ketones and high-molecular-weight pyrolytic lignin compounds not detectable by GC-MS containing both aldehyde and ketone groups. All further conclusions are based on the assumption that all carbonyl compounds are oximated quantitatively.

The sharp drop in the carbonyl content in nonvolatile fractions (GC-MS not detectable) between the feed and the 300/2 product (Figure 10), points to a significant content of carbonyls, especially aldehydes, in the pyrolytic lignin molecules. The presence of the aldehyde groups in pyrolytic lignin could be expected based on the research of Patil et al.[40] The results also showed that the number of the carbonyl groups in the nonvolatile fractions was higher than that of the carboxyl groups (higher ratio in Figure 9). Compared to the carboxylic acids, the nonvolatile carbonyls were removed more easily than the volatile carbonyls, which could be attributed to the higher presence and reactivity of aldehydes in the pyrolytic lignin molecules compared to both the low- and high-molecular-weight ketones. Therefore, the ratio of the carbonyls quantified by GC-MS vs the total carbonyls rose (Figure 10). At 320 °C and 8 MPa, all the high-boiling carbonyls were removed. Because of this, the sum of all the carbonyls quantified by GC-MS was almost equal to the results of the Faix method (ratio of 107%). A ratio higher than 100% was probably caused due to the measurement error of these methods.

Total Content of Phenols in the Organic Liquid Phase by the Folin−Ciocalteu Method. Phenolics are in general among the least reactive oxygenates present in the bio-oils as known from literature.[31] On the other hand, 1,3-di-, 1,3,4-tri-, and 1,2,3-tri-hydroxybenzenes were identified together with aldehydes as the most reactive compounds contributing to the aging of the bio-oils during storage.[39]

The small decrease in the total phenolic content (Figure 11) was probably caused by the deoxygenation of di- and trihydroxyl benzenes to phenols. Because, as known from literature,[18] monohydroxybenzenes provide method about 2/3 of absorbance in the Folin−Ciocalteu (FC) compared to the gallic acid (trihydroxybenzoic acid) used for the calibration. Moreover, the presence of the alkyl chain in phenolics further reduces the absorbance to one-third of the Gallic acid absorbance.[18] For this reason, it is obvious that the results from the FC method are not able to give us an absolute number and it is problematic to draw other conclusions, than those already drawn in the previous sections. Nevertheless, the FC method was found as a good indicator of the antioxidant capacity of the bio-oil as a whole.[41] We plan to provide a more detailed comparison of the response of the wider range of the phenolic compounds in the FC method, typically present in bio-oils and the HDO bio-oils, in a dedicated study in the future.

CONCLUSIONS

We presented the first detailed quantitative study mapping the fate of the individual key oxygenates during the one-stage hydrotreatment of straw bio-oil over a sulfided catalyst in a wide range of reaction conditions. Using a complex analysis of the aqueous and organic phases based on the combination of GC-MS analysis with functional-group-specific analytical methods (i.e., carboxylic acids, carbonyls and phenols determined by the carboxylic acid number, Faix, and Folin−Ciocalteu methods, respectively), we obtained a comprehensive understanding of the formation and/or consumption of oxygenates and hydrocarbons as a function of the reaction conditions used. Among the tested reaction conditions, one-stage bio-oil upgrading at 340 °C and 4 MPa is to be preferred, as there was no significant saturation of the aromatic ring while a majority of the oxygenates was removed. Thus, a sustainable product with minimum hydrogen consumption suitable for the subsequent coprocessing with petroleum fractions in a refinery was obtained. Moreover, the biobased aromatics are very desired components of the gasoline and jet-fuel blending pools The results will allow further optimization of the sulfided NiMo catalyst to ensure the more efficient removal of carboxylic acids and, thus, additional enhancement of its stability during long-term bio-oil hydrotreatment.

ASSOCIATED CONTENT

Ⓢ Supporting Information

The Supporting Information is available free of charge on the ACS Publications website at DOI: 10.1021/acssuschemeng.8b06860.

> Properties of the aqueous phases, overview of standards used for GC-MS quantitative analysis, results for all directly quantified compounds by GC-MS in the products organic and aqueous phase, solubility of chosen compounds, volatile oxygenates group analysis, cumulative changes in C15 + C16 and C17 + C18 alkyl chain molecules, scheme of the decomposition of possible pyrolytic lignin molecule, and photo of aqueous phase aging (PDF)

AUTHOR INFORMATION

Corresponding Author

*E-mail: Milos.Auersvald@vscht.cz. Telephone: +420220444238. Fax: +420220444321.

ORCID

Miloš Auersvald: 0000-0002-2449-6173
Martin Staš: 0000-0002-3106-8601
David Kubička: 0000-0003-2996-7824

Notes

The authors declare no competing financial interest.

ACKNOWLEDGMENTS

The results were obtained in the BioMates project. This project has received funding from the European Union's Horizon 2020 research and innovation program under grant agreement no. 727463. The authors are grateful to Tim Schulzke and Stefan Conrad (Fraunhofer UMSICHT) for providing the straw bio-oil used in the hydrotreatment experiments. The publication reflects only the authors' view and the Commision is not responsible for any use that may be made of the information it contains. Financial support was received from specific university research (MSMT No 21-SVV/2018).

ABBREVIATIONS

AP	aqueous phase
CAN	carboxylic acid number
FC	Folin−Ciocalteu
HDO	hydrodeoxygenation
LOD	limit of detection
LOQ	limit of quantification
MCR	micro Conradson carbonization residue
RSD	relative standard deviation
TIC	total ion current

REFERENCES

(1) Bridgwater, A. V. Review of fast pyrolysis of biomass and product upgrading. *Biomass Bioenergy* **2012**, *38*, 68−94.

(2) Mohan, D.; Pittman, C. U.; Steele, P. H. Pyrolysis of wood/biomass for bio-oil: a critical review. *Energy Fuels* **2006**, *20* (3), 848−889.

(3) Mortensen, P. M.; Grunwaldt, J. D.; Jensen, P. A.; Knudsen, K. G.; Jensen, A. D. A review of catalytic upgrading of bio-oil to engine fuels. *Appl. Catal., A* **2011**, *407*, 1−19.

(4) Bi, Y.; Wang, G.; Shi, Q.; Xu, C.; Gao, J. Compositional changes during hydrodeoxygenation of biomass pyrolysis oil. *Energy Fuels* **2014**, *28* (4), 2571−2580.

(5) Staš, M.; Kubička, D.; Chudoba, J.; Pospíšil, M. Overview of analytical methods used for chemical characterization of pyrolysis bio-oil. Energy Fuels **2014**, *28* (1), 385−402.

(6) Elliott, D. C.; Hart, T. R.; Neuenschwander, G. G.; Rotness, L. J.; Olarte, M. V.; Zacher, A. H.; Solantausta, Y. Catalytic hydroprocessing of fast pyrolysis bio-oil from pine sawdust. Energy Fuels **2012**, *26* (6), 3891−3896.

(7) De Miguel Mercader, F.; Koehorst, P. J. J.; Heeres, H. J.; Kersten, S. R. A.; Hogendoorn, J. A. Competition Between Hydrotreating and Polymerization Reactions During Pyrolysis Oil Hydrodeoxygenation. *AIChE J.* **2011**, *57*, 3160−3170.

(8) de Miguel Mercader, F.; Groeneveld, M. J.; Kersten, S. R.; Geantet, C.; Toussaint, G.; Way, N. W.; Schaverien, C. J.; Hogendoorn, K. J. Hydrodeoxygenation of pyrolysis oil fractions: process understanding and quality assessment through co-processing in refinery units. Energy Environ. Sci. **2011**, *4* (3), 985−997.

(9) Elliott, D. C.; Wang, H.; Rover, M.; Whitmer, L.; Smith, R.; Brown, R. Hydrocarbon liquid production via catalytic hydroprocessing of phenolic oils fractionated from fast pyrolysis of red oak and corn stover. *ACS Sustainable Chem. Eng.* **2015**, *3* (5), 892−902.

(10) Nowakowski, D. J.; Bridgwater, A. V.; Elliott, D. C.; Meier, D.; de Wild, P. Lignin fast pyrolysis: results from an international collaboration. J. Anal. Appl. Pyrolysis **2010**, *88* (1), 53−72.

(11) Elliott, D. C.; Hart, T. R.; Neuenschwander, G. G.; Rotness, L. J.; Zacher, A. H. Catalytic Hydroprocessing of Biomass Fast Pyrolysis Bio-oil to Produce Hydrocarbon Products. Environ. Prog. Sustainable Energy **2009**, *28*, 441−449.

(12) Routray, K.; Barnett, K. J.; Huber, G. W. Hydrodeoxygenation of pyrolysis oils. Energy Technol. **2017**, *5* (1), 80−93.

(13) Stankovikj, F.; Tran, C.-C.; Kaliaguine, S.; Olarte, M. V.; Garcia-Perez, M. Evolution of Functional Groups during Pyrolysis Oil Upgrading. Energy Fuels **2017**, *31* (8), 8300−8316.

(14) Sanna, A.; Vispute, T. P.; Huber, G. W. Hydrodeoxygenation of the aqueous fraction of bio-oil with Ru/C and Pt/C catalysts. Appl. Catal., B **2015**, *165*, 446−456.

(15) Ferrell, J. R.; Olarte, M. V.; Christensen, E. D.; Padmaperuma, A. B.; Connatser, R. M.; Stankovikj, F.; Meier, D.; Paasikallio, V. Standardization of chemical analytical techniques for pyrolysis bio-oil: history, challenges, and current status of methods. Biofuels, Bioprod. Biorefin. **2016**, *10* (5), 496−507.

(16) Christensen, E.; Ferrell, J.; Olarte, M. V.; Padmaperuma, A. B.; Lemmon, T. *Acid Number Determination of Pyrolysis Bio-oils using Potentiometric Titration: Laboratory Analytical Procedure (LAP)*; National Renewable Energy Lab. (NREL): Golden, CO (United States), 2016.

(17) Black, S.; Ferrell, J.; Olarte, M. V.; Padmaperuma, A. B. *Determination of Carbonyls in Pyrolysis Bio-oils by Potentiometric Titration. Faix Method. Laboratory Analytical Procedure (LAP)*; National Renewable Energy Lab. (NREL), Golden, CO (United States), 2016.

(18) Rover, M. R.; Brown, R. C. Quantification of total phenols in bio-oil using the Folin−Ciocalteu method. J. Anal. Appl. Pyrolysis **2013**, *104*, 366−371.

(19) Patel, M.; Kumar, A. Production of renewable diesel through the hydroprocessing of lignocellulosic biomass-derived bio-oil: A review. *Renewable Sustainable Energy Rev.* **2016**, *58*, 1293−1307.

(20) Romero, Y.; Richard, F.; Brunet, S. Hydrodeoxygenation of 2-ethylphenol as a model compound of bio-crude over sulfided Mo-based catalysts: Promoting effect and reaction mechanism. Appl. Catal., B **2010**, *98* (3), 213−223.

(21) Hellinger, M.; Carvalho, H. W.; Baier, S.; Wang, D.; Kleist, W.; Grunwaldt, J.-D. Catalytic hydrodeoxygenation of guaiacol over platinum supported on metal oxides and zeolites. Appl. Catal., A **2015**, *490*, 181−192.

(22) Wang, H.; Male, J.; Wang, Y. Recent advances in hydrotreating of pyrolysis bio-oil and its oxygen-containing model compounds. ACS Catal. **2013**, *3* (5), 1047−1070.

(23) French, R. J.; Stunkel, J.; Black, S.; Myers, M.; Yung, M. M.; Iisa, K. Evaluate Impact of Catalyst Type on Oil Yield and Hydrogen Consumption from Mild Hydrotreating. Energy Fuels **2014**, *28*, 3086−3095.

(24) Zacher, A. H.; Elliott, D. C.; Olarte, M. V.; Santosa, D. M.; Preto, F.; Iisa, K. Pyrolysis of woody residue feedstocks: upgrading of bio-oils from mountain-pine-beetle-killed trees and hog fuel. Energy Fuels **2014**, *28* (12), 7510−7516.

(25) Auersvald, M.; Shumeiko, B.; Vrtiška, D.; Straka, P.; Staš, M.; Šimáček, P.; Blažek, J.; Kubička, D. Hydrotreatment of straw bio-oil from ablative fast pyrolysis to produce suitable refinery intermediates. Fuel **2019**, *238*, 98−110.

(26) Schulzke, T.; Conrad, S.; Westermeyer, J. Ablative Flash Pyrolysis of Straw—Conversion Process and Valorization Options for Solid and Liquid Products. In *Biorefinery for Food & Fuels & Materials*; Montpellier, France, 2015.

(27) Yoshimura, Y.; Sato, T.; Shimada, H.; Matsubayashi, N.; Nishijima, A. Influences of oxygen-containing substances on deactivation of sulfided molybdate catalysts. Appl. Catal. **1991**, *73* (1), 55−63.

(28) Michailof, C.; Sfetsas, T.; Stefanidis, S.; Kalogiannis, K.; Theodoridis, G.; Lappas, A. Quantitative and qualitative analysis of hemicellulose, cellulose and lignin bio-oils by comprehensive two-dimensional gas chromatography with time-of-flight mass spectrometry. *J. Chromatogr. A* **2014**, *1369*, 147−160.

(29) Stankovikj, F.; McDonald, A. G.; Helms, G. L.; Garcia-Perez, M. Quantification of bio-oil functional groups and evidences of the presence of pyrolytic humins. Energy Fuels **2016**, *30* (8), 6505−6524.

(30) Gunawan, R.; Li, X.; Lievens, C.; Gholizadeh, M.; Chaiwat, W.; Hu, X.; Mourant, D.; Bromly, J.; Li, C.-Z. Upgrading of bio-oil into advanced biofuels and chemicals. Part I. Transformation of GC-detectable light species during the hydrotreatment of bio-oil using Pd/C catalyst. *Fuel* **2013**, *111*, 709−717.

(31) Elliott, D. C. Historical developments in hydroprocessing bio-oils. Energy Fuels **2007**, *21* (3), 1792−1815.

(32) Zacher, A. H.; Olarte, M. V.; Santosa, D. M.; Elliott, D. C.; Jones, S. B. A review and perspective of recent bio-oil hydrotreating research. Green Chem. **2014**, *16* (2), 491−515.

(33) Chaiwat, W.; Gunawan, R.; Gholizadeh, M.; Li, X.; Lievens, C.; Hu, X.; Wang, Y.; Mourant, D.; Rossiter, A.; Bromly, J.; Li, C.-Z. Upgrading of bio-oil into advanced biofuels and chemicals. Part II. Importance of holdup of heavy species during the hydrotreatment of bio-oil in a continuous packed-bed catalytic reactor. Fuel **2013**, *112*, 302−310.

(34) Laurent, E.; Delmon, B. Study of the hydrodeoxygenation of carbonyl, carboxylic and guaiacyl groups over sulfided CoMo/γ-Al2O3 and NiMo/γ-Al2O3 catalysts: I. Catalytic reaction schemes. Appl. Catal., A **1994**, *109* (1), 77−96.

(35) Stankovikj, F.; McDonald, A. G.; Helms, G. L.; Olarte, M. V.; Garcia-Perez, M. Characterization of the Water-Soluble Fraction of Woody Biomass Pyrolysis Oils. Energy Fuels **2017**, *31* (2), 1650−1664.

(36) Gevert, B.; Otterstedt, J.; Massoth, F. Kinetics of the HDO of methyl-substituted phenols. Appl. Catal. **1987**, *31* (1), 119−131.

(37) Bunch, A. Y.; Ozkan, U. S. Investigation of the reaction network of benzofuran hydrodeoxygenation over sulfided and reduced Ni−Mo/Al2O3 catalysts. J. Catal. **2002**, *206* (2), 177−187.

(38) Elliott, D. C.; Neuenschwander, G. G. Liquid fuels by low-severity hydrotreating of biocrude. In *Developments in Thermochemical Biomass Conversion*; Springer Science & Business Media, 1997; Vol. *1*.

(39) Joseph, J.; Rasmussen, M. J.; Fecteau, J. P.; Kim, S.; Lee, H.; Tracy, K. A.; Jensen, B. L.; Frederick, B. G.; Stemmler, E. A. Compositional changes to low water content bio-oils during aging: an NMR, GC/MS, and LC/MS study. Energy Fuels **2016**, *30* (6), 4825−4840.

(40) Patil, S. K.; Heltzel, J.; Lund, C. R. Comparison of structural features of humins formed catalytically from glucose, fructose, and 5-hydroxymethylfurfuraldehyde. Energy Fuels **2012**, *26* (8), 5281−5293.

(41) Everette, J. D.; Bryant, Q. M.; Green, A. M.; Abbey, Y. A.; Wangila, G. W.; Walker, R. B. Thorough study of reactivity of various

compound classes toward the Folin– Ciocalteu reagent. *J. Agric. Food Chem.* **2010**, *58* (14), 8139−8144.

Catalysis Science & Technology

ROYAL SOCIETY OF CHEMISTRY

PAPER

View Article Online
View Journal | View Issue

CrossMark click for updates

Cite this: *Catal. Sci. Technol.*, 2016, **6**, 1829

Towards understanding the hydrodeoxygenation pathways of furfural–acetone aldol condensation products over supported Pt catalysts

R. Ramos, Z. Tišler, O. Kikhtyanin and D. Kubička*

Aiming at the valorisation of furfural-derived compounds, the hydrodeoxygenation of furfural–acetone condensation products has been studied using supported platinum catalysts. The influence of the catalytic properties of different supports, such as SiO_2, Al_2O_3, TiO_2, hydrotalcite (HTC), Beta zeolite, Al-SBA-15 and WO_3–ZrO_2, was evaluated in a batch reactor for 480 min at 200 °C and 50 bar of H_2. The used feed consisted of a mixture of furfural–acetone adducts (C_8–C_{19}), obtained in previous experiments using a continuous flow reactor and hydrotalcite as a catalyst. Except for Pt/SiO_2, all catalysts showed high conversion of the reactants, especially due to the hydrogenation of all the aliphatic C=C bonds. However, the extent of further hydrogenation (furan C=C and ketone C=O bonds) was limited, particularly when HTC and Al_2O_3 were used as supports. The higher accessibility of Pt/TiO_2 and the smaller Pt particle size shown by Pt/Al-SBA-15, Pt/WO_3–ZrO_2 and Pt/Beta in comparison with the other catalysts led to an improvement in the hydrogenation of furanic and ketonic groups, likely due to lower adsorption constraints. The higher acid character of the latter group of catalysts promotes dehydration and ring opening steps, thus enhancing the selectivity towards linear alcohols. Likewise, a significant increase in the extent of aldol condensation reactions was also observed with these catalysts, yielding longer carbon chain compounds. Based on this study, a reaction scheme for the transformation of 4-(2-furyl)-3-buten-2-one (C_8) into octane has been proposed in order to establish a valuable correlation between the main conversion pathways and the catalytic properties of the employed heterogeneous catalyst, thus contributing to further development of efficient deoxygenation catalysts.

Received 27th August 2015,
Accepted 19th October 2015

DOI: 10.1039/c5cy01422k

www.rsc.org/catalysis

Introduction

The efficient conversion of lignocellulose-derived platform compounds, such as furfural and hydroxymethylfurfural, into liquid fuels and value-added chemicals could contribute to the development of more sustainable and environmentally-friendly alternative renewable sources and energy technologies.[1,2] Furfural ($C_5H_4O_2$) is an oxygenated compound obtained through dehydration of hemicellulose building blocks (*e.g.*, xylose and arabinose) derived from lignocellulosic biomass by acid-catalyzed treatments.[3] Since lignocellulose is the main component of agricultural waste and forest residues, the synthesis and subsequent transformation of furfural (and its derivatives) has become an active research area in recent years.[3–5] However, the carbon chain length of furfural, once hydrodeoxygenated, is in general too short for fuel applications. In this respect, aldol condensation of furfural with small ketones affords larger organic molecules (≥C_8) by forming C–C bonds between carbonyl-containing compounds. Recently, this strategy has been proposed for the direct condensation of furfural (F) with acetone (Ac) as a promising approach to yield alkane precursors.[6–10] Accordingly, the formation of the F–Ac monomer (C_8) and the F_2–Ac dimer (C_{13}) mostly takes place in the presence of a base or acid catalyst at low temperatures (25–70 °C). It should be noted that acetone itself is also available from renewable biomass through fermentation[11] or ketonization strategies.[12,13]

In order to yield valuable liquid hydrocarbons, furfural–acetone condensate products have to be deoxygenated, typically at high hydrogen pressures (20–80 bar) and mild temperatures (170–300 °C). During deoxygenation, the furfural–acetone adducts are subjected to hydrogenation, ring opening and dehydration reactions, yielding numerous intermediate products according to diverse reaction pathways.[10,14–16] Some authors have studied the deoxygenation of furfural–acetone condensation adducts into alkanes as a one-step process using bifunctional catalysts.[15–17] However, due to the complexity of this process, the majority of authors suggest carrying out the hydrogenation step individually, *i.e.* as an intermediary transformation step between the aldol condensation reaction and the final deoxygenation stage.[10,14,18–20]

Research Institute of Inorganic Chemistry, RENTECH-UniCRE, Chempark Litvínov, Záluží-Litvínov, 436 70, Czech Republic. E-mail: David.Kubicka@vuanch.cz

The hydrogenation of furfural–acetone aldol condensation products plays an important role in the multi-step catalytic transformation into liquid alkanes as it increases the feedstock stability as a result of the elimination of the unsaturated monomer and dimer (F–Ac and F_2–Ac, respectively). Consequently, the stabilization allows more severe deoxygenation reaction conditions and thus better yields of alkanes, *i.e.* fully deoxygenated products. In this sense, there are three different kinds of double bonds to be hydrogenated: aliphatic C=C, furanic C=C and ketonic C=O bonds. Thermodynamic and kinetic considerations favour hydrogenation of the C=C bond over C=O,[21,22] whereas steric constrains usually limit the hydrogenation rates of C=C in comparison with C=O hydrogenation.[23] Moreover, the furanic ring of furfural may also cause steric hindrance, reducing the hydrogenation of the C=C furanic ring compared to the aliphatic C=C bonds.[24] Similarly, the hydrogenation of the furanic C=O bond is generally more restricted, inhibiting ring opening reactions which are a fundamental step towards the formation of linear alcohols.[25]

The selection of the catalyst plays a critical role in the conversion pathways. Among the different metal phases studied, platinum has been revealed as one of the most suitable metals for hydrogenating both double bonds and ketone bonds, at moderate temperatures and pressures.[17,26] Concerning the support, its main function is to achieve optimum dispersion, stabilize suitably the metal species and provide sufficient mass transfer rates, *i.e.* the consideration of the textural properties of the supports is crucial. Additionally, support materials can exhibit acidic or basic properties, which promote different reactions and intermediate formation, altering the efficiency, and therefore, changing the overall activity and selectivity of the transformation.[26]

Within this context, the main scope of this contribution is to investigate the influence of different supported platinum catalysts on the deoxygenation of furfural–acetone condensation products. The research is focused on the use of real furfural–acetone aldol condensation products obtained in large scale using a flow reactor and basic hydrotalcite as a catalyst.[27] The activity of seven different supports (SiO_2, Al_2O_3, TiO_2, hydrotalcite, Beta zeolite, Al-SBA-15 and WO_3–ZrO_2) loaded with platinum was compared at 200 °C and 50 bar. The support selection covers a wide range of acidity and textural properties, allowing us to evaluate the effect of the nature of active sites and pore morphology on the reaction mechanism. The understanding of this conversion is particularly useful for the design of novel catalysts that will allow development of a competitive technology for the production of valuable alkanes from furfural condensation adducts.

Experimental

Feedstock

The used feed consisted of a mixture of furfural–acetone aldol condensation products obtained from the experiments described elsewhere,[27] using a continuous flow fixed bed reactor at 50 °C and hydrotalcite (Mg/Al = 3) as a catalyst. The aldol condensation reactions of furfural and acetone led to the formation of a heterogeneous mixture of compounds, resulting not only from the cross aldol condensation of the aldehyde and the ketone groups, but also from acetone self-condensation, affording diacetone alcohol (DAA) and mesityl oxide (MSO). In order to achieve a more appropriate ratio between the reactant molecules (F–Ac and derivatives, *i.e.* various aldol condensation products) and the amount of catalyst, the initial feed was diluted by adding more acetone. Thus, the final feedstock loaded into the batch reactor consisted of 50 ml of aldol condensation products and 100 ml of acetone. The molar concentration of the main compounds present in the feedstock (X_i), determined by GC and GC-MS analyses, is given in Table 1.

Catalyst preparation

Different supports were used for studying the effect of their catalytic properties on the deoxygenation of furfural–acetone adducts. The influence of their textural and acido-basic properties was evaluated by investigating a wide range of materials including commercial supports SiO_2 (Astin Catalysts and Chemicals), Al_2O_3 (Astin Catalysts and Chemicals), TiO_2 (Euro Support), Beta zeolite (Zeolyst Int., Si/Al = 12.5), and WO_3–ZrO_2 (Euro Support), and in-house synthesized hydrotalcite[27] and Al-SBA-15 (Si/Al = 50).

The incorporation of platinum to the supports was carried out by wetness impregnation of tetraammineplatinum(II) nitrate ($Pt(NH_3)_4(NO_3)_2$) to prepare catalysts with a nominal metal loading in the range 0.2–0.8 wt%. The deposition of Pt was carried out by adding an aqueous solution of the precursor to the supports. After impregnation, the catalysts were dried at 120 °C overnight and then calcined at 500 °C in air for 6 h (heating rate 1 °C min^{-1}).

Catalyst characterization

The catalysts were characterized by different physicochemical characterization methods in order to determine their main textural and acido-basic properties.

The textural properties were measured using nitrogen adsorption–desorption isotherms at 77 K with a

Table 1 Composition of the used feedstock

Compound	Molecular mass (g mol^{-1})	Molar fraction (X_i)
Acetone	58	9.7×10^{-1}
DAA	116	3.86×10^{-3}
MSO	98	2.48×10^{-4}
F–Ac	136	1.95×10^{-2}
F–Ac_2	176	2.06×10^{-3}
F_2–Ac	214	2.71×10^{-3}
$(F–Ac)_2$	272	5.79×10^{-4}
F_2–Ac_2	254	1.35×10^{-3}
F_2–Ac_3	294	7.34×10^{-4}

Quantachrome AUTOSORB instrument. Prior to the analyses, the samples were treated at 250 °C for 3 h under nitrogen flow in order to remove the adsorbed compounds. The BET equation was used for the specific surface area calculation, whereas the pore volume and pore size were determined by the BJH method.

The acidic and basic properties of the catalysts were evaluated by temperature-programmed desorption (TPD) of ammonia and carbon dioxide, respectively, in a Micromeritics Autochem 2950 apparatus. Prior to the TPD analyses, the catalyst samples were reduced *in situ* under 10 vol% H_2/Ar (25 cm^3 min^{-1}) at 350 °C (10 °C min^{-1}) for 60 min to reproduce the condition of the catalyst at the beginning of the catalytic experiments. Before reduction, the sample was outgassed under a He flow of 25 cm^3 min^{-1} with a heating ramp of 10 °C min^{-1} up to 500 °C.

The NH_3 TPD experiments were started by cooling the sample after reduction down to 180 °C followed by treating it with an ammonia stream (10 vol% in He) of 25 cm^3 min^{-1} for 30 min. Once the sample was saturated, the physically adsorbed NH_3 was removed by flowing He (25 cm^3 min^{-1}) for 60 min. Finally, temperature-programmed desorption was performed by subjecting the sample to a heating rate of 15 °C min^{-1} in flowing He (25 cm^3 min^{-1}) up to 500 °C and maintaining this temperature for 30 min.

In the case of the CO_2 TPD analyses, the sample was cooled after reduction down to 50 °C and saturated under a CO_2 flow (10 vol% in He) of 50 cm^3 min^{-1} for 30 min. Subsequently, the physically adsorbed carbon dioxide was removed by flowing He (25 cm^3 min^{-1}) at 50 °C for 60 min. Finally, the chemically adsorbed CO_2 was desorbed by heating up the sample to 850 °C (heating rate of 15 °C min^{-1}) in flowing He (25 cm^3 min^{-1}) and maintaining this temperature for 30 min. The amounts of desorbed species were quantified using calibration standards.

The platinum content of the catalysts was determined by X-ray Fluorescence Spectroscopy (XRF) using a Philips PW 1404 UniQuant apparatus. The reducibility of the Pt phase was examined by temperature-programmed reduction (TPR) using a Micromeritics Autochem 2950 unit. The catalyst samples (0.1 g) were pretreated at 500 °C in flowing Ar (25 cm^3 min^{-1}) for 60 min, then cooled down to 40 °C, and finally reduced under a stream of 10 vol% H_2/Ar (25 cm^3 min^{-1}) while increasing the temperature by 10 °C min^{-1} up to 500 °C. H_2 uptake as a function of temperature was measured online using a TCD detector.

The metal dispersion and particle size were determined by CO pulse chemisorption at 50 °C. Prior to the chemisorption, the samples were reduced *in situ* under 10 vol% H_2/Ar (20 cm^3 min^{-1}) at 350 °C. After reduction, the sample was cooled down to 50 °C and then 5 vol% CO/He gas was introduced by pulse dosing in a He flow (50 cm^3 min^{-1}). Metal dispersion was determined by measuring the amount of adsorbed CO, sample metal loading and using the adsorption stoichiometry factor 1 (M + CO → M–CO).

Catalytic experiments

The performance of the catalysts was studied in a high-pressure 300 ml batch reactor (Parr Instrument Co.) equipped with digital controllers of stirring speed, temperature and pressure and gas flow meters. All data were collected and monitored continuously during the reaction by a Parr 4848B acquisition interface.

Prior to the reaction, the catalyst (1 g) was reduced *in situ* under H_2 flow (80 cm^3 min^{-1}) at 350 °C for 90 min. After cooling down, the reactor was loaded with 150 ml of the feedstock mixture described above (Table 1) and purged thoroughly with hydrogen. Subsequently, heating of the reactor was performed under moderate conditions – pressure (15 bar) and stirring (100 rpm). Once the desired temperature (200 °C) was reached, the vessel was pressurized to 50 bar of H_2 and the stirring speed was increased to 1000 rpm to prevent external mass transfer limitations. The samples of products were collected at different intervals during the course of the reaction (480 min) in order to evaluate the kinetic behaviour. The product mixtures were analyzed by an Agilent 7890A GC unit equipped with a flame ionization detector (FID) using an HP-5 capillary column (30 m, 0.32 ID, 0.25 μm). The hydrogenated products were identified by using standard reference compounds along with GC-MS analyses using a Thermo Scientific ITQ 1100 unit.

The evolution of the concentrations of the reactants and products, and the yields of the products were calculated by GC analysis of the feedstock and the liquid product samples as follows:

$$[X_{\mathrm{i}}]_t\,\% = \frac{[X_{\mathrm{i}}]_t}{[X_{\mathrm{i}}]_{t=0}} \times 100$$

$$[Y_{\mathrm{i}}]_t\,\% = \frac{[X_{\mathrm{i}}]_t - [X_{\mathrm{i}}]_{t=0}}{[X_{\mathrm{F-Ac}}]_{t=0}} \times 100$$

where $[X_i]_t$% represents the relative molar concentration of species i at time *t*, $[X_i]_t$ is the molar concentration of i, $[Y_i]_t$% is the yield of species i (derived from F–Ac) at time *t* and $[X_{F-Ac}]_{t=0}$ is the molar concentration of compound F–Ac (C_8) at the beginning of the reaction.

Results and discussion

Catalyst properties

The catalysts prepared by impregnation of platinum on different supports were characterized by a number of techniques in order to determine their main physico-chemical properties. The characterization results are summarized in Table 2.

The results of XRF analysis show a Pt content similar to the theoretical value from the starting solution, indicating that complete incorporation of metal species has been achieved by the wetness impregnation process. The textural

Table 2 Physicochemical properties of the studied catalysts

	Pt content[a]	Pt dispersion[b]	Pt particle size[b]	Active metal surface area[b]	S_{BET}[c]	Pore volume[d]	Pore size[d]	Acid/basic sites		
Catalyst	(wt.%)	(%)	(nm)	(m^2 g^{-1})	(m^2 g^{-1})	(cm^3 g^{-1})	(Å)	(meq NH_3 g^{-1})[e]	(meq CO_2 g^{-1})[f]	T_{max} (°C)[g]
Pt/SiO_2	0.35	0.8	141.6	0.01	46	0.648	49	—	—	—
Pt/Al_2O_3	0.54	14.6	7.7	0.19	207	0.431	38	0.138	—	240
Pt/TiO_2	0.48	7.9	14.3	0.09	77.6	0.403	302	0.110	0.160	238/110
Pt/HTC	0.73	3.8	29.4	0.07	179	0.730	31	—	0.796	110
Pt/Beta	0.48	34.6	3.2	0.42	529	0.116[h]	6–7[h]	0.648	—	271
Pt/Al-SBA-15	0.29	65.3	1.7	0.47	672	1.283	78	0.221	—	261
$Pt/WO_3–ZrO_2$	0.08	41.4	2.7	0.08	90.3	0.272	78	0.258	—	268

[a] XRF measurements. [b] CO pulse chemisorption at 50 °C of samples reduced at 350 °C. [c] Nitrogen adsorption at 77 K. [d] BJH method. [e] NH_3 TPD experiments (180–500 °C) of samples reduced at 350 °C. [f] CO_2 TPD experiments (50–850 °C) of samples reduced at 350 °C. [g] Temperature maxima of the peak as determined by TPD experiments. [h] Micropore volume and BEA framework pore size.

properties of the samples present a wide variety of values, ranging from the low porosity shown by Pt/SiO_2 (56 m^2 g^{-1}) to the high specific surface area shown by Pt/Beta and Pt/Al-SBA-15 (529 and 672 m^2 g^{-1}, respectively). The higher values of the BET surface area play an important role since they help to achieve a better platinum dispersion and metal interaction with the support, improving the metal site activity. Similarly, the pore size values vary within a broad interval from microporous (6–7 Å in the case of Pt/Beta) to mesoporous materials (30–300 Å), which may affect considerably the accessibility of the reactant molecules to the active sites due to steric limitations. Thus, according to the data given in Table 2, Pt/TiO_2 (302 Å) should provide good access to its active sites, whereas Pt/Beta zeolite, despite its remarkable specific surface area, may suffer from major diffusional problems. Regarding the pore volume, Pt/Al-SBA-15 shows the highest value (1.28 cm^3 g^{-1}) due to the combination of high specific surface area and pore size.

The acidity/basicity of the catalysts, as determined by NH_3/CO_2 desorption, is included in Table 2. The total amount of acid/basic sites (meq NH_3/CO_2 g^{-1}) is related to the amount of ammonia/carbon dioxide desorbed, whereas the maximum desorption temperature (T_{max}) is an indication of the acid/basic site strength. Pt/Al-SBA-15, $Pt/WO_3–ZrO_2$ and Pt/Beta show the highest acidity; the remarkable acid character (0.648 meq NH_3 g^{-1}) of the latter material is related to the low Si/Al ratio (12.5) of the BEA zeolite framework. Regarding the acid strength, these materials show a similar maxima value for the desorption temperature (268–271 °C). Pt/Al_2O_3 and Pt/TiO_2 catalysts also exhibit acid character although in a lower range both in the amount (0.110–0.138 meq NH_3 g^{-1}) and in the strength (238–240 °C) of the acid sites. In the case of the latter, a significant amount of basic sites was also established by CO_2 desorption analysis (0.160 meq CO_2 g^{-1}), mostly corresponding to the presence of weak basicity (110 °C). As expected, the highest basicity is exhibited by Pt/HTC (0.796 meq CO_2 g^{-1}), which indicates the major basic character of this material.

Regarding the size and dispersion of platinum particles, Table 2 shows the important differences in these values among the studied catalysts. Both parameters are essential features in bifunctional catalysts, since their activities and selectivities are not only influenced by the nature of the metal species, but can also be controlled by their size and distribution.[25,26,28] As expected, a noticeable dispersion was found for catalysts with the highest specific surface area, *i.e.* Pt/Beta and Pt/Al-SBA-15 (34.6 and 65.3%, respectively), while Pt/SiO_2, which shows the lowest BET surface area, has a very low metal dispersion (0.8%). These values imply great differences in Pt particle sizes, ranging from 1.7 nm for Pt/Al-SBA-15 to 141 nm for Pt/SiO_2. Equally, the presence of Brønsted acid sites in Pt/Beta and Pt/Al-SBA-15 may enhance the Pt dispersion due to the stronger interaction between the metal phase and the support.[29] The last aspect may also be responsible for the significant degree of dispersion and the small particle size observed in the case of $Pt/WO_3–ZrO_2$ (41.4% and 2.7 nm). Nevertheless, the lower metal loading of this catalyst may have affected these values. In this sense, Pt/Al_2O_3, Pt/TiO_2 and Pt/HTC show higher values of Pt particle sizes (7.7–29.4 nm), likely due to the combination of higher metal loading, middle textural properties and lower acid character. Finally, the estimated active metal surface areas may constitute a useful parameter for the evaluation of the studied catalytic activities.

Conversion of furfural–acetone condensation products

A series of preliminary tests were performed in order to establish the most appropriate conditions for the hydrodeoxygenation experiments. Despite the exothermic character of the hydrogenation reactions, an increase in reactant conversion was observed with increasing reaction temperature, within the experimental range. A maximum temperature of 200 °C was set in order to keep the reactants and products in the liquid phase. In addition, harsher conditions (>200 °C) led to undesirable severe C–C bond cleavage and coke formation, making the whole process less energy-efficient. During the course of the reaction, hydrogen was consumed and, consequently, more was supplied to keep the pressure constant. The selected pressure value (50 bar) ensures excess of hydrogen during the whole course of the experiment. The amount of catalyst (1 g) and overall reaction time (480 min) were also optimized to observe significant changes in the product distribution. The results of these initial studies allowed the definition of a standard reaction procedure (described above) for all the subsequent experiments presented in this work.

Fig. 1 shows the variations in the relative molar concentration (X_i%) of the main components of the feedstock (Table 1)

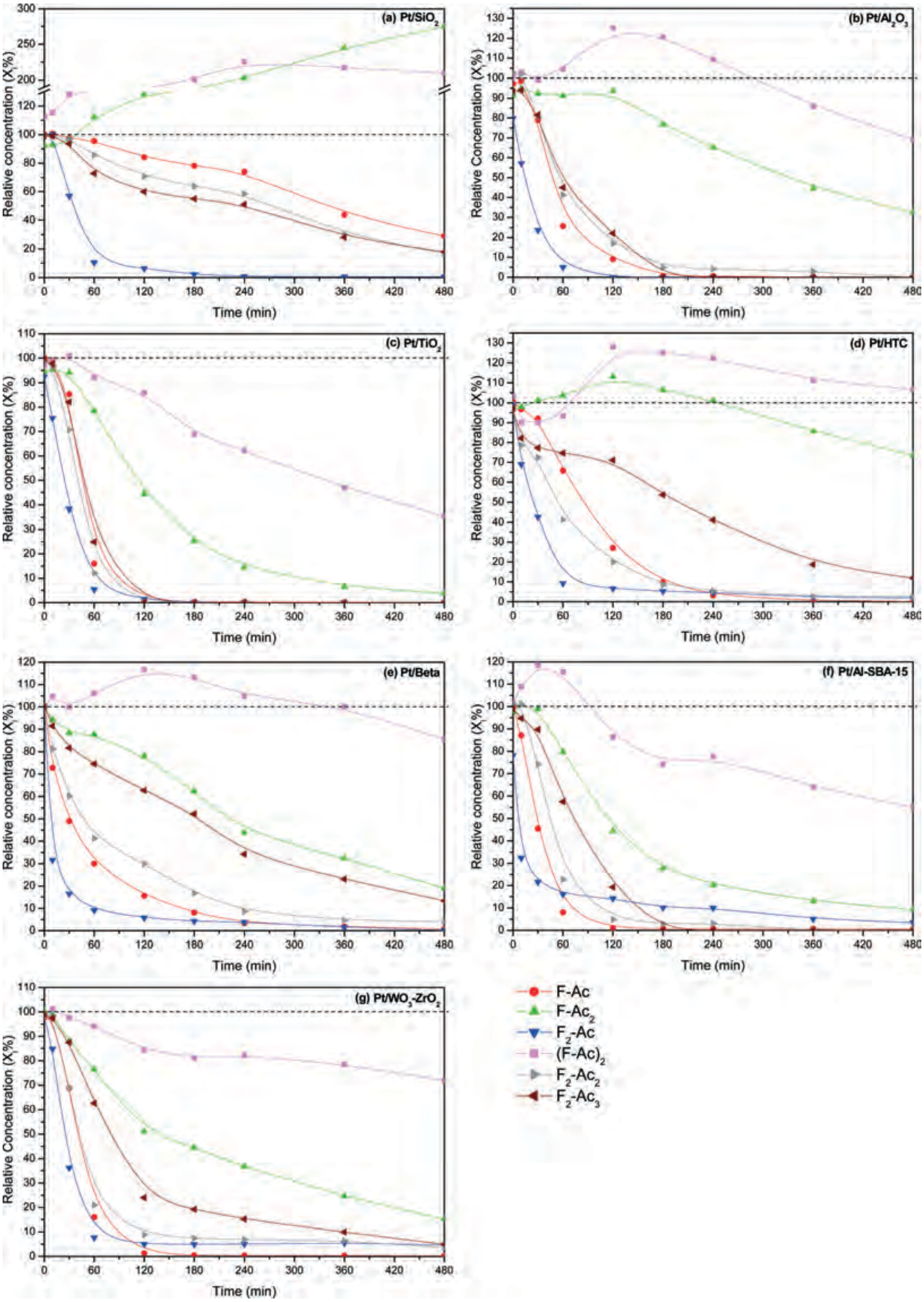

Fig. 1 Evolution of the relative concentration (X_i%) of the reactants (furfural–acetone condensation products) during hydrodeoxygenation over different catalysts (T = 200 °C; P = 50 bar; t = 480 min).

as a function of reaction time. Due to the significant differences in the molar fraction concentrations between these compounds, the results depicted in Fig. 1 are referred to by their percentage variation (relative concentration) with the purpose of appreciating more clearly their evolution with reaction time. Most of the reactants show a decreasing tendency as a result of the progressive hydrogenation of their bonds (aliphatic C=C, ketonic C=O and furanic C=C). The highest rate of conversion for all tested catalysts corresponded to the compound F_2–Ac, which in the experiments carried out with Pt/Al_2O_3 and Pt/TiO_2 completely disappeared after 120 min. A similar behaviour was observed for F–Ac, F_2–Ac_2 and F_2–Ac_3, showing a continuous decrease in their molar fractions as the reaction proceeded, although with a lower hydrogenation rate. Thus, except for Pt/SiO_2, the relative concentration values of these reactants after 480 min were close to zero, indicating an almost full conversion to hydrogenated compounds. The lowest hydrogenation rate of Pt/SiO_2 may be associated with the absence of acid/basic sites, as well as with its low active metal surface area (0.01 $m^2\ g^{-1}$), which implies a poor hydrogenation activity. Likewise, the significant value of X_i% observed for F_2–Ac_3 after 480 min when the Pt/Beta catalyst was used (13.3 X_i%) is very likely related to the steric limitations in microporous materials for bulky molecules such as F_2–Ac_3. Thus, in spite of the fact that most of the Pt particles are probably located on the external surface, the lower accessibility to acid sites reduces the activity of this catalyst. In this respect, the kinetic curves observed for Pt/TiO_2 demonstrate clearly that large pores (mean pore size ≈ 300 Å) facilitate the access of the reactants to the active sites. The influence of mass transfer limitations on the reaction was minimized by applying suitable experimental conditions as those suggested in a similar process,[30] as well as by using small catalyst particles (<100 μm) and vigorous stirring (1000 rpm).

The active metal surface area does not correlate with the initial hydrogenation conversion rate of the reactants. For example, for Pt/Beta and Pt/Al-SBA-15, which showed considerably high active metal surface areas (0.42 and 0.47 $m^2\ g^{-1}$, respectively), presented similar or even lower conversion rates than the rest of the studied catalysts. This fact may be attributed to the participation of acid/basic sites in the initial reactant conversion or to the plausibly different structures of Pt particles due to their different sizes and locations.

On the other hand, the extent of the hydrogenation of F–Ac_2 and $(F–Ac)_2$ seems to be limited, even showing an increase in their relative molar fractions after 480 min when Pt/SiO_2 is used. This fact may be associated with the formation of these compounds, due to the consecutive aldol condensation reactions of acetone with F–Ac or self-condensation of F–Ac. In the case of some other catalysts, like Pt/Al_2O_3, Pt/HTC, Pt/Beta and Pt/Al-SBA-15, the concentration of $(F–Ac)_2$ shows a maximum at short reaction times (60–120 min). This behaviour indicates that these condensation reactions are faster than the hydrogenation of these reactants over fresh catalysts. The formation of F–Ac_2 and $(F–Ac)_2$ is observed even on Pt/SiO_2, *i.e.* in the absence of acid and basic sites, which implies that the condensation of F–Ac adducts takes place probably through a thermal route. Due to the poor hydrogenation performance of this catalyst (caused by the low specific surface area of Pt), the consecutive conversion of these condensation products is only partial.

The extent of aldol condensation reactions over the studied catalysts is evidenced by the increasing concentration of diacetone alcohol (DAA) formed by acetone self-condensation. Subsequently, DAA undergoes successive dehydration and hydrogenation reactions yielding mesityl oxide (MSO), methyl isobutene ketone (MIBK) and methyl isobutyl carbinol (MIBC). This conversion process is schematically depicted in Fig. 2, along with the variation of the concentration of these products in one of the performed experiments. Importantly, direct hydrogenation of acetone to isopropanol was not observed. Since the concentration of MIBK was increasing in all experiments as the reaction progressed and DAA and MSO showed a maximum in their concentrations, it can be inferred that the rate of the selective hydrogenation of DAA and MSO is faster than the rate of formation of MIBC, under the given experimental conditions. It is interesting to note that no higher molecular-weight products, such as dimethyl heptanone, derived from the further condensation of acetone with MIBK, were observed.

The motivation for performing hydrogenation/deoxygenation in the presence of acetone is to couple the aldol condensation of furfural with acetone with the subsequent hydrogenation without any intermediate separation steps, such as distillation of solvents that might be very demanding due to the high reactivity of the aldol condensation products. Although it is not the main objective of this work to analyse the influence of the tested catalysts on acetone conversion, it is worth mentioning that Pt/Beta, Pt/Al-SBA-15 and Pt/WO_3–ZrO_2 gave the highest yields of MIBK. This result indicates a direct relation between the acidity of the used catalysts and the extent of the acetone self-condensation and consecutive hydrogenation represented in Fig. 2.

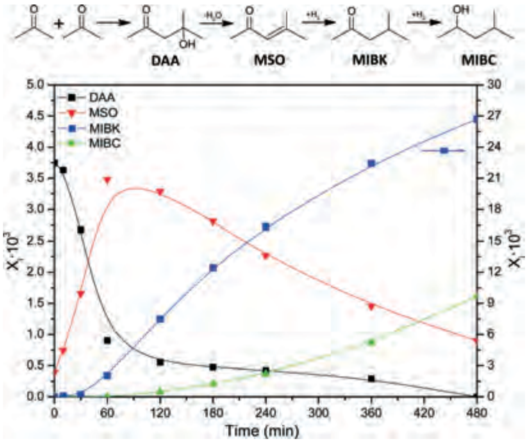

Fig. 2 Aldol condensation and further hydrogenation of acetone itself (T = 200 °C; P = 50 bar; t = 480 min).

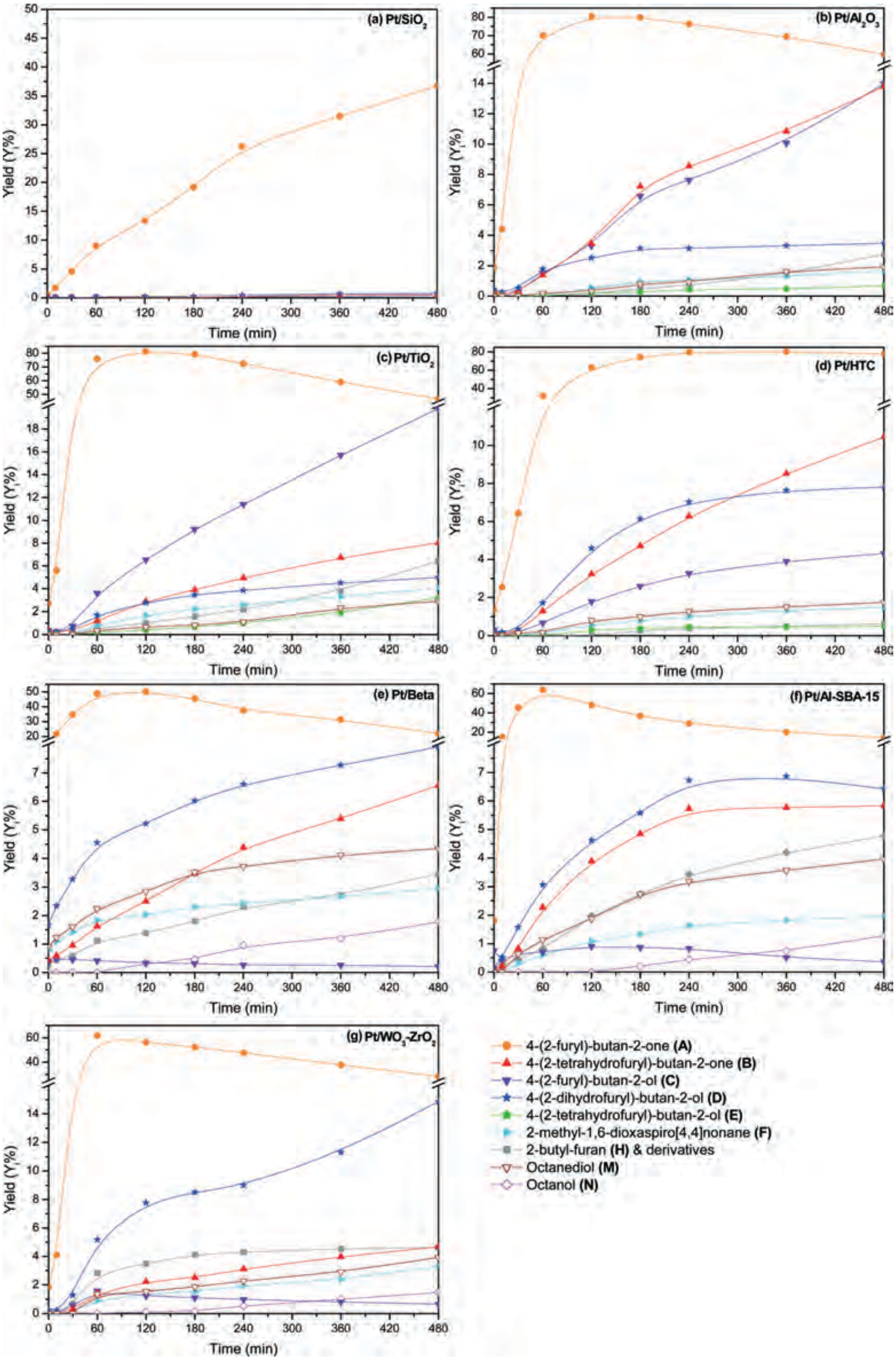

Fig. 3 Evolution of the yield (Y_i%) of F–Ac hydrodeoxygenated products over different catalysts (T = 200 °C; P = 50 bar; t = 480 min).

Hydrodeoxygenation selectivity

The multicomponent nature of the initial feedstock led to a complex mixture of products, derived from the successive hydrogenation steps of the different bonds (aliphatic C═C, furanic C═C and ketonic C═O), ring opening and dehydration reactions. Furthermore, some additional side reactions such as condensation, isomerization or cyclization may occur, resulting in a diverse product distribution within a wide range of molecular weights. Therefore, in order to simplify the discussion, the GC and GC-MS analyses of the collected samples were focused on the fraction of compounds originated from 4-(2-furyl)-3-buten-2-one (F–Ac), which constituted 72% of the reactants (without taking into consideration acetone). The study of the reaction pathways of F–Ac transformation can be used as a case study for the estimation of the conversion pathways of heavier furfural–acetone condensation products.

Fig. 3 depicts the yields of the main products obtained from the hydrogenation of F–Ac as a function of reaction time for the different studied catalysts. In all cases, the high yield of 4-(2-furyl)-butan-2-one (**A**) stands out among the other hydrogenated products. The yield of this compound reaches a maximum at short reaction times, followed by a smooth decrease as it is consumed to afford more deeply hydrogenated products. This fact suggests that the hydrogenation of this conjugated C═C bond is very fast, whereas the further hydrogenation steps, *i.e.* of the ketone group and the furan ring, are the rate-determining hydrogenation steps. This behaviour is common for all tested catalysts except for Pt/SiO_2, which shows a slow and continuous increase in the yield of **A**, indicating again the very poor hydrogenation performance of this material. This observation is also confirmed by the absence of the other intermediate products resulting from the consecutive hydrogenation of **A** in Pt/SiO_2 experiments.

The consecutive formation of hydrogenated compounds from the primary product (**A**) was also observed although to a lower extent. These included products such as 4-(2-tetrahydrofuryl)-butan-2-one (**B**) and 4-(2-furyl)-butan-2-ol (**C**), which are derived from furanic ring and ketonic bond hydrogenation, respectively. For some catalysts, like Pt/Al_2O_3 and Pt/TiO_2, the yield of these products reached significant values, >7.9%, through a continuous increase as the reaction proceeded. However, in the case of Pt/Beta, Pt/Al-SBA-15 and Pt/WO_3–ZrO_2, the formation of **C** seems to be limited, not exceeding yields of 0.7%. This fact may be correlated with a faster transformation of **C** into 4-(2-dihydrofuryl)-butan-2-ol (**D**) and 2-butyl-furan (**H**), *via* partial hydrogenation of the furan ring and deoxygenation, respectively. The formation of **D** may be promoted by the smaller particle sizes observed in these catalysts, which may modify the surface chemical adsorption of the reactant and the subsequent hydrogenation steps.[25,31]

Thus, the smaller Pt particles may favour the interactions with the furanic ring, allowing the unconstrained adsorption of the most accessible double bond.[22,32] On the other hand, the higher acidic character shown by Pt/Beta, Pt/Al-SBA-15 and Pt/WO_3–ZrO_2 may have enhanced the deoxygenation reactions, increasing the formation of **H** (3.4–4.8%). Overall, it is concluded that the selectivity to **C** decreased due to the combination of smaller Pt particles and the presence of acid sites.

The complete hydrogenation of the original molecule (F–Ac) led to the production of 4-(2-tetrahydrofuryl)-butan-2-ol (**E**), which only appeared in limited yields (<3.2%). The low formation of this product might not only be related to the slower kinetics of furanic ring and ketonic bond hydrogenation, but also to the higher reactivity of their precursors, promoting side reactions which reduce the selectivity to this compound. On the other hand, the continuous increase in the yield of **E** can be explained by its higher stability, caused by the limitation of the ring-opening steps of the saturated ring.[33] Among the mentioned side reactions, the formation of 2-methyl-1,6-dioxaspiro[4,4]nonane (**F**) took place, likely through the intramolecular addition of the hydroxyl group on the double bond of **D**.[34]

The extent of oxygen removal steps was confirmed by the formation of compounds such as 2-butyl-furan (**H**), 2-butyl-dihydrofuran (**I**), 2-propyl-tetrahydropyran (**J**) and 2-butyl-tetrahydrofuran (**K**). The deoxygenation steps took place mostly through dehydration or hydrogenolysis reactions which usually imply the interaction of Brønsted acid sites with the hydroxyl group.[35] Thus, the yield of deoxygenated compounds reached higher values with those catalysts that exhibited stronger acidity, like Pt/Beta, Pt/Al-SBA-15 and Pt/WO_3–ZrO_2 (Fig. 4a). In contrast, low acid materials or no-acid materials, such as Pt/Al_2O_3 and Pt/HTC, respectively, show a lower extent of deoxygenation steps. However, Pt/TiO_2 also exhibited a remarkable deoxygenation activity indicating that even mild acidity together with improved accessibility is equally important for furanic ring interaction with the active sites.

The formation of linear alcohols like octanediols (**M**) and octanols (**N**) occurs *via* ring opening reactions through hydrogenolysis of the C–O bond of the furanic ring, leading to the formation of a new hydroxyl group. The significant yields of octanediols at short reaction times (<60 min) in the case of Pt/Beta, Pt/Al-SBA-15 and Pt/WO_3–ZrO_2 indicate that the formation of octanediols likely occurs through ring opening of the primary intermediates, like **C**, since the yields of further hydrogenated precursors (**B**, **D** and **E**) are too low or non-existent at the beginning of the reactions. This observation is in accordance with Vlachos *et al.*,[36] who reported that the ring opening reactions preferentially take place through non-saturated rings because of the higher energy barriers associated with the ring opening of **D**, **B** and **E**. This behaviour may also be related to the observed low concentration of **C** with Pt/Beta, Pt/Al-SBA-15 and Pt/WO_3–ZrO_2, since in the presence of acid sites the hydrogenolysis of the C–O bond of the non-saturated furanic ring is promoted. A similar behaviour is observed in the production of octanols (**M**), whose yields

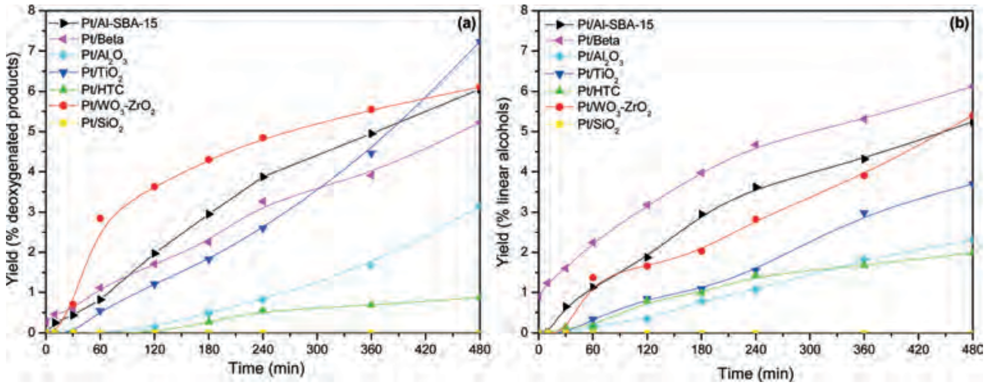

Fig. 4 Evolution of the yield (Y_i%) of (a) deoxygenated products (**H** + **I** + **J** + **K** + **N**) and (b) linear alcohol products (**M** + **N**), from the hydrodeoxygenation of F–Ac over different catalysts (T = 200 °C; P = 50 bar; 480 min).

seem to be linked to the formation of **H** (2-butyl-furan) and enhanced by the presence of acid sites (Pt/Beta, Pt/Al-SBA-15 and Pt/WO_3–ZrO_2). Fig. 4b shows the variation in the yield of octanediols and octanols with reaction time for all studied catalysts. The continuous increase in the yield of linear alcohols implies that dehydration/hydrogenolysis could be the rate-determining step in the conversion pathway to octane over the investigated set of platinum-containing catalysts.

Proposal of a reaction scheme

To shed light on the transformation pathways of furfural–acetone condensation products into hydrocarbons and to understand the role of different catalyst functionalities, an analysis of the kinetic curves exhibited in Fig. 3 and in previously published works,[14,17] was performed. As a result, a reaction scheme has been proposed to describe, in the most simplified way possible, the major routes in the conversion of 4-(2-furyl)-3-buten-2-one (F–Ac) into *n*-octane. The reaction scheme of the studied transformation is rather complicated, since it includes numerous intermediate products, side reactions, competitive and non-competitive steps, adsorption of solvent, formation of coke, *etc.* The product distribution consists of a mixture of compounds with different degrees of hydrogenation, indicating that there is a step by step mechanism through which various intermediates are formed. Fig. 5 shows the essential features of the reaction pathway for the production of octane from F–Ac, comprising the hydrogenation, condensation, isomerization, cyclization and dehydration/hydrogenolysis steps. Likewise, Table 3 displays the yield of F–Ac hydrogenated products obtained after 480 min, using the different prepared catalysts and the experimental procedure describe above.

Firstly, the hydrogenation of the aliphatic C═C bond takes place, yielding 4-(2-furyl)-butan-2-one (**A**). The fast hydrogenation of this bond is enhanced by its favourable thermodynamic conditions, and also due to the absence of steric limitations, unlike the case of the furanic ring bonds.[19]

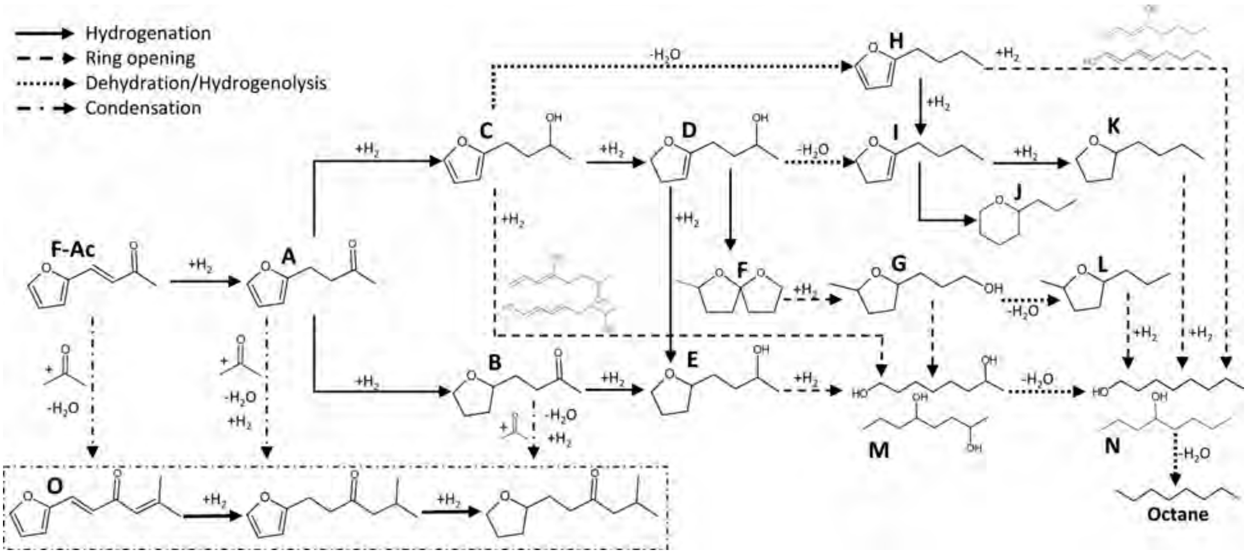

Fig. 5 Proposed reaction scheme for the hydrodeoxygenation of 4-(2-furyl)-3-buten-2-one (F–Ac) into octane.

Table 3 4-(2-Furyl)-3-buten-2-one (F–Ac) hydrodeoxygenation products after 480 min at 200 °C and 50 bar[a]

	Yield (Y_i%)													
Catalysts	F–Ac	**A**	**B**	**C**	**D**	**E**	**F**	**G**	**H**	**I**	**J**	**M**	**N**	**O**
Pt/ SiO_2	29.2	36.7	0.5	0.4	0.7	—	—	—	—	—	—	—	—	12.7
Pt/Al_2O_3	0	59.7	13.8	14.0	3.5	0.8	1.6	1.4	—	0.2	2.7	1.9	0.4	—
Pt/TiO_2	0	46.4	7.9	19.6	5.0	3.2	4.0	3.4	—	0.6	6.3	2.9	0.8	0.0
Pt/HTC	0.2	74.0	9.9	4.1	7.4	0.5	1.4	—	0.6	—	—	1.6	0.2	0.0
Pt/Beta	0.8	22.0	6.5	0.2	7.9	0.3	2.9	—	3.4	—	—	4.3	1.8	32.9
Pt/Al-SBA-15	0.6	14.2	5.8	0.3	6.4	0.6	2.0	1.2	4.8	—	—	4.0	1.3	39.7
Pt/WO_3–ZrO_2	0.2	28.3	4.7	0.7	14.7	1.1	3.3	2.2	4.6	0.3	—	3.9	1.5	34.6

[a] 4-(2-Furyl)-butan-2-one (**A**), 4-(2-tetrahydrofuryl)-butan-2-one (**B**), 4-(2-furyl)-butan-2-ol (**C**), 4-(2-dihydrofuryl)-butan-2-ol (**D**), 4-(2-tetrahydrofuryl)-butan-2-ol (**E**), 2-methyl-1,6-dioxaspiro[4,4]nonane (**F**), 5-methyl-2-tetrahydrofuranpropanol (**G**), 2-butyl-furan (**H**), 2-butyl-dihydrofuran (**I**), 2-propyl-tetrahydropyran (**J**), 2-butyl-tetrahydrofuran (**K**), 2-methyl-5-propyl-tetrahydrofuran (**L**), octanediols (**M**), octanols (**N**) and heavier condensation products (**O**).

The subsequent hydrogenation of **A** may proceed by two parallel routes: hydrogenation of the ketonic C═O bond or hydrogenation of the furanic ring C═C bonds. The latter yields 4-(2-tetrahydrofuryl)-butan-2-one (**B**), which is an intermediate of the completely hydrogenated molecule 4-(2-tetrahydrofuryl)-butan-2-ol (**E**). The former affords 4-(2-furyl)-butan-2-ol (**C**) that can undergo many different side reactions in addition to its transformation into **E**. The yield of this intermediate furan alcohol (**C**) is very low (negligible) when acid catalysts are used (Pt/Beta, Pt/Al-SBA-15 and Pt/WO_3–ZrO_2), most likely as a result of its immediate consumption yielding **D**, **H** and **M**. Specifically, the initial hydrogenation of the furanic ring of **C** produces a reactive intermediate, 4-(2-dihydrofuryl)-butan-2-ol (**D**), which may undergo cyclization due to the interaction between the –OH group and the partially hydrogenated ring yielding 2-methyl-1,6-dioxaspiro[4,4]nonane (**F**).[34] In addition, **D** may undergo hydrogenation of the remaining double bond in the furanic ring, thus yielding **E**, or dehydration reactions forming 2-butyl-dihydrofuran (**I**). A similar step may occur directly from **C**, yielding 2-butyl-furan (**H**), which can be further hydrogenated to **I**. Alternatively, the furan C–O bond present in **C** may be hydrogenolysed resulting in the opening of the furanic ring. This option yields linear unsaturated octanediols, which are rapidly hydrogenated to saturated octanediols (**M**). Otherwise, the formation of **M** can also occur *via* the ring opening of **E** or 5-methyl-2-tetrahydrofuranpropanol (**G**), affording saturated octanediols directly. The latter was derived from the ring opening steps of **F**, *via* hydrogenolysis of one of the C–O bonds. In this respect, C–C bond scission is generally unfavourable upon ring opening *via* C–O bond cleavage.[36,37]

The formation of **H** and **I** is a consequence of the dehydration of the primary intermediates. This reaction implies the formation of water through the loss of the –OH group from **C** or **D** intermediates. However, in the case of Pt/Al_2O_3 and Pt/TiO_2, the presence of **H** is a bit controversial, since although it is clearly observed at short reaction times, as the reaction progresses the GC retention time of the peak decreases gradually (*i.e.* **H** is co-eluting with a product of consecutive reactions and is itself consumed in the course of the reaction). According to the GC-MS pattern, the co-eluting compound is 2-propyl-tetrahydropyran (**J**) and it seems to be formed at the expense of **H**, likely *via* a fast formation of **I**.[38] The reason for the significant yield of **J** over TiO_2 and Al_2O_3 supported Pt is not yet fully understood. Nonetheless, the formation of **J** has been reported in similar processes by other authors, who have suggested its formation *via* isomerization and hydrogenation of **H**.[13,39] From the point of view of our results, the production of **J** seems to be linked to the presence of 2-butyl-dihydrofuran (**I**), since both products are obtained in the same experiments, suggesting that their formation by hydrogenation of **H** is closely related. On the other hand, the absence of **J** with the more acidic materials (Pt/Beta, Pt/Al-SBA-15 and Pt/WO_3–ZrO_2) indicates that with these catalysts the ring opening of **H** to form octanols (**N**) is more favoured by the presence of Brønsted acid sites. In any case, the formation of **J** constitutes an undesired side reaction since it reduces the selectivity to octane by forming a stable compound. Despite the fact that some oxygen removal steps (deoxygenation) took place, the dehydration of octanediols and octanols towards octane was very restricted since the presence of the hydrocarbon was not detected by GC-MS analyses. Therefore, it is also likely that the formation of **N** take places mostly through **H** rather than by dehydration of **M**.

In addition to the hydrogenation route of F–Ac, the significant formation of heavier products (**O**) catalyzed by Pt/SiO_2, Pt/Beta, Pt/Al-SBA-15 and Pt/WO_3–ZrO_2 was observed. These compounds are products of aldol condensation of acetone either with F–Ac, or with other intermediate ketone compounds such as **A** and **B**. Thus, this route leads to the formation of longer carbon chain intermediates which, once deoxygenated, would ultimately yield larger alkenes (C_{11+}), *i.e.* the overall hydrocarbon yield would not be affected in the case of total hydrodeoxygenation. However, it should be considered that these reactions may lead to the production of a heavy fraction that can be involved in the formation of carbon deposits. Therefore, this aspect must be taken into consideration for the performance of longer experiments as a possible cause of catalyst deactivation. Likewise, the successive hydrogenation steps of **O** indicate the possibility of performing simultaneously aldol-condensation and hydrogenation reactions, although this process is technically very demanding since the optimal conditions for both reactions are different.[40] Particularly, in the case of acid catalysts, the yields of these heavier products were very significant (32.9–39.7%), thus reducing considerably the maximum attainable selectivity to octane. One possibility to prevent these side reactions is the use of solvents other than acetone (*e.g.* alcohols), which can be expected to limit the extent of aldol condensation reactions. It is also worth noting that despite almost one third of F–Ac undergoes further condensation, Pt/Beta, Pt/Al-SBA-15 and Pt/WO_3–ZrO_2 afford the highest yields of octanols (1.3–1.8%) among the studied catalysts. This indicates superior ring opening and deoxygenation activity of platinum supported on acid supports in comparison with platinum supported on non-acidic or basic supports.

The abovementioned results suggest that employing acid catalysts, such as Pt/Beta, Pt/Al-SBA-15 and Pt/WO_3–ZrO_2, with hydrogenated intermediate products (*i.e.* products less prone to condensation), may improve the final yield of linear alcohols and octane. Hence, an additional longer experiment (16 h) was carried out consisting of two stages. Firstly, an 8 hour reaction was performed using Pt/TiO_2 and the original feedstock (Table 1). Secondly, Pt/Al-SBA-15 was added to the obtained product from the first stage and the experiment was continued for another 8 hours. In this way the good hydrogenation activity of Pt/TiO_2 was combined with the good deoxygenation activity of Pt/Al-SBA-15. At the same time, it was expected that the decrease in the concentration of F–Ac and intermediates **A** and **B** during the first stage would limit the extent of acetone condensation reactions and favour a higher yield of C_8 intermediates. The yields of products are shown in Fig. 6 as a function of reaction time.

In line with the previous results, **A** and **C** are the main products obtained as a result of the hydrogenation of F–Ac on Pt/TiO_2. Both of the products are rapidly consumed when Pt/Al-SBA-15 is used as a catalyst. In the case of **C**, which is completely absent at the end of the reaction (960 h), it is mostly due to the high promotion of ring opening and dehydration steps in the presence of Brønsted acid sites, yielding **M** (19.7%) and **H**, respectively. The latter is also quickly converted to **J** (23%) and **K** (10.8%), *via* hydrogenation and isomerization reactions. The increasing amount of these products, together with **G**, indicates a significant limitation for opening saturated rings. Similarly, despite the high increase in **M**, the yield of **E** does not show any decrease, confirming the lower reactivity of this compound. Thus, in order to optimize the production of octane, the formation of fully hydrogenated species, such as **E**, should be avoided due to the more demanding conditions required to open their tetrahydrofuran ring in comparison with furan and dihydrofuran rings.

Fig. 6 also reveals the intermediate character of compound **B** and **D** showing a decreasing trend when the concentration of their respective precursors (**A** and **C**) is too low. The formation of heavier products with Pt/Al-SBA-15 is not completely inhibited (**O** = 6%), due to the extent of condensation reactions between acetone and the remaining intermediate ketones, *i.e.* **A** and **B** after hydrogenation over Pt/TiO_2. However, the yield of these compounds is considerably reduced in comparison with the experiment over Pt/Al-SBA-15 when F–Ac was used as feedstock, *i.e.* when F–Ac was in contact with the acid sites of the Al-SBA-15 support. Consequently, the selectivity to C_8 intermediates that can be hydrodeoxygenated is enhanced, which together with the higher ring opening and dehydration activity of Pt/Al-SBA-15 lead to an increase in the formation of octanediols (19.7%) and octanols (3.5%).

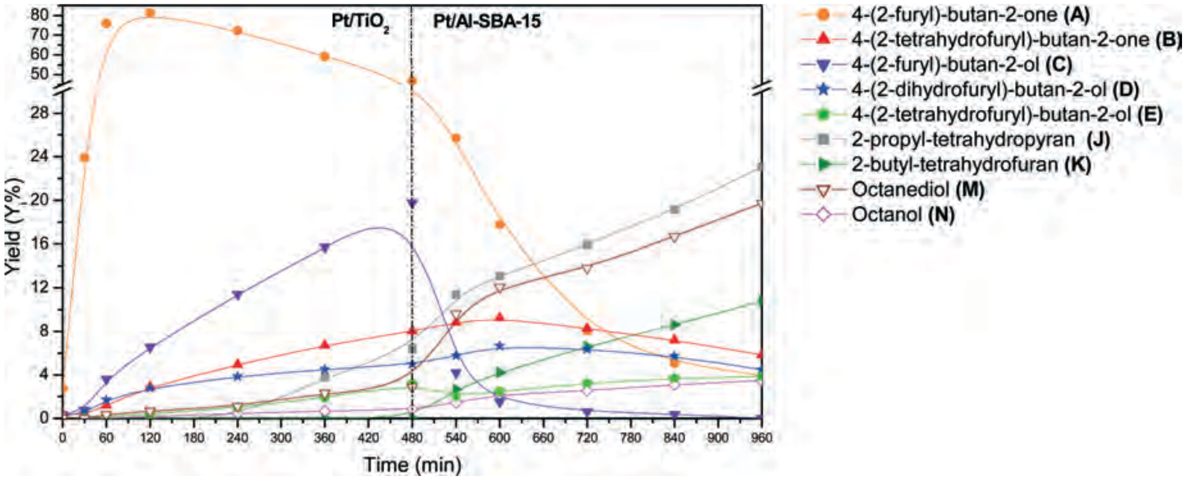

Fig. 6 Evolution of the yield (Y_i%) of F–Ac hydrogenated products (T = 200 °C; P = 50 bar) in a two stage experiment: Pt/TiO_2 (8 h) and Pt/Al-SBA-15 (8 h).

The significantly higher concentration of octanediols (**M**) over octanols (**N**) suggests that the dehydration of linear alcohols is more restricted than furanic ring molecules. However, the higher hydrodeoxygenation rate achieved in the two stage experiment also afforded a low yield of octane (1.5%), formed presumably by the dehydration of **N**. The formation of green octane completes the proposed reaction scheme (Fig. 5), setting the groundwork for future development of catalysts capable of efficiently deoxygenating furfural condensation products into green hydrocarbons.

Conclusions

The hydrodeoxygenation of furfural–acetone condensation products has been studied using different supported Pt catalysts. The studied materials show a wide range of textural and acid properties which significantly affect the activity and selectivity of the process. The multicomponent nature of the initial feedstock (derived from furfural–acetone aldol condensation experiments) led to a complex mixture of products, formed mainly by different extent of hydrogenation, ring opening and dehydration/hydrogenolysis reactions. Based on the study of the conversion rates and the kinetic behaviours shown by the main reactants and intermediates, a reaction scheme for the conversion of 4-(2-furyl)-3-buten-2-one (F–Ac) into octane has been proposed. The performed experiments indicated that the conversion pathways and product distribution may be significantly modified by the catalytic properties of the studied supports.

Except for Pt/SiO_2, all catalysts showed high conversion of the reactants, mostly due to the complete hydrogenation of the aliphatic C═C bonds. However, the extent of the conversion of furanic C═C and ketonic C═O bonds was more limited, particularly when HTC and Al_2O_3 were used as supports. The use of Pt/TiO_2 further promoted the hydrogenation, although the selectivity to linear alcohols seemed to be limited by the slow rate of dehydration and ring-opening steps. In all cases, ring-opening reactions occurred preferentially through non-saturated rings, indicating the possible convenience of a selective hydrogenation to aliphatic C═C and ketonic C═O bonds in the early steps. Likewise, in the case of Pt supported on Beta, Al-SBA-15, WO_3–ZrO_2, aldol condensation reactions took place between carbonyl-containing intermediates and acetone, yielding longer carbon chain compounds. Although the formation of these molecules reduced the concentration of C_8 molecules, a remarkable selectivity to linear alcohols was observed due to the higher extent of ring-opening and dehydration reactions in the presence of Brønsted acid sites.

The production of octanols and octanediols having potential as valuable petrochemical feedstocks was improved by performing a two stage experiment, using Pt/TiO_2 (8 h) and Pt/Al-SBA-15 (8 h). The further hydrogenation of the primary reactants using Pt/TiO_2, along with the higher promotion of ring-opening and dehydration reactions with Pt/Al-SBA-15, enhanced the hydrodeoxygenation rate of C_8 intermediates, achieving final production of an octane fraction.

Acknowledgements

This publication is a result of project no. P106/12/G015 supported by the Czech Science Foundation which is being carried out in the UniCRE center (CZ.1.05/2.1.00/03.0071) whose infrastructure was supported by the European Regional Development Fund and the state budget of the Czech Republic.

Notes and references

1 S. De, B. Saha and R. Luque, *Bioresour. Technol.*, 2015, **178**, 108.

2 J. J. Bozell and G. R. Petersen, *Green Chem.*, 2010, **12**, 539.

3 K. Yan, G. Wu, T. Lafleur and C. Jarvis, *Renewable Sustainable Energy Rev.*, 2014, **38**, 663.

4 K. J. Zeitsch, *The chemistry and technology of furfural and its many by-products (Vol. 13)*, Elsevier, 2000.

5 S. Dutta, S. De, B. Saha and M. I. Alam, *Catal. Sci. Technol.*, 2010, **2**(10), 2025.

6 L. Faba, E. Díaz and S. Ordóñez, *Appl. Catal., B*, 2012, **113**, 201.

7 O. Kikhtyanin, V. Kelbichová, D. Vitvarová, M. Kubů and D. Kubička, *Catal. Today*, 2014, **227**, 154.

8 L. Hora, V. Kelbichová, O. Kikhtyanin, O. Bortnovskiy and D. Kubička, *Catal. Today*, 2014, **223**, 138.

9 J. N. Chheda and J. A. Dumesic, *Catal. Today*, 2007, **123**(1), 59.

10 R. Xing, A. V. Subrahmanyam, H. Olcay, W. Qi, G. P. van Walsum, H. Pendse and G. W. Huber, *Green Chem.*, 2010, **12**(11), 1933.

11 H. van der Wal, B. L. Sperber, B. Houweling-Tan, R. R. Bakker, W. Brandenburg and A. M. López-Contreras, *Bioresour. Technol.*, 2013, **128**, 431.

12 M. Gliński, J. Kijeński and A. Jakubowski, *Appl. Catal., A*, 1995, **128**(2), 209.

13 T. N. Pham, D. Shi, T. Sooknoi and D. E. Resasco, *J. Catal.*, 2012, **295**, 169.

14 W. Xu, Q. Xia, Y. Zhang, Y. Guo, Y. Wang and G. Lu, *ChemSusChem*, 2011, **4**(12), 1758.

15 Q. N. Xia, Q. Cuan, X. H. Liu, X. Q. Gong, G. Z. Lu and Y. Q. Wang, *Angew. Chem., Int. Ed.*, 2014, **53**(37), 9755.

16 L. Faba, E. Díaz and S. Ordóñez, *Catal. Sci. Technol.*, 2015, **5**(3), 1473.

17 L. Faba, E. Díaz and S. Ordóñez, *Appl. Catal., B*, 2014, **160**, 436.

18 W. Xu, X. Liu, J. Ren, P. Zhang, Y. Wang, Y. Guo and G. Lu, *Catal. Commun.*, 2010, **11**(8), 721.

19 C. J. Barrett, J. N. Chheda, G. W. Huber and J. A. Dumesic, *Appl. Catal., B*, 2006, **66**(1), 111.

20 A. D. Sutton, F. D. Waldie, R. Wu, M. Schlaf, A. Louis III and J. C. Gordon, *Nat. Chem.*, 2013, **5**(5), 428.

21 R. Zanella, C. Louis, S. Giorgio and R. Touroude, *J. Catal.*, 2004, **223**(2), 328.

22 M. Englisch, A. Jentys and J. A. Lercher, *J. Catal.*, 1997, **166**(1), 25.

23 T. B. L. W. Marinelli, J. H. Vleeming and V. Ponec, *Stud. Surf. Sci. Catal.*, 1993, **75**, 1211.

24 J. Lee, Y. Xu and G. W. Huber, *Appl. Catal., B*, 2013, **140**, 98.

25 P. Claus, *Top. Catal.*, 1998, **5**(1–4), 51.

26 P. Mäki-Arvela, J. Hajek, T. Salmi and D. Y. Murzin, *Appl. Catal., A*, 2005, **292**, 1.

27 O. Kikhtyanin, L. Hora and D. Kubička, *Catal. Commun.*, 2015, **58**, 89.

28 W. Zang, G. Li, L. Wang and X. Zhang, *Catal. Sci. Technol.*, 2015, 5(5), 2532.

29 B. Delmon, P. Grange and G. F. Froment, *Hydrotreatment and hydrocracking of oil fractions*, Elsevier, 1997.

30 P. A. Ramachandran and R. V. Chaudhari, *Three-phase catalytic reactors (Vol. 2)*, Gordon & Breach Science Pub, 1983.

31 C. J. Kliewer, C. Aliaga, M. Bieri, W. Huang, C. K. Tsung, J. B. Wood, K. Komvopoulos and G. A. Somorjai, *J. Am. Chem. Soc.*, 2010, **132**(37), 13088.

32 U. K. Singh and M. A. Vannice, *Stud. Surf. Sci. Catal.*, 2000, **130**, 497.

33 S. Sitthisa and D. E. Resasco, *Catal. Lett.*, 2011, **141**(6), 784.

34 K. Alexander, L. S. Hafner and L. E. Schniepp, *J. Am. Chem. Soc.*, 1951, **73**(6), 2725.

35 P. M. Mortensen, J. D. Grunwaldt, P. A. Jensen and A. D. Jensen, *ACS Catal.*, 2013, 3(8), 1774.

36 S. Wang, V. Vorotnikov and D. G. Vlachos, *Green Chem.*, 2014, **16**(2), 736.

37 C. R. Waidmann, A. W. Pierpont, E. R. Batista, J. C. Gordon, R. L. Martin, R. M. West and R. Wu, *Catal. Sci. Technol.*, 2013, 3(1), 106.

38 D. Robin, M. Sarraf, H. E. Audier and M. Fetizon, *Tetrahedron Lett.*, 1984, **25**(35), 3815.

39 K. L. Luska, J. Julis, E. Stavitski, D. N. Zakharov, A. Adams and W. Leitner, *Chem. Sci.*, 2014, 5(12), 4895.

40 L. Faba, E. Díaz and S. Ordóñez, *ChemSusChem*, 2014, **7**, 2816.

Applied Catalysis A: General 530 (2017) 174–183

Contents lists available at ScienceDirect

Applied Catalysis A: General

journal homepage: www.elsevier.com/locate/apcata

Solvent effects in hydrodeoxygenation of furfural-acetone aldol condensation products over Pt/TiO_2 catalyst

Rubén Ramos[a,*], Zdeněk Tišler[a], Oleg Kikhtyanin[a], David Kubička[a,b]

[a] *Unipetrol Centre of Research and Education (UNICRE), Chempark Litvínov, Záluží-Litvínov, 436 70, Czechia*
[b] *Technopark Kralupy, University of Chemistry and Technology Prague, Žižkova 7, 27801 Kralupy nad Vltavou, Czechia*

ARTICLE INFO

Article history:
Received 26 September 2016
Received in revised form
14 November 2016
Accepted 15 November 2016
Available online 17 November 2016

Keywords:
Furfural
Aldol condensation
Hydrodeoxygenation
Solvent effects
Platinum titania catalyst

ABSTRACT

The solvent effects on hydrodeoxygenation (HDO) of 4-(2-furyl)-3-buten-2-one (F-Ac) over Pt/TiO_2 catalyst were investigated at $T = 200\,^{\circ}C$ and $P(H_2) = 50$ bar. The initial reactant is the main product of aldol condensation between furfural and acetone, which constitutes a promising route for the production of bio-based chemicals and fuels. A sequence of experiments was performed using a selection of polar solvents with different chemical natures: protic (methanol, ethanol, 1-propanol, 2-propanol, 1-pentanol) and aprotic (acetone, tetrahydrofuran (THF), *n*,*n*-dimethylformamide (DMF)). In case of protic solvents, a good correlation was found between the polarity parameters and conversion. Consequently, the highest hydrogenation rate was observed when 2-propanol was used as a solvent. In contrast, the hydrogenation activity in presence of aprotic solvents was related rather to solvent-catalyst interactions. Thus, the initial hydrogenation rate declined in order Acetone > THF > DMF, *i.e.* in accordance with the increase in the nucleophilic donor number and solvent desorption energy. Regarding the product distribution, a complex mixture of intermediates was obtained, owing to the successive hydrogenation (aliphatic C═C, furanic C═C and ketonic C═O bonds), ring opening (via C—O hydrogenolysis) and deoxygenation reactions. Based on the proposed reaction scheme for the conversion of F-Ac into octane, the influence of the studied solvents over the cascade catalytic conversion is discussed. A significant formation of cyclic saturated compounds such as 2-propyl-tetrahydropyran and 2-methyl-1,6-dioxaspiro[4,4]nonane took place via undesirable side reactions of cyclization and isomerization. The best catalytic performance was found when using acetone and 2-propanol as solvents, achieving significant yields of 4-(2-tetrahydrofuryl)-butan-2-ol (28.5–40.4%) and linear alcohols (6.3–10.4%). The better performance of these solvents may be associated with a lower activation energy barrier for key intermediate products, due to their moderate interaction with the reactant and the catalyst. In case of methanol and DMF, undesired reactions between the reactant and the solvent took place, leading to a lower selectivity towards the targeted hydrodeoxygenated products.

1. Introduction

Biomass is a key renewable resource with the potential to satisfy at least partially the growing energy demand and to provide alternative technologies to petroleum-based ones. Hemicellulose is one of the major components (25–35 wt%) of non-food lignocellulose biomass, which can be transformed into C_5 and C_6 sugars monomers via acid-catalyzed hydrolysis [1,2]. This sugar fraction can be further processed to furanic compounds (via acid-catalyzed dehydration), leading to the production of lignocellulosic platform molecules (e.g. furfural and 5-hydroxymethylfurfural) that could play the role of basic building blocks in future biorefineries [3,4]. Therefore, in order to produce valuable green chemicals and fuels from sustainable sources, the catalytic transformation of furan derivatives is regaining the attention of different research groups in recent years [5,6].

Among the different conversion strategies, aldol condensation allows increasing carbon chain length of furanic compounds by forming larger bio-based molecules, more appropriate for upgrading to gasoline and diesel fuels. Aldol condensation is a well-known organic synthesis, which generally takes place between carbonyl groups at low temperatures (25–70 °C) and atmospheric pressure. This route has been successfully used for the condensation of furfural (C_5) with acetone in presence of solid basic catalysts, yielding mostly 4-(2-furyl)-3-buten-2-one (F-Ac) and 1,5-difuryl-

---

[*] Corresponding author. Present address: Department of Chemistry, University of Liverpool, Crown Street, Liverpool, L69 7ZD, UK.
E-mail address: R.Ramos-Velarde@liverpool.ac.uk (R. Ramos).

http://dx.doi.org/10.1016/j.apcata.2016.11.023
0926-860X/© 2016 Elsevier B.V. All rights reserved.

1,4-pentadien-3-one (F-Ac-F) [7,8]. However, compared with most petrochemical products, furfural-acetone condensation products are multifunctionalized oxygenated compounds which require challenging chemical transformations *i.e.* hydrogenation (C=C aliphatic, C=O ketone and C=C furanic ring bonds), ring opening (C—O hydrogenolysis) and deoxygenation (via dehydration or C—OH hydrogenolysis) in order to yield liquid transportation fuels. Hence, the overall conversion of these adducts into alkanes may be performed by hydrodeoxygenation (HDO), generally at mild temperatures (150–300 °C) and high hydrogen pressures (20–100 bar) [9,10].

The presence of heterogeneous catalysts in the HDO processing of furfural-acetone condensation products favours the conversion rates (thermodynamic and kinetic considerations) and allows tailoring the product distribution through the selection of the catalyst features. In a previous work, we have investigated the influence of different supported Pt catalysts on the HDO of furfural-acetone condensation products [11]. Similarly, different studies from the literature have reported the performance of metal-based catalysts on this process, exploring the effects of different parameters such as; nature of the metal phase [10], catalyst morphology [12–14], reaction system [13,15,16] and operation conditions [9,17,18]. Most of these studies have been carried out in the liquid phase, using different kinds of solvents to dissolve the solid reactants and to dissipate the heat generated from exothermic reactions. Thus, Dumesic and co-workers investigated the hydrogenation of furfural-acetone adducts employing Pd/MgO-ZrO_2 as catalyst in aqueous environment [15,18]. From the same research group, another work investigated the activity of Pt/SiO_2-Al_2O_3 in dehydration of these compounds using tetrahydrofuran (THF) as solvent [16]. In the same way, Lu et al. [14,17,19] carried out a series of experiments combining different solvents such as isopropanol, ethanol, THF and cyclohexane. Similarly, Gordon et al. [9] compared the results obtained using acetic acid and methanol as solvents in deoxygenation reactions under mild operating conditions. Additionally, HDO of furfural-acetone condensation products has been carried out in hexane [10,12] and, also using ionic liquids [20]. Nevertheless, due to the lack of systematic experimental data, the influence of the reaction media (solvents) on the activity and selectivity in the HDO of furfural-acetone condensation products has been scarcely discussed.

According to preceding works [21–24], it is expected that solvent effects have a strong influence on hydrogenation reactions, which constitute an essential initial step in the HDO processing. A general reaction scheme for F-Ac hydrogenation is shown in Fig. 1. The primary C=C aliphatic hydrogenation (4-(2-furyl)-butan-2-one; **A**) is followed by further hydrogenation steps of C=C furanic ring bonds (4-(2-tetrahydrofuryl)-butan-2-one; **B**) or C=O ketone bond (4-(2-furyl)-butan-2-ol; **C**). On the pathway to the completely hydrogenated compound (4-(2-tetrahydrofuryl)-butan-2-ol; **E**), the partial hydrogenation of the latter yields a reactive intermediate (4-(2-dihydrofuryl)-butan-2-ol; **D**), which may undergo different reactions [11].

In spite of the progress in understanding solvent effects on hydrogenation reactions, much work remains to be done to unravel the influence of solvents in multi-step catalytic transformations, such as the HDO of F-Ac towards valuable alkanes, which further comprises: ring opening reactions (on metal and possibly acid sites), dehydration/hydrogenolysis (most likely on Brønsted acid sites), as well as different side reactions. Likewise, the regular use of bifunctional catalysts in such processes may increase the complexity of solvent effects owing to the likely interactions between the metal phases and the solvent [25].

In the present contribution, we aim to investigate the solvent effects on the HDO of 4-(2-furyl)-3-buten-2-one (F-Ac) in terms of conversion rates and product distribution. Pt/TiO_2 was selected as a reference catalyst due to the well-known hydrodeoxygenation activity of this metal phase and the enhanced accessibility provided by the titania support. A sequence of experiments was performed using a selection of polar solvents with different chemical nature: protic (methanol, ethanol, 1-propanol, 2-propanol, 1-pentanol) and aprotic (acetone, tetrahydrofuran, n,n-dimethylformamide). The initial hydrogenation rate and further transformations through furan ring opening and deoxygenation steps, are discussed considering the solvent-reactant and the solvent-catalyst interactions. To our knowledge, such systematic investigation of solvent effects on HDO of furfural-acetone condensation products has not been described previously. Therefore, this work may provide a better understanding of the role of a solvent in this catalytic conversion, contributing to a rational solvent selection that would improve the overall process efficiency.

2. Experimental

2.1. Chemicals

Methanol (Sigma Aldrich, >99.9%), Ethanol (Sigma Aldrich, >99.8%), 1-propanol (Sigma Aldrich, >99.5%), 2-propanol (Lach-Ner, >99.7%), 1-pentanol (Sigma Aldrich, >99%), acetone (Sigma Aldrich, >99.5%), tetrahydrofuran (Sigma Aldrich, >99.9%) and *n*,*n*-dimethylformamide (Sigma Aldrich, >99.8%) were used without further treatment. The TiO_2 support and tetraammine-platinum(II) nitrate were purchased from Eurosupport Manufacturing Czechia and Sigma Aldrich, respectively, and used as received. Hydrogen was supplied from an external reservoir (Linde, >99%).

2.2. Catalyst preparation

The catalyst, Pt/TiO_2, was prepared by incipient wetness impregnation using tetraammine-platinum(II) nitrate ($Pt(NH_3)_4(NO_3)_2$) to obtain a nominal metal loading of 2 wt% (referred to mass catalyst). The deposition of Pt was carried out by adding dropwise an aqueous solution of the precursor to the support at ambient temperature. After metal incorporation, the catalyst was dried at 120 °C overnight and calcined at 500 °C in air for 6 h (heating rate 1 $°C\,min^{-1}$).

2.3. Catalyst characterization

The properties of Pt/TiO_2 were analyzed by different physico-chemical characterization methods. The amount of incorporated Pt was determined by X-ray Fluorescence Spectroscopy (XRF) using a Philips PW 1404 UniQuant apparatus. Textural properties were determined from N_2 physisorption isotherms at 77 K obtained by using a Quantachrome AUTOSORB unit. Prior to the analyses, the sample was outgassed at 250 °C for 3 h flowing N_2. BET equation and BJH method were used to calculate the specific surface area and the average pore size, respectively.

Acid and base sites were evaluated by temperature programmed desorption (TPD) of ammonia and carbon dioxide, respectively, employing a Micromeritics Autochem 2950 equipment. Prior to the TPD analyses, the sample (0.1 g) was reduced in situ under 10 vol% H_2/Ar (25 $cm^3\,min^{-1}$) at 350 °C for 60 min. Then, the catalyst was outgassed in flowing helium (25 $cm^3\,min^{-1}$) with a heating ramp of 10 $°C\,min^{-1}$ up–500 °C. The NH_3 TPD measurement was started by cooling the sample down to 180 °C and saturating it with ammonia (25 $cm^3\,min^{-1}$ of 10 vol% NH_3/He) for 30 min. Subsequently, the physically adsorbed NH_3 was removed by flowing He (25 $cm^3\,min^{-1}$) for 60 min. Finally, TPD was performed heating the Pt/TiO_2 catalyst in flowing He (25 $cm^3\,min^{-1}$) with a rate of 15 $°C\,min^{-1}$ up to 500 °C, and maintaining this temperature for

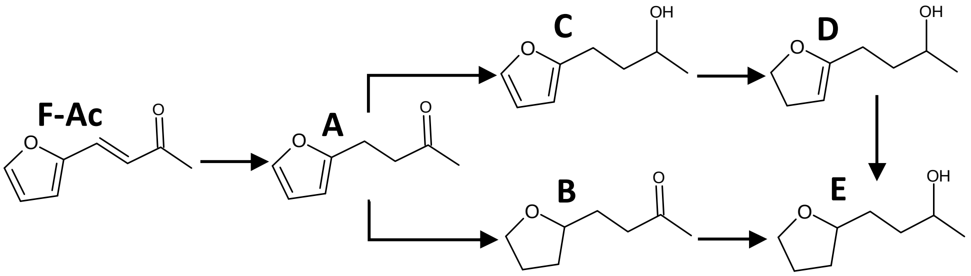

Fig. 1. Reaction scheme for the hydrogenation of 4-(2-furyl)-3-buten-2-one over bifunctional catalysts; (A) 4-(2-furyl)-butan-2-one, (B) 4-(2-tetrahydrofuryl)-butan-2-one, (C) 4-(2-furyl)-butan-2-ol, (D) 4-(2-dihydrofuryl)-butan-2-ol, (E) 4-(2-tetrahydrofuryl)-butan-2-ol.

30 min. The CO_2 TPD experiment was initiated by cooling the sample to 50 °C followed by saturating it with a flow of 10 vol% CO_2/He (50 $cm^3\,min^{-1}$) at 50 °C for 30 min. Afterward, the physisorbed carbon dioxide was removed by flowing He (25 $cm^3\,min^{-1}$) at 50 °C for 60 min. Finally, the chemically adsorbed CO_2 was desorbed by heating up the sample to 900 °C (heating rate of 15 °C min^{-1}) in flowing He (25 $cm^3\,min^{-1}$) and maintaining this temperature for 30 min.

The metal dispersion of Pt in the Pt/TiO_2 catalyst was determined by CO pulse chemisorption using a Micromeritics Autochem 2950 equipment. After the reduction treatment, the sample was degassed under He flow at 500 °C for 1 h and then cooled down to 50 °C. Subsequently, a sequence of 5 vol% CO/He pulses (500 μl) was introduced in a flow of He (50 $cm^3\,min^{-1}$) and passed through the sample until the areas of the successive peaks remained constant. The relation between the areas of the different chemisorbed CO pulses allowed evaluating the metal dispersion as a function of metal loading and defined adsorption stoichiometry factor (1 CO/Pt atom).

Solvent interactions with Pt/TiO_2 catalyst were investigated by temperature programmed desorption (TPD) of the pre-adsorbed solvent. A sample of reduced Pt/TiO_2 catalysts was saturated at 50 °C by pulse dosing of a gaseous stream of He (20 $cm^3\,min^{-1}$) bubbled through the solvent. Then, the adsorbed solvent was removed under a flow of He (25 $cm^3\,min^{-1}$) by increasing the temperature from 50 to 500 °C. Different heating rates (10, 15 and 20 °C min^{-1}) were used during the TPD resulting in a variation in the temperature of the desorption peak maximum. The desorption enthalpy (E_d) was then calculated from the slope of the linear relationship between the heating rate and the temperature of the desorption peak maximum, according to the method reported by Cvetanovic and Amenomiya [26].

2.4. Catalytic experiments

The catalytic conversion of 4-(2-furyl)-3-buten-2-one (Alfa Caesar, 98%) was studied in a steel 300 ml batch reactor (Parr Instrument Co.). Temperature, pressure and stirring speed were monitored and logged through a Parr 4848 B acquisition interface. Prior to the experiments, the catalyst (0.2 g) was reduced in situ by H_2 flow (80 $cm^3\,min^{-1}$) at 350 °C for 90 min. After cooling down, a prepared solution of 1 g of 4-(2-furyl)-3-buten-2-one (F-Ac) and 150 ml of the solvent was loaded into the reactor. Then, the system was heated up to 200 °C and pressurized with H_2 to 50 bar, under a slow stirring speed (100 rpm). The initial reaction time was taken when the reactor reached the desired temperature and the stirring speed was increased to 1000 rpm. The hydrogen consumed during the reaction (480 min) was replenished from an external source to maintain a constant reaction pressure. Samples of products were collected at different reaction times in order to study the progress of the reaction. The identification of the resulting compounds was done by means of GC–MS analyses using a Thermo Scientific ITQ 1100 apparatus. The quantification of the product mixtures were analyzed by an Agilent 7890A GC unit (FID detectors) equipped with a HP-5 capillary column (30 m, 0.32 ID, 0.25 μm). To this end, standard reference compound like 4-(2-furyl)-3-buten-2-one (Sigma Aldrich, >95%) was used for calibration measurements, assuming the same GC sensitivity for the rest of C_8 furan/tetrahydrofuran derived compounds.

Table 1
Physicochemical properties of Pt/TiO_2 catalyst.

Pt content	(wt%)	1.8
BET surface	($m^2\,g^{-1}$)	95
Pore size	(nm)	30.4
Amount of acid sites	(meq $NH_3\,g^{-1}$)	0.134
NH_3 desorption maximum	(°C)	234
Amount of base sites	(meq $CO_2\,g^{-1}$)	0.416
CO_2 desorption maximum	(°C)	105/194
Pt dispersion	(%)	15.6
Average Pt particle size	(nm)	7.2

F-Ac conversion at time t (X_t) was calculated using Eq. (1):

$$X_t = \frac{[C_{\text{F-Ac}}]_{t=0} - [C_{\text{F-Ac}}]_t}{[C_{\text{F-Ac}}]_{t=0}} \times 100 \tag{1}$$

where $[C_{\text{F-Ac}}]_{t=0}$ and $[C_{\text{F-Ac}}]_t$ are the initial molar concentration and the molar concentration at time t of F-Ac in solution, respectively. The yield of the specie *i* at time t ($[Y_i]_t$) was given by Eq. (2):

$$[Y_i]_t = \frac{[C_i]_t - [C_i]_{t=0}}{[C_{\text{F-Ac}}]_{t=0}} \times 100 \tag{2}$$

where $[C_i]_{t=0}$ and $[C_i]_t$ are the initial molar concentration and the molar concentration at time t of the specie *i*, respectively.

3. Results and discussion

3.1. Catalyst characterization

The main physicochemical properties of Pt/TiO_2, characterized by the instrumental techniques described in Section 2.3, are reported in Table 1.

The final Pt content in the catalysts was determined by XRF at to be 1.8 wt%, indicating an almost complete incorporation of the metal phase on the support by the used impregnation method. The nitrogen adsorption-desorption isotherm of Pt/TiO_2 (Fig. S1 in the Supporting information) exhibited a profile characteristic of mesoporous materials, with a noticeable adsorption at high relative pressures ($P/P_0 > 0.8$). Based on the experimental data provided by this isotherm, BET surface area (95 $m^2\,g^{-1}$) and average pore size (30.4 nm) were determined. The obtained textural properties provide an appropriate specific surface area for the dispersion of the metal phase, as well as an extensive pore size, capable of accommodating the F-Ac molecules into the mesopore system without steric limitations.

Fig. 2 illustrates the temperature programmed desorption curves obtained for the desorption of NH_3 (Fig. 2a) and CO_2 (Fig. 2b).

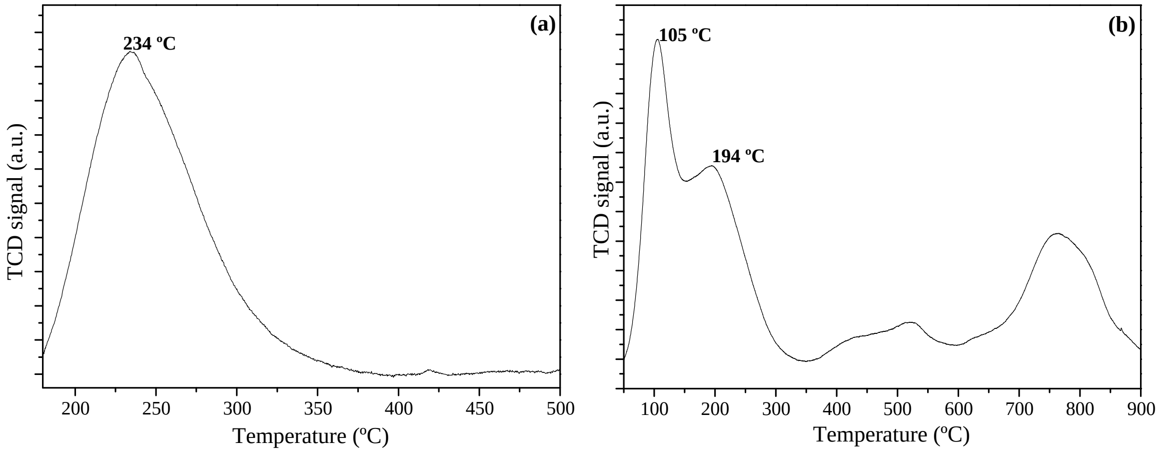

Fig. 2. TPD curves of Pt/TiO$_2$ catalyst; (a) ammonia TPD and (b) carbon dioxide TPD.

The integration of the NH$_3$ TPD curve revealed presence of acidic sites (0.134 meq NH$_3$ g^{-1}) of weak strength (maximum desorption at 234 °C). On the contrary, the total amount of basic sites, calculated from the CO$_2$ TPD curve, was considerably higher (0.416 meq CO$_2$ g^{-1}). This value was estimated without considering the CO$_2$ desorbed above 500 °C, since, according to some authors [27,28] and, also in agreement to the performed blank test, the TPD signal obtained at those temperatures is associated with residual carbonates not removed during the calcination or outgassing steps (500 °C). Thus, only the chemisorbed CO$_2$ in form of bicarbonate anions of weak basic strength (90–110 °C) and bidentate species (190–220 °C) of medium strength, were taken into account for the quantification of the catalyst basic properties.

Finally, Pt dispersion (15.6%) and average Pt particle size (7.2 nm) were estimated by CO pulse chemisorption measurements (Fig. S2). These features may be crucial for catalyst performance, since the activation of the intermediate compounds over metal centers is strongly influenced by the dispersion degree and particle size of the metal phase [29,30].

3.2. Conversion and initial hydrogenation rate

Following the experimental procedure defined in the Section 2.4, the effects arising from the use of different solvents in the HDO of F-Ac were evaluated in terms of the reactant conversion and the initial hydrogenation rate. Control experiments without catalysts and with non-impregnated TiO$_2$ were performed in acetone, showing a negligible conversion (<5%) and suggesting that it is the presence of Pt^0 particles which allows for H$_2$ uptake on the surface and catalyses F-Ac hydrogenation. Likewise, catalyst particle size (<30 μm) and vigorous stirring (1000 rpm) were chosen to avoid mass transfer limitations and internal diffusion resistance. The first hydrogenation step usually corresponds to the fast hydrogenation of the aliphatic C=C bond, which is favoured by thermodynamic conditions and the absence of steric limitations (unlike the case of the furanic ring bonds) [12,15,16]. An overview of the conversion results obtained from the performed experiments is represented in Fig. 3, where the studied polar solvents were grouped according to their chemical nature into (a) protic and (b) aprotic.

Fig. 3a shows a clear difference between the conversion rates of experiments carried out in methanol and 1-pentanol, and in the rest of the studied alcohols (ethanol, 1-propanol and 2-propanol). The latter group of solvents showed higher hydrogenation rates, achieving a full conversion of F-Ac already after 180 min of reaction. However, the hydrogenation rates of F-Ac when using 1-pentanol and methanol were substantially lower, leading to an incomplete conversion even after 480 min of reaction (97 and 92.5%, respectively). Similar behaviour was observed in Fig. 3b for aprotic solvents, where in acetone and tetrahydrofuran (THF) a complete conversion was reached at 240 min, whereas, due to a considerably lower hydrogenation rate, the final conversion (480 min) in *n*,*n*-dimethylformamide (DMF) was around 93%.

Table 2
Solvent polarity parameters of the studied solvents (Dipole moment (μ), dielectric constant (ε_r)) and initial hydrogenation rates of HDO conversion of F-Ac over Pt/TiO$_2$.

Solvent	μ Debye	ε_r (at 25 °C)	$r_0 \times 10^{-4}$ (mmol g_{cat}^{-1} min^{-1})
Methanol	1.70	32.7	0.80
Ethanol	1.69	24.3	4.31
1-propanol	1.68	20.1	7.77
2-propanol	1.66	18.3	8.08
1-pentanol	1.70	13.9	2.44
THF	1.63	7.6	1.72
Acetone	2.88	20.5	8.70
DMF	3.86	36.7	0.35

The factors responsible for these variations may in principle originate from different phenomena, such as: interaction of the solvent with the reactant, competitive adsorption on the catalyst surface, or reactant and hydrogen solubilities. The effects related to the solubility of the reactant can be considered negligible due to the high reaction temperature (200 °C) and the excess of solvent used (1 g of F-Ac per 150 ml solvent), ensuring a complete solvation of the reactant in all performed experiments. On the other hand, although in some cases solvent effects have been attributed to different hydrogen solubility measurements [31], most of the authors agree that a clear correlation cannot be established between hydrogenation activity and hydrogen solubility [22,24,32,33]. In this respect, it is worth to note that accurate data of hydrogen solubility under the operating conditions are difficult to obtain, and a limited information is available in the literature to correlate the obtained results for the whole set of studied solvents.

Concerning the influence of the solvent-reactant interactions, Table 2 summarizes polarity parameters of each solvent and the initial hydrogenation rates exhibited in them. The dipole moment (μ) provides information about the structure of the molecule, whereas dielectric constant (ε_r) is a useful macroscopic measurement of the solvent polarity. The initial hydrogenation rates were determined from the change in the molar concentration of F-Ac during the first 30 min.

The experimental results presented in Table 2 do not show any correlation between the initial hydrogenation rates and the polarity parameters when the complete series of the tested solvents is

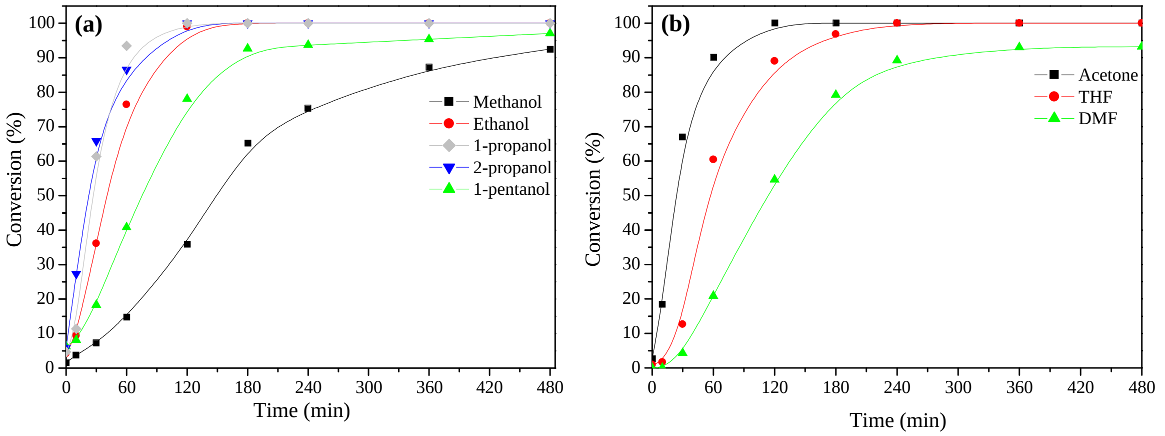

Fig. 3. Solvent effects on the conversion of 4-(2-furyl)-3-buten-2-one over Pt/TiO_2 catalyst; (a) protic and (b) aprotic solvents.

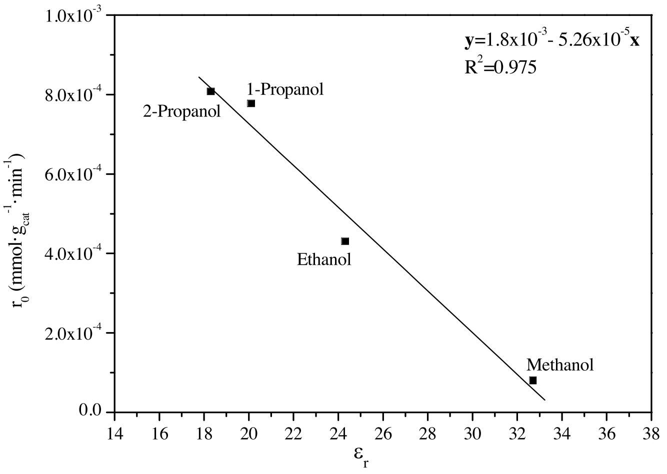

Fig. 4. Initial hydrogenation rates as a function of solvent dielectric constants of polar protic solvents.

considered. For instance, the highest hydrogenation activity was observed in acetone and 2-propanol in spite of the significant differences in their dipole moment (1.66 and 2.88 D, respectively). In contrast, a satisfactory correlation was found between the solvent polarity and the initial hydrogenation rate when considering only protic solvents. In general, the initial hydrogenation rate of F-Ac decreased as the polarity of the alcohol solvents increased. Thus, the variation in the dielectric constant values (ε_r) fitted reasonably well with the estimated initial hydrogenation rates. A linear correlation was found (Fig. 4) with the exception of 1-pentanol, which despite having a relatively low value of ε_r (13.9), presented a low initial hydrogenation rate (2.44×10^{-4} mmol g_{cat}^{-1} min^{-1}). The trend showed by most of the studied alcohols may be explained considering the hydrogen bond donors nature of protic solvents. This fact may be responsible for stronger bonding between the hydroxyl group of the alcohols and the reactant (F-Ac). Thus, as the polarity increases the solvent-reactant interaction becomes more important, improving the solvation effects and hindering the adsorption of F-Ac on the catalytic surface [24,33]. The unusually lower hydrogenation activity in 1-pentanol corresponds well with similar results obtained in hydrogenation of 1-phenyl-1,2-propanedione [22]. This behaviour may be related with the higher bulkiness of 1-pentanol, which can hinder the adsorption of the molecules, leading to a lower reaction rate [34]. Nevertheless, in this particular case probably other effects such as hydrogen solubility or adsorption strength may be involved as well.

Regarding the polar aprotic solvents, the initial hydrogenation rate pattern followed the trend: Acetone > THF > DMF, differing from the polarity correlation. Thus, no relationship between the initial hydrogenation rate and polarity parameters was found for the series of polar aprotic solvents. In particular, the highest initial hydrogenation rate was observed in acetone, which has an intermediate value of both μ and ε_r. Therefore, even though polarity parameters may play a significant role in the liquid phase hydrogenation of F-Ac, other physicochemical phenomena must be considered in order to explain the observed behaviour with polar aprotic solvents. In this respect, solvent adsorption on Pt/TiO_2 surface may have a strong influence on the catalytic activity. Despite the polar aprotic solvents are unable to act as hydrogen donors, they are good electron pair donor solvents. Thus, in case of working with bifunctional catalysts, the formation of strong complexes EPD/EPA (electron pair donor/electron pair acceptor) may occur through an electron transfer between the aprotic solvent (*n*-EPD) and the metal phase (υ-EPA) [35]. Consequently, a competitive solvent-reactant adsorption may arise, blocking partially the access of F-Ac molecules to the active sites and hindering the reaction progress. Fig. 5a shows the hydrogenation rates as a function of the nucleophilic donor number (DN), which represents a quantitative measure of the electron pair donor ability [36].

The initial hydrogenation rates showed a continuous decrease as DN of the polar aprotic solvents increased. For example, the best initial hydrogenation rate exhibited in acetone corresponded with the lowest DN (71 kJ mol^{-1}), whereas the limited hydrogenation activity showed by DMF is related to the highest DN (111.2 kJ mol^{-1}). These results may also be described as a coordinative Lewis base/acid interaction between the solvent (Lewis base) and the catalyst. Consequently, considering the accepted Lewis acid character of the Pt/TiO_2 catalyst (Fig. 2a), a series of chemisorption experiments was performed in order to confirm the strength of the solvent-catalyst interactions. Thus, following the method reported by Amenomiya et. al [26], the desorption enthalpy was calculated for each solvent and plotted as a function of the initial hydrogenation rate (Fig. 5b). The maximum desorption enthalpy was found for DMF, showing a value of 263 kJ mol^{-1}. On the contrary, acetone and THF presented considerably lower desorption enthalpies of 108 and 150 kJ&903;mol^{-1}, respectively. These results were consistent with DN data for polar aprotic solvents [36], showing a close correlation, and consequently, a very similar decreasing tendency of the initial hydrogenation rates (r_0) as energy of desorption (E_d) increased (Fig. 5a and b). These facts suggest that DMF interacts much stronger than THF and acetone with Pt/TiO_2 surface, promoting a competitive solvent/reactant adsorption on the catalyst active sites. Similarly, the higher hydrogenation rate observed in

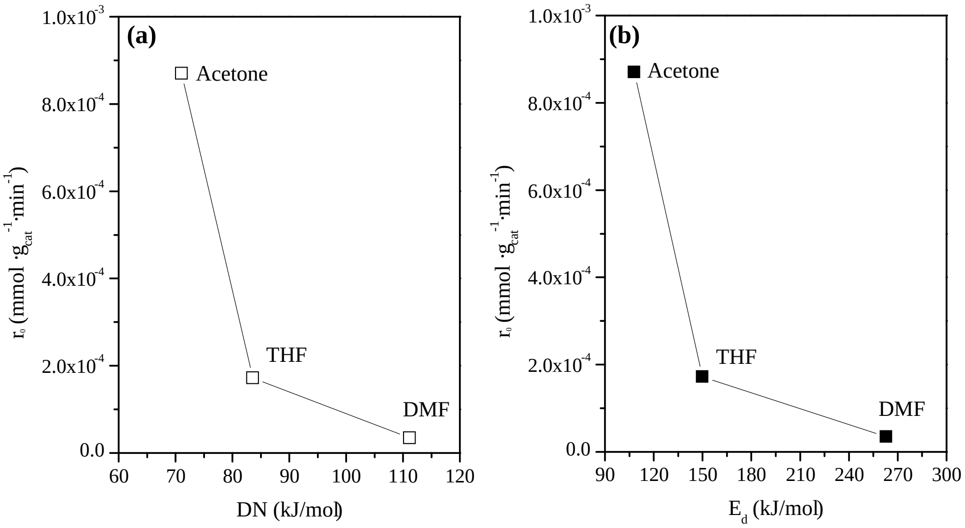

Fig. 5. Initial hydrogenation rate of F-Ac in aprotic solvents as a function of: (a) nucleophilic donor number [36] and (b) solvent desorption energy (calculated by TPD).

acetone would be related to the weaker adsorption of this solvent on Pt/TiO_2. In summary, we can conclude that solvent adsorption strength played an essential role in determining the F-Ac initial hydrogenation rate when polar aprotic solvents were used. On contrary, in the case of polar protic solvents the desorption enthalpies are not a so useful parameter due to the existence of other larger interactions like hydrogen bonding [35].

Obviously, it would have been interesting to complete the study using some apolar solvents, which are expected to show very weak interactions with both the reactant and the catalyst. However, from our own experience, 4-(2-furyl)-3-buten-2-one is nearly immiscible in both apolar solvents and in water, limiting the F-Ac concentration in the vicinity of the accessible active sites and inducing mass transfer limitations.

3.3. Hydrodeoxygenation products

The experimental data allowed elucidating that the transformation of F-Ac on bifunctional catalysts started with the initial hydrogenation of aliphatic C=C bond followed by further hydrogenation steps catalyzed by metals and continued by subsequent ring opening and deoxygenation reactions on acid and metal sites, respectively. According to a previous study [37], the further hydrogenation of the carbonyl group is more demanding since it is limited by the presence of the furan ring, which causes significant steric hindrances. In this respect, the hydrogenation of the furan ring is strongly influenced by the reactant adsorption mode on the metal sites, which is closely related to the metal dispersion and metal particle size [38]. Regarding the ring-opening and deoxygenation reactions, they typically require the presence of strong acid sites that facilitate C—O hydrogenolysis and dehydrations steps [39]. Fig. 6 displays an example of the evolution of the yields of the main products from the HDO of F-Ac when using acetone as a solvent. Based on the information provided by these kinetic curves, a reaction scheme was proposed in a previous work, demonstrating that a very complex mixture of products related through different catalytic transformations is formed [11].

Fig. 6 clearly shows that the first hydrogenation step of C=C aliphatic bond, forming 4-(2-furyl)-butan-2-one (**A**), is followed by formation of further hydrogenated products such as: 4-(2-tetrahydrofuryl)-butan-2-one (**B**), 4-(2-furyl)-butan-2-ol (**C**) and 4-(2-dihydrofuryl)-butan-2-ol (**D**). The presence of a maximum in the yield of those compounds reveals their intermediate character on the pathway towards the fully hydrogenated molecule 4-(2-tetrahydrofuryl)-butan-2-ol (**E**), which shows a continuous increase as the reaction proceeds. A similar trend is observed in the case of 2-butyl-dihydrofuran (**G**) and 2-butyl-tetedrahydrofuran (**H**), which are formed most probably by dehydration steps and subsequent ring hydrogenation of the primary products. The continuously increasing yield of these compounds (**E**, **G** and **H**) indicates a limitation in the subsequent ring opening steps on the conversion pathway of F-Ac to linear alcohols over Pt/TiO_2 catalyst. This fact is likely associated with the absence of stronger acid sites (mainly Brønsted), which, in combination with metal sites, are mostly responsible for ring-opening reactions typically through C—O hydrogenolysis. Nevertheless, in case of acetone as a solvent, a significant formation of octanediols and octanols (**J**) took place (≈10%), suggesting that ring opening takes place though to a limited extent.

The use of Pt/TiO_2 as a catalyst for the study of the solvent effects is justified by its multi-functional properties (metal sites and weak acidity/basicity) as well as by the absence of stronger basic/acid sites, which usually, under the selected operation conditions, promote side reactions with the solvent [11,40]. This selection was based on our previous work [11], in which Pt/TiO_2 catalyst showed the best conversion rate of furfural-acetone adducts and the lowest formation of solvent-reactants condensates. Thus, the use of weakly basic/acid support can be a suitable strategy to modify the catalyst performance, as long as the basicity/acidity is not strong enough to catalyze undesired reaction steps like aldol condensation, etherification or acetalization.

The above presented differences in F-Ac conversion rates could be also applied when discussing the concentration of intermediate compounds derived from the tandem reaction pathway of the studied HDO conversion [11,12]. Thus, solvent-reactant and solvent-catalyst interactions may affect the kinetics of each step, leading to major changes as the reaction proceeds. Fig. 7a shows the yields of the main hydrogenated products at the end of the reaction time (480 min). Thereby, important differences in the product distribution may be appreciated between the tested solvents. For example, the yield of **A** varies from 0% in case of 2-propanol to 60.5% for methanol. Similar deviations can be found in the production of **B**, **C** and **E** showing their maximum yields in ethanol (16%), THF (47.8%) and 2-propanol (40.4%), respectively. However, these variations may be considerably reduced if we refer to the results in terms of selectivity. Since the reaction time needed to reach full

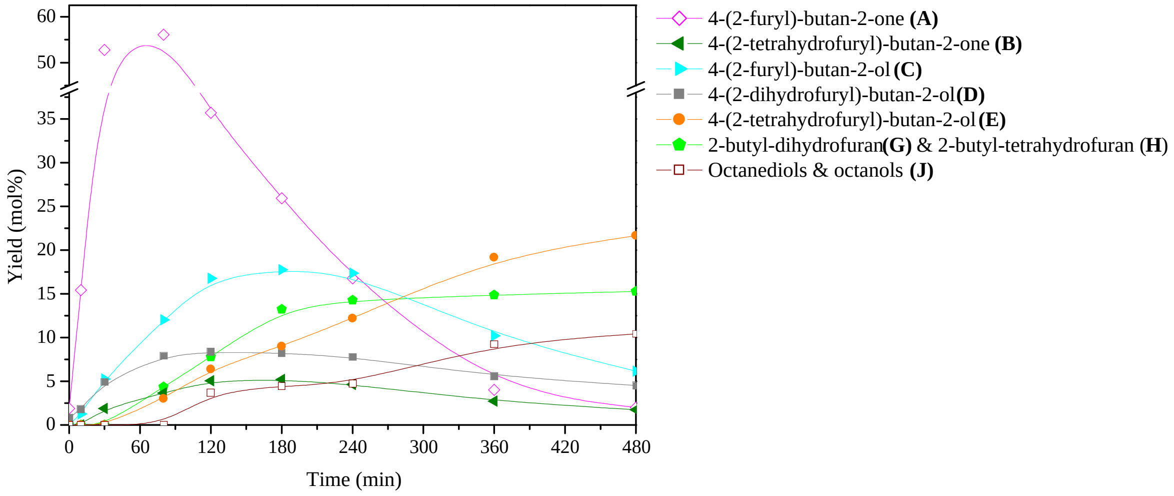

Fig. 6. Evolution of the yields of the main products from the HDO of 4-(2-furyl)-3-buten-2-one over Pt/TiO_2 using acetone as solvent.

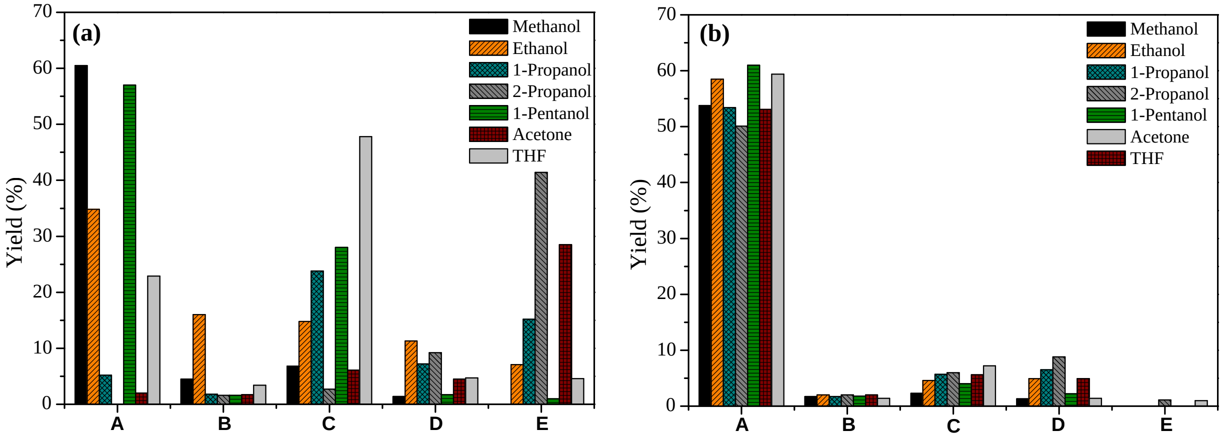

Fig. 7. Yields of the hydrogenated products from HDO of F-Ac at (a) the end of the reaction (480 min) and (b) considering the same conversion degree of F-Ac (70%).

conversion of the initial reactant (F-Ac) is very different in each experiment depending on the solvent used, the yields of the hydrogenated products showed in Fig. 7a could be strongly influenced by the conversion degree of F-Ac. In this respect, Fig. 7b represents the product distribution obtained with each solvent when considering the same conversion degree of F-Ac (i.e. 70%). Thus, for instance, the yield of **A** varies within a much narrower range (50–61%). Likewise, the yield variations of **B**, **C**, **D** and **E** are substantially reduced when the conversion of F-Ac is the same for each solvent. Hence, the results presented in Fig. 7 suggest that the yields of the products are strongly dependent on the conversion rates showed by each solvent, having a deeper impact due to the cascade reaction of the studied HDO conversion.

Table 3 summarizes the final yields (after 480 min) of the products from HDO of F-Ac in experiments using different solvents. As discussed above, it is important to mention that these results are primarily affected by the different hydrogenation rates showed by each solvent. The results derived from the use of DMF were not included in this table owing to the totally different product distribution obtained in this solvent media. This behaviour will be discussed in detail separately hereafter.

The catalytic performance of Pt/TiO_2 varied significantly depending on the applied solvent. In case of methanol, the reaction practically seized after the primary hydrogenation (**A** = 60.5%) and did not proceed further. As it has been previously reported [23,41], the smaller and more reactive is the alcohol the stronger is the hydrogen bonding between the carbonyl oxygen of the reactant and the hydroxy group of the solvent. Thus, in case of methanol the interaction was the most pronounced among the used solvents, reducing thus the preference towards C=O hydrogenation intermediate (**C**), which constitutes the preferred pathway in the following hydrogenation steps. The hydrogenation of the C=C furanic bonds (yielding **B**) is relatively limited in F-Ac due to the aromatic nature of the furan ring and also owing to the presence of the C=O bond in the same adsorption plane [42]. Thus, a selective hydrogenation of the C=O bond (**C**) took usually preference over the hydrogenation of furanic C=C (**B**) in most of the performed experiments. On the other hand, a significant yield (19.3%) of heavier products (molecular mass over 146 g mol^{-1}) were found in case of using methanol. This fact is in agreement with previous works reporting that shorter chain alcohols favour side reactions like acetalization [33] or etherification [41,43] between the reactant and the solvent. The formed acetal and ether intermediates may undergo further conversions at longer reaction times and/or higher temperatures, producing equally interesting hydrodeoxygenated by-products [44,45].

Similarly to methanol, the experiment carried out with 1-pentanol showed a high selectivity to the primary hydrogenated product (**A** = 57%), although in this case a significant hydrogenation of the C=O bond (**C** = 28%) was also observed. This fact can be attributed to the less effective hydrogen bonding between the solvent OH group and the reactant, due to the larger molecular size of 1-pentanol. In any case, according to these results, both protic sol-

Table 3
Yields of F-Ac hydrodeoxygenation products after 480 min (T = 200 °C; P(H_2) = 50 bar).

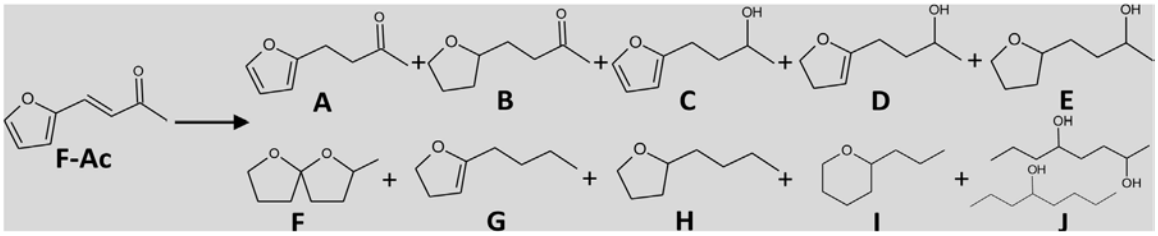

Solvent	Conv. (mol%)	Yield (mol%)								
		A	B	C	D	E	F	G + H	I	J
Methanol	92.5	60.5	4.5	6.8	1.4	0	0	0	0	0
Ethanol	100	34.8	16	14.8	11.3	7.1	7.2	6.5	0	2
1-Propanol	100	5.2	1.8	23.8	7.2	15.2	19.6	9.7	17.3	0
2-Propanol	**100**	**0**	**1.6**	**2.6**	**9**	**40.4**	**8.2**	**0**	**31.7**	**6.3**
1-Pentanol	92	57	1.6	28	1.7	1	2.5	0	0	0
THF	100	22.9	3.4	47.8	4.7	4.6	3.1	0	13.3	0
Acetone	**100**	**2**	**1.7**	**6.1**	**4.5**	**28.5**	**10.3**	**15.3**	**20.9**	**10.4**

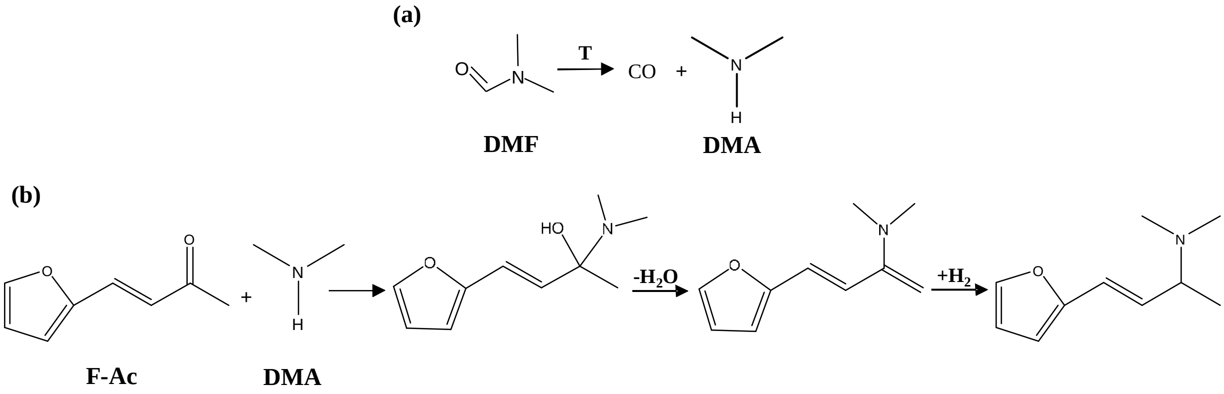

Fig. 8. Reaction scheme for (a) thermal decomposition of *n*,*n*-dimethylformamide and (b) addition of 4-(2-furyl)-3-buten-2-one and dimethylamine.

vents showed a limited HDO activity due to different causes namely strong reactant-alcohol interaction (methanol) and higher bulkiness (1-pentanol) which retarded F-Ac adsorption on the catalyst [34,41].

The hydrogenation degree of F-Ac was gradually enhanced when using ethanol, 1-propanol and 2-propanol, reaching yields of **E** equal to 7.1, 15.2 and 40.4% after 480 min, respectively. The better performance of 2-propanol over the rest of alcohols agrees well with the higher hydrogenation activity observed when secondary alcohols are used as solvents instead of primary alcohols [24,46]. This improvement in the hydrogenation ability has been attributed to an additional reduction mechanism involving H_2 transfer from the alcohol hydroxy group on the metal surface [24] or to the more effective hydrogen donor via inter-hydride transfer on Lewis acid catalysts [47,48]. The noticeable production of **B** in ethanol (16%) is probably related to the mentioned stronger hydrogen bonding (between the ketone group of the reactant and the solvent OH group) as the alcohol molecular size is reduced, preventing thereby the formation of further hydrodeoxygenated intermediates. Likewise, an important yield of 2-methyl-1,6-dioxaspiro[4,4]nonane (**F**) was observed, especially with 1-propanol (19.6%). The formation of this compound occurs via cyclization of **D** due to the interaction between the OH group and the partially hydrogenated furanic ring [49]. Dehydration also took place resulting in the elimination of hydroxyl groups from **C**, **D** and **E**, and consequently yielding products such as: 2-butyl-dihydrofuran (**G**), and 2-butyl-tetrahydrofuran (**H**) and 2-propyl-tetrahydropyran (**I**). Similarly to the production of **F**, the formation of **I** is associated with fast hydrogenation and isomerization of the partially hydrogenated furanic ring (**G**) [50]. The concentration of **I** was quite significant in 1-propanol (17.3%) and 2-propanol (31.7%), suggesting a pronounced extent of isomerization/cyclization steps when using these solvents. Nevertheless, both **F** and **I** constitute an important fraction of cyclic saturated products formed by undesirable side reactions that are difficult to transform into linear hydrocarbons due to the limited ring opening activity of the Pt/TiO_2 catalyst.

In case of aprotic solvents, pronounced differences were found between the product distribution showed by acetone and THF. In case of THF, along with aliphatic bond hydrogenation (**A** = 23%), a prominent yield of **C** was observed (47.8%). Equally, in spite of the low production of partially deoxygenated products (**G** and **H**), a remarkable formation of **I** was obtained (13.3%). This fact is likely a consequence of fast isomerization/cyclization reactions when using THF as a solvent. On the other hand, the HDO of F-Ac in acetone presents the highest production of both linear alcohols (**J** = 10.3%) and partially deoxygenated products (**G** + **H** + **I** = 36.2%). It also needs to be mentioned that a significant extent of acetone self-condensation was observed, yielding mesityl oxide (0.01 g cm^{-3}) and methyl isobutyl ketone (0.03 g cm^{-3}). Moreover, partial hydrogenation of acetone took place (<5%) forming 2-propanol in the reaction media. Both acetone and 2-propanol showed the highest yield of products found at the end of the HDO cascade reaction network (**J**, **G**, **H**, **I**,), which is in agreement with the higher conversion rates observed with these solvents. Therefore, the better performance of these solvents may be associated with a lower activation energy barrier for the key intermediate products, leading to enhanced reactions rates. Nevertheless, unlike in 2-propanol in which only octanediols were present, the use of acetone favoured the production of **G** and **H** (15.3%) which are the direct precursors for the formation of octanol. Its concentration in the final product mixture was 3.2%.

The product distribution observed when using DMF differed completely from the rest of the tested solvents, showing a high selectivity (>80%) to the formation of two isomers of 4-(2-furyl)-3-buten-2-dimethylamine. These compounds were likely formed via thermal decomposition of DMF into carbon dioxide and dimethylamine (Fig. 8a) [51], followed by the subsequent ketone amine addition between F-Ac and dimethylamine (Fig. 8b). This reaction involves the formation of the corresponding hemiaminal and enamine intermediates which are rapidly converted by dehydration and hydrogenation steps, respectively. Thus, despite the high conversion of F-Ac achieved with DMF (93%), the negligible yield of the targeted hydrodeoxygenated products discourages the use of this solvent. This fact illustrates the importance of a proper solvent selection not only with respect to conversion rates but also in terms of supressing undesirable side reactions.

4. Conclusions

Solvents influence the catalytic hydrodeoxygenation of 4-(2-furyl)-3-buten-2-one (F-Ac) by altering solvent-reactant and solvent-catalyst interactions. The use of Pt/TiO_2 as a catalyst allowed an almost complete conversion of F-Ac (>92%) with all the tested solvents after 480 min under $P(H_2) = 50$ bar and at $T = 200\,^{\circ}C$. The solvent polarity of protic solvents correlated well with the observed hydrogenation activity, indicating the importance of solvent-reactant interactions. Specifically, F-Ac conversion increased with decreasing protic solvent polarity. On the other hand, a strong interaction between the catalysts and the solvents could inhibit hydrogenation rate in case of aprotic polar solvents.

The differences in conversion rates have a strong influence on the obtained product distribution due to the complex network of reactions involved in the studied transformation. Thus, important differences were observed among the investigated solvents, achieving the best HDO activities when using 2-propanol and acetone. Despite the formation of stable cyclic intermediates such as 2-methyl-1,6-dioxaspiro[4,4]nonane (**F**) and 2-propyltetrahydropyran (**I**), the use of these solvents led to a significant production of 4-(2-tetrahydrofuryl)-butan-2-ol (28.5–40.4%) and linear alcohols (6.3–10.4%). The production of the latter demonstrated that, besides hydrogenation reactions, ring opening took place when using acetone and 2-propanol as solvents. Likewise, undesirable condensation reactions between the solvent and the reactant were also observed with methanol (etherification) and DMF (ketone-amine addition). The results indicate that in addition to the development and design of the catalysts, the appropriate selection of the solvent media is essential in order to optimise the HDO of furan derivatives compounds.

Acknowledgments

This publication is a result of the project no. P106/12/G015 supported by the Czech Science Foundation which is being carried out in the UniCRE center (CZ.1.05/2.1.00/03.0071) whose infrastructure was supported by the European Regional Development Fund and the state budget of the Czech Republic.

Appendix A. Supplementary data

Supplementary data associated with this article can be found, in the online version, at http://dx.doi.org/10.1016/j.apcata.2016.11.023.

References

[1] R.W. Torget, J.S. Kim, Y.Y. Lee, Ind. Eng. Chem. Res. 39 (2000) 2817–2825.
[2] K. Karimi, S. Kheradmandinia, M.J. Taherzadeh, Biomass Bioenergy 30 (2006) 247–253.
[3] Y. Román-Leshkov, J.N. Chheda, J.A. Dumesic, Science 312 (2006) 1933–1937.
[4] J.J. Bozell, G.R. Petersen, Green Chem. 12 (2010) 539–554.
[5] A.S. Dias, S. Lima, M. Pillinger, A.A. Valente, Adv. Synth. Chem. 8 (2010) 167–186.
[6] K.J. Zeitsch, The Chemistry and Technology of Furfural and Its Many By-products, vol. 13, Elsevier, 2000.
[7] G.W. Huber, J.N. Chheda, C.J. Barrett, J.A. Dumesic, Science 308 (2005) 1446–1450.
[8] L. Hora, V. Kelbichová, O. Kikhtyanin, O. Bortnovskiy, D. Kubička, Catal. Today 223 (2014) 138–147.
[9] A.D. Sutton, F.D. Waldie, R. Wu, M. Schlaf, A. Louis III, J.C. Gordon, Nat. Chem. 5 (2013) 428–432.
[10] L. Faba, E. Díaz, S. Ordónez, Appl. Catal. B: Environ. 160 (2014) 436–444.
[11] R. Ramos, Z. Tišler, O. Kikhtyanin, D. Kubička, Catal. Sci. Technol. 6 (2016) 1829–1841.
[12] L. Faba, E. Díaz, S. Ordóñez, Catal. Sci. Technol. 5 (2015) 1473–1484.
[13] L. Faba, E. Díaz, S. Ordóñez, Chem. Sus. Chem. 7 (2014) 2816–2820.
[14] Q.N. Xia, Q. Cuan, X.H. Liu, X.Q. Gong, G.Z. Lu, Y.Q. Wang, Ang. Chem. Int. Ed. 53 (2014) 9755–9760.
[15] C.J. Barrett, J.N. Chheda, G.W. Huber, J.A. Dumesic, Appl. Catal. B: Environ. 66 (2006) 111–118.
[16] R. Xing, A.V. Subrahmanyam, H. Olcay, W. Qi, G.P. van Walsum, H. Pendse, G.W. Huber, Green Chem. 12 (2010) 1933–1946.
[17] W. Xu, Q. Xia, Y. Zhang, Y. Guo, Y. Wang, G. Lu, Chem. Sus. Chem. 4 (2011) 1758–1761.
[18] J.N. Chheda, J.A. Dumesic, Catal. Today 123 (2007) 59–70.
[19] W. Xu, X. Liu, J. Ren, P. Zhang, Y. Wang, Y. Guo, G. Lu, Catal. Comm. 11 (2010) 721–726.
[20] K.L. Luska, J. Julis, E. Stavitski, D.N. Zakharov, A. Adams, W. Leitner, Chem. Sci. 5 (2014) 4895–4905.
[21] P. Mäki-Arvela, L.P. Tiainen, A.K. Neyestanaki, R. Sjöholm, T.K. Rantakylä, E. Laine, T. Salmi, D.Y. Murzin, Appl. Catal. A: Gen. 237 (2002) 181–200.
[22] E. Toukoniitty, P. Mäki-Arvela, J. Kuusisto, V. Nieminen, J. Päivärinta, M. Hotokka, T. Salmi, D. Murzin, J. Mol. Cat. A: Chem. 192 (2003) 135–151.
[23] J. Hájek, N. Kumar, P. Mäki-Arvela, T. Salmi, D.Y. Murzin, J. Mol. Cat. A: Chem. 217 (2004) 145–154.
[24] N.M. Bertero, A.F. Trasarti, C.R. Apesteguía, A.J. Marchi, Appl. Catal. A: Gen. 394 (2011) 228–238.
[25] P. Mäki-Arvela, J. Hajek, T. Salmi, D.Y. Murzin, Appl. Catal. A: Gen. 292 (2005) 1–49.
[26] R.J. Cvetanovic, Y. Amenomiya, Advan. Catal. Relat. Subj. 17 (1967) 103–149.
[27] M. Di Serio, M. Ledda, M. Cozzolino, G. Minutillo, R. Tesser, E. Santacesaria, Ind. Eng. Chem. Res. 45 (2006) 3009–3014.
[28] M. Bolognini, F. Cavani, D. Scagliarini, C. Flego, C. Perego, M. Saba, Catal. Today 75 (2002) 103–111.
[29] B. Coq, A. Tijani, F. Figuéras, J. Mol. Catal. 68 (1991) 331–345.
[30] A. Giroir-Fendler, D. Richard, P. Gallezot, Catal. Lett. 5 (1990) 175–181.
[31] P.A. Rautanen, J.R. Aittamaa, A.O.I. Krause, Ind. Eng. Chem. Res. 39 (2000) 4032–4039.
[32] A. Drelinkiewicza, A. Waksmundzka, W. Makowski, J.W. Sobczak, A. Król, A. Zieba, Catal. Lett. 94 (2004) 143–156.
[33] J. He, C. Zhao, J.A. Lercher, J. Catal. 309 (2014) 362–375.
[34] I. Kun, G. Szöllösi, M. Bartók, J. Mol. Catal. A: Chem. 169 (2001) 235–246.
[35] C. Reichardt, Verlag Chem. (1979).
[36] V. Gutmann, Electrochim. Acta 21 (1976) 661–670.
[37] H. Wan, A. Vitter, R.V. Chaudhari, B. Subramaniam, J. Catal. 309 (2014) 174–184.
[38] W. Zang, G. Li, L. Wang, X. Zhang, Catal. Sci. Technol. 5 (2015) 2532–2553.
[39] C.R. Waidmann, A.W. Pierpont, E.R. Batista, J.C. Gordon, R.L. Martin, R.M. West, R. Wu, Catal. Sci. Technol. 3 (2013) 106–115.
[40] P. Panagiotopoulou, D.G. Vlachos, Appl. Catal. A: Gen. 480 (2014) 17–24.
[41] P. Panagiotopoulou, N. Martin, D.G. Vlachos, J. Mol. Catal. A: Chem. 392 (2014) 223–228.
[42] R. Rao, A. Dandekar, R.T.K. Baker, M.A. Vannice, J. Catal. 171 (1997) 406–419.
[43] X. Hu, R.J. Westerhof, L. Wu, D. Dong, C.Z. Li, Green Chem. 17 (2015) 219–224.
[44] J. Luo, M. Monai, H. Yun, L. Arroyo-Ramírez, C. Wang, C.B. Murray, P. Fornasiero, R.J. Gorte, Catal. Lett. 146 (2016) 711–717.

[45] J. Luo, L. Arroyo-Ramírez, R.J. Gorte, D. Tzoulaki, D.G. Vlachos, AIChE J. 61 (2015) 590–597.
[46] J.I. Di Cosimo, A. Acosta, C.R. Apesteguía, J. Mol. Catal. A: Chem. 234 (2005) 111–120.
[47] M.A. Aramendıía, V. Borau, C. Jiménez, J.M. Marinas, J.R. Ruiz, F.J. Urbano, J. Mol. Catal. A: Chem. 171 (2001) 153–158.
[48] A. Martin, U. Armbruster, I. Gandarias, P.L. Arias, Eur. J. Lipid Sci. Technol. 115 (2013) 9–27.
[49] K. Alexander, L.S. Hafner, L.E. Schniepp, J. Am. Chem. Soc. 73 (1951) 2725–2726.
[50] A.A. Anderson, S.P. Simonyan, E. Lukevics, Chem. Het. Comp. 34 (1998) 1406–1408.
[51] J. Muzart, Tetrahedron 65 (2009) 8313–8323.

Catalysis Communications 114 (2018) 42–45

Contents lists available at ScienceDirect

Catalysis Communications

journal homepage: www.elsevier.com/locate/catcom

Short communication

Catalytic conversion of furfural-acetone condensation products into bio-derived C_8 linear alcohols over Ni—Cu/Al-SBA-15

Rubén Ramos[a], José M. Hidalgo[a], Michael Göpel[a], Zdeněk Tišler[a], Francine Bertella[b], Agustín Martínez[b], Oleg Kikhtyanin[a,c], David Kubička[c,*]

[a] Unipetrol Centre of Research and Education (UNICRE), Chempark Litvínov, Záluží-Litvínov 436 70, Czechia
[b] Instituto de Tecnología Química, Universitat Politècnica de Valencia (UPV-CSIC) - Consejo Superior de Investigaciones Científicas, Avda. de los Naranjos, s/n, 46022 Valencia, Spain
[c] Technopark Kralupy, University of Chemistry and Technology Prague, Žižkova 7, 27801 Kralupy nad Vltavou, Czechia

ARTICLE INFO

Keywords:
Furfural
Aldol condensation
Hydrogenation
SBA-15
Ni-Cu catalysts

ABSTRACT

The production of C_8 linear diols from a furfural-acetone condensation product has been achieved for the first time using a non-noble metal based catalyst. In particular, SBA-15 supported Ni—Cu bimetallic catalyst showed the best hydrogenating activity reaching an outstanding yield (*ca.* 63%) of the fully saturated product. The incorporation of acidity by the preparation of Ni—Cu/Al-SBA-15 resulted in the promotion of ring-opening steps, which led to a remarkable yield of C8 linear diols (28%). These results establish a competitive catalytic route for the production of bio-based diols over cost-efficient 3d transition metal-based catalysts.

1. Introduction

Within the context of future biorefineries, furanic compounds, such as furfural (C_5) and 5-hydroxymethylfurfural (C_6), are expected to play an essential role as bio-platform molecules for the production of chemicals and fuels. These compounds can be obtained by acid-catalysed hydrolysis and dehydration of C_5-C_6 carbohydrates, which constitute the main building blocks of lignocellulosic biomass [1, 2]. To obtain larger organic molecules, more suitable for the upgrading to biofuels, furan derivatives can be transformed by aldol condensation with other carbonyl-containing molecules forming C—C bonds [3–5]. This approach has been successfully applied for the condensation of furfural with acetone, yielding as main product: 4-(2-furyl)-3-buten-2-one (F—Ac) [6, 7]. The subsequent hydrogenation and C—O hydrogenolysis of this over-functionalized adduct leads to the production of versatile C_8 linear diols suitable for the synthesis of both biofuels and bio-derived polyesters (Fig. 1) [8]. This challenging transformation involves several chemical reactions, which require the use of high temperatures (170–300 °C), hydrogen pressures (20–80 bar) and the participation of heterogeneous catalysts capable of reducing the number of separate catalytic steps by allowing transformation of a wide variety of functionalities; *i.e.* furan rings, olefins and carbonyl groups [9].

Porous materials with easy accessibility of bulky reactants to surface acid and supported metal sites have attracted much attention in the conversion of furfural-acetone adducts. The presence of reduced metal phase(s) is required to promote the hydrogenation steps, whereas acid sites have been proved to be necessary for C—O hydrogenolysis reactions. Hence, Pd has shown a significant performance over supports such as: $NbOPO_4$ [10], cobalt aluminate [11], HZSM-5 [12], MgO-ZrO_2 [13] and Beta zeolite [14]. Equally, Pt has extensively studied using as carriers: $CoAl_2O_4$ and $NbOPO_4$ [15], SiO_2-Al_2O_3, zeolites, MgZr mixed oxide and activated carbons [16]. Likewise, promising results were obtained using Ru/C and Ru nanoparticles supported onto an ionic liquid phase [17].

Opposed to the use of noble-metal-based catalysts, the catalytic conversion of furfural-acetone adducts with readily available 3d transition metals has been scarcely studied. Likewise, to the best of our knowledge, the use of SBA-15 based catalysts has not been reported in the literature yet. This ordered mesoporous material exhibits excellent support properties advantageous for the aimed transformation, *e.g.*; high (hydro)thermal stability, large specific surface area ($> 700\,m^2\,g^{-1}$) and a well-defined mesoporous system (4–30 nm) [18]. Furthermore, the variable framework composition allows the incorporation of species such as Al or Zr [19], which provide the required surface acidity for further conversion towards the targeted alcohols.

In this work, we address further catalyst development in the conversion of furfural-acetone adducts using SBA-15 supported Ni and Cu catalysts. The obtained product distributions were correlated with physico-chemical properties of the catalysts. This study aims to establish a rational design of more efficient heterogeneous catalysts for the

---

[*] Corresponding author.
E-mail address: David.Kubicka@vscht.cz (D. Kubička).

https://doi.org/10.1016/j.catcom.2018.06.006
Received 12 February 2018; Received in revised form 29 May 2018; Accepted 6 June 2018

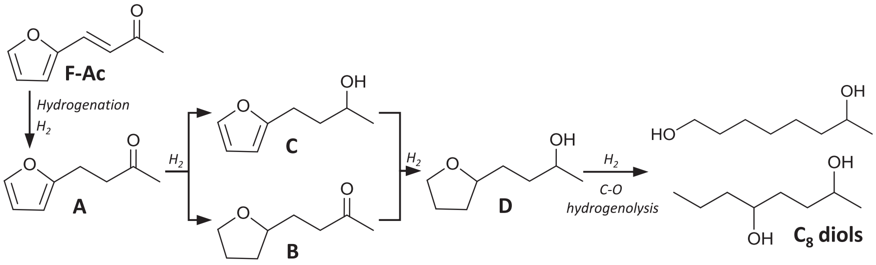

Fig. 1. Reaction pathway for the transformation of F—Ac into C_8 linear diols.

Table 1
F—Ac conversion over SBA-15 supported metal catalysts[a].

Catalyst	Metal[b] (wt%)	d_M[c] (nm)	Conv. (%)	Yield (%)					
				A	B	C	D	E	C_8 diols
Cu/SBA-15	3.4	–	59	59	–	–	–	–	–
Ni/SBA-15	10.2	39.4	100	0	3	52	25	9	–
Ni-Cu/SBA-15	10–3.1	41.9	100	–	–	8	**63**	16	–
Ni-Cu/Al-SBA-15	7–2.5	44.7	100	1	4	13	7	10	**17**
Pt/SBA-15	1	20.7	100	7	1	68	5	2	–
Pd/SBA-15	0.7	10.2	100	5	2	87	1	1	–
Ru/SBA-15	1.3	20.2	100	–	–	28	57	6	–

[a] Reaction conditions: 1 $g_{(F-Ac)}$, 150 ml acetone, 0.25 g_{cat}, T = 200 °C, P = 50 bar H_2, 1000 rpm, t = 8 h.

[b] Metal content calculated from ICP/TEM-EDX measurements.

[c] Mean metal crystallite size based on TEM images.

production of C_{8+} linear alcohols from lignocellulose-derived furanic compounds.

2. Experimental

2.1. Catalysts synthesis and preparation

Mesoporous all-silica SBA-15 and Al-containing (Si/Al = 30) SBA-15 materials were synthesised according to the method reported by Zukal et al. [20]. The incorporation of metal phases was carried out by incipient wetness impregnation. After impregnation, the samples were dried at 120 °C overnight and calcined in air at 550 °C for 6 h. Further details related to the synthesis and preparation methods are given in the ESI.

2.2. Catalysts characterization

The prepared catalysts were characterized for their chemical composition (ICP-OES, FESEM-EDX), BET area and pore size distribution (N_2 physisorption isotherms), surface acidity (NH_3-TPD) and morphology (HAADF-STEM), as described in the ESI.

2.3. Catalytic experiments

All reactions were performed in a high-pressure autoclave reactor system. Prior to the reaction, the catalyst was reduced in a flow of H_2. Afterwards, the reactor was cooled to room temperature and loaded with a solution of F—Ac (1 g) in acetone or 2-propanol (150 ml). Subsequently, the reactor was heated to 200 °C and the reaction started by pressuring the autoclave to 50 bar of hydrogen. The identification and quantification of the products were done using standard reference compounds and chromatographic methods (see ESI).

3. Results and discussion

Table 1 shows the product distributions obtained from the conversion of F—Ac over different SBA-15 supported metal catalysts using acetone as solvent. The reaction conditions (T = 200 °C, P_{H2} = 50 bar and 1000 rpm) were based on our previous findings regarding the conversion of F—Ac with different supported Pt catalysts [9]. In addition to the products listed in Table 1, other compounds, like 2-methyl-1,6-dioxaspiro[4,4]nonane and 2-propyltetrahydropyran were also identified with yields < 3%.

The Cu/SBA-15 sample showed an incomplete conversion of the F—Ac reactant after 8 h (59%) forming 4-(2-furyl)-butan-2-one (A) as the only product. The hydrogenation of the furan ring and the ketone group was completely impeded, in accordance with the poor catalytic performance of similar Cu-containing catalysts in hydrogenation of furfural [21, 22] and ketone-containing reactants [23, 24]. On the other hand, the Ni/SBA-15 catalyst exhibited a remarkable hydrogenation of F—Ac, affording a significant yield of the fully hydrogenated 4-(2-tetrahydrofuryl)-butan-2-ol (D = 25%). These differences can be attributed to the different in structure and nature preferential adsorption sites over Cu and Ni. Thus, while Cu metal surfaces have very weak affinity for the C=C bonds of the furan ring, the stronger adsorption of these bonds over Ni metal surfaces promotes the hydrogenation of the furan ring and the C=O group, which is in the same plane [22]. These results highlight the good performance of the Ni loaded catalyst showing a higher hydrogenation activity than SBA-15 supported Pt and Pd catalysts (D = 1–5%). On the other hand, the Ru/SBA-15 catalyst showed a higher production of D (57%), consistent with the reported high selectivity of this metal for furan ring hydrogenation [25]. Likewise, a noticeable production of 2-butyl-furan and 2-butyl-tetrahydrofuran (E = 6–9%) was observed when using supported Ni and Ru catalysts, indicating that C—OH hydrogenolysis reactions occurred to some extent on these supported metals.

The Ni—Cu/SBA-15 bimetallic catalyst exhibited a significantly different catalytic activity compared to Ni and Cu monometallic catalysts. Particularly, the Ni—Cu/SBA-15 sample showed the highest yield of D (63%) and E (16%) among the tested materials. Similar synergetic catalytic effects from the combination of Ni and Cu were previously proven in ethanol steam reforming [26, 27], glycerol hydrogenolysis [28] and hydrogenation of furfural and aromatics [29, 30]. According

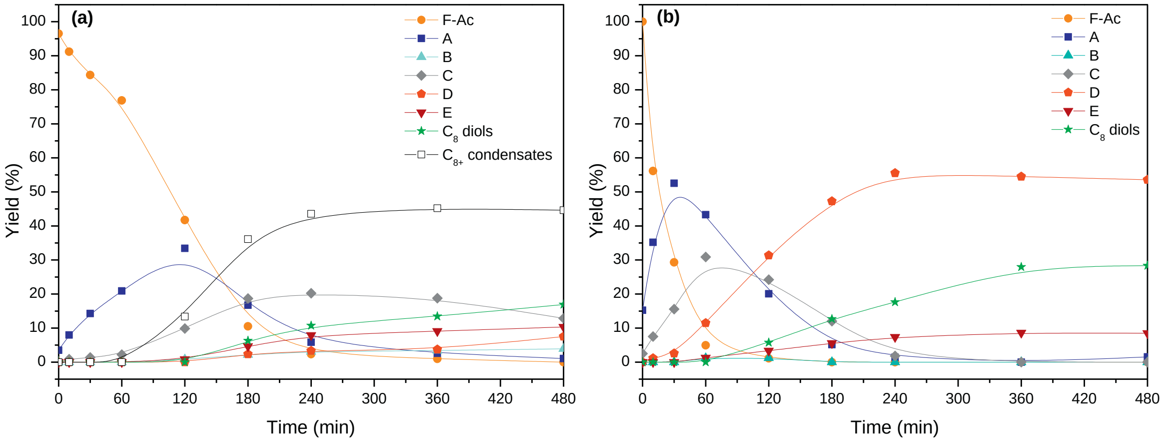

Fig. 2. Time evolution of F—Ac conversion and yield of products over the Ni—Cu/Al-SBA-15 catalyst in (a) acetone and (b) 2-propanol. $T = 200$ °C and $P = 50$ bar H_2.

to these studies, the improved performance was due to an active Ni—Cu binary phase exhibiting electronic properties different from the monometallic counterparts [31]. Because of the fewer d-band holes in the Ni—Cu bimetallic phase compared to Ni, the adsorption strength of active hydrogen is weakened, enhancing its diffusion on the catalyst surface and facilitating hydrogenation reactions [32]. Hence, the Ni—Cu bimetallic catalyst enhanced the hydrogenation rate of F—Ac, along with a higher promotion of C-OH hydrogenolysis reactions.

Despite the superior hydrogenation activity shown by the Ni—Cu/SBA-15 catalyst, no linear compounds were detected in the product mixture, suggesting the inhibition of ring-opening steps over this material. This behaviour can be related to the absence of surface acid sites, since those are usually required to promote the C—O hydrogenolysis of furanic rings [9]. Thus, the purely siliceous SBA-15 support was modified by incorporating Al during the synthesis procedure to introduce mild surface acidity (Al-SBA-15, Si/Al = 30). The subsequent impregnation with Ni and Cu metal phases resulted in a bifunctional Ni—Cu/Al-SBA-15 catalyst, which combined surface acid sites and the hydrogenating metal phase (see characterization of this catalyst by N_2 physisorption, NH_3-TPD and electron microscopy in Figs. 1–3 of the ESI).

The obtained product distribution using Ni—Cu/Al-SBA-15 showed a significant yield of 2,5-octanediol and 1,7-octanediol (C_8 diols = 17%), together with a low yield of D (7%). The formation of further deoxygenated octanols was not observed, suggesting that C—O hydrogenolysis/dehydration of the produced diols are limited under the reaction conditions. However, the main fraction of products corresponded to longer carbon chain compounds $C_{8+} \approx 44\%$ (not listed in Table 1). The formation of these heavier by-products is likely due to the aldol condensation between ketone-containing compounds (mostly A) and acetone (Fig. 5 of the ESI). This reaction has been reported to prevail in the presence of acid sites and at moderate temperatures [9, 33]. Accordingly, despite yielding linear compounds through C—O hydrogenolysis, the extent of aldol condensation as side reaction over the Ni—Cu/Al-SBA-15 catalyst reduced the selectivity towards the targeted C_8 diols.

In order to prevent the formation of the heavier by-products, we tested the performance of the Ni—Cu/Al-SBA-15 catalyst using 2-propanol instead of acetone as a solvent to limit condensation reactions. In this sense, 2-propanol has been revealed as an excellent solvent in the conversion of F—Ac due to its protic nature, intermediate polarity ($\varepsilon_r = 18.3$) and secondary alcohol character [34]. Fig. 2 depicts the reaction progress profiles over Ni—Cu/Al-SBA-15 in acetone (Fig. 2a) and 2-propanol (Fig. 2b). In both experiments, A was the first intermediate due to the favoured hydrogenation of the C=C aliphatic bond, reaching a maximum at short reaction times (30–120 min). The following hydrogenation of A formed products like B, C and D. The yield of the latter was considerably different in acetone (7%) and 2-propanol (53%) after 480 min of reaction. This fact could be related with the formation of condensate products when using acetone and with the promotion of catalytic hydrogen transfer reactions (based on the Meerwein-Ponndorf-Verley reduction) in 2-propanol (Fig. 2a). On the contrary, aldol condensation reactions did not take place in 2-propanol (C_{8+} compounds were not detected), showing a higher selectivity towards the fully hydrogenated product D. Both C_{8+} condensates (in Fig. 2a) and D (in Fig. 2b) exhibited a similar yield over time behaviour, showing a continuous increase in the interval 60–240 min and no significant change at reaction times > 240 min. The latter trend is likely associated with the total consumption of their main precursors after 240 min, *i.e.* F—Ac, A and B. On the other hand, the lack of further conversion of D suggests that the C—O hydrogenolysis of this compound is not favoured under the reaction conditions applied. Thus, the noticeable production of C_8diols reached in 2-propanol (28%) likely occurs *via* ring opening of other intermediates like A or C. This observation agrees with previous studies which report that C—O hydrogenolysis of furanic compounds preferentially takes place through non-saturated rings (such as hydrofuranic) due to the higher activation energy required for tetrahydrofuran intermediates [35–37].

4. Conclusions

A direct catalytic process for the partial defunctionalisation of furfural-acetone adducts using non-noble metal-based catalysts under mild reaction conditions has been reported. A bimetallic Ni—Cu phase supported on Al-SBA-15 has been demonstrated as an effective catalyst to produce C_8 linear diols. The combination of a highly redox-active metal phase and acid sites promotes the required hydrogenation and C—O hydrogenolysis reactions. Likewise, the noticeable differences between acetone and 2-propanol reveal the great impact of the solvent on the obtained product distribution, affecting both activity and selectivity. Nevertheless, more studies of the non-precious Ni—Cu/Al-SBA-15 catalysts are required for deeper understanding, mainly of the catalytic chemistry and stability. Equally, the use of alternative solvents with lower H_2 solubility and slower hydrogenation kinetics could be explored in order to promote acid-ring opening over furan hydrogenation reactions. This work improves the understanding of the conversion of furfural-acetone adducts, and may enable the design of 3d transition metals-based catalysts for the transformation of furanic compounds to fuels and commodity chemicals.

Acknowledgements

This work was supported by the Czech Science Foundation (project No. P106/12/G015).

References

[1] J.N. Chheda, Y. Román-Leshkov, J.A. Dumesic, Green Chem. 9 (2007) 342–350.
[2] I. Agirrezabal-Telleria, I. Gandarias, P.L. Arias, Catal. Today 234 (2014) 4–58.
[3] A. Bohre, S. Dutta, B. Saha, M.M. Abu-Omar, ACS Sustain. Chem. Eng. 3 (2015) 1263–1277.
[4] M.I. Alam, S. Gupta, A. Bohre, E. Ahmad, T.S. Khan, B. Saha, M.A. Haider, Green Chem. 18 (2016) 6431–6435.
[5] S. Dutta, A. Bohre, W. Zheng, G.R. Jenness, M. Núñez, B. Saha, D.G. Vlachos, ACS Catal. 7 (2017) 3905–3915.
[6] L. Faba, E. Díaz, S. Ordóñez, Appl. Catal. B Environ. 113 (2012) 201–211.
[7] L. Hora, V. Kelbichová, O. Kikhtyanin, O. Bortnovskiy, D. Kubička, Catal. Today 223 (2014) 138–147.
[8] X. Tang, J. Wei, N. Ding, Y. Sun, X. Zeng, L. Hu, L. Lin, Renew. Sustain. Energy Rev. 77 (2017) 287–296.
[9] R. Ramos, Z. Tišler, O. Kikhtyanin, D. Kubička, Catal. Sci. Technol. 6 (2016) 1829–1841.
[10] Q.N. Xia, Q. Cuan, X.H. Liu, X.Q. Gong, G.Z. Lu, Y.Q. Wang, Angew. Chem. Int. Ed. 53 (2014) 9755–9760.
[11] W. Xu, X. Liu, J. Ren, P. Zhang, Y. Wang, Y. Guo, G. Lu, Catal. Commun. 11 (2010) 721–726.
[12] J. Yang, N. Li, S. Li, W. Wang, L. Li, A. Wang, X. Wang, Y. Cong, T. Zhang, Green Chem. 16 (2014) 4879–4884.
[13] J.N. Chheda, J.A. Dumesic, Catal. Today 123 (2007) 5970.
[14] A. Bohre, B. Saha, M.M. Abu-Omar, ChemSusChem 8 (2015) 4022–4029.
[15] W. Xu, Q. Xia, Y. Zhang, Y. Guo, Y. Wang, G. Lu, ChemSusChem 4 (2011) 1758–1761.
[16] L. Faba, E. Díaz, S. Ordóñez, Catal. Sci. Technol. 5 (2015) 1473–1484.
[17] K.L. Luska, J. Julis, E. Stavitski, D.N. Zakharov, A. Adams, W. Leitner, Chem. Sci. 5 (2014) 4895–4905.
[18] Y. Yang, C. Ochoa-Hernández, V.A. de la Peña, J.M. O'Shea, D.P. Serrano Coronado, ACS Catal. 2 (2012) 592–598.
[19] J.A. Melero, L.F. Bautista, J. Iglesias, G. Morales, R. Sánchez-Vázquez, Catal. Today 195 (2012) 44–53.
[20] A. Zukal, J. Pastva, J. Čejka, Microporous Mesoporous Mater. 167 (2013) 44–50.
[21] S. Sitthisa, D.E. Resasco, Catal. Lett. 141 (2011) 784–791.
[22] R.S. Rao, R.T.K. Baker, M.A. Vannice, Catal. Lett. 60 (1999) 51–57.
[23] R. Ramos, A. Grigoropoulos, N. Perret, M. Zanella, A.P. Katsoulidis, T.D. Manning, J.B. Claridge, M.J. Rosseinsky, Green Chem. 19 (2017) 1701–1713.
[24] X.L. Li, J. Deng, J. Shi, T. Pan, C.G. Yu, H.J. Xu, Y. Fu, Green Chem. 17 (2015) 1038–1046.
[25] R. Alamillo, M. Tucker, M. Chia, Y. Pagán-Torres, J.A. Dumesic, Green Chem. 14 (2012) 1413–1419.
[26] A.J. Vizcaíno, A. Carrero, J.A. Calles, Int. J. Hydrog. Energy 32 (2007) 1450–1461.
[27] A. Carrero, J.A. Calles, A.J. Vizcaíno, Appl. Catal. A Gen. 327 (2007) 82–94.
[28] I. Gandarias, J. Requies, P.L. Arias, U. Armbruster, A. Martin, J. Catal. 290 (2012) 79–89.
[29] R.M. Lukes, C.L. Wilson, J. Am. Chem. Soc. 73 (1951) 4790–4794.
[30] A.G. Boudjahem, W. Bouderbala, M. Bettahar, Fuel Process. Technol. 92 (2011) 500–506.
[31] S.D. Robertson, B.D. McNicol, J.H. De Baas, S.C. Kloet, J.W. Jenkins, J. Catal. 37 (1975) 424–431.
[32] Y. Yao, D.W. Goodman, J. Mol. Catal. A Chem. 383 (2014) 239–242.
[33] O. Kikhtyanin, V. Kelbichová, D. Vitvarová, M. Kubů, D. Kubička, Catal. Today 227 (2014) 154–162.
[34] R. Ramos, Z. Tišler, O. Kikhtyanin, D. Kubička, Appl. Catal. A Gen. 530 (2017) 174–183.
[35] S. Wang, V. Vorotnikov, D.G. Vlachos, Green Chem. 16 (2014) 736–747.
[36] A.D. Sutton, F.D. Waldie, R. Wu, M. Schlaf, A. Louis III, J.C. Gordon, Nature 5 (2013) 428–432.
[37] S. Yao, X. Wang, Y. Jiang, F. Wu, X. Chen, X. Mu, A.C.S. Sustain, Chem. Eng. 2 (2013) 173–180.